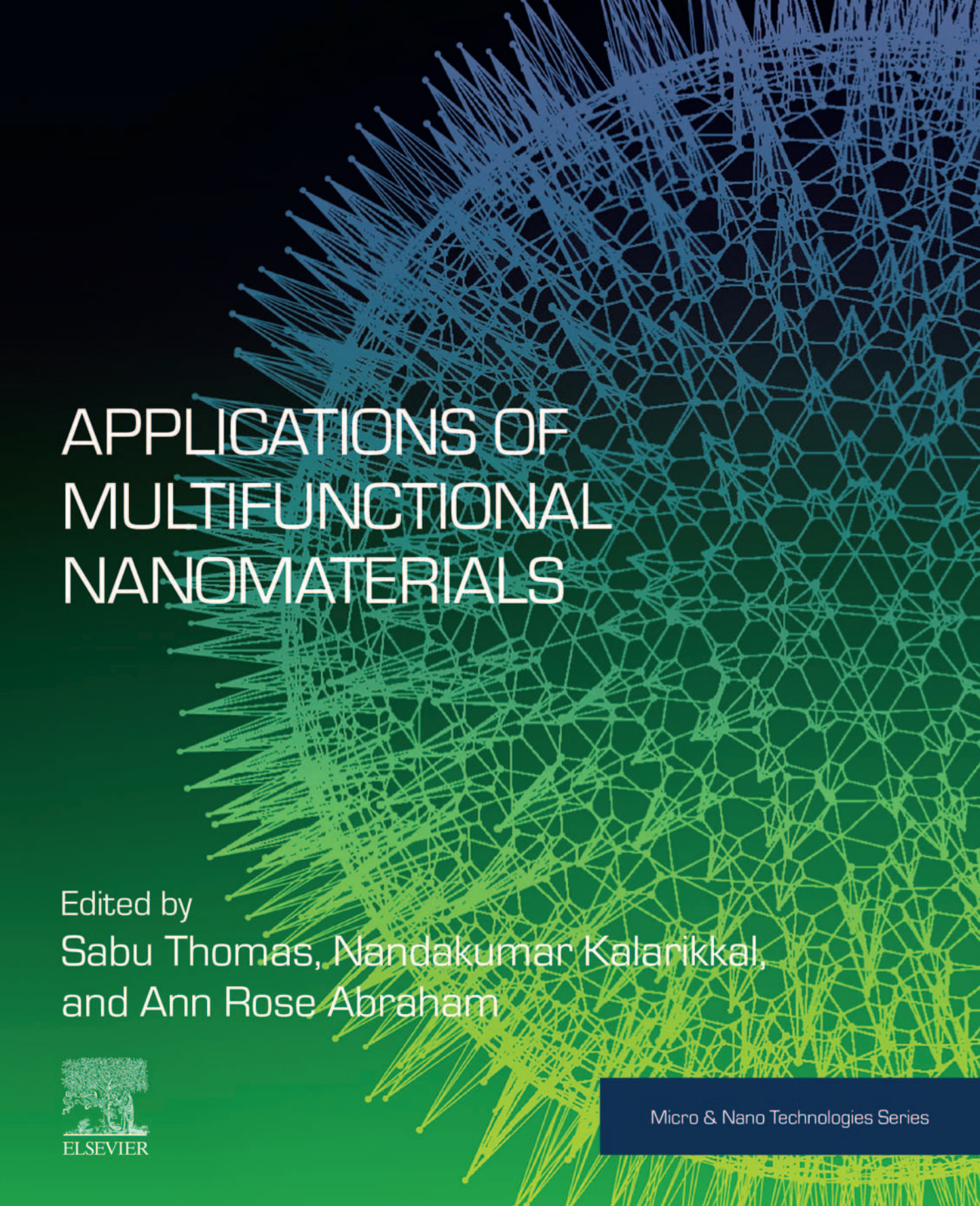

APPLICATIONS OF MULTIFUNCTIONAL NANOMATERIALS

Edited by
Sabu Thomas, Nandakumar Kalarikkal, and Ann Rose Abraham

ELSEVIER

Micro & Nano Technologies Series

APPLICATIONS OF MULTIFUNCTIONAL NANOMATERIALS

This page intentionally left blank

MICRO AND NANO TECHNOLOGIES

APPLICATIONS OF MULTIFUNCTIONAL NANOMATERIALS

Edited by

SABU THOMAS
School of Energy Materials, Mahatma Gandhi University, Kottayam, Kerala, India

NANDAKUMAR KALARIKKAL
International and Inter University Centre for Nanoscience and Nanotechnology, School of Pure and Applied Physics, Mahatma Gandhi University, Kottayam, Kerala, India

ANN ROSE ABRAHAM
Department of Physics, Sacred Heart College (Autonomous), Thevara, Kochi, India

ELSEVIER

Elsevier
Radarweg 29, PO Box 211, 1000 AE Amsterdam, Netherlands
The Boulevard, Langford Lane, Kidlington, Oxford OX5 1GB, United Kingdom
50 Hampshire Street, 5th Floor, Cambridge, MA 02139, United States

Notices

Knowledge and best practice in this field are constantly changing. As new research and experience broaden our understanding, changes in research methods, professional practices, or medical treatment may become necessary.

Practitioners and researchers must always rely on their own experience and knowledge in evaluating and using any information, methods, compounds, or experiments described herein. In using such information or methods they should be mindful of their own safety and the safety of others, including parties for whom they have a professional responsibility.

To the fullest extent of the law, neither the Publisher nor the authors, contributors, or editors, assume any liability for any injury and/or damage to persons or property as a matter of products liability, negligence or otherwise, or from any use or operation of any methods, products, instructions, or ideas contained in the material herein.

ISBN: 978-0-12-820557-0

Publisher: Matthew Deans
Acquisitions Editor: Glyn Jones
Editorial Project Manager: Tom Mearns
Production Project Manager: Sreejith Viswanathan
Cover Designer: Mark Rogers

Typeset by TNQ Technologies

Contents

18. Nanoparticles in oral health care: clinical insights and future perspectives

Anurag Satpathy, Punyatoya Panda, Reetuparna Nanda, Subhashree Priyadarsini, and Monalisa Mishra

19. Nebulizer spray delivery of phytopharmaceutical nanosuspension via oral and nasal route: a challenging approach to fight against COVID-19

Abhishek Bhattacharjee, Sabu Thomas, and Partha Palit

IV

Biomedical applications of nanomaterials

20. Bio-nanomaterials and their applications

Mohd Talha, Nishit Pathak, Sanjib Bhattacharyya, and Yuanhua Lin

21. Can bio-nanotechnology be effective against multi drug resistant (MDR) pathogens?

Divya P. Sukumaran, and Mohamed Hatha Abdulla

22. Nanomaterials in bioimaging and cell labeling

K. Sapna, P.P. Manzur Ali, and A.A. Mohamed Hatha

29. Bio-nanomaterials: applications and utility in agricultural and medical field

V
Environmental applications

30. Enhanced cocatalysis of bimetallic nanostructures for catalytic and photocatalytic applications

31. Nanomaterials incorporated electrospun membranes for membrane distillation

32. Application of multifunctional carbon-based silver nanocomposites for environmental remediation

Contributors

Mohamed Hatha Abdulla Department of Marine Biology, Microbiology and Biochemistry, School of Marine Sciences, Cochin University of Science and Technology, Kochi, Kerala, India

Ann Rose Abraham Department of Physics, Sacred Heart College (Autonomous), Thevara, Kochi, Kerala, India

Pinky Abraham St. Gregorious College, Kottarakkara, Kollam, Kerala, India

Jiji Abraham Vimala College (Autonomous), Thrissur, Kerala, India

Arjun Ajith Mohan Nanoscience Research Laboratory, School of Materials Science and Engineering, National Institute of Technology Calicut, Kozhikode, Kerala, India

A. Anil Center for Materials for Electronics Technology [C-MET], MeitY, Government of India, Thrissur, Kerala, India

P. Anitha College of Veterinary and Animal Sciences, Kerala Veterinary and Animal Sciences University, Mannuthy, Thrissur, Kerala, India

Pius Augustine Materials Research Laboratory, Department of Physics, Sacred Heart College (Autonomous), Thevara, Kochi, India; Materials Research Centre, Indian Institute of Science, Bangalore, Karnataka, India

Saji Augustine Department of Physics, St. Thomas College, Kottayam, Kerala, India; Department of Physics, Deva Matha College, Kottayam, Kerala, India

S. Balasubramanian Department of Inorganic Chemistry, University of Madras, Chennai, Tamil Nadu, India

Aadil Bathla School of Chemistry and Biochemistry, Thapar Institute of Engineering & Technology, Patiala, Punjab, India

Abhishek Bhattacharjee Department of Pharmaceutical Sciences, Assam University, Silchar, Assam, India

Sanjib Bhattacharyya Department of Pharmaceutical Science and Chinese Traditional Medicine, Southwest University, Chongqing, China

M. Bindu Polymer Science and Technology Laboratory, Department of Chemistry, National Institute of Technology Calicut, Kozhikode, Kerala, India

Subir Kumar Biswas Laboratory of Active Bio-based Materials, Research Institute for Sustainable Humanosphere, Kyoto University, Uji, Kyoto, Japan; Pulp and Paper Division, Bangladesh Forest Research Institute, Sholoshahor, Chattogram, Bangladesh

Suryasarathi Bose Department of Materials Engineering, Indian Institute of Science, Bangalore, Karnataka, India

Sandeep Chaudhary Department of Chemistry, Visvesvaraya National Institute of Technology Nagpur, Nagpur, Maharashtra, India

Suchitra Rajput Chauhan Centre for Advanced Materials and Devices (CAMD), School of Engineering and Technology, BML Munjal University, Kapriwas, Haryana, India

Ashwini Chauhan Department of Microbiology, Tripura University (A Central University), Tripura, India; Invisiobiome, New Delhi, Delhi, India

Jincemon Cyriac Department of Physics, St. Thomas College, Kottayam, Kerala, India; Department of Physics, Sree Narayana College, Chengannur, Alappuzha, Kerala, India; Department of Physics, Marian College Kuttikkanam (Autonomous), Peermade, Idukki, Kerala, India

Mónica Cristina García Universidad Nacional de Córdoba, Facultad de Ciencias Químicas, Departamento de Ciencias Farmacéuticas, Ciudad Universitaria, Haya de la Torre and Medina Allende, Córdoba, Argentina; Consejo Nacional de Investigaciones Científicas y Técnicas, CONICET, Unidad de Investigación y Desarrollo en Tecnología Farmacéutica, UNITEFA, Córdoba, Argentina

Soney C. George Centre for Nanoscience and Technology, Amal Jyothi College of Engineering, Kottayam, Kerala, India

Sumana Ghosh Bio-ceramics and Coating Division, CSIR-Central Glass and Ceramic Research Institute (CSIR-CGCRI), Kolkata, West Bengal, India

Sruthi Gopal Membrane Separation Group, Department of Chemical Engineering, National Institute of Technology Calicut, Kozhikode, Kerala, India

K.P. Greeshma Sri Ramakrishna College of Arts and Sciences (Autonomous) Coimbatore, Tamil Nadu, India

Noel Jacob Kaleekkal Membrane Separation Group, Department of Chemical Engineering, National Institute of Technology Calicut, Kozhikode, Kerala, India

Sam John Department of Chemistry, St. Berchmans College, Mahatma Gandhi University Kottayam, Kerala, India

Shiny Joseph Department of Chemical Engineering, National Institute of Technology Calicut, Kozhikode, Kerala, India

Khasthi Ballabh Joshi Department of Chemistry, School of Chemical Science and Technology, Harisingh Gour Vishwavidyalaya (A Central University), Sagar, Madhya Pradesh, India

Nandakumar Kalarikkal School of Pure and Applied Physics, Mahatma Gandhi University, Kottayam, Kerala, India; International and Inter University Centre for Nanoscience and Nanotechnology, Mahatma Gandhi University, Kottayam, Kerala, India; School of Nanoscience and Nanotechnology, Mahatma Gandhi University, Kottayam, Kerala, India

Mohd Jahir Khan Diatom Nanoengineering and Metabolism (DNM) Laboratory, School of Applied Sciences, Harisingh Gour Vishwavidyalaya (A Central University), Sagar, Madhya Pradesh, India

S. Kiran Polymer Science and Engineering Division, CSIR-National Chemical Laboratory, Pune, Maharashtra, India; Academy of Scientific and Innovative Research (AcSIR), Ghaziabad, India

Indradeep Kumar Department of Aeronautical Engineering, Institute of Aeronautical Engineering, Hyderabad, Telangana, India

Yuanhua Lin School of New Energy and Materials, Southwest Petroleum University, Chengdu, Sichuan, China; State Key Laboratory of Oil and Gas Reservoir Geology and Exploitation, Southwest Petroleum University, Chengdu, Sichuan, China

Mary R. Louis Department of Chemistry, Visvesvaraya National Institute of Technology Nagpur, Nagpur, Maharashtra, India

S. Malathi Department of Inorganic Chemistry, University of Madras, Chennai, Tamil Nadu, India; Crystal Growth Centre, Anna University, Chennai, Tamil Nadu, India

Akshit Malhotra Department of Microbiology, Tripura University (A Central University), Tripura, India; Invisiobiome, New Delhi, Delhi, India

P.P. Manzur Ali MES Mampad College, Malappuram, Kerala, India

Muthuchamy Maruthupandy Laboratorio de Nanocelulosa y Biomateriales, Departamento de Ingeniería Química, Biotecnología y Materiales, Facultad de Ciencias Físicas y Matemáticas, Universidad de Chile, Santiago, Chile

Sunny Mathew Department of Physics, Marian College Kuttikkanam (Autonomous), Peermade, Idukki, Kerala, India

Aishwarya V. Menon Department of Materials Engineering, Indian Institute of Science, Bangalore, Karnataka, India

Monalisa Mishra Neural Developmental Biology Lab, Department of Life Science, NIT Rourkela, Rourkela, Odisha, India; Siksha O Anusandhan University, Bhubaneshwar, Odisha, India

A.A. Mohamed Hatha Department of Marine Biology, Microbiology and Biochemistry, School of Marine Sciences, Cochin University of Science and Technology, Kochi, Kerala, India

Sumit Mukherjee Neural Developmental Biology Lab, Department of Life Science, NIT Rourkela, Rourkela, Odisha, India

Thillaichidambaram Muneeswaran Laboratorio de Nanocelulosa y Biomateriales, Departamento de Ingeniería Química, Biotecnología y Materiales, Facultad de Ciencias Físicas y Matemáticas, Universidad de Chile, Santiago, Chile

Vimal Antony Muttathettu College of Veterinary and Animal Sciences, Kerala Veterinary and Animal Sciences University, Mannuthy, Thrissur, Kerala, India; College of Avian Sciences and Management, Kerala Veterinary and Animal Sciences University, Thiruvazhamkunnu, Palakkad, Kerala, India

Giuvanni Mutton Chimie ParisTech, PSL University, CNRS, Institut de Recherche de Chimie Paris, Paris, France

Sonali Naik Polymer Science and Engineering Division, CSIR-National Chemical Laboratory, Pune, Maharashtra, India; Academy of Scientific and Innovative Research (AcSIR), Ghaziabad, India

Reetuparna Nanda Siksha O Anusandhan University, Bhubaneshwar, Odisha, India

S. Narayana Kalkura Crystal Growth Centre, Anna University, Chennai, Tamil Nadu, India

Bonamali Pal School of Chemistry and Biochemistry, Thapar Institute of Engineering & Technology, Patiala, Punjab, India

Shiny Palatty Department of Chemistry, Bharata Mata College, Kochi, Kerala, India

Partha Palit Department of Pharmaceutical Sciences, Assam University, Silchar, Assam, India

Punyatoya Panda Neural Developmental Biology Lab, Department of Life Science, NIT Rourkela, Rourkela, Odisha, India; Siksha O Anusandhan University, Bhubaneshwar, Odisha, India

Nishit Pathak Department of Pharmaceutical Science and Chinese Traditional Medicine, Southwest University, Chongqing, China

Subhashree Priyadarsini Siksha O Anusandhan University, Bhubaneshwar, Odisha, India

Franck Quero Laboratorio de Nanocelulosa y Biomateriales, Departamento de Ingeniería Química, Biotecnología y Materiales, Facultad de Ciencias Físicas y Matemáticas, Universidad de Chile, Santiago, Chile; Millennium Nucleus on Smart Soft Mechanical Metamaterials, Santiago, Chile

K.R. Rekha Mol Department of Marine Biology, Microbiology & Biochemistry, School of Marine Sciences, Cochin University of Science and Technology, Kochi, Kerala, India

B.P. Resmi Centre for Nanoscience and Technology, Amal Jyothi College of Engineering, Kottayam, Kerala, India; TKM Institute of Technology, Ezhukone, Kollam, Kerala, India

N. Sandhyarani Nanoscience Research Laboratory, School of Materials Science and Engineering, National Institute of Technology Calicut, Kozhikode, Kerala, India

K. Sapna Department of Marine Biology, Microbiology and Biochemistry, School of Marine Sciences, Cochin University of Science and Technology, Kochi, Kerala, India

Anurag Satpathy Neural Developmental Biology Lab, Department of Life Science, NIT Rourkela, Rourkela, Odisha, India; Siksha O Anusandhan University, Bhubaneshwar, Odisha, India

Vincent Semetey Chimie ParisTech, PSL University, CNRS, Institut de Recherche de Chimie Paris, Paris, France

Md. Iftekhar Shams Forestry and Wood Technology Discipline, Life Science School, Khulna University, Khulna, Bangladesh

Sreekala S. Sharma Department of Chemistry, Bharata Mata College, Kochi, Kerala, India; Department of Chemistry, Sree Sankara Vidyapeetom College, Ernakulam, Kerala, India

Devansh Sharma Department of Materials Engineering, Indian Institute of Science, Bangalore, Karnataka, India

Laxmi Gayatri Sorokhaibam Department of Chemistry, Visvesvaraya National Institute of Technology Nagpur, Nagpur, Maharashtra, India

Sreelakshmi Rajeevan Centre for Nanoscience and Technology, Amal Jyothi College of Engineering, Kottayam, Kerala, India

Rajesh Srivastava Department of Biotechnology, GIT, Gitam Institute of Technology and Management (GITAM), Visakhapatnam, Andhra Pradesh, India

Alagappan Subramaniyan Department of Physics, Thiagarajar College of Engineering, Madurai, Tamil Nadu, India

Divya P. Sukumaran Department of Marine Biology, Microbiology and Biochemistry, School of Marine Sciences, Cochin University of Science and Technology, Kochi, Kerala, India

Sathyavathi Sundararaju Department of Pathology, Division of Pathology Sciences, Sidra Medicine, Doha, Qatar

Mohd Talha School of New Energy and Materials, Southwest Petroleum University, Chengdu, Sichuan, China; State Key Laboratory of Oil and Gas Reservoir Geology and Exploitation, Southwest Petroleum University, Chengdu, Sichuan, China

Sabu Thomas School of Chemical Sciences, Mahatma Gandhi University, Kottayam, Kerala, India; International and Inter University Centre for Nanoscience and Nanotechnology, Mahatma Gandhi University, Kottayam, Kerala, India; School of Energy Materials, Mahatma Gandhi University, Kottayam, Kerala, India

Arun Torris Polymer Science and Engineering Division, CSIR-National Chemical Laboratory, Pune, Maharashtra, India

G. Unnikrishnan Polymer Science and Technology Laboratory, Department of Chemistry, National Institute of Technology Calicut, Kozhikode, Kerala, India

Ruby Varghese Department of Chemistry, School of Sciences, Jain Deemed to be University, Bangalore, Karnataka, India

Thirumalaisamy Vennila Department of Chemistry, Sri Sairam Engineering College, Chennai, Tamil Nadu, India

Vandana Vinayak Diatom Nanoengineering and Metabolism (DNM) Laboratory, School of Applied Sciences, Harisingh Gour Vishwavidyalaya (A Central University), Sagar, Madhya Pradesh, India

Xianpeng Yang Laboratory of Active Bio-based Materials, Research Institute for Sustainable Humanosphere, Kyoto University, Uji, Kyoto, Japan

Hiroyuki Yano Laboratory of Active Bio-based Materials, Research Institute for Sustainable Humanosphere, Kyoto University, Uji, Kyoto, Japan

Foreword to applications of multifunctional nanomaterials

What multifunctional nanomaterials can do for future technologies

Nanomaterials are not new any longer. They have infiltrated all fields of technology and penetrated our daily life, as they are widely used in devices ranging from mobile phones and computers to cars that we drive and medicines that we take. This means that they have become practically useful and important. Nanomaterials are nanoscale building blocks that provide new properties and enable new technologies. Many materials change their properties at the nanoscale. For example, thin metal films become transparent, keeping their conductivity. Nanoscale gold particles may have different colors, depending on their size. Electrons are confined in nanoparticles, giving rise to quantum effects. Medicine uses nanosized particles that can penetrate cellular membranes. Much of the biology occurs at the nanometer scale. Water purification is done by nanomaterials having a large specific surface area. Some of those are new, some are very old. For example, activated carbon (charcoal) is known from ancient time, but we now understand that it works as a good sorbent because of nanometer and even subnanometer pores in carbon particles, and we have learned how to control the size of those pores to accommodate molecules of different sizes. However, to move beyond the currently available technologies, we need better materials, we need new materials, and we need materials that can perform more than one function, so known multifunctional nanomaterials. The examples include structural batteries that can transform the body of a car into an energy storage device eliminating the need for a large battery in the trunk or under the car. On the opposite size of the length scale are theranostic (therapeutic and diagnostic) nanoparticles capable of carrying a drug and its targeted delivery to the required location in the body. Those nanoparticles can perform additional functions like being fluorescent to enable their tracking and transform light to heat to destroy tumors. Building multiple functionalities into nanomaterials opens new horizons for medical and many other technologies.

What do we expect from the future nanomaterials? It is, first of all, precise control over the size, composition, structure, and properties. Nano is not so much about the size as it is about nanoscale control of materials that allows us to finely tune their properties. Moreover, the goal is often to achieve new and unusual properties that are not available in conventional bulk materials. If one nanomaterial cannot have all the required properties and perform multiple functions, nanomaterials are combined to form hybrid materials (e.g., catalytic metal or oxide particles supported on electrically conductive and mechanically strong graphene or nanotubes) or nanocomposites (e.g., conducting nanoparticles in a dielectric polymer matrix).

We already have many nanoparticles/nanostructures to choose from. Zero-

dimensional nanoparticles include fullerenes, metal and ceramic nanopowders, and colloidal metal, ceramic, and organic particles, such as proteins. One-dimensional nanostructures include DNA, carbon and other nanotubes, nanofibers, and nanowires. Two-dimensional (2D) structures, with graphene being the leader, are probably currently the fastest expanding group, as many new and previously unknown 2D materials, such as silicene, germanene, borophene, and MXenes (2D carbides and nitrides of transition metals), have been discovered. However, they also include many well-known materials such as boron nitride, transition metal dichalcogenides, and oxides/hydroxides, including clays, which are receiving renewed attention. 2D materials attract attention not only because of a variety of useful properties but also because they are easy to assemble into continuous films and coatings. Moreover, 2D sheets with very different properties (metallic, dielectric, semiconducting, etc.) can be combined into hybrids, like bricks in a wall or Lego stones, producing new multifunctional materials with almost any imaginable combination of compositions and properties. As long as we have a sufficient variety of those building blocks, we can build anything we need. This drives search for new 2D materials with different properties that can add to the existing variety. New technologies, such as wearable and flexible electronics, and Internet of Things lead to an increasing demand for solution processable and printable nanoparticles and can be used to manufacture flexible, multifunctional nanomaterials.

This book covers many classes of multifunctional nanomaterials. For example, it discusses the use of magnetic nanoparticles for electromagnetic interference shielding. With increasing number of transmitting devices around us, we need better protection from electromagnetic noise that they create. It talks about application of nanoparticles in health care. Nanoparticles on face masks and other surfaces can kill viruses, like COVID-19, and bacteria. Hydroxyapatite and some other nanoparticles can promote bone growth. Many advances in biomedical field have been achieved due to use of nanoparticles for imaging. Those are new synthetic nanoparticles. However, there is plenty of room for inexpensive natural nanoparticles, like clays, for use in animal nutrition, agriculture, water purification, environmental technologies, and also structural polymer nanocomposites. Again, the key to their proper use is understanding and control of properties, such as the size and degree of exfoliation of two-dimensional clay nanosheets. Having this wealth of multifunctional nanomaterials for a variety of applications collected in one book should help readers navigate this large, important, and quickly expanding field.

Yury Gogotsi, Ph.D., D.Sc., Dr.h.c.
Charles T. and Ruth M. Bach,
Distinguished University Professor
Director, A.J. Drexel Nanomaterials Institute
Drexel University, Philadelphia, Pennsylvania, USA

CHAPTER

1

The ample gamut of applications of multifunctional nanomaterials

Ann Rose Abraham[1], *Nandakumar Kalarikkal*[2,3,4] *and Sabu Thomas*[3,5]

[1]Department of Physics, Sacred Heart College (Autonomous), Thevara, Kochi, Kerala, India; [2]School of Pure and Applied Physics, Mahatma Gandhi University, Kottayam, Kerala, India; [3]International and Inter University Centre for Nanoscience and Nanotechnology, Mahatma Gandhi University, Kottayam, Kerala, India; [4]School of Nanoscience and Nanotechnology, Mahatma Gandhi University, Kottayam, Kerala, India; [5]School of Energy Materials, Mahatma Gandhi University, Kottayam, Kerala, India

1. Applications of multifunctional nanomaterials: an overview

The distinct and exceptional physicochemical properties exhibited by nanomaterials have contributed to its significant advancements in nanoparticle systems capable of providing the necessary functionalities. The chapter briefly describes new avenues opened up by nanomaterials for various applications.[1–3] The present chapter provides an overview of promising applications of nanomaterials and their role for next generation futuristic applications. It is quite evident that there is a great prospect for engineered hybrid nanomaterials in all fields like physics, chemistry, biomedicine,[3] sensor, energy,[4–6] engineering,[7,8] optics,[9] and industrial applications.[10]

Multifunctional nanomaterials are of increased interest in various industrial applications. This book highlights the revolutionary applications made possible by nanoparticles in fields of energy devices, energy generation and storage,[10] electromagnetic interference shielding,[11] biomedicine,[12,13] environment remediation,[14] photcatalysis,[14] and industrial applications.[15] The role of nanomaterials in the fight against COVID is highlighted in the book. Various biomedical[16–23] applications like nanoparticles as drug delivery agents, oral health care and in agricultural field are also emphasized. Hybrid nanomaterials for electromechanical applications, electrochemical sensing, photocatalytic applications, fuel cell applications, and environmental remediation[24] are also discussed.

Applications of Multifunctional Nanomaterials
https://doi.org/10.1016/B978-0-12-820557-0.00033-3

The book chapters highlighting the diverse applications of nanomaterials can be introduced as follows. The book is specifically divided into different sections which deal with applications of different applications of diverse classes of nanomaterials like magnetic nanoferrites, carbon-based nanomaterials, bionanomaterials, polymer nanocomposites, etc. The book chapters are introduced briefly as follows. Part I of the book, dealing with Chapters 2–9, gives a description of various energy applications of nanomaterials exploiting magnetic nanomaterials, multiferroics, and also carbon nanomaterials. Part II of the book, dealing with Chapters 10–14, focuses on various industrial applications of nanomaterials like electromechanical applications, photodetection, etc. Part III of the book dealing with Chapters 15–18 gives emphasis to the nanoparticles in health care. Part IV of the book dealing from Chapters 19–29 describing the biomedical applications of nanomaterials illuminates the role of bionanomaterials in bioimaging, cell labeling, therapeutic, diagnostic applications and also nano minerals, in animal nutrition. Part V of the book divided into Chapters 30–32 describes environmental applications of nanomaterials. A brief schematic of the different applications of nanomaterials described in the book is illustrated in Fig. 1.1.

Chapter 2 entitled "Nanoferrites for electromagnetic shielding applications" discusses the appealing potential of ferrites in shielding electromagnetic waves. This chapter comprehensively describe the various types of ferrites that have been popularly used over the past decade as well as the modifications made to them to extend the electromagnetic wave shielding properties over a wider frequency window.

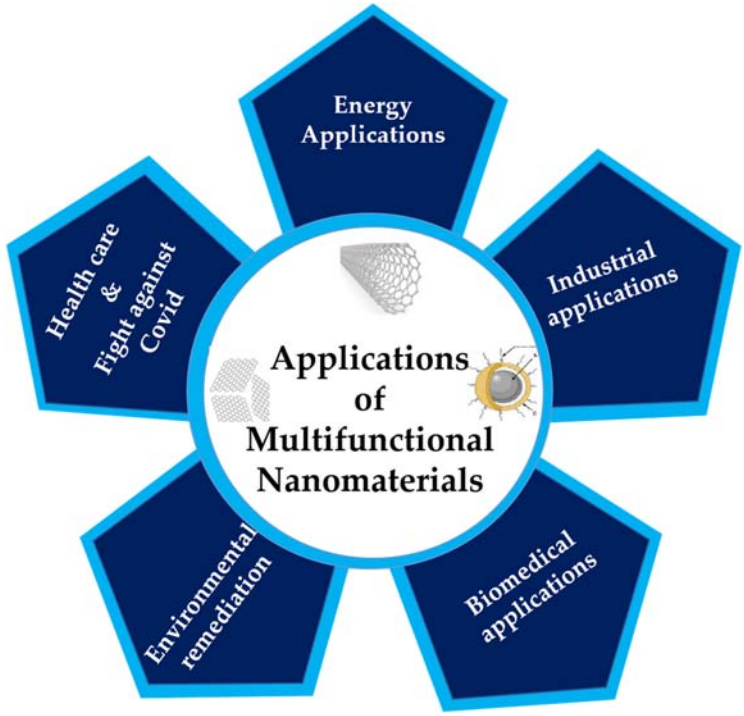

FIGURE 1.1 Applications of multifunctional nanomaterials.

Chapter 3 entitled "Rare earth doped $BiFeO_3$ multiferroic system: optical, dielectric and magnetoelectric coupling applications" describes the dielectric, optical, and magnetoelectric coupling properties of Bismuth ferrite multiferroic system. Rare earth doping enhances the dielectric properties and the magneto electric coupling coefficient of the system and indicates its potential applications in spintronics and ferroelectric nonvolatile memory applications.

Chapter 4 entitled "Carbon nanostructures for energy generation and storage" highlights the exceptional prospects of carbon-based nanomaterials in the field of clean energy generation and storage technologies. Significant emphasis is given in the chapter to hydrogen production through water splitting, fuel cells, giving focus to direct methanol fuel cells and enzymatic fuel cells and supercapacitors.

Chapter 5 entitled "Nano engineering diatoms in microfluidic lab on chip devices" discusses a technology to upscale sun-based fuel generation and separation from living microalgal cells. The chapter describes the development of efficient, economical and sensitive nano-engineered diatom microfluidic devices that keep a check on dead cells and bacterial contamination, permitting only high lipid containing diatoms to grow and multiply thus keeping them in living state.

Chapter 6 entitled "Nano composite membrane for direct methanol fuel cell" exemplifies the current status of research and the role played by nanocomposite polymer electrolyte membrane for performance of direct methanol fuel cells.

Chapter 7 entitled "Elastomeric foam for energy applications: Energy devices" describes the improved properties of polymer foams, production pathways and applications in the energy sector. A brief overview of different types of elastomeric foams for energy application and energy devices are highlighted in the chapter.

Chapter 8 entitled "Nanocellulose-based polymer composites for energy applications" illustrates nanocellulose as an ideal architecture block for connecting with a variety of capacitive energy storage substrates. The chapter highlights the impressive characteristics and applications of cellulose-modified composite materials and carbon materials used as independent element for high-performance sodium ion capacitors or sodium ion batteries.

Chapter 9 entitled "Advances in functionalized Polyaniline nanocomposites for electrochemical sensing and energy storage applications" presents a brief overview of developments in Polyaniline-based nanocomposites for energy storage, conversion devices as well as other electrochemical applications. The development of nanocomposites of functionalized polyaniline with carbon nanotube, metal organic framework, and transition metal oxide composites in the development of clean energy storage devices, particularly supercapacitors are also discussed in the chapter.

Chapter 10 entitled "Multifunctional hydroxylapatite nanofillers for fine-tuning of elastomer characteristics" focuses on the characteristics of nanoreinforcements and the importance of fine tuning the properties of some elastomeric matrices. The chapter highlights the role of hydroxylapatite nanoparticles in modulating the mechanical, dielectric, viscoelastic properties, and in vitro biocompatibility of elastomers.

Chapter 11 entitled "Emerging applications of nanofluids" describes the applications of nanofluids on enhanced heat transfer and design of cooling requirements in Electronics industry. It focuses on emerging applications of nanofluids including, industrial cooling, oil recovery, machining process, improving natural gas storage, and others including sensor fabrication.

Chapter 12 titled "Promising inorganic nanomaterials for future generation" deals with different kinds of inorganic nanomaterials such as metallic, inorganic nanomaterials, nonmetallic inorganic nanomaterials, carbon-based nanomaterials, nanopolymers, dendrimers, quantum dots, magnetic nanomaterials, composite inorganic nanomaterials, ceramic-based nanomaterials, and other recently developed nanomaterials having great prospects for versatile applications in future. The chapter describes the prospects of these inorganic nanomaterials in radiotherapy, chemotherapy sensitization, biomedical, and other industrial applications.

Chapter 13 entitled "Two-dimensional layered materials for efficient photodetection" describes utilization of Transition metal dichalcogenides as ideal candidates for photodetection over conventional silicon-based technology. The effectiveness of MoS_2-based thin-film photodetectors in photodetection and also the efficacy of the Pulsed Laser Deposition in realizing MoS_2-based thin-film heterostructure photodetectors are analyzed in the chapter.

Chapter 14 entitled "Electromechanical application of magnetite nanomaterials blended with single-walled carbon nanotubes" addresses the nanotechnology applications in electromechanical components. The synthesis and development of physically stable, thermally robust, and environmentally friendly nanosheets using nanopowder of iron oxide and single-walled carbon nanotubes for electromechanical component applications like transformers, inductors, bobbins, etc. are highlighted in the chapter.

Chapter 15 titled "Nanoparticles as drug delivery agents for managing diabetic retinopathy" describes the applications of nanoparticles in ocular delivery and to prevent progression of diabetic retinopathy. The chapter also discusses various strategies to deliver nanoparticle-based drugs and their toxic effects. This chapter highlights current treatment strategies of diabetic retinopathy using nanotechnology and also to formulate nano-based therapeutics that will be helpful in the future.

Chapter 16 entitled "Stimuli responsive self-assembled nanocarriers based on amphiphilic block copolymers for cancer therapy" describes stimuli-driven ABCP-based self-assembled nanostructures, which recognize changes in external or internal environment that trigger the release of the payload, thus, conducting *on-demand* release behavior. Special emphasis is given to polymersomes and the recent advances in their biomedical applications in the treatment of cancer.

Chapter 17 entitled "Nanoparticles in oral health care: clinical insights and future perspectives" provides a comprehensive overview of the application of nanoparticles in advanced dental materials, drugs, and techniques that are currently exploited for prevention and treatment of ailments such as dental caries, periodontal disease, dentinal hypersensitivity, tooth discoloration, maxillofacial prosthesis, oral cancer, etc.

Chapter 18 entitled "Nanosuspension based Intra-nasal, or Intra-oral Nebulizer spray with phytopharmaceuticals: challenging fight against COVID-19" discusses the profound antimicrobial activity of nanosuspension of phytopharmaceuticals like curcumin, piperine, sinigrin, etc. on inhibiting the infection of SARS, influenza, and coronavirus.

Chapter 19 entitled "Bio-nanomaterials and applications" application of nanomaterials in medicine, treatment of diseases, effective drug delivery, and other clinical applications. The chapter emphasizes the unique properties like surface plasmon resonance exhibited by metallic nanoparticles which makes them applicable as markers for the optical detection of bio-molecules.

Chapter 20 entitled "Can bio-nanotechnology be effective against multi-drug resistant (MDR) pathogens?" describes nanoparticles as the most promising tools to curb antibiotic resistant bacteria, which do not allow bacteria to acquire resistance. The chapter highlights the potential of silver nanoparticles as the most effective nanomaterial against multidrug resistant bacteria.

Chapter 21 entitled "Nanomaterials in bioimaging and cell labeling" summarizes the progress in nanoparticle-based cell labeling which has emerged as an important aspect of disease diagnostics and therapeutics for efficient labeling of stem, immune, and cancer cells and as dyes to facilitate tracking of tissue-specific cells.

Chapter 22 entitled "Biological prospects and potential of nanoparticles in animal nutrition" briefly describes the potential of nanoparticles, their activity, and significance in animal applications. The use of nanominerals for enhancing the bioavailability of the mineral feed supplements in the livestock industry is highlighted in the chapter.

Chapter 23 entitled "Use of lectin-functionalized and lectin-targeted nanomaterials for multiple therapeutic applications" addresses the biotechnological potential of lectin-based nanoparticles in the pharmaceutical applications, diagnosis, and therapeutic effect and other innovative biomedical applications, highlighting recent advances in this emerging field.

Chapter 24 entitled "Construction and application of bionanomaterials" briefs the role of smart, functional nanomaterials and nonobots that provide an adaptable platform in exploring several chronic illnesses and other therapeutic applications in a more noninvasive route.

Chapter 25 entitled "Medical device associated-biofilm eradication strategies: use of multifunctional nanomaterials" illuminates the potential of multi-functional nanomaterials to prevent bacterial adhesion, interfere bacterial colonization, and mediate drug delivery to eradicate bacterial biofilm aggregates relevant to medical devices and clinical settings.

Chapter 26 entitled "Bionanofiber-reinforced transparent nanocomposites for future applications" describes the preparation, properties, and potential applications of transparent nanocomposites reinforced by bio-derived nanocelluloses, nanochitins, and their nanostructured mesoporous microfibers/microparticles. The prospects of these bio-based, transparent, light-weight, strong and flexible, nanocomposites as substrates and structural windows for photonics, optoelectronics, vehicles, and buildings are described in the chapter.

Chapter 27 entitled "Nano-biomaterials for therapeutic and diagnostic applications" focuses on the potential biomedical applications of metal and metal oxide nanoparticles in treating infections and targeted drug delivery systems. It also describes the functionalization of these nanoparticles to be used as nanovaccines for cancer immunotherapy.

Chapter 28 entitled "Polymeric nanoparticles for biomedical applications" describes the drug delivery and therapeutic applications of nanomaterials. The chapter highlights the recent advancements in Curcumin loaded PLGA nanoformulations that are attractive candidates for tumor targeted therapy and imaging. The functional properties exhibited by the nanoformulations toward different cancer types are also highlighted.

Chapter 29 entitled "Bio-nanomaterials application for best utility in agricultural and medical field" describes the different nanotechnology approaches for sustainable agriculture for better yield and productivity of crops, and also development of biosensors for pollutant detection in biological bodies.

Chapter 30 entitled "Enhanced co-catalysis of bimetallic nanostructures for catalytic and photocatalytic applications" explains the catalytic/photocatalytic applications of bimetallic core-shell nanostructure and TiO_2 nanocomposites for degradation, hydrogenation, oxidation, and reduction in important industrial compounds.

Chapter 31 entitled "Nanomaterials incorporated electrospun membranes for membrane distillation" illuminates the role of engineered nanoparticles in nanofibrous membranes developed by electrospinning process for membrane distillation process. Nanoparticle coated membranes, membranes with nanoparticles incorporated into the matrix, and membranes with surface modifications through functionalization are all being explored to improve membrane hydrophobicity.

Chapter 32 entitled "Applications of multifunctional carbon-based silver nanocomposites for environmental remediation" reports the effectiveness of multifunctional silver loaded activated carbon composite, with higher surface area and temperature stability in comparison with the nascent carbon, to remove organic pollutants like dyes and pharmaceuticals through a simple adsorption process. Silver loading on activated carbon has been observed to be a suitable way to prepare multifunctional adsorbent material for effective water purification, as discussed in the chapter.

2. Conclusion

This chapter is a short reflection of multifunctional efficiency of nanomaterials that are currently evolving as next generation nanobots, memory or energy devices or even nanocarriers for drug delivery. Herein this chapter, we highlight using various illustrations the multifunctional applications of nanomaterials. It has been clearly illustrated by the energy, industrial, environmental, biomedical implications, and the agro-technological revolution brought about by the unique properties of nanomaterials. The major scientific impacts offered by nanomaterials, one-dimensional nanofibres, and 2D materials are illustrated in the book. The significant impact of nanomaterials in health care is also explored in the book, in this scenario when the world is under the threat of the lethal Corona virus, and the development of nanovaccines for treatment has become an acute necessity.

References

1. Rackauskas S, Cesano F, Uddin MJ. Multifunctional nanomaterials for energy applications. *Nano Mater* 2022;**12**(13):2170.
2. Kappadan S, Gebreab TW, Thomas S, Kalarikkal N. Tetragonal $BaTiO_3$ nanoparticles: an efficient photocatalyst for the degradation of organic pollutants. *Mater Sci Semicond Process* 2016;**51**:42–7.
3. Apu EH, Nafiujjaman M, Sandeep S, Makela AV, Khaleghi A, Vainio S, et al. Biomedical applications of multifunctional magnetoelectric nanoparticles. *Mater Chem Front* 2022;**6**(11):1368–90.
4. Abraham AR, Raneesh B, Das D, Oluwafemi OS, Thomas S, Kalarikkal N. *Interface engineered ferrite@ ferroelectric core-shell nanostructures: a facile approach to impart superior magneto-electric coupling*. *AIP Conf Proc*, **1942**. AIP Publishing LLC; 2018. p. 020002.
5. Paunović N, Dohčević-Mitrović Z, Djokić DM, Aškrabić S, Lazović S, Abraham AR, et al. Revealing plasmon-phonon interaction in nanocrystalline $MgFe_2O_4$ spinels by far-infrared reflection spectroscopy. *Mater Sci Semicond Process* 2022;**149**:106889.

6. Abraham AR, Raneesh B, Woldu T, Aŝkrabić S, Lazović S, Dohčević-Mitrović Z, et al. Realization of enhanced magnetoelectric coupling and Raman spectroscopic signatures in 0−0 type hybrid multiferroic core−shell geometric nanostructures. *J Phys Chem C* 2017;**121**(8):4352−62.
7. Yaragalla S, Chandran CS, Kalarikkal N, Subban RHY, Chan CH, Thomas S. Effect of reinforcement on the barrier and dielectric properties of epoxidized natural rubber−graphene nanocomposites. *Polym Eng Sci* 2015;**55**(11):2439−47.
8. Abraham J, Xavier P, Bose S, George SC, Kalarikkal N, Thomas S. Investigation into dielectric behaviour and electromagnetic interference shielding effectiveness of conducting styrene butadiene rubber composites containing ionic liquid modified MWCNT. *Polym* 2017;**112**:102−15.
9. Esteso MA, Ribeiro ACF, George SC, Abraham AR, Haghi AK, editors. *Optical and Molecular Physics: Theoretical Principles and Experimental Methods*. CRC Press; 2021.
10. Kodolov VI, Mukbaniani O, Abraham AR, editors. *Nanostructured Carbon for Energy Generation, Storage, and Conversion*. CRC Press; 2022.
11. Poothanari MA, Abraham J, Kalarikkal N, Thomas S. Excellent electromagnetic interference shielding and high electrical conductivity of compatibilized polycarbonate/polypropylene carbon nanotube blend nanocomposites. *Ind Eng Chem Res* 2018;**57**(12):4287−97.
12. Augustine R, Dominic EA, Reju I, Kaimal B, Kalarikkal N, Thomas S. Electrospun poly (ε-caprolactone)-based skin substitutes: i n vivo evaluation of wound healing and the mechanism of cell proliferation. *J Biomed Mater Res B Appl Biomater* 2015;**103**(7):1445−54.
13. Joseph B, Sagarika VK, Sabu C, Kalarikkal N, Thomas S. Cellulose nanocomposites: fabrication and biomedical applications. *J Bioresour Bioprod* 2020;**5**(4):223−37.
14. Komaraiah D, Radha E, Kalarikkal N, Sivakumar J, Reddy MR, Sayanna R. Structural, optical and photoluminescence studies of sol-gel synthesized pure and iron doped TiO_2 photocatalysts. *Ceram Int* 2019;**45**(18):25060−8.
15. Balakrishnan P, Gopi S, Geethamma VG, Kalarikkal N, Thomas S. Cellulose nanofiber vs nanocrystals from pineapple leaf fiber: a comparative studies on reinforcing efficiency on starch nanocomposites. *Macromol Symp* August 2018;**380**(1):1800102.
16. Mohan S, Oluwafemi OS, Kalarikkal N, Thomas S, Songca SP. Biopolymers−application in nanoscience and nanotechnology. *Recent Adv Biopolym* 2016;**1**(1):47−66.
17. Klostergaarda J, Banksonb J, Woodwardc W, Gibsond D, Seeneyd C. Magnetically responsive nanoparticles for vectored delivery of cancer therapeutics. *AIP Conf Proc* 2010;**1311**(1):382−7.
18. Pramanik P, Krishnan P, Maity A, Mridha N, Mukherjee A, Vikas R. *Application of nanotechnology in agriculture, environmental nanotechnology*, **4**. Springer; 2020. p. 317−48.
19. Allaker R. The use of nanoparticles to control oral biofilm formation. *J. Dental Res.* 2010;**89**(11):1175−86.
20. Wu S, Li Y, Ding W, Xu L, Ma Y, Zhang L. Recent advances of persistent luminescence nanoparticles in bioapplications. *Nano-Micro Lett* 2020;**12**(1).
21. Gutierrez MF, et al. Mechanical and microbiological properties and drug release modeling of an etch-and-rinse adhesive containing copper nanoparticles. *Dent Mater* 2017;**33**(3):309−20.
22. Lim EK, Kim T, Paik S, Haam S, Huh YM, Lee K. Nanomaterials for theranostics: recent advances and future challenges. *Chem. Rev.* 2015;**115**:327−94.
23. Ramazanzadeh B, et al. Comparison of antibacterial effects of ZnO and CuO nanoparticles coated brackets against *Streptococcus mutans*. *J Dent* 2015;**16**(3):200−5.
24. Dominic M, Joseph R, Begum PM, Kumar AS, Jeemol PA, Jose T, et al. Cellulosic bionanocomposites based on acrylonitrile butadiene rubber and *Cuscuta reflexa*: adjusting structure-properties balance for higher performance. *Cell* 2021;**28**(11):7053−73.

This page intentionally left blank

PART I

Energy applications of nanomaterials

This page intentionally left blank

CHAPTER

2

Nanoferrites for electromagnetic interference shielding application

Aishwarya V. Menon, Devansh Sharma and Suryasarathi Bose

Department of Materials Engineering, Indian Institute of Science, Bangalore, Karnataka, India

1. Introduction

In present times, mankind is dependent on various electronic equipment for their day to day activities. Since the discovery of the capabilities of electromagnetic (EM) waves, they have found potential use in various fields such as military application, communication, medical devices, etc., to name a few. Presently, there is a great demand to miniaturize electronic devices which is why researchers are working in the small wavelength microwave frequency region. However, with the growing use of these devices, there is an increase in unwanted and stray EM radiations in the ambient environment, creating EM pollution, which is proven to seriously impact the working of other nearby electronic devices by EM coupling and cross-talk. Therefore, current research 54321`is being focused on the development of EM shields which can protect electronic devices from stray EM waves.[1]

According to the classical theory of electromagnetic induction by faraday, changing the electric field can generate a magnetic field or vice-versa. Thus, from the theory, the energy of the incoming EM waves can be absorbed by incorporating conducting, magnetic or dielectric material which can either reflect or absorb the incoming EM waves.[2] In the beginning, metallic shields were used predominantly due to their excellent conductivity since the free electron cloud in metals reflects incoming EM waves. This was not desirable since the reflected wave can always interfere with some other unshielded device or component. Magnetic metals were the other alternatives to conducting metallic reflectors; however, their shielding efficiency was quite limited to low frequencies (<1 GHz) since their permeability drops to unity at such high frequencies as the magnetic dipoles cannot keep up with the rapidly changing field direction at higher frequencies hence ceasing to produce any significant losses. This was when the research was diverted to the more versatile magnetic nanoferrites which when incorporated in a suitable matrix shields EM waves through more than just one mechanism.[3–6]

Applications of Multifunctional Nanomaterials
https://doi.org/10.1016/B978-0-12-820557-0.00005-9

Ferrites are generally referred to as oxides of iron which show magnetic properties and hence are widely used for electromagnetic damping. These ferrites can be classified as spinel ferrites, garnets, hexagonal ferrites, and ortho ferrites depending on their crystal structure.[7,8] Their properties mainly depend upon their synthesis method,[9] nature of dopant,[10] and concentration of doping[11] which in turn results in changes in the microwave absorption properties of the ferrite.

1.1 Mechanism of EMI shielding

EM waves consist of two different components: electric and magnetic components. These components interact in different ways with different types of materials, resulting in loss of EM wave'senergy. Below are the various ways in which EM waves can interact with different materials.

1.1.1 Losses in conducting materials

In conductors, major losses occur due to two factors. Firstly, under the influence of the alternating electric field, the electrons are forced to oscillate which results in the EM energy loss. Also, due to the magnetic field, there is a movement of electrons in response to the applied field which results in eddy currents and leads to the generation of a counter magnetic field such that it cancels the applied magnetic field.[12] These losses are more prominent at higher frequencies.

1.1.2 Losses in dielectric materials

In dielectric material, major losses are due to the interaction between dipoles and electric vector. These dipoles start orienting in the direction of the alternating electric field. In the microwave frequency region, these dipoles are unable to cope with the rapidly changing field thus, causing dissipation of energy. Also, in a quest to align according to the alternating field, these dipoles collide with each other causing dissipation of EM energy in the form of heat.[13]

1.1.3 Losses in magnetic materials

Losses in a magnetic material are majorly in low-frequency range as their permeability decreases at high frequency as discussed earlier. At higher frequencies, major losses are due to hysteresis, which occurs due to the irreversible rotation of magnetic dipoles in the presence of the alternating external field. In lower frequencies, the majority of losses are due to domain wall resonance which occurs due to the movement of domain wall under the influence of the alternating magnetic field.[14,15]

Magnetic losses from magnetic metals like Fe, Ni, or Co and magnetic oxides like Ferrites, gadolinium oxide (Gd_2O_3) etc., arise from various factors including hysteresis losses, domain wall losses, natural resonance, eddy current losses and exchange resonance. Additionally, defective crystal structure causes polarization losses as discussed earlier. However, at high frequencies, magnetic losses such as hysteresis losses and domain wall losses do not contribute toward the overall shielding performance. However, natural resonance (at < 10 GHz), eddy current losses and exchange resonance (>10 GHz) do play a predominant role in absorption.[16–23] Magnetic eddy current plays a crucial role in causing magnetic loss, which is inevitable especially at high frequencies. Induced currents are formed in an

alternating EM field, which forms a closed loop inside the magnetic particle. The magnetic eddy current is characterized as $\mu''(\mu') - 2f^{-1}$. Generally, the value of $\mu''(\mu')^{-2}f^{-1}$ is constant in investigated frequency range, indicating that magnetic eddy currents dominates magnetic loss. However, if the value of $\mu''(\mu')^{-2}f^{-1}$ changes with frequency, it demonstrates that there are other magnetic loss mechanisms which dominate in the system.[24–27]

In the case of ferrites, their efficiency at high-frequency decreases due to a decrease in their permeability as governed by Snoek's limit.[28] Therefore, these ferrites are often coupled with different conducting or dielectric materials to enhance their performance in the microwave range. Researchers have mainly explored graphene oxide (GO) as a template for growing such ferrites and dispersing them in the polymeric matrix.[22] Also, conducting nanoparticles like MWCNT (Multiwalled Carbon Nanotube) are one of the most explored conducting filler due to their high aspect ratio and excellent electrical conductivity.[29] Doping ferrites with other elements is another technique that has been widely used to extend its shielding bandwidth. We have discussed the role of various types of ferrites and their hybrid heterostructures with carbonaceous fillers as well as with conducting polymers for EMI shielding in this chapter.

2. Spinel ferrites for EMI shielding

Spinel ferrites have the formula PFe_2O_4, whereby the tetrahedral and octahedral interstitial sites are designated as P (divalent metal ions like Cu, Co, Mn, Ni, Zn, Fe). They are characterized by large magnetic losses and semiconducting property.[7]

2.1 Ferric and ferrous oxides

Among the oxides of iron, magnetite (Fe_3O_4) and Fe_2O_3 are the most comprehensively investigated because of their ease of synthesis, high chemical stability, low toxicity, etc. Mashuri et al.[30] synthesized ferrites based on iron sands by high energy ball milling at room temperature. They achieved a high reflection loss of up to −7.28 dB in at 7.50 GHz. Jia et al.[31] developed magnetite nanoparticles where the loose magnetic nanoparticles assembled in the form of Fe_3O_4 spheres of ~300 nm in size. The synthesized loose spheres exhibit two magnetic loss peaks at 4.0–5.0 GHz and 16.0–17.0 GHz when compared with the solid Fe_3O_4 spheres, which show only one peak at 4.0–5.0 GHz which belongs to magnetite. The latter peak in the case of the loose spheres is attributed to the effect of the morphology. Phadtare et al.[32] developed a lightweight and porous polymer foam composites by controlling the scaffold structure using a surfactant and varying the amount of Fe_3O_4 nanoparticles. The microwave absorption of the foams was enhanced to as high as 82% with the addition of 15 wt% Fe_3O_4. Biswas et al.[33] fabricate Fe_3O_4 nanoparticles of different shapes (spherical, cubic, cluster, and flower, for example) and studied the effect of shape anisotropy and size of Fe_3O_4 on the microwave shielding properties by incorporating them in polycarbonate (PC)/Polyvinylidene fluoride (PVDF) blend matrix along with MWCNTs as conducting nanofillers. They found that spherically shaped Fe_3O_4 nanomaterials exhibited superior performance of −38 dB at 18 GHz which was attributed to the excellent dispersibility of the small-sized nanospheres. Zhang et al.[34] synthesized crystalline Fe_3O_4 nanowire arrays 200 nm in diameter and 6–10 μm in length and composited them in PC porous membranes by one-step

electrochemical deposition without heating. They found that the ferromagnetic resonance frequencies of ferrite arrays reached up to 25 GHz under a magnetic field of 9 kG, and it could also be tuned in a wide frequency range by an external magnetic field. Han et al.[35] developed Fe_3O_4 and Fe nanowires by electrospinning followed by reduction process of approximately 50−60 nm and 30−40 nm, in diameter respectively. The paraffin-based composite containing 50 wt% weight concentration of Fe_3O_4 nanowires, exhibited a minimum reflection loss of (RL_{min}) of −17.2 dB at 6.2 GHz with the matching thickness of 5.5 mm. Gong et al.[36] developed Fe−ferrite composite nanotubes of 100 nm diameter and lengths of tens of micrometers by thermal hydrogen reduction of α-FeOOH nanowires. Due to the effective eddy current suppression by the thin wall characteristic of nanotubes, the composite nanotubes exhibit high permeability resulting in RL_{min} of about −18 dB and the effective absorption band (frequency range for $RL_{min} < -10$ dB) of 12.5−17.5 GHz.

Jia et al.[37] synthesized a lightweight and flexible composite aerogel composed of CNTs and mesoporous Fe_3O_4 using an in-situ growth method. CNTs served as frameworks for the growth of Fe_3O_4 and the growth of Fe_3O_4 crosslinked CNTs into an integrated structure which lead to the formation of monolithic porous magnetic foam with a high particle loading of 88 wt%. The aerogel exhibited an excellent EMI shielding performance in the low-frequency range of 3−5 GHz. An et al.[38] fabricated a multigranule Fe_3O_4 nanocluster of various sizes and placed them on graphene-based composites. The absorption coefficient was found to increase by incorporation of ferrite compared to bare nanocomposite with only graphene. Cheng et al.[39] developed flexible PVDF nanocomposite-based films using Fe_3O_4 and carbonaceous nanoparticles like Carbon Nanotubes (CNTs) and Graphenes through solution processing and compression molding method. Due to the synergetic effect of Fe_3O_4 nanoparticles and CNTs or GNPs, the total shielding of the 8 wt% CNTs and GNPs filled PVDF/Fe_3O_4 composites increased from −14.1 to −32.7 dB, and −16.2 to −35.6 dB, while the film thickness was increased from 0.5 to 1.1 mm, respectively. The mechanism of shielding of the composites was mainly attributed to the absorption process. Liu et al.[40] developed a trilayer-type laminated epoxy nanocomposite containing a matching layer with 15 wt% nano-Fe_3O_4, an absorbing layer with 5 wt% CNTs and a reflecting layer with 10 wt% CNTs. The laminated nanocomposite exhibited excellent microwave absorption from 13 to 40 GHz up to −40 dB.

Biswas et al.[41] probed into the mechanism of shielding in polymer nanocomposites containing a conducting phase like MWCNTs, and a magnetic phase based on inverse-spinel ferrites, MFe_2O_4 (M = Fe, Co, Ni). The study revealed that high saturation magnetization and hysteresis loss, better impedance matching, high consolidated loss, higher attenuation constant and comparable eddy current loss help Fe_3O_4 shield the EM wave in the X and Ku band when compared to the other ferrites based on Ni and Co as shown in Fig. 2.1. Moreover, the enhanced dielectric and/or interfacial polarization losses because of π-electrons in MWCNTs produce a synergistic effect. The composites in a biphasic PC/PVDF blend resulted in shielding ability of −31 dB for Fe_3O_4+MWCNTs, which is 19% and 24% higher when compared to $CoFe_2O_4$ + MWCNT and $NiFe_2O_4$ + MWCNT containing blends.

Kim et al.[42] developed silver (Ag)-decorated poly (vinyl alcohol) (PVA)/Fe_2O_3 composite nanofibrous webs by electrospinning and metal-deposition methods. The concentration of Fe_2O_3 and the thickness of Ag-decorated on PVA/Fe_2O_3 composite nanofiber webs were systematically varied. 200 nm thick Ag-decorated PVA nanofiber webs showed excellent EMI

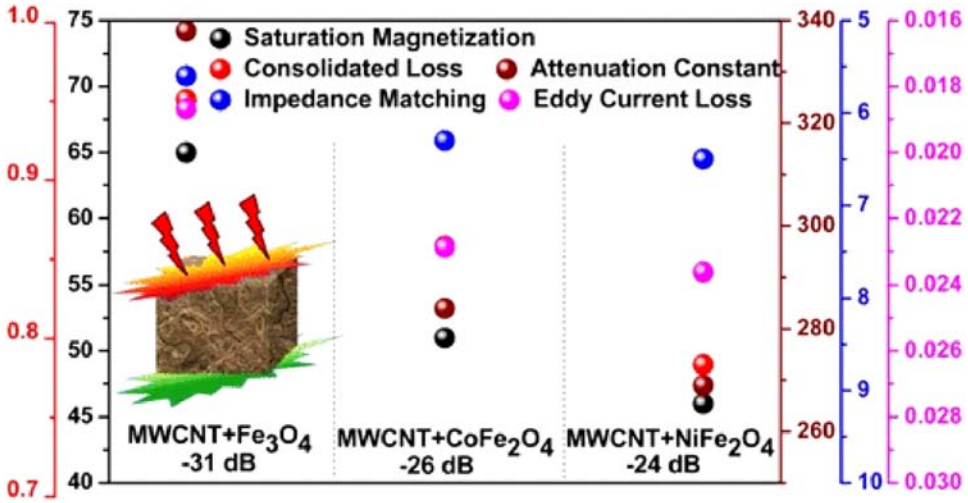

FIGURE 2.1 Mechanism of EMI shielding in Co and Ni ferrite composites with MWCNT. *Reprinted from Biswas S, Panja SS, Bose S. Physical insight into the mechanism of electromagnetic shielding in polymer nanocomposites containing multiwalled carbon nanotubes and inverse-spinel ferrites.* J Phys Chem C *2018;**122**(34):19425–19437. Copyright © 2018, with permission from American Chemical Society.*

shielding of −42.5 dB while 200 nm thick Ag-decorated PVA/10%−Fe_2O_3 composite nanofibers showed EMI shielding as high as −45.2 dB at 10 GHz; the mechanism of shielding being absorption-based. Arun Prakash et al.[43] studied the effect on microwave shielding of adding silanized fine Fe_2O_3 particle of sizes 800, 200, and < 100 nm into E-glass fiber-reinforced epoxy composites. Tong et al.[44] compared the EMI shielding properties of urchin-like α-Fe_2O_3 and Fe_3O_4 nanostructures prepared from the precursor urchin-like α-FeOOH under reducing atmosphere. Urchin-like α-Fe_2O_3 exhibited an RL_{min} value of −9.2 dB between 14 and 18 GHz while the urchin-like Fe_3O_4 showed an enhanced RL_{min} of −29.96 dB and below −20 dB in 3.76–8.15 GHz.

2.2 Nickel-based ferrites

Mandal et al.[45] synthesized nanohollow spheres and bulk nanoparticles of Nickel ferrite ($NiFe_2O_4$) to study the effect of morphology on the microwave absorption properties in the X-Band. Composites were prepared with 25 wt% nanoparticles and a thickness of 2 mm. They found that the hollow nanoparticles lead to lower density (∼3.91 g/cc) and multiple internal reflections thereby enhancing EM wave absorption with an RL_{min} of −59.2 dB at ∼11.7 GHz with an absorption bandwidth between 9.18 and 12 GHz. Fu et al.[46] prepared pompon flower-like $NiFe_2O_4$ (PF−$NiFe_2O_4$) by a vapor diffusion-deposition method followed by its annealing. The PF-$NiFe_2O_4$ nanoparticles exhibited RL_{min} of −18.3 dB while its bulk counterpart $NiFe_2O_4$ only yielded RL_{min} of −9.2 dB. This was attributed to the unique pompon flower-like morphology of PF-$NiFe_2O_4$. The incident EM waves get trapped and undergo multiple scattering and absorption in the ordered array of acicular "petal" thus minimizing direct reflections of EM waves. Biswas et al.[47] used a compartmentalized approach to

disperse $NiFe_2O_4$ and MWCNTs in a biphasic polymer blend of PVDF and PC by suitable functionalization of both the nanoparticles. They observed that when the $NiFe_2O_4$ nanoparticles were localized in PC phase and MWCNTs were localized in PVDF phase, the highest shielding effectiveness of −67 dB was achieved.

Zhang et al.[48] developed a novel double-layer microwave absorber composed of spinel ferrite $Ni_{0.8}Co_{0.2}Fe_2O_4$ nanofibers (NCFO NFs) and Ni−C hybrid NFs via electrospinning method combined with subsequent heat treatment for EMI shielding in 2−18 GHz frequency range. The double-layer absorbers consisting of 1.5 mm thick 50 wt% NCFO NFs/paraffin composite (matching layer) and 0.8 mm thick 5 wt% Ni−C NFs/paraffin composite (absorbing layer) exhibited higher absorption compared to individual layers with an RL_{min} of −84.9 dB at 17.0 GHz and an effective absorption bandwidth of 7.4 GHz ranging from 10.6 to 18 GHz. Nikzad et al.[49] synthesized Co- and Gd-substituted $NiFe_2O_4$ ferrite nanoparticles with the formula $Ni_{1-x}Co_xFe_{2-y}Gd_yO_4$ ($x = 0.0-1.0$ and $y = 0.0-0.1$) using hydrothermal approach. They found an enhancement in the magnetization and coercive field with an increase in cobalt and gadolinium content which was attributed to the redistribution of cations in the spinel nano ferrite structure. RL_{min} of −26.7 dB was obtained at 9.4 GHz for ferrites with $x = 1.0$ and $y = 0.1$ with an absorption bandwidth of 3.6 GHz at 1.8 mm thickness.

Saha et al.[50] synthesized $Ni_{0.40}Zn_{0.40}Cu_{0.20}Fe_2O_4$ (NZCF) nanoparticles and incorporated them in the PVDF matrix to prepare microwave shielding composites. They achieved an RL_{min} of -49.7 dB at 13.2 GHz at 10 wt% loading of NZCF. The EM wave absorption properties were attributed to the mutual contribution of magnetic dipoles from NZCF and electric dipoles resulting from the enhancement in the electroactive β phase in PVDF. Liu et al.[51] synthesized $Ni_{0\cdot5-x}Zn_{0\cdot3-x}Mn_{0\cdot2+2x}Fe_2O_4$ ferrites by sol-gel auto combustion process followed by annealing at 1200°C for 3 h in air, which resulted in improved grain size. For samples with $x = 0\cdot1$, a RL_{min} of −27·57 dB was observed at 11 GHz with an absorption bandwidth of 8·0 GHz at 3.8 mm thickness. Qian et al.[52] synthesized Ni−Zn ferrites with different neodymium substitutions ($Ni_{0.5}Zn_{0.5}Nd_xFe_{2-x}O_4$) with a combination of sol-gel route and self-propagating combustion (SPC) method. They obtained an RL_{min} of −20.8 dB at 4.4 GHz and an effective absorption bandwidth of 3.2 GHz at $x = 0.04$ and 8.5 mm thickness.

Jocobo et al.[53] synthesized a hybrid nanostructure composed of hard and soft magnetic phases. $NiFe_2O_4$ was synthesized by a self-combustion method over nanocrystalline powders of Nd−Co substituted strontium hexaferrite with the composition $Sr_{0.5}Nd_{0.5}Co_{0.5}Fe_{10.5}O_{19}$ at different mass ratios. Strong exchange-coupling between the two magnetic phases was found in the magnetization studies for the composition 30/70 and 50/50 for $Sr_{0.5}Nd_{0.5}Co_{0.5}Fe_{10.5}O_{19}/NiFe_2O_4$ (hard/soft magnetic phase). The 50/50 composition exhibited the highest EM wave blocking performance with an RL_{min} of −34.4 dB at 11.1 GHz and an absorption bandwidth of 3.5 GHz.

2.3 Cobalt based ferrites

Yan et al.[54] synthesized monodisperse cobalt ferrite ($CoFe_2O_4$) nanospheres of about 100−200 nm in size using a simple solvothermal method. The nanospheres were composited with paraffin wax in the ration 3:1 and an RL_{min} of −11.96 dB (at 9.00 GHz for 100 nm), −23.02 dB (at 5.55 GHz for 125 nm) and −32.79 dB (at 10.47 GHz for 200 nm) was obtained.

Li et al.[55] synthesized $CoFe_2O_4$ fibers and particles by directly annealing electro spun citric acid-based precursor fibers and drying the precursor gel under a protective atmosphere. Composites were prepared in paraffin by adding 33 wt% of the nanofibers. When the matching thickness approached 3 mm, the absorption bandwidth reached up to 10.0 GHz over the entire X-band and Ku-band. Cole–Cole plot suggests the presence of multiple dielectric relaxation processes. The electromagnetic coupling between the EM wave and $CoFe_2O_4$ fibers enhances the microwave absorption.

Huang et al.[56] synthesized the $Co_xZn_{(1-x)}Fe_2O_4$ (x = 0.2, 0.4, 0.6, 0.8) nanofibres by electrospinning method and they found that the saturation magnetization and coercivity could be enhanced by tuning the Co^{2+} content. 15 wt% of the composition $Co_{0.6}Zn_{0.4}Fe_2O_4$ in polymer matrix showed the highest microwave attenuation ability with 90% and 80% EM wave absorption in the X—band and Ku—band frequencies, respectively, with a surface density of only 2.4 kg/m^2. Liu et al.[57] developed single and double layer absorbers by synthesizing spherical NiO and Ni substituted $CoFe_2O_4$ (CNZF) of the formula $Co_{0.2}Ni_{0.4}Zn_{0.4}Fe_2O_4$ by sol-gel autoignition process for microwave absorption in the frequency range 2–18 GHz. They found that the double-layer absorbers of thickness 3.2 mm consisting of 30 wt% NiO as a matching layer and 30 wt% CNZF as absorption layer exhibited an RL_{min} of −67.0 dB at 9.2 GHz and effective absorbing bandwidth of 3.9 GHz from 7.0 to 10.9 GHz.

Li et al.[58] synthesized monodisperse hollow $CoFe_2O_4$ microspheres with an average size of 150 nm and a shell thickness of 50 nm using a solvothermal approach. The particles were thermally reduced to obtain hollow $CoFe_2O_4$–Co_3Fe_7 microspheres which will improve EM wave absorption. They found that hollow $CoFe_2O_4$–Co_3Fe_7 exhibited better shielding properties compared to $CoFe_2O_4$ nanoparticles with an RL_{min} of −41.6 dB and absorption bandwidth of 3 GHz at a thickness of 1.3 mm in the Ku band. Salimkhani et al.[59] deposited $CoFe_2O_4$ nanoparticles carbon fibers as a 3D structure using the electrophoretic method by varying the deposition parameters to study their magnetic and EM wave absorption properties. They observed that by optimizing voltage amount and time to 25 V and 6 min respectively coating uniformity was maintained and this led to the highest EM wave attenuation of −10.25 dB in the X band region.

2.4 Manganese-based ferrites

Wang et al.[60] synthesized spherical manganese ferrite ($MnFe_2O_4$) colloidal nanocrystal assemblies (CNAs) on a wood substrate using a solvothermal method with assize ranging from 50 to 360 nm. The as-prepared $MnFe_2O_4$/wood hybrids exhibited RL_{min} of −12 dB at 15.52 GHz. Katiyar et al.[61] developed a composite of EPDM rubber with different ratios of manganese-zinc ferrite for application as EM wave absorbers in the frequency range of 2–18 GHz. The maximum absorption bandwidth obtained was −7.4 GHz at 2.5 mm absorber. Biswas et al.[62] incorporated $MnFe_2O_4$ nanoparticles, synthesized using a hydrothermal approach along with MWCNTs in PVDF matrix to develop multi-layered assemblies for EM wave shielding. The resulting ultrathin (0.60 mm) multilayered EM wave absorber was able to block >99.999% (ca. −50 dB) of the incoming EM waves. Biswas et al.[62] made multilayered thin polymer films by the rational arrangement of tailor-made nanocomposites that were designed to absorb electromagnetic (EM) radiation. $MnFe_2O_4$ nanoparticles were incorporated in the PVDF matrix, along with conductive multiwall carbon nanotubes (MWCNTs)

and treated as outer layers of the multilayer assembly. The resulting ultrathin (0.60 mm) multi-layered architecture was able to block >99.999% ($SE_T = -50$ dB) of the incoming EM radiation. Bhattacharjee et al.[63] constructed of ultrathin multilayer polymer nanocomposite films by layer-by-layer (LbL) architectural assembly. $MnFe_2O_4$ nanoparticles were incorporated in PVDF along with conductive MWCNTs (PNTMn-Fe) by a facile solution blending process and used as outer layers of the LbL assembly. In order to scavenge the transmitted radiation through the top layers, PVDF films sandwiched with a Ni (nickel)- deposited woven carbon fiber mat was designed using a facile electroless deposition technique and used as inner layers of the LbL assembly. The different layers were then stacked and hot pressed into a composite structure which resulted in an extraordinary (−52 dB at 18 GHz) shielding effectiveness at only 0.60 mm thickness.

3. Hexaferrites for EMI shielding

Hexagonal ferrites are characterized by high magnetocrystalline anisotropy field and a planar anisotropy which improves their natural resonance in the upper GHz range. They crystallize in a hexagonal structure and are of six types, namely, M, U, W, X, Y, and Z type. These ferrite with hexagonal structures are anisotropic and possess a larger intrinsic magnetocrystalline anisotropy field and large in-plane anisotropy. This causes their natural resonance to occur in the GHz range.[64]

3.1 Barium based ferrites

Barium ferrites ($BaFe_{12}O_{19}$) are a class of hard magnetic materials, which are used for various applications such as magnetic recording media, permanent magnets, and microwave devices. $BaFe_{12}O_{19}$ possesses high saturation magnetization, high Curie temperature, good chemical, as well as corrosion resistance. Hexagonal ferrites like $BaFe_{12}O_{19}$ are well-known magnetic microwave absorbers however they possess high density and lower dielectric loss which restrict their widespread applications as microwave absorbers. Iqbal et al.[65] reported the synthesis of $BaFe_{12}O_{19}$ nanoparticles via sol-gel technique followed by annealing at 400°C, 700°C, and 850°C to investigate the effect of annealing temperature on the morphology and EMI shielding efficiency. They found that $BaFe_{12}O_{19}$ nanoparticles annealed at 850°C exhibited pure crystalline phase hexagonal structure with a high magnetic moment (31.32 emu g−1) and coercivity (2.7 kOe). The total shielding effectiveness achieved was −17.57 dB at 11.58 GHz which was at par with existing literature.[65–68] Biswas et al.[69] used a compartmentalized approach to disperse $BaFe_{12}O_{19}$ and MWCNTs in a biphasic PC/PVDF blend by suitably modifying the nanoparticles with functional groups. They found that when ionic liquid modified MWCNTs were placed in PVDF phase and the $BaFe_{12}O_{19}$ was placed in PC phase, the highest shielding effectiveness of −37 dB was achieved as can be seen from Fig. 2.2.

Rana et al.[70] synthesized cobalt substituted M-type barium nanoferrite of composition $BaCo_xFe_{12-x}O_{19}$ with $x = 0.4$, 0.8, and 1.0 via a coprecipitation method. The as-obtained powders were pressed into toroidal samples and the maximum reflection loss obtained was −45 dB for the composition at $x = 1.0$ in the Ku band. Similarly, Guo et al.[71] synthesized

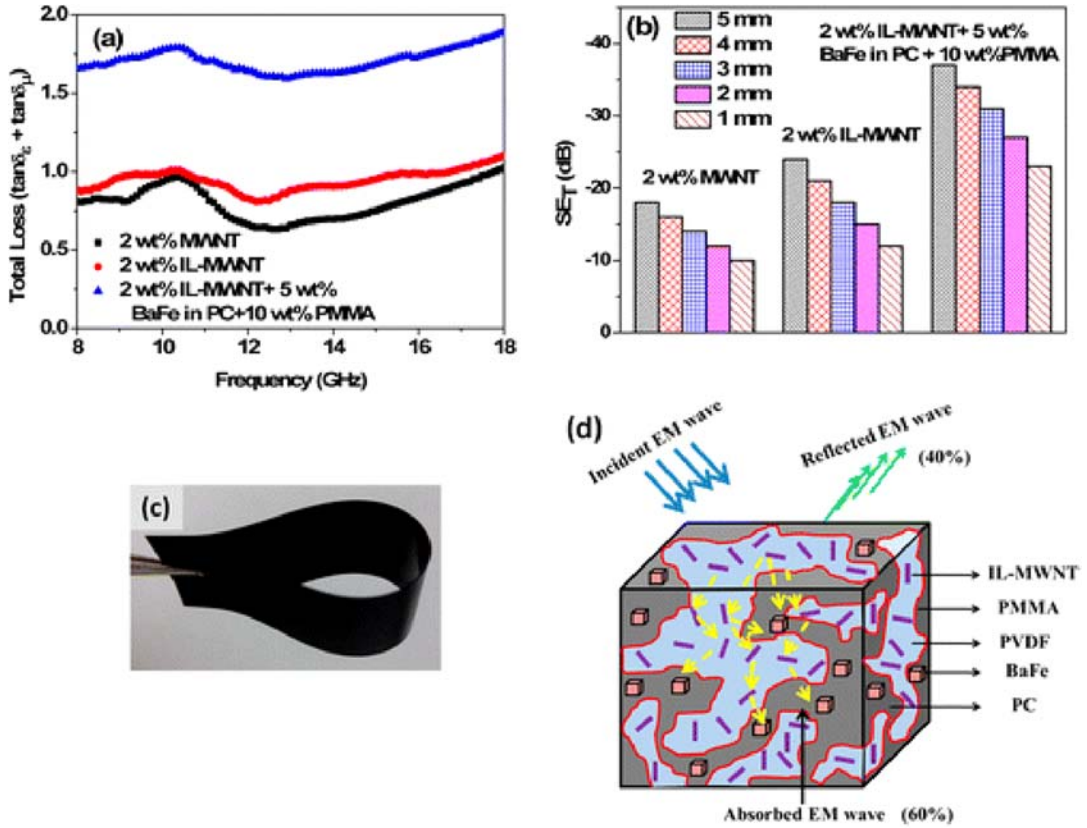

FIGURE 2.2 (A) Total loss tangent (B) total shielding effectiveness at various thickness (C) flexibility of prepared film composite and (D) cartoon illustrating the mechanism of EM attenuation for blends containing 2 wt% ionic liquid modified MWCNT in PVDF phase and 5 wt% $BaFe_{12}O_{19}$ in the PC phase. *Reprinted from Biswas S, Kar GP, Bose S. Tailor-made distribution of nanoparticles in blend structure toward outstanding electromagnetic interference shielding*. ACS Appl Mater Interfaces *2015;7(45):25448−25463. Copyright © 2015, with permission from American Chemical Society.*

$Ba_3Co_2Fe_{24}O_{41}$ Z-type hexaferrite by the citric acid sol-gel method and a composite was prepared in paraffin with ferrite to paraffin ratio of 5:1. The RL_{min} obtained was −50 dB at 4.1 GHz for a sample thickness of 5 mm. Similar studies were conducted on multiple substitutions such as $Ba_{0.8}Al_{0.2}Co_{0.9}Zn_{1.1}Fe_{19}O_{27}$,[72,73] $Ba_{0.5}Ce_{0.5}Fe_{11}CoO_{19}$,[74] $BaCo_{2-x}Ni_xFe_{16}O_{27}$,[75] $Ba_3Co_2Cr_{2x}Fe_{24-2x}O_{41}$,[76] $BaCo_xTi_xFe_{12-2x}O_{19}$,[77,78] etc.

Zhang et al.[79] synthesized W-type $BaZn_2Fe_{16}O_{27}$ by ball milling the precursors. A RL_{min} of −17.02 dB was obtained at 9.04 GHz with an absorption bandwidth from 7.28 to 11.44 GHz at a sample thickness of 3.5 mm. In a similar study, they doped $BaZn_2Fe_{16}O_{27}$ with antimony-doped tin oxide (ATO) by coprecipitation method in different mole ratios. When the mole ratio of $BaZn_2Fe_{16}O_{27}$/ATO was 1:2, the minimum RL_{min} obtained was −31.14 dB at 12.4 GHz, with an absorption bandwidth of 9.6 GHz in the Ku-band.[80] Kaur et al.[81] synthesized M-type $Ba_{0.5}Sr_{0.5}Co_xLa_xFe_{12-2x}O_{19}$ hexagonal ferrite for shielding in the X band frequency range. They found that doping improves impedance matching

and microwave absorption characteristics of Ba−Sr based ferrites. The powder obtained was pelleted and sintered to obtain samples for shielding measurement and the RL_{min} obtained was −43.33 dB in composition x = 0.2 at 10.75 GHz at a sample thickness of 1.9 mm.

Kaur et al.[82] developed $Ba_{0.5}Sr_{0.5}Co_xIn_xFe_{12-2x}O_{19}$ hexaferrite and found that both Co^{2+} and In^{3+} increased microwave absorption, impedance matching as well as the absorption bandwidth of the samples. RL_{min} obtained was −39.99 dB at 11.14 GHz in the composition x = 0.2 at a thickness of 1.6 mm. In a similar study they developed $Ba_{0.5}Sr_{0.5}Co_xRu_xFe_{(12-2x)}O_{19}$ and obtained a RL_{min} of −12.02 dB at 9.0 GHz in the composition x = 0.2.[83] Joshi et al.[84] developed M-type $Ba_{0.5}Sr_{0.5}Co_xGd_xFe_{12-2x}O_{19}$ and obtained a RL_{min} of −15.0 dB at 8.2 GHz for a thickness of 2.9 mm in the X band in the composition x = 0.8.

Liu et al.[85] synthesized M-type barium ferrite powders doped with Zr^{4+} ions ($BaFe_{12-x}Zr_xO_{19}$) by the sol-gel process. They found that the anisotropic field (H_a) of the ferrites decreased from 15.75 kOe to 8.13 kOe with increasing Zr^{4+} from x = 0 to 0.4. A strong RL_{min} of ∼-50 dB in the frequency window of 18−40 GHz was obtained with an absorptivity of electromagnetic (EM) power per unit thickness reaching as high as 0.156% μm^{-1}, which is about 2−5 times higher than those of most reported in the literature. They obtained multiple-resonance permeability peaks which were suggested to be originating from Fe^{3+} ions. As shown in Fig. 2.3, the resonant frequencies obtained for $BaFe_{11.8}Zr_{0.2}O_{19}$, $BaFe_{11.7}Zr_{0.3}O_{19}$ and $BaFe_{11.6}Zr_{0.4}O_{19}$ samples are (33.0 GHz, 34.1 GHz, 36.5 GHz, and 39.2 GHz), (27.1 GHz, 28.0 GHz, 30.3, and 33.1 GHz) and (22.6 GHz, 23.9 GHz, 26.5 GHz, and 29.5 GHz), respectively. The exchange couplings among Fe^{3+}, Fe^{2+}, and O^- also contributed toward multiple reflection loss peaks resulting in a broad absorption bandwidth of ∼12 GHz. In a similar study, they doped barium ferrite with Nb^{5+} to enhance the EM absorption around atmospheric window of 35 GHz by sintering Nb doped barium ferrite precursors at 1400 °C for 3 h in air, Ar and N_2. The magnetic loss region as well as the complex permittivity was found to be highest for samples sintered in N_2 with an RL_{min} of −37 dB at 35 GHz with an absorption bandwidth of more than 12 GHz at a very low thickness of 0.55 mm.[86]

Liu et al.[87] reported the microwave absorption properties of a La-substituted $Ba_{12}Fe_{28-}Ti_{15}O_{84}$ quaternary ferrite which was prepared via a modified sol-gel method. They found that the introduction of La into $Ba_{12}Fe_{28}Ti_{15}O_{84}$ had a remarked influence on conductivity, dielectric and magnetic properties of the ferrites which resulted in RL_{min} of −16.6 dB with an effective bandwidth from 8.24 to 12.16 GHz in the composition x = 3 within the X band.

3.2 Strontium-based ferrites

M-type strontium ferrites are characterized by its strong magneto-crystalline anisotropy which induces high cut-off frequency. Chen et al.[88] synthesized uniform urchin-like $SrFe_{12}O_{19}$ with a diameter of 3−4 μm via facile surfactant assisted hydrothermal approach. The urchins exhibited an RL_{min} of −22.8 dB was observed at 15.1 GHz at a thickness of 3 mm with an absorption bandwidth ranging from 12.4 to 18.0 GHz in the X and Ku band. They stated that the absorbing property of the urchin-like $SrFe_{12}O_{19}$ was better than that of bulk particles because firstly the prickly urchin-like structure can trap incident EM waves inhibiting direct reflections and secondly, the urchin causes multiple scattering and absorption which again improves absorption performance as shown in Fig. 2.4.

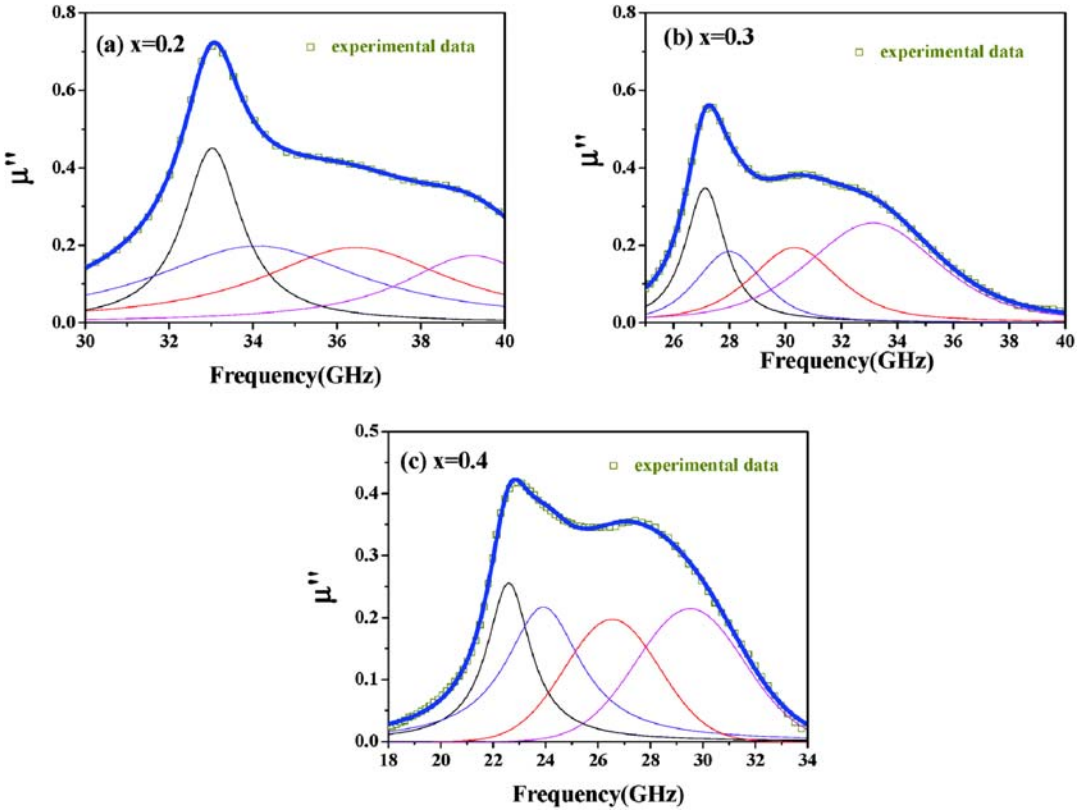

FIGURE 2.3 Resolved natural resonance peaks for $BaFe_{12-x}Zr_xO_{19}$ with (A) x = 0.2, (B) x = 0.3, and (C) x = 0.4. *Reprinted from Liu C, Xu Q, Tang Y, Wang Z, Ma R, Ma N, Du P. Zr 4+ doping—controlled permittivity and permeability of BaFe 12− x Zr x O 19 and the extraordinary EM absorption power in the millimeter wavelength frequency range. J Mater Chem C 2016;**4**(40):9532−9543. Copyright © 2016, with permission from Royal Society of Chemistry.*

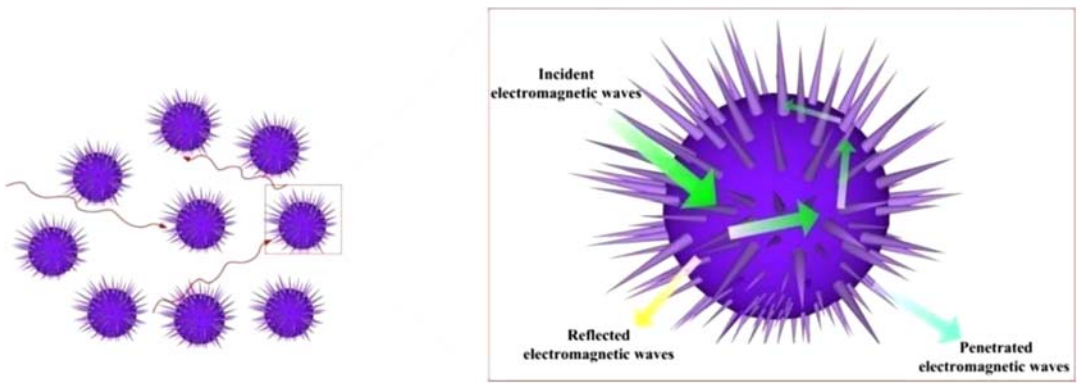

FIGURE 2.4 Schematic diagram of EM wave absorbing mechanism for the urchin-like $SrFe_{12}O_{19}$. *Reprinted from Chen W, Zhu X, Liu Q, Fu M. Preparation of urchin-like strontium ferrites as microwave absorbing materials.* Mater Lett *2017;**209**:425−428. Copyright © 2017, with permission from Elsevier.*

Yu et al.[89] synthesized mesoporous Ag_3PO_4 nanorods/$SrFe_{12}O_{19}$ hexagonal nanoflake and dispersed it in 60 wt% paraffin. The composites resulted in high RL_{min} of −63.18 dB at 4.72 GHz at 5.1 mm thickness. The effective absorption bandwidth obtained was about 6.24 GHz at 2.3 mm. Mesoporous nature of the nanoparticles induces multiple scattering of the incident EM waves thereby increasing the propagation path of the incident microwaves inside the absorbers. Moreover, the large surface area also results in a higher interfacial polarization effect, which accelerates microwave absorption intensity. Kaur et al.[90] developed M-type lanthanum-doped $SrFe_{12}O_{19}$ with general formula $Sr_{1-y}La_yFe_{12}O_{19}$ (y = 0.00, 0.10, 0.15, 0.20 and 0.25) for application in the frequency range of 18−40 GHz. The ferrites exhibited a high RL_{min} of −30 dB with an absorption bandwidth of about 2 GHz. Min-HyeokPark et al.[91] synthesized Zn-substituted Z-type Sr hexaferrites ($Sr_3Co_{2-x}Zn_xFe_{24}O_{41}$, $x = 0$, 0.5, 1.0, 1.5) via solid-state reaction route and dispersed them in an epoxy matrix. They observed a double hysteresis behavior in ferrites with $x = 1.0$ and 0.5, shifts in μ' and μ'' values to lower frequencies accompanied by increasing EM wave absorption intensities with increasing Zn substitution content which was assigned to the decrease in the magnetocrystalline anisotropy. The composites exhibited low loss factors (μ'' and $\varepsilon'' \approx 0$) under 1 GHz and high EM wave absorption bandwidth between 1.5 and 7.5 GHz. Nikzad et al.[92] synthesized Y-type hexagonal $Sr_2Co_2Fe_{12-y/2}Al_{y/2}O_{22}$ (where y = 0.0−3.0 in a step of 0.5) nanoparticles by chemical coprecipitation and the particle size was found to increase with Al^{3+} ion substitution. The samples with y = 3.0 exhibit highest RL_{min} of −30.7 dB with an absorption bandwidth of 3.3 GHz at X-band.

4. Garnets for EMI shielding

Garnets are described by the formula $Pe_3Fe_5O_{12}$, where Pe is a trivalent ion like a rare earth (RE) element. They have a similar structure to spinel ferrites; however, they have an extra dodecahedral c axis where cations can be doped to tune the lattice interaction for desired physical properties.[7]

Sharma et al.[93] studied the effect of the synthesis method on the EMI shielding properties of the yttrium iron garnet (YIG: $Y_3Fe_5O_{12}$). In the study, they synthesized YIG by sol-gel and solid-state method. They observed that the morphology of the particles differs with the synthesis method. They found that the nanoparticle prepared by sol-gel method exhibited an RL_{min} of −28 dB at 20 GHz for 300 μm thickness which was superior to the solid-state sample. Akhtar et al.[94] synthesized Al-doped spinel and garnet ferrites of the formula $Ni_{0.5}Zn_{0.3}Al_{0.2}$-$_{Fe2O4}$ and $Y_{2.8}Al_{0.2}Fe_5O_{12}$ by sol-gel technique. They obtained circular morphology for spinel ferrite and cubic morphology for the garnet structure. Toroidal samples were prepared by sintering for studying EM wave shielding properties in the C and X band. They concluded that Al doped garnets are excellent materials for filters, oscillators, waveguides, and high-frequency applications. Li et al.[95] synthesized YIG nanoparticles using a solid-state reaction method with a particle size of 68.2 nm. Thus, the prepared particle showed RL_{min} of as −34.5 dB at 20 GHz.

Choudhary et al.[96] synthesized coral-shaped YIG through the solution combustion method. PANI was synthesized using a chemical oxidative method. A composite in 50 wt% paraffin-wax was prepared by varying the concentration of YIG and PANI. The

composite consisting of 20 wt% YIG and 30 wt% PANI resulted in SE_T of −44.8 dB for 3 mm thick sample. They claimed that at the above critical concentration, the coral shape of YIG helps in multiple scattering of EM waves through the YIG-PANI interfaces. These scattered waves are then trapped within the dense coral network of YIG until they are absorbed by the PANI phase via conduction loss resulting in synergistic EM wave attenuation.

5. Hybrid nanostructures of ferrites for EMI shielding

As discussed previously, ferrites alone may not be able to provide shielding effectiveness over a wide frequency range, more so in the upper GHz frequency range. Therefore, they are often conjugated with carbonaceous fillers like MWCNTs, Graphene, etc., or with conducting polymers like Polyaniline (PANI), Polythiophene, Polypyrrole (PPy), etc. Conjugation with conducting or dielectric materials provides multiple interfaces with differing dielectric properties that help weaken the inherent power of the incoming EM waves.[19,20,97] Moreover, the overlapping conducting interfaces causes multiple reflections which further promote losses in EM wave power.

5.1 Nanostructures with carbonaceous materials

Biswas et al.[98] synthesized "flower-like" ferrite nanoparticles and conjugated it with MWCNTs. On incorporation of these heterostructures in PC/PVDF blends, shielding effectiveness of −64 dB at 18 GHz was obtained for 0.9 mm thick samples. The conjugation of flower-like Fe_3O_4 nanoclusters on the defect sites of the surface-functionalized MWCNTs absorbed the incident EM waves due to the interfacial polarization of different heterogeneous structures. Zhang et al.[99] synthesized Fe_3O_4 nanoparticles decorated MWCNTs@C ferrite nanocomposites using a coprecipitation method followed by a calcination process. The heterostructures with approximately 60 wt% Fe_3O_4 nanoparticles showed the best electromagnetic absorption properties with an RL_{min} of −52.47 dB at a thickness of 2.0 mm at 10.4 GHz. Menon et al.[18,21] grafted Fe_3O_4 nanoparticles onto graphene oxide (GO) sheets using a one-pot hydrothermal method and its 5 wt% composite in Polyurethane matrix along with MWCNTs resulted in shielding effectiveness of −36 dB at 18 GHz. Codoping reduced graphene oxide (rGO)/Fe_3O_4 with semiconducting MoS_2 resulted in improved shielding performance of −43 dB at 18 GHz due to improved polarization losses.[97,100] Pawar et al.[101] grafted dopamine modified Fe_3O_4 onto MWCNTs via diazotization reaction and dispersed them in PC/SAN blends to achieve high shielding effectiveness of −32.5 dB at 18 GHz. They also grafted Fe_3O_4 onto reduced GO (rGO) using a one-pot hydrothermal method and dispersing them in PC/SAN blends along with MWCNTs, resulted in high shielding efficiency of −50.7 dB at 18 GHz.[102] Sushmita et al.[16] provided a mechanistic insight on how different types of dopant on GO effects EMI shielding properties. They used ferrimagnetic Fe_3O_4 and paramagnetic Gd_2O_3 to dope GO. In a PC matrix when coupled with MWCNTs SE_T achieved for Gd_2O_3 and Fe_3O_4 hybrid was −28 and −33 dB at 18 GHz, respectively. They concluded that irrespective of the dopant, various magnetic and dielectric losses govern the EM wave shielding in polymeric nanocomposites when facilitated by multiple internal reflections from MWCNTs and GO.

Shu et al.[103] synthesized an MWCNT/$ZnFe_2O_4$ hybrid by a facile one-step solvothermal method. They observed that $ZnFe_2O_4$ microspheres were anchored to the surface of MWCNTs and the microspheres acted as bridges linking the neighboring MWCNTs resulting in 3D conductive networks as shown in Fig. 2.5. They obtained RL_{min} of −55.5 dB at 13.4 GHz with an absorption bandwidth of 3.6 GHz with a thickness of only 1.5 mm and particle loading of 50 wt% in wax. The same group also synthesized a nitrogen-doped rGO/$ZnFe_2O_4$ hybrid nanocomposites through a facile one-pot hydrothermal strategy and their composites with 40 wt% wax resulted in RL_{min} of −54.6 dB at 10.0 GHz (X-band) and effective absorption bandwidth achieved was 4.2 GHz (11.8−16.0 GHz) with a thickness of only 2.0 mm.[104] They also developed a rGO/MWCNT/$ZnFe_2O_4$ hybrid by the solvothermal route which resulted in twisting of MWCNTs around $ZnFe_2O_4$ microspheres and their interlinking with rGO forming highly connected 3D conductive networks. The composites in 50 wt% wax resulted in RL_{min} of −22.2 dB with an absorption bandwidth of 2.3 GHz for a thickness of only 1.0 mm.[105−107]

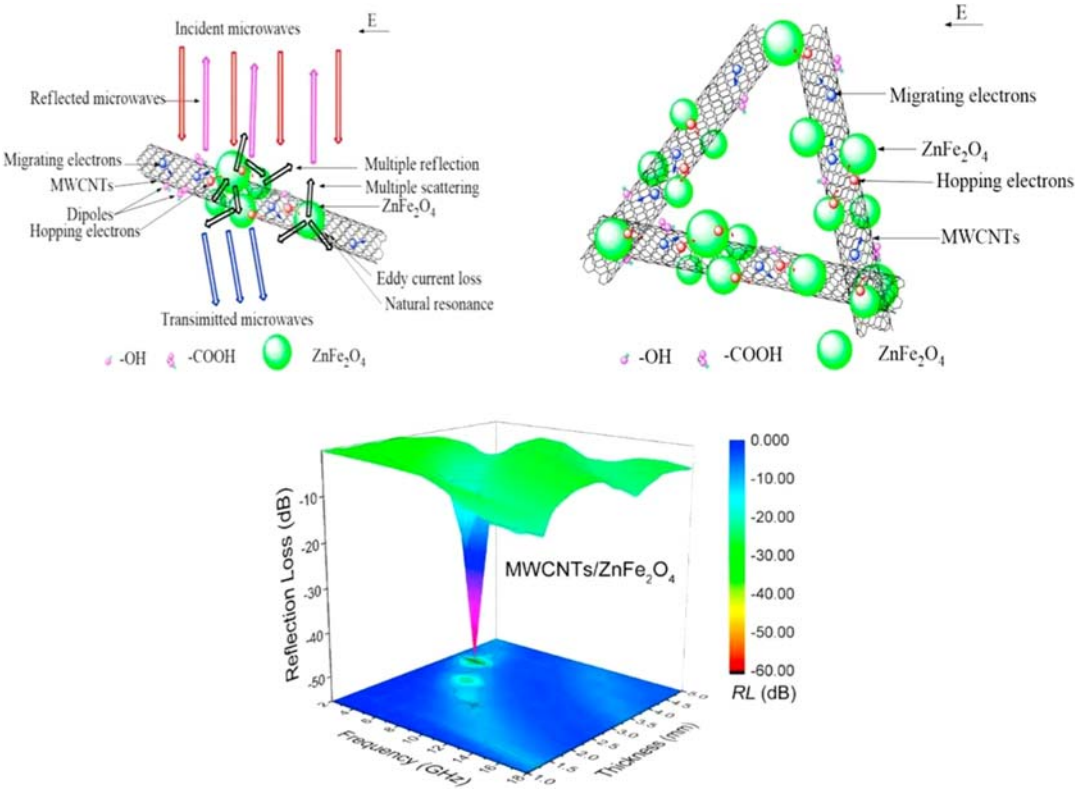

FIGURE 2.5 Mechanism of EMI shielding in MWCNTs/ZnFe2O4 hybrid composites. *Reprinted from Shu R, Zhang G, Wang X, Gao X, Wang M, Gan Y, Shi J, He J. Fabrication of 3D net- like MWCNTs/ZnFe2O4 hybrid composites as high-performance electromagnetic wave absorbers.* Chem Eng J *2018;**337**:242−255. Copyright © 2018, with permission from Elsevier.*

Zhang et al.[108] synthesized an MWCNTs/$NiFe_2O_4$ hybrid heterostructure by a facile one-pot solvothermal strategy. Through incorporating these heterostructures in 50 wt% wax, they achieved a RL_{min} of −42.3 dB with a thickness of 1.2 mm and the effective absorption bandwidth was 3.8 GHz. Yadav et al.[109,110] prepared rGO/$NiFe_2O_4$ heterostructures and composited them in 50 wt% of an elastomeric matrix which resulted in maximum shielding effectiveness was up to −28.5 dB with the shielding mechanism being absorption. In another study, Wu et al.[111] used amphiphilic GO as the "surfactant" to directly disperse MWCNTs in aq. dispersions and they further synthesized a reduced GO/MWCNT/$NiFe_2O_4$ ternary nanocomposites by a facile one-pot hydrothermal strategy. The results revealed that the ternary nanocomposites exhibited the enhanced EM wave absorption compared with the binary nanocomposite of rGO/MWCNT and single $NiFe_2O_4$. RL_{min} reached −50.2 dB with a thickness of just 1.4 mm and effective absorption bandwidth was 5.0 GHz (13−18 GHz). Liu et al.[112] synthesized rGO/$NiFe_2O_4$ clusters by using polyethylene oxide as a structure-directing reagent whereby rGO/$NiFe_2O_4$ clusters with diameters of 40−70 nm is composed of $NiFe_2O_4$ nanoparticles with diameters of 3−5 nm. The composites exhibited RL_{min} of up to −47.3 dB at 11.9 GHz and an absorption bandwidth of 4.7 GHz with a thickness of 2.5 mm. Fu et al.[113] synthesized $NiFe_2O_4$ nanorod/graphene composites by a facile one-step hydrothermal process in the presence of an ionic liquid, 1-propyl-3-hexadecylimidazolium bromide ([PHeIm][Br]). The RL_{min} obtained was −29.2 dB at 16.1 GHz with a thickness of 2.0 mm, and absorption bandwidth ranged from 13.6 to 18 GHz. Xiong et al.[114] anchored MWCNTs on the surface of silica-coated porous rod-like $NiFe_2O_4$ ($NiFe_2O_4$@SiO_2). They observed high EMI shielding efficiency with an RL_{min} of −67.8 dB and an absorption bandwidth of 4.5 GHz spanning from 13.5 to 18 GHz at a filler loading of 40 wt% and a thickness of only 1.9 mm.

Liu et al.[115,116] synthesized hierarchical cobalt ferrite ($CoFe_2O_4$)/rGO nanocomposites with a porous structure through in situ solvothermal reaction by varying the weight fraction of rGO. The hierarchical porous structure and proper electromagnetic parameters resulted in the improvement of impedance matching and attenuation ability. Their composites with 50 wt% wax resulted in strong RL_{min} of −57.7 dB and absorption bandwidth of 5.8 GHz (8.3−14.1 GHz) at a thickness of 2.8 mm. Zhang et al.[117] developed a unique covalently bonded $CoFe_2O_4$/graphene nanocomposites through an amino-ester-amide reaction process. Compared to noncovalently bonded nanocomposites, the covalently bonded nanocomposites exhibited outstanding electromagnetic wave absorption properties resulting in RL_{min} of −55.2 dB, and the absorption bandwidth achieved was about 5.4 GHz at 1.7 mm of thickness. They proposed that the absorption observed is due to the introduction of amide bonds in the nanocomposites which promote the migration rate of electrons between $CoFe_2O_4$ and graphene nanosheets as a stable carrier channel, which impacts the electromagnetic parameters and polarization modes of the materials. The rGO/$CoFe_2O_4$ composites developed by Zong et al.[118] exhibited an RL_{min} of −44.1 dB at 15.6 GHz with a thickness of 1.6 mm, and the absorption bandwidth of 4.7 GHz (from 13.3 to 18.0 GHz) with a thickness of only 1.5 mm. Biswas et al.[119] anchored $CoFe_2O_4$ onto MWCNTs using a pyrene derivative by chemical modification and selectively localized them in co-continuous blends of PVDF and poly(styrene-co-acrylonitrile) (SAN) which resulted in RL_{min} of −55 dB in the Ku band.

Zhang et al.[120] synthesized rGO/$MnFe_2O_4$ hybrids by a facile one-pot hydrothermal method. The obtained $MnFe_2O_4$ particles had a unique cubic morphology and were uniformly attached to rGO with an average particle size of 100 nm. Their composites with 70 wt% filling ratio resulted in RL_{min} of −47.5 dB with an absorption bandwidth of 5.2 GHz for a thickness of only 1.7 mm. Sun et al.[121] grew $MnFe_2O_4$ nanoparticles on graphene by a facile one-step solution-phase route. The as-synthesized heterostructures resulted in excellent microwave absorbability exhibiting a RL_{min} of −31.3 dB at 11.5 GHz with a thickness of 2 mm. Srivastava et al.[122] reported EMI shielding effectiveness of rGO-$MnFe_2O_4$ hybrids synthesized by a one-pot hydrothermal route, in presence of MWCNTs as conductive filler in PVDF matrix. Excellent absorption and a SE_T of −38 dB at 18 GHz were obtained for 5 wt% rGO-$MnFe_2O_4$ and 3 wt%MWCNTs.

Verma et al.[123] synthesized rGO/$BaFe_{12}O_{19}$ hybrids by high energy ball milling which resulted in $BaFe_{12}O_{19}$ nanoparticles with an average particle size of 20−30 nm is well distributed and firmly anchored onto the surface of the rGO. The composites exhibited high shielding effectiveness of −32 dB (∼99.9% attenuation) at a thickness of 3 mm in the Ku band. The mechanism of shielding was proposed to be the enhancement of the space charge polarization, natural resonance, multiple scattering, and the effective anisotropy energy of $BaFe_{12}O_{19}$ nanoparticles. He et al.[124] developed three-phase composites of PVDF-$BaFe_{12}O_{19}$- rGO by a facile wet chemical method and hot-pressing approach. In the X band, the composites showed excellent RL_{min} of −32 dB at 11 GHz and with an absorption bandwidth from 9.6 to 12.8 GHz.

Gao et al.[125] synthesized 100-150 nm-sized pod-like 3D $Ni_{0.33}Co_{0.67}Fe_2O_4$/rGO using a solvothermal reaction followed by cold quenching in liquid nitrogen which caused the $Ni_{0.33}Co_{0.67}Fe_2O_4$ to be encapsulated in rGO rolls due to the shrinkage of rGO in liquid nitrogen. The RL_{min} obtained was −47.5 dB and the absorption bandwidth obtained was 5.02 GHz at a loading of 20 wt% in the frequency range 1−18 GHz. They observed that $Ni_{0.33}Co_{0.67}Fe_2O_4$/rGO show much better absorbing performances than pure $Ni_{0.33}Co_{0.67}Fe_2O_4$ microspheres and $Ni_{0.33}Co_{0.67}Fe_2O_4$-rGO mixture prepared by mechanically blending of cold quenched pure rGO and $Ni_{0.33}Co_{0.67}Fe_2O_4$ microspheres. Zhang et al.[126] surface-modified MWCNTs by Ar plasma and $Co_{0.5}Ni_{0.5}Fe_2O_4$ nanoparticles were doped onto the surface of the MWCNTs by a chemical coprecipitation method. The composites of 0.75 wt% modified MWCNTs with Polyimide resulted in RL_{min} of −24.37 dB and an absorption bandwidth of 5.1 GHz from 7.8 to 12.9 GHz. After plasma modification, the surface of the MWCNTs produced carboxyl groups, which are beneficial for interfacial bonding between the MWCNTs and Polyimide. Zhou et al.[127] fabricated NiZn ferrite nanofibers via electrospinning technique and then physically converted them into rGO/NiZn ferrite nanocomposites whereby the graphene nanosheets were uniformly decorated with NiZn ferrite without aggregation. They found that these nanocomposites had remarkable improvements in both permittivity and permeability, which was attributed to the combination of the good conductivity of rGO and high magnetocrystalline anisotropy of NiZn ferrites which led to superior RL_{min} of −37.71 dB at 12.5 GHz, and an absorption bandwidth of 3.68 GHz. Liu et al.[128–131] synthesized a silane coupling agent modified $Ni_{0.4}Zn_{0.4}Co_{0.2}Fe_2O_4$ covered rGO hybrids via a simple, efficient and controllable three-step method which resulted in firm and uniform decoration of $Ni_{0.4}Zn_{0.4}Co_{0.2}Fe_2O_4$ on the rGO nanosheets. Microwave adsorption properties evaluated in the frequency range of 2−18 GHz showed a RL_{min} of −51.8 dB at 15.1 GHz with

an absorption bandwidth of 5.3 GHz (from 12.7 to 18 GHz) at a thickness of 2.1 mm. As shown in Fig. 2.6, they have explained the possible mechanism of EM wave shielding in the rGO/$Ni_{0.4}Zn_{0.4}Co_{0.2}Fe_2O_4$ composites. Zhou et al.[132] used a combined precipitation-hydrothermal method to fabricate MWCNT/$Ni_{0.5}Zn_{0.5}Fe_2O_4$ hybrid powders and found that when the MWCNT content was 5 wt% the RL_{min} obtained was −32.5 dB with an absorption bandwidth of 3.9 GHz in 2−9 GHz frequency range.

Peymanfar et al.[133] fabricated a magnetic composite of $SrAl_{1.3}Fe_{10.7}O_{19}$ nanoparticles and MWCNTs using a modified sol−gel method. The MWCNTs were first functionalized using a mixture of nitric and sulfuric and then coated with $SrAl_{1.3}Fe_{10.7}O_{19}$ in the presence of poly (methyl methacrylate) (PMMA) in an argon atmosphere furnace. They achieved a RL_{min} of −44.08 dB at 9.56 GHz and an absorption bandwidth of 2.21 GHz in the X band with a thickness of only 3.1 mm diameter and using 30 wt% of the heterostructure. Acharya et al.[134] report fabrication rGO/$SrAl_4Fe_8O_{19}$ heterostructure by one port chemical reduction of GO in the presence of $SrAl_4Fe_8O_{19}$ and they prepared composites of these heterostructures in PVDF. By varying the concentration of rGO and $SrAl_4Fe_8O_{19}$ they observed that rGO

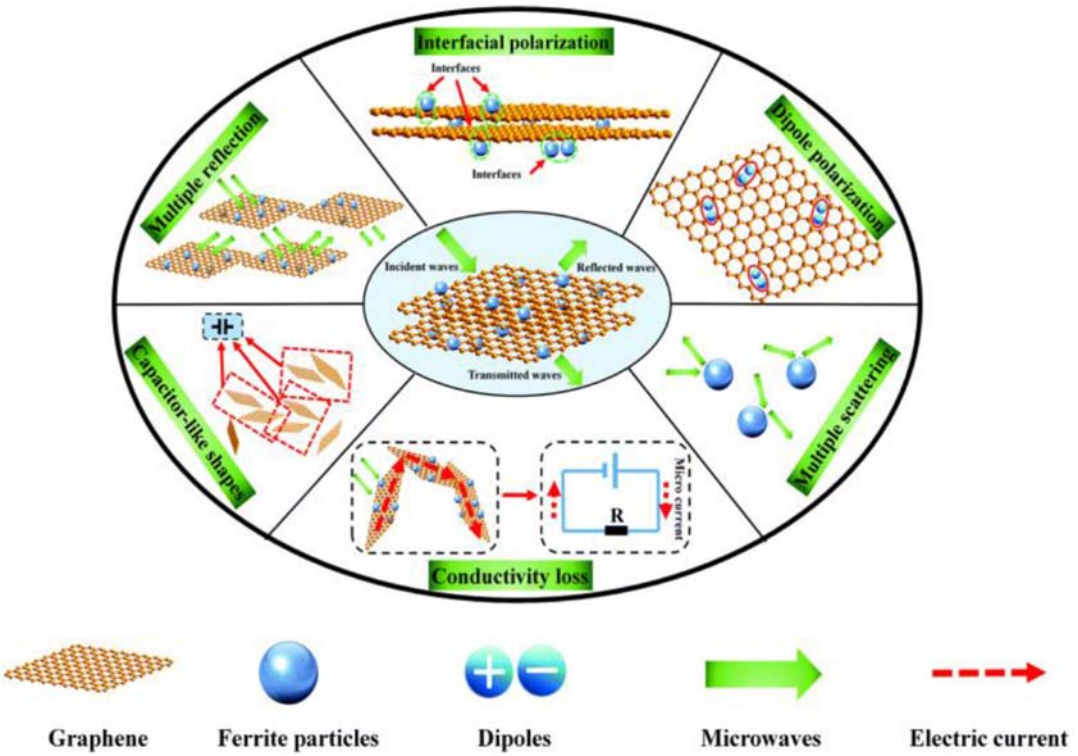

FIGURE 2.6 EM wave absorption mechanisms for the rGO/$Ni_{0.4}Zn_{0.4}Co_{0.2}Fe_2O_4$ nanocomposites. *Reprinted from Liu P, Yao Z, Zhou J, Yang Z, Kong LB. Small magnetic Co-doped NiZn ferrite/graphene nanocomposites and their dual-region microwave absorption performance.* J Mater Chem C *2016;4(41):9738−9749. Copyright © 2016, with permission from Royal Society of Chemistry.*

plays a crucial role in not only providing the conductive paths in the EM wave absorption but also in the magnetic domain communication of magnetic entities within the rGO network which resulted in high shielding effectiveness of −40 dB in X band with shielding mechanism being absorption type. Jamalian et al.[135] developed Mn−Sn−Ti substituted strontium ferrite nanoparticles attached on varying concentrations of MWCNTs by sol-gel method. The composites with 30 wt% polyvinyl chloride exhibited a RL_{min} of −28 dB at 8.8 GHz and an absorption bandwidth of 4 GHz.

Lin et al.[136] synthesized a graphene/$CoFe_2O_4$/YIG (with $CoFe_2O_4$: YIG mass ratio of 4:1 and graphene: $CoFe_2O_4$/YIG mass ratio of 1:5) nanocomposite by a deoxidation technique. The $CoFe_2O_4$ and YIG were synthesized separately via sol-gel and physically combined after which they were combined with GO via hydrothermal route. They observed a RL_{min} of −32.9 dB at 13.6 GHz which was much higher in composites without graphene.

5.2 Nanostructures with conducting polymers

Hosseini et al.[137] synthesized polyaniline (PANI)−$MnFe_2O_4$ core-shell nanostructure by in situ polymerization in the presence of dodecyl benzene sulfonic acid (DBSA) as the surfactant and dopant and ammonium persulfate (APS) as the oxidant. The size of $MnFe_2O_4$ was about 24 nm while the PANI coating content was about 15 wt%. The nanostructures were dispersed in acrylic resin and a coating thickness of 1.4 mm yielded a RL_{min} of −15.3 dB at 10.4 GHz in the X band. Gandhi et al.[138] synthesized PANI−$CoFe_2O_4$ nanostructures via one-step chemical oxidative polymerization of aniline in the presence of $CoFe_2O_4$ nanoparticles (30−40 nm). The ratio of PANI to $CoFe_2O_4$ was varied and the best shielding effectiveness with an absorption coefficient of −21.5 dB (more than 99% attenuation of microwaves) was exhibited by PANI: $CoFe_2O_4$ ratio of 1:2. Ma et al.[139] synthesized PANI/$Co_{0.5}Zn_{0.5}Fe_2O_4$ nanostructures by an in situ polymerization method with a particle size of 70 nm. Composites were prepared by dispersing 2 g of the nanostructure in 50 mL epoxy resin and the RL_{min} was measured in X-band (8.2−12.4 GHz), U-band (12.4−18 GHz) and K-band (18−26.5 GHz) by radar cross-sectional method according to the national standard GJB-2038−94. The RL_{min} obtained of the about −39.9 dB at 22.4 GHz with a bandwidth of 5 GHz. Lei et al.[140] co doped FeNi ferrites and coated PANI on them by varying reaction conditions including the polymerization temperature and reaction time to develop composites with high shielding ability. They observed that at an optimized polymerization condition of 20°C for 12 h the highest microwave absorption with an RL_{min} of −54.3 dB, and effective bandwidth of about 6.02 GHz at a thickness of 6.8 mm was achieved. Li et al.[141] synthesized $CoFe_2O_4$ hollow microspheres with protrusions by reduction of Co and Fe salts with a base in the presence of polystyrene (PS) microspheres followed by calcination as shown in Fig. 2.7. The obtained nanoparticles were then coated with polythiophene by in-situ polymerization method. The as-obtained nanoparticles were dispersed in wax in 8:3 ratio and were tested for shielding performance. They observed that at a thickness of 3.0 mm the composites exhibited a strong RL_{min} of −33.8 dB at 9.5 GHz with an absorption bandwidth of 3.1 GHz (8.2−11.3 GHz). Fang et al.[142] synthesized a heterostructure consisting of chopped carbon fibers (CF), $Co_{0.2}Fe_{2.8}O_4$ and PANI via a layer by layer (LBL) assembly for EMI shielding in the frequency range 2−18 GHz. The heterostructures when dispersed in wax in a ratio of 1:2 demonstrated RL_{min} of −38.2 dB at 12.7 GHz with a thickness of 4.1 mm. The shielding observed was attributed to

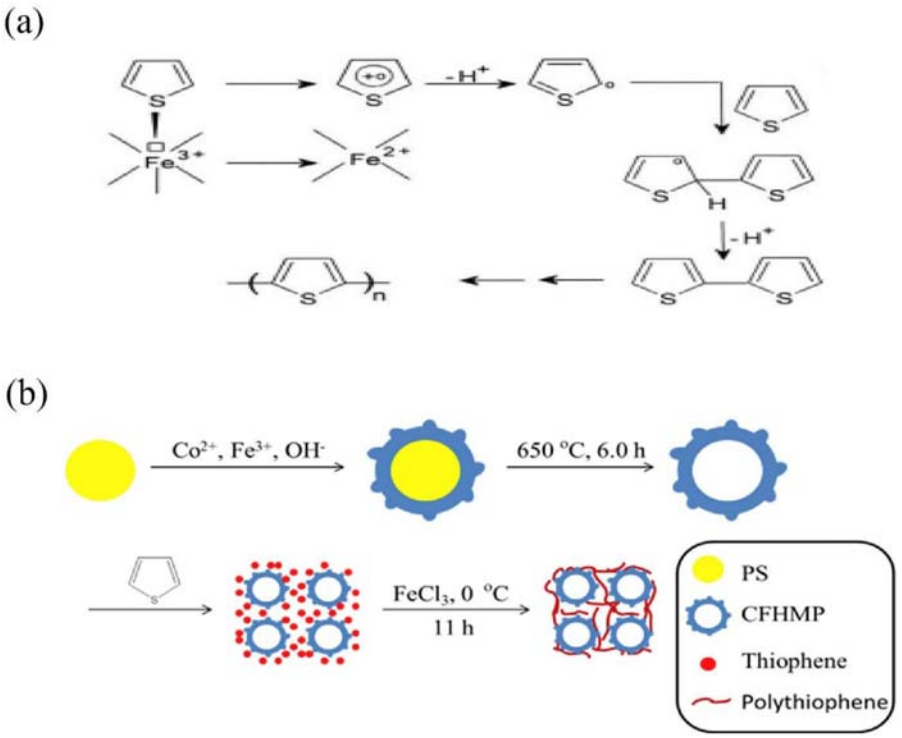

FIGURE 2.7 (A) Polymerization of polythiophene (B) synthesis of polythiophene coated $CoFe_2O_4$ hollow microspheres with protrusions. *Reprinted from Li L, Liu S, Lu L. Synthesis and significantly enhanced microwave absorption properties of cobalt ferrite hollow microspheres with protrusions/polythiophene composites.* J Alloys Compd *2017;**722**:158–165. Copyright © 2017, with permission from Elsevier.*

the combined effect of magnetic loss and dielectric losses from the synergistic combination of the three phases.

Li et al.[143] synthesized $NiFe_2O_4$ spinel ferrites by polyacrylamide sol-gel method, and its nanostructures with PANI and polypyrrole (PPy) were prepared via in situ emulsion polymerization. Composites were prepared in 70 wt% wax and the RL_{min} of $NiFe_2O_4$/PPy composite was found to be better than that of $NiFe_2O_4$/PANI composite with a value of −42 dB at 8 GHz and an absorption bandwidth of 4.5 GHz at a thickness of 3.5 mm. Saini et al.[144] synthesized PANI encapsulated Cd^{2+} substituted $NiFe_2O_4$ nanocomposites via in situ polymerization. Composites containing 30 wt% of particles showed the maximum SE_T of −42.7 dB for 2.3 mm thickness in the X-band range which was attributed to the synergistic tuning of magnetic and conductive inclusions. Didehban et al.[145] synthesized $Ni_{0.5}Zn_{0.5}Fe_2O_4$ by first preparing a nitrate–citrate gel was metallic nitrates and citric acid followed by sol–gel synthesis and auto-combustion. Then 15 and 35 wt% PANI was coated by in-situ polymerization of aniline. The composites were prepared in equal mass ratios of epoxy and the composite with 35 wt% PANI coating resulted in best shielding performance in X band exhibiting an RL_{min} −20 dB at 9.1 GHz. Ali et al.[146] developed $Mn_{0.1}Ni_{0.45}Zn_{0.45}Fe_2O_4$ by sol-gel method and then coated them with PANI in-situ chemical oxidative polymerization. Their

75 wt% composites with wax exhibit an absorption bandwidth from 2.60 to 3.74 GHz at a low surface density ranging from 2.5 to 3.1 kg/m^2. The RL_{min} achieved was −31.32 dB at 11.13 GHz with a matching thickness of 3 mm.

Li et al.[147] synthesized nanosized $Zn_{0.6}Cu_{0.4}Cr_{0.5}Fe_{1.46}Sm_{0.04}O_4$ by a rheological phase reaction method. These nanoparticles were further coated with PANI and PPy via in situ polymerization method. When the relative content of $Zn_{0.6}Cu_{0.4}Cr_{0.5}Fe_{1.46}Sm_{0.04}O_4$ in the nanostructures with PANI and PPy was approximately 20 wt%, the RL_{min} obtained for 1:1 composite with wax was −22.46 dB at 14.07 GHz and −20.90 dB at 14.05 for $Zn_{0.6}Cu_{0.4}Cr_{0.5}Fe_{1.46}Sm_{0.04}O_4$/PANI and $Zn_{0.6}Cu_{0.4}Cr_{0.5}Fe_{1.46}Sm_{0.04}O_4$/PPy, respectively. Elahi et al.[148] synthesized $Zn_{0.5}Ni_{0.4}Cr_{0.1}Fe_2O_4$ nanoparticles by sol−gel method and then coated 5, 15 and 25 wt% of PANI by in situ polymerization. The as-obtained powders were pressed for shielding measurement, and the results show that nanostructures with 25 wt% PANI coating show the best RL_{min} of −26.3 dB at 13.6 GHz in the Ku band. Zuo et al.[149] synthesized coralliform PANI nanorods and they were grafted onto the surface of $Li_{0.35}Zn_{0.3}Fe_{2.35}O_4$ (prepared by sol-gel method) by interfacial polymerization. At an optimized weight ratio of 1:2 of ferrite to aniline monomer, the RL_{min} value reached for their 70 wt% composite in wax was −36.9 dB at 12.4 GHz with the thickness of 2.1 mm and absorption bandwidth achieved was 4.24 GHz (11.26−15.5 GHz). The enhanced microwave absorption was chiefly attributed to the coralliform structure and improved impedance matching between the dielectric and magnetic loss.

Liu et al.[150] synthesized $BaFe_{12}O_{19}$/PANI core−shell nano-composites with PANI shell thickness varying from 25 to 60 nm by in-situ polymerization. The shell thickness variation helped in tuning the electric and magnetic characteristics of the nanostructures which helped refining impedance match, conductance loss, magnetic resonance loss and interfacial loss. The best EMI shielding performance was exhibited by the 70/30 (nanostructure/wax) composite with 30−40 nm shell thickness resulting in RL_{min} of −28 dB at 12.8 GHz with an absorption bandwidth of 3.8 GHz (11.8−15.6 GHz) at a thickness of 2.0 mm.

Peymanfar et al.[151] synthesized aluminum- doped strontium hexaferrite nanoparticle ($SrAl_{1.3}Fe_{10.7}O_{19}$) by sol-gel method. Further, $SrAl_{1.3}Fe_{10.7}O_{19}$/MWCNT/PANI multiphasic nanostructure was synthesized through a sonochemical method by in situ polymerization. The composites in 80 wt% wax resulted in RL_{min} of −24.93 dB at 16.40 GHz with a bandwidth of 2.81 GHz at a thickness of 6.5 mm in Ku band and were attributed to the interactive effect of the three components. Luo et al.[152] synthesized M-type strontium ferrite substituted by rare-earth ions Sm^{3+} and Er^{3+} via a sol-gel method. The ferrites were coated with 50−100 nm thick coating of PPy by in situ polymerization method using ammonium persulfate as oxidant. The nanostructures showed an increase in coercivity with PPy coating. The shielding efficiency of a 1:1 mass ratio composite of $SrEr_{0.3}Fe_{11.7}O_{19}$ was higher than that of $SrSm_{0.3}Fe_{11.7}O_{19}$ composite resulting in RL_{min} of −24.01 dB in 13.8 GHz for 3.0 mm with an absorption bandwidth of 7.2 GHz over the Ku band. He et al.[153] developed a PANI/Ag/$SrFe_{12}O_{19}$ heterostructure via a three-step method whereby, first, $SrFe_{12}O_{19}$ was synthesized via coprecipitation, then Ag was coated onto $SrFe_{12}O_{19}$ particles via chemical plating method and finally, PANI was coated onto Ag/$SrFe_{12}O_{19}$ particles via in-situ polymerization. The particles were dispersed in 70 wt% paraffin and the RL_{min} obtained was −14.86 dB at 9.98 GHz with an absorption bandwidth between 8.7 and 12.1 GHz for a thickness of 2 mm in the X band frequency range.

Bhingardive et al.[154] synthesized $CaFe_2O_4$ nanoparticles using Pechini method and coated it with PANI by in-situ polymerization. They compared the properties of PANI coated

$CaFe_2O_4$ with that of PANI-coated MWCNTs, and they observed that the former approach yielded the best results by achieving shielding effectiveness of −57 dB at 18 GHz and exhibiting 80% absorption of the incident EM radiation. From their study, they concluded that conducting PANI layer on magnetic $CaFe_2O_4$ results in highly lossy materials as compared to coating a conducting layer onto conducting MWCNTs.

Shen et al.[155] synthesized a copolymer composed of two conducting polymers: (N- methylpyrrole and pyrrole). The polymerization was carried out in situ in the presence of $Ba_{0.9}Nd_{0.1}Cr_{0.5}Fe_{11.5}O_{19}$ ferrite. This resulted in the $Ba_{0.9}Nd_{0.1}Cr_{0.5}Fe_{11.5}O_{19}$ ferrite particles being coated by the (N-methylpyrrole-co-pyrrole) copolymer as shown in Fig. 2.8. The dopant used for the conducting copolymer was H_3PO_4 which can make the N atom in the copolymer positively charged and can bond with the negatively charged $Ba_{0.9}Nd_{0.1}Cr_{0.5}$-$Fe_{11.5}O_{19}$ through H-bonding and electrostatic interaction. The EM wave absorbing properties of the poly(N-methylpyrrole-co-pyrrole)/$Ba_{0.9}Nd_{0.1}Cr_{0.5}Fe_{11.5}O_{19}$ composites was found to be better than that of individual-components which resulted in a RL_{min} of −26.57 dB and absorption bandwidth of 8.36 GHz in the frequency range of 2−18 GHz for a ratio of 5/3 (polymer/filler) and a thickness of 2 mm.

Cheng et al.[156] synthesized PPy/YIG heterostructure via in situ polymerization. They observed a negative permittivity behavior combined with metal-like conduction in the composites, which was attributed to the low-frequency plasmonic state of free electrons in the conducting PPy networks. The combined effect of magnetic resonance of YIG and the

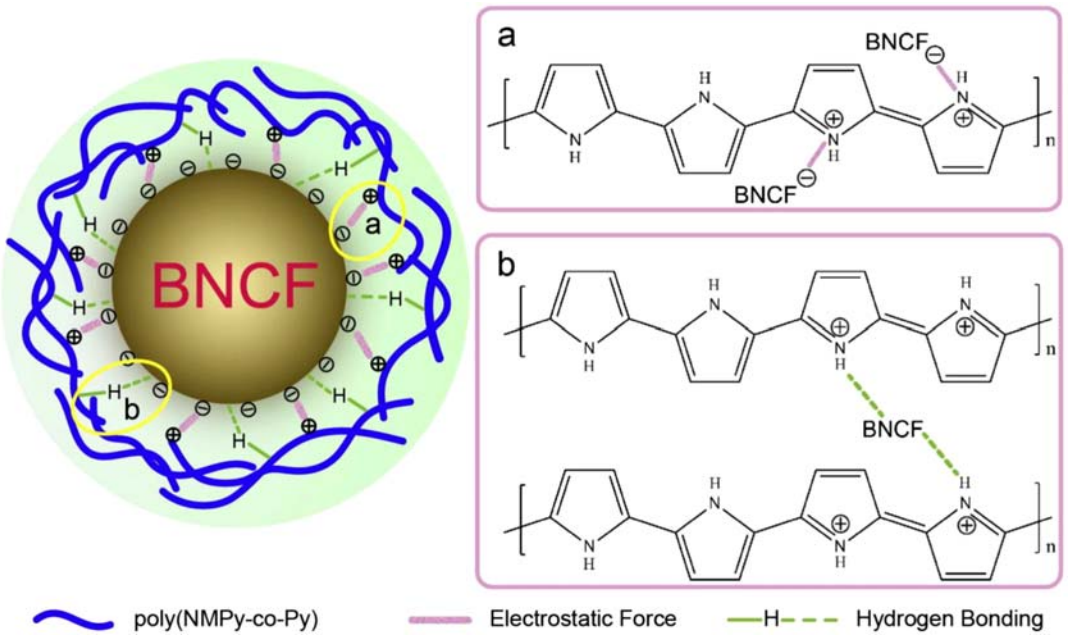

FIGURE 2.8 Schematic for synthesize of poly(N-methylpyrrole-co- pyrrole)/$Ba_{0.9}Nd_{0.1}Cr_{0.5}Fe_{11.5}O_{19}$ composites. *Reprinted from Shen J, Feng J, Li L, Tong G, He Y. Synthesis and excellent electromagnetic absorbing properties of copolymer (N-methylpyrrole-co-pyrrole) and Ba−Nd−Cr ferrite.* J Alloys Compd *2015;**632**:490−499. Copyright © 2015, with permission from Elsevier.*

diamagnetic response of PPy conducting networks resulted in a relaxation-type frequency dispersion in the permeability plots. Lin et al.[157] synthesized a PANI/$CoFe_2O_4$/YIG composite via in situ polymerization method for EMI shielding in 2−18 GHz range. They observed that when the mass ratio of $CoFe_2O_4$: YIG powders is 6:4, the highest RL_{min} of −23.4 dB at 7.7 GHz was obtained. Yang et al.[158] synthesized a hard/soft $BaFe_{12}O_{19}/Y_3Fe_5O_{12}$ heterostructure via was a one-step sol-gel method. These when then coated with PANI through the in situ polymerization method. Composites were prepared at 1:1 ratio in wax. They observed an exchange-coupling effect between $BaFe_{12}O_{19}$ and $Y_3Fe_5O_{12}$ at a ratio of 0.9: 0.1 which led to an excellent RL_{min} of −40.8 dB at 9.9 GHz and an absorption bandwidth between 6.8 and 12.3 GHz.

5.3 Core-shell nanostructures

Pawar et al.[159] synthesized carbon encapsulated "brick-like" Fe_3O_4 nanoparticles (Fe_3O_4@C) through a simple hydrothermal approach using Glucose as the carbon source. When incorporated in a PC matrix along with MWCNTs, they achieved RL_{min} of −41.3 dB at 17.7 GHz and with an absorption bandwidth of 4.4 GHz for a thickness of 1 mm. They claimed that the encapsulation of Fe_3O_4 with carbon prevented the disruption of conducting pathways facilitated by MWCNTs. Bhattacharjee et al.[160] reported a high EMI shielding effectiveness of −40 dB in the Ku-band for a film of 600 μm thickness using a unique core-shell heterostructure consisting of a Fe_3O_4 core and a conducting MWCNT shell, supported onto a dielectric SiO_2 spacer. The core-shell heterostructures were incorporated into a PVDF matrix along with conducting MWCNTs as shown in Fig. 2.9.

Feng et al.[161] prepared core/shell-structured, hard/soft spinel-ferrite-based $CoFe_2O_4$/$NiFe_2O_4$ nanocapsules with an average diameter of 17 nm by a facile two-step hydrothermal process using $CoFe_2O_4$ cores of ∼15 nm diameter as the hard magnetic phase and $NiFe_2O_4$ shells of ∼1 nm thickness as the soft magnetic phase. They observed that compared to $CoFe_2O_4$ and $NiFe_2O_4$ nanoparticles the core/shell structure enabled a significant reduction in electric resistivity and an enhancement in dipole and interfacial polarization in resulting in an obvious increase in dielectric permittivity and loss in the whole S−Ku bands of microwaves of 2−18 GHz, respectively. The exchange-coupling interaction between the core and shell led to enhanced exchange resonances in magnetic permeability and loss above 10 GHz manifesting in RL_{min} of −20.1 dB at 9.7 GHz at a thickness of 4.5 mm with an absorption bandwidth of 8.4 GHz (7.8−16.2 GHz).

Li et al.[162] developed $Ti_3C_2T_x$/NiZn ferrite composites with high reflection loss using a facile in situ coprecipitation method. The as-synthesized Ti3C2Tx/NiZn ferrite composite with a 5 wt% $Ti_3C_2T_x$ MXenes loading exhibited high RL_{min} of −42.5 dB at 13.5 GHz with an absorption bandwidth about 3 GHz (12−15 GHz) in the K-band. The potential electromagnetic wave absorption mechanisms were proposed to be a magnetic loss, dielectric loss, conductivity loss, multiple reflections, and scattering.

Wang et al.[163] developed a core/shell-structured CeO_2/Fe_3O_4 and Fe_3O_4/CeO_2 nanocapsules by interchange assembly of diluted magnetic semiconductor CeO_2 and ferromagnetic Fe_3O_4 as the core and the shell, and vice versa, using a facile two-step polar solvothermal method. The CeO_2/Fe_3O_4 (core/shell) nanocapsules showed enhanced permittivity and permeability in the Ku band with an RL_{min} of −28.9 dB at 15.3 GHz due to interfacial polarization and natural resonance at ∼15 GHz.

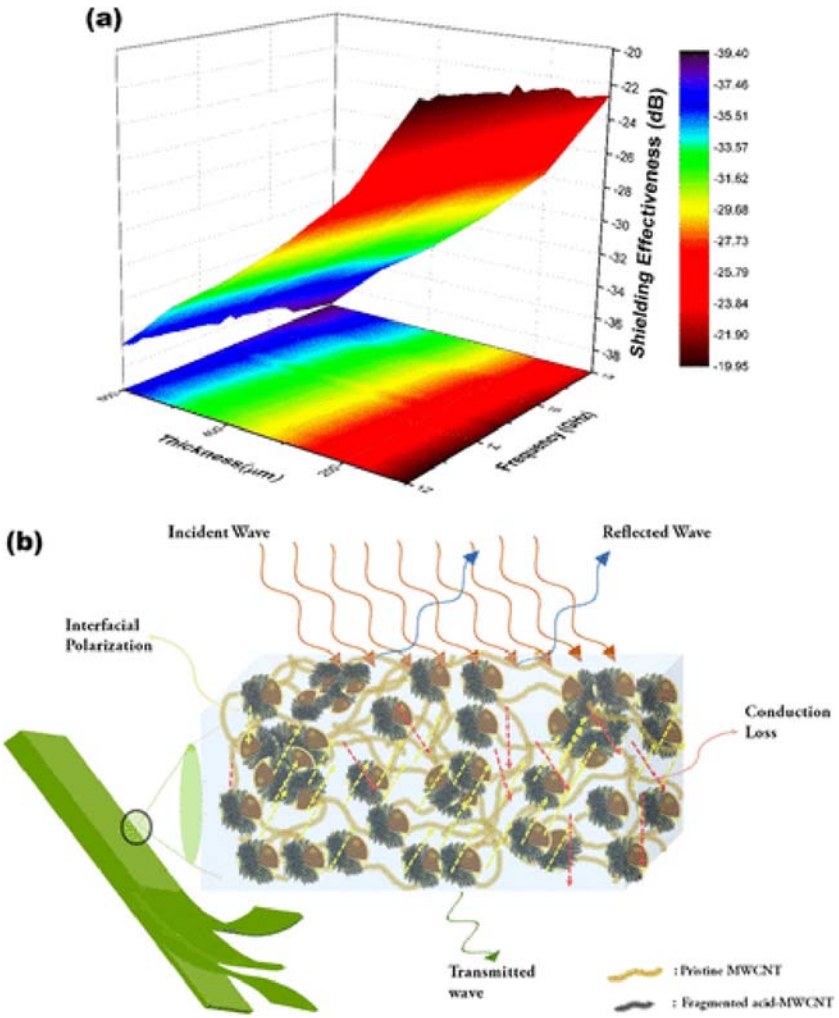

FIGURE 2.9 (A) SE_T for PVDF/core-shell heterostructure/MWCNT nanocomposites as a function of thickness (B) EMI shielding mechanism in the developed composite. *Reprinted from Bhattacharjee Y, Chatterjee D, Bose S. Core–multishell heterostructure with excellent heat dissipation for electromagnetic interference shielding.* ACS Appl Mater Interfaces *2018;**10**(36):30762–30773.Copyright © 2018, with permission from American Chemical Society.*

He et al.[164] synthesized (00h) $BaFe_{12}O_{19}$ filled $Ba_2Co_2Fe_{12}O_{22}$@PANI composite with oriented microstructure by an in situ polymerization reaction and a tape-casting method. The nanostructures were composited with polyvinyl butyral (PVB) (volume fraction of the powder to PVB being 30%) and composites sheets were prepared through the tape-casting process. Under the shear forces during the tap-casting, the $BaFe_{12}O_{19}$ templates were orderly dispersed in the composite to form an oriented microstructure to enhance the scattering effect. The RL_{min} obtained was −66.9 dB at 11.6 GHz with an absorption bandwidth of about 6.32 GHz at a thickness of 1.9 mm.

6. Conclusions

From the above discussion, it can be safely concluded that ferrites, as a class of magnetic materials are highly versatile in shielding EM waves. Two of the most important factors required for EM wave absorption especially as high frequencies are: magnetic and dielectric losses. Although ferrites do not impart appreciable magnetic losses except for significant eddy current losses at high frequencies, they can, however, contribute toward dielectric losses due to the presence of crystal defects that lead to the formation of dipole centers. Under an alternating EM field, these dipoles perform orientated rotation causing polarization losses leading to EM energy conversion to thermal energy. Doping ferrites with other metals can improve their coercivity leading to an increase in magnetic hysteresis losses, shifts the resonance frequency to higher frequencies, the ions with larger radiuses cause lattice distortions that improve dielectric loss. RE metal ions have unpaired 4f electrons, that causes the occurrence of 4f−3d couplings with ferrites which improve the EM properties.[152] To enhance the losses, dielectric and conducting inclusions are incorporated along with ferrites either separately or via suitable conjugation which further leads to a synergistic improvement in shielding efficiency. We hope that this consolidated review will help guide researchers from both academia and industry in designing suitable ferrite-based EM shields at the required frequency and application window.

References

1. Pomposo JA, Rodrıgúez J, Grande H. Polypyrrole-based conducting hot melt adhesives for EMI shielding applications. *Synth Met* 1999;**104**(2):107−11.
2. Fishbane PM, Gasiorowicz S, Thornton ST. *Physics for Scientists and Engineers Prentice Hall*. 1993. p. 0−13. New Jersey.
3. Chen Z, Xu C, Ma C, Ren W, Cheng H-M. Lightweight and flexible graphene foam composites for high-performance electromagnetic interference shielding. *Adv Mater* 2013;**25**(9):1296−300.
4. Pawar SP, Biswas S, Kar GP, Bose S. High frequency millimetre wave absorbers derived from polymeric nanocomposites. *Polymer* 2016;**84**:398−419.
5. Arief I, Biswas S, Bose S. FeCo-anchored reduced graphene oxide framework-based soft composites containing carbon nanotubes as highly efficient microwave absorbers with excellent heat dissipation ability. *ACS Appl Mater Interfaces* 2017;**9**(22):19202−14.
6. Biswas S, Panja SS, Bose S. Tailored distribution of nanoparticles in bi-phasic polymeric blends as emerging materials for suppressing electromagnetic radiation: challenges and prospects. *J Mater Chem C* 2018;**6**(13):3120−42.
7. Shukla V. Review of electromagnetic interference shielding materials fabricated by iron ingredients. *Nanoscale Adv* 2019;**1**(5):1640−71.
8. Özgür Ü, Alivov Y, Morkoç H. Microwave ferrites, part 1: fundamental properties. *J Mat Sci: Mat Elect* 2009;**20**(9):789−834.
9. El-Sayed K, Mohamed MB, Hamdy S, Ata-Allah SS. Effect of synthesis methods with different annealing temperatures on micro structure, cations distribution and magnetic properties of nano-nickel ferrite. *J Magn Magn Mater* 2017;**423**:291−300.
10. Bayrakdar H, Yalçın O, Vural S, Esmer K. Effect of different doping on the structural, morphological and magnetic properties for Cu doped nanoscale spinel type ferrites. *J Magn Magn Mater* 2013;**343**:86−91.
11. Aakash, Choubey R, Das D, Mukherjee S. Effect of doping of manganese ions on the structural and magnetic properties of nickel ferrite. *J Alloys Compd* 2016;**668**:33−9.
12. Celozzi S, Araneo RJ EoR, Engineering M. *Electromagnetic shielding*. 2005.
13. Ping EX. Transmission of electromagnetic waves in planar, cylindrical, and spherical dielectric layer systems and their applications. *J Appl Phy* 1994;**76**(11):7188−94.

14. Dilon. Jr JF, Earl. Jr HE. Domain wall motion and ferrimagnetic resonance in a manganese ferrite. *J Appl Phy* 1959;**30**(2):202−13.
15. Kwon HJ, Shin JY, Oh JH. The microwave absorbing and resonance phenomena of Y- type hexagonal ferrite microwave absorbers. *J Appl Phy* 1994;**75**(10):6109−11.
16. Sushmita K, Menon AV, Sharma S, Abhyankar AC, Madras G, Bose S. Mechanistic insight into the nature of dopants in graphene derivatives influencing electromagnetic interference shielding properties in hybrid polymer nanocomposites. *J Phys Chem C* 2019;**123**(4):2579−90.
17. Gebrekrstos A, Biswas S, Menon AV, Madras G, Pötschke P, Bose S. Multi-layered stack consisting of PVDF nanocomposites with flow-induced oriented MWCNT structure can supress electromagnetic radiation. *Composites, Part B* 2019;**166**:749−57.
18. Menon AV, Madras G, Bose S. Ultrafast self-healable interfaces in polyurethane nanocomposites designed using Diels−Alder "click" as an efficient microwave absorber. *ACS Omega* 2018;**3**(1):1137−46.
19. Menon AV, Madras G, Bose S. Phase specific dispersion of functional nanoparticles in soft nanocomposites resulting in enhanced electromagnetic screening ability dominated by absorption. *Phys Chem Chem Phys* 2017;**19**(1):467−79.
20. Menon AV, Madras G, Bose S. Magnetic Alloy-MWNT heterostructure as efficient electromagnetic wave suppressors in soft nanocomposites. *ChemistrySelect* 2017;**2**(26):7831−44.
21. Menon AV, Madras G, Bose S. Shape memory polyurethane nanocomposites with porous architectures for enhanced microwave shielding. *Chem Eng J* 2018;**352**:590−600.
22. Menon AV, Madras G, Bose S. Light weight, ultrathin, and "thermally-clickable" self- healing MWNT patch as electromagnetic interference suppressor. *Chem Eng J* 2019;**366**:72−82.
23. Sharma M, Singh D, Menon A, Madras G, Bose S. Suppressing electromagnetic radiation by trapping ferrite nanoparticles and carbon nanotubes in hierarchical nanoporous structures designed by crystallization-induced phase separation. *ChemistrySelect* 2018;**3**(4):1189−201.
24. Sun J, Wang W, Yue Q. Review on microwave-matter interaction fundamentals and efficient microwave-associated heating strategies. *Materials* 2016;**9**(4):231.
25. Zhang Y, Wang X, Cao M. Confinedly implanted NiFe2O4-rGO: cluster tailoring and highly tunable electromagnetic properties for selective-frequency microwave absorption. *Nano Res* 2018;**11**(3):1426−36.
26. Liu J, Cao M-S, Luo Q, Shi H-L, Wang W-Z, Yuan J. Electromagnetic property and tunable microwave absorption of 3D nets from nickel chains at elevated temperature. *ACS Appl Mater Interfaces* 2016;**8**(34):22615−22.
27. Ma J, Wang X, Cao W, Han C, Yang H, Yuan J, Cao M. A facile fabrication and highly tunable microwave absorption of 3D flower-like Co3O4-rGO hybrid-architectures. *Chem Eng J* 2018;**339**:487−98.
28. Snoek JL. Dispersion and absorption in magnetic ferrites at frequencies above one Mc/s. *Physica* 1948;**14**(4):207−17.
29. Al-Saleh MH, Sundararaj U. Electromagnetic interference shielding mechanisms of CNT/polymer composites. *Carbon* 2009;**47**(7):1738−46.
30. Mashuri X, Lestari W, Triwikantoro X, Darminto X. Preparation and microwave absorbing properties in the X-band of natural ferrites from iron sands by high energy milling. *Mater Res Express* 2018;**5**(1):014003.
31. Jia K, Zhao R, Zhong J, Liu X. Preparation and microwave absorption properties of loose nanoscale Fe3O4 spheres. *J Magn Magn Mater* 2010;**322**(15):2167−71.
32. Phadtare VD, Parale VG, Lee K-Y, Kim T, Puri VR, Park H-H. Flexible and lightweight Fe3O4/polymer foam composites for microwave-absorption applications. *J Alloys Compd* 2019;**805**:120−9.
33. Biswas S, Arief I, Panja SS, Bose S. Electromagnetic screening in soft conducting composite-containing ferrites: the key role of size and shape anisotropy. *Mater Chem Front* 2017;**1**(12):2574−89.
34. Zhang Y, Zhang J, Yuan L, Li G, Zhang X, Yue Z, Li L. Synthesis and microwave magnetic properties of magnetite nanowire arrays in polycarbonate templates. *Ceram Int* 2017;**43**:S403−6.
35. Han R, Li W, Pan W, Zhu M, Zhou D, Li F-s. 1D magnetic materials of Fe3O4 and Fe with high performance of microwave absorption fabricated by electrospinning method. *Sci Rep* 2014;**4**(1):7493.
36. Gong Y-X, Zhen L, Jiang J-T, Xu C-Y, Wang W-S, Shao W-Z. Synthesis of Fe−ferrite composite nanotubes with excellent microwave absorption performance. *CrystEngComm* 2011;**13**(22):6839−44.
37. Jia X, Wang J, Zhu X, Wang T, Yang F, Dong W, Wang G, Yang H, Wei F. Synthesis of lightweight and flexible composite aerogel of mesoporous iron oxide threaded by carbon nanotubes for microwave absorption. *J Alloys Compd* 2017;**697**:138−46.

38. An BH, Park BC, Yassi HA, Lee JS, Park J-R, Kim YK, Ryu JE, Choi DS. Fabrication of graphene-magnetite multi-granule nanocluster composites for microwave absorption application. *J Compos Mater* 2019. 0021998319853032.
39. Cheng H, Wei S, Ji Y, Zhai J, Zhang X, Chen J, Shen C. Synergetic effect of Fe3O4 nanoparticles and carbon on flexible poly (vinylidence fluoride) based films with higher heat dissipation to improve electromagnetic shielding. *Composites, Part A* 2019;**121**:139–48.
40. Liu Y, Song D, Wu C, Leng J. EMI shielding performance of nanocomposites with MWCNTs, nanosized Fe3O4 and Fe. *Composites, Part B* 2014;**63**:34–40.
41. Biswas S, Panja SS, Bose S. Physical insight into the mechanism of electromagnetic shielding in polymer nanocomposites containing multiwalled carbon nanotubes and inverse-spinel ferrites. *J Phys Chem C* 2018;**122**(34):19425–37.
42. Kim H-R, Kim B-S, Kim I-S. Fabrication and EMI shielding effectiveness of Ag-decorated highly porous poly(-vinyl alcohol)/Fe2O3 nanofibrous composites. *Mater Chem Phys* 2012;**135**(2):1024–9.
43. Arun Prakash VR, Rajadurai A, Jayaseelan V, Jerome Das S, Murali M, Julyes Jaisingh S. Role of silanized magnetic Fe2O3 particle in heat dissipation and microwave shielding behavior of E-glass fibre-reinforced epoxy resin composite. *Mater Res Express* 2019;**6**(7):076113.
44. Tong G, Wu W, Guan J, Qian H, Yuan J, Li W. Synthesis and characterization of nanosized urchin-like α-Fe2O3 and Fe3O4: microwave electromagnetic and absorbing properties. *J Alloys Compd* 2011;**509**(11):4320–6.
45. Mandal D, Gorai A, Mandal K. Electromagnetic wave trapping in NiFe2O4 nano-hollow spheres: an efficient microwave absorber. *J Magn Magn Mater* 2019;**485**:43–8.
46. Fu M, Zhu Z, Zhou Y, Xu W, Chen W, Liu Q, Zhu X. Multifunctional pompon flower- like nickel ferrites as novel pseudocapacitive electrode materials and advanced absorbing materials. *Ceram Int* 2020;**46**(1):850–6.
47. Biswas S, Kar GP, Bose S. Engineering nanostructured polymer blends with controlled nanoparticle location for excellent microwave absorption: a compartmentalized approach. *Nanoscale* 2015;**7**(26):11334–51.
48. Zhang X, Xiang J, Wu Z, Gong L, Chen X, Guan G, Wang Y, Zhang K. Enhanced absorbing properties and structural design of microwave absorbers based on Ni0. 8Co0. 2Fe2O4 nanofibers and Ni-C hybrid nanofibers. *J Alloys Compd* 2018;**764**:691–700.
49. Nikzad A, Parvizi R, Rezaei G, Vaseghi B, Khordad R. Structural, magnetic and microwave properties of nanocrystalline Ni-Co-Gd ferrites. *J Elect Mat* 2018;**47**(2):1302–10.
50. Saha P, Das S, Sutradhar S. Influence of Ni-Zn-Cu-ferrite on electroactive β- phase in poly (vinylidene fluoride)-Ni-Zn-Cu-ferrite nanocomposite film: unique metamaterial for enhanced microwave absorption. *J Appl Phys* 2018;**124**(4):045303.
51. Liu Y, Liu X, Wang X. Synthesis and microwave absorption properties of Ni− Zn−Mn spinel ferrites. *Adv Appl Ceram* 2015;**114**(2):82–6.
52. Qian K, Yao Z, Lin H, Zhou J, Haidry AA, Qi T, Chen W, Guo X. The influence of Nd substitution in Ni−Zn ferrites for the improved microwave absorption properties. *Ceram Int* 2020;**46**(1):227–35.
53. Jacobo SE, Bercoff PG, Herme CA, Vives LA. Sr hexaferrite/Ni ferrite nanocomposites: magnetic behavior and microwave absorbing properties in the X-band. *Mater Chem Phys* 2015;**157**:124–9.
54. Yan A, Liu H. In A NH4Ac-assisted solvothermal fabrication and properties of size-controlled cobalt ferrite nanospheres. In: *IOP conference series: materials science and engineering*. IOP Publishing; 2015. p. 012092.
55. Li J, Feng Y, Wu Y, Yuan Y. Fiber-guided and particle-localized microwave absorption of nanoscale CoFe2O4 derived from citric acid-based precursor. *Phys B Condens Matter* 2019;**561**:16–22.
56. Huang X, Zhang J, Xiao S, Chen G. The cobalt zinc spinel ferrite nanofiber: lightweight and efficient microwave absorber. *J Am Ceram Soc* 2014;**97**(5):1363–6.
57. Liu P-J, Yao Z-J, Ng VMH, Zhou J-T, Yang Z-H, Kong L-B. Enhanced microwave absorption properties of double-layer absorbers based on spherical NiO and Co 0.2 Ni 0.4 Zn 0.4 Fe 2 O 4 ferrite composites. *J Alloy Comp* 2018;**31**(2):171–9.
58. Li W, Wang L, Li G, Xu Y. Hollow CoFe2O4−Co3Fe7 microspheres applied in electromagnetic absorption. *J Magn Magn Mater* 2015;**377**:259–66.
59. Salimkhani H, Motei Dizaji A, Hashemi E, Palmeh P, Sabeghi G, Salimkhani S. Magnetic and microwave absorptive properties of electrophoretically deposited nano-CoFe2O4 as a 3D structure on carbon fibers. *Ceram Int* 2016;**42**(11):12709–14.
60. Wang H, Wang C, Xiong Y, Yao Q, Chang Q, Chen Y, Jin C, Sun Q. Solvothermal fabrication and growth behavior study of spherical MnFe 2 O 4 through a bottom-up method on wood substrate with effective microwave absorption. *RSC Adv* 2017;**7**(40):24764–70.

61. Katiyar M, Prasad M, Agarwal K, Singh RK, Kumar A, Prasad NE. Study and characterization of E.M. absorbing properties of EPDM ferrite composite containing manganese zinc ferrite. *J Reinforc Plast Compos* 2017;**36**(10):754–65.
62. Biswas S, Bhattacharjee Y, Panja SS, Bose S. Rational design of multilayer ultrathin nano-architecture by coupling of soft conducting nanocomposite with ferrites and porous structures for screening electromagnetic radiation. *ChemistrySelect* 2017;**2**(3):1094–101.
63. Bhattacharjee Y, Bhingardive V, Biswas S, Bose S. Construction of a carbon fiber based layer-by-layer (LbL) assembly—a smart approach towards effective EMI shielding. *RSC Adv* 2016;**6**(113):112614–9.
64. Ghasemi A, Hossienpour A, Morisako A, Saatchi A, Salehi M. Electromagnetic properties and microwave absorbing characteristics of doped barium hexaferrite. *J Magn Magn Mater* 2006;**302**(2):429–35.
65. Iqbal S, Kotnala G, Shah J, Ahmad S. Barium ferrite nanoparticles: a highly effective EMI shielding material. *Mater Res Express* 2019;**6**(5):055018.
66. Handoko E, Sugihartono I, Budi S, Randa M, Jalil Z, Alaydrus M. The effect of thickness on microwave absorbing properties of barium ferrite powder. *J Phys Conf* 2018;**1080**:012002.
67. Ozah S, Bhattacharyya NS. Nanosized barium hexaferrite in novolac phenolic resin as microwave absorber for X-band application. *J Magn Magn Mater* 2013;**342**:92–9.
68. Peymanfar R, Rahmanisaghieh M. Preparation of neat and capped BaFe2O4 nanoparticles and investigation of morphology, magnetic, and polarization effects on its microwave and optical performance. *Mater Res Express* 2018;**5**(10):105012.
69. Biswas S, Kar GP, Bose S. Tailor-made distribution of nanoparticles in blend structure toward outstanding electromagnetic interference shielding. *ACS Appl Mater Interfaces* 2015;**7**(45):25448–63.
70. Rana K, Thakur P, Tomar M, Gupta V, Thakur A. Investigation of cobalt substituted M- type barium ferrite synthesized via co-precipitation method for radar absorbing material in Ku-band (12–18GHz). *Ceram Int* 2018;**44**(6):6370–5.
71. Guo D, Kong W, Feng J, Li X, Fan X. Synthesis, electromagnetic and microwave absorption properties of Ba3Co2Fe24O41 hexaferrites for GHz application. *Mater Sci Eng, B* 2018;**228**:213–7.
72. Mohammad FZ, Siddiqui JJ, Ali K, Arshad H, Mudsar M, Ijaz A. Magnetic and microwave absorption properties of W-type nanoferrite in X and Ku band. *J Mater Sci Mater Electron* 2019;**30**(3):2278–84.
73. Ozah S, Bhattacharyya NS. Development of BaAlxFe12−xO19-NPR nanocomposite as an efficient absorbing material in the X-band. *J Magn Magn Mater* 2015;**374**:516–24.
74. Araz İ. The effect of Ce–Co substitution on the structural and the electromagnetic properties of barium hexaferrite. *J Mater Sci Mater Electron* 2019;**30**(5):5130–6.
75. Cho H-S, Kim S-S. The effect of Zn and Ni substitution on magnetic and microwave absorbing properties of Co2W hexagonal ferrites. *Ceram Int* 2019;**45**(7, Part B):9406–9.
76. Magham SBS, Sharma M, Shannigrahi SR, Tan HR, Sharma V, Meng YS, Idapalpati S, Ramanujan RV, Repaka DVM. Development of Z-type hexaferrites for high frequency EMI shielding applications. *J Magn Magn Mater* 2017;**441**:303–9.
77. Narang SB, Pubby K. Electromagnetic characterization of Co-Ti-doped Ba-M ferrite- based frequency-tunable microwave absorber in 12.4–40 GHz. *J Supercond Nov Magnetism* 2017;**30**(2):511–20.
78. Li W, Lv J, Zhou X, Zheng J, Ying Y, Qiao L, Yu J, Che S. Enhanced and broadband microwave absorption of flake-shaped Fe and FeNi composite with Ba ferrites. *J Magn Magn Mater* 2017;**426**:504–9.
79. Zhang J. Interference effects on microwave absorbing properties of W-type BaZn2Fe16O27 prepared by solid method. *J Mater Sci Mater Electron* 2019;**30**(9):8437–44.
80. Zhang J, Wang L-X, Huang X-G, Zhang Q-T. Electromagnetic properties of BaZn 2 Fe 16 O 27/antimony-doped tin oxide composite absorbing materials by co-precipitation method. *Rare Met* 2014;**33**(6):697–702.
81. Kaur H, Marwaha A, Singh C, Narang SB, Jotania R, Jacobo S, Sombra ASB, Trukhanov SV, Trukhanov AV, Dhruv P. Investigation of structural, hysteresis and electromagnetic parameters for microwave absorption application in doped Ba–Sr hexagonal ferrites at X-band. *J Alloys Compd* 2019;**806**:1220–9.
82. Kaur H, Marwaha A, Singh C, Narang SB, Jotania R, Bai Y, et al. Tailoring of electromagnetic absorption in substituted hexaferrites from 8.2 GHz to 12.4 GHz. *J Electron Mater* 2020;**49**:1646–53.
83. Kaur R, Dhillon N, Singh C, Narang SB, Chandra M. Microwave and electrical characterization of M-type Ba0.5Sr0.5CoxRuxFe(12−2x)O19 hexaferrite for practical applications. *Solid State Commun* 2015;**201**:72–5.
84. Joshi R, Singh C, Singh J, Kaur D, Narang SB, Jotania RB. A study of microwave absorbing properties in Co–Gd doped M-type Ba–Sr hexaferrites prepared using ceramic method. *J Mater Sci Mater Electron* 2017;**28**(16):11969–78.

85. Liu C, Xu Q, Tang Y, Wang Z, Ma R, Ma N, Du P. Zr 4+ doping- controlled permittivity and permeability of BaFe 12− x Zr x O 19 and the extraordinary EM absorption power in the millimeter wavelength frequency range. *J Mater Chem C* 2016;**4**(40):9532−43.
86. Liu C, Fang G, Li Z, Zhang Y, Zhao X, Peng K, Zhang Y, Zou J. Achieving impressive millimeter-wave absorption properties in Nb5+ doped barium ferrite by simply controlling the sintering atmosphere. *Mater Lett* 2019;**244**:147−50.
87. Liu S, Wei K, Cheng Y, Yan S, He L, Deng L. Structural, magnetic and microwave electromagnetic properties in La-substituted quaternary ferrite. *J Alloys Compd* 2019;**791**:469−76.
88. Chen W, Zhu X, Liu Q, Fu M. Preparation of urchin-like strontium ferrites as microwave absorbing materials. *Mater Lett* 2017;**209**:425−8.
89. Yu J, Yu J, Ying T, Cui C, Sun Y, Liu X. The design and the preparation of mesoporous Ag3PO4 nanorod/SrFe12O19 hexagonal nanoflake heterostructure for excellent microwave absorption. *J Alloys Compd* 2019;**775**:225−32.
90. Kaur P, Bahel S, Narang SB. Electromagnetic wave absorption properties of La-doped strontium M-type hexagonal ferrite in a 18−40 GHz frequency range. *J Electron Mater* 2020;**49**(3):1654−9.
91. Park M-H, Kang Y-M. Fabrication and properties of Z-type Sr3Co2−xZnxFe24O41 hexaferrites and their composites with epoxy. *J Magn Magn Mater* 2019;**491**:165628.
92. Nikzad A, Ghasemi A, Tehrani MK, Gordani GR. Correlation between structural features and microwave analysis of substituted Sr-Co2Y ceramic nanoparticles. *J Supercond Nov Magnetism* 2016;**29**(6):1657−64.
93. Sharma V, Saha J, Patnaik S, Kuanr BK. YIG based broad band microwave absorber: a perspective on synthesis methods. *J Magn Magn Mater* 2017;**439**:277−86.
94. Akhtar MN, Saleem M, Khan MA. Al doped spinel and garnet nanostructured ferrites for microwave frequency C and X- band applications. *J Phys Chem Solid* 2018;**123**:260−5.
95. Li H, Guo Y. High microwave absorption characteristic nanomaterial preparation and mechanism analysis. *J Alloys Compd* 2018;**765**:936−42.
96. Choudhary HK, Kumar R, Pawar SP, Anupama AV, Bose S, Sahoo B. Effect of coral- shaped yttrium iron garnet particles on the EMI shielding behaviour of yttrium iron garnet- polyaniline-wax composites. *ChemistrySelect* 2018;**3**(7):2120−30.
97. Menon AV, Choudhury B, Madras G, Bose S. 'Trigger-free' self-healable electromagnetic shielding material assisted by co-doped graphene nanostructures. *Chem Eng J* 2020;**382**:122816.
98. Biswas S, Panja SS, Bose S. Unique multilayered assembly consisting of "flower-like" ferrite nanoclusters conjugated with MWCNT as millimeter wave absorbers. *J Phys Chem C* 2017;**121**(26):13998−4009.
99. Zhang K, Gao X, Zhang Q, Chen H, Chen X. Fe3O4 nanoparticles decorated MWCNTs @ C ferrite nanocomposites and their enhanced microwave absorption properties. *J Magn Magn Mater* 2018;**452**:55−63.
100. Menon AV, Madras G, Bose S. Mussel-inspired self-healing polyurethane with "flower—like" magnetic MoS2 as efficient microwave absorbers. *ACS Appl Poly Mater* 2019;**1**(9):2417−29.
101. Pawar SP, Marathe DA, Pattabhi K, Bose S. Electromagnetic interference shielding through MWNT grafted Fe3O4 nanoparticles in PC/SAN blends. *J Mater Chem* 2015;**3**(2):656−69.
102. Pawar SP, Gandi M, Bose S. High performance electromagnetic wave absorbers derived from PC/SAN blends containing multiwall carbon nanotubes and Fe3O4 decorated onto graphene oxide sheets. *RSC Adv* 2016;**6**(44):37633−45.
103. Shu R, Zhang G, Wang X, Gao X, Wang M, Gan Y, Shi J, He J. Fabrication of 3D net- like MWCNTs/ZnFe2O4 hybrid composites as high-performance electromagnetic wave absorbers. *Chem Eng J* 2018;**337**:242−55.
104. Shu R, Zhang J, Wu Y, Wan Z, Zheng M. Facile design of nitrogen-doped reduced graphene oxide/zinc ferrite hybrid nanocomposites with excellent microwave absorption in the X- band. *Mater Lett* 2019;**255**:126549.
105. Shu R, Zhang G, Zhang J, Wang X, Wang M, Gan Y, Shi J, He J. Fabrication of reduced graphene oxide/multiwalled carbon nanotubes/zinc ferrite hybrid composites as high- performance microwave absorbers. *J Alloys Compd* 2018;**736**:1−11.
106. Shu R, Li W, Zhou X, Tian D, Zhang G, Gan Y, Shi J, He J. Facile preparation and microwave absorption properties of RGO/MWCNTs/ZnFe2O4 hybrid nanocomposites. *J Alloys Compd* 2018;**743**:163−74.
107. Liu Z, Xing H, Liu Y, Wang H, Jia H, Ji X. Hydrothermally synthesized Zn ferrite/multi- walled carbon nanotubes composite with enhanced electromagnetic-wave absorption performance. *J Alloys Compd* 2018;**731**:745−52.

108. Zhang J, Shu R, Guo C, Sun R, Chen Y, Yuan J. Fabrication of nickel ferrite microspheres decorated multi-walled carbon nanotubes hybrid composites with enhanced electromagnetic wave absorption properties. *J Alloys Compd* 2019;**784**:422–30.
109. Yadav RS, Kuřitka I, Vilcakova J, Skoda D, Urbánek P, Machovsky M, Masař M, Kalina L, Havlica J. Lightweight NiFe2O4-Reduced Graphene Oxide-Elastomer Nanocomposite flexible sheet for electromagnetic interference shielding application. *Composites, Part B* 2019;**166**:95–111.
110. Yadav RS, Kuřitka I, Vilčáková J, Machovský M, Škoda D, Urbánek P, Masař M, Gořalik M, Urbánek M, Kalina L, Havlica J. Polypropylene nanocomposite filled with spinel ferrite NiFe2O4 nanoparticles and in-situ thermally-reduced graphene oxide for electromagnetic interference shielding application. *Nanomaterials* 2019;**9**(4):621.
111. Wu Y, Shu R, Li Z, Guo C, Zhang G, Zhang J, Li W. Design and electromagnetic wave absorption properties of reduced graphene oxide/multi-walled carbon nanotubes/nickel ferrite ternary nanocomposites. *J Alloys Compd* 2019;**784**:887–96.
112. Liu P, Huang Y, Sun X. NiFe2O4 clusters on the surface of reduced graphene oxide and their excellent microwave absorption properties. *Mater Lett* 2013;**112**:117–20.
113. Fu M, Jiao Q, Zhao Y. Preparation of NiFe2O4 nanorod–graphene composites via an ionic liquid assisted one-step hydrothermal approach and their microwave absorbing properties. *J Mater Chem* 2013;**1**(18):5577–86.
114. Xiong Y, Luo H, Nie Y, Chen F, Dai W, Wang X, Cheng Y, Gong R. Synergistic effect of silica coated porous rodlike nickel ferrite and multiwalled carbon nanotube with improved electromagnetic wave absorption performance. *J Alloys Compd* 2019;**802**:364–72.
115. Liu Y, Chen Z, Zhang Y, Feng R, Chen X, Xiong C, Dong L. Broadband and lightweight microwave absorber constructed by in situ growth of hierarchical CoFe2O4/reduced graphene oxide porous nanocomposites. *ACS Appl Mater Interfaces* 2018;**10**(16):13860–8.
116. Liu Z, Xu G, Zhang M, Xiong K, Meng P. Synthesis of CoFe2O4/RGO nanocomposites by click chemistry and electromagnetic wave absorption properties. *J Mater Sci Mater Electron* 2016;**27**(9):9278–85.
117. Zhang N, Liu X, Huang Y, Wang M, Li S, Zong M, Liu P. Novel nanocomposites of cobalt ferrite covalently-grafted on graphene by amide bond as superior electromagnetic wave absorber. *J Colloid Interface Sci* 2019;**540**:218–27.
118. Zong M, Huang Y, Zhang N. Reduced graphene oxide-CoFe2O4 composite: synthesis and electromagnetic absorption properties. *Appl Surf Sci* 2015;**345**:272–8.
119. Biswas S, Kar GP, Bose S. Microwave absorbers designed from PVDF/SAN blends containing multiwall carbon nanotubes anchored cobalt ferrite via a pyrene derivative. *J Mater Chem* 2015;**3**(23):12413–26.
120. Zhang G, Shu R, Xie Y, Xia H, Gan Y, Shi J, He J. Cubic MnFe2O4 particles decorated reduced graphene oxide with excellent microwave absorption properties. *Mater Lett* 2018;**231**:209–12.
121. Sun G, Liu H, Yuan M, Liao Q, Zhang Y. Enhanced electromagnetic performance of MnFe2O4 nanocrystals grown on graphene via a one-step solution route. *Sci Adv Mater* 2019;**11**(2):283–90.
122. Srivastava RK, Xavier P, Gupta SN, Kar GP, Bose S, Sood AK. Excellent electromagnetic interference shielding by graphene- MnFe2O4-multiwalled carbon nanotube hybrids at very low weight percentage in polymer matrix. *ChemistrySelect* 2016;**1**(18):5995–6003.
123. Verma M, Singh AP, Sambyal P, Singh BP, Dhawan SK, Choudhary V. Barium ferrite decorated reduced graphene oxide nanocomposite for effective electromagnetic interference shielding. *Phys Chem Chem Phys* 2015;**17**(3):1610–8.
124. He H, Luo F, Qian N, Wang N. Improved microwave absorption and electromagnetic properties of BaFe12O19-poly(vinylidene fluoride) composites by incorporating reduced graphene oxides. *J Appl Phys* 2015;**117**(8):085502.
125. Gao M, Zhao Y, Wang S, Xu Y, Feng C, Shi D, Jiao Q. Preparation of pod-like 3D Ni0.33Co0.67Fe2O4@rGO composites and their microwave absorbing properties. *Ceram Int* 2019;**45**(6):7188–95.
126. Zhang L, Shi C, Rhee KY, Zhao N. Properties of Co0.5Ni0.5Fe2O4/carbon nanotubes/polyimide nanocomposites for microwave absorption. *Composites, Part A* 2012;**43**(12):2241–8.
127. Zhou X, Chuai D, Zhu D. Electrospun synthesis of reduced graphene oxide (RGO)/NiZn ferrite nanocomposites for excellent microwave absorption properties. *J Supercond Nov Magnetism* 2019;**32**(8):2687–97.
128. Liu P, Yao Z, Zhou J. Controllable synthesis and enhanced microwave absorption properties of silane-modified Ni0.4Zn0.4Co0.2Fe2O4 nanocomposites covered with reduced graphene oxide. *RSC Adv* 2015;**5**(114):93739–48.

129. Liu P, Yao Z, Zhou J. Preparation of reduced graphene oxide/Ni0.4Zn0.4Co0.2Fe2O4 nanocomposites and their excellent microwave absorption properties. *Ceram Int* 2015;**41**(10, Part A):13409–16.
130. Liu P, Ng VMH, Yao Z, Zhou J, Lei Y, Yang Z, Kong LB. Microwave absorption properties of double-layer absorbers based on Co0.2Ni0.4Zn0.4Fe2O4 ferrite and reduced graphene oxide composites. *J Alloys Compd* 2017;**701**:841–9.
131. Liu P, Yao Z, Zhou J, Yang Z, Kong LB. Small magnetic Co-doped NiZn ferrite/graphene nanocomposites and their dual-region microwave absorption performance. *J Mater Chem C* 2016;**4**(41):9738–49.
132. Zhou X-B, Shen L, Li L, Huang T-M, Hu C-F, Pan W-M, Jin X-H, Sun J, Gao L, Huang Q. Preparation of nanocrystalline-coated carbon nanotube/Ni0. 5Zn0. 5Fe2O4 composite with excellent electromagnetic property as microwave absorber. *J Phys D Appl Phys* 2013;**46**(14):145002.
133. Peymanfar R, Afghahi SSS, Javanshir S. Preparation and investigation of structural, magnetic, and microwave absorption properties of a SrAl1.3Fe10.7O19/multiwalled carbon nanotube nanocomposite in X and Ku-band frequencies. *J Nanosci Nanotechnol* 2019;**19**(7):3911–8.
134. Acharya S, Alegaonkar P, Datar S. Effect of formation of heterostructure of SrAl4Fe8O19/RGO/PVDF on the microwave absorption properties of the composite. *Chem Eng J* 2019;**374**:144–54.
135. Jamalian M, Ghasemi A, Paimozd E. Influence of multiwalled carbon nanotube addition on the magnetic and reflection-loss characteristics of Mn–Sn–Ti substituted strontium ferrite nanoparticles. *J Alloys Compd* 2014;**604**:373–8.
136. Lin Y, Liu X, Ye T, Yang H, Wang F, Liu C. Preparation and microwave absorption property of graphene-supported CoFe2O4/Y3Fe5O12 nanocomposite. *J Mater Sci Mater Electron* 2016;**27**(8):8177–82.
137. Hosseini SH, Mohseni SH, Asadnia A, Kerdari H. Synthesis and microwave absorbing properties of polyaniline/MnFe2O4 nanocomposite. *J Alloys Compd* 2011;**509**(14):4682–7.
138. Gandhi N, Singh K, Ohlan A, Singh DP, Dhawan SK. Thermal, dielectric and microwave absorption properties of polyaniline–CoFe2O4 nanocomposites. *Compos Sci Technol* 2011;**71**(15):1754–60.
139. Ma RT, Zhao HT, Zhang G. Preparation, characterization and microwave absorption properties of polyaniline/Co0.5Zn0.5Fe2O4 nanocomposite. *Mater Res Bull* 2010;**45**(9):1064–8.
140. lei Y, Yao Z, Lin H, Zhou J, Haidry AA, liu P. The effect of polymerization temperature and reaction time on microwave absorption properties of Co-doped ZnNi ferrite/polyaniline composites. *RSC Adv* 2018;**8**(51):29344–55.
141. Li L, Liu S, Lu L. Synthesis and significantly enhanced microwave absorption properties of cobalt ferrite hollow microspheres with protrusions/polythiophene composites. *J Alloys Compd* 2017;**722**:158–65.
142. Fang J, Chen Z, Wei W, Li Y, Liu T, Liu Z, Yue X, Jiang Z. A carbon fiber based three-phase heterostructure composite CF/Co 0.2 Fe 2.8 O 4/PANI as an efficient electromagnetic wave absorber in the K u band. *RSC Adv* 2015;**5**(62):50024–32.
143. Li Z, Ye M, Han A, Du H. Preparation, characterization and microwave absorption properties of NiFe2O4 and its composites with conductive polymer. *J Mater Sci Mater Electron* 2016;**27**(1):1031–43.
144. Saini M, Shukla R, Kumar A. Cd2+ substituted nickel ferrite doped polyaniline nanocomposites as effective shield against electromagnetic radiation in X-band frequency. *J Magn Magn Mater* 2019;**491**:165549.
145. Didehban K, Yarahmadi E, Nouri-Ahangarani F, Mirmohammadi SA, Bahri-Laleh N. Radar absorption properties of Ni0.5Zn0.5Fe2O4/PANI/epoxy nanocomposites. *J Chin Chem Soc* 2015;**62**(9):826–31.
146. Ali NN, Al-Qassar Bani Al-Marjeh R, Atassi Y, Salloum A, Malki A, Jafarian M. Design of lightweight broadband microwave absorbers in the X-band based on (polyaniline/MnNiZn ferrite) nanocomposites. *J Magn Magn Mater* 2018;**453**:53–61.
147. Li L, Xiang C, Liang X, Hao B. Zn0.6Cu0.4Cr0.5Fe1.46Sm0.04O4 ferrite and its nanocomposites with polyaniline and polypyrrole: preparation and electromagnetic properties. *Synth Met* 2010;**160**(1):28–34.
148. Elahi A, Shakoor A, Irfan M, Niaz NA, Mahmood K, Awan MS. Effect of loading ZnNiCrFe2O4 nanoparticles on structural and microwave absorption properties of polyaniline nanocomposites. *J Mater Sci Mater Electron* 2016;**27**(9):9489–95.
149. Zuo Y, Yao Z, Lin H, Zhou J, Liu P, Chen W, Shen C. Coralliform Li0.35Zn0.3Fe2.35O4/polyaniline nanocomposites: facile synthesis and enhanced microwave absorption properties. *J Alloys Compd* 2018;**746**:496–502.
150. Liu J, Zhang J, Li Y, Zhang M. Microwave absorbing properties of barium hexa- ferrite/polyaniline core-shell nano-composites with controlled shell thickness. *Mater Chem Phys* 2015;**163**:470–7.

151. Peymanfar R, Javidan A, Javanshir S. Preparation and investigation of structural, magnetic, and microwave absorption properties of aluminum-doped strontium ferrite/MWCNT/polyaniline nanocomposite at KU-band frequency. *J Appl Polym Sci* 2017;**134**(30):45135.
152. Luo J, Xu Y, Mao H. Magnetic and microwave absorption properties of rare earth ions (Sm3+, Er3+) doped strontium ferrite and its nanocomposites with polypyrrole. *J Magn Magn Mater* 2015;**381**:365–71.
153. He Z, Qi S, Zhong X, Ma H, Wang P, Qiu H. Preparation and microwave-absorbing properties of silver-coated strontium ferrite with polyaniline via in situ polymerization. *J Alloys Compd* 2015;**621**:194–200.
154. Bhingardive V, Woldu T, Biswas S, Kar GP, Thomas S, Kalarikkal N, Bose S. Microwave absorption in MWNTs-based soft composites containing nanocrystalline particles as magnetic core and intrinsically conducting polymer as a conductive layer. *ChemistrySelect* 2016;***1***(15):4747–52.
155. Shen J, Feng J, Li L, Tong G, He Y. Synthesis and excellent electromagnetic absorbing properties of copolymer (N-methylpyrrole-co-pyrrole) and Ba–Nd–Cr ferrite. *J Alloys Compd* 2015;**632**:490–9.
156. Cheng C, Fan R, Fan G, Liu H, Zhang J, Shen J, Ma Q, Wei R, Guo Z. Tunable negative permittivity and magnetic performance of yttrium iron garnet/polypyrrole metacomposites at the RF frequency. *J Mater Chem C* 2019;**7**(11):3160–7.
157. Lin Y, Liu X, Ye T, Yang H, Wang F, Liu C. Synthesis and characterization of CoFe2O4/Y3Fe5O12 composites based on polyaniline. *J Mater Sci Mater Electron* 2016;**27**(5):4833–8.
158. Yang H, Ye T, Lin Y, Liu M. Exchange coupling behavior and microwave absorbing property of the hard/soft (BaFe12O19/Y3Fe5O12) ferrites based on polyaniline. *Synth Met* 2015;**210**:245–50.
159. Pawar SP, Gandi M, Saraf C, Bose S. Polycarbonate composites containing carbon encapsulated "brick-like" Fe3O4 nanoparticles as efficient microwave absorbers with a large bandwidth. *ChemistrySelect* 2016;**1**(13):3829–38.
160. Bhattacharjee Y, Chatterjee D, Bose S. Core–multishell heterostructure with excellent heat dissipation for electromagnetic interference shielding. *ACS Appl Mater Interfaces* 2018;**10**(36):30762–73.
161. Feng C, Liu X, Or SW, Ho SL. Exchange coupling and microwave absorption in core/shell-structured hard/soft ferrite-based CoFe2O4/NiFe2O4 nanocapsules. *AIP Adv* 2017;**7**(5):056403.
162. Li Y, Zhou X, Wang J, Deng Q, Li M, Du S, Han Y-H, Lee J, Huang Q. Facile preparation of in situ coated Ti 3 C 2 T x/Ni 0.5 Zn 0.5 Fe 2 O 4 composites and their electromagnetic performance. *RSC Adv* 2017;**7**(40):24698–708.
163. Wang J, Zhu P, Wang J, Or SW, Ho S, Tan J. Interchange core/shell assembly of diluted magnetic semiconductor CeO2 and ferromagnetic ferrite Fe3O4 for microwave absorption. *AIP Adv* 2017;**7**(5):055811.
164. He L, Wang J, Zhao Y, Liu J, Zhong Z, Zhang C. (00h) BaM filled core-shell Co2Y@PANI ferrite-polymer composite for enhanced microwave absorption performances. *Mater Chem Phys* 2018;**219**:390–8.

This page intentionally left blank

CHAPTER

3

Rare earth doped $BiFeO_3$ multiferroic system: optical, dielectric, and magnetoelectric coupling properties and applications

Jincemon Cyriac[1,3,5], *Nandakumar Kalarikkal*[4], *Sunny Mathew*[5] *and Saji Augustine*[1,2]

[1]Department of Physics, St. Thomas College, Kottayam, Kerala, India; [2]Department of Physics, Deva Matha College, Kottayam, Kerala, India; [3]Department of Physics, Sree Narayana College, Chengannur, Alappuzha, Kerala, India; [4]International and Inter University Centre for Nanoscience and Nanotechnology, Mahatma Gandhi University, Kottayam, Kerala, India; [5]Department of Physics, Marian College Kuttikkanam (Autonomous), Peermade, Idukki, Kerala, India

1. Introduction

1.1 Multiferroic materials and magnetoelectric coupling

Multiferroic materials have numerous applications in the field of low power consuming devices such as spintronics, storage media, microwave devices, miniature antennas, etc.[1,2] It exhibits the combined nature of multiple (charge and spin) order parameters of ferroelectricity, ferromagnetism, and ferroelasticity.[3] The term "multiferroic" was first introduced in 1994 by H. Schmid, to describe crystals with multiple ferroic order parameters simultaneously.[4] The distinct ferroic behaviors are (1) ferroelectric—a spontaneous electric polarization by an applied electric field (2) ferromagnetic—a spontaneous magnetization by an applied magnetic field (3) ferroelastic—a spontaneous deformation by an applied stress. The relation between ferroelectric, ferromagnetic, and multiferroic is depicted in Fig. 3.1.

Applications of Multifunctional Nanomaterials
https://doi.org/10.1016/B978-0-12-820557-0.00001-1

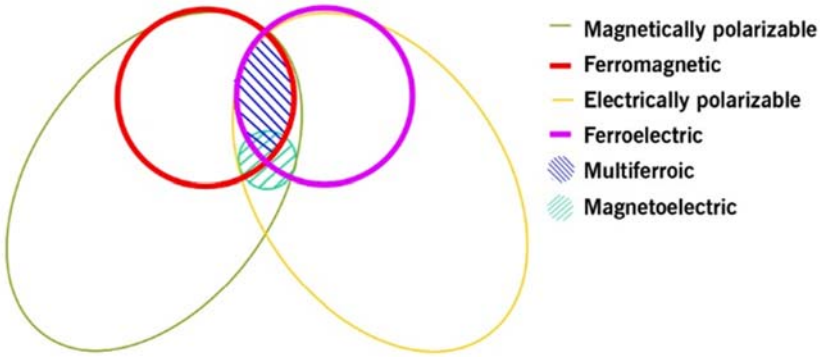

FIGURE 3.1 Schematic diagram: The relationship between magnetically polarizable, ferromagnetic, electrically polarizable, ferroelectric, multiferroic, and magnetoelectric materials.

The simultaneous combination of two different phenomena ferroelectricity and ferromagentism are called multiferroicity. This multiferroic effect was first introduced in antiferromagnetic Cr_2O_3 oxides by Dzyaloshinskii et al. in 1959.[5] Because of the difficulty in bringing ferroelectricity and magnetism together, there are very few materials that exhibit multiferroic characteristics. Thus, researches are underway to develop multiferroic materials with high coupling coefficient at moderate temperature for device applications. The multiferroic materials are designed using different methods includes doping of rare earth elements in the appropriate host matrix. The magnetoelectric coupling between electric and magnetic order parameters is explained by theoretical approach on the basis of Landau theory,

$$-F(E,H) = \frac{1}{2}\varepsilon_0\,\varepsilon_{ij}E_iE_j + \frac{1}{2}\mu_0\,\mu_{ij}H_iH_j + \alpha_{ij}E_iH_j + \frac{\beta_{ijk}}{2}E_iH_jH_k + \frac{\gamma_{ijk}}{2}H_iE_jE_k + \ldots \quad (3.1)$$

where $\boldsymbol{F}(\boldsymbol{E},\boldsymbol{H})$ represents the free energy in terms of the applied electric field ($\boldsymbol{E}$) and the magnetic field ($\boldsymbol{H}$), the magnetoelectric (ME) coupling coefficients are represented by α_{ij}, β_{ij} and γ_{ij}, respectively.

$$\alpha_{ij} = \partial P/\partial H \quad 3.2$$

where $\partial P/\partial H$ represents the linear magneto electric coupling coefficient, which have maximum value for $BiFeO_3$ (BFO) multiferroic system.[6,7]

1.2 $BiFeO_3$—multiferroic system

Bismuth ferrite-$BiFeO_3$ (abbreviation - BFO) is an inorganic eco-friendly, single phase, type-1 category multiferroic material, which possess both ferroelectric and magnetic properties at room temperature.[8] It possesses ferroelectric transition temperature at $T_c \sim 1103$ K and ferromagnetic transition temperature (G-type anti ferromagnetism) $T_N \sim 643$ K.[8–10] BFO possess rhombohedrally distorted perovskite (ABO_3) structure of $R3c$ phase group with lattice parameters $a = b = 5.5775$ Å, $c = 13.8616$ Å , $\alpha = \beta = 90$degree and $\gamma = 120$degree

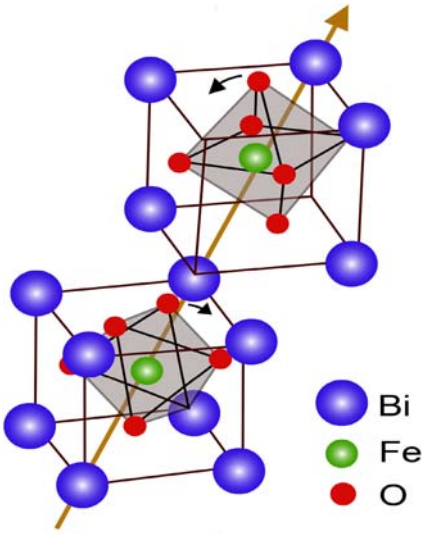

FIGURE 3.2 Crystal structure of $BiFeO_3$. The Bi, Fe, and O ions are represented with blue, green, and red colored circles, respectively. The two oxygen octahedra (*shaded in gray color*) rotate opposite directions around the [1 1 1] axis.

as given in Fig. 3.2. The simultaneous multiferroic property is explained by Dzyaloshinskii-Moriya (DM) interaction in the BFO crystal system.[11,12] The BFO has a weak ferromagnetic ordering and eight structural transitions. The spatially modulated spin structure exhibits its antiferromagnetic proeprties and inhibits the magnetoelectric effect. The ferroelectricity is due to the $6s^2$ lone pair electrons of the bismuth ions and G-type antiferromagnetic property is due to the cycloidal spin structure of the partially filled 3 d^5 orbitals of Fe^{3+} ions.[13]

To solve some of the problems in multiferroic materials such as high leakage current, formation of new multiphase during preparation, structural transitions, etc. and some efforts have been made to increase dielectric constant and to reduce the leakage current to improve the ferroelectric polarization in the BFO. This is possible through rare earth doping at the Bi or Fe site. But it is difficult to synthesis single phase $BiFeO_3$ multiferroic systems due to the high volatile nature of the Bi^{3+} ions. This high volatile nature creates the bismuth vacancies ($V_{Bi^{3+}}$) and that leads to the reduction of Fe^{3+} to Fe^{2+} and also to the formation of oxygen vacancies, it causes the dielectric properties in the $BiFeO_3$ multiferroic system. We can enhanced this dielectric, magneto electric coupling properties by doping rare earth ions such as Eu^{3+}, Dy^{3+}, and Pr^{3+} in Bi^{3+} site in very low concentration.

2. Experimental methods

In place of Bi^{3+}, rare-earth-doped (RE = Eu^{3+}) $Bi_{1-x}RE_xFeO_3$ nanocrystalline multiferroic perovskite samples were synthesized through a sol-gel method. It is a wet chemistry method that can produce highly homogeneous and pure samples. For the synthesis of europium

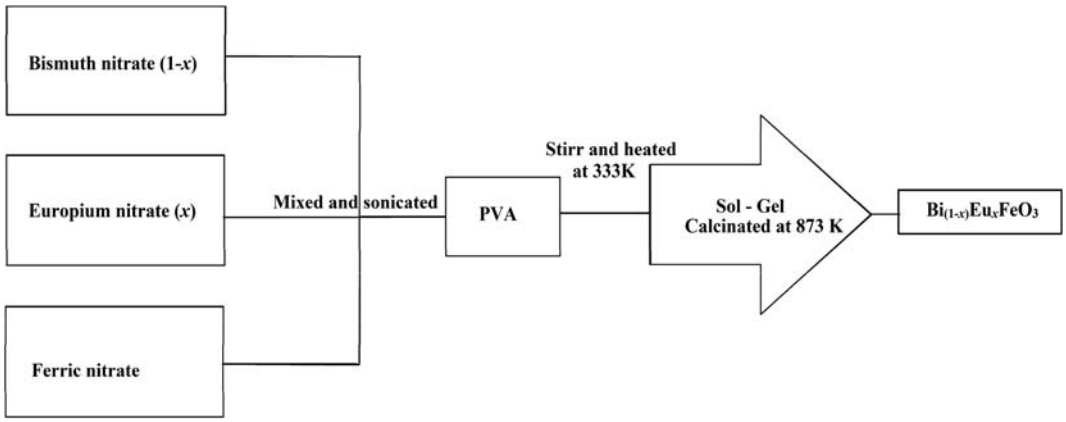

FIGURE 3.3 Flowchart of the synthesis of europium doped $Bi_{1-x}Eu_xFeO_3$ ($x = 0$, 0.01, and 0.02) samples.

doped $Bi_{1-x}Eu_xFeO_3$ ($x = 0$, 0.01, and 0.02) samples, 99.9% pure bismuth nitrate $Bi(NO_3)_3 \cdot 5H_2O$, ferric nitrate $Fe(NO_3)_2 \cdot 9H_2O$, europium nitrate $Eu(NO_3)_3 \cdot 5H_2O$ and poly vinyl alcohol (PVA) are used as the precursors. Stoichiometric amounts of $Bi(NO_3)_3 \cdot 5H_2O$ (molecular weight 485.07 g/mol) dissolved in 70%-concentrated HNO_3 and $Fe(NO_3)_2 \cdot 9H_2O$ (molecular weight 404.00 g/mol), and $Eu(NO_3)_3 \cdot 5H_2O$ (molecular weight 428.06 g/mol) were diluted in double distilled water, and all these solutions were sonicated separately for 20 min.

PVA (chelating agent) of weight equal to the weight of the metal ions was then added to the mixed solution and stirred for 12 h until it got completely dissolved. Thereafter the solution was evaporated at 333K for 6 to 7 days till it gradually turned into a viscous sol and then to dark brown gel. The final dried gel was heated to 873K for 2 h and $Bi_{1-x}Eu_xFeO_3$ powder samples were obtained.[14–16] The other rare-earth doped samples were prepared in the same way, replacing the rare-earth precursor and its stoichiometric calculations. The complete experimental procedure is illustrated in the flowchart shown in Fig. 3.3.

3. Result and discussion

3.1 X-ray diffraction

Fig. 3.4 represents the X-ray diffraction spectra of $Bi_{1-x}Eu_xFeO_3$ ($x = 0$, 0.01, and 0.02) samples. All the diffraction peaks (0 1 2), (1 0 4), (1 1 0), (2 0 2), (0 2 4), (1 1 6), (1 2 2), (3 0 0), (2 2 0), (0 3 6), (1 3 4) are indexed and well matched with the ICDD card no: 01-086-1518, with rhombohedral distorted structure with *R3C* space group. In the pure (BFO) sample the impurity peak (1 2 1) of $*Pbam\text{-}Bi_2Fe_4O_9$ phase is present, but the rare-earth ($\mathbf{Eu^{3+}}$) doping helped to the removal of this impurity phase.[15]

The crystallite size of the samples are calculated using Scherrer equation, $= \frac{0.9\,\lambda}{\beta \cos\theta}$, where $\lambda = 1.546$ Å ($CuK\alpha$ − X-ray source) and β is the full width at half maximum (FWHM measured in degree) of the maximum intense peak of the spectrum ($2\theta \sim 32$degrees).[17]

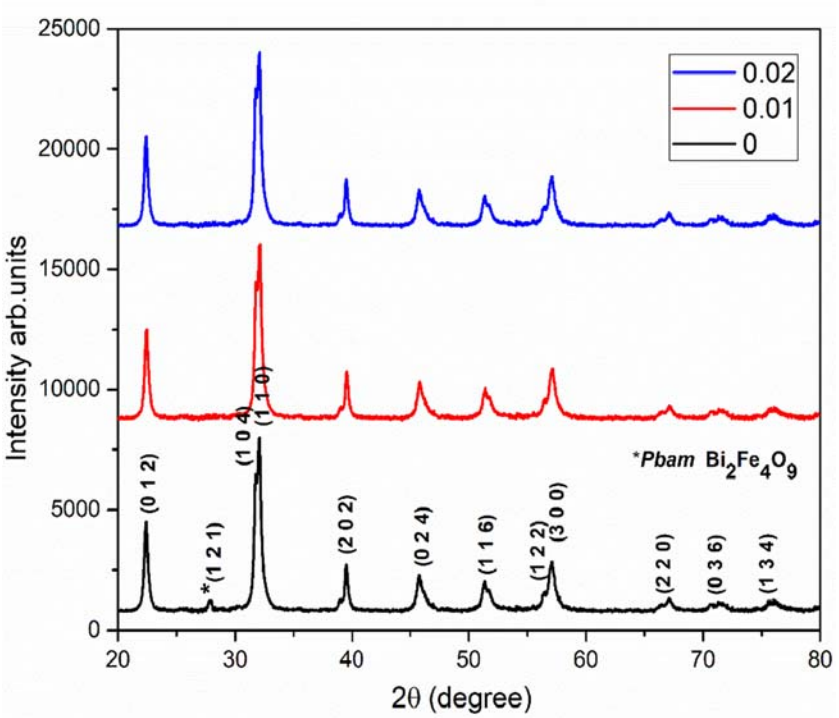

FIGURE 3.4 XRD patterns of the $Bi_{1-x}Eu_xFeO_3$ ($x = 0$, 0.01, and 0.02) samples.

The calculated crystallite size of the prepared samples is shown in Table 3.1. The crystallite size (~ 13 nm)decreases with the increase in the doping concentration of the europium ions. This is due to the lower ionic radius of the Eu^{3+} (ionic radius = 1.07 Å) ions instead of Bi^{3+} ions (ionic radius = 1.17 Å). The lattice parameters and the unit cell volume of the samples are calculated, which decreases as the doping concentration increases and are illustrated in Fig. 3.5.

Wonderful results have been observed on Eu^{3+} doping at Bi site. It eliminates the impurity phases present in the undoped BFO. The doping also causes the compression of Fe-O and Eu-O bonds and affects the lattice strain in the material.[18] To reduce this lattice strain, the two

TABLE 3.1 The calculated crystallite size using Scherrer equation.

Sample	2θ	FWHM β (degree)	Crystallite size (nm)
$BiFeO_3$	32.0771	0.6345	13.0295
$Bi_{0.09}Eu_{0.01}FeO_3$	32.1365	0.6373	12.9735
$Bi_{0.08}Eu_{0.02}FeO_3$	32.0847	0.6428	12.8615

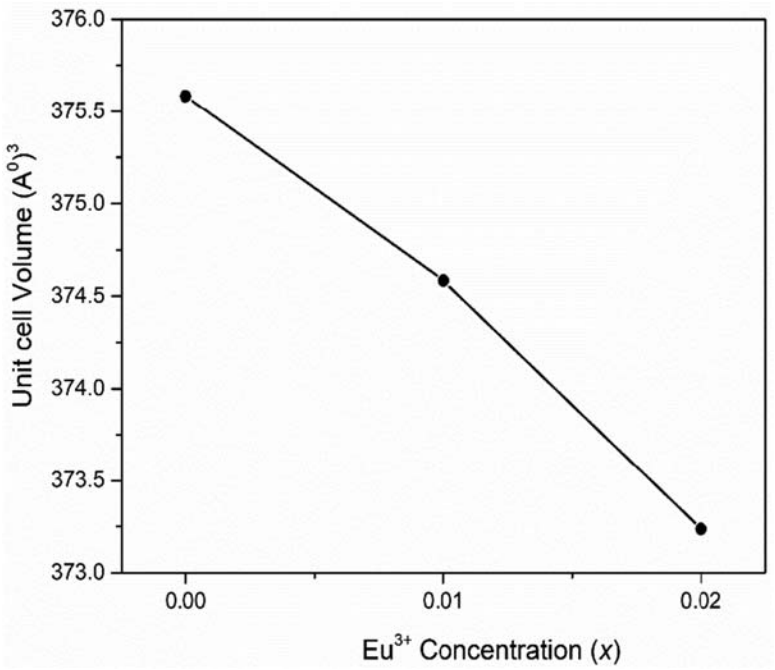

FIGURE 3.5 Unit cell volume of the $Bi_{1-x}Eu_xFeO_3$ ($x = 0$, 0.01, and 0.02) samples.

adjacent oxygen octahedra are rotated around the polarization axis [1 1 1]. This rotation induces a net polarization in the crystal lattice and it enhances the optical, dielectric, magneto electric coupling, and magnetic properties of the BFO system.[19,20]

3.2 Optical properties

The optical properties of the $Bi_{1-x}Eu_xFeO_3$ ($x = 0$, 0.01, and 0.02) samples were studied using UV-Vis diffused reflectance spectroscopy. The obtained reflectance spectra of the powder samples are depicted in the following Fig. 3.6.

The band gap energies of these samples are calculated using Kubelka-Munk function.$f(R)$[21]

$$f(R) = \frac{(1-R)^2}{2R} \tag{3.3}$$

where R if the percentage of reflection of the UV-Vis light from the samples. Using $f(R)$, the band gap energy is calculated from the $(f(R)h\nu)^2$ versus $h\nu$ *(eV)* plot and tangents meeting at $(f(R)h\nu)^2 = 0$ is the band gap energy of the prepared samples and is given in the following Fig. 3.7.[22]

The obtained band gap energy values of the samples are given in Table 3.2. As the concentration of the Eu^{3+} ions increase, the band gap energy of the samples decreases. This decrease

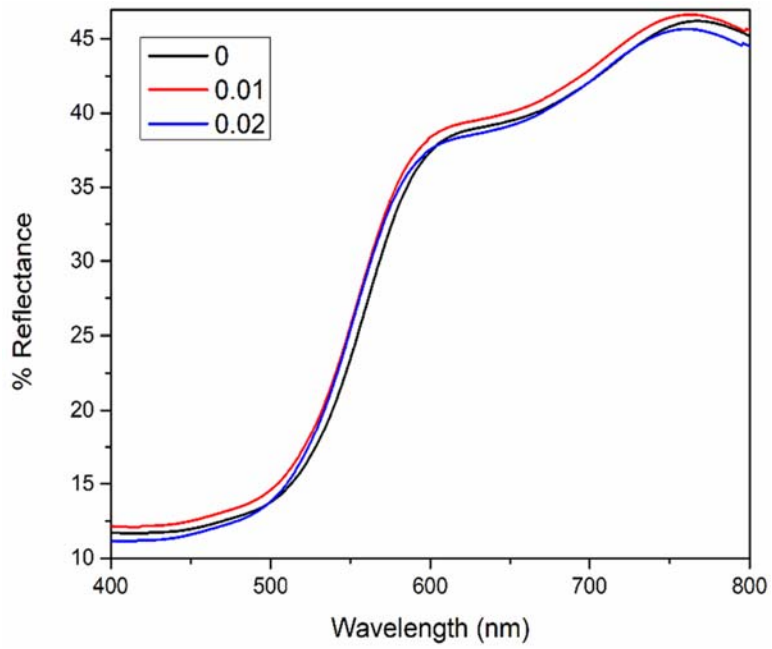

FIGURE 3.6 The UV-Vis diffused reflectance spectra of the $Bi_{1-x}Eu_xFeO_3$ ($x = 0$, 0.01, and 0.02).

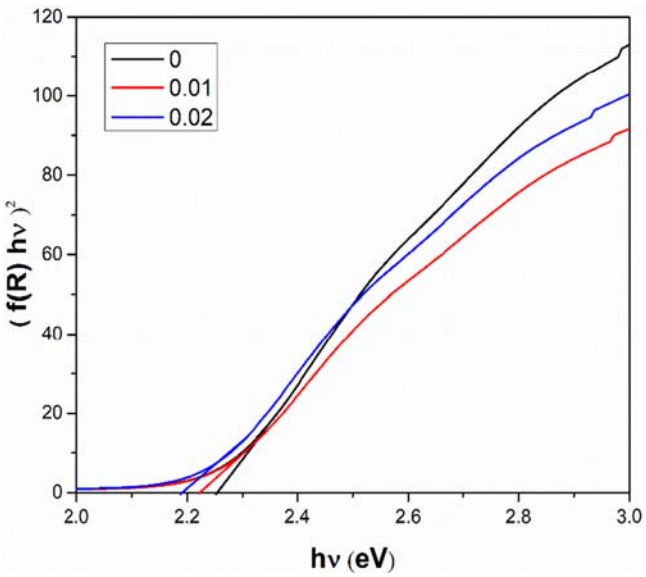

FIGURE 3.7 $(f(R)h\nu)^2$ versus $h\nu$ plot of the $Bi_{1-x}Eu_xFeO_3$ ($x = 0$, 0.01, and 0.02) samples.

TABLE 3.2 The band gap energy values of the samples calculated from Fig. 3.7.

Sample	Bandgap (eV)
$BiFeO_3$	2.255
$Bi_{0.09}Eu_{0.01}FeO_3$	2.224
$Bi_{0.08}Eu_{0.02}FeO_3$	2.191

in the band gap energy is due to the formation of the new energy levels between the valance band of the O *2p* states to the conduction band of the Fe *3d* state and these materials are very relevant in the field of photovoltaic applications due to the rare earth doping.[16]

3.3 Dielectric properties

The dielectric materials have wide range of applications in the field of charge storage devices like capacitors due to its electric polarization. The dielectric property of a material depends on its structure, density, porosity, and temperature. When an external electric field is applied to a dielectric material, ionic, electric, and bipolar polarization occurred in it due to the orientation of the charged particles. This orientation produces a torque (τ), which causes the bound charges to form and aligned within the materials. This polarization in the material due to the presence of the external *ac* electric field (E) produces an instantaneous dielectric constant and capacitance in the material.

The dielectric constant (ε^*) is a complex quantity and is expressed as[23]

$$\varepsilon^* = \varepsilon' - j\varepsilon'' \tag{3.4}$$

where ε' and ε'' are the real and imaginary part of dielectric constant, j is the current density.

The real part is represented as,

$$\varepsilon' = \frac{C_p d}{\varepsilon_0 A} \tag{3.5}$$

where C_p is the capacitance, A is the area of cross section, d is the thickness of the sample (in pellet form) of the sample, and ε_0 is the permittivity of free space.

$$\varepsilon_0 = 8.854 \times 10^{-12}\ \mathrm{F/m}$$

The imaginary part (dielectric leakage) is represented as,

$$\varepsilon'' = \varepsilon' \tan\delta \tag{3.6}$$

where $\tan\delta$ is the dissipation factor,[24]

$$\tan(\delta) = {}^{1}/_{2\pi f R_p C_p} \tag{3.7}$$

where R_p is the parallel resistance and C_p is the parallel capacitance of the pelleted samples measured.

This is due to the phase change of the dipole and the applied electric field. The frequency depended dielectric constant of the $Bi_{1-x}Eu_xFeO_3$ ($x = 0$, 0.01, and 0.02) samples in the ac frequencies (100 Hz − 2 MHz) are illustrated in Fig. 3.8.

The dielectric constant of all samples decreases sharply with the increase in the applied ac frequency, which can be explained in terms of the dielectric-relaxation phenomenon. At low frequencies, atomic, electronic orientation and the space charge polarization cause values of the dielectric constant. In $Bi_{1-x}Eu_xFeO_3$ samples, the space charges are due to the presence of bismuth (V_{Bi}^{-3}) and oxygen (V_O^{+2}) vacancies. Due to this space charges the Fe^{3+} ions may be converted to Fe^{2+} ions to maintain the charge balance as in the following equations.[25]

$$2Fe^{3+} + O^{2-} \rightarrow 2Fe^{2+} + V_o^{2+} + 1/2O_2 \tag{3.8}$$

$$2Bi^{3+} + 3O^{2-} \rightarrow 2(V_{Bi})^{3+} + 3(V_O)^{2+} + Bi_2O_3 \tag{3.9}$$

But at higher frequencies, this space charge polarizations disappear, so the value of the dielectric constant decreases. The values of the dielectric constant increased with the Eu^{3+} doping and the values of ε' at the frequency 1 KHz given in Table 3.3.

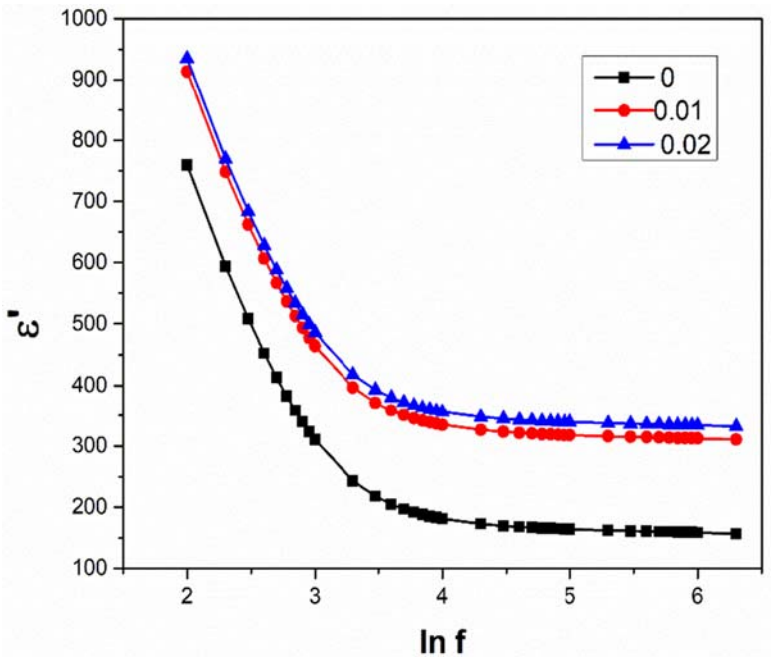

FIGURE 3.8 The variation of dielectric constant of the $Bi_{1-x}Eu_xFeO_3$ ($x = 0$, 0.01, and 0.02) samples in the ac (100 Hz−2 MHz) frequencies.

TABLE 3.3 The values of dielectric constant and leakage at 1 KHz of the $Bi_{1-x}Eu_xFeO_3$ samples.

Sample	ε'	ε''
$BiFeO_3$	310.4066	400.3394
$Bi_{0.09}Eu_{0.01}FeO_3$	464.2871	598.803
$Bi_{0.08}Eu_{0.02}FeO_3$	485.6705	626.3817

The dielectric leakage of the $Bi_{1-x}Eu_xFeO_3$ ($x = 0$, 0.01, and 0.02) samples are also decreases with an increase in applied ac frequency, and it is illustrated in Fig. 3.9. This decrease in ε'' with increase in frequency is explained by the Koop's phenomenological theory.[26] The value of the ε'' (1 MHz) increases with increase in concentration of the Eu^{3+} ions, given in Table 3.3. This is due to the increase in the migration of the ions by structural inhomogeneity and vacancy type defects in the samples.[16,26]

3.4 Magnetoelectric coupling properties

The electric polarization in a material in the presence of external magnetic field is referred as the magnetoelectric (ME) coupling property of the material.[27,28] The

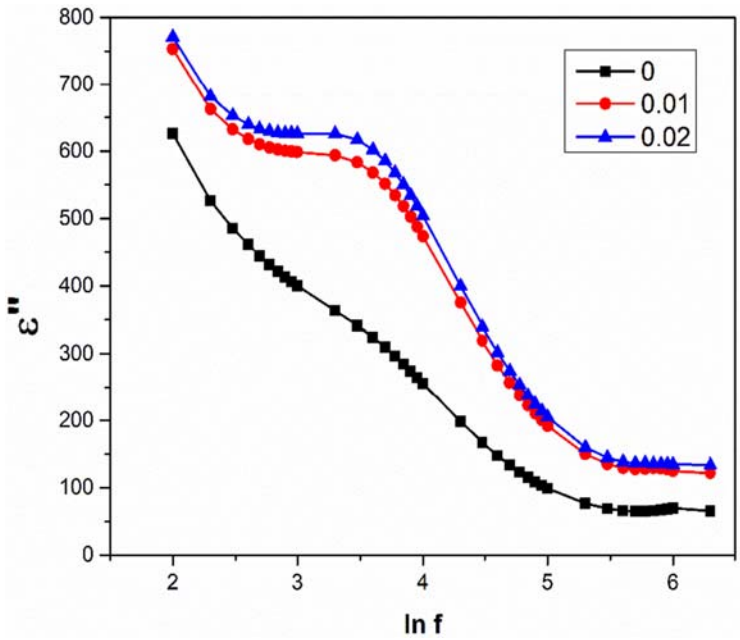

FIGURE 3.9 The variation of dielectric leakage ε'' of the $Bi_{1-x}Eu_xFeO_3$ ($x = 0$, 0.01, and 0.02) samples in the ac (100Hz − 2 MHz) frequencies.

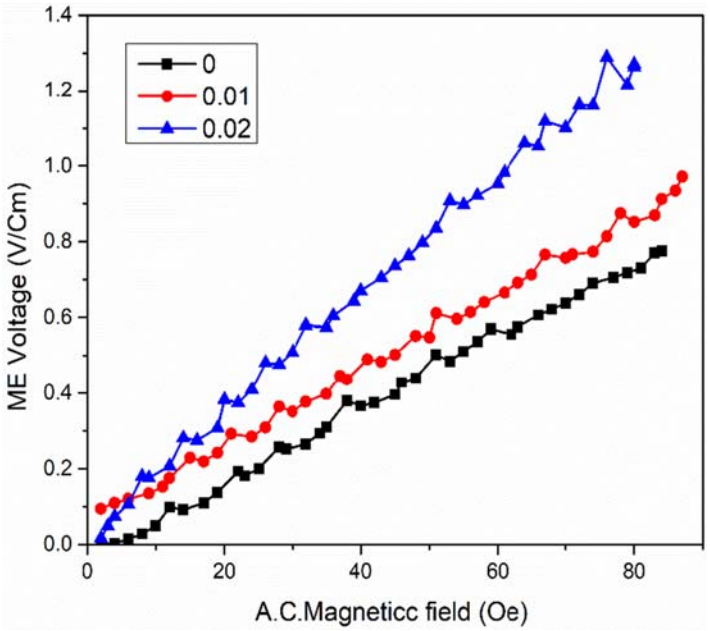

FIGURE 3.10 The magnetoelectric coupling voltage of $Bi_{1-x}Eu_xFeO_3$ ($x = 0$, 0.01, and 0.02) samples as a function of applied ac magnetic field frequencies.

multiferroic material possess ME coupling properties at room temperature. The synthesized nanoparticle samples are pelletized and make electric contact by pasting silver paste on the both sides of the pellet. It placed in the middle of the Helmholtz coil that excited by an external ac magnetic field (H_{ac} in Oested). Fig. 3.10 represents the magnetoelectric coupling voltage of $Bi_{1-x}Eu_xFeO_3$ ($x = 0$, 0.01, and 0.02) samples as a function of applied ac magnetic field (H_{ac}) at a fixed frequency of 750 Hz with a dc constant bias field (H_{dc}) of 3500 Oesterd.

The magnetoelectric coupling coefficient (α_E) can be calculated from the slope of the *ME* voltage versus H_{ac} curve, the valueα_E of the samples is given in Table 3.4.

The value of α_E increases with doping Eu^{3+} because the ferroelectric and magnetic interactions in the lattice increase with the presence of rare-earth ions.[16]

TABLE 3.4 The values of magnetoelectric coupling coefficient of the $Bi_1-_xEu_xFeO_3$ samples.

Sample	ME coupling coefficient (α_E)
$BiFeO_3$	0.009
$Bi_{0.09}Eu_{0.01}FeO_3$	0.010
$Bi_{0.08}Eu_{0.02}FeO_3$	0.016

4. Conclusion

Replacing the rare earth ion in place of the Bi^{3+} ions helps to improve the uniformity and purity of the samples. The impurity phase of Pbam-$Bi_2Fe_4O_9$ was eliminated by doping of Eu^{3+} ions. Crystalline size, lattice parameter, and unit cell volume were also reduced by this rare-earth doping. The optical property is increased as the band gap decreases due to the formation of additional energy levels between the valence and the conduction band. Therefore, these materials have extensive applications in semiconductor device manufacturing and nanophotonics. Eu^{3+} ions in the BFO system enhance the electrical and magnetoelectric coupling properties. Overall, these rare-earth doped BFO nanoparticles are important in the field of smart nanotechnology and in the field of spintronics.

References

1. X. Liang, H. Chen, N.X. Sun, Magnetoelectric materials and devices, APL Mater 9 (2021) 041114, https://doi.org/10.1063/5.0044532.
2. A. Hirohataa, K. Yamadab, Y. Nakatanic, I.-L. Prejbeanud, D. Bernard, P. Pirroe, B. Hillebrandse, Review on spintronics: principles and device applications, J Magn Magn Mater 509 (2020) 166711, https://doi.org/10.1016/j.jmmm.2020.166711.
3. X. Yang, Z. Zhou, T. Nan, Y. Gao, G.M. Yang, M. Liu, N.X. Sun, Recent advances in multiferroic oxide heterostructures and devices, J Mater Chem C 4 (2016) 234–243, https://doi.org/10.1039/C5TC03008K.
4. H. Schmid, Multi-ferroic magnetoelectrics, Ferroelectrics 162 (1) (1994), https://doi.org/10.1080/00150199408245120.
5. Dzyaloshinskii IE. *J. Exp. Theor. Phys. (USSR)* (1959), **37** , p. 881, Sov Phys JETP, 10 (1960), p. 628.
6. S. Narayan Tripathy, K.K. Mishra, S. Sen, B.G. Mishra, D.K. Pradhan, R. Palai, D.K. Pradhan, Phase transition and magneto-electric coupling of $BiFeO_3$–$YMnO_3$ multiferroic nanoceramics, J Appl Phys 114 (14) (2013) 144104, https://doi.org/10.1063/1.4824061.
7. M.A. Tamerd, B. Abraime, A. Kadiri, A. Lahmar, M. El Marssi, M. Hamedoun, A. Benyoussef, A. El Kenz, Prediction of magnetoelectric properties of defect $BiFeO_3$ thin films using Monte Carlo simulations, J Magn Magn Mater 539 (2021) 168402, https://doi.org/10.1016/j.jmmm.2021.168402.
8. AshalataPuhan, BhavyaBhushan, Arpan KumarNayak, DibyaranjanRout, Chapter 12- BiFeO3 – Based Materials and Their Properties, in: Fundamentals and Properties of Multifunctional Nanomaterials, Micro and Nano Technologies, 2021, pp. 275–293.
9. Y. Hong, J. Li, H. Bai, Z. Song, M. Wang, Z. Zhou, Effect of octahedron tilt on the structure and magnetic properties of bismuth ferrite, J Advan Ceram 9 (2020) 641–646, https://doi.org/10.1007/s40145-020-0398-1.
10. V.R. Palkar, D.C. Kundaliya, S.K. Malik, Effect of Mn substitution on magnetoelectric properties of bismuth ferrite system, J Appl Phys 93 (7) (2003) 4337–4339, https://doi.org/10.1063/1.1558992.
11. V.G. Prokhorov, G.G. Kaminsky, J.M. Kim, T.W. Eom, J.S. Park, Y.P. Lee, V.A. Khokhlov, Evidence of non-Dzyaloshinskii–Moriya ferromagnetism in epitaxial $BiFeO_3$ films, Low Temp Phys 37 (2) (2011) 129–133, https://doi.org/10.1063/1.3555838.
12. C.Y. Kuo, Z. Hu, J.C. Yang, S.C. Liao, Y.L. Huang, R.K. Vasudevan, M.B. Okatan, S. Jesse, S.V. Kalinin, L. Li, H.J. Liu, C.H. Lai, T.W. Pi, S. Agrestini, K. Chen, P. Ohresser, A. Tanaka, L.H. Tjeng, Y.H. Chu, Single-domain multiferroic $BiFeO_3$ films, Nat Commun 7 (2016) 12712, https://doi.org/10.1038/ncomms12712.
13. M. Pugaczowa-Michalska, J. Kaczkowski, Bonding analysis of $BiFeO_3$ substituted by Gd^{3+}, proceedings of the European conference physics of magnetism, Acta Phys Pol 2 (127) (2005), https://doi.org/10.12693/APhysPolA.127.362.
14. J. Cyriac, M.T. Rahul, N. Kalarikkal, P.M.G. Nambissan, Positron annihilation spectroscopic studies of multiferroic $Bi_{1-x}Pr_xFeO_3$ nanocrystalline compounds, J Phys Conf 618 (2015) 012012, https://doi.org/10.1088/1742-6596/618/1/012012.
15. J. Cyriac, S. Augustine, N. Kalarikkal, S. Mukherjee, M. Ahmed, P.M.G. Nambissan, Dysprosium-substitution-induced structural changes of multiferroic nanocrystalline bismuth ferrite and the investigation through positron

annihilation and other studies, Physica B: Phys Condens Matter Phys B 599 (2020) 412431, https://doi.org/10.1016/j.physb.2020.412431.
16. J. Cyriac, S. Mathew, S. Augustine, P.M.G. Nambissan, Defects characterization studies of europium-substituted bismuth ferrite nanocrystals by positron annihilation and other methods, J Phys D Appl Phys 51 (2018) 435303, https://doi.org/10.1088/1361-6463/aadfa7.
17. M.Y. Shami, M.S. Awan, Anis ur Rehman M, Phase pure synthesis of $BiFeO_3$, Nanopowders using diverse precursor coprecipitation method, J Alloys Compd 509 (2011) 10139–10144, https://doi.org/10.1016/j.jallcom.2011.08.063.
18. T. Durga Rao, R. Ranjith, S. Asthana, Enhanced magnetization and improved insulating character in Eu substituted $BiFeO_3$, J Appl Phys 115 (12) (2014) 124110, https://doi.org/10.1063/1.4869775.
19. P. Suresh, P.D. Babu, S. Srinath, Role of La, Gd codoping on the enhanced dielectric and magnetic properties of $BiFeO_3$ ceramics, Ceram Int 42 (2016) 4176–4184, https://doi.org/10.1016/j.ceramint.2015.11.091.
20. M. Muneeswaran, R. Dhanalakshmi, N.V. Giridharan, Effect of Tb substitution on structural, optical, electrical and magnetic properties of $BiFeO_3$, J Mater Sci Mater Electron 26 (6) (2015) 3827–3839, https://doi.org/10.1007/s10854-015-2909-3.
21. S. Hussain, S.K. Hasanain, Chemical pressure induced red shift in band gap and d-d transition energies in Sr doped $BiFeO_3$, J Alloys Compd 688 (2016) 1151–1156, https://doi.org/10.1016/j.jallcom.2016.07.158.
22. B. Ramachandran, A. Dixit, R. Naik, G. Lawes, M.S.R. Rao, Charge transfer and electronic transitions in polycrystalline $BiFeO_3$, Phys Rev B 82 (1) (2010), https://doi.org/10.1103/PhysRevB.82.012102.
23. P. Singh, V.K. Babbar, A. Razdan, S.L. Srivastava, V.K. Agrawal, T.C. Goel, Dielectric constant, magnetic permeability and microwave absorption studies of hot-pressed Ba-CoTi hexaferrite composites in X-band, J Mater Sci 41 (21) (2006) 7190–7196, https://doi.org/10.1007/s10853-006-0921-y.
24. P. Godara, A. Agarwal, N. Ahlawat, S. Sanghi, R. Dahiya, Crystal structure transformation, dielectric and magnetic properties of Ba and Co modified $BiFeO_3$ multiferroic, J Alloys Compd 594 (2014) 175–181, https://doi.org/10.1016/j.jallcom.2014.01.103.
25. N. Kumar, S. Kumar, B. Narayan, S.A.K. Bansal, Effect of Dy^{3+} substitution on structural, magnetic and dielectric properties of $BiFeO_3$-$PbTiO_3$ multiferroics, IEEE -NMDC, 2018, https://doi.org/10.1109/NMDC.2018.8605908.
26. M. Kumar, K.L. Yadav, Magnetoelectric characterization of $xNi_{0.75}Co_{0.25}Fe_2O_{4-(1-x)}BiFeO_3$ nanocomposites, J Phys Chem Solid 68 (9) (2007) 1791–1795, https://doi.org/10.1016/j.jpcs.2007.05.006.
27. A. Das, S. De, S. Bandyopadhyay, S. Chatterjee, D. Das, Magnetic, dielectric and magnetoelectric properties of $BiFeO_3$-$CoFe_2O_4$ nanocomposites, J Alloys Compd 697 (2017) 353–360, https://doi.org/10.1016/j.jallcom.2016.12.128.
28. M. Kumar, K.L. Yadav, Study of room temperature magnetoelectric coupling in Ti substituted bismuth ferrite system, J Appl Phys 100 (7) (2006) 074111, https://doi.org/10.1063/1.2349491.

This page intentionally left blank

CHAPTER

4

Carbon nanostructures for energy generation and storage

Arjun Ajith Mohan and N. Sandhyarani

Nanoscience Research Laboratory, School of Materials Science and Engineering, National Institute of Technology Calicut, Kozhikode, Kerala, India

1. Introduction

One of the most serious problems being faced by humanity today is the rise of carbon dioxide (CO_2) levels in the atmosphere. The level of CO_2 in the atmosphere in September 2022 is 415.95 ppm as per the information from the website *co2.earth*. Another surprising fact is that it is the highest level of CO_2 that has been observed in the past 800,000 years. Even if the CO_2 emissions stop today, this level would take another 1000 years or more to self-mitigate! Carbon dioxide is one of the major greenhouse gases causing global warming. Another impact of the increase in CO_2 is the acidification of ocean water. Ocean acidification is defined as the decrease in pH of the ocean as a result of CO_2 uptake (Fig. 4.1A). This could lead to the dissolution of shells of marine organisms thus impacting biodiversity adversely (Fig. 4.1B).[1] In this scenario, the CO_2 emissions due to anthropological activities need to decelerate. This can be done only by shifting the emphasis on fossil fuels to renewable energy generation and storage techniques. Some of these techniques have been prevalent since the early times. However, the gap between the power generation efficiencies and cost considerations of these renewable energy devices is the main factor for their limited availability in the commercial market. The advent of nanotechnology has opened many attractive avenues for better construction and efficiencies in addition to the reduced cost of these devices. This could pave way for a sustainable energy infrastructure.

The application of nanomaterials in energy generation and storage has been studied extensively. Graphene,[2] carbon nanotubes,[3] fullerenes,[4] and carbon onions,[5] are some commonly used carbon-based nanomaterials. These materials exhibit interesting properties like good electrical conductivity, high surface area to volume ratio, and high porosity. In addition to this, they also act as good supports for both organic and inorganic catalysts.[6]

Applications of Multifunctional Nanomaterials
https://doi.org/10.1016/B978-0-12-820557-0.00010-2

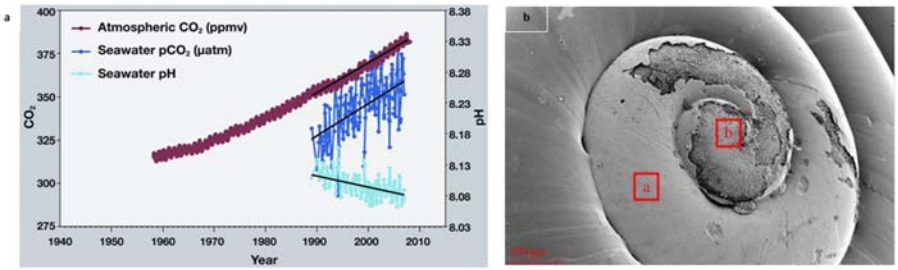

FIGURE 4.1 (A) Data acquired by PMEL carbon program, national oceanic and atmospheric administration (NOAA), United States government; (B) SEM image showing shell dissolution in a pteropod. *Adapted with permission from The Royal Society Publishing: Proceedings of the Royal Society B, Limacina helicina shell dissolution as an indicator of declining habitat suitability owing to ocean acidification in the California Current Ecosystem, Bednaršek N, Feely RA, Reum JCP, Peterson B, Menkel J, Alin SR, Hales B. Limacina Helicina shell dissolution as an indicator of declining habitat suitability owing to ocean acidification in the California current ecosystem.* Proceed Royal Soci B: Biol Sci *2014;**281**(1785):20140123. https://doi.org/10.1098/rspb.2014.0123. (Copyright, 2014).*

This chapter will discuss the basics and applications of nanomaterials with regard to some highly researched energy generation devices like methanol and enzyme fuel cells, photocatalytic, electrochemical, and photoelectrochemical hydrogen evolution reactions through water splitting and energy storage devices like supercapacitors.

2. Energy generation

Renewable energy generation techniques have been the object of extensive research as a green energy technology. Some of the major technologies are the production of hydrogen through water splitting, electrochemical energy conversion devices like fuel cells, solar energy harvesting, vibrational energy derivation using piezoelectric materials, wind energy harvesting using wind turbines, and energy from biomass. Among these techniques, this chapter focuses on energy from hydrogen produced through water splitting and electrochemical energy harvesting and storage devices.

2.1 Production of hydrogen through water splitting

Hydrogen is a highly flammable diatomic gas that possesses a high energy density (120−140 MJ/kg). Hydrogen can be produced from water and the combustion product of hydrogen is water. A combination of these factors makes hydrogen fuel of choice for powering the transport sector. The first successful demonstration of hydrogen evolution through water splitting was reported by Akira Fujishima and Kenichi Honda in 1972.[7] The Honda and Fujishima model involved light falling on a TiO_2 electrode whose band gap is in the range of the incident photons (Fig. 4.2). This led to electron-hole pair (exciton) formation. The electrons are shuttled through the outer circuit to the platinum black (PB) electrode and the holes formed oxidize water into H^+ ions and O_2 at the TiO_2 electrode. The H^+ ions formed move over to the PB electrode and undergo reduction to form hydrogen.

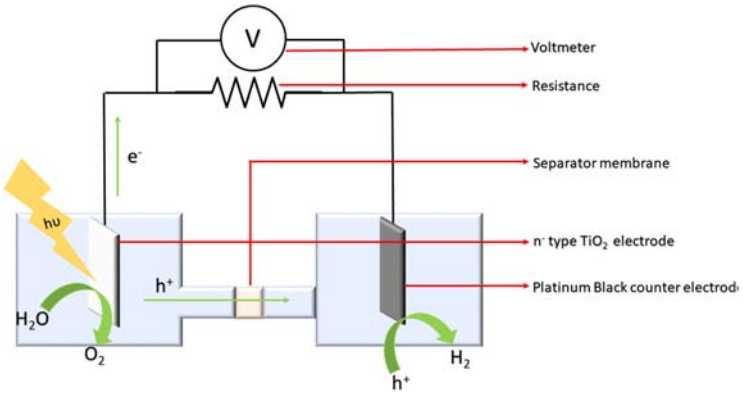

FIGURE 4.2 Schematic of the photoelectrochemical cell for water splitting used. *Redrawn by permission from Fujishima A, Honda K. Electrochemical photolysis of water at a semiconductor electrode.* Nature *1972;**238**(5358):37–38. https://doi.org/10.1038/238037a0 (Copyright, 1972).*

Some of the major challenges that are associated with hydrogen production through water splitting are the bandgap of the catalyst involved, the surface area of the electrodes, and the electron-hole recombination.

2.1.1 Types of water splitting reactions

Water splitting can be achieved through many routes such as photocatalytic, electrocatalytic, and photo electrocatalytic water splitting.

(1) Photocatalytic water splitting: In the photocatalytic method, water splitting occurs as a result of the formation of excitons by the absorption of incident photons. Here the bandgap of the material is very important. Depending on the energy of the incident photon, a careful selection of the material needs to be carried out. In the case of UV light-harvesting a band gap of above 3 eV is required. However, for visible light harvesting a band gap of <3 eV is sufficient.

An ideal photocatalyst is such that:

(a) It should have a bandgap that exceeds the free energy of water splitting i.e., 1.23 eV,
(b) The valence and conduction band edges for the photocatalyst should be lower than the water oxidation potential and higher than the hydrogen reduction potential, respectively,
(c) The photon absorption coefficients of the material should be high so as to generate a high yield of charge carriers, and
(d) Low recombination rate of the electron-hole pair.

The use of carbon-based nanomaterials like graphene, carbon nanotubes (CNTs), carbon quantum dots, and graphitic-carbon nitride (g-C_3N_4) can improve the performance of photocatalytic water splitting by decreasing charge recombination, enhancing visible light absorption, and enhancing the surface area of the catalyst.[8,9]

(2) Electrocatalytic water splitting: Electrocatalytic water splitting is a process where the splitting of water is done electrochemically. The electrocatalytic water splitting involves

the hydrogen evolution (HER) on the cathode and the oxygen evolution reaction (OER) on the anode. The energy required for water splitting is 237 kJ/mol under standard conditions. A potential of 1.23 V is required/electron that is transferred.

The reactions taking place in acidic and alkaline media are:

	Total reaction	
	$H_2 + O_2 \rightarrow H_2O$	(4.1)
In acidic medium,		
Cathode	$2H^+ + 2e^- \rightarrow H_2$	(4.2)
Anode	$H_2O \rightarrow 2H^+ + \frac{1}{2}O_2 + 2e^-$	(4.3)
In alkaline medium		
Cathode	$2H_2O + 2e^- \rightarrow H_2 + 2OH^-$	(4.4)
Anode	$2OH^- \rightarrow H_2O + \frac{1}{2}O_2 + 2e^-$	(4.5)

The HER process can be divided into three steps in both these media, Volmer reaction (hydrogen adsorption reaction), Heyrovsky reaction (electrochemical hydrogen desorption reaction), and Tafel reaction (chemical desorption reaction).

In the selection of the materials for electrocatalytic water splitting, Trasatti plotted a logarithm of exchange current densities vs metal hydrogen bond strength, which is known as the volcano plot. This plot enables one to compare the activities of various catalysts.[10,11] The use of conducting carbon-based nanomaterials materials like CNT, and graphene in conjunction with both platinum group metals (PGM) and transition metal catalysts can bring about a revolution in electrocatalytic water splitting.

(3) **Photoelectrocatalytic water splitting (PEC):** This process is a combination of photocatalytic and electrocatalytic water splitting. In photoelectrocatalytic water splitting, the material is coated onto a conducting electrode. Applying potential in presence of light leads to HER. The potential that needs to be applied here is shifted to lower values in the case of appropriately modified electrodes. Here the photogenerated holes migrate to the anode and oxidize H_2O. The reaction sites i.e., the two electrodes in this process are separated spatially, and hence products H_2 and O_2 can be collected separately. A major highlight of this method is that its performance is at par with the fossil fuel-based technologies provided the solar light is used as the light source and solar to hydrogen (STH) conversion efficiency reaches 10%. In terms of performance evaluation for a PEC system, the STH is a product of light absorption efficiency (η_{abs}), charge separation efficiency(η_{sep}), and the injection efficiency of the photogenerated charge carriers (η_{inj}). In summary, in order to achieve an efficient PEC water splitting there must be (i) a broad light absorption range for efficient light utilization, (ii) efficient transfer of charge from the bulk of the photoelectrode to the surface, (iii) rapid consumption of

the photogenerated carriers for the surface reaction with minimum overpotential, and (iv) Excellent durability for practical applications.

2.1.2 Carbon nanomaterials for water splitting reactions

The inclusions of carbon nanomaterials mainly MWCNT, reduced graphene oxide (rGO) and carbon nitride(C_3N_4) for water splitting reactions have been reported to enhance the efficiency of the process. These materials are known to improve the efficiency of HER and OER. The general advantages of carbonaceous materials are their good electrical conductivity, good mechanical properties, and light weight, which is hard to be matched by other catalysts. Among the carbon nanomaterials, the most commonly reported ones for water splitting include rGO, CNTs, and graphitic carbon nitride(g-C_3N_4). A concise account of their applications for water splitting is given in the succeeding sections.

2.1.2.1 Carbon nitrides

Carbon nitrides contain tris-triazine rings connected by planar amino groups. It consists of a network of sp^2 bonded C−N structures and behaves like a semiconductor. Carbon nitride exists in many analogous structures α forms, β forms, and graphite-like carbon nitride, which is also called graphitic carbon nitride (g-C_3N_4). The bandgap of g-C_3N_4 is 2.7 eV, which is energetically favorable for visible light water splitting reactions.[12,13] It has been proved using density functional theory (DFT) that even without the absence of any metal centers it is possible to split water using this catalyst. The carbon act as centers for proton reduction to H_2 gas and nitrogen acts as surfaces for oxidation of water to oxygen (O_2). Wang et al. reported H_2 production from water for the first time for g- C_3N_4 from cyanamide at a rate of 0.1−4 $\mu molh^{-1}$. This was increased further by the same group by adding a small amount of platinum (Pt), which facilitates electron transfer from the conduction band of g-C_3N_4 to Pt. This was reported to improve the H_2 production by about a factor of 7.[12] Concomitantly, Chen et al. synthesized a mesoporous g-C_3N_4 (similar to Vinu et al.[14]). They synthesized ordered mesoporous polymeric g- C_3N_4 (from cyanamide) and was investigated for hydrogen evolution from water splitting in the presence of visible light and Pt as the cocatalyst. The rate of evolution was 8.5 $\mu molh^{-1}$, which was greater than bulk g- C_3N_4.[15] Among a lot of preliminary work on carbon nitride (CN) done by Markus Antonietti et al., the synthesis of different morphologies of CN was also reported.[16] These morphologies were generated using diatom frustules which acts as nucleation sites. Depending on the ratio of the precursor (cyanamide) to the diatom different morphologies were obtained. The H_2 evolution reaction of the different morphologies that were obtained was highest for diatom to cyanamide ratio of 0.5 which is in the range of 14 $\mu molh^{-1}$.[17] The iodine doping has been shown to improve the photocatalytic activity.[18] On adding functionalities to g- C_3N_4, the absorption wavelength range of the material was found to vary.[19] Hong et al. observed that the use of sulfur-containing precursors like thiourea (TU) resulted in the presence of sulfur in the final product, which led to the modification of the electronic band gap. The synthesis was carried out in the presence of SiO_2 as the template, which led to the formation of mesoporosity. A synergy between the porosity and sulfur content led to a hydrogen evolution rate of 136 $\mu molh^{-1}$, which was one of the highest reported in the literature.[20] Doping of C_3N_4 with P, S, O, and N atoms is a versatile method to improve it's hydrogen evolution activity.[21−24]

Metal-doped carbon nitrides have also been reported like the cobalt phthalocyanine (Co-Pc) based g-C_3N_4, which has been inspired by chlorophyll and protohematin in which the structures are formed using metal (Mg and Fe) and N bonds. The same ideology has been used here where the Co -Pc and melamine on subjecting to high-temperature forms bonds between Co and nitrogen of the melamine, followed by polymerization to form Co-doped g-C_3N_4. The metal phthalocyanine can also form a π -π bond with the carbon nanostructures leading to improved hydrogen evolution activity (Fig. 4.3).[25] The HER activity of this material was found to be 28 $\mu molh^{-1}$ which is higher than pristine g-C_3N_4.

In addition to doping the formation of assemblies of various morphologies of low dimensional g-C_3N_4s is reported. Jun et al. have reported on the synthesis of nanoparticles, nanotubes, and nanosheets of g-C_3N_4s and used for HER.[26] The HER evolution rates of the developed materials are in the range of 200−300 $\mu molh^{-1}$. The composite of metal oxide semiconductors with g-C_3N_4 also have been reported with improved activity.[27]

There have been multiple studies based on the HER of g-C_3N_4 synthesized using a variety of techniques. In all of these it has been found that the alteration of the band structure of g-C_3N_4 in addition to an increase in surface area has contributed to optimum performance. In addition to the above-mentioned techniques, there have been innumerable reports on the improvement of HER using g-C_3N_4 like defect engineering where the structure of a purely crystalline material is disrupted by a chemical modification,[28] composites with plasmonic metals like Au and Ag,[29] composites of g-C_3N_4 with bimetallic crystals etc. There have also been reports of composites of g-C_3N_4 with CdS where the nanosheets of the C_3N_4 were decorated on the lateral surface of the CdS. The HER, in this case, was 83 $\mu molh^{-1}$. This was attributed to the synergy between the well-matched overlapping band structures, which facilitates charge separation.[30] A comprehensive report of the different strategies of application of C_3N_4 can be obtained from the review works by Guangfu Liao et al.[31] A summary of the existing literature reported for HER using g-C_3N_4 is presented in Fig. 4.3B.

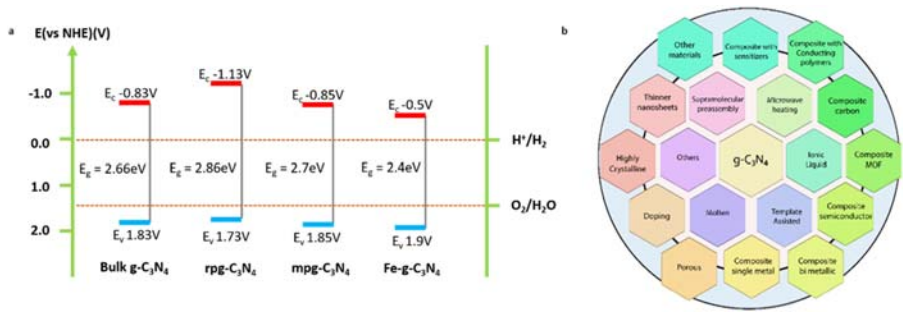

FIGURE 4.3 (A) Band structures of different carbon nitrides (rpg—regenerated g-C_3N_4 by protonation and deprotonation; mpg—mesoporous g-C_3N_4; Fe-g-C_3N_4—iron doped g-C_3N_4). (B) Schematic diagram of the synthetic methods of g-C_3N_4 (inner circle) and it's different nanostructures and composites applied for HER (outer circle).[31] *Redrawn by permission from John Wiley and sons; Zhang Y, Antonietti M. Photocurrent generation by polymeric carbon nitride Solids: an initial step towards a novel photovoltaic system.* Chem Asian J *2010;**5**(6):1307−1311. https://doi.org/10.1002/asia.200900685, (Copyright, 2010), Chen PW, Li K, Yu YX, Zhang WD. Cobalt-doped graphitic carbon nitride photocatalysts with high activity for hydrogen evolution.* App Surf Sci *2017;**392**:608−615.*

2.1.2.2 Carbon nanotubes, their modifications, composites as catalysts for water splitting reactions

One of the initial reports about the use of CNTs for water splitting was performed by Guo et al. who used a camera flash as the excitation point for the splitting of water between channels of single-walled carbon nanotubes (SWCNTs). This was attributed to the absorption of photons by the water molecules and the SWCNTs leading to the generation of O and H atoms. The basis for this was thermo splitting of water.[32] In order to enhance the visible light activity of TiO_2 and also to enable better separation of electron-hole pairs, a composite of multi-walled carbon nanotubes (MWCNTs) and TiO_2 have been prepared by Dai et al.[33] The visible light hydrogen evolution rates of 8092.5 μmol/g/h were reported. PEC cells are a conventional way of exploring water-splitting reactions.[7] Kim et al. fabricated a PEC cell that used CNT decorated with metals as cathode instead of the conventional metal-based electrodes. the p-type character of CNTs is explored here. Conventional *P* types of electrodes were found to be highly corrosive in water whereas, CNTs are found to be noncorrosive.

A crucial strategy to improve the efficiency of water splitting reaction (water oxidation) was reported by Toma et al. They modified MWCNT with polyamidoamine ammonium (PAMAM) dendrimer. Later an electrostatic immobilization strategy was used by using the positive charge on top of the dendrimers to trap anionic ruthenium-containing clusters. The improvement in the number of these clusters would improve the water oxidation capability. The oxygen production efficiency was found to enhance in the case of the MWCNT modified PAMAM dendrimers that contained the ruthenium clusters (Fig. 4.4).[34] Another report on the same ideology was reported by Fei Li et al. who used a single ruthenium

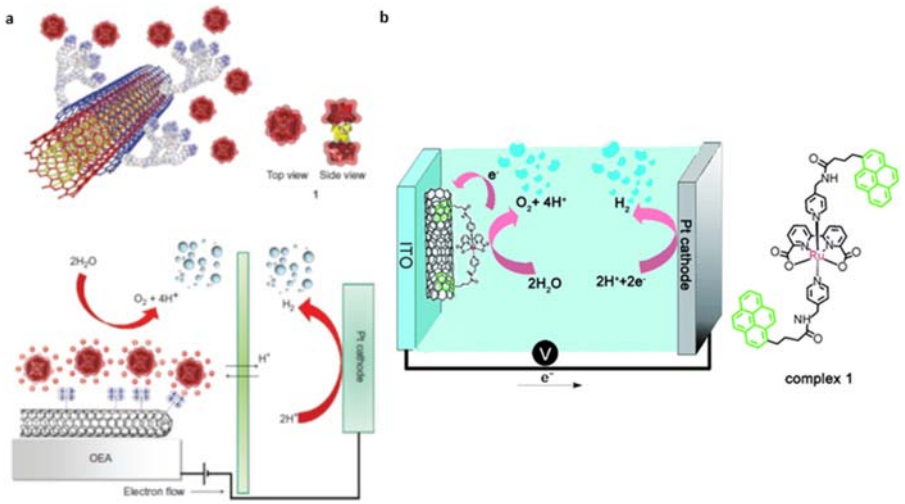

FIGURE 4.4 (A), (B) Schematic diagram of the mechanism of water oxidation using ruthenium cluster embedded in organic molecules which are used to modify MWCNT. *Reprinted with permission from Toma F, Sartorel A, Iurlo M et al. Efficient water oxidation at carbon nanotube–polyoxometalate electrocatalytic interfaces.* Nat Chem *2010;**2**(10):826–831. https://doi.org/10.1038/nchem.761 (Copyright, 2010); Reprinted by permission from John Wiley and Sons; Li F, Zhang B, Li X, Jiang Y, Chen L, Li Y, Sun L. Highly efficient oxidation of water by a molecular catalyst immobilized on carbon nanotubes.* Angew Chem Int Ed *2011;**50**(51):12276–12279 (Copyright, 2011).*

catalyst linked with CNT-modified ITO for water splitting. This catalyst was linked to MWCNT using pyrene linkages which further improved the conductivity of the material. The onset for water oxidation was found to be 1.15 V (0.3 V over potential). The highest catalytic current was observed at an overpotential of 0.28 V. At 1.4 V however, both O_2 and H_2 bubbles were seen at the working and counter electrode respectively (Fig. 4.4).[35]

A visible light active polymer catalyst was synthesized by the polymerization of the 1,3,5 triazine-2,4,6 trithiol as the precursor in the presence of iodine.[36] HER experiments were performed using this catalyst in combination with ruthenium and SWCNT as cocatalysts. The HER rate was found to improve on using CNTs and ruthenium which was attributed to the efficient charge separation achieved by using these materials as cocatalysts.

It can be seen from the report that semiconducting CNTs contributed more toward the photocatalytic activity than their metallic counterparts.[37] The polymerization of cyanamide to synthesize g-C_3N_4 in the presence of CNTs create a reinforcement that leads to better activity. The % of MWCNT impacts this HER rate which is found to be highest at 0.5% of MWCNT. Beyond this value, the MWCNT was found to be detrimental to HER.[38]

A composite of CNTs and graphene can form a conduction expressway that facilitates charge separation.[39] The presence of CNT acts as a spacer to induce the separation of graphene sheets. Furthermore, the presence of insulating edges in polycrystalline graphene can hinder the charge transfer process. The CNTs can act as subpercolation networks and induce efficient charge separation. The contact area between catalytic nanoparticles is also increased by using this 3D composite. As a result of using this composite, the efficiency of HER is increased up to 530% at 1.23V (325 mA/cm^2). An enhancement factor of 3–7 was reported for acid-treated materials in the case of HER. Single-walled CNTs showed enhanced properties before and after acid treatment.[40] Transition metal chalcogenides have always exhibited a higher photocatalytic activity.[41] A composite of MWCNT and MoS_3 is a good catalyst for water-splitting reactions. Lin et al. used this composite to optimize the loading of MoS_3 on MWCNT and were successful in producing HER with a smaller over potential of 0.13 V.[42] CNTs have also been used in quaternary composites of CdS, Pt, and TiO_2. The role of Pt and CNT is that of charge separators where the loading of these two should be optimized for optimum HER.[43]

In addition to this, another N-doped CNT based polyhedron was used to embed CoP nanoparticles.[44] The CoP embedded carbon is responsible for exhibiting HER processes. The CNTs, which are present on the surface of the catalyst play a positive role in terms of functionality. Works on transition metal carbides along with CNTs have also been reported recently. Ouyang et al. reported cobalt and β-Mo_2C embedded in N-doped carbon nanotubes for HER reactions. The overpotential to achieve 10 mA/cm^2 was 170 mV. The role of CNTs, in this case, was the protection of the nanoparticles from alkaline corrosion and also the provision of fast electron transport between the carbon matrix and nanoparticles.[46]

Very recently C_{60} was adsorbed on SWCNT for use as a metal-free and pH universal catalyst for HER. The role of CNT is that of an electron acceptor. This can be explained in terms of the bandgaps for SWCNT and C_{60}, which have bandgaps in the visible region. This enabled the catalyst to perform well for HER in visible light. The onset overpotential for this catalyst was reported to be 60mV. The catalyst was reported to be a trifunctional catalyst for HER, OER, and ORR.[47]

In summary, there are many effective strategies that have been employed to use CNTs as part of water splitting reactions. Some of the methodologies have been discussed above. In addition to this, there are more avenues that have been explored for the application of CNTs in water splitting. One of the major roles of using CNT in almost all reports is to act as an effective charge separation agent in case of photocatalytic water splitting. In the remaining two cases i.e., photoelectro catalytic and electrocatalytic water splitting it has been shown extensively that CNTs help in enhancing the transfer of electrons to the active sites in addition to acting as protecting agents from the high pH environments that are present in the electrolytes in case of acid and basic pH electrolytes. The recent trends in literature can be summarized as pointing toward N doping of CNTs which has shown immense potential for HER applications.

2.1.2.3 Graphene-based materials, their composites as catalysts for water splitting reactions

The addition of graphene sheets improves the electronic conductivity and surface area of the catalyst. Zhang et al. have synthesized a TiO_2—graphene sheets (GSs) based composite for HER. The effect of annealing temperatures and annealing atmospheres was also studied. The highest HER was reported for the 5wt% of GSs. N_2 atmosphere has been preferred for annealing because of the creation of O_2 vacancies which act as electron traps and cause efficient HER.[48] The addition of graphene in many cases is to acts as a separator of the electron-hole pairs that are generated during the irradiation process. A similar explanation for the role of graphene was reported by Cheng et al. who used a solvothermal method for the synthesis of rGO, TiO_2 nanocomposite.[49] The doping of nitrogen is reported to induce high HER activity in the materials.[50]

Graphene has always attracted attention in the water splitting area because of it's layered structure, low cost, structural tunability, and high conductivity. More importantly, doped-graphene has been gaining momentum because of its n-type characteristics which assist in the promotion of hole transfer for water oxidation. It also helps in the tailoring of the band gap of semiconducting photocatalysts and also in hindering the electron pair recombination rates. More importantly, graphene derivatives like reduced graphene oxide are negatively charged which makes it an ideal material for metal oxides to adsorb on.[51,52]

Recently other 2D materials like exfoliated black phosphorous (EBP) have been reported for making composites with nitrogen-doped graphene. This composite has shown to be a good catalyst for overall water splitting (a combination of both OER and HER). This composite has displayed an enhancement in its activities due to the lower fermi level of EBP relative to N-doped graphene. A directional interfacial electron transfer is induced, which improves the electron density over EBP and enhances the adsorption/desorption of H. The overpotential for HER reported for this material is 191 mV to afford a current density of 10 mA/cm^2.[53]

Transition metal sulfides like MoS_2—NiS_2 have been deposited over 3D graphene foam for overall water-splitting reactions. The 3D graphene presents a unique 3D interconnected structure leading to better water splitting. The catalyst loading can be increased because of the large surface area and also fast kinetics for mass and electron transfer is possible. An overpotential of 172 mV has been attained for achieving a current density of 10 mA/cm^2. The pathway followed here is the Volmer-Heyrovsky pathway for the HER process.[54] The N doping of CNTs had resulted in lowering energies for the adsorption of H* on an N doped CNT-rGO composite.[55]

It was reported that the oxygen dopants would improve the activity of OER and HER.[56] There have been many interesting works reported with doped graphene and transition metal phosphides. They have shown improved HER characteristics.[57–59] Taking advantage of the defect sites in carbon quantum dots and combining this with graphene has also shown to be good catalysts for HER with an overpotential of 194 mV.[60] Different morphologies of graphene have also been combined together, for instance, hydrogels of graphene have been combined with B-doped graphene quantum dots which exhibited an overpotential of 130 mV.[61] Heteroatom codoped graphene has been used for electrochemical water splitting. The N, S codoped graphene was activated by $ZnCl_2$ to enlarge the specific surface areas. The HER overpotential reported in this case was 0.29 V (vs. RHE).[62] Graphene has also been used in combination with CNTs and TiO_2 for water-splitting reactions. The role of graphene and MWCNT was to promote the generation of Ti^{3+} and also promote oxygen vacancy formation in turn reducing the bandgap of anatase TiO_2.[63] Recently there also have been ternary and quaternary junctions of other materials with graphene which have been utilized for the same process. A detailed account of various literature published in this area can be studied from various reviews published on this topic which elucidate various trends in this field (Fig. 4.5).[64,65]

In summary, the role of carbon-based nanomaterials for water splitting is a long-standing success story that could be attributed to the cost effectiveness, resistance to corrosive conditions, high conductivity, and easily tailorable morphologies that can be attained. From a comprehensive understanding of the literature, it can be concluded that the role of carbon nanostructures is increasing and is currently aligned toward hetero atom doping of different carbon nanostructures working synergistically with transition metal-based compounds for achieving efficient overall water splitting.

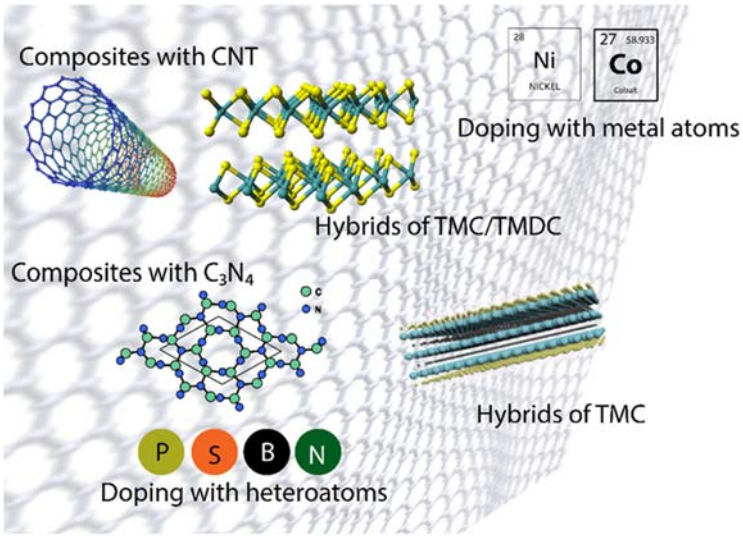

FIGURE 4.5 Schematic diagram of doping and hybrids of graphene applied for HER (outer circle).[64,65]

2.2 Fuel cells

The history of fuel cells is one avenue that has been continuously developing. The first fuel cell was developed by William Grove in 1839. This was followed by the development of a 5 kW system by Professor Francis Bacon in 1932. A 15 kW bacon cell was fitted to an Allis-Chalmers tractor. Later on, these fuel cells developed by General Electric were used to power manned space missions on the Apollo spacecraft. These fuel cells were proton exchange membrane fuel cells (PEMFCs).

Succeeding this many fuel cell technologies were devised, which were mainly aimed at alternative energy-powered drive trains for automotive. These include the PEMFCs devised by Ballard, soldier-borne fuel cell devices to power electronics, and many other industries, which came up due to the rise in optimism related to the fuel cell industry. Car makers like Daimler, Toyota, and General Motors were prime players in this process. This interest in fuel cell technology has resulted in a huge amount of funding in this area, particularly in the area of stationary and mobile fuel cell technologies.

A fuel cell is an electrochemical energy generator that uses the chemical energy present in fuel and converts it into electricity through an oxidizing agent like air or O_2. Depending on the kind of electrochemical reactions, the electrolytes that are used, and the operation temperatures there are different types of fuel cells. In order to cover the scope of this chapter, we will be classifying fuel cells depending on the power densities which can give us a clear idea regarding the applications they can be used for.

Since this chapter deals with both energy generation and storage devices a basic understanding of the position of various energy generation and storage devices in terms of energy density and power density is essential. A plot that makes this comparison (between energy density and power density) is known as the Ragone plot where the energy available per unit mass (energy density) is plotted against how quickly the energy can be delivered (power per unit mass, power density) (Fig. 4.6A). It can be observed that fuel cells possess a high energy density whereas supercapacitors possess a higher power density. This means that fuel cells are capable of delivering their performance over longer durations whereas supercapacitors have a very short discharge per unit time. Li-ion batteries bridge the space between supercapacitors and batteries. However, in comparison to fossil fuel-based internal combustion systems, these renewable energy systems are less efficient and research in these areas are aiming to fill this gap by developing more efficient nanomaterial-enhanced systems. To start with, we will be discussing more fuel cells in the upcoming sections.

2.2.1 Direct methanol fuel cells (DMFC)

Among the different types of fuel cells that exist (Fig. 4.6B) the direct methanol fuel cells (DMFCs) are suitable for portable applications ranging from a few millwatts (mW) to kilowatts (kW). The major reason for the selection of methanol as a fuel is due to its high energy density, operational safety, low cost, and ease of transportation. More importantly, the relative ease with which it can be stored compared to hydrogen is a decisive factor in the popularity of this fuel.

Fig. 4.6C shows a schematic diagram for the general setup of a methanol fuel cell. Methanol is fed into the anode compartment where it is oxidized to CO_2, H^{+}, and e^{-}. The H^{+} ions pass through the proton exchange membrane (PEM) and enter the cathode compartment

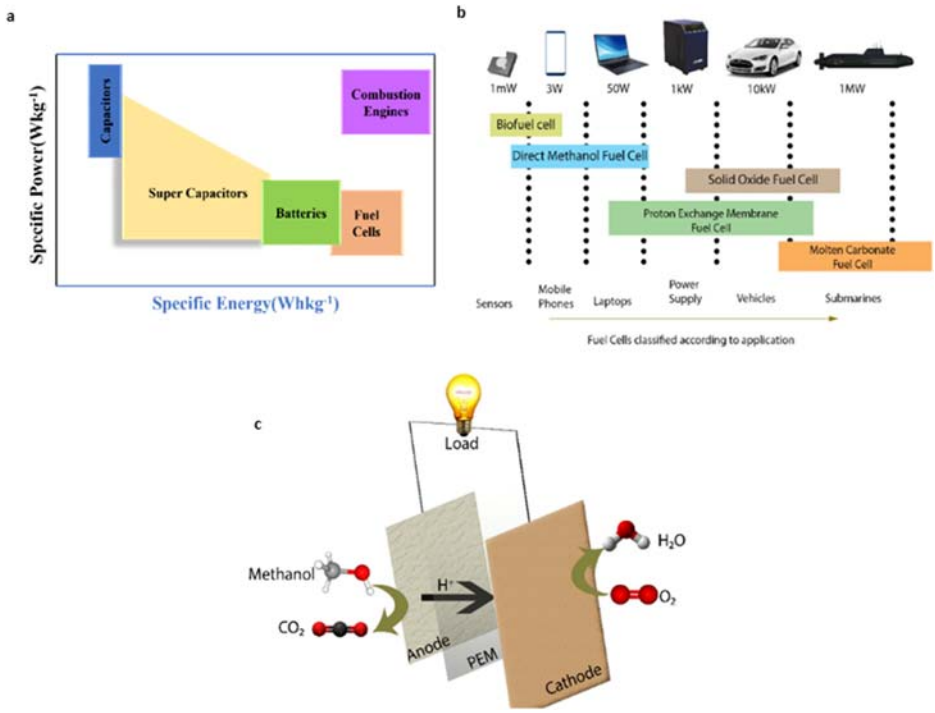

FIGURE 4.6 (A) Ragone plot showing the comparison between carious energy generation and storage devices (B) Schematic diagram of the classification of fuel cells according to their applications (B) (C) Schematic representation of a methanol fuel cell. *Redrawn with permission from Martin Winter, Ralph J Brodd. What are batteries, fuel cells, and supercapacitors?* Chem Rev *2004;**104**(10):4245–4270, (Copyright, 2004) American chemical society.*

where it combines with oxygen to form water. The reactions that take place in a methanol fuel cell in the acidic medium are given below:

$$CH_3OH + H_2O \rightarrow CO_2 + 6H^+ + 6e^- \quad E^o_{anode} = 0.046V \tag{4.6}$$

$$\frac{3}{2}O_2 + 6H^+ + 6e^- \rightarrow 3H_2O \quad E^o_{cathode} = 1.23V \tag{4.7}$$

The overall reaction is given by:

$$CH_3OH + 1\tfrac{1}{2}O_2 + H_2O \rightarrow CO_2 + 3H_2O \quad E_{cell} = 1.18V \tag{4.8}$$

The oxidation of methanol on the anode side takes place on the surface of catalysts. The common catalyst employed for methanol oxidation reaction (MOR) is platinum (Pt). The cost involved in using this material for MOR is high and hence research is currently progressing to find an alternative catalyst. The active surface of Pt is prone to poisoning due to the adsorption of carbon monoxide (an intermediate formed during methanol oxidation). This

process is commonly referred to as "poisoning". This happens at potentials below 450 mV where CO is bonded on the surface which impedes the further chemisorption of methanol on the catalyst surface. In order to avoid this process and also induce cost-effectiveness of the catalyst, research is directed toward reducing the loading of platinum and also finding out other alternatives to this catalyst. The role of carbon-based materials in this context is very important as primarily materials like CNT, graphene-based materials are being used as support materials for this for the alternative catalysts that are being studied. From the cathode point of view, a lot of carbon-based materials have been used as catalysts for oxygen reduction reaction (ORR). There are extensive reviews that have been written on using carbon-based materials for ORR reactions.[66] This section aims to briefly summarize the application of carbon materials on anode and cathode side of the DMFC.

2.2.2 *Carbon-based materials for methanol oxidation reactions (MOR)*

2.2.2.1 Carbon nanotubes (CNTs) and related structures for MOR

The primary carbon materials that are actively considered as a support for catalysts are CNTs. The combination of CNTs with different catalytic materials has been reported extensively.

CNTs were used as anchors for one-dimensional Pt nano thorns. The nano thorns were synthesized by an air-water interface process. A synergistic effect of the Pt and CNTs contributed to a high current density for MOR. An increase in electrochemical active surface area due to the presence of CNTs is seen from the higher activity of the Pt nano thorns assembled on CNTs.[67] In another work, TiN nanoparticles were anchored on CNTs, and deposition of platinum was done over this material. The current density of this material was 6.22 times higher than that obtained for Pt/C.[68] Palladium is another commonly reported catalyst for methanol oxidation. Yan et al. have used Pd−Pt nanoparticles deposited over polyaniline-coated CNTs. The MOR current reported for this catalyst was 62.3 mA/cm^2 at a low onset potential of 0.36 V(vs. SCE).[69] In all of these reports, the role of CNTs is that of efficient catalyst support by reducing the poisoning effect of CO intermediate on Pt nanoparticles. The high conductivity of carbon materials is also leading to better electronic communication between the electrode and the deposited catalyst.

Among the transition metal-based compounds, MoS_2 and M-Xenes have been capturing attention recently because of their layered structure. A combination of the quantum dots of these materials was combined with MWCNT for acting as a dual catalyst for both MOR and ORR. Yang et al. reported a current density of 160 A/g for this material which was higher than that of all constituent combinations. In this case, the activity was linked to the mass of MoS_2 where an excess of MoS_2 would lead to aggregation and when maintained at an optimum ratio this value would lead to an increase in the active site for catalysis.[70]

Another area that is witnessing a high influx of reports in the case of MWCNT is the doping of MWCNT with heteroatoms. This leads to modification of the electronic structure thus increasing the surface binding sites. It also leads to decreasing of the activation of energy of the reactions and also takes part in the destruction of poisoning intermediates. Doping with both S and N leads to the generation of a greater number of electrochemically active sites leading to more efficient catalysis. NiO nanoparticles loaded onto S, N dual

doped CNTs lead to a MOR current of 2200 mA/mg which was higher than the same nanoparticles loaded on pristine CNTs. The doping was reported to provide a greater number of sites for the anchoring of the NiO nanoparticles. In addition to this doping also acted as size restraint to limit the size growth of the nanoparticle thus exposing a greater number of catalytic surfaces. It also served to promote electron transportation from the electrode surface in addition to the oxidation of adsorbed intermediate species thus increasing the stability of the catalyst.[71] An S-doped CNT material was used to support Pt nanoparticles. S doping was carried out by poly (3,4-ethylenedioxythiophene) (PEDOT). The Pt nanoparticles of size 2 nm were uniformly distributed over the doped CNTs. The current density of this material was 322.44 mA/mg of Pt.[72] Zhou et al. reported a novel Ni doped TiN modified N doped CNTs as a support for Pt catalysts. There existed a strong electrical coupling between TiN and N CNTS network which enabled the fast electron transfer during MOR.[73]

2.2.2.2 Graphene and related structures for MOR

Graphene possesses a layered structure that can act as support for catalytic nanoparticles. Defect-free graphene synthesized by electrochemical exfoliation of a graphite rod in PSS solution was reported and Pt was deposited on this. It was also proven that the CO tolerance of graphene Pt is greater than bare Pt leading to improved performance of the material.[74] (100) plane of Pt was reported to possess lower poisoning and hence higher MOR capability. Utilizing this strategy we have coelectrodeposited Pt (100) on reduced graphene oxide (rGO). This report also showed the influence of the number of electrochemical cycles for deposition. When this material was deposited for one cycle a high mass activity of 2.54 A/mg at 0.67 V was obtained for MOR.[75] In addition to Pt nanostructures of Pd in combination with Pt were also grown on top of graphene. Xie et al. carried out the alternate deposition of Pt and Pd on graphene and used the resultant material for MOR. It was found that the material possessed tolerance to CO because of the presence of Pd. The current density for MOR was found to be 25 mA/cm^2.[76] Recently platelets of Pd were prepared by Yang et al. and used for MOR.[77] The use of MXenes ($Ti_3C_2T_x$) in combination with reduced graphene oxide was prepared in a bottom-up approach. Platinum nanoparticles were self-assembled on these structures using hydrothermal treatment. This material displayed a high MOR mass activity of 1200 mA/mg.[78] There have been numerous reports in addition to these representative examples where a combination of precious metals has been used for MOR.

Because of the high cost associated with the use of precious metal catalysts, there has been an increasing trend toward the use of transition metal catalysts for MOR. Qiu et al. reported a strategy for the decoration of allowing nanoparticles of Pt, M (= Fe, Co, Ni) on graphene support. SiO_2 nanospheres were used as sacrificial templates for the deposition of rGO. The removal of SiO_2 led to the formation of rGO nanospheres. Prior to this, the nanoparticles of Pt, M (= Fe, Co, and Ni) were deposited on this support. This led to the formation of rGO sphere with Pt, M (= Fe, Co, Ni) deposition. This material was then used for MOR and mass activity of 461.54 A/g of Pt was obtained for the Pt−Fe-based material because of the improved electrochemical active surface area in the case of Fe-based material.[79] It was also shown that the presence of metal-organic framework (MOF) enhances the surface area and charge transfer properties.[80] Another important class of material that could be considered for MOR among the transition metal-based catalysts is the transition metal dichalcogenides (TMDCs).

A nonnoble metal electrocatalyst (CoS_2/MoS_2) was embedded into rGO. A fuel cell was built using this catalyst as the anode material and Pt–Ru/C as the cathode catalyst. The power density of the fuel cell was reported to be 20 mW/cm^2 with an OCV of 0.35 V.[81]

As with the hetero atom doping of CNTs, there has been a large number of reports on the doping of graphene also. N, S doped graphene was used as the support material for Pd nanoparticles. A thermal treatment process is followed for the doping of the graphene. A current density of 14 mA/cm^2 is achieved for this material which could be attributed to the N, S doping.[82] Recently An et al. reported the synthesis of an S, P codoped graphene as a support for Pt nanoparticles (Fig. 4.7). A freeze-drying procedure was utilized for the development of a 3D porous structure that supported Pt nanoparticles. The porous structure helped in the enhancement of the catalytic activity due to the ability of the reactants to percolate inside the pores. A MOR current density of 2.82 mA/cm^2 with good tolerance to CO was observed due to the presence of hydroxyl groups on the surface of the 3D structure.[83] In a similar work, N-doped rGO was used as the support for anchoring PtPd alloy nanoparticles. Hydroxyproline was used as the N dopant, reductant, and swelling agent for rGO. The PtPd alloy nanoparticles were anchored using a hydrothermal technique. A very high MOR activity of 115.5 mA/mg was obtained using this material.[84]

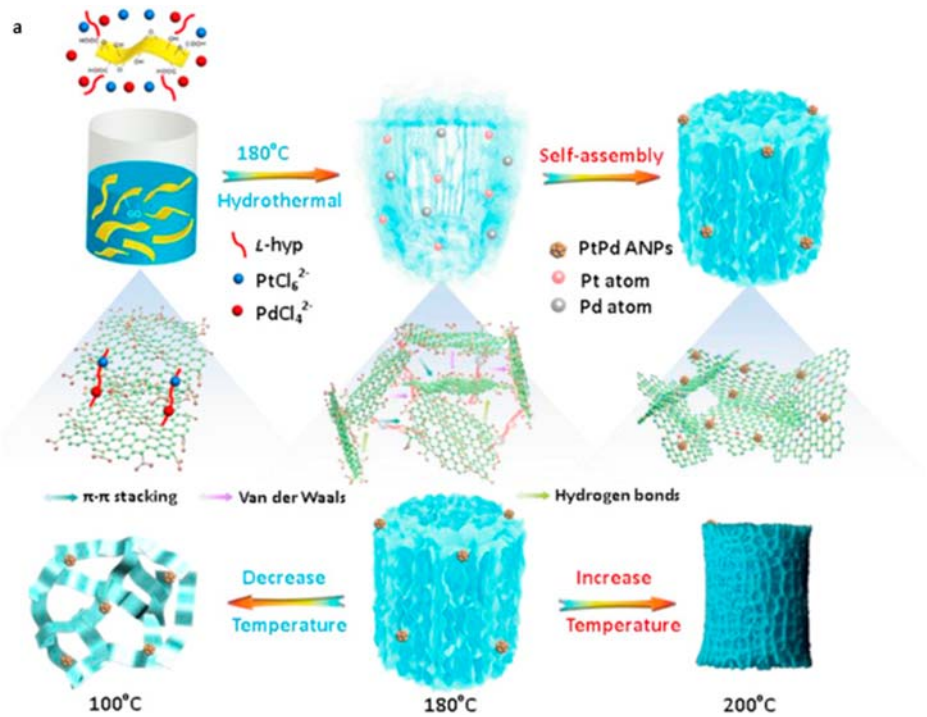

FIGURE 4.7 Representation of the mechanism for synthesis of the catalyst. *Reprinted with permission from Ya-Cheng Shia, Jiu-Ju Feng, Xiao-Xiao Lin, Lu Zhang, Junhua Yuan, Qian-Li Zhang, Ai-Jun Wang. One-step hydrothermal synthesis of three-dimensional nitrogen-doped reduced graphene oxide hydrogels anchored PtPd alloyed nanoparticles for ethylene glycol oxidation and hydrogen evolution reactions. Elsevier: Electrochimica Acta. (Copyright, 2019); Reported by An et al.*

2.2.2.3 Fullerenes and related structures for MOR

Fullerenes are another supporting material for anchoring catalytic nanoparticles for MOR. It was found that the oxidation current for C_{60}–Pt composite is nearly double than that of bare Pt.[85] Very recently a composite of Au nanoparticles and fullerenes was synthesized by Bhavani et al.[86] The fullerenes were electro-reduced in KOH solutions to make them more conductive followed by electrodeposition of gold nanoparticles. The material exhibited a high current density of 48 mA/cm^2. A graphene fullero pyrrolidone hybrid was synthesized by Zhang et al. who used this material as a support for Pd nanoparticles. This material when applied as a catalyst for MOR produced a mass activity of 483 mA/mg.[87] The applicability of this material toward MOR is limited by its solubility in solvents. Substitution of the cage surface of this material can be considered an effective strategy for it's uses as electrode material for MOR.

2.2.2.4 Carbon nitrides and related structures for MOR

Carbon nitrides have also had immense applications in the field of MOR. The presence of nitrogen-containing atoms in this material enhances the electron accepting ability which leads to the polarization of the adjacent carbon atoms. A covalently coupled hybrid of rGO and g-C_3N_4 was synthesized by Wenyao Zhang et al. The material exhibited a peak current density of 1770 mA/mg which was higher than other combinations of the constituents (Fig. 4.8).[88] Carbon nitride-based catalysts were also reported to possess an intermediate removal ability because of the presence of electron-accepting nitrogen atoms.[89,90]

This section summarized in a concise manner the application of various carbon nanostructures for MOR applications. It could be seen that the application of these structures was as support materials for the anchoring of catalysts. More importantly, another observation that could be made was that the application of carbonaceous nanostructures improved the poisoning

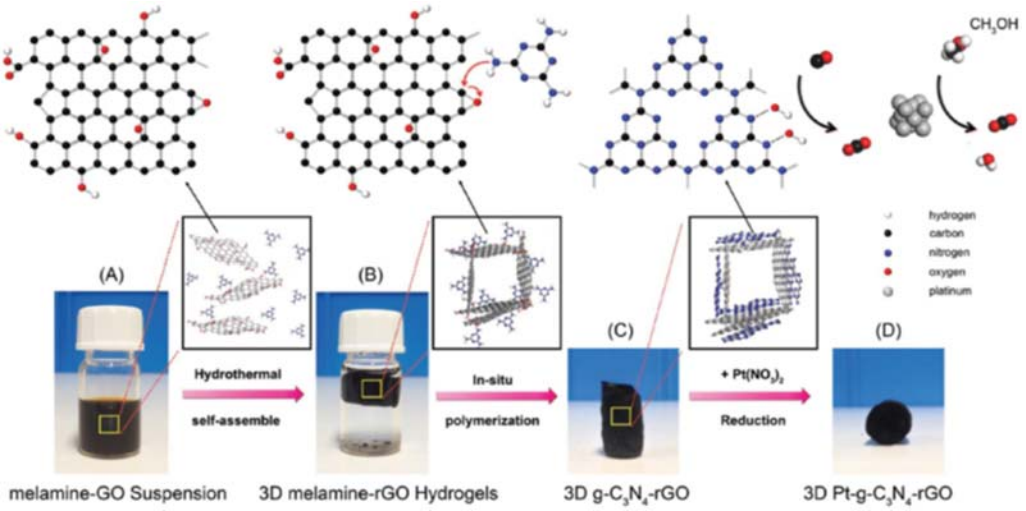

FIGURE 4.8 Representation of the mechanism for synthesis of the catalyst. *Reprinted with permission from John Wiley and Sons; Zhang W, Fu Y, Wang J, Wang X. 3D Hierarchically Porous Graphitic Carbon Nitride Modified Graphene-Pt Hybrid as Efficient Methanol Oxidation Catalysts.* Advanced Materials Interfaces *2017;4(12):1601219. https://doi.org/10.1002/admi.201601219, (Copyright, 2017).*

resistance of the catalyst because of the presence of functional groups. The next section will be dealing with the use of carbon nanostructures as ORR catalysts.

2.2.3 Carbon-based materials for oxygen reduction reactions (ORR)

The cathode side of a fuel cell receives the H^+ ions, which are produced in the anode compartment through the proton exchange membrane. Reduction of O_2 takes place according to Eq. (4.8) leading to the formation of water in the cathode compartment. Briefly, ORR in aqueous solutions takes place in two pathways: one is the four e^- pathway from O_2 to H_2O and the other is the 2 e^- pathway through the formation of hydrogen peroxide. In nonaqueous protic solvents, there is a possibility of the formation of superoxides also. The rate of ORR reaction is a very slow process hence catalysts are employed in order to speed it up.[91]

The oxygen reduction reactions can be represented by the equations given below:

In acidic aqueous electrolyte:

➢ $4e^-$ pathway

$$O_2 + 4H^+ + 4e^- \rightarrow 2H_2O \quad 1.229V(\text{vs SHE}) \tag{4.9}$$

➢ $2e^-$ pathway

$$O_2 + 2H^+ + 2e^- \rightarrow 2H_2O_2 \quad 0.70V(\text{vs SHE}) \tag{4.10}$$

$$2H_2O_2 + 2H^+ + 2e^- \rightarrow 2H_2O \quad 1.76V(\text{vs SHE}) \tag{4.11}$$

In alkaline aqueous electrolyte:

➢ $4e^-$ pathway

$$O_2 + H_2O + 4e^- \rightarrow 4OH \quad 0.401V(\text{vs SHE}) \tag{4.12}$$

➢ $2e^-$ pathway

$$O_2 + H_2O + 2e^- \rightarrow HO_2^- + OH^- \quad -0.065V(\text{vs SHE}) \tag{4.13}$$

$$HO_2^- + H_2O + 2e^- \rightarrow 3OH^- \quad 0.867V(\text{vs SHE}) \tag{4.14}$$

Carbon-based nanostructures have been used extensively as ORR catalysts or as catalyst support. A very brief account of this application using representative examples will be given in the following sections.

2.2.3.1 Carbon nanotubes (CNTs) and related structures for ORR

Literature abounds in the applications of CNTs for ORR. The advantages of using these nanostructures for ORR are that they are essentially metal free (or contain very small amounts of metal impurities); pristine carbon is inert to the adsorption/activation of O_2 and other intermediates. This activity can be improved by the adsorption of polyelectrolytes, chemical doping, and introduction structural defects. A polyelectrolyte functionalized CNT was reported for creating a net positive charge around the carbon atoms in the CNTs. This functionalization was found to have ORR capability both in the aligned and nonaligned form. The functionalized CNT exhibited an onset potential of −0.12 V (vs. SCE) in comparison to the −0.29 V (vs. SCE) displayed by the pristine CNTs. This was also accompanied by an increase in the ORR current density for the functionalized CNTs. A vertically aligned counterpart of the functionalized CNT displayed an even better positive shift in the ORR at −0.07 (vs. SCE) with higher current density.[92] Recent trends in ORR literature exhibit a trend toward the use of doped CNTs. A few examples of this application are mentioned in the upcoming paragraph.

Vertically aligned nitrogen-containing CNTs were synthesized by Gong et al. These vertically aligned CNTs were produced by the pyrolysis of iron phthalocyanine in the presence of NH_3 vapor. Removal of the Fe catalyst was carried out using electrochemical techniques. The ORR performed by this metal-free material takes the 4 e^- pathway with a much lower over potential. The material exhibited peaks at −1 V (vs. Ag/AgCl) and −0.65 V (vs. Ag/AgCl) before the removal of the iron catalyst and the peaks were featureless after the removal of the Fe. The material was shown to possess better ORR characteristics than Pt−C material because of the large surface area and also the better facilitating of the electrolyte diffusion.[93] In continuation to this work Yasuda et al. synthesized an iron nitrogen-doped CNT using the same molecule. However, the difference here was that the phthalocyanine (FePC) adsorbed CNTs were pyrolyzed (Fig. 4.9).

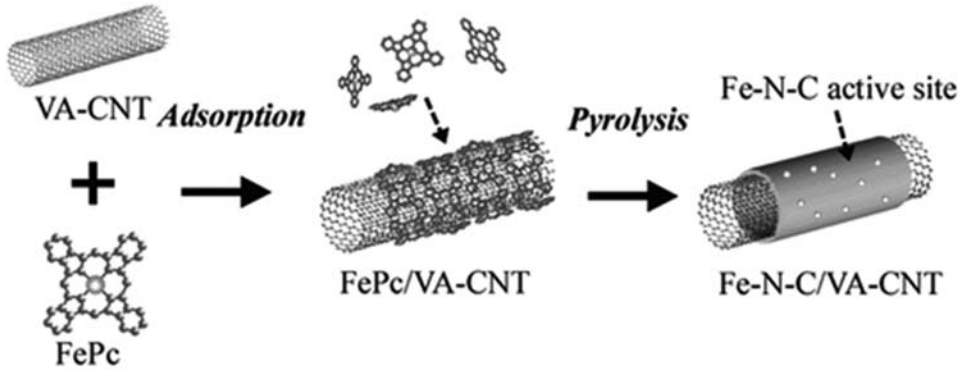

FIGURE 4.9 Representation of the mechanism for synthesis of the catalyst. *Reprinted with permission from John Wiley and Sons; Yasuda S, Furuya A, Uchibori Y, Kim J, Murakoshi K. Iron−nitrogen-doped vertically aligned carbon nanotube electrocatalyst for the oxygen reduction reaction.* Adv Funct Mater *2016,* **26***(5), 738−744. https://doi.org/10.1002/adfm.201503613. (Copyright, 2015).*

The CNTs and FePC were combined because of the strong affinity because of the π- π interaction between the CNTs and phthalocyanine groups. The ORR measurements were carried out in acidic media. The ORR peaks at 0.78 V were shown by this material. The electron transfer number showed a value of 2.98.[94]

In addition to the metal-free ORR capability of this material, there have also been reports using MWCNT in combination with transition metals. One such example is the work by Jianian Chen et al. A ZIF 67 based on cobalt was grown on Ti_3AlC_2-based MXene. Pyrolysis was carried out on this material which resulted in the formation of Co-tipped CNT growing across the MXene sheets. The ORR capability of this material was dependent on the amount of MXene. The limiting current density of this material was 5.55 mA/cm^2. The electron transfer number for this material was estimated to be 3.9 which points to the $4e^-$ based ORR pathway.[95]

These representative examples illustrate the significance of the use of CNTs as catalyst materials for ORR. The succeeding section will deal with the use of graphene and it's derivatives for ORR.

2.2.3.2 Graphene and related structures for ORR

It has been reported extensively that ultrapure graphene is not a good catalyst for ORR because of its zero bandgap properties. It also has been shown to possess the low electrocatalytic activity and was not suitable for ORR.[96] Mazánek and coworkers have proved that the activity of pristine graphene is due to the presence of metal impurities that are adsorbed on it' s surface from reaction mixtures. They developed a reactive thermal treatment, which led to the removal of metallic impurities and led to the loss of electrocatalytic activity.[97] This phenomenon has been reported extensively in various reports. Han et al. synthesized high-loading single atom Cu on graphene.[98] The Cu atoms are introduced into the matrix by a highly active gaseous Cu-containing intermediate. This material displayed ORR characteristics. The Cu loading in this case of 5.4wt%. The limiting current density, in this case, was 5.6 mA/cm^2.

Another important strategy for the application of graphene in ORR is heteroatom doping. Recently many reports have appeared on this topic. Wang et al. have reported the synthesis of a Fe—N impregnated carbon in a hybrid with in situ grown graphenes. The Fe—N based HPC graphene N doped. This material was used as an ORR catalyst. The ORR peak position of this material is more positive than Pt/C. The presence of Fe and N has resulted in the increase in efficiency of the catalytic process from a $2e^-$ pathway to a $4e^-$ pathway.[99]

In another work, a graphene nanomesh was prepared by the thermal exfoliation and shape-modified MOF.[100] This material was synthesized using a facile technique where Zn ZIL MOF was carbonized and then exfoliated in a nitrogen atmosphere at 900°C. A very thin sheet-like structure is obtained, which was used for ORR. An onset potential was applied at 0.860 V (vs. RHE) and a current density of 4.243 mA/cm^2 was obtained. The electron transfer number for this process was found to be 3.85 which is closer to 4 implying that a $4e^-$ reduction process is obtained.

Another example of the application of ORR in the case of graphene is the use of plasmonic nanoparticles for enhancement in ORR. A plasmon-induced hot electron enhancement method for ORR enhancement has been used by Fenglei Shi et al. An optical excitation in the form of a laser light source was used during the ORR studies. It was seen in this study

that upon laser excitation the ORR increased. The highest enhancement in catalytic activity was found for Ag nanotriangles which have stronger fields confined at the corners. The enhancement can be explained as the electrons from the Ag preferring to move into the lower energy band on the graphene resulting in enhancement.[101]

In a novel strategy, nitrogen-doped graphene oxide was used as the catalyst for ORR. In this work nitrogen-doped graphene oxide is used as the catalyst for ORR. The initial phase of the study focused on the exposing of GO nanosheets in water to different solvents. Depending on Hansen's solubility parameters various solvent-treated GO displayed various interplanar distances. These sheets were then treated with a high-temperature ammonia treatment (850°C) resulting in the formation of N-doped reduced graphene oxide. In terms of onset potentials, water treated with N rGO showed an onset potential of 1.03 V (vs. RHE) whereas that treated with noncyclic solvents like ethanol and ether exhibited an onset of 1.07 V (vs. RHE) and 1.10 V (vs. RHE) respectively. A comparatively lower onset was recorded in the case of pyridine, which showed an onset of 1.03 V (vs. RHE). Pyridine showed the highest electron transfer number of 4 and also the highest selectivity and performance in alkaline electrolytes. This could be attributed to the formation of microporous holes in the sheets leading to edge defects and also inducing a 3D structure in the sheets that promotes ORR.[102]

In conclusion, the application of graphene for ORR is a highly active area due to the scalability, and tailor ability that is possible in the case of graphene. The presence of functional groups in the structure and also the ease with which doping can be done is another advantage of using graphene for ORR. A detailed account of the advances in nonmetal doped graphene for ORR can be found in the review article by Shao et al.[96]

2.2.3.3 Other carbon-based nanostructures for ORR

In addition to CNT and graphene, there are also other morphologies that are used for ORR catalysis. One such area is the use of microporous and mesoporous carbon-based structures. An example of this is the micro and mesoporous carbons. Among these Fe−N doped carbons are a commonly used class of materials. Hanzeng Zou used Fe−N codoped carbon spheres synthesized by electrospinning and thermal treatment. This material was first electrospun and then heat treated at 220°C under air for 120 min/s. The ORR performance of this material was −0.018 V (vs. Ag/AgCl), which was close to Pt/C.[103] Atomically dispersed Fe atoms have been anchored on N-doped carbon nanospheres. The N doping was carried out using histidine. A templating strategy was adopted for this purpose. The ORR performance of the catalyst was studied in .1M KOH solution. The onset potential of this material was a measure to be 1.046 V(vs. RHE).[104]

g-C_3N_4 is another material that can be used as a catalyst for ORR. Fu et al. synthesized spheres of g-C3N4/carbon composite. The spherical morphology is obtained by the addition of glucose to a mixture of melamine and cyanuric acid. After calcination polymerization of glucose happens and a spherical structure of carbon core and C_3N_4 shell is formed. The material was used as a catalyst for ORR in 0.1 M KOH. The onset potential of the material was 0.9 V (vs. RHE) and it also exhibited a nearly 4 electron reduction process which is lower than other materials discussed in this section.[105]

A brief account of the carbon-based materials that have been used for ORR is presented. It is evident that carbon-based materials exhibit a high efficiency for oxygen reduction reaction and they possess huge potential for commercialization. The use of these nanomaterials can

bring down the cost and most importantly the absence of metals in many of these materials, they can exhibit a high methanol tolerance which cannot be seen in the case of metal-based ORR catalysts.

2.3 Enzyme fuel cells

A biofuel cell is a fuel cell that uses biological components (Microorganisms or Enzymes) to produce energy by the oxidation of the fuel supplied. This section deals with biofuel cells, which are more biologically safe, comparatively nonpolluting, and also cheaper to operate as the electrolyte is a biomolecule that is readily available in the environment.

Biofuel cells are classified into two groups: Microbial fuel cells (MFC) if the catalyst is a microbe and enzymatic fuel cell (EFC) if the enzyme carries out the feed (fuel) oxidation. The fuel that is supplied is oxidized and the resulting electrons are transferred to the anode. The electron transfer mechanism can happen through two routes. One route is the mediated electron transfer (MET) where the electrons are transferred to the anode through a mediator molecule. The second route is the direct electron transfer (DET) in which the electrons are directly transferred onto the anode.

In MET for enzymatic fuel cells, the electrons are transferred through some mediator molecule that is in contact with the redox site of the enzyme. In the case of DET, the enzyme needs to have strong adsorption with the electrode through a specific type of bonding and the redox center of the electrode needs to be in contact with the electrode to promote electron tunneling.

Biofuel cells can be used in miniature biological devices, which rely on the breakdown of a macromolecule for energy for example use of enzymatic fuel cells in heart implants is hypothesized to work on the breakdown of glucose molecules (Fig. 4.10).

Biological fuel cells have been known for a century starting from the first biofuel cell (BFC) that was demonstrated in 1912. The first enzyme-based fuel cell was only reported in 1964,

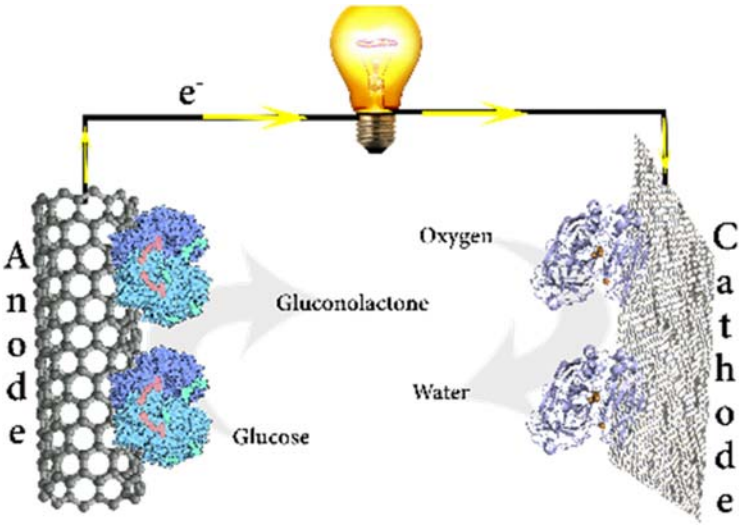

FIGURE 4.10 Schematic of a biofuel cell with glucose oxidase as the anode enzyme oxidizing glucose to gluconolactone and bilirubin oxidase as the cathodic enzyme which reduces oxygen to water.

which was a glucose oxidase (GOx) enzyme-based fuel cell that used glucose as the fuel.[106] The individual cell reactions happening in a general glucose-based fuel cell are given below.

$$\text{Glucose} \rightarrow \text{Gluconolactone} + 2H^+ + 2e^- \tag{4.15}$$

$$O_2 + 4H^+ + 4e^- \rightarrow 2H_2O \tag{4.16}$$

In microbial fuel cells, the enzyme of an enzymatic fuel cell is replaced by the bacteria. This bacterium is used to oxidize the feed that is given to the cell. There are two kinds of bacterial species that can be utilized for the realization of a microbial fuel cell (MFC). The mediated MFC is where the microbes are electrochemically inactive. The electron transfer from the cells to the electrode is facilitated by mediators such as thionine, methyl viologen, methyl blue, humic acid, or neutral red. The mediator-free MFC is where the use of a mediator is not required and they use electrochemically active bacteria to transfer electrons to the electrode. Among the electrochemically active bacteria are, Shewanella putrefaciens, Aeromonas hydrophila, and others. Some bacteria have extensions (pili) on their membrane, and are able to transfer their electrons via pili. Mediator-less microbial fuel cells derive energy directly from certain plants. This fuel cell is known as a plant microbial fuel cell. The power being thus derived can provide additional ecological advantages. These fuel cells use inorganic mediators to channel the electrons produced.

Although the route of feed/fuel oxidation is different the components of these cells are the same viz Anode, cathode, mediators, PEM, and bacteria/enzyme for fuel digestion. Taking into the huge volume of reports when considering the bacterial and enzyme fuel cell, this section will discuss the application of carbon nanomaterials with respect to enzyme fuel cells only. In addition to this, the contents of this section will proceed to examine examples of glucose oxidase (GOx) anode based; carbon nanomaterial-modified whole biofuel cells. The use of nanotechnology to modify these components has been reported to improve the efficiency i.e., the current densities produced by these cells for a definite volume of fuel supplied.

2.3.1 Structure of enzymes

In order to better understand the working of these fuel cells, a brief glance over the structure of GOx, horse radish peroxidase (HRP), and multicopper oxidase (MCO) enzymes like bilirubin oxidase (BOx) and laccase (LAc) are highly essential.

Glucose oxidase is crystallized from *Aspergillus Niger*. Each monomer in this enzyme has a deeply buried flavin adenine dinucleotide cofactor ($FAD/FADH_2$), which is the redox site of the enzyme (Fig. 4.11A). The location of this cofactor is ~15 Å from the surface of the enzyme. The total size of the enzyme is 60 Å × 52 Å × 77 Å with a hydrodynamic diameter of 89 Å and an isolelectric point of ~4.3. The optimum working pH for this enzyme is 5.5–7.4 at a temperature of 37°C.[107] GOx can also be used in mediated conditions where redox mediators like ferrocene,[108] osmium-based redox polymers,[109] quinone-based mediators,[110] can establish contact between the electrode and the enzyme redox center. The redox mediator gets regenerated as part of the redox reaction.

HRP is a heme-containing metalloenzyme which has two metal centers one of which is a heme group and the other comprises of calcium. A heme group is a planar group that is held in the middle of a porphyrin ring with four pyrrole molecules (Fig. 4.11). There are two

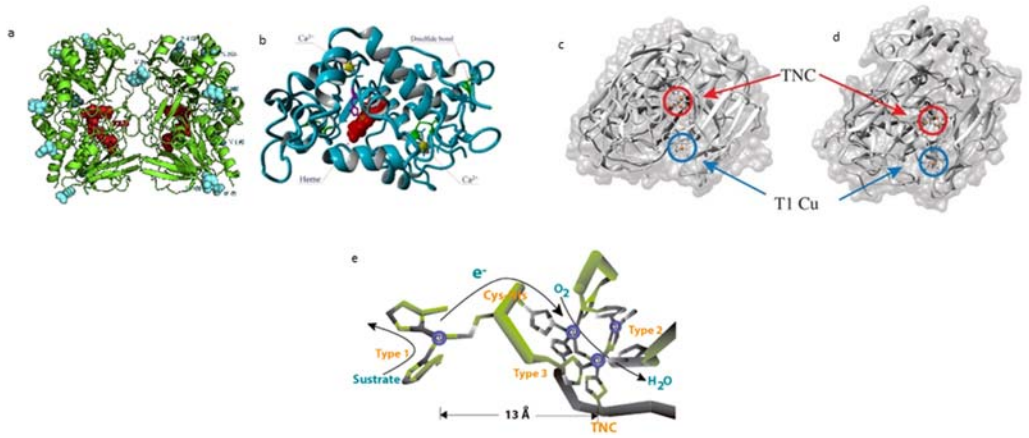

FIGURE 4.11 (A) Structure of GOx from *Aspergillus* Niger constructed using Pymol (B)Three-dimensional structure of HRP, Crystal structure of (C) Laccase (Lac) and (D) Bilirubin oxidase (BOx), (E) Schematic representation of electron flow in the active site from T1 to the trinuclear site.[115] *(A) Reprinted with permission from Elsevier: Bioelectrochemistry, engineering glucose oxidase for bio electrochemical applications, nicolas Mano. (Copyright, 2019); Haddad R, Mattei JG, Thery J, Auger A. Novel ferrocene-anchored ZnO nanoparticle/carbon nanotube Assembly for glucose oxidase wiring: application to a glucose/air fuel cell.* Nanoscale *2015;**7**(24):10641–10647. https://doi.org/10.1039/C5NR00497G; (B) Bo Zhu, Takuro Mizoguchi, Takaaki Kojima, Hideo nakano. Ultra-high-Throughput screening of an In Vitro-synthesized horseradish peroxidase displayed on Microbeads using cell sorter* PLOS ONE ***10**(5):e0127479 licensed under CC BY; (D) Adapted by permission from the Royal society publishing; Ross D, Milton and shelley D. Minteer. Direct enzymatic bioelectrocatalysis: Differentiating between myth and reality* Journal of the Royal society Interface. *(Copyright, 2017); (E) Tasca F, Farias D, Castro C, acuna-Rougier C, antiochia R. Bilirubin oxidase from Myrothecium verrucaria Physically absorbed on graphite electrodes. Insights into the alternative resting form and the sources of activity loss* PLOS ONE ***10**(7):e0132181 licensed under CC BY.*

binding sites for the iron molecule above and below the heme group. There is a histidine residue, which is located below the heme group. The second histidine group in the distal side of the heme group is vacant in the resting state and it is this site that is open for H_2O_2 during redox reactions. The Fe atom's sixth octahedral position is considered the active site of the enzyme.[111,112] Some reports have been published recently, which show that GOx and HRP can work in the cathode side of an enzymatic fuel cell also because of the reducing action of HRP which can reduce the peroxide formed by GOx in oxygenated conditions.[113]

MCO is one of the most commonly used reducing enzymes for cathodes of enzyme fuel cells. MCOs contain multiple types of Cu centers termed T1, T2, and T3 (binuclear) (Fig. 4.11C and D). The T1 site is located close to the surface and is responsible for single electron reductions and it is the T2 and T3 site which is a trinuclear cluster (TCN) where O_2 undergoes $4e^-$ reduction to H_2O_2 once this site is located favorably.[114,115] These enzymes have been known to exhibit DET when immobilized with the T1 site close to the electrode surface (Fig. 4.11). Bilirubin oxidase and laccase are the commonly reported enzymes for the oxygen reduction reaction.

Serge Cosnier et al. have perfected a pelleting technique of MWCNT by a soft grinding process. In this process, GOx, MWCNT, and catalase (an enzyme for disproportionation of H_2O_2) were soft ground and made into pellets (Fig. 4.12). The cathode of the enzyme in this case was HRP, which was made into electrodes using the same technique.

This enzyme fuel cell used both mediated and nonmediated reactions at the anode side. The mediator used was naphthoquinone. The role of the CNTs was to wire the enzymes properly and cause an efficient electron transfer. A flow-through enzyme fuel cell was fabricated and a power of 0.7 mW was obtained. The fuel cell gave an OCV of 0.6 V.[116] The same group also reported biofuel cells using the same 3D electrodes. Changes were made to the cathode enzyme where laccase was used as the cathode. A power density of 1.54 mW/cm^2 was obtained with an OCV of 0.76 V.[110]

The use of a 3D electrode of graphene-carbon nanotube composite has been reported by Prasad et al. (Fig. 4.12).[117] An acrylic glass-based construction has been used to construct the fuel cell. The graphene used in this work was grown using chemical vapor deposition (CVD) on nickel foam. The nickel form was eroded using HCl. SWCNT was loaded into this suspension by dipping the foam overnight in a carboxylate functionalized CNT solution. The immobilization of the anode enzyme was carried out by the EDC-NHS strategy which is covalent in nature. The inclusion of MWCNT into the anode has resulted in an improvement in the OCV of the electrode. The cathode electrode consisted of ABTS as mediator and laccase enzyme as cathode with graphene and MWCNT as the support. The developed device has shown a high-power density of 2.5 mW/cm^2 at a peak current density of 5 mA/cm^2.

The use of modified MWCNTs are also common. In an attempt to replace conventional mediators, which are not cyto-friendly, Saravanan et al. have reported the use of manganese phenanthroline chloride for the immobilization of glucose oxidase on functionalized multiwalled carbon nanotubes. This complex was anchored on functionalized MWCNT, which was coated on a glassy carbon electrode and used for the oxidation of glucose. More importantly, this mediator complex is independent of oxygen dependency of glucose oxidase which has been proved. The electrode with the glucose oxidase immobilized has also shown an appreciable increase in oxidation current. In conjunction with a platinum cathode a biofuel cell was constructed and an OCV of 250 mV was obtained with a power density of 7.3 $\mu W/cm^2$. The glucose selectivity of the cathode toward ORR has not been proved which may result in a cross-potential formation.[118]

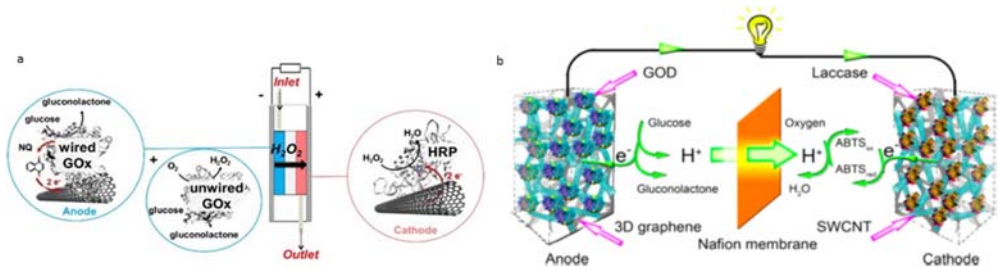

FIGURE 4.12 (A) Schematic representation of the fuel cell (B) schematic representation of the fuel cell. *(A) Abreu et al.; Reprinted by permission from Elsevier; Abreu C, Nedellec Y, Ondel O, Buret F, Cosnier S, Le Goff A, Holzinger M, Glucose oxidase bioanodes for glucose conversion and H_2O_2 production for horseradish peroxidase biocathodes in a flow through glucose biofuel cell design.* J Power Sources,*2018;**392**:176–180. https://doi.org/10.1016/j.jpowsour.2018.04.104 (Copyright, 2018); (B) Reprinted with permission from Kenath Priyanka Prasad, Yun Chen Peng Chen. Three-dimensional graphene-carbon nanotube hybrid for high-performance enzymatic biofuel cells,* ACS Appl Mater Interfaces *2014;**6**:5, (Copyright, 2014) American Chemical Society. ACS.*

In addition to a combination of CNT and rGO reports on the use of magnetic nanoparticles for the immobilization of glucose oxidase have also been reported. A composite of GO and Fe_3O_4 was synthesized by a solvothermal method.[119] The NH_2 functionalized Fe_3O_4 nanoparticles obtained by the solvothermal method were anchored on GO using EDC/NHS chemistry. The obtained composite was separated from the solution magnetically and washed several times. The glassy carbon electrode used in this case is a magnetic glassy carbon electrode. The ORR capability of the BOD was characterized and was found to be close to the redox potential of T1 copper site of the BOD. The assembled fuel cell produced an OCV of 0.6 V with a peak power density of 74 $\mu W/cm^2$ at a current density of 180 $\mu A/cm^2$. The use of a composite of rGO and Fe_3O_4 has reportedly increased the surface area, and electron transfer resistance and also prevented leakage of enzymes because of the paramagnetic properties of the nanoparticle. Our group is also involved in the development of compact enzyme fuel cells. Arjun et al. have recently fabricated a sandwich-type enzyme fuel cell (Fig. 4.13A). This fuel cell was fabricated by immobilization of GOx on a pyrene carboxylic acid—MWCNT composite. The cathode of the fuel cell was made of rGO-Ceria nanocomposite which is glucose tolerant. A hydrogel based on agar-PVA was used to store and supply glucose in addition to acting as a separator membrane. The fuel cell was able to produce a power density of 6.25 $\mu W/cm^2$ and an OCV of 140 mV.[120]

The combination of carbon-based materials with gold nanoparticles can improve resistances in enzyme-modified electrodes. Toward this end, Pengfei et al. have used bacterial cellulose to construct a 3D electrode that acts as the base electrode to immobilize MWCNT.[121] This MWCNT is then covered with PEI using a facile technique. This was followed by the reduction of gold leading to the formation of a dense gold surface which the authors claim to act as plugs to induce DET. The reports are based on the electrostatic immobilization of glucose oxidase and laccase. A 2- compartment device was assembled where the anode compartment could act as a glucose sensor. The fuel cell developed a power of 325 $\mu W/$

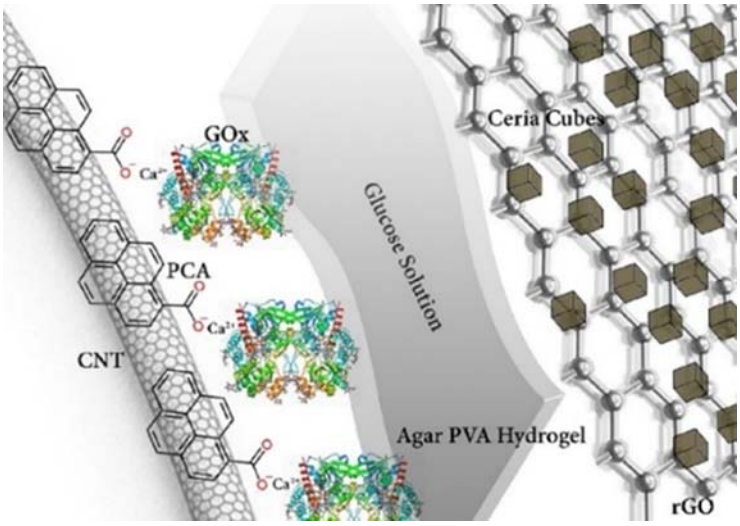

FIGURE 4.13 (A) Schematic representation of the fuel cell fabricated by our group. *Reprinted by permission from Elsevier; Arjun AM, Vimal M, Sandhyarani N. A hybrid hydrogel separated biofuel cell with a novel enzymatic anode and glucose tolerant cathode.* Int J Hydrogen Energy *2019;44(49), 27056–27066.* https://doi.org/10.1016/j.ijhydene.2019.08.131. *(Copyright, 2019).*

cm^3 at a current density of 3 mA/cm^3. The fuel cell could act as a sensor for the detection of glucose until 500 mM of glucose. A maximum OCV of 500 mV was obtained in this case.

Carbon dots also have been used for the immobilization of enzymes. Zhao et al. prepared carbon quantum dots using the candle soot technique and glucose oxidase was immobilized. The electrode was immersed in 20 mM PBS containing different concentrations of glucose in both oxygen and nitrogen saturated conditions. A fuel cell was made with this electrode as the anode and bilirubin oxidase on carbon quantum dots as a cathode. The fuel cell was capable of producing an OCV of 0.9 V and a power density of 40 $\mu W/cm^2$ at 100 $\mu A/cm^2$. The use of these carbon dots provides 3D scaffolds for enzyme immobilization in addition to them acting as electron relays.[122] In addition to carbon dots mesoporous carbon nanoparticles have also been reported. The work by Trifonov et al. elaborated the implanting of Pt nanoclusters in glucose oxidase immobilized on mesoporous carbon nanoparticles (Fig. 4.13B). The role of the pores is to confine the growth of the nanoclusters so that they become electrically wired to the GOx core. This system leads to the formation of an inside out synthesized platinum cluster, which has direct contact with the enzymatic redox core. More importantly, it was found that after 60 min of operation the current density was found to be higher for this system. This system could generate an OCV of 600 mV and a short circuit current of 140 $\mu A/cm^2$. A power density of 50 $\mu W/cm$ could be produced.[123]

A very brief account of the construction of enzyme fuel cells using carbon nanostructures has been presented. The use of these structures has led to an improvement in the electron transfer rates and also reachability in terms of connections to enzyme redox cores. There are gaps in the literature for the construction of enzyme fuel cells when compared with materials used for other methods of energy generation. This can be filled by a systematic approach to addressing the performance enhancements, which can be bought about when using these nanostructures. A very systematic literature discussion can be obtained from the many reviews that have been published in this field.[124,125]

3. Energy storage

Renewable energy generation is an intermittent process that cannot satisfy our demands for sustainable energy infrastructure. In such a scenario the only solution is to store the energy produced by renewable energy devices. However, energy storage has been synonymous with batteries for a very long time. Particularly, lithium-ion batteries have revolutionized the way the present society function. Their use in everything ranging from small sensors to heavy transportation is invaluable. Nevertheless, batteries suffer from disadvantages like swelling of active materials, volumetric modulation, and safety aspects. Moreover, in terms of applications batteries are suitable for a continuous long-term supply at a constant rate. In contrast, electrochemical supercapacitors are safer and are capable of proving 100−1000 times more power density than batteries (They however possess 3−30 times lesser energy density than batteries). Supercapacitors are safer and can sustain a huge number of charge-discharge cycles. In layman's terms, they are typically used for bursts of power. This comparison can be represented in terms of the Ragone plot. The supercapacitors occupy areas of higher specific power whereas the batteries occupy areas of higher specific energy. The Ragone plot

indicates that the supercapacitor has higher specific power but lower specific energy. The comparison for this in layman's terms can be made with a torch light which is synonymous with a battery where light (in the case of a battery it will be energy) lasts for a long time whereas in a camera flash which is synonymous to a supercapacitor (in case of supercapacitor it will be power) lasts only for a short time that too with maximum intensity. This energy storage section is dedicated to supercapacitors which have benefitted immensely from the application of carbon nanomaterials.

In terms of construction; an electrochemical supercapacitor possesses two electrodes separated by a separator. If the two electrodes are identical the device is named a symmetric supercapacitor and in the case of different electrodes, the device is named an asymmetric supercapacitor. The separator that separates the two electrodes is not only permeable to ions but also prevents contact between the two electrodes. The separators used usually are polymer-based or paper-based separators and they are soaked in electrolytes to allow for ion flow. Depending on the charge storage mechanism supercapacitors can be divided into two. Electrical double layer capacitors (EDLC) in which the charge storage takes place on the interface between the electrode and electrolyte (Fig. 4.14). The second category of supercapacitors is pseudo capacitors, which involve reversible faradaic redox reactions for charge storage (Fig. 4.14). A third category also exists which combines a carbon electrode or a pseudocapacitive electrode it is termed a hybrid capacitor.

The application of carbon-based nanomaterials in supercapacitors has led to improvement in the efficiencies of their operation. The application of nanomaterials in both the categories of supercapacitors is discussed briefly in the succeeding sections.

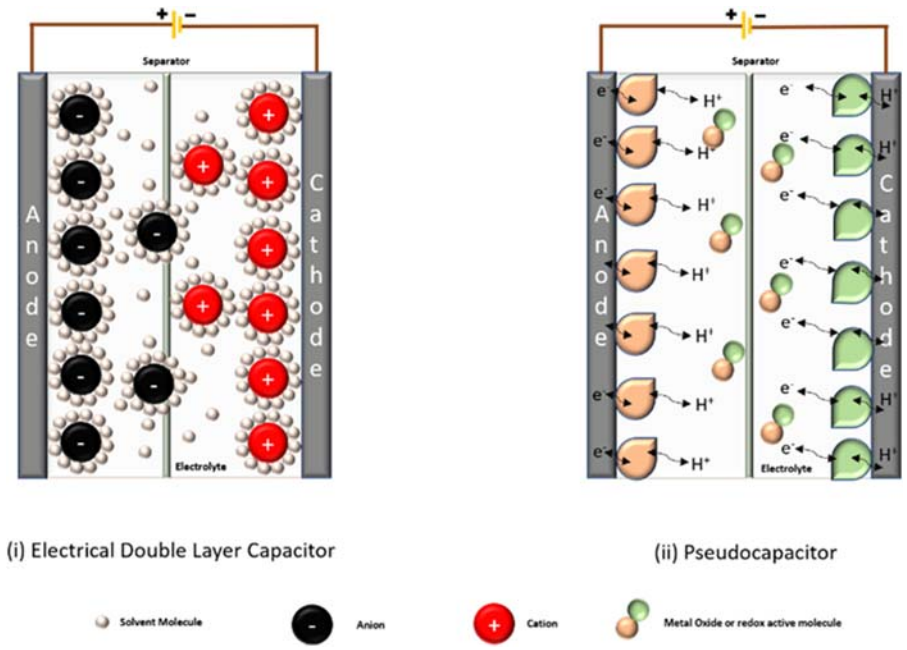

FIGURE 4.14 (A) Schematic diagram of electrical double-layered capacitor and (B) Pseudocapacitor.

3.1 Electrical double layer capacitors (EDLC)

Similar to conventional capacitors EDLCs work on charge separation. However, they possess two separate charge layers between the electrolyte and electrode surfaces. Because of this, they have high capacitance in comparison to conventional capacitors. It is important to note that the process is a nonfaradaic process with no charge transfer involved. In order to make this process more efficient, carbon-based materials are used. Among the most common carbon nanomaterials CNTs, graphene has been studied extensively followed by other morphologies with high surface area. A brief discussion about the use of carbon nanotubes in EDLC follows.

3.1.1 Carbon nanotubes and related materials in EDLC

Aerogels of SWCNT were fabricated by Van Aken et al. using a critical point drying of hydrated precursors. The electrodes were found to be free-standing, which negated the use of a binder. A room temperature-based ionic liquid electrolyte was used. The capacitance of the material was about 40 F/g at a current density of 30 A/g. This could be attributed to the high surface area ($900 m^2/g$) of the material with pore diameters in the range of 2–50 nm.[126] In another work based on SWCNT flexible transparent films an optically transparent film with high transmittance was fabricated by Kanninen et al. The films were able to reach maximum potential of only 0.6 V which was attributed to the Fe impurities in the CNT film. A high mass-specific capacitance of 178 F/g was obtained using this material.[127] An increase in the surface area of the electrodes would lead to an increase in the capacitance. Wang et al. realized this using ZIF-8 MOF nanocrystals strung on MWCNTs. A carbonization process was used for this stringing process. The surface area of this material was reported to be 569.3 m^2/g. The capacitance properties of the material were tested in an acidic medium. The specific capacitance of the material was 225.5 F/g, which was attributed to the mesoporous architectures and high surface area polyhedral carbons. Capacitance retention of 91.6% was reported at a high current density of 10 A/g.[128]

Nitrogen doping of carbon nanotubes is another methodology for improving charge storage efficiency. For this Dubal et al. synthesized 1D polypyrrole (PPY) nanotubes, which when carbonized resulted in the formation of N-doped CNTs. An asymmetric supercapacitor with the PPY nanotubes as positive electrodes and N-doped CNTs as negative electrodes yielded a voltage window of 1.4V. The N doped CNT electrode demonstrated a high capacitance of 228 F/g. The assembled supercapacitor had good cyclic stability of 89.98%.[129] In another work Yang et al. prepared sulfur-doped bamboo-like CNTs. The sulfur doping was done by the carbonization of a sulfonated polymer nanotube. The capacitance of this material was shown to be 259 F/g with capacitance retention of 97.7%.[130]

In conclusion, the use of CNTs and their doped versions have bought about an increase in the capacitance of these material-modified electrodes. More importantly, the doping of CNTs helped in bringing an increase in electrical conductivity along with increased active sites.

3.1.2 Graphene and related materials in EDLC

Very recently vertically oriented graphene (graphene nanowalls (GNWs)) were reported. These nanowalls were electrochemically activated to enhance their specific capacitances. This material was used for developing an EDLC-based electrode. A comparison of the charge

storage was made before and after activation and it was found that there was a 150% increase in specific capacitance after the activation process.[131] A combination of rGO with carbon dots resulted in an increase in surface area (130% of initial). An increased capacitance value of 214 F/g was obtained after the rGO was combined with the carbon dots.[132] Graphene was deposited electrochemically using a single-step controllable process for exfoliating and depositing graphene oxide by Khakpour et al.[133] The electrochemical analysis of this material revealed an areal capacitance of 1.932 mF/cm^2.

Doping of graphene oxide is another technique that can impart high energy storage capability. Lee et al. synthesized imine-rich nitrogen-doped graphene in which pyrrole and pyridine groups were selectively incorporated. The material was used for supercapacitor application on 6M KOH solution. The material displayed a specific capacitance of 174 F/g in the case of the pyrrole-modified N-doped graphene due to the change in electronic structure.[134]

3.1.3 Other carbon-based materials in EDLC

Among the other carbon materials for EDLCs, some of the important contributions have been reported from porous carbon derived from natural precursors. One such example is the porous carbon nano onions prepared from rice husk by nickel-assisted graphitization. The material possessed a very high surface area of 3821 m^2/g. This material was used as a super-capacitor electrode and it exhibited a high specific capacitance of 350 F/g and a superior cyclic performance of 99% retention after 10,000 cycles.[135] A thiophene-based sulfur doped carbon nano onion was synthesized by Mohapatra et al. This material displayed a high specific surface area of 950 m^2/g and an ordered mesoporous structure. The sulfur incorporation led to a high specific capacitance value of 305 F/g which was almost 3 times higher than the pristine carbon-based nano onion. The two-electrode configuration showed high capacitance retention of 95% even after 10,000 cycles.[136]

The use of carbon-based materials in EDLC has been synonymously linked to an increase in surface area in the case of EDLC. The electrical conductivity of the materials and high capacitance retention is another advantage that has encouraged the emergence of a large number of reports in this area. Another area in the research on supercapacitors is the pseudo capacitors. This will be discussed in the succeeding sections.

3.2 Pseudocapacitors

These capacitors work on faradaic charge transfer involving redox reactions in the interface between electrodes and electrolytes. For redox reactions to occur efficiently high surface area and highly conductive electrodes are required. This is where the application of carbon-based nanomaterials is significant. The use of carbon-based materials like CNTS, graphene, and other carbon-based materials contribute to improvement in potential window, stability, and energy density, and cost-effectiveness of the final device.

3.2.1 Carbon nanotubes and related materials in pseudocapacitors

The combination of conducting polymers with CNTs has been used for supercapacitor applications. Tahir et al. fabricate poly(3,4-ethylenedioxythiophene) (PEDOT) coated MWCNT as microcapacitor electrode materials. The capacitor was able to deliver a specific capacitance of 20.6 F/cm^2 with a 99.9% capacitance retention after 20,000 cycles.[137]

3.2.2 Graphene and related materials in pseudocapacitors

A Nile blue conjugated 3D graphene aerogel was synthesized by a facile hydrothermal approach. The conjugation is a strong noncovalent bonding between the π electrons of the Nile blue and the graphene. The nanocomposite possessed an area of 154 m^2/g. The structure was found to be a combination of macropores, mesopores, and micropores which act as ion buffering reservoirs and also minimize the transport distances of electrolytes of ions into graphene. This electrode was used for charge storage in 1M H_2SO_4.[138] A specific capacitance of 483 F/g was obtained with capacitance retention of 73.5%.

Layered double hydroxides of Ni−Co with the growth of Zn and Co-nanoparticles have been grown on a graphene foam. The electrode displayed an areal capacitance of 7485 mF/cm^2. A symmetric supercapacitor built using this device was able to exhibit an areal capacitance of 1278 mF/cm^2 with capacitance retention of 108% over 5000 cycles.[139]

3.2.3 Other carbon-based materials in pseudocapacitors

A combination of tungsten nitride and phosphorous-modified carbon fabric was reported by Dubal et al.[140] The use of transition metal nitrides has been justified because of the high electrical conduction of the material in addition to it's corrosion resistance. Since symmetric devices based on the use of tungsten nitride is able to work only in low potential windows, an asymmetric device based on PPY positive electrode and EDLC-based tungsten nitride was taken. The device exhibited a wide potential window of 1.6V with a volumetric capacity of 7.1 mF/cm^3. The capacitance retention of this material was 20,000 cycles.

This very brief account of the use of different nanostructures for supercapacitor applications has been done using representative examples and it can be inferred from them that the addition of carbon-based nanomaterials as platforms for the growth of nanoparticles in the case of pseudo particles has led to better capacitance values because of the better connectivity of the underlying material with the grown nanoparticles. In addition to this as mentioned in earlier sections, these materials also bring about a conductivity enhancement that impacts the device fabrication process in a positive manner.

4. Conclusion

The area that encompasses the use of carbon-based nanostructures for energy generation is one that has spanned a very long time. The advantage of using these nanostructures are that they are economical, and their morphologies can be tailored in a multitude of ways to suit our applications. Researchers across the globe have made use of these advantages to report advancements in performance for energy generation. An analysis of the literature volume in this area shows that more than 18,000 articles have been published in the past 10 years. This itself shows the prospect that these materials hold in terms of energy generation. In conclusion, carbon-based materials have shown exceptional promise in the energy generation area and a further effort to commercialize these materials for real-life application is necessary so that this research can be used to alleviate the energy problems faced by society.

The use of carbon-based nanomaterials in the energy storage arena has been prevalent for a long time. Literature abounds in examples where these materials have been used for various

enhancements in charge storage properties. The approximate number of articles utilizing carbon as a constituent material is more than 10,000 in the last 10 years alone. As with the case for energy generating materials even though there is an abundance in published scientific data a commercially viable device is yet to emerge. More importantly, areas in energy storage like using biomass-derived carbon for energy storage hold great promise in terms of cost-effective materials. To conclude, the future is very bright for carbon-based energy storage materials.[45]

References

1. N. Bednaršek, R.A. Feely, J.C.P. Reum, B. Peterson, J. Menkel, S.R. Alin, B. Hales, Limacina helicina shell dissolution as an indicator of declining habitat suitability owing to ocean acidification in the California current Ecosystem, Proc Biol Sci 281 (1785) (2014) 20140123, https://doi.org/10.1098/rspb.2014.0123.
2. A.N. Geim, K. Novoselov, Graphene calling, Nat Mater 6 (3) (2007), https://doi.org/10.1038/nmat1858, 169–169.
3. S. Iijima, Carbon nanotubes: past, present, and future, Phys B Condens Matter 323 (1) (2002) 1–5, https://doi.org/10.1016/S0921-4526(02)00869-4.
4. H.W. Kroto, J.E. Fischer, D. Cox, The fullerenes, Newnes, 2012.
5. N. Sano, H. Wang, M. Chhowalla, I. Alexandrou, G.A.J. Amaratunga, Synthesis of carbon "onions" in water, Nature 414 (6863) (2001) 506–507, https://doi.org/10.1038/35107141.
6. Q. Wu, L. Yang, X. Wang, Z. Hu, From carbon-based nanotubes to nanocages for advanced energy conversion and storage, Acc Chem Res 50 (2) (2017) 435–444, https://doi.org/10.1021/acs.accounts.6b00541.
7. A. Fujishima, K. Honda, Electrochemical Photolysis of water at a semiconductor electrode, Nature 238 (5358) (1972) 37–38, https://doi.org/10.1038/238037a0.
8. H. Ahmad, S.K. Kamarudin, L.J. Minggu, M. Kassim, Hydrogen from photo-catalytic water splitting process: a review, Renew Sustain Energy Rev 43 (2015) 599–610, https://doi.org/10.1016/j.rser.2014.10.101.
9. N. Syed, J. Huang, Y. Feng, X. Wang, L. Cao, Carbon-based nanomaterials via heterojunction serving as photocatalyst, Front Chem 7 (2019), https://doi.org/10.3389/fchem.2019.00713.
10. X. Li, X. Hao, A. Abudula, G. Guan, Nanostructured catalysts for electrochemical water splitting: current state and prospects, J Mater Chem 4 (31) (2016) 11973–12000, https://doi.org/10.1039/C6TA02334G.
11. Y. Yan, B. Yu Xia, B. Zhao, X. Wang, A review on noble-metal-free bifunctional heterogeneous catalysts for overall electrochemical water splitting, J Mater Chem 4 (45) (2016) 17587–17603, https://doi.org/10.1039/C6TA08075H.
12. X. Wang, K. Maeda, A. Thomas, K. Takanabe, G. Xin, J.M. Carlsson, K. Domen, M. Antonietti, A metal-free polymeric photocatalyst for hydrogen production from water under visible light, Nat Mater 8 (1) (2009) 76–80, https://doi.org/10.1038/nmat2317.
13. Y. Xu, M. Kraft, R. Xu, Metal-free carbonaceous electrocatalysts and photocatalysts for water splitting, Chem Soc Rev 45 (11) (2016) 3039–3052, https://doi.org/10.1039/C5CS00729A.
14. A. Vinu, K. Ariga, T. Mori, T. Nakanishi, S. Hishita, D. Golberg, Y. Bando, Preparation and characterization of well-ordered hexagonal mesoporous carbon nitride, Adv Mater 17 (13) (2005) 1648–1652, https://doi.org/10.1002/adma.200401643.
15. X. Chen, Y.-S. Jun, K. Takanabe, K. Maeda, K. Domen, X. Fu, M. Antonietti, X. Wang, Ordered mesoporous SBA-15 type graphitic carbon nitride: a semiconductor host structure for photocatalytic hydrogen evolution with visible light, Chem Mater 21 (18) (2009) 4093–4095, https://doi.org/10.1021/cm902130z.
16. Y. Zhang, M. Antonietti, Photocurrent generation by polymeric carbon nitride Solids: an initial step towards a novel photovoltaic system, Chem Asian J 5 (6) (2010) 1307–1311, https://doi.org/10.1002/asia.200900685.
17. J. Liu, J. Huang, D. Dontosova, M. Antonietti, Facile synthesis of carbon nitride micro-/nanoclusters with photocatalytic activity for hydrogen evolution, RSC Adv 3 (45) (2013) 22988–22993, https://doi.org/10.1039/C3RA44490B.
18. G. Zhang, M. Zhang, X. Ye, X. Qiu, S. Lin, X. Wang, Iodine modified carbon nitride semiconductors as visible light photocatalysts for hydrogen evolution, Adv Mater 26 (5) (2014) 805–809, https://doi.org/10.1002/adma.201303611.

19. J. Zhang, G. Zhang, X. Chen, S. Lin, L. Möhlmann, G. Dołega, G. Lipner, M. Antonietti, S. Blechert, X. Wang, Co-monomer control of carbon nitride semiconductors to optimize hydrogen evolution with visible light, Angew Chem Int Ed 51 (13) (2012) 3183–3187, https://doi.org/10.1002/anie.201106656.
20. J. Hong, X. Xia, Y. Wang, R. Xu, Mesoporous carbon nitride with in situ sulfur doping for enhanced photocatalytic hydrogen evolution from water under visible light, J Mater Chem 22 (30) (2012) 15006–15012, https://doi.org/10.1039/C2JM32053C.
21. S. Guo, Z. Deng, M. Li, B. Jiang, C. Tian, Q. Pan, H. Fu, Phosphorus-doped carbon nitride tubes with a layered micro-nanostructure for enhanced visible-light photocatalytic hydrogen evolution, Angew Chem Int Ed 55 (5) (2016) 1830–1834, https://doi.org/10.1002/anie.201508505.
22. C. Rajkumar, P. Veerakumar, S.-M. Chen, B. Thirumalraj, K.-C. Lin, Ultrathin sulfur-doped graphitic carbon nitride nanosheets as metal-free catalyst for electrochemical sensing and catalytic removal of 4-nitrophenol, ACS Sustain Chem Eng 6 (12) (2018) 16021–16031, https://doi.org/10.1021/acssuschemeng.8b02041.
23. Z.-F. Huang, J. Song, L. Pan, Z. Wang, X. Zhang, J.-J. Zou, W. Mi, X. Zhang, L. Wang, Carbon nitride with simultaneous porous network and O-doping for efficient solar-energy-driven hydrogen evolution, Nano Energy 12 (2015) 646–656, https://doi.org/10.1016/j.nanoen.2015.01.043.
24. J. Fang, H. Fan, M. Li, C. Long, Nitrogen self-doped graphitic carbon nitride as efficient visible light photocatalyst for hydrogen evolution, J Mater Chem 3 (26) (2015) 13819–13826, https://doi.org/10.1039/C5TA02257F.
25. P.W. Chen, K. Li, Y.X. Yu, W.D. Zhang, Cobalt-doped graphitic carbon nitride photocatalysts with high activity for hydrogen evolution, Appl Surf Sci 392 (2017) 608–615, https://doi.org/10.1016/j.apsusc.2016.09.086.
26. Y.-S. Jun, J. Park, S.U. Lee, A. Thomas, W.H. Hong, G.D. Stucky, Three-dimensional macroscopic assemblies of low-dimensional carbon nitrides for enhanced hydrogen evolution, Angew Chem Int Ed 52 (42) (2013) 11083–11087, https://doi.org/10.1002/anie.201304034.
27. N. Guo, Y. Zeng, H. Li, X. Xu, H. Yu, X. Han, Novel mesoporous TiO_2@g-C3N4 hollow Core@shell heterojunction with enhanced photocatalytic activity for water treatment and H2 production under simulated sunlight, J Hazard Mater 353 (2018) 80–88, https://doi.org/10.1016/j.jhazmat.2018.03.044.
28. W. Ren, J. Cheng, H. Ou, C. Huang, M.-M. Titirici, X. Wang, Enhancing visible-light hydrogen evolution performance of crystalline carbon nitride by defect engineering, Chem Sus Chem 12 (14) (2019) 3257–3262, https://doi.org/10.1002/cssc.201901011.
29. S. Samanta, S. Martha, K. Parida, Facile synthesis of Au/g-C3N4 nanocomposites: an inorganic/organic hybrid plasmonic photocatalyst with enhanced hydrogen gas evolution under visible-light irradiation, Chem Cat Chem 6 (5) (2014) 1453–1462, https://doi.org/10.1002/cctc.201300949.
30. J. Zhang, Y. Wang, J. Jin, J. Zhang, Z. Lin, F. Huang, J. Yu, Efficient visible-light photocatalytic hydrogen evolution and enhanced photostability of core/shell CdS/g-C3N4 nanowires, ACS Appl Mater Interfaces 5 (20) (2013) 10317–10324, https://doi.org/10.1021/am403327g.
31. G. Liao, Y. Gong, L. Zhang, H. Gao, G.-J. Yang, B. Fang, Semiconductor polymeric graphitic carbon nitride photocatalysts: the "holy grail" for the photocatalytic hydrogen evolution reaction under visible light, Energy Environ Sci 12 (7) (2019) 2080–2147, https://doi.org/10.1039/C9EE00717B.
32. D.-Z. Guo, G.-M. Zhang, Z.-X. Zhang, Z.-Q. Xue, Z.-N. Gu, Visible-light-induced water-splitting in channels of carbon nanotubes, J Phys Chem B 110 (4) (2006) 1571–1575, https://doi.org/10.1021/jp055929q.
33. K. Dai, T. Peng, D. Ke, B. Wei, Photocatalytic hydrogen generation using a nanocomposite of multi-walled carbon nanotubes and TiO2 nanoparticles under visible light irradiation, Nanotechnology 20 (12) (2009) 125603, https://doi.org/10.1088/0957-4484/20/12/125603.
34. F.M. Toma, A. Sartorel, M. Iurlo, M. Carraro, P. Parisse, C. Maccato, S. Rapino, B.R. Gonzalez, H. Amenitsch, T.D. Ros, L. Casalis, A. Goldoni, M. Marcaccio, G. Scorrano, G. Scoles, F. Paolucci, M. Prato, M. Bonchio, Efficient water oxidation at carbon nanotube–polyoxometalate electrocatalytic interfaces, Nat Chem 2 (10) (2010) 826–831, https://doi.org/10.1038/nchem.761.
35. F. Li, B. Zhang, X. Li, Y. Jiang, L. Chen, Y. Li, L. Sun, Highly efficient oxidation of water by a molecular catalyst immobilized on carbon nanotubes, Angew Chem Int Ed 50 (51) (2011) 12276–12279, https://doi.org/10.1002/anie.201105044.
36. Z. Zhang, J. Long, L. Yang, W. Chen, W. Dai, X. Fu, X. Wang, Organic semiconductor for artificial photosynthesis: water splitting into hydrogen by a bioinspired C3N3S3polymer under visible light irradiation, Chem Sci 2 (9) (2011) 1826–1830, https://doi.org/10.1039/C1SC00257K.

37. N. Li, Y. Ma, B. Wang, Y. Huang, Y. Wu, X. Yang, Y. Chen, Synthesis of semiconducting SWNTs by arc discharge and their enhancement of water splitting performance with TiO_2 photocatalyst, Carbon 49 (15) (2011) 5132–5141, https://doi.org/10.1016/j.carbon.2011.06.097.
38. A. Suryawanshi, P. Dhanasekaran, D. Mhamane, S. Kelkar, S. Patil, N. Gupta, S. Ogale, Doubling of photocatalytic H2 evolution from G-C3N4 via its nanocomposite formation with multiwall carbon nanotubes: electronic and morphological effects, Int J Hydrogen Energy 37 (12) (2012) 9584–9589, https://doi.org/10.1016/j.ijhydene.2012.03.123.
39. J.Y. Kim, J.-W. Jang, D.H. Youn, J.Y. Kim, E.S. Kim, J.S. Lee, Graphene – carbon nanotube composite as an effective conducting scaffold to enhance the photoelectrochemical water oxidation activity of a hematite film, RSC Adv 2 (25) (2012) 9415–9422, https://doi.org/10.1039/C2RA21169F.
40. Y.K. Kim, H. Park, How and to what extent do carbon materials catalyze solar hydrogen production from water? Appl Catal B Environ 125 (2012) 530–537, https://doi.org/10.1016/j.apcatb.2012.06.018.
41. C.K. Sumesh, S.C. Peter, Two-dimensional semiconductor transition metal based chalcogenide based heterostructures for water splitting applications, Dalton Trans 48 (34) (2019) 12772–12802, https://doi.org/10.1039/C9DT01581G.
42. T.-W. Lin, C.-J. Liu, J.-Y. Lin, Facile synthesis of MoS3/carbon nanotube nanocomposite with high catalytic activity toward hydrogen evolution reaction, Appl Catal B Environ 134–135 (2013) 75–82, https://doi.org/10.1016/j.apcatb.2013.01.004.
43. G. Khan, S.K. Choi, S. Kim, S.K. Lim, J.S. Jang, H. Park, Carbon nanotubes as an auxiliary catalyst in heterojunction photocatalysis for solar hydrogen, Appl Catal B Environ 142–143 (2013) 647–653, https://doi.org/10.1016/j.apcatb.2013.05.075.
44. Y. Pan, K. Sun, S. Liu, X. Cao, K. Wu, W.-C. Cheong, Z. Chen, Y. Wang, Y. Li, Y. Liu, D. Wang, Q. Peng, C. Chen, Y. Li, Core–shell ZIF-8@ZIF-67-derived CoP nanoparticle-embedded N-doped carbon nanotube hollow polyhedron for efficient overall water splitting, J Am Chem Soc 140 (7) (2018) 2610–2618, https://doi.org/10.1021/jacs.7b12420.
45. X. Zhang, X. Zhang, H. Xu, Z. Wu, H. Wang, Y. Liang, Iron-doped cobalt monophosphide nanosheet/carbon nanotube hybrids as active and stable electrocatalysts for water splitting, Adv Funct Mater 27 (24) (2017) 1606635, https://doi.org/10.1002/adfm.201606635.
46. T. Ouyang, Y.-Q. Ye, C.-Y. Wu, K. Xiao, Z.-Q. Liu, Heterostructures composed of N-doped carbon nanotubes encapsulating cobalt and β-Mo2C nanoparticles as bifunctional electrodes for water splitting, Angew Chem Int Ed 58 (15) (2019) 4923–4928, https://doi.org/10.1002/anie.201814262.
47. R. Gao, Q. Dai, F. Du, D. Yan, L. Dai, C60-Adsorbed single-walled carbon nanotubes as metal-free, PH-universal, and multifunctional catalysts for oxygen reduction, oxygen evolution, and hydrogen evolution, J Am Chem Soc 141 (29) (2019) 11658–11666, https://doi.org/10.1021/jacs.9b05006.
48. X.-Y. Zhang, H.-P. Li, X.-L. Cui, Y. Lin, Graphene/TiO 2 nanocomposites: synthesis, characterization and application in hydrogen evolution from water photocatalytic splitting, J Mater Chem 20 (14) (2010) 2801–2806, https://doi.org/10.1039/B917240H.
49. P. Cheng, Z. Yang, H. Wang, W. Cheng, M. Chen, W. Shangguan, G. Ding, TiO_2–Graphene nanocomposites for photocatalytic hydrogen production from splitting water, Int J Hydrogen Energy 37 (3) (2012) 2224–2230, https://doi.org/10.1016/j.ijhydene.2011.11.004.
50. X. Zou, X. Huang, A. Goswami, R. Silva, B.R. Sathe, E. Mikmekova, T. Asefa, Cobalt-embedded nitrogen-rich carbon nanotubes efficiently catalyze hydrogen evolution reaction at all PH values, Angew. Chem.-Int. Edit. 53 (17) (2014) 4372–4376, https://doi.org/10.1002/anie.201311111.
51. M.I. Fadlalla, S.G. Babu, Chapter 5 - role of graphene in photocatalytic water splitting for hydrogen production, in: M. Jawaid, A. Ahmad, D. Lokhat (Eds.), Graphene-based nanotechnologies for energy and environmental applications, Micro and nano technologies, Elsevier, 2019, pp. 81–108, https://doi.org/10.1016/B978-0-12-815811-1.00005-3.
52. A. Pérez del Pino, A. González-Campo, S. Giraldo, J. Peral, E. György, C. Logofatu, A.J. deMello, J. Puigmartí-Luis, Synthesis of graphene-based photocatalysts for water splitting by laser-induced doping with ionic liquids, Carbon 130 (2018) 48–58, https://doi.org/10.1016/j.carbon.2017.12.116.
53. Z. Yuan, J. Li, M. Yang, Z. Fang, J. Jian, D. Yu, X. Chen, L. Dai, Ultrathin black phosphorus-on-nitrogen doped graphene for efficient overall water splitting: dual modulation roles of directional interfacial charge transfer, J Am Chem Soc 141 (12) (2019) 4972–4979, https://doi.org/10.1021/jacs.9b00154.

54. P. Kuang, M. He, H. Zou, J. Yu, K. Fan, 0D/3D MoS2-NiS2/N-doped graphene foam composite for efficient overall water splitting, Appl Catal B Environ 254 (2019) 15–25, https://doi.org/10.1016/j.apcatb.2019.04.072.
55. W. Wan, S. Wei, J. Li, A.C. Triana, Y. Zhou, R.G. Patzke, Transition metal electrocatalysts encapsulated into N-doped carbon nanotubes on reduced graphene oxide nanosheets: efficient water splitting through synergistic effects, J Mater Chem 7 (25) (2019) 15145–15155, https://doi.org/10.1039/C9TA03213D.
56. Q. Hu, G. Li, G. Li, X. Liu, B. Zhu, X. Chai, Q. Zhang, J. Liu, C. He, Trifunctional electrocatalysis on dual-doped graphene nanorings–integrated boxes for efficient water splitting and Zn–air batteries, Adv Energy Mater 9 (14) (2019) 1803867, https://doi.org/10.1002/aenm.201803867.
57. J. Yang, D. Guo, S. Zhao, Y. Lin, R. Yang, D. Xu, N. Shi, X. Zhang, L. Lu, Y.-Q. Lan, J. Bao, M. Han, Cobalt phosphides nanocrystals encapsulated by P-doped carbon and married with P-doped graphene for overall water splitting, Small 15 (10) (2019) 1804546, https://doi.org/10.1002/smll.201804546.
58. F. Bu, W. Chen, M.F.A. Aboud, I. Shakir, J. Gu, Y. Xu, Microwave-assisted ultrafast synthesis of adjustable bimetal phosphide/graphene heterostructures from MOFs for efficient electrochemical water splitting, J Mater Chem 7 (24) (2019) 14526–14535, https://doi.org/10.1039/C9TA03146D.
59. R.-Q. Li, B.-L. Wang, T. Gao, R. Zhang, C. Xu, X. Jiang, J. Zeng, Y. Bando, P. Hu, Y. Li, X.-B. Wang, Monolithic electrode integrated of ultrathin NiFeP on 3D strutted graphene for bifunctionally efficient overall water splitting, Nano Energy 58 (2019) 870–876, https://doi.org/10.1016/j.nanoen.2019.02.024.
60. M. Zhao, J. Zhang, H. Xiao, T. Hu, J. Jia, H. Wu, Facile in situ synthesis of a carbon quantum dot/graphene heterostructure as an efficient metal-free electrocatalyst for overall water splitting, Chem Commun 55 (11) (2019) 1635–1638, https://doi.org/10.1039/C8CC09368G.
61. T.V. Tam, S.G. Kang, M.H. Kim, S.G. Lee, S.H. Hur, J.S. Chung, W.M. Choi, Novel graphene hydrogel/B-doped graphene quantum dots composites as trifunctional electrocatalysts for Zn–Air batteries and overall water splitting, Adv Energy Mater 9 (26) (2019) 1900945, https://doi.org/10.1002/aenm.201900945.
62. X. Li, X. Duan, C. Han, X. Fan, Y. Li, F. Zhang, G. Zhang, W. Peng, S. Wang, Chemical activation of nitrogen and sulfur Co-doped graphene as defect-rich carbocatalyst for electrochemical water splitting, Carbon 148 (2019) 540–549, https://doi.org/10.1016/j.carbon.2019.04.021.
63. S. Bellamkonda, N. Thangavel, H.Y. Hafeez, B. Neppolian, G. Ranga Rao, Highly active and stable multi-walled carbon nanotubes-graphene-TiO_2 nanohybrid: an efficient non-noble metal photocatalyst for water splitting, Catal Today 321–322 (2019) 120–127, https://doi.org/10.1016/j.cattod.2017.10.023.
64. J. Li, Z. Zhao, Y. Ma, Y. Qu, Graphene and their hybrid electrocatalysts for water splitting, ChemCatChem 9 (9) (2017) 1554–1568, https://doi.org/10.1002/cctc.201700175.
65. J. Albero, D. Mateo, H. García, Graphene-based materials as efficient photocatalysts for water splitting, Molecules 24 (5) (2019) 906, https://doi.org/10.3390/molecules24050906.
66. L. Yang, J. Shui, L. Du, Y. Shao, J. Liu, L. Dai, Z. Hu, Carbon-based metal-free ORR electrocatalysts for fuel cells: past, present, and future, Adv Mater 31 (13) (2019) 1804799, https://doi.org/10.1002/adma.201804799.
67. W. Zhang, L. Zhang, G. Zhang, P. Xiao, Y. Huang, M. Qiang, T. Chen, Air/water interfacial growth of Pt nanothorns anchored in situ on macroscopic freestanding CNT thin film for efficient methanol oxidation, New J Chem 43 (15) (2019) 6063–6068, https://doi.org/10.1039/C9NJ00437H.
68. Y. Zheng, H. Zhan, H. Tang, J. Luo, D. Dang, T. Shu, J. Ren, X. Tian, S. Liao, Atomic platinum layer coated titanium copper nitride supported on carbon nanotubes for the methanol oxidation reaction, Electrochim Acta 248 (2017) 349–355, https://doi.org/10.1016/j.electacta.2017.07.065.
69. R. Yan, X. Sun, X. Zhang, J. Zheng, B. Jin, High quality electrocatalyst by Pd-Pt alloys nanoparticles uniformly distributed on polyaniline/carbon nanotubes for effective methanol oxidation, Nanotechnology (2019), https://doi.org/10.1088/1361-6528/ab5e94.
70. X. Yang, Q. Jia, F. Duan, B. Hu, M. Wang, L. He, Y. Song, Z. Zhang, Multiwall carbon nanotubes loaded with MoS2 quantum dots and MXene quantum dots: non–Pt bifunctional catalyst for the methanol oxidation and oxygen reduction reactions in alkaline solution, Appl Surf Sci 464 (2019) 78–87, https://doi.org/10.1016/j.apsusc.2018.09.069.
71. H. Sun, J. Liu, C. Zhang, Q. Yuan, Y. Ye, W. Yan, Z. Tian, C.S. Liang, N dual-doped carbon nanotubes as substrate to enhance the methanol oxidation performance of NiO nanoparticles, Carbon 152 (2019) 114–119, https://doi.org/10.1016/j.carbon.2019.06.007.

72. J.-J. Fan, Y.-J. Fan, R.-X. Wang, S. Xiang, H.-G. Tang, S.-G. Sun, A novel strategy for the synthesis of sulfur-doped carbon nanotubes as a highly efficient Pt catalyst support toward the methanol oxidation reaction, J Mater Chem 5 (36) (2017) 19467–19475, https://doi.org/10.1039/C7TA05102F.
73. Q. Zhou, K. Yu, Z. Pan, Z. Huang, Y. Xu, G. Hu, S. Wu, C. Chen, L. Lin, Y. Lin, Research on a novel Ni-doped TiN modified N-doped CNTs supported Pt catalysts and their synergistic effect for methanol electrooxidation, Int J Hydrogen Energy 43 (50) (2018) 22519–22528, https://doi.org/10.1016/j.ijhydene.2018.10.081.
74. D.B. Gorle, V. Velacheri Kumman, M.A. Kulandainathan, Highly efficient, large surface area and spherically shaped Pt particles deposited electrolytically synthesized graphene for methanol oxidation with impedance spectroscopy, Int J Hydrogen Energy 42 (25) (2017) 16258–16268, https://doi.org/10.1016/j.ijhydene.2017.05.160.
75. T. Radhakrishnan, N. Sandhyarani, Three dimensional assembly of electrocatalytic platinum nanostructures on reduced graphene oxide – an electrochemical approach for high performance catalyst for methanol oxidation, Int J Hydrogen Energy 42 (10) (2017) 7014–7022, https://doi.org/10.1016/j.ijhydene.2016.12.132.
76. W. Xie, F. Zhang, Z. Wang, M. Yang, J. Xia, R. Gui, Y. Xia, Facile preparation of PtPdPt/graphene nanocomposites with ultrahigh electrocatalytic performance for methanol oxidation, J Electroanal Chem 761 (2016) 55–61, https://doi.org/10.1016/j.jelechem.2015.12.007.
77. H. Yang, L. Geng, Y. Zhang, G. Chang, Z. Zhang, X. Liu, M. Lei, Y. He, Graphene-templated synthesis of Palladium nanoplates as novel electrocatalyst for direct methanol fuel cell, Appl Surf Sci 466 (2019) 385–392, https://doi.org/10.1016/j.apsusc.2018.10.050.
78. C. Yang, Q. Jiang, W. Li, H. He, L. Yang, Z. Lu, H. Huang, Ultrafine Pt nanoparticle-decorated 3D hybrid architectures built from reduced graphene oxide and MXene nanosheets for methanol oxidation, Chem Mater 31 (22) (2019) 9277–9287, https://doi.org/10.1021/acs.chemmater.9b02115.
79. X. Qiu, T. Li, S. Deng, K. Cen, L. Xu, Y. Tang, A general strategy for the synthesis of PtM (M=Fe, Co, Ni) decorated three-dimensional hollow graphene nanospheres for efficient methanol electrooxidation, Chem Eur J 24 (6) (2018) 1246–1252, https://doi.org/10.1002/chem.201704959.
80. T. Noor, N. Zaman, H. Nasir, N. Iqbal, Z. Hussain, Electro catalytic study of NiO-MOF/RGO composites for methanol oxidation reaction, Electrochim Acta 307 (2019) 1–12, https://doi.org/10.1016/j.electacta.2019.03.116.
81. M.B. Askari, P. Salarizadeh, M. Seifi, S.M. Rozati, Electrocatalytic properties of CoS2/MoS2/RGO as a non-noble dual metal electrocatalyst: the investigation of hydrogen evolution and methanol oxidation, J Phys Chem Solid 135 (2019) 109103, https://doi.org/10.1016/j.jpcs.2019.109103.
82. X. Zhang, J. Zhu, C.S. Tiwary, Z. Ma, H. Huang, J. Zhang, Z. Lu, W. Huang, Y. Wu, Palladium nanoparticles supported on nitrogen and sulfur dual-doped graphene as highly active electrocatalysts for formic acid and methanol oxidation, ACS Appl Mater Interfaces 8 (17) (2016) 10858–10865, https://doi.org/10.1021/acsami.6b01580.
83. M. An, C. Du, L. Du, Y. Wang, Y. Wang, Y. Sun, G. Yin, Y. Gao, Enhanced methanol oxidation in acid media on Pt/S, P Co-doped graphene with 3D porous network structure engineering, Chemelectrochem 6 (4) (2019) 1157–1165, https://doi.org/10.1002/celc.201801395.
84. Y.-C. Shi, J.-J. Feng, X.-X. Lin, L. Zhang, J. Yuan, Q.-L. Zhang, A.-J. Wang, One-step hydrothermal synthesis of three-dimensional nitrogen-doped reduced graphene oxide hydrogels anchored PtPd alloyed nanoparticles for ethylene glycol oxidation and hydrogen evolution reactions, Electrochim Acta 293 (2019) 504–513, https://doi.org/10.1016/j.electacta.2018.10.068.
85. K. Vinodgopal, M. Haria, D. Meisel, P. Kamat, Fullerene-based carbon nanostructures for methanol oxidation, Nano Lett 4 (3) (2004) 415–418, https://doi.org/10.1021/nl035028y.
86. K.S. Bhavani, T. Anusha, P.K. Brahman, Fabrication and characterization of gold nanoparticles and fullerene-C60 nanocomposite film at glassy carbon electrode as potential electro-catalyst towards the methanol oxidation, Int J Hydrogen Energy 44 (47) (2019) 25863–25873, https://doi.org/10.1016/j.ijhydene.2019.08.005.
87. X. Zhang, J.-W. Zhang, P.-H. Xiang, J. Qiao, Fabrication of graphene-fullerene hybrid by self-assembly and its application as support material for methanol electrocatalytic oxidation reaction, Appl Surf Sci 440 (2018) 477–483, https://doi.org/10.1016/j.apsusc.2018.01.150.
88. W. Zhang, Q. Yao, X. Wu, Y. Fu, K. Deng, X. Wang, Intimately coupled hybrid of graphitic carbon nitride nanoflakelets with reduced graphene oxide for supporting Pd nanoparticles: a stable nanocatalyst with high catalytic

activity towards formic acid and methanol electrooxidation, Electrochim Acta 200 (2016) 131–141, https://doi.org/10.1016/j.electacta.2016.03.169.
89. W. Zhang, Y. Fu, J. Wang, X. Wang, 3D hierarchically porous graphitic carbon nitride modified graphene-Pt hybrid as efficient methanol oxidation catalysts, Adv Mater Interfac 4 (12) (2017) 1601219, https://doi.org/10.1002/admi.201601219.
90. Q. Zhang, Z. Yang, J. Yang, X. Yu, Y. Ling, Y. Zhang, W. Cai, H. Cheng, Carbon nitride simultaneously boosted a PtRu electrocatalyst's stability and electrocatalytic activity toward concentrated methanol, Chem Commun 54 (67) (2018) 9282–9285, https://doi.org/10.1039/C8CC03752C.
91. F. Si, Y. Zhang, L. Yan, J. Zhu, M. Xiao, C. Liu, W. Xing, J. Zhang, 4 - electrochemical oxygen reduction reaction, in: W. Xing, G. Yin, J. Zhang (Eds.), Rotating electrode methods and oxygen reduction electrocatalysts, Elsevier, Amsterdam, 2014, pp. 133–170, https://doi.org/10.1016/B978-0-444-63278-4.00004-5.
92. S. Wang, D. Yu, L. Dai, Polyelectrolyte functionalized carbon nanotubes as efficient metal-free electrocatalysts for oxygen reduction, J Am Chem Soc 133 (14) (2011) 5182–5185, https://doi.org/10.1021/ja1112904.
93. K. Gong, F. Du, Z. Xia, M. Durstock, L. Dai, Nitrogen-doped carbon nanotube Arrays with high electrocatalytic activity for oxygen reduction, Science 323 (5915) (2009) 760–764, https://doi.org/10.1126/science.1168049.
94. S. Yasuda, A. Furuya, Y. Uchibori, J. Kim, K. Murakoshi, Iron–nitrogen-doped vertically aligned carbon nanotube electrocatalyst for the oxygen reduction reaction, Adv Funct Mater 26 (5) (2016) 738–744, https://doi.org/10.1002/adfm.201503613.
95. J. Chen, X. Yuan, F. Lyu, Q. Zhong, H. Hu, Q. Pan, Q. Zhang, Integrating MXene nanosheets with cobalt-tipped carbon nanotubes for an efficient oxygen reduction reaction, J Mater Chem 7 (3) (2019) 1281–1286, https://doi.org/10.1039/C8TA10574J.
96. Y. Shao, Z. Jiang, Q. Zhang, J. Guan, Progress in nonmetal-doped graphene electrocatalysts for the oxygen reduction reaction, ChemSusChem 12 (10) (2019) 2133–2146, https://doi.org/10.1002/cssc.201900060.
97. V. Mazánek, J. Luxa, S. Matějková, J. Kučera, D. Sedmidubský, M. Pumera, Z. Sofer, Ultrapure graphene is a poor electrocatalyst: definitive proof of the key role of metallic impurities in graphene-based electrocatalysis, ACS Nano 13 (2) (2019) 1574–1582, https://doi.org/10.1021/acsnano.8b07534.
98. G. Han, Y. Zheng, X. Zhang, Z. Wang, Y. Gong, C. Du, M.N. Banis, Y.-M. Yiu, T.-K. Sham, L. Gu, Y. Sun, Y. Wang, J. Wang, Y. Gao, G. Yin, X. Sun, High loading single-atom Cu dispersed on graphene for efficient oxygen reduction reaction, Nano Energy 66 (2019) 104088, https://doi.org/10.1016/j.nanoen.2019.104088.
99. S. Wang, X. Yan, K.-H. Wu, X. Chen, J.-M. Feng, P. Lu, H. Feng, H.-M. Cheng, J. Liang, S.X. Dou, A hierarchical porous Fe-N impregnated carbon-graphene hybrid for high-performance oxygen reduction reaction, Carbon 144 (2019) 798–804, https://doi.org/10.1016/j.carbon.2018.12.066.
100. W. Xia, J. Tang, J. Li, S. Zhang, K.C.-W. Wu, J. He, Y. Yamauchi, Defect-rich graphene nanomesh produced by thermal exfoliation of metal–organic frameworks for the oxygen reduction reaction, Angew Chem 131 (38) (2019) 13488–13493, https://doi.org/10.1002/ange.201906870.
101. F. Shi, J. He, B. Zhang, J. Peng, Y. Ma, W. Chen, F. Li, Y. Qin, Y. Liu, W. Shang, P. Tao, C. Song, T. Deng, X. Qian, J. Ye, J. Wu, Plasmonic-enhanced oxygen reduction reaction of silver/graphene electrocatalysts, Nano Lett 19 (2) (2019) 1371–1378, https://doi.org/10.1021/acs.nanolett.8b05053.
102. J.H. Dumont, U. Martinez, K. Artyushkova, G.M. Purdy, A.M. Dattelbaum, P. Zelenay, A. Mohite, P. Atanassov, G. Gupta, Nitrogen-doped graphene oxide electrocatalysts for the oxygen reduction reaction, ACS Appl Nano Mater 2 (3) (2019) 1675–1682, https://doi.org/10.1021/acsanm.8b02235.
103. H. Zou, S. Pei, Z. Zhou, Z. Chen, X. Xiong, Y. Sun, Y. Zhang, Fe, N-doped carbon spheres prepared by electrospinning method as high efficiency oxygen reduction catalyst, RSC Adv 10 (2) (2020) 779–783, https://doi.org/10.1039/C9RA08951A.
104. Y. Chen, Z. Li, Y. Zhu, D. Sun, X. Liu, L. Xu, Y. Tang, Atomic Fe dispersed on N-doped carbon hollow nanospheres for high-efficiency electrocatalytic oxygen reduction, Adv Mater 31 (8) (2019) 1806312, https://doi.org/10.1002/adma.201806312.
105. X. Fu, X. Hu, Z. Yan, K. Lei, F. Li, F. Cheng, J. Chen, Template-free synthesis of porous graphitic carbon nitride/carbon composite spheres for electrocatalytic oxygen reduction reaction, Chem Commun 52 (8) (2016) 1725–1728, https://doi.org/10.1039/C5CC08897F.
106. A.T. Yahiro, S.M. Lee, D.O. Kimble, Bioelectrochemistry: i. Enzyme utilizing bio-fuel cell studies, Biochim Biophys Acta (BBA) - Spec Sect Biophys Subj 88 (2) (1964) 375–383, https://doi.org/10.1016/0926-6577(64)90192-5.

107. N. Mano, Engineering glucose oxidase for bioelectrochemical applications, Bioelectrochemistry 128 (2019) 218–240, https://doi.org/10.1016/j.bioelechem.2019.04.015.
108. R. Haddad, J.-G. Mattei, J. Thery, A. Auger, Novel ferrocene-anchored ZnO nanoparticle/carbon nanotube Assembly for glucose oxidase wiring: application to a glucose/air fuel cell, Nanoscale 7 (24) (2015) 10641–10647, https://doi.org/10.1039/C5NR00497G.
109. A. Ruff, Redox polymers in Bioelectrochemistry: common playgrounds and novel concepts, Cur Opin Electrochem 5 (1) (2017) 66–73, https://doi.org/10.1016/j.coelec.2017.06.007.
110. B. Reuillard, A.L. Goff, C. Agnès, M. Holzinger, A. Zebda, C. Gondran, K. Elouarzaki, S. Cosnier, High power enzymatic biofuel cell based on naphthoquinone -mediated oxidation of glucose by glucose oxidase in a carbon nanotube 3D matrix, Phys Chem Chem Phys 15 (14) (2013) 4892–4896, https://doi.org/10.1039/C3CP50767J.
111. G.I. Berglund, G.H. Carlsson, A.T. Smith, H. Szöke, A. Henriksen, J. Hajdu, The catalytic pathway of horseradish peroxidase at high resolution, Nature 417 (6887) (2002) 463–468, https://doi.org/10.1038/417463a.
112. N.C. Veitch, Horseradish peroxidase: a modern view of a classic enzyme, Phytochemistry 65 (3) (2004) 249–259, https://doi.org/10.1016/j.phytochem.2003.10.022.
113. A. Ruff, J. Szczesny, N. Marković, F. Conzuelo, S. Zacarias, I.A.C. Pereira, W. Lubitz, W. Schuhmann, A fully protected hydrogenase/polymer-based bioanode for high-performance hydrogen/glucose biofuel cells, Nat Commun 9 (1) (2018) 1–10, https://doi.org/10.1038/s41467-018-06106-3.
114. R.D. Milton, F. Giroud, A.E. Thumser, S.D. Minteer, R.C.T. Slade, Bilirubin oxidase bioelectrocatalytic cathodes: the impact of hydrogen peroxide, Chem Commun 50 (1) (2013) 94–96, https://doi.org/10.1039/C3CC47689H.
115. R.D. Milton, F. Giroud, A.E. Thumser, S.D. Minteer, R.C.T. Slade, Hydrogen peroxide produced by glucose oxidase affects the performance of laccase cathodes in glucose/oxygen fuel cells: FAD-dependent glucose dehydrogenase as a replacement, Phys Chem Chem Phys 15 (44) (2013) 19371–19379, https://doi.org/10.1039/C3CP53351D.
116. C. Abreu, Y. Nedellec, O. Ondel, F. Buret, S. Cosnier, A. Le Goff, M. Holzinger, Glucose oxidase bioanodes for glucose conversion and H2O2 production for horseradish peroxidase biocathodes in a flow through glucose biofuel cell design, J Power Sources 392 (2018) 176–180, https://doi.org/10.1016/j.jpowsour.2018.04.104.
117. K.P. Prasad, Y. Chen, P. Chen, Three-dimensional graphene-carbon nanotube hybrid for high-performance enzymatic biofuel cells, ACS Appl Mater Interfaces 6 (5) (2014) 3387–3393, https://doi.org/10.1021/am405432b.
118. N. Saravanan, P. Mayuri, A. Senthil Kumar, Improved electrical wiring of glucose oxidase enzyme with an in-situ immobilized Mn(1,10-phenanthroline)2Cl2-complex/multiwalled carbon nanotube-modified electrode displaying superior performance to Os-complex for high-current sensitivity bioelectrocatalytic and biofuel cell applications, ACS Appl Bio Mater 1 (5) (2018) 1758–1767, https://doi.org/10.1021/acsabm.8b00584.
119. S. Pakapongpan, R.P. Poo-arporn, Self-assembly of glucose oxidase on reduced graphene oxide-magnetic nanoparticles nanocomposite-based direct electrochemistry for reagentless glucose biosensor, Mater Sci Eng C 76 (2017) 398–405, https://doi.org/10.1016/j.msec.2017.03.031.
120. A.M. Arjun, M. Vimal, N. Sandhyarani, A hybrid hydrogel separated biofuel cell with a novel enzymatic anode and glucose tolerant cathode, Int J Hydrogen Energy 44 (49) (2019) 27056–27066, https://doi.org/10.1016/j.ijhydene.2019.08.131.
121. P. Lv, H. Zhou, A. Mensah, Q. Feng, D. Wang, X. Hu, Y. Cai, L. Amerigo Lucia, D. Li, Q. Wei, A highly flexible self-powered biosensor for glucose detection by epitaxial deposition of gold nanoparticles on conductive bacterial cellulose, Chem Eng J 351 (2018) 177–188, https://doi.org/10.1016/j.cej.2018.06.098.
122. M. Zhao, Y. Gao, J. Sun, F. Gao, Mediatorless glucose biosensor and direct electron transfer type glucose/air biofuel cell enabled with carbon nanodots, Anal Chem 87 (5) (2015) 2615–2622, https://doi.org/10.1021/acs.analchem.5b00012.
123. A. Trifonov, A. Stemmer, R. Tel-Vered, Enzymatic self-wiring in nanopores and its application in direct electron transfer biofuel cells, Nanoscale Adv 1 (1) (2019) 347–356, https://doi.org/10.1039/C8NA00177D.
124. X. Xiao, H. Xia, R. Wu, L. Bai, L. Yan, E. Magner, S. Cosnier, E. Lojou, Z. Zhu, A. Liu, Tackling the challenges of enzymatic (Bio)Fuel cells, Chem Rev 119 (16) (2019) 9509–9558, https://doi.org/10.1021/acs.chemrev.9b00115.
125. A. Ruff, F. Conzuelo, W. Schuhmann, Bioelectrocatalysis as the basis for the design of enzyme-based biofuel cells and semi-artificial biophotoelectrodes, Nat Catal 1–11 (2019), https://doi.org/10.1038/s41929-019-0381-9.

126. K.L. Van Aken, C.R. Pérez, Y. Oh, M. Beidaghi, Y. Joo Jeong, M.F. Islam, Y. Gogotsi, High rate capacitive performance of single-walled carbon nanotube Aerogels, Nano Energy 15 (2015) 662–669, https://doi.org/10.1016/j.nanoen.2015.05.028.
127. P. Kanninen, N.D. Luong, L.H. Sinh, I.V. Anoshkin, A. Tsapenko, J. Seppälä, A.G. Nasibulin, T. Kallio, Transparent and flexible high-performance supercapacitors based on single-walled carbon nanotube films, Nanotechnol 27 (23) (2016) 235403, https://doi.org/10.1088/0957-4484/27/23/235403.
128. Y. Wang, B. Chen, Y. Zhang, L. Fu, Y. Zhu, L. Zhang, Y. Wu, ZIF-8@MWCNT-Derived carbon composite as electrode of high performance for supercapacitor, Electrochim Acta 213 (2016) 260–269, https://doi.org/10.1016/j.electacta.2016.07.019.
129. D.P. Dubal, N.R. Chodankar, Z. Caban-Huertas, F. Wolfart, M. Vidotti, R. Holze, C.D. Lokhande, P. Gomez-Romero, Synthetic approach from polypyrrole nanotubes to nitrogen doped pyrolyzed carbon nanotubes for asymmetric supercapacitors, J Power Sources 308 (2016) 158–165, https://doi.org/10.1016/j.jpowsour.2016.01.074.
130. Y. Yang, L. Liu, Y. Tang, Y. Zhang, D. Jia, L. Kong, Bamboo-like carbon nanotubes containing sulfur for high performance supercapacitors, Electrochim Acta 191 (2016) 846–853, https://doi.org/10.1016/j.electacta.2016.01.149.
131. D.-J. Hsu, Y.-W. Chi, K.-P. Huang, C.-C. Hu, Electrochemical activation of vertically grown graphene nanowalls synthesized by plasma-enhanced chemical vapor deposition for high-voltage supercapacitors, Electrochim Acta 300 (2019) 324–332, https://doi.org/10.1016/j.electacta.2019.01.134.
132. V. Strauss, M. Muni, A. Borenstein, B. Badamdorj, T. Heil, D.M. Kowal, R. Kaner, Patching laser-reduced graphene oxide with carbon nanodots, Nanoscale 11 (26) (2019) 12712–12719, https://doi.org/10.1039/C9NR01719D.
133. I. Khakpour, A. Rabiei Baboukani, A. Allagui, C. Wang, Bipolar exfoliation and in situ deposition of high-quality graphene for supercapacitor application, ACS Appl Energy Mater 2 (7) (2019) 4813–4820, https://doi.org/10.1021/acsaem.9b00479.
134. M.S. Lee, D.R. Whang, Y.H. Song, J.T. Kim, M.H. Yang, U.H. Choi, D.W. Chang, Effects of pyridine and pyrrole moieties on supercapacitive properties of imine-rich nitrogen-doped graphene, Carbon 152 (2019) 915–923, https://doi.org/10.1016/j.carbon.2019.06.082.
135. H. Jin, S. Wu, T. Li, Y. Bai, X. Wang, H. Zhang, H. Xu, C. Kong, H. Wang, Synthesis of porous carbon nano-onions derived from rice husk for high-performance supercapacitors, Appl Surf Sci 488 (2019) 593–599, https://doi.org/10.1016/j.apsusc.2019.05.308.
136. D. Mohapatra, G. Dhakal, M.S. Sayed, B. Subramanya, J.-J. Shim, S. Parida, Sulfur doping: unique strategy to improve the supercapacitive performance of carbon nano-onions, ACS Appl Mater Interfaces 11 (8) (2019) 8040–8050, https://doi.org/10.1021/acsami.8b21534.
137. M. Tahir, L. He, W. Ali Haider, W. Yang, X. Hong, Y. Guo, X. Pan, H. Tang, Y. Li, L. Mai, Co-electrodeposited porous PEDOT–CNT microelectrodes for integrated micro-supercapacitors with high energy density, high rate capability, and long cycling life, Nanoscale 11 (16) (2019) 7761–7770, https://doi.org/10.1039/C9NR00765B.
138. Y. Shabangoli, M.S. Rahmanifar, A. Noori, M.F. El-Kady, R.B. Kaner, M.F. Mousavi, Nile blue functionalized graphene aerogel as a pseudocapacitive negative electrode material across the full PH range, ACS Nano 13 (11) (2019) 12567–12576, https://doi.org/10.1021/acsnano.9b03351.
139. D.S. Patil, S.A. Pawar, J.C. Shin, H.J. Kim, Layered double hydroxide based on ZnCo@NiCo- nano-architecture on 3D graphene scaffold as an efficient pseudocapacitor, J Power Sources 435 (2019) 226812, https://doi.org/10.1016/j.jpowsour.2019.226812.
140. D.P. Dubal, N.R. Chodankar, S. Qiao, Tungsten nitride nanodots embedded phosphorous modified carbon fabric as flexible and robust electrode for asymmetric pseudocapacitor, Small 15 (1) (2019) 1804104, https://doi.org/10.1002/smll.201804104.

CHAPTER

5

Nanoengineering diatoms in microfluidic lab on chip devices

Vandana Vinayak[1], *Mohd Jahir Khan*[1] *and Khasthi Ballabh Joshi*[2]

[1]**Diatom Nanoengineering and Metabolism (DNM) Laboratory, School of Applied Sciences, Harisingh Gour Vishwavidyalaya (A Central University), Sagar, Madhya Pradesh, India;**
[2]**Department of Chemistry, School of Chemical Science and Technology, Harisingh Gour Vishwavidyalaya (A Central University), Sagar, Madhya Pradesh, India**

Abbreviations

AFM Atomic force microscopy
APES 3-aminopropyltriethoxysilane
Diafuel© Diatom biofuel copyright
DIV Diatom infecting viruses
DSSC Dye sensitized solar cells
EV Electric vehicles
FITC Fluoroscein isothiocyanate
GMRs Guided mode resonance
LED Light emitting diode
LOC Lab on chip
MBA 4 Mercaptobenzoic acid
ME Microchannel efficiency
MEMS Microelectroporation mechanical system
MF Microfluidic
MOSCAP Metal oxide semiconductor capacitor
PDMS Polydimethylsiloxane
PMF Pulsed magnetic field
PZT Piezo electric disc
RPT Resistive pulse sensors
SEM Scanning electron microscopy
SERS Surface resonance enhancement
TMAH Tetramethylammonium hydroxide
TNT 2,4,6 trinitrotoulene
μDAD Microfluidic diatom analytical device
μPAD Microfluidic paper-based analytical device

Applications of Multifunctional Nanomaterials
https://doi.org/10.1016/B978-0-12-820557-0.00030-8

1. Introduction

Diatoms are microalgae widely distributed in different water bodies and geographies having about 100,000 species.[1] They vary in size from 2 to 2000 μm all having distinctive morphologies.[2] The peculiar feature of diatoms is that their cell wall is made up of silica.[3] This makes their cell wall rigid which can tolerate a shearing force of about 750 μN.[4] The shear strain required to break diatom frustules varies for different diatom types. The elastic modulus for *Coscinodiscus* varies from 3.4 to 15.6 GPa thus establishing that centric diatoms could tolerate some elastic deformation.[4] The ability to undergo elastic deformation and endurance has indeed great potential in microelectromechanical systems (MEMS) and microfluidic systems. Wang et al.[5] study on three different diatoms (*Coscinodiscus* sp., *N. palea*, *D. brightwellii*) showed that ringent girdle bands of *Coscinodiscus* sp. were more flexible than the complete frustules. Though, the long chain clusters of *N. palea* and central spines of *D. brightwellii* also have some elasticity.[5] This elastic behavior of diatoms has great applications for their uses in Lab-on-chip devices (LOC) to endure elastic deformation during water flow, in pharmaceutical as well as in optical fiber technology. Diatoms are in fact luminescent silicon nanostructures that constitute dead diatoms known as diatomite and live diatom cells.[6] The diatomite mainly consists of 70%−80% of silicon dioxide, and few metallic oxides mainly alumina and ferric oxide.[7] Not to forget, the first ever use of diatomite was by Swedish chemist 'Alfred Nobel' in a mixture of nitroglycerine and kieselguhr to make Dynamite.[8]

Since diatoms have well-aligned pores of size up to 40 nm they have well-organized nano architecture which adds to their applications in wide variety of nanotechnology and material science studies.[9] Besides these pores help in exchange of gases and adding surface area to the diatoms (>200 m^2/g).[10] Fig. 5.1 shows the nanoarchitecture of two groups of diatoms *Cyclotella meneghiniana* and *Pinnularia borealis*.

The indepth study of diatom nanoporous architecture study is required to know the size of pores, their arrangement, to take their usage in preparation of different nanomaterials. *Sellaphora* sp. for example, shows a good array of pores moving radially from center to periphery at elongating sizes. Its porous architecture is elaborated in different state of art microscopy SEM, TEM and AFM images as can be seen in Fig. 5.2. Owning to these properties these diatoms are employed for their application in microdevices and diatom-based materials.[11] Much of these microdevices use diatomite in the microfluidic application as biosensors,[9] solar cells,[6a,11b] photobioreactors,[13] cell sorters,[14] drug vehicle,[15] etc. Many times such diatom simulated complete LOC are used for cell culture,[12,16] selection of strain and also for detection of secondary metabolites.[17]

2. Diatoms in micro-electroporation/electro mechanical system (MEMS)

The art of introducing foreign molecules like genes and proteins into biological cells is a very significant technique.[15] This involves a lot of applications including metabolic engineering,[18] gene therapy,[19] *invitro* fertilization,[20] cancer treatment,[21] induced pluripotent cells,[22] etc. Diatoms among microalgae are metabolically engineered to act as a potential vector or

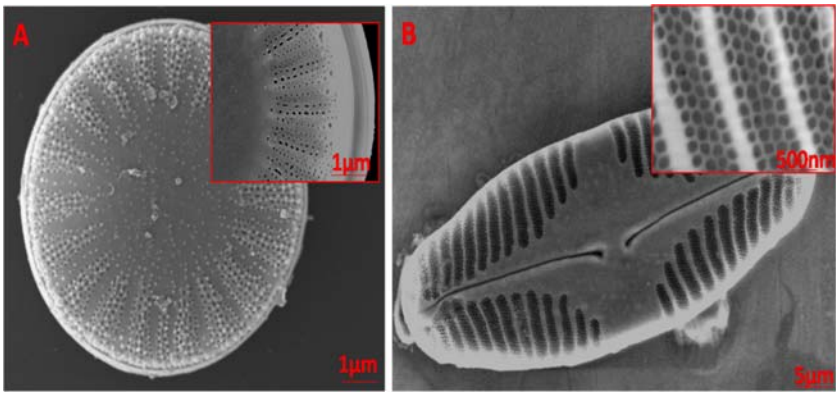

FIGURE 5.1 SEM image of (A) *Cyclotella menighiniana* inset pores at scale of 1 µm and (B) *Pinnularia borealis*. Inset pores at scale of 500 nm.

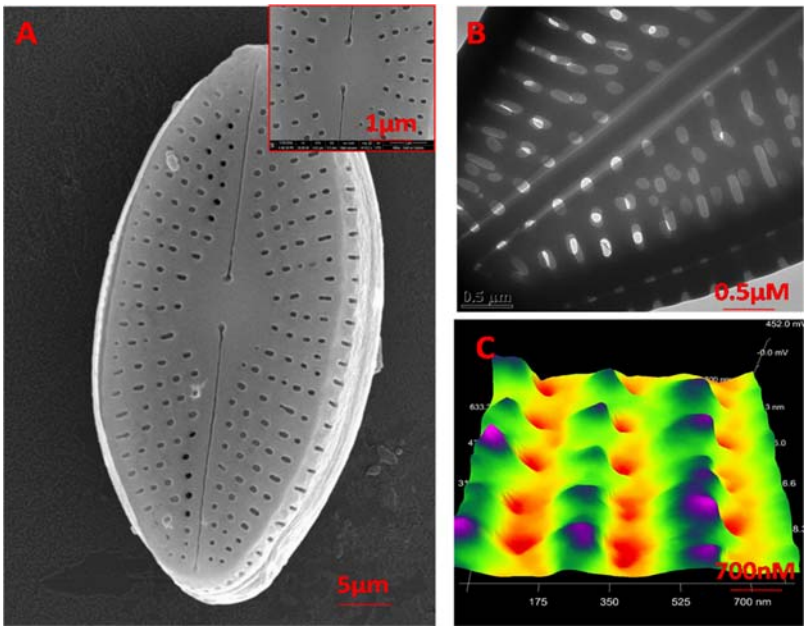

FIGURE 5.2 *Sellaphora* sp. showing porous nanoarchitecture revealed by (A) SEM image at scale 5 µm with inset at the scale of 1 µm; (B) TEM image at scale 0.5 µm and (C) High-resolution 3D AFM image of diatom pores.

drug carrier to heal a tumourous or cancerous cell line.[23] But this is also done to alter or introduce genes via plasmids with antibiotics in diatoms so as to target the diseased cell.[24] Alternately the same is done to increase the production of lipids and other secondary metabolites in diatom and microalgae.[25] The major reason is being that cell membranes are not permeable to the foreign molecules hence techniques like electroporation,[26] bombardments via gene

gun,[27] chemical treatment,[22a] viral vector,[28] etc., are employed. However, among them, the cuvette-type electroporation method employed in transfecting biological cell, requires high voltage,[29] metal ion dissolution,[30] and irreversible electroporation.[29,31] The high voltage, however, results into low efficiency. The efficiency can, however, be improved if the distance between the electrodes, to minimizes the problems often coming in cuvette electrode electroporation. This automatically reduces the voltage however, maintaining the same electric field strength.[15] Kang and co-workers fabricated a microelectroporation mechanical system (MEMS) which reduces the distance between the electrodes to height of ~0.1 mm. They checked their MEMS device electroporating only small volume of *Chlamydomonas reinhardtii* samples in order to check their cell viability and delivery efficiency.[15,32] *Chlamydomonas reinhardtii* is a standard microalgae model which is used for the production of biodiesel, since it has lipids between 20% and 50% of their cell body.[33] The fabricated MEMS is of aluminum metal which is economical and has high conductivity. The aluminum not only lowers the joule heat but also improves the transfection efficiency of microalgae necessary for genetic engineering.[15]

Kang et al.[15,34] used three kinds of tracer molecules (calcein, FITC-BSA, and plasmid DNA) to study electroporation with 3D microelectroporation system and that with a conventional cuvette system.[35] Fig. 5.3 shows delivery efficiency with the three tracer molecules and it was found that in calcein and FITC-BSA; the delivery efficiency increased by 1.5 and seven folds using MEMS microelectrode.[15] However, in case of intracellular delivery by plasmid DNA, the delivery efficiency increased by 4.85 folds using MEMS.[15,34] Diatoms on the other hand have been used as diatom infecting viral (DIV) promoters for engineering of marine

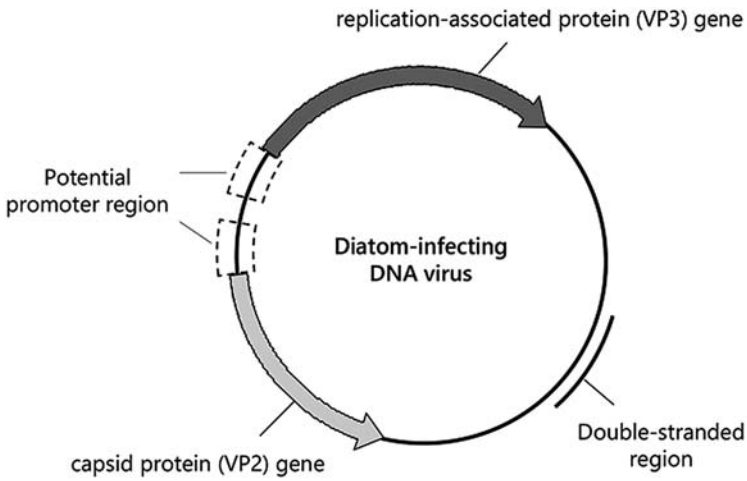

FIGURE 5.3 The genome structures of marine diatom-infecting DNA viruses. Modified from the ClorDNAV genome. *Reproduced with permission from Kadono T, Tomaru Y, Suzuki K, Yamada K, Adachi M. The possibility of using marine diatom-infecting viral promoters for the engineering of marine diatoms.* Plant Sci *2020, 110475.*

diatoms like *Phaeodactylum tricornutum*.[36] DIV have both double-stranded DNA and single-stranded RNA with atleast two open reading frames. DIV's target the diatoms host cells and influence the metabolic machinery. DIV carry the targeted promoter region of the ClorDNAV VP3 gene (ClP1) as shown in Fig. 5.3. In this case they targeted *P. tricornutum* machinery so that ClP1 gene could be used for producing maximum secondary metabolites at low nutrition conditions.[36] This leaves an interesting application of diatoms as microelectroporation and electro-machine application in the treatment of virus-based infections in humans.

Besides the injection of genes, diatoms have been metabolically engineered for a variety of other MEMS having their application in the drugs industry, optical systems, solar cells, etc. We had shown how metabolically engineered two-way diatoms cultures with TiO_2 have increased the efficiency of conventional dye-sensitized solar cells (DSSC).[37] Encouraged by this we made a facile way of decorating diatoms with peptides and silver nanoparticles doping further on titanium dioxide anode and found equivalent efficiency; as we found in metabolically engineered live diatoms with TiO_2 in DSSCs.[38] Other than this, diatoms doped metals (lanthanides, zinc, gold) acted as microcontainers to inhibit the gram-positive and gram-negative bacterial infections.[39] They also acted as nature absorbents to monitor water quality by absorbing heavy metals[40] as revealed by a change in their valve formation. Not the least, they act as pollution indicators by changing their cell growth, lipids and altering the physical and chemical parameters of fluids in wastewater.[41]

3. Why diatoms in microfluidics?

Diatoms because of their small pore size and dimensions are suitably used in sorting and separations.[42] Since they survive in slow moving environments, they thus have <1 Reynold number in the fluid surrounding them.[43] In such situation, they are dragged by viscous forces that help them in transporting and separating molecules coming their way.[44] Additionally, due to their distinctive porous structure, they have the ability to selectively sieve biomolecules of interest. This feature in microfluidic is responsible for frequent clogging, low flow rates, and back pressures. However, porous structure of diatoms allows the transport of molecules in a fluid by diffusion and also due to its tangential flow.[42] Losic et al.[42] used this selective transport property of diatom by fixing diatoms at the end of microcapillary tube. They checked the transport of fluorescein nanoparticles of different sizes (20 and 100 nm) through the frustules pores of diatom *Coscinodiscus* sp. and *Thallosiosra eccenterica* in the permeate solution contained in a microfluidic device.[42] Both these diatom species differed in the arrangement of pores with respect to their size, shape, density, and arrangement.[42] The experimental flux of these fluorescein nanoparticles was found to be 1.02 ± 0.20 nmoles $min^{-1}cm^{-2}$ ($n = 3$) which was in agreement with the theoretical flux rates estimated by Fick's law as 0.5 nmol min^{-1} cm^{-2} (Berg, 1983). The fluorescence signal of nanoparticles of size 20 nm was found within 8 h; however, no signal was diagnosed for the 100 nm- sized fluorescence nanoparticles.[42] This selective diffusion transport among the diatom frustules is of great use in microfluidics and lab-on-chip (LOC) devices for various potential applications.

4. Diatom lab on chip (LOC) and biosensing

Diatoms have great potential for photoluminescence and electrochemical detection. To make this possible diatom needs to be cultured. However, the most common method to do it is by culturing them in flasks and later removing the organic matter by filtration and acid washing.[45] This however destroys the diatom frustules and thus different way of culturing them should be designated. Cai et al.[46] used polydimethylsiloxane (PDMS) to fabricate a microfluidic chip via lithography to culture diatoms in a single chamber. The PDMS made microfluidic LOC device transparent to light and permeable to gases allowing diatoms to grow.[47] Growing diatoms in such closed microcosms may be used for biosensing and construction of diatom solar panels as well.[1,46] Cai et al.[46] used soft lithography methods to study the gliding motion in diatom *Bacillaria paradoxa.* The microchannels were made on the PDMS microfluidic LOC device and culture conditions of diatom were standardized. Diatoms were injected into 24 chips at different times with same speed in order to analyze the initial cell density of diatom cells with that of increase in their cell number. The cells of *B. paradoxa Gmelin* usually remain connected to each other forming chains and clusters.[48] The motility of *Bacillaria* under alternating dark and light exhibited rhythms with majority of the colonies being motile under light conditions and nonmotile under dark conditions.[48,49] Cai et al.[46] demonstrated this by two *Bacillaria* colonies with different status in still and moving water, since flow of water can be controlled in a microfluidic chip. In still water the stretch amplitude declines to near zero (0.5 μm) in 0.2 h having vibration period of 29±3s. The *Bacillaria* colony moves toward fluid flow direction assuming "a" as the angle to express the flow direction, many of the colonies tend to be 0 in about 10 min. This clearly established that diatom *Bacillaria* vibrates along the less shear force or liquid with least resistance. Thus it was proved that it is possible to culture diatoms *B. paradoxa Gmelin* in the customized microfluidic chip. They additionally proved that the motion of 2 cell *Bacillaria* colony in a still and moving water in microfluidic chip. It was seen that the cells vibrate and follow the direction of water offering least resistance.

Subsequently Cai et al.; fabricated a LOC in which diatoms were grown to maximum amount and cleaned with sulfuric acid and H_2O_2 to get rid of organic matter.[5,46] The cleaned diatoms were irradiated with ultraviolet light to let the diatoms bond to PDMS microchambers strongly.[46]

Cai et al.[50] showed microfluidic LOC which has central inlet of diameter 6 mm, 12 culture chambers of 2 mm each and three outlets. The width of the channels was 120 μm allowing diatom *Coscinodiscus excentricus* to cross the chambers and outlets. The diatoms were cultured in culture room till the cell density reached 3.6×10^4 cells mL^{-1} which were then injected into LOC via micropumps at variable speeds of 0.1 mLh^{-1} to 2.0 mLh^{-1}.[51]

To study the biosensing capability of diatom on a LOC, the diatom chip was modified by 2% of 3-aminopropyltriethoxysilane (APES) in acetone. This bonds the diatoms with APES resulting in the formation of siloxane bonds so as to form aminopropyl-terminated surface bonds.[50,51] The SEM image of LOC clearly showed that diatom was well on the surface of it bonded firmly. Further SEM images of diatom *Coscinodiscus excentricus* also established that diatoms frustules were firm, complete and not broken.

In order to check the detection of proteins in the diatom bonded APES LOC; fluoroscein isothiocyanate (FITC) was added. FITC conjugates with the proteins which bond with the APES diatomite LOC and was observed under fluorescence microscopy. It was observed that before FITC was injected diatoms were localized in the chamber as no fluorescence could be seen. However, after the FITC was injected, the location of diatom had not changed. The fluorescence was detected and was highest among the whole diatom frustules than from the surrounding area. The optical intensity measured using Image pro-plus software revealed that diatom frustules showed fluorescence with optical intensity of 1300 as compared to 300 from the surrounding area which is roughly 4 times stronger. This certainly is a great feature via which diatoms could probably bind many biomolecules which could help in detection of biomolecules of interest. Such diatom microfluidic LOC would help making 3 D micro as well as nano porous channels for not only biosensing but also molecular sensing the molecules of interest.[50]

Apart from using PDMS in the microfluidic LOC devices, researchers have used paper based microanalytical devices (μPAD).[52] This has been done to lower the cost and capillary flow. Also it certainly won't allow the use of syringe or micropump for injecting the cells or chemical dose shots. μPAD on the other hand can be fabricated using conventional soft lithographic techniques utilizing either photoresists or wax printing.[53] The technique has utilized detection of glucose, protein, cholesterol and heavy metals.[54] Besides this, silica microanalytical devices have attracted much attention due to its porosity and large surface area.[55] The reason being that the high porosity of silica enables detection of biomolecules not only on the surface but also inside the pores. Additionally, the optical density and compatibility of surface groups enhances the attachment and detection of biomolecules. Moon et al. synthesized silica colloidal particles for detection of nucleic acid.[56] Yang et al. used them for detecting glucose, however the lack of high degree order in these colloidal solutions results in nonuniform diffusion of analytes and hence poor spatial resolutions.[57] Since, diatoms are organic silica frustules bodies found abundantly on the earth in the form of diatomite.[11b]

Zhen et al. used diatom-based sensors to detect 2,4,6 trinitrotoulene (TNT).[58] De stafno modified diatoms (*Coscinodiscus concinnus*) with antibodies for immunocomplex detection.[59] They found that the photonic crystals of diatom could enhance surface resonance enhancement (SERS) when hybridized with plasmonic nanostructures. Kong et al. have developed diatoms doped with silver nanoparticles for label free TNT testing.[60] Later on they developed microfluidic diatom analytical device (μDAD) to detect illicit drugs. They chose cocaine as the target molecule which is one of the most widely used illicit drug all over the world.[61] The μDAD was fabricated in a very simple way in which diatomaceous earth substrate was fabricated by simply spin coating diatomite on the glass slides. The diatomite is first heated at 150°C for 6 h in an oven and then dispersed on aqueous solution of carboxy methyl cellulose dispersed on the glass slide and spin-coated as per the protocol described by Kong et al.[60] The μDAD are fabricated in such a way that the analyte to be traced is placed in the center of the reservoir and thereafter the chip is dried as seen in Fig. 5.4. The tip ends of the μDAD are then immersed into the solvent which migrates through the microchannels via capillary force. The separated analyte spots are marked under ultraviolet light at 380 nm and visualized by iodine colorimetry as seen in Fig. 5.4A. Thereafter, AuNP is dropped on the spots, and fluorescence spectra are recorded.

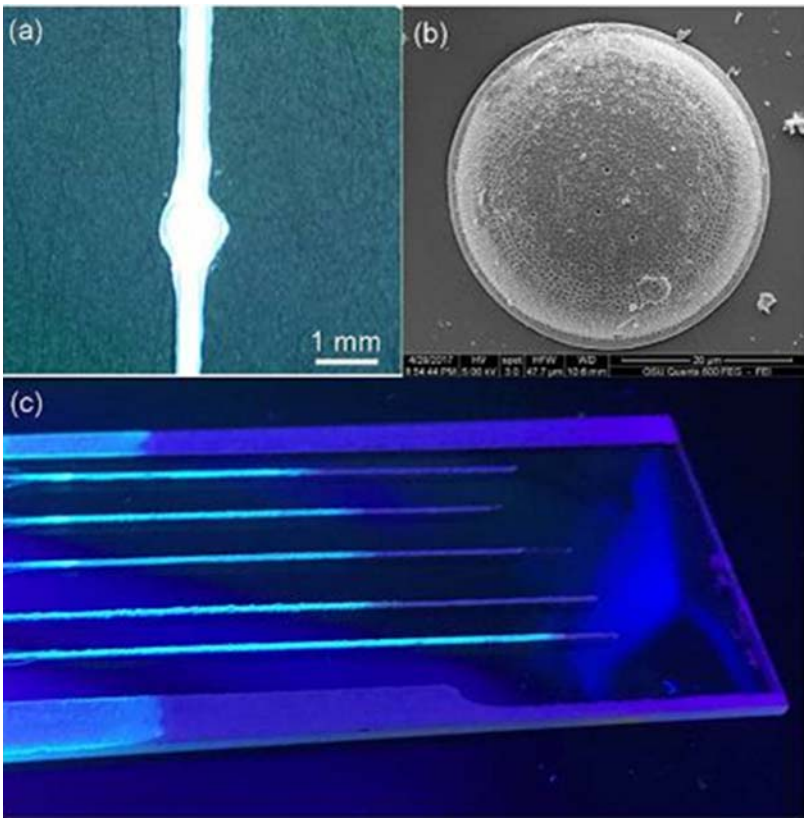

FIGURE 5.4 (A) Optical image of the μDADs; (B) SEM image of the honeycomb-like diatomite, which forms the microchannels of μDADs, and (C) optical image of μDADs after 100 ppm pyrene migration illuminated by UV light. *Reproduced with permission from Kong X, Chong X, Squire K, Wang AX. Microfluidic diatomite analytical devices for illicit drug sensing with ppb-level sensitivity.* Sensor Actuator B Chem *2018;**259**:587–595.*

Fig. 5.4B shows the SEM image of μDAD, the width of the microchannels is about 400 μm. The two dimensional uniformly arranged pores on the diatomite are responsible for guided mode resonance (GMRs). The highly porous nanostructure of the diatomite is responsible for the photonic effects and the uniform pore size allows homogenous fluid flow into the pores of the diatomite. This allows the eluent to flow smoothly and uniformly in the μDAD via capillary action. It was seen that when 100ppm of pyrene was allowed to flow in the μDAD, the fluorescence color of pyrene was observed against the glass substrate thus demonstrating that the μDAD allowed uniform pump-free flow of the fluid as can be seen in Fig. 5.4C. Therefore, when a fluid flows across a μDAD; diatomite acts as a stationary phase because hydroxyl group on diatomite makes it highly polar. This simply means a polar compound would be having more affinity with diatomite. Thereafter, Kang et al.[60] used μDAD to separate pyrene and 4 mercaptobenzoic acid (MBA). Pyrene moves further in the μDAD than MBA due to weak affinity with polar diatomite. The SERS spectra showed peaks at 590 cm^{-1} and 1230 cm^{-1} establishing that diatomite in LOC is working as a stationary phase as seen in

Fig. 5.5. Further, the detection limits of pyrene and MBA mixture were down to 1ppb on DAD and 2 ppm on normal diatomite chromatography. This establishes that μDAD is 1000 times more sensitive compared to normal diatomite plates. μDAD were also used by Kang et al. to separate illicit drug cocaine from plasma sample. They intentionally added cocaine into human plasma both purchased from Sigma and tried separating them using μDAD. It was found that since serum proteins are heavier they couldn't move into the microchannels of μDAD. However, good separation of cocaine was observed to the level of 10 ppb. This was remarkably better than what earlier workers did by using column switching liquid chromatography method to detect cocaine which showed limit of detection of 80 ppb.[62] This certainly would be having its potential application in drug testing and forensic testing which is far much sensitive and economical than high performance liquid chromatography and gas chromatography.

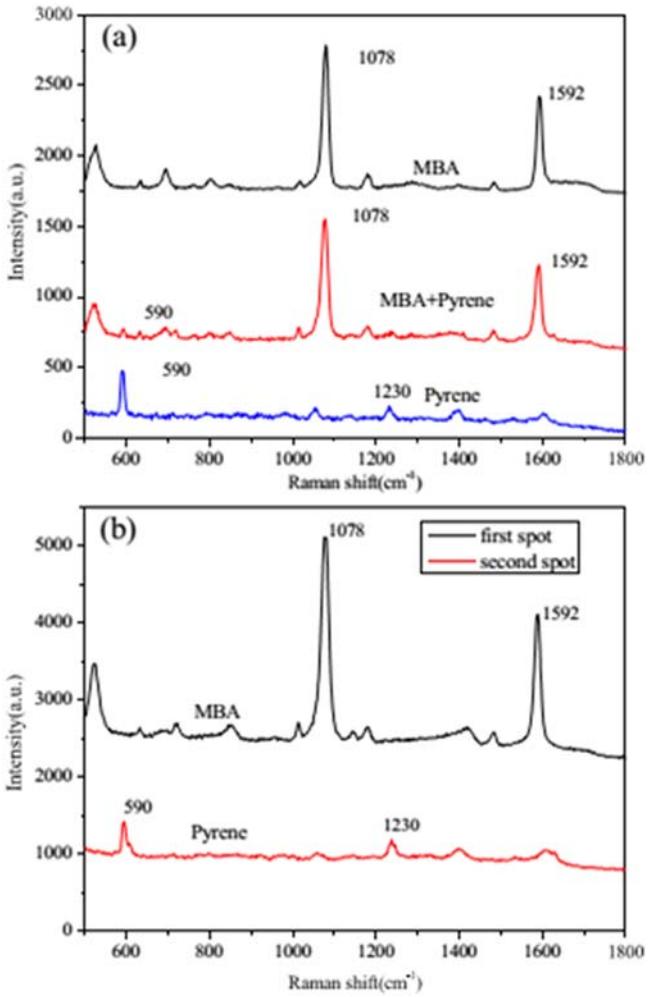

FIGURE 5.5 (A) SERS spectra of pure substance of MBA, pyrene and the mixture; and (B) SERS spectra of different spots on μDADs after chromatography separation. *Reproduced with permission from Kong X, Chong X, Squire K, Wang AX. Microfluidic diatomite analytical devices for illicit drug sensing with ppb-level sensitivity.* Sensor Actuator B Chem *2018;**259**:587–595.*

5. Diatom template and microfluidics

Diatoms because of their patterned structure also have great application for biometric and bioinspired nanomaterials. Even though large number of fabrication techniques are available in microelectronics which includes high cost set ups for UV photolithography, phase shift photolithography,[63] electron beam writing,[64] focused ion beam lithography,[65] and X-ray lithography[66] against the economical imprint[67] and soft lithography techniques which are quiet economical. Generally soft lithography using PDMS has been widely used to transfer patterns for microcontact printing.[68] This has its applications in optical devices,[69] microfluidic devices[70] and biosensors.[50] Nature has always been a source of inspiration to fabricate devices. A wide range of materials is inspired to be made from bioresources available in the nature. There are varieties of microorganisms which have well-ordered symmetry of their cell wall or pores but it has been difficult to mimic them synthetically in the laboratory. Losic et al.[71] used soft lithography techniques to form diatom replica nanostructures for the first time. Diatoms frustules are source of biotemplating their frustules for nanoarchitectured microfluidic devices.[71] Since diatoms have nanostructured architecture made up of amorphous silica their replicas can be made on PDMS and polymers by negative and positive photoresist. The diatom replica were first transferred onto PDMS via soft lithography and then to some hard surface or hard curable polymer, or some colloidal salt by positive photo resist.

Coscinodiscus sp. frustules and its polymer replicas was formed by molding. In the negative replicas on PDMS and the positive replicas by mercapto ester photocurable polymer (NOA60). The stepwise replication transforms the concave shaped *Coscinodiscus* sp. diatoms into convex replica on PDMS and concave mold or diatom replica on polymer NOA60. The fabricated replicas have optical and photonic properties similar to diatoms and can be used and replicated for their use in potential techno applications.[71] The honeycomb porous domes of their replicas frustules were beautifully demonstrated by SEM and AFM images. The domes had two different kind of pores smaller (190 nm) and larger (400−500 nm) arranged in a hexagonal nanoarchitecture. The AFM of negative replica clearly demonstrated that the shape and architecture of frustules size and shape are irreversibly patterned on PDMS replica. The AFM of final replication of negative replica as positive replica on desired applied material established that the high resolution topography is similar to the master template of the frustules. Losic's work of replicating diatoms on PDMS mold was reproduced by Hlúbiková, D et al.[72] on diatoms having bilateral symmetry, for example, *Fragilaria biceps* and *Fragilaria* sp. Unlike Losic who used 2 mm space for micromanipulating the replicas on centric diatom, Wang, Pan et al. worked on larger surface on pinnate diatoms. Fig. 5.6 shows the AFM images of master diatom replica and their corresponding PDMS negative replica in *F. biceps*. Even though high resolution SEM and AFM images were produced the replicas were not very stable. They tried to reduce the viscosity of PDMS by increasing the ratio of curing agent/elastomer and degassed it. This was done so that the less viscous PDMS easily entered into the pores of diatoms. Degassing made the diatom frustules fragile and also without it resolution of 50 nm was possible. They, however, advised that the PDMS replication of diatom frustules is more reproducible for small and flat diatoms as compared to large and long diatoms as the later tends to break from the cast and are highly fragile.

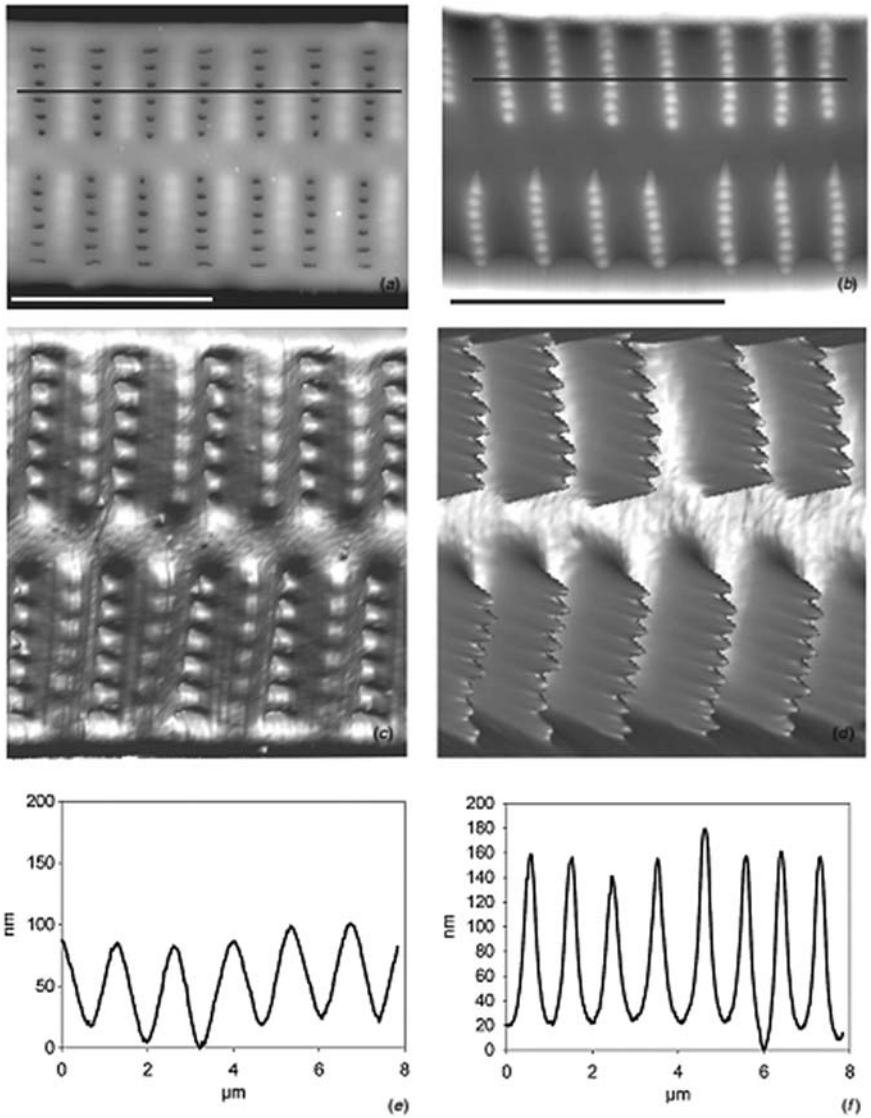

FIGURE 5.6 Micrographs of AFM comparing the structure morphology of diatom valves of *F. biceps* (A),(C),(E) and their negative replicas in PDMS mold (B),(D), (F) shows the topography of valves and distances between the pores (E),(F). Axes were normalized. Scale bar: 5 μm. *Reproduced with permission from Hlúbiková D, Luís A, Vaché V, Ector L, Hoffmann L, Choquet P. Optimization of the replica molding process of PDMS using pennate diatoms.* J Micromech Microeng *2012;**22**(11):115019.*

Even then many researchers have used diatom template for fabrication of variety of nanomaterials in microfluidics. A fine replica of *Thallosiosera pseudonana* biotemplated with carbon by initially treating it with $AlCl_3.6H_2O$, immersed in furfuryl alcohol and calcinated at 900°C for 3 h as per the protocol mentioned by Pérez-Cabero et al.[73] It was finally replicated by

degrading of all its mesosporous SiO_2 by chemical etching protocols (NaOH, HF (5%) and HF (10%)). This resulted in to well organized nanoarchitecture of pores as in diatom *T. pseudonana* besides having void gaps among adjacent pores. Fig. 5.7 show SEM images

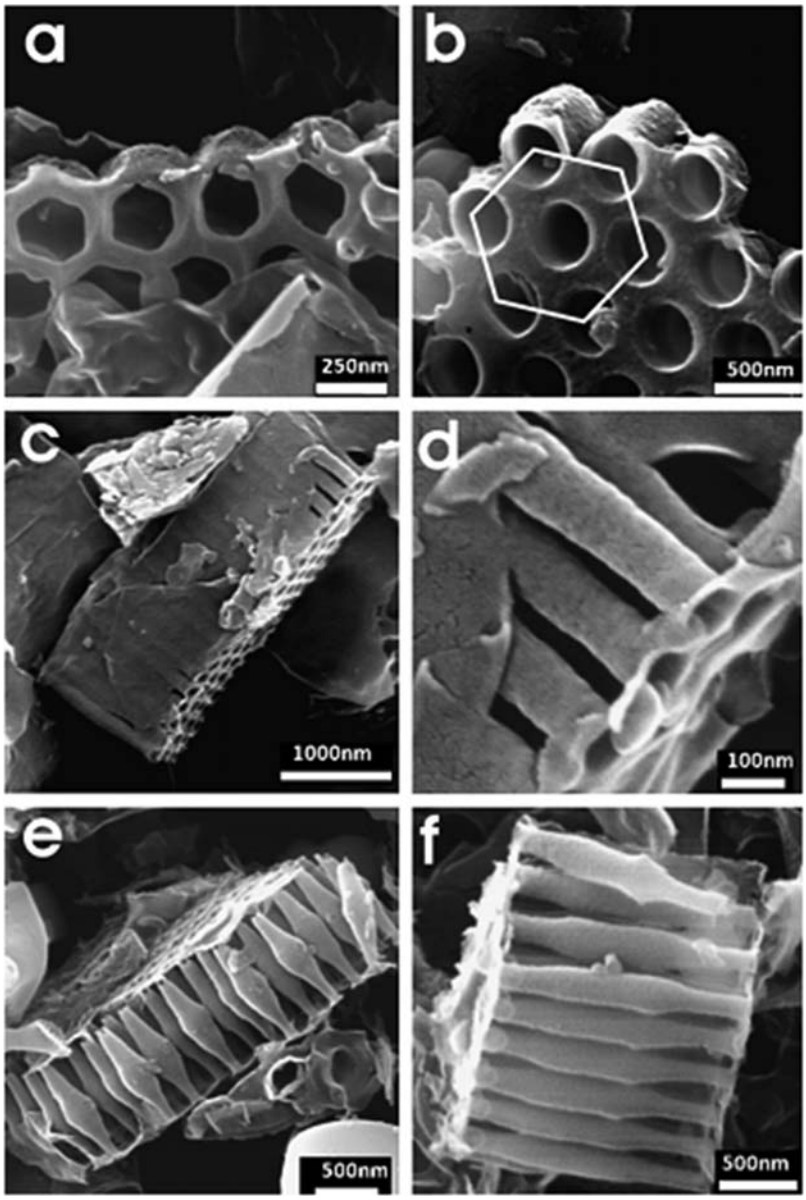

FIGURE 5.7 SEM images of carbonaceous *Thallosiosera pseudonana* after etching with HF (5%) at different contact times. (A–B) t = 6 h; (C–D) t = 12 hand (E–F) t = 24 h. *Reproduced with permission from Pérez-Cabero M, Puchol V, Beltran D, Amoros P. Thalassiosira pseudonana diatom as biotemplate to produce a macroporous ordered carbon-rich material.* Carbon *2008;**46**(2):297–304.*

of *T. pseudonana* after treatment with 5% HF at different times. During 6 h treatment with 5% HF, there is not much difference in the voids among the tubes in the porous frustules of diatom as can be seen in Fig. 5.7A–B. However, as the time period of exposure is increased the SiO_2 of the diatom gets degraded showing progressive SiO_2 etching (C–D); and after 24 h revealing fine macroporous carbonaceous replicas of *T. pseudonana* (E–F). Li et al.[74] further showed that controlled synthesis of manganese iron oxide hybrid replica on diatomite helps by two step hydrothermal process in fabricating high performance supercapacitors. Eynde et al.[75] showed how diatom *Pinnularia* sp. titania made biotemplates by sol gel hydrolysis shows high photocatalytic properties for absorbing pollutant gases like carbon monoxide and nitrous oxide.

6. Microfluidic cell culture

Microfluidic cell culture essentially refers to growth of cells in laboratory conditions which often needs to set conditions to minimize the contaminations and maintenance of pure cell lines.[76] The application of microfluidic cell culture has evolved its application essentially to the cell biology and medicine.[77] It evolves the cell culture at microscale level to monitor the individual cell growth and metabolism.[78] Thus unlike the macroscopic methods, microfluidic cell cultures involve few hundred or single cells. This thus helps in monitoring the cell growth via time lapse microscopy more closely with minimum nutrients requirements.[32a] They also have ability to analyze chemicals added as biosensors in the culture platform in order to detect the cellular and physiological parameters *in-situ*.[14] Such biosensors have ability to test on minimal number of cells with low dosage and quantity.[79] The culture material on a microfluidic chips are generally made up using polydimethylsiloxane [$(CH_3)_2Si–O$], abbreviated as PDMS. The major advantage of PDMS is that it's permeable to gases (O_2 and CO_2) and even water vapors. However, untreated PDMS can be toxic for different cell types. The only way to block the toxicity is by coating the PDMS with concentrated protein solutions.[80] The protein like poly D-Lysine leaves a net positive charge on the PDMS leaving it hydrophilic.[81] Similarly PDMS coated with carboxy methyl cellulose polysaccharides allows the cell attachment, growth, and its movement on PDMS surface in microfluidic devices.[82] Microfluidic and LOC devices thus because of their temporal control over the single cell cultures and their reagents have been used for their high throughput screening. They have been used for variety of applications like cell and drug screening and detection, bioenergy, diagnostics, etc.[83] Therefore, screening single microalgae cells is very much crucial in selecting drug resistant cells and mutagenic algal cells to be used off chip and re-grown.[84] Similarly microfluidic cell culture plays a vital role in selecting the strains which are efficient in producing secondary metabolites like lipids.[14]

7. High throughput screening and cell sorting of diatoms in microfluidics

Though microfluidic cell sorters and microdroplet-based microsystems are widely used for single cell sorting but they lack time course analysis capabilities.[85] They also lack capability to monitor single cell growth rate. The microdroplet-based microfluidic systems, however, lack

long-term culture manipulation. A high throughput microfluidic screening platform with 1024 trapping sites were, however, analyzed for long-term cell culture and growth in *Chlamydomonas reinhardtii*.[85] This was followed by chip fluorescent tagging along with selective retrieval of target cells in this unicellular green microalga.[85] The microfluidic device or logic gate allowed only selectively screened cells of interest to work off the chip. The device was made up of three PDMS layers; a top and middle control layer and bottom of cell culture or analysis layer. The bottom layer (height: 16 μm) had 1024 single cell trapping gates vide which single cell can be trapped, analyzed and cultured. The cell of interest can be selectively collected to an off chip reservoir while closing the remaining gates while simultaneously applying back flow for easy transfusion of selected cell. Single cell of *Chlamydomonas reinhardtii* undergoes change in shape, size due to reproduction. *In-situ* fluorescence studies analyzing the lipid bodies in the algal cells stained with Nile red (*yellow*) and autofluoroscence from chlorophyll as red in color. Single cell algal monitoring on LOC for their rate of reproduction, change in metabolism, and production of lipid bodies serves as the facile platform, before advancing to commercial scale for harvesting the algae. This is comparatively much better than lab flask scale culturing which not only face shading effect but flocculation, contamination, difficult studying single cell.[86]

Among various techniques employed to harvest diatoms, centrifugation is the most common way since it is simple and efficient.[86] However, the investments cost for large scale application makes it very expensive method inspite of it also being nonselective and concentrating the unwanted materials. Besides this, care is needed to standardize different species of same genera of microalgae as high shear force and gravitation may damage the biomass.[87] Diatoms on the other hand are also responsible for 30% crude oil on this earth; they could be nano factories if oil could be harvested from them.[1] They, unlike other agricultural oil producing plants, grow, and multiply rapidly thus making 10 times more lipid per hectare of land with theoretical estimates reaching 200 times.[88] The present high cost of algal biofuels is due to extraction procedures including crushing or drying of algal cells which require high energy inputs.[89]

The eventual depletion of non-renewable fossil fuels has directed interest toward developing ways of efficiently producing biofuel.[90] However, the cost of production of biofuel is high because it utilizes extraction and crushing procedures from microalgae that can require a substantial energy input.[89b,91] It is important to mimic nature's way in cell culturing, biosensing, making nanobots, and manufacturing crude oil from microalgae.[25]

7.1 Trilobite chips to screen size-based algae (diatoms)

According to Barros et al.,[92] "The optimization of a pre-concentration step before dewatering process is the most promising approach toward lowering microalgal harvesting costs." Hønsvall et al.[86] used a trilobite (earliest known arthropods) structure inspired microfluidic chip for concentrating the moving particles in a moving fluid specially for harvesting microalgae in a culture. The chip was designed based on hydrodynamic principle in which the suspended particles are continuously added or sorted as the liquid in it flows through as seen in Fig. 5.8A. In this there is one outlet for concentrated cells and other fraction for the purified cells fraction. The units in this chip known as terrace ridges and are arranged at intervals of 190−800 μm based on the trilobite structure as can be seen in Fig. 5.8B. These terrace ridges

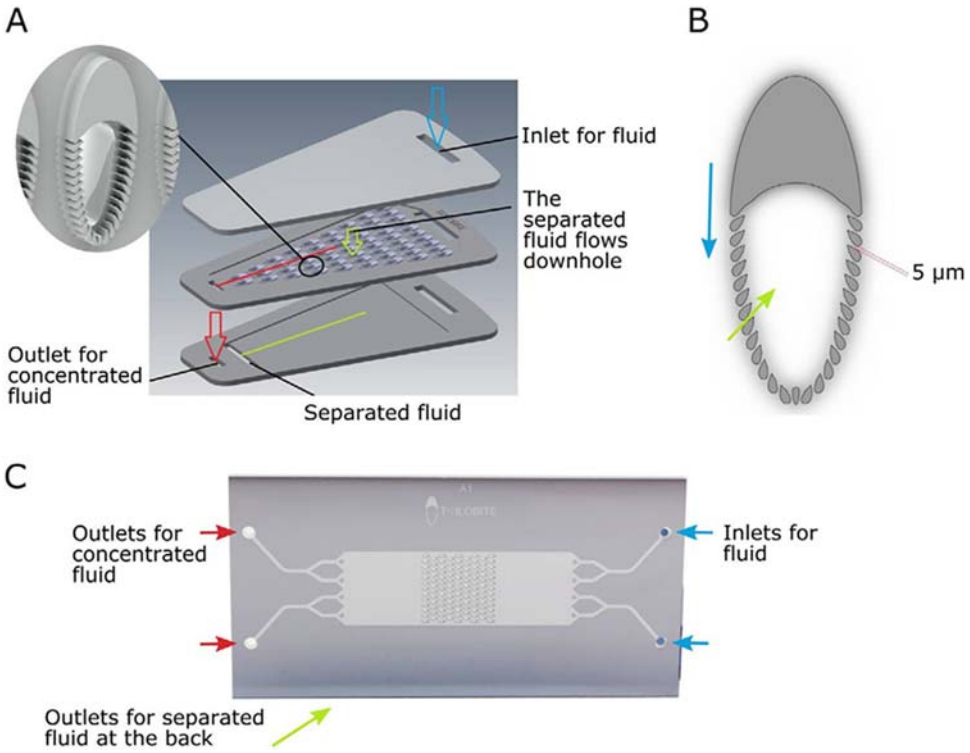

FIGURE 5.8 (A) Structure and principle of the trilobite microfluidic chip. Inlet suspension (*blue arrow*) enters on top. Most of the liquid flows into the units and down the holes (*green arrow*), and is collected at the outlet in the bottom layer. Particles that are larger than the gaps in the units are carried with the flow through the separation field, and collected at the outlet at the end of the chip (*red arrow*); (B) Structure of the trilobite unit. The liquid flow (*blue*) carries large particles past the unit, while smaller particles and liquid flows into the units (*green arrow*). The gap between the blades (or feet) of the unit (here 5 lm) defines the size of particles that flows into the unit; (C) Chip used in experiments. Note that the main channel and the placement of the field of separation units differ slightly from that presented in (A). The outlets for the separated fluid (permeate) are not visible from this side of the chip. Also note that there are two holes for each outlet and inlet in this chip. *Reproduced with permission from Hønsvall BK, Altin D, Robertson LJ. Continuous harvesting of microalgae by new microfluidic technology for particle separation.* Bioresour Technol *2016;**200**:360–365.*

reduce the surface drag force and maintain a uniform and ambient flow at velocity of 0.05–0.15 ms^{-1} and even greater than 0.20 ms^{-1}.[94] The drag force exhibited by these ridges is, however, greater than the gravitational forces hence not affected by the positioning of a living trilobite.[86] The terrace ridges are arranged so as to allow the liquid to flow past head first and rest of the body later. In the middle of the trilobite, the hole manages the collecting of the fluid at the collecting layer. The particles in the liquid which are greater than the gap between the terrace ridges get collected at the bottom of the trilobite field. Such trilobite LOC photo-bioreactor was specially designed for microalgae (green algae and diatom) *Rhodomonas baltica, Chaetoceros* sp. and *Thalassiosira weissflogii*. The LOC in a way sorted the cells according to their size. Though LOC proved difficult to sort diatom cells of *Thalassiosira*

weissflogii which caused clogging due to extra polysaccharides produced by them as compared to other microalgae.[93] However, few bacterial species may also interfere with the continuous harvesting of diatoms as they clog or flocculate with them[94] or sometime block by utilizing the extra polymer materials.[95] In such cases where bacterial species are present along with algae the Trilobite chips may not be useful. However, in cases where the cell size is small and there is no contamination (pure algal culture), the chance of regular harvesting without the recycling of nutrient media via these LOC Trilobite chips is viable. The group has also demonstrated that since the cells are regularly harvested, there is no need to clean the filter end as there is no dead end filtration required. Since the chip screens the under sized algae it is possible to harvest the under sized algae from the group of large sized algae for re-growth in the harvest chamber.

7.2 Microfluidic algal phobioreactors

The microalgae have been cultured for a variety of secondary metabolites which include lipids, pigments and drugs related to antiinflammatory and anticancerous treatments.[25] Even though initial cell culture is done in Petri plates and flasks the large-scale production of these metabolites require photo bioreactors. The purpose of which is to increase the biomass production for their potential applications. These photo bioreactors generally are customized as per the requirement but basically all are run using batteries whose life is not more than 5 years.[96] Moreover the process of extraction of the secondary metabolites from the microalgae requires regular feed of inoculums and nutrients.[97] Furthermore cross contamination and selective strain screening is the most faced challenge in large scale production of biomass from microalgae.[98] However, miniaturizing these photo bioreactors will avoid the initial screening and quality as well as yield of end products. The introduction of microfluidics in microalgae cell culture might be an answer for cell screening, optimizing the production of secondary metabolites and selection for high throughputs. Since microalgae are moving with stream, trapping them in order to study them at cell scale is a prerequisite. The cell trapping and microdevices to study the microalgae at cell scale are of three types: (1) mechanical traps; (2) microfluidic droplets; and (3) microchambers.[25] These traps have multi micropillars closely arranged of size less than that of the microalgae in C or U shape to allow the desired sized cells to pass and refrain others.[99] This has though been applied to trap *Botryococcus braunii; Chlamydomonas reinhardtii; Synechococcus elongatus; Chlorella sorokiniana; C. sorokiniana;* however, no study revealed trapping diatoms. The trapping via microfluidic droplets involve droplets in a continuous flow emulsion and those having electro wetting properties. Among these two, flow of droplets via emulsion reaches up to 1×10^6 min^{-1} whereas electro wetting depends upon dielectric properties of electrode.[100] However, microfluidic droplets via emulsion fail in long-term lipid accumulation.[101] These studies have been done on *Chlamydomonas reinhardtii* and *Chlorella vulgaris*; whereas electrowetting droplets were examined in diatom *Cyclotella cryptica*.[25] In this the size of electrowetting droplet varies from 10 to 70 μL, and droplets from the reservoir containing the medium or fluorescence dyes are divided and transported to the microalgal reservoir by changing the dielectric constant of the electrode. However, Wang et al.[102] generated an air bubble via syringe pump directed to a T junction. In third trapping method i.e., the microchambers the algal cells are cultured on a PDMS fabricated microfluidic device for the first time in *Tetraselmis chuii* and *Neochloris*

oleoabundans. The cells are sealed inside the chamber; however the permeability of PDMS allows easy exchange of gases. Furthermore, addition of BODIPY dye helps in monitoring the accumulation of lipids while still in the sealed microfluidic device. As per the choice microcolumns are fitted with an inlet and an outlet for maximum growth of microalgal cells. The highest growth rate was observed in *Chlamydomonas reinhardtii* where a single trap system was made having continuous supply of medium and 12:12 h of light and dark period with light of about 100 μmol m^2 s^{-1}.[105] However, it was observed that a deeper trap resulted in slow growth as large number of microalgal cells were in depths experiencing shaded areas. The study of single cell of diatoms captured in microdroplets showed much better results than in single cell traps. The microfluidic growth of microalgal cells specially the lipid rich diatoms may be very useful further to increase the lipid content by varying the chemical kinetics of the medium and by individually studying the division of cells. The microfluidic device culturing the microalgal cells including the diatoms can be further integrated to flow cytometer for selection and screening of the desired microlalgal or diatom strain. Such labs on chip device will in situ monitor the presence of lipid bodies, viability of cells and selection of strains of interest.[25]

7.3 Opto-microfluidics for cell screening

Much early in 2006, Hu and Davis developed a technique of automated image processing the diatom image.[103] This was done to collect the light scattered by the diatom cells exposed to laser light so as to designate them different shapes and sizes. In a microfluidic optical sensing of microalgal cells, the cells are illuminated with light emitting diode (LED) or laser light source. This may simultaneously involve staining the cells with fluorescence dye in order to detect the secondary metabolites like lipid and pigments.[101] A microfluidic optical set up generally involves a blue laser (470−490 nm) for illumination and a red laser (630−675 nm) for measuring the chlorophyll contents in the living microalgal cell culture. Holmes et al.[104] fabricated an optical set up where microalgae cells culture are illuminated by laser of 532 and 633 nm. This was compared with commercial cytometry intensity of fluorescence by these cells for identification of microalgae species. The pigments in the microalgae like chlorophyll and phycoery therin were identified at 660 and 575 nm. The elongated shape of diatom *Pseudo-nitzschia* showed the varying light scattering as it enters the different microchannels of a microfluidic chamber. However, an efficient optical system involves a slow uptake of liquid culture at the rate of about 10 μLmin^{-1} against that of 200 μLmin^{-1} and replacing lasers lights with LED and photomultiplier tubes (PMT) for illumination, to avoid big optical microfluidic set ups. Besides this, resistive pulse sensors (RPT) monitors cell number and size and detect the viable cells.[105] They also developed resonance frequencies (200−500 kHz) which helps in distinguishing living and dead cells.

7.4 Resonating microfluidic chamber to harvest diatoms

Use of resonance and ultrasonications has been a way of extraction techniques for oil and other secondary metabolites from diatom cells.[89b] We can reduce the cost of production for Diafuel[106] from these diatoms at affordable and cheap price. In our earlier work we showed that if instead of crushing or extracting diatoms, oil could be harvested so as to lower the cost

of production. Since diatoms have an automated mechanical strength of about 750 μN[4] laying pressure on them allows the oil to come out as it was seen in *Terpsinoë musica*.[89b]

Also earlier we designed a class of resonating microfluidic (MF) chambers for diatom containing different microchannels of various shape and sizes. The different patterns or designs on masks were prepared for the fabrications of silicon wafers in a microfluidic chamber of size 30 mm × 30 mm x 200 μm following Metal-Oxide-Semiconductor capacitor (MOSCAP) wet oxidation method[107] as seen in Fig. 5.9II. The microfluidic chamber was then microfabricated following a standard photolithography method on a chromium mask with wet etching of Si wafers in tetramethylammonium hydroxide (TMAH) solution checked using a Dekstat profilometer.

SEM micrographs of four different mask pattern code 1, 4, 5, and 6 as seen in Fig. 5.9II A−D on etched four different silicon wafer giving the clear view of the size and shape of cylindrical micropillars. The etched Si wafer was fixed to two PZT discs (diameter 10 mm and thickness 5 mm) on the back side by glue bond. The surface of one PZT disc was connected to a function generator and that to an oscilloscope[108] and as shown in Fig. 5.10A−B. The diatoms were injected from one inlet chamber to an area of microchannels of varying size and shape resonating and harvesting lipid on a chip device (Fig. 5.10C).

When the function generator delivered an adequate electrical wave at the fixed parameters (350 kHz and 500 mV), the fabricated micropillars resonated and generated mechanical pressure on the diatoms present in its chamber. It was seen that both *Nitzschia palea* and *Pinnularia borealis* behaved like *Terpsinoë musica* when put under mechanical stress and produced oil

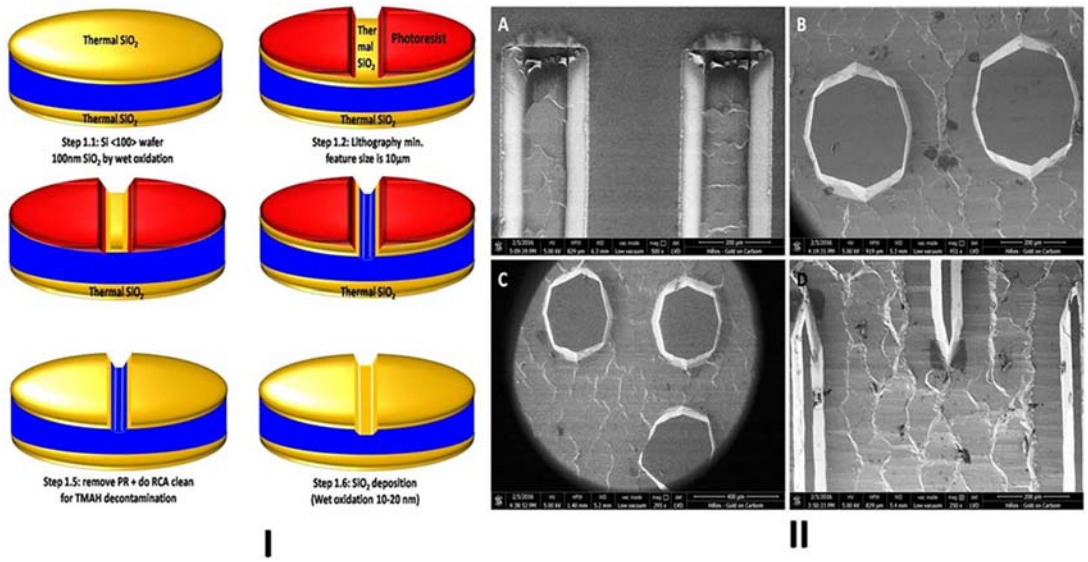

FIGURE 5.9 (I) MOSCAP (metal oxide semiconductor capacitor) fabrication of resonating microfluidic (MF) chamber for biofuel production; (II) Scanning electron micrographs of microchannels consisting of microwalls (A) masks code-1 (B) cylindrical micropillars masks code-4, (C) Mask code-5 and (D) Mask code −6.

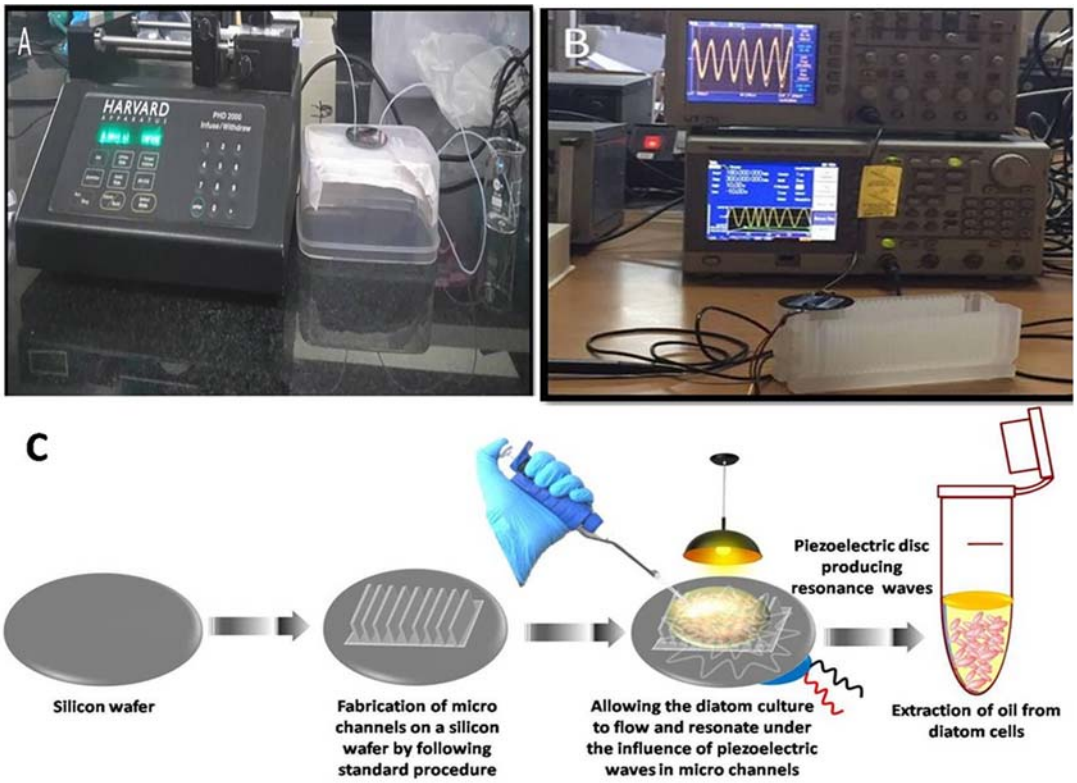

FIGURE 5.10 Image (A) showing injection of diatoms via syringe pump at the rate of 10 μL min^{-1} which allows about 5×10^5 cells min^{-1} to enter the resonating chamber, (B) showing a resonating device further attached with piezoelectric (PZT) disc at its opposite ends. The device was connected to a function generator and oscilloscope. *Reproduced with permission from Vinayak V, Kumar V, Kashyap M, Joshi KB, Gordon R, Schoefs B. In* Fabrication of resonating microfluidic chamber for biofuel production in diatoms (Resonating device for biofuel production), 2016 3rd international conference on emerging electronics (ICEE), IEEE: *2016; pp. 1–6 and (C) Schematic representation of Resonating microfluidic chamber.*

without itself undergoing lyses. The device with same diatom inoculums injected on to it was run for different time periods (5, 10, 20, 30, 40 min).

Since the requirement of diatom solar panels is to let the diatoms ooze lipid without letting them lose their viability therefore, the selection of the design will depend upon maximum cell viability and also high efficiency in terms of lipid oozed and collected in the supernatant after resonance in the device. It is obvious that the pellet has more cells and compared to that in the supernatant this might be the reason why most of the pellet samples had high amounts of lipid percentage in the pellet.

In our experiment we used a resonating devise to mechanically harvest oil without sacrificing the cells completely. The devices from designs **1**, **4** and **5** in which *Pinnularia borealis* was used showed overall higher lipid dry weight percentage in the pellet as compared to the lipid %age from the supernatant for same sample. However, *Pinnularia borealis* in design

1 showed highest lipid content in the supernatant (1.76%) in comparison to that in the pellet (0.58%) and cell viability up to 50.51% at 40 min of continuous resonance frequency of 350 kHz in the MF chamber. On the other hand in design **4** for the same culture sample (*Pinnularia borealis*) for the same duration of time (40 min), the amount of lipid content in the supernatant was 1.75% in comparison to that in the pellet 0.49% with cell viability reaching up to 45.36%. Further MF device **5** for *Pinnularia borealis* didn't show efficient lipid harvesting from the supernatant as it is seen that it took just 10 min for oil to come out fast from the cells but the difference of biofuel percentage was low (0.23%) as compared to two samples from design **1** and design **4,** respectively thus lowering the efficiency to 15.46%. A similar reduced viability of cells was observed for design **6** for same culture sample with no increase in lipid harvested from the diatom cells. A similar experiment was conducted using *Nitzschia palea*, tested for design **4** and **6** only. The results regarding cell viability were coherent with that of *Pinnularia borealis* and it was observed that design **4** showed maximum cell viability with maximum lipid harvested at 30 min for design **4** whereas design **6** showed no harvesting of lipid and poor cell viability. Further the efficiency of microchannels fabricated in the silica wafer was checked. Here we had proposed a quantity "Micro channel Efficiency" (M.E) to compare the oozing of lipid by different microchannels in the MF chamber at different time durations. The microchannel efficiency of device was calculated only for these diatoms as they maintained the cell integrity, easy to culture and show moderate visible lipid content under microscope. The microchannel efficiency was calculated by using the following hypothetical formula:

$$\textit{Microchannel efficiency} = \frac{\textit{Lipid content of supernantant}}{\textit{Lipid content of pellet}} \times \frac{\textit{Cell integrity}}{\textit{Times in minutes}}$$

$$\textit{Cell integrity} = \frac{\textit{Sample cell count}}{\textit{Mother culture cell count}} \times 100$$

Table 5.1 shows "Microchannel Efficiency" calculated for those mask patterns in MF chambers/devices in which the cell viability was found to be high.

TABLE 5.1 Comparative "micro channel efficiency" in *Pinnularia borealis* and *Nitzschia palea* using different MF devices.

Sample with diatom	Time (min)	Micro channel efficiency %
Mask 1 (*Pinnularia borealis*)	40	3.83
Mask 4 (*Pinnularia borealis*)	40	4.05
Mask 5 (*Pinnularia borealis*)	10	1.9
Mask 4 (*Nitzschia palea*)	30	6.01
Mask 6 (*Nitzschia palea*)	30	5.72

Reproduced with permission from Vinayak V, Kumar V, Kashyap M, Joshi KB, Gordon R, Schoefs B. In Fabrication of resonating microfluidic chamber for biofuel production in diatoms (Resonating device for biofuel production), 2016 3rd international conference on emerging electronics (ICEE), IEEE: *2016; pp. 1–6.*

It is evident from the "Microchannel Efficiency" Table 5.1 that design **4** is the best design showing M.E of 4.05% when resonated at the standardized parameters for a time period of 40 min. The resonance and the voltage applied together create a mechanical pressure appropriate for diatoms to milk lipid with the least cell sacrifice. The "Microchannel Efficiency" from samples of different designs gives us an idea of relative lipid content with respect to time using the resonating device fabricated from different masks. The resonating microfluidic device is characteristic as not only it harvests the lipid from diatoms without killing it but also is economical a facile template for diatom solar panels.[1] They can be simulated to a large prototype at industrial level for production of diafuel at commercial scale so as to meet the increasing energy demand.

Yuan et al.,[110] fabricated a microfluidic device fixed with PZT disc, function generator, and oscilloscope to trap microalgae and diatom in order to do live water monitoring. The LOC device is economical like MF device fabricated by[109] but here instead to harvest oil from diatoms it traps the algae and diatoms (Fig. 5.11). The microfluidic channel on the LOC was fabricated to form a standing wave and a reflector thickness as recommended by Lund et al.[111] so as to trap the particle. The PZT device having resonance frequency of 8.58 MHz is used to give a sound velocity of 1475 ms^{-1} in water. The channel of dimensions 2700 × 800 × 85 μm with PZT disc of size 800 × 800 μm was fixed on the trapping site. A glass substrate has been used for the trapping device, and syringe pumps are fitted for injecting the sample at speed of 0.5 $\mu Lmin^{-1}$ to 2.7 $\mu Lmin^{-1}$ and 0.5 $\mu Lmin^{-1}$ to 4 $\mu Lmin^{-1}$ for both *Chlorella* and diatoms, respectively, as per the protocol of Yuan et al.[110]

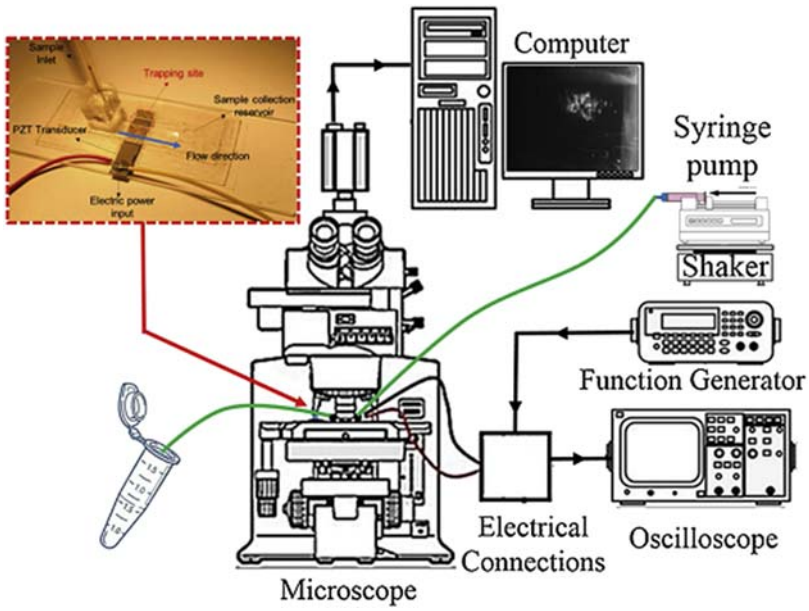

FIGURE 5.11 Experimental setup constructed for experimental measurements and device characterization. *Reproduced with permissions from Yuan Q, Mirzajani H, Evans B, Greenbaum E, Wu J. A disposable bulk-acoustic-wave microalga trapping device for real-time water monitoring*. Sensor Actuator B Chem *2020;**304**:127388.*

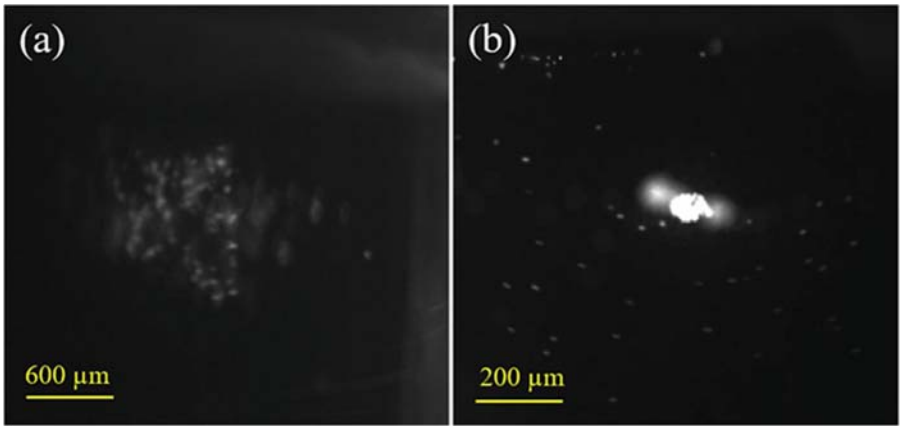

FIGURE 5.12 Diatom and chlorella trapping area, (A) Trapping area of diatom and (B) Trapping area of chlorella. *Reproduced with permissions from Yuan Q, Mirzajani H, Evans B, Greenbaum E, Wu J. A disposable bulk-acoustic-wave microalga trapping device for real-time water monitoring.* Sensor Actuator B Chem *2020;**304**:127388.*

Two different experiments were set up for green algae Chlorella and diatom (*Thallosiosira* sp.), and it was seen that when the algae and diatom reach the center reservoir where PZT is fixed only few escape the trapping area (Fig. 5.12). It was observed that immediately after AC signal was turned on, *Chlorella* cells immediately move to the trapping region and are trapped. However, diatom cells start swirling and form clusters which increase in size reaching 275 × 168 μm in 60 s. This is due to the chitin fibrils low fluorescence polysaccharides in diatoms which act as spacers to keep them apart. Since Chlorella does not have chitin they exhibit high fluorescence intensity and gets concentrated in the trapping site occupying an area of 44 × 100 μm. The particle trapping efficiency for Chlorella was 82%−74% whereas for diatom *Thallosiosira* sp. it was 85%−79%. Also importantly due to gravity different particles stay at different heights in the trapping area. It was found that vertical trapping position was 28 μm from bottom for Chlorella and 34 μm that for diatom. This certainly establishes that diatoms are at higher position than Chlorella. Thus, this device could trap different sized particles at different heights and can screen at real time the quality of water yet being economical and disposable.

8. Integrated hypothesis

Earlier we had shown that the diatom cells doped with magnetite nanoparticles helps in easy separation of oil which could be harvested in diatom solar panel.[112] If in a PDMS and glass fabricated LOC such magnetite doped diatom strike the walls of serpentine micropillars in microfluidic device it may ooze oil under the influence of solenoid magnet. The serpentine microfluidic device further integrated with yellow and red filters to measure the changes in chlorophyll via autofluorescence could be one such LOC which will monitor not only diatom screening for lipid production, but also initialize its easy harvest and separation. An integrated microfluidic device which enables to measure the auto fluorescence of chlorophyll

in the cells helps in screening different diatom strains for their chlorophyll and phycoerythrin content at 488 nm, 575 nm, 532 nm and 660 nm. This further allows for checking the cell viability thus keeping a check on the dead and living cells. The LOC device can be kept between two copper electrodes to separate strains with different lipid content by dielectrophoresis.[113] As the magnetite doped diatoms strike the micropillar designed in serpentine microfluidic device; the mechanical pressure exerted on the walls of micropillars allows the oil to come out which gets collected in the reservoir tank. The device may be a one closed chip miniature prototype for a future industrial level photobioreactor which would not require continuous nutrient feed and, diafuel (biofuel from diatoms) may be harvested continuously at low cost. The integrated microfluidic device will resonate due to a pulsed magnetic field (PMF) involving three major process as follows:

i. The serpentine channels in the device allows the measurement of chlorophyll in the diatoms to show autofluorescence while crossing the red and yellow filters in optomicrofluidic system.
ii. The resonance frequency in the system alters the dielectric properties of cytoplasm and lipid allowing only lipid rich diatoms to follow a hydrodynamic stream under the influence of negative dielectrophoresis.
iii. The magnetite doped diatom cells help in clean separation of oil; as the cells move out under the influence of PMF. Since PDMS is a hydrophobic and lipophilic it allows the oil to get absorbed repelling water in the media. Recently, we proved this by fabricated a low cost Luffa TiO_2 doped PDMS nanosponge to absorb oil.[114] The clean oil thus moves out of the device across the polydimethylsiloxane (PDMS) nano sponge layer on the top of the reservoir and is collected separately as seen in Fig. 5.13.

The microfluidic LOC device is projected to be: cheap, made up of glass and low cost Luffa TiO_2 _PDMS nanosponge, closed, fully automated and fast.

The technology may require zero energy input and with intact cell viability at almost zero nutrients can be fed at intervals of approximate 60 days. Since the system is further closed and integrated with filters to check dead cells and contamination; the two PDMS layer permits gaseous exchange and oil adsorption of lipid rich strains via dielectrophoresis as shown in Fig. 5.13. The self-automated system will pave the way toward the development of easy-to-use and plug-and-play technologies based on microfluidics, cell perfusion and resonance frequency generated by pulse magnetic fields in one integrated LOC device.

9. Conclusion

The integrated microfluidic device to harvest value added from diatoms involves living microalgal cells with frugal requirements of nutrients and absolutely no requirement of feeding new cell inoculums.[86] The closed bio-microfluidic system biomimics nature way of making crude oil from microalgal cells which does not requires any external feed of nutrients or new cells; nor cells are crushed, extracted,[85] electroporated,[15] ultrasonicated, etc., for crude oil.[86] Cells would be multiplying continuously whereas the dead cells would serve as the nutrient requirement for the new ones. We therefore propose a microfluidic device which

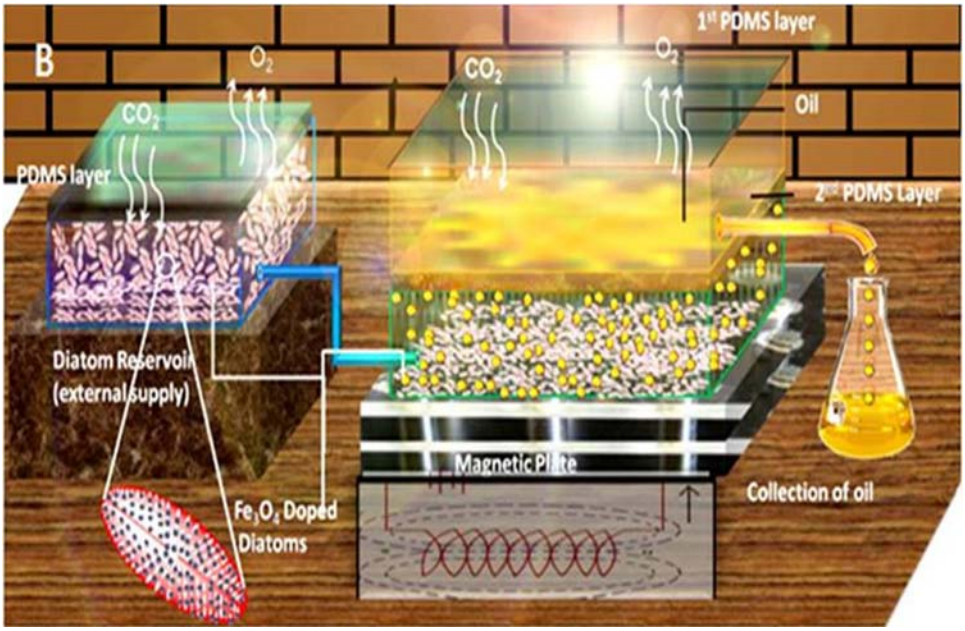

FIGURE 5.13 Schematic sketch of integrated microfluidic device for live cell perfusion system for biofuel production in the presence of light.

will keep a check on dead cells, bacterial contamination allowing only lipid rich diatoms to grow and multiply maintaining their living state. The technology aims for optofluidics to upscale sun based fuel generation and its separation from living microalgal cells.[86] Diatoms like other microalgae also produce variety of high value metabolites especially fucoxanthin besides producing oil. Since harvesting diatoms for its high value and low value metabolites is a big challenge economically due to its small size and thick silica wall. However, for large-scale production of byproducts from microalgal cultures their is increase in its cost of production.[92,115] Even though a substantial work is done with regard to diatoms in microfluidics and as nanomaterials, still much need to explore easy diatom culture and its harvesting for secondary metabolites in situ at facile and economic techniques.

10. Conflict of interest

Authors declare no conflict of interest.

Acknowledgments

MJK thank DST-Nanomission, Government of India. Dr. Vikas Kumar is acknowledged for the art work used wherever necessary. This work is supported by DST-Nanomission, Government of India Project No. SR/NM/NT-1090/2014(G), CEFIPRA Indo French project PPMB 7133/2020, and INUP IIT Bombay project no. Pid: P989423752/2016 to VV (Principal Investigator) and KBJ.

References

1. Ramachandra TV, Mahapatra DM, B K, Gordon R. Milking diatoms for sustainable energy: biochemical engineering versus gasoline-secreting diatom solar panels. *Ind Eng Chem Res* 2009;**48**(19):8769–88.
2. Round FE, Crawford RM, Mann DG. *Diatoms: biology and morphology of the genera*. Cambridge university press; 2007.
3. Srinivasarao M. Nano-optics in the biological world: beetles, butterflies, birds, and moths. *Chem Rev* 1999;**99**(7):1935–62.
4. Hamm CE, Merkel R, Springer O, Jurkojc P, Maier C, Prechtel K, Smetacek V. Architecture and material properties of diatom shells provide effective mechanical protection. *Nature* 2003;**421**(6925):841–3.
5. Wang Y, Zhang D, Cai J, Pan J, Chen M, Li A, Jiang Y. Biosilica structures obtained from Nitzschia, Ditylum, Skeletonema, and Coscinodiscus diatom by a filtration-aided acid cleaning method. *Appl Microbiol Biotechnol* 2012;**95**(5):1165–78.
6. (a) Jeffryes C, Campbell J, Li H, Jiao J, Rorrer G. The potential of diatom nanobiotechnology for applications in solar cells, batteries, and electroluminescent devices. *Energy Environ Sci* 2011;**4**(10):3930–41;
   (b) Qin T, Gutu T, Jiao J, Chang C-h, Rorrer GL. Biological Fabrication of Photoluminescent Nanocomb Structures by Metabolic Incorporation of Germanium into the Biosilica of the Diatom Nitzschia frustulum. *ACS Nano* 2008;**2**(6):1296–304.
7. Goren R, Baykara T, Marsoglu M. A study on the purification of diatomite in hydrochloric acid. *Scand J Metall* 2002;**31**:115–9.
8. Lichtman MA. Alfred nobel and his prizes: from dynamite to DNA. *Rambam Maimonides Med J* 2017;**8**(3):e0035.
9. Khan MJ, Rai A, Ahirwar A, Sirotiya V, Mourya M, Mishra S, et al. Diatom microalgae as smart nanocontainers for biosensing wastewater pollutants: recent trends and innovations. *Bioengineered* 2021;**12**(2):9531–49.
10. (a) De Stefano L, Rendina I, De Stefano M, Bismuto A, Maddalena P. Marine diatoms as optical chemical sensors. *App Phy Lett* 2005;**87**:233902;
    (b) Stefano LD, Rea I, Rendina I, Stefano MD, Moretti L. Lensless light focusing with the centric marine diatom Coscinodiscus walesii. *Opt Express* 2007;**15**(26):18082–8.
11. (a) Gordon R, Losic D, Tiffany MA, Nagy SS, Sterrenburg FA. The Glass Menagerie: diatoms for novel applications in nanotechnology. *Trends Biotechnol* 2009;**27**(2):116–27;
    (b) Yang W, Lopez PJ, Rosengarten G. Diatoms: Self assembled silica nanostructures, and templates for bio/chemical sensors and biomimetic membranes. *Analyst* 2011;**136**(1):42–53.
12. Zong S, Wang Z, Chen H, Yang J, Cui Y. Surface Enhanced Raman Scattering Traceable and Glutathione Responsive Nanocarrier for the Intracellular Drug Delivery. *Anal Chem* 2013;**85**(4):2223–30.
13. Nassif N, Livage J. From diatoms to silica-based biohybrids. *Chem Soc Rev* 2011;**40**(2):849–59.
14. Halldorsson S, Lucumi E, Gomez-Sjoberg R, Fleming RMT. Advantages and challenges of microfluidic cell culture in polydimethylsiloxane devices. *Biosens Bioelectron* 2015;**63**:218–31.
15. Kang S, Kim K-H, Kim Y-C. A novel electroporation system for efficient molecular delivery into Chlamydomonas reinhardtii with a 3-dimensional microelectrode. *Sci Rep* 2015;**5**(1):15835.
16. Cai J, Pan J, Chen M, Wang Y, Zhang D. Culturing and Bonding of Diatom on a Microfluidic Chip for Biosensing Application. *Appl Mech Mater* 2013;**461**:809–13.
17. (a) Archibald JM. The puzzle of plastid evolution. *Curr Biol* 2009;**19**(2):R81–8;
    (b) Kang S, Kim K-H, Kim Y-C. A novel electroporation system for efficient molecular delivery into Chlamydomonas reinhardtii with a 3-dimensional microelectrode. *Sci Rep* 2015;**5**:15835.
18. Jang JH, Rives CB, Shea LD. Plasmid delivery in vivo from porous tissue-engineering scaffolds: transgene expression and cellular transfection. *Mol Ther: J American Soc Gene Therapy* 2005;**12**(3):475–83.
19. Mansouri S, Cuie Y, Winnik F, Shi Q, Lavigne P, Benderdour M, Beaumont E, Fernandes JC. Characterization of folate-chitosan-DNA nanoparticles for gene therapy. *Biomaterials* 2006;**27**(9):2060–5.
20. Wang C-H, Lee Y-H, Kuo H-T, Liang W-F, Li W-J, Lee G-B. Dielectrophoretically-assisted electroporation using light-activated virtual microelectrodes for multiple DNA transfection. *Lab Chip* 2014;**14**(3):592–601.
21. (a) Mahmoodi Chalbatani G, Dana H, Gharagouzloo E, Grijalvo S, Eritja R, Logsdon CD, Memari F, Miri SR, Rad MR, Marmari V. Small interfering RNAs (siRNAs) in cancer therapy: a nano-based approach. *Int J Nanomedicine* 2019;**14**:3111–28;
    (b) Lee SJ, Huh MS, Lee SY, Min S, Lee S, Koo H, Chu JU, Lee KE, Jeon H, Choi Y, Choi K, Byun Y, Jeong SY,

Park K, Kim K, Kwon IC. Tumor-homing poly-siRNA/glycol chitosan self-cross-linked nanoparticles for systemic siRNA delivery in cancer treatment. *Angew Chem* 2012;**51**(29):7203–7.
22. (a) Lee CH, Kim JH, Lee HJ, Jeon K, Lim H, Choi H, Lee ER, Park SH, Park JY, Hong S, Kim S, Cho SG. The generation of iPS cells using non-viral magnetic nanoparticle based transfection. *Biomaterials* 2011;**32**(28):6683–91;
(b) Okita K, Nakagawa M, Hyenjong H, Ichisaka T, Yamanaka S. Generation of mouse induced pluripotent stem cells without viral vectors. *Science* 2008;**322**(5903):949–53.
23. (a) Daboussi F, Leduc S, Maréchal A, Dubois G, Guyot V, Perez-Michaut C, Amato A, Falciatore A, Juillerat A, Beurdeley M. Genome engineering empowers the diatom Phaeodactylum tricornutum for biotechnology. *Nat Commun* 2014;**5**(1):1–7;
(b) Huang W, Daboussi F. Genetic and metabolic engineering in diatoms. *Philos Trans R Soc Lond B Biol Sci* 2017;**372**(1728):20160411.
24. Diner RE, Bielinski VA, Dupont CL, Allen AE, Weyman PD. Refinement of the Diatom Episome Maintenance Sequence and Improvement of Conjugation-Based DNA Delivery Methods. *Front Bioeng Biotechnol* 2016;**4**:65.
25. Bodénès P, Wang H-Y, Lee T-H, Chen H-Y, Wang C-Y. Microfluidic techniques for enhancing biofuel and biorefinery industry based on microalgae. *Biotechnol Biofuels* 2019;**12**(1):33.
26. (a) Choi SO, Kim YC, Lee JW, Park JH, Prausnitz MR, Allen MG. Intracellular protein delivery and gene transfection by electroporation using a microneedle electrode array. *Small* 2012;**8**(7):1081–91;
(b) Jeon K, Suresh A, Kim Y-C. Highly efficient molecular delivery into Chlamydomonas reinhardtii by electroporation. *Kor J Chem Eng* 2013;**30**(8):1626–30.
27. (a) Day A, Debuchy R, van Dillewijn J, Purton S, Rochaix J-D. Studies on the maintenance and expression of cloned DNA fragments in the nuclear genome of the green alga Chlamydomonas Reinhardtii. *Physiol Plantarum* 1990;**78**(2):254–60;
(b) Kindle KL, Schnell RA, Fernandez E, Lefebvre PA. Stable nuclear transformation of Chlamydomonas using the Chlamydomonas gene for nitrate reductase. *J Cell Biol* 1989;**109**(6 Pt 1):2589–601.
28. Karimi M, Inze D, Depicker A. GATEWAY vectors for Agrobacterium-mediated plant transformation. *Trends Plant Sci* 2002;**7**(5):193–5.
29. Geng T, Lu C. Microfluidic electroporation for cellular analysis and delivery. *Lab Chip* 2013;**13**(19):3803–21.
30. (a) Lee WG, Demirci U, Khademhosseini A. Microscale electroporation: challenges and perspectives for clinical applications. *Integr Biol (Camb)* 2009;**1**(3):242–51;
(b) Kim JA, Cho K, Shin MS, Lee WG, Jung N, Chung C, Chang JK. A novel electroporation method using a capillary and wire-type electrode. *Biosens Bioelectron* 2008;**23**(9):1353–60.
31. Luo D, Saltzman WM. Synthetic DNA delivery systems. *Nat Biotechnol* 2000;**18**(1):33–7.
32. (a) Huang Y-H, Shih Y-J, Cheng F-J. Novel KMnO4-modified iron oxide for effective arsenite removal. *J Hazard Mater* 2011;**198**:1–6;
(b) Adamo A, Arione A, Sharei A, Jensen KF. Flow-Through Comb Electroporation Device for Delivery of Macromolecules. *Anal Chem* 2013;**85**(3):1637–41.
33. Chisti Y. Biodiesel from microalgae. *Biotechnol Adv* 2007;**25**(3):294–306.
34. Azencott HR, Peter GF, Prausnitz MR. Influence of the cell wall on intracellular delivery to algal cells by electroporation and sonication. *Ultrasound Med Biol* 2007;**33**(11):1805–17.
35. (a) Kim JA, Cho K, Shin MS, Lee WG, Jung N, Chung C, Chang JK. A novel electroporation method using a capillary and wire-type electrode. *Biosens Bioelectron* 2008;**23**(9):1353–60;
(b) Kim J, Ryu B-G, Kim B-K, Han J-I, Yang J-W. Continuous microalgae recovery using electrolysis with polarity exchange. *Bioresour Technol* 2012;**111**:268–75.
36. Kadono T, Tomaru Y, Suzuki K, Yamada K, Adachi M. The possibility of using marine diatom-infecting viral promoters for the engineering of marine diatoms. *Plant Sci* 2020:110475.
37. Gautam S, Kashyap M, Gupta S, Kumar V, Schoefs B, Gordon R, Jeffryes C, Joshi KB, Vinayak V. Metabolic engineering of tio 2 nanoparticles in nitzschia palea to form diatom nanotubes: an ingredient for solar cells to produce electricity and biofuel. *RSC Adv* 2016;**6**(99):97276–84.
38. Gupta S, Kashyap M, Kumar V, Jain P, Vinayak V, Joshi KB. Peptide mediated facile fabrication of silver nanoparticles over living diatom surface and its application. *J Mol Liq* 2018;**249**:600–8.
39. (a) Singh R, Kumar Mishra N, Kumar V, Vinayak V, Ballabh Joshi K. Transition metal ion–mediated tyrosine-based short-peptide amphiphile nanostructures inhibit bacterial growth. *Chembiochem* 2018;**19**(15):1630–7;

(b) Singh R, Khan MJ, Rane J, Gajbhiye A, Vinayak V, Joshi KB. Biofabrication of diatom surface by tyrosine-metal complexes: smart microcontainers to inhibit bacterial growth. *ChemistrySelect* 2020;**5**(10):3091–7;
(c) Singh R, Suryavashi V, Vinayak V, Joshi KB. Gold-ions-mediated diproline peptide nanocarpets and their inhibition of bacterial growth. *ChemistrySelect* 2019;**4**(19):5810–6.
40. Gautam S, Pandey LK, Vinayak V, Arya A. Morphological and physiological alterations in the diatom Gomphonema pseudoaugur due to heavy metal stress. *Ecol Indicat* 2017;**72**:67–76.
41. Ahirwar A, Gupta S, Kashyap M, Shukla P, Vinayak V. Differential cell viability in Nitzschia palea on exposure to different organic and inorganic environmental effluents. *Int J Environ Sci Technol* 2020;**17**(1):493–504.
42. Losic D, Rosengarten G, Mitchell J, Voelcker N. Pore Architecture of diatom frustules: potential nanostructured membranes for molecular and particle separations. *J Nanosci Nanotechnol* 2006;**6**:982–9.
43. Matthias S, Müller F. Asymmetric pores in a silicon membrane acting as massively parallel brownian ratchets. *Nature* 2003;**424**(6944):53–7.
44. Peterson DS. Solid supports for micro analytical systems. *Lab Chip* 2005;**5**(2):132–9.
45. Losic D, Mitchell JG, Voelcker NH. Diatomaceous lessons in nanotechnology and advanced materials. *Adv Mater* 2009;**21**(29):2947–58.
46. Cai J, Chen M, Wang Y, Pan J, Li A, Zhang D. Culture and motion analysis of diatom bacillaria paradoxa on a microfluidic platform. *Curr Microbiol* 2013;**67**(6):652–8.
47. Huh D, Torisawa YS, Hamilton GA, Kim HJ, Ingber DE. Microengineered physiological biomimicry: organs-on-chips. *Lab Chip* 2012;**12**(12):2156–64.
48. Kapinga M, Gordon R. Cell attachment in the motile colonial diatom Bacillaria paxillifer. *Diatom Res* 1992;**7**:215–20.
49. Kapinga M, Gordon R. Cell motility rhythms in bacillaria paxillifer. *Diatom Res* 1992;**7**:221–5.
50. Cai J, Pan JF, Chen ML, Wang Y, Zhang DY. *In culturing and bonding of diatom on a microfluidic chip for biosensing application, applied mechanics and materials, trans tech publ*. 2014. p. 809–13.
51. Acres RG, Ellis AV, Alvino J, Lenahan CE, Khodakov DA, Metha GF, Andersson GG. Molecular structure of 3-aminopropyltriethoxysilane layers formed on silanol-terminated silicon surfaces. *J Phys Chem C* 2012;**116**(10):6289–97.
52. (a) Li X, Ballerini DR, Shen W. A perspective on paper-based microfluidics: current status and future trends. *Biomicrofluidics* 2012;**6**(1):011301;
(b) Fu E, Downs C. Progress in the development and integration of fluid flow control tools in paper microfluidics. *Lab Chip* 2017;**17**(4):614–28.
53. Martinez AW, Phillips ST, Butte MJ, Whitesides GM. Patterned paper as a platform for inexpensive, low-volume, portable bioassays. *Angew Chem Int Ed* 2007;**46**(8):1318–20.
54. (a) Carrilho E, Martinez AW, Whitesides GM. Understanding wax printing: a simple micropatterning process for paper-based microfluidics. *Anal Chem* 2009;**81**(16):7091–5;
(b) Martinez AW, Phillips ST, Carrilho E, Thomas SW, Sindi H, Whitesides GM. Simple telemedicine for developing regions: camera phones and paper-based microfluidic devices for real-time, off-site diagnosis. *Anal Chem* 2008;**80**(10):3699–707;
(c) Nie Z, Deiss F, Liu X, Akbulut O, Whitesides GM. Integration of paper-based microfluidic devices with commercial electrochemical readers. *Lab Chip* 2010;**10**(22):3163–9;
(d) Nie Z, Nijhuis CA, Gong J, Chen X, Kumachev A, Martinez AW, Narovlyansky M, Whitesides GM. Electrochemical sensing in paper-based microfluidic devices. *Lab Chip* 2010;**10**(4):477–83.
55. Xu C, Liu Y, Su F, Liu A, Qiu H. Nanoporous PtAg and PtCu alloys with hollow ligaments for enhanced electrocatalysis and glucose biosensing. *Biosens Bioelectron* 2011;**27**(1):160–6.
56. Moon JH, McDaniel W, Hancock LF. Facile fabrication of poly(p-phenylene ethynylene)/colloidal silica composite for nucleic acid detection. *J Colloid Interface Sci* 2006;**300**(1):117–22.
57. Yang H, Zhu Y. Size dependence of SiO2 particles enhanced glucose biosensor. *Talanta* 2006;**68**(3):569–74.
58. Zhen L, Ford N, Gale DK, Roesijadi G, Rorrer GL. Photoluminescence detection of 2,4,6-trinitrotoluene (TNT) binding on diatom frustule biosilica functionalized with an anti-TNT monoclonal antibody fragment. *Biosens Bioelectron* 2016;**79**:742–8.
59. De Stefano L, Rotiroti L, De Stefano M, Lamberti A, Lettieri S, Setaro A, Maddalena P. Marine diatoms as optical biosensors. *Biosens Bioelectron* 2009;**24**(6):1580–4.

60. Kong X, Chong X, Squire K, Wang AX. Microfluidic diatomite analytical devices for illicit drug sensing with ppb-level sensitivity. *Sensor Actuator B Chem* 2018;**259**:587–95.
61. Degenhardt L, Chiu W-T, Sampson N, Kessler RC, Anthony JC, Angermeyer M, Bruffaerts R, De Girolamo G, Gureje O, Huang Y. Toward a global view of alcohol, tobacco, cannabis, and cocaine use: findings from the WHO World Mental Health Surveys. *PLoS Med* 2008;**5**(7).
62. Brunetto MR, Cayama YD, García LG, Gallignani M, Obando MA. Determination of cocaine and benzoylecgonine by direct injection of human urine into a column-switching liquid chromatography system with diode-array detection. *J Pharmaceut Biomed Anal* 2005;**37**(1):115–20.
63. Aizenberg J, Rogers JA, Paul KE, Whitesides GM. Imaging profiles of light intensity in the near field: applications to phase-shift photolithography. *Appl Opt* 1998;**37**(11):2145–52.
64. Huth M, Porrati F, Gruszka P, Barth S. Temperature-dependent growth characteristics of Nb-and CoFe-based nanostructures by direct-write using focused electron beam-induced deposition. *Micromachines* 2020;**11**(1):28.
65. Li W, van Baren J, Berges A, Bekyarova E, Lui CH, Bardeen CJ. Shaping organic microcrystals using focused ion beam milling. *Cryst Growth Des* 2020;**20**(3):1583–9.
66. Mahajan S, Sharkins JA, Hunter AH, Avishai A, Ereifej ES. Focused ion beam lithography to etch nano-architectures into microelectrodes. *JoVE* 2020;(155):e60004.
67. Barbero DR, Saifullah MS, Hoffmann P, Mathieu HJ, Anderson D, Jones GA, Welland ME, Steiner U. High-resolution nanoimprinting with a robust and reusable polymer mold. *Adv Funct Mater* 2007;**17**(14):2419–25.
68. Wilbur JL, Jackman RJ, Whitesides GM, Cheung EL, Lee LK, Prentiss MG. Elastomeric optics. *Chem Mater* 1996;**8**(7):1380–5.
69. Xia Y, McClelland JJ, Gupta R, Qin D, Zhao X-M, Sohn LL, Celotta RJ, Whitesides GM. Replica molding using polymeric materials: a practical step toward nanomanufacturing. *Adv Mater* 1997;**9**(2):147–9.
70. McDonald JC, Whitesides GM. Poly(dimethylsiloxane) as a material for fabricating microfluidic devices. *Acc Chem Res* 2002;**35**(7):491–9.
71. Losic D, Mitchell JG, Lal R, Voelcker NH. Rapid fabrication of micro- and nanoscale patterns by replica molding from diatom biosilica. *Adv Funct Mater* 2007;**17**(14):2439–46.
72. Hlúbiková D, Luís A, Vaché V, Ector L, Hoffmann L, Choquet P. Optimization of the replica molding process of PDMS using pennate diatoms. *J Micromech Microeng* 2012;**22**(11):115019.
73. Pérez-Cabero M, Puchol V, Beltran D, Amoros P. Thalassiosira pseudonana diatom as biotemplate to produce a macroporous ordered carbon-rich material. *Carbon* 2008;**46**(2):297–304.
74. Li K, Liu X, Zheng T, Jiang D, Zhou Z, Liu C, Zhang X, Zhang Y, Losic D. Tuning MnO2 to FeOOH replicas with bio-template 3D morphology as electrodes for high performance asymmetric supercapacitors. *Chem Eng J* 2019;**370**:136–47.
75. Van Eynde E, Tytgat T, Smits M, Verbruggen SW, Hauchecorne B, Lenaerts S. Biotemplated diatom silica–titania materials for air purification. *Photochem Photobiol Sci* 2013;**12**(4):690–5.
76. Wlodkowic D, Faley S, Skommer J, McGuinness D, Cooper JM. Biological Implications of Polymeric Microdevices for Live Cell Assays. *Anal Chem* 2009;**81**(23):9828–33.
77. Mehta G, Mehta K, Sud D, Song JW, Bersano-Begey T, Futai N, Heo YS, Mycek M-A, Linderman JJ, Takayama S. Quantitative measurement and control of oxygen levels in microfluidic poly(dimethylsiloxane) bioreactors during cell culture. *Biomed Microdevices* 2007;**9**(2):123–34.
78. Meyvantsson I, Beebe DJ. Cell culture models in microfluidic systems. *Annu Rev Anal Chem* 2008;**1**(1):423–49.
79. Liu Q, Wu C, Cai H, Hu N, Zhou J, Wang P. Cell-based biosensors and their application in biomedicine. *Chem Rev* 2014;**114**(12):6423–61.
80. Grossmann G, Guo W-J, Ehrhardt DW, Frommer WB, Sit RV, Quake SR, Meier M. The RootChip: an integrated microfluidic chip for plant science. *Plant Cell* 2011;**23**(12):4234.
81. Wang M, Thanou M. Targeting nanoparticles to cancer. *Pharmacol Res* 2010;**62**(2):90–9.
82. Yang L, Li L, Tu Q, Ren L, Zhang Y, Wang X, Zhang Z, Liu W, Xin L, Wang J. Photocatalyzed surface modification of poly(dimethylsiloxane) with polysaccharides and assay of their protein adsorption and cytocompatibility. *Anal Chem* 2010;**82**(15):6430–9.
83. (a) Yin H, Marshall D. Microfluidics for single cell analysis. *Curr Opin Biotechnol* 2012;**23**(1):110–9;
(b) Lindström S, Andersson-Svahn H. Overview of single-cell analyses: microdevices and applications. *Lab Chip* 2010;**10**(24):3363–72;
(c) Lecault V, White AK, Singhal A, Hansen CL. Microfluidic single cell analysis: from promise to practice. *Curr*

Opin Chem Biol 2012;**16**(3-4):381–90;
(d) Teh S-Y, Lin R, Hung L-H, Lee AP. Droplet microfluidics. *Lab Chip* 2008;**8**(2):198–220;
(e) Lagus TP, Edd JF. A review of the theory, methods and recent applications of high-throughput single-cell droplet microfluidics. *J Phys Appl Phys* 2013;**46**(11):114005;
(f) Han A, Hou H, Li L, Kim HS, de Figueiredo P. Microfabricated devices in microbial bioenergy sciences. *Trends Biotechnol* 2013;**31**(4):225–32;
(g) Kim HS, Weiss TL, Thapa HR, Devarenne TP, Han A. A microfluidic photobioreactor array demonstrating high-throughput screening for microalgal oil production. *Lab Chip* 2014;**14**(8):1415–25.
84. Huesemann MH, Hausmann TS, Bartha R, Aksoy M, Weissman JC, Benemann JR. Biomass productivities in wild type and pigment mutant of Cyclotella sp.(Diatom). *Appl Biochem Biotechnol* 2009;**157**(3):507–26.
85. Kim HS, Devarenne TP, Han A. A high-throughput microfluidic single-cell screening platform capable of selective cell extraction. *Lab Chip* 2015;**15**(11):2467–75.
86. Hønsvall BK, Altin D, Robertson LJ. Continuous harvesting of microalgae by new microfluidic technology for particle separation. *Bioresour Technol* 2016;**200**:360–5.
87. Ahmad AL, Yasin NHM, Derek CJC, Lim JK. Comparison of harvesting methods for microalgae Chlorella sp. and its potential use as a biodiesel feedstock. *Environ Technol* 2014;**35**(17):2244–53.
88. (a) Clarke A, Skadsheim A, Holmes LJ. Lipid biochemistry and reproductive biology in two species of Gammaridae (Crustacea: Amphipoda). *Mar Biol* 1985;**88**(3):247–63;
(b) Levitan O, Dinamarca J, Hochman G, Falkowski PG. Diatoms: a fossil fuel of the future. *Trends Biotechnol* 2014;**32**(3):117–24.
89. (a) Dassey AJ, Theegala CS. Harvesting economics and strategies using centrifugation for cost effective separation of microalgae cells for biodiesel applications. *Bioresour Technol* 2013;**128**:241–5;
(b) Vinayak V, Manoylov KM, Gateau H, Blanckaert V, Herault J, Pencreac'h G, Marchand J, Gordon R, Schoefs B. Diatom milking: a review and new approaches. *Mar Drugs* 2015;**13**(5):2629–65.
90. Nigam P, Singh A. Production of liquid biofuels from renewable resources. *Prog Energy Combust Sci* 2011;**37**:52–68.
91. Armbrust EV. The life of diatoms in the world's oceans. *Nature* 2009;**459**(7244):185–92.
92. Barros AI, Gonçalves AL, Simões M, Pires JCM. Harvesting techniques applied to microalgae: A review. *Renew Sustain Energy Rev* 2015;**41**:1489–500.
93. Mopper K, zhou J, Sri Ramana K, passow U, dam HG, Drapeau DT. The role of surface-active carbohydrates in the flocculation of a diatom bloom in a mesocosm. *Deep Sea Res Part II Top Stud Oceanogr* 1995;**42**(1):47–73.
94. (a) Gärdes A, Iversen MH, Grossart H-P, Passow U, Ullrich MS. Diatom-associated bacteria are required for aggregation of Thalassiosira weissflogii. *ISME J* 2011;**5**(3):436–45;
(b) de Gouvion Saint Cyr D, Wisniewski C, Schrive L, Farhi E, Rivasseau C. Feasibility study of microfiltration for algae separation in an innovative nuclear effluents decontamination process. *Separ Purif Technol* 2014;**125**:126–35.
95. (a) Bar-Zeev E, Rahav E. Microbial metabolism of transparent exopolymer particles during the summer months along a eutrophic estuary system. *Front Microbio* 2015;**6**:403;
(b) Seebah S, Fairfield C, Ullrich MS, Passow U. Aggregation and sedimentation of Thalassiosira weissflogii (diatom) in a warmer and more acidified future ocean. *PLoS One* 2014;**9**(11):e112379.
96. Holcomb RE, Mason LJ, Reardon KF, Cropek DM, Henry CS. Culturing and investigation of stress-induced lipid accumulation in microalgae using a microfluidic device. *Anal Bioanal Chem* 2011;**400**(1):245–53.
97. Kim H, Devarenne T, Han A. Microfluidic systems for microalgal biotechnology: a review. *Algal Res* 2017;**30**.
98. Markou G, Nerantzis E. Microalgae for high-value compounds and biofuels production: A review with focus on cultivation under stress conditions. *Biotechnol Adv* 2013;**31**(8):1532–42.
99. Kim HS, Weiss TL, Thapa HR, Devarenne TP, Han A. A microfluidic photobioreactor array demonstrating high-throughput screening for microalgal oil production. *Lab Chip* 2014;**14**(8):1415–25.
100. Lim J, Caen O, Vrignon J, Konrad M, Taly V. Parallelized ultra-high throughput microfluidic emulsifier for multiplex kinetic assays. *Biomicrofluidics* 2015;**9**(3):034101.
101. Kim HS, Devarenne TP, Han A. Microfluidic systems for microalgal biotechnology: a review. *Algal Res* 2018;**30**:149–61.
102. Wang J, Meng X, Song Y, Pan X, Li D-D. Detection of activity of single microalgae cells in a new microfluidic cell capturing chip. *Meas Sci Technol* 2016;**27**:125701.

103. Hu Q, Davis C. Accurate automatic quantification of taxa-specific plankton abundance using dual classification with correction. *Mar Ecol Prog Ser* 2006;**306**:51–61.
104. Benazzi G, Holmes D, Sun T, Mowlem MC, Morgan H. Discrimination and analysis of phytoplankton using a microfluidic cytometer. *IET Nanobiotechnol* 2007;**1**(6):94–101.
105. (a) Kim Y-H, Park S, Kim MH, Choi Y-K, Yang Y-H, Kim HJ, Kim H, Kim H-S, Song K-G, Lee SH. Ultrasound-assisted extraction of lipids from Chlorella vulgaris using [Bmim][MeSO4]. *Biomass Bioenergy* 2013;**56**:99–103;
(b) Song JL, Au KH, Huynh KT, Packman AI. Biofilm responses to smooth flow fields and chemical gradients in novel microfluidic flow cells. *Biotechnol Bioeng* 2014;**111**(3):597–607;
(c) Wang J, Song Y, Maw M, Pan X, Sun Y, Li D-D. Detection of size spectrum of microalgae cells in an integrated underwater microfluidic device. *J Exp Mar Biol Ecol* 2015;**473**:129–37.
106. Vinayak V, Gordon R, Joshi K, Schoefs B. *"Diafuel." 2018 Trademark application no 3778882. Trade Marks Journal No: 1846, 23/04/2018 Class 4*. 2018.
107. Yano H, Katafuchi F, Kimoto T, Matsunami H. Effects of wet oxidation/anneal on interface properties of thermally oxidized SiO/sub 2//SiC MOS system and MOSFET's. *IEEE Trans Electron Dev* 1999;**46**(3):504–10.
108. Vinayak V, Kumar V, Kashyap M, Gordon R, Schoefs B. *FFabrication of resonating microfluidic chamber for biofuel production in diatoms*. 2016.
109. Vinayak V, Kumar V, Kashyap M, Joshi KB, Gordon R, Schoefs B. In Fabrication of resonating microfluidic chamber for biofuel production in diatoms (Resonating device for biofuel production). In: *2016 3rd International Conference on Emerging Electronics (ICEE), IEEE*; 2016. p. 1–6.
110. Yuan Q, Mirzajani H, Evans B, Greenbaum E, Wu J. A disposable bulk-acoustic-wave microalga trapping device for real-time water monitoring. *Sensor Actuator B Chem* 2020;**304**:127388.
111. (a) Evander M, Johansson L, Lilliehorn T, Piskur J, Lindvall M, Johansson S, Almqvist M, Laurell T, Nilsson J. Noninvasive acoustic cell trapping in a microfluidic perfusion system for online bioassays. *Anal Chem* 2007;**79**(7):2984–91;
(b) Guo S, Zhao L, Zhang K, Lam K, Lau ST, Zhao X, Wang Y, Chan HL, Chen Y, Baigl D. Ultrasonic particle trapping in microfluidic devices using soft lithography. *Appl Phys Lett* 2008;**92**(21):213901.
112. Kumar V, Singh R, Thakur S, Joshi K, Vinayak V. Doping of magnetite nanoparticles facilitates clean harvesting of diatom oil as biofuel for sustainable energy. *Mater Res Express* 2018;**5**.
113. Khoshmanesh K, Nahavandi S, Baratchi S, Mitchell A, Kalantar-zadeh K. Dielectrophoretic platforms for bio-microfluidic systems. *Biosens Bioelectron* 2011;**26**(5):1800–14.
114. Khan MJ, Singh R, Joshi KB, Vinayak V. TiO 2 doped polydimethylsiloxane (PDMS) and Luffa cylindrica based photocatalytic nanosponge to absorb and desorb oil in diatom solar panels. *RSC Adv* 2019;**9**(39):22410–6.
115. Molina Grima E, Belarbi EH, Acién Fernández FG, Robles Medina A, Chisti Y. Recovery of microalgal biomass and metabolites: process options and economics. *Biotechnol Adv* 2003;**20**(7):491–515.

Further reading

1. Shiino Y, Kuwazuru O, Suzuki Y, Ono S. Swimming capability of the remopleuridid trilobite Hypodicranotus striatus: Hydrodynamic functions of the exoskeleton and the long, forked hypostome. *J Theor Biol* 2012;**300**:29–38.
2. Lapierre F, Wu N, Zhu Y. Influence of flow rate on the droplet generation process in a microfluidic chip. *SPIE* 2011;**8204**.

CHAPTER

6

Nanocomposite membrane for direct methanol fuel cell

Shiny Joseph

Department of Chemical Engineering, National Institute of Technology Calicut, Kozhikode, Kerala, India

1. Introduction

The present regulations in environmental protection demand clean energy production methods which lead to the development of fuel cells. Direct methanol fuel cell (DMFC) employs a polymer electrolyte membrane (PEM) and is operated at low temperatures using a liquid fuel methanol. The heart of the fuel cell is the membrane electrode assembly (MEA), which consists of an anode, PEM and a cathode. The membrane is sandwiched between the anode and cathode. The performance of the DMFC is limited by the PEM. The function of PEM is to transfer protons from anode to cathode and block the passage of fuel/oxidants and electrons. The permeation of methanol through the PEM results in mixed potential, catalyst poisoning, and low fuel utilization efficiency. The working principle of DMFC is illustrated in Fig. 6.1. By the electrochemical reaction at the anode, the methanol and water molecule split into protons, electrons, and CO_2. The generated protons reach to the cathode through the PEM and electrons through the external circuit. The protons and electrons combine with oxygen to produce water at the cathode.

The reactions taking place in DMFC is shown below:

$$\text{Anode: } CH_3OH + H_2O \rightarrow 6H^+ + 6e^- + CO_2$$

$$\text{Cathode: } 3/2\ O_2 + 6H^+ + 6e^- \rightarrow 3H_2O$$

$$\text{Overall: } CH_3OH + 3/2\ O_2 \rightarrow 3H_2O + CO_2$$

Due to these drawbacks, the commercialization of DMFC is a huge task. Several researchers have focused their attention to develop a reliable, high performing polymer electrolyte with high proton conductivity, less or no methanol crossover, high chemical and electrochemical stability, good thermal and mechanical stability, and low cost. The cation exchange membrane based on perfluorosulfonic acid ionomer called Nafion was developed by

Applications of Multifunctional Nanomaterials
https://doi.org/10.1016/B978-0-12-820557-0.00007-2

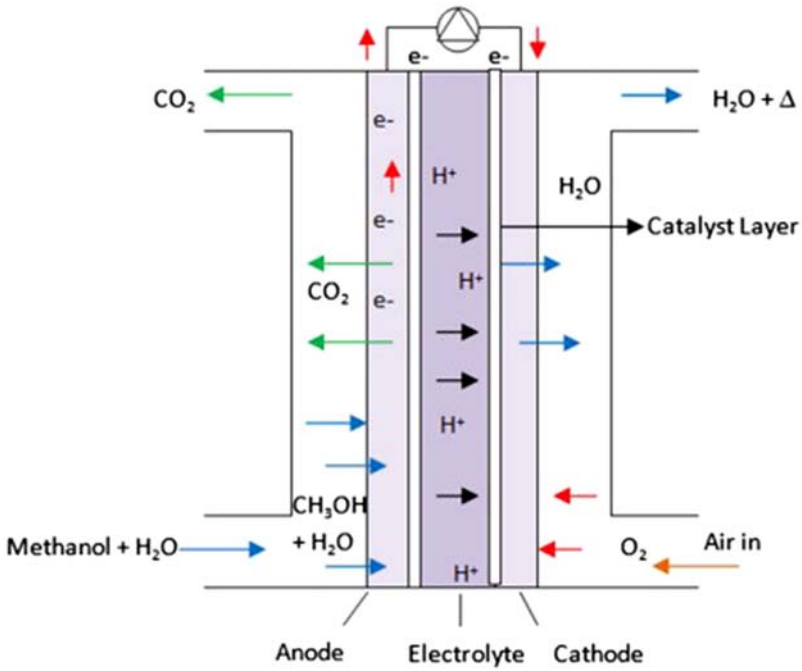

FIGURE 6.1 Schematic representation of DMFC.

Dupont. It is used in fuel cells due to its high protonic conductivity and thermal and chemical stability. Nevertheless, Nafion has several disadvantages such as high methanol crossover and decrease in ionic conductivity when operated at higher temperatures due to the dehydration of the membrane. Due to this, several types of proton exchange membranes were investigated using sulfonated aromatic hydrocarbons, acid-base complexes and by modification of these membranes using hygroscopic inorganic nanomaterial. The polymeric materials, inorganic materials, and the polymer electrolyte nanocomposite developed during the past years are briefly covered and discussed in the following sections.

2. Proton transport mechanism

Proton conductivity is the essential characteristic of a proton exchange membrane. The resistance to ionic conductivity of the PEM is proportional to the resistive losses in fuel cell and limits its performance. The PEM contains a nonconducting hydrophobic backbone and an ion conducting hydrophilic side chains distributed in the polymer matrix. In the presence of water, the proton and the sulfonic acid group enter into a solvated state. The transport processes in an ion exchange membrane may be due to the four possible mechanisms, namely, diffusion due to concentration gradient, electro-migration as a result of electric potential

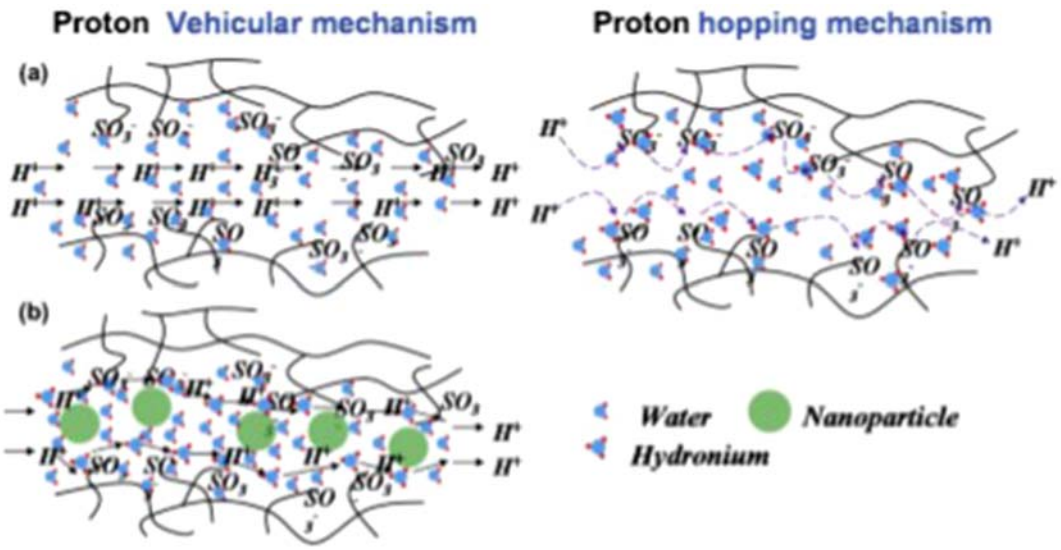

FIGURE 6.2 The schematic representation of the vehicular mechanism and Grotthus mechanism in (A) pristine membranes and (B) polymer/nano-particle composite membranes.[2]

gradient, convection due to electroosmotic solvent transfer and surface site hopping.[1] In the surface site hopping mechanism, also known as Grotthus mechanism, the protons generated at the anode reaches the membrane surface and hop from one hydrolyzed ionic site (such as H_3O^+, SO_3−H) to another across the membrane. Whereas in convective/vehicular mechanism, the proton is adsorbed on to the vehicle site (i.e., on water and form H_3O^+) and diffuses through the water filled channels as the result of the electrochemical driving force. The Grotthus mechanism and vehicular mechanism is schematically presented in Fig. 6.2.[2] Hsu and Gierke modeled the transport of ions through the Nafion membrane by constructing an elastic cluster model for ion cluster formation. The developed cluster network model is shown in Fig. 6.3. According to this model, the polymeric ions and absorbed water separate from the fluorocarbon matrix into approximately spherical domains connected by short narrow channels. The polymeric charges are imbedded in the water phase very near the water/fluorocarbon interface. This structure corresponds to the structure of an inverted micelle.[3] When hydrophilic surface modified nanoparticles are introduced into sulfonated polymer matrix, the interfacial properties of the polymer and the additives get improved. This generates additional conducting paths for the proton and thus the conductivity increases.

3. Polymer electrolyte membranes

Generally, the proton conducting electrolyte membrane IS classified into three categories: perfluorosulfonic acid membranes, nonfluorinated hydrocarbon membrane, and acid-base complexes.

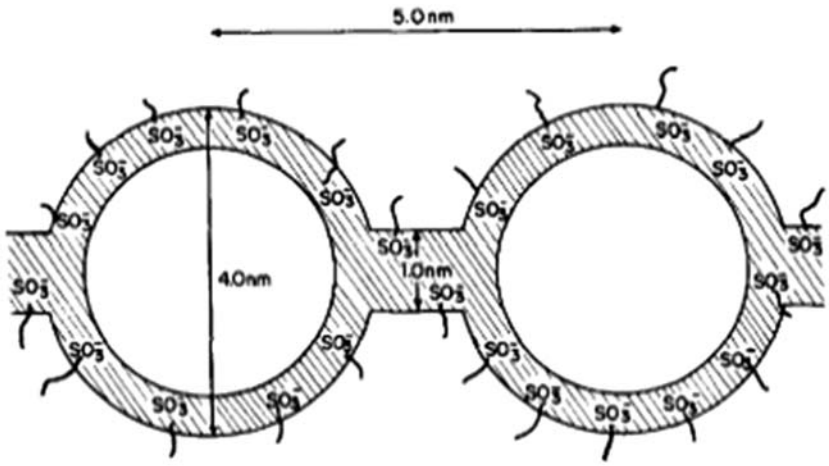

FIGURE 6.3 Cluster-network model for nafion membranes.[3]

3.1 Perfluorinated sulfonic acid membranes

Perfluorinated sulfonic acid membranes are fluorocarbon based ion exchange membranes first developed by Dupont in 1966 (Nafion). Fluorocarbon based membranes are homogeneous membranes with uniformly distributed sulfonic acid ionic charge group throughout the highly acidic tetrafluoroethylene polymer matrix. These membranes have strong hydrophobic backbone and strong hydrophilic side chains. The strong hydrophobic and hydrophilic domains create a microphase separation at the interface in presence of water. The uniform distribution of these strong hydrophilic sulfonic acid units form ionic clusters with interconnected channel. These uniform and effective channels cause high ionic conductivity at fully hydrated condition. The similar types of flurocarbon membranes include Aciplex developed by Asahi Chemical Company, Flemion by Asahi Glass Company, fumapem by Fumatech GmbH, and Dow by Dow Chemicals. The chemical structure of these membranes is shown in Fig. 6.4.[4] They have high thermal and chemical stability and good proton conductivity at fully hydrated condition.

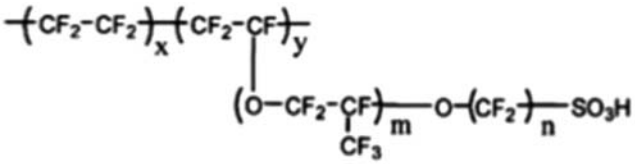

Nafion®117	$m \geq 1$, n=2, x=5-13.5, y=1000
Flemion®	m=0, 1; n=1-5
Aciplex®	m=0, 3; n=2-5, x=1.5-14
Dow membranc	m=0, n=2, x=3.6-10

FIGURE 6.4 Chemical structures of perfluorinated polymer electrolyte membranes.[4]

3.2 Nonfluorinated hydrocarbon membranes

Hydrocarbon membranes have certain advantage over fluorocarbon membranes. They are cheap, commercially available, and their structure can be modified easily by introducing polar sites. The hydrocarbon based PEMs usually contain sulfonic acid groups, phosphoric acid groups, sulfonamides, and azole derivatives as polar groups. Diverse polymer materials including poly(ether sulfone) (PES), poly(ether ketone) (PEK), polybenzimidazole (PBI), polyimide (PI), poly(phenylene), polyphosphazene, and polyvinylidene fluoride (PVDF) were examined for the backbones of PEMs. The overall performance of PEMs is affected by the disparity in the topological architectures of polymeric ionomers. Block side chain type, comb-shaped, and densely functionalized cation exchange membranes (CEM) have been shown in Fig. 6.5.[5] Even though these PEMs provide higher proton conductivity, it has weak dimensional stability due to increased water channel formation and lower chemical stability. Hydrocarbon-based polymers have a distinct microstructure depending on their chemical structure. The water uptake capacity and swelling behavior depends strongly on the polymer morphology. The rigid structure of the sulfonated hydrocarbon polymers allows them to be thermally and mechanically stable up to 200°C. They also have great fuel barrier properties. For a given ion exchange capacity, sulfonated polymers have lower proton conductivity and higher dimensional swelling than fluorocarbon polymers due to their lower acidity and hydrophobicity of the polymer back bone. The weak interaction between the hydrophobic and hydrophilic moieties results in less effective microphase separation, channel formation and lower chemical stability, especially for structures with ether linkage.[6]

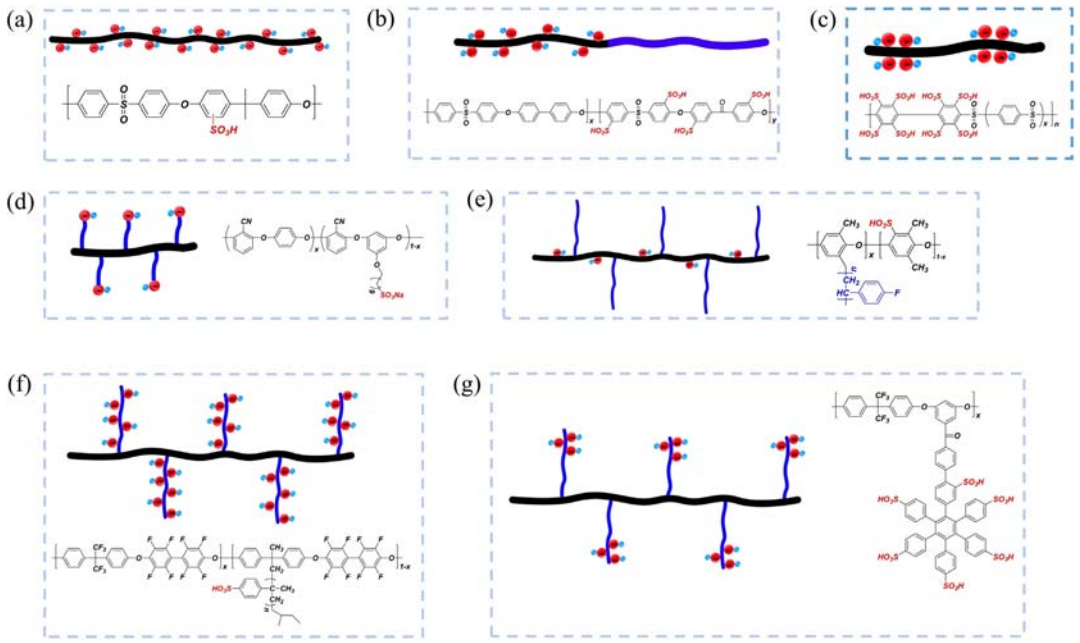

FIGURE 6.5 The topological architecture of hydrocarbon based proton exchange membrane.[5]

Hydrocarbon PEMs belong to four categories, namely, random copolymers, block copolymers, graft copolymers, and densely sulfonated copolymer. In sulfonated random copolymers, the hydrophobic and hydrophilic moieties are of low strength and are randomly distributed. The morphology of these random polymers depends on chemical nature of the polymer structure and external processing conditions like solution casting, acidification and hot pressing. The proton conductivity of random copolymers is much lower due to the random dispersion of ionic clusters in the hydrophilic domains and the less interconnectivity of the clusters. The studies on sulfonated poly ethers (SPE) show that small and planar hydrophobic components facilitate aggregation of hydrophobic and hydrophilic moieties and help in the formation of well-developed hydrophobic ionic clusters.[7] The high degree of sulfonation (DS) of random copolymer improves its proton conductivity due to the formation of concentrated hydrophilic ionic cluster and interconnection.[8] The hydrophilic clusters become more sparsely distributed as the distance between the adjacent sulfonic acid groups increases.

Block copolymers consist of hydrophilic and hydrophobic homosequences which creates well defined microphase separation of hydrophilic and hydrophobic regions. Their morphological orientation causes anisotropic water swelling in them. Badami et al.[9] studied a block copolymer based on SPAE using a fluorine based coupling agent, hexafluoro benzene HFB, and decafluorobiphenyl (DFBP). The DFBP containing block polymers exhibit more well-developed morphology with well-connected ionic channels. The fluorine increases its hydrophobicity due to which the DFBP shows better proton conductivity at various ranges of RH (300%−100%).

The sulfonated ABA triblock copolymers based on hydrophilic sulfonated poly(ether ether sulfone) (SPEES) and hydrophobic poly(methyl methacrylate) (PMMA) and poly(pentafluorostyrene) (PPFS) were synthesized using direct self-assembly method and infiltration of the polymers into anodized aluminum oxide (AAO) templates method[10] ABA. They reported that the chemical structure and preparation method affect the morphology, thermal stability, water uptake, and proton conductivity. The fluorinated membranes prepared by self-assembly exhibited a phase segregated morphology improved proton conductivity than the infiltration into the AAO templates method. Both the polymers show an improved methanol permeability resistance than Nafion 117. The ABA triblock copolymer consists of two hydrophilic A oligomers based on sulfonated poly phenyline oxide and a hydrophobic B oligomer SPAE. They show a well-connected worm like hydrophilic ionic channel. The proton conductivity of the triblock copolymer was comparable to Nafion operating at room temperature even at medium temperature of 100°C and low RH. The proton conductivity was greater when RH was greater than 70%. The block length of the hydrophilic and hydrophobic repeating units and the number of blocks influence the protonic conductivity and mechanical property of the polymers. The crystallinity of the polymer increases the mechanical and chemical stabilities of the membrane but impedes ionic transport. So, a balance between the crystallinity and amorphicity has to be maintained to balance the stability and ionic conductivity.[11] Block copolymers have definite hydrophilic ionic clusters (5−9 nm). The densely sulfonated block copolymer with increased proton conductivity is less dependent on RH. The oxidation of the sulfide linkage in hydrophilic block is oxidized to sulfone which increases the acidity of the sulfonic acid group and improves the oxidative chain stability.[12] Highly dense sulfonated block copolymers with short hydrophobic block length provide well-defined morphology and oxidative stability to the polymeric electrolyte membrane.

Graft copolymers are synthesized by linking hydrophilic aromatic or aliphatic side chain to the hydrophobic main chain. It contains ion conducting and nonion conducting units, forming difficult homosequences. The morphology can be controlled by adjusting the length and periodicity of the side chains. The size of ionic clusters and channels can be controlled by the length and rigidity of the side chains, whereas the cluster density is controlled by the periodicity of the side chains.[13]In a densely sulfonated copolymer, the hydrophilic−hydrophobic phase separation is created by isolation and localization of ion conducting functional group. The repeating unit of these polymers will have more than two sulfonic acid group which promote clustering and isolation of ion conducting group.[14]

3.3 Acid- base complexes

Acid-base complexes are considered to be promising materials to be used as PEMs in fuel cell application. These provide high proton conductivity at higher temperature without any dehydration of the membrane. These types of PEMs provide better chemical, mechanical and oxidative stability of the membrane. The much investigated polybenzimidazole(PBI)− H_3PO_4 complex shows promise as it offers good proton conductivity, mechanical and oxidative stability even to a temperature of 200°C. It was also found that the proton conductivity increases with increasing dope concentration of H_3PO_4 and decreases with temperature.[15] The interaction forces between the acid-base membranes control the membrane swelling without affecting its flexibility. Hence, these membranes generally possess low water uptake, good mechanical strength, better thermal stability, and high proton conductivity. Some of the more investigated acid-base membrane includes polyvinyl alcohol (PVA)/H_3PO_4, sulfonated polymers such as SPEEK/PBI, SPPENK, SPBEK. The chemical structures of the acid and base polymers are shown in Fig. 6.6.[16]

4. Inorganic nanomaterials

The inorganic nanomaterials investigated for the preparation of nanocomposite polymer electrolyte of fuel cell include metal oxides (TiO_2, SiO_2, ZrO_2), metal phosphates (ZrP, BPO_4), heteropolyacids (HPAs- $H_aZ_bM_cO_n$) (Z = heteroatom; M = Mo, W, V in their higher oxidation states), layered silicate minerals (nanoclays, zeolite), and carbon based nanomaterials(CNTs, GO). These materials generally improve the water uptake capacity, thermal and mechanical stability of the PEMs.

4.1 Zirconium phosphate

The zirconium phosphate both in its amorphous and crystalline forms exhibit excellent chemical and physical properties. The superb ion exchange characteristics, thermal stability, and high aspect ratio along with its easily controllable morphology make it suitable for fuel cell application. Amorphous zirconium phosphates can be synthesized in various forms such as powders, gels, granules and films. Depending on the synthesis process and functionalization techniques, various morphologies such as spheres, cubes, globules, irregular shapes can be produced (Fig. 6.7).[17] The crystalline zirconium phosphate has a layered structure which

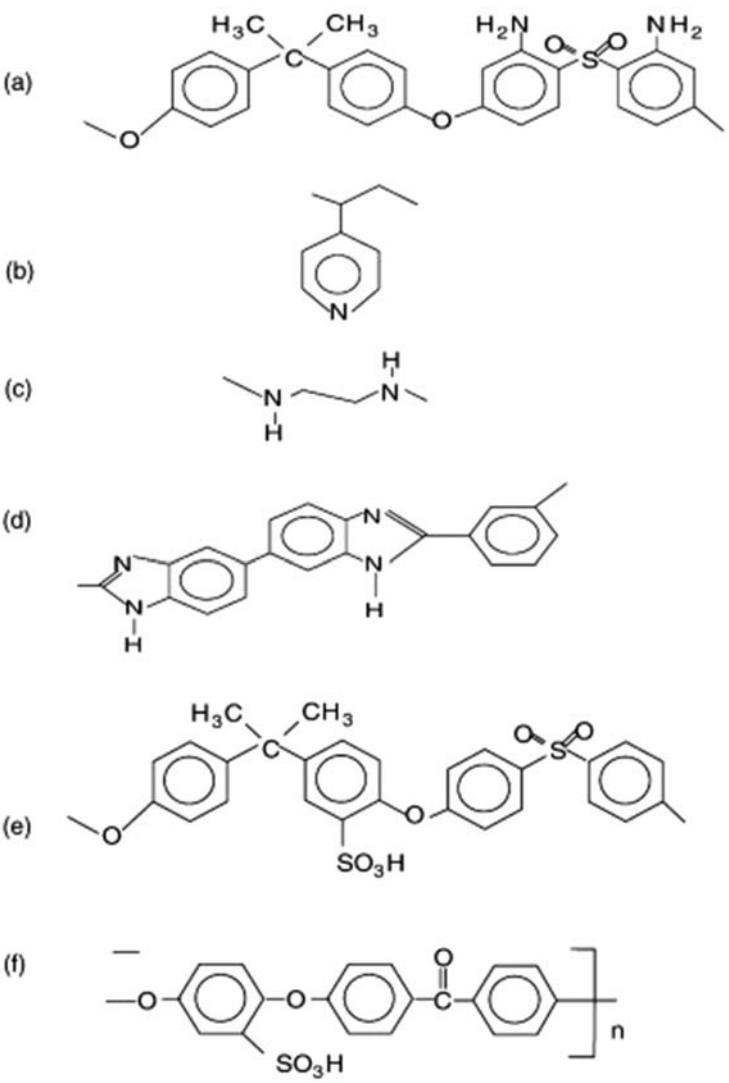

FIGURE 6.6 Structure of basic polymers (A–D) and acidic polymers (E, F).

makes it more attractive due to its more easily controlled structure, exfoliation and intercalation properties. The schematic representation of crystalline zirconium phosphate αZrP is shown in Fig. 6.8.[17]

4.2 Heteropolyacids

Heteropolyacids (HPA) are polyoxometalate compounds having acid, base, and redox properties. The general formula of the basic structural unit, known as Keggin structure, of this class of compound is $H_nXM_{12}O_{40}$; where X is the heteroatom—P, Si, Ge, and As; M is the addenda

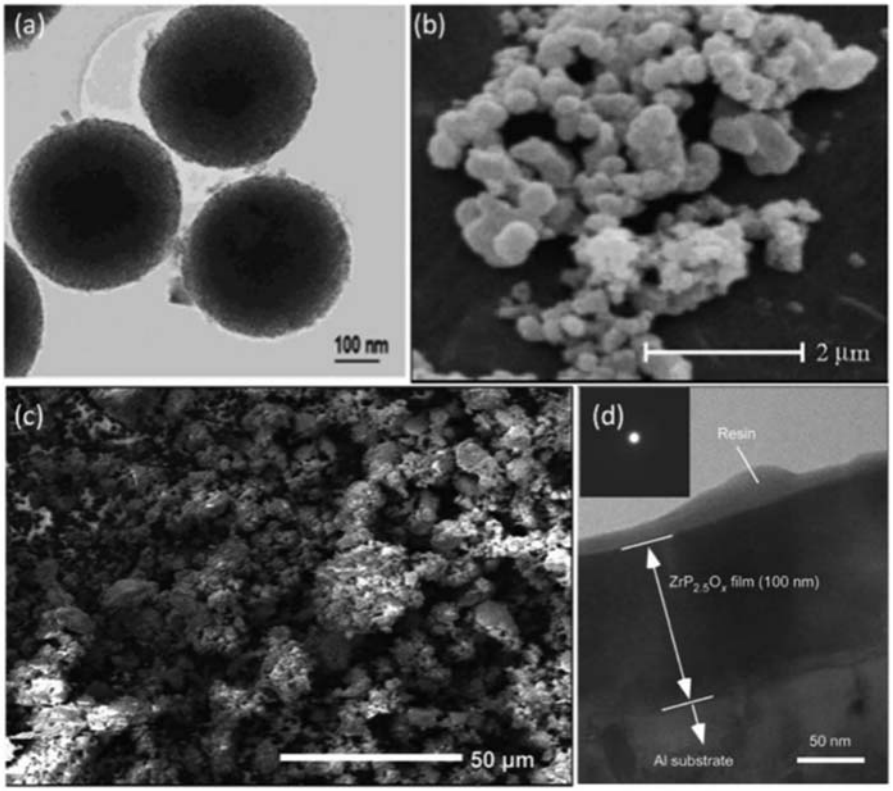

FIGURE 6.7 Morphologies of different types of amorphous ZrP: (A) ZrP spheres, (B) wormhole-like structure, (C) globule agglomerates, and (D) amorphous ZrP thin film.[17]

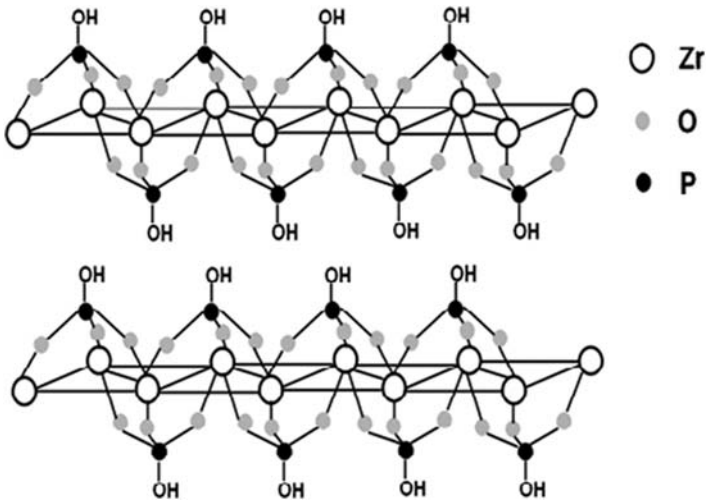

FIGURE 6.8 Schematic expression of molecular structure of α-ZrP.[18]

atom—Mo, W, and V. Typical HPA include phosphotungstic acid [$H_3PW_{12}O_{40}.nH_2O$] (PWA), phosphomolybdic acid [$H_3POMo_{12}O_4.nH_2O$] (PMOA) and silicotungstic acid [$H_4SiW_{12}O_{40}.nH_20$] (SIWA). The crystalline form exhibits high proton conductivity.[19] Among these PWA is largely selected for study due to its strong acidity. However, its high water solubility may lead to the leakage of PWA and instability of performance during operation. Conduction of HPA is due to the protons located on the bridging oxygen atom and its conductivity is related to the number of water molecules coordinated to the unit. The degree of hydration in HPA varies from 6 to 29 molecules of water per HPA molecule. The extremely high solubility and their large particle size within the membrane matrix make ineffective bridging between the ionic domains and limit the performance of nanocomposite membrane.

4.3 Solid acids

Solid acids are good candidates for proton conducting membranes due to their high proton conductivity in the anhydrous state. But it is brittle and has very narrow temperature range for the super protonic phase (i.e., between the transition temperature and melting temperature). The general formula is $MmHn(XO_4)$ $(m + n)/2$, where M = K, Rb, NH_4, Cs; X = S, Se, P, As. It undergoes structural phase change at certain temperature.[20] This compound does not contain water molecules in their structure and its conductivity is independent of the atmospheric humidity and it has high thermal and electrochemical stability. The most well-known compound of this class is $CsHSO_4$.

4.4 Metal oxides

The metal oxides, such as TiO_2, SiO_2, and ZrO_2, are hydrophilic in nature and increase the water holding capacity of the membrane and also block the passage of methanol through the membrane. TiO_2 nanoparticle, a polymorph material, exists in both crystalline and amorphous forms. Its major crystalline phases rutile, anatase, and brookite are stable at atmospheric conditions. The relative stability TiO_2 depends on its particle size. There are different types of nanostructure for multiphase TiO_2 such as nanoparticles, whiskers, fibers, spindle. The amorphous TiO_2 is synthesized as nanoparticles, nanotubes thin film and nanotube arrays. The amorphous and crystalline forms of TiO_2 nanostructure of controlled size and shape are prepared by sol gel process.

4.4.1 Nanoclay

Nanoparticles of layered mineral silicates consisting of layered structural units are called Nanoclays. They can form complex clay crystallites by stacking one layer upon another. The widely studied nanoclays montmorillonite (MMT) has a plate like structure and belongs to smectite family. They have been thus much researched because of their properties such as high cation swelling behavior, exchange capacity, and large surface area. They are dispersed in polymer matrix as fillers or additives in polymer-nanoclay composite to improve the polymer properties. The interfacial interaction between the nanoclay and polymer matrix significantly influences the performance of the polymer nanoclay composite. The interaction can be further modified by surface functionalization of the nanoclays.[21] The structure of MMT is shown in Fig. 6.9.

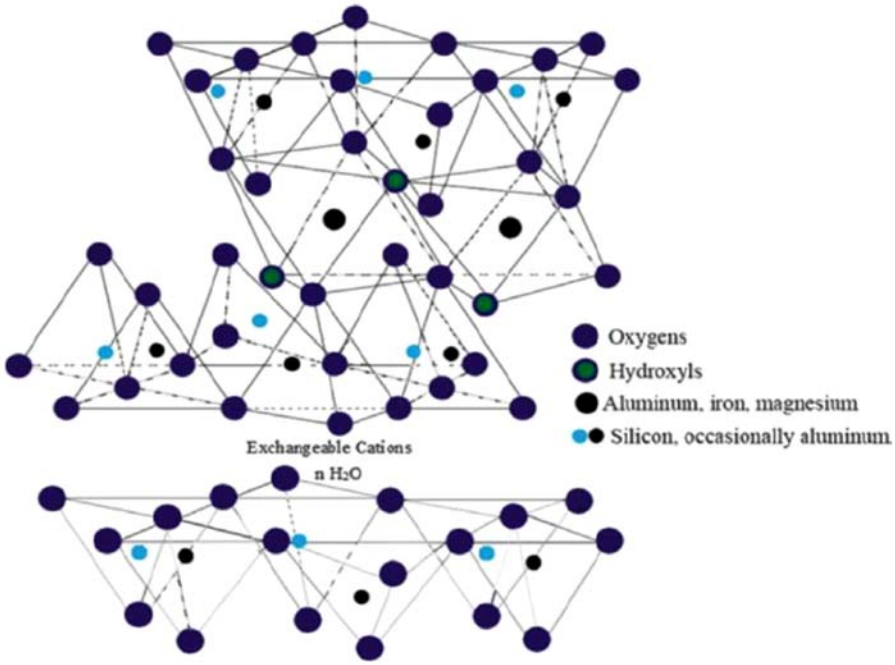

FIGURE 6.9 The structure of montmorillonite clay.

5. Composite membranes

The hydrophilic and proton conducting inorganic fillers are added to the PEM to enhance the proton conducting and methanol blocking properties. The composite membranes based on the Nafion inorganic material, aromatic and aliphatic hydrocarbon, and inorganic acid–organic base polymer mainly used for PEM is reviewed.

5.1 Nafion-based nanocomposites

The limited availability of water at the anode, electroosmotic drag of water from anode to cathode and insufficient water back diffusion causes membrane dehydration. The membrane dehydration increases the protonic resistance which in turn increases the ohmic resistance of the cell and reduces cell efficiency. Nafion–SiO_2 composites were prepared using several methods such as solution recast, sol-gel method, self-assembling method, and in situ sol-gel methods. Sahu et al.[22] developed Nafion–Silica composite membrane using a novel water hydrolysis process. A homogenous, transparent and less viscous inorganic sol was prepared by water hydrolysis to prepare silicon alkoxide. This sol is incorporated into the polymer matrix and heated at 90°C under vacuum. The transparent polymer film obtained is tested for PEFC with varying RH between 100% and 18% at elevated temperature and atmosphere pressure. When tested at 100% RH and 60°C temperature under ambient pressure, Nafion 1135–Silica (10%) composite membrane showed a peak power density of 720 mW/cm^2,

whereas the Nafion 1135 membrane had a peak power density of 550 mW/cm^2. An excess silica phase in Nafion matrix brings down the performance by causing electrode flooding. Since Nafion-inorganic composite membrane exhibits lower resistance, the membrane sustains higher load current density especially under low RH condition. Chang et al.[23] prepared Nafion/SiO_2 composite membrane with controlled sizes of SiO_2 nanoparticles by an in situ sol gel process. These composite membranes were tested at 110°C and 59% RH. A 10% increase in power density for composite membrane with 10 nm SiO_2 nanoparticle was reported. They also reported that at 100% RH and 30°C, Nafion 212 membrane has higher proton conductivity than the nanocomposite membrane. Weilin et al.[24] studied the Nafion−SiO_2−PWA nanocomposite membrane prepared by sol-gel method. The proton conductivity of the Nafion−SiO_2−PWA composite increased with increase in SiO_2 concentration. But in Nafion−SiO_2, the proton conductivity reduced with increase in SiO_2 concentration. The methanol permeability of the composite membrane was always lower than pristine membrane. The decrease in proton conductivity with increasing silica content is due to the inhibition of the proton conduction in composite membrane. But in Nafion−SiO_2−PWA composite, the increased silica network holds more proton conducting PWA molecule. The immersion time of the membrane in TEOS/methanol solution influences the methanol permeation and methanol permeability of the composite membrane. The nonpolar TEOS molecular will dissolve Nafion C−F backbone to lose the conducting $^{-}SO_3$- group.

A surface functionalized mesoporous Zirconium phosphate (MZP) was synthesized by Sahu et al.[25] The mesoporous MZP is impregnated with Nafion ionomer to prepare a Nafion−MZP composition membrane. The PEFCs with Nafion 1135−MZP (5%) composite membrane operated at 100% RH at 70°C produces a peak power density of 725 mW/cm^2 compared to 655 mW/cm^{-2} of the PEFC with Nafion 1135 membrane. The performance of the composite membrane increases with increase in MZP concentration and attains maximum power density at 5% concentration. The membrane at 18% RH produces a peak power density of 353 mW/cm^2, whereas pristine Nafion produces 224 mW/cm^2 under the same condition. The Nafion−MZP composite membrane performs better than pristine membrane under identical condition.

The surface characteristics of the TiO_2 (5%) nanoparticle, incorporated in the Nafion matrix affect the proton conductivity and hence the performance of DMFC at high temperature of 145°C and standard atmospheric pressure.[26] Its high surface area and the hydroxyl group on the surface of TiO_2 promote the proton conductivity of the membrane at high temperature. The crystalline structure of the filler does not affect the proton conductivity of the composite. The composite membrane operated at 80°C does not significantly influence the performance of the PEFC[27] in the range of RH (26%−100%). But at 120°C, its performance was affected by both RH and TiO_2 content. The TiO_2 particle in the polymer electrolyte increases the water retention and proton conductivity due to the adsorption of H^{+}.

5.2 Hydrocarbon-based composite membrane

Nanocomposite sulfonated hydrocarbons membranes have several required properties of PEM such as reduced methanol permeability, high morphological stability even at high degree of sulfonation, and less water swelling. Sulfonated aromatic polymers such as poly ether ether ketone, poly arylene ether sulfone, poly imides, poly phosphazene, polybenzimidazole, and polyphenylenes are extensively investigated as PEMs. These aromatic hydrocarbons have

high mechanical, thermal and chemical stability, good film forming ability, and low fuel crossover.

Inorganic fillers such as heteropolyacids, zirconium sulfate, and sulfonated silica are used with random copolymers and block copolymers in order to compensate the disadvantages of pure polymers. Well-dispersed fillers interact with the sulfonic acid group and form ionic clusters. However, incompatibility of the inorganic material with the polymer may result in macrophase separation. This will lead to poor mechanical strength and lower proton conductivity due to blockage of the transport path way. Composite SPAE membrane incorporated with sulfated zirconia was evaluated for its morphological changes and proton conductivity. The morphology of the membrane depends highly on the percentage of the filler and its dispersity in the polymer matrix. The size of the ionic cluster does not depend on the content of the filler. The 5% concentration of the filler gave maximum ionic conductivity. Higher than 5% of the filler results in aggregation of the particle and restrict the channel of the hydrophilic domain. Similar observation is made for composite made using sulfonated silica and SPAE.[28]

The size of the ionic cluster depends on the type of the filler. The composite membrane had a lower water uptake and higher proton conductivity compared to the pristine membrane. Also, the electrochemical performance was higher for the composite membrane both at 80°C and 100% RH and at 120°C and 50% RH. Hsu et al.[29] investigated the effect of pyrene sulfonic acid (PSA) filler added to sulfonated poly (styrene-b-isoprene-b-styrene) (S—SIS) triblock copolymer. A 2% concentration of the filler enhanced the ionic conductivity about 9 times more than the unfilled triblock polymer. With the addition of PSA, the ionic clusters became increasingly small and connected due to the interaction of the filler with hydrophobic polystyrene. With an increase in filler concentration, the ionic cluster size increases due to the aggregation of the hydrophilic domain.

Pandey and Shahi[30] investigated the application of composite membrane prepared from sulfonated poly imide (SPI) and sulfonated silica precursor (SSP) in DMFC. SPI/SSP-40, i.e., composite membrane with 40% SSP shows 6.34×10^{-2} S/cm proton conductivity.

Park et al.[31] incorporated ionic liquid, an ion conducting liquid having high boiling point and low volatility, into sulfonated poly(styrene-b-methanebutane) (SMB) block copolymers. They explored the use of these membranes in medium temperature fuel cell application. The study was conducted using three ionic liquids, namely, trifluoromethane sulfonate (OTF), methane sulfonate (MS), and tetrafluoroborate (BF4). In all cases, the proton conductivity of the composite membrane is always higher than the pristine polymer membrane. The hydrophilic ionic domain slightly more improved in composite membrane. The more fluorinated ionic liquid showed higher conductivity over all temperature ranges.

5.3 Acid-base complexes

The mechanical properties of the blended membrane are improved by the acid-base complexes. In acid base blend system, sulfonated acidic polymer complexes with a basic polymer. Na et al.[32] blended SPEEK, acidic polymer with PBI, a basic polymer to form the acid-base complex. Even though the proton conductivity of the acid-base complex is lower than the sulfonated PEEK membrane, the ionic conductivity was independent of temperature.

S. Changkhanchom and A Sirivat[33] synthesized sulfonated PEKES and sulfonated graphene oxide (GO) composite membrane with high degree of sulfonation which showed an

improved proton conductivity of 0.0593 S/cm which is 7 times higher than Nafion 117 membrane. A small quantity of the sulfonated GO (0.5%) added to SPEKES improved the mechanical stability and proton conductivity of the composite. It also reduced the methanol permeability in composite membrane compared to pristine SPEKES membrane. Rambabu and Bhat[34] studied SPEEK–amino acid functionalized GO (1%) composite membrane for DMFC and reported an improved ion conductivity, decreased methanol permeability, higher peak power density and a comparable open cell voltage to Nafion 117. Thirayu at al[35] investigated SPEEK/sY Zeolite (15%) which exhibited improved water uptake, proton conductivity (0.0520 S/cm), mechanical property, oxidative stability, and reduced methanol permeability (1.02×10^{-6} cm^2/s) compared to the pristine SPEEK. Avanish et al.[36] studied covalently grafted PSSA–GO nanoplatelet (0.15%)–SPEEK composite membrane and its performance in DMFC. It showed a peak power density of 170 mW/cm^2 (Fig. 6.10B) which was better than pristine SPEEK membrane and Nafion 117. The composite membrane also showed better durability and a 40% reduction in methanol crossover. Nuha et al.[37] investigated cloisite incorporated SPEEK electrospun nanocomposite prepared for DMFC application. The tortuosity developed by the cloisite layer in the membrane decreased the methanol crossover by improving the barrier properties. The size of the cloisite particle and the degree of dispersion influenced the properties of the composite membrane. However, it showed an open cell voltage of 0.4 V which was much lower than expected. Sasikala et al.[38] prepared a composite membrane incorporating functionalized Bentonite clay in SPEEK and compared its performance with pristine SPEEK (Fig. 6.10A). It showed an open cell voltage of 0.85 V and a power density of 140 mW/cm^2. The proton conductivity, methanol crossover reduction and OCV, improved at the temperature of 70°C compared to 30°C.

Pandey and Shahi[39] prepared a nucleophilic attack resistant sulfonated PI using diamines with high basicity and dianhydride with low electron affinity. Sulfonated silica precursor (SSP) was incorporated into this sulfonated PI and the composite membrane was used in DMFC for investigation. SPI–SSP (40%) showed a proton conductivity of 0.0634 S/cm and a methanol permeability of 4.8×10^{-7} cm^2/s for 40% SSP concentration.

Swati et al.[40] tested composite membrane prepared using SPES–SGO for proton conductivity in the temperature range of 30–90°C and methanol crossover to use in a DMFC. The high degree of sulfonation of PES causes swelling of the membrane. In order to overcome this problem, sulfonated graphene oxide having excellent mechanical, thermal and structural properties have been incorporated in SPES. The substitution of epoxy and hydroxyl functional groups on GO by HSO_3 enhances the properties of the composite membrane. Incorporation of small amount of GO improves the ionic conductivity, selectivity, and the methanol crossover resistance. The composite containing 5% SGO has a proton conductivity of 0.058 S/cm and a methanol permeability of 1.556×10^{-7} cm^2/s.

An SPES–PVA–exfoliated tungsten disulfide (E-WS_2) nanosheet composite membranes was tested for DMFC application.[41] The E-WS_2 nanosheet imparts excellent mechanical and thermal stability. It showed a methanol permeability of 3.42×10^{-8} cm^2/s and a proton conductivity of 1.18×10^{-2} S/cm. Esam et al.[42] studied a PVA/TiO_2 nanocomposite membrane and reported a reduction in methanol permeability due to filling of the cavities by Ti^{3+} and O^- ions and due to the complex formation. They noticed that the ionic conductivity reduces with increasing crosslinking of the PVA/TiO_2 matrix. Yang[43] studied the use of PVA –MMT – PSSA composite membrane for DMFC

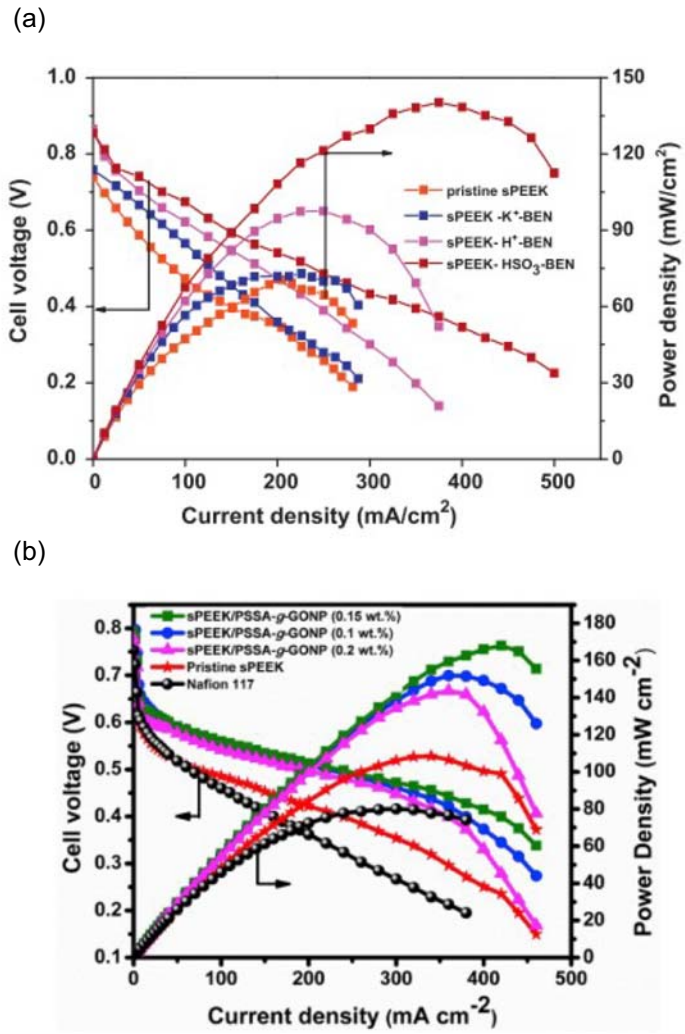

FIGURE 6.10 (A) Cell polarization studies for DMFCs with pristine SPEEK and composite membranes at 70°C[38] and (B) Comparative DMFC polarization for pristine SPEEK, SPEEK/PSSA-g-GONP and nafion 117 at 80°C.[36]

application. By introducing proton carrier PSSA, the ionic conductivity of the PVA/PSSA blend membrane is increased and by introducing MMT, the methanol permeability is reduced.

6. Conclusion

The cation exchange membranes considered as PEM in DMFC are perfluorosulfonic acid membrane, hydrocarbon-based electrolyte membrane, and acid–base complexes. The PEM contains hydrophobic and hydrophilic moieties in their structure. Microlevel phase

separation depends on the strength of the moieties. The hydrophilic moieties create ionic clusters with interconnected microchannel. The size of ionic clusters and the interconnected channel depends on the strength and arrangement of these moieties in the matrix. The ionic conductivity is facilitated by this water filled interconnected channel. In per fluorinated sulfonic acid membrane, the addition of the hydrophilic inorganic material in the polymer matrix increases the water holding capacity of the membrane and also creates a tortuous path for methanol which reduces the permeability through the membrane. The sulfonated polymers have lower ionic conductivity and higher dimensional swelling compared to PFSAs. The hydrocarbon membrane can be grouped into four categories, namely, random copolymers, block copolymers, grafted copolymers, and densely sulfonated copolymers, depending on the arrangement of hydrophobic and hydrophilic moieties. When hydrophilic inorganic materials are added to these polymers, these will interact with sulfonic acid group and improve the water retention capacity of the composite. The acid−base complexes membranes are obtained by the introduction of acidic inorganic material such as H_3PO_4, heteropolyacids, solid acids SiO_2, TiO_2, etc., to the basic polymers. Hence, it can be concluded that the composite membrane is a better choice for the PEM of the DMFC as it helps in improving ionic conductivity and reduction in permeability of methanol.

References

1. Luo T, Abdu S, Wessling M. Selectivity of ion exchange membranes: a review. *J Membr Sci* 2018;**555**:429−54. https://doi.org/10.1016/j.memsci.2018.03.051.
2. Kim DJ, Jo MJ, Nam SY. A review of polymer-nanocomposite electrolyte membranes for fuel cell application. *J Ind Eng Chem* 2015;**21**:36−52. https://doi.org/10.1016/j.jiec.2014.04.030.
3. Hsu WY, Gierke TD. Ion transport and clustering in nafion perfluorinated membranes. *J Membr Sci* 1983;**13**:307−26. https://doi.org/10.1016/S0376-7388(00)81563-X.
4. Peighambardoust SJ, Rowshanzamir S, Amjadi M. *Review of the proton exchange membranes for fuel cell applications*. Elsevier Ltd; 2010. https://doi.org/10.1016/j.ijhydene.2010.05.017.
5. Ran J, Wu L, He Y, Yang Z, Wang Y, Jiang C, Ge L, Bakangura E, Xu T. Ion exchange membranes: new developments and applications. *J Membr Sci* 2017;**522**:267−91. https://doi.org/10.1016/j.memsci.2016.09.033.
6. Shin DW, Guiver MD, Lee YM. Hydrocarbon-based polymer electrolyte membranes: importance of morphology on ion transport and membrane stability. *Chem Rev* 2017;**117**:4759−805. https://doi.org/10.1021/acs.chemrev.6b00586.
7. Bae B, Miyatake K, Watanabe M. Effect of the hydrophobic component on the properties of sulfonated poly(arylene ether sulfone)s. *Macromolecules* 2009;**42**:1873−80. https://doi.org/10.1021/ma8026518.
8. Shin DW, Lee SY, Lee CH, Lee KS, Park CH, McGrath JE, Zhang M, Moore RB, Lingwood MD, Madsen LA, Kim YT, Hwang I, Lee YM. Sulfonated poly(arylene sulfide sulfone nitrile) multiblock copolymers with ordered morphology for proton exchange membranes. *Macromolecules* 2013;**46**:7797−804. https://doi.org/10.1021/ma400889t.
9. Badami AS, Lane O, Lee HS, Roy A, McGrath JE. Fundamental investigations of the effect of the linkage group on the behavior of hydrophilic-hydrophobic poly(arylene ether sulfone) multiblock copolymers for proton exchange membrane fuel cells. *J Membr Sci* 2009;**333**:1−11. https://doi.org/10.1016/j.memsci.2008.12.066.
10. Agudelo NA, Palacio J, López BL. Effect of the preparation method on the morphology and proton conductivity of membranes based on sulfonated ABA triblock copolymers. *J Mater Sci* 2019;**54**:4135−53. https://doi.org/10.1007/s10853-018-3115-5.
11. Li N, Lee SY, Liu YL, Lee YM, Guiver MD. A new class of highly-conducting polymer electrolyte membranes: aromatic ABA triblock copolymers. *Energy Environ Sci* 2012;**5**:5346−55. https://doi.org/10.1039/c1ee02556b.
12. Titvinidze G, Kreuer KD, Schuster M, De Araujo CC, Melchior JP, Meyer WH. Proton conducting phase-separated multiblock copolymers with sulfonated poly(phenylene sulfone) blocks for electrochemical

applications: preparation, morphology, hydration behavior, and transport. *Adv Funct Mater* 2012;**22**:4456–70. https://doi.org/10.1002/adfm.201200811.
13. Balog S, Gasser U, Jetsrisuparb K, Gubler L. Structure of the hydrophilic phase and its impact on the conductivity of graft copolymer ionomers at low hydration level. *Polymer* 2013;**54**:4266–75. https://doi.org/10.1016/j.polymer.2013.06.015.
14. Tian S, Meng Y, Hay AS. Membranes from poly(aryl ether)-based ionomers containing randomly distributed nanoclusters of 6 or 12 sulfonic acid groups. *Macromolecules* 2009;**42**:1153–60. https://doi.org/10.1021/ma802456m.
15. Qingfeng L, Hjuler HA, Bjerrum NJ. Phosphoric acid doped polybenzimidazole membranes: physiochemical characterization and fuel cell applications. *J Appl Electrochem* 2001;**31**:773–9. https://doi.org/10.1023/A:1017558523354.
16. Smitha B, Sridhar S, Khan AA. Solid polymer electrolyte membranes for fuel cell applications - a review. *J Membr Sci* 2005;**259**:10–26. https://doi.org/10.1016/j.memsci.2005.01.035.
17. Xiao H, Liu S. Zirconium phosphate (ZrP)-based functional materials: synthesis, properties and applications. *Mater Des* 2018;**155**:19–35. https://doi.org/10.1016/j.matdes.2018.05.041.
18. Zhang F, Xie Y, Lu W, Wang X, Xu S, Lei X. Preparation of microspherical α-zirconium phosphate catalysts for conversion of fatty acid methyl esters to monoethanolamides. *J. Colloid Interface Sci.* 2010;**349**(2):571–7.
19. Molchanov VV, Maksimov GM, Maksimovskaya RI, Goidin VV, Buyanov RA. Synthesis of heteropoly acids and their salts using mechanochemical activation. *Inorg Mater* 2003;**39**:687–93. https://doi.org/10.1023/A:1024579507330.
20. Rhee HW, Ghil LJ. *Polymer nanocomposites in fuel cells*. Woodhead Publishing Limited; 2012. https://doi.org/10.1533/9780857096241.3.433.
21. Guo F, Aryana S, Han Y, Jiao Y. A review of the synthesis and applications of polymer-nanoclay composites. *Appl Sci* 2018;**8**:1–29. https://doi.org/10.3390/app8091696.
22. Sahu AK, Pitchumani S, Sridhar P, Shukla AK. Nafion and modified-Nafion membranes for polymer electrolyte fuel cells: an overview. *Bull Mater Sci* 2009;**32**:285–94. https://doi.org/10.1007/s12034-009-0042-8.
23. Ke CC, Li XJ, Shen Q, Qu SG, Shao ZG, Yi BL. Investigation on sulfuric acid sulfonation of in-situ sol-gel derived Nafion/SiO_2 composite membrane. *Int J Hydrogen Energy* 2011;**36**:3606–13. https://doi.org/10.1016/j.ijhydene.2010.12.030.
24. Xu W, Lu T, Liu C, Xing W. Low methanol permeable composite Nafion/silica/PWA membranes for low temperature direct methanol fuel cells. *Electrochim Acta* 2005;**50**:3280–5. https://doi.org/10.1016/j.electacta.2004.12.014.
25. Sahu AK, Pitchumani S, Sridhar P, Shukla AK. Co-assembly of a nafion-mesoporous zirconium phosphate composite membrane for PEM fuel cells. *Fuel Cell* 2009;**9**:139–47. https://doi.org/10.1002/fuce.200800178.
26. Baglio V, Aricò AS, Di Blasi A, Antonucci V, Antonucci PL, Licoccia S, Traversa E, Fiory FS. Nafion-TiO2 composite DMFC membranes: physico-chemical properties of the filier versus electrochemical performance. *Electrochim Acta* 2005;**50**:1241–6. https://doi.org/10.1016/j.electacta.2004.07.049.
27. Chalkova E, Pague MB, Fedkin MV, Wesolowski DJ, Lvov SN. Nafion/TiO[sub 2] proton conductive composite membranes for PEMFCs operating at elevated temperature and reduced relative humidity. *J Electrochem Soc* 2005;**152**:A1035. https://doi.org/10.1149/1.1895225.
28. Kim T, Choi YW, Kim CS, Yang TH, Kim MN. Sulfonated poly(arylene ether sulfone) membrane containing sulfated zirconia for high-temperature operation of PEMFCs. *J Mater Chem* 2011;**21**:7612–21. https://doi.org/10.1039/c1jm10577a.
29. Hsu HM, Hsu CH, Kuo PL. The intensively enhanced conductivity of polyelectrolytes by amphiphilic compound doping. *Polym Chem* 2015;**6**:2717–25. https://doi.org/10.1039/c4py01672f.
30. Pandey RP, Shahi VK. Sulphonated imidized graphene oxide (SIGO) based polymer electrolyte membrane for improved water retention, stability and proton conductivity. *J Power Sources* 2015;**299**:104–13. https://doi.org/10.1016/j.jpowsour.2015.08.093.
31. Kim O, Jo G, Park YJ, Kim S, Park MJ. Ion transport properties of self-assembled polymer electrolytes: the role of confinement and interface. *J Phys Chem Lett* 2013;**4**:2111–7. https://doi.org/10.1021/jz4009536.
32. Zhang H, Li X, Zhao C, Fu T, Shi Y, Na H. Composite membranes based on highly sulfonated PEEK and PBI: morphology characteristics and performance. *J Membr Sci* 2008;**308**:66–74. https://doi.org/10.1016/j.memsci.2007.09.045.

33. Changkhamchom S, Sirivat A. Sulfonated (graphene oxide/poly(ether ketone ether sulfone) (S-GO/S-PEKES) composite proton exchange membrane with high proton conductivity for direct methanol fuel cell. *Polym. Technol. Mater.* 2019;**58**:1900–13. https://doi.org/10.1080/25740881.2019.1587770.
34. Rambabu G, Bhat SD. Amino acid functionalized graphene oxide based nanocomposite membrane electrolytes for direct methanol fuel cells. *J Membr Sci* 2018;**551**:1–11. https://doi.org/10.1016/j.memsci.2018.01.026.
35. Chuesutham T, Sirivat A, Paradee N, Changkhamchom S, Wattanakul K, Anumart S, Krathumkhet N, Khampim J. Improvement of sulfonated poly(ether ether ketone)/Y zeolite -SO3H via organo-functionalization method for direct methanol fuel cell. *Renew Energy* 2019;**138**:243–9. https://doi.org/10.1016/j.renene.2019.01.107.
36. Shukla A, Dhanasekaran P, Sasikala S, Nagaraju N, Bhat SD, Pillai VK. Covalent grafting of polystyrene sulfonic acid on graphene oxide nanoplatelets to form a composite membrane electrolyte with sulfonated poly(ether ketone) for direct methanol fuel cells. *J Membr Sci* 2020;**595**:117484. https://doi.org/10.1016/j.memsci.2019.117484.
37. Awang N, Jaafar J, Ismail AF, Othman MHD, Rahman MA. Performance of void-free electrospun SPEEK/Cloisite as a function of degree of dispersion state on nanocomposite proton exchange membrane for direct methanol fuel cell application. *Membranes* 2019;**9**. https://doi.org/10.3390/membranes9010007.
38. Sasikala S, Meenakshi S, Bhat SD, Sahu AK. Functionalized Bentonite clay-sPEEK based composite membranes for direct methanol fuel cells. *Electrochim Acta* 2014;**135**:232–41. https://doi.org/10.1016/j.electacta.2014.04.180.
39. Pandey RP, Shahi VK. Aliphatic-aromatic sulphonated polyimide and acid functionalized polysilsesquioxane composite membranes for fuel cell applications. *J Mater Chem A* 2013;**1**:14375–83. https://doi.org/10.1039/c3ta12755a.
40. Gahlot S, Sharma PP, Kulshrestha V, Jha PK. SGO/SPES-based highly conducting polymer electrolyte membranes for fuel cell application. *ACS Appl Mater Interfaces* 2014;**6**:5595–601. https://doi.org/10.1021/am5000504.
41. Divya K, Sri Abirami Saraswathi MS, Alwarappan S, Nagendran A, Rana D. Sulfonated poly (ether sulfone)/poly (vinyl alcohol) blend membranes customized with tungsten disulfide nanosheets for DMFC applications. *Polymer* 2018;**155**:42–9. https://doi.org/10.1016/j.polymer.2018.09.010.
42. Abdel-Hady EE, Mohamed HFM, Abdel-Hamed MO, Gomaa MM. Physical and electrochemical properties of PVA/TiO 2 nanocomposite membrane. *Adv Polym Technol* 2018;**37**:3842–53. https://doi.org/10.1002/adv.22167.
43. Yang CC. Fabrication and characterization of poly(vinyl alcohol)/montmorillonite/poly(styrene sulfonic acid) proton-conducting composite membranes for direct methanol fuel cells. *Int J Hydrogen Energy* 2011;**36**:4419–31. https://doi.org/10.1016/j.ijhydene.2011.01.011.

Further reading

1. Gopi KH, Bhat SD, Sahu AK, Sridhar P. Quaternized poly(phenylene oxide) anion exchange membrane for alkaline direct methanol fuel cells in KOH-free media. *J Appl Polym Sci* 2016;**133**:1–11. https://doi.org/10.1002/app.43693.
2. Parthiban V, Akula S, Sahu AK. Surfactant templated nanoporous carbon-Nafion hybrid membranes for direct methanol fuel cells with reduced methanol crossover. *J Memb Sci* 2017;**541**:127–36. https://doi.org/10.1016/j.memsci.2017.06.081.

CHAPTER

7

Nano and micro elastomeric foams in energy and other related applications

B.P. Resmi[1,2], *Pinky Abraham*[3], *Jiji Abraham*[4] *and Soney C. George*[1]

[1]**Centre for Nanoscience and Technology, Amal Jyothi College of Engineering, Kottayam, Kerala, India;** [2]**TKM Institute of Technology, Ezhukone, Kollam, Kerala, India;** [3]**St. Gregorious College, Kottarakkara, Kollam, Kerala, India;** [4]**Vimala College (Autonomous), Thrissur, Kerala, India**

1. Introduction

Science is the systematic study of natural phenomena and their applications to human welfare. Natural processes also produce polymeric foams. Due to their excellent properties when compared to competing materials, they may be found almost everywhere. These are the materials of choice for a variety of uses including thermal insulation, food and beverage packing, construction, electronics, sound attenuation, filtration, automotive, electronics, aerospace, toys and furnishing, etc.[1–3] Being elastomeric, flexible, and rigid, these types of polymer foams can be made from a variety of polymers such as polystyrene (PS), polyisocyanurate (PIR), polyethylene (PE), polypropylene (PP), polyurethane (PU), poly(ethylene-vinyl acetate) (EVA), etc. Nowadays PU foams (PUFs), influence world foam production very effectively, followed by PS and PVC foams. PS foam is the first created and usually used foam material that shows lower mechanical features like low fracture strain. However, a type of foamed polymeric substance has molded to different formulations, even though costlier when compared to PS or polyolefinic foamed material. Recently there are copolymer based foams that lead to elastic and resilient foamed materials in which elastomeric foamed ones exhibited a comparatively huge difference in cell size because of diffusing of blowing agents while in the foam process. Furthermore, mechanical and electrical properties decrease considerably at low bulk densities of foams sign. Moreover, there will be cell orientation in the foam, which will improve the resistance toward toughness, tear and puncture.

Applications of Multifunctional Nanomaterials
https://doi.org/10.1016/B978-0-12-820557-0.00027-8

The need for elastomer foams enhanced considerably in the last 2 decades because of their smooth surface, non-particulating, and moisture-resistant properties. In addition, this type of foamed material has very low volatile organic compounds (VOCs) and does not contain formaldehyde or fibers, making the product, a worldwide accepted one. Elastomer-based foamed substances are completed without the use of chlorofluorocarbons (CFCs), hydrochlorofluorocarbons (HCFCs), or hydrofluorocarbons (HFCs), causing it favorable regarding the toughest environmental requirements. The production of elastomeric foam is progressing several times and is thus apt in especially needed conditions. A nonhalogenated foam appropriate in high-temperature applications on stainless steel (up to 250°F), Foams with high-temperature can withstand a temperature up to 300°F, accessibility of extra colors, which include white that keeps handlers the additional time and cost of priming or painting on interior applications, laminated insulation regarding outdoor use where ultraviolet (UV) exposure, weather, and physical abuse are a concern.

Moreover, the current accessibility of insulation with an in-built antimicrobial additive serves as one of the most stimulating developments in elastomeric foam. Insulation, which is clearly designed and placed provides immediate and long-term benefits. Insulation protects people, equipment, systems, and finally one's budget. Energy expenses are considerably reduced when a system is correctly constructed, insulated, and maintained, which saves money and also guards the environment. The insulation of elastomeric foam expanded in the year 1950s. The establishment of elastomeric foams and other materials based on polymer signaled a significant shift in the industry from natural materials, such as cork, to synthetic materials and chemicals for use. The insulation of elastomer rapidly gained popularity, owing to the fact that it removed the demand for vapor barrier for blocking any transfer of moisture. The insulating feature become more widely available in various forms (such as sheets, rolls, and tubes), and it grew in prominence as an insulator, particularly in refrigerators, pipes, and ductwork uses.

Thus enhanced properties like weightlessness, great impact strength, and improvement in the insulating features make polymer foam find enormous applications. The enhancement in properties of the foam resulting from the cell size and morphological characteristics leads to microcellular and nanocellular foams.[4,5] The lightweight and great strength are the potential factors that determine the quality of polymer. The microstructure of the foam like the density of the bubble, size of the bubble, and bubble size distribution, as well as the intrinsic properties of the polymers that affect the mechanical property of polymer foams.[6,7]

Rubber foams are cured elastomers or expanded rubbers that play a major part in the rubber industry. Rubber foams are classified into two groups: open-cell foams and closed-cell foams depending on their cell structure. The gas phases (cells) are connected to each other in open cell foams and the cells are isolated or separated by cell walls in closed cell foams.[8] Rubber foams exhibit thermal and sound insulating properties, absorption of energy, and structural application due to its properties viz low cost and low-density.[9] Chemical blowing agents(CBA) can be used for synthesizing both types of foams, which will undergo thermal decomposition with the evolution of vapors and physical blowing agents that attains expansion through decompression or the reaction based on heat, undergoing nonchemical change.

2. Classification of elastomeric foams

The morphology and cell structure of the material undergoing foaming are often classified as open cells and closed cells, and they made noteworthy effects regarding the properties of the foams.[10,11] The effectiveness of energy absorption of the microcellular polymeric foams highly hinges on the cell structure and size at the same time. Foam is an open-cell, lightweight material, which is commonly used for insulation, filtration, and cushioning. These foamed materials possess low density to allow air to flow through the cell structure. High-density foams have been created for fluid sealing applications in addition to the typical applications for traditional foam. The cells are more concentrated in higher-density foamed materials. The concentration of cells is lower in medium and low-density foamed materials. The complex microstructure of foams will have a strong impact on the mechanical property of foams. The relative density, the extent to which the cells are opened or closed, and the geometric anisotropy of the foams are some remarkable structural features of foams. A flexible material packed with cavities, or bubbles makes up foam structures. By creating gas bubbles in a liquid foundation, which then begins to set over a short period of time, revealing the final foam structure based on the properties of the liquid and gas. Open-cell foam and closed-cell foam come under the first category of foams and there is a combination of the two, which is usually named as semi-open cell foam.

2.1 Open cell foams

The cells of open-cell foams are aligned one below the other, and they are in contact with the surrounding air if there is no outer membrane. The flow of liquids and gases through these foams is quite easy. Its cell structure has sound-absorbing properties and when flexible, it exhibits cushioning characteristics.[12] As a result, these foams are suited for sound absorption and cushioning applications (Fig. 7.1).

Open cell foam, on the other hand, has its applications. Being softer and springier, providing excellent comfort and support for a variety of applications it offers, open cell is employed in a variety of sofas, chairs, lower seats, and mattresses because of its outstanding comfort level. Apart from that, open-cell foam comes in differing levels of stiffness and density, it can be incredibly soft or harder for more support. It can be seen in a variety of products such as support aids, pillows, pet beds, etc.

Open-cell foam has no easily vaporizable organic compounds or ozone-depleting gases. It is suitable for soundproofing and will not shrink, break or fade over time. It expands 100 times its original size while density ranges from 0.4 to 1.2 lbs./ft3.

2.1.1 Benefits of open cell foams

This type of foam has enormous applications in several areas such as soundproofing, packaging with a protective layer, furniture upholstery, interior designs etc.

2.2 Closed cell foams

Closed cell foams consist of tiny cavities, which are totally surrounded by their walls and therefore these are nothing as exchange with other cells.[3,13] The water absorption capacity

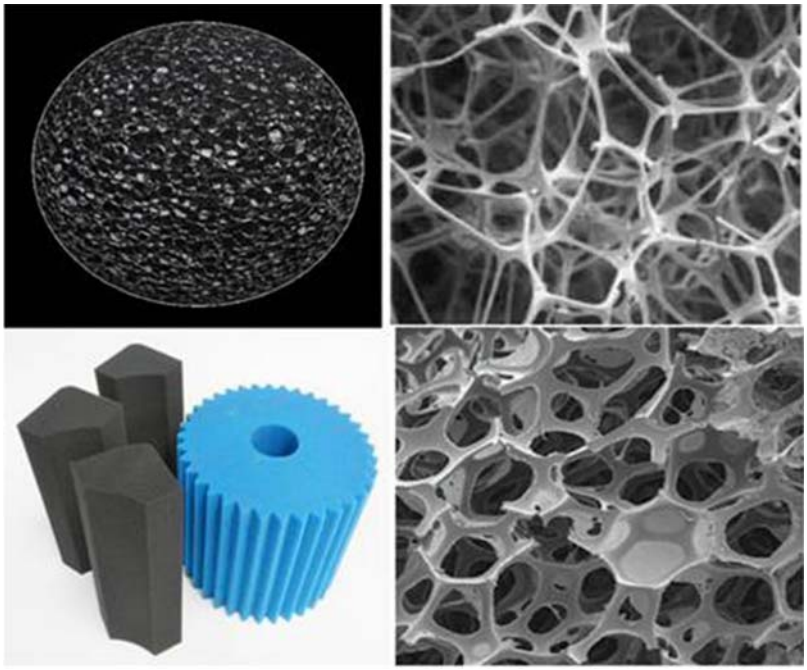

FIGURE 7.1 Open cell foams. *Athavale S.* The role of elastomeric foams in thermal insulation*; 2018*. *https://doi.org/10.13140/RG.2.2.33539.76325*.

and water vapor permeability properties are lower when compared with open-cell foams. These foams are also applied for numerous uses where a sturdier structure is needed such as packaging and shipping needs, protection barriers, and more. As it is harder, closed cells are good enough for purposes demanding added stability like transporting breakable items from one place to another. It generates a good barrier to entrap heat and air conditioning inside a building in order to reduce utility costs. So this type of foam can be used in construction as building insulation. Some electrical and automotive applications too can be utilized by these closed-cell foams (Fig. 7.2).

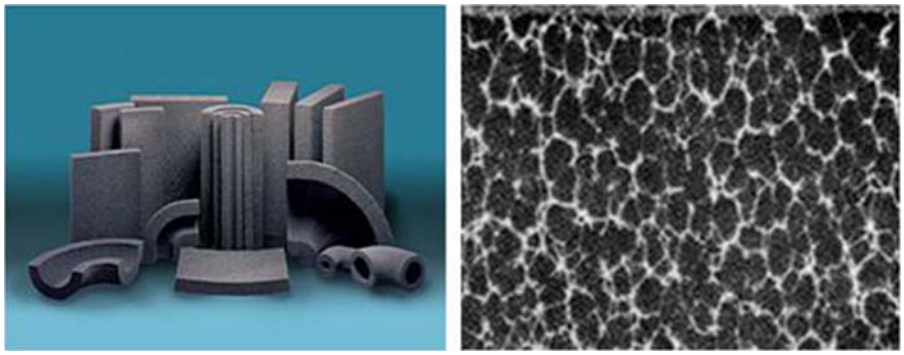

FIGURE 7.2 Closed cell foams. *Athavale S.* The role of elastomeric foams in thermal insulation*; 2018*. *https://doi.org/10.13140/RG.2.2.33539.76325*.

The closed-cell foam can be applied in inside and outside environments due to its high reliability and structural strength. It is good for imparting heat and sound insulation as well as reducing vapor transmission. Leakage is also prevented due to the structure of the foam while it acts as a barrier to moisture transport. Closed cell foam is widely used in sealing and insulation in several areas in addition to their application as disposable medical devices.

The properties, as well as performance of open-cell foam and closed-cell foam products, may be different even if they are in similar appearances and also they should be treated as two varying products. Some characteristics are common for both foams like shock absorbing ability, thermal insulating property, and noise deadening, etc. 90% and above closed cells are found in closed-cell foams, for open-cell foam, out of which there is as still any official definition, the figure is generally under 20%, even though it is having larger proportions. In addition, the basic features of the foamed material, viz tear strength, thermal conduction, average density, water absorbing ability and water tightness, and permeability of vapor or compressive strength directly depend upon closed cell content.

3. Nonlinear stress-strain behavior of elastomeric foam

Due to their light weight, designability, and good noise/vibration isolation/attenuation features, polymeric foams are used in nonstructural applications all over the world. Generally foamed material experiences large recoverable deformations when compared to solid materials, so it can perform as cushioning or buffering components.[14] Elastomeric foams are highly nonlinear in their mechanical property. Three types of compressive processes are taking place in elastomeric foam such as linear elastic deformation at low strains (<5%) due to the bending of cell walls, a plateau of deformation having a relatively low range of stress owing to elastic buckling of cell walls and finally, there will be densification at higher strains, due to crushing of cell walls, causing a sudden rise of compressive stress. An elastomeric foam under deformation under tension can be divided into two stages: the first stage is the foam deformation, which happens in a linear elastic manner that resembles the first stage of the compression process, because of cell wall bending, and the second stage of tension, the stiffness enhances gradually owing to cell wall rotation and alignment.[1] Diene et al. have suggested in creating constitutive relations regarding largely nonlinear material behavior by superposition principle about strain rates. For elastomeric foams, the nonlinear region of the stress-strain relation was recalculated based on ab-initio approximation. Polymers like polyethylene, polyurethane, and silicone foams features will be in agreement with this formulation by incorporating fillers that act as nucleating agents to impart porosity and shear modulus behavior.[15]

The behavior of elastomeric foam is susceptible to strain rate based on the visco-hyperelastic material model and it was discussed by Yang et al.[16] Quasi-static response and strain energy potentials are discussed in this model in terms of compressible hyperelasticity and suggested polynomial series by the help of three independent parameters. A nonlinear Maxwell relaxation model having four parameters are utilized to describe strain rate sensitivity. This study mainly concentrated on the polyurethane elastomer-based foams bearing two densities—PORON-4701−59-25,045−1648 (0.4 g/cm^{3}density) (PORON-1) and

PORON-4701−59-20,093−1648 (0.32 g/cm^3 density) ((PORON-2). The comparison of the responses of two foams revealed that the above-said model will be beneficial to explain compressible elastomeric materials visco-hyperelasticity loaded at increased strain rates.

The nonlinear stress-strain features for elastomeric expanded materials with large porous nature were studied regarding different kinds of biaxial tension, uniaxial tension, and compression by Iba et al.[17] Regarding the expense and mass of the materials, the study emphasized that porous elastomeric foams are superior to use. Their mechanical properties derive from low-density cellular structures of corresponding polymer solids. In addition, open cell foams containing air phase produce viscoelastic effects due to airflow caused by stress. The air enhances the rigidity of the foamed material in a small period of time that will be smaller when compared with typical time based on stress-driven airflow but will give no rigidity for a large period of time because there, the outflow of the air will be easy across cells.[18,19] Moreover, on-linearity in compression is due to the stress-strain connections, similar to thin beam bucking.[18,20−22] As a result of the bucking and collapsing of each cell that facilitates the elastomeric polymer undergoing compression with extremely little load, and the compression associating bucking of the cell brings not any considerable lateral expansion. Moreover, noncellular traditional elastomers under compression need limited load, which leads to a significant level of lateral expansion by volume conservation. Elastomeric foams with exceptional characteristics in compression behavior will be the cause behind their widespread use in shock absorption. In addition, the mechanical properties of elastomeric foamed materials are obviously compressible and undertake determinate modification in volume before and after deformation. Herein they have taken the two types of cellular elastomeric foams (Fig. 7.3) such as polyurethane open cell foam (PU) (PU-75-O) and natural rubber filled with carbon black as the closed cells of (NR) (NR-100-C).

The nonlinear stress-strain feature of elastomeric foams with large pores ($\rho^*/\rho s < 0.1$) based on biaxial extension, uniaxial extension, and compression are experimentally determined. The Poisson's ratio quantities for elastomeric foams are evaluated under finite tensile deformation from the dimensional change and have been found to be around 0.24, which is not depending upon its kind and magnitude of executed strain. Regarding planar extension, there observed some exciting features, which will be derived from finite compressibility where the dimension in one direction will not be changed.

Liu et al. proposed a nonlinear phenomenological model linked to large deformed structural foams.[14] The stress-strain response, plasticity-like stress plateau, and densification phases were explained using a model under compressive loads. In addition, in order to determine the effect of initial foam density, this model parameter should be systematically varied resulting in stress yield and hard-like or soft-like performance based on different confinement situations. In order to validate the proposed constitutive model, two foam types were with varying initial bulk densities. This model was also used fruitfully for capturing the stress-strain response of two structural foams having varied initial densities while exposed to uniaxial compression lacking lateral confinement as well as uniaxial compression under rigid confinement. Foams of this type are heat-activated structural foams that are now being used in automotive structures to modify the strength and/or stiffness of structural members.

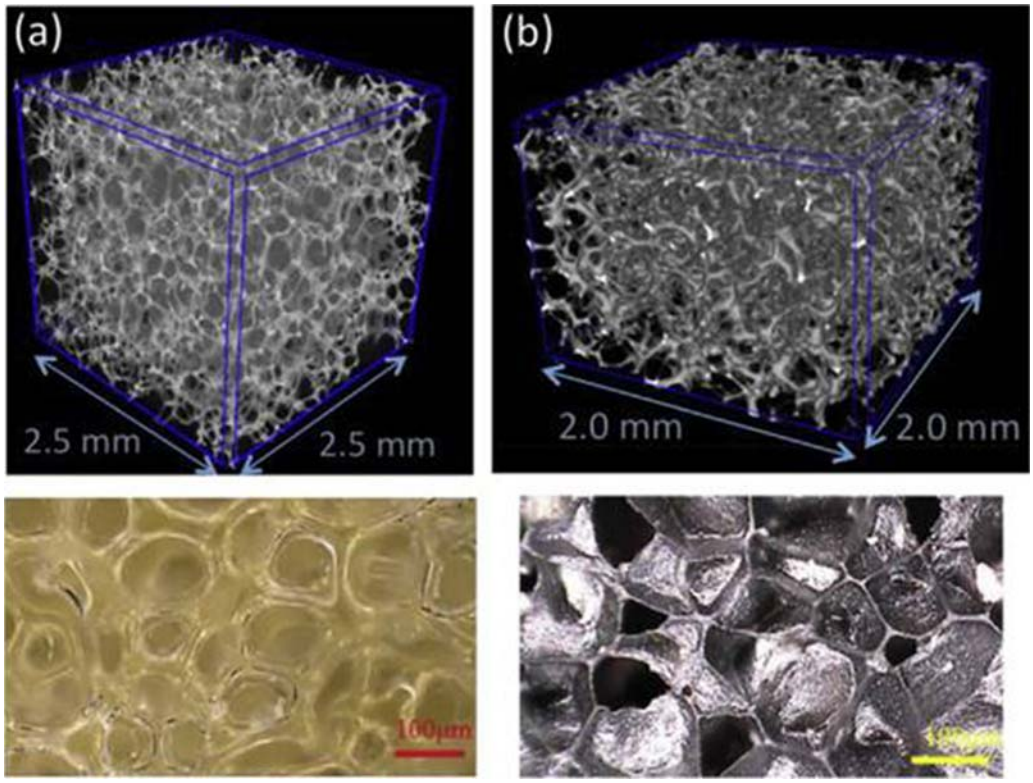

FIGURE 7.3 The images of X-ray CT (*upper*) and optical microscopy (*bottom*) for (A) PU-75-O (open-cell foam) and (B) NR-100-C (closed-cell foam). *Iba H, Nishikawa Y, Urayama K. Nonlinear stress-strain behavior of elastomer foams investigated by various types of deformation.* Polymer *2016;**83**:190–198. Copy right 2015 Elsevier.*

4. Different types of elastomeric foam for energy application; energy devices

Polymeric foam structures have been used in practice since the 1940 and 1950s and now because of their novel structural properties, these types of foams can be progressively applied in the engineering field due to physical ease in use, successful packaging, comforting energy absorption, fine insulating and cushioning properties. These returns show the way regarding a lot of uses, like buoyancy, heat-insulating, packing, and gaskets. Thus, the microstructure of the foamed material undergoes large deformations when it is utilized for general purposes. Different types of rubbers such as styrene-butadiene rubber, polyisoprene rubber, natural rubber, acrylonitrile butadiene rubber, poly (ethylene propylene diene), chlorinated polyethylene rubber, chloroprene rubber, poly(ethylene vinyl acetate), polyurethane, Poly dimethyl siloxane, Silica reinforced Poly siloxane, polymer blends and polymer composite are also using to make foams in the academic world as well as in the industrial world.

4.1 Poly dimethylsiloxane based foam

Polydimethylsiloxane (PDMS) refers to one kind of polymer based on organosilicon, which is represented by a formula $CH_3[Si(CH_3)_2O]_nSi(CH_3)$. If the organic material is a product of silicon, then there will be an effective chemical bonding existing among silicon and oxygen atoms in the backbone of the siloxane system as it promotes elasticity, optical transparency, inertness toward chemical reactions, thermal stability, biocompatibility, and PDMS has been the best effective supporting material, which can be used like an alternative in traditional silicon for microchip fabrication regarding the existing study of microelectromechanical systems (MEMS) and microfluidic devices.

Due to its exceptional surface properties, PDMS has a lot more applications like adulterations in environmental conditions, defending coating against flame, also in corrosion/oxidation.[23,24] PDMS having silanol groups makes covalent bonds of metallo-siloxane (Si—O-metal) on the surface of metals in order to attain strong adhesion at the interface, helping the material more applicable for controlling corrosion of metals and alloys.[25,26] PDMS has also been used as antiicing as well as a self-cleaning agent for buildings and car surfaces because of the instinctive hydrophobicity,[27,28] moreover antireflection coatings if combined with optical gridding as well as patterning.[29,30] However, they have low density, a high area of surface, and improved flexibility compared to bulk material due to the presence of air voids inside the PDMS material. These increased properties effectively widen the application of porous PDMS into different areas.[31—34]

Choi et al. created porous PDMS with the help of sugar particles having varying sizes and showed that enhancing the template crystals nonuniformity made finer absorptivity of organics.[35] A 3D and metal-coated interconnected Ag/Cu-PDMS sponges with the help of an electroless deposition method was also created by Liang and coworkers.[36] The as-synthesized composite showed high electrical conductivity for supporting LED lightings as stretchable circuits as shown in Fig. 7.4.

Porous carbon/PMDS are also been an important component for secondary batteries and soft conductors. Li and coworkers have synthesized GO/PDMS sponges through the process of sugar leaching, hydroiodic acid reduction, and graphene oxide infiltration.[37] Wang et al. fabricated polydimethylsiloxane (PDMS) composite foams having macroscopic porous

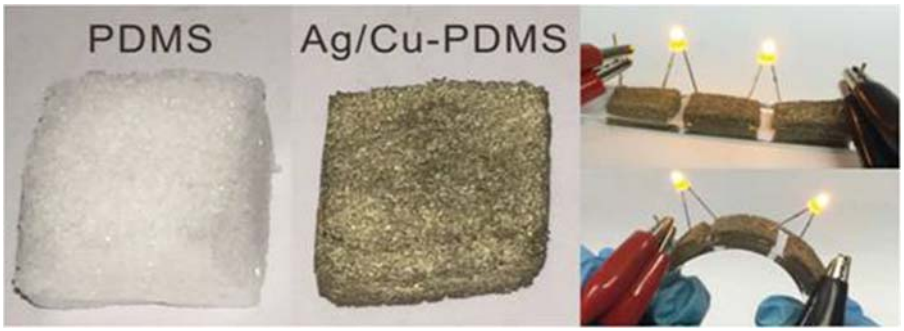

FIGURE 7.4 Optical images of the original PDMS sponge and Ag/Cu-PDMS sponge, and the LED circuits built with the Ag/Cu-PDMS sponge. *PDMS*, polydimethylsiloxane.

open cell-structures and better-quality wettability CNP/PDMS composite foams and that is behaving like an interfacial solar receiver for capturing solar energy. This composite exhibited efficient localization of heat, excellent photo-thermal features, fine floatability, and chemical stability for aiding effective interfacial solar heating. This CNPs and PDMS composite having open cell-porosity brings outstanding photo-thermal efficacy as well as thermal energy preservation for attaining efficacy in solar-powered vaporization to cost-effective manufacture of interfacial solar receivers. Thus PDMS and its composite foam served as excellent candidates and find many applications in energy-related processes.

4.2 Ethylene propylene diene terpolymer-based foam

The ethylene–propylene–diene terpolymer (EPDM) involves an important role owing to its better resisting power toward aging, high chemical stability, also greater resisting power to breakdown while performing mechanical operations. Wang et al. have developed ethylene propylene diene terpolymer foams through two varying treatments by using carbon black N330 as a reinforced particle with a high-surface area. In order to understand the microstructure and mechanical properties of the foamed materials possessing relative density varying from 0.11 to 0.62, scanning electron microscopy analysis and mechanical testing were utilized effectively. This study also mentioned the compression characteristics of EPDM foamed material having a varied relative density between 0.11 and 0.62. EDPM matrix was assessed based on properties like ideality, effectiveness, and absorption of energy-based diagram in order to optimize the selection of foams toward hands-on purposes like cushioning and packaging.[38]

4.3 Elastomeric nanoclay-based foam

The addition of nanoparticles into elastomeric materials leads to improvement in the characteristics of the host matrix. Nanoclay (NC), owing to its properties like degradation resistance toward heat and its improvement in mechanical features makes the particles one of the most efficient ones.[39,40] In addition, expanded and cured elastomeric materials called rubber foams/sponges plays a major part in the industry of rubber. Being low cost and low-density value, the foamed product will be appropriate to use in heat and sound insulating situations, absorption of energy as well as in structural purposes. Moreover, the presence of particle added as fillers affect the morphology and general characteristics of natural rubber (NR) having closed-cell foams. The reported method exhibited that nano-based carbon black (NCB) plays a vital role in the cure characteristics, morphological characteristics, and mechanical properties of rubber-based foams.[41,42]

Fig. 7.5 showed the influence of NC content on the NR/NC/NCB hybrid foams and its compressive stress-strain behavior is shown in Table 7.1. It can be noticed that NC has a well reinforcing nature and thereby it modifies the modulus of foam. The rubber-foamed materials can be compared with a composite regarding a continuous nanocomposite matrix (NR/NC/NCB)and a dispersed phase (gas cells). These results confirmed that the mechanical properties of both individual phases are not only the factors for the compressive stress-strain behavior of these foams but depends also on their morphologies.

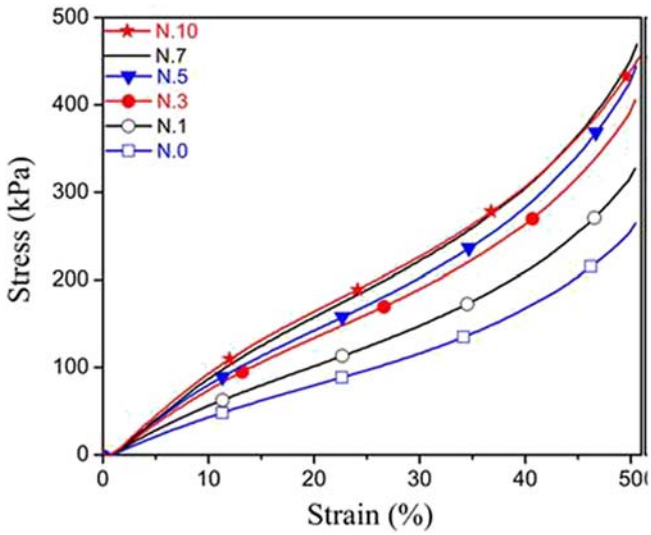

FIGURE 7.5 Stress–strain curves of NR/NC/NCB hybrid nanocomposite foams under uniaxial compression. *NC*, nanoclay; *NCB*, nanocarbon black; *NR*, natural rubber. *Ariff ZM, Zakaria Z, Tay LH, Lee SY. Effect of foaming temperature and rubber grades on properties of natural rubber foams.* J Appl Polym Sci *2008;**107**:2531–2538. Color figure can be viewed at wileyonlinelibrary.com.*

TABLE 7.1 Effect of nanoclay content on the mechanical properties of NR/NC/NCB hybrid nanocomposite foams.[43]

Sample	Elastic Modulus (kPa)	Stress at 50% Strain (kPa)	Resilience(%)	Hardness (Shore D)
N.0	500	258	79	18.1
N.1	666	320	69	21.5
N.3	841	395	63	25.9
N.5	887	432	58	32.0
N.7	911	453	51	38.0
N.10	918	448	37	37.0

These results showed that nanoclay-based foams can find novel applications owing to their better properties in engineering like lower density, great damping, large specific strength, stiffness, large fatigue strength, and greater thermal thermal stability.

4.4 Silica reinforced poly siloxane 3-D-based foam

Silicone elastomer or polysiloxane is an elastomeric polymeric material, which is having silica as the reinforcing agent. Polysiloxane with silica fillers has high stability toward heat, which enable it to function as good heat insulator.[43] However, the polymers are versatile

in nature, which makes them applicable in daily experiences like automotive parts, machines, packaging of materials, fabrics, and telephones. Others are having lesser visibility, including circuit boards, composites for spaceships, and medicinal applications.

Insulators with silicone rubber coatings are also fabricated by Seyedmehdi et al.[44] Polysiloxane rubbers are having worldwide industrial use because of outstanding stability. The mechanical properties like tensile strength, modulus, tear strength, elongation at break, hardness, compression set, rebound resilience, and abrasion resistance of silicone rubbers are commonly increased by inserting fillers. Fig. 7.6 shows the silicone rubber chain.

The excellent mechanical and physical properties of polymer composites find application both in fundamental science and industrial fields. The elastomer is having silica as filler and explore application as a heat insulator extensively for cars, house, and also day-to-day appliances.

4.5 Supercritical Co_2 based foam

Supercritical fluid technology produced remarkable steps in the previous epoch regarding commercial use and a vital understanding of solution behavior. Many of these polymers undergo a foaming process by supercritical carbon dioxide (SC CO_2) includes plastics, like polyethylene, polypropylene, polystyrene, and biodegradable polyester poly (lacticacid), poly [(1,4-butylene terephthalate)-c-(1,4-butylene adipate) (BTA). It can be seen that rubber-like or elastomeric materials involve difficulty in foaming with traditional foaming agents (chemicals).[45] But the function of falling glass transition temperature, melting of temperatures together with significant drop regarding the viscosity of polymers by SC CO_2 offers an opening to elastomer based foam materials as the movement of molecules and its orientation took place while at the time of melting state at a lowered temperature. Depending on the thermodynamic instability the foaming procedure comprises three steps: (1) formation of gas/polymer solution; (2) cell nucleation; and (3) cell growth. This is so because CO_2 will be largely undergoing diffusion, which leads to amorphous elastomeric materials without any difficulty. The advantage of foaming is expressed in terms of its greater viscoelastic feature (elongational viscosity) of elastomers. The foaming process with CO_2 can be divided into two steps as shown in Scheme 7.1.

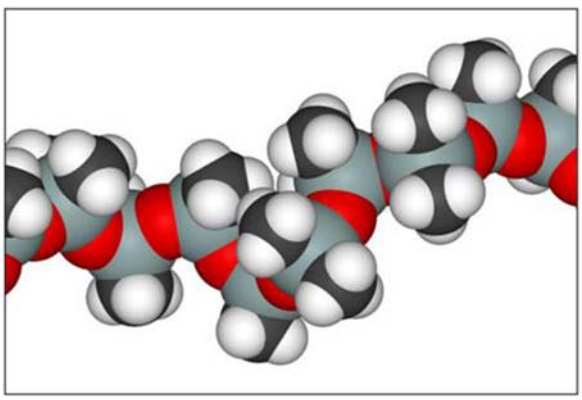

FIGURE 7.6 Silicone rubber chain. *Seyedmehdi SA, Zhang H, Zhu J. Superhydrophobic RTV silicone rubber insulator coatings.* Appl Surf Sci *2011;**258**:2972–2976. https://doi.org/10.1016/j.apsusc.2011.11.020. Copyright 1986, Wiley.*

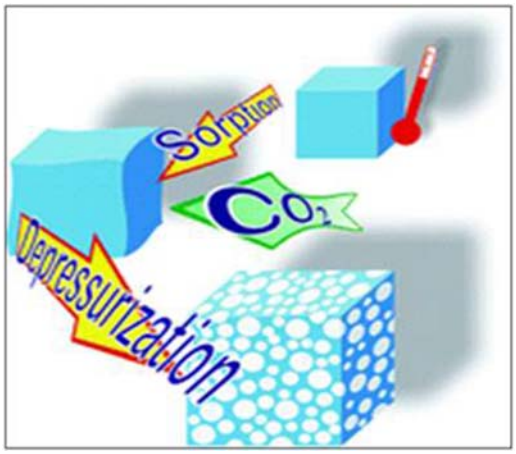

SCHEME 7.1 Schematic representation of the CO_2-foaming process. *Tomasko DL, Li H, Liu D, Han X, Wingert MJ, Lee LJ, Koelling KW. A review of CO_2 applications in the processing of polymers.* Ind Eng Chem Res *2003;**42**:6431–6456. https://doi.org/10.1021/ie030199z. Copyright 2008, RSC Publishing.*

In the current situation, CO_2 methods have developed like a potential process in order to precipitate constituent parts from solutions with the conventional environmental and tunable solvent benefits while also leaving particles solvent-free. Furthermore, these innovative methods offer reasonable means to formulate thermally labile or biologically not stable compounds, which find uses in drug-delivery systems as a progress.[46] Moreover CO_2 is a nonhazardous foaming agent, which is greener. As a result, the latest usages are to be found in foaming decomposable or biocompatible polymers to produce porous supports or other medical appliances. Sheridan et al. discussed CO_2 to foam a highly amorphous biodegradable copolymer of polylactide and polyglycolide having applications as three-dimensional tissue engineering supports. The porosity was evaluated as high as 95%.[47]

4.6 Poly urethane based foam

Polyurethane thermoset foams (PUF) are widely used in the chemical industry, electronics, textiles, medical and other fields owing to their large strength, outstanding wear resistance, and varied hardness range. Polyurethane contains a bond (NHCOO) of the urethane repeating unit. This is formed through the process of polymerization of isocyanates, polyols, and other additives (Scheme 7.1). PUFs in general categorized into flexible foams and rigid or inelastic foams. In addition, further categorizing are flexible PU slabs, flexible molded foams, reaction injection molding (RIM), carpet backing, or two-component formulations, etc.[48–50] Polyurethane has hydrogen bonding, which involves the natural link between polymer series thereby increasing total functioning and characteristics. Moreover, polymer composite comprising foams with nanosized fillers develops a high need in order to get weightless and highly functioning foams for developing areas like aviation, automobile, and electronic industry.[51,52] It is also seen that polyurethane foams (RPUFs) with rigidity showed a choice of remarkable properties such as sound mechanical properties, prominent weather capacity, and reduced thermal conductivity. RPUFs have a variety of uses as in automobile, packing, and building fields.[53]

RPUFs features are modified to meet the demands of evolving applications. Likewise, PU foams with flexibility have also synthesized for the purpose of varying outstanding features. Moreover generally applied strategies for modifying the features of foam contains different filler particles as reinforcement.[54,55] The nanofillers are generally added in polyol, prepolymer, or chain extender at the time of synthesis of PU, previous to the addition of the foaming agent. Carbon nanotube(CNT), graphene, and carbon black are nanoparticles having enormous applications owing to their excellent mechanical and physical properties. Combining nanosized subdivisions with useful properties in traditional multifunctional PU foam is familiar to developing the material functioning.

Foams of polyurethane with exceptional benefits of weightlessness, low cost, reduced density, superior manufacturability, change in shape, decomposition nature, and adjustable glass transition temperature when compared with PU polymer. Due to their unique properties, PUFs find application in various fields as follows.

4.6.1 Aerospace and automotive industry

Things like hinges, truss booms, and coilable truss booms based on PU have been investigated in the aerospace industry in addition to solar displays, deployable panels, and an antenna having reflection was also found out.[56]

4.6.2 Radar absorbing and EMI shielding

Due to the high strength-to-weight ratio of materials the radar absorbing properties can be attained in sandwich structures. So polyurethane-based foaming materials are getting the tremendous application. By adding filler particles in PU foams, sandwich structures of the core and face skins are synthesized. The spreading of reinforcing agents like fillers disturbs the material toughness as well as boosts its absorption features. It is also noticeable that polymer composites found application in EMI shielding owing to their weightlessness, and corrosion resistance.[57] There are varieties of nanofillers that can be utilized to reinforce the composite of PU foams viz CNT, graphene and GO. Bernal et al. showed polyurethane nanocomposite foamed one with rigidity inserting MWCNT fillers, which is conducting electrically and behave as EMI shielding materials.[58] Cell structure, density, and filler content are the factors that affect electrically based characteristics of PU nanocomposite foams with rigidity. EMI shielding effectiveness in PU foam-based composite objects are concentrated by the dispersion of filler and its direction in conduction-based composites.

4.6.3 Fire proof materials

Polyurethane foams generally are igneous and highly combustible cellular materials. The combustibility characteristics owing to foams based on polyurethane were the key factor to limit their important applications. The property of fire retardancy of polyurethane foams should be essential for packing, construction and building, and automotive needs. Polyurethane foams undergoing burning emit large quantity smoke and highly concentrated hydrogen cyanide and carbon monoxide toxic products, which will be hazardous when compared with common ignition outcomes. Numerous methods can be applied for increasing its fire retardancy in polyurethane foams, which are the incorporation of fire-retardant additives, adding on materials having fire-retardancy like fillers in nanorange, and finishing a layer with fire-retardant materials on PU surface.[59–61]

4.6.4 Shape memory appliance

Polymer foams with porosity, lower-density, shape memory materials are active and have tremendous applications on the technical side. Shape memory foams exist as things efficient of keeping shape, which is not permanent by the use of a thermal, chemical, and another stimulus regaining their original shape.[56,62] Singhal et al. fabricated shape memory foams of polyurethane from small molecular weight and branched hydroxyl monomers.[63] There are many reports on PU foams that highlights the effects of stimuli on shape memory and thermal and thermomechanical characteristics regarding the material.

4.6.5 Sensor

The micro-structured elastomers and polymer nanocomposites find application in sensing technologies and are being applied in capacitive devices, ferroelectric sensors, microfluidics, optical waveguides, and semiconductor nanomembranes. Dielectric films based on PU elastomeric foam, also stretchable metal electrodes exhibited strength to extremity situations containing stretching and tissue-like folding and autoclaving. Due to their good elastic behavior and large porous nature, foams having conductivity showed fine compressibility, also stable piezoresistive sensing signals have strain up to 90%. The graphene-based porous foams focus in a way on obtaining lightweight piezo resistive sensors having ultrahigh compressibility and exciting sensing performances.[64,65]

4.6.6 Biomedical application

The fabrication of new biomaterials is a great demand for curing therapeutics accomplished by minimum enveloping surgical techniques. Both biocompatibility as well as biodegradability of polyurethane-based foams encourage their usefulness both in vivo and in vitro. As a result, PU foams are greatly applicable in bone tissue engineering, nerve agent hydrolyzing enzymes, biocatalytic air filtering, absorption of biological fluids, injectable delivery systems, and other various substitutes. The injectable drug delivery systems and bone tissue engineering make use of Graphene- and PU-based foams to achieve good results. All applications of PUF-based composite are summarized and shown in Figs. 7.7 and 7.8.

4.7 Chlorinated polyethylene/chlorinated PVC-based foam

Chlorinated polyethylene(CPE)/chlorinated polyvinyl chloride (CPVC) is the low-cost alternative of polyethylene holding chlorine substance from 34% to 44%. It is used as blends of polyvinyl chloride (PVC) with soft chlorinated polyethylene enhancing the impact resistance. In addition to its resistant power to the weather. In addition to this can be utilized in PVC-based foils to make them softer, without risking plasticizer migration. The rubber industry utilizes chlorinated polyethylene, which is cross-linked peroxidically yielding elastomers. Flammability will be reduced by adding chlorinated polyethylene to another polyolefin. Like an outer jacket, chlorine-based polyethylene can be applied in power cords at times. The integration of CPVC into CPE immediately enhances the foam properties, thereby increasing the mechanical as well as fire functioning. Because of its acceptable cross-linking like intermolecular and intramolecular chains of the polymer, the dense network structure of CPE/CPVC having greater strength causes an enhanced size of the cell, lower

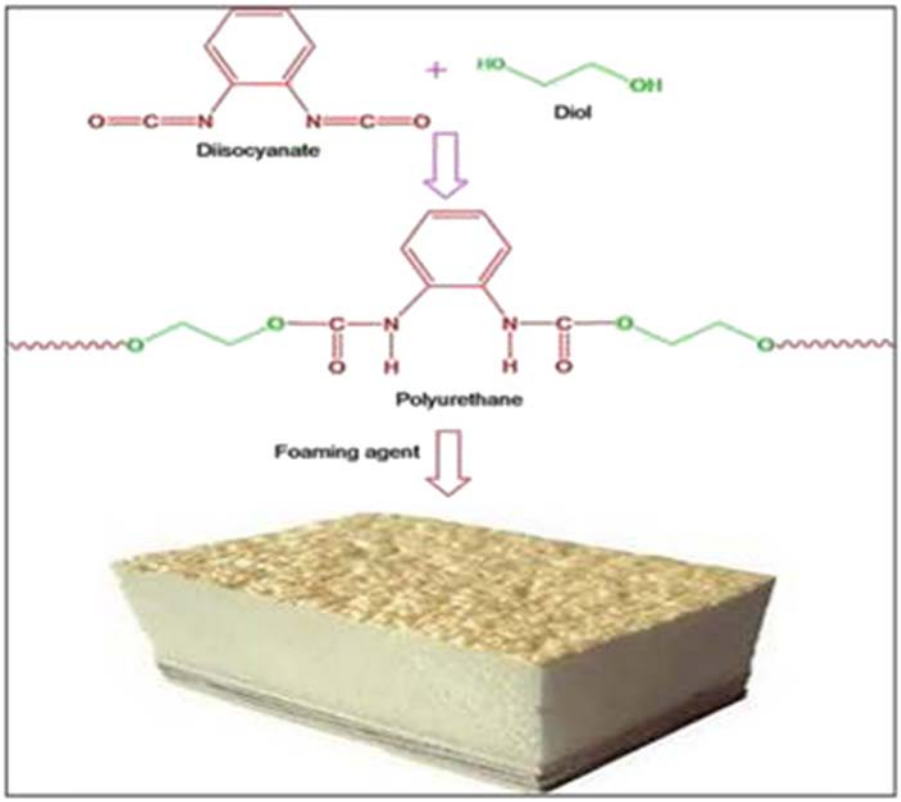

FIGURE 7.7 Polyurethane foam. *Kausar A. Polyurethane composite foams in high-performance applications: a review.* Polym-Plast Technol Eng *2018;**57**:346–369. https://doi.org/10.1080/03602559.2017.1329433. Copyright 2017, Taylor and Francis.*

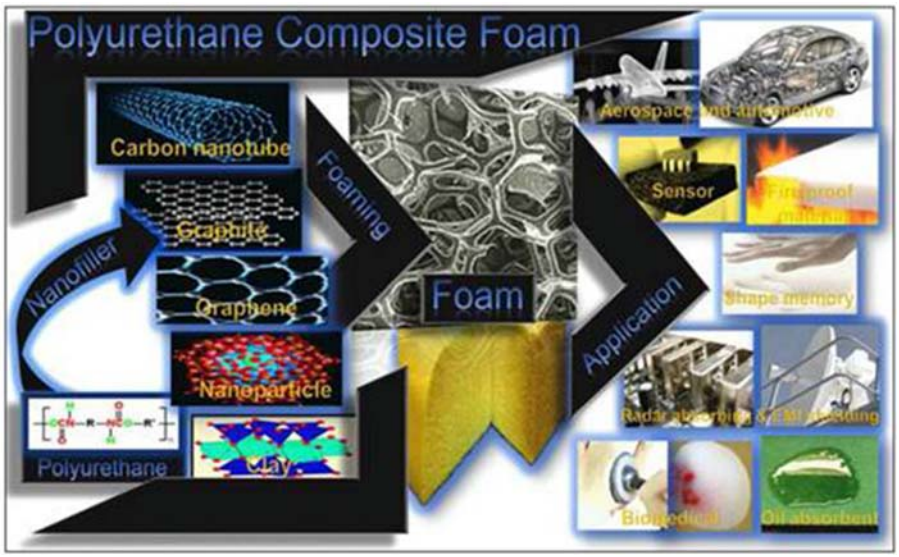

FIGURE 7.8 Polyurethane foam and its application. *Kausar A. Polyurethane composite foams in high-performance applications: a review.* Polym-Plast Technol Eng *2018;**57**:346–369. https://doi.org/10.1080/03602559.2017.1329433. Copyright 2017, Taylor and Francis.*

density of cell, also modified dimensional stability of CPE/CPVC foams (CCFs). Moreover, the flame-retardancy characteristics of foamed material (i.e., limiting oxygen index and cone calorimeter combustion) may be supposed as being enhanced by the rise of CPVC content. The (CPVC) is a nonnatural polymeric product formed through additional chlorinating PVC, which will enhance the heat and flame retardant nature of PVC.[66]

4.8 A hybrid core/solid—shell spherical-based foam

The usual cellular materials viz cancellous bone, beehive, wood, sponge, and plant parenchyma cell comprise of lightweight having unusual mechanical functioning with extra-greater toughness and specific stiffness, strong energy absorption density. Yang et al. fabricated an innovative hybrid foam-core/solid-shell spherical (FSS)structure. Super strength and great absorption of energy are attributed to their hierarchical and hybrid architectures. The planned FSS structure is probable to suggest a capable guide to plan protective structures with extraordinary functioning capacities and super performances in the coming future.[67]

4.9 Polyethylene (flexible elastomer) based foam

As this material is a long-lasting, lightweight, resilient, closed-cell material, Polyethylene (PE) foam has always been in need for packing delicate goods owing to its outstanding vibration-dampening as well as insulation characteristics. This one correspondingly advances strong resistant power to chemicals and moisture. Chemically cross-linked polyethylene foam has high thermal and mechanical resistance. Moreover, this belongs to a class of closed-cell foams utilized in varying applications. The important uses of PE foam comprising of packing, controlling insulation as well as vibrations in aerospace, flotation devices, sporty equipment's and appliances insulation. As this type of foam usually involves better selection owing to its closed-cell structure creating the material to produces more resistance toward mold, water, mildew, and further moisture-related pollutants. It has good shock absorption and vibrations, in addition to being a strong effective insulator. The important applications are enlisted as follows.

4.10 Appliances

PE foam can be employed as thermal insulator and to reduce noise in many applications. This type of foamed material is good in appliances in watery conditions, like washing machines or bathroom purposes as the foam contains cell structures as closed, which can obstruct mold and several pollutants by microorganisms. This class of foams is good for lowering the sound pollution of engines as well as their vibrations.

4.11 Insulation

Foams based on PE not only does it resist thermal energy well, but also put a stop to the disturbance of bacteria, moisture, insects, and small creatures. Mainly the animals and bugs must not cross the foam. This is the reason that PE-foamed material behaves like an excellent pest barrier in homes.

4.12 Packaging

PE foam is a great quality material for packing due to its efficacy in absorbing vibrations and weather influences. It is also sufficiently better for insulation as well as protecting oversensitive objects and is usually used for packing sensitive parts in electronics.

4.13 Aerospace equipment

Owing to its outstanding features, PE foam can be used as an insulator in aerospace. The aerospace industry chose PE foam as an insulator because the weightlessness behavior makes the foam to be a better one for use in situations where weight/mass comprises a significant parameter. The foam will also be in the absorption of vibrations and noise even though in flight.

5. Elastomeric foams in energy devices

The elastomeric foams are excellent in their properties and make them progress at a rapid pace all over the world. These properties include lightweight, outstanding strength-to-weight ratio, higher thermal and insulating abilities, energy absorption capacity, and suitable cushioning and comfort characteristics.

The fabrication of completely foldable energy storage devices is an important challenge in science as well as in the technical field, if foldable or wearable electronic appliances are to be realized for the future generation. So it is essential to create novel electrically conductive materials, which are having super flexibility in order to gain folding or crumpling ability. Huang et al. have fabricated reduced graphene oxide (RGO) layers with fixed porous nature showing an elastomer scaffold-viz folding through graphene oxide (GO) layers. Their action has shown an abundance of graphene layers with micro voids. On the basis of the folding solid-state supercapacitors, these freer RGO films act dual functions as a current collector and electroactive material. These RGO films with porous nature were utilized to synthesize a foldable solid-state supercapacitor, showing stability toward electrochemically efficient 2000 uni and bi-folding cycles.[68]

Andrea Lamberti et al. also demonstrated that flexible supercapacitor electrodes use laser-induced graphene (LIG), which acts as excellent material for activity.[19,20] It exhibits a 3D network consisting of multilayer graphene obtained by a process called laser writing process on the surface of the polymer. Herein they displace the layer of LIG with porosity produced upon a sheet of polyimide into a base PDMS (polydimethylsiloxane). The resulting composite material exhibited exceptional mechanical properties characteristic of elastomers and possess fine electrical conductivity, along with a large surface area naturally existing in the structures of LIG. Asa result, electrochemical storage with improved functioning of symmetric supercapacitor could be attained. Thus host matrix possessing elastomer-based feature allows large deformation regarding made-up appliances where it demonstrates high possibilities regarding the progress of wearable and stretchable sources of energy-storage strongly apt for the use like artificial skin and other conformal electronic systems.[69]

Furthermore, One-dimensional supercapacitors yarn/fiber for electronics with miniature equipment, implantable medical gadgets, and textile-based electronics are the most desirable sources of energy compared with traditional three- or two-dimensional foam or film-type. However, the majority of supercapacitors based on fibers (FBSs) basically hold elasticity having inadequate stretchability and tensile strain. Choi et al. fabricated coils, pseudo capacitive yarns as capable electrodes to achieve stretchable supercapacitors with high efficiency. In this case, the bare CNT coiled yarns are introduced by incorporating a giant twist (50,000 twists/m) in CNT spun yarns, that are taken as of multi-walled carbon nanotube (MWNT) forest. These CNT coiled yarns are utilized like stretchable electrodes in electrochemical double-layer capacitance (EDLC). EDLC-based supercapacitors with MnO2 will be considered since MnO_2 is a material capable of having pseudocapacitive behavior owing to their large theoretical capacitance, small rate, and environmental friendliness. They are used in stretchable in addition to strongly efficient supercapacitors based on the yarn, which use unexceptional core−shell-structured coiled electrodes in order to increase dramatically its energy storing capability. Moreover, structured yarns of the Pseudo capacitive core(CNT)−shell(MnO2) have been shown to have great elasticity, specific capacitance, mechanical and electrochemical cyclability.[70]

Jiayi Yang, exhibited liquid metal elastomer (LMEF) with very soft mechanical properties, upright compressibility, and both positive and negative piezo permittivity.[71] They illustrated the mechanism of the piezo permittivity of the LMEF from the foam structure (providing positive piezopermittivity) and the occurrence of deformable liquid metal (LM) fillers (providing negative piezopermittivity). High positive permittivity will be needed for sensing meanwhile it increases the difference in capacitance emerging from geometric differences to a capacitor, although negative piezo permittivity possesses a path to develop capacitors that will not change capacitance in reaction to deformation. Herein they reported a capacitive tactile sensor having LMEF, establishing a large capacitance difference, great sensitivity, and large initial capacitance. The capacitive tactile sensor is applied to quantify the movement of the human body or identify the place in a sensor array. Based on the LMEF piezo permittivity, an overall high-efficiency correction was demonstrated by changing the dielectric characteristics of the LMEF in response to touch.[71]

NaNi and Ling Zhang illustrated Dielectric elastomers (DEs) included in electroactive polymeric type (EAPs) showing noteworthy electromechanical impact, that finished as incredibly impressive across the last several decades as an application in soft actuators, generators, and sensors. Dielectric elastomeric sensors are made up of an elastic and flexible dielectric polymer sandwiched between two compliant electrodes, which are grounded based on the plane-parallel capacitors principle. Mechanical deformations, like pressure, strain, shear, and torsion have to be measured by using elastic and sensitive dielectric elastomer tactile sensors, akin to human skin as a result of the progress in stretchable polymers and stretchable conductors. For extreme sensitivity as well as rapid response, dielectric layers with air gaps and microstructure are utilized in pressure sensors or multiaxial force sensors. Multimodal-based dielectric elastomeric sensors have been stated in such a way as it will spot mechanical distortion nevertheless it again detects temperature, and humidity, in addition to chemical and biological stimulation in human-action examining and personal healthcare. Henceforth, dielectric elastomer sensors generally involve high capacity use in wearable appliances, soft robotics, diagnosis in the medical field, and structural health observation,

due to their high distortion, reduced expense, effortlessness in creation, also easiness of incorporation regarding monitored structures.[72]

Alan Fletcher et al. fabricated CNTs-based elastomer nanocomposite foams within fluorocarbon polymer creating outstanding capacity in the production of electromagnetic static discharge (ESD) and electromagnetic interference EMI shielding materials. It also added the benefit of its flexible and weightlessness nature.[73]

Ecoflex-0030 elastomer and liquid metal alloy, a soft porous composite was developed first time by Suryakantam Nayak, where the composite contains unsystematic porosities, which act like tiny triboelectric nanogenerators.[74] The triboelectric foam formed an extreme peak-to-peak short-circuit current having ~466 nA and open circuit voltage having ~78 V regarding a sample of size 5 ×5 ×1 cm, where the output current is ~20% advanced when comparing to formerly informed triboelectric foams grounded within polydimethylsiloxane and lead zirconate titanate/carbon nanotube having equal area. Moreover, the quality of the surface enhances its softness and increases the formation of charges resulting progress of 36% triboelectric charge. In jogging, shoe insole having porosity with 3 wt parts of LMA in Ecoflex matrix, generate a sudden power of ~2.6 mW. Also, this insole displays capacitive stimuli to distortion, which aids this sensor owing in accomplishing force, motion, and weight calculations. Thus, the shoe insole creates an immediate power of 2.6 mW during jogging situations, which is applied to power ECG chips and another wearable sensor based on a small scale. Thus, gained rapid power density seems to be considerably larger than formerly stated foams with triboelectric nature depending on PDMS and CNT/PZT. However, loading in different static or cyclic forces leads to a change in capacitance. Consequently, this kind of composite material has been utilized as a sensor to measure force as well as weight. These porous material composites with porous nature produce energy from stretching, bending, and twisting making them wearable energy harvesters to power wearable sensors.[74]

6. Conclusions and out look

Varieties of elastomeric foam, its energy applications, and energy devices are presented in this chapter owing to its novel properties like lightweight and flexibility. Polymeric foams occupy a major role in the industry as well as in commercial applications. This chapter also highlights the incorporation of varieties of organic and inorganic nanofillers in polymeric foam and its impact on enhancing its properties. In foaming, foams with exact cellular structure are created by embedding nanoparticles as fillers inside cell walls or within the cavities. The total performance of the polymer foam can be measured by the influence of the density of the cell, density of the foam, nucleation impact of nano ranged particles along with enhancing the concentration of nanofiller. As a result of the electrical conduction, thermal conduction, large specific surface area, and mechanical strength, polymer foams are widely used for multifunctional applications. The technological improvements in processing and advanced developments regarding sustainable solutions based on polymeric composite foams will produce important outcomes with the greatest applications in many areas, especially in energy devices.

Acknowledgments

All India Council for Technical Education (Order No. 8–41/FDC/RPS (POLICY-I)/2019–20), New Delhi, India is greatly acknowledged for the financial support.

References

1. Liang G, Chandrashekhara K. Neural network based constitutive model for elastomeric foams. *Eng Struct* 2008;**30**:2002–11. https://doi.org/10.1016/j.engstruct.2007.12.021.
2. Das S, Heasman P, Ben T, Qiu S. Porous organic materials: strategic design and structure–function correlation. *Chem Rev* 2017;**117**:1515–63. https://doi.org/10.1021/acs.chemrev.6b00439.
3. Khemani KC. Polymeric foams: an overview. In: Khemani KC, editor. *Polymeric foams*. Washington, DC: American Chemical Society; 1997. p. 1–7. https://doi.org/10.1021/bk-1997-0669.ch001.
4. Naguib HE, Park CB, Panzer U, Reichelt N. Strategies for achieving ultra low-density polypropylene foams. *Polym Eng Sci* 2002;**42**:1481–92. https://doi.org/10.1002/pen.11045.
5. Fujimoto Y, Ray SS, Okamoto M, Ogami A, Yamada K, Ueda K. Well-controlled biodegradable nanocomposite foams: from microcellular to nanocellular. *Macromol Rapid Commun* 2003;**24**:457–61. https://doi.org/10.1002/marc.200390068.
6. Saha MC, Mahfuz H, Chakravarty UK, Uddin M, Kabir MdE, Jeelani S. Effect of density, microstructure, and strain rate on compression behavior of polymeric foams. *Mater Sci Eng, A* 2005;**406**:328–36. https://doi.org/10.1016/j.msea.2005.07.006.
7. Alvarez P, Mendizabal A, Petite MM, Rodríguez-Pérez MA, Echeverria A. Finite element modelling of compressive mechanical behaviour of high and low density polymeric foams. *Mater Werkst* 2009;**40**:126–32. https://doi.org/10.1002/mawe.200900417.
8. Lee PC, Wang J, Park CB. Extruded open-cell foams using two semicrystalline polymers with different crystallization temperatures. *Ind Eng Chem Res* 2006;**45**:175–81. https://doi.org/10.1021/ie050498j.
9. Xu Y, Zhang S, Peng X, Wang J. Fabrication and mechanism of poly(butylene succinate) urethane ionomer microcellular foams with high thermal insulation and compressive feature. *Eur Polym J* 2018;**99**:250–8. https://doi.org/10.1016/j.eurpolymj.2017.12.032.
10. Ameli A, Nofar M, Jahani D, Rizvi G, Park CB. Development of high void fraction polylactide composite foams using injection molding: crystallization and foaming behaviors. *Chem Eng J* 2015;**262**:78–87. https://doi.org/10.1016/j.cej.2014.09.087.
11. Yuan M, Turng L-S. Microstructure and mechanical properties of microcellular injection molded polyamide-6 nanocomposites. *Polymer* 2005;**46**:7273–92. https://doi.org/10.1016/j.polymer.2005.06.054.
12. Athavale S. *The role of elastomeric foams in thermal insulation*. 2018. https://doi.org/10.13140/RG.2.2.33539.76325.
13. Lopez-Pamies O, Castañeda PP, Idiart MI. Effects of internal pore pressure on closed-cell elastomeric foams. *Int J Solid Struct* 2012;**49**:2793–8. https://doi.org/10.1016/j.ijsolstr.2012.02.024.
14. Liu Q, Subhash G. A phenomenological constitutive model for foams under large deformations. *Polym Eng Sci* 2004;**44**:463–73. https://doi.org/10.1002/pen.20041.
15. Dienes JK, Solem JC. Nonlinear behavior of some hydrostatically stressed isotropic elastomeric foams. *Acta Mech* 1999;**138**:155–62. https://doi.org/10.1007/BF01291841.
16. Yang LM, Shim VPW. A visco-hyperelastic constitutive description of elastomeric foam. *Int J Impact Eng* 2004;**30**:1099–110. https://doi.org/10.1016/j.ijimpeng.2004.03.011.
17. Iba H, Nishikawa Y, Urayama K. Nonlinear stress-strain behavior of elastomer foams investigated by various types of deformation. *Polymer* 2016;**83**:190–8. https://doi.org/10.1016/j.polymer.2015.12.021.
18. Dong L, Lakes RS. Frequency dependence of Poisson's ratio of viscoelastic elastomer foam. *Cell Polym* 2011;**30**:277–86. https://doi.org/10.1177/026248931103000601.
19. Lakes R, Lakes RS. *Viscoelastic materials*. Cambridge University Press; 2009.
20. Gibson LJ. Modelling the mechanical behavior of cellular materials. *Mater Sci Eng, A* 1989;**110**:1–36. https://doi.org/10.1016/0921-5093(89)90154-8.
21. Messinger RJ, Marks TG, Gleiman SS, Milstein F, Chmelka BF. Molecular origins of macroscopic mechanical properties of elastomeric organosiloxane foams. *Macromolecules* 2015;**48**:4835–49. https://doi.org/10.1021/acs.macromol.5b00532.

22. Zhang BS, Zhang ZX, Lv XF, Lu BX, Xin ZX. Properties of chlorinated polyethylene rubber/ethylene vinyl acetate copolymer blend-based foam. *Polym Eng Sci* 2012;**52**:218–24. https://doi.org/10.1002/pen.22071.
23. Ryu B-H, Kim D-E. Development of highly durable and low friction micro-structured PDMS coating based on bio-inspired surface design. *CIRP Annals* 2015;**64**:519–22. https://doi.org/10.1016/j.cirp.2015.03.004.
24. Eduok U, Faye O, Szpunar J. Recent developments and applications of protective silicone coatings: a review of PDMS functional materials. *Prog Org Coating* 2017;**111**:124–63. https://doi.org/10.1016/j.porgcoat.2017.05.012.
25. Wu L-K, Zhang J-T, Hu J-M, Zhang J-Q. Improved corrosion performance of electrophoretic coatings by silane addition. *Corrosion Sci* 2012;**56**:58–66. https://doi.org/10.1016/j.corsci.2011.11.018.
26. Jiang M-Y, Wu L-K, Hu J-M, Zhang J-Q. Silane-incorporated epoxy coatings on aluminum alloy (AA2024). Part 1: improved corrosion performance. *Corrosion Sci* 2015;**92**:118–26. https://doi.org/10.1016/j.corsci.2014.11.046.
27. Yu D, Zhao Y, Li H, Qi H, Li B, Yuan X. Preparation and evaluation of hydrophobic surfaces of polyacrylate-polydimethylsiloxane copolymers for anti-icing. *Prog Org Coating* 2013;**76**:1435–44. https://doi.org/10.1016/j.porgcoat.2013.05.036.
28. Kapridaki C, Maravelaki-Kalaitzaki P. TiO2–SiO2–PDMS nano-composite hydrophobic coating with self-cleaning properties for marble protection. *Prog Org Coating* 2013;**76**:400–10. https://doi.org/10.1016/j.porgcoat.2012.10.006.
29. Davaasuren G, Ngo C-V, Oh H-S, Chun D-M. Geometric study of transparent superhydrophobic surfaces of molded and grid patterned polydimethylsiloxane (PDMS). *Appl Surf Sci* 2014;**314**:530–6. https://doi.org/10.1016/j.apsusc.2014.06.170.
30. Trespidi F, Timò G, Galeotti F, Pasini M. PDMS antireflection nano-coating for glass substrates. *Microelectron Eng* 2014;**126**:13–8. https://doi.org/10.1016/j.mee.2014.03.043.
31. Gupta RK, Dunderdale GJ, England MW, Hozumi A. Oil/water separation techniques: a review of recent progresses and future directions. *J Mater Chem A* 2017;**5**:16025–58. https://doi.org/10.1039/C7TA02070H.
32. Li X, Li Y, Huang Y, Zhang T, Liu Y, Yang B, He C, Zhou X, Zhang J. Organic sponge photocatalysis. *Green Chem* 2017;**19**:2925–30. https://doi.org/10.1039/C6GC03558B.
33. Khosravi M, Azizian S. Synthesis of a novel highly oleophilic and highly hydrophobic sponge for rapid oil spill cleanup. *ACS Appl Mater Interfaces* 2015;**7**:25326–33. https://doi.org/10.1021/acsami.5b07504.
34. Nguyen DD, Tai N-H, Lee S-B, Kuo W-S. Superhydrophobic and superoleophilic properties of graphene-based sponges fabricated using a facile dip coating method. *Energy Environ Sci* 2012;**5**:7908–12. https://doi.org/10.1039/C2EE21848H.
35. Choi S-J, Kwon T-H, Im H, Moon D-I, Baek DJ, Seol M-L, Duarte JP, Choi Y-K. A polydimethylsiloxane (PDMS) sponge for the selective absorption of oil from water. *ACS Appl Mater Interfaces* 2011;**3**:4552–6. https://doi.org/10.1021/am201352w.
36. Liang S, Li Y, Yang J, Zhang J, He C, Liu Y, Zhou X. 3D stretchable, compressible, and highly conductive metal-coated polydimethylsiloxane sponges. *Adv Mater Technol* 2016;**1**:1600117. https://doi.org/10.1002/admt.201600117.
37. Li H, Ding Y, Ha H, Shi Y, Peng L, Zhang X, et al. An all-stretchable-component sodium-ion full battery. *Adv Mater* 2017;**29**(23):1700898. https://doi.org/10.1002/adma.201700898.
38. Wang B, Peng Z, Zhang Y, Zhang Y. Compressive response and energy absorption of foam EPDM. *J Appl Polym Sci* 2007;**105**:3462–9. https://doi.org/10.1002/app.26399.
39. Esmizadeh E, Naderi G, Arezoomand S, Mazinani S. Fabrication and characterization properties of polypropylene/polycarbonate/clay nanocomposites prepared with twin-screw extruder. *Sci Eng Compos Mater* 2018;**25**:31–9. https://doi.org/10.1515/secm-2015-0406.
40. Arroyo M, López-Manchado MA, Herrero B. Organo-montmorillonite as substitute of carbon black in natural rubber compounds. *Polymer* 2003;**44**:2447–53. https://doi.org/10.1016/S0032-3861(03)00090-9.
41. Ariff ZM, Zakaria Z, Tay LH, Lee SY. Effect of foaming temperature and rubber grades on properties of natural rubber foams. *J Appl Polym Sci* 2008;**107**:2531–8. https://doi.org/10.1002/app.27375.
42. J.-H. Kim, K.-C. Choi, J.-M. Yoon, The foaming characteristics and physical properties of natural rubber foams: effects of carbon black content and foaming pressure, (n.d.) vol. 7.
43. Advani SG, Hsaio K-T. *Manufacturing techniques for polymer matrix composites (PMCs)*. Woodhead Publishing Limited; 2012. https://doi.org/10.1533/9780857096258.
44. Seyedmehdi SA, Zhang H, Zhu J. Superhydrophobic RTV silicone rubber insulator coatings. *Appl Surf Sci* 2011;**258**:2972–6. https://doi.org/10.1016/j.apsusc.2011.11.020.

45. Jacobs LJM, Kemmere MF, Keurentjes JTF. Sustainable polymer foaming using high pressure carbon dioxide: a review on fundamentals, processes and applications. *Green Chem* 2008;**10**:731–8. https://doi.org/10.1039/B801895B.
46. Tomasko DL, Li H, Liu D, Han X, Wingert MJ, Lee LJ, Koelling KW. A review of CO2 applications in the processing of polymers. *Ind Eng Chem Res* 2003;**42**:6431–56. https://doi.org/10.1021/ie030199z.
47. Sheridan M, Shea LD, Peters MC, Mooney DJ. Bioabsorbable polymer scaffolds for tissue engineering capable of sustained growth factor delivery. *J Contr Release : Official J ContrRelease Society* 2000;**64**(1–3):91–102. https://doi.org/10.1016/S0168-3659(99)00138-8.
48. Ge C, Lian D, Cui S, Gao J, Lu J. Highly selective CO2 capture on waste polyurethane foam-based activated carbon. *Processes* 2019;**7**:592. https://doi.org/10.3390/pr7090592.
49. Harikrishnan G, Patro TU, Khakhar DV. Polyurethane Foam–Clay nanocomposites: nanoclays as cell openers. *Ind Eng Chem Res* 2006;**45**:7126–34. https://doi.org/10.1021/ie0600994.
50. Gama N, Ferreira A, Barros-Timmons A. Polyurethane foams: past, present, and future. *Materials* 2018;**11**:1841. https://doi.org/10.3390/ma11101841.
51. Hu L, Wang Z, Zhao Q. Flame retardant and mechanical properties of toughened phenolic foams containing a melamine phosphate borate. *Polym-Plast Technol Eng* 2017;**56**:678–86. https://doi.org/10.1080/03602559.2016.1227844.
52. Antunes M, Velasco JI. Multifunctional polymer foams with carbon nanoparticles. *Prog Polym Sci* 2014;**39**:486–509. https://doi.org/10.1016/j.progpolymsci.2013.11.002.
53. Zieleniewska M, Leszczyński MK, Szczepkowski L, Bryśkiewicz A, Krzyżowska M, Bień K, Ryszkowska J. Development and applicational evaluation of the rigid polyurethane foam composites with egg shell waste. *Polym Degrad Stabil* 2016;**132**:78–86. https://doi.org/10.1016/j.polymdegradstab.2016.02.030.
54. Widya T, Macosko CW. Nanoclay-modified rigid polyurethane foam. *J Macromol Sci, Part B* 2005;**44**:897–908. https://doi.org/10.1080/00222340500364809.
55. Kausar A. Polyurethane composite foams in high-performance applications: a review. *Polym-Plast Technol Eng* 2018;**57**:346–69. https://doi.org/10.1080/03602559.2017.1329433.
56. Liu Y, Du H, Liu L, Leng J. Shape memory polymers and their composites in aerospace applications: a review. *Smart Mater Struct* 2014;**23**:023001. https://doi.org/10.1088/0964-1726/23/2/023001.
57. Zhang H-B, Yan Q, Zheng W-G, He Z, Yu Z-Z. Tough Graphene–Polymer microcellular foams for electromagnetic interference shielding. *ACS Appl Mater Interfaces* 2011;**3**:918–24. https://doi.org/10.1021/am200021v.
58. Bernal MM, Martin-Gallego M, Molenberg I, Huynen I, Manchado MAL, Verdejo R. Influence of carbon nanoparticles on the polymerization and EMI shielding properties of PU nanocomposite foams. *RSC Adv* 2014;**4**:7911–8. https://doi.org/10.1039/C3RA45607B.
59. Zammarano M, Krämer RH, Harris R, Ohlemiller TJ, Shields JR, Rahatekar SS, Lacerda S, Gilman JW. Flammability reduction of flexible polyurethane foams via carbon nanofiber network formation. *Polym Adv Technol* 2008;**19**:588–95. https://doi.org/10.1002/pat.1111.
60. Chen M-J, Shao Z-B, Wang X-L, Chen L, Wang Y-Z. Halogen-free flame-retardant flexible polyurethane foam with a novel nitrogen–phosphorus flame retardant. *Ind Eng Chem Res* 2012;**51**:9769–76. https://doi.org/10.1021/ie301004d.
61. Qian L, Feng F, Tang S. Bi-phase flame-retardant effect of hexa-phenoxy-cyclotriphosphazene on rigid polyurethane foams containing expandable graphite. *Polymer* 2014;**55**:95–101. https://doi.org/10.1016/j.polymer.2013.12.015.
62. Singhal P, Boyle A, Brooks ML, Infanger S, Letts S, Small W, Maitland DJ, Wilson TS. Controlling the actuation rate of low-density shape-memory polymer foams in water. *Macromol Chem Phys* 2013;**214**:1204–14. https://doi.org/10.1002/macp.201200342.
63. Singhal P, Rodriguez JN, Small W, Eagleston S, de Water JV, Maitland DJ, Wilson TS. Ultra low density and highly crosslinked biocompatible shape memory polyurethane foams. *J Polym Sci B Polym Phys* 2012;**50**:724–37. https://doi.org/10.1002/polb.23056.
64. Schwartz G, Tee BC-K, Mei J, Appleton AL, Kim DH, Wang H, Bao Z. Flexible polymer transistors with high pressure sensitivity for application in electronic skin and health monitoring. *Nat Commun* 2013;**4**:1–8. https://doi.org/10.1038/ncomms2832.
65. Pang C, Kwak MK, Lee C, Jeong HE, Bae W-G, Suh KY. Nano meets beetles from wing to tiptoe: versatile tools for smart and reversible adhesions. *Nano Today* 2012;**7**:496–513. https://doi.org/10.1016/j.nantod.2012.10.009.

66. Zhang ZX, Dai X, Luo P, Sinha TK, Kim JK, Li H. Lightweight, elastomeric, and flame-retardant foams from expanded chlorinated polymers. *Macromol Mater Eng* 2019;**304**:1900145. https://doi.org/10.1002/mame.201900145.
67. Yang W, Yue Z, Xu B. A hybrid elastomeric foam-core/solid-shell spherical structure for enhanced energy absorption performance. *Int J Solid Struct* 2016;**92**–**93**:17–28. https://doi.org/10.1016/j.ijsolstr.2016.05.001.
68. Huang R, Huang M, Li X, An F, Koratkar N, Yu Z-Z. Porous graphene films with unprecedented elastomeric scaffold-like folding behavior for foldable energy storage devices. *Adv Mater* 2018;**30**:1707025. https://doi.org/10.1002/adma.201707025.
69. Lamberti A, Clerici F, Fontana M, Scaltrito L. A highly stretchable supercapacitor using laser-induced graphene electrodes onto elastomeric substrate. *Adv Energy Mater* 2016;**6**:1600050. https://doi.org/10.1002/aenm.201600050.
70. Choi C, Sim HJ, Spinks GM, Lepró X, Baughman RH, Kim SJ. Elastomeric and dynamic MnO2/CNT core–shell structure coiled yarn supercapacitor. *Adv Energy Mater* 2016;**6**:1502119. https://doi.org/10.1002/aenm.201502119.
71. Yang J, Tang D, Ao J, Ghosh T, Neumann TV, Zhang D, Piskarev E, Yu T, Truong VK, Xie K, Lai Y-C, Li Y, Dickey MD. Ultrasoft liquid metal elastomer foams with positive and negative piezopermittivity for tactile sensing. *Adv Funct Mater* 2020;**30**:2002611. https://doi.org/10.1002/adfm.202002611.
72. Ni N, Zhang L. Dielectric elastomer sensors. In: Cankaya N, editor. *Elastomers*. InTech; 2017. https://doi.org/10.5772/intechopen.68995.
73. Fletcher A, Gupta MC, Dudley KL, Vedeler E. Elastomer foam nanocomposites for electromagnetic dissipation and shielding applications. *Compos Sci Technol* 2010;**70**:953–8. https://doi.org/10.1016/j.compscitech.2010.02.011.
74. Nayak S, Li Y, Tay W, Zamburg E, Singh D, Lee C, Koh SJA, Chia P, Thean AV-Y. Liquid-metal-elastomer foam for moldable multi-functional triboelectric energy harvesting and force sensing. *Nano Energy* 2019;**64**:103912. https://doi.org/10.1016/j.nanoen.2019.103912.

This page intentionally left blank

CHAPTER

8

Nanocellulose-based polymer composites for energy applications

Sam John[1], *Sreelakshmi Rajeevan*[2], *K.P. Greeshma*[3] and *Soney C. George*[2]

[1]Department of Chemistry, St. Berchmans College, Mahatma Gandhi University Kottayam, Kerala, India; [2]Centre for Nanoscience and Technology, Amal Jyothi College of Engineering, Kottayam, Kerala, India; [3]Sri Ramakrishna College of Arts and Sciences (Autonomous) Coimbatore, Tamil Nadu, India

1. Introduction

Cellulose is considered one of the most naturally occurring organic polymers and its annual production is estimated as greater than 7.5×10^{10} tons and used as a sustainable raw material used in the paper industry. The various sources of cellulose are wood, agriculture residues, and annual plants. The amount of cellulose in wood is approximately 40%–45% by weight depending on the species. The cell wall of plants is made up of cellulose which is present in the form of microfibrils and packed to form cellulose fibers. Every individual unit of cellulose fiber is an element in the cellulose microfibrils and is seen as embedded in a matrix that is made up of lignin and hemicellulose. Lignin can be immediately oxidized by a basic medium at a high temperature and cannot be hydrolyzed in an acid medium, whereas hemicellulose constitutes an amorphous structure and contains polysaccharides.

There are various types of nanocellulose such as nano fibrillated cellulose, cellulose nanocrystals, and bacterial cellulose that are attained from different procedures. Nanofibrillated cellulose is isolated by mechanical processes under high-pressure homogenization, crushing, and filtering, while cellulose nanocrystal isolation is done by acid hydrolysis. Upon acid hydrolysis, nanofibrillated cellulose undertakes transverse splitting in the amorphous regions upon sonication resulting in rod-like materials that are denoted as cellulose whiskers. The properties of natural plant-derived cellulose nanofibers are affected by various components like cell dimensions, chemical structures, microfibril angles, and internal fiber structures which vary among the different parts of a plant. Bacterial cellulose is manufactured by a series of biotechnological processes from low-molecular-weight carbon sources (Fig. 1).

Applications of Multifunctional Nanomaterials
https://doi.org/10.1016/B978-0-12-820557-0.00031-X

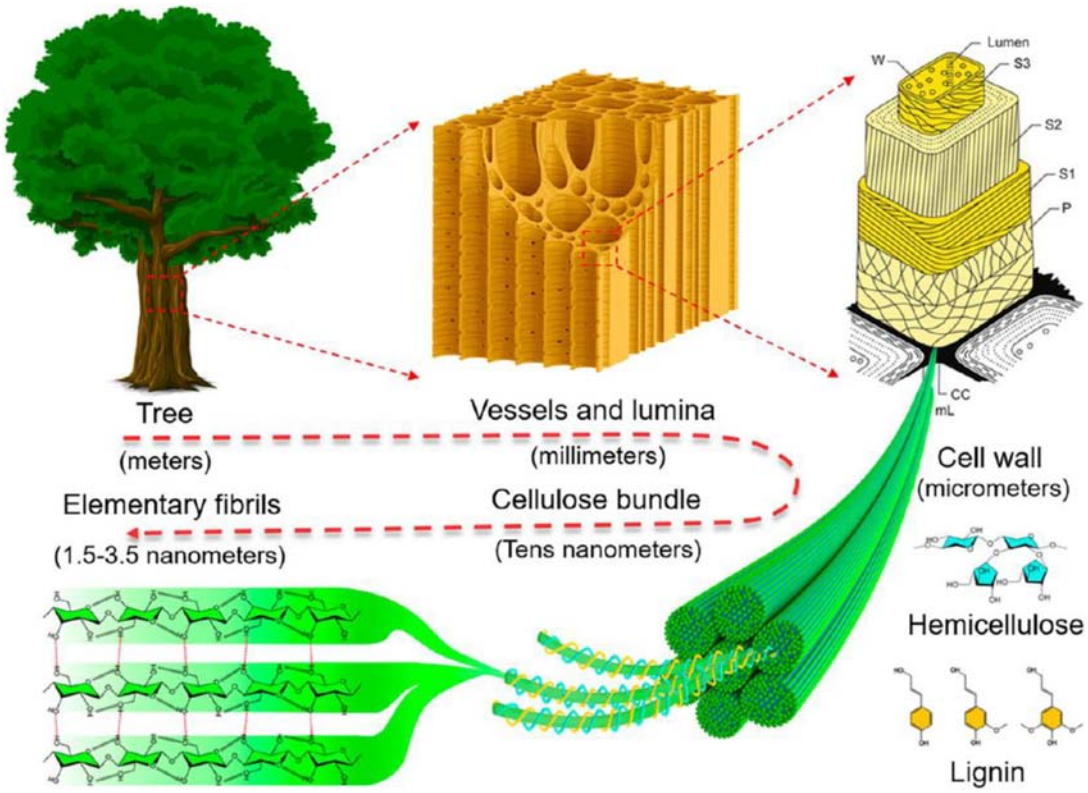

FIGURE 1 Graphical illustration of the hierarchical structure of wood, from macroscopic to molecular scale. *Tree image is adapted from ref [1]. Copyright 2017 American Chemical Society. The cell wall comprised of multilayers is adapted with permission from ref [2]. Copyright 2006 Springer Nature.*

1.1 Methods for nanocellulose isolation

The isolation of nanocellulose is from the secondary cell walls of plants, and its production is done by several procedures. The lactase enzyme can reduce or modify the lignin and hemicellulose contents without disturbing the cellulose content.

The mechanical treatment is applied in cellulosic materials for defibrillation. Chemical and enzymatic treatments are carried out to increase the ease of mechanical fibrillation. The defibrillation techniques including refining, grinding, bleaching, ultrasonication, and homogenization depend on the morphology of nanocellulose. Li and Wei tested sugarcane residue with ionic liquids (1-butyl-3-methylimidazolium chloride) under a high-pressure homogenization technique to prepare nano fibrillated cellulose. Minimize energy usage in nanocellulose production by mechanical processes usually requires chemical pretreatments including alkaline, acid, oxidation, and the enzymatic treatment of cellulose. The removal of lignin, hemicellulose, and pectin solubilization is achieved by acid-alkaline pretreatment prior to the mechanical isolation of nanofibrillated cellulose. The extraction of nanofibers from jute fibers by

treatments with DMSO is followed by acid hydrolysis.[1] The simple and fast technique to regenerate nanocellulose is of electrospinning method, and it can be potentially scaled up to industrial applications.[2]

1.2 Nanocellulose-based functional materials energy applications

Global demand for energy usage is growing because of the higher living standards of modern society. The part of energy storage systems is based on inorganic, carbonaceous substances, hydrocarbon-derived petroleum products, and metal compounds. Fossil fuel is a major source of energy that is being used to meet greater global demand for fuel. However, the usage of fossil fuels exacerbates pollution and global warming. A shift from the use of fossil fuels to renewable energy sources is inevitable while considering the current and future environmental challenges we will face over the next few decades.

One of the most abundant and almost inexhaustible natural bio-polymers is cellulose. Cellulose is considered an alternative to fossil fuel-based polymers which is a bio-degradable, bio-compatible, and renewable natural polymers. The glycosidic oxygen bridges of cellulose monomers are joined by β-1,4-linked glucopyranose (Fig. 2). The monomer unit in cellulose is twined by an angle of 180 degrees with respect to its neighbors. Cellobiose is a dimer of this natural polymer, and it is the repeating unit. Depending upon the source, the degree of polymerization of wood-derived cellulose may change and it is approximately 10,000 glucose units while cotton-derived cellulose is 15,000 units. The characteristics such as hydrophilicity, chirality, and biodegradability of cellulose are due to the presence of three hydroxyl groups in glucopyranose.

Cellulose is a unique, sustainable, functional material with appealing mechanical and electrochemical characteristics: it has a high surface area and fibrous structures, is economically feasible, has excellent stability in most solvents, thermal stability, hydrophilicity, high specific modulus ($\sim$100 GPa/(g/cm^3). Nanocellulose has been widely used as a separator, electrolyte, binder, and substrate material for energy storage. In addition to this, nanocellulose-derived carbon materials have gained scientific attention in sustainable energy storage due to their raw-material abundance, low-cost, high conductivity, and sensible electrochemical performance. The derivatives of nanocellulose are inexpensive and environmentally friendly, make them as promising candidate for the fabrication of green renewable energy storage devices.

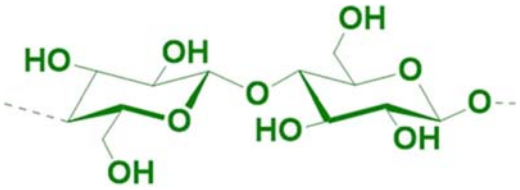

FIGURE 2 The chemical structure of cellulose, which is a linear polymer made up of β-D-glucopyranose units covalently linked with (1−4) glycosidic bonds.

1.3 Cellulose-based supercapacitors

A supercapacitor is referred to as an electrochemical energy storage device possessing high power, a long life cycle, and low maintenance cost. Supercapacitors are classified as electrical double-layer (EDL) capacitors and pseudocapacitors. In EDL capacitors, the electrochemical energy is accumulated by the adsorption/desorption of ions, and the pseudocapacitor works based on redox reactions.[3] There is another type of supercapacitor available: hybrid supercapacitor, a small-footprint, high-power energy storage device that comprises two kinds of electrodes. Hence, hybrid supercapacitors have a high energy density, high power density, and high cycling stability.

The unique chemical structure of nanocellulose is (1) good mechanical stability and a high aspect ratio modifies the nanocellulose highly for flexible energy storage applications (2) ample of −OH groups on the surface of nanocellulose permitting a wide possibility of hybridization to convert nanocellulose into composite electrodes and separators, (3) nanocellulose possess good structural, thermal stability, and wettability in different electrolytes makes it as a good candidate for the applications of electrochemical energy storage (4) Because of high porous structure, doping nature, high surface area, tunable microstructure, high carbon content, and easily modifiable properties of nanocellulose making it an outstanding candidate for the preparation of electrode material. The nanocellulose hydrogels/aerogels with tunable surface structures enable the deposition of electroactive and conducting materials to produce electrode sheets and supercapacitor systems.

1.3.1 1D supercapacitors

Nanocellulose fibers have flexibility, good mechanical robustness, and numerous pores which enable the nanocellulose network for active material loading making it a perfectly strong and flexible material for 1D energy storage devices. Gogotsi et al. reported porous carbon materials that can be embedded into cellulose-based yarns for wearable supercapacitors.[4] The functional modification of biopolymer is achieved by adding a controlled amount of molecular cosolvents and ionic liquids. They suggested that the natural fiber welding process converts cellulose yarn into supercapacitors. In this way, the natural fibers are combined with functional materials (e.g., nano carbons) to generate hybrid macroscopic fiber electrodes, which reveal both high capacitance (up to 37 mF /cm) and flexibility.

1.3.2 2D supercapacitors

2D flexible supercapacitors are highly attractive and used in portable and wearable electronics. The relatively high specific surface area and multifunctional electronic structure of two-dimensional (2D) materials, such as MXene, molybdenum disulfide (MoS_2), and graphene, make it an ideal candidate for applications in flexible energy storage devices. Nanocellulose contains a hydrophobic C−H part that can interact with the hydrophobic part of 2D material and the hydrophilic part of the nano cellulose forms H-bonding with the hydrophilic OH group at the defective edges of 2D material. A simple 2D paper supercapacitor was prepared by applying carbon nanotube ink on A4-sized cellulose paper.

In the same way, flexible supercapacitors are designed by printing, filtration, or coating methods engaging various carbonaceous materials, conductive polymers, or metal oxides. The preparation of electrodes in the form of films of graphene and nanocellulose was

proposed by many researchers. Such supercapacitors exhibit high mechanical strength, high specific surface area, high cyclic stability, fast charging, and discharging rate, and high-power density.[5,6]

1.3.3 3D supercapacitors

Flexible energy storage systems have recently gained attention in terms of portable electronic devices. In situ polymerization of three-dimensional cellulose/graphene, tailoring its nanostructure and functional modification of graphene provides a massive platform for energy storage. The nanocellulose/graphene oxide 3D supercapacitors were developed by Liu et al. The bond between the carboxyl group of graphene oxide and the hydroxyl group of nanocellulose has not allowed the piling of graphene oxide layers thus preventing the aggregation of nanocellulose in the platform. The nanocellulose-based aerogel is used as substrates of energy devices due to the advantages of high porous structure, large specific surface area, and extremely low density. The H-bonding interaction between water and cellulose, the fabricated nanocellulose aerogels could remain in their shape in the water. The support material used for electrochemical energy storage devices is bacterial cellulose-derived carbon nanofiber aerogel with high porosity, large surface area, large thickness, and controllable doping structure.

Wu et al. made a 3D scaffold aerogel with increased porosity and surface area.[7] In addition to aerogel, three-dimensional electrodes are also prepared from wood-based materials, and it is possible to increase the thickness and mass loading of the electrodes as well.

Naturally obtained wood-based materials are relatively abundant and renewable energy sources, the merit of wood-based materials consists of large thickness, long channels with small tortuosity, rich pathways for electrons and ions, and mass loading capacity.

The strategies of constructing wood-based energy storage devices can be divided into three types: (1) direct utilization of wood and its carbonaceous products as separators and electrode active materials, (2) carbonization process of the wood membrane to perform as a three-dimensional current collector, enables various types of electrode active materials to be penetrated or coated into the pores, (3) the three-dimensional electrodes are fabricated from the single multi-channelled structure of wood. The manufacturing of various wood-based electrodes and devices with multiple functions depends on the variety of these construction strategies which helps encompass the scope in the field of energy storage applications.

1.4 Cellulose-based separators and electrolytes

Nowadays lithium-ion batteries are used as one of the important and most promising energy storage devices. Lithium-ion batteries are not only used in laptops, digital cameras, and portable electronic devices but also used in wearable/flexible devices, large-scale power sources, and hybrid electrical vehicles. In lithium-ion batteries, the anode and cathode are separated by a permeable membrane. The important function of a permeable membrane is to prevent an electrical short circuit between the anode and cathode of electrochemical cell. The permeable membrane allows the passage of ionic charge carriers that are essential to close the circuit in an electrochemical cell during the passage of current.

The critical components used in liquid electrolyte batteries are separators. Separators should be chemically stable to nonaqueous organic solvent and electrochemically stable with regard to the electrolyte and electrode materials and mechanically strong enough to resist the high tension during battery construction. The structure and properties of separators play a key role in influencing the energy density, and cell performance, including service life, power density, and safety.

The excellent mechanical strength and chemical stability of polyethylene and polypropylene are used for the manufacture of membrane separators. The natural abundance and structural configuration of cellulose make it a favorable applicant for the manufacture of separators, reinforcing agents in gel polymer, solid polymer electrolytes, and electrodes. The lithium-ion battery separators are made up of a large variety of cellulose including nanocrystalline cellulose, ordinary cellulose, cellulose nanofibrils, and bacterial cellulose. The derivative of cellulose such as cellulose acetate butyrate, cellulose acetate, methylcellulose, cellulose di acetate, hydroxy propyl methyl cellulose, carboxy methyl cellulose, and hydroxy ethyl cellulose, etc., are commonly used.

Cellulose microfibers are the most common substrate in commercial paper. Paper is the most exploited and cheapest substrate that exhibits favorable properties such as low price, recyclability, mechanical flexibility, and biocompatibility. The cellulose microfibers in paper form a rough, mesoporous platform with many surface functional groups which is helpful for binding electroactive and conducting materials and the porous structure enables the fast mass transport of chemical species. In the case of lithium metal/liquid electrolyte systems, where uneven lithium dendrites grow during electrochemical cycling and can lead to an explosion.

A good electrolyte must satisfy several conditions,[8] it neither react nor degrade in the normal voltage range nor leak or vaporize during the cell operation. The physicochemical robust nature helps the formation of iron pair and promotes + vely charged lithium-ion. It should also be suitable with the electrode and penetrate the pores of the separator. Above such characteristics need to be maintained over many charge/discharge cycles. Today the most used electrolytes are the mixtures of ethylene carbonate and ethyl methyl carbonate, dimethyl carbonate, and diethyl carbonate. These mixed electrolytes are volatile polar, very low thermal stability, polar, flammable, and low electrochemical stability together with high reduction potential. Due to this inherent drawbacks scientists are looking for new alternatives such as solid-type gel-type electrolytes. Several methods are, but nanocellulose has been used as a new substrate for solid-state electrolytes. A. Chiappone et al. developed micro fibrillated cellulose polymer electrolytes for Li-ion batteries. Nair et al. reported that polymer electrolyte membranes with cellulose possess good mechanical stabilities.[9,10]

1.5 Nanocellulose for metal−air batteries

In the future energy network, the electrochemical energy storage devices are essential components to safeguard the unpredictable energy generation and supplies from renewable sources. When compared to lithium-ion batteries, metal-O_2 batteries have much higher theoretical energy density and are frequently promoted as the solution for next-generation electrochemical energy storage applications in electric vehicles or grid energy storage. For achieving electrochemical reliability, the active and durable electrocatalysts in metal−air rechargeable

batteries can accelerate the evolution reaction and oxygen reduction reaction. The electrocatalysts can be generally divided into seven: (1) transition metal oxides, containing single-metal oxides, noble metal oxides like $RuO_2$and mixed-metal oxides; (2) functional carbon materials consist of nanostructured carbons and doped carbons; (3) metal oxide−nanocarbon hybrid materials; (4) metal−nitrogen complex including nonpyrolyzed and pyrolyzed; (5) conductive polymers; (6) transition metal nitrides; (7) noble metals Pt, Ag, Au, and its alloys.

The development of electrocatalysts for both primary and rechargeable metal−air batteries have gained great attention in recent years. The chemical kinetics of the reaction is very low; therefore, metals such as platinum, ruthenium, and iridium, and their alloys are used to enhance the rate of electrochemical reaction. At the same time, the relatively high amount of precious metals and inadequate electrocatalyst impose a hurdle to practical application. Recently, the precious metal catalyst is replaced by cost-effective cellulose derives air catalyst. The electrocatalytic spots are generated by the pyrolysis of nano cellulose.

Heteroatom doping is usually used to change the nature and chemical properties of pure carbon materials and attain advanced metal-free carbon catalysts for rechargeable metal−air batteries to promote electrochemical properties. Doping carbon with hetero atoms such as N, P, S, and B can modify the properties of carbon. The structure-engineered nanocarbon doped with a heteroatom, nitrogen (N) has facilitated catalytic reactions. Because nitrogen has a larger electronegativity value than carbon, relatively small covalent radii, and a similar atomic size to carbon, five valence electrons of nitrogen are used for bonding with carbon atoms. Nitrogen has a higher electronegativity value than carbon that can attract electrons from carbons creating defects and induce conductivity of the carbon material and thus enhancing battery performance.

Nitrogen-doped bacterial cellulose carbon nanofiber aerogel was reported by Yu et al. for zinc-air batteries. This nitrogen can induce defects at the graphene edges or basal planes. Structurally these defective sites act as active regions for the reduction of oxygen and show good electrochemical stability in basis media.[11]

Cellulose nanofibril-based alkaline anion exchange film was announced by Chen and coworkers. Surface modification of cellulose nanofibril with quaternary ammonium salts brings about 2-QAFC exhibiting high hydroxide ion conductivity and a separator for metal-air battery. The membrane allows the passage of −OH ions between the metal and air, and the water holding capacity of the membrane, low anisotropic swelling boosted the specific capacities; and improved cycling performance.[12]

1.6 Nanocellulose fabricated solar cell

Low cost, compatibility with flexible substrates, and lightweight organic photovoltaics have developed as an economic potential substitute for silicon-based solar cells. Conventional and inverted are the two configurations of organic photovoltaics. The inverted configuration is inert to both oxygen and humidity, so they favor long-term stability. Nanocrystalline cellulose and nano fabrillated cellulose have low thermal expansion coefficients, dimensional stability, transparency, dominant reinforcing potential, and unique value of high Young's modulus. Smooth and highly transparent films are prepared from cellulose fibers. These

transparent films are used as an alternative and interesting substrate material for organic solar cells, light-emitting diodes, thin film transistors, and touch screens.[13–16]

An efficient and well-organized polymeric solar cell was prepared by Zhou et al. in 2013 with nanocrystals of cellulose as the substrate. The polymeric solar cell showed an efficiency of 2.7% and exhibit good rectification in the dark. An alternate work conducted by Zhou et al. shows an efficiency of 4%. The solar cell is also prepared by depositing conducting polymer to nanocrystals of cellulose via a film-transfer lamination process.[17]

To achieve the light scattering ability, solar cell materials have high light scattering and excellent optical clearness or haze. Approximately 96% transparency and 60% ultrahigh haze novel wood-based nanocellulose paper were developed by Fang et al. To attach the carboxyl group in to wood fiber, it is treated with an oxidizing agent TEMPO/NaBr/NaClO. This process reduces the H-bonds between the cellulose fibrils and converts it into a high-density material having excellent optical properties. The power conversion efficiency of wood fiber-based transparent paper increased from 5.34% to 5.88% as compared to regular cellulose-based materials.[18]

1.7 Conclusion

Especially cellulose is an auspicious material for the preparation of economically cheap, lightweight, soft, and viable supercapacitors. The most naturally rich renewable organic bio-polymer cellulose has several interesting qualities including good porosity, hydrophilicity, and mechanical flexibility. These countenances make cellulose an ideal architecture block for connecting with a variety of capacitive energy storage substrates. Methylcellulose an eco-friendly polymer material was successfully used in lithium-ion batteries. Conductive materials derived from nanocellulose have been extensively adopted in the area of energy materials, such as solar cells and lithium-ion batteries. The impressive characteristics of cellulose-modified composite materials and carbon materials used as independent elements for high-performance sodium-ion capacitors or sodium-ion batteries.

References

1. Wang B, Sain M. Dispersion of soybean stock-based nanofiber in a plastic matrix. *Polym Int* 2007;**56**:538–46.
2. George J, Sabapathi SN. Cellulose nanocrystals: synthesis, functional properties, and applications. *Nanotechnol Sci Appl* 2015;**8**:45–54.
3. Chen W, Yu H, Lee SY, Wei T, Li J, Fan Z. Nanocellulose: a promising nanomaterial for advanced electrochemical energy storage. *Chem Soc Rev* 2018;**47**:2837–72.
4. Jost K, Durkin DP, Haverhals LM, Brown EK, Langenstein M, De Long HC, Trulove PC, Gogotsi Y, Dion G. Natural fiber welded electrode yarns for knittable textile supercapacitors. *Adv Energy Mater* 2015;**5**:1401286–93.
5. Ma Q, Cheng H, Fane AG, Wang R, Zhang H. Recent development of advanced materials with special wettability for selective oil/water separation. *Small* 2016;**12**:2186–202.
6. Wan C, Jiao Y, Li J. Flexible, highly conductive, and free-standing reduced graphene oxide/polypyrrole/cellulose hybrid papers for supercapacitor electrodes. *J Mater Chem* 2016;**5**:3819–31.
7. Wu ZY, Liang HW, Chen LF, Hu BC, Yu SH. Bacterial cellulose: a robust platform for design of three dimensional carbon-based functional nanomaterials. *Acc Chem Res* 2016;**49**:96–105.
8. Xu K. Nonaqueous liquid electrolytes for lithium-based rechargeable batteries. *Chem Inform* 2004;**35**.

9. Nair JR, Chiappone A, Gerbaldi C, Ijeri VS, Zeno E, Bongiovanni R, Bodoardo S, Penazzi N. Novel cellulose reinforcement for polymer electrolyte membranes with outstanding mechanical properties. *Electrochim Acta* 2011;**57**(15):104–11.
10. Chiappone A, Jijeesh JR, Gerbaldi C, Jabbour L, Bongiovanni R, Zeno E, Beneventi DN. Penazzi, Microfibrillated cellulose as reinforcement for Li-ion battery polymer electrolytes with excellent mechanical stability. *J.Jpow Sour* 2011;**196**:10280–8.
11. Liang HW, Zhen-Yu Wu ZY, Chen LF, Li C, Yu SH. Bacterial cellulose derived nitrogen-doped carbon nanofiber aerogel: an efficient metal-free oxygen reduction electrocatalyst for zinc-air battery. *Nano Energy* 2015;**11**:366–76.
12. Fu J, Zhang J, Song X, Zarrin H, Tian X, Qiao J, Rasen L, Li K, Chen Z. A flexible solid-state electrolyte for wide-scale integration of rechargeable zinc–air batteries. *Energy Environ Sci* 2016;**9**:663–70.
13. Zhu H, Fang Z, Preston C, Li Y, Hu L. Transparent paper: fabrications, properties, and device applications. *Energy Environ Sci* 2014;**7**:269–87.
14. Klemm D, Kramer F, Moritz S, Lindstrom T, Ankerfors M, Gray D, Dorris A. Nanocelluloses: a new family of nature-based materials. *Angew. Chem. Int. Ed* 2011;**50**:5438–46.
15. Chinga-Carrasco G, Tobjork D, Osterbacka R. Inkjet-printed silver nanoparticles on nano-engineered cellulose films for electrically conducting structures and organic transistors: concept and challenges. *J Nanopart Res* 2012;**14**:1213–22.
16. Zhu H, Xiao Z, Liu D, Li Y, Weadock NJ, Fang Z, Huang J, Hu L. Biodegradable transparent substrates for flexible organic-light-emitting diodes. *Energy Environ Sci* 2013;**6**:2105–11.
17. Zhou Y, Khan TM, Liu JC, Fuentes-Hernandez C, Shim JW, Najafabadi E, Youngblood JP, Moon RJ, Kippelen B. Recyclable organic solar cells on cellulose nanocrystal substrates. *Sci Rep* 2013;**3**:1536–40.
18. Fang ZQ, Zhu HL, Yuan YB, Ha D, Zhu SZ, Preston C, Chen QX, Li YY, Han XG, Lee S, Chen G, Li T, Munday J, Huang JS, Hu LB. Novel nanostructured paper with ultrahigh transparency and ultrahigh haze for solar cells. *Nano Lett* 2014;**14**(2):765–73.

This page intentionally left blank

CHAPTER

9

Advances in functionalized polyaniline nanocomposites for electrochemical sensing and energy storage applications

Sreekala S. Sharma[1,2] *and Shiny Palatty*[1]

[1]Department of Chemistry, Bharata Mata College, Kochi, Kerala, India; [2]Department of Chemistry, Sree Sankara Vidyapeetom College, Ernakulam, Kerala, India

1. Introduction

Polyaniline (PANi) is a conducting polymer that has been widely explored for electrochemical applications in the field of energy storage and as a sensing platform for the detection of various moieties. The properties of PANi such as economical and feasible methods of synthesis, appreciable conductivity that can be modulated, better environmental stability, alterable doping/dedoping chemistry, and fascinating redox properties due to the existence of variable oxidation states make PANi attractive for diverse applications.[1–4] The functionalization of PANi by forming composites with nanomaterials like metal oxides, metal nanoparticles, metal sulfides, metal-organic frameworks, carbon nanomaterials, etc. has improved the many-fold properties of PANi and widened the scope of application in different arenas.[5–8]

The need for alternate clean energy sources to solve the problems of energy catastrophe arising from the exhaustion of fossil fuels necessitated the development of supercapacitors as energy storage devices.[9] Among the conducting polymers, polyaniline can be considered the most prospective choice for developing electrode materials compared to the high molecular weight counterparts such as polythiophene and polypyrrole.[10] Polyaniline possesses the properties vital for developing electrode materials for supercapacitors such as good electrochemical activity, high specific capacitance, and appreciable stability in acid medium.[11] The drawbacks of polyaniline such as structural instability due to swelling and shrinkage of

Applications of Multifunctional Nanomaterials
https://doi.org/10.1016/B978-0-12-820557-0.00004-7

individual polymer chains during the charge-discharge process can be significantly improved to a great extent by forming composites with nanomaterials and carbonaceous materials.[12,13]

Another provoking challenge faced by the scientific community is the development of sensing materials competent for sensing environmental pollutants ranging from toxic gases to persistent organic pollutants.[14] In this aspect also, polyaniline has been utilized as the sensing platform for fabricating electrochemical sensors on account of the peculiar optical properties of the polymer and the existence of three oxidation states having a different color, electrical conductivity, and stability.[15,16]

2. Fundamental principles

2.1 Electrochemical sensing

Electrochemical (EC) sensors belong to the subclass of chemical sensors, which senses the concentration of an analyte based on a chemical reaction. The EC sensors detect the information allied with chemical reactions and convert it into the form of measurable current (amperometric/voltammetric method), conductivity (conductometric method), and voltage or potential (potentiometric method).[17,18] The working of EC sensors involves the pairing of a chemically selective layer capable of recognizing the electrocatalyzed chemical reactions with an electrochemical transducer, which converts the chemical changes into electrical signals.[19] The basic setup for the electrochemical sensor can be schematically represented as shown in Fig. 9.1.

2.2 Energy storage devices

The energy crisis and the need for alternate energy storage devices have always baffled the scientific community for the past few decades. Supercapacitors have emerged as a promising technology for energy storage since they can store energy by the conversion of electrical energy to chemical energy.[20] Supercapacitors have the advantages of prolonged cycle life, good

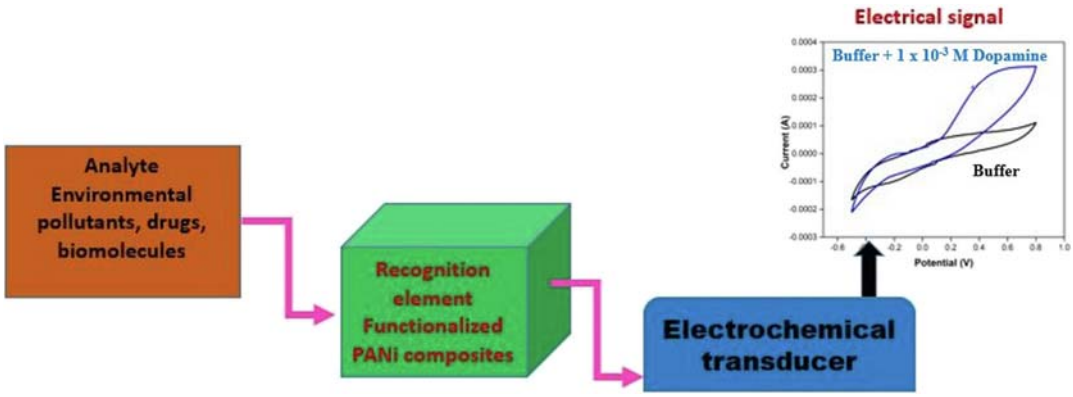

FIGURE 9.1 Schematic representation of the basic set up of an electrochemical sensor

power density, and a wider range of operation compared to conventional batteries and dielectric capacitors.[21] The main criterion that classifies supercapacitors is the energy storage mechanism and based on this two categories are possible viz. the Electrical double layer capacitors (EDLCs) and pseudocapacitors. In EDLCs the charge storage is influenced by the separation of charges at the boundary between the electrolyte and electrode whereas in pseudo capacitors charge storage relies on rapid and Faradaic redox reactions (reversible) happening in the bulk of the material or on the surface.[22,23] Polyaniline belonging to the family of pseudocapacitors is widely employed as electrode material for supercapacitors on account of its higher values of specific capacitance.[24] However, deprived cycling stability and poor rate capability of polyaniline during charge-discharge cycles impose the need for developing functionalized composites of polyaniline with other EDLCs such as carbon nanotubes, graphene, and its derivatives and also with pseudocapacitive metal oxides, metal sulfides and metal nanoparticles.[25–27] The classification of supercapacitors can be better understood on the basis of the schematic representation as shown in Fig. 9.2.

3. Functionalized polyaniline nanocomposites for electrochemical sensing applications

3.1 Polyaniline-based electrochemical sensors for biomolecules

Functionalized Polyaniline composites have widely received appreciation as a recognition element in electrochemical sensors for detecting a wide variety of analytes spanning from biomolecules to environmental contaminants due to the simple methods of synthesis, redox chemical properties, and ease of functionalization.[28] A glucose sensor without employing enzymes based on PANI-reduced graphene oxide (RGO) with silver nanoparticle functionalization has been reported by Deshmukh et al. The PANI-Ag-RGO composite was prepared by electrochemical polymerization technique and exhibited remarkable sensitivity (2.7664 $\mu A/\mu M/cm^2$),

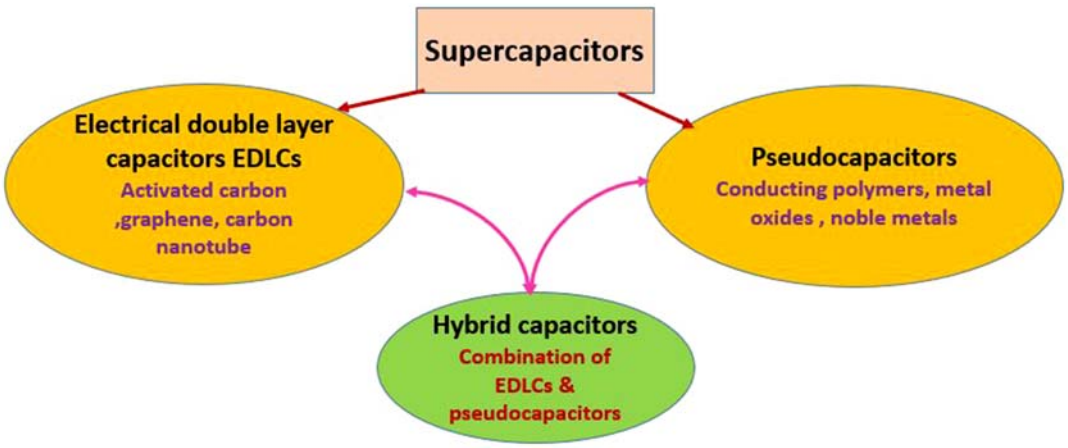

FIGURE 9.2 Classification of supercapacitors

broad detection range (50−0.1 μM), and lower response time. The mechanism underlying glucose detection was also clearly explained and the incorporation of metal nanoparticles and RGO in the PANi matrix has significantly increased the electron transfer and surface area, which resulted in high sensitivity. The sensor's practicability was also analyzed by real-time detection of glucose levels in various commercially available organic fluids.[29] In another report, an enzyme-free glucose sensor was developed employing cobalt oxide (Co_3O_4) nanosheet webbed PANi by chemical oxidative polymerization. The composite was deposited on a glassy carbon electrode and glucose sensing was done using cyclic voltammetry and amperometric technique. The biosensor's limit of detection ranged from 0.1 to 0.8 mM of glucose and the lowest limit of detection (LOD) was found to be 0.06 mM with admirable sensitivity and reproducibility were also assessed for real-time serum analysis of glucose.[30] A glucose biosensor was fabricated using a multistep simple process by initial deposition of PANi and graphene oxide (GO) on platinum and subsequent deposition of copper nanoparticles followed by oxidation to CuO nanoparticles resulting in Pt-PANI-rGO-CuO hybrid composite. The sensor unveiled a sensitivity of 1252 μA/mM/cm^2 with LOD 1.5 μM and excellent selectivity in presence of intrusive species like uric acid, dopamine, and ascorbic acid.[31] Polyaniline − nickel oxide (NiO) composite-based amperometric sensor for sensing glucose in a nonenzymatic manner was also reported and the sensor demonstrated a sensitivity of (5625 μA/mM/cm^2), good stability, and was proved to be effective in real-time analysis of serum samples.[32]

Polyaniline-based sensors for simultaneous detection tow biomolecules have also been reported. A functionalized polyaniline thin film impregnated with glucose oxidase and urease enzymes was developed and an enzyme-based field-effect transistor (FET) centered technology was used for sensing glucose and urea. Potential data measurements indicated a sensitivity of 14.7 ± 0.9 mV/decade and a detection range of 10^{-5} to 10^{-1} mol/L (for urea) and 7.4 ± 0.5 mV/decade with a detection range of 10^{-5} to 10^{-1} mol/L (for glucose).[33] Another group reported an enzyme-free biosensor based on hollow CuO and PANI nanofibre hybrid for selective and sensitive detection of hydrogen peroxide and glucose using cyclic voltammetry. The sensor exhibited a wide range of detection (0.001−20 mM) with LOD (0.45 μM) for glucose and (0.005−9.255 mM) with LOD (0.11 μM) for hydrogen peroxide.[34]

Detection of dopamine is crucial in the case of diseases like Parkinson's disease, Alzheimer's, and other neurological disorders. A highly selective nonenzymatic sensor for detecting dopamine in presence of uric acid was developed using polyaniline nanofibre composite functionalized using cobalt hydroxide. The developed sensor has a significant linear detection range between 0.1 and 200 μM, LOD value (0.03 μM), and sensitivity of 790.7 μA/mM/cm^2.[35] A core-shell type composite with hollow tin oxide (SnO_2) as core and PANi as a shell with a uniform coating of nitrogen-doped graphene quantum dot (NGQD) was deposited on GCE to fabricate the dopamine sensor. The sensing was done using differential pulse voltammetry (DPV) in the range of 0.5−200 μM and the sensor showed excellent sensitivity even when interfering molecules like ascorbic acid and uric acid were present.[36]

Other biomolecules, which are frequently detected using electrochemical methods of sensing include uric acid, ascorbic acid, creatinine, and hydrogen peroxide. The detection of uric acid employing α-Fe_2O_3- PANI nanotube composite by DPV technique afforded the following results. The fabricated sensor unveiled excellent selectivity and sensitivity

(0.433 $\mu A \mu M^{-1}$) along with interfering species (ascorbic acid, citric acid, and succinic acid) in the detection range 0.01−5 μM with a LOD of 0.038 μM. The composite was also used in the real-time analysis of urine samples and the recovery was found to be greater than 98% for all the samples proposing its practical applicability.[37] Ascorbic acid detection employing a ternary composite of PANI- Cu (II) phthalocyanine and graphene was reported by S.Pakapongpan et al. The composite was prepared by electrolytic exfoliation of graphite in presence of the copper phthalocyanine and then rapid mixing polymerization with aniline resulted in the hybrid PANI/Gr/CuPc composite. The composite was drop cast on a screen-printed electrode and sensing was performed using the amperometric technique. The sensing was also done for real samples by determining the concentration of ascorbic acid in commercial vitamin tablets with a recovery of 99%−116% for the three vitamin samples. The incorporation of metal phthalocyanine enhanced the electron transfer in PANi and graphene thereby displaying excellent sensitivity, wide range detection limits, and selectivity.[38] Creatinine is another biomolecule whose concentration in blood samples requires analysis for monitoring kidney and thyroid malfunctions. An amperometric method was used in the highly sensitive detection of creatinine with the aid of creatinine deaminase enzyme immobilized PANi nanostructure functionalized with Nafion. The sensing was based on measuring the ammonium ion doping level in PANi produced by electrocatalysis of creatinine by the immobilized enzyme. The sensitivity of the sensor increased drastically to 1300 $mA/mM\ cm^{-2}$) after the immobilization of enzyme on Nafion modified PANI.[39]

Detection of hydrogen peroxide produced as a result of enzyme-catalyzed reactions of other biomolecules such as cholesterol, glucose, lactates, and glutamates is essential in many pharmaceutical and clinical applications. A ternary composite system in which reduced graphene oxide (RGO) was initially functionalized with PANi to activate the hydrophilic amino groups to enhance composite formation with silver nanoparticles was utilized in sensing hydrogen peroxide. The PANi-RGO-AgNP composite was then loaded on GCE for making an amperometric sensor. The sensor showed an appreciable detection range of 0.01−1000 μM and LOD of 50 nm. The sensing was based on the electronic interaction between PANI and silver nanoparticles enhanced by the presence of RGO, which increased the electrochemical reduction of hydrogen peroxide.[40]

3.2 Polyaniline-based electrochemical sensors for environmental pollutants

Water pollution has created serious health issues in humans such as brain and lung disorders, cancer, and so on and higher concentration are even lethal. In addition, the discharge of pollutants into water bodies has harmful effects on the water ecosystem. The detection of environmental contaminants has become increasingly important and critical to developing inexpensive and robust sensors with remarkable sensitivity and a wide range of detection. Electrochemical methods of sensing have been proven to be a proficient substitute compared to conventional detection methods owing to their outstanding sensitivity, selectivity, simple operation, and rapid response time. Among the various types of electrochemical sensors, polyaniline-based sensors have emerged as a promising platform for sensing environmental pollutants.[41]

Phenolic compounds like 2-nitrophenol, 2-amino phenol, 4-nitro phenol, etc. released from numerous industries can be considered persistent aromatic pollutants, which can cause high

risks of toxicity due to their mutagenic or carcinogenic nature at concentrations above the permissible limits. Functionalized composites of polyaniline −graphene and cerium tungstate for sensing 2-nitrophenol were prepared by chemically grafting polyaniline on the surface of graphene oxide by chemical oxidative polymerization followed by reducing of graphene oxide to graphene and coupling it with cerium tungstate. The hybrid ternary composite was fabricated to form the sensor by coating it on a glassy carbon electrode. The composite sensor exhibited excellent sensitivity (1.229 $\mu A/\mu M/cm^2$), quicker response, and detection range from 1.0 nM to 1 mM demonstrating its potential as an electrochemical sensor for screening phenolic compounds.[42] The capability of silver nanowire (AgNW) −polyaniline composite system for selectively and sensitively detecting 4-nitrophenol was evaluated by differential pulse voltammetric method. The sensor's stability was tested by keeping the modified electrode for 20 days and monitoring the current response to 0.01 mM of 4-nitrophenol every 5 days; the sensor retained 87% of the response after the test period. The analysis was also extended to real water samples collected from four different water resources and the recoveries were excellent in the range of 97%−101%.[43] The fabrication of an electrochemical sensor for 4-amino phenol was done employing a polyaniline-graphene-MWCNT composite and the sensing was done by a reliable I−V electrochemical method. The method of sensing 4-amino phenol by the I−V technique has shown to be a prospective method for sensing phenolic compounds with high levels of selectivity, sensitivity, and lower response time compared to other electrochemical methods.[44]

A biosensor based on polyphenol oxidase (enzyme) entrapped into the hybrid assembly of polyaniline-polyacrylonitrile (pan) and graphene obtained by phase inversion was evaluated for screening phenolic pollutants by using p-cresol as a model pollutant. The amperometric responses of the sensor showed a sensitivity of (6.46 $\mu A/\mu M/cm^2$) in the range of 2×10^{-6} to 1.16×10^{-5} M and good antiinterference stability in the presence of 10 inorganic interfering ions as well as organic molecules such as glucose, aniline, and ascorbic acid. The real-time analysis of p-cresol envisages the utility of hybrid biosensor for developing marketable sensors for phenolic compound determination.[45]

The admirable sensitivity of PANi combined with the enhanced surface area of macroporous silicon was utilized in developing a functionalized PANi composite for sensing naphthalene, a potential chemical causing damage to tissues and nerves, and also has been reported to be carcinogenic. For developing the chemosensor, the composite was immersed in 1M potassium chloride solution in ethanol and the changes in impedance with the addition of parts per billion (ppb) amounts of naphthalene were monitored to quantify the amount of naphthalene. The chemosensor so developed was able to sense the low concentration of naphthalene in the order of 30 ppb.[46] Detection of hydrazine is crucial since in lower concentrations it is neurotoxic and high concentrations are reported to be carcinogenic. An amperometric sensor based on polyaniline, copper nanoparticles and graphene oxide was fabricated by drop casting the composite (CuNPs-PANi-GO) on a glassy carbon electrode (GCE). The sensing capability was initially evaluated by cyclic voltammetric technique for optimizing the pH of the solution to 7.0 since at pH above 7.0 hydrazine exists as a neutral molecule and below 7.0 in the protonated form. The selectivity of the fabricator was studied by choosing both inorganic and organic interfering species (500-fold excess) and the results indicate that the sensor is highly selective toward hydrazine even with the addition of higher levels of the species interfering with hydrazine. The sensitivity (359.93 $\mu A/mM/cm^2$) and lower LOD value

(0.0045 μM) with appreciable stability and reproducibility validates the use of the sensor for real-time monitoring of toxic hydrazine in environmental samples.[47]

Residues of insecticides and pesticides in freshly consumed fruits, vegetables, soil, and water resources cause several types of diseases in human beings as well as other living beings. Polyaniline-based sensors have received extensive attention as electrochemical sensors on account of their large surface area and presence of amino groups, which can interact with the analyte thereby improving the sensitivity and selectivity. A highly functionalized composite was fabricated by click chemistry using manganese phthalocyanine (terminal alkyl substituted) and 4-azido polyaniline on indium-coated glass as working electrodes for selectively detecting pesticides. The sensor was employed for the detection of fenitrothion, eserine, and diazinon by square wave voltammetric technique. The sensor demonstrated a highly selective and stable response to the three variants of pesticides and it has shown greater sensitivity of 4.67 $A/M/cm^2$ in the case of fenitrothion making it ideal for developing fenitrothion sensors for viable applications.[48] In another study, a sensor was developed for detecting Imidacloprid, an insecticide utilizing a quaternary composite of polyaniline, ionic liquid (IL), graphene quantum dots (GQD), and multiwalled carbon nanotubes (MWCNT). The working electrode was fabricated using a GCE on which a 5 μL solution (with varying amounts of GQD (5.0 mg), MWCNT (5.0 mg), and IL (10 mg) dispersed in 15 mL water) was drop cast initially and then polyaniline film was grown using electropolymerization process. The electrode exhibited a linear range of detection from 0.03 to 12μmol/L with a LOD as low as 9 nmol/L and was also evaluated for selectivity by sensing in presence of seven variants of pesticides. The sensor was also shown to be feasible in sensing real samples of apple, tomato, and cucumber with good levels of recovery.[49]

4. Functionalized polyaniline nanocomposites for energy storage applications

4.1 Polyaniline—graphene composites for supercapacitor applications

Graphene, a two-dimensional one-atom dense monolayer of carbon atoms with a honeycomb lattice structure and its derivative graphene oxide have widely received acceptance in the construction and development of electrode materials for supercapacitor applications.[50] The distinctive properties of graphene such as massive surface area (2630 m^2/g), good electrical conductivity (10^7 Sm^{-1}), improved mechanical strength, and flexibility have been extensively employed for devising electrode materials for energy storage. However, the accumulation of neighboring sheets as a result of noncovalent interaction (π-π interaction) leads to the reduced surface area, conductivity, and specific capacitance.[51] The derivative of graphene viz. graphene oxide (GO) has a layered sheet-like structure with hydroxyl and epoxy functional groups at the plane and edge basal positions. The presence of oxygen functional groups in GO hinders the agglomeration of individual sheets as well as improves the hydrophilic nature of GO thus enhancing its dispersion in water and other solvents.[52] Several strategies have been adopted by researchers in overcoming the undesirable aspects of graphene and augment its electrochemical activity. The most effective approach to improvise the properties of both graphene and PANi for practical applications is to develop

functionalized composites by utilizing the better properties of both counterparts resulting in hybrid composites with synergistic qualities vital for electrochemical applications.

A self-assembly approach employing GO solution as a surfactant was used in fabricating PANi—GO composite, which resulted in the formation of a porous three−dimensional framework of GO with a molecular level uniform coating of PANi. The porous structure enabled the diffusion of electrolytes and also helped in the mobility of electrons in the network of composite material causing elevated values of specific capacitance (824 F/g at 2.22 A/g current density) and excellent capacitance retention.[53] In another report, reduced graphene oxide (three −dimensional) was grafted on dendritic structures of PANi resulting in the formation of PANI-RGO composite aerogels endowed with high values of specific capacitance (1600 F/g at 12 A/g current density), energy (545 Wh/kg) and power densities (1538 W/kg).[54] A low-cost electrode material with higher specific capacitance (763 F/g) ideal for energy storage applications was fabricated by using light-weight (0.2 g/cm^3) PANi-graphene paper composite with high flexibility and conductivity. PANi nanorods were deposited on flexible graphene paper using the electrodeposition technique to form the free-standing electrode material relevant and highly beneficial for handy electronic devices.[55] Zhou et al. reported the synthesis of PANi—GO composites by in-situ polymerization of aniline on stacked GO sheets resulting in the formation of PANi nanofibres confined inside the GO network with improved pathways for ion and electron transport. The material exhibited a specific capacitance value (780 F/g at a current density of 0.5 A/g) with 91% cycling stability at higher current densities.[56]

Conductive polymer hydrogels (CPHs) are another option in developing flexible supercapacitors with good attributes such as higher values of specific capacitance, prolonged cycle stability, better power, and energy density. A conducting polymer gel based on PANi, GO and sodium alginate was prepared by in-situ polymerization method and then coated on a hydrophilic carbon cloth to produce the flexible electrode material. The solid-state capacitor was then assembled by packing two CPH electrodes with a polyester mesh filled with electrolyte as a separator. The as-prepared capacitor exhibited a specific capacitance of 780 F/g at 0.5mA/g current density and with significant electrochemical stability (88.2% of initial capacitance after 1000 cycles).[57] In another study, graphene hydrogels with a density of 0.01 g/cm^3 were synthesized by hydrothermal process and were then used in the preparation PANI—graphene hydrogel composite films. The direct polymerization of PANi on graphene hydrogels resulted in enhancing the electrochemical stability with 99% specific capacitance (323.9 F/g) retention after 1000 cycles.[22]

Functionalization of PANi was done by sulfonation using m-amino benzene sulfonic acid to improve the electrochemical properties and then a composite was synthesised with graphene oxide. The sulfhonic acid groups performed the function of dopant and a surfactant as well as it helped in preventing the agglomeration of graphene sheets. A three-electrode setup as well as an asymmetric supercapacitor (ASC) has been fabricated to test the efficiency of SPANi-GO composites. The 3-electrode setup delivered a specific capacitance of 1107 F/g at 1 A/g current density and the ASC constructed with SPANi-GO as anode and RGO as cathode displayed excellent values for power density (14,764 W/kg), energy density (31.4 Wh/kg) and outstanding cycling stability (94% retention after 5000 cycles) signifying its efficacy for high power consuming energy storage devices.[58]

Yan Liu et al. exploited the oxygenated groups in the basal positions of GO to form composites with PANi by first converting the epoxide groups in the basal plane to hydroxyl groups and then transforming them to carboxyl groups by an esterification reaction with oxalic acid. The heavily carboxylated sheets of GO can then form stable structures with PANi as a result of the affinity between the carboxyl groups of GO and amine nitrogen of PANi. The method validated an effective strategy for carboxyl functionalization of GO sheets and the composite exhibited remarkable capacitance.[59]

4.2 Polyaniline—carbon nanotube composites for supercapacitor applications

The framing of flexible and wearable supercapacitors entails the development of electrode materials that are mechanically stable and possess a large surface area and high values of conductivity. Polyaniline when used alone as an electrode material possesses the disadvantages such as restricted cycling stability, limited available surface area, and low electrical conductivity. The limitations of PANi can be amended to a greater extent by combining it with carbon materials. Among the carbon materials, carbon nanotubes have been a predominant alternative principally due to their peculiar properties like improved surface area, noteworthy mechanical stability, and electrical conductivity. Moreover, the incorporation of even lesser amounts of carbon nanotubes in the polyaniline matrix can significantly improve the mechanical stability of the polymer as well as it can also provide an interconnected three-dimensional structure, which facilitates electron transport within the composite.

A biomimetic template derived from polydimethylsiloxane (PDMS) cross-linked with Xanthosoma sagittifolium leaves was fabricated for the synthesis of PANi-carbon nanotube composites by Chang et al. for supercapacitor applications.[60] The composite exhibited enhanced capacitive behavior with retention of capacitance even at higher current densities. The leaf-scale morphology of the composites helped in improving the surface area and roughness thereby increasing the transport of ions and electrons leading to improved electronic conductivity and better electrochemical activity meeting the requirements for supercapacitor applications. In another study,[61] vertically aligned nitrogen doped carbon nanotube (NCNT) arrays possessing three-dimensional porous architecture were employed as a scaffold for the synthesis of PANi—NCNT composites by electrodeposition. The composite's practical feasibility as a supercapacitor was evaluated using cyclic voltammetry (CV), galvanostatic charge-discharge studies (GCD) electrochemical impedance spectroscopy (EIS), and also by constructing a symmetric capacitor with the PANi-NCNT composite as both anode and cathode using polyvinyl alcohol (PVA)/H_2SO_4 hydrogel as electrolyte and separator. The fabricated supercapacitor displayed appreciable specific capacitance (128 F/g at 2.47 A/g current density) and preserved 92% of initial capacitance at 24.7 A/g current density following up to 10,000 cycles.

In a recent report, Hyaluronic acid (HA) was utilized as a surfactant and binder for better dispersion of single-walled carbon nanotubes (SWCNT) by a wet-spinning process for the fabrication of a ternary core-shell composite with carbon nanotube assimilated HA as the core and PANi as the shell by electrodeposition. The core part consisting of CNT incorporated HA acted as a scaffold or template for efficient deposition of PANi thereby increasing the surface area and porosity of the composite. The composite electrode exhibited excellent stability

under bending and twisting with over 90% of preservation of initial capacitance after 3000 cycles validating the composite material's flexibility as ideal for wearable electronic equipment.[62]

In another study,[63] PANi−CNT core-shell hybrid composites grown by layer-by-layer deposition on a carbon cloth and tested for supercapacitor application in the presence of a redox-active electrolyte (1 M H_2SO_4 with PVA/Fe^{2+}/Fe^{3+}gel electrolyte). The specific capacitance value was enhanced from 1005 F/g to 1547 F/g at 2 A/g current density in the presence of the redox additive in 1M H_2SO_4. The symmetric supercapacitor employing three electrodes (PANi−CNT) connected in series was used to light an LED (1.8V, 20 mA) indicating it's perspective as a power source. Additionally, the fabricated flexible symmetric supercapacitor was able to deliver power and energy density values of 700 W/kg and 22.9 Wh/kg respectively.

Lia Hou et al.[64] detailed the fabrication of PANi−CNT composites using functionalized carbon nanotubes, two types of functionalization were performed to create carboxylated carbon nanotubes; acid treating and the other by chemical vapor deposition (CVD). The results indicate that the incorporation of highly carboxylated CNTs obtained by acid treating enhanced the electrochemical performance of the composite as well as the cycle life with excellent retention (88.2%) of capacitance even after 10,000 cycles of galvanostatic charge-discharge.

The cycling stability, as well as the rate capability of polyaniline, was shown to be boosted by covalently implanting PANi on the surface of CNTs and by generating an interpenetrated porous architecture using calcium carbonate as a template. The porous composite demonstrated a higher specific capacitance of 1266 F/g at 1 A/g with a rate performance of 83% retention after 10,000 cycles and a lower charge transfer resistance.[65]

In an attempt to investigate the methods for improving the cycling stability of PANi-based electrodes, Taina Rauhavala et al.[66] used two different approaches viz. heating under vacuum and incorporation of acid-treated carbon nanotubes in the polymer matrix. The results of the study give a clear picture of the changes in the morphology and oxidation states of PANi during cyclic charge-discharge studies. The incorporation of acid-treated carbon nanotubes significantly enhances the specific capacitance value as well as the mechanical stability while heat-treated electrodes cannot retain capacitance for a prolonged time. The investigation clearly gives a detailed systematic insight into the changes occurring during the electrode's interaction with electrolyte and demonstrates a scheduled aging stability study well-suited for real-time applications.

Another study reported the scope of engineering the interface between the electrode and collector to facilitate quicker electron transport as an operational methodology to upgrade the electrochemical characteristics of supercapacitors. The PANi-CNT composites were codeposited on expanded graphite (ExGP) by electrodeposition process and the electrochemical studies revealed that the composite showed a specific capacitance value of 826.7 F/g with substantial energy and power densities. The expanded graphite helped in creating an interface with ample contact points between the electrode and collector resulting in better values of specific capacitance. The symmetric supercapacitor developed using PANi-CNT-ExGP was found to be flexible for use in portable and wearable equipment.[67]

4.3 Polyaniline—metal organic framework (MOF) composites for supercapacitor applications

Metal organic frameworks (MOFs) may be defined as a type of inorganic—organic hybrid materials in which the inorganic part comprises mostly transition metal centers and the organic part is made up of electron-donating ligands such as 2-methyl imidazole,1,4 benzene dicarboxylic acid 2,2′- bipyridyl and so on.[68] The most striking features of MOFs include highly manageable surface area, tunable pore sizes with highly ordered crystalline structures with excellent stability, and the ability to accommodate guest molecules in their large pore volumes. However, many of the reported MOFs are insulators as a single-phase material. Studies on the use of MOFs as a sole entity or in combination with other conductive materials such as conducting polymers, metal oxides, and metal sulfides for supercapacitor applications have experienced fabulous progress in the past 5–6 years. The surface area and the ordered porous structure with mesopores enabling ion and electron diffusion are the main features of MOFs exploited to develop supercapacitor electrodes.[69]

In an attempt to exploit the porosity of MOFs, a PANI–Cu (II) MOF was synthesized by a two-step process involving the chemical oxidative polymerization of polyaniline as the first step and the second step consisting of the synthesis of Cu (II)–MOF in presence of the PANI prepared in the initial step. The composite was able to retain the initial value of specific capacitance (734 F/g) up to 98% even after 4000 cycles. It can be concluded from the study that the association of Cu (II) MOF and PANI resulted in an increase in both specific capacitance and cycle life of both components significantly.[70] A ternary composite based on zinc oxide Co-MOF and PANI on carbon cloth was fabricated as electrode material for supercapacitor applications by Chunmei Zhu et al. The synthesis adopted for preparing the core-shell composite on carbon cloth consists of electrodeposition followed by a hydrothermal process. The highly ordered core-shell morphology of the composite with the MOF support retarded the volume changes of PANI thereby improving the cycling stability (82.5% after 5000 cycles).[71] In another report, carbon nanotube, Zeolitic imidazole framework (ZIF-67), and PANI composites (PANi-CNT-ZIF-67-CC) were deposited on carbon cloth (CC) as a substrate for developing a flexible electrode material. The material so developed exhibited a higher value of specific capacitance (3511 mF/cm^2 at 10 mVs^{-1}) on account of its enhanced surface area, porous structure, and pooled pseudo capacitance of PANI and ZIF-67.[72]

Supercapacitor electrode materials based on impregnating electroactive materials on textiles have gained popularity owing to their flexible and lightweight properties along with their porosity and mechanical durability. A three-dimensional (3-D) quaternary composite was assembled using PANI, ZnO, Zeolitic imidazole framework-ZIF-8 and two-dimensional graphene sheets on polyester material. The significant improvement in electrical conductivity of ZIF-8 by the porous network of conductive materials such as PANI, ZnO, and graphene as well as the synergic effect of pseudocapacitive materials (PANI, ZnO, and ZIF-8) and EDLC capacitance associated with graphene-enhanced the electrochemical activity of the composite leading to an areal capacitance of 1.378 F/cm^2. The supercapacitor device delivered an energy density of 235 μW H/cm^3 and power density of 1542 $\mu W/cm^3$ and was evaluated for potential practical applications by employing it to light LED and for powering calculators.[73] Interlacing of molecular organic frameworks with polyaniline was done by electrochemically depositing PANI on MOF crystals on carbon cloth for fabricating textile

electrode materials. The as-prepared composite disclosed an exceptional areal capacitance value of 2146 mF cm^{-2} and was able to perform without any decline in capacitance under twisting and bending revealing its practical applications as a flexible and handy solid-state energy storage device.[74]

4.4 Polyaniline—transition metal oxide composites for supercapacitor applications

The research on electrode materials based on polyaniline and transition metal oxides has made numerous contributions to the development of versatile energy storage devices possessing higher values of capacitance, energy, and power densities. The promising advantage of incorporating transition metal oxides in polyaniline matrix is the redox chemistry of the transition metals with variable oxidation states leading to higher values of capacitance and energy densities. The most frequently employed transition metal oxides representing each group in the transition metal series for developing hybrid composites for supercapacitor applications are discussed in the forthcoming section.

Among the metals of the fourth group Titanium oxide (TiO_2) and Zirconium oxide (ZrO_2) have been reported in combination with PANi for developing electrode materials. The electrochemical studies of mesoporous TiO_2 incorporated PANi matrix showed that the intercalation of TiO_2 resulted in a higher surface area and faster diffusion of ions due to the mesoporous nature of TiO_2. The obtained results indicate that the developed composite with a specific capacitance of 935 F/g possessing remarkable cycling stability and improved energy and power characteristics is a perfect aspirant for practical applications.[75] A ternary composite of ZrO_2 anchored graphene-highly oriented PANI was proposed as a novel material with good electrochemical characteristics. The enhancement in the capacitance arises as a result of the harmonizing effect of the three components; ZrO_2 helped in preventing the collapsing of PANI and aggregation of graphene sheets and the transport of electrons as well as ion-diffusion supported by enhanced conductivity of PANI. The attained values of specific capacitance (1178.6 F/g at 0.3 A/g current density), high power (0.8 kW/kg) and energy (104.76 Wh/kg) densities with better retention of capacitance (93. 2%, 1000 cycles) can be considered as a low-cost synthetic strategy for developing functional designs with better electrochemical traits in the field of energy storage devices.[76]

Vanadium pentoxide (V_2O_5) has gained a lot of consideration among transition metal oxides in developing supercapacitor electrodes due to its ability to achieve higher values of specific capacitance and the layered structure, which supports ion diffusion. A flexible, textile-based electrode was assembled by the codepositing of PANi and V_2O_5 on carbon cloth (CC) adopting the electrodeposition technique. The working electrode made up of the composite exhibited a specific capacitance of 443 F/g (at 0.5mA/cm^2 current density) and the symmetric supercapacitor device developed using PANI- V_2O_5 composite was able to deliver maximum energy (69.2 Wh/kg) and power density (0.72 kW/kg) with excellent retention of capacitance (92%) after 5000 cycles.[77] The effect of the generation of oxygen vacancies in V_2O_5 to modify its electrochemical properties was investigated by making composites with three different conducting polymers such as PANI, Polypyrrole (Ppy), and Poly (3,4—ethylene dioxy thiophene) PEDOT. Among the three composites, the PANI- V_2O_5 composite exhibited

a specific capacitance of 523 F/g and better restoring of initial capacitance (100% after 15,000 cycles) compared to Ppy (437 F/g) and PEDOT (614 F/g).[78]

Among the metals belonging to the chromium group, Molybdenum oxide (MoO_3) and tungsten oxide (WO_3) have also been experimented in developing composites with PANi for energy storage applications. A supercapacitor electrode with a wider potential window of operation (1.4 V) was fabricated using self-doped polyaniline (SPAN) and MoO_3 by electrodeposition. The composite exhibited better electro activity as a result of the coalescence of the organic—inorganic components with the highest value of specific capacitance (570 F/g), energy density (35 Wh/kg), and power density (4.7 kW/kg) respectively.[79] In another study,-PANi-PPy-MoO_3 composites bio-inspired from the structure of Setaria virdis were assembled by a two-step process in which the core-shell Ppy-MoO_3 part was synthesized by oxidative polymerization of aniline on MoO3 belts followed by polymerization of aniline in the core-shell structure. The composite exhibited a structure greatly resembling the plant in which MoO_3 served as the stalk part surrounded by PANi nanowire arrays in the form of bristles and Ppy as a grain linking PANI and MoO_3. The composite with magnificent composition and structure helped in improving the specific capacitance (1315 F/g at 0.5 A/g), energy density (63 Wh/kg), and cycling stability (86% after 20,000 cycles.[80] In a very recent report, an asymmetric roll-type fiber supercapacitor device (FSC) was made-up using PANI (anode) and MoO_3 as the cathode on a carbon fiber (CF) substrate and PVA/1M H_2SO_4 as electrolyte. The asymmetric fiber supercapacitor configuration exhibited a higher energy density (67.51 μWh/cm^3) than the symmetrical SC using PANI nanofibre electrode (25.12 μWh/cm^3) having roll type orientation.[81]

Manganese oxide (both MnO_2 and Mn_3O_4) has been reported in combination with conducting polymers to mend the drawbacks of using them alone. Polyaniline −MnO_2 composites with enormous specific surface area (480 m^2/g) obtained by single-step chemical oxidative polymerization of aniline in presence of potassium permanganate showed a specific capacitance of 497 F/g with 88.2% restoration of initial capacitance even up to 5000 cycles.[82] A composite hydrogel based on PANI with embedded MnO_2 having a three-dimensional porous structure has shown an appreciable specific capacitance with good cycling stability (81% after 1000 cycles).[83] In another approach, a ternary composite that can exhibit a specific capacitance of 1240 F/g at 2 A/g current density was constructed by using PANI −Mn_3O_4 and graphene. The enhancement in capacitance arises as a result of the collective effect of the pseudo capacitance of PANI and Mn_3O_4 along with surplus surface area and the layered structure of graphene.[84]

Ruthenium oxide (RuO_2) and Iridium oxide (IrO_2) are widely employed in electrochemical applications due to their outstanding specific capacitance, steady chemical reversibility, and rate capability. However, their highly expensive nature and complex multistep synthetic processes impede their practical applications. Iron oxide is the sole member commonly engaged in developing composites with conducting polymers. An economical method for synthesizing PANi- RuO_2 composite by sequential adsorption of ionic layer andand reaction process (SILAR) was demonstrated by Deshmukh et al. The obtained composite demonstrated 664 F/g (specific capacitance) with 89% of capacitance remaining after 5000 cycles. Though the composite showed the decreased value of specific capacitance, its cycling stability was significantly improved.[85] An asymmetric supercapacitor devised with a composite of pyrolyzed polyaniline tubes (PPNT) and Fe_2O_3 as negative electrodes and Zn−Co sulfide

decorated hydrothermally derived carbon spheres as positive electrode revealed higher energy density of 85.12 Wh/kg at a power density of 460 W/kg and also with favorable cycling stability making them effective for high performance supercapacitors.[86]

Hybrid composites possessing hierarchical nanostructure obtained by integrating Co_3O_4 with PANi were used as supercapacitor electrode material and the results disclosed that the PNI nanoshrubs over Co_3O_4 meet the features such as specific capacitance (1151 F/g), power and energy density crucial for a supercapacitor for developing high performing supercapacitors.[87]

A ternary composite of PANI-$NiCo_2O_4$-and reduced graphene oxide with an outstanding value of specific capacitance (1235 F/g) was employed as the cathode in an asymmetric supercapacitor (ASC) device to test its practical viability. The assembled ASC with activated carbon as electrode showed commendable cycle life and specific capacitance.[88] In another report, a PANi-$NiCo_2O_4$ binary composite prepared by hydrothermal process on nickel substrate has shown a maximum of 3108 F/g specific capacitance with 96% cycling stability. The composite's practical application was tested by fabricating an asymmetric supercapacitor with activated carbon and the energy density (77.6 Wh/kg) delivered by the ASC at a higher power density of 800 w/kg.[89]

Binary metal oxide-based conducting polymers have also been identified as potential nominees for electrochemical applications. Binary metal oxides based on vanadates having the general formula $M_3V_2O_8$ (M = Co. Ni, Li, Na, Fe, etc.) have been used by Liu et al. for developing flexible as well as transparent symmetric SC devices. The synthesis strategy adopted for obtaining $Ni_3V_2O_8$—PANI hybrid was a chemical bath deposition process. The $Ni_3V_2O_8$—PANI demonstrated remarkable electrochemical performance with the values of specific capacitance and areal capacitance being 2565.7 F/g at 5mV/s and 58.5 mF/cm^2. The device also has excellent cycle life with 88% restoration of areal capacitance following 20,000 charge-discharge cycles.[90]

Nickel oxide is another transition metal oxide frequently employed in forming composites with polyaniline for supercapacitor applications. In two different studies, Polyaniline—nickel oxide binary composites were synthesized, and evaluated for supercapacitor electrode material fabrication. Both the groups' synthesized PANi-NiO nanosheets as electrode materials, one group achieved a specific capacitance of 514 F/g while the other group obtained a maximum value of 936.63 F/g respectively.[91,92] A ternary composite of PANI-NiO and graphene was synthesized via a two-step process involving a hydrothermal method (for the formation of NiO layer on graphene) and an in-situ oxidative polymerization (for obtaining a PANI coating on the NiO-graphene surface) was employed as electrode material for developing flexible supercapacitors. The flexible thin film electrode so developed exhibited an enhanced specific capacitance of 1409 F/g with 92% cycling stability up to 2500 cycles.[93]

Copper oxides are also reported in combination with polyaniline for energy storage applications.[94–96] A ternary composite system encompassing PANI, RGO, and copper oxide was assessed for supercapacitor applications and the results obtained clearly envisage improved specific capacitance of 684.93 F/g and 84% cycling stability after 5000 cycles. The composite was also demonstrated to be effective as a secondary backup source of power.[97]

5. Conclusion

Polyaniline has been acknowledged as the most suitable conducting polymer with appropriate properties employable for electrochemical applications. In this chapter, we have mainly focused on the development of functionalized Polyaniline composites suitable for next-generation energy storage devices (mainly supercapacitors) and as sensitive platforms for environmental monitoring as well as biomedical applications. The significant developments in the field of electrochemical sensing employing polyaniline composites have been highlighted in the initial section of the chapter. The various functionalization strategies aiming at improving the electrochemical performance of polyaniline using carbon nanomaterials, molecular organic frameworks, and transition metal oxides are discussed in detail in this chapter. The research works published so far on polyaniline composites have recommended that the cautious selection of nanomaterials combined with modifying the synthesis procedures can pave a novel way for materializing highly electroactive, low-cost PANi based composites suitable for energy storage and conversion devices as well as other electrochemical applications.

References

1. *High-throughput template-free continuous flow synthesis of polyaniline nanofibers*. 2018. https://doi.org/10.1021/acs.iecr.8b04507.
2. Pal N, Chauhan S. *Functionalized polyaniline and composites*. Elsevier Inc.; 2019. https://doi.org/10.1016/B978-0-12-817915-4.00011-7.
3. Sun B, Ma W, Wang N, Xu P, Zhang L, Zhao H, Lin KA, Du Y. *Polyaniline : a new metal-free catalyst for peroxymonosulfate activation with highly efficient and durable removal of organic pollutants*. 2019. https://doi.org/10.1021/acs.est.9b03374.
4. Mu Y, Xie Y. *Theoretical and experimental comparison of electrical properties of nickel (II) coordinated and protonated polyaniline*. 2019. https://doi.org/10.1021/acs.jpcc.9b04550. No. Ii.
5. Gabal MA, Al-Juaid AA, El-Rashed S, Hussein MA, Al Angari YM. Polyaniline/Co0.6Zn0.4Fe2O4core-Shell nano-composites. Synthesis, characterization and properties. *J Alloys Compd* 2018;**747**:83–90. https://doi.org/10.1016/j.jallcom.2018.02.316.
6. Idrees M, Razaq A, Islam A, Yasmeen S, Sultana K, Asif MH, Nadeem M. Morphology and dielectric properties of directly collected and polyaniline coated lignocelluloses fibers. *Synth Met* 2017;**232**(May):138–43. https://doi.org/10.1016/j.synthmet.2017.08.009.
7. Puthirath AB, Methattel Raman S, Varma SJ, Jayalekshmi S. Exceptionally crystalline and conducting acid doped polyaniline films by level surface assisted solution casting approach. *Appl Phys Lett* 2016;**108**(16):12–7. https://doi.org/10.1063/1.4947083.
8. Bhandari S. *Polyaniline*. Elsevier Inc.; 2018. https://doi.org/10.1016/b978-0-12-809551-5.00002-3.
9. Manuscript A. *Chem Comm* 2020;**56**(28):4003–6. https://doi.org/10.1039/D0CC01028F.
10. Zhang W, Kong Y, Jin X, Yan B, Diao G, Piao Y. Supramolecule-assisted synthesis of cyclodextrin polymer functionalized polyaniline/carbon nanotube with core-shell nanostructure as high-performance supercapacitor. *Mater Electrochim Acta* 2019;**135345**. https://doi.org/10.1016/j.electacta.2019.135345.
11. Jin K, Zhang W, Wang Y, Guo X, Chen Z, Li L, et al. *Electrochim Acta* 2018;**285**:221–9. https://doi.org/10.1016/j.electacta.2018.07.220.
12. Online VA, Tang J, Xu H. *RSC Adv* 2016. https://doi.org/10.1039/C5RA22208G.
13. Li Y, Xing R, Zhang B, Bulin C. Fluoro-functionalized graphene oxide/polyaniline composite electrode material for supercapacitors. *Poly Poly Comp* 2019;**27**(7):76–81. https://doi.org/10.1177/0967391118817404.
14. Hanif F, Tahir A, Akhtar M, Waseem M, Haider S, Aly MF, Shakir I, Imran M, Farooq M. Ultra-selective detection of Cd 2 + and Pb 2 + using glycine functionalized reduced graphene oxide/polyaniline nanocomposite electrode. *Synth Met* 2019;**257**(September):116185. https://doi.org/10.1016/j.synthmet.2019.116185.

15. Gumpu MB, Nesakumar N, Sethuraman S, Krishnan UM, Rayappan JBB. Development of electrochemical biosensor with ceria-PANI core-shell nano-interface for the detection of histamine. *Sensor Actuator B Chem* 2014;**199**:330–8. https://doi.org/10.1016/j.snb.2014.04.009.
16. Liu C, Tai H, Zhang P, Yuan Z, Du X, Xie G, Jiang Y. A high-performance flexible gas sensor based on self-assembled PANI-CeO2 nanocomposite thin film for trace-level NH3 detection at room temperature. *Sensor Actuator B Chem* 2018;**261**:587–97. https://doi.org/10.1016/j.snb.2017.12.022.
17. Radhakrishnan S, Mathiyarasu J. *Graphene—carbon nanotubes modified electrochemical sensors*. Elsevier Inc.; 2019. https://doi.org/10.1016/B978-0-12-815394-9.00008-X.
18. Zhihua L, Xucheng Z, Jiyong S, Xiaobo Z, Xiaowei H, Tahir HE. Preparation of conducting polyaniline/proto-porphyrin composites and their application for sensing VOCs. *Food Chem* 2019;**276**(May 2018):291–7. https://doi.org/10.1016/j.foodchem.2018.10.029.
19. Wang S, Zhang K, Wang Q, Fan Y, Shen J, Li L, Yang L, Zhang W. *Graphical abstract SC*. 2018. https://doi.org/10.1016/j.electacta.2018.10.135.
20. Rose A, Prasad KG, Sakthivel T, Gunasekaran V, Maiyalagan T, Vijayakumar T. PT postal address. *Appl Surf Sci* 2018;**449**:551–7. https://doi.org/10.1016/j.apsusc.2018.02.224.
21. Wang H, Ma G, Tong Y, Yang Z. *Biomass carbon/polyaniline composite and WO 3 nanowire-based asymmetric supercapacitor with superior performance*. 2018.
22. Liu AD, Du P, Wei W. Flexible and robust sandwich-structured S-doped reduced graphene oxide/carbon composite nanotubes/polyaniline membranes : excellent (S-RGO/CNTs/PANI) candidate as free-standing electrodes for high-performance supercapacitors. *Electrochim Acta* 2017;**233**:201–9. https://doi.org/10.1016/j.electacta.2017.03.040.
23. Mensing JP, Lomas T, Tuantranont A. Electrochimica acta ammonia strengthened graphene/CNT-wrapped polyaniline- nano fi ber composites loaded with palladium nanoparticles for coin cell supercapacitors. *Electrochim Acta* 2018;**263**. https://doi.org/10.1016/j.electacta.2017.12.193. e35–e35.
24. Chandran M, Shamna I, Anusha A, Bhagiyalakshmi M. Synthesis of mesoporous carbon-polymeric hybrid material for energy storage application. *SN Appl Sci* 2019;**1**(6). https://doi.org/10.1007/s42452-019-0509-1.
25. Eftekhari A, Li L, Yang Y. Polyaniline supercapacitors. *J Power Sources* 2017;**347**:86–107. https://doi.org/10.1016/j.jpowsour.2017.02.054.
26. Farid M, Basha MAF, Zaki AH, Khedr MH. Nanocomposite system of simultaneously-thiolated graphene oxide and polyaniline nanofibers for energy storage applications. *Electrochim Acta* 2019;**300**:1–8. https://doi.org/10.1016/j.electacta.2019.01.075.
27. Li W, Gao F, Wang X, Zhang N, Ma M. Strong and robust polyaniline-based supramolecular hydrogels for flexible supercapacitors. *Angew Chem Int Ed* 2016;**55**(32):9196–201. https://doi.org/10.1002/anie.201603417.
28. Applications B, Pirzada M, Altintas Z. *Nanomaterials for healthcare*. 2019.
29. Deshmukh MA, Kang BC, Ha TJ. Non-enzymatic electrochemical glucose sensors based on polyaniline/reduced-graphene-oxide nanocomposites functionalized with silver nanoparticles. *J Mater Chem C* 2020;**8**(15):5112–23. https://doi.org/10.1039/c9tc06836h.
30. Yassin MA, Shrestha BK, Ahmad R, Shrestha S, Park CH, Kim CS. Exfoliated nanosheets of Co 3 O 4 webbed with polyaniline nanofibers: a novel composite electrode material for enzymeless glucose sensing application. *J Ind Eng Chem* 2019;**73**:106–17. https://doi.org/10.1016/j.jiec.2019.01.011.
31. Fang L, Zhu Q, Cai Y, Liang B, Ye X. 3D porous structured polyaniline/reduced graphene oxide/copper oxide decorated electrode for high performance nonenzymatic glucose detection. *J Electroanal Chem* 2019;**841**(January):1–9. https://doi.org/10.1016/j.jelechem.2019.04.032.
32. Kailasa S, Rani BG, Bhargava Reddy MS, Jayarambabu N, Munindra P, Sharma S, Venkateswara Rao K. NiO nanoparticles -decorated conductive polyaniline nanosheets for amperometric glucose biosensor. *Mater Chem Phys* 2020;**242**:122524. https://doi.org/10.1016/j.matchemphys.2019.122524.
33. Mello HJNPD, Mulato M. Enzymatically functionalized polyaniline thin films produced with one-step electrochemical immobilization and its application in glucose and urea potentiometric biosensors. *Biomed Microdevices* 2020;**22**(1). https://doi.org/10.1007/s10544-020-00478-4.
34. Liu T, Guo Y, Zhang Z, Miao Z, Zhang X, Su Z. Fabrication of hollow CuO/PANI hybrid nanofibers for non-enzymatic electrochemical detection of H2O2 and glucose. *Sensor Actuator B Chem* 2019;**286**:370–6. https://doi.org/10.1016/j.snb.2019.02.006.

35. Li Z, Qian W, Guo H, Jin R, Taoliu J, Zheng J. Sensitive electrochemical sensing platform for selective determination of dopamine based on amorphous cobalt hydroxide/polyaniline nanofibers composites. *Nanotechnology* 2020;**31**(27):275501. https://doi.org/10.1088/1361-6528/ab84a2.
36. Hsu WF, Wu TM. Electrochemical sensor based on conductive polyaniline coated hollow tin oxide nanoparticles and nitrogen doped graphene quantum dots for sensitively detecting dopamine. *J Mater Sci Mater Electron* 2019;**0**(0):0. https://doi.org/10.1007/s10854-019-01165-8.
37. Mahmoudian MR, Basirun WJ, Sookhakian M, Woi PM, Zalnezhad E, Hazarkhani H, Alias Y. Synthesis and characterization of α-Fe2O3/polyaniline nanotube composite as electrochemical sensor for uric acid detection. *Adv Powder Technol* 2019;**30**(2):384–92. https://doi.org/10.1016/j.apt.2018.11.015.
38. Pakapongpan S, Mensing JP, Phokharatkul D, Lomas T, Tuantranont A. Highly selective electrochemical sensor for ascorbic acid based on a novel hybrid graphene-copper phthalocyanine-polyaniline nanocomposites. *Electrochim Acta* 2014;**133**:294–301. https://doi.org/10.1016/j.electacta.2014.03.167.
39. Do JS, Chang YH, Tsai ML. Highly sensitive amperometric creatinine biosensor based on creatinine deiminase/nafion®-nanostructured polyaniline composite sensing film prepared with cyclic voltammetry. *Mater Chem Phys* 2018;**219**:1–12. https://doi.org/10.1016/j.matchemphys.2018.07.057.
40. Kumar V, Gupta RK, Gundampati RK, Singh DK, Mohan S, Hasan SH, Malviya M. Enhanced electron transfer mediated detection of hydrogen peroxide using a silver nanoparticle-reduced graphene oxide-polyaniline fabricated electrochemical sensor. *RSC Adv* 2018;**8**(2):619–31. https://doi.org/10.1039/c7ra11466d.
41. Dakshayini BS, Reddy KR, Mishra A, Shetti NP, Malode SJ, Basu S, Naveen S, Raghu AV. Role of conducting polymer and metal oxide-based hybrids for applications in ampereometric sensors and biosensors. *Microchem J* 2019;**147**:7–24. https://doi.org/10.1016/j.microc.2019.02.061.
42. Khan A, Khan AAP, Rahman MM, Asiri AM, Inamuddin, Alamry KA, Hameed SA. *Preparation and characterization of PANI@G/CWO nanocomposite for enhanced 2-nitrophenol sensing*, vol 433. Elsevier B.V.; 2018. https://doi.org/10.1016/j.apsusc.2017.09.219.
43. Zhang C, Govindaraju S, Giribabu K, Huh YS, Yun K. AgNWs-PANI nanocomposite based electrochemical sensor for detection of 4-nitrophenol. *Sensor Actuator B Chem* 2017;**252**:616–23. https://doi.org/10.1016/j.snb.2017.06.039.
44. Rahman MM, Hussein MA, Alamry KA, Al-Shehry FM, Asiri AM. Polyaniline/graphene/carbon nanotubes nanocomposites for sensing environmentally hazardous 4-aminophenol. *Nano-Struct Nano-Objects* 2018;**15**:63–74. https://doi.org/10.1016/j.nanoso.2017.08.006.
45. Zheng H, Yan Z, Wang M, Chen J, Zhang X. Biosensor based on polyaniline-polyacrylonitrile-graphene hybrid assemblies for the determination of phenolic compounds in water samples. *J Hazard Mater* 2019;**378**(January):120714. https://doi.org/10.1016/j.jhazmat.2019.05.107.
46. Toledo RP, Dias CES, Huanca DR, Salcedo WJ. Physical and chemical characterization of PANI/SiO2/MPS heterostructure to Be used as high sensitivity chemosensor for naphthalene. *Sensor Actuator B Chem* 2018;**277**(September):445–55. https://doi.org/10.1016/j.snb.2018.09.043.
47. Vellaichamy B, Periakaruppan P, Ponnaiah SK. A new in-situ synthesized ternary CuNPs-PANI-GO nano composite for selective detection of carcinogenic hydrazine. *Sensor Actuator B Chem* 2017;**245**:156–65. https://doi.org/10.1016/j.snb.2017.01.117.
48. Akyüz D, Koca A. An electrochemical sensor for the detection of pesticides based on the hybrid of manganese phthalocyanine and polyaniline. *Sensor Actuator B Chem* 2019;**283**:848–56. https://doi.org/10.1016/j.snb.2018.11.155.
49. Nasr-Esfahani P, Ensafi AA, Rezaei B. Fabrication of a highly sensitive and selective modified electrode for Imidacloprid determination based on designed nanocomposite graphene quantum dots/ionic liquid/multiwall carbon nanotubes/polyaniline. *Sensor Actuator B Chem* 2019;**296**(May):1–8. https://doi.org/10.1016/j.snb.2019.126682.
50. Zou Y, Zhang Z, Zhong W, Yang W. Hydrothermal direct synthesis of polyaniline, graphene/polyaniline and N-doped graphene/polyaniline hydrogels for high performance flexible supercapacitors. *J Mater Chem* 2018;**6**(19):9245–56. https://doi.org/10.1039/c8ta01366g.
51. Luo Y, Zhang Q, Hong W, Xiao Z, Bai H. A high-performance electrochemical supercapacitor based on a polyaniline/reduced graphene oxide electrode and a copper(ii) ion active electrolyte. *Phys Chem Chem Phys* 2017;**20**(1):131–6. https://doi.org/10.1039/c7cp07156f.

52. Asen P, Shahrokhian S, Zad AI. *Transition metal ions-doped polyaniline/graphene oxide nanostructure as high performance electrode for supercapacitor applications*. 2018. p. 983–96.
53. Wu J, Zhang Q, Wang J, Huang X, Bai H. A self-assembly route to porous polyaniline/reduced graphene oxide composite materials with molecular-level uniformity for high-performance supercapacitors. *Energy Environ Sci* 2018;**11**(5):1280–6. https://doi.org/10.1039/C8EE00078F.
54. Hoa N Van, Thi T, Quyen H, Hieu N Van, Quang T. Three-dimensional reduced graphene oxide-grafted polyaniline aerogel as an active material for high performance supercapacitors. *Synth Met* 2016;**223**:192–8. https://doi.org/10.1016/j.synthmet.2016.11.021.
55. Manuscript A. *Energy _ environmental science volume issue*. 2013 [Doi 10.1039_c2ee24203f] Cong, Huai-Ping; Ren, Xiao-Chen; Wang, Ping; Yu, Shu-Hong—Flexible Grapheneâ€"polyaniline Composite Paper for High-Performance Supercapaci.Pdf. 2010, No. 207890.
56. Zhou Q, Wei T, Yue J, Sheng L, Fan Z. Polyaniline nanofibers confined into graphene oxide architecture for high-performance supercapacitors. *Electrochim Acta* 2018;**291**:234–41. https://doi.org/10.1016/j.electacta.2018.08.104.
57. Guo G, Sun Y, Ma Y, Zhou Y, Xiong Z, Liu Y. Facile synthesis of conducting hydrogels based on polyaniline fiber and graphene oxide for application in all-solid-state supercapacitors. *Int J Electrochem Sci* 2016;**14**(6):5899–912. https://doi.org/10.20964/2019.06.220.
58. Bandyopadhyay P, Kuila T, Balamurugan J, Nguyen TT, Kim NH, Lee JH. Facile synthesis of novel sulfonated polyaniline functionalized graphene using M-aminobenzene sulfonic acid for asymmetric supercapacitor application. *Chem Eng J* 2017;**308**:1174–84. https://doi.org/10.1016/j.cej.2016.10.015.
59. Lyu W, Yu M, Feng J, Yan W. Facile synthesis of coral-like hierarchical polyaniline micro/nanostructures with enhanced supercapacitance and adsorption performance. *Polymer (Guildf)* 2019;**162**:130–8. https://doi.org/10.1016/j.polymer.2018.12.037.
60. Chang CM, Weng CJ, Chien CM, Chuang TL, Lee TY, Yeh JM, Wei Y. Polyaniline/carbon nanotube nanocomposite electrodes with biomimetic hierarchical structure for supercapacitors. *J Mater Chem* 2013;**1**(46):14719–28. https://doi.org/10.1039/c3ta13758a.
61. Malik R, Zhang L, McConnell C, Schott M, Hsieh YY, Noga R, Alvarez NT, Shanov V. Three-dimensional, free-standing polyaniline/carbon nanotube composite-based electrode for high-performance supercapacitors. *Carbon N. Y.* 2017;**116**:579–90. https://doi.org/10.1016/j.carbon.2017.02.036.
62. Zheng T, Wang X, Liu Y, Bayaniahangar R, Li H, Lu C, Xu N, Yao Z, Qiao Y, Zhang D, Pour Shahid Saeed Abadi P. Polyaniline-decorated hyaluronic acid-carbon nanotube hybrid microfiber as a flexible supercapacitor electrode material. *Carbon N. Y.* 2020;**159**:65–73. https://doi.org/10.1016/j.carbon.2019.11.074.
63. Xia C, Leng M, Tao W, Wang Q, Gao Y, Zhang Q. Polyaniline/carbon nanotube core–shell hybrid and redox active electrolyte for high-performance flexible supercapacitor. *J Mater Sci Mater Electron* 2019;**30**(5):4427–36. https://doi.org/10.1007/s10854-019-00731-4.
64. Hou L, Zhang W, Zhou H, Zhai HJ. Facile preparation of polyaniline-carbon nanotube hybrid electrodes and dependence of their supercapacitive properties on degree of carboxylation of carbon nanotubes. *J Nanoparticle Res* 2020;**22**(1). https://doi.org/10.1007/s11051-019-4737-5.
65. Che B, Li H, Zhou D, Zhang Y, Zeng Z, Zhao C, He C, Liu E, Lu X. Porous polyaniline/carbon nanotube composite electrode for supercapacitors with outstanding rate capability and cyclic stability. *Compos B Eng* 2019;**165**(January):671–8. https://doi.org/10.1016/j.compositesb.2019.02.026.
66. Rauhala T, Davodi F, Sainio J, Sorsa O, Kallio T. On the stability of polyaniline/carbon nanotube composites as binder-free positive electrodes for electrochemical energy storage. *Electrochim Acta* 2020;**336**:135735. https://doi.org/10.1016/j.electacta.2020.135735.
67. Zhou H, Zhi X, Zhai HJ. A facile approach to improve the electrochemical properties of polyaniline-carbon nanotube composite electrodes for highly flexible solid-state supercapacitors. *Int J Hydrogen Energy* 2018;**43**(39):18339–48. https://doi.org/10.1016/j.ijhydene.2018.07.168.
68. Fang X, Zong B, Mao S. Metal–organic framework-based sensors for environmental contaminant sensing. *Nano-Micro Lett* 2018;**10**(4):1–19. https://doi.org/10.1007/s40820-018-0218-0.
69. Chen Y, Ni D, Yang X, Liu C, Yin J, Cai K. Electrochimica acta microwave-assisted synthesis of honeycomblike hierarchical spherical Zn-doped Ni-MOF as a high-performance battery-type supercapacitor electrode material. *Electrochim Acta* 2018;**278**:114–23. https://doi.org/10.1016/j.electacta.2018.05.024.

70. Neisi Z, Ansari Z, Amin A, Dezfuli S. Polyaniline/Cu (II) metal - organic frameworks composite for high performance supercapacitor electrode. *J Inorg Organomet Polym Mater* 2019:18–21. https://doi.org/10.1007/s10904-019-01145-9. No. Ii.
71. Chunmei Z, Ying H, Yijun L, Kazantseva N, Saha P, Qilin C. High-performance supercapacitor electrodes. *J Energy Chem* 2018;**35**:124–31. https://doi.org/10.1016/j.jechem.2018.11.006. No. xxxx.
72. Wang L, Yang H, Pan G, Miao L, Chen S, Song Y. Electrochimica acta polyaniline-carbon nanotubes @ zeolite imidazolate Framework67- carbon cloth hierarchical nanostructures for supercapacitor electrode. *Electrochim Acta* 2017;**240**:16–23. https://doi.org/10.1016/j.electacta.2017.04.035.
73. Liu Y, Jin L, Wang H, Kang X, Bian S. Fabrication of three-dimensional composite textile electrodes by metal-organic framework, zinc oxide, graphene and polyaniline for all-solid-state supercapacitors. *J Colloid Interface Sci* 2018;**530**:29–36. https://doi.org/10.1016/j.jcis.2018.06.062.
74. Wang L, Feng X, Ren L, Piao Q, Zhong J, Wang Y, Li H, Chen Y, Wang B. *Flexible solid-state supercapacitor based on a metal—organic framework interwoven by electrochemically-deposited PANI*. 2015. https://doi.org/10.1021/jacs.5b01613.
75. Parveen N, Ansari MO, Cho MH. Route to high surface area, mesoporosity of polyaniline-titanium dioxide nanocomposites via one pot synthesis for energy storage applications. *Ind Eng Chem Res* 2016;**55**(1):116–24. https://doi.org/10.1021/acs.iecr.5b02907.
76. Giri S, Ghosh D, Das CK. Growth of vertically aligned tunable polyaniline on graphene/ZrO 2 nanocomposites for supercapacitor energy-storage application. *Adv Funct Mater* 2014;**24**(9):1312–24. https://doi.org/10.1002/adfm.201302158.
77. Bai M, Liu T, Luan F, Liu X. *Electrodeposition of vanadium oxide—polyaniline composite nanowire electrodes for high energy density supercapacitors***1**; 2014. p. 10882–8. https://doi.org/10.1039/c3ta15391f.
78. Bi W, Huang J, Wang M, Jahrman EP, Seidler GT, Wang J, Wu Y, Gao G. *In local electric field derived from interfacial oxygen vacancies for high energy density*. 2019. https://doi.org/10.1039/c9ta04264d.
79. Online VA, He H, Liu X. *RSC Adv* 2015;**5**(92):75374–9. https://doi.org/10.1039/C5RA12075F.
80. Manuscript A. *Materials chemistry A*. 2018. https://doi.org/10.1039/C8TA04218G.
81. Yu S, Patil B, Ahn H. PANI//MoO 3 fiber-shaped asymmetric supercapacitors with roll-type configuration. *Fibers Poly* 2020;**21**(3):465–72. https://doi.org/10.1007/s12221-020-9811-1.
82. Zhao Y, Wang CA. Nano-network MnO2/polyaniline composites with enhanced electrochemical properties for supercapacitors. *Mater Des* 2016;**97**:512–8. https://doi.org/10.1016/j.matdes.2016.02.120.
83. Huang H, Chen R, Yang S, Li L, Liu Y, Huang J. Facile fabrication of MnO2-embedded 3-D porous polyaniline composite hydrogel for supercapacitor electrode with high loading. *High Perform Polym* 2019;**32**(3):286–95. https://doi.org/10.1177/0954008319860893.
84. Haldar P, Biswas S, Sharma V, Chowdhury A, Chandra A. Mn3O4-Polyaniline-Graphene as distinctive composite for use in high-performance supercapacitors. *Appl Surf Sci* 2019;**491**(May):171–9. https://doi.org/10.1016/j.apsusc.2019.06.106.
85. Deshmukh PR, Patil SV, Bulakhe RN, Sartale SD, Lokhande CD. Inexpensive synthesis route of porous polyaniline—ruthenium oxide composite for supercapacitor application. *Chem Eng J* 2014;**257**:82–9. https://doi.org/10.1016/j.cej.2014.06.038.
86. Hekmat F, Hosseini H, Shahrokhian S, Unalan HE. Hybrid energy storage device from binder-free zinc-cobalt sulfide decorated biomass-derived carbon microspheres and pyrolyzed polyaniline nanotube-iron oxide. *Energy Storage Mater* 2020;**25**(June):621–35. https://doi.org/10.1016/j.ensm.2019.09.022.
87. S CP, R BE, Pillai S, C M, Aravind A, J. Devaki S. Polyaniline-cobalt oxide nano shrubs based electrodes for supercapacitors with enhanced electrochemical performance. *Electrochim Acta* 2019;**324**:134876. https://doi.org/10.1016/j.electacta.2019.134876.
88. Rashti A, Wang B, Hassani E, Feyzbar-Khalkhali-Nejad F, Zhang X, Oh T-S. Electrophoretic deposition of nickel cobaltite/polyaniline/RGO composite electrode for high performance all-solid-state asymmetric supercapacitors. *Energy Fuels* 2020;**34**:6448–61. https://doi.org/10.1021/acs.energyfuels.0c00408.
89. Li Y, Zhang Z, Chen Y, Chen H, Fan Y, Li Y, Cui D, Xue C. Facile synthesis of a Ni-based NiCo 2 O 4 -PANI composite for ultrahigh specific capacitance. *Appl Surf Sci* 2019:144646. https://doi.org/10.1016/j.apsusc.2019.144646.

90. Liu X, Wang J, Yang G. In situ growth of the Ni3V2O8@PANI composite electrode for flexible and transparent symmetric supercapacitors. *ACS Appl Mater Interfaces* 2018;**10**:20688–95. https://doi.org/10.1021/acsami.8b04609.
91. Singu BS, Palaniappan S, Yoon KR. Polyaniline–nickel oxide nanocomposites for supercapacitor. *J Appl Electrochem* 2016;**46**(10):1039–47. https://doi.org/10.1007/s10800-016-0988-3.
92. Navale YH, Navale ST, Dhole IA, Stadler FJ, Patil VB. Specific capacitance, energy and power density coherence in electrochemically synthesized polyaniline-nickel oxide hybrid electrode. *Org Electron* 2018;**57**(January):110–7. https://doi.org/10.1016/j.orgel.2018.02.037.
93. Wu X, Wang Q, Zhang W, Wang Y, Chen W. Nano nickel oxide coated graphene/polyaniline composite film with high electrochemical performance for flexible supercapacitor. *Electrochim Acta* 2016;**211**:1066–75. https://doi.org/10.1016/j.electacta.2016.06.026.
94. Omar FS, Numan A, Duraisamy N, Ramly MM, Ramesh K, Ramesh S. Binary composite of polyaniline/copper cobaltite for high performance asymmetric supercapacitor application. *Electrochim Acta* 2017;**227**:41–8. https://doi.org/10.1016/j.electacta.2017.01.006.
95. Viswanathan A, Shetty AN. Facile in-situ single step chemical synthesis of reduced graphene oxide-copper oxide-polyaniline nanocomposite and its electrochemical performance for supercapacitor application. *Electrochim Acta* 2017;**257**:483–93. https://doi.org/10.1016/j.electacta.2017.10.099.
96. Li X, Demartino GN. *Ac Ce pte us cri Pt us Pt*. 2009 [No. May].
97. Viswanathan A, Shetty AN. Single step synthesis of RGO, copper oxide and polyaniline nanocomposites for high energy supercapacitors. *Electrochim Acta* 2018;**289**:204–17. https://doi.org/10.1016/j.electacta.2018.09.033.

PART II

Industrial applications of nanomaterials

This page intentionally left blank

CHAPTER

10

Multifunctional hydroxylapatite nanofillers for fine-tuning of elastomer characteristics

M. Bindu[1], A. Anil[2] and G. Unnikrishnan[1]

[1]Polymer Science and Technology Laboratory, Department of Chemistry, National Institute of Technology Calicut, Kozhikode, Kerala, India; [2]Center for Materials for Electronics Technology [C-MET], MeitY, Government of India, Thrissur, Kerala, India

1. Need of fine tuning of elastomers

Elastomers are typically characterized by excellent chain flexibility, mobility, and large deformation.[1,2] They can be stretched to several times than their unstretched length, and the original dimensions can be almost regained when the deforming stress is released. Elastomers possess a viscoelastic nature and weak intermolecular forces.[3,4] They are usually used in cross-linked forms. Upon crosslinking, the segmental mobility gets restricted to a significant extent.[5] Nano particles are often introduced into elastomer matrices in order to improve the mechanical properties, viz., modulus, tensile and tear strength, compression properties, and abrasion resistance. The effectiveness of the reinforcement depends on the filler characteristics and also on the strength of the polymer-filler interactions.[6–8]

Four types of arrangements of nanoparticles in a polymer matrix have been reported by Kickelbick et al., viz; (1) inorganic nanoparticles embedded in inorganic polymers, (2) nanoparticles bonded onto polymer backbone, (3) interpenetrating network with chemical bonds, and (4) inorganic-organic hybrid polymer as shown in Fig. 10.1.[9]

The degree of reinforcement increases with a decrease in particle size which obviously provides higher polymer-filler interfaces. Reinforcing fillers usually have a particle size in the range of 10–100 nm.[10]

Biocompatible nano-composites are now receiving substantial consideration as novel materials for biomedical applications. Rubbers viz; polyurethanes, silicone rubbers and polypeptide elastomers are extensively being employed as biomaterials because of the easiness in

Applications of Multifunctional Nanomaterials
https://doi.org/10.1016/B978-0-12-820557-0.00018-7

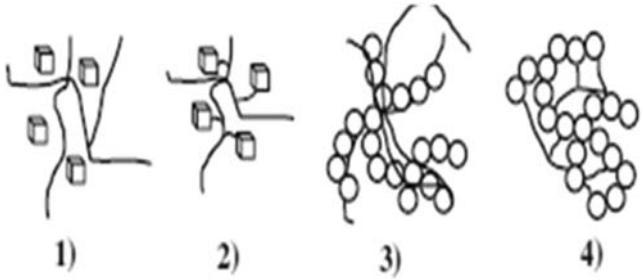

FIGURE 10.1 Different ways of arrangement of nanoparticles in a matrix (1) inorganic nanoparticles embedded in inorganic polymers, (2) nanoparticles bonded onto polymer backbone, (3) interpenetrating network with chemical bonds and (4) inorganic-organic hybrid polymer [Ref. 9].

their synthesis, bio-durability and biocompatibility.[11–13] However, these elastomers frequently flop to cross the physical and mechanical requirements for suitable applications, when they are used alone. Nano reinforcements dispersed within the elastomeric matrix have shown to improve the basic properties of the matrices making them suitable for different applications. Fig. 10.2 represents an overall view of different elastomers and the types of nanoparticles being used for reinforcement for biomedical applications.

Mechanical and barrier property improvements of elastomeric poly-caprolactone (PCL) matrix have been achieved by the incorporation of organically modified silicate nanoparticles.[14] It has been reported that the modulus and ultimate strength increase with an increase in nano-silicate loading, whereas the elongation at break and permeability significantly decrease. Kim et al. explored the biodegradation and biocompatibility of PCL elastomers for bone regeneration.[15] Oleic acid modified PCL nano-composites were developed and the morphological, mechanical and cellular response studies were performed by them. The results indicate that the modified systems exhibit excellent mechanical properties and improved cellular interactions than the conventional composites and virgin PCL. The organic modifier oleic acid was supposed to increase the osteoblastic responses. Biocompatibility assessments were performed using umbilical vein endothelial cells. The HA/PCL system has been found to enhance the growth of endothelial cells and primary osteoblast. Also, the cell cultures and osteoblast were observed to be dependent on PCL loading and contact time.

Excellent physico-mechanical characteristics viz; toughness, fatigue resistance, durability and chemical versatility make thermoplastic polyurethanes (PU) suitable for many applications.[16] The PUs have a segmented copolymer chemistry derived from a mixture of a diisocyanate, a macro-diol and a chain extender. PU based nano-composites have been used for infection control, controlled drug delivery etc.[17,18] Bioactive montmorillonite (MMT) nanoparticles have been reported to provide biological characteristics to a PU matrix.[19] It has been concluded from literature that the organic fillers having suitable structures may be used to modify the biological responses of PU-based systems. Antibacterial properties can be imparted to PU matrix upon nanofiller loading. Hung et al. reported the improvement in biocompatibility and cell proliferation of PU matrix upon incorporating silver

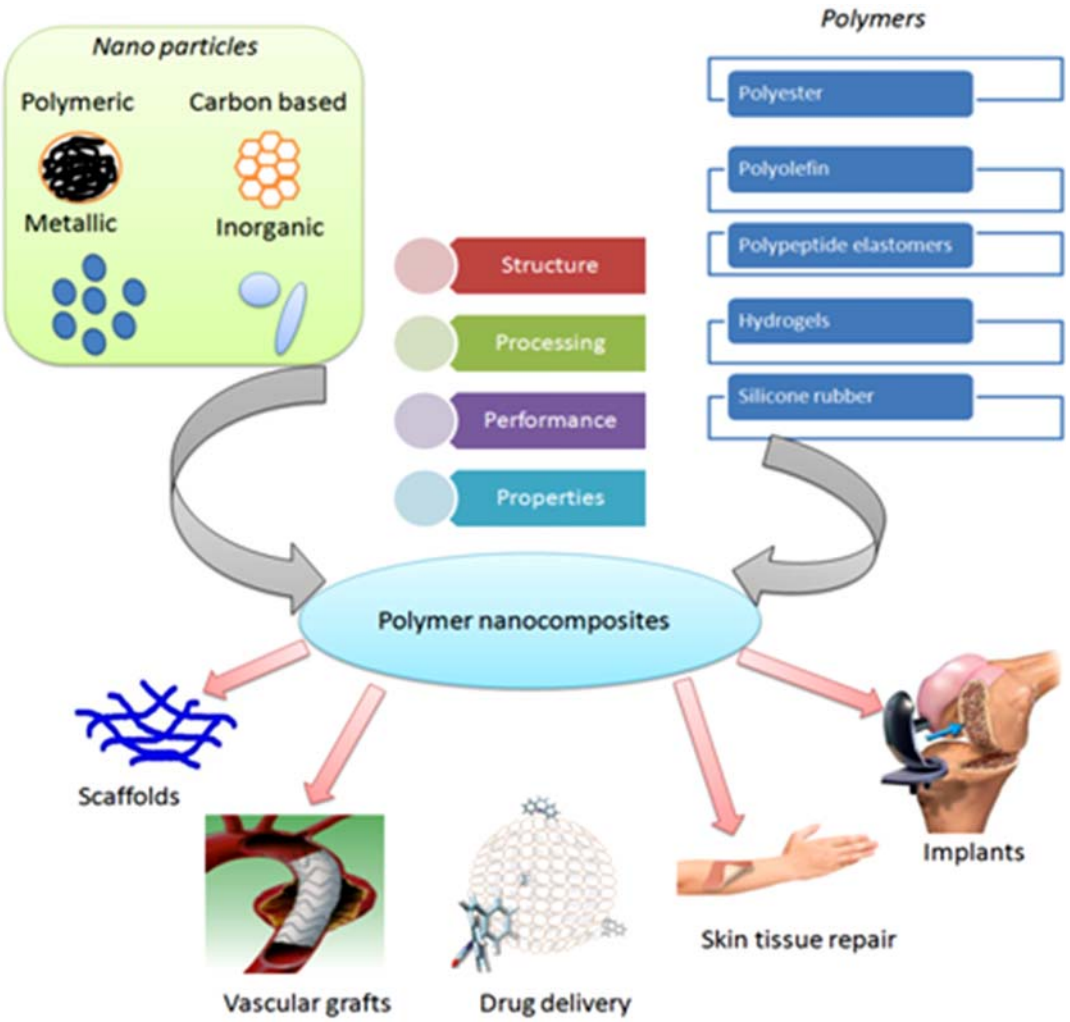

FIGURE 10.2 Biomedical applications of polymer nano-composites.

nanoparticles.[20] Williams et al. investigated the potential of integrating multiwalled carbon nanotubes (CNT) with PU for electrical interfacing with neural tissues.[21]

Poly (trimethylene carbonate) (PTMC) elastomers have been used as long term degradable devices for soft tissue engineering as they are both biocompatible and mechanically resilient.[22] They have been used as surgical sutures, controlled drug delivery vehicles, bone cement and tissue engineering scaffolds.[23] Ribeiro et al. reported the utilization of PTMC reinforced with HA and multiwalled CNT (MWCNT) for joint repair.[24] The features of HA were carefully tapped to inspire osteo-conduction while the MWCNT was used as a reinforcing agent. The results suggested that the friction coefficient and surface behavior of PTMC reinforced systems were near to those of the cartilage. The mechanical properties' improvement

in poly (diol citrates) (POC) has been achieved upon incorporating a nanofibrous PLLA nanophase into POC matrix.[25] The results showed an enhancement in tensile strength, modulus, and elongation at break; interestingly the mechanical properties were observed to be comparable to those of blood vessels, ligaments and human cartilage.

Improvement in the conductivity of insulating polymeric scaffolds has been reported; from the angle of the biocompatibility.[26] The induction of appropriate electrical properties by the addition of filler, in a viscoelastic system, can fine-tune its inherent characteristics including biocompatibility. The embedding of an elastomeric matrix with biocompatible filler could be an ideal option to trigger the desired elastic features while improving the basic visco-elastic properties.[27]

2. Hydroxylapatite: a promising filler for elastomers

Hydroxylapatite (HA) is a major component of human bone, where it is entwined with collagen fibers. The constituents of HA are primarily calcium (Ca) and phosphorous (P), with a stoichiometric ratio of $Ca/P = 1.667$.[28] Fig. 10.3 shows the components of bone, showing the presence of HA. The synthetic HA has been of great interest to researchers, due to its outstanding biocompatibility and affinity toward biopolymers.[30,31] It has been reported that the HA can support new bone in growth through osteo-conduction, without producing any local or systemic toxicity, irritation, or foreign body responses.[29]

Several reports reveal that HA and its derivatives can be used to investigate the biomineralization in human body. Outstanding reports are available in literature, on the biomineralization activity of HA particles.[32–34] It has been reported that the HA can act as a nuclei for the apatite formation. The amount of apatite formed is directly related to the

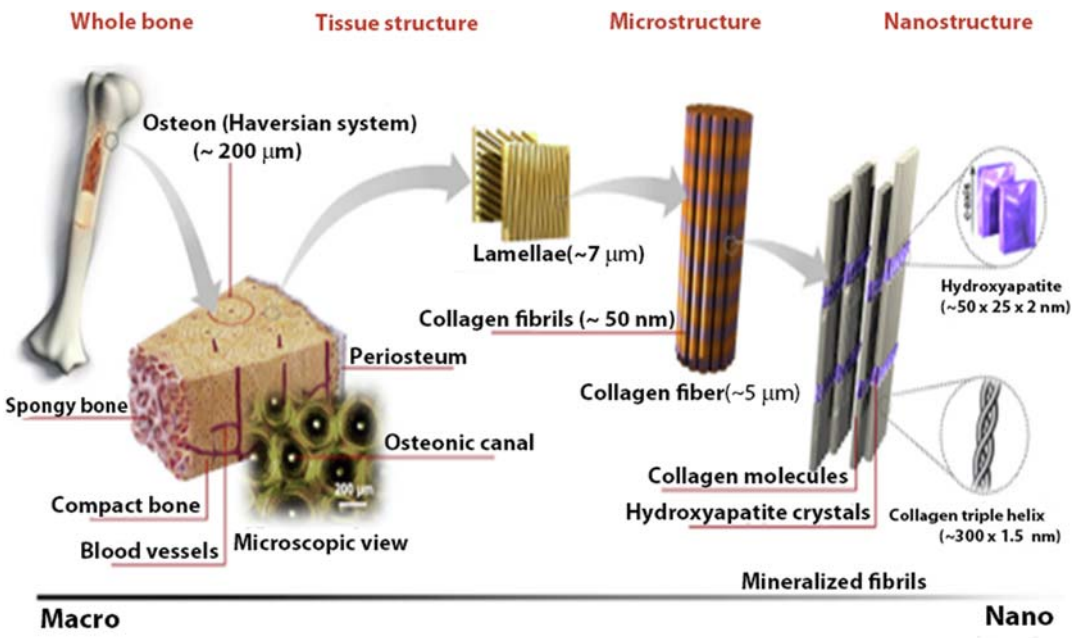

FIGURE 10.3 Components of bone [Ref. 29].

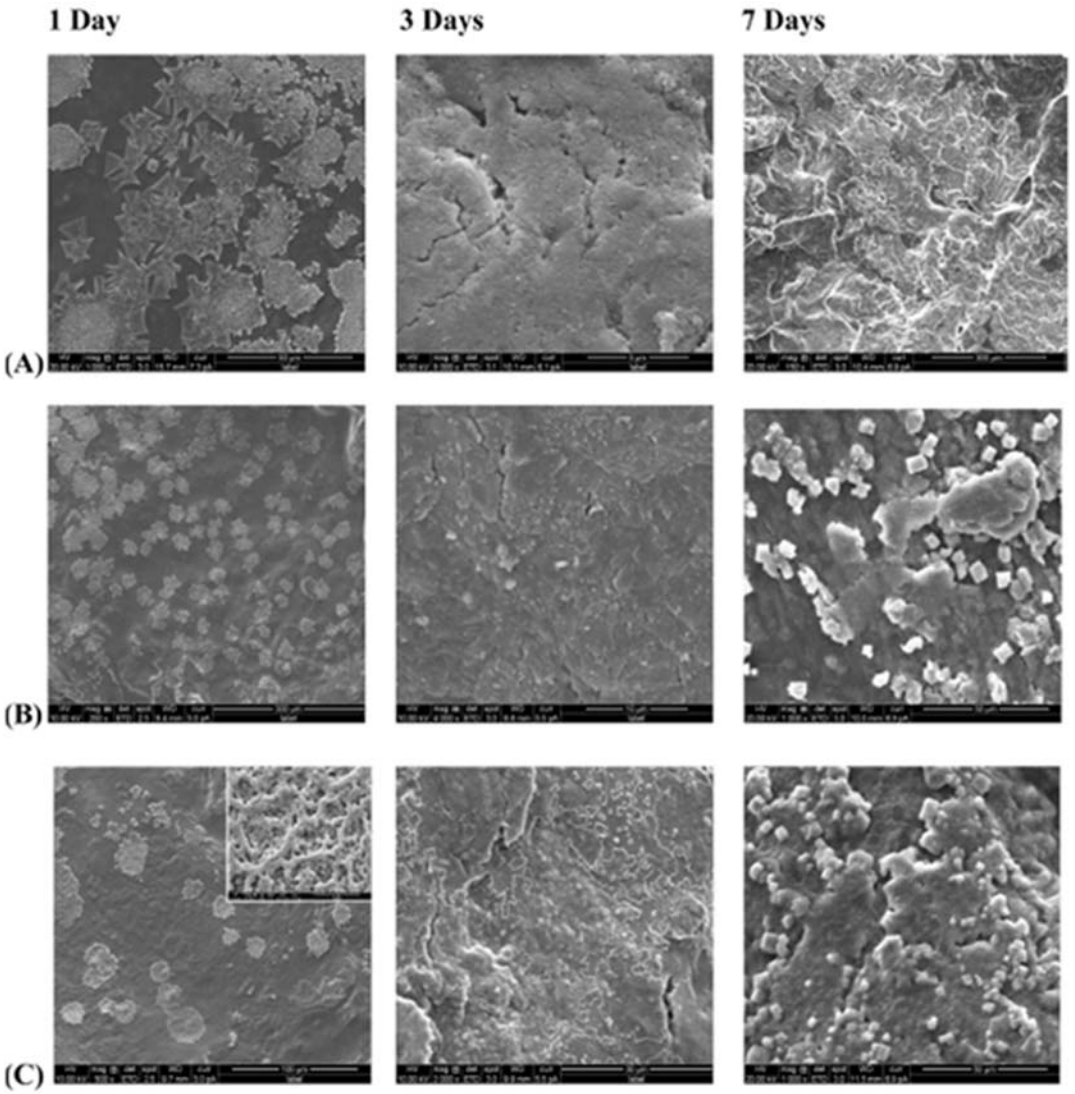

FIGURE 10.4 SEM images of chitosan/HA composites showing apatite formation after immersing in simulated body fluid for 1, 3 and 7 days (A): 5% n-HA (B) 8% n-HA (C) 10% n-HA [Ref. 34].

concentration of HA. The apatite layer structure is also influenced by the viability and differentiation of preosteoblast cells.[35] The SEM images of a chitosan/HA composite showing apatite formations have been presented in Fig. 10.4.

HA is a promising material for several applications such as bone and periodontal defects' replacement, ear implanting, tissue engineering, drug delivery and bio-active coating on metallic osseous implants.[36–39] The broad-spectrum significance of HA and its derivatives has also led to many engineering and technological purposes; as catalysts for chemical reactions such as Michael addition and methane oxidation, host materials for laser, fluorescence

materials, gas sensors, ion conductors, etc.[40–43] Synthetic HA also finds applications in column chromatography, for rapid fractionation of proteins and nucleic acids, and also for water management practices and remediation of heavy metals and polluted soils.[44–46]

Muller et al. reported the influence of HA particles on the human monocyte derived macrophages (HMMs), by incubating them with HMMs in serum and serum free conditions.[47] It has been observed that the HA addition does not produce any inflammation, irrespective of its concentrations used. The overall bioactivity of HA has been found to be influenced by factors such as the amount of proteins adsorbed, size, surface charge, morphology, formation of agglomerates and hydrophilicity.[48–52]

Excellent reports are available in literature, on the usage of HA as drug delivery agents. The drugs so delivered are protected from disintegration and are usually released at a slow rate. The kinetics of cisplatin release by HA has been reported by Barroug et al.[53] The results showed that a cumulative release of 58% of adsorbed drug occurred within 2 weeks. Palazzo et al. reported the kinetics of release of cisplatin, di (ethylene diammine platinum) medronate (DPM) and bisphosphonate alendronate from HA.[54] The HA having needle morphology favored ligand exchange induced binding to negatively charged alendronate. Irrespective of the surface area and shape, the HA could load almost 90% of the initial concentration of alendronate and cisplatin.

A novel approach to vaccination based on HA as an antigen carrier is currently in practice. Goyal et al. reported the use of HA particles coated with cellobiose, to deliver a hepatitis B surface antigen (HBsAg).[55] It has been observed that the HA coated system delivers approximately 20% of HBsAg effectively. HA can also be used for bio-imaging applications. Ong et al. reported the use of HA, conjugated with the radio isotopes of technetium, for bio-imaging purpose.[56] Clunie et al. performed experiments using HA-Sm^{153} (Sm- Samarium) particles, as a carrier to obtain bio-distribution data.[57]

Among several HA structures, nano-sized HAs, with appropriate morphology, stoichiometry, and purity have now gained boundless attention in various bio-medical applications and in basic research areas.[58–61] An observed improvement in cell proliferation and differentiation associated with n-HA compared to conventional HA can be attributed to the increased surface area and surface roughness, resulting in better cell adhesion and cell matrix interactions.[62,63]

3. Synthesis strategies for n-HA

The properties of synthetic n-HA are strongly dependent on its crystallinity, particle size, particle size distribution, morphology and surface area, which in turn depend up on the route for its synthesis. A variety of synthetic strategies for the synthesis of n-HA particles are available in literature such as:

3.1 Dry methods

Dry methods may be executed by solid state synthesis and mechano-chemical methods.[64–66] They are having the advantages of obtaining n-HA crystals with high crystallinity, from relatively cost-effective raw materials. The major draw backs associated with them are the larger particle size (in solid state reaction) and low phase purity (in mechano-chemical process).

3.2 Wet methods

n-HA crystals are normally prepared by precipitation from aqueous solutions of Ca and phosphate ion sources. The wet chemical method can be classified into six categories as follows[67–71]:

1. Conventional chemical precipitation
2. Hydrolysis method
3. Sol-gel method
4. Hydrothermal method
5. Emulsion method
6. Sonochemical method

A strong advantage of this strategy is a clear-cut control over the morphology and particle size. However, the crystallinity and phase purity control are very difficult. In order to obtain HA with high phase purity, a precipitation reaction is usually carried out at high p^H or high temperature or both.[72,73] When the p^H is dropped, the temperature should be elevated and vice versa. This can causes an intense reduction in the formation of phase impurities, such as dicalcium phosphate anhydrous (DCPA) and octa calcium phosphate (OCP), ensuring HA as the dominant phase. Fig. 10.5 shows the influence of p^H and temperature on the morphology and particle size of n-HA.[74]

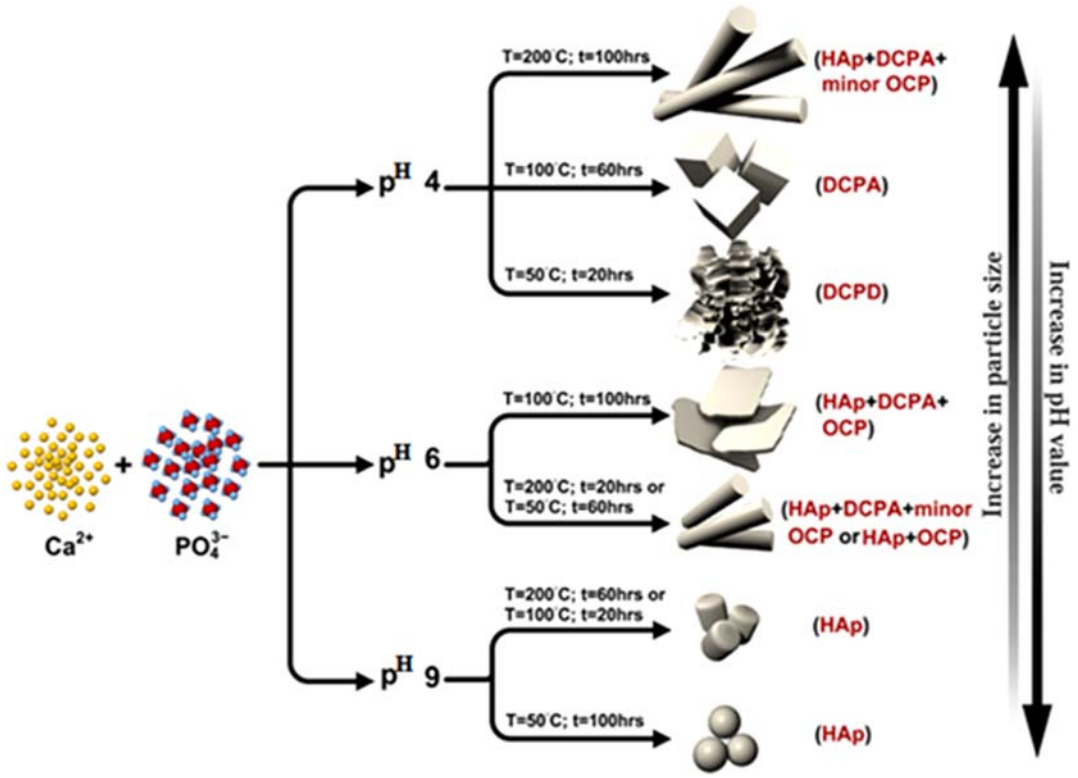

FIGURE 10.5 Effect of temperature and p^H on the morphology and particle size of n-HA [Ref. 74].

3.3 High temperature process

The routes for high temperature synthesis of n-HA particles include combustion method and pyrolysis, of which the former has received more attention.[75–77] By this method, good chemical homogeneity and excellent crystallinity can be achieved. Unwanted CaP phases can be eliminated by high temperature processes. Poor control over the processing variables and the generation of secondary aggregates (especially during pyrolysis) are the major drawbacks.

3.4 Synthesis from biogenic sources

Naturally available substances such as bone waste, egg shells, skeleton of marine organisms, naturally derived biomolecules etc have been extensively employed for the synthesis of n-HA over the past decades. This method may attract more consideration in the near future because of the possible achievement of enhanced physicochemical properties.[78–80]

4. Structure and dispersion behavior of hydroxylapatite nanoparticles

Fig. 10.6 shows a typical crystal structure of HA. HA crystallizes in hexagonal system with unit cell dimensions a = 9.41 A^0, c = 6.88 A^0, z = 2 (Space group: $P6_3/m$).[81] Lower crystallographic symmetry causes anisotropy along different directions. It has been observed that the c axis of HA crystals and collagen fibers showed a preferred orientation along the

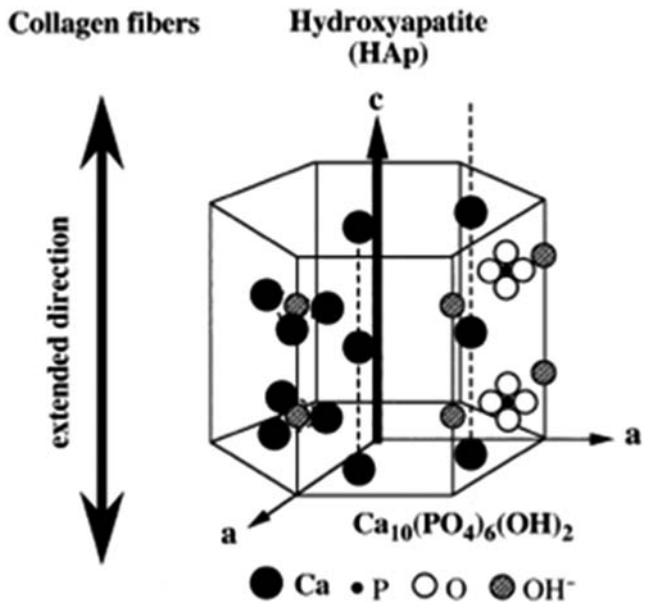

FIGURE 10.6 Crystal structure of HA nanoparticles [Ref. 81].

longitudinal direction of the bone, whereas weak poles for the c axis of HA were noted in both the radial and tangential directions.

It has been reported that the "a" and "b" planes are bioactive, whereas "c" is bio-inert. Thus, in-order to use HA for biomedical applications, a specific orientation of the crystal is required.[82] Owing to the presence of polar groups, the crystals are susceptible to ion exchange easily.

The properties of the elastomers can be modulated by the nanofillers, if there is considerable extent of interaction between the components. Lack of adhesion between the components, however, may lead to the failure of the system. The surface wettability plays a crucial role in determining the overall performance of the nanoparticle reinforced elastomeric systems.[83] The wettability further depends on the hydrophilicity/polarity of the partners. For a wetting surface, the surface energy should be minimum. The wettability is expressed in terms of contact angle values θ_c, the angle at which the gas-liquid interface, γ_{GL} meets the solid-liquid interface γ_{SL}. The surface may be considered as hydrophilic, if the fluid spreads over a large area on the surface ($\theta_c < 90^0$). A nonwettable surface is characterized by a contact angle $\theta_c > 90^0$ (hydrophobic).[84] Fig. 10.7 shows typical images of water droplets on (a) a hydrophobic and (b) a hydrophilic surface, respectively.

The degree of wetting is expressed by the spreading parameter S, which is defined as[83]:

$$S = \gamma_{SG} - (\gamma_{SL} + \gamma_{GL}) \tag{10.1}$$

The conditions for complete wetting of the surface is $S > 0$ and, and for partial wetting is $S < 0$.

It has been reported the surface tension and wettability directly influences the thrombogenicity, and protein adsorption behavior.[85]

The mechanical properties of the n-HA modified elastomeric system depends upon the size, shape and size distribution of n-HA. Various shapes of n-HA are available viz; irregular, acicular (nano rods, nano tubes) and platey.[86] It has been reported that our natural bone is made up of blade like nano hydroxylapatite crystals.[87] Irregular shapes are preferred over

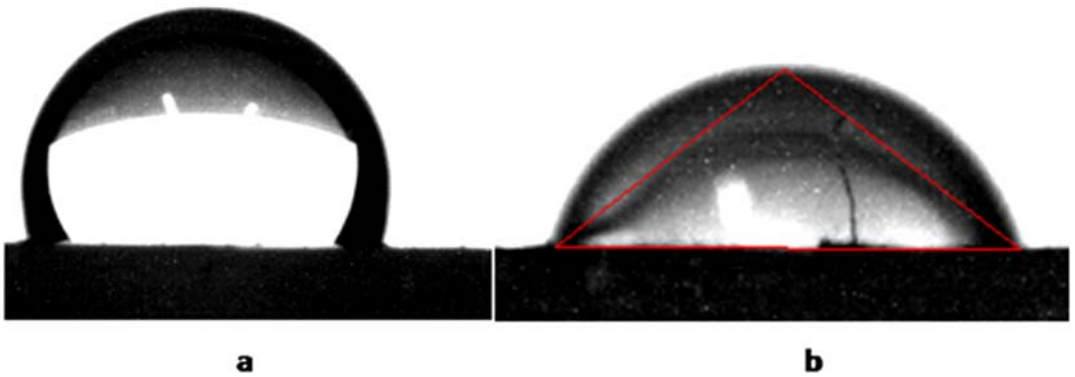

FIGURE 10.7 Images of water droplets on (A) silicone rubber (B) silicone rubber/nano hydroxylapatite surface [Ref. 84].

regular shapes, since the polymer can form mechanical interlock with the nano fillers, whereas it is not possible with the spherical fillers. The chemical bonding between the polymer and n-HA particle will certainly influence the mechanical properties of the system.[88,89] If the interfacial interactions are very strong, the stress transfer from the polymer to the reinforcement has been observed to very effective.

The amount of nano filler can influence the mechanical properties of the nano filler filled polymeric systems. Espirages et al. proved that the n-HA loading in a bioactive acrylic bone cement would increase the tensile modulus and compressive strength.[90] However, as the n-HA loading exceeded 20 wt%, the homogeneity of the systems was found to be lost. Then the entire stress would be concentrated on the n-HA particles, giving rise to a brittle system, with lower tensile properties. The finer particles may tend to combine together to form strongly bonded aggregates, which may change into larger structures known as agglomerates. Typical adhesion forces, viz., interlocking, electrostatic, van der Waals may be applied with increasing agglomerate strength.[91]

A high quality and high performance polymer nanocomposites would require homogeneous dispersion of nanofillers within the matrix. The efficiency of particle dispersion in a matrix can be assessed by scanning electron microscopy (SEM), transmission electron microscopy (TEM) and image analysis technique. TEM image of polysiloxane/HA systems having a particle size of 20–70 nm, with (a) relatively homogenous distribution of HA particles and (b) HA agglomerates have been shown in Fig. 10.8.[92]

For every nanoparticle filled polymeric system, there would be a maximum volume fraction of the filler that could be incorporated into the matrix. In actual practice, the nanofillers have a broad or bi model size distribution.[92] In this model, the smaller particles may assume to occupy the space between the larger particles, leading to high content of the filler per unit volume in the resulting composites.

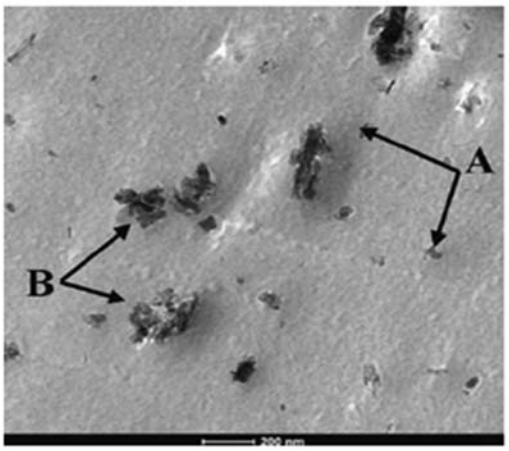

FIGURE 10.8 TEM image of polysiloxane/HA systems having a particle size of 20–70 nm, with (A) relatively homogenous distribution of HA particles and (B) HA agglomerates [Ref. 92].

5. Surface modification of hydroxylapatite nanoparticles

The surface treatments ensure a relatively uniform distribution of n-HA particles, even at higher filler loadings. The surface modifiers should be nontoxic, biocompatible, and they would not alter the physicochemical as well as the biological properties of n-HA. Various strategies have been adopted for the surface modification of n-HA particles. The surface modifications by carboxylic acids were well established.[93] The carboxylic acids form hydrogen bond with the surface −OH group of n-HA. It has been observed that the higher homologous carboxylic acids are more effective compared to lower members. The carboxylic acids, viz., oleic acid and stearic acid, belong to the fatty acid series can be used up to 3 wt%, without altering the particle size and bio-activity of n-HA.[94] The use of surfactants sodium dodecyl sulfate (SDS) for n-HA surface modifications are available in literature.[95] The negative charge of SDS may interact with the localized surface charge of n-HA particles.

Esterification reactions constitute an alternative method for the surface modification of n-HA particles.[96] The alkyl part in the alcohol may react with acidic phosphate site of the n-HA, to form esterified n-HA. The surface modification by this strategy could bring changes in properties viz; acidity, basicity, catalytic activity, electrophoretic mobility and protein adsorption behavior. The surface modification of n-HA by pyrophosphoric acid (PP) have been reported by Tanaka et al.[97] The surface P−OH groups of n-HA are being attacked by PP to form additional surface P−OH groups and phosphoric acids. As the concentration of PP increases, more surface P−OH groups are attacked by PP as per the reaction:

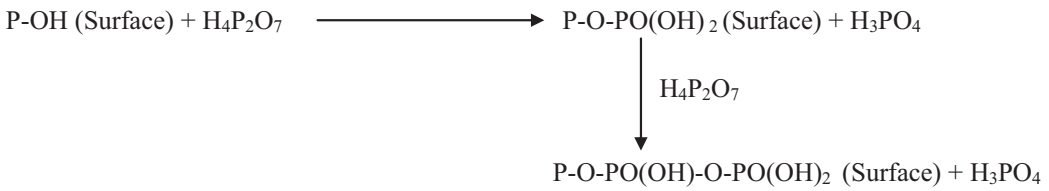

The modified n-HA particles were found to be more aggregated compared to the unmodified ones. With an increase in the modifier (PP) concentration, the amount of phosphate group increases, leading to a reduction in the Ca: P ratio from 1.62 to 1.35.

Silanes have been widely employed as a coupling agent between the inorganic and organic components.[98,99] It has been reported that the silanes do not enhance the cytocompatibility of the final products. Its application have been reported in the surface modification of n-HA for the fabrication of dental composites and bone repairing materials.[100] Borum et al. modified the n-HA particle's surface by silica with varying amounts, which is obtained by the hydrolysis of tetraethyl orthosilicate.[101] Excellent reports are available in the literature, based on the role of silica in the osteogenic and bioactivity of the bioglass.[102] The surface silanol groups (Si−OH) on the amorphous silica has been found to be more effective compared to the highly crystalline or heat treated silica. The n-HA particles were also modified by hexamethyldisilazane [$(CH_3)_3Si]_2NH$ (HMDS), followed by heat treatments.[103] This was driven by the thought that the surface P−OH group of n-HA particles would react with HMDS and form $Si(CH_3)_3$ groups on the surface. As a result of this, the hydrophilic surface may change

into hydrophobic. When the modified surfaces are heated, they may be converted into surface Si−OH groups. The Si−OH groups formed in this way and the remaining surface P−OH groups again may react with HMDS. Owing to this, there may be an increase in the surface Si atom according to the mechanism as shown below[103]:

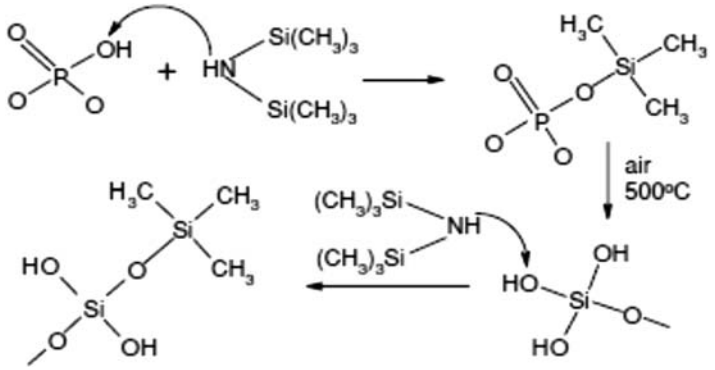

Mechanism of surface modification of n-HA particles by HMDS

The surface silanol groups can also be formed by the hydrolysis of triethoxysilane in ethanol as per the reaction shown below.[104]

$$CH_2{=}CHSi(OCH_2CH_3)_3 + 3\ H_2O \rightarrow CH_2{=}CHSi(OH)_3 + 3\ CH_3CH_2OH$$

The active groups of the n-HA particles viz; OH^-, PO_4^{-3} and Ca^{+2} may react with the hydrolysate. Owing to this, the hydrophilic surfaces of the n-HA changes into hydrophobic. The n-HA particles can be modified by using γ-aminopropyltriethoxysilane by exploring the amino groups.[105] The modifier, γ-methacroyl oxytrimethyl silane, have been employed in the surface modification of the n-HA particles for the fabrication of bioactive bone cement.[106]

Wang et al. reported two strategies to improve the interfacial adhesion between the constituents[107]; use of silanes for the n-HA surface modification and grafting for the polyethylene matrix. It has been shown that the coupling agent, silane, enhances the penetration of polymer chains into the voids of n-HA, during the processing. As a result of this, the interlocking between the n-HA and the matrix gets enhanced, leading to a system, which functions in a synergic way. Various isocyanates were grafted onto n-HA particles at different temperatures and the reactivity of isocyanates toward −OH group of n-HA have been compared.[108] It was found that the hexamethylene diisocyanate (HMDI) and isocyanatoethyl methacrylate (ICEM) have more affinity toward n-HA, while ethyl isocyanate acetate (EIA) and butyl isocyanate (BIC) have less affinity toward n-HA particles. Therefore, ICEM and HMDI are ideal for introducing polyethylene glycol (PEG) on to the n-HA particles.

Lee et al. reported a novel strategy for the surface modification of n-HA particles by using 3-mercaptopropoinic acid.[109] It was followed by the grafting of ethylene glycol methacrylate phosphate (EGMP) to create sulfur free radicals at the surface of n-HA. A schematic representation of the surface modification process has been shown as Fig. 10.9.

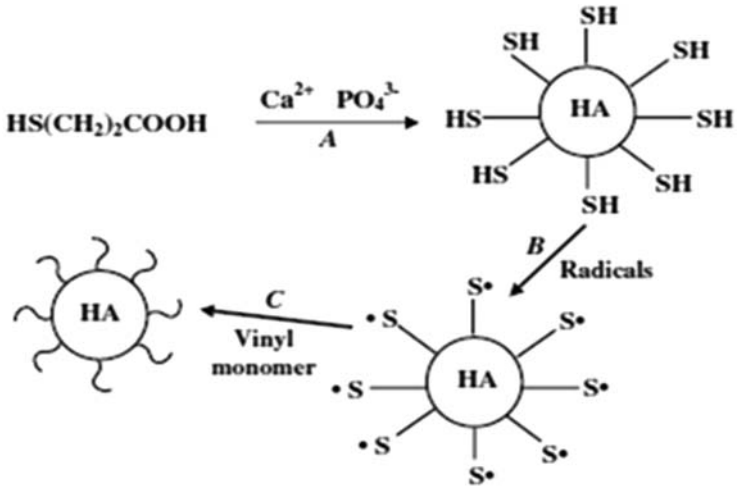

FIGURE 10.9 Surface modification of n-HA by grafting polmerization (A: Thiol functionalized n-HA, B: S radicals on n-HA surface, C: Surface grafting polymerization of EGMP) [Ref. 109].

6. Nano-hydroxylapatite modified elastomeric systems

Liu et al. developed polymer nanocomposite membranes based on polyurethane (PU) elastomers and n-HA particles by solvent casting and freeze drying strategies.[110] PU/n-HA membranes were then subjected to different characterization techniques viz; SEM, XRD, IR, mechanical test and in-vitro biocompatibility. The results substantiate that the incorporation of n-HA into PU matrix increases the tensile strength by 186% and elongation at break by 107% compared to virgin PU. MTT assay and cell culture studies reveal that the n-HA particles in PU matrix creates a positive environment for adhesion and proliferation of cells. The developed system has been proposed to use as bone regeneration membranes.

The surface of the composite membrane was observed to be rough with irregular pores, compared to neat PU and the surface roughness increases with increase in n-HA loading. The SEM images of the systems have been shown in Fig. 10.10. The rough surface and porous structures are highly desirable for the cell adhesion and proliferation.[111]

It is reported that the pore sizes greater than 20 μm are essential for the tissue in-growth.[112] In the study, the developed PU/n-HA system has a pore size of <10 μm, and it has been found to possess the potential to prevent the escaping of osteogenic components and maintain a suitable environment for the migration of osteogenic cells in the defect, while preventing the connective tissue migration into the bony defect site.

The mechanical properties of the systems have been presented in Table 10.1. It has been observed that as the n-HA content increases from 0 to 30 wt%, the tensile strength increases from 4.91 to 14.04 MPa and the elongation at break increases from 370% to 766%. As the n-HA loading exceeds 30 wt%, both the tensile strength and the elongation at break exhibit a decreasing trend.

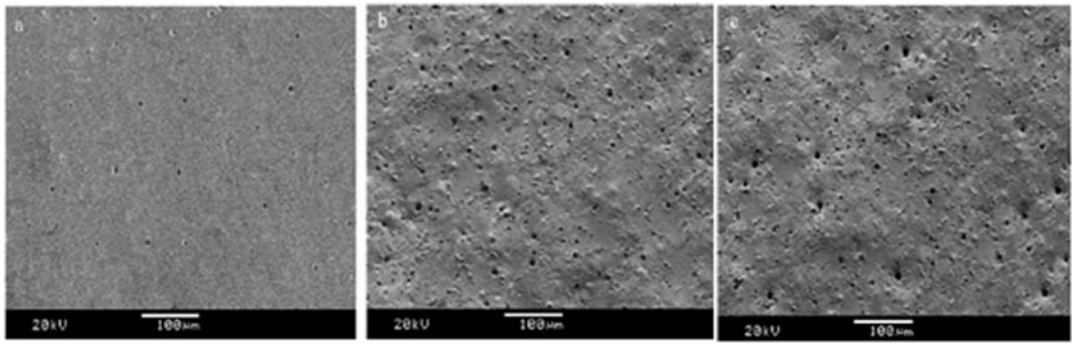

FIGURE 10.10 SEM images of PU/n-HA systems as a function of n-HA loading: (A) PU (B) 30 wt% n-HA (C) 40 wt% n-HA [Ref. 110].

TABLE 10.1 Mechanical properties of PU/n-HA systems [Ref. 110].

HA content (wt%)	Tensile strength (MPa)	Elongation-at-break (%)	Tensile modulus (MPa)	Bending strength (MPa)	Bending modulus (MPa)
0	4.91 ± 0.49	370 ± 30	1.23 ± 0.10	0.45 ± 0.07	5.64 ± 0.26
20	9.52 ± 0.58	619 ± 33	2.32 ± 0.09	1.36 ± 0.02	13.21 ± 0.35
30	14.04 ± 0.74	766 ± 32	3.69 ± 0.19	1.76 ± 0.13	17.38 ± 0.50
40	12.84 ± 0.69	597 ± 29	8.45 ± 0.42	2.42 ± 0.18	21.24 ± 0.34

The surface −OH groups of n-HA particles are highly reactive and they can make covalent linkages with a polymer matrix. These covalent linkages are often responsible for the improved interfacial interactions between the polymer matrix and the n-HA particles, leading to an enhancement in the tensile properties. The enhancement in mechanical properties, upon the incorporation of nanofillers have been reported by many researchers.[113–116] The nanoparticles are capable of transferring the stress among them, during the deformation process. As the concentration of n-HA increases, there are chances for particle agglomeration and the particles would be loosely bonded to each other. Owing to this, the mechanical properties exhibit a decreasing trend. The in-vitro biocompatibility tests reveal that the added n-HA particles plays an important role in improving the biocompatibility of PU based membranes. The n-HA particles in PU matrix creates an osteo-conductive environment compared to the sample without n-HA. The n-HA may be employed either in the form of granules, blocks or cements for bone regeneration applications.[117–119] As the n-HA content increases, the number of cells which adhering on the membrane was observed to be increased. The n-HA weight ratio of 30% has been found to be optimum, to use the developed system as bone regeneration membranes.

In another report, the PU matrix was reinforced by n-HA particles, after the surface modification of n-HA by multifunctional isocyanates.[120] The surface modification process improves the adhesion between the PU matrix and n-HA particles. The surface properties of n-HA may change after the surface modification; which may prevent the particles from agglomerating and ensures a relatively homogenous distribution in the matrix. Owing to this, the surface modified composite systems often exhibit excellent mechanical features, compared to the untreated n-HA containing samples. The stress-strain plots of the systems have been shown as Fig. 10.11.

Tetteh et al. reported the fabrication of PU/n-HA composites for bone tissue engineering applications by electro spinning technique and evaluated the role of particle size of hydroxylapatite on the fiber morphology and mechanical properties.[121] It has been shown that the HA with smaller particle size and higher surface area, blends very well with the PU matrix, and results in a uniform distribution of fibers compared to those having μ-HA (Fig. 10.12). It was reported that the n-HA particles with higher surface area compared to μ-HA would offer better bonding to the PU matrix, enabling greater reinforcement and eventually excellent mechanical and functional properties compared to conventional microcomposites.

The n-HA fibers are more consistent in size and morphology, and the particles would be better distributed within, and bound to the matrix. HA has been reported to facilitate quicker bone regeneration and exhibit the capability to bond directly with the regenerated bone.[122] The PU/n-HA systems possess excellent cell viability; meaning that the cell proliferation rate is higher. This may be due to the bioactive nature of HA, combined with a higher surface area and crystallinity.

A higher surface area of HA would make it suitable to adsorb more amount of proteins.[123] It has been shown that the initial calcium absorption onto the nanofillers would enhance the binding of some of the proteins, which further would promote adhesion and proliferation of

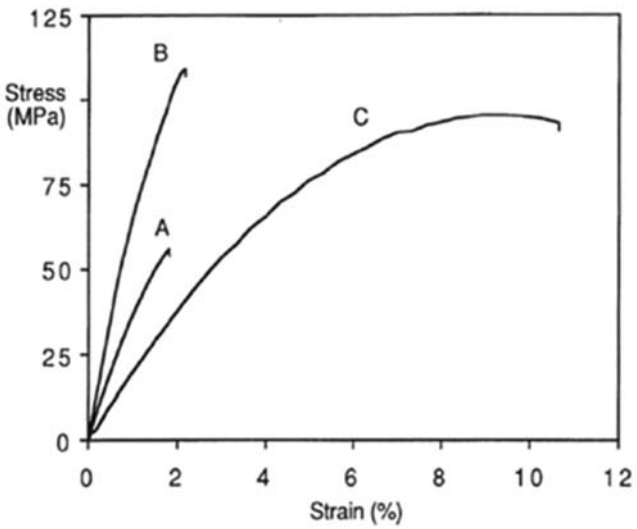

FIGURE 10.11 Stress-strain curves of the PU/n-HA systems (A) PU/untreated n-HA (B) PU/surface modified n-HA (C) unfilled PU [Ref. 120].

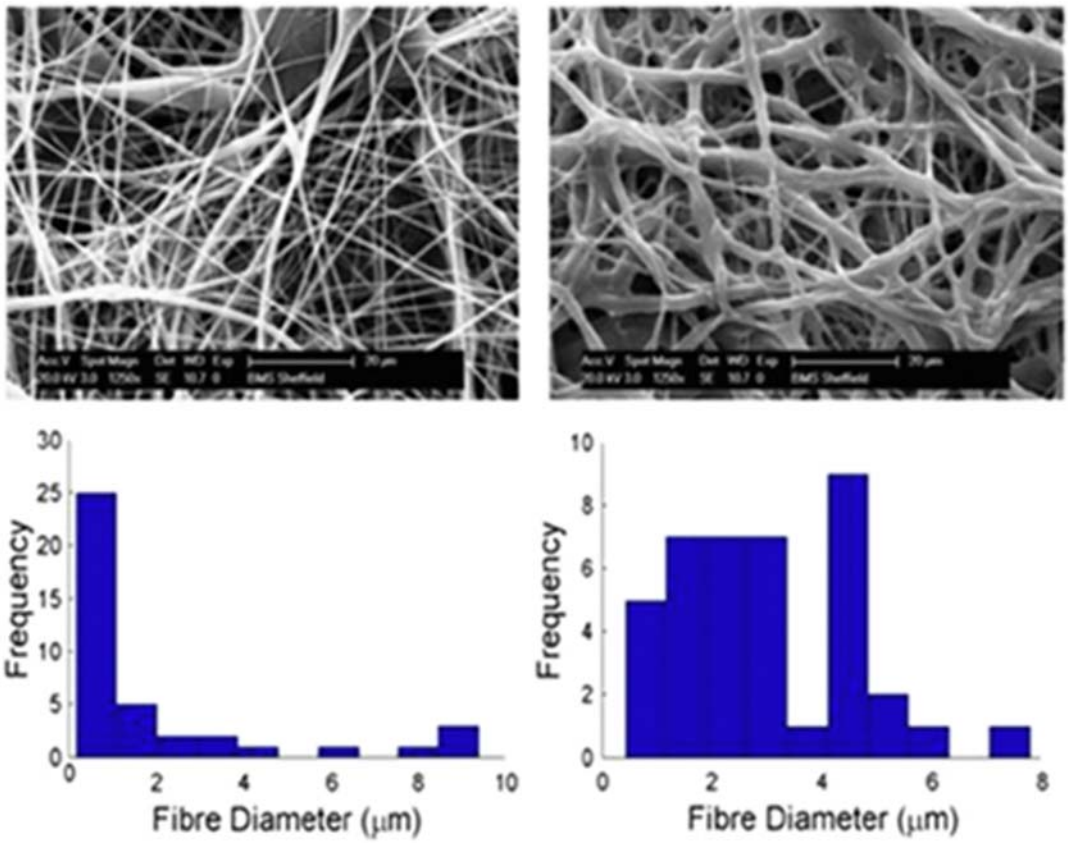

FIGURE 10.12 SEM images: Column A- Electrospun PU/ μ-HA composites and a histogram of fiber diameter; column B- Electrospun PU/ *n*-HA composites and a histogram of fiber diameter [Ref. 121].

cells. The porosity of HA also has a strong influence on the cell viability. A Low porosity would hinder the cell proliferation and decrease the rate of migration and nutrient transfer. Fig. 10.13 shows the MTT assay of various systems, viz., PU/n-HA, PU/μ-HA and PU elastomers using MLO-A5 cells.

In one of our efforts, silicone rubber (SR) was modified by embedding it with n-HA particles to evaluate the dielectric and viscoelastic features.[124] The properties viz; dielectric constant, dissipation factor, volume resistivity, electrical conductivity, storage modulus and mechanical damping were investigated. The aim is the simultaneous modulation of conducting and visco-elastic features to enable SR to function effectively in more challenging ambience than that of its regular and current utilizations. It has been observed that the dielectric constant increases with an increase in n-HA loading, for all the frequencies. The dielectric constant has contributions from both the interfacial and orientation polarizations.[125]

In the interfacial polarization (Maxwell–Wagner polarization) mechanism, dipoles can be induced at the interface between the dielectric SR and the conducting n-HA, in the presence

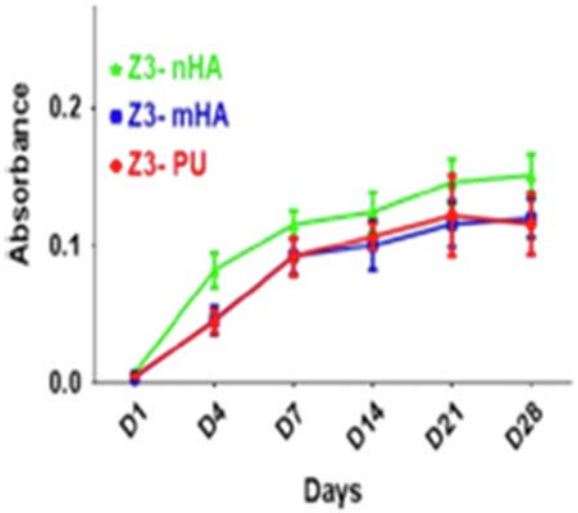

FIGURE 10.13 MTT assay of the PU/n-HA, PU/μ-HA and PU elastomers [Ref. 121].

of an electric field (due to the difference in polarization). In addition, when polar n-HA molecules are subjected to an electric field, the randomly distributed dipole fields can orient themselves with the applied field causing orientation polarization. The observed enhancement in dielectric constant with n-HA loading can be attributed to the increment in orientation and interfacial polarization originating from the polar groups of n-HA. The dipole moment of OH in n-HA has a major contribution to the dielectric features. A scheme demonstrating the polarization effect of n-HA is shown in Fig. 10.14.

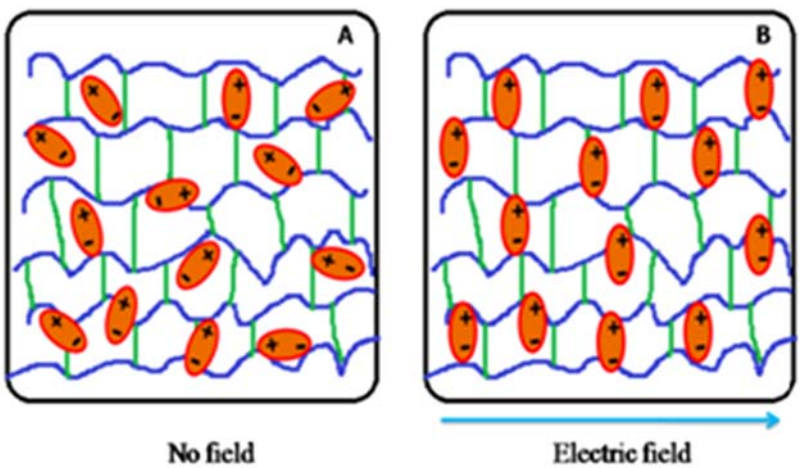

FIGURE 10.14 Orientation of dipoles of n-HA in SR matrix, in presence of an electric field [Ref. 124].

Loading of n-HA into SR matrix has been found to result in a significant improvement in the room temperature storage modulus of SR/n-HA systems. The n-HA particles have been found to be almost homogenously distributed within the SR matrix, reducing discontinuities for stress transfer; under a sinusoidal load. The embedding of n-HA particles into viscoelastic SR matrix restricts the segmental mobility and deformability of the matrix. This has been shown in Fig. 10.15.

Fig. 10.16 shows the loss factor, the ratio of loss modulus to storage modulus, of SR/n-HA systems. In a composite system, the loss factor is affected by the incorporation of fillers.[126] This can be attributed to the shear stress concentrations at the filler ends in association with the additional viscoelastic energy dissipation within the matrix.

In the case of the unfilled system (pure SR), three peaks have been observed in the tan δ versus temperature plot; one at −110°C corresponding to Tg; a prominent peak at −56°C, characteristic of the crystalline domains in SR and a peak at −30°C corresponding to the melting of the crystalline domains. However, for the filled systems, the tan δ peaks have been found to be reduced in height with a broadening. This is a clear evidence of the embedding effect of n-HA in SR matrix. Interestingly, the crystallites of n-HA with SR macromolecular chains gives an effective reinforcement and the system functions in a synchronized way under the dynamic load. This is schematically shown in Fig. 10.17.

The simultaneous modulation of visco-elastic and dielectric properties achieved through the above work can contribute to the expansion of the spectrum of applications of SR. When a voltage is applied across SR/n-HA system, which is placed between two electrodes,

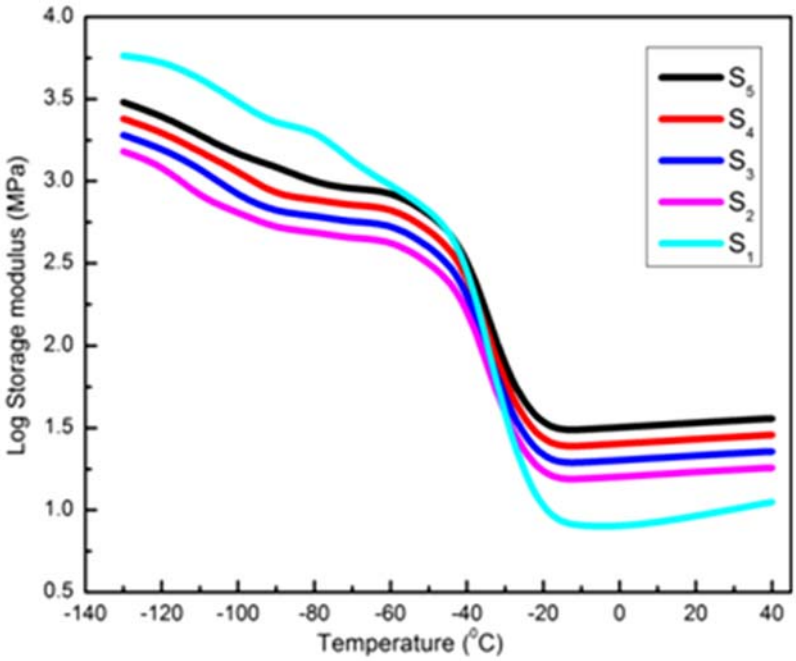

FIGURE 10.15 Storage modulus of SR/n-HA systems [Ref. 124].

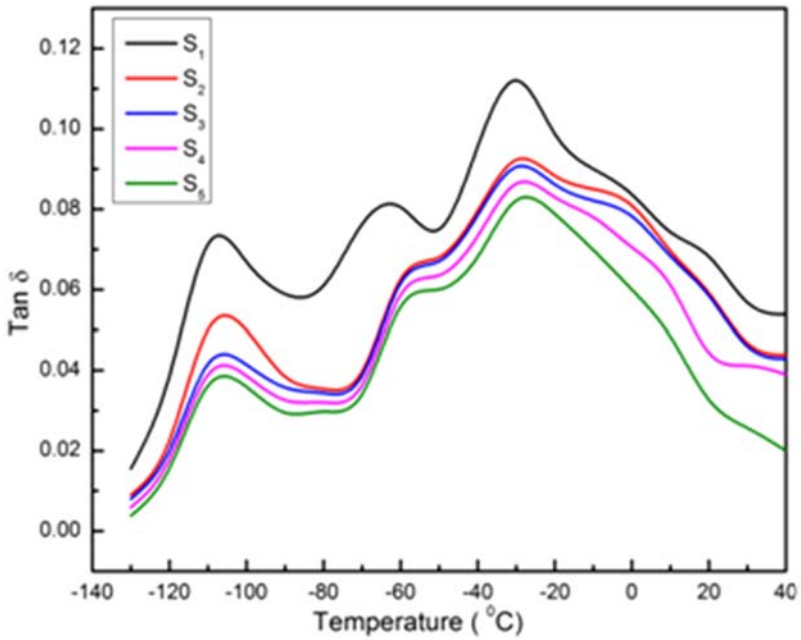

FIGURE 10.16 Tan δ versus temperature of SR/n-HA systems [Ref. 124].

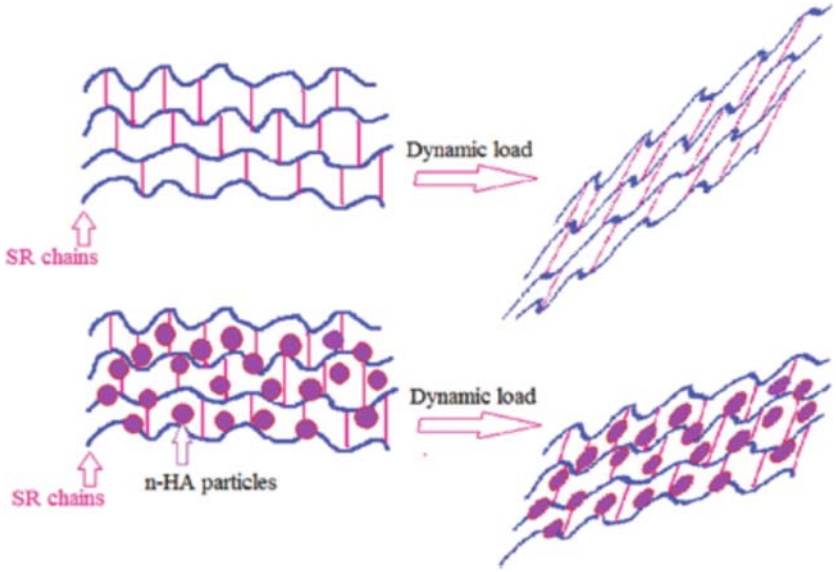

FIGURE 10.17 Schematic representation of behavior of SR and SR/n-HA systems under a dynamic load [Ref. 124].

the attraction between opposite charges and the repulsion of like charges would generate a stress (known as Maxwell stress) causing the compression and elongation of it as shown in Fig. 10.18. This effect can effectively be utilized for the development of blood pumps and robotic instruments for minimally invasive surgery.

Roy et al. reported the fabrication of fibrous n-HA/poly dimethyl siloxane (n-HA/PDMS) composites and evaluated the role of nano filler aspect ratio, crystallinity and surface interactions on the functional performance of the developed systems.[127] A soft template method has been employed for the fabrication of n-HA fibers. Nanofibers of varying aspect ratio and crystallinity have been synthesized by varying the pH and calcination time. The tensile strength and tensile modulus of the n-HA fibers prepared under normal pH, showed a dramatic increase, when compared with those prepared under an acidic pH.

Further, uncalcined samples were observed to offer a better reinforcement compared with the calcined samples. A comparison has been presented as Fig. 10.19.

The physicomechanical properties of the polymer nanocomposites are highly influenced by the aspect ratio of the nano filler.[128] The enhancement in the mechanical properties has been observed to be directly proportional to the aspect ratio of the filler, which further depends on its geometry and dispersion behavior. An enormous discrepancy in magnitude of various properties was obtained for the nanocomposites prepared with calcined and uncalcined n-HA fillers. This has been attributed to the high crystallinity of n-HA, ease the regularity in arrangement of the atoms, and attainment of regular shape with smooth surfaces. It was shown that n-HA with low crystallinity are irregular, but upon calcination, the smoothness of the surface increased.[129]

Irregular surfaces of n-HA are capable of establishing polymer-filler interactions, by mechanical interlocking phenomena.[130] Thus stronger filler-polymer interfaces are established with uncalcined samples, owing to the presence of more anchoring sites due to the surface

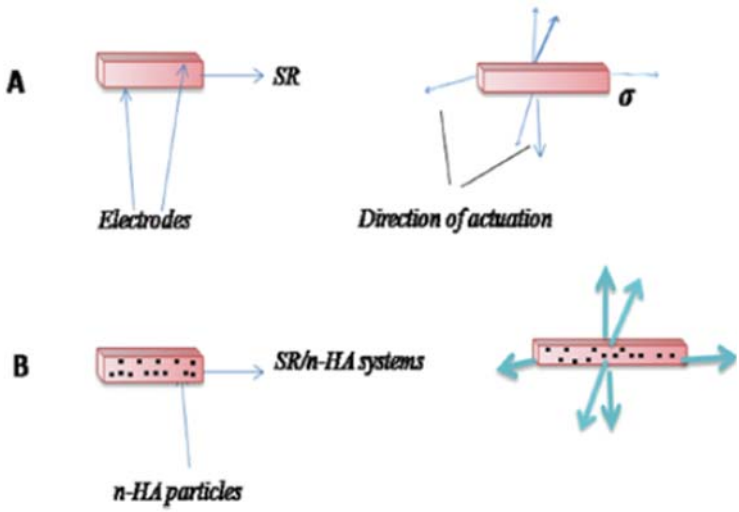

FIGURE 10.18 Actuation in: (A) SR (B) SR/n-HA systems [Ref. 124].

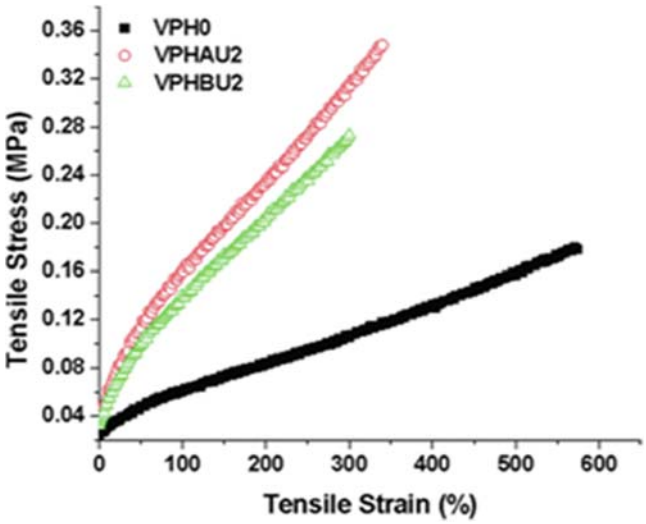

FIGURE 10.19 Stress-strain plots of unfilled PDMS (VPH0) and n-HA filled PDMS nanocomposites (VPHAU2: n-HA prepared at normal pH and uncalcined; VPHBU2: n-HA prepared at acidic pH and uncalcined) [Ref. 127].

irregularities. The FESEM images of the samples (Fig. 10.20) show the difference in the dispersion behavior of the nanofillers prepared at normal pH and an acidic pH. The n-HA fibers prepared at normal pH shows a relatively uniform distribution, whereas significant agglomeration has been observed in the samples prepared at an acidic pH.

In another interesting report, poly (1, 2-propanediol-sebacate) citrate [PPSC] elastomers have been modified by varying the amount of n-HA (5–20 wt%) for tissue engineering applications.[131] The DMA study reveals that the developed system is mechanically stable under dynamic load. The addition of n-HA into PPSC matrix leads to a reduction in the tangent of loss angle (tan δ), owing to the volume effect.

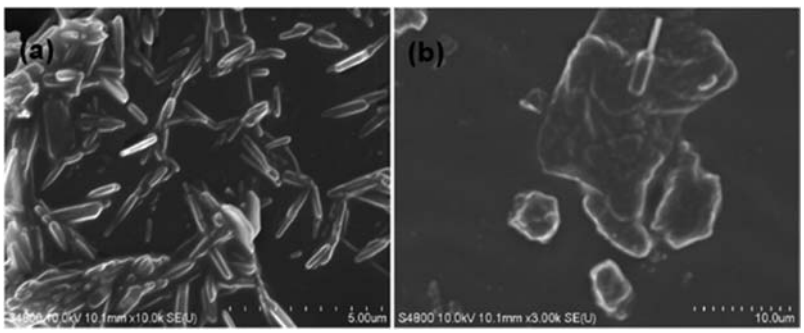

FIGURE 10.20 FESEM images of the n-HA fibers prepared at: (A) Normal pH (B) acidic pH [Ref. 127].

Besides, the interaction between the n-HA particles and the matrix causes a decrease in the height of the tan δ peak. In addition, the glass transition temperature (Tg), which is determined from the peak of the tan δ curve, gets shifted to a lower temperature. The reduction in the Tg has been attributed to the decrease in the crosslink density of the system, upon n-HA loading.[132] The storage modulus represents the ability of a material to store the mechanical energy and oppose deformation.[133] It has been shown that the PPSC/n-HA systems possess a higher storage modulus compared to the virgin PPSC. The addition of rigid n-HA particles restricts the free segmental mobility of the elastomeric chains and causes an increase in the storage modulus. The variations of tan δ and storage modulus upon n-HA loading have been shown as Fig. 10.21.

It has been reported that, as the n-HA content in the PPSC matrix increases, the water contact angles decreases and the systems become more hydrophilic. This can be attributed to the formation of hydrogen bonds between the surface −OH groups of n-HA water molecule.

The water uptake (%) of the samples were determined by comparing the initial weight (W_0), with the weight after swelling (W_1) in phosphate buffer solution at pH 7.4, as shown in Eq. (10.2).

$$\text{Water uptake\%} = \frac{W_1 - W_0}{W_0} \tag{10.2}$$

From Fig. 10.22, it is clear that the water absorption of the composites offers a decreasing trend with increasing n-HA content in the PPSC matrix. This may be attributed to the strong interfacial interactions between the filler and the matrix and the volume effect induced by the filler would reduce the degree of swelling.

The cell viability has been assessed by MTT assay by using L929 cells. The cell relative growth rate (RGR) was calculated as[131]:

$$\text{RGR}(\%) = \frac{\text{Absorbance of the material} - \text{Absorbance of the blank}}{\text{Absorbance of the negative} - \text{Absorbance of the blank}} \times 100 \tag{10.3}$$

The RGR has been classified into six numerical grades as shown in Table 10.2. Attainment of a grade 0−1 was accepted as qualified.

Fig. 10.23 shows that the cell morphology is not very much different from as in the case of negative controls. The cells show good growing conditions. It has been proved that the addition of n-HA improves the biocompatibility of PPSC matrix.

An elastomeric hydrogel has been developed by embedding polyethylene glycol (PEG) with n-HA particles for diverse tissue engineering applications.[134] The developed systems possessed a pore size of 100−300 nm. The PEG hydrogels and PEG/n-HA nanocomposites hydrogels were subjected to loading and unloading cycles to determine the hysteresis. The results indicate that, for the PEG hydrogel, there is an almost complete overlapping of the loading and unloading cycles. However, for the nanocomposites, hysteresis has been observed as shown as Fig. 10.24.

The addition of n-HA particles into PEG gel increased the compressive strength and modulus of the nanocomposites. The modulus increased by twice, when the n-HA concentrations increased from 0 to 15 wt%. The effect of n-HA loading, on the visco-elastic features of PEG hydrogel, was evaluated from the energy required for the permanent deformation. This

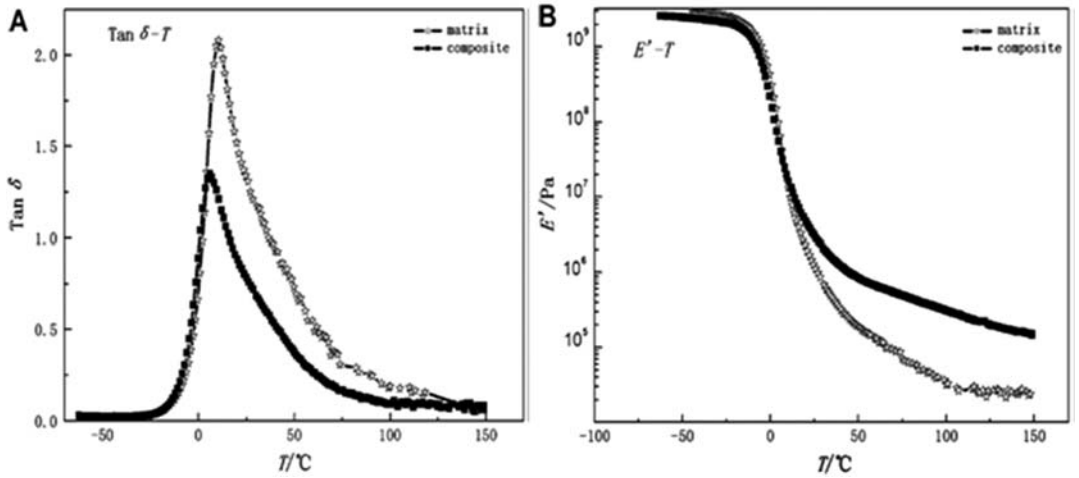

FIGURE 10.21 Variations of tan δ and storage modulus upon n-HA loading in the PPSC matrix [Ref. 131].

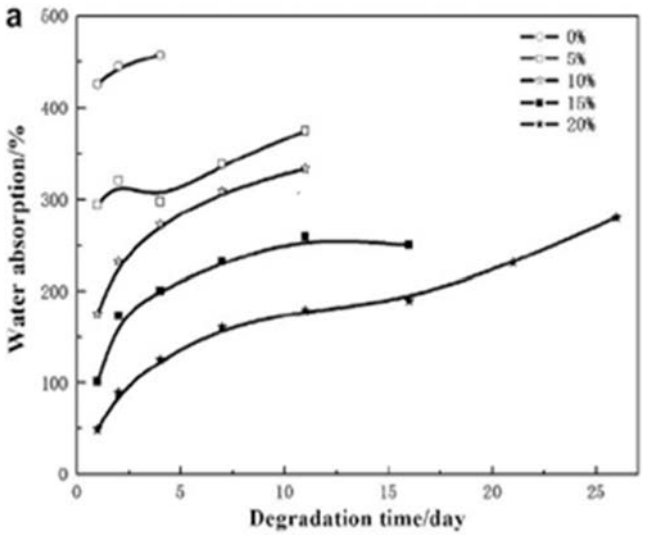

FIGURE 10.22 Water absorption of PPSC/n-HA composites [Ref. 131].

TABLE 10.2 The standard of RGR response grades [Ref. 131].

Grades	0	1	2	3	4	5
RGR	≥100	75–99	50–74	25–49	1–25	0

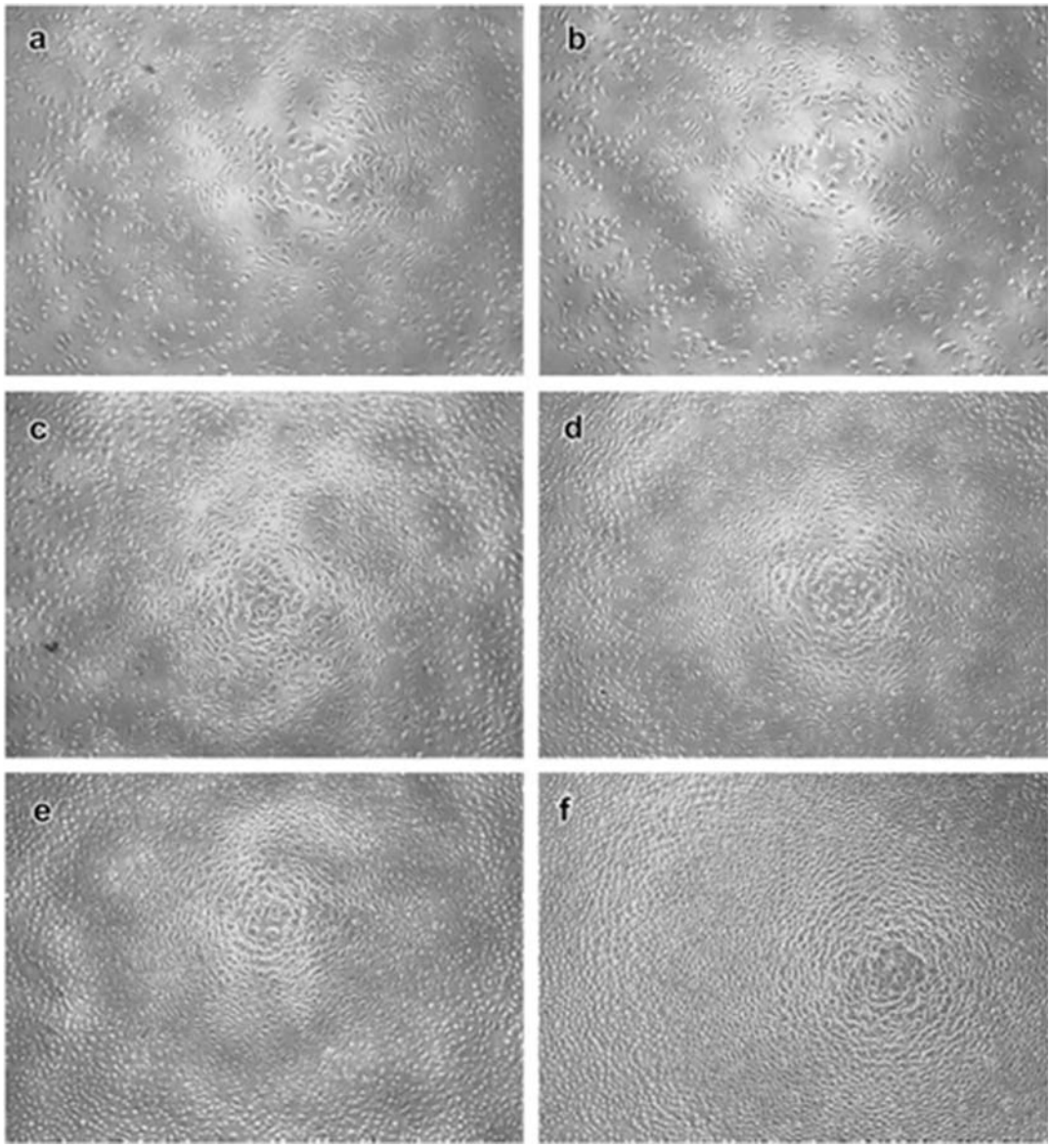

FIGURE 10.23 Images of cells after incubation for (A) 2 days (C) 4 days (E) 7 days (b,d,f) the negative control [Ref. 131].

has been obtained from the area of the hysteresis loop in the stress-strain plot. The virgin PEG hydrogel remains elastic at low deformation and thus experiences low energy loss during the loading and unloading cycle. As the n-HA content increases from 0− to 15 wt%; the energy loss observed is 25-fold. This has been an indication that the n-HA particles could induce some viscoelastic changes for the PEG hydrogel.

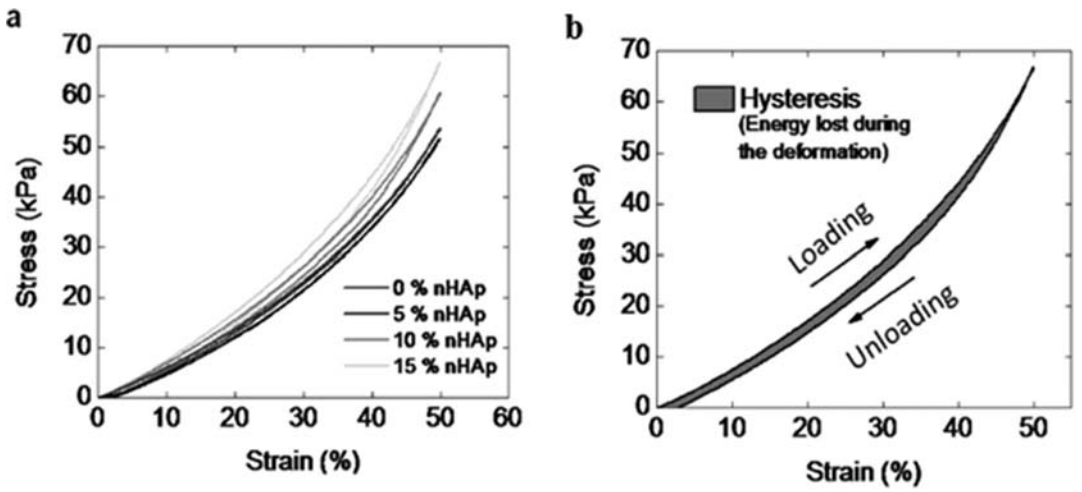

FIGURE 10.24 (A) Compressive properties as a function of n-HA loading (B) typical hysteresis plot of PEG/n-HA systems [Ref. 134].

It has been reported that the PEG is a biocompatible polymer, having a low rate of protein adsorption and cell adhesion.[135] The addition of n-HA particles into PEG matrix would interestingly provide cell adhesion sites that may lead to the attachment of more number of cells on the surface of hydrogel nanocomposites as shown in Fig. 10.25.

Some other studies show that the n-HA can promote adhesion of osteoblasts cells and facilitate differentiation of mesenchymal stem cells into osteoblast cells.[136,137] Song et al. fabricated elastomeric nanocomposites composed of poly (2-hydroxyethyl methacrylate) and high amounts of n-HA.[138] The osteoblastic differentiation of the bone marrow stromal cells on these materials was observed to be significantly influenced by the addition of n-HA.

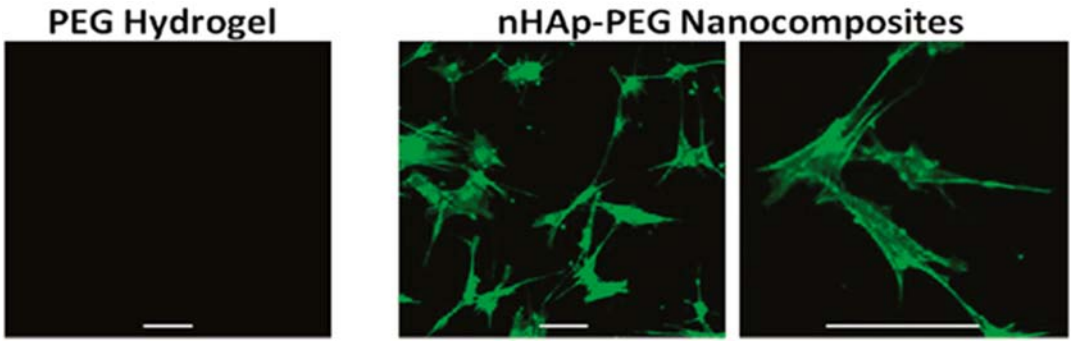

FIGURE 10.25 Cell cultured on PEG and n-HA/PEG nanocomposites [Ref. 134].

7. Conclusions

One of the most charming phenomena in material science is the reinforcement of elastomers by rigid entities such as dispersed particulate fillers. The reinforced elastomeric systems can play a crucial role in the fabrication of many devices for technological applications. Nanosized reinforcements in elastomeric systems allow the modulation of a wide range of materials' properties. It offers a higher degree of interfacial interactions and lower stress concentrations.

There have been many achievements in the field of multifunctional nanocomposites' technology. Great efforts have been undertaken to modify these materials at the nanoscale to optimize their performance. It is believed that the multifunctional polymer nanocomposites would play a key role in our lives in the near future.

References

1. Mark JE. *Applied plastics engineering handbook*. 2011. p. 93–107.
2. Mark JE. Elastomeric networks with bimodal chain-length distribution. *Acc Chem Res* 1994;**27**:271–8.
3. Kluppel M. Evaluation of viscoelastic master curves of filled elastomers and applications to fracture mechanics. *J Phys Condens Matter* 2009;**21**:35104–13.
4. Feldman D. Elastomer nanocomposites. *J Macromol Sci* 2012;**49**:784–93.
5. Munch E, Pelletier JM, Sixou B, Vigier G. Molecular mobility of crosslinked elastomers stretched above T_g. *Polymer* 2006;**47**:3477–85.
6. Dannenberg EM. The effects of surface chemical interactions on the properties of filler-reinforced rubbers. *Rubber Chem Technol* 1975;**48**:410–44.
7. Bhattacharyya S, Sinturel C, Bahloul O, Saboungi ML, Thomas S, Salvetat JP. Improving reinforcement of natural rubber by networking of activated carbon nanotubes. *Carbon* 2008;**46**:1037–45.
8. Bokobza L. Mechanical and electrical properties of elastomer nanocomposites based on different carbon nanomaterials. *Vib Spectrosc* 2009;**51**:52–9.
9. Kickelbick G. Concepts for the incorporation of inorganic building blocks into organic polymers on a nanoscale. *Prog Polym Sci* 2003;**28**:83–114.
10. Bokobza L. Elastomeric composites. I. Silicone composites. *J Appl Polym Sci* 2004;**93**:2095–104.
11. Wang E, Lee SH, Lee SW. Elastin-like polypeptide based hydroxyapatite bio-nanocomposites. *Biomacromolecules* 2011;**12**(3):672–80.
12. Saralegi A, Rueda L, Martin L, Arbelaiz A, Eceiza A, Corcuera MA. From elastomeric to rigid polyurethane/cellulose nanocrystal Bionanocomposites. *Compos Sci Technol* 2013;**88**:39–47.
13. Thakur S, Karak N. A tough, smart elastomeric bio-based hyperbranched polyurethane nanocomposite. *New J Chem* 2015;**39**:2146–54.
14. Gorrasi G, Tortora M, Vittoria V, Polletb E, Lepoittevin B, Alexandre M, Dubois P. Vapor barrier properties of polycaprolactone montmorillonite nanocomposites: effect of clay dispersion. *Polymer* 2003;**44**:2271–9.
15. Won Kim H. Biomedical nanocomposites of hydroxyapatite/polycaprolactone obtained by surfactant mediation. *J Biomed Mater Res* 2007;**83A**:169–77.
16. Tabuani D, Bellucci F, Terenzi A, Camino G. Flame retarded thermoplastic polyurethane (TPU) for cable jacketing application. *Polym Degrad Stabil* 2012;**97**:2594–601.
17. Saha K, Butola BS, Joshi M. Drug-loaded polyurethane/clay nanocomposite nanofibers for topical drug-delivery application. *J Appl Polym Sci* 2014;**131**:40230–8.
18. Ashjari HR, Dorraji MSS, Fakhrzadeh V, Eslami H, Rasoulifard MH, Houjaghan MR, Gholizadeh P, Kafil HS. Starch-based polyurethane/CuO nanocomposite foam: antibacterial effects for infection control. *Int J Biol Macromol* 2018;**111**:1076–82.
19. Silva GRD, Cunha Jr ADS, Vieira LC, Silva LM, Ayres E, Oréfice RL, Fialho SL, Saliba JB, Cohen FB. Montmorillonite clay based polyurethane nanocomposite as substrate for retinal pigment epithelial cell growth. *J Mater Sci Mater Med* 2013;**24**:1309–17.

20. Hung HS, Wu CC, Chien S, Hsu S. The behavior of endothelial cells on polyurethane nanocomposites and the associated signaling pathways. *Biomaterials* 2009;**30**:1502–11.
21. Williams CM, Nash MA, Laura A, Warren P. Electrically conductive polyurethanes for biomedical applications. *Proc SPIE Biomed Appl Micro Nano Eng II* February 2005. https://doi.org/10.1117/12.585321.
22. Song Y, Wennink JWH, Kamphuis MMJ, Sterk LMT, Vermes I, Poot AA, Feijen J, Grijpma DW. Dynamic culturing of smooth muscle cells in tubular poly(trimethylene carbonate) scaffolds for vascular tissue engineering. *Tissue Eng* 2011;**17**:381–7.
23. Bat E, van Kooten TG, Feijen J, Grijpma DW. Resorbable elastomeric networks prepared by photocrosslinking of high-molecular-weight poly(trimethylene carbonate) with photoinitiators and poly(trimethylene carbonate) macromers as crosslinking aids. *Acta Biomater* 2011;**7**:1939–48.
24. Ribeiro R, Ganguly P, Darensbourg D, Usta M, Ucisik AH, Liang H. Biomimetic study of a polymeric composite material for joint repair applications. *J Mater Res* 2007;**22**:1632–9.
25. Qiu H, Yang J, Kodali P, Koh J, Ameer G. A novel citric acid based poly(diol citrate)-composite for orthopaedic implants. *Biomaterials* 2006;**27**:5845–54.
26. Balint R, Cassidy NJ, Cartmell SH. Conductive polymers: towards a smart biomaterial for tissue engineering. *Acta Biomater* 2014;**10**:2341–53.
27. Chen DZ, Tang CY, Chan KC, Tsui CP, Yu PHF, Leung MCP, Uskokovic PS. Dynamic mechanical properties and in vitro bioactivity of PHBHV/HA nanocomposite. *Compos Sci Technol* 2007;**67**:1617–26.
28. Asghar ASS, Qasim M. Synthesis and characterization of nano-hydroxyapatite powder using wet chemical precipitation reaction. *J Mater Sci Technol* 2014;**30**:307–10.
29. Shojai MS, Khorasani MT, Khoshdargi ED, Jamshidi A. Synthesis methods for nanosized hydroxyapatite with diverse structures. *Acta Biomater* 2013;**9**(8):7591–621.
30. Wang Y, Liu L, Guo S. Characterization of biodegradable and cytocompatible nano-hydroxyapatite/polycaprolactone porous scaffolds in degradation invitro. *Polym Degrad Stabil* 2010;**95**:207–13.
31. Dong Z, Li Y, Zou Q. Degradation and biocompatibility of porous nano- hydroxyapatite/polyurethane composite scaffold for bone tissue engineering. *Appl Surf Sci* 2009;**255**:6087–91.
32. Lao L, Wang Y, Zhu Y, Zhang Y, Gao C. Poly(lactide-co-glycolide)/hydroxyapatite nanofibrous scaffolds fabricated by electrospinning for bone tissue engineering. *J Mater Sci Mater Med* 2011;**22**:1873–84.
33. Min Kim H, Himeno T, Kawashita M, Kokubo T, Nakamura T. The mechanism of biomineralization of bone-like apatite on synthetic hydroxyapatite: an in vitro assessment. *J R Soc Interface* 2004;**1**:17–22.
34. Roy P, Sailaja RRN. Chitosan–nanohydroxyapatite composites: mechanical, thermal and bio-compatibility studies. *Int J Biol Macromol* 2015;**73**:170–81.
35. Lehmann G, Cacciotti I, Palmero P, Montanaro L, Bianco A, Campagnolo L, Camaioni A. Differentiation of osteoblast and osteoclast precursors on pure and silicon-substituted synthesized hydroxyapatites. *Biomed Mater* 2012;**7**:1–13.
36. van Blitterswijk CA, Hesseling SC, Grote JJ, Koerten HK, de Groot K. The biocompatibility of hydroxyapatite ceramic: a study of retrieved human middle ear implants. *J Biomed Mater Res* 1990;**24**:433–53.
37. Zhou H, Lee J. Nanoscale hydroxyapatite particles for bone tissue engineering. *Acta Biomater* 2011;**7**:2769–81.
38. Andronescu E, Ficai A, Albu MG, Mitran V, Sonmez M, Ficai D, Ion R, Cimpean A. Collagen-hydroxyapatite/Cisplatin drug delivery systems for locoregional treatment of bone cancer. *Technol Cancer Res Treat* 2013;**12**:275–84.
39. Baker MI, Eberhardt AW, Martin DM, McGwin G, Lemons JE. Bone properties surrounding hydroxyapatite-coated custom osseous integrated dental implants. *J Biomed Mater Res Part B Appl Biomater* 2010;**95B**:218–24.
40. Tahir R, Banert K, Solhy A, Sebti S. Zinc bromide supported on hydroxyapatite as a new and efficient solid catalyst for Michael addition of indoles to electron deficient olefins. *J Mol Catal Chem* 2006;**246**:39–42.
41. Hasna K, Kumar SS, Komath M, Varma MR, Jayaraj MK, Kumar KR. Synthesis of chemically pure, luminescent Eu^{3+} doped HAp nanoparticles: a promising fluorescent probe for in vivo imaging applications. *Phys Chem Chem Phys* 2013;**15**:8106–811.
42. Mene RU, Mahabole MP, Khairnar RS. Surface modified hydroxyapatite thick films for CO_2 gas sensing application: effect of swift heavy ion irradiation. *Radiat Phys Chem* 2011;**80**. 682–682.
43. Yashima M, Kubo N, Omoto K, Fujimori H, Fujii K, Ohoyama K. Diffusion path and conduction mechanism of protons in hydroxyapatite. *J Phys Chem C* 2014;**118**:5180–7.

44. Jana K, Lacher NA, Svec F. Control of selectivity via nanochemistry: monolithic capillary column containing hydroxyapatite nanoparticles for separation of proteins and enrichment of phosphopeptides. *Anal Chem* 2010;**82**:8335–41.
45. Cummings LJ, Snyder MA, Brisack K. Chapter 24, protein chromatography on hydroxyapatite columns. *Methods Enzymol* 2009;**463**:387–404.
46. Li Z, Zhou M, Lin W. The research of nanoparticle and microparticle hydroxyapatite amendment in multiple heavy metals contaminated soil remediation. *J Nanomater* 2014;**2014**:1–8.
47. Müller KH, Motskin M, Philpott AJ, Routh AF, Shanahan CM, Duer MJ, Skepper JN. The effect of particle agglomeration on the formation of a surface-connected compartment induced by hydroxyapatite nanoparticles in human monocyte-derived macrophages. *Biomaterials* 2014;**35**(3):1074–88.
48. Kulanthaivel S, Mishra U, Agarwal T, Giri S, Pal K, Pramanik K, Banerjee I. Improving the osteogenic and angiogenic properties of synthetic hydroxyapatite by dual doping of bivalent cobalt and magnesium ion. *Ceram Int* 2015;**41**:11323–33.
49. Kumar GS, Rajendran S, Karthi S, Govindan R, Girija EK, Karunakaran G, Kuznetsov D. Green synthesis and antibacterial activity of hydroxyapatite nanorods for orthopedic applications. *MRS Commun* 2017;**7**:183–8.
50. Han Y, Wang X, Dai H, Li S. Nanosize and surface charge effects of hydroxyapatite nanoparticles on red blood cell suspensions. *ACS Appl Mater Interfaces* 2012;**4**:4616–22.
51. Dey S, Das M, Balla VK. Effect of hydroxyapatite particle size, morphology and crystallinity on proliferation of colon cancer HCT116 cells. *Mater Sci Eng C* 2014;**39**:336–9.
52. Abdal-hay A, Pant HR, Lim JK. Super-hydrophilic electrospun nylon-6/hydroxyapatite membrane for bone tissue engineering. *Eur Polym J* 2013;**49**:1314–21.
53. Barroug A, Glimcher MJ. Hydroxyapatite crystals as a local delivery system for cisplatin: adsorption and release of cisplatin in vitro. *J Orthop Res* 2002;**20**:274–80.
54. Palazzo B, Iafisco M, Laforgia M, Margiotta N, Natile G, Bianchi CL, Walsh D, Mann S, Roveri N. Biomimetic hydroxyapatite–drug nanocrystals as potential bone substitutes with antitumor drug delivery properties. *Adv Funct Mater* 2007;**17**:2180–8.
55. Goyal AK, Rawat A, Prem SM, Gupta N, Khatri K, Vyas SP. Nanodecoy system: a novel approach to design hepatitis B vaccine for immunopotentiation. *Int J Pharm* 2006;**309**:227–33.
56. Ong H, Loo JSC, Boey FYC, Russell SJ, Ma J, Peng KW. Exploiting the high-affinity phosphonate–hydroxyapatite nanoparticle interaction for delivery of radiation and drugs. *J Nano Res* 2008;**10**:141–50.
57. Clunie G, Liu D, Cullum I, Edwards J. Samarium-153-particulate hydroxyapatite radiation synovectomy: biodistribution data for chronic knee synovitis. *J Nucl Med* 1995;**36**:51–7.
58. Tripathi A, Saravanan S, Pattnaik S, Moorthi A, Partridge NC, Selvamurugan N. Bio-composite scaffolds containing chitosan/nano-hydroxyapatite/nano-copper–zinc for bone tissue engineering. *Int J Biol Macromol* 2012;**50**:294–9.
59. Jayachandran V, Kwon KS. Nano-Hydroxyapatite composite biomaterials for bone tissue engineering-a review. *J Biomed Nanotechnol* 2014;**10**:3124–40.
60. Kumar GS, Thamizhavel A, Yokogawa Y, Narayana Kalkura S, Girija EK. Synthesis, characterization and *in vitro* studies of zinc and carbonate co-substituted nano-hydroxyapatite for biomedical applications. *Mater Chem Phys* 2012;**134**:1127–35.
61. Surmeneva MA, Surmenev RA, Nikonova YA, Selezneva II, Ivanova AA, Putlyaev VI, Prymak O, Epple M. Fabrication, ultra-structure characterization and in vitro studies of RF magnetron sputter deposited nano-hydroxyapatite thin films for biomedical applications. *Appl Surf Sci* 2014;**30**:172–80.
62. Kokkinos PA, Koutsoukos PG, Deligianni DD. Detachment strength of human osteoblasts cultured on hydroxyapatite with various surface roughness, Contribution of integrin subunits. *J Mater Sci Mater Med* 2012;**23**:1489–98.
63. Khalili AA, Ahmad R. A review of cell adhesion studies for biomedical and biological applications. *Int J Mol Sci* 2015;**16**:18149–84.
64. Pramanik S, Agarwal AK, Rai K, Garg A. Development of high strength hydroxyapatite by solid-state-sintering process. *Ceram Int* 2007;**33**:419–26.
65. Zhang HG, Zhu Q. Preparation of fluoride-substituted hydroxyapatite by a molten salt synthesis route. *J Mater Sci Mater Med* 2006;**17**:691–5.

66. Teshima K, Lee SH, Sakurai M, Kameno Y, Yubuta K, Suzuki T. Well-formed one-dimensional hydroxyapatite crystals grown by an environmentally friendly flux method. *Cryst Growth Des* 2009;**9**:2937–40.
67. Kim DW, Cho IS, Kim JY, L Jang H, Han GS, Ryu HS. Simple large-scale synthesis of hydroxyapatite nanoparticles: insitu observation of crystallization process. *Langmuir* 2009;**26**:384–8.
68. Graham S, Brown PW. Reactions of octacalcium phosphate to form hydroxyapatite. *J Cryst Growth* 1996;**165**:106–15.
69. Padmanabhan SK, Balakrishnan A, Chu MC, Lee YJ, Kim TN, Cho SJ. Sol–gel synthesis and characterization of hydroxyapatite nanorods. *Particuology* 2009;**7**:466–70.
70. Zhang G, Chen J, Yang S, Yu Q, Wang Z, Zhang Q. Preparation of amino-acid- regulated hydroxyapatite particles by hydrothermal method. *Mater Lett* 2011;**65**:572–4.
71. Murray M, Wang J, Ponton C, Marquis P. An improvement in processing of hydroxyapatite. *J Mater Sci* 1995;**30**:3061–74.
72. Catros S, Guillemot F, Lebraud E, Chanseau C, Perez S, Bareille R. Physico-chemical and biological properties of a nano-hydroxyapatite powder synthesized at room temperature. *IRBM* 2010;**31**:226–33.
73. Zhang Y, Lu J. A simple method to tailor spherical nanocrystal hydroxyapatite at low temperature. *J Nano Res* 2007;**9**:589–94.
74. Shojai MS, Khorasani MT, Jamshidi A. Hydrothermal processing of hydroxyapatite nanoparticles–a Taguchi experimental design approach. *J Cryst Growth* 2012;**361**:73–84.
75. Cho JS, Kang YC. Nano-sized hydroxyapatite powders prepared by flame spray pyrolysis. *J Alloys Compd* 2008;**464**:282–7.
76. Aizawa M, Hanazawa T, Itatani K, Howell F, Kishioka A. Characterization of hydroxyapatite powders prepared by ultrasonic spray-pyrolysis technique. *J Mater Sci* 1999;**34**:2865–73.
77. Itatani K, Tsugawa T, Umeda T, Musha Y, Davies IJ, Koda S. Preparation of submicrometer-sized porous spherical hydroxyapatite agglomerates by ultrasonic spray pyrolysis technique. *J Ceram Soc Jpn* 2010;**118**:462–6.
78. Zhao H, He W, Wang Y, Zhang X, Li Z, Yan S. Biomineralization of large hydroxyapatite particles using ovalbumin as biosurfactant. *Mater Lett* 2008;**62**:3603–5.
79. Han Y, Li S, Wang X. A novel thermolysis method of colloidal protein precursors to prepare hydroxyapatite nanocrystals. *Cryst Res Technol* 2009;**44**:336–40.
80. Nayar S, Guha A. Waste utilization for the controlled synthesis of nanosized hydroxyapatite. *Mater Sci Eng C* 2009;**29**:1326–9.
81. Nakano T, Kabara K, Tabata Y, Nagata N, Enomoto S, Marukawa E, Umakoshi Y. Unique alignment and texture of biological apatite crystallites in typical calcified tissues analyzed by microbeam x-ray diffractometer system. *Bone* 2002;**31**:479–87.
82. Inoue K, Sassa K, Yokogawa Y, Sakka Y, Okido M, Asai S. Control of crystal orientation of hydroxyapatite by imposition of a high magnetic field. *Mater Trans* 2003;**44**:1133–7.
83. Chow TS. Wetting of rough surfaces. *J Phys Condens Matter* 1998;**10**:445–51.
84. Bindu M, Unnikrishnan G. A gateway to tune the mechanical properties and surface features of silicone rubber. *Polym Compos* 2019. https://doi.org/10.1002/pc.24445.
85. Supova M, Martynkova GS, Barabaszova KC. Effect of nanofillers dispersion in polymer matrices: a review. *Sci Adv Mater* 2010;**3**:1–25.
86. Liu Q, Wijn JR, Blitterswijk CA. Nano-apatite/polymer composites: mechanical and physicochemical characteristics. *Biomaterials* 1997;**18**:1263–70.
87. Lowenstam HA, Weiner S. *On bio-mineralization*. New York: Oxford University Press; 1989.
88. Bhowmik R, Katti KS, Katti D. Influence of mineral on the load deformation behavior of polymer in hydroxyapatite- polyacrylic acid nanocomposite biomaterials: a steered molecular dynamics study. *J Nanosci Nanotechnol* 2008;**8**:2075–84.
89. Bhowmik R, Katti KS, Katti D. Molecular dynamics simulation of hydroxyapatite–polyacrylic acid interfaces. *Polymer* 2007;**48**:664–74.
90. Espigares I, Elvira C, Mano JF, Vazquez B, San Roman J, Reis RL. New partially degradable and bioactive acrylic bone cements based on starch blends and ceramic fillers. *Biomaterials* 2003;**23**:1883–95.
91. Wang M. Developing bioactive composite materials for tissue replacement. *Biomaterials* 2003;**24**:2133–51.
92. Supova M. Problem of hydroxyapatite dispersion in polymer matrices: a review. *J Mater Sci Mater Med* 2009;**20**:1201–13.

93. Tanaka H, Watanabe T, Chikazawa M, Kandori K, Ishikawa T. TPD, FTIR, and molecular adsorption studies of calcium hydroxyapatite surface modified with hexanoic and decanoic acids. *J Colloid Interface Sci* 1999;**214**:31–7.
94. Li Y, Weng W. Surface modification of hydroxyapatite by stearic acid: characterization and in vitro behaviors. *J Mater Sci Mater Med* 2008;**19**:19–25.
95. Shimabayashi S, Uno T, Nakagaki M. Formation of a surface complex between polymer and surfactant and its effect on the dispersion of solid particles. *Colloids Surf A Physicochem Eng Asp* 1997;**123**:283–95.
96. Nicholas LB, Wilson Jr OC. Surface modification of hydroxyapatite. Part I. Dodecyl alcohol. *Biomaterials* 2003;**24**:3671–9.
97. Tanaka H, Futaoka M, Hino R. Surface modification of calcium hydroxyapatite with pyrophosphoric acid. *J Colloid Interface Sci* 2004;**269**:358–63.
98. Zhao JL, Fu T, Han Y, Xu KW. Reinforcing hydroxyapatite/thermosetting epoxy composite with 3-D carbon fiber fabric through RTM processing. *Mater Lett* 2004;**58**:163–8.
99. Dupraz AMP, Vandenmeer SAT, Dewijn JR, Goedemoed JH. Biocompatibility screening of silane-treated hydroxyapatite powders, for use as filler in resorbable composites. *J Mater Sci Mater Med* 1996;**7**:731–8.
100. Santos C, Clarke RL, Braden M, Guitian F, Davy KWM. Water absorption characteristics of dental composites incorporating hydroxyapatite filler. *Biomaterials* 2002;**23**:1897–904.
101. Borum L, Wilson Jr OC. Surface modification of hydroxyapatite. Part II. Silica. *Biomaterials* 2003;**24**:3681–8.
102. Hench LL, Paschall HA. Direct chemical bond of bioactive glass-ceramic materials to bone and muscle. *J Biomed Mater Res* 1973;**7**:25–42.
103. Tanaka H, Watanabe T, Chikazawa M, Kandori K, Ishikawa T. Surface structure and properties of calcium hydroxyapatite modified by hexamethyldisilazane. *J Colloid Interface Sci* 1998;**206**:205–11.
104. Wen J, Li Y, Zuo Y, Zhou G, Li J, Jiang L, Xu W. Preparation and characterization of nano-hydroxyapatite/silicone rubber composite. *Mater Lett* 2008;**62**:3307–9.
105. Furuzono T, Wang PL, Korematsu A, Miyazaki K, Oido-Mori M, Kowashi Y, Obuta K, Tanaka J, Kishida A. Physical and biological evaluations of sintered hydroxyapatite/silicone composite with covalent bonding for a percutaneous implant material. *J Biomed Mater Res* 2003;**65B**:217–26.
106. Deb S, Aiyathurai L, Roether JA, Luklinska ZB. Development of high-viscosity, two-paste bioactive bone cements. *Biomaterials* 2005;**26**:3713–8.
107. Wang M, Bonfield W. Chemically coupled hydroxyapatite–polyethylene composites: structure and properties. *Biomaterials* 2001;**22**:1311–20.
108. Liu Q, De Wijn JR, Blitterswijk CA. A study on the grafting reaction of isocyanates with hydroxyapatite particles. *J Biomed Mater Res* 1998;**40**:358–64.
109. Lee SC, Choi HW, Lee HJ, Kim KJ, Chany JH, Kim SY, Choi J, Oh KS, Neony YK. In-situ synthesis of reactive hydroxyapatite nano-crystals for a novel approach of surface grafting polymerization. *J Mater Chem* 2007;**17**:174–80.
110. Liu H, Zhang L, Li J, Zou Q, Zuo Y, Tian W, Li Y. Physicochemical and biological properties of nano-hydroxyapatite-reinforced aliphatic polyurethanes membranes. *J Biomater Sci* 2010;**21**:1619–36.
111. Bružauskaitė I, Bironaitė D, Bagdonas E, Bernotienė E. Scaffolds and cells for tissue regeneration: different scaffold pore sizes-different cell effects. *Cytotechnology* 2016;**68**:355–69.
112. Pineda LM, Busing M, Meinig RP, Gogolewski S. Bone regeneration with resorbable polymeric membranes. III. Effect of poly (L-lactide) membrane pore size on the bone healing process in large defects. *J Biomed Mater Res* 1996;**31**:385–94.
113. Katritzky AR, Sakhuja R, Huang L, Gyanda R, Wang L, Carnaby Jackson D, Ciaramitaro DA, Bedford CD, Duran RS. Effect of filler loading on the mechanical properties of crosslinked 1,2,3-triazole polymers. *J Appl Polym Sci* 2010;**118**:121–7.
114. Azizah AB, Rozman HD, Azniwati AA, Tay GS. The effect of filler loading and silane treatment on kenaf core reinforced polyurethane composites: mechanical and thermal properties. *J Polym Environ* 2020;**28**:517–31.
115. Zhou1 YX, Wu PX, Cheng ZY, Ingram J, Jeelani S. Improvement in electrical, thermal and mechanical properties of epoxy by filling carbon nanotubes. *EXPRESS Polym. Lett* 2008;**2**:40–8.
116. Benli S, Yilmazer Ü, Pekel F, Özkar S. Effect of fillers on thermal and mechanical properties of polyurethane elastomer. *J Appl Polym Sci* 1998;**68**:1057–65.

117. Kim JM, Son JS, Kang SS, Kim G, Choi SH. Bone regeneration of hydroxyapatite/alumina bilayered scaffold with 3 mm passage-like medullary canal in canine tibia model. *BioMed Res Int* 2015:1–6. https://doi.org/10.1155/2015/235108.
118. Kattimani VS, Kondaka S, Lingamaneni KP. Hydroxyapatite-past, present, and future in bone regeneration. *Bone Tissue Regen Insights* 2016;**7**:9–19.
119. Panday V, Upadhyaya V, Berwal V. Comparative evalution of G bone (hydroxyapatite) and G-graft (hydroxyapatite with collagen) as bone graft material in mandibular III molar extraction socket. *J Clin Diagn Res* 2015;**9**:ZC48–52.
120. Bos M, Dam GWV, Jongsma T, Bruin P, Pennings AJ. The effect of filler surface modification on the mechanical properties of hydroxyapatite-reinforced polyurethane composites. *Compos Interfac* 1995;**3**:169–76.
121. Tetteh G, Khan AS, Smith RMD, Reilly GC, Rehman IU. Electrospun polyurethane/hydroxyapatite bioactive Scaffolds for bone tissue engineering: the role of solvent and hydroxyapatite particles. *J Mech Behav Biomed* 2014;**39**:95–110.
122. Amini AR, Laurencin CT, Nukavarapu SP. Bone tissue engineering: recent advances and challenges. *Crit Rev Biomed Eng* 2012;**40**:363–408.
123. Wang K, Zhou C, Hong Y, Zhang X. A review of protein adsorption on bioceramics. *Interface Focus* 2012;**2**:259–77.
124. Bindu M, Unnikrishnan G. Modulation of dielectric and viscoelastic features of silicone rubber (SR) by nano-hydroxylapatite (n-HA) embedding. *New J Chem* 2018;**42**:6441–8.
125. Hongbo L. *Dielectric under electric field. Electric field*. 2018. https://doi.org/10.5772/intechopen.72231.
126. Lago ED, Cagnin E, Boaretti C, Roso M, Lorenzetti A, Modesti M. Influence of different carbon-based fillers on electrical and mechanical properties of a PC/ABS blend. *Polymers* 2020;**12**:29–44.
127. Roy N, Bhowmick AK. Tailor-made fibrous nanohydroxyapatite/polydimethylsiloxane composites: excavating the role of nanofiller aspect ratio, amorphicity, and noncovalent surface interaction. *J Phys Chem C* 2012;**116**:8763–72.
128. Peng F, Shaw MT, Olson JR, Wei M. Hydroxyapatite needle shaped particles/poly (L-lactic acid) electrospun scaffolds with perfect particle-along nanofiber orientation and enhanced mechanical properties. *J Phys Chem C* 2011;**115**:15743–51.
129. Pang YX, Bao XJ. Influence of temperature, ripening time and calcination on the morphology and crystallinity of hydroxyapatite nanoparticles. *Eur Ceram Soc* 2003;**23**:1697–704.
130. Ramanathan T, Abdala AA, Stankovich S, Dikin DA, Alonso MH, Piner RD, Adamson DH, Schniepp HC, Chen X, Ruoff RS, Nguyen ST, Aksay IA, Prud'homme R, Brinson LCN. Functionalized graphene sheets for polymer nanocomposites. *Nanotechnology* 2008;**3**:327–31.
131. Lei L, Li L, Zhang L, Chen D, Tian W. Structure and performance of nano-hydroxyapatite filled biodegradable poly((1,2-propanediol-sebacate)-citrate) elastomers. *Polym Degrad Stabil* 2009;**94**:1494–502.
132. Tonpheng B, Yu J, Andersson O. Effects of cross-links, pressure and temperature on the thermal properties and glass transition behaviour of polybutadiene. *Phys Chem Chem Phys* 2011;**3**:15047–54.
133. Ni J, Wang M. In vitro evaluation of hydroxyapatite reinforced polyhydroxybutyrate composite. *Mater Sci Eng C* 2002;**20**:101–9.
134. Gaharwar AK, Dammu SA, Canter JM, Wu CJ, Schmidt G. Highly extensible, tough, and elastomeric nanocomposite hydrogels from poly(ethylene glycol) and hydroxyapatite nanoparticles. *Biomacromolecules* 2011;**12**:1641–50.
135. Ratner BD. *Biomaterials science: an introduction to materials in medicine*. New York: Academic Press; 1996.
136. Anselme K. Osteoblast adhesion on biomaterials. *Biomaterials* 2000;**21**:667–81.
137. Hu Q, Tan Z, Liu Y, Tao J, Cai Y, Zhang M, Pan H, Xu X, Tang RJ. Effect of crystallinity of calcium phosphate nanoparticles on adhesion, proliferation, and differentiation of bone marrow mesenchymal stem cells. *Mater Chem* 2007;**17**:4690–8.
138. Song J, Xu J, Filion T, Saiz E, Tomsia AP, Lian JB, Stein GS, Ayers DC, Bertozzi CR. Elastomeric high-mineral content hydrogel-hydroxyapatite composites for orthopedic applications. *J Biomed Mater Res Part A* 2009;**89A**:1098–107.

This page intentionally left blank

CHAPTER

11

Emerging applications of nanofluids

Alagappan Subramaniyan

Department of Physics, Thiagarajar College of Engineering, Madurai, Tamil Nadu, India

1. Introduction to nanofluids

Nanofluids are colloidal engineered suspensions of nanoparticle in a suitable base fluid. The tailoring of nanoparticle size, shape, chemical composition, volume fraction of the nanoparticle can affect the properties of nanofluid. Nanofluid are nanoparticles suspended in a liquid medium which enhance the properties of the base medium. When nanoparticles are dispersed in a liquid medium, they can also create an interfacial layer between the particle and liquid medium

Fig. 11.1 depicts the constituents of nanofluid. We could just consider a combination of nanoparticle, interfacial layer, and base fluid to constitute a nanofluid

$$\text{Nanofluid} = \text{Base fluid} + \text{Nanoparticle} + \text{Interfacial layer surrounding nanoparticle.}$$

The first indication of nanofluid was given by S.U.S Choi in 1995 at Argonne National Laboratory, the USA.[1] Nanofluids are attributed as accidental discovery when Choi was not able

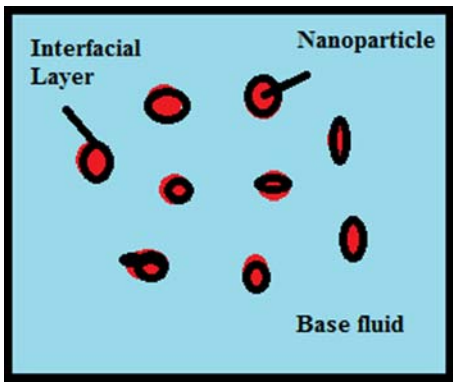

FIGURE 11.1 The constituents of nanofluid.

Applications of Multifunctional Nanomaterials
https://doi.org/10.1016/B978-0-12-820557-0.00032-1

to separate the copper nanoparticles synthesized by Chemical Vapor Deposition. Due to recent advancements in manufacturing process of nanoparticles and commercial availability of nanoparticles, nanofluid preparation has become extremely easy. Nanofluids can be prepared by two major methods. The one step method and two step method.

In one-step process, the nanoparticle is prepared in the liquid medium to get a nanofluid. In two-step process, the nanoparticles are first synthesized by any of the top-down or bottom-up manufacturing process. This is followed by dispersing nanoparticles in select liquid medium of desired volume fraction.

Due to wide synthesis methods available over a range of composition for nanoparticles, a variety of nanofluids can be prepared. Nanofluids can be metallic, ceramic, or carbon based. In recent years, polymeric nanofluids have also been synthesized. Some of the typical nanofluids which have attracted attention of researchers are ZnO nanofluid (ZnO nanoparticles dispersed in water), TiO_2 nanofluids, Ag nanofluid, copper oxide nanofluids, Al_2O_3 nanofluids, etc. The efficient applications of nanofluid lie in their stability[2]. The nanoparticles need to be dispersed in the liquid medium. Optimizing the nanoparticle volume fraction, volume of base liquid, shape and size along with inclusion of surfactants are recommended techniques. The characterization of nanofluid is done through the Zeta potential measurements using the dynamic light scattering procedures. The potential is measured across the interfacial layer, and a potential value of 30−60 mV can indicate a stable nanofluid. A stable nanofluid can be put to engineering, medical, and agricultural applications.

2. Tuning the application of nanofluids

It is a well proved fact that the size of nanoparticle of a particular shape and composition can affect the number of surface atoms and change the properties of nanoparticle. For example, decreasing size can introduce more number of surface atoms and alter the melting point of nanomaterials. Thus the size of the nanoparticle can tune any desired property and affect the extent of applications. The tuning of the color of gold by changing its nanosize is a remarkable example in the history of nanotechnology. Since nanoparticles are a major constituent of nanofluids, there is a possibility to tune the properties of nanofluid and explore their exciting applications. Figs. 11.2 and 11.3 show the tenability of nanoparticle and nanofluid application.

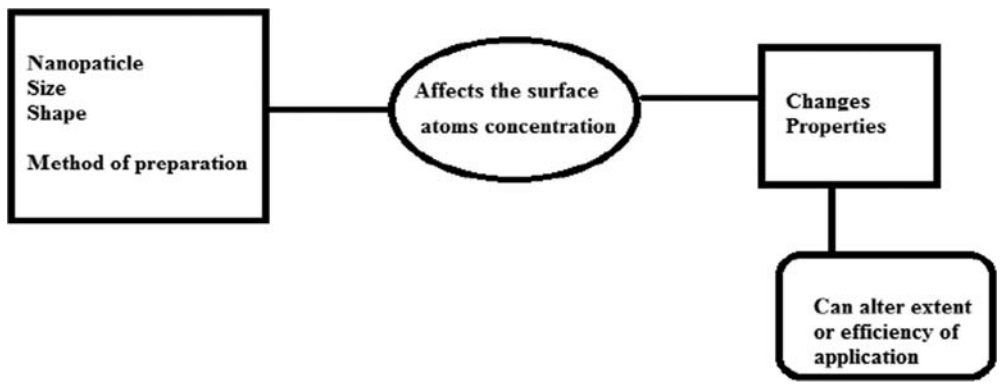

FIGURE 11.2 Tuning the application of nanoparticle.

3. Application of nanofluid

When nanofluids were first discovered, they were identified as a heat transfer medium which could accelerate cooling process. Adding small volume fraction of nanoparticles in a liquid can change the thermal conductivity by enormous amounts. Thus there is efficient heat transfer from the device to the surroundings due to the presence of nanofluid. For example, during cutting steel enormous volume of water is used to prevent the distortion of steel due to high temperature. If small amount of nanoparticles are added in water, the thermal conductivity of water increases and lesser amount of water is required. With the extensive research in nanofluid synthesis, properties, stability investigations their applications also extended over a wide range from engineering to medicine and agriculture. The objective of this chapter is to introduce the readers to emerging and evolving applications of nanofluid which can save energy, natural resources, and even reduce the high-risk cancer treatments. A brief list of new and emerging applications of nanofluid includes the following:

1. Industrial cooling
2. Oil recovery.
3. Machining process.
4. Improving natural gas storage
5. Solar energy harvesting applications
6. Carbon dioxide capture
7. Safe surgery and sensor fabrication

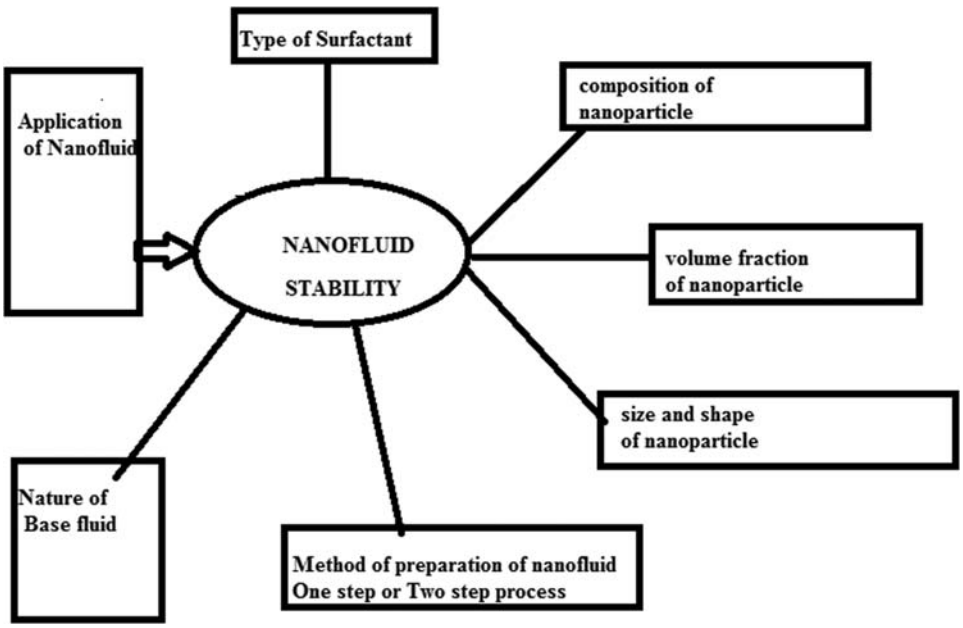

FIGURE 11.3 Tuning the application of nanofluids.

3.1 Nanofluids for industrial cooling

Many electronic and electrical devices produce heat when the usage time is high. Proper cooling is required for smooth running of machine and avoids overheating. PC desktop, laptop, and smart phone of the current generation are cooled by air itself. A fan is necessary to remove the heat, thus maintaining the temperature of the CPU. It increase their lives and also reduces the risk of damage. A CPU cooling fan works on principle of convection. Modern CPU also consists of sensors which can alter the speed of fan to achieve the desired cooling rate. Exponentially increasing heat generation has been cited as a problem with industrial electronics.[3]

Several industrial applications like boiler power plant, laser, nuclear power plants, and machining process require cooling mechanisms. Here cooling is the process of transfer of heat energy for source to sink or device to surroundings to avoid overheating, The most abundant used cooling medium is water, because of its high boiling point and high specific heat in addition to low cost and easy availability. Industrial cooling can be done through open or closed circulating systems. Water can be used to cool nuclear power plants, automobile internal combustion engine, hydro electric generators, and laser systems. The principle behind water cooling is convective heat transfer mechanisms. Large volumes of water are required for cooling high temperature devices or for cooling large volume of heat sources. Water cooling can also reduce the operating temperature of the PV cell, thereby improving efficiency of PV panel.

Adding small volume of nanoparticles to water (nanofluid with water as base fluid) can improve the thermal conductivity of water by large amounts thus providing an efficient cooling system. Nanofluids can potentially enhance the efficiency of heat exchangers used in the industrial sectors, Thus nanofluids are necessary for efficient heat transfer and can also aid the reduction in the size of heat transfer device. Prior to nanofluids, microfluids (micron size particles dispersed with fluids) were used. The idea of microfluid suspension was proposed almost in 1831 by Maxwell.[3] Nanofluids eliminated the problems associated with microfluids like sedimentation, abrasion of pipe walls, and low thermal conductivity.[4,5] Eastman investigated the properties of copper nanofluids (nanoparticles of copper with ethylene glycol) and reported approximately 40% increase in thermal conductivity of ethylene glycol, for a very small volume fraction of 0.3vol% of copper nanoparticles.[6] Thus small volume fractions of nanoparticle produced a big impact in cooling technologies by increasing the thermal conductivity of existing fluid. A review on heat transfer characteristics of nanofluid and their theoretical models, preparation of nanofluid, types of nanofluid, methods of measurement of thermal conductivity is given by Xiang-Qi-Wang and Arun S Mujumdar.[7]

In automobile cooling, nanofluids can be used as engine coolant, fuel additive, shock absorber, and as lubricant. The details of nanofluids application in automobile till the year 2010 are discussed by S. SenthilRaja.[8] The major conclusions of the review indicate an increase in efficiency in IC combustion engine within a range of 5%−10% along with an increase in combustion of the fuel. Efficient cooling system in automobiles can lower the weight of automobile and increase its efficiency. Ethylene glycol and ethylene glycol/water in ratio 1:1 are used as automobile coolants. But adding nanoparticles to the existing coolant, we can raise the boiling point of the working coolant there by transferring more heat to the surroundings.

A critical review on electronic cooling is reported by Mehdi Bahiraei.[9] With the failure of conventional cooling methods for high heat flux electronic devices, nanofluids have gained importance. The review reports the use of carbon base nanofluids, alumina nanofluids, zinc oxide, silica nanofluids, copper oxide nanofluids, diamond nanofluids, and hybrid nanofluids. A comparison between heat transfer enhancement of various nano-particles in cooling of electronic devices is reported by Khaleduzzaman.[10] Three different water base nanofluids containing SiC, CuO, and alumina nanoparticles were investigated. The CuO and alumina nanofluids showed highest enhancement values of approximately 11.5% and 12%, respectively. A 10% increase in heat transfer can minimize the size of equipment and also indicate a longer life span of the electronic device. Nanofluids are a sure solution to the rising heat current density associated with a single chip. The single chip heat current density is reported to increase from 320 W/cm^2 to 530 W/cm^2 during a period of 2007–2011 by Lee J.H.[11] For a 4-year period, the heat current density is increased almost by 50%, which forces the engineers to try alternatives like nanofluid. Moore's law predicts that the number of transistors doubles in almost 18 months. Thus the heat flux will also increase with the number of transistors. The use of nanofluids not only increases the thermal conductivity of the liquid but also the heat capacity of the liquid for a given volume. Minimal clogging, better stability, and reduced pumping power are other added advantages of nanofluid technology for electronic cooling. The nano particle size and shape dependence which could enhance the electronic cooling capacity is yet to be explored to its fullest potential. Many anomalies in results exist for the same shape, size, and volume fraction due to method of preparation and impurities.

3.2 Nanofluids for oil recovery

Oil recovery is the process of cleaning and recovery of oil after an oil spill. Oil recovery can be classifies as primary, secondary, tertiary, and quaternary. They also include thermal method, chemical methods, and electromagnetic methods, etc. The worldwide oil recovery is approximately at an average of 30%. The petroleum industry is also focusing on potential use of nanofluids for enhanced oil recovery.[12] An experimental study of nanofluids intended for enhanced oil recovery was conducted by B.A Suleimanov[13] and coworkers. The nanofluid was made by an aqueous solution of anionic surface-active agents with addition of light nonferrous metal nanoparticles. It was proved that the use of the nanofluid permitted a 70%–90% reduction in surface tension on an oil boundary in comparison with surface-active agent aqueous solution. They also reported a considerable increase in enhanced oil recovery. Alomair[14] and coworkers investigated the nanofluids for heavy oil recovery. Their primary focus was to investigate the effect of nanofluid for heavy crude oil recovery in comparison to water flooding. They used silicon oxide, aluminum oxide, nickel oxide, and titanium oxide nanoparticles at different concentrations with saline water as base fluid. They also investigated the effects of nanofluids on the interfacial tension and emulsion viscosity. Their experimental results proved that the aluminum oxide nanofluid at a concentration of 0.05 wt.% reduced the emulsion viscosity by 25%. The mixed nanofluid of silicon and aluminum oxide at 0.05 wt.% showed the highest incremental oil recovery among the fluids they investigated.

Oil recovery can also be done by using electromagnetic waves by M. Kashif and coworkers.[15] They used electromagnetic transmitter with three magnetic feeders for oil recovery. It was observed that with three magnetic feeders, the magnetic field increases to a mximum of two times. The principle of using electromagnetic waves involves absorbption of electromagnetic waves by the core rock samples. The absorption increases the heat in core samples which further reduce the viscosity of the oil. M.kashif[15] and coworkers reported oil recovery of 40%−60% of the samples they investigated. Hassan Ali[16] and co workers have done a review on enhanced oil recovery by using electromagnetic-assisted nanofluids. The effect of dielectric and magnetic nanoparticle for enhanced oil recovery is discussed. Viscosity effects of nanofluids which influence enhance oil recovery process are reported. The interaction of electromagnetic waves with nanoparticle is also explained.

Sayed Ameenuddin Irfann[17] and coworkers have given a review on enhanced oil recovery by using nanofluids based on mathematical modeling and simulations. Their aim was to understand the flow characteristics of nanoparticles in porous media and the behavior of nanoparticles under high temperatures, pressures, and salinity levels due to external electric and magnetic fields. The reported that the experimental approaches for nanofluid enhanced oil recovery are not only time-consuming, but also complicated and expensive. Hence mathematical models are required for understanding the transport and interaction of nanofluids in a reservoir. Further simulations offer an advantage of optimization to get maximum oil recovery with less cost. Their manuscript critically analyzes the latest developments in mathematical modeling and simulation techniques that have been reported for nanofluid-assisted enhanced oil recovery. They have also discussed the challenges ahead in nanofluid oil recovery. The injection of nanofluids into oil reservoirs is now considered as a frontier chemical technique for oil recovery. It has the potential to produce to produce more than 50%, which is currently not possible by traditional primary and secondary recovery techniques. The role of nanofluid in oil recovery process is to improve injectivity and aid the displacement of oil, altering interfacial tension and viscosity as discussed in a review by Baoliang Peng and coworkers.[18] The technique of using nanofluids for oil recovery is also called as nanoflooding. The effect of different dimensions of nanomaterials (0,1,2,3 D) and the nanostructure morphology, intrinsic material properties, temperature, and pH are discussed in the same review. They also concluded the mechanism of nanoflooding as wettability alteration, reducing interfacial tension, controllable viscosity, disjoint pressure for oil displacement, and a stable foam and emulsion.[18] According to Baoliang Peng and coworkers,[18] the most successful applications of nanomaterials in oil field use are encapsulated breakers and tracers. Successful nanofloodings are reported in laboratories scale.

3.3 Nanofluids for machining process

Machining is a manufacturing process in which materials are removed using cutting tools from some workpiece. The final objective of a machining process is to converting raw material into a desired shape. Machining process include drilling, turning, milling, grinding, facing, boring, and knurling. Machining is also done on forged cast or rolled components and is referred to as a secondary machining process or metal cutting process. Each machining process has its own advantages and disadvantages, but they all have a drawback of large time

consumption. Nanofluids play the role as cutting fluids for machining process there by reducing the time of operation. A review on the various machining process, factors affecting machining process, and the impact of various nanofluids for machining process in reducing time of operation, energy, and material consumption is discussed by Y. Shokoohi.[19] The lubrication and cooling features of nanofluid play important role when they are used for machining process. Application of nanofluid in machining process can also increase the quality of surface finish of the material. The quality is better than dry condition or when base fluids like water alone are used for cooling The reason is attributed to more efficient lubricating, decrease in machining forces, depletion in friction, and higher heat transfer coefficient.[20] The composition of nanoparticle, shape, size, volume fraction of nanoparticle in base fluid, the combination of nanoparticle, and base fluid will affect the lubricating and cooling characteristics of nanofluid. Considerable variation of machining forces is reported with the nanosize and volume fraction of aluminum oxide-water base nanofluid.[20] It is also cited that nanofluids have higher thermal conductivity and convection heat transfer factors along with less environmental hazards.[21] The high cost of nanoparticles clustering and sedimentation are negative aspects of nanofluids for machining process.[19] Since nanoparticles have high surface area, their chemical activity increases and formation of microparticles is favored which is responsible for sedimentation. Nanofluids can be described as heat controlling agents in machining process and maintaining the temperature of work piece and tool piece along with reducing friction.[22] Nanofluids of titanium dioxide nanoparticles[23] have been used to reduce the surface roughness by approximately 30%. Multiwalled carbon nanotubes[24] with deionized water as base fluid can also provide the same reduction in roughness to titanium dioxide with vegetable oil. N.S.M Sahid has reported on the experimental investigation on the performance of the TiO_2 and ZnO hybrid nanocoolant in ethylene glycol mixture toward AA6061-T6 machining.[25] The effect of the base fluid water and ethylene glycol mixture to a prepared hybrid nanocoolant was investigated in their experiment. The hybrid nanocoolant consisted of 80:20 of volume concentration up to 0.1%. The particle size of TiO_2 was close to 20 nm and heterogeneous ZnO with a range of 10−30 nm was used for machining process. Their research finding suggests that a hybrid nanocoolant using a minimum quantity lubrication is a suitable alternative for an economically and environmentally compatible production. They also concluded that the cutting parameters and the hybrid nanocoolant play a crucial role in determining surface roughness, material removal rate, and tool wear. The nanoparticle application in some of the green technologies such as MQL (Minimum Quantity Lubricant) and MQCL(Minimum Quantity cooling lubricant) using vegetable oils proves superior cooling and lubricating properties and also minimizes the use of cutting fluids. It has also been reported to create new solutions for machining, especially for difficult-to-cut materials.[26] There different nanoparticles, such as Al_2O_3, MoS_2, SiO_2, ZrO_2, CuO, TiO_2, and CNT, are shown to improve the tribological property, thermal conductivity, and viscosity.[27] Lee Gong[28] and coworkers have performed turning machining operations on nickel alloys using graphene nanofluids. They have stressed the difficulty in machining operations with a nickel alloy Inconel 18. Nickel-alloys are classified as difficult to machine metals due to their low thermal conductivity and strength even at high temperatures. The surface complexity and intricate shapes is crucial for these alloys since they are used in aerospace and petroleum industries. Nanofluids serve the purpose of cutting fluids for obtaining intricate shape and maintaining dimensional tolerance to a minimum. In this context, Lee Gong group[28]

evaluates the feasibility of sustainable turning of the Inconel 718 alloy using the MQL strategy with graphene nanofluids. Nanofluids were prepared with vegetable oil as base fluid and graphene plates of 5 and 10 μm range. Their results showed that the nanofluid with the lowest size of graphene nanoplatelets promoted the best surface quality Their findings indicate that the nanoparticles inclusion and efficiency as additives in a machining operation depends on their size, which can influence their thermo-physical characteristics.

3.4 Nanofluids for improving natural gas storage

Natural gas is a fuel source consisting primarily of methane. It is a mixture of gasses rich in hydrocarbons. It is often found associated with other fossil fuels in coal beds. It can also be naturally created in a biological process. The risk of natural gas is it is highly combustible, but offers the advantage that when effectively burned, gives a tremendous amount of energy. In comparison with other fossil fuels, it burns cleanly and emits low levels of potentially harmful waste and by-products into the air. Natural gas exists in reservoirs beneath the earth's surface. It usually exists in large volumes in the vicinity of oil deposits. Natural gas can be stored for an indefinite period of time. The purpose of storing natural gas is twofold. One is meeting base load requirements (seasonal requirements), and other is meeting peak load requirements (unexpected requirements). There are three main types of underground natural gas storage facilities, that is, depleted reservoirs, aquifers, and salt caverns. As a basic principle, any underground storage facility is altered before injection, to create a type of storage vessel underground. Natural gas is injected into the formation which builds up pressure. The pressure increases with addition of natural gas. With increasing pressure, the gas may be easily extracted when required. If the built in pressure drops to below a critical level, there is no pressure difference because of which gas cannot be pushed out. Thus in any underground storage facility, there is a certain amount of gas that may never be extracted which is called as physically unrecoverable gas. Burning natural gas can release an appreciable amount of carbon dioxide which can lead to air and water pollution. Natural gas can be stored and transmitted as compressed natural gas (CNG), liquefied natural gas, and solidified natural gas (SNG). Storing and transporting natural gas as clathrate hydrates is referred as SNG. It is going to be a promising alternative due to several advantages that are given below as elaborated by H.P. Velusamy in the first review in SNG storage.[29] Since SNG is based on Clathrate hydrate formation process, it is environmentally friendly and nontoxic because it uses water. The methane is stored in its respective molecular form which gives complete recovery or utilization. The major advantage being that it requires moderate temperature and pressure conditions during formation and storage. It is also highly compact mode of storage with relatively high energy density, and it is also an extremely safe mode of storage due to its nonexplosive nature. H.P Velusamy[29] and coworkers also suggest in their review that SNG technology is well suited for stationary applications handling lower volumes of methane (natural gas). A promising option will be to employ the SNG technology for storing and transporting methane produced from biomass gasification plant. Improvement in the kinetics of gas hydrate formation is essential for the further development of this novel technology as suggested by Yi Yu Lu[30] and coworkers. Graphite nanofluids were used for enhancing the methane hydrate formation. Their experiments were conducted in a stirred tank reactor at

277 K and 6.0 MPa. They studied the methane hydrate nucleation and growth in graphite nanofluids using microscopy techniques. Their results indicate that the gas storage capacity obtained in graphite nanofluids increased by 3% in comparison to base fluid water. They also observed reduction in induction time close to 90% and the total time for hydrate formation was decreased two-thirds. They probed the effect of graphite nanoparticles concentrations such as 0.2, 0.5, and 1.0 wt% and found that the concentration of 0.5 wt% is optimal for the enhancement of methane hydrate formation. They also reported that gas storage capacity obtained for the 0.5 wt% graphite nanofluids was higher than that obtained in other nanofluids such as the iron oxide and zinc oxide nanofluids. Hence, graphite nanofluids have proven an effective approach to enhance hydrate formation for SNG storage by Yi Yu Lu and coworkers.[30]

3.5 Nanofluid for solar energy harvesting applications

It is well known fact that sun in an unlimited renewable energy that can support mankind and is the best alternative source to fossil fuel. Only 50% of the suns energy reach the earth and effective collection, storage, and utilization of the energy could solve all the human demands. The biggest advantage of solar energy is its renewable nature and green energy. However it suffers from the drawback of collecting adequate energy during seasonal changes. In this aspect, the storage of solar energy may play a crucial role. Solar energy technologies have been classified as photovoltaic technology and solar thermal technology. In photovoltaic technology, the sun light falling on panel generates electricity. The photons from solar radiation strike the semiconductor panel to generate electrons and give electricity. This is usually observed on roof tops but can be installed on open area grounds or walls. The extent of panel and the orientation of panel type of panel(static or dynamic) can have effect on the electricity generated. Photovoltaic technology can be considered as a great success in residential domains across the globe. Solar thermal technology deals with collection of solar energy through reflectors and focuses the collected sunlight on the receivers, where sun light is converted to heat. The heat is used to drive an engine or perform specific task. Solar energy is used for solar cookers, solar lightning systems, solar energy-based vehicles, etc. The importance of solar energy technologies for development of rural areas in India is reported by A. Renuka Prasad and coworkers.[31] In rural areas, solar energy can be used for water heating, solar distillation, solar lightning, solar drying, solar cooking, and in design of energy efficient buildings, and solar photovoltaics-based pump sets for irrigation. Solar energy can also be used for constructing solar ponds which can aid the salt production, water desalination and aqua culture. Solar energy has also aided the educational domain through the use of solar calculators since 1970s.

The solar collector plays a crucial role in collecting solar energy. Solar collector is any material which collects energy from sun and further focuses it to for water heating. The use of solar collectors provides an alternative for domestic water heating with a water heater. The advantage is it reduces energy costs over time. Also in a residential settings, many collectors can be combined in an array, which is to generate electricity in solar thermal power plants. Solar collectors are classified as low, medium, or high-temperature heat energy exchangers. There are broadly two types of thermal solar collectors: concentrating and nonconcentrating.

The exit in different geometries as Flat plate solar collectors, parabolic solar collectors, evacuated tube solar collectors, and direct absorption solar collectors (DASC). An in-depth review of various solar collectors and their application is discussed by Younnes menni and coworkers.[32] J. Fan and coworkers[33] discussed the efficiency and life time of solar collectors. They reported that within a period of 5 years, from 2002 to 2007, the performance of solar collector has been increased by 30%–80% for a mean solar collector fluid temperature of 40 to 100°C, respectively. The success was attributed due to improvement of the collector design. Patric E Phelan and coworkers[34] emphasized on direct absorption solar collectors, in which incident sunlight is absorbed directly by a working fluid. In conventional solar thermal collectors, the sunlight is absorbed by a receiver, which then transfers heat to the working fluid. Patric E Phelan and coworkers[34] proposed that DASC could be developed further, it can expand the emerging opportunities including refrigeration. In DASC, nanofluids have been proposed as working fluid due to their high thermal conductivity and minimization of radiation losses. It is interesting to note that nanofluids are used in both the solar technologies-Photovoltaics (PV) and solar thermal. In solar thermal, they are used a working fluid for DASC and in solar PV they are used as a cooling medium.

Metal oxide–water base nanofluids are mainly used for PV cooling technologies because of low cost and nontoxicity. The main advantage of nanofluid for these cooling technologies involves high thermal conductivity and increased specific heat capacity. Karami and Rahimi[35] used Boehmite nanofluid for cooling polycrystalline cells. Cooling was done on the back side of the module through cooling ducts of different shapes. It was shown that small percentage of nanofluid in water enhances temperature difference of module surface. Even for a small concentration of 0.1% wt. of Boehmite nanoparticles in water fluid, a decrease in temperature in the range of 4.5°C was observed. Copper tubing with silica nanofluid[36] was also used to cool down a polycrystalline PV module from back side. It was shown that nanofluid with 3.0% wt. of silica nano particles enhances the efficiency by 1.5%. The effective use of hybrid nanofluids in solar energy systems as working fluid has been very gainful in terms of performance, mainly due to novel thermal transportation characteristics of nanofluid. Hybrid nanofluids-based solar systems have shown great performance nearly twice, as a result of good thermal and optical properties' of nanofluid.

Enhancement in friction factor/pumping power of hybrid nanofluid-based solar systems is one of the major concerns.[37] Hybrid nanofluids have also been mainly investigated with metal oxide nanofluids. After a detailed review on hybrid nanofluids, Tayyab Raza Shah and Hafiz Ali[37] have reported that the scope of hybrid nanofluids in practical systems is limited because of stability issues and have recommended extensive investigation on combination of hybrid nanoparticles and base fluids. The heating-cooling cycles of hybrid nanofluids in a solar thermal system could cause nanoparticle to microparticle phase transformation because of instability of nanoparticles.

The efficiency of DASC collectors is limited by the absorption properties of the working fluid. It has been shown that mixing nanoparticles in a liquid to form a nanofluid can create enhanced effect on the base liquid thermal conductivity. Nanoparticles also offer the advantage of improving the radiative properties of liquids because of solid phase inclusions. The enhanced thermal conductivity and radiative properties is responsible for the increase in the efficiency of direct absorption solar collectors. Todd. P. Ottanicar[38] and group have report on the experimental results on direct absorption solar collectors based on nanofluids made

from of nanoparticles like carbon nanotubes, graphite, and silver. They observed maximum efficiency improvements of up to 5% in solar thermal collectors in their investigations. Further they compared the experimental and numerical results and demonstrated an initial rapid increase in efficiency with increasing volume fraction followed by a saturation limit.

Munzer S. Y. Ebaid[39] and coworkers performed investigation on enhancement of PV cells using two types of metal oxide nanofluids like Al_2O_3 and TiO_2 with water as base fluid. They communicated that controlling operating temperature of PV panels can enhance efficiency. Temperature control was done with nanofluids. They reported that the overheating of a PV module decreases the performance of the output power by 0.4%−0.5% per 1°C. To achieve cooling, nanofluids could be considered as an effective method. In their study, two types of nanofluids, namely, Al_2O_3 and TiO_2/water base nanofluids of different volume flow rates and three different concentrations of 0.01%, 0.05%, and 0.1% by weight were used. Three PV panels were cooled simultaneously using nanofluids, water, and natural air, respectively. Their results indicated that nanofluids for cooling enhanced heat transfer rate much superior than water and air. They observed best results for TiO_2 nanofluids at 0.1 wt.% concentration. Their results represent the first application of nanofluid cooling in the turbulent flow regimes along with outdoor conditions including real solar irradiation. The use of nanofluids in cooling PV panels is thus gaining momentum and can become an ideal solution in near future.

K.Mallikarjuna and coauthors[40] reviewed the use of nanocoating and nanofluids for solar energy harvesting. Their paper critically reviewed and conveyed the up-to-date literature available till 2020 for usage of nanofluids and nanocoating's in solar energy harvesting operating in low, medium, and high temperature ranges for enhancement and effectiveness in performance. They also reported that the nanofluids could improve the optical performance of solar cells other than speeding up the process of heat transfer.

3.6 Nanofluids for carbon dioxide capture

Carbon dioxide is a harmful gas and well known that it can cause global warming. Carbon Capture and Storage (CCS) has evolved as a technology where a maximum of 90% of the carbon dioxide (CO_2) emitted is captured.It is known that carbon dioxide is produced from the use of fossil fuels in electricity generation and industrial processes. Emission of carbon dioxide can enter the atmosphere and cause global warming. The process of carbon dioxide capture technology consists of capturing transporting and storing carbon dioxide in underground. Carbon dioxide capture can be done by precombustion or postcombustion techniques. Nanofluids can help the effective capture of carbon dioxide.

Cameron Hepburn and coworkers[41] have review 10 pathways for the utilization of carbon dioxide. They reported on pathways that involve chemicals, fuels, and microalgae which might reduce emissions of carbon dioxide but also commented on its limited potential removal, whereas they also dealt with pathways that involve construction materials which can utilize and remove carbon dioxide. Land-based pathways could increase agricultural output and remove carbon dioxide. Their assessment suggested that each pathway could scale to over 0.5 gigatons of carbon dioxide utilization annually.

Recently, the absorption of carbon dioxide using nanofluids has attracted more attention from scientists, engineers, and academicians. Basavaraj Devakki and Shijo Thomas[42]

conducted absorption test of carbon dioxide in a custom designed high-pressure stainless steel 316 L vessel, in which CO_2 and nanofluid were in direct contact at static state. They investigated TiO_2 and Al_2O_3 water-based nanofluids with very small concentrations of 0.02−0.14wt.%. Their results show that relative absorption index of CO_2 absorption has increased to a maximum and then decreased with increase in nanoparticle concentration. The aqueous-based TiO_2, Al_2O_3 nanofluids were reported to be most effective at 0.1 and 0.14wt.%. The relative absorption index showed nearly 40% and 22% increase in CO_2 absorption as compared to water. Experiments were also performed with salt water. Salt concentration can alter the nanoparticle interactions and interface interactions, thereby decreasing the stability of nanofluid. Decreasing stability indicated a decrease in carbon dioxide absorption. When the slat content was varied from 1% to 3% approximately, the carbon dioxide absorption rate decreases by almost 12%. These results again indicate that the success of nanofluid technology largely relies on preparing stable nanofluids.

3.7 Role of nanofluids in safe surgery and sensing applications

The effective utilization of nanoparticles in healthcare industry can improve the life span of humans. Nanotechnology can improve the diagnosis of the disease and also help in fast and safe recovery. The applications of nanofluids in drug delivery, medical treatment, disease diagnosis, antibacterial cases, wound dressing, and cryopreservation are discussed by Mojan Sheikpour and coworkers.[43] Magnetic fluid hyperthermia for cancer treatment, magnetic fluid for anemia treatment, the antibacterial activity of metal oxide nanoparticles is also discussed. The authors have recommended that future work involves identifying new applications of nanofluids in biomedical and medical issues and testing different types of nanofluids in drug delivery, treatment, and diagnosis.

Nanofluids are mainly being implemented for medical treatments like cancer therapy. Nanofluids can be used to increase the heat generated or increase the heat transfer and give cooling. Thus nanofluids help in medical treatments mainly in taking control over the heat at localized or desired spots. Nanofluids have been used to produce high temperature in a local region, which assist in killing cancerous cells without affecting the nearby normal tissues. Nanofluids are useful in safer surgery because of their cooling properties. The success of medical operation may increase due to use of nanofluids and it may also prevent organ damage.

Magnetic nanoparticles are preferred for biomedical applications because they can tailor the required magnetic force.

Nanofluids have also been used in design of optical sensors. These sensors have been used for rapid visual inspection of defects in ferromagnetic materials. V. Mahendran and John Philip[44] developed a sensor for studying internal defects in material based on polarizable nanoemulsion through magnetic field variations. These sensors have advantages over existing flux leakage sensors in terms of cost, reusability, and complexity. A.W Zaibudeen and John Philip[45] have reported a magnetic nanofluid sensor for urea detection. The sensing technique is simple nonenzymatic and inexpensive and based on large wavelength shift in visible range for urea's presence. They also reported the depandance of Bragg peak position on concentration of urea. The method offers rapid urea detection in small time intervals. For normal urea level the sensor worked in linear range. The optical sensor developed could detect urea

concentration of 0.001−100 g/L. A.W Zaibudeen and John Philip[46] have also designed magnetic nanofluid-based optical sensors for detection of temperature and pH. Their sensing technique is based on changes in conformation of adsorbed macro molecular groups followed by change in optical properties of nanoemulsions induced through magnetic field. The temperature measuring capability was between 5 and 90C and pH was in the range of 3−11.5. The fast response time of approximately 1s, minimum cross interference due to other condition and low cost are attractive features of this sensor. John Philip, V. Mahendran, and Leona G Felicia[47] have reported a simple inexpensive ultrasensitive magnetic nanofluid-based sensor for detection of cation, anion, and ammonia. Their sensor showed selectivity to a large number of ions and was several times faster than the 3D crystal sensors. The sensor could detect ions of sodium, potassium, copper, iron, lead cadmium, manganese, and nickel. They also reported that nanofluid sensors could become an excellent tool for analytes recognition. Besides the temperature, pH, cation, anion, ammonia, urea, and defects, John Philip group at IGCAR also developed magnetic nanofluid-based glucose[48] and methanol[49] sensors. The response time for methanol detection in aqueos solution was about 1 s, and the sensor showed a linear variation from 0 to 5000 ppm. A Simple inexpensive laboratory scale nanofluid-based optical sensing investigation is done by A.L. Subramaniyan[50] and coworkers to predict the stability of nanofluid. Water base TiO_2 nanofluid was used as a medium for optical sensing and semiconductor diode was used as the optical source. A photo detector was used as sensing element. The sedimentation of prepared nanofluid was due to gravity sedimentation and transmitted intensity of the nanofluid sample is recorded by a photo detector. A profile between the transmitted intensity and distance of nanofluid from laser source is obtained which can predict the stability of nanofluid.

4. Conclusion

Since the accidental discovery of nanofluids by S.U.S Choi in 1995, they were primarily used as heat transfer fluids. The enormous increase in thermal conductivity of nanofluids due to addition of small volume fraction of nanoparticles opened the gate way for nanofluids in thermal management systems. The primary applications of nanofluid were focused on enhanced heat transfer and design of cooling requirements in electronics. Over the past 20 years, the applications of nanofluid have drifted from cooling applications to various sectors like oil recovery, renewable energy, carbon dioxide capture, and health care.

In addition to these, nanofluids are also finding applications in direct methanol fuel cell membranes, inhibiting corrosion, energy efficient buildings, and enhancing battery life. The applications of nanofluid technology continue to grow at a rapid pace from serving miniature electronic goods to large and efficient buildings with economic solar based lightning systems. The tremendous improvement in fabrication techniques of nanoparticles of desired shape and size can further enhance the applications of nanofluids. The only hindrance to the ever growing applications of nanofluids in all regimes can be due to stability issues. Hence, it can be concluded that more attention has to be given by scientists, engineers, and academics to develop stable nanofluids of any chemical composition, size, and volume fraction for the complete success in emerging applications.

References

1. Choi US. Enhancing thermal conductivity of fluids with nanoparticles, developments and applications of non-Newtonian flows. In: Siginer DA, Wang HP, editorsvol 231; 1995. p. 99–105. 66.
2. Ghadimi, Saidur R, Metselaar HSC. A review of nanofluid stability properties and characterization in stationary conditions. *Int J Heat Mass Tran* 2011;**54**:4051–68.
3. Rotkin SV. Thermal Moore's law and near-field thermal conductance incarbon-based electronics. Proc. SPIE. 2009, 7399, 73990F SPIE. https://doi.org/10.1117/12.826326.
4. Maxwell JC. *A treatise on electricity and magnetism*. 2nd ed., vol 1. Oxford, UK: Clarendon Press; 1881. p. 440.
5. Thomas S, Sobhan BP. A review of experimental investigation on thermal properties of nanofluids. Nanoscale Res Lett 2011;6:377.
6. Eastman JA, Choi SUS, Li S, Thompson LJ. Anomalously increased effective thermal conductivity of ethylene glycol based nanofluids containing copper nanoparticles. *Appl Phys Lett* 2001;**78**(6):718–20.
7. Wang XQ, Mujumdar AS. Heat transfer characteristics of nanofluids: a review. *Int J Therm Sci* 2007;**46**:1–19.
8. Senthilraja S, Karthikeyan M, Gangadevi R. Nanofluid applications in future automobiles: comprehensive review of existing data. *Nano-Micro Lett* 2010;**2**:306–10.
9. Bahiraei M, Hesmatian S. Electronics cooling with nanofluids – a critical review. *Energy Convers Manag* 2018;**172**:438–56.
10. Khaleduzzaman SS, Saidur R, Selvaraj J, Mahbubul IM, Sohel MR, Shahrul IM. Nanofluids for thermal performance improvement in cooling of electronic device. *Adv Mater Res* 2014;**832**:218–2232013.
11. Lee JH. *Convection performance of nanofluids for electronics cooling. PhD thesis*. Stanford University; 2009.
12. Hamouda AA, Karoussi O. Effect of temperature, wettability and relative permeability on oil recovery from oil-wet chalk. *Energies* 2008;**1**:19–34.
13. Suleimanov A, Ismailov FS, Veliyev F. Nanofluid for enhanced oil recovery. *J Pet Sci Eng Volume* 2011;**78**:431–7.
14. Alomair OA, Matar KM, Alsaeed YH. *Nanofluids application for heavy oil recovery*. Society of Petroleum Engineers; 2014. https://doi.org/10.2118/171539-MS.
15. Kashif M, Yahya N, Zaid HM, Shafie A, Jasamai M, Nasir N, Akhter MN. Oil recovery by using electromagnetic waves. *J Appl Sci* 2011;**11**:1366–70.
16. Ali H, Soleimani H, Yahya N, Demirald BM, Hussaine T, Adebayoa L. Enhanced oil recovery by using electromagnetic-assisted nanofluids: a review. *Rev J Mol Liq* 2020;**309**:113095.
17. Ameenuddin Irfan S, Shafie A, Yahya N, Zainuddin N. Mathematical modeling and simulation of nanoparticle-assisted enhanced oil recovery—a review. *Energies* 2019;**12**:1575.
18. Peng B, Zhang L, Luo J, Wang P, Ding B, Zeng M, Cheng Z. A review of nanomaterials for nanofluid enhanced oil recovery. *RSC Adv* 2017;**7**:32246.
19. Shokoohi Y, Shekarian E. Application of nanofluids in machining processes – a review. *J. Nanosci Tech.* 2016;**2**(1):59–63.
20. Shen B, Shih AJ, Tung SC. Application of nanofluids in minimum quantity lubrication grinding. *Tribol Trans* 2008;**51**:730–7.
21. Setti D, Ghosh S, Rao PV. Application of nano cutting fluid under minimum quantity lubrication (MQL) technique to improve grinding of Ti–6Al–4V alloy. *Proc World Acad Sci Eng Technol* 2012;**70**:512–6.
22. Saravanakumar N, Prabu L, Karthik M, Rajamanickam A. Experimental analysis on cutting fluid dispersed with silver nano particles. *J Mech Sci Technol* 2014;**28**(2014):645–51.
23. Yogeswaran M, Kadirgama K, Rahman MM, Devarajan R. Temperature analysis when using ethylene-glycol-based TiO2 as a new coolant for milling. *Int J Automotive Mechanical Eng* 2015;**11**:2272–81.
24. Roy S, Ghosh A. High speed turning of AISI 4140 steel using nanofluid through twin jet SQL system. In ASME 2013 international manufacturing science and engineering conference. *J Adv Res Fluid Mech Therm Sci* 2013;**69**(1):163–73.
25. Sahid NSM, Rahman MM, Kadirgama K, Ramasamy D, Maleque MA, Noor MM. Experimental investigation on the performance of the TiO_2 and ZnO hybrid nanocoolant in ethylene glycol mixture towards AA6061-T6 machining. *Int J Automot Mech Eng* 2017;**14**(1):3913–26.
26. Tran TL, Tran M. *Duc the characteristics and application of nanofluids in MQL and MQCL for sustainable cutting processes*. *Advances in Microfluidic Technologies for Energy and Environmental Applications*. 2020. https://doi.org/10.5772/intechopen.90362.

27. Lee P-H, Nam JS, Li C, Lee SW. An experimental study on micro-grinding process with nanofluid minimum quantity lubrication (MQL). *Int J Precis Eng Manuf* 2012;**13**:331–3.
28. Gong L, Bertolini R, Ghiotti A, Ning H, Bruschi S. Sustainable turning of Inconel 718 nickel alloy using MQL strategy based on graphene nanofluids. *Int J Adv Manuf Technol* 2020;**108**:3159–74.
29. Prakash Veluswamy H, Kumar A, Seo Y, Lee JD, Linga P. A review of solidified natural gas (SNG) technology for gas storage via clathrate hydrates. *Appl Energy* 2018:262–85.
30. Lu YY, Ge BB, Zhong D-L. Investigation of using graphite nanofluids to promote methane hydrate formation: application to solidified natural gas storage. *J Energy* 2020. https://doi.org/10.1016/j.energy.2020.117424.
31. Renuka Prasad A, Sumer Singh D, Harish Nagar D. Importance of solar energy technologies for development of rural area in India. *IJSRST* 2017;**3**(6):585–99.
32. Menni Y, Ahmed A, Ali C. A review of solar energy collectors: models and applications. *J Appl Comput Mech* 2018;**4**(4):375–401.
33. Fan J, Chen Z, Fubro S, Perers B, Karlsson B. Efficiency and life time of solar collectors for solar water heating plants. In: *Proceedings of the ISES solar world congress 2009, renewable energy shaping our future*; 2009.
34. Phelan P, Otanicar T, Taylor R, Tyagi H. Trends and opportunities in direct-absorption solar thermal collectors. *J Therm Sci Eng Appl* 2013;**5**.
35. Karami N, Rahimi M. Heat transfer enhancement in a PV cell using Boehmite nanofluid. *Energy Convers Manag* 2014;**86**:275–85.
36. Sardarabadi M, Passandideh-Fard M, Heris SZ. Experimental investigation of the effects of silica/water nanofluid on PV/T (photovoltaic thermal units). *Energy* 2014;**66**:264–72.
37. Shah TR, Hafiz Muhammad AL. Applications of hybrid nanofluids in solar energy, practical limitations and challenges: a critical review. *Sol Energy* 2019;vol 183:173–203.
38. Otanicar TP, Phelan PE, Prasher RS, Gary R, Taylor RA. Nanofluid-based direct absorption solar collector. *J Renew Sustain Energy* 2010;**2**:033102.
39. Ebaid MSY, Al-busoul M, Ayoup M. Ghrair Performance enhancement of photovoltaic panels using two types of nanofluids. *J Heat transfer* 2020;**49**(5):2789–812.
40. Mallikarjuna K, Santhoshkumar Reddy Y, Hemachandra Reddy K, Sanjeeva Kumar PV. A nanofluids and nanocoatings used for solar energy harvesting and heat transfer applications: a retrospective review analysis. *Mater Today Proc* 2021. https://doi.org/10.1016/j.matpr.2020.05.833.
41. Hepburn C, Adlen E. Beddington the technological and economic prospects for CO_2 utilization and removal. *Nature* 2019;**575**:87–97. https://doi.org/10.1038/s41586-019-1681-6.
42. Devakki B, Thomas S. Experimental investigation on absorption performance of nanofluids for CO_2 capture. *Int J Air-Cond Refrig* 2020;**28**(2).
43. Sheikhpour M, Arabi M, Kasaeian A, Rabei AR, Zahra T. Role of nanofluids in drug delivery and biomedical technology: methods and applications. *Nanotechnol Sci Appl* 2020;**13**:47–59.
44. Vellaichamy M, Philip J. Nanofluid based optical sensor for rapid visual inspection of defects in ferromagnetic materials. Appl Phys Lett 2012;100(7):073104.
45. Zaibudeen AW, Philip J. Magnetic nanofluid based non enzymatic sensor for urea detection. *Sens Actuators Chem B* 2018;**255**(1):720–8.
46. Zaibudeen AW, Philip J. Temperature & pH sensor based on functionalized magnetic field. *Sens Actuators Chem B* 2018;**268**(1):338–49.
47. Philip J, Mahendran V, Felicia LG. A simple simple inexpensive ultrasensitive magnetic nanofluid based sensor for detection of cation ,anion and ammonia. *J Nanofluids* 2013;**2**:113–9.
48. Mahendran V, Philip J. Non-enzymatic glucose detection using magnetic nanoemulsions. *Appl Phys Lett* 2014;**105**:123110. https://doi.org/10.1063/1.4896522.
49. Mahendran V, Philip J. methanol sensor based on stimulus-responsive magnetic nanoemulsions. *Sens Actuators Chem B* 2013;**185**:488–95.
50. Subramaniyan AL, Kottaisamy M, Ilangovan R. Optical sensing of TiO2 nanofluids for self stability. *Mater Sci Forum* 2015;**87**:143–9.

This page intentionally left blank

CHAPTER

12

Promising inorganic nanomaterials for future generation

Sumana Ghosh

Bio-ceramics and Coating Division, CSIR-Central Glass and Ceramic Research Institute (CSIR-CGCRI), Kolkata, West Bengal, India

1. Introduction

Multifunctional nanomaterials are of considerable interest in the field of energy applications such as energy generation, storage, saving, conversion, and transmission. Various energy applications need a specific combination of electrical, thermal, mechanical, optical, and catalytic functions of materials. Several properties e.g., electrical conductivity, thermal conductivity, large surface area, and chemical stability of the inorganic nanomaterials have made them suitable for energy applications.[1] Inorganic nanoparticles have also received increased attention in the field of oncology. Huang et al.[2] showed the successful use of semiconductor fluorescent quantum dots, carbon nanotubes, gold nanoparticles, iron oxide magnetic nanoparticles, and ceramic nanoparticles in photothermal therapy, imaging, tumor targeting, and drug delivery applications. They also mentioned the limitations and toxicity issues associated with inorganic nanoparticles in living organisms. Nanotechnology has the potential to improve the early diagnosis, treatment, and monitoring of disease progression. Recently, there is a new trend to use nanoparticles (NPs) as nanomedicine in cancer therapy. The multifunctional nanoparticle can be effectively utilized for the diagnosis and treatment of cancer.[3] The structural characteristics of NPs make them excellent modes for targeting cancer cells. They can potentially enter the abnormal cells causing DNA damage and determining the defects in the genes. Apart from targeting cancer cells they also assist in the release and monitoring of therapeutic agents against cancer.[4]

Additionally, progress has been made on cancer theranostic strategies using mesoporous silica nanoparticles and carbon-based nanomaterials.[5] Several studies have indicated the beneficial effects of using these nanoparticles. However, detailed and long-term in vivo clinical trials are essential. Nanobiomaterials have attracted tremendous attention in the biomedical field.[6] Three-dimensional (3D) nanofiber scaffolds have attracted attention in tissue

Applications of Multifunctional Nanomaterials
https://doi.org/10.1016/B978-0-12-820557-0.00006-0

regeneration. Moreover, many 3D scaffolds displayed bone and cartilage regeneration abilities. Therefore, it is required to develop multifunctional 3D nanobiomaterials for obtaining tumor therapy and tissue regeneration abilities.[6] Nanomaterials-based sensors can be used for checking environmental pollution owing to their excellent properties. Various nanomaterials such as carbon nanotubes, gold nanoparticles, silicon nanowires, and quantum dots have been extensively explored in detecting and measuring toxic gases, toxic metal ions, pesticides, and harmful industrial compounds with high sensitivity.[7]

The objective of this chapter was to present an overview of different kinds of inorganic nanomaterials being utilized for suitable applications or having great prospects for future generation utility. Although there are excellent review articles and book chapters in this field, still the current chapter has been perceived to provide deep insight into the broad perspective of inorganic materials for future use.

2. Present status

2.1 Nonmetallic inorganic nanomaterials

Silica has been used for dental applications because of its physical, and optical properties and compatibility with composites. Engineered silica nanomaterials have superior physical and mechanical properties, which make them suitable for dental applications. The specific physicochemical properties of silica-based nanomaterials such as surface properties, mechanical properties, and biocompatibility have enabled their application in potential biological applications.[8] The phytotoxicity of nano-CeO_2, nano-La_2O_3, nano-Gd_2O_3 and nano-Yb_2O_3 on different plant species such as radish, rape, tomato, lettuce, wheat, cabbage, and cucumber were investigated. Their effects on root growth varied significantly.[9] Rare earth oxides account for 59% of the total worldwide consumption of rare earth elements in the market of catalysts, glassmaking, and metallurgy while in high-growth markets (such as battery alloys, ceramics, and permanent magnets) rare earth oxides account for 41% of the total worldwide consumption of rare earth elements.[10] Nanomaterials (NMs) can be utilized for a human health problem. However, a detailed understanding of their intracellular behavior and related toxic effects is urgently needed. Recently, ferroptosis has been found to be iron-mediated cell death. There is no evidence for the effect of iron-free engineered NMs on ferroptosis. Zhang et al.[11] showed that zinc oxide nanoparticles (ZnO NPs)-induced cell death involves ferroptosis. They established ferroptosis as a novel cell death phenotype induced by engineered NMs. Flowerlike α-Fe_2O_3 nanostructures were synthesized by microwave-assisted solvothermal method.[12] These flowerlike α-Fe_2O_3 nanostructures had a high surface area with abundant hydroxyl groups on their surface and thereby, showed excellent adsorption properties as an adsorbent for arsenic and chromium removal. The results suggested that ion exchange between surface hydroxyl groups and AsV or CrVI species was responsible for the adsorption. Liang et al.[13] prepared polymer-stabilized tetragonal ZrO_2 nanopowders by using microwave heating. They examined that the photoluminescence property of the synthesized ZrO_2 fine particles was quite good.

Malhotra et al.[14] evaluated chronic ecotoxicities of magnetic nanoparticles (MNPs) exposure on the brain of adult zebrafish. They studied the behavioral changes related to neuronal

functions in contact with two different concentrations of MNPs, which revealed that MNPs at environmental concentration caused a slight influence on behavioral and biochemical activities of the fish brain. This study showed some minor behavioral modifications owing to exposure to highly concentrated, bare Fe_3O_4 MNPs and thereby, indicating the necessity of more surface modification to increase its water solubility and biocompatibility in order to decrease its biotoxicity.[14] Yang et al.[15] fabricated CaO-based ceramic mold for investment casting by stereolithography (SLA) and nonaqueous gel casting technique using CaO-based slurry. The resulting ceramic mold showed excellent thermal stability, reaction-resistance to molten active alloys, and enhanced efficiency and economy than other ceramic molds. Researchers have already carried out in-depth research on the interactions between the TiO_2-based materials and the cell wall of the microorganisms and reported elsewhere.[16] Morphological examinations were made to detect the physical damage on the cell wall that indicated the death of the microorganism. Thus, it was clear that the photocatalytic approach was good for the effective inhibition of microorganisms.[16]

2.2 Metal based inorganic nanomaterials

The necessity of biocompatible materials for different applications has attracted more attention to nanobiotechnology. Manganese (Mn) metal has numerous applications in the area of medicine, biomedicine, biosensors, water treatment/purification, electronics, electrochemistry, photo electronics, and catalysis. Green synthesis of Mn NPs has been investigated and reported elsewhere. Manganese oxides (Mn-oxides) in various forms such as MnO, Mn_5O_8, Mn_2O_3, MnO_2, and Mn_3O_4 can be used in a variety of fields. Mn-oxide NPs have great potential for sustainable nanotechnology.[17] Manganese-containing nanoparticles have promising applications in the field of nanomedicine.[18] However, it is true that more research on Mn-based nanoparticles is needed to ensure their biosafety. Thus, comparative studies are further necessary to assess the advantages of Mn-based nanoparticles. There is a great demand for clean and sustainable energy sources due to the exhaustion of fossil fuels and environmental pollution. In recent decades, platinum (Pt)-based fuel cells have achieved tremendous advances as a green energy source. However, there is still a lack of energy production efficiency. Conventional Pt electrocatalysts are usually inadequate in catalytic activity and the selectivity of electrochemical reactions. On the contrary, metal alloy nanocatalysts exhibited exceptional electrocatalytic performance on fuel cells compared to that of pure Pt catalysts. This was ascribed to the modification of the surface geometry and electronic structure of the catalytically active metal component.[19] The metallic nanoparticles show worthy antimicrobial activity against gram-positive bacterium bacillus subtilus. It has been found that Ag−Cu bimetallic nano-particle shows high antimicrobial activity. Investigation in this direction will help to prepare nano-medicines and targeted drug delivery. Nazeruddin et al.[20] have confirmed that Ag−Cu bimetallic NPs are capable of providing high antibacterial efficiency. Henceforth, these NPs have great potential in the preparation of drugs against bacteria.

Metal nanoparticles, bimetallic alloy nanoparticles, and composite materials made of metal nanoparticles have a great prospect for future generation usage. Alloy metal nanoparticles exhibit exciting optical responses. Surface-plasmon resonance frequencies of bimetallic alloy

nanoparticles can be controlled precisely through the variation of alloy compositions. Researchers showed that the photoluminescence intensity of semiconductors was increased or decreased in the metal-semiconductor composite nanostructures depending upon the compositions and sizes of the nanomaterials. It was observed that metallic alloy nanoparticles exhibited fine-tuning of optical responses over a broad wavelength range than pure metals. Remarkable photoluminescence and chemical properties of metal-semiconductor nanocomposite materials were revealed by stimulating quasi-particle interactions among plasmons and excitons.[21] Tabassum et al.[22] developed new functional materials with unique physical and chemical properties through nano-confinement of metal-based nanostructures in one-dimensional carbon nanotubes (M@CNTs) for various energy applications. They emphasized the future prospects of M@CNTs for electrochemical energy conversion and storage devices. Advanced nano-confinement methods have been invented for different functional nanoparticles e.g., metals, metal oxides, metal sulfides, metal phosphides, metal carbides, etc. Particularly, the focus is being made on their catalytic activities and stabilities. Further, new strategies are being thought to increase storage capacities of Zn−air batteries, Li−O_2 batteries, and lithium-ion batteries.[22] Pulsed laser ablation method was found to be a promising alternative for many conventional methods in synthesizing nanoparticles as this synthesis route provides totally ligand-free nanoparticles.[23] Binary and ternary alloy nanoparticles with totally homogeneous elemental distribution could be fabricated by this method. Moreover, the composition of these nanoparticles was similar to bulk implant material. The model AuAg was used to evaluate composition-related toxicological effects of alloy nanoparticles. The feasible mechanism of toxicity was recognized as the release of Ag^+ ion considering recent toxicological investigations with mammalian cells, gametes, and bacteria.[23]

The possibility to use metal-based nanoparticles in medicine and related field has been reported by some researchers.[24] The noble metal-based nanoparticles (Au NPs and Ag NPs) showed great possibilities for improving the quality of radiation-based anticancer therapy, using as drug delivery systems, supporting molecular imaging as well as forming compounds with bactericidal, fungicidal, and antiviral properties. However, it is necessary to overcome certain barriers to the biodegradability or porosity of some nanoparticles. Moreover, there is relatively little information about the toxicity and interaction of these nanoparticles with living normal cells. Indeed, the development of nanotechnology has enabled effective treatment and diagnosis of various diseases. However, the degradation and elimination of metal nanoparticles from the body have to be solved.[24] Currently, there is a lack of knowledge regarding nanoparticle immunotoxicity, biodistribution, and pharmacokinetics.[25] The interaction of nanomaterials with the immune system is very motivating. The physicochemical properties of nanoparticles influence the immunological effects. Extensive studies are needed to correlate the effects of physicochemical properties with the immune toxicity of metal-based nanoparticles as well as the overall evaluation of nanodrug toxicity. Further, a knowledge base should be developed on the physicochemical properties of nanoparticles that controls the immune system. The materials science in association with immunology, and immune bioengineering can help in developing prophylactic and therapeutic vaccine applicants.[25]

It has been seen that antimicrobial textiles have gained considerable interest for use in different application fields.[26] Therefore, antimicrobial agents e.g., quaternary ammonium compounds, heterocyclic compounds with anionic groups, triclosan, *N*-halamine siloxanes,

polybiguanides, metal salts, and synthetic colorants have been used to impart antimicrobial properties to different textile materials. However, most of these antimicrobial agents suffer from several disadvantages along with low durability. They give rise to environmental toxicity and act on nontarget microorganisms. To overcome these problems, silver nanoparticles with long-term durability, strong cytotoxicity toward microorganisms, low toxicity to human cells, high selectivity, increased dyeability and biocompatibility are drawing a tremendous level of attention in both academic research and industry. Therefore, silver nanomaterials utilized for the production of textiles surfaces having certain enchanting properties including antimicrobial activity, UV protection competency, water resistance property, and self-cleaning ability. Recent studies have described the use of silver nanomaterials as novel colorants and antimicrobial agents for different textile materials.[27] Nanoparticles can penetrate into the human body through the skin, respiratory, and digestive systems.[27] Silver nanoparticles tend to accumulate in various organs, especially in the liver, kidneys, and lungs. Particularly, the presence of silver nanoparticles in the liver may be dangerous. The suspected accumulation of silver nanoparticles in the lungs can also have negative effects, which are likely to be noticeable in the future. Thus, further research on the toxicity of silver nanoparticles in relation to living organisms is very much necessary. A suitable method of environment renaturalization is needed to avoid possible threats as silver nanoparticles have great prospects for future generation.[27]

Additionally, there are some difficulties and challenges around the nanomaterials in complex media.[28] Hence, initially proper chemical separation and biological assays of nanomaterials from nanoproducts needs to be developed. A simple and rapid method to separate and analyze gold nanomaterials in cosmetics was reported by Cao et al.[28] Quantification of gold by inductively coupled plasma mass spectrometry and thorough characterization of size distribution, morphology, and the surface property was conducted. Preliminary toxicity assessment indicated that highly concentrated gold nanomaterials in cosmetic creams had no visible toxicity to human keratinocytes even after 24 h exposure. They revealed that the gold nanomaterials were mostly attached to the cell membrane.[28] It is well-known that nonnoble metal catalysts mainly focus on tuning their surface functionality and increasing surface area to exploit metal loading for high catalytic reduction of 4-nitrophenol. However, the inefficient hydride is formed on the metal surface due to the passive role of these supports that restricts the catalytic activity. Fe_3O_4@porous-conductive carbon (Fe_3O_4@C-A) core-shell structure was utilized as active support for Co, Ni, Fe, and Mn nanoparticles. The significant difference in catalytic activity was ascribed to the synergistic effect amid Fe_3O_4, conductive carbon, and metal nanoparticles, which resulted in efficient hydride formation. It was observed that active support with nonnoble metals assisted hydride formation, accelerating the catalytic reduction of 4-nitrophenol.[29]

Bimetallic nanoparticles of noble metals are suitable for application in certain areas e.g., heterogeneous catalysis, imaging, biomedical devices, and nanomedicine. Loza et al.[30] showed the applicability of nanoparticles e.g., Ag, Au, and platinum group metals than the corresponding monometallic nanoparticles. The ratio of two metals, homogeneity, and internal distribution of the elements played a great role in the resultant properties (light absorption, antibacterial effects, and catalytic activity) in the case of bimetallic nanoparticle.[30] Applications of copper nanoparticles are gradually increasing in account of cost-effectiveness and availability of Cu nanoparticles.[31] Although colloidal Cu NPs have

considerably catalytic activity still synthesis of copper nanoparticles is very challenging due to transformation of Cu nanoparticles to copper oxide in air. Extensive research carried out on the synthesis of copper nanoparticles showed some promising methods such as microemulsion, microoven assisted decomposition, wet chemical, and thermal decomposition. The copper nanoparticles showed possible biological applications for antimicrobial and wound healing purposes.[31]

2.3 Carbon-based nanomaterials

Several functional properties of carbon-based nanomaterials (CBNs) such as thermal and electrical conductivity, high mechanical strength, and optical properties are being used for various industrial applications that utilize electronics along with high-strength materials. These unique properties of CBNs are also being thought of used in several areas of biomedical engineering.[32] New technologies based on carbon-based nanomaterials enable the identification and tackling of environmental challenges. Contributions of carbon-based nanomaterials to a broad range of environmental applications such as antimicrobial agents, environmental sensors, sorbents, high-flux membranes, depth filters, renewable energy technologies, and pollution prevention strategies have been already reported.[33] The bacterial resistance to currently available antibiotics shows the urgent need for new alternative antibacterial agents. Nanomaterials can be used as antibacterial agents for the management of infectious diseases. Among these antibacterial nanomaterials, CBNs have appealed much consideration due to their unique physicochemical properties and relatively higher biosafety. The inhibition of bacterial metabolism, photothermal effect, photocatalytic effect, physical damage, mechanical damage, oxidative stress, lipid extraction, and isolation by wrapping have been studied. The synergistic effect of using CNMs with other antibacterial materials as well as the effects of the physicochemical properties of CNMs on antibacterial activity has been also investigated by researchers and reported elsewhere.[34] Carbon-based nanomaterials are being widely used either in the chemical industry catalysts/catalyst supports or in the energy/environmental applications because of their high surface areas, tunable porosity, and functionalization. Recently, the newly developing metal-organic frameworks (MOFs) made from metal ions and polyfunctional organic ligands have shown promising precursors for preparing various carbon-based nanomaterials. This may be attributed to their high BET surface areas, large pore volumes, abundant metal/organic species, and rare tunability of compositions and structures. MOF-derived carbon-based nanomaterials have great advantages in terms of controlled morphologies, graded porosity, and easy functionalization with other heteroatoms and metal/metal oxides as compared to other carbon-based catalysts. Hence, these nanomaterials can be used as highly efficient catalysts or as catalyst supports for numerous significant reactions.[35]

Extensive research is being conducted regarding the application of various carbon nanomaterials (CNMs) such as graphene, graphene oxide (GO), reduced graphene oxide (rGO), carbon nanotubes (CNTs), activated carbon fiber and expanded graphite (EG) or functionalized CNMs including functionalized graphene and C_{60}-fullerene in energetic materials (EMs).[36] Although EG had only been used in chemical heat pumps still it has other applications as an additive in nanothermites and flame retardant additive in cladding materials for

solid propellant charges. C_{60}-fullerene can be functionalized with energetic groups to form energetic compounds with excellent thermal stability. However, the variety of energetic compounds used for C_{60}-fullerene functionalization is yet limited. C_{60}-fullerene derivatives can either be used as combustion catalysts, energetic binders, or additives. Generally, graphene and its aerogels combined with either catalysts or oxidizers can be used as advanced oxidizers and combustion catalysts. GO and rGO have been found to be energetic by themselves. These CNMs are used as matrices to bind many other energetic compounds (e.g., nitrocellulose (NC), HMX, and FOX-7). Various energetic compounds can be deposited on GO or rGO for improving their performance. Functionalized CNTs have been developed as combustion catalysts or energetic additives to propellants like C_{60}-fullerene. Some of these nanomaterials have been also used in new formulations of thermites and ignitors. A variety of synthetic techniques such as chemical vapor deposition (CVD), hydrothermal, microemulsion, reductive deposition, ultrasonic compositing, and chemical reaction methods have been used to prepare CNM-containing EMs. The combination of CNTs with highly sensitive EMs has improved the sensitivity and performance of these EMs. Detonation nanodiamonds (DnDs) are gaining popularity, yet their application in EMs is limited. Recently, researchers are taking great challenges to functionalize DnDs with energetic or other functional groups.[36]

2.4 Nanopolymers and dendrimers

The unique physicochemical properties of polymeric nanomaterials (nanoscale size, high reactivity, large surface area to mass ratio) customize them in many application fields. Polymeric nanomaterials are specifically engineered materials. Thus, their use in nanomedicine has greatly changed the therapeutic and diagnostic modalities.[37] Conducting polymers (CPs) have been widely applied in various organic devices.[38] CPs have to be nanostructured in order to improve their performance. Electrosynthesis is an effective and one-step approach to synthesizing CP nanomaterials. The properties of the resulting materials can be controlled easily. Li et al.[38] synthesized CP nanostructures and nanocomposites by electrochemical polymerization for their probable applications in organic devices such as sensors, actuators, and memory devices. Most of the newly developed drugs fail to achieve adequate bioavailability in the brain due to low water solubility and low permeability.[39] Drug delivery systems are required to aid the access of molecules to the selected location within the body. Dendrimers are customizable nanopolymers with uniform, well-defined particle sizes, and shapes. Dendrimers are of renowned interest for biomedical applications because of their ability to cross cell membranes. This potential pharmaceutical delivery system can cross the blood-brain barrier (BBB) and other important target points. Beg et al.[39] mentioned that the high level of control over the dendritic design (size, branching density, surface functionality) makes dendrimers perfect carriers in the field of brain drug delivery of anticancer, antiinflammatory, and antimicrobial agents. Dendrimers such as poly(propylene imine) (PPI), polyethercopolyester (PEPE), poly(amidoamine) (PAMAM), Glyco, PEGylated, peptide, and pH dendrimers carry the drug molecules either by means of physical interactions or by chemical bonding. The pH-sensitive dendrimers are able to deliver drug molecules at the tumor site through modification of ionic exchange in the brain microenvironment.[39] Fu et al.[40] studied cholesterol (Chol)-modified dendrimer system for targeted chemotherapy of folate (FA)

receptor-expressing cancer cells. The synthesized dendrimers were used to arrest 10-hydroxycamptothecin (HCP), which was a hydrophobic anticancer drug. They assumed that Chol-modified dendrimers might be adopted as a promising carrier for application in targeted cancer therapy.[40]

2.5 Quantum dots

The development of two-dimensional (2D) inorganic materials-based quantum dots (QDs) is still in its early stages but attracted attention due to their high chemical stability, excellent optical property, good aqueous dispersibility, good biocompatibility, and easy functionalization.[41] There are several 2D-QDs based on graphene, silicene, phosphorene, carbides, nitrides, transition metal oxides, transition metal dichalcogenide and MXenes, which have a possible application in bioimaging, fluorescent sensing, optoelectronics, and cancer therapy. Further studies are needed for 2D-QDs to meet their increasing demands in diverse applications. Cadmium telluride quantum dots (CdTe QDs) are used as near-infrared probes in biologic and medical applications.[42] However, their cytological effects and mechanism of potential toxicity are not been properly understood up to now. Fan et al.[42] evaluated the toxicity of cadmium telluride (CdTe) QDs of different sizes and investigated their mechanism of toxicity in the yeast *Saccharomyces cerevisiae*. Further studies on toxicity mechanisms revealed that orange-emitting CdTe (O−CdTe QDs) could partially inhibit autophagy at a late stage, which varied from the results obtained in the case of mammalian cells. Moreover, autophagy inhibited at a late stage by O-CdTe QDs could be partially recovered by enhancing autophagy with the aid of an autophagy activator (rapamycin) in combination with increasing living cells. These results indicated that inhibition of autophagy acted as a toxicity mechanism of CdTe QDs in *Saccharomyces cerevisiae*.[42] Therefore, the present work demonstrates an innovative toxicity mechanism of CdTe QDs in yeast and provides valuable information on the effect of CdTe QDs on living cells.

Recent advancement in the chemistry of colloidal semiconductor nanocrystal doping has led to an effort to dope CdSe quantum dots with Mn^{2+}. Beaulac et al.[43] synthesized Mn^{2+} doped CdSe and evaluated the physical properties of this material that included excitonic magnetic polaron formation, spin-polarizable excitonic photoluminescence, magnetic circular dichroism, and exciton storage. The physical properties of the colloidal quantum dots were shown to compare suitably with those of the similar self-assembled Mn^{2+}-doped quantum dots developed by molecular beam epitaxy. However, attractive physical properties displayed by colloidal Mn^{2+}-doped CdSe quantum dots suggested that the material can be effectively utilized for future fundamental and applied research.[43] Lead halide perovskite quantum dots (QDs) are very promising for lighting and display applications because of their color-tunable and narrow-band emissions. But, they suffer from lead toxicity and instability. Although lead-free Sn-based and Bi-based perovskite QDs are previously described, they all show low photoluminescence quantum yield (PLQY) and poor stability. Leng et al.[44] synthesized $Cs_3Bi_2Br_9$ perovskite QDs with high PLQY and excellent stability. As-synthesized $Cs_3Bi_2Br_9$ QDs showed a blue emission at 410 nm with a PLQY up to 19.4%. The whole series of $Cs_3Bi_2X_9$ (X = Cl, Br, and I) QDs by mixing precursors can cover the photoluminescence emission range from 393 to 545 nm. Furthermore, $Cs_3Bi_2Br_9$ QDs show excellent

photostability and moisture stability due to the all-inorganic nature and the surface passivation by bismuth oxybromide (BiOBr). Thus, the one-pot synthesis of $Cs_3Bi_2Br_9$ QD/silica composite was possible. A lead-free perovskite white light-emitting diode was fabricated by combining the composite of $Cs_3Bi_2Br_9$ QD/silica with $Y_3Al_5O_{12}$ phosphor. $Cs_3Bi_2Br_9$ QDs exposed a new direction for the fabrication of optoelectronic devices as lead-free perovskite QDs owing to their excellent stability and photophysical characteristics.[44]

An effective method to improve reliability and decrease the price of perovskite solar cells (PSCs) is the utilization of an inorganic hole-transport layer (HTL). However, the preparation of high-quality inorganic HTL films is really a problem. Liu et al.[45] proposed a modest surface modification approach for the preparation of stable, hydrophobic cuprous oxide (Cu_2O) quantum dots as top hole-transport materials for efficient PSCs. The efficiency of PSCs with surface-modified Cu_2O was significantly higher than that of PSCs with unmodified Cu_2O. The performance of PSCs was improved due to the superior film properties obtained by surface modification. Cu_2O-based PSCs displayed better stability than other PSCs due to dopant-free technology and hydrophobic surface.[45] The size-dependent optical properties of quantum dots (QDs) are frequently exploited for use in medical imaging and labeling applications. Cadmium telluride quantum dots (3.2 nm) were shown to have an intense anticoagulant effect focused around the intrinsic coagulation pathway than their 3.6 nm counterparts. Several clinical diagnostic tests were carried out over a concentration range of the QDs, which demonstrated that the 3.2 nm QDs stimulated their response on the intrinsic pathway. But, it was found that the activity of the individual intrinsic coagulation factors was not affected. In addition, it was established that the mechanism was strongly influenced by the concentration of calcium ions and not cadmium ions trickled from the QDs. Static and shear-based primary hemostasis assays were also carried out that revealed profound anticoagulant effects independent of platelets and phospholipids. Maguire et al.[46] carried out a study on the anticoagulant properties of cadmium telluride quantum dots. Their investigation suggested that the physical-chemical properties of the QDs might have an influence in hemostasis and coagulation.[46] However, the mechanism has not been fully understood. In vivo testing of similar QDs is essential in respect of safety before their actual application as diagnostic tools.

2.6 Composite inorganic nanomaterials

Separators are needed to improve the performance of lithium-ion batteries. Commercial lithium-ion battery separators are mainly polyolefin organic diaphragms, but their temperature instability leads to battery short circuits and fire risk. Xu et al.[47] utilized an electrospinning method to prepare a flexible SiO_2 nanofiber membrane combined with a poly(vinylidene fluoride-hexafluoropropylene) (PVDF-HFP) nanofiber membrane. The mechanical strength of the SiO_2/PVDF-HFP composite nanofiber membrane (SPF) was significantly high with full dimensional stability at 200°C. SPF demonstrated high porosity, outstanding thermal stability as well as large-area closed cells at 180°C during actual use in lithium-ion battery separators than polyethylene (PE) separators. The liquid absorption rate of SPF was much higher than a PE separator. Furthermore, the performance of lithium-ion batteries prepared by SPF has made SPF an ultimate choice for high-power battery separators.[47] A composite material consisting of Sm, Ag, and TiO_2 inorganic nanomaterials was synthesized by Wu et al.[48] using

supercritical fluid drying (SCFD) combined with sol-gel techniques. $Sm/Ag/TiO_2$ showed optimal properties at 600°C. It was observed that the inorganic composite nanomaterials $Sm/Ag/TiO_2$ had high-temperature resistance, and good photocatalytic and antibacterial characteristics in visible light. Recently, interest has grown among researchers to apply various materials for the treatment of bone-related diseases and syndromes by using biodegradable polymer-ceramic composites.[49] Biomaterials used to repair or replace damaged parts of the human body are mainly metals, ceramics, and polymers. Composites can be manufactured by combining two or more materials to achieve enhanced biocompatibility and biomechanical properties for specific applications. Metals and their alloys such as titanium, stainless steel, and cobalt-based alloys have been widely investigated for implant-device applications because of their excellent mechanical properties. However, these materials have certain drawbacks e.g., toxicity, poor tissue adhesion, and stress shielding effect due to their high elastic modulus. Thus, hydroxyapatite (HA) coatings have been applied on metals as their chemical composition is comparable to that of bone and teeth. Recently, a wide range of synthetic polymers has been studied for different biomedical applications on account of their promising biocompatibility and biodegradability. There is an enormous prospect of synthetic polymer-ceramic composites (e.g., PLLA/HA and PCL/HA) for eradicating the stress shielding effect and thereby, resulting in revision surgery.[49]

Atif et al.[50] investigated the structures, morphologies, phototoxicities, and antibacterial activities of undoped and Mn-doped ceria nanocomposite materials. They found that the undoped nanocomposites had lower cytotoxicities and inhibitions than those of the doped nanocomposites toward pathogens. The manganese-doped ceria nanocomposite enhanced the antibacterial activity and effectiveness for photodynamic therapy. This was attributed to the connection of the extreme reactive oxygen species generation for targeted toxicity and supreme antioxidant property in the inhibition of bacteria growth. It was assumed that the optimized cell viability dosage and doping concentration would be utilized for treating cancer and bacterial infections.[50] Nanocellulose obtained from natural renewable resources is very useful for different applications due to its superb mechanical strength, morphological features, biocompatibility, and biodegradability. Their high specific surface area, template structure, and active surface groups cause surface modification and accommodate various nanostructured materials by physical deposition and chemical deposition. Zhang et al.[51] showed various procedures for loading different nano-structured materials such as metals, nanocarbons, oxides, mineral salt, quantum dots, and nonmetallic elements into nanocellulose. The nanocellulose composites can be used in the fields of catalysis, optical-electronic devices, biomedicine, sensors, composite reinforcement, photoswitching, flame retardancy, and oil/water separation.[51] Ionescu et al.[52] prepared polymer-derived ceramic nanocomposites based silicon oxycarbide-based materials (SiOC) and ZrO_2 by two synthetic approaches. Annealing experiments were performed in the temperature range of 1300°−1600°C. They perceived that the inclusion of ZrO_2 into the SiOC matrix increased the thermal stability of the composites. Therefore, the experimental results indicated the vast potential of polymer-derived $SiOC/ZrO_2$ composites for high-temperature applications.[52]

A high-efficient catalyst is needed for the catalytic oxidation of volatile organic compounds (VOCs). MnO_2 nanoparticles encapsulated in spheres of Ce−Mn solid solution are an efficient catalyst for the catalytic oxidation of a typical VOC, toluene.[53] It was observed that the said composite catalyst had much better toluene oxidation activity than the original MnO_2 and

CeO_2. In addition to this, the shell of the Ce−Mn solid solution provided superior thermal stability and resistance against 5 vol. % H_2O. The resultant composite offered high BET surface area, good reducibility, and fast oxygen mobility leading to outstanding catalytic performance.[53] Great demand exists for functional composite materials with desired properties in a variety of applications. The formation of homogenous composite material by conventional mixing methods is problematic because of agglomeration. The research was carried out to form homogeneous poly(methylmethacrylate) (PMMA)-indium tin oxide (ITO) composite by electrostatic assembly method. The consequential composite showed high visible light transparency and tremendous shielding effect of infrared (IR). Hence, this PMMA-ITO composite has good potential to be used in the automobile industry. The IR shielding rate could be tuned by controlling the amount of ITO nanoparticles.[54] Some researchers synthesized Au_{core}-Co_{shell} nanoparticles by wet chemical method and subsequently characterized.[55] They demonstrated significant improvement in coercivity of Au_{core}-Co_{shell} nanoparticles at 10 K compared to the pure cobalt sample. This happened due to the pinning effect of cobalt spins at the Au/Co interface. They suggested that the pinning mechanisms were strain pinning and demagnetizing field pinning.[55] Study has been already made on the synthesis of TiO_2 composite nanomaterials for various applications.[56] Usually, composite materials have been fabricated by adding metal, metal oxide, and metal sulfide with TiO_2 in the form of either layered or core-shell structures. The said composites can be prepared by various methods such as chemical synthesis, solution/gas-phase deposition, and templated fabrication.[56]

2.7 Recent developments

Printed electronics are widely being used in the field of the manufacturing industry for electronic devices. Researchers worked on the inorganic nanomaterials, which can be involved in PE applications e.g., inorganic nanomaterials-based inks for preparation of printed conductive patterns, electrodes, sensors, thin film transistors (TFTs), and other micro/nanoscale devices.[57] Inorganic NMs have been proven to induce autophagy perturbation in cells. There is a great role of inorganic NMs in modulating autophagy. Guo et al.[58] studied the potential mechanisms for NMs-induced autophagy perturbation and the effect of autophagy perturbation in resolving the destiny of the cells. They also detected the probable roles of inorganic NMs-modulated autophagy for the diagnosis and treatment of various diseases. Inorganic nanomaterials are suitable for advanced theranostics to attain stimuli-responsive drug release as well as synergetic, combinatory, and multimodality therapies. NMs-induced autophagy is a potential mechanism of nanotoxicity. But, it may be a cellular defensive mechanism against nanotoxicity. Furthermore, both autophagy inhibition and activation have been reported as powerful anticancer therapeutic strategies. Autophagy helps in cancer therapy either by hindering cell transformation, enabling existence under severe conditions, and chemotherapy.[58] Inorganic complexes and metal-based nanomaterials enable infectious disease detection in low-resource settings. Markwalter et al. [59] showed the role of inorganic biomarkers and their advantageous properties for infectious disease detection. The metal-based technologies were employed for sample preparation and biomarker isolation from sample matrices. They showed that the inorganic nanomaterial-based probes were exploited for signal generation.[59]

The tuning of the morphology of inorganic materials grown by rapid precipitation during their crystallization from one to three-dimensional (1D to 3D) structures was done by Lai et al.[60] without ant capping agents or templates. The balance between the electrolytic dissociation (α) of the reactants and the supersaturation (S) of the solutions was made to control the morphology. They prepared metal oxides, hydroxides, carbonates, molybdates, oxalates, phosphates, fluorides, and iodate by using this method with varied morphologies.[60] Balasubramanian et al.[61] synthesized various nano-biomaterials and characterized. According to them nanostructured ceramics, cement, and coatings are suitable for orthopedic, dental, and other medical applications. Novel biocompatible ceramic materials with improved biomedical functions are the materials, which would be used for future generation health-related applications. Promising ceramic nanomaterials for biomedical applications are tricalcium phosphate (TCP), calcium phosphate (CaP), hydroxy-apatite (HAP), TCP + HAP, Si substituted HAP, calcium sulfate and carbonate, bioactive glasses, bioactive glass-ceramics, titania-based ceramics, alumina ceramics, zirconia ceramics and ceramic polymer composites.[61] Ghosh et al.[62] prepared and characterized micron sized fluorapatite based bioactive glass-ceramic material for biomedical applications. The studied glass-ceramics had good bioactivity as evidenced by SEM-EDX and chemical analysis, which showed a reaction of the glass-ceramic specimen with the SBF solution and the formation of an apatite layer on its surface.[62] Ghosh et al.[63] also prepared bioactive glass-ceramic coatings of varied microstructure and properties by suitable adjustments of the crystallization parameters for suitable application on biocompatible titanium alloys. The mechanical properties such as microhardness and scratch resistance were affected significantly by the crystallization parameters. It was observed that fluroapatite based glass-ceramic coating showed good bioactivity and thereby, indicating its possible to use in-vivo applications onto the Ti-based biomedical implants.[63] Similar glass-ceramics were applied onto Ti6Al4V substrates by microwave processing and conventional processing techniques by Ghosh et al.[64] Microwave processed coating showed enhanced bioactivity compared to conventional ones. Based on their research work it is expected that promising results may be achieved by using the same glass ceramics on a nano-scale.

Some researchers described new nanotechnology-based methods to deliver DNA and small interfering RNAs into biological systems. Nanotechnology has helped to use novel DNA and RNA delivery systems for gene therapy, which can be used instead of viral vectors. The nonviral vectors can be made of inorganic nanoparticles, liposomes, carbon nanotubes, protein/peptide-based nanoparticles, and nanosized polymeric materials. The advantages of nonviral vectors were identified to be diminished immunity. Furthermore, flexible design permits them to be functionalized and targeted to specific sites in a biological system with low cytotoxicity.[65] Currently, nanotechnology is being used for drug delivery in many areas of medicine. Various nanoparticle platforms are under various stages of preclinical and clinical development including various liposomes, polymeric micelles, dendrimers, quantum dots, gold nanoparticles, and ceramic nanoparticles. Multifunctional nanoparticles are capable of targeting, imaging, and therapy. However, potential ethical issues need anticipated solutions. The recently approved nanoparticle systems have improved the therapeutic index of drugs either by reducing drug toxicity or by enhancing drug efficacy. Future research efforts need to be directed toward finding new methods for nanotoxicology, recognition of biological effects of nanoparticles in the environment, and creation of the bases of

nanobiomonitoring.[66] Wang et al.[67] made pattern technologically important materials directly by using DUV light, 365 nm i-line UV light, 405 nm h-line blue light, and 450 nm visible light. These approaches could be used to further improve direct optical lithography of functional inorganic nanomaterials (DOLFIN) and direct electron-beam lithography of functional inorganic nanomaterials (DELFIN) methods, which would be utilized as an alternative to traditional photopolymer lithography. Therefore, this study helps in the enhancement of nanomanufacturing abilities.[67] Ceramic nanomaterials have immense potential in terms of their low density, hardness, corrosion resistance, and high-temperature resistance properties.[68] It has been seen that ceramic nanomaterials have great prospect in high-temperature applications. Several technologies have been developed for enhancing high-temperature properties of a metal substrate, and more specifically, improving the oxidation resistance. Indeed, there is no doubt that ceramic coatings are an excellent option for enhancing the high-temperature properties of metallic substrates as having been used in combustion elements, hot gas path components, and even for tip nozzles inside automotive engines. However, the fabrication of homogenous, uniform, dense and crack-free coatings is very much challenging and possible only with established and standardized manufacturing process.[68]

Magnetic nanoparticles (MNPs) have been widely studied by researchers for their potential applications in nanomedicine. Apart from this, MNPs are being used for different applications e.g., magnetic imaging, magnetic biosensing, magnetic separation, drug delivery, gene delivery, and hyperthermia therapy. Wu et al.[69] reviewed some emerging techniques in magnetic diagnostics such as magneto-resistive (MR), micro-Hall (μHall) biosensors, magnetic particle spectroscopy, magnetic relaxation switching, and surface-enhanced Raman spectroscopy (SERS)-based bioassays. Recently, MNPs are also used as contrast agents in magnetic resonance imaging and as tracer materials in magnetic particle imaging.[69] Currently, biosensors are being fabricated by using electrochemical methods. High-sensitivity sensors have been developed using nanomaterials for the bio-detection of proteins.[70] The sensors worked on the basis of the interaction of biomaterials with the type of nanostructures. It has been established that one-dimensional (1-D) structures such as nanowires, nanotubes, and nanorods have a high potential for bio-applications. Polymers, carbon, and zinc oxide have been widely used for the fabrication of nanostructures due to their high sensitivity, biocompatibility as well as ease of preparation.[70] Lee et al.[71] proposed a novel material for simple and fast detection of pesticide residue on fruits or vegetables. Gold nanoparticle-coated ZrO_2-nanofiber surface has been proven to be SERS-active for trace detection of pesticide residue. Further, Au NPs/ZrO_2 NFs can be made on a large surface area and are thus promising for flexible and extensible applications.[71] ZrO_2 films were in situ prepared using the anodic passivation of a ZrB_2 ceramic in alkaline solutions. The film obtained was found to significantly improve the corrosion resistance of ZrB_2 Ceramics when dissolved in an 8M NaOH solution. When the film was put in a 0.1 M $H_2C_2O_4$ solution the corrosion resistance was improved by almost one order of magnitude compared with the bare ceramics.[72] Nanotechnology has established itself as a key supporting technology for a wide range of applications, thus becoming very important among the industrial sectors e.g., electronic, healthcare, chemical, cosmetics, composites, and energy. Despite the latest development, the possibility of adverse influences of nanotechnology on the environment, human health, safety, and sustainability is still a challenge.[73]

2.8 Conclusions

The present review provides an overview of a variety of promising inorganic nanomaterials including metallic/nonmetallic inorganic nanomaterials, carbon-based nanomaterials, nanopolymers, dendrimers, quantum dots, ceramic-based nanomaterials, composite inorganic nanomaterials, magnetic nanomaterials, and other currently developed inorganic nanomaterials and their role for possible futuristic applications for next generation. It is quite evident that there is a great prospect for inorganic nanomaterials in radiotherapy, chemotherapy sensitization, biomedical, pharmacology, medicine, sensor, energy applications, and industrial applications. However, further research on inorganic nanomaterial is still required as many ambiguities have to be cleared in near future before exploring the benefits of these unique materials in actual applications.

Acknowledgments

The present author is thankful to Director, CSIR-Central Glass and Ceramic Research Institute for his permission to publish this review paper.

References

1. Wang H, Liang X, Wang J, Jiao S, Xue D. Multifunctional inorganic nanomaterials for energy applications. *Nanoscale* 2020;**12**:14–42.
2. Huang H-C, Barua S, Sharma G, Dey SK, Rege K. Inorganic nanoparticles for cancer imaging and therapy. *J Contr Release* 2011;**155**:344–57.
3. Parvanian S, Mostafavi SM, Aghashiri M. Multifunctional nanoparticle developments in cancer diagnosis and treatment. *Sens Bio-Sens Res.* 2017;**13**:81–7.
4. Pugazhendhi A, Edison TNJI, Karuppusamy I, Kathirvel B. Inorganic nanoparticles: a potential cancer therapy for human welfare. *Int J Pharm* 2018;**539**:104–11.
5. Chen Y-C, Huang X-C, Luo Y-L, Chang Y-C, Hsieh Y-Z, Hsu H-Y. Non-metallic nanomaterials in cancer theranostics: a review of silica- and carbon-based drug delivery systems. *Sci Technol Adv Mater* 2013;**14**:044407, 1–23.
6. Liu Y, Yu Q, Chang J, Wu C. Nanomaterials: from 0D to 3D for tumor therapy and tissue regeneration. *Nanoscale* 2019;**11**:13678–708.
7. Su S, Wu W, Gao J, Lu J, Fan C. Nanomaterials-based sensors for applications in environmental monitoring. *J Mater Chem* 2012;**22**:18101–10.
8. Ha S-W, Weiss D, Weitzmann MN, Beck Jr GR. Applications of silica-based nanomaterials in dental and skeletal biology. In: *Nanomaterials in clinical dentistry*. 2nd ed. Micro and Nano Technologies; 2019. p. 77–112.
9. Ma Y, Kuang L, He X, Bai W, Ding Y, Zhang Z, Zhao Y, Chai Z. Effects of rare earth oxide nanoparticles on root elongation of plants. *Chemosphere* 2010;**78**:273–9.
10. Charalampides G, Vatalis KI, Apostoplos B, Ploutarch-Nikolas B. Rare earth elements: industrial applications and economic dependency of europe. *Procedia Econ Finance* 2015;**24**:126–35.
11. Zhang C, Liu Z, Zhang Y, Ma L, Song E, Song Y. "Iron free" zinc oxide nanoparticles with ion-leaking properties disrupt intracellular ROS and iron homeostasis to induce ferroptosis. *Cell Death Dis* 2020;**11**:183–98.
12. Cao C-Y, Qu J, Yan W-S, Zhu J-F, Wu Z-Y, Song W-G. Low-cost synthesis of flowerlike α-Fe2O3 nanostructures for heavy metal ion removal: adsorption property and mechanism. *Langmuir* 2012;**28**:4573–9.
13. Liang J, Deng Z, Jiang X, Li F, Li Y. Photoluminescence of tetragonal ZrO2 nanoparticles synthesized by microwave irradiation. *Inorg Chem* 2002;**41**:3602–4.
14. Malhotra N, Chen J-R, Sarasamma S, Audira G, Siregar P, Liang S-T, Lai Y-H, Lin G-M, Ger T-R, Hsiao C-D. Ecotoxicity assessment of Fe_3O_4 magnetic nanoparticle exposure in adult zebrafish at an environmental pertinent concentration by behavioral and biochemical testing. *Nanomaterials* 2019;**9**:873–97.

15. Yang Q, Zhu W, Lu Z, Li D, Wang Z, Wang F. Rapid fabrication of high-performance CaO-based integral ceramic mould by stereolithography and non-aqueous gelcasting. *Materials* 2019;**12**:934–48.
16. Rodríguez-González V, Obregón S, Patrón-Soberano OA, Terashima C, Fujishima A. An approach to the photocatalytic mechanism in the TiO_2-nanomaterials microorganism interface for the control of infectious processes. *Appl Catal B Environ* 2020;**270**:118853. 1-21.
17. Hoseinpour V, Ghaemi N. Green synthesis of manganese nanoparticles: applications and future perspective–a review. *J Photochem Photobiol B Biol* 2018;**189**:234–43.
18. Zhen Z, Xie J. Development of manganese-based nanoparticles as contrast probes for magnetic resonance imaging. *Theranostics* 2012;**2**:45–54.
19. Kim M, Lee C, Ko SM, Nam J-M. Metal alloy hybrid nanoparticles with enhanced catalytic activities in fuel cell applications. *J Solid State Chem* 2019;**270**:295–303.
20. Nazeruddin GM, Prasad RN, Shaikh YI, Shaikh AA. Synergetic effect of Ag-Cu bimetallic nanoparticles on antimicrobial activity. *Der Pharm Lett* 2014;**6**:129–36.
21. Gangopadhyay P. Metallic alloy nanoparticles and metal-semiconductor nanomaterials. *NanoWorld J* 2018;**4**:31–42.
22. Tabassum H, Mahmood A, Zhu B, Liang Z, Zhong R, Guo S, Zou R. Recent advances in confining metal-based nanoparticles into carbon nanotubes for electrochemical energy conversion and storage devices. *Energy Environ Sci* 2019;**12**:2924–56.
23. Rehbock C, Jakobi J, Gamrad L, van der Meer S, Tiedemann D, Taylor U, Kues W, Rath D, Barcikowski S. Current state of laser synthesis of metal and alloy nanoparticles as ligand-free reference materials for nanotoxicological assays. *Beilstein J Nanotechnol* 2014;**5**:1523–41.
24. Klebowski B, Depciuch J, Parlińska-Wojtan M, Baran J. Applications of noble metal-based nanoparticles in medicine. *Int J Mol Sci* 2018;**19**:4031–48.
25. Luo Y-H, Chang LW, Lin P. Metal-based nanoparticles and the immune system: activation, inflammation, and potential applications. *BioMed Res Int* 2015;**2015**:1–12. Article ID 143720.
26. Islam S-u, Butola BS, Mohammad F. Silver nanomaterials as future colorants and potential antimicrobial agents for natural and synthetic textile materials. *RSC Adv* 2016;**6**:44232–47.
27. Pulit-Prociak J, Banach M. Silver nanoparticles-a material of the future…? *Open Chem* 2016;**14**:76–91.
28. Cao M, Li J, Tang J, Chen C, Zhao Y. Gold nanomaterials in consumer cosmetics nanoproducts: analyses, characterization, and dermal safety assessment. *Small* 2016;**12**:5488–96.
29. Baye AF, Appiah-Ntiamoah R, Kim H. Synergism of transition metal (Co, Ni, Fe, Mn) nanoparticles and "active support" Fe3O4@C for catalytic reduction of 4-nitrophenol. *Sci Total Environ* 2020;**712**:135492.
30. Loza K, Heggen M, Epple M. Synthesis, structure, properties, and applications of bimetallic nanoparticles of noble metals. *Adv Funct Mater* 2020;**30**:1909260. 1-14.
31. Powar NS, Patel VJ, Pagare PK, Pandav RS. Cu nanoparticle: synthesis, characterization and application. *Chemical Methodol* 2019;**3**:457–80.
32. Cha C, Shin SR, Annabi N, Dokmeci MR, Khademhosseini A. Carbon-based nanomaterials: multifunctional materials for biomedical engineering. *ACS Nano* 2013;**7**:2891–7.
33. Mauter MS, Elimelech M. Environmental applications of carbon-based nanomaterials. *Environ Sci Technol* 2008;**42**:5843–59.
34. Xin Q, Shah H, Nawaz A, Xie W, Akram MZ, Batool A, Jan LTSU, Boddula R, Guo B, Liu Q, Gong JR. Antibacterial carbon-based nanomaterials. *Adv Mater* 2018;**31**(45):e1804838.
35. Shen K, Chen X, Chen J, Li Y. Development of MOF-derived carbon-based nanomaterials for efficient catalysis. *ACS Catal* 2016;**6**:5887–903.
36. Yan Q-L, Gozin M, Zhao F-Q, Cohen A, Pang S-P. Highly energetic compositions based on functionalized carbon nanomaterials. *Nanoscale* 2016;**8**:4799–851.
37. Vasile C. Chapter 1 - polymeric nanomaterials: recent developments, properties and medical applications. In: *Polymeric nanomaterials in nanotherapeutics, micro and nano technologies*; 2019. p. 1–66.
38. Li C, Bai H, Shi G. Conducting polymer nanomaterials: electrosynthesis and applications. *Chem Soc Rev* 2009;**38**:2397–409.
39. Beg S, Samad A, Alam MI, Nazish I. Dendrimers as novel systems for delivery of neuropharmaceuticals to the brain. *CNS Neurol Disord - Drug Targets* 2011;**10**:576–88.

40. Fu F-F, Zhou B-Q, Ouyang Z-J, Wu Y-L, Zhu J-Y, Shen M-W, Xia J-D, Shi X-Y. Multifunctional cholesterol-modified dendrimers for targeted drug delivery to cancer cells expressing folate receptors. *Chin J Polym Sci* 2019;**37**:129–35.
41. Xu Y, Wang X, Zhang WL, Lv F, Guo S. Recent progress in two-dimensional inorganic quantum dots. *Chem Soc Rev* 2018;**47**:586–625.
42. Fan J, shao M, lai L, liu Y, Xie Z. Inhibition of autophagy contributes to the toxicity of cadmium telluride quantum dots in *Saccharomyces cerevisiae*. *Int J Nanomed* 2016;**11**:3371–83.
43. Beaulac R, Archer PI, Ochsenbein ST, Gamelin DR. Mn2+-doped CdSe quantum dots: new inorganic materials for spin-electronics and spin-photonics. *Adv Funct Mater* 2008;**18**:3873–91.
44. Leng M, Yang Y, Zeng K, Chen Z, Tan Z, Li S, L J, Xu B, D. L, Hautzinger MP, Fu Y, Zhai T, Xu L, Niu G, Jin S, Tang J. All-inorganic bismuth-based perovskite quantum dots with bright blue photoluminescence and excellent stability. *Adv Funct Mater* 2017;**1704446**:1–11.
45. Liu C, Zhou X, Chen S, Zhao X, Dai S, Xu B. Hydrophobic Cu_2O quantum dots enabled by surfactant modification as top hole-transport materials for efficient perovskite solar cells. *Adv Sci* 2019;**6**:1801169, 1–9.
46. Maguire CM, Lavin M, Doyle M, Byrne M, Prina-Mello A, O'Donnell JS, Volkov Y. The anticoagulant properties of cadmium telluride quantum dots. *J Interdiscip Nanomed* 2018;**3**:16–28.
47. Xu Y, Zhu J-W, Fang J-B, Li X, Yu M, Long Y-Z. Electrospun high-thermal-resistant inorganic composite nonwoven as lithium-ion battery separator. *J Nanomate* 2020;**2020**:1–10. Article ID 3879040.
48. Wu J, Zhang G, Liu J, Gao H, Song C, Du H, Zhang L, Gong Z, LÜ Y. Synthesis, characteristics, and antibacterial activity of a rare-earth samarium/silver/titanium dioxide inorganic nanomaterials. *J Rare Earths* 2014;**32**:727–32.
49. Alizadeh-Osgouei M, Li Y, Wen C. A comprehensive review of biodegradable synthetic polymer-ceramic composites and their manufacture for biomedical applications. *Bioact Mater* 2019;**4**:22–36.
50. Atif M, Iqbal S, Fakhar-E-Alam M, Ismail M, Mansoor Q, Mughal L, Aziz MH, Hanif A, Farooq WA. Manganese-doped cerium oxide nanocomposite induced photodynamic therapy in MCF-7 cancer cells and antibacterial activity. *BioMed Res Int* 2019;**2019**:1–13. Article ID 7156828.
51. Zhang Q, Zhang L, Wu W, Xiao H. Methods and applications of nanocellulose loaded with inorganic nanomaterials: a review. *Carbohydr Polym* 2020;**229**:115454.
52. Ionescu E, Linck C, Fasel C, Müller M, Kleebe H–J, Ried R. Polymer-derived SiOC/ZrO2 ceramic nanocomposites with excellent high-temperature stability. *J Am Ceram Soc* 2009;**93**:241–50.
53. Luo Y, Lin D, Zheng Y, Feng X, Chen Q, Zhang K, Wang X, Jiang L. MnO2 nanoparticles encapsuled in spheres of Ce-Mn solid solution: efficient catalyst and good water tolerance for low-temperature toluene oxidation. *Appl Surf Sci* 2019;**504**:144481.
54. Tan WK, Yokoi A, Kawamura G, Matsuda A, Muto H. PMMA-ITO composite formation via electrostatic assembly method for infra-red filtering. *Nanomaterials* 2019;**9**:886. 1-9.
55. Wen T, Krishnan KM. Magnetic properties of Aucore-Coshell nanoparticles. *J Appl Phys* 2011;**109**:07B515-1–3.
56. Dahl M, Liu Y, Yin Y. Composite titanium dioxide nanomaterials. *Chem Rev* 2014;**114**:9853–89.
57. Wu W. Inorganic nanomaterials for printed electronics: a review. *Nanoscale* 2017;**9**:7342–72.
58. Guo L, He N, Zhao Y, Liu T, Deng Y. Autophagy modulated by inorganic nanomaterials. *Theranostics* 2020;**10**:3206–22.
59. Markwalter CF, Kantor AG, Moore CP, Richardson KA, Wright DW. Inorganic complexes and metal-based nanomaterials for infectious disease diagnostics. *Chem Rev* 2019;**119**:1456–518.
60. Lai W-H, Wang Y-X, Wang Y, Wu M, Wang J-Z, Liu H-K, Chou S-L, Chen J, Dou S-X. Morphology tuning of inorganic nanomaterials grown by precipitation through control of electrolytic dissociation and supersaturation. *Nat Chem* 2019;**11**:695–701.
61. Balasubramanian S, Gurumurthy B, Balasubramanian A. Biomedical applications of ceramic nanomaterials: a review. *Int J Pharmaceut Sci Res* 2017;**8**:4950–9.
62. Ghosh S, Dandapat N, Balla VK. Preparation and in vitro characterization of fluroapatite based bioactive glass-ceramics for biomedical applications. *Mater Today Proc* 2015;**2**:1326–31.
63. Sanyal S, Shukla M, Dandapat N, Ghosh S. In vitro evaluation of bioactive glass ceramic coating for application on Ti6Al4V based biomedical implants. *J Non-Cryst Solids* 2018;**500**:22–9.
64. Ghosh S, Nandi Majumdar S, Shukla M. Enhanced bioactive glass-ceramic coating on Ti6Al4V substrate by microwave processing technique for biomedical applications. *Mater Lett* 2018;**218**:60–6.

65. Riley MK, Vermerris W. Recent advances in nanomaterials for gene delivery-a review. *Nanomaterials* 2017;**7**:94–113.
66. I Moreno-Vega A-, Gómez-Quintero T, Nuñez-Anita R-E, Acosta-Torres L-S, Castaño V. Polymeric and ceramic nanoparticles in biomedical applications. *J Nanotechn* 2012;**2012**:10 pages. Article ID 936041.
67. Wang Y, Pan J-A, Wu H, Talapin DV. Direct wavelength-selective optical and electron-beam lithography of functional inorganic nanomaterials. *ACS Nano* 2019;**13**:13917–31.
68. Gamero M. Ceramic nanomaterials for high temperature applications. *Res Develop Mater Sci* 2017;**2**:126–30.
69. Wu K, Su D, Liu J, Saha R, Wang J-P. Magnetic nanoparticles in nanomedicine: a review of recent advances. *Nanotechnology* 2019;**30**:502003.
70. Kumar A, Jung MS, Ji T. Protein biosensors based on polymer nanowires, carbon nanotubes and zinc oxide nanorods. *Sensors* 2011;**11**:5087–111.
71. Lee H, Liao J-D, Sivashanmugan K, Liu BH, Fu W-e, Chen C-C, Chen GD, Juang Y-D. Gold nanoparticle-coated ZrO_2-nanofiber surface as a SERS-active substrate for trace detection of pesticide residue. *Nanomaterials* 2018;**8**:402–13.
72. Yang H, Zhang J, Li J, Shen Q, Zhang L. In situ preparation and corrosion resistance of a ZrO_2 film on a ZrB_2 ceramic. *Coatings* 2019;**9**:455–66.
73. Santos CSC, Gabriel B, Blanchy M, Menes O, García D, Blanco M, Arconada N, Neto V. Industrial applications of nanoparticles-a prospective overview. *Mater Today Proc* 2015;**2**:456–65.

This page intentionally left blank

CHAPTER

13

Two-dimensional layered materials for efficient photodetection

Pius Augustine[1,2]

[1]Materials Research Laboratory, Department of Physics, Sacred Heart College (Autonomous), Thevara, Kochi, India; [2]Materials Research Centre, Indian Institute of Science, Bangalore, Karnataka, India

1. Introduction

Photodetectors (PDs) are optoelectronic devices that convert the optical signal into an equivalent amount of detectable electrical signal through light-matter interaction. Significant research is being carried out in the field of photodetectors across the globe due to their utility in various applications like imaging,[1] optical communication[2] solar energy harvesting,[3] photoelectric memory,[4] etc. A good photodetector should display a high sensitivity at the operating wavelengths, high fidelity, fast response, and above all should be cost-effective.

Traditionally three-dimensional (3D) bulk material systems like GaN, Si, Ge, InGaAs, etc., have been used for the detection of a wide spectrum of electromagnetic radiations. Even though the process of photodetection using 3D material technology is well established, it experiences various challenges in improving the precision and quality of detection required due to low absorption coefficient, poor carrier mobility, and defective interface. Cost is another concern in 3D bulk systems. However, the recent research on two-dimensional (2D)-layered materials revealed characteristics like enhanced carrier mobility[5] pronounced quantum confinement effect,[6] outstanding mechanical properties,[7] excellent compatiabilites[8] dangling-bond free surface,[9] etc., and hence can be developed into a promising new generation photodetection technology. The scientific research witnessed this novel material science on 2D layered materials after the groundbreaking discovery of graphene (Gr) by Novoselov and Geim, which fetched them Nobel Prize in Physics. 2D layered materials (2DLM) encompass chalcogenides, nitrides, halides, 2DLM based heterostructures, and composites.[10–15] The

Applications of Multifunctional Nanomaterials
https://doi.org/10.1016/B978-0-12-820557-0.00015-1

exotic material characteristics exhibited by nanolayered materials became a matter of inquiry for fundamental research as well as engineering applications. 2D layered nanosystems include materials with bandgap ranging from 0 to 6 eV and hence can be utilized for the photodetection of a wide range of electromagnetic spectrum and replace the conventional 3D bulk materials in photodetection applications.

Despite the significant advance in material processing, various hurdles are being faced by the researchers in realizing device quality 2D crystal systems for upscaling the technology and achieving improved device performance. The quality and crystallinity of the 2D nano-thin films play a significant role in the photoresponse exhibited by the nanosystems and the performance of the device. Controlling the crystal orientation, thickness, and morphology, etc., can be tuned by optimizing the thin film growth process to maximize the photoresponsivity and reliability in detection. Pulsed laser deposition is an excellent thin film growth process for realizing quality nano-thin films of TMDC compared to other conventional techniques like micromechanical exfoliation, chemical vapor deposition, molecular beam epitaxy (MBE), liquid-phase exfoliation, etc. Even though PLD is a versatile technology for the growth of quality TMDC nanofilms for photodetection, a detailed review or analysis of the PLD technique for TMDC is sparse.

This chapter will present a broad overview of the classification of 2D-layered material, various possible mechanisms in photodetection, the figures of merit that determine the quality of photodetectors, the pulsed laser deposition as a versatile thin-film technology to realize nano-thin films, and analysis of a few results on promising photodetector nano system MoS_2 based nano heterostructures, which were realized through pulsed laser ablation, for efficient photodetection application.

2. Classification of 2D-layered material

2D-layered materials is broadly classified based on the transport property displayed by the charge carriers, which is also a yardstick for the optoelectronic prospects of the system. The electrical or electronic characteristics or transport properties of a material system can be well described by analyzing the band structure of the material. The electronic band structure can proclaim the functional characteristics of the nano-thin films viz: metallic, semiconducting, insulating, or even superconducting. In 2D semiconducting systems, the electron confinement can be directly related to the band structure, which distinguishes the materials with different photoresponsivity as well. Also, a better understanding of the modulations in the band structure of the semiconducting 2D layers will enable the researchers to design quality heterostructures for efficient photodetection. A general classification of various types of 2D-layered photodetectors along with a few examples is given for reference.

1. Metallic 2DLMs, which show negligible bandgap and high electrical conductivity.
2. Dirac Semimetals—for example, graphene, which is one atom thick and displays excellent carrier mobility of 20,000 $cm^2 V^{-1}S^{-}$,[116] is an ideal candidate for photosensitive

material.[17–19] One of the major drawbacks of pristine graphene as photosensitive material is the reduced photoresponsivity. However, an improved photoresponsivity ~ 1000 A/W could be achieved in graphene through a carrier tunneling mechanism.[18] In spite of the exposition of unparalleled properties by graphene, the gapless energy bandgap of graphene limits its suitability in a variety of applications. This triggered the search for 2DLMs with a sizable energy band gap which leads to the discovery of conventional van der Waal's materials called TMDCs which are highly abundant and hence cost-effective and exhibit stable and eco-friendly characteristics.

3. Semiconducting 2DLMs

As the name suggests, they possess moderate electrical conductivity due to reduced energy bandgap (below 3 eV) but comparatively lesser than metallic 2DLMs. In the periodic table of elements, group number IV—XI is named as transition metals or transition elements, based on the typical chemistry exhibited by these materials. In general, 2DLMs exhibit relatively strong intralayer covalent interaction and very weak interlayer van der Waals interactions and the material properties exhibited by them are greatly layer dependent.

a. Transition metal dichalcogenide (TMDC): TMDC unit cell is three atoms thick and consists of a layer of transition metal atoms sandwiched between two layers of chalcogen atoms. This three atoms thick unit cell in layer form is known as one layer of the material. Excellent modulations in semiconducting response exhibited by many of the TMDCs in nano form have been explored for a variety of optoelectronic applications, which is described in the table given at the end of the chapter.

The prominent members of this group include group VIB dichalcogenides like MoS_2, WS_2, $MoSe_2$, WSe_2, $MoTe_2$, WTe_2 with a moderate bandgap of 1–2 eV. Of these, MoS_2 is a highly explored system, which exhibits layer dependant bandgap and shows an indirect-to-direct bandgap transition when thinned from the bulk to ML to a single layer (~1.3–1.9 eV)[20] and is found to be an excellent material system for photoelectric detection. Record high responsivity 1.4×10^5 A W^{-1} and detectivity of 9×10^{15} Jones (several orders of magnitude higher than commercial Si and Ge PDs) have been reported in MoS_2-based PDs.[21,22]

b. Semiconducting transition metal trichalcogenide (TMTC): It exhibits general formula MX_3 and M_2X_3, where M is a transition metal and X is a chalcogen.

Eg.for MX_3 TMTCs for optoelectronic applications - TiS_3, $TiSe_3$, ZrS_3, $ZrSe_3$, HfS_3 and $HfSe_3$

Eg.for M_2X_3 TMTCs - Pd_2Se_3, Co_2Se_3 and Ni_2Se_3.

c. Group IIIA chalcogenides - GaS, GaSe, GaTe, InSe, In_2Se_3

d. Group IVA chalcogenides - SiS, SiSe, Si_2Te_3, GeS, GeSe, etc., and

e. Group VA chalcogenides-phosphorene oxide, antimonene oxides, Bi_2S_3, SbO, etc., also exhibit excellent photodetection characteristics. InSe and GaSe have been reported to exhibit extremely high photo-responsivity of 5000 A $W.^{-1}$[23,24]

3. Mechanism of photoelectric detection

Photodetection is a conversion of an optical signal or information into an electrical signal and hence is a kind of energy conversion. The spectral range of detection by a device depends on the bandgap of the photosensitive material, and the generated photocurrent/photovoltage depends on the photodetector architecture. The prominent mechanisms in the photodetection process could be the photoconductive effect, photovoltaic effect, photogating effect, photothermoelectric effect, and bolometric effect. Each one of these mechanisms will have some advantage over the other types in a particular situation and accordingly, it would be utilized in the device architecture.

3.1 Photoconductive effect

The photoconductive effect utilizes the variation in electrical conductivity to the change in the number of the electrical carrier when e-m radiation impinges on the material.[25] The energy of the light photons will be absorbed by the electrons in the valence band and get excited to the conduction band, which modulate the equilibrium charge carriers in the material. If a potential difference is applied across the material, charge carriers can be separated and driven in the external circuit. It is a kind of photoelectric effect. So, there is a threshold wavelength which is decided by the bandgap of the material, above which no photoconductive effect or photodetection, can be observed in the material. The basic design of a photoconductor consists of a semiconductor photosensitive material with two Ohmic metal contacts at the opposite ends. Since an external voltage is needed for getting appreciable photodetection, a large dark current will be generated in the device which distorts the performance of the device working in photoconductive mode.[26,27]

3.2 Photovoltaic effect

It is a kind of spontaneous generation photocurrent/photovoltage under the illumination of light, which takes place across the photosensitive heterojunction. The built-in electric field available in the heterojunction will be the driving force for the photocarriers to move in the external circuit and to constitute photocurrent. The photovoltaic effect is also a kind of photoelectric effect and hence a threshold frequency of the incident light is inevitable for the process to take place. However, there are recent developments in photovoltaics, which confirm the possibility of photovoltaics at lower frequencies through interband excitation.[28] Also, self-powered photodetectors are possible in devices operating in photovoltaic mode, which facilitate energy saving and reduced dark current during its operation.

3.3 Photogating effect

The photogating effect arises when photocarriers are captured by localized electron/hole traps created in the system due to doping, and in a way, external photocurrent can be modulated.[29] Generally, those photodetectors which work based on the photogating effect will exhibit reasonably higher photo gain due to the extended life time of the generated

photocarriers. However, the increased photo gain would adversely affect the response speed of the device due to the de-trapping process which takes place at a slower pace.

3.4 Photothermoelectric effect

It arises due to the temperature gradient that is created across the detector device under photo illumination, which will drive the photocurrent through the circuit.[30] The thermoelectric response is developed either due to the uneven or localized light illumination or due to the difference in the thermoelectric coefficients of the two-component materials which participate in the heterojunction. Generally, the thermoelectric current so produced will flow between the hot and cold junctions and it will be significantly low to be used for any practical photodetection applications.

3.5 Bolometric effect

It is due to the heating of the photosensitive material when irradiated with heat radiation, preferably in the infra-red region of the electromagnetic spectrum. In the bolometric effect, under the illumination of light, the variation in the mobility of the charge carriers will induce a change in the electrical conductivity of the photosensitive material.[31] With an increase in temperature, the amplitude of the vibration of the atoms will increase which will act as scattering centers for the moving electrons. Therefore, the temperature coefficient of the photosensitive material decide the bolometric response in a photosensitive material under photo illumination.

4. Figures of merits for photodetectors

Semiconductor-based photodetectors are being used for a variety of applications. Each photosensitive material will have certain merits and a few demerits, which depend upon the fabrication processes, stability, and performance. The quality of the photodetector is quantified in terms of certain parameters known as figures of merit of the photodetector, to assess the utility of the device for applications. Important figures of merits in photodetection are outlined in brief.

4.1 External quantum efficiency (EQE or η)

It is defined as the ratio of the rate (r_e) of electrons collected at the detector terminals to the rate (r_p) of photons incident on the device ($\eta = r_e/r_p$).

η—depends on 3 parameters.

1. Lesser the light reflected, the better will be the detection.
2. In the expression for variation in the intensity of light with distance inside the material $I(x) = I_0e^{-\alpha x}$, if the product αx is much larger than unity, η will be improved. (α—absorption coefficient).
3. η depends on the photon wavelength.

Efficiency can also be expressed as

1. $\eta = I_{ph}/\varphi\ I_{ph}$—photon current and φ—photon flux

The flux of photon depends upon the power of the incident radiation (P_{optic}) and its energy (hν)

$$\varphi = (P_{optic} \times e)/h\nu$$

2. $\eta = R_\lambda hc/e\lambda$

Where R_λ—responsivity, e—elementary charge, h—Planck's constant, c—speed of incident light, and λ—wavelength of the incident light.

EQE is a direct indication of the optical gain of the device.[32,33]

4.2 Responsivity (R_λ)

Responsivity is a quantitative measure of the detector quality which quantifies the output signal (photocurrent) generated per input signal power. It depends on the speed of diffusion of the photogenerated carriers through the material to reach the electrodes and produce photocurrent i.e., it depends on the diffusion coefficient and mobility of electrons and holes. A higher photoresponsivity is an indication of the ability of the device to detect even the weak input light signal.[33,34]

Generally, responsivity exhibited by the photodetector increases monotonically with increasing the wavelength of the light until it reaches the cut off wavelength, above which energy of the radiation will be insufficient to cause photoexcitation. Also, the light absorption coefficient of the material is a function of the wavelength which increases with wavelength. So, a trade-off between wavelength and absorption coefficient of the material plays a role in photodetection. A general expression for the responsivity of a photodetector is expressed as. $R = \frac{\eta q\lambda}{hc}\frac{1}{\sqrt{1+\omega^2\tau^2}}G$

Where η is quantum efficiency, q is the electronic charge, λ—wavelength of the incident light, h—Planck's constant, c—speed of light in vacuum, ω—electrical modulation frequency, τ—response time, G—photoconductive gain. At low modulation frequency, the above expression may be given as. $R = \frac{\eta q\lambda}{hc}G$

Responsivity may also be defined as $R_\lambda = I_\lambda/(P_\lambda S)$, where I_λ is the photocurrent ($I_{llumination}$—I_{dark}), P_λ is the light power or intensity of the incident light, S is the effective illuminated area of the device and λ is the wavelength of the incident light. It is measured in A/W.[35,36]

4.3 Response/recovery time

Response time is a measure of the quickness in response when the device is turned on or off. It is measured as the time taken for the signal to rise from 10% to 90% when the incident light is turned on (rising edge) or time is taken for the current to decrease from 90% to 10% when the light switched off (falling edge).[37,38]

5. Noise in detectors

Noise is any undesired signal which weakens the signal. The output photocurrent due to the signal will be fluctuated or superseded by the current or voltage generated due to noise. Fluctuations arise due to noise is generated externally or internally and the corresponding variations in the V and I will be statistical in nature. Also, the noise will generate a current in the circuit even in the absence of the light signal. Generally, three different types of noise sources are encountered in the photodetection, which would constitute current in the circuit.

They are (1) dark noise, (2) shot noise, and (3) Johnson or Nyquist noise.

Dark current or dark noise current, as the name indicates, is the constant response exhibited by a photodetector due to thermal generation of e-h pairs when it is not actively being exposed to light.

Shot noise (quantum noise) arises due to the randomness in the arrival of light quanta and exhibits the variation as a statistical response which may be well expressed as a Poisson distribution. This statistical random fluctuation of the input light signal cannot be eliminated, and hence identical randomness in the generation e-h pairs and the current so produced is expected.

The third one is the thermal Noise in Photodetectors also known as Johnson noise or Nyquist noise. It is generated in the detector due to the thermal agitation of the electrons in the light detecting material. The constantly moving electrons collide with each other and with the atoms of the material and the motion between two collisions represents a tiny current. These random fluctuations at short intervals constitute Johnson or Nyquist noise.

5.1 Signal to noise ratio (SNR)

Noise in detectors cannot be eliminated, and will constitute a dark current (nA or pA) in the detector even in the absence of the input light. For the detector to be able to differentiate between the random noise and the input signal, the power of the light signal should be greater than that of the noise signal.

SNR = Signal power/noise power.

5.2 Noise equivalent power (NEP) and detectivity (D)

It is an important figure of merit for a detector and is defined as the rms value of incident power which can generate a signal current of voltage whose rms value is equal to the rms value of current or voltage due to noise effects.

Or it is the minimum detectable optical power of bandwidth 1 Hz, at which SNR in the detector is unity and can be measured as the ratio of current generated due to noise to the responsivity of the device.

i.e., $NEP = I_{noise}/R$[33,39]

For a photodetector, NEP is specified at a particular wavelength and temperature. Bandwidth of the incident radiation for the measurement of NEP is generally taken as 1 Hz.

Noise power within a bandwidth of Δf is proportional to Δf itself. Since current or voltage is proportional to the square root of power, the noise current is proportional to $(\Delta f)^{1/2}$ and the unit of NEP is Watts/$(Hz)^{1/2}$.

NEP may be measured through the following relation.

$NEP = [hc(2eI_d)^{1/2}]/\eta e\lambda$.

I_d—dark current η—efficiency and the rest are standard parameters.

5.3 Detectivity (D)

Detectivity is defined as the inverse of NEP and specific detectivity (D*) is the inverse of NEP normalized to the unit area of the detector. It is useful for comparing the quality of different photodetectors made up of different materials and having different geometries. A better photodetector will exhibit higher detectivity.

$Detectivity\ (D) = 1/NEP = \eta e\lambda/[hc(2eI_d)^{1/2}]$

Both NEP and detectivity depend on the active area of the photodetector and hence varies as the defining area is changing. So, an area independent parameter called specific detectivity (D*) is defined to compare the sensitivity of the materials.

5.4 Specific detectivity (D*)

$D^* = (A\ B)^{1/2}/NEP$. A—is device area and B—electrical bandwidth.

It may also be expressed as $D^* = R\ (A\ B)^{1/2}/i_n$. where i_n is noise current.

Specific detectivity is expressed in the unit (cm $Hz^{1/2}\ W^{-1}$) also known as Jones.

6. Photodetector classification

1. Powered or self-powered PDs: It is based on whether the detector needs an external power supply to drive generated photocurrent in the external circuit or not.
2. Broadband or narrow band PDs: Based on the range of wavelengths that can be detected by the PD.
3. Organic or inorganic PDs: based on the composition of photosensitive material used in PD.
4. MSM PDs and HJ PDs: based on device structure.

7. Photodetector—device architecture

7.1 Metal–semiconductor–metal (MSM) PDs

Two metal electrodes are given at the ends of photosensitive channel material to form a planar geometry, which facilitates easy flow of photocarriers through the channel material. A large photocurrent, higher photocurrent gain, enhanced responsivity, and high efficiency

are expected in MSM architecture.[40] Notable drawbacks with MSM architecture are high energy consumption due to large dark current and low on/off ratio.

7.2 Heterojunction photodetectors (HJPDs)

Heterojunction photodetectors use photosensitive heterostructures composed of two materials having different Fermi levels. Based on the types of components, HJPDs can be divided into Schottky, p-n, and homotype junction PDs. Schottky junction PD uses semiconductor-metal junctions. In p-n junction type, p-type and n-type materials form junctions and in homotype junction PDs, semiconductors with similar carrier types will participate in the junction formation.[41] The dark current due to thermal excitation will be considerably suppressed in heterojunction due to the formation of the depletion barrier. Also, it exhibits reduced energy consumption, high on/off ratio, high detectivity, and fast response. However, it generally exhibits low photoresponsivity.

8. Pulsed laser deposition

Historical development of PLD goes back to mid 1960s when Smith and Turner used a ruby laser to deposit thin films. Since laser technology was in its nascent stage, the development of PLD in thin-film fabrication was quite slow in the initial years compared to other deposition techniques like MBE (low energy ≈ 0.1 eV), which was good to produce better quality thin films. However, the following decades witnessed the fast advances in laser technology, which made available lasers with a higher repetition rate than early ruby lasers, and thin-film deposition using PLD moved to the forefront. Lasers with highly reliable and very short optical pulses enabled the congruent evaporation of the target and stoichiometric deposition of multicomponent thin films. Further development in laser technology brought out high efficient harmonic generators and excimer lasers (10 ns pulses) delivering powerful UV radiation with less absorption depth, which started a new era of nonthermal and highly efficient laser ablation. PLD systems generally use focused pulsed excimer or Nd: YAG laser to ablate the target. Pulsed laser deposition (PLD) is a superior thin film deposition technique originally designed for multi-component materials. A focused high power pulsed laser beam is used for the ablation of solid target material and deposition of a stoichiometric thin film on the substrate. Target (anything! metal, semiconductors, etc.) and substrates are seated in a highly evacuated chamber having a narrow window for the laser beam to fall on the rotating target. Since the laser is used as an external clean energy source and no filament is involved, deposition can be carried out in both inert and reactive background gases. Rapid evaporation of the solid target results from the absorption of the electromagnetic laser beam and subsequent energy transfer to the phonons of the target leads to a high heating rate of 10^8 K/s on the target surface. The temperature developed is so high that, congruent evaporation of the target will be established. Highly excited and ionized evaporated species form a well-directed, transient ($\sim$ns time-scales), and highly luminous plasma plume normal to the target surface.

Compared to other deposition techniques like sputtering, PLD needs only a small target. Multilayered films of different materials can be achieved by sequential ablation of assorted targets. The target carousel, housing several targets of different materials, enables multilayer film deposition without breaking the vacuum when changing the materials. Since film thickness is directly related to the number of pulses used to ablate, even an atomic monolayer can be realized by fine control of laser frequency (repetition rate). Film thickness can be controlled in real-time even, by simply turning the laser on and off. Also, the stoichiometry of the multicomponent system can be obtained in PLD deposition at comparatively lower substrate temperature due to the excessive heating rate of the ablated species, which is a favorable condition for the semiconductor industry as it avoids possible thermal degradation. The properties of the film are affected by a number of parameters such as laser fluence, background gas pressure, substrate temperature, etc., which allows an operator to manipulate the film properties for various applications by tuning the variables.

8.1 PLD grown 2DLM photodetectors (PDs)

Many researchers across the globe have successfully fabricated both MSM PDs and heterojunction photodetectors of 2D layered materials using pulsed laser ablation. These devices are available in different forms like photoresistors or phototransistors. Photodetectors that can detect the polarization of the incident light are useful for application in imaging, remote sensing, communication, and military uses.[42] There are photodetectors designed to study the polarization of the incident light. When polarized light is allowed to fall on such a detector, an asymmetric nonequilibrium steady state is created which induces photocurrent in the device.[43]

The PLD device used in our studies is shown in the Fig. 13.1(i). The first study on the photodetection of PLD-grown 2D TMDC was reported by Late et al. in 2014,[44] in which they could grow MoS_2 on Kapton substrate using PLD. Recently, Deependra et al.,[45] could realize self-powered photodetectors of MoS_2 on AlN buffered Si wafer through pulsed laser deposition. The device architecture or photodetector exhibited improved figures of merits and the detector demonstrated stable photoswitching and enhanced photoresponsivity in MoS_2-based photodetectors realized through pulsed laser ablation. The author is also working on growing MoS_2 heterostructures on Si and Si/AlN wafers with different buffer layers like ZnO, SnO_2, CuO, etc., through pulsed laser ablation and to realize heterostructures for efficient photodetection. PLD parameters are optimized for quality thin film growth. The thickness of the film depends on the number of laser shots. It was found that some 300 laser shots produce a few layers (5–6) of MoS_2. A substrate temperature of 400 °C and above during deposition and high-temperature annealing for more than 30 min were found to be ideal for realizing quality thin film having improved photodetection. In our experiments, the throw distance was fixed to be 4.5 cm and deposition was carried out at 1.2×10^{-5} mbar pressure. Self powered and broadband photodetection as well as photoswitching response could be realized in our PLD grown heterostructure and MSM devices (Fig. 13.1(ii)).

There are also promising reports available on the PLD grown WS_2 photodetectors. A few of the reports on MoS_2 photodetectors available in the literature are analyzed below. PLD grown systems are also analyzed separately (Table 13.1).

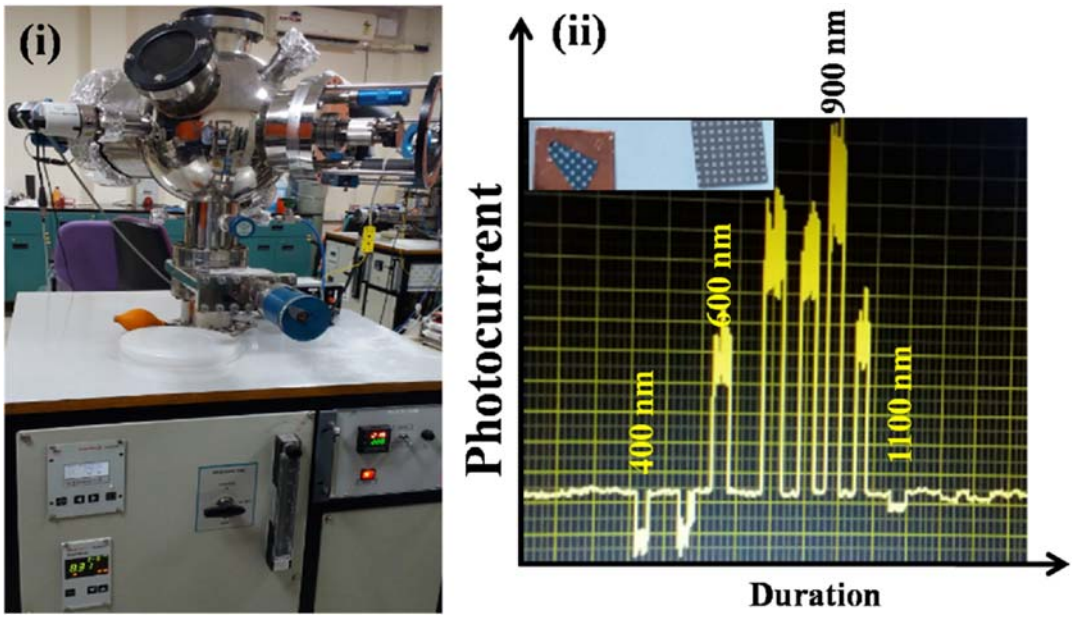

FIGURE 13.1 (i) Pulsed laser deposition unit used for MoS_2 thin film growth (ii) Photoresponse acquired in MoS_2 based device under illumination (400–1200 nm) (data without processing). PLD grown device is shown inset.

TABLE 13.1 Photodetector structure, highest detection wavelength (nm), responsivity (A/W), and response/recovery time exhibited by MoS_2-based systems are analyzed.

Photodetector structure	Highest detection wavelength (nm)	Responsivity (A/W)	Response/recovery time
$MA_3Bi_2Br_9$passivated few-layer MoS_2[46]	530	~512	0.3/0.3 ms
P(VDF-TrFE) driven MoS_2[47]	635	~2570	1.8/2.0 ms
$MoS_2/CsPbBr_3$[48]	442	~4.4	0.72/1.01 ms
MoS_2/CuO[49]	570	~157.6	~34.6/51.9 ms
MoS_2/Si[50]	808	~0.9082	56/825 ns
$GaSe/MoS_2$[51]	532	~3	50 ms
$MoTe_2/MoS_2$[52]	637	0.046	60/25 μs
$MoS_2/MoSe_2$[53]	633	~350	10 ms
MoS_2/P^+ Si[59]	808	~0.746	178/198 μs
MoS_2/Graphene QDs[55]	405	$\sim 10^4$	0.07/1.23 s
Single-layer MoS_2[56]	450	$\sim 7.5 \times 10^{-3}$	50/50 ms
CNT-MoS_2 p-n junction[57]	650	~0.1	15/15 μs
MoS_2/Si[58]	780	~23.1	21.6/65.5 μs

(*Continued*)

TABLE 13.1 Photodetector structure, highest detection wavelength (nm), responsivity (A/W), and response/recovery time exhibited by MoS_2-based systems are analyzed.—cont'd

Photodetector structure	Highest detection wavelength (nm)	Responsivity (A/W)	Response/recovery time
ZnPc treated MoS_2 with Al_2O_3 passivation layer[59]	532	~430	100 ms
MoS_2/p-Si[60]	455	~0.03	38.78/43.07 μs
n-MoS_2/p-Si[61]	808	~0.3	3/40 μs
n-MoS_2/n-Si[61]	650	~11.9	30.5/71.6 μs
MoS_2/h-BN/graphene[62]	405	~180	0.23/0.25 s
3D r-GO-MoS_2/pyramid Si[63]	808	~21.8	2.8/46.6 ms
Pd–MoS_2/Si[64]	950	~0.654	2.1/173.8 μs
$CH_3NH_3PbI_3$/MoS_2 with r-GO as HT[65]	660	~1.08×10^4	<45 ms
Pd-single layer MoS_2[66]	425	~0.88	24.2/24.5 ms
MoS_2–CdTe[67]	780	~0.0366	43.7/82.1 μs
PLD grown systems			
MoS_2[68]	445–2717	0.0507	–
WS_2/Bi_2Te_3[69]	370–1550	30.7	20/20 ms
MoS_2[70]	300–800	1.96	98/98 ms
MoS_2/Si[71]	400–980	–	150 ns/2.1 μs
WS_2[72]	370–1064	0.51	4.1/4.4 s
WSe_2[73]	370–1064	0.92	0.9/2 s
InSe[74]	370–980	27	0.5/1.7 s
GaSe[75]	240–900	1.4	5/20 s
SnSe[76]	370–808	5.5	–
$Mo_{0.5}W_{0.5}S_2$[77]	370–1064	5.8	150/150 ms
In_2Se_3/$CuInSe_2$[78]	370–1064	20.1	8/8 ms
MoS_2[79]	7200–8000	–	10/9.6 s
In_2Se_3[80]	254–1064	20.	24.6/57.4 ms
SnS[81]	370–808	115	–

9. Conclusion

Miniaturization of electronic products demands the requirement of photodetectors at nanometer size for induction in novel technology. MoS2-based thin film photodetectors are found to be effective in quality photodetection over a wide range of the electromagnetic spectrum. Novel device architecture using TMDC-based photodetectors is highly promising for enhanced photodetection. It has been understood from the recent scientific inquiry that pulsed laser deposition can be used for growing MoS2-based nano-films and heterostructures to realize excellent photodetection, photoswitching, etc., for various applications.

Declaration of interests

The author declares that he has no known competing financial interests or personal relationships that could have appeared to influence the work reported in this paper.

Acknowledgments

Pius is thankful to Science and Engineering Research Board (SERB), DST, Govt. of India for granting Teacher Associate for Research Excellence (TARE- TAR/2020/000241) award, to carry out research in association with Prof. Karuna Kar Nanda, Material Research Center, Indian Institute of Science Bangalore. Also, the financial assistance received from the SH college Major Research Project (SHMRP/2021/001) is acknowledged.

References

1. Sun B, Edgar MP, Bowman R, Vittert LE, Welsh S, Bowman A, et al. 3D computational imaging with single-pixel detectors. *Science* 2013;**340**:844–7.
2. Assefa S, Xia F, Vlasov YA. Reinventing germanium avalanche photodetector for nanophotonic on-chip optical interconnects. *Nature* 2010;**464**:80–4.
3. Burschka J, Pellet N, Moon S-J, Humphry-Baker R, Gao P, Nazeeruddin MK, et al. Sequential deposition as a route to high-performance perovskite-sensitized solar cells. *Nature* 2013;**499**:316–9.
4. Lu MP, Lu MY, Chen LJ. Multibit programmable optoelectronic nanowire memory with sub-femtojoule optical writing energy. *Adv Funct Mater* 2014;**24**:2967–74.
5. Kaasbjerg K, Thygesen KS, Jacobsen KW. Phonon-limited mobility in n-type single-layer MoS2 from first principles. *Phys Rev B* 2012;**85**:115317.
6. Quereda J, Biele R, Rubio Bollinger G, Agraït N, D'Agosta R, Castellanos Gomez A. Strong quantum confinement effect in the optical properties of ultrathin α-In2Se3. *Adv Opt Mater* 2016;**4**:1939–43.
7. Zhou X, Zhang Q, Gan L, Li H, Zhai T. Large-size growth of ultrathin SnS2 nanosheets and high performance for phototransistors. *Adv Funct Mater* 2016;**26**:4405–13.
8. Wang P, Liu S, Luo W, Fang H, Gong F, Guo N, et al. Arrayed van der Waals broadband detectors for dual-band detection. *Adv Mater* 2017;**29**:1604439.
9. Lee YT, Jeon PJ, Han JH, Ahn J, Lee HS, Lim JY, et al. Mixed-dimensional 1D ZnO–2D WSe2 van der Waals heterojunction device for photosensors. *Adv Funct Mater* 2017;**27**:1703822.
10. Geim AK. Graphene: status and prospects. *Science* 2009;**324**:1530–4.
11. Singh V, Joung D, Zhai L, Das S, Khondaker SI, Seal S. Graphene based materials: past, present and future. *Prog Mater Sci* 2011;**56**:1178–271.
12. Brent JR, Savjani N, O'Brien P. Synthetic approaches to two-dimensional transition metal dichalcogenidenanosheets. *Prog Mater Sci* 2017;**89**:411–78.
13. Chaika AN, Aristov VY, Molodtsova OV. Graphene on cubic-SiC. *Prog Mater Sci* 2017;**89**:1–30.

14. Papageorgiou DG, Kinloch IA, Young RJ. Mechanical properties of graphene and graphene-based nanocomposites. *Prog Mater Sci* 2017;**90**:75–127.
15. Tan C, Lai Z, Zhang H. Ultrathin two-dimensional multinary layered metal chalcogenidenanomaterials. *Adv Mater* 2017;**29**:1701392.
16. Bolotin KI, Sikes KJ, Jiang Z, Klima M, Fudenberg G, Hone J, et al. Ultrahigh electron mobility in suspended graphene. *Solid State Commun* 2008;**146**:351–5.
17. Zhang Y, Liu T, Meng B, Li X, Liang G, Hu X, et al. Broadband high photoresponse from pure monolayer graphene photodetector. *Nat Commun* 2013;**4**:1811.
18. Yang X, Ayaz A, Khurram S, Nan M, Mingsheng X, Yuhan Z, et al. Solvent-based soft-patterning of graphene lateral heterostructures for broadband high-speed metal-semiconductor-metal photodetectors. *Adv Mater Technol* 2017;**2**:1600241.
19. Liu CH, Chang YC, Norris TB, Zhong Z. Graphene photodetectors with ultra-broadband and high responsivity at room temperature. *Nat Nanotechnol* 2014;**9**:273–8.
20. Mak KF, Lee C, Hone J, Shan J, Heinz TF. Atomically thin MoS2: a new direct-gap semiconductor. *Phys Rev Lett* 2010;**105**:136805.
21. Peize H, Luke SM, Qing XW, Nicholas Q, Abdel El F, Masahiro I, et al. Highly sensitive MoS2 photodetectors with graphene contacts. *Nanotechnology* 2018;**29**:20LT01.
22. Saran R, Curry RJ. Lead sulphidenanocrystalphotodetector technologies. *Nat Photonics* 2016;**10**:81–92.
23. Cao Y, Cai K, Hu P, Zhao L, Yan T, Luo W, et al. Strong enhancement of photoresponsivity with shrinking the electrodes spacing in few layer GaSephotodetectors. *Sci Rep* 2015;**5**:8130.
24. Di Bartolomeo A, Grillo A, Urban F, Iemmo L, Giubileo F, Luongo G, et al. Asymmetric Schottky contacts in bilayer MoS2 field effect transistors. *Adv Funct Mater* 2018;**28**:1800657.
25. Lopez Sanchez O, Lembke D, Kayci M, Radenovic A, Kis A. Ultrasensitive photodetectors based on monolayer MoS2. *Nat Nanotechnol* 2013;**8**:497–501.
26. Xing Z, Lin G, Wenming T, Qi Z, Shengye J, Huiqiao L, et al. Ultrathin SnSe2 flakes grown by chemical vapor deposition for high-performance photodetectors. *Adv Mater* 2015;**27**:8035–41.
27. Hafeez M, Gan L, Li H, Ma Y, Zhai T. Chemical vapor deposition synthesis of ultrathin hexagonal ReSe2 flakes for anisotropic Raman property and optoelectronic application. *Adv Mater* 2016;**28**:8296–301.
28. Wang G, Li L, Fan W, Wang R, Zhou S, Lü JT, et al. Interlayer coupling induced infrared response in WS2/MoS2 heterostructures enhanced by surface Plasmon resonance. *Adv Funct Mater* 2018;**28**:1800339.
29. Huang H, Wang J, Hu W, Liao L, Wang P, Wang X, et al. Highly sensitive visible to infrared MoTe2 photodetectors enhanced by the photogating effect. *Nanotechnology* 2016;**27**:445201.
30. Buscema M, Barkelid M, Zwiller V, van der Zant HSJ, Steele GA, Castellanos-Gomez A. Large and tunable photothermoelectric effect in single-layer MoS2. *Nano Lett* 2013;**13**:358–63.
31. Freitag M, Low T, Xia F, Avouris P. Photoconductivity of biased graphene. *Nat Photonics* 2013;**7**:53–9.
32. Mueller T, Xia F, Freitag M, Tsang J, Avouris P. Role of contacts in graphene transistors: a scanningphotocurrent study. *Phys Rev B Condens Matter* 2009;**79**:245430.
33. Xie C, Mak C, Tao X, Yan F. Photodetectors based on two-dimensional layered materials beyond graphene. *Adv Funct Mater* 2017;**27**:1603886.
34. Huang Y, Xu K, Wang ZX, Shifa TA, Wang QS, Wang F, Jiang C, He J. Designing the shape evolution of SnSe2 nanosheets and their optoelectronic properties. *Nanoscale* 2015;**7**:17375–80.
35. Hinds S, Levina L, Ethan J, Klem D, Konstantatos G, Sukhovatkin V, Sargent EH. Smooth-morphology ultrasensitive solution-processed photodetectors. *Adv Mater* 2008;**20**:4398.
36. Soci C, Zhang A, Xiang B, Dayeh SA, Aplin DPR, Park J, Bao XY, Lo YH, Wang D. ZnO nanowire UV photodetectors with high InternalGain. *Nano Lett* 2007;**7**:1003.
37. Buscema M, Island JO, Groenendijk DJ, Blanter SI, Steele GA, van der Zant HSJ, Castellanos-Gomez A. Photocurrent generation with two-dimensional van der Waals semiconductors. *Chem Soc Rev* 2015;**44**:3691–718.
38. Sun Z, Chang H. Graphene and graphene-like two-dimensional materials in photodetection: mechanismsand methodology. *ACS Nano* 2014;**8**:4133–56.
39. Huo N, Konstantatos G. Recent progress and future prospects of 2D-based photodetectors. *Adv Mater* 2018;**30**:e1801164.
40. Li L, Wang W, Chai Y, Li H, Tian M, Zhai T. Few-layered PtS2 phototransistor on h-BN with high gain. *Adv Funct Mater* 2017;**27**:1701011.

41. Zeng LH, Wang MZ, Hu H, Nie B, Yu YQ, Wu CY, et al. Monolayer graphene/germanium Schottky junction as high-performance self-driven infrared light photodetector. *ACS Appl Mater Interfaces* 2013;**5**:9362–6.
42. Tyo JS, Goldstein DL, Chenault DB, Shaw JA. Review of passive imaging polarimetry for remote sensing applications. *Appl Opt* 2006;**45**:5453–69.
43. Zhang X, Wang J, Zhang SC. Topological insulators for high-performance terahertz to infrared applications. *Phys Rev B* 2010;**82**:245107.
44. Late DJ, Shaikh PA, Khare R, Kashid RV, Chaudhary M, More MA, et al. Pulsed laser-deposited MoS2 thin films on W and Si: field emission and photoresponse studies. *ACS Appl Mater Interfaces* 2014;**6**:15881–8.
45. Singh DK, Pant R, Chowdhury AM, Roul B, Nanda KK, Krupanidhi SB. Defect-mediated transport in self-powered, broadband, and ultrafast photoresponse of a MoS2/AlN/Si-based photodetector. *ACS Appl Elect Mater* 2020;**2**(4):944–53.
46. He J, Yang Y, He Y, Ge C, Zhao Y, Gao L, Tang J. Low noise and fast photoresponse of few-LayeredMoS2 passivated by MA3Bi2Br9. *ACS Photonics* 2018;**5**:1877–84.
47. Wang X, Wang P, Wang J, Hu W, Zhou X, Guo N, Huang H, Sun S, Shen H, Lin T, et al. Ultrasensitive and broadband MoS2 photodetector driven by ferroelectrics. *Adv Mater* 2015;**27**:6575–81.
48. Stoumpos CC, Malliakas CD, Peters JA, Liu Z, Sebastian M, Im J, Chasapis TC, Wibowo AC, Chung DY, Freeman AJ, et al. Crystal growth of the perovskite semiconductor CsPbBr3: a new materialfor high-energy radiation detection. *Cryst Growth Des* 2013;**13**:2722–7.
49. Um DS, Lee Y, Lim S, Park S, Lee H, Ko H. High-performance MoS2/CuO nanosheet-on-one-dimensional Heterojunction Photodetectors. *ACS Appl Mater Interfaces* 2016;**8**:33955–62.
50. Qiao S, Cong R, Liu J, Liang B, Fu G, Yu W, Ren K, Wang S, Pan C. A vertically layered MoS2/Siheterojunction for an ultrahigh and ultrafast photoresponse photodetector. *J Mater Chem C* 2018;**6**:3233–9.
51. Islam A, Lee J, Feng PX-L. Atomic layer GaSe/MoS2 van der Waals heterostructure photodiodes withLow noise and large dynamic range. *ACS Photonics* 2018;**5**:2693–700.
52. Chen Y, Wang X, Wu G, Wang Z, Fang H, Lin T, Sun S, Shen H, Hu W, Wang J, et al. High-performance photovoltaic detector based on MoTe2/MoS2 van der Waals heterostructure. *Small* 2018;**14**:1870038.
53. Yang Y, Huo N, Li J. Gate modulated and enhanced optoelectronic performance of MoSe2 and CVD-grownMoS2 heterojunctions. *RSC Adv* 2017;**7**:41052–6.
54. Guo J, Li S, Ke Y, Lei Z, Liu Y, Mao L, Gong T, Cheng T, Huang W, Zhang X. Broadband Photodetector based on vertically stage-liked MoS2/Si heterostructure with ultra-high sensitivity and fastresponse speed. *Scripta Mater* 2020;**176**:1–6.
55. Chen C, Qiao H, Lin S, Man Luk C, Liu Y, Xu Z, Song J, Xue Y, Li D, Yuan J, et al. Highly responsiveMoS2 photodetectors enhanced by graphene quantum dots. *Sci Rep* 2015;**5**:11830.
56. Yin Z, Li H, Li H, Jiang L, Shi Y, Sun Y, Lu G, Zhang Q, Chen X, Zhang H. Single-layer MoS2phototransistors. *ACS Nano* 2012;**6**:74–80.
57. Jariwala D, Sangwan VK, Wu C-C, Prabhumirashi PL, Geier ML, Marks TJ, Lauhon LJ, Hersam MC. Gate-tunable carbon nanotube-MoS2 heterojunction p-n diode. *Proc Natl Acad Sci USA* 2013;**110**:18076–80.
58. Lou Z, Zeng L, Wang Y, Wu D, Xu T, Shi Z, Tian Y, Li X, Tsang YH. High-performance MoS2/Siheterojunction broadband photodetectors from deep ultraviolet to near infrared. *Opt Lett* 2017;**42**:3335.
59. Huang Y, Zhuge F, Hou J, Lv L, Luo P, Zhou N, Gan L, Zhai T. Van der Waals coupled OrganicMolecules with monolayer MoS2 for fast response photodetectors with gate-tunable responsivity. *ACS Nano* 2018;**12**:4062–73.
60. Kim HS, Kumar MD, Kim J, Lim D. Vertical growth of MoS2 layers by sputtering method for efficient photoelectric application. *Sens. Actuators A Phys.* 2018;**269**:355–62.
61. Wang L, Jie J, Shao Z, Zhang Q, Zhang X, Wang Y, Sun Z, Lee ST. MoS2/Si heterojunction with vertically standing layered structure for ultrafast, high-detectivity, self-driven visible-near infrared photodetectors. *Adv Funct Mater* 2015;**25**:2910–9.
62. Vu QA, Lee JH, Nguyen VL, Shin YS, Lim SC, Lee K, Heo J, Park S, Kim K, Lee YH, et al. Tuning carrier tunneling in van der Waals heterostructures for ultrahigh detectivity. *Nano Lett* 2017;**17**:453–9.
63. Xiao P, Mao J, Ding K, Luo W, Hu W, Zhang X, Zhang X, Jie J. Solution-processed 3DRGO–MoS2/pyramid Si heterojunction for ultrahigh detectivity and ultra-broadband photodetection. *Adv Mater* 2018;**30**:1801729.
64. Hao LZ, Gao W, Liu YJ, Liu YM, Han ZD, Xue QZ, Zhu J. Self-powered broadband, high-detectivity and ultrafast photodetectors based on Pd-MoS2/Si heterojunctions. *Phys Chem Chem Phys* 2015;**18**:1131–9.

65. Peng Z-Y, Xu J-L, Zhang J-Y, Gao X, Wang S-D. Solution-processed high-performance Hybrid Photodetectors enhanced by perovskite/MoS2 bulk heterojunction. *Adv Mater Interfac* 2018;**5**:1800505.
66. Wang X-F, Zhao H-M, Shen S-H, Pang Y, Shao P-Z, Li Y-T, Deng N-Q, Li Y-X, Yang Y, Ren T-L. High performance photodetector based on Pd-single layer MoS2 Schottky junction. *Appl Phys Lett* 2016;**109**:201904.
67. Wang Y, Huang X, Wu D, Zhuo R, Wu E, Jia C, Shi Z, Xu T, Tian Y, Li X. A room-temperaturenear-infrared photodetector based on a MoS2/CdTe p-n heterojunction with a broadband response up to1700 nm. *J Mater Chem C* 2018;**6**:4861−5.
68. Xie Y, Zhang B, Wang S, Wang D, Wang A, Wang Z, et al. Ultrabroadband MoS2 photodetector with spectral response from 445 to 2717 nm. *Adv Mater* 2017;**29**:1605972.
69. Yao J, Zheng Z, Yang GW. Layered-material WS2/topological insulator Bi2Te3 heterostructure photodetector with ultrahigh responsivity in the range from 370 to 1550 nm. *J Mater Chem C* 2016;**4**:7831−40.
70. Jiao L, Jie W, Yang Z, Wang Y, Chen Z, Zhang X, et al. Layer-dependent photoresponse of 2D MoS2 films prepared by pulsed laser deposition. *J Mater Chem C* 2019;**7**:2522−9.
71. Hu C, Wang X, Miao P, Zhang L, Song B, Liu W, et al. Origin of the ultrafast response of the lateral photovoltaic effect in amorphous MoS2/Si junctions. *ACSAppl Mater Interfaces* 2017;**9**:18362−8.
72. Yao JD, Zheng ZQ, Shao JM, Yang GW. Stable, highly-responsive and broadband photodetection based on large-area multilayered WS2 films grown by pulsedlaser deposition. *Nanoscale* 2015;**7**:14974−81.
73. Zheng Z, Zhang T, Yao J, Zhang Y, Xu J, Yang G. Flexible, transparent and ultra-broadband photodetector based on large-area WSe2 film for wearable devices. *Nanotechnology* 2016;**27**:225501.
74. Yang Z, Jie W, Mak CH, Lin S, Lin H, Yang X, et al. Wafer-scale synthesis of high-quality semiconducting two-dimensional layered InSe with broadband photoresponse. *ACS Nano* 2017;**11**:4225−36.
75. MahjouriSamani M, Gresback R, Tian M, Wang K, Puretzky AA, Rouleau CM, et al. Pulsed laser deposition of photoresponsive two-dimensional GaSenanosheet networks. *AdvFunct Mater* 2014;**24**:6365−71.
76. Yao J, Zheng Z, Yang G. All-layered 2D optoelectronics: a high-performance UV-Vis-NIR broadband SnSephotodetector with Bi2Te3 topological insulatorelectrodes. *AdvFunct Mater* 2017;**27**:1701823.
77. Yao J, Zheng Z, Yang GW. Promoting the performance of layered-material photodetectors by alloy engineering. *ACS Appl Mater Interfaces* 2016;**8**:12915−24.
78. Zheng Z, Yao J, Yang G. Self-assembly of the lateral In2Se3/CuInSe2 heterojunction for enhanced photodetection. *ACS Appl Mater Interfaces* 2017;**9**:7288−96.
79. Goswami A, Dhandaria P, Pal S, McGee R, Khan F, Antić Ž, et al. Effect of interface on mid-infrared photothermal response of MoS2 thin film grown by pulsedlaser deposition. *Nano Res* 2017;**10**:3571−84.
80. Zheng ZQ, Yao JD, Yang GW. Growth of centimeter-scale high-quality In2Se3 films for transparent, flexible and high performance photodetectors. *J Mater Chem C* 2016;**4**:8094−103.
81. Yao J, Yang G. Flexible and high-performance all-2D photodetector for wearable devices. *Small* 2018;**14**:1704524.

CHAPTER

14

Electromechanical application of magnetite nanomaterials blended with single-walled carbon nanotubes

Indradeep Kumar

Department of Aeronautical Engineering, Institute of Aeronautical Engineering, Hyderabad, Telangana, India

1. Introduction

Graphene is a new member of the allotropes of the carbon family, with famous members like diamond, graphite, fullerene, nanotubes, and graphene. Graphene has much attention since the earlier research by Germ and Novoseloi, for which they received the Noble prize in 2010. Graphene and its derivatives, such as graphite oxide, reduced graphene oxide, and graphene oxides, have been used in scientific research. Graphene is a 3-D layer of sp^2 hybridized carbon atoms that exhibits exceptional magnetic, mechanical, thermal, electronic, and optical properties with a large surface area. The compelling interest in carbon nanotubes (CNTs) has kindled research activity since their discovery in 1991.[1–3] Its fabulous properties have opened numerous applications in field emission transistors, and catalysis.

Irrespective of the stunning technological development, there is still much struggle in the synthesis aspect, which is a significant drawback in complying with these unique materials in a commercial application. Apart from the various known catalytic chemical vapor deposition (CCVD) methods, SWCNTs can be produced with varying diameters, large-scale production, high purity, variable temperature, and, most importantly, economical. Single-Wall Carbon Nanotubes (SWCNTs) are CNTs with a single layer or single graphene sheet-shaped or rolled cylindrical tube form. The other kind of CNTs, a family of concentric tubes with a position perpendicular to the axis, is termed MultiWall Carbon Nanotubes (MWCNTs). The Young's Modulus of SWCNTs is greater than 1 TPa, and the Tensile strength is around 200Gpa. The thermal conductivity can be higher up to 2500 W/mK. SWCNTs have proven that it is a beautiful candidate for emission with a perfect mass-to-weight ratio, a minimum radius of the curvature tip, and sensible heat emitting properties.[4–11]

Applications of Multifunctional Nanomaterials
https://doi.org/10.1016/B978-0-12-820557-0.00003-5

SWCNTs consist of a single graphene sheet rolled in cylindrical form. Its remarkable structural and physical properties lead to various potential applications in electrical, electronic, and mechanical devices. Doping, adsorption, or growing on the surface of metal nanoparticles can improve, change, or manipulate metal nanoparticles' physical and chemical properties; hence, the newly prepared hybrid composite can open new application opportunities. In the nanoscale domain, the nanoparticles' properties cannot be observed in bulk or the counterpart of atoms. Iron oxide nanostructure-based material is exploited for various research purposes because of its magnetic, optical, electrical, and catalytic behaviors. However, IONs must always be combined with other nanostructured materials to create increased properties. nanocomposites.[12,13] Therefore it is a great deal to prepare nanomaterials that provide desired characteristics. Because of its synthesizing simplicity in the laboratory and its elegant features, iron oxide nanoparticles (IONs) gain a unique place between other oxides of metal nanosized. This valuable SWCNTs option has excellent potential for synthesizing nanocomposites. In other words, electromechanical applications include transformers, inductors, bobbins, and other electromechanical components. These hybridized nanocomposites can create a new class of electrical and mechanical components, extending their useful lives and reducing the risk of malfunction-related hazards such as overheating, causing fire, etc. This chapter describes Fe_3O_4(IONs)-SWCNTs nanocomposites for electrical and mechanical applications.

Many researchers used earlier hematite, maghemite, and magnetite iron oxides to form nanocomposites. Therefore, this chapter mainly focuses on Magnetite (Fe_3O_4) and its composites for electromechanical applications. Magnetite (Fe_3O_4) ($Fe^{II}Fe^{III}{}_2O_4$) is also named ferrous ferrite or Iron (II, III). Magnetite molecular formula Fe_3O_4 can be depicted as $FeO.Fe_2O_3$. Magnetite has the most vital magnetism among all the natural minerals. It differs from other iron oxides because it simultaneously has Fe++ and Fe+++ ions. Fe_3O_4 has a CCP structure forming a cubic inverse spinal structure. Hematite (α-Fe2O3) is one of the oldest members with promising capabilities in rocks and soil.

Hematite is highly stable; hence, it is generally the final product of other oxides of Iron after the transformation. Hematite is coarsely crystalline, it shows a gray or black color, but it offers a red color if it is finely divided. After the Hematite, maghemite (γ-Fe_2O_3) is the second most stable among all other iron oxides found in soil and other natural resources. While ferrites include divalent and trivalent cations, maghemite and magnetite have a spinel crystal structure.[3] Maghemite shows n-type semiconductor behaviors and antiferromagnetic.[14–20] Magnetic SWCNTs' properties have yet to be reviewed in detail instead of a few original reports. Hence, their importance is undoubtful because of various potential and current medicine, chemistry, physics, and biology through nanotechnology. This chapter's main objective is to highlight current and potential applications.[14,15,21–23]

2. Metal-SWCNTs composites

In the periodic table, few magnetic metals are present. Paramagnetic properties have been found in a few typical metals with SWCNTs like Iron, nickel, or cobalt. Iron/SWCNTs hybrids and iron oxides like Fe_3O_4 are undoubtedly very well studied as central metals.[16–20,24] This hybrid can obtain by various methods via both greener and classic chemicals. Green

chemical-focused solar radiation can be applied to prepare three-dimensional oxides of metals dispersed with SWCNTs by simultaneous exfoliation and reduction. This method allows the insertion of SWCNTs in between the metal oxides. These SWCNTs, dispersed with metal oxide nanoparticles, might be used in energy storage sensing, conversion devices, and environmental fields.[25–36]

3. Magnetic behavior of iron oxides

The iron atom's magnetic moments are extreme because, in their 3d orbital, four unpaired electrons are present. When iron atoms getting crystallizes, various magnetic states can be arises. In the state of paramagnetism, the magnetic moment of individual atoms is aligned randomly to each other, and hence overall, the crystal possesses zero magnetic moments. Some of these atom moments will be aligned when an external magnetic field is introduced; hence, the crystal possesses a small net magnetic moment.[37] All individual atoms' moments can be aligned in a ferromagnetic material without introducing the external electric field. Atoms in ferrimagnetic materials having two types of moments are antiparallel to one another. Net magnetic moments are therefore present, and if their magnitudes are the same, the object is antiferromagnetic, which has no net magnetic moments. Above the Curie temperature of 956 K, the Hematite shows paramagnetic nature. While still ferromagnetic at ambient temperature, it transitions to an antiferromagnetic state at Morin temperature (260 K). Hematite magnetic properties depend on the particle size, crystallinity, and the cation substitution extent. As the particle size decreases Morin temperature of the Hematite decreases and vanishes for very smaller particles. At room temperature, magnetite shows ferrimagnetic nature and has 850 K Ci temperature. At room temperature, magnetite particles smaller than 6 nm exhibit superparamagnetic nature. Their magnetic characteristics depend highly on the synthesis method employed to create them. Margulies et al. looked at how much the magnetism of the nanosized magnetite affects the crystal shape. The coercivity order affected by crystal morphology are: octahedral > cubes > Spheres.[38,39] Maghemite has ferrimagnetic properties at room temperature but gradually becomes unstable at higher temperatures and loses its susceptibility. Maghemite's Curie temperature is challenging to measure experimentally since the loss of magnetism causes an irreversible structural shift to Hematite. According to this theory, the Curie temperature of maghemite lies between 820 and 986 K. Maghemite particles exhibit superparamagnetic properties at temperatures below 10 nm.[40,41]

4. Iron oxide-SWCNTs composites

Magnetic SWCNTs nanocomposites can be prepared to form a core in the nanocomposites double-shell structure in which Fe is the core, iron oxide as the inner shell, and SWCNTs the outer shell. This composite is very stable even in strong acid also. Other magnetic SWCNTs nanocomposites can be prepared in which Fe is used as a core, iron oxides are used as shells, and SWCNTs are used as nanofillers.[42–46]

4.1 Fe_2O_3-SWCNTs composites

SWCNTs can be iron oxide composites in the form of the element or core-shell nanoparticles. The ratio of iron nanoparticles in different oxide states depends on the oxygen present. Due to their abundant oxygen, SWCNTs nanoparticles were loaded on magnetic iron oxide sheets. SWCNTs nanoparticles changed the Fe_2O_3 lattice structure and their intrinsic properties, depending on the SWCNTs precursor. pH can adjust by effectively charging attraction or repulsion between SWCNTs and Fe_2O_3 nanoparticles since pH is crucial for the composite's stability. The double-layer electrical forces can explain the adsorption of Fe_2O_3 at low pH between the Fe_2O_3 and SWCNTs shown in Fig. 14.1.[47–55] At higher pH, due to similar charge repulsion, dispersions are stable. With SWCNTs, an intriguing effect was observed. Greater concentrations result in the restabilization of Fe_2O_3, whereas lower concentrations result in the flocculation of Fe_2O_3. This composite can enhance the electrode's electrical and chemical performance, which is iron-oxide-based in high-rate Lithium-ion batteries.[56,57]

4.2 Magnetite(Fe_3O_4)-SWCNTs composites

Adding carbon-derived materials like graphene or CNTs to the magnetite helps in phase changes and volume accommodation and helps improve the electrical conductivity of the synthesized sheet significantly. This chapter will see the effect on magnetite properties by adding SWCNTs to improve the physical and chemical properties. Adding SWCNT in the magnetite (Fe_3O_4), which is in IONs, electrical conductivity, volume accommodation, and phase change other physical and chemical properties can be improved for performance and long-term stability. In most methods like hydrothermal, sol-gel, pyrolysis, etc., fabrication binders can be used to form Fe_3O_4 composites with SWCNTs.[58,59] Binder in the fabrication method may impede electron and iron transport, reducing capacity. These fabrication methods may be complex and completed in multiple steps, which increases the cost of production. The supersonic cold spray method can fabricate Fe_3O_4IONs-SWCNTs composites in which both Fe_3O_4IONs and SWCNTs can be deposited simultaneously without using any

FIGURE 14.1 Synthesized nanosheets using nanopowder of iron oxide and single walls carbon nanotubes.

binder. A film with uniformity and superior adhesion property can be formed quickly across the substrate by merely sweeping a nozzle. In between substrate and material being deposited, the supersonic impact produces excellent adhesion of the film deposited. Further densification and compaction of the materials deposited by subsequently impacted material increases the cohesion between Fe_3O_4IONs and SWCNTs composites, as shown in Fig. 14.2.[60–62]

The magnetic properties of IONs have been exploited in various applications like magnetic resonance imaging, therapeutic agents, magnetic recording media, and various other electrical and mechanical components. Nanomaterials of a specific shape, size, magnetic properties, and surface characteristics are required in these applications. For storing data, the particle must be stable and have a switchable magnetic state that should not be affected by temperature variations.[63] They must resist corrosion, friction, and temperature fluctuation and be uniformly small. Magnetite can be used in data storage and recording because of its stable physical and chemical nature. It can combine with SWCNTs to improve their storage capacity and coercivity. Incorporated nanoparticles have excellent thermal stability compared to conventional ones. As a result, SWCNTs blended IONs are predominant for magnetic discs, high bias audiotapes, and videotapes.

It can also be utilized in magnetometers as a sensing element and recording. Fe_3O_4IONs-SWCNTs composite embedded in the nonmagnetic matrix exhibits enormous resistance to the magnet, resulting in decreased resistance due to the applied magnetic field. Fe_3O_4IONs-SWCNTs in ferrofluids can be used in space applications for high-performance sealing. Ferrofluids contain Fe_3O_4IONs-SWCNTs in superparamagnetic nanoparticles dispersed in an organic or aqueous medium.[64,65] Ferrofluids show magnetic moment only in applied electric fields; otherwise, it shows zero net magnetic moments, and hence an external magnet can trap the fluid in a specific location to act as a seal. This fluid can be used in optical switches and tunable diffraction gratings because it has magnetic field-dependent optical anisotropy properties. This can also be used in vibrating environments and sealing computer disk units instead of conventional sealing materials.

Fe_3O_4IONs-SWCNTs blends receive attention in the formation of immunoassays, contrast agents for magnetic resonance imaging, hyperthermia, and targeted drug delivery vehicles at

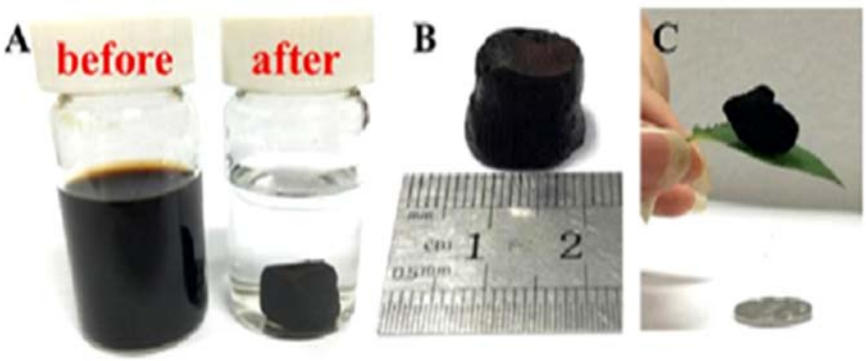

FIGURE 14.2 Formation of composite.

room temperature Fe_3O_4IONs-SWCNTs particles can exhibit super magnetic behavior. Functionalized Fe_3O_4IONs-SWCNTs, which are super magnetic with the help of an electric field, allow the drug delivery to the required target where the local release of medicine is required. The Fe_3O_4IONs-SWCNTs nanoparticles surface be used in drug delivery, functionalized with drug genetic materials or protein to deliver these locally.[66–75]

4.2.1 Fe_3O_4-SWCNTs aerogels

Aerogels have the most considerable attention compared to the all magnetic SWCNTs hybrid among all mixed valent of iron oxides with SWCNTs. Magnetite and other Aerogels and their synthesizing procedures are very well known. Introducing SWCNTs can lead to various unusual potential applications and their properties; for example, pollutants can be removed easily, like crude oil. These composites can be in simple composition (i.e., Fe_3O_4-SWCNTs) or other functional groups like a composite. Hence, 3D N-doped Fe_3O_4 aerogel (N- FA)- supported SWCNTs nanoparticles (SWCNTs/N-FA) are well known as an efficient cathode catalyst for the oxygen reduction reaction. These composites can be synthesized through thermal treatment, freeze-drying, and combined hydrothermal self-assembly processes. The resultant product showed excellent electro-catalytic behavior for the oxygen reduction reaction in alkaline electrolytes, including better durability, high electron transfer number, lower H_2O_2 yield, high current density, and lower ring current. 3D magnetite aerogel having SWCNTs nanoparticles is reported to be the lightest magnetic elastomer ever. In strain-dependent electrical resistance and reversible magnetic field induced, this can monitor stretching and compression in the material. Among various aerogel hydrophobic Fe_3O_4-SWCNTs, the solvothermal process can form aerogel composites with very low density and significantly higher porosity with a reticulated sheet structure. This composite can be used by allowing 30–40 times greater mass intake after 10–12 water-oil separation cycles in crude oil remediation.[49,50,56,57,76]

4.2.2 Bi-component magnetite-SWCNTs

Solvothermal and hydrothermal synthesis procedures are widely used to synthesize the nonaerogel type magnetite -SWCNTs composites, although various synthesis procedures like atomic layer deposition can be used frequently. Magnetic Fe_3O_4 foam with hierarchical porous structures by combining the SWCNTs nanoparticles can prepare by a hydrothermal system by gaseous reduction. It can be used as adsorption of organic and oil solvent; hence it can be used for oil spill clean-up. Under mild conditions, while controlling the reduction degree of Fe_3O_4, SWCNTs nanoparticles on Fe_3O_4 foam have different morphologies, cubic structures, or nanosheet arrays. A particular ratio of Fe_3O_4/SWCNTs is significant for various applications. As a result, solvothermal techniques can be utilized to generate Fe_3O_4/SWCNTs nanocomposites with various SWCNTs to Fe_3O_4 ratios, which can then be used to remove the methylene blue dye from aqueous solutions. You can see the following morphologies: SWCNTs nanoparticles spread uniformly and uniformly over the Fe_3O_4 sheet in a sheet-like structure without clumping together. A decrease in adsorption capacity coincided with an increase in magnetization due to adding more SWCNTs nanoparticles to the surface of the Fe_3O_4 sheet. Size influences mitochondrial activity during reduction. The chemical functionalization of Fe_3O_4 and SWCNTs increase the biocompatibility and makes the system independent of the size distribution of nanoparticles.[77–81]

4.2.3 Multi-component Magnetite-SWCNTs

Systems having complex SWCNTs/F_e3O_4 and inorganic or organic are also ubiquitous. Thus, Fe_3O_4 sheet double side coating mesoporous nanocomposites with greater pore volume and surface area may be obtained. Each side of Fe_3O_4 sheet was coated with a layer of silica materials; the mesoporous, sol-gel method assisted with CTAB and subsequent calcinations. Prepared composites can identify or analyze peptides in human urine, specific enrichment, size selectiveness where required, and protein digest solution.[82] Few researchers also investigated magnetic materials with chitosan in biomedical applications.[66,83–87] Thus, an SWCNTs/Fe_3O_4/Chitosan composite was prepared by the technique of mixing-evaporation of solution. By using 0.5% SWCNTs by weight and 1% Fe_3O_4 by weight, Young's modulus can be enhanced by up to 30%, and tensile strength can be improved by up to 80% of the chitosan. It can be used as an excellent electrochemical biosensor catalyst for glucose detection because nitrogen in chitosan when SWCNTs are introduced in biocompatible and water-dispersible chitosan functionalized Fe_3O_4 is prepared by one-step ball milling of chitosan and Fe_3O_4. Bio-adsorbent can also be prepared by magnetic composite based on chitosan and SWCNTs-Fe_3O_4 composites.[88,89]

5. Applications

5.1 Fe_3O_4-SWCNTs in biofuels

It is urgent to reduce greenhouse gas emissions. At the same time, the energy supply should be increased due to the rising global demand for energy, higher economic growth, higher commodity prices in developing nations, and scientific evidence that the presence of carbon dioxide in the atmosphere is one of the primary causes of climate change. Biofuel is a renewable resource, and if adequately converted and produced, it can provide liquid fuels that can reduce the greenhouse gas emissions like NOx more than petroleum oil. Fischer-Tropsch Synthesis (FTS) is a well-known catalytic process for preparing liquid fuels by efficiently gasifying biomass feedstock and valuable organic compounds like diesel. Derived diesel is up to 30% more efficient and is clean burning than gasoline. However, most available catalysts are costly, produce a comprehensive hydrocarbon array product and CO_2 CH_4, and are not readily recyclable. Due to the production of CH_4 as byproducts of waste H_2, lowering methane selectivity and increasing the formation of long-chain hydrocarbons are the most important reason for producing a new type of FTS catalyst.[90]

Iron-based catalysts can provide a great value in FTS because of their high activity over a wide temperature range relative to the other catalyst. Lower cost allows producing gasoline at a higher temperature and diesel at a lower temperature. They can catalyze water-gas shift reaction, enabling hydrocarbons' formation in liquid form from synthesis gas with a lower H_2 to CO ratio. In sources of coal and biomass, the ratio of H_2 to CO is around 1.15–1.20. In FTS, most iron-based catalysts are supported on higher surface area oxides, like Al_2O_3, SiO_2, and zeolites. When reinforced with alumina or silica, iron forms mixed oxides because of the solid metal-support interaction influences, which results in the formation of iron aluminate or iron silicate, which is challenging to reduce. Besides, the liquid fuels prepared by the FTS method impose expensive separation. The process of purification and upgrading makes it costlier

because of the present catalyst's lack of selectivity. Therefore, forming a new generation nanocatalyst can provide higher activity, better selectivity, recyclability, and stability. The formation of such a catalyst is an essential aim for heterogeneous catalysis, which can significantly impact the fuel industry and chemical industries. Recently researchers are focusing on preparing a new and highly efficient, selective nanocatalyst with nanocarbons and nanofiber for FTS with iron or cobalt-based catalysts. These days nanocarbon has become an emerging area informing the advanced supported catalyst due to the limited interaction with the metal catalysts. In a few cases, nanocarbons can provide tunable support for catalyst interactions. For example, with the help of carbon nanofibers, researchers recently developed a highly selective catalyst to form lower olefins from the synthesis gas by FT to Olefins process. Many researchers reported higher activity in FTS with an iron-based catalyst in which CNTs are supported to produce hydrocarbons with a longer chain.[91–94]

This chapter will discuss SWCNT' application as a higher surface area support for Fe_3O_4-based nanoparticle catalyst to form hydrocarbons with longer chains. In heterogeneous catalysis, SWCNTs have recently shown remarkable tunability and unique property in supporting various metallic and bimetallic nanoparticle catalysts. Because of the SWCNTs' well-defined structure, they can have more defined and controlled types of defects tuned better to get the desired catalytic surface properties of functionalities. Researchers postulated that incorporating defect sites in the sp^2-bonded carbon network of SWCNTs might provide thermal stability against the particle growth in the Iron-based catalyst without hindering their activation. Besides, due to the extended π-system in SWCNTs and the higher electron density, it might be easier to reduce the IONs on the surface of SWCNTs, generating a catalytically active iron oxides catalyst with SWCNTs. This can have an impact on product selectivity and catalyst activity. This technique gives a homogeneous distribution of IONs within the surface of the SWCNTs support. Compared to conventional heating, microwave irradiation's main advantages are reaction mixture getting rapid and uniformly heated.[95,96]

5.2 Fe_3O_4-SWCNTs in electromechanical applications

As we know, the nanomaterials' shape and size, surface properties, and size distribution significantly impact the nanosheets' behavior and characteristics, with the formation method having a pivotal role in practical purposes. Formation methods also determine impurity in the nanosheet, the degree of defects in the structure, and their distribution over the surface can achieve. This research aimed to synthesize low-cost or cost-effective Iron-based highly dispersive nanosheets that can be used in electromechanical applications.[27,44] Regarding the use of nanotechnology in electromechanical components, SWCNTs and Nanopowder of Iron Oxide can be combined to create a new class of nanosheets physically stable, thermally resilient, and environmentally beneficial. A cost-effective, higher strength to weight technology based on the latest materials was developed for electrical components like transformers, inductors, bobbins, and other electromechanical components to increase the components' life span and prevent it happening hazards because of malfunctioning, like overheating causes fire, etc. Using the nano emulsion method in which thermodynamically stable two immiscible substances stabilized by nonionic, anionic, or cationic surfactants, the nanoclay of mixture can be obtained nanopowder of Iron oxide and SWCNTs.[73] The nanosheet formed from the nano clay has improved electromechanical properties like high

strength to weight ratio, almost negligible rusting ability, Damage-tolerance, and thermal protection and control.

The aim can achieved by (1) synthesizing a new type of stabilized iron-based nanoparticle using a green stabilizer at a lower cost. (2) testing the stabilized nanoparticles' effectiveness for making small electrical components, and (3) testing the feasibility of the formed sheet's electrical components. In the work, we have tested the following three key research hypotheses: (1) high strength to weight ratio (>5); (2) almost negligible rusting ability; the stabilized nanoparticles will offer much greater resistivity and longevity over currently used nonstabilized iron particles for rusting; (3) damage-tolerant systems: damage-tolerant systems are consists of nanoscale approaches to increase system robustness through improved interlaminar interfaces, repair mechanisms, and health monitoring and (4) thermal protection and control: Thermal management system gives the lightweight approach to protect systems from getting damaged due to uncontrolled thermal cycling.

A new member of the carbon family called SWCNTs, which has higher thermal and electrical conductivity, a larger surface area, and electro-catalytic properties can be simulated with much interest in reducing the difficulty in realizing the new ideas for improving the performance of many current and potential devices. Unique properties of Fe_3O_4 nanoparticles, such as lox toxicity, strong magnetic properties, higher adsorption capacity for required biomolecules immobilization, etc. This section will discuss the application of Fe_3O_4-SWCNTs composites in biomedical determination. The catalytic activity of Fe_3O_4-SWCNTs composites can improve because of enhancing electronic communication. For example, the transfer of charge between catalyst and support. Synergistic effects of SWCNTs and IONs components give nanocomposites with novel physical and chemical properties and consequently increase electrical and chemical performance. Fe_3O_4-SWCNTs composites can be considered one of the most promising hybrid composites to boost the formation of more efficient electrochemical sensors.[83]

5.3 Fe_3O_4-SWCNTs in electrochemical sensors

A device that can continuously and reversibly provide real-time and reliable information to the surrounding medium about its chemical composition is called a chemical sensor. These sensors' advantages are the recognition part, which can be biological or chemical elements, and a transducer to provide a visual signal. The interaction between recognition elements and targets is converted to the electrical signal for getting the analytical information in electrochemical sensors, among the various transducers that can be used in chemical sensors like piezoelectric, thermal, electrical, etc. Electrochemical transducers offer low detection limits and repeatability, high sensitivity, strong stability, wide linear response range, simplicity, downsizing capability, and low cost. Electrochemical sensors have been successfully incorporated into field applications and commercialization.[27] Usually, an electrochemical sensor is an assembly of a working electrode in which Fe_3O_4-SWCNTs composites can be used, a reference in which Ag/AgCl and calomel can be used as a counter electrode, namely, cathode or anode. Electrochemical sensors, based on recognition elements, can be classified as:

Immuno-sensors: electrochemical immunoassay techniques take advantage of higher selectivity of recognizing the antibody and antigen molecule. Since it is a relatively simple

device, miniaturization, and higher sensitivity, this can be used in and developed in disease biomarkers detection fields and other diagnostic tests.[73]

Chemically modified electrochemical sensors: the electrode in these sensors made up of Fe_3O_4-SWCNTs composites are chemically modified deliberately. Typically, the electrode modification consists of either coating the electrode or on the surface of electrode bounding of required modifiers, which can alter the electrochemical properties of the Fe_3O_4-SWCNTs composites electrodes. For modifying electrodes within the electrode, the electro-catalytic medium's inclusion is one of the attractive approaches. Organic, inorganic, or hybrid composites can change the electrode composition to achieve specific sensing requirements.[83]

Enzymatic electrochemical sensor: by immobilizing the enzyme layer on the electrode surface, which is made by Fe_3O_4-SWCNTs composites for responding to the interactions occurring because of the bicatalytic reaction in the presence of the target substrate, this type of sensor can fabricate. In a few biosensors, enzymes and targets can be involved in the reduction or oxidation of the reaction with the help of an electrochemical transducer which can convert it into an electrical signal. Enzymes provide various advantages like higher selectivity, higher sensitivity, and relatively faster response because enzymes show catalytic activity, decreasing response time and hence sensitivity increases but losing its activity because of immobilization.[92]

5.4 Some other applications of Fe_3O_4-SWCNTs

Magnetite/SWCNTs synthesized with solvothermal methods can effectively eliminate both bacteriophage and bacteria in water. It is also capable of removing a variety of pathogens. Iron oxide, mainly Fe_3O_4/SWCNTs nanoparticles, can be used as an adsorbent in treating wastewater. Various other applications of Fe_3O_4/SWCNTs hybrids are shown in Table 14.1.

TABLE 14.1 Some other applications of Fe_3O_4-SWCNTs.

Compositions	Applications	References
Fe_3O_4-SWCNTs aerogel	Arsenic ions can remove from the water.	74
Fe_3O_4-SWCNTs	Higher electrochemical adsorption ability of inorganic arsenic species.	75
Fe_3O_4-SWCNTs supported with cyclodextrin	From wastewater, heavy metals can remove.	76
Magnetic mesoporous silica and Fe_3O_4-SWCNTs modified with polyethylenimine	These hierarchical composites can be used for the synthetic adsorptive simultaneous removal of humic acid and metal ions.	77
Magnetic and conductive- Fe_3O_4-SWCNTs based multifunctional membrane or film	It can be used in water desalination. It can also use in catalysis, biomedical fields, radiation shielding devices, and supercapacitors.	78
SWCNTs- Fe_3O_4	This act as a super adsorbent for removing 1-naphthol, naphthalene, and 1-naphthylamine with different polarity.	79
3D Fe_3O_4 foam supported with SWCNTs	It can be used as an anode in a lithium battery	80

6. Conclusion and future scope

The composites of IONs and SWCNTs, in unique morphological forms like Fe_2O_3-SWCNTs and Magnetite (Fe_3O_4)-SWCNTs Composites, Fe_3O_4-SWCNTs Aerogels, bicomponent magnetite-SWCNTs and multi-component magnetite- SWCNTs, etc., can be blend together by various techniques like solvothermal and hydrothermal techniques. The synthesized composites can be used in many current and future applications, including sensor, biosensor, and analytical applications and the degradation and removal of water pollutants in environmental remediation. These applications include electrical components like transformers, inductors, bobbins, and other electromechanical components, materials for Li-Ion battery anodes, supercapacitors, SWCNTs-ferrofluid-cement for construction.[97–101]

References

1. Kumar I, Dhanasekaran C. Nanomaterial-based energy storage, and supply system in aircraft. In: *Materials today: proceedings*. vol 18. Elsevier Ltd; 2019. p. 4341–50.
2. Kumar I. Nanomaterial-based energy storage and supply system in aircraft systems. *Nanomater Compos Energy Appl* 2019:283–302. https://doi.org/10.1201/9780429265051-12.
3. 3Kumar I, Dhanasekaran C. Materials today: proceedings Iron-based nanomaterial sheets for electromechanical applications. *Mater Today Proc* 2020:2–6. https://doi.org/10.1016/j.matpr.2020.06.280.
4. Kumar I, Dhanasekaran C. Materials today: proceedings Synthesizing helical-single walled carbon nanotubes by chemical vapour decomposition for engine. *Mater Today Proc* 2020:2–7. https://doi.org/10.1016/j.matpr.2020.04.209.
5. Kumar I, Dhanasekaran C. A review on nano-casing of jet engine and diesel engine using single-walled carbon nanotubes. *Mater Today Proc* 2019;**18**.
6. Kumar I, Dhanasekaran C. Science direct behaviour of cottonseed oil blended with single-walled carbon nanotubes in , direct injection single cylinder diesel engine. *Mater Today Proc* 2020;**24**:2157–62.
7. Hu FM, Ma T, Lin H-Q, Gubernatis JE. Magnetic impurities in graphene. *Phys Rev B* 2011;**84**:075414.
8. Voloshina E, Dedkov Y. Electronic and magnetic properties of the graphene ferromagnet interfaces: theory vs. experiment. In: Mikhailov S, editor. *Physics and applications of graphene- experiments*. Rijeka, Croatia: Intech; 2011.
9. Le HM, Hirao H, Kawazoe Y, Nguyen-Manh DJ. Nanostructures of C60-metalgraphene (metal = Ti, Cr, Mn, Fe, or Ni): a spin-polarized density functional theory study. *Phys Chem C* 2014;**118**:21057–65.
10. Raji AT, Lombardi EB. Stability, magnetic and electronic properties of cobalt- vacancy defect pairs in graphene: a first-principles study. *Physica B* 2015;**464**:28–37.
11. Li B, Xu D, Zhao J, Zeng H. First principles study of electronic and magnetic properties of co-doped armchair graphene nanoribbons. *J Nanomater* 2015;**538180**:9.
12. Donati F, Dubout Q, Autes G, Patthey F, Calleja F, Gambardella P, Yazyev OV, Brune H. Magnetic moment and anisotropy of individual Co atoms on graphene. *Phys Rev Lett* 2013;**236801**:5.
13. Vita H, Bottcher S, Leicht P, Horn K, Shick AB, Maca F. Electronic structure and magnetic properties of cobalt intercalated in graphene on Ir(111). *Phys Rev B* 2014;**90**:165432.
14. Afshar M, Doosti H. Magnetic properties of cobalt single layer added on graphene: a density functional theory study. *Mod Phys Lett B* 2015;**29**(2):9. 1450262.
15. Zhidkov IS, Skorikov NA, Korolev AV, Kukharenko AI, Kurmaev EZ, Fedorov VE, Cholakh SO. Electronic structure and magnetic properties of graphene/Co composites. *Carbon* 2015;**91**:298–303.
16. Lin K-YA, Hsu F-K, Lee W-D. Magnetic cobalt–graphene nanocomposite derived from self-assembly of MOFs with graphene oxide as an activator for peroxymonosulfate. *J Mater Chem* 2015;**3**:9480–90.
17. Zhang L, Huang Y, Zhang Y, Ma Y, Chen Y. Sol–gel autocombustion synthesis of graphene/cobalt magnetic nanocomposites. *J Nanosci Nanotechnol* 2013;**13**:1129–31.
18. Yang S, Cui G, Pang S, Cao Q, Kolb U, Feng X, Maier J, Mullen K. Fabrication of cobalt and cobalt oxide/graphene composites: towards high-performance anode materials for lithium ion batteries. *ChemSusChem* 2010;**3**:236–9.

19. Yao Y, Xu C, Qin J, Wei F, Rao M, Wang S. Synthesis of magnetic cobalt nanoparticles anchored on graphene nanosheets and catalytic decomposition of Orange II. *Ind Eng Chem Res* 2013;**52**:17341–50.
20. Umair A, Raza H. Controlled synthesis of bilayer graphene on nickel. *Nanoscale Res Lett* 2012;**7**:437.
21. Decker R, Brede J, Atodiresei N, Caciuc V, Blugel S, Wiesendanger R. Atomicscale magnetism of cobalt-intercalated graphene. *Phys Rev B* 2013;**87**:041403(R).
22. Rougemaille N, N'Diaye AT, Coraux J, Vo-Van C, Fruchart O, Schmid AK. Perpendicular magnetic anisotropy of cobalt films intercalated under graphene. *Appl Phys Lett* 2012;**101**:142403.
23. Vermisoglou EC, Devlin E, Giannakopoulou T, Romanos G, Boukos N, Psycharis V, Lei C, Lekakou C, Petridis D, Trapalis C. Reduced graphene oxide/iron carbide nanocomposites for magnetic and supercapacitor applications. *J Alloys Compd* 2014;**590**:102–9.
24. Dlubak B, Martin M-B, Weatherup RS, Yang H, Deranlot C, Blume R, Schloegl R, Fert A, Anane A, Hofmann S, Seneor P, Robertson J. Graphene-passivated nickel as an oxidation-resistant electrode for spintronics. *ACS Nano* 2012;**6**(12):10930–4.
25. Sicot M, Bouvron S, Zander O, Rudiger U, Dedkov VS, Fonin M. Nucleation and growth of nickel nanoclusters on graphene Moire on Rh(111). *Appl Phys Lett* 2010;**96**:093115.
26. Mural PKS, Pawar SP, Jayanthi S, Madras G, Sood AK, Bose S. Engineering nanostructures by decorating magnetic nanoparticles onto graphene oxide sheets to shield electromagnetic radiations. *ACS Appl Mater Interfaces* 2015;**7**:16266–78.
27. Qu W, Zhang L, Chen G. Magnetic loading of graphene–nickel nanoparticle hybrid for electrochemical sensing of carbohydrates. *Biosens Bioelectron* 2013;**42**:430–3.
28. Fang J, Zha W, Kang M, Lu S, Cui L, Li S. Microwave absorption response of nickel/graphene nanocomposites prepared by electrodeposition. *J Mater Sci* 2013;**48**:8060–7.
29. Aravind SSJ, Eswaraiah V, Ramaprabhu S. Facile and simultaneous production of metal/metal oxide dispersed graphene nano composites by solar exfoliation. *J Mater Chem* 2011;**21**(43):17094–7.
30. Lee S-H, Sridhar V, Jung J-H, Karthikeyan K, Lee YS, Mukherjee R, Koratkar N, Oh I-K. Graphene nanotube iron hierarchical nanostructure as lithium ion battery anode. *ACS Nano* 2013;**785**:4242–51.
31. Takahashi K, Wang Y, Chiba S, Nakagawa Y, Isobe S, Ohnuki S. Low temperature hydrogenation of iron nanoparticles graphene. *Sci Rep* 2014;**4**:4598.
32. Kumar H, Shukla AK. Fabrication Fe/Fe_3O_4/graphene nanocomposite electrode material for rechargeable Ni/Fe batteries in hybrid electric vehicles. *Int Lett Chem Phys Astron* 2013;**2013**:15–25.
33. Jabeen H, Chandra V, Jung S, Woo Lee J, Kim KS, Bin Kim S. Enhanced Cr(VI) removal using iron nanoparticle decorated graphene. *Nanoscale* 2011;**3**:3583–5.
34. Guo J, Wang R, Weei Tjiu W, Pan J, Liu T. Synthesis of Fe nanoparticles@graphene composites for environmental applications. *J Hazard Mater* 2012;**225–226**:63–73.
35. Li Y, Zhou W, Wang H, Xie L, Liang Y, Wei F, Idrobo J-C, Pennycook SJ, Dai H. An oxygen reduction electrocatalyst based on carbon nanotube-graphene complexes. *Nat Nanotechnol* 2012;**7**:394–400.
36. Parvez K, Yang S, Hernandez Y, Winter A, Turchanin A, Feng X, Mullen K. Nitrogen-doped graphene and its iron-based composite as efficient electrocatalysts for oxygen reduction reaction. *ACS Nano* 2012;**6**(11):9541–50.
37. Zhu J, Sadu R, Wei S, Chen DH, Haldolaarachchige N, Luo Z, Gomes JA, Young DP, Guo Z. Magnetic graphene nanoplatelet composites toward arsenic removal. *ECS J. Solid State Sci. Technol.* 2012;**1**(1):M1–5.
38. Zhu J, Wei S, Gu H, Rapole SB, Wang Q, Luo Z, Haldolaarachchige N, Young DP, Guo Z. One-pot synthesis of magnetic graphene nanocomposites decorated with core@double-shell nanoparticles for fast chromium removal. *Environ Sci Technol* 2012;**46**:977–85.
39. Zhang X, Alloul O, He Q, Zhu J, Joseph Verde M, Li Y, Wei S, Guo Z. Strengthened magnetic epoxy nanocomposites with protruding nanoparticles on the graphene nanosheets. *Polymer* 2013;**54**:3594–604.
40. Wang Y, He Q, Qu H, Zhang X, Guo J, Zhu J, Zhao G, Colorado HA, Yu J, et al. Magnetic graphene oxide nanocomposites: nanoparticles growth mechanism and property analysis. *J Mater Chem C* 2014;**2**:9478–88.
41. McCoy TM, Brown P, Eastoe J, Tabor RF. Noncovalent magnetic control and reversible recovery of graphene oxide using iron oxide and magnetic surfactants. *ACS Appl Mater Interfaces* 2015;**7**:2124–33.
42. Sun Z, Madej E, Wiktor C, et al. One-pot synthesis of carbon-coated nanostructured iron oxide on few-layer graphene for lithium-ion batteries. *Chem Eur J* 2015;**21**:16154–61.
43. Jang B, Chae OB, Park S-K, Ha J, Oh S-M, Na HB, Piao Y. Solventless synthesis of an iron-oxide/graphene nanocomposite and its application as an anode in high-rate Li-ion batteries. *J Mater Chem* 2013;**1**:15442–6.

44. Tae Kim I, Magasinski A, Jacob K, Yushin G, Tannenbaum R. Synthesis and electrochemical performance of reduced graphene oxide/maghemite composite anode for lithium ion batteries. *Carbon* 2013;**52**:56–64.
45. Zhu X, Zhu Y, Murali S, Stoller MD, Ruoff RS. Nanostructured reduced graphene oxide/Fe2O3 composite as a high-performance anode material for lithium ion batteries. *ACS Nano* 2011;**5**(4):3333–8.
46. Eeu YC, Lim HN, Lim YS, Zakarya SA, Huang NM. Electrodeposition of polypyrrole/reduced graphene oxide/iron oxide nanocomposite as supercapacitor electrode material. *J Nanomater* 2013;**2013**:6. 653890.
47. Sinh A, Jan NR. Separation of microcystin-LR by cyclodextrin-functionalized magnetic composite of colloidal graphene and porous silica. *ACS Appl Mater Interfaces* 2015;**7**:9911–9.
48. agadeesh RV, Natte K, Junge H, Beller M. Nitrogen-doped graphene-activated iron-oxide-based nanocatalysts for selective transfer hydrogenation of nitroarenes. *ACS Catal* 2015;**5**:1526–9.
49. Jung SM, Jung HY, Dresselhaus MS, Jung JJ, Kong J. A facile route for 3D aerogels from nanostructured 1D and 2D materials. *Sci Rep* 2012;**2**:849.
50. Zhou S, Jiang W, Wang T, Lu Y. Highly hydrophobic, compressible, and magnetic polystyrene/Fe_3O_4/graphene aerogel composite for oil–water separation. *Ind Eng Chem Res* 2015;**54**:5460–7.
51. Ren L, Huang S, Fan W, Liu T. One-step preparation of hierarchical superparamagnetic iron oxide/graphene composites via hydrothermal method. *Appl Surf Sci* 2011;**258**:1132–8.
52. Fu C, Zhao G, Zhang H, Li S. A facile route to controllable synthesis of Fe_3O_4/graphene composites and their application in lithium-ion batteries. *Int J Electrochem Sci* 2014;**9**:46–60.
53. Wang G, Gao Z, Wan G, Lin S, Yang P, Qin Y. Supported high-density magnetic nanoparticles on graphene by atomic layer deposition used as efficient synergistic microwave absorbers. *Nano Res* 2014;**7**(5):704–16.
54. Yang S, Chen L, Mu L, Ma PC. Magnetic graphene foam for efficient adsorption of oil and organic solvents. *J Colloid Interface Sci* 2014;**430**:337–44.
55. Farghali MA, Salah El-Din TA, Al-Enizi AM, El Bahnasawy RM. Graphene/magnetite nanocomposite for potential environmental application. *Int J Electrochem Sci* 2015;**10**:529–37.
56. Wu Z-S, Yang S, Sun Y, Parvez K, Feng X, Müllen K. 3D nitrogen-doped graphene aerogel-supported Fe_3O_4 nanoparticles as efficient electrocatalysts for the oxygen reduction reaction. *J Am Chem Soc* 2012;**134**:9082–5.
57. Xu X, Li H, Zhang Q, Hu H, Zhao Z, Li J, Li J, Qiao Y, Gogotsi Y. Selfsensing, ultralight, and conductive 3D graphene/iron oxide aerogel elastomer deformable in a magnetic field. *ACS Nano* 2015;**9**(4):3969–77.
58. Xue Y, Chen H, Yu D, et al. Oxidizing metal ions with graphene oxide: the in situ formation of magnetic nanoparticles on self-reduced graphene sheets for multifunctional applications. *Chem Commun* 2011;**47**:11689–91.
59. He H, Gao C. Supraparamagnetic, conductive, and processable multifunctional graphene nanosheets coated with high-density Fe_3O_4 nanoparticles. *Appl Mater Interf* 2010;**2**(11):3201–10.
60. Urbas K, Aleksandrzak M, Jedrzejczak M, Jedrzejczak M, Rakoczy R, Chen X, Mijowska E. Chemical and magnetic functionalization of graphene oxide as a route to enhance its biocompatibility. *Nanoscale Res Lett* 2014;**9**:656.
61. Yin P, Sun N, Deng C, Li Y, Zhang X, Yang P. Facile preparation of magnetic graphene double-sided mesoporous composites for the selective enrichment and analysis of endogenous peptides. *Proteomics* 2013;**13**:2243–50.
62. Huang D, Wang X, Deng C, Song G, Cheng H, Zhang X. Facile preparation of raisin-bread sandwich-structured magneticgraphene/mesoporous silica composites with C18-modified pore-walls for efficient enrichment of phthalates in environmental water. *J Chromatogr A* 2014;**1325**:65–71.
63. Yadav M, Rhee KY, Park JS, Hui D. Mechanical properties of Fe_3O_4/GO/chitosan composites. *Composites Part B* 2014;**66**:89–96.
64. Zhang W, Li X, Zou R, Wu H, Shi H, Yu S, Liu Y. Multifunctional glucose biosensors from Fe_3O_4 nanoparticles modified chitosan/graphene nanocomposites. *Sci Rep* 2015;**5**:11129.
65. Ou Y, Wang F, Huang Y, Li D, Jiang Y, Qin Q-H, Stachurski ZH, Tricoli A, Zhang T. Fabrication and cytocompatibility of Fe_3O_4/SiO2/graphene–CdTeQDs/CS nanocomposites for drug delivery. *Colloids Surf B Biointerfaces* 2014;**117**:466–72.
66. Fan L, Luo C, Li X, Lu F, Qiu H, Sun M. Fabrication of novel magnetic chitosan grafted with graphene oxide to enhance adsorption properties for methyl blue. *J Hazard Mater* 2012:272–9.
67. Fan L, Luo C, Sun M, Li X, Lu F, Qiu H. Preparation of novel magnetic chitosan/graphene oxide composite as effective adsorbents toward methylene blue. *Bioresour Technol* 2012;**114**:703–6.
68. Jovici N, Calatayud MP, Sanz B, Montone A, Goya GF. Ex situ integration of iron oxide nanoparticles onto exfoliated expanded graphite flakes in aqueous suspension. *J Serb Chem Soc* 2014;**79**(9):1155–67.

69. Wang N, Hu B, Chen M-L, Wang J-H. Polyethylenimine mediated silver nanoparticle-decorated magnetic graphene as a promising photothermal antibacterial agent. *Nanotechnology* 2015;**26**:8. 195703.
70. Zhan S, Zhu D, Ma S, Yu W, Jia Y, Li Y, Yu H, Shen Z. Highly efficient removal of pathogenic bacteria with magnetic graphene composite. *ACS Appl Mater Interfaces* 2015;**7**:4290–8.
71. Kyzas GZ, Deliyanni EA, Matis KA. Graphene oxide and its application as an adsorbent for wastewater treatment. *J Chem Technol Biotechnol* 2014;**89**:196–205.
72. Ye Y, Yin D, Wang B, Zhang Q. Synthesis of three-dimensional Fe_3O_4/graphene aerogels for the removal of arsenic ions from water. *J Nanomater* 2015;**864864**:6.
73. Mishra AK, Ramaprabhu S. Ultrahigh arsenic sorption using iron oxide-graphene nanocomposite supercapacitor assembly. *J Appl Phys* 2012;**112**:104315.
74. Hu X-j, Liu Y-g, Wang H, Zeng G-m, Hua X, Guo Y-m, Li T-t, Chen A-w, Jiang L-h, Guo F-y. Adsorption of copper by magnetic grapheneoxide-supported-cyclodextrin: effects of pH, ionicstrength, background electrolytes, and citric acid. *Chem. Chem. Eng. Res. Design* 2015;**93**:675–83.
75. Wang Y, Liang S, Chen B, Guo F, Yu S, Tang Y. Synergistic removal of Pb(II), Cd(II) and humic acid by Fe_3O_4@-mesoporous silica-graphene oxide composites. *PLoS One* 2013;**8**(6):e65634.
76. Narayanan TN, Liu Z, Lakshmy PR, Gao W, Nagaoka Y, Sakthi Kumar D, Lou J, Vajtai R, Ajayan PM. Synthesis of reduced graphene oxide– Fe_3O_4 multifunctional freestanding membranes and their temperature dependent electronic transport properties. *Carbon* 2012;**50**:1338–45.
77. Yang X, Li J, Wen T, Ren X, Huang Y, Wang X. Adsorption of naphthalene and its derivatives on magnetic graphene composites and the mechanism investigation. *Colloids Surf A Physicochem Eng Asp* 2013;**422**:118–25.
78. Luo J, Liu J, Zeng Z, et al. Three-dimensional graphene foam supported Fe_3O_4 lithium battery anodes with long cycle life and high rate capability. *Nano Lett* 2013;**13**:6136–43.
79. Yoon T, Kim J, Kim J, Kyoo Lee J. Electrostatic self-assembly of Fe_3O_4 nanoparticles on graphene oxides for high capacity lithium-ion battery anodes. *Energies* 2013;**6**:4830–40.
80. Zhao DF, Yang H, Li RS, Ma JY, Feng WJ. Fabrication of nickel ferrite–graphene nanocomposites and their photocatalytic properties. *Mater Res Innovat* 2014;**18**(7):519–23.
81. Zhu P, Liu S, Xie J, Zhang S, Cao G, Zhao X. Facile synthesis of NiFe2O4/reduced graphene oxide hybrid with enhanced electrochemical lithium storage performance. *J Mater Sci Technol* 2014;**30**(11):1078–83.
82. Wang W, Hao Q, Lei W, Xia X, Wang X. Ternary nitrogen-doped graphene/nickel ferrite/polyaniline nanocomposites for high-performance supercapacitors. *J Power Sources* 2014;**269**:250–9.
83. Xiao Y, Li X, Zai J, Wang K, Gong Y, Li B, Han Q, Qian X. CoFe2O4-graphene nanocomposites synthesized through an ultrasonic method with enhanced performances as anode materials for Li-ion batteries. *Nano-Micro Lett* 2014;**6**(4):307–15.
84. Suwanchawalit C, Somjit V. Hydrothermal synthesis of magnetic CoFe2O4-graphene nanocomposite with enhanced photocatalytic performance. *Digest J. Nanomater. Biostruct* 2015;**10**(3):769–77.
85. Li N, Zheng M, Chang X, Ji G, Lu H, Xue L, Pan L, Cao J. Preparation of magnetic CoFe2O4-functionalized graphene sheets via a facile hydrothermal method and their adsorption properties. *J Solid State Chem* 2011;**184**:953–8.
86. Ramesh Kumar P, Kollu P, Santhosh C, Eswara Varaprasada Rao K, Kim DK, Nirmala Grace A. Enhanced properties of porous CoFe2O4–reduced graphene oxide composites with alginate binders for Li-ion battery applications. *New J Chem* 2014;**38**:3654–61.
87. Fei P, Zhong M, Lei Z, Su B. One-pot solvothermal synthesized enhanced magnetic zinc ferrite–reduced graphene oxide composite material as adsorbent for methylene blue removal. *Mater Lett* 2013;**108**:72–4.
88. Zhang W, Quan B, Lee C, et al. One-step facile solvothermal synthesis of copper ferrite–graphene composite as a high-performance supercapacitor material. *ACS Appl Mater Interfaces* 2015;**7**:2404–14.
89. Shahnavaz Z, Woi PW, Aliasn Y. A hydrothermally prepared reduced graphene oxide-supported copper ferrite hybrid for glucose sensing. *Ceram Int* 2015;**41**:12710–6.
90. Cheng G, Yu X, Zhou MD, Zheng S-Y. Preparation of magnetic graphene composites with hierarchical structure for selective capture of phosphopeptides. *J Mater Chem B* 2014;**2**:4711–9.
91. Peng E, Shi Guang Choo E, Chandrasekharan P, et al. Synthesis of manganese ferrite/graphene oxide nanocomposites for biomedical applications. *Small* 2012;**8**(23):3620–30.

92. Yang Y, Shi H, Wang Y, et al. Graphene oxide/manganese ferrite nanohybrids for magnetic resonance imaging, photothermal therapy and drug delivery. *J Biomater Appl* January 2016;**30**(6):810–22. http://www.ncbi.nlm.nih.gov/pubmed/26296777.
93. Panwar R, Puthucheri S, Singh D, Agarwala V. Design of ferrite–graphene-based thin broadband radar wave absorber for stealth application. *IEEE Trans Magn* 2015;**51**(1):4. 2802804.
94. Durmus Z, Durmus A, Kavas H. Synthesis and characterization of structural and magnetic properties of graphene/hard ferrite nanocomposites as microwave-absorbing material. *J Mater Sci* 2015;**50**:1201–13.
95. Gao T, Chen Z, Huang Q, Niu F, Huang X, Qin L, Huang Y. A review: preparation of bismuth ferrite nanoparticles and its applications in visible-light induced photocatalyses. *Rev Adv Mater Sci* 2015;**40**:97–109.
96. Dai JF, Xian T, Di LJ, Yang H. Preparation of BiFeO3-graphene nanocomposites and their enhanced photocatalytic activities. *J Nanomater* 2013:5. 642897.
97. Li T, Shen J, Li N, Ye M. Hydrothermal preparation, characterization and enhanced properties of reduced graphene-BiFeO3 nanocomposite. *Mater Lett* 2013;**91**:42–4.
98. Candini A, Klyatskaya S, Ruben M, Wernsdorfer w, Affronte M. Graphene spintronic devices with molecular nanomagnets. *Nano Lett* 2011;**11**:2634–9.
99. Lopes M, Candini A, Urdampilleta M, et al. Surface-enhanced Raman signal for terbium single-molecule magnets grafted on graphene. *ACS Nano* 2010;**4**(12):7531–7.
100. Govan J, Gun'ko YK. Recent advances in the application of magnetic nanoparticles as a support for homogeneous catalysts. *Nanomaterials* 2014;**4**:222–41.
101. Gan N, Zhang J, Lin S, Long N, Li T, Cao Y. A novel magnetic graphene oxide composite absorbent for removing trace residues of polybrominated diphenyl ethers in water. *Materials* 2014;**7**:6028–44.

This page intentionally left blank

CHAPTER

15

Bionanofiber-reinforced transparent nanocomposites for future applications

Subir Kumar Biswas[1,2], *Xianpeng Yang*[1], *Hiroyuki Yano*[1] *and Md. Iftekhar Shams*[3]

[1]**Laboratory of Active Bio-based Materials, Research Institute for Sustainable Humanosphere, Kyoto University, Uji, Kyoto, Japan;** [2]**Pulp and Paper Division, Bangladesh Forest Research Institute, Sholoshahor, Chattogram, Bangladesh;** [3]**Forestry and Wood Technology Discipline, Life Science School, Khulna University, Khulna, Bangladesh**

1. Introduction

Nanocomposites are ubiquitously found in nature. Almost all the stiff biological materials, such as wood, bone, teeth, insect cuticles, crustacean shells, mollusk shells, silk, antlers, fish scales, etc., are nanocomposites.[1,2] These materials are light-weight but have high strength, stiffness and/or toughness primarily to serve the structural function, thanks to their nanoscale reinforcement phase combined with intelligently designed composite structure from nano-to-macroscale. In some materials, for example, wood and insect cuticles, a polymer matrix is reinforced by nanoscale polymer fibers—cellulose or chitin. Whereas, in some materials, for example, crustacean shells, mollusk shells, bone and teeth, a polymer (including nanoscale fibrous) matrix is reinforced by nanoscale mineral particles. Geared from the outstanding properties of these biological nanocomposite materials, there has been a recent research hype to synthesize novel light-weight and high-strength nanocomposite materials with added functionalities by utilizing nanoscale reinforcement phase.

Today, diverse kinds of nanoscale reinforcements are known to us, either organic-natural origin (such as cellulose and chitin nanofibers),[3–7] inorganic-natural origin (such as clay nanoplatelets),[8] organic-synthetic origin (such as Kevlar, polyester, and silk nanofibers),[9–12] inorganic-synthetic origin (such as carbon nanomaterials—carbon nanotubes, carbon nanofibers, graphene nanoribbons, etc.),[8] or hybrid origin (such as silk-clay composite

Applications of Multifunctional Nanomaterials
https://doi.org/10.1016/B978-0-12-820557-0.00026-6

nanofibers).[10,12] Cellulose nanofibers (CNFs) that are readily extractable from plants,[3–5] and chitin nanofibers (ChNFs) that are readily extractable predominantly from crustacean sources,[7] both being the most earth-abundant natural reinforcement nanomaterials, renewable, and biodegradable, they already have received a substantial attention in the first-quarter of the 21st century. Moreover, because CNFs and ChNFs are highly crystalline in nature having hydrogen-bonded extended polysaccharide chains, they have very high mechanical strength and thermal stability, especially which of CNFs are comparable to or even better than Kevlar, carbon fiber, or steel (Table 15.1). In addition, they have the unique ability to form strong network via hydrogen bonding in the polymer matrix that promotes the mechanical properties, and are amenable to chemical modification to introduce further functionalities.

CNFs were first utilized as the reinforcement in the polymer matrix by Favier et al. in 1995.[35,36] They used mixed-aspect-ratio tunicate cellulose nanowhiskers having a width of 10–20 nm and a length ranging from 100 nm to several micrometers. The nanowhiskers (0–14 wt%) were mixed with the styrene-butyl-acrylate copolymer latex. A 6 wt% nanowhiskers content in the composite film achieved more than two orders of magnitude higher mechanical properties than that of the neat copolymer film. A major breakthrough in obtaining CNF-reinforced "functional" nanocomposites was made by Yano et al. in 2005.[37] They used long, high-aspect-ratio CNFs (~50 nm wide and several micrometers long) from bacteria (BCNFs) to prepare a (nano)paper followed by impregnation and polymerization of the transparent monomer resins into it. Apart from the high mechanical improvement over the neat polymers, the nanocomposites were highly flexible, optically transparent (>80% light

TABLE 15.1 Properties of crystalline cellulose, chitin, and various other reinforcing materials.

Material	Density (G CM^{-3})	Tensile strength (GPA)	Elastic modulus (GPA)	Coefficient of thermal expansion (CTE) (ppm k^{-1})	References
KEVLAR-49 FIBER	1.4	3.6–4.1	124–131	−2.0	13,14
CARBON FIBER	1.8	1.5–5.5	150–500	−0.6	14
MILD STEEL	–	0.4–0.6	194–243	–	15
HIGH STRENGTH STEEL	–	0.8–0.9	207–242	–	15
STAINLESS STEEL	7.8	0.4–1.8	193–204	10.2–17.2	14
CLAY NANOPLATELETS	–	–	170	–	16
CARBON NANOTUBES	–	11–63	270–950	–	17,18
BORON NANOWHISKERS	–	2–8	250–360	–	19
CNF (crystalline)	**1.6**	**2–7.7**	**~140**	**0.1[a], 6[b]**	20–31
ChNF (crystalline)	**1.6**	**1.6–3**	**41–70**	**21**	32–34

[a]*CTE was measured in an all-cellulose composite using a thermomechanical analyzer.*[24]
[b]*CTE of the wood cellulose crystal was measured using X-ray diffraction.*[31]
Adapted with permission from Moon RJ, Martini A, Nairn J, Simonsen J, Youngblood J. Cellulose nanomaterials review: structure, properties and nanocomposites. Chem Soc Rev *2011;**40**:3941–3994 © 2011 The Royal Society of Chemistry.*

transmittance), combined with a coefficient of thermal expansion (CTE) as low as 6 ppm K^{-1} (about 8–33 times lower than that of the most transparent and flexible plastics). Because the width of the BCNFs was one-10th of the visible light wavelengths, the nanocomposite was highly optically transparent even at a BCNFs content as high as 70 wt%. The CTE was comparable to that of "brittle" glass (7–10 ppm K^{-1}),[38] which is the mostly used transparent substrate in the optoelectronic devices such as solar cells, displays, organic light-emitting diodes (OLEDs), etc. Because of their desirable material properties and amenability for the "roll-to-roll" processing, the BCNF-reinforced transparent nanocomposite films were regarded as the suitable substrate for the optoelectronic devices.[39–41]

After the great achievement by Yano et al.,[37] there has been a boom in the nanocellulose-based (transparent) materials research that still continues. Note that, nanocellulose is the collective term of all forms of the nanoscale cellulose, such as CNFs, cellulose nanowhiskers, cellulose nanocrystals (CNCs), or cellulose nanorods (CNs). Inspired by the optically transparent nanocomposites reinforced by CNFs, research on the nanocomposites reinforced by ChNFs (extracted predominantly from crustacean shells) followed. Note that, chitin is the second most abundant biopolymer after cellulose with an annual production between 10^{10} to 10^{12} tons.[42] In this chapter, we describe preparation of nanocelluloses and nanochitins in general, and give an overview of the earliest to latest studies on their optically transparent nanocomposites and the future application thereof, with a particular focus on the pioneering works done at the Research Institute for Sustainable Humanosphere, Kyoto University in Japan.

2. Preparation of nanocelluloses

Nanocellulose, which generally refers to all types of nanometric cellulosic fibers, can be classified into two main subcategories.(1) CNFs, which have a semi-crystalline structure, a width of 3 ~ <100 nm, and a length of several micrometers; therefore, they have a very high aspect ratio (ca. >100). (2) Cellulose nanowhiskers, nanocrystals, or nanorods (CNCs or CNs), which have a very high crystallinity, but much shorter length (usually <1 μm). The nanocelluloses can be obtained from wood, plants, tunicate, algae, and bacteria.[3–5] The most viable sources are the woods and plants, considering a global production of approximately 100 billion tons per annum through photosynthesis.[43]

2.1 Preparation of CNFs

Shortly after the appearance of the first report on BCNF-reinforced optically transparent nanocomposite by Yano et al.,[37] the research was exaggerated to extract CNFs from more readily available sources, that is, wood and nonwood plants. Note that, in Wood Science, CNFs are commonly known as the elementary fibrils or microfibrils (3–5 nm wide) and their bundles (15–50 nm wide). CNFs are the main component of the plant cell (fiber) wall (Fig. 15.1). To extract CNFs, the cellulose fibers (i.e., pulp fibers) are first liberated by chemically removing and/or degrading the matrix substances—lignin and hemicelluloses. The water/fiber slurry is then mechanically nano-fibrillated by passing several times through a

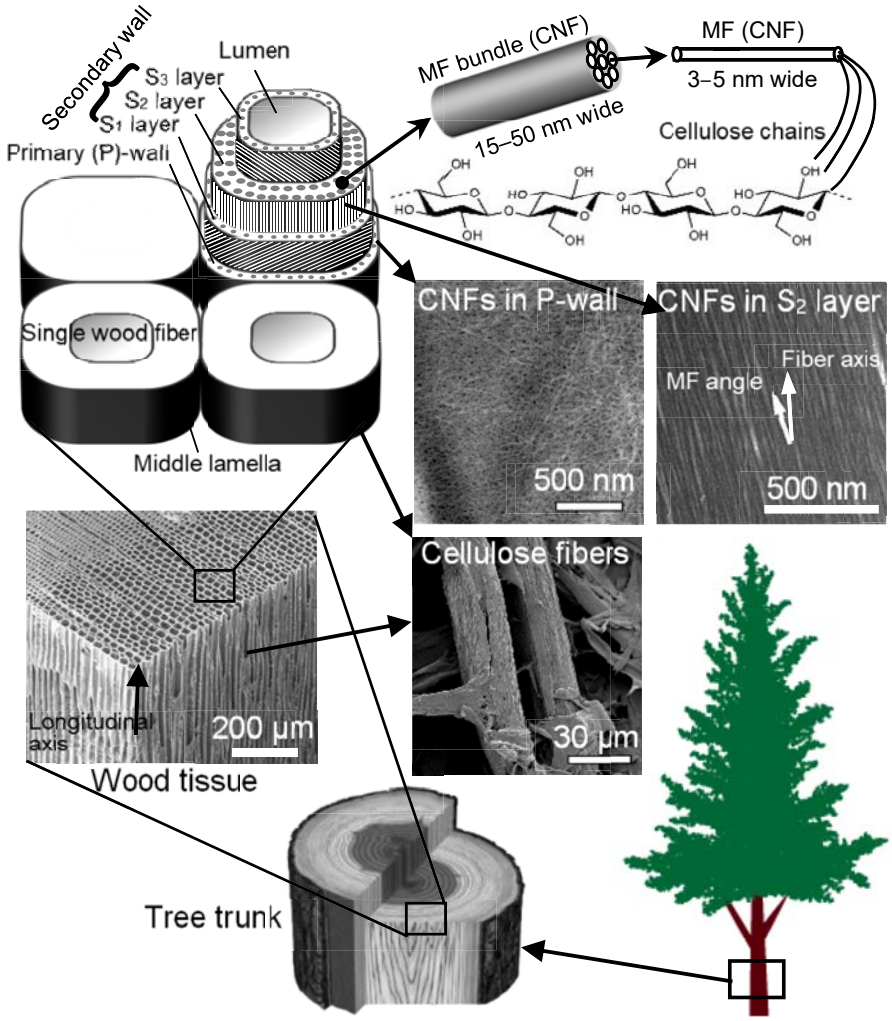

FIGURE 15.1 Illustration of the hierarchical structure of wood on different length scales.

grinder,[44] high-pressure homogenizer or microfluidizer,[45–49] or high intensity ultrasonic equipment.[50,51] Due to the strong mechanical treatment, the original crystalline structure of the cellulose fibrils get damaged that results in lowering the strength of the nanocelluloses. In 2007, Abe et al.[44] developed a method to obtain CNFs in native (unmodified) state with a uniform 15 nm width via "one-pass" grinder treatment (Fig. 15.2A). The CNFs obtained were high in crystallinity (~80%), owing to the much milder mechanical treatment.

The mechanical nano-fibrillation of cellulose fibers can be facilitated by swelling and loosening the interfibrillar hydrogen bonds via chemical or enzymatic pretreatments.[48–50,52–54] A chemical pretreatment usually modifies the cellulose surface by introducing electrostatic repulsive charges that facilitate liberation of the thin individualized CNFs during the mild

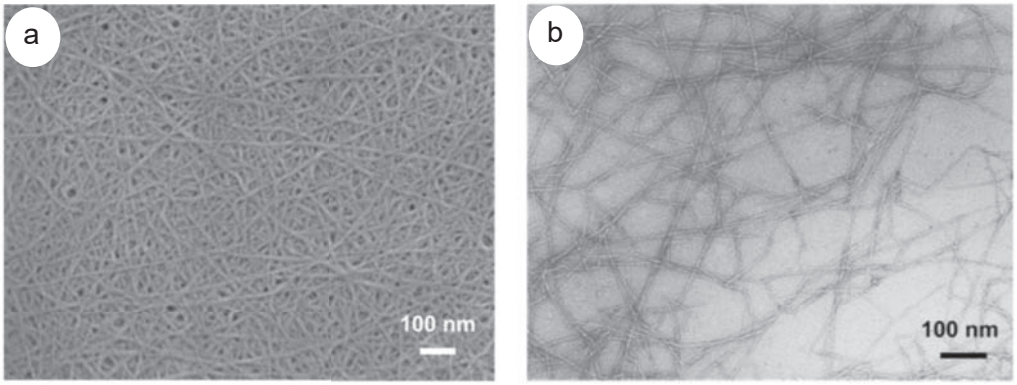

FIGURE 15.2 (A) FE-SEM micrograph of the isolated native CNFs from wood. (B) TEM micrograph of TEMPO-oxidized CNFs (surface modified; carboxylate content 1.5 mmol g^{-1}) with 3–4 nm in width. Both nanofibers were prepared under a never-dried condition. *Reproduced/adapted with permission from (A) Zimmermann T, Bordeanu N, Strub E. Properties of nanofibrillated cellulose from different raw materials and its reinforcement potential.* Carbohydr Polym *2010;**79**:1086–1093; and (B) Henriksson M, Henriksson G, Berglund LA, Lindström T. An environmentally friendly method for enzyme-assisted preparation of microfibrillated cellulose (MFC) nanofibers.* Eur Polym J *2007;**43**:3434–3441* © *2007 American Chemical Society.*

mechanical treatment. As for example, TEMPO (2,2,6,6-tetramethylpiperidine-1-oxyl radical)-mediated oxidation introduces carboxylate groups to the cellulose surface,[50,52] which facilitates liberation of CNFs having an elementary width (3–5 nm) even by simple magnetic stirring (Fig. 15.2B). On the other hand, the enzymes preferentially attack the amorphous part of the cellulose microfibrils but do not modify the cellulose, and hence reduce the energy consumption during the mechanical nano-fibrillation.[48,49,53]

2.2 Preparation of CNCs

CNFs are highly crystalline in nature and contain both highly ordered, highly hydrogen bonded crystalline regions, and disordered amorphous regions (Fig. 15.3A). The amorphous regions can be cleaved by acid hydrolysis to retrieve the crystalline parts, that is, CNCs (Fig. 15.3B–D).[55,56] CNCs are also known as cellulose nanowhiskers or cellulose nanorods (CNs). Due to the high order and intimate packing of the cellulose molecules via hydrogen bonding, the CNCs have a high axial modulus (stiffness) of ~140 GPa. However, it has been found that the CNFs promote strength and modulus of the nanocomposites better than the CNCs, owing to their larger aspect ratio and extensive fiber entanglement.[57]

Hydrolysis of the amorphous regions has been performed by sulfuric acid (H_2SO_4),[58] hydrochloric acid (HCl),[56,59,60] maleic acid,[61] and formic acid.[62] An important aspect of H_2SO_4 hydrolysis is that it introduces the sulfonate ester charge groups on the CNC surface, thereby, leads to a stable CNC/water suspension via electrostatic repulsion.[5,56] In contrast, CNCs can be obtained in an unmodified state by using other acids such as HCl.[56] The width, length and crystallinity of the CNCs can be tweaked by varying the hydrolysis condition, for example, acid concentration, time and temperature. Typically, the width varies between 3 and 20 nm, and length is <500 nm (but may vary between 50 and 4000 nm).[5] The crystallinity

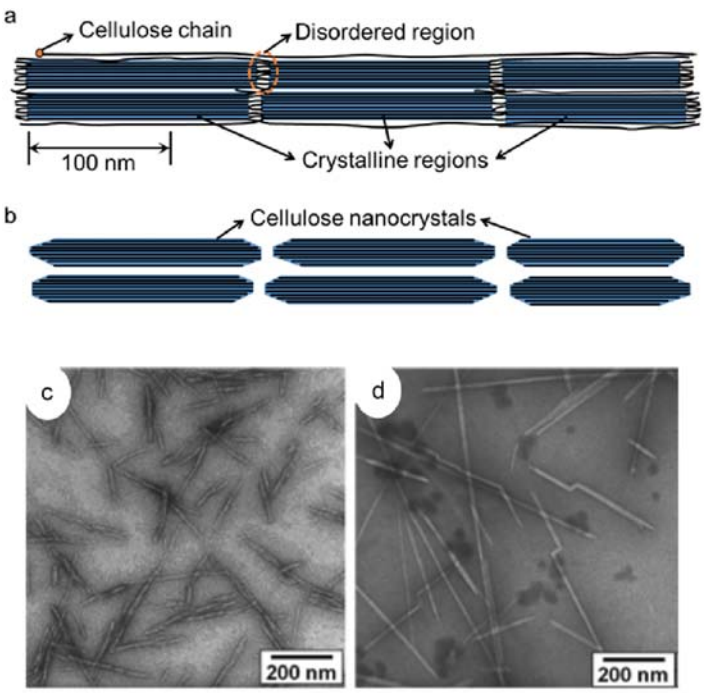

FIGURE 15.3 (A) Model CNFs with the semi-crystalline configuration, (B) CNCs that can be retrieved after the removal of amorphous (disordered) regions via acid hydrolysis, (C) CNCs retrieved from wood fibers, and (D) CNCs retrieved from tunicin. *Adapted/reproduced with permission from Ref. Moon RJ, Martini A, Nairn J, Simonsen J, Youngblood J. Cellulose nanomaterials review: structure, properties and nanocomposites.* Chem Soc Rev *2011;**40**:3941–3994 © 2011 The Royal Society of Chemistry.*

of wood- and plant-based CNCs can be 54%–88%, while the crystallinity of tunicate CNCs can be 85%–100%.[5] Note that the early introduction of nanocelluloses as the reinforcement was in the form of CNCs, perhaps, because of their ease of isolation via acid hydrolysis.

3. Preparation of nanochitins

Chitin is a linear natural polysaccharide of β-(1-4)-2-acetamido-2-deoxy-D-glucopyranose. It is structurally and chemically similar to cellulose, but an acetoamide group is present at the C-2 position of the anhydroglucose unit instead of the hydroxyl group (Fig. 15.4). After cellulose, chitin is the most abundant naturally occurring polysaccharide on earth.[6,7] Like

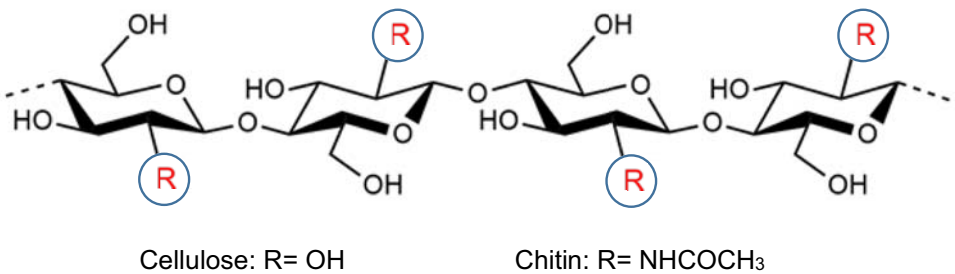

FIGURE 15.4 Chemical structure of cellulose and chitin.

cellulose, chitin is also highly crystalline (mostly α-chitin). The α-chitin (with antiparallel molecular arrangement) is mainly found in the external skeletons (shells) of mollusks, crabs, shrimp, and insects, and in the fibrous material of cellular walls of mushrooms and algae.[6,7,32,63,64] The β-chitin (with parallel molecular arrangement) is mainly found in the squid pens and tubeworms.[7,32,65] The crustacean shells (crabs, shrimps, lobsters, etc.) are composed of around 15%–40% chitin,[66] and the main source of industrial chitin. Inspired by the reinforcing effect provided by nanocelluloses, study on the isolation and utilization of nanochitins as the reinforcing element in the nanocomposites followed.

3.1 Preparation of ChNFs

Fig. 15.5 shows the hierarchical structure of the crustacean shell. Similar to cellulose, chitin also occurs in nature as the ordered nanofibrils of 2–5 nm in width, which are clustered into thicker chitin-protein nanofibers of 50–300 nm in width and embedded in a variety of proteins, lipids and minerals.[67] To isolate ChNFs from such a complex matrix, the mineral is removed first typically using a dilute HCl that produces a water-soluble salt. In the next step, removal of protein and lipid is done. Typically, sodium hydroxide (NaOH) or KOH solution is used with variations in the reaction temperature and time. Alkaline reaction condition usually resulted in the partial deacetylation of chitin into chitosan with the amino ($-NH_2$) group at the C-2 position. Therefore, the concentration of alkali should be chosen wisely so that a trace amount of deacetylation occurs. Generally, 4%–5% alkali is used with a suitable combination of reaction temperature and time.[68,69] The final step of the chitin purification is either the removal of pigment composition using an organic solvent (such as ethanol),[68] or bleach the chitin sample using an acidified $NaClO_2$ solution.[69]

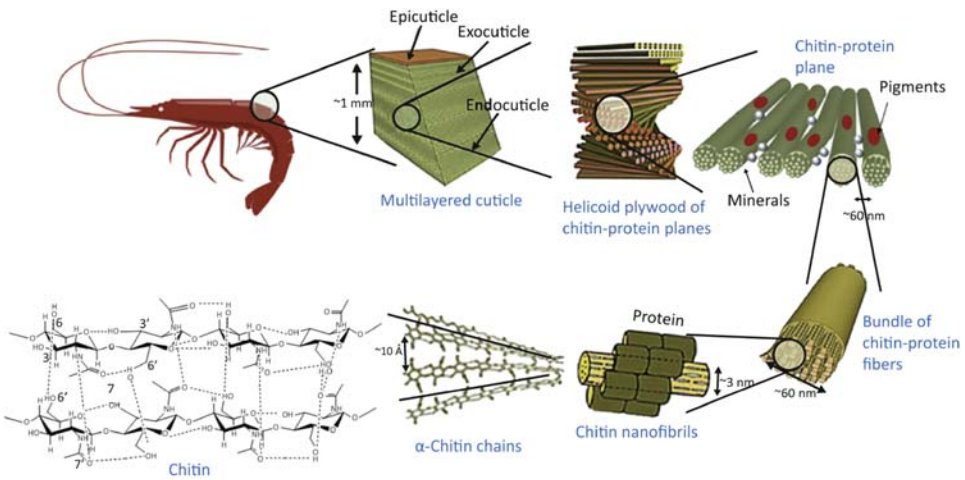

FIGURE 15.5 Illustration of the hierarchical structure of crustacean shell on different length scales. *Reproduced with permission from Ref. Hülsey MJ. Shell biorefinery: a comprehensive introduction. Green Ener Environ 2018 3:318–327 © 2018 Elsevier.*

After chitin purification from the source materials, the mechanical nanofibrillation method is same as for the CNFs as described above. However, the most important condition to obtain uniform and well-dispersed ChNFs is to introduce electrostatic repulsive charges on the surface of the chitin. Like cellulose, TEMPO-mediated oxidation can form C-6 carboxylate group on the chitin molecule, which gives negative repulsive charge in water.[7,70] Therefore, uniform and well-dispersed ChNFs can be obtained after the mechanical treatment. Another facile way to introduce electrostatic (positive) repulsive charge is to add few drops of acids (such as acetic acid or HCl) to maintain the pH of the chitin/water slurry at 3-4 during the mechanical treatment.[7,71] The isolated chitin usually contains small amounts of the C-2 amino group (due to the deacetylation during the chemical purification), which become suitably cationized at pH 3-4 and facilitate nanofibrillation in a width of 3–4 nm (Fig. 15.6A).[71] Shams and his coworkers[68,72,73] took this advantage to fibrillate ChNFs in a uniform width of 20–30 nm simply by using a house-hold food blender (Fig. 15.6B and C).

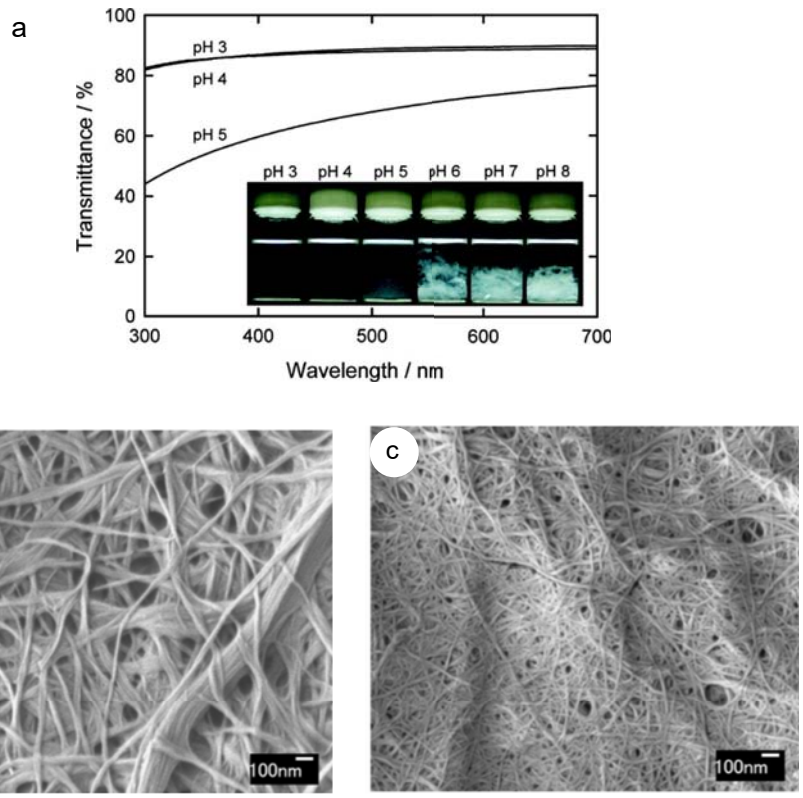

FIGURE 15.6 (A) Photographs of dispersions of squid pen β-chitin prepared by ultrasonication in water at pH 3–8 with their corresponding transmittance spectra. At pH 3–4, the dispersions are optically clear due to the thinner and well-dispersed ChNFs. (B) SEM image of ChNFs extracted from crab shells via a high-speed blender in water at pH 7. (C) SEM image of ChNFs extracted from crab shells via a high-speed blender in water at pH 3–4. *Reproduced with permission from (A) Fan Y, Saito T, Isogai A. Preparation of chitin nanofibers from squid pen β-chitin by simple mechanical treatment under acid conditions.* Biomacromolecules *2008;**9**:1919–1923 © 2008 American chemical society; and (B,C) Shams MI, Ifuku S, Nogi M, Oku T, Yano H. Fabrication of optically transparent chitin nanocomposites. Appl Phys A 2010;**102**:325–331.*

3.2 Preparation of ChNCs

Chitin nanocrystals or nanowhiskers (ChNCs) can be obtained by acid hydrolysis of purified chitin.[74–78] The early chitin nanocomposites were reinforced by ChNCs.[74,75] Typically, 3N HCl is used at 90–95°C for 90 min to prepare ChNCs of 15–20 nm in width and 200–300 nm in length. Fan et al.[70] reported the preparation of ChNCs using TEMPO-mediated oxidation followed by ultrasonic treatment. These ChNCs can be considered as the surface-modified ChNCs as carboxylate groups are present on the crystal surface. The ChNCs prepared by this method are thinner in width (8 nm) with a length of 340 nm. However, we noticed that, in literature, mostly ChNFs were used as the reinforcement in the transparent nanocomposites rather than ChNCs, probably owing to their facile extraction from bioresources (compared to CNFs) and their larger aspect ratio than ChNCs that promote extensive nanofiber entanglement and hence mechanical performance of the nanocomposites.

4. Bionanofiber-reinforced optically transparent composites

4.1 Transparent nanocomposites reinforced by individualized nanofibers

4.1.1 BCNFs-reinforced transparent nanocomposites

The first report on the fabrication of optically transparent nanocomposites reinforced with CNFs was published by Yano et al. in 2005.[37] CNF-scaffold spun by bacteria (Acetobacter xylinum) was compressed and dried to form a (nano)paper, and subsequently submerged into the transparent resin monomers (such as epoxy and acrylic resin) followed by polymerization. The small pores in the (nano)paper were replaced by the resin, and the nanocomposites (Fig. 15.7A) thus obtained with a BCNF-content of 60–70 wt% had an astonishing

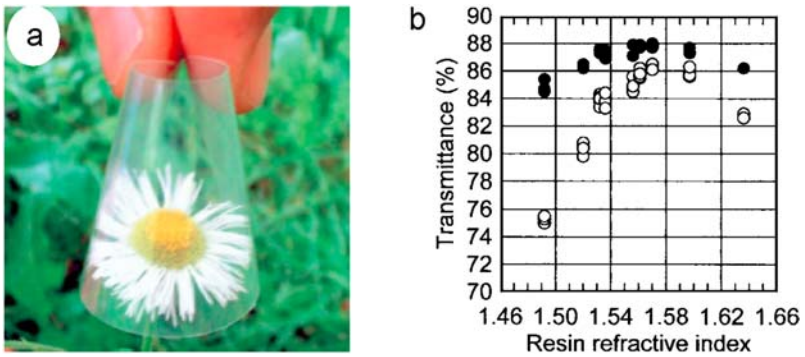

FIGURE 15.7 (A) Photograph of a 65-μm-thick BCNFs/acrylic resin nanocomposite (BCNF content 60 wt%). (B) Total (filled circle) and regular (open circle) light transmittances of the nanocomposites in relation to the refractive index of the corresponding acrylic resin at 20°C and 590 nm wavelength. *Reproduced with permission from (A) Yano H, Sugiyama J, Nakagaito AN, Nogi M, Matsuura T, Hikita M, Handa K. Optically transparent composites reinforced with networks of bacterial nanofibers.* Adv Mat *2005;**17**:153–155 © 2005 willey; and (B) Nogi M, Handa K, Nakagaito AN, Yano H. Optically transparent bionanofiber composites with low sensitivity to refractive index of the polymer matrix.* Appl Phys Lett *2005;**87**:243110 © 2005 American Institute of Physics.*

combination of material properties: (1) a high optical transparency (>80%), about 10% lower than that of the neat resin, (2) a high flexibility similar to the neat resin, (3) an elastic modulus of up to 21 GPa, five times higher than that of the engineered plastics, (4) a high strength of up to 325 MPa, and (5) an incredibly low CTE of 6 ppm K^{-1} (BCNFs/epoxy nanocomposite), 20 times lower than that of the neat epoxy. Because the width of the BCNFs in the bacteria-spun scaffold was about one-10th of the visible light wavelengths (~50 nm), the light propagated through the nanocomposites was almost free from scattering.[79] Therefore, the nanocomposites were highly optically transparent even at a BCNFs content as high as 70 wt%. As for the high mechanical and thermomechanical properties, the strong and thermally stable nanofibers (see Table 15.1) produced a strong, highly entangled network via hydrogen bonding in the (nano)paper, which was still maintained after the polymer impregnation. The intact strong network gave the nanocomposites a high mechanical strength and stiffness, and drastically restricted the high thermomechanical deformation of the polymer matrix. These nanocomposites can be simply described as the unique materials that are as transparent and thermally stable as glass, as strong as steel, and as flexible as plastic.

Realizing the potential of the nanocellulose-reinforced nanocomposites in application such as the substitute substrate of glass in flexible and light-weight optoelectronic devices such as flexible displays and solar cells, Yano's research group did further studies using BCNFs as the model. First, they studied the effect of refractive index variations between the resin and BCNFs on their nanocomposites.[80] Acrylic resins with refractive indices from 1.492 to 1.636 were used. Note that the refractive index of cellulose is 1.618 along the fiber and 1.544 in the transverse direction. The nanocomposites were 56−63 μm thick, and the nanofiber content was 56−62 wt%. Fig. 15.7B shows that even the refractive indices of the nanofibers and the resins were not exactly matching, the nanocomposites were still optically transparent due to the much less width of the nanofibers than the visible wavelength.[79] However, the highest transparency was obtained with the resin having a refractive index right about the same as the average of the refractive indices of the cellulose along and perpendicular to the fiber direction.

Further studies revealed that some properties of the BCNF-reinforced nanocomposites can be improved by surface acetylation of the BCNFs.[81,82] A practical disadvantage of cellulose is that it is naturally hydrophilic due to the presence of hydroxyl groups in their molecular chains, making nanocelluloses less compatible in the hydrophobic polymer matrix (note that most resins are hydrophobic in nature) in addition with high susceptibility of the nanocomposites to moisture. These issues may cause phase-separation between the resin and nanofibers, resulting in degradation of the nanocomposite properties (both mechanical and optical). Surface acetylation of cellulose can introduce hydrophobic nature to it by replacing hydroxyl groups with acetyl groups (Fig. 15.8A) and resolve those issues. Fig. 15.8B shows that the moisture content of the BCNFs/acrylic resin nanocomposites reduced up to an optimum acetyl degree of substitution (DS) of ~0.6. However, more acetylation to BCNFs beyond DS = 0.6 increased the moisture content of the nanocomposites, demonstrating that increased acetylation degree can degrade the crystalline structure of cellulose making it more susceptible to moisture.

Surface acetylation also helps to fine tune the refractive index of cellulose to match that of the suitable or desirable resin matrix in order to obtain high optical transparency in the nanocomposites.[81,82] For example, acetylated BCNFs nanocomposites with the tricyclodecane

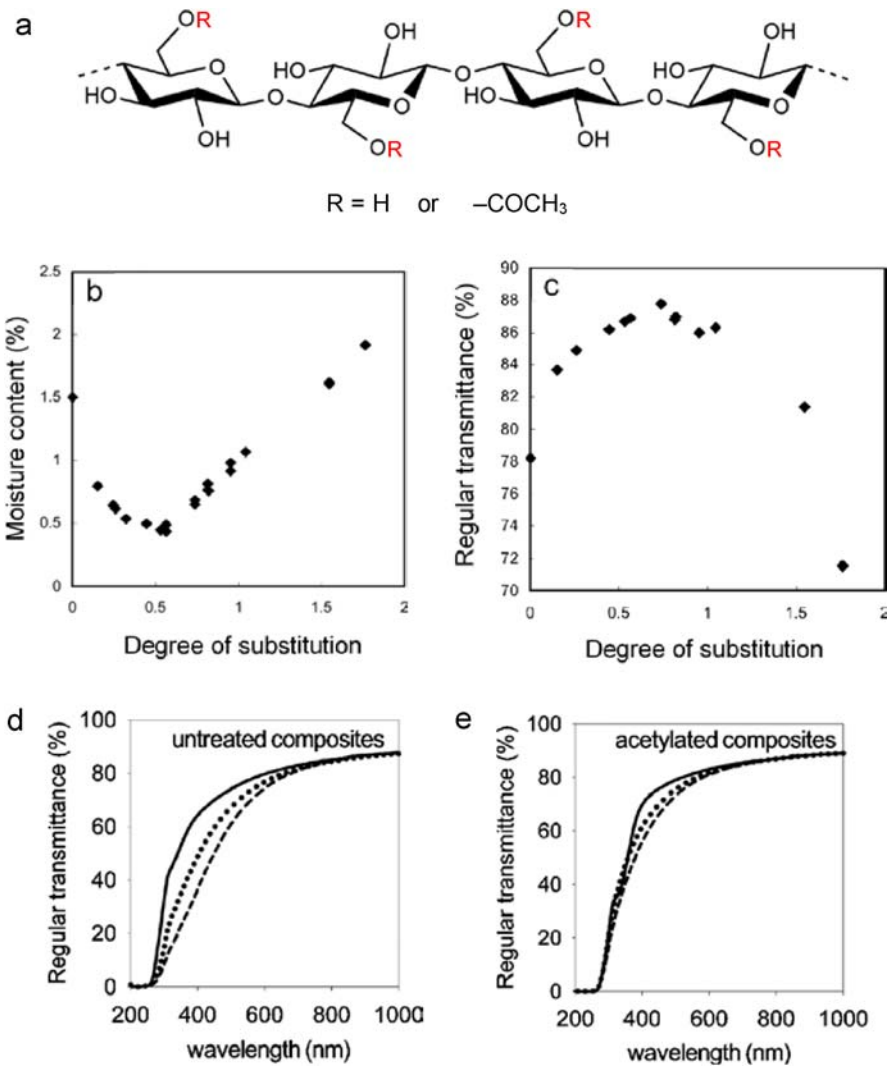

FIGURE 15.8 (A) Chemical structure of acetylated cellulose. Note that the presence of acetyl groups only at C-6 position is shown here, but depending on the severity of acetylation treatment, the acetyl group may present at C-2 and/or C-3 position. Moisture content (B) and optical transmittance at 580 nm (C) of the BCNFs/acrylic resin nanocomposites as the function of acetylation DS of BCNFs. (D, E) optical transmittance spectra of the nanocomposites before (solid line) and after heating at 200°C for 1 h (dotted line) and 3 h (broken line). The DS of BCNFs in (E) was only 0.17. The acrylic resin used in (B–E) was tricyclodecane dimethanol dimethacrylate (TCDDMA). *(B,C) Reproduced with permission from Ifuku S, Nogi M, Abe K, Handa K, Nakatsubo F, Yano H. Surface modification of bacterial cellulose nanofibers for property enhancement of optically transparent composites: Dependence on acetyl-group DS. Biomacromolecules 2007;**8**:1973–1978. © 2007 American chemical society; and (D,E) Reproduced/adapted with permission from Nogi M, Abe K, Handa K, Nakatsubo F, Ifuku S, Yano H. Property enhancement of optically transparent bionanofiber composites by acetylation.* Appl Phys Lett *2006;**89**:233123 © 2006 American institute of physics.*

dimethanol dimethacrylate (TCDDMA) resin matrix had an optimum DS of ~0.7 for highest optical transparency (Fig. 15.8C). At this acetylation DS, the refractive index of cellulose suitably changed to closely match that of the TCDDMA (1.532). Therefore, the optical transparency loss of neat TCDDMA (91.2%) was only 3.4% for acetylated BCNFs nanocomposites compared to 13.0% for untreated one, even at a BCNFs content as high as 63%. Furthermore, the degradation in optical transparency of the nanocomposites at elevated temperature (200 °C) was significantly reduced by acetylation treatment (Fig. 15.8D and E), which is a desirable trait for the flexible and transparent substrates for optoelectronic devices. However, acetylation of BCNFs did not improve the CTE of the nanocomposites (~10 ppm K^{-1}), because the interaction among the nanofibers was weak due to the reduced interfibrillar hydrogen bonding from acetylated surface.[82]

Nogi and Yano[39] developed an interesting strategy to further reduce the CTE of the BCNFs reinforced nanocomposites to the level of that of silicon crystals (3 ppm K^{-1})—the mostly used semiconducting material in optoelectronic devices. Instead of compressing the CNF-scaffold spun by bacteria (Acetobacter xylinum), they utilized its natural anisotropic porous structure along with the meticulous choice of a transparent resin (2.2-bis[4-(acryloxypolyethoxy)phenyl]propane; ABPE-10). The elastic modulus of the resin used was only 0.025 GPa, therefore, the negligible thermomechanical stress generated in the planar direction of the nanocomposites was effectively restricted by the highly entangled planar BCNFs network (Fig. 15.9A and B). Only a 5 wt% BCNFs was enough to reduce the CTE of the resin

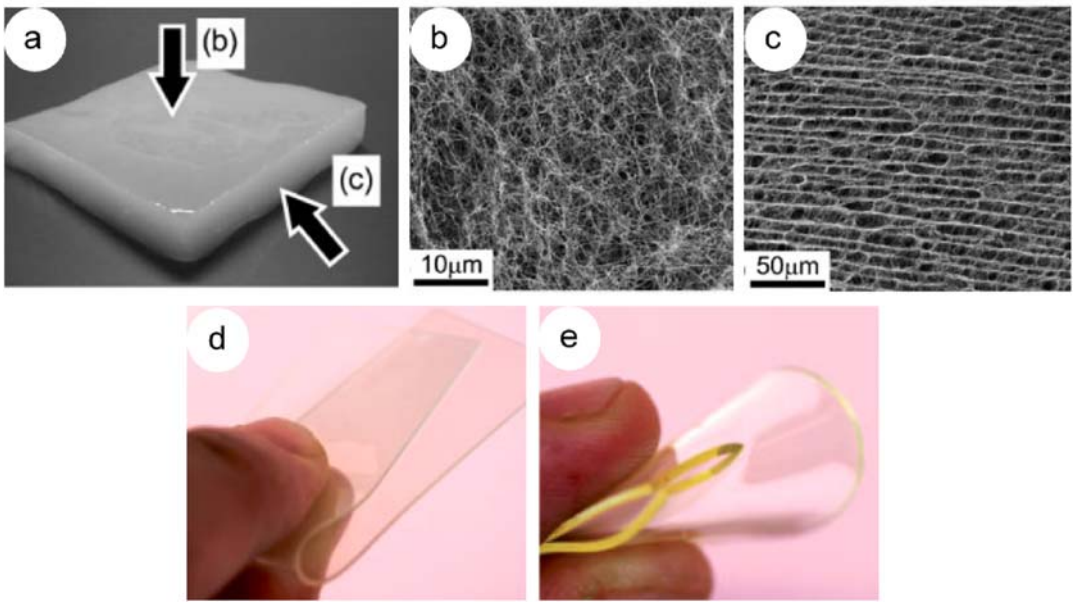

FIGURE 15.9 (A) Macroscopic and (B,C) FE-SEM images of BCNF-scaffold, where (B) shows the planar extensively entangled structure, and (C) shows the relatively weak interaction of BCNFs in the thickness direction. (D) Photograph of the nanocomposite containing only 5 wt% BCNFs but having a CTE of only 4 ppm K^{-1}. (E) Photograph of the weak neat resin film. *Reproduced/adapted with permission from Nogi M, Yano H. Transparent nanocomposites based on cellulose produced by bacteria offer potential innovation in the electronics device industry.* Adv Mater *2008;**20**:1849–1852 © 2008 Willey.*

from 245 ppm K^{-1} to 4 ppm K^{-1}; in contrast, when a resin (TCDDMA) with an elastic modulus of 2.5 GPa was used, an addition of 7.4 wt% BCNFs only reduced the CTE from 86 ppm K^{-1}–38 ppm K^{-1}[183] However, the CTE of the nanocomposite in the thickness direction was very high at 555 ppm K^{-1} due to the weak interaction of the BCNFs (Fig. 15.9C). But, the high CTE in thickness direction should not be a big issue in the practical application due to the thinness of the nanocomposite. Also, due to the use of low BCNFs content, the transparency (82% @ 700 μm thickness) and flexibility (elastic modulus only 0.3 GPa) of the nanocomposite were satisfactorily high (Fig. 15.9D), and the foldability of the nanocomposite was improved compared to that of the neat resin film (Fig. 15.9E).

4.1.2 Plant/wood-based CNFs-reinforced transparent nanocomposites

In the early stage of the research on CNF-reinforced optically transparent nanocomposites, BCNFs served as the perfect and ready-made model of the CNFs. But, the plants and wood are the most viable and industrially upscalable source of CNFs (also see Fig. 15.1). Therefore, attempt to extract CNFs from the commercial pulps by Yano's research group started immediately after their success using BCNFs. The commercial pulps were mechanically nanofibrillated using a grinder having two grind stones assembled in a rotor-stator configuration. It was found that more than 5 passes through the grinder are needed to achieve sufficient nanofibrillation of the pulp to obtain a nanocomposite having a similar transparency (80%–85% at 600 nm wavelength) as the BCNF-reinforced nanocomposites at a similar or even higher nanofiber content (73–88 wt%) (Fig. 15.10A–C).[84,85] However, the increased number of grinder passes of the pulp mechanically degraded the crystal structure of cellulose resulting in the gradual decrease in strength and elastic modulus, and the corresponding increase in CTE of the nanocomposites (Fig. 15.10D–F). Compared to the low CTE (6 ppm K^{-1}) and high elastic modulus (up to 21 GPa) of the BCNF-reinforced nanocomposites, the plant/wood-based CNFs-reinforced transparent nanocomposites had a CTE of ca. 17–23 ppm K^{-1} and an elastic modulus of ca. 7–8 GPa.

To obtain CNFs in unmodified state with minimal damage, Abe et al. developed a simple technique in which the pulp was kept in a never-dried state until the grinder treatment.[44] Therefore, they could avoid the hornification (generation of strong hydrogen bonds among the microfibrils), which occurs during the drying processes in a typical pulping method. As a result, they succeeded in extracting CNFs with a uniform width of 15 nm from wood pulp by passing it only once through the grinder (Fig. 15.2A). The thinner and high-quality CNFs resulted in a nanocomposite (with TCDDMA matrix) with a high transparency (81% @ 85 wt% CNFs content), low CTE (~10 ppm K^{-1}), high strength (up to ~300 MPa), and high elastic modulus (up to ~16 GPa). Later, Okahisa et al.[40] utilized a combination of surface acetylated wood CNFs and low-modulus resin (ABPE-10) to produce a nanocomposite of high optical transmittance (up to 85%), high flexibility, and low CTE (12 ppm K^{-1}), only at a CNFs content 35–40 wt%. Note that, the wood CNFs (nano)paper prepared in that study was most probably similar in microstructure as that of a compressed BCNF-scaffold, rather than that of an uncompressed porous one (Fig. 15.9C).

4.1.3 ChNFs reinforced transparent nanocomposites

The first report of an optically transparent nanocomposite reinforced by ChNFs is due to Ifuku et al. in 2010.[86] The grinder-extracted ChNFs (10–20 nm in width) from commercial

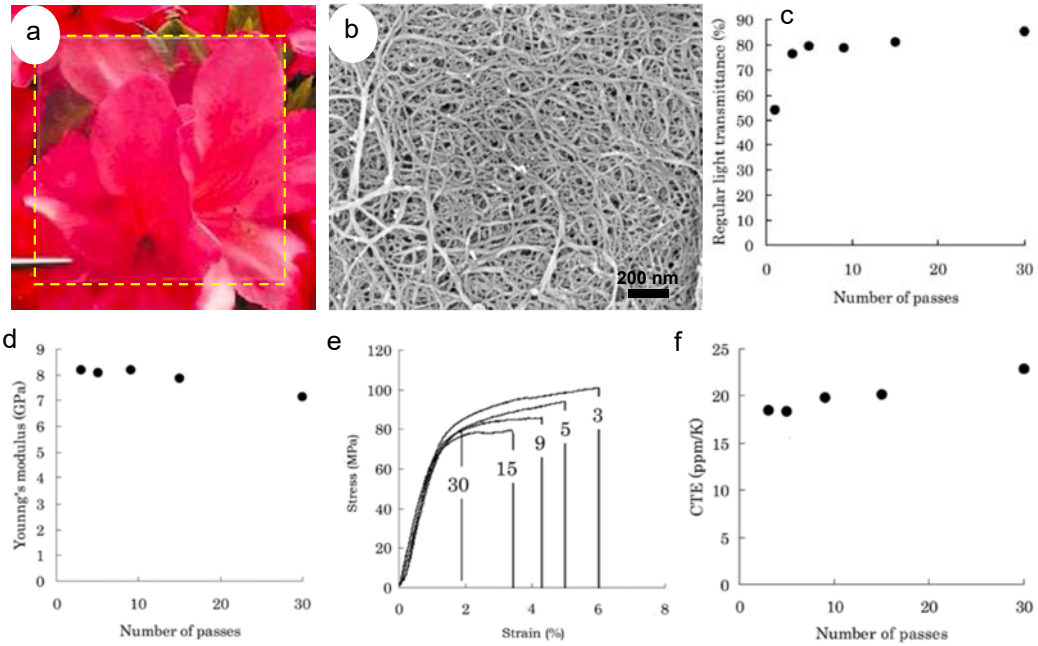

FIGURE 15.10 (A) The first transparent nanocomposite reinforced by 70 wt% plant/wood-based CNFs. (B) FE-SEM image of the 15-pass grinder treated CNFs from commercial pulp fibers. Regular transmittance at 600 nm (C), elastic modulus (D), stress-strain behavior (E) and CTE (F) of the nanocomposites in relation to the grinding pass number. (B–F) The acrylic resin used in (A and C–F) was TCDDMA. *(A) Reproduced with permission from Iwamoto S, Nakagaito AN, Yano H, Nogi M. Optically transparent composites reinforced with plant fiber-based nanofibers.* Appl Phys A *2005;**81**:1109–1112 © 2005 springer-verlag; and (B–F) Reproduced/adapted with permission from Iwamoto S, Nakagaito AN, Yano H. Nano-fibrillation of pulp fibers for the processing of transparent nanocomposites.* Appl Phys A *2007;**89**:461–466 © 2007 Springer-Verlag.*

crab shell powder were used at a content of 60 wt% to reinforce the TCDDMA acrylic resin following the (nano)paper impregnation method described above. The nanocomposites obtained had a high optical transparent of 88%–90% at 600 nm wavelength (Fig. 15.11A). Interestingly, the optical transparency of the ChNF-reinforced nanocomposites was similar to that of acetylated-BCNF-reinforced nanocomposites at a similar nanofibers content. It may indicate that the naturally acetylated ChNFs are less hydrophilic than CNFs, therefore, had a close affinity to the hydrophobic resin, and also, the refractive index of them was probably suitably close to that of the TCDDMA resin (1.532). Fig. 15.11B shows that the suitable refractive index of the transparent resin to obtain ChNF-reinforced nanocomposites with highest optical transparency is between 1.50 and 1.53.[87]

More detailed studies by Shams et al.[68,88] and Ifuku et al.,[87] revealed that ChNFs (extracted from crab shell using a simple high-speed blender and a grinder, respectively) are better reinforcements for transparent resins than the nonacetylated CNFs (extracted from wood using a grinder) in terms of high optical transparency (Fig. 15.11C) and high resistance to heating to a temperature as high as 200 °C (Fig. 15.11D). The elastic moduli and tensile strengths of the

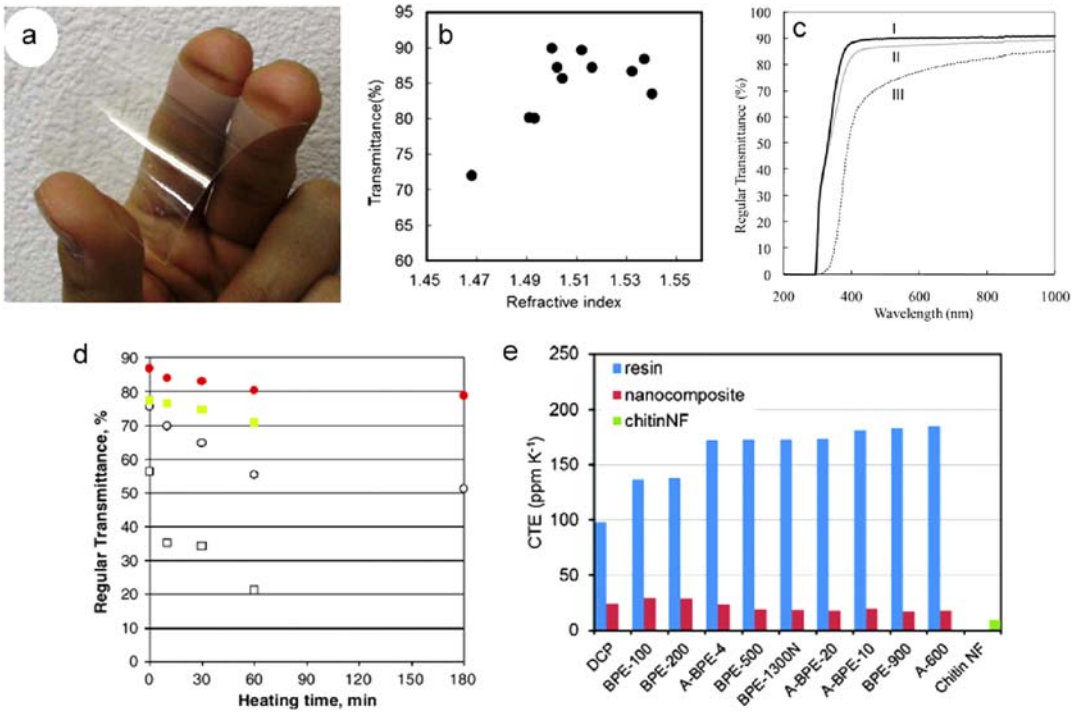

FIGURE 15.11 (A) The first transparent nanocomposite reinforced by 60 wt% crab-shell ChNFs. (B) Regular light transmittance of the ChNF-reinforced nanocomposites at 600 nm wavelength versus the refractive index of their corresponding acrylic resin matrices. (C) Regular light transmittance of acrylic resin film (I), ChNF nanocomposite (II), and CNF nanocomposite (III). (D) Regular light transmittance of ChNF nanocomposite and CNF nanocomposite against heating time at 200°C. ChNF nanocomposite: 600 nm wave length (circle filled) and 400 nm (circle open). CNF nanocomposite: 600 nm (square filled) and 400 nm (square open). (E) CTE of different acrylic resin films and their ChNF-reinforced nanocomposites. In (B–E), the nanocomposites had a nanofiber-content of ~40 wt%. *Reproduced with permission from (A, E) Ifuku S, Nogi M, Yoshioka M, Morimoto M, Yano H, Saimoto H. Fibrillation of dried chitin into 10–20 nm nanofibers by a simple grinding method under acidic conditions.* Carbohydrate Polym *2010;**81**:134–139© 2010 Elsevier; (B) Ifuku S, Morooka S, Nakagaito AN, Morimoto M, Saimoto H. Preparation and characterization of optically transparent chitin nanofiber/(meth)acrylic resin composites.* Green Chem *2011;**13**:1708–1711 © 2011 The Royal Society of Chemistry; (C) Shams MI, Ifuku S, Nogi M, Oku T, Yano H. Fabrication of optically transparent chitin nanocomposites.* Applied Physics A *2010;**102**:325–331 © 2010 springer-verlag; and (D) Shams, M. I.; Yano, H. Simplified fabrication of optically transparent composites reinforced with nanostructured chitin.* J Polym Environ *2013;**21**:937–943 © 2013 springer.*

resins were significantly increased by up to 3 GPa and 44 MPa, respectively, at a ChNF-content of 40 wt%. The CTE of the resins was drastically decreased up to 90% to a lowest value of 16–18 ppm K^{-1} (Fig. 15.11E), slightly higher than that of CNF-based nanocomposites. Again, it was observed that the CTE of low-elastic-modulus resins reduced significantly compared to that of rigid resins, because the thermomechanical deformation stress generated in the low-modulus resins was negligible enough to almost completely suppress by the ChNFs network. Later, Biswas et al.[72,73] demonstrated transparent nanocomposites with an above similar set of properties reinforced by ChNFs extracted from shrimp shell using a simple kitchen blender. Meanwhile, acetylation of ChNFs extracted from crab shell did not

improve the transparency and CTE of the nanocomposites with the TCDDMA matrix compared to that of the raw-ChNFs/TCDDMA nanocomposites.[89] Therefore, ChNFs are equally potential reinforcements to transparent resins as the CNFs, which do not need any sophisticated equipment to extract from the source materials nor any chemical modification to fabricate highly optically transparent nanocomposites.

4.1.4 A new method to obtain bionanofibers-reinforced transparent nanocomposites

It is known that nanocelluloses are intrinsically hydrophilic and typically extracted in water that pose difficulties to mix them with hydrophobic resins (most resins are hydrophobic). Problems include nanocellulose agglomeration (uneven dispersion), phase separation between components, etc., that may cause inferior mechanical and optical properties of nanocomposites. Hydrophobic surface modification of nanocelluloses is a typical route to resolve these issues, which is time consuming and requires hazardous chemicals. In this respect, impregnation (IM) method described above can be considered as a facile and versatile method, because any liquid resin can be imbibed through the micro (air) gaps by capillary action in the (nano)paper that has an already well-dispersed nanofiber-network interlocked by strong hydrogen bonds. Yet, surface modification to nanocelluloses can improve some properties of the nanocomposites prepared by this method as discussed above.

However, surface of the IM nanocomposites usually contains extraresin layers on both sides without nanofiber reinforcement,[40] similar to the nanocomposites prepared by coating/depositing a transparent resin on the surface of the (nano) paper.[90] These extraresin layers may peel-off and crack during device fabrication owing to the large CTE mismatch.[40] In a recent study, Shams and Yano[91] additionally proposed that both CNFs and ChNFs reinforced optically transparent composites are difficult to mold into three-dimensional (3D) complex shapes during the resin impregnation process because of the presence of strong inter-nanofibrillar hydrogen bonds in the (nano)paper. The transparent nanocomposites with 3D complex shapes having a high mechanics, high flexibility, and low CTE are desired for next-generation optically transparent precision parts. For example, a smart contact lens equipped with a nano/microelectronic sensor that can monitor blood-glucose level of a person from the eye fluid or take a picture with a blink of an eye.[92,93]

Therefore, Shams and Yano introduced a new technique based on the concept of emulsification of oil and water.[91] They produced a Pickering emulsion (PE) of resin-in-water, in which the microsized (<10 μm) liquid resin droplets are covered and stabilized solely by the ChNFs (Fig. 15.12A). Note that, an emulsion is a system of dispersed droplets of one immiscible liquid in another stabilized by surfactant/emulsifier molecules, while PEs are solely stabilized by small particles.[94] Subsequently, the emulsion was filtered and dried to obtain a liquid-resin/ChNFs nanocomposite mat. Interestingly, even the emulsion contained resin droplets in the liquid state, the 10 wt% ChNFs (based on the total weight of resin and ChNFs) provided sufficient protection that a negligible amount of the resin was lost during the filtration. Because the nanocomposite mat contained resin droplets in liquid state that also might help to prevent or at least severely limit the formation of strong hydrogen bonds among the ChNFs, it could easily be formed into desired shapes with high optical transparency (Fig. 15.12B and C) simply by hot-pressing using an appropriate die. The regular (86%–87%) and total (~90%) light transmittances were at a similar level as the IM nanocomposites having a same resin (ABPE-10). This indicates that the ChNFs were uniformly

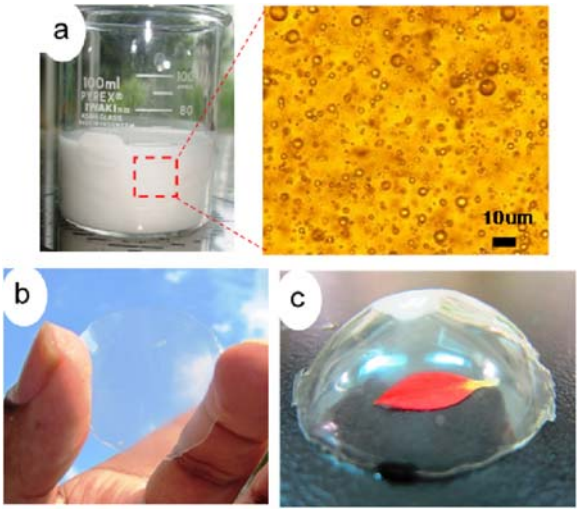

FIGURE 15.12 (A) A resin-in-water pickering emulsion in which microresin droplets are covered and stabilized by the ChNFs. (B,C) pphotographs of ChNF-reinforced flat-shaped (B) and 3D complex-shaped (C) transparent nanocomposites prepared from pickering emulsion. *Reproduced/adapted with permission from (C) Shams MI, Yano H. Doubly curved nanofiber-reinforced optically transparent composites.* Sci Rep *2015;5:16421 © 2015 Springer Nature.*

dispersed in the nanocomposite prepared by the PE method. Most fascinatingly, the CTE obtained for the PE transparent nanocomposites having a ChNF-content of 14 wt% was similar (15–16 ppm K^{-1}) to that of the IM nanocomposites having ca. 35–40 wt% ChNFs. Note that the CTE of the neat resin was 213 ppm K^{-1}.

To further clarify the advantage of PE method, Biswas et al.[95–97] conducted detailed studies using both long CNFs and short rod-like CNCs. They found that the PE transparent nanocomposites possess a self-assembled hierarchical structure (Fig. 15.13A and B), which was generated by interconnection of numerous nanocellulose-covered droplets. Because of having a hierarchical structure, PE nanocomposites showed an improved strength, toughness, and flexibility compared to those of IM nanocomposites at a similar nanocellulose content (Fig. 15.13C). Remarkably, the PE nanocomposites containing only 10 wt% CNCs had a CTE of 3.4 ppm K^{-1}, which was very low compared to many known substrate materials and almost same as the CTE of semiconducting silicon crystals (Fig. 15.13D). This excellent outcome was achieved due to a combination of factors such as: (1) the resin used (ABPE-10) was very soft as described earlier, (2) CNCs that intrinsically had a drastically low CTE (Table 15.1), and (3) the hierarchical structure obtained by PE method that gave an anisotropic thermal deformation character to the nanocomposites, very similar to the IM nanocomposite reinforced by an uncompressed BCNF-scaffold as explained above (also see Fig. 15.9C and Fig. 15.13A and B). Furthermore, the modulus of the PE nanocomposite remained high (~2 GPa) even at a temperature as high as 150°C.

In addition, Biswas et al.[95,96] demonstrated that the PE method not only facilitates the nanocomposites to be 3D-molded in macroscale (as shown in Fig. 15.12C) but also in nano/microscale with a precise control of shapes and dimensions. The micro- and nano-patterned nanocomposites displayed in Fig. 15.14A–C, respectively, were fabricated simply by placing the nanocomposite mats on the respective oppositely patterned substrates followed by hot-pressing and polymerization of the resin. Note that the nano- and microscale surface features support strong optical resonance and reduce plasmonic loss, which can

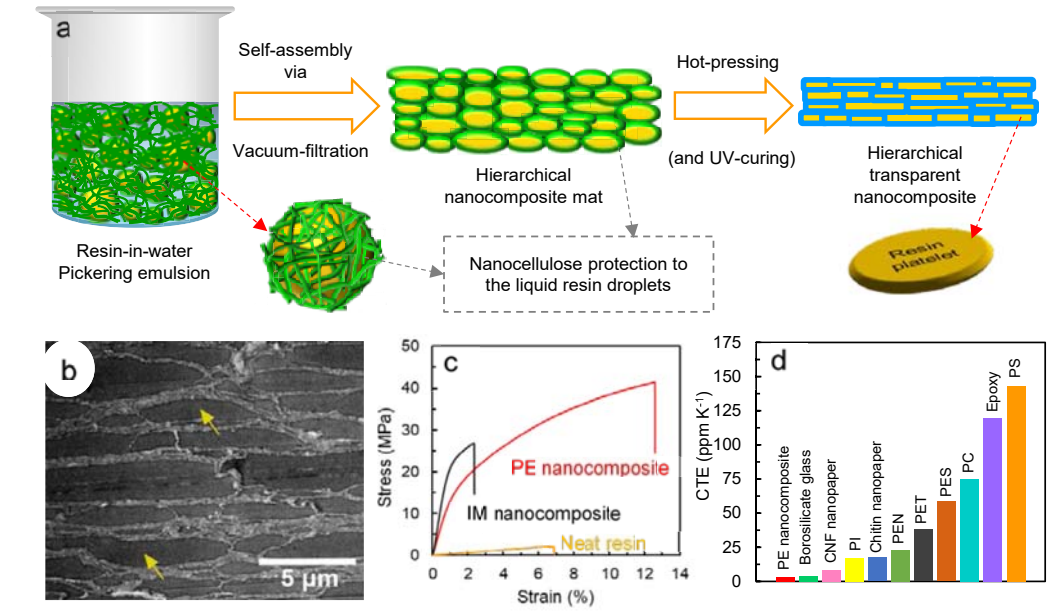

FIGURE 15.13 (A) Schematic of the PE method to obtain self-assembled hierarchical transparent nanocomposites. (B) A TEM image of the cross-section of a transparent nanocomposite. The darker parts consisted of resin (represented by the arrows) and lighter parts consisted of nanocellulose network. (C) Tensile stress-strain curves of PE nanocomposite (CNFs ~16 wt%), IM nanocomposite (CNFs ~20 wt%), and ABPE-10 resin. (D) CTE of PE nanocomposite (CNC 10 wt%) compared to a list of known transparent optoelectronic substrates. PI = polyimide, PEN = polyethylene naphthalate, PET = polyethylene terephthalate, PES = polyether sulfone, PC = polycarbonate, and PS = polystyrene. *Reproduced/adapted with permission from (A–C) Biswas SK, Sano H, Shams MI, Yano H. Three-dimensional-moldable nanofiber-reinforced transparent composites with a hierarchically self-assembled "reverse" nacre-like architecture.* ACS Appl Mater Interfaces *2017;**9**:30177–30184; and (D) Biswas SK, Tanpichai S, Witayakran S, Yang X, Shams MI, Yano H. Thermally superstable cellulosic-nanorod-reinforced transparent substrates featuring microscale surface patterns.* ACS Nano *2019;**13**:2015–2023 © 2019 American Chemical Society.*

enhance and effectively control light absorption, scattering, and outcoupling to improve the performance of the optoelectronic devices such as solar cells, light-emitting diodes (LEDs), etc.[98] Therefore, the easy-made surface-patterned nanocomposite materials having a high transparency, strength, toughness, and flexibility, and a drastically low CTE could favorably be applied as the high-performance substrates in future flexible optoelectronics.

4.2 Transparent nanocomposites reinforced by "nanostructured" particles/fibers

4.2.1 Transparent nanocomposites reinforced by "nanostructured" chitin microparticles

While the great merits of extracted nanocelluloses and nanochitins from bioresources to reinforce transparent resins/polymers have been justified, an important consideration is to

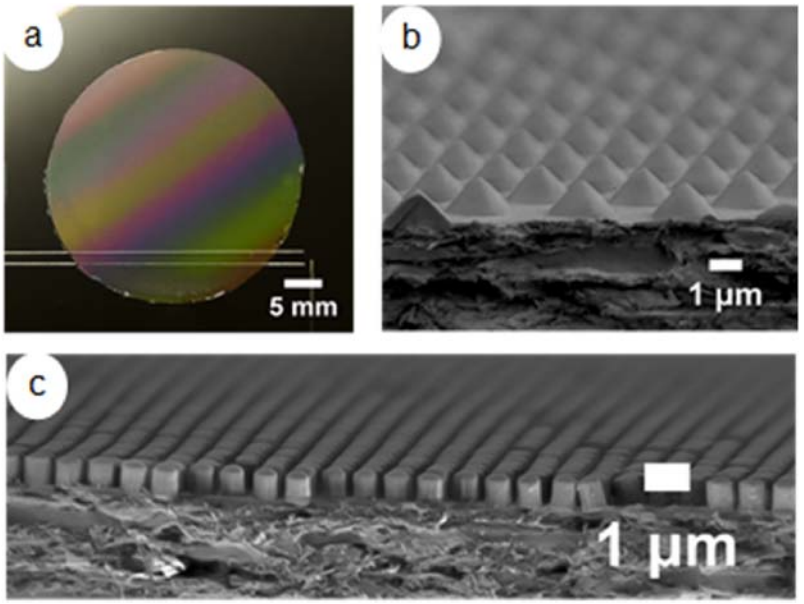

FIGURE 15.14 (A) A surface-patterned transparent PE nanocomposite showing diffraction induced rainbow color. FE-SEM images of a microlens array (B) and nanopillar array (C) molded on the surface of the PE nanocomposite. *Reproduced with permission from Biswas SK, Sano H, Shams MI, Yano H. Three-dimensional-moldable nanofiber-reinforced transparent composites with a hierarchically self-assembled "reverse" nacre-like architecture.* ACS Appl Mat Interf *2017;**9**:30177−30184 © 2017 American chemical society.*

reduce processing energy and time for nanocomposite fabrication. Nanofibrillation of cellulose and chitin requires energy-intensive and time-consuming mechanical treatments. Additionally, dehydration of suspension and Pickering emulsion of CNFs and ChNFs is time consuming owing to their very high specific surface area. Shams et al.[88,99] did pathfinding works in that respect, where they proved that nanofibrillation is in fact not necessary to obtain an optically transparent, mechanically strong, and thermal-dimensionally stable composite. They turned a whole carb transparent by keeping its original shape intact (Fig. 15.15A−C).[99] As mentioned earlier that almost all stiff biological materials are nanocomposites, crab shell is composed of ChNF-scaffold reinforced by mineral nanoparticles and embedded in a matrix of proteins and lipids (Fig. 15.5). After removal of minerals, proteins, lipids, and pigments by typical chemical treatments (see Preparation of nanochitins), the white crab shell composed of nanoporous ChNF-scaffold was submerged into the resin that turned it into a transparent material with its intact original shape and morphological details (Fig. 15.15B and C). This finding indicates that nanocomposites based on particles with a larger size than the optical wavelength would not cause light scattering provided that the particles are composed of nanostructured networks that allow resin impregnation.

Subsequently, inspired by the transparent crab, Shams et al.[88,99] demonstrated transparent nanocomposite films reinforced by mildly fibrillated chitin microparticles (diameter: ~350 μm). The mildly fibrillated chitin microparticles were dispersed in water followed by

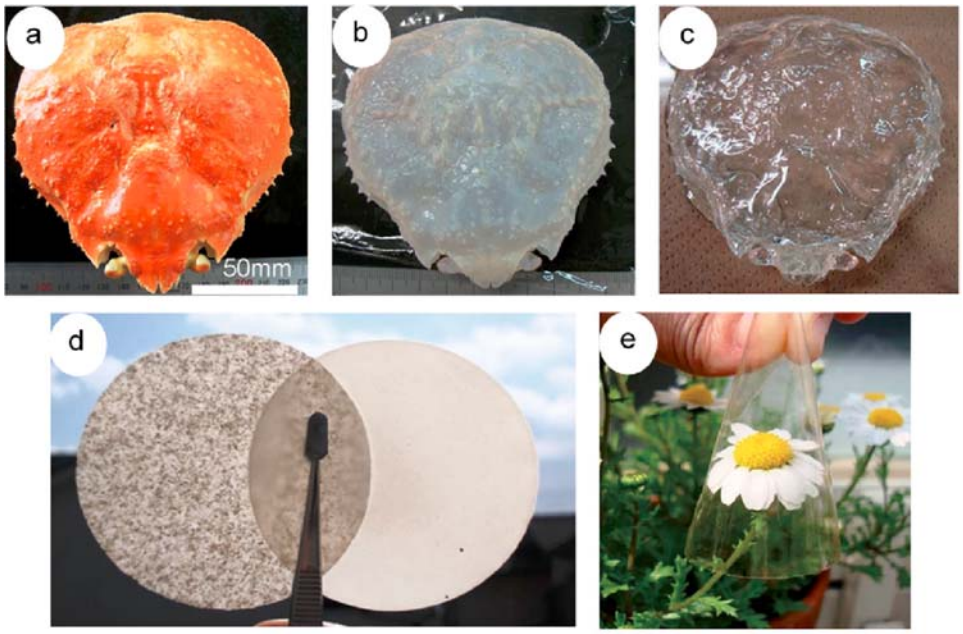

FIGURE 15.15 (A) Original crab shell, (B) crab shell after removal of matrix substances, and (C) transparent crab shell after immersion in ABPE-10 acrylic resin. (D) Appearance of chitin microparticle paper (*left*) and ChNFs (nano) paper (*right*). (E) A transparent and flexible chitin microparticle nanocomposite (chitin content: 22 wt%; resin: ABPE-10). *Reproduced with permission from (A–C and E) Shams MI, Yano H. Simplified fabrication of optically transparent composites reinforced with nanostructured chitin.* J Polym Environ *2013;**21**:937–943 © 2012; Iftekhar Shams M, Nogi M, Berglund LA, Yano H. The transparent crab: preparation and nanostructural implications for bioinspired optically transparent nanocomposites.* Soft Matter *2012;**8**:1369–1373 © 2013 Springer.*

filtration and drying to form a paper (Fig. 15.15D), and subsequently, immersed it into the resin to impregnate into the pores to obtain a transparent nanocomposite (Fig. 15.15E). The nanocomposites were similar in transparency (regular transmittance: ~82% @ 600 nm) and thermal-dimensionally stability (CTE: 18–25 ppm K^{-1}) as ChNF-reinforced nanocomposites, but took much less time and energy to prepare. The modulus of the resin was also increased enormously, which was stable over a wide temperature range from 20 to 200°C. This is inspiring that "nanostructured" chitin microparticles can improve the mechanical and thermal properties of a resin while maintaining its optical transparency, which is counterintuitive to the notion that the filler size should be one-10th of the visible wavelength to obtain a transparent composite,[37,79] but a positive aspect in terms of upscaling the nanocomposite production for commercial utilization in optoelectronic devices.

4.2.2 *Transparent nanocomposites reinforced by "nanostructured" cellulose (pulp) fibers*

Following the pioneering work on chitin microparticles reinforced optically transparent nanocomposites, Yano et al.[100] focused on fabricating cellulose (pulp) fiber-based transparent nanocomposites. Typically, wood fibers are ~3 mm long and ~30 μm in diameter, and are

composed of CNFs (Fig. 15.1 and Fig. 15.16A and B). Because the CNFs are embedded in lignin and existed individually in the wood cell (fiber) walls, the impregnation of the transparent resin could be achieved into the mesopores produced after the removal of lignin. Additionally, to facilitate further impregnation of the resin, the pulp fibers were refined first by bead milling to induce internal fibrillation (a typical process in pulp and paper making). After that, the pulp fibers were acetylated and formed into a paper. The acetylation and internal fibrillated allowed good penetration of the resin into the cell (fiber) walls, that is, in between the CNFs, as well as in the whole paper sheet. As a result, the flexible nanocomposites obtained were highly optically transparent (regular transmittance: 80%–84%) and thermal-dimensionally stable (CTE: 13–19 ppm K^{-1}) at a fiber content of 17–25 wt% (Fig. 15.16C). In comparison, the IM nanocomposites reinforced with acetylated wood-extracted CNFs and having a same resin matrix showed regular transmittance of 82% and CTE of 12 ppm K^{-1} at a CNFs content of 35–40 wt%.[40] It should be noted that the CTE of the pulp fiber-based transparent nanocomposite at a low fiber content is similar to that of the CNF-based nanocomposite at a relatively high CNFs content, which was probably due to the much less damage to the almost intact CNFs in the pulp fibers than in the nanofibrillated individualized CNFs.

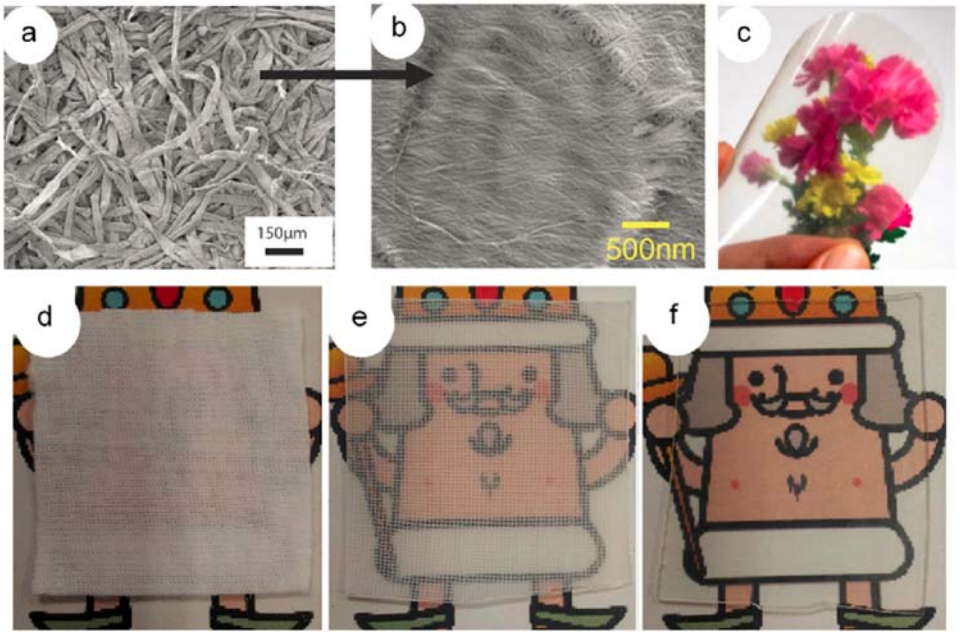

FIGURE 15.16 FE-SEM micrographs of (A) wood (pulp) fibers and (B) nanostructure of the fiber, the cellulose microfibrils (i.e., CNFs) can be directly seen on the fiber surface. (C) An optically transparent flexible nanocomposite reinforced with acetylated pulp (fiber content: 17 wt%; DS: 1.25; resin: ABPE-10). Appearances of a cotton cloth (D), ABPE-10 resin-impregnated composite cotton cloth (E), and ABPE-10 resin-impregnated composite cotton cloth prepared by chemically swelling the cotton fibers in order to facilitate resin impregnation (F). *Reproduced with permission from (A–C) Yano H, Sasaki S, Shams MI, Abe K, Date T. Wood pulp-based optically transparent film: a paradigm from nanofibers to nanostructured fibers.* Adv Opt Mat *2014;**2**:231–234 © 2014 Wiley-VCH; and (D-F) (D–E) Abe, K.; Morita, M.; Yano, H. Fabrication of optically transparent cotton fiber composite.* J Mater Sci *2018;**53**:10872–10878 © 2018 Springer.*

Meanwhile, aiming to apply the above technique to cotton fibers and then cotton fabrics in order to produce large-sized transparent and flexible nanocomposites, Abe et al.[101] found some difficulties and proposed the ways to overcome those. Cotton fibers do not contain lignin, and the CNFs form strong aggregates by hydrogen bonding with a high degree of crystallinity. As a result, cotton fibers are difficult to fibrillate internally and hence only acetylation was not enough to produce a transparent cotton composite. Therefore, a series of swelling pretreatments such as alkali treatment and surface carboxylation by TEMPO-mediated oxidation have been employed that promoted surface acetylation and hence impregnation of resin deep into the cotton cell walls. The treated cotton fibers were formed into a paper and then immersed into the resin to obtain a transparent composites with a regular light transmittance of 83% (at 600 nm) and CTE of 19.5 ppm K^{-1}. Finally, the process was employed to a commercial cotton cloth to demonstrate an optically transparent cotton cloth composite (Fig. 15.16D–F). When an untreated cotton cloth was used, it became translucent due to the impregnation of resin into the cotton fabric mesh and the fabric could be observed visually (Fig. 15.16E). On contrary, a completely transparent composite was obtained with the treated cotton fabric due to easy impregnation of the transparent resin into the cotton fibers (Fig. 15.16F).

The above results imply that the nanofibrillation steps to produce CNFs are in fact not necessary, and hence the energy and time for the production of high-performance transparent nanocomposites can be drastically reduced, which make these bio-based unique nanomaterials exceedingly closer to industrial application with prospects ready to be realized.

5. Potential commercial applications of the bionanofiber-reinforced transparent nanocomposites

5.1 Substrate for optoelectronic devices

One of the most potential commercial applications of the nanocellulose- and nanochitin-reinforced transparent nanocomposites is considered to be as the substrate for optoelectronic devices, such as photovoltaics, displays, smart windows, touch screens, smart contact lens, and so forth. It is noteworthy that the substrates play a crucial role in determining the device performance and reliability. Glass is the conventional choice for the substrate material owing to its high transparency, high thermal stability, and a low CTE of ~7–10 ppm K^{-1}[138] However, glass is intrinsically brittle, therefore, would never comply with the recent unprecedented requirement for transparent and flexible substrates for light-weight, thin-film, bendable, and wearable consumer optoelectronics.

The CTE is one of the most pivotal factors to consider in the fabrication of optoelectronic devices. It is important for the substrates to have a very small CTE like the glass or even lower. But, most flexible and soft plastics have extremely large CTEs, often exceeding 200 ppm K^{-1}. As multilayers of different functional materials (such as silver nanowires, indium-tin-oxide, semi-conducting silicon, etc.) are deposited on the plastic substrate by thermal processes, the thermal cycling induces high thermomechanical deformation in the plastic substrate, subjecting the functional materials to strain and eventual cracking.[39,40,97] In that respect, the bionanofiber-reinforced nanocomposites possess all the traits desired for the

flexible optoelectronic substrate as discussed above. Meanwhile, different optoelectronic devices based on these nanocomposite substrates (especially, nanocellulose-based nanocomposite substrates) have already been demonstrated successfully in the literature.[39–41,97,102,103] A flexible OLED display and a smart transparency modulating film are shown in Fig. 15.17 for instance.

One more positive aspect of the bionanofiber-reinforced transparent nanocomposites is that they exhibit excellent thermal conductivity compared to most transparent plastics.[104,105] For example, a CNC-reinforced transparent nanocomposite exhibited thermal conductivity as high as 5.7 W m^{-1} K^{-1}.[105] This high-level thermal conductivity is advantageous in quick dissipation of heat generated in the electronic components that would enhance the lifespan of the device. Therefore, taking all the desirable characteristics in account, it can be hypothesized that the bionanofiber-based transparent nanocomposites are exceedingly closer to commercial application in optoelectronic devices.

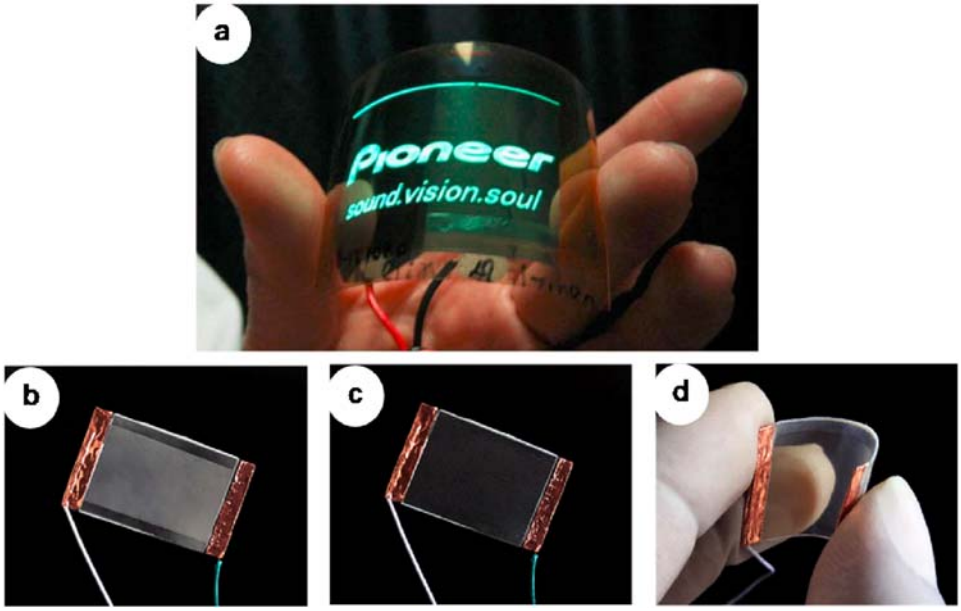

FIGURE 15.17 (A) A flexible OLED display fabricated on a transparent CNF-reinforced nanocomposite. (B–D) A flexible transparency modulating smart film fabricate on a transparent CNC-reinforced nanocomposite. (B) Off state, (C) on state, and (D) on state under bending. *Reproduced with permission from (A) Okahisa Y, Yoshida A, Miyaguchi S, Yano H. Optically transparent wood–cellulose nanocomposite as a base substrate for flexible organic light-emitting diode displays.* Composites Sci Tech *2009;**69**:1958–1961 © 2009 Elsevier. (B–D) Biswas SK, Sano H, Yang X, Tanpichai S, Shams MI, Yano H. Highly thermal-resilient agnw transparent electrode and optical device on thermomechanically superstable cellulose nanorod-reinforced nanocomposites.* Adv Opt Mat *2019;**7**:1900532 © 2019 Wiley.*

5.2 Light-weight shatter-proof windows

Another commercially viable potential application of the bionanofiber-reinforced transparent nanocomposites is as the high-performance, light-weight, and shatter-proof windows for vehicles (cars, aircraft, etc.) and buildings. Today, mostly glass and laminated-glass are used as the windows and windshields. Glass itself is very brittle and heavy (density: $\sim$2.5 g cm^{-3}). To reduce the brittleness and weight, laminated-glass (glass-plastic-glass three-ply structure) is used in the vehicles. However, for structural requirements, thickness of the laminated-glass is needed to be high, which in turn increase the weight.

An important consideration of the vehicle manufacturers is to reduce the weight of the vehicle in order to increase the fuel efficiency and reduce the carbon emission. In order to reduce the weight of the vehicle by 10% by 2020, the Ministry of the Environment of Japan partnered with Toyota and other industries and academia produced a car, named Nanocellulose Vehicle (NCV), of which most parts are made up of nanocellulose-reinforced composites.[106] The roof panel and back door glass of the NCV are transparent composites of PC and CNFs with a CNFs share of 15 wt% (Fig. 15.18). These PC/CNFs composites are 50% lighter than inorganic glass and 20% lighter than ordinary glass-PC-glass laminates. It is noteworthy that owing to CNFs reinforcement to PC, the composite achieved the required structural and mechanical properties at a relatively lower thickness and weight.

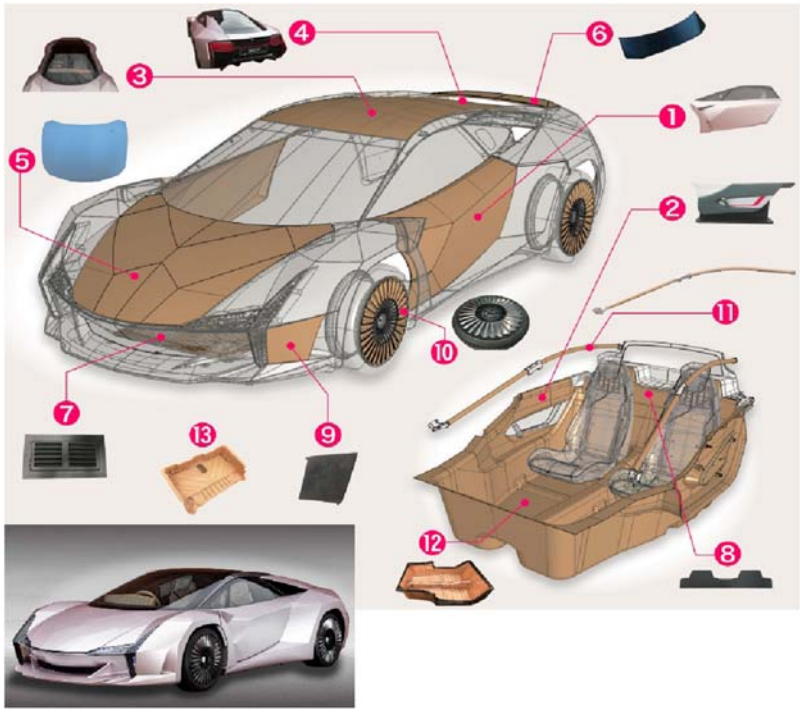

FIGURE 15.18 Nanocellulose vehicle (NCV), most parts of which are made up of nanocellulose-reinforced composites as represented by numbers. The roof panel[3] and back door glass[4] of the NCV are transparent PC/CNFs composites. The CNF-content of these composites is 15 wt%. The inset shows the actual picture of the NCV prototype car. Photos and drawings/sketches are provided by the ministry of the Environment, Japan.

6. Concluding remarks

In this chapter, we described the preparation, properties, and potential applications of transparent nanocomposites reinforced by bio-derived nanocelluloses, nanochitins, and their nanostructured mesoporous microfibers/microparticles. These bio-derived reinforcements have incredible strength, modulus, and thermal stability and are abundantly available from nature, renewable, biodegradable, and carbon neutral, which are required for environmentally sound material technologies. Further, their reinforced transparent nanocomposites are light-weight, strong, flexible, moldable in nano to macroscale, and incredibly thermally and thermal-dimensionally stable. Therefore, prospects of these bio-based transparent nanocomposites as the substrates and structural windows for photonics, optoelectronics, vehicles, and buildings are enormous; some of these applications are already maturing toward commercial level.

References

1. Fratzl P, Weinkamer R. Nature's hierarchical materials. *Prog Mater Sci* 2007;**52**:1263–334.
2. Wegst UG, Bai H, Saiz E, Tomsia AP, Ritchie RO. Bioinspired structural materials. *Nat Mater* 2015;**14**:23–36.
3. Klemm D, Kramer F, Moritz S, Lindstrom T, Ankerfors M, Gray D, Dorris A. Nanocelluloses: a new family of nature-based materials. *Angew Chem Int Ed* 2011;**50**:5438–66.
4. Dufresne A. Nanocellulose: potential reinforcement in composites (chapter 1). In: John MJ, Sabu T, editors. *Natural polymers: vol. 2. Nanocomposites*. The Royal Society of Chemistry; 2012. p. 1–32.
5. Moon RJ, Martini A, Nairn J, Simonsen J, Youngblood J. Cellulose nanomaterials review: structure, properties and nanocomposites. *Chem Soc Rev* 2011;**40**:3941–94.
6. Nawawi W, Jones M, Murphy RJ, Lee KY, Kontturi E, Bismarck A. Nanomaterials derived from fungal sources-is it the new hype? *Biomacromolecules* 2020;**21**:30–55.
7. Ifuku S, Saimoto H. Chitin nanofibers: preparations, modifications, and applications. *Nanoscale* 2012;**4**:3308–18.
8. Naskar AK, Keum JK, Boeman RG. Polymer matrix nanocomposites for automotive structural components. *Nat Nanotechnol* 2016;**11**:1026–30.
9. Kamiyama M, Soeda T, Nagajima S, Tanaka K. Development and application of high-strength polyester nanofibers. *Polym J* 2012;**44**:987–94.
10. Sahay R, Kumar PS, Sridhar R, Sundaramurthy J, Venugopal J, Mhaisalkar SG, Ramakrishna S. Electrospun composite nanofibers and their multifaceted applications. *J Mater Chem* 2012;**22**:12953–71.
11. Xue X, Jiang K, Yin Q, Zhang X, Zhang W, Jia H, Ji Q. Tailoring the structure of Kevlar nanofiber and its effects on the mechanical property and thermal stability of carboxylated acrylonitrile butadiene rubber. *J Appl Polym Sci* 2019;**136**:47698.
12. Kim H, Che L, Ha Y, Ryu W. Mechanically-reinforced electrospun composite silk fibroin nanofibers containing hydroxyapatite nanoparticles. *Mater Sci Eng C* 2014;**40**:324–35.
13. Kawabata S, Sera M, Kotani T, Katsuma K, Niwa M, Xiaoxin C. Anisotropic mechanical properties of advanced high performance fibers obtained by a single fiber testing system. In: Miravete A, editor. *Composites properties and applications: proceedings of the ninth international conference on composite materials (ICCM/9)*. vol. 6. Madrid, Spain: University of Zaragoza and Woodhead Publishing Ltd.; 1993. p. 671.
14. Callister Jr WD, Rethwisch DG. *Materials science and engineering: an introduction*. 9th ed. New York: John Wiley & Sons; 2013. p. 882–900.
15. Yan J-B, Liew JYR, Zhang M-H, Wang J-Y. Mechanical properties of normal strength mild steel and high strength steel S690 in low temperature relevant to Arctic environment. *Mater Des* 2014;**61**:150–9.
16. Hussain F, Hojjati M, Okamoto M, Gorga RE. Review article: polymer-matrix nanocomposites, processing, manufacturing, and application: an overview. *J Compos Mater* 2006;**40**:1511–75.
17. Yu M-F, Lourie O, Dyer MJ, Moloni K, Kelly TF, Ruoff RS. Strength and breaking mechanism of multiwalled carbon nanotubes under tensile load. *Science* 2000;**287**:637–40.

18. Salvetat JP, Bhattacharyya S, Pipes RB. Progress on mechanics of carbon nanotubes and derived materials. *J Nanosci Nanotechnol* 2006;**6**:1857–82.
19. Ding W, Calabri L, Chen X, Kohlhaas KM, Ruoff RS. Mechanics of crystalline boron nanowires. *Compos Sci Technol* 2006;**66**:1112–24.
20. Nishino T, Takano K, Nakamae K. Elastic modulus of the crystalline regions of cellulose polymorphs. *J Polym Sci B Polym Phys* 1995;**33**:1647–51.
21. Šturcová A, Davies GR, Eichhorn SJ. Elastic modulus and stress-transfer properties of tunicate cellulose whiskers. *Biomacromolecules* 2005;**6**:1055–61.
22. Wohlert J, Bergenstråhle-Wohlert M, Berglund LA. Deformation of cellulose nanocrystals: entropy, internal energy and temperature dependence. *Cellulose* 2012;**19**:1821–36.
23. Cintrón MS, Johnson GP, French AD. Young's modulus calculations for cellulose Iβ by MM3 and quantum mechanics. *Cellulose* 2011;**18**:505–16.
24. Nishino T, Matsuda I, Hirao K. All-cellulose composite. *Macromolecules* 2004;**37**:7683–7.
25. Page DH, EL-Hosseny F. The mechanical properties of single wood pulp fibres. Part VI: fibril angle and the shape of the stress-strain curve. *J Pulp Pap Sci* 1983;**9**:99–100.
26. Saito T, Kuramae R, Wohlert J, Berglund LA, Isogai A. An ultrastrong nanofibrillar biomaterial: the strength of single cellulose nanofibrils revealed via sonication-induced fragmentation. *Biomacromolecules* 2013;**14**:248–53.
27. Tashiro K, Kobayashi M. Theoretical evaluation of three-dimensional elastic constants of native and regenerated celluloses: role of hydrogen bonds. *Polymer* 1991;**32**:1516–26.
28. Eichhorn SJ, Davies GR. Modelling the crystalline deformation of native and regenerated cellulose. *Cellulose* 2006;**13**:291–307.
29. Mark RE. *Cell wall mechanics of tracheids*. New Haven: Yale University Press; 1968. p. 119–52.
30. Lahiji RR, Xu X, Reifenberger R, Raman A, Rudie A, Moon RJ. Atomic force microscopy characterization of cellulose nanocrystals. *Langmuir* 2010;**26**:4480–8.
31. Hori R, Wada M. The thermal expansion of wood cellulose crystals. *Cellulose* 2005;**12**:479–84.
32. Bamba Y, Ogawa Y, Saito T, Berglund LA, Isogai A. Estimating the strength of single chitin nanofibrils via sonication-induced fragmentation. *Biomacromolecules* 2017;**18**:4405–10.
33. Ogawa Y, Hori R, Kim U-J, Wada M. Elastic modulus in the crystalline region and the thermal expansion coefficients of α-chitin determined using synchrotron radiated X-ray diffraction. *Carbohydr Polym* 2011;**83**:1213–7.
34. Nishino T, Matsui R, Nakamae K. Elastic modulus of the crystalline regions of chitin and chitosan. *J Polym Sci B Polym Phys* 1999;**37**:1191–6.
35. Favier V, Canova GR, Cavaillé JY, Chanzy H, Dufresne A, Gauthier C. Nanocomposite materials from latex and cellulose whiskers. *Polym Adv Technol* 1995;**6**:351–5.
36. Favier V, Chanzy H, Cavaillé JY. Polymer nanocomposites reinforced by cellulose whiskers. *Macromolecules* 1995;**28**:6365–7.
37. Yano H, Sugiyama J, Nakagaito AN, Nogi M, Matsuura T, Hikita M, Handa K. Optically transparent composites reinforced with networks of bacterial nanofibers. *Adv Mater* 2005;**17**:153–5.
38. Ashby MF. *Materials selection in mechanical design*. Oxford: Pergamon Press; 1993. p. 44–121.
39. Nogi M, Yano H. Transparent nanocomposites based on cellulose produced by bacteria offer potential innovation in the electronics device industry. *Adv Mater* 2008;**20**:1849–52.
40. Okahisa Y, Yoshida A, Miyaguchi S, Yano H. Optically transparent wood–cellulose nanocomposite as a base substrate for flexible organic light-emitting diode displays. *Compos Sci Technol* 2009;**69**:1958–61.
41. Ummartyotin S, Juntaro J, Sain M, Manuspiya H. Development of transparent bacterial cellulose nanocomposite film as substrate for flexible organic light emitting diode (OLED) display. *Ind Crop Prod* 2012;**35**:92–7.
42. Roberts GAF. *Chitin chemistry*. London: Macmillan Press Ltd.; 1992.
43. Puranen T, Alapuranen M, Vehmaanperä J. Trichoderma enzymes for textile industries (chapter 26). In: Gupta VK, Schmoll M, Herrera-Estrella A, Upadhyay RS, Druzhinina I, Tuohy MG, editors. *Biotechnology and biology of trichoderma*. New York: Elsevier; 2014. p. 351–62.
44. Abe K, Iwamoto S, Yano H. Obtaining cellulose nanofibers with a uniform width of 15 nm from wood. *Biomacromolecules* 2007;**8**:3276–8.
45. Zimmermann T, Bordeanu N, Strub E. Properties of nanofibrillated cellulose from different raw materials and its reinforcement potential. *Carbohydr Polym* 2010;**79**:1086–93.

46. Dufresne A, Cavaille JY, Vignon MR. Mechanical behavior of sheets prepared from sugar beet cellulose microfibrils. *J Appl Polym Sci* 1997;**64**:1185–94.
47. Stelte W, Sanadi AR. Preparation and characterization of cellulose nanofibers from two commercial hardwood and softwood pulps. *Ind Eng Chem Res* 2009;**48**:11211–9.
48. Sehaqui H, Zhou Q, Ikkala O, Berglund LA. Strong and tough cellulose nanopaper with high specific surface area and porosity. *Biomacromolecules* 2011;**12**:3638–44.
49. Galland S, Andersson RL, Salajková M, Ström V, Olsson RT, Berglund LA. Cellulose nanofibers decorated with magnetic nanoparticles—synthesis, structure and use in magnetized high toughness membranes for a prototype loudspeaker. *J Mater Chem C* 2013;**1**:7963–72.
50. Johnson RK, Zink-Sharp A, Renneckar SH, Glasser WG. A new bio-based nanocomposite: fibrillated TEMPO-oxidized celluloses in hydroxypropylcellulose matrix. *Cellulose* 2008;**16**:227–38.
51. Wang S, Cheng Q. A novel process to isolate fibrils from cellulose fibers by high-intensity ultrasonication, Part 1: process optimization. *J Appl Polym Sci* 2009;**113**:1270–5.
52. Saito T, Kimura S, Nishiyama Y, Isogai A. Cellulose nanofibers prepared by TEMPO-mediated oxidation of native cellulose. *Biomacromolecules* 2007;**8**:2485–91.
53. Henriksson M, Henriksson G, Berglund LA, Lindström T. An environmentally friendly method for enzyme-assisted preparation of microfibrillated cellulose (MFC) nanofibers. *Eur Polym J* 2007;**43**:3434–41.
54. Yang X, Biswas SK, Han J, Tanpichai S, Li M-C, Chen C, Zhu S, Das AK, Yano H. Surface and interface engineering for nanocellulosic advanced materials. *Adv Mater* 2020:2002264. https://doi.org/10.1002/adma.202002264. 2020 (in press).
55. Thygesen A, Oddershede J, Lilholt H, Thomsen AB, Ståhl K. On the determination of crystallinity and cellulose content in plant fibres. *Cellulose* 2005;**12**:563–76.
56. Agustin MB, Nakatsubo F, Yano H. The thermal stability of nanocellulose and its acetates with different degree of polymerization. *Cellulose* 2015;**23**:451–64.
57. Xu X, Liu F, Jiang L, Zhu JY, Haagenson D, Wiesenborn DP. Cellulose nanocrystals vs. cellulose nanofibrils: a comparative study on their microstructures and effects as polymer reinforcing agents. *ACS Appl Mater Interfaces* 2013;**5**:2999–3009.
58. Oliveira FBd, Bras J, Pimenta MTB, Curvelo AAdS, Belgacem MN. Production of cellulose nanocrystals from sugarcane bagasse fibers and pith. *Ind Crop Prod* 2016;**93**:48–57.
59. Wang B, Sain M. Isolation of nanofibers from soybean source and their reinforcing capability on synthetic polymers. *Compos Sci Technol* 2007;**67**:2521–7.
60. Montanari S, Rountani M, Heux L, Vignon MR. Topochemistry of carboxylated cellulose nanocrystals resulting from TEMPO-mediated oxidation. *Macromolecules* 2005;**38**:1665–71.
61. Filson PB, Dawson-Andoh BE. Sono-chemical preparation of cellulose nanocrystals from lignocellulose derived materials. *Bioresour Technol* 2009;**100**:2259–64.
62. Lv D, Du H, Che X, Wu M, Zhang Y, Liu C, Nie S, Zhang X, Li B. Tailored and integrated production of functional cellulose nanocrystals and cellulose nanofibrils via sustainable formic acid hydrolysis: kinetic study and characterization. *ACS Sustainable Chem Eng* 2019;**7**:9449–63.
63. Vincent JF, Wegst UG. Design and mechanical properties of insect cuticle. *Arthropod Struct Dev* 2004;**33**:187–99.
64. Ifuku S, Nomura R, Morimoto M, Saimoto H. Preparation of chitin nanofibers from mushrooms. *Materials* 2011;**4**:1417–25.
65. Cuong HN, Minh NC, Van Hoa N, Trung TS. Preparation and characterization of high purity beta-chitin from squid pens (Loligo chenisis). *Int J Biol Macromol* 2016;**93**:442–7.
66. Hülsey MJ. Shell biorefinery: a comprehensive introduction. *Green Ener Environ* 2018;**3**:318–27.
67. Raabe D, Sachs C, Romano P. The crustacean exoskeleton as an example of a structurally and mechanically graded biological nanocomposite material. *Acta Mater* 2005;**53**:4281–92.
68. Shams MI, Ifuku S, Nogi M, Oku T, Yano H. Fabrication of optically transparent chitin nanocomposites. *Appl Phys A* 2010;**102**:325–31.
69. Ifuku S, Nogi M, Abe K, Yoshioka M, Morimoto M, Saimoto H, Yano H. Preparation of chitin nanofibers with a uniform width as α-chitin from crab shells. *Biomacromolecules* 2009;**10**:1584–8.
70. Fan Y, Saito T, Isogai A. Chitin nanocrystals prepared by TEMPO-mediated oxidation of α-chitin. *Biomacromolecules* 2008;**9**:192–8. https://doi.org/10.1021/bm700966g.

71. Fan Y, Saito T, Isogai A. Preparation of chitin nanofibers from squid pen β-chitin by simple mechanical treatment under acid conditions. *Biomacromolecules* 2008;**9**:1919–23. https://doi.org/10.1021/bm800178b.
72. Biswas SK, Shams MI, Das AK, Islam MN, Nazhad MM. Flexible and transparent chitin/acrylic nanocomposite films with high mechanical strength. *Fibers Polym* 2015;**16**:774–81.
73. Biswas SK, Das AK, Yano H, Shams MI. Development of high performance transparent nanocomposites reinforced with nanofibrillated chitin extracted from shrimp wastes. *J Chitin Chitosan Sci* 2013;**1**:138–43.
74. Paillet M, Dufresne A. Chitin whisker reinforced thermoplastic nanocomposites. *Macromolecules* 2001;**34**:6527–30.
75. Nair KG, Dufresne A. Crab shell chitin whisker reinforced natural rubber nanocomposites. 1. Processing and swelling behavior. *Biomacromolecules* 2003;**4**:657–65.
76. Tzoumaki MV, Moschakis T, Biliaderis CG. Metastability of nematic gels made of aqueous chitin nanocrystal dispersions. *Biomacromolecules* 2010;**11**:175–81.
77. Goodrich JD, Winter WT. α-chitin nanocrystals prepared from shrimp shells and their specific surface area measurement. *Biomacromolecules* 2007;**8**:252–7.
78. Lin N, Wei S, Xia T, Hu F, Huang J, Dufresne A. Green bionanocomposites from high-elasticity "soft" polyurethane and high-crystallinity "rigid" chitin nanocrystals with controlled surface acetylation. *RSC Adv* 2014;**4**:49098–107.
79. Novak BM. Hybrid nanocomposite materials–Between inorganic glasses and organic polymers. *Adv Mat* 1993;**5**:422–33.
80. Nogi M, Handa K, Nakagaito AN, Yano H. Optically transparent bionanofiber composites with low sensitivity to refractive index of the polymer matrix. *Appl Phys Lett* 2005;**87**:243110.
81. Nogi M, Abe K, Handa K, Nakatsubo F, Ifuku S, Yano H. Property enhancement of optically transparent bionanofiber composites by acetylation. *Appl Phys Lett* 2006;**89**:233123.
82. Ifuku S, Nogi M, Abe K, Handa K, Nakatsubo F, Yano H. Surface modification of bacterial cellulose nanofibers for property enhancement of optically transparent composites: dependence on acetyl-group DS. *Biomacromolecules* 2007;**8**:1973–8.
83. Nogi M, Ifuku S, Abe K, Handa K, Nakagaito AN, Yano H. Fiber-content dependency of the optical transparency and thermal expansion of bacterial nanofiber reinforced composites. *Appl Phys Lett* 2006;**88**:133124.
84. Iwamoto S, Nakagaito AN, Yano H, Nogi M. Optically transparent composites reinforced with plant fiber-based nanofibers. *Appl Phys A* 2005;**81**:1109–12.
85. Iwamoto S, Nakagaito AN, Yano H. Nano-fibrillation of pulp fibers for the processing of transparent nanocomposites. *Appl Phys A* 2007;**89**:461–6.
86. Ifuku S, Nogi M, Yoshioka M, Morimoto M, Yano H, Saimoto H. Fibrillation of dried chitin into 10–20 nm nanofibers by a simple grinding method under acidic conditions. *Carbohydr Polym* 2010;**81**:134–9.
87. Ifuku S, Morooka S, Nakagaito AN, Morimoto M, Saimoto H. Preparation and characterization of optically transparent chitin nanofiber/(meth)acrylic resin composites. *Green Chem* 2011;**13**:1708–11.
88. Shams MI, Yano H. Simplified fabrication of optically transparent composites reinforced with nanostructured chitin. *J Polym Environ* 2013;**21**:937–43.
89. Ifuku S, Morooka S, Morimoto M, Saimoto H. Acetylation of chitin nanofibers and their transparent nanocomposite films. *Biomacromolecules* 2010;**11**:1326–30.
90. Nogi M, Yano H. Optically transparent nanofiber sheets by deposition of transparent materials: a concept for a roll-to-roll processing. *Appl Phys Lett* 2009;**94**:233117.
91. Shams MI, Yano H. Doubly curved nanofiber-reinforced optically transparent composites. *Sci Rep* 2015;**5**:16421.
92. Kim J, Kim M, Lee MS, Kim K, Ji S, Kim YT, Park J, Na K, Bae KH, Kyun Kim H, Bien F, Young Lee C, Park JU. Wearable smart sensor systems integrated on soft contact lenses for wireless ocular diagnostics. *Nat Commun* 2017;**8**:14997.
93. Sako Y, Iwasaki M, Hayashi K, Kon T, Nakamura T, Onuma T, Tange A. *Contact lens and storage medium*. Sony Corporation, U.S. Patent 20160097940A1; 2016.
94. Pickering SU. Emulsions. *J Chem Soc, Transact* 1907;**91**:2001–21.
95. Biswas SK, Sano H, Shams MI, Yano H. Three-dimensional-moldable nanofiber-reinforced transparent composites with a hierarchically self-assembled "reverse" nacre-like architecture. *ACS Appl Mater Interfaces* 2017;**9**:30177–84.

96. Biswas SK, Tanpichai S, Witayakran S, Yang X, Shams MI, Yano H. Thermally superstable cellulosic-nanorod-reinforced transparent substrates featuring microscale surface patterns. *ACS Nano* 2019;**13**:2015–23.
97. Biswas SK, Sano H, Yang X, Tanpichai S, Shams MI, Yano H. Highly thermal-resilient agnw transparent electrode and optical device on thermomechanically superstable cellulose nanorod-reinforced nanocomposites. *Adv Opt Mater* 2019;**7**:1900532.
98. Brongersma ML, Cui Y, Fan S. Light management for photovoltaics using high-index nanostructures. *Nat Mater* 2014;**13**:451–60.
99. Iftekhar Shams M, Nogi M, Berglund LA, Yano H. The transparent crab: preparation and nanostructural implications for bioinspired optically transparent nanocomposites. *Soft Matter* 2012;**8**:1369–73.
100. Yano H, Sasaki S, Shams MI, Abe K, Date T. Wood pulp-based optically transparent film: a paradigm from nanofibers to nanostructured fibers. *Adv Opt Mater* 2014;**2**:231–4.
101. Abe K, Morita M, Yano H. Fabrication of optically transparent cotton fiber composite. *J Mater Sci* 2018;**53**:10872–8.
102. Song X, Yang S, Liu X, Wu M, Li Y, Wang S. Transparent and water-resistant composites prepared from acrylic resins ABPE-10 and acetylated nanofibrillated cellulose as flexible organic light-emitting device substrate. *Nanomaterials* 2018;**8**:648.
103. Wang R, Yu H, Dirican M, Chen L, Fang D, Tian Y, Yan C, Xie J, Jia D, Liu H, Wang J, Tang F, Asiri AM, Zhang X, Tao J. Highly transparent, thermally stable, and mechanically robust hybrid cellulose-nanofiber/polymer substrates for the electrodes of flexible solar cells. *ACS Appl Energy Mater* 2020. https://doi.org/10.1021/acsaem.9b01943.
104. Shimazaki Y, Miyazaki Y, Takezawa Y, Nogi M, Abe K, Ifuku S, Yano H. Excellent thermal conductivity of transparent cellulose nanofiber-epoxy resin nanocomposites. *Biomacromolecules* 2007;**8**:2976–8.
105. Wu X, Gao Y, Yao H, Sun K, Fan R, Li X, An Y, Lei Y, Zhang Y. Flexible and transparent polymer/cellulose nanocrystal nanocomposites with high thermal conductivity for thermal management application. *J Appl Polym Sci* 2019:48864. https://doi.org/10.1002/APP.48864.
106. Nano Cellulose Vehicle Project of the Ministry of the Environment, Japan; Research Institute for Sustainable Humanosphere (RISH), Kyoto University, Japan. http://www.rish.kyoto-u.ac.jp/ncv/special/> Accessed 20.12.19.

This page intentionally left blank

PART III

Nanoparticles in health care

This page intentionally left blank

CHAPTER

16

Nanoparticles as drug delivery agents for managing diabetic retinopathy

Sumit Mukherjee, Punyatoya Panda and Monalisa Mishra

Neural Developmental Biology Lab, Department of Life Science, NIT Rourkela, Rourkela, Odisha, India

Abbreviations

ACCORD Action to Control Cardiovascular Risk in Diabetes
AMD Age-related Macular Degeneration
Ang-2 Angiopoietins
ARB Angiogenesis-Related Blindness
ARI Inhibitors of Aldose reductase
AuNP Gold Nanoparticles
BBB Blood-Brain Barrier
bFGF basic Fibroblast Growth Factor-2
BRB Blood Retinal Barrier
CD Cyclodextrin
CeO_2 Cerium Oxide
CNV Choroidal Neovascularization
DME Diabetic Macular Edema
DR Diabetic Retinopathy
DXR Doxorubicin
ER Endoplasmic Reticulum
ETDRS Early Treatment Diabetic Retinopathy Study
FA Fluocinolone Acetonide
HGF Hepatocyte Growth Factor
HIF 1α Hypoxia Inducing Factor 1α
HUVEC Human Umbilical Vein Endothelial Cells
iBRB Inner Blood Retinal Barrier
ICAM-1 Intercellular Adhesion Molecule-1
IGF Insulin-like Growth Factor
LDL Low-Density Lipoprotein
MNPs Magnetic Nanoparticles
NGF Nerve Growth Factor
NLC Nanostructured Lipid Carriers
NP Nanoparticle
NPDR Non-proliferative Diabetic Retinopathy

Applications of Multifunctional Nanomaterials
https://doi.org/10.1016/B978-0-12-820557-0.00014-X

OCT Octriotide
ODN-1 Oligonucleotide
PACA Poly(alkyl cyanoacrylates)
PACAP Pituitary Adenylate Cyclase-Activating Peptide
PAMAM Polyamidoamine
PCEP Poly-[(cholesteryl oxocarbonylamido ethyl) methyl bis(-ethylene) ammonium iodide]-ethyl phosphate
PEG Poly(ethylene glycol)
PEG-PSA Poly(ethylene glycol)- Poly(sebacic acid)
PKC Protein Kinase C
PLA Poly-lactic Acid
PLGA Poly(lactic-co-glycolic acid)
PMMA Poly(methyl methacrylate)
PVA Polyvinyl Alcohol
PVD Posterior Vitreous Detachment
QD Quantum Dot
RAS Rennin-Angiotensin System
RES Reticulo Endothelial System
RGD Arginine-Glycine-Aspartic acid
ROP Retinopathy of Prematuration
ROS Reactive Oxygen Species
RPE Retinal Pigment Epithelium
RVE Retinal Vascular Epithelium
SDF-1 Stromal derived growth factor
SiNP Silicon dioxide Nanoparticles
SLN Solid Lipid Nanoparticle
SOD Superoxide Dismutase
TiO_2 Titanium oxide
TNF Tumor Necrosis Factor
tPA Tissue Plasminogen Activator
UKPDS UK Prospective Diabetes Study
VEGF Vascular Endothelial Growth Factor
VEGFR-2 VEGF receptor-2
WESDR Wisconsin Epidemiologic Study of Diabetic Retinopathy

1. Introduction

Diabetes has emerged as a disease of utmost concern posing threat among the one-third population of the world.[1] The chronic disease is characterized by elevated blood glucose level that arises from the nonfunctionality of the pancreas to synthesize insulin or resistance of the peripheral cells to insulin, the hormone responsible for maintaining glucose homeostasis.[2] Diabetes can be classified into two main types: (1) Type I and (2) Type II. Type I diabetes prevails due to the failure of the pancreas to produce insulin which is mainly diagnosed in children and youths.[3] Whereas, type II, is called as the diabetes of adults, that occurs due to reduced insulin synthesis or the cell's inability to respond to it.[4] The third type of diabetes, known as gestational diabetes may also arise at pregnancy that mainly results from the placental hormones. These hormones interfere with the insulin receptor and create a hyperglycemic condition.[5]

The occurrence of diabetes for a longer period may result in some serious issues including the micro- and macrovascular complications linked to heart disease and peripheral arterial

diseases.[6] The common complications in all types of diabetes involve diabetic neuropathy,[7] retinopathy,[8] and nephropathy.[9] Of them, diabetic retinopathy is a microvascular complication that has major effects on a patient's life quality, particularly the visual acuteness which subsequently leads to the loss of visual ability.[10]

To understand the pathophysiology of various eye disorders, we need to know about the eye structures and the functionality of every part (Fig. 16.1).[11] The outer membrane of the eye is made of a clear and concaved membrane known as cornea.[12] As light crosses the cornea, it passes through the anterior chamber, pupil, and then through a lens which enhances the focus of the light. At the final stage, light passes through the vitreous humor in the center and hits the retina, located in the posterior eye.[13] The retina comprises a fine layer of photosensitive tissue that receives light and converts it to electrical signals that are perceived by the brain for visual recognition.[14] Retina possesses the blood retina barrier (BRB), which contains the retinal pigment epithelium (RPE) and retinal vascular epithelium (RVE). The outer blood retinal barrier (BRB) is maintained by RPE cells and the tight junctions present in RPE from the inner BRB.[15] The endothelial cells of the retina are covered by glial cells and pericytes. Pericytes maintain vascular stability and control the proliferation of the endothelial cells, whereas the main role of glial cells is to process retinal vascular components and stabilize blood flow in the retina.[16,17] The two main glial cells that are present in the retina are the Muller cell and astrocyte. Muller cells maintain retinal functioning as well as the pH in the

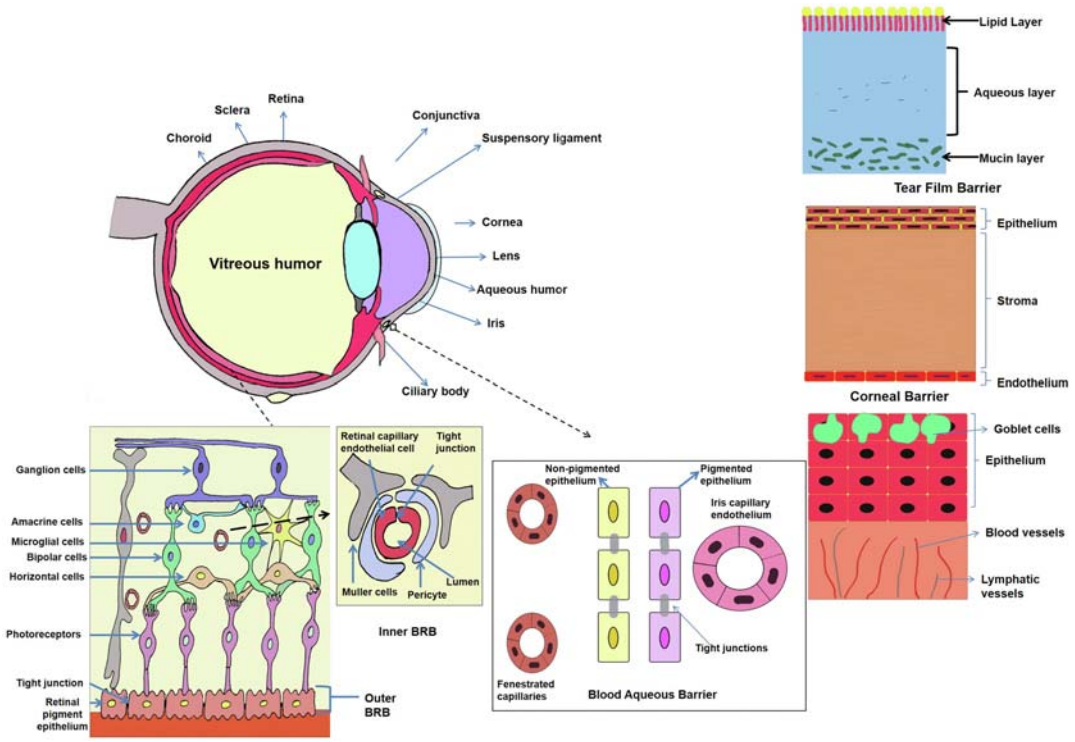

FIGURE 16.1 Overview of the whole eye. Magnified structure of a transverse section of different parts of the eye and ocular barriers.

retina. On the other hand, astrocytes control retinal vasculature development.[18] Anatomical and structural changes in the BRB and its associated companions result in pathophysiological alterations in DR.[19]

DR possesses a serious threat to the healthcare system due to the high economic burden of treatment and other complications and thus is a challenge for the future. As the human eye bears many complex barriers, the cure of DR is quite challenging.[20] Current therapies of DR involve laser photocoagulation, surgical interventions, and pharmacotherapies.[21] Although these treatments have remained a standard care system for the management of DR over the last few decades, they generally do not restore the lost vision completely and there are certain limitations. Although these therapies are well effective, the cost of treatment is very high, involves invasive procedures, and shows ocular and systemic complications.[22,23] To prevent the drug's systemic exposure, scientists have developed intravitreal steroid implants which again involve invasive methods and show complexities such as elevated ocular pressure, glaucoma, and cataract.[24,25] Various inhibitors like inhibitors of protein kinase C (PKC),[26] inhibitors of aldose reductase (ARI),[27] inhibitors of growth hormone,[28] an inhibitor of inflammatory agents,[29] carbonic anhydrase inhibitors,[30] blockers of renin -angiotensin system (RAS)[31] are also used for treatment. Various antioxidants, enzymatic vitreolysis, gene, and stem cell therapy are combined with any two or three therapies to lower the progress of DR.[21] Besides this, treatment of DR requires a longer duration and thus it includes repeated invasive methods which result in more severe ocular problems like vitreous hemorrhage, endophthalmitis, retinal detachment, and cataract.[32] To overcome this difficulty, novel noninvasive treatment approaches are needed.

Last few decades many advanced nanomaterials have been developed to treat various diseases including DR. Nanoparticles have a size range of 1−100 nm and they have important roles in drug delivery, gene therapy, and biological imaging.[33] Nanoparticles have certain advantages as a drug carrier which include, (1) prolonged and target-specific delivery, (2) improved delivery of large and hydrophobic drugs, and (3) less toxic reactions and complications.[34,35] Current nano-based systems provide a chance to cope with the disadvantages of the conventional approaches that include uncontrolled drug release, not suitable for targeted delivery, invasive, poor penetration, less retention time, poor bioavailability, and adverse effects. Delivering drugs to the posterior part, the potential site for DR is often limited by the ocular barriers. Nanoparticle-loaded drugs can permeate these barriers, and provide a better therapeutic efficacy compared to the classical systems.[21]

The current chapter describes the use of nanoparticles in ocular delivery followed by the nanomaterials used to prevent DR progression. Various strategies to deliver nanoparticle-based drugs and their toxic effects have also been discussed here. This chapter will help to understand the current treatment strategies of DR using nanotechnology and to formulate nano-based therapeutics that will be helpful in the future.

2. Diabetic retinopathy

Diabetic retinopathy appears as a complication of chronic diabesity for 10 years or above and is the major cause of adult blindness.[36] The hyperglycemic condition in diabetes leads to metabolic imbalance and activates low-grade, chronic inflammatory signaling pathways which have distinctive roles in the progress of DR (Fig. 16.2).[37]

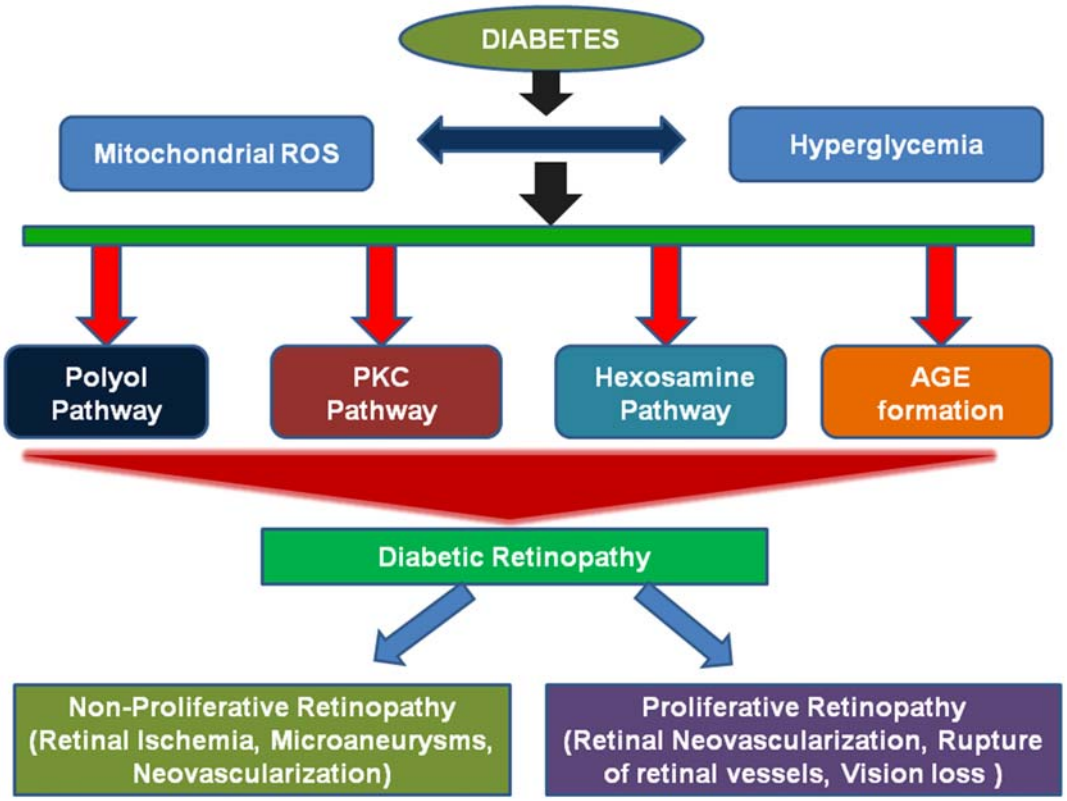

FIGURE 16.2 Various pathways via which diabetes induces diabetic retinopathy.

Clinical signs of this disease are retinal hemorrhage, formation of microaneurysms, capillary blockage, cotton-wool spots, macular edema, hard exudates, and finally the formation of abnormal blood vessels (Fig. 16.3).[38,39] Multiple metabolic pathways are associated with DR pathogenesis, such as the polyol pathway, protein glycation, PKC pathway activation, and hexosamine pathway (Fig. 16.2).[40] All these events upregulate proangiogenic and inflammatory factors like vescular endothelial growth factor (VEGF),[41] Insulin-like Growth Factor (IGF),[42] Angiopoietins (Ang-2),[43] Stromal derived growth factor (SDF-1),[44] basic Fibroblast Growth Factor-2 (bFGF-2),[45] Hepatocyte Growth Factor (HGF),[46] Tumore necrosis factor (TNF)[47] and interleukin-6.[48]

Based on the severity and clinical signs associated with the disease, DR is mainly divided into two classes: 1) Nonproliferative and 2) Proliferative (Fig. 16.3).[49] Retinopathy of nonproliferative origin was earlier called background DR. It is the beginning stage of DR, which may lead to proliferative DR if remain unnoticed. Nonproliferative DR can be mild, modest, or advanced type. Mild type is identified by noticeable damage to the small vessels of the retina which may grow balloon-like bulging called microaneurysms.[50,51] In the moderate type, some small retinal blood vessels are blocked, causing oxygen depletion and nutrient supply

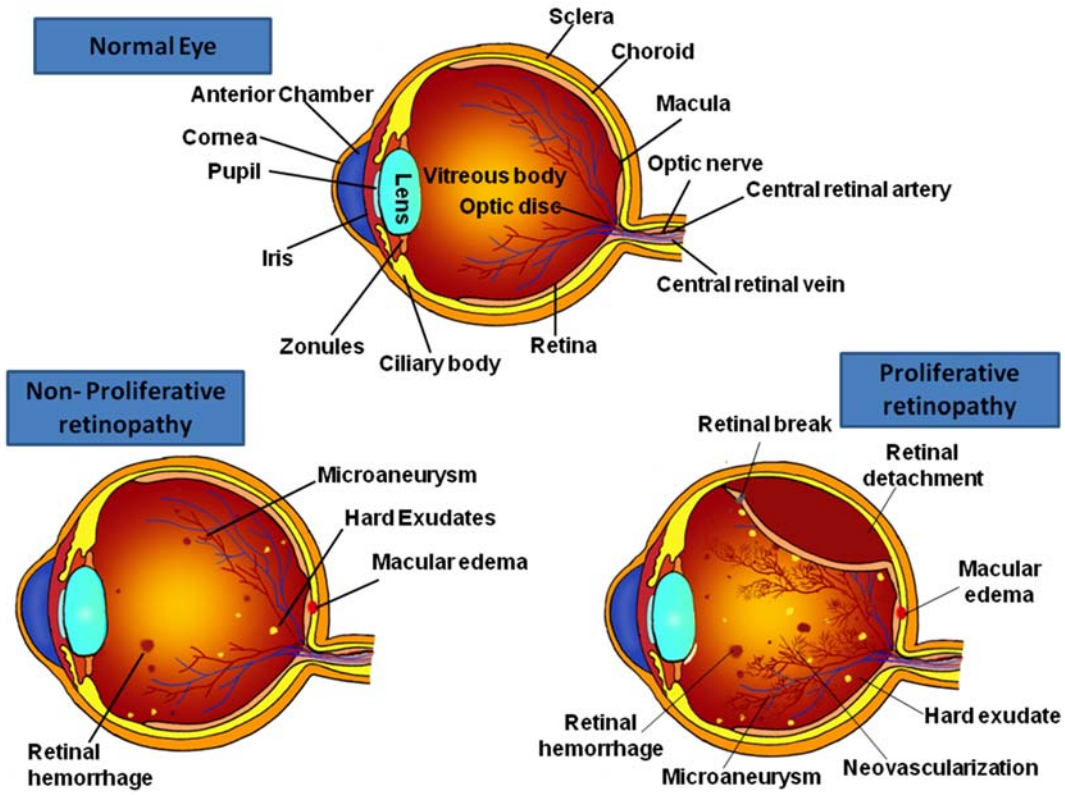

FIGURE 16.3 Types of diabetic retinopathy and the common physiological changes that occur during DR.

to some areas of the retina. Advanced retinopathy is identified by blockage of considerable blood vessels resulting in a shortage of nutrition and oxygen in areas of the retina. This condition is called retinal ischemia.[52] The hypoxic condition in these areas induces neovascularization to restore the oxygen supply. The most severe stage of this disease is proliferative DR, identified by severe damage to the small blood vessels of the retina and a hypoxic condition.[53] This results in abnormal retinal vessels, which are fragile and cause internal bleeding into the vitreous. This condition may lead to sudden blindness. Proliferative DR can also lead to detachment of the retina with profound vision loss.[21]

3. Disease progression and complications

The molecular and biochemical pathways of DR are identified in various studies.[54,55] The hyperglycemic condition of diabetes triggers various metabolic pathways, like the hexosamine and polyol pathways, free radical production, and advanced glycation end products which appear to play vital roles in the pathogenesis of DR (Fig. 16.2).[49,56]

Additional investigations have also pointed out the role of neurodegeneration, neuroinflammation, and RAS.[57–59] Moreover, the anomalous generation of ER stress and mitochondrial ROS are the contributing factors of the DR pathogenesis.[60] ER stress results from protein misfolding which causes the unfolded or misfolded proteins to build up in the ER lumen, thereby elevating oxidative stress, inflammation, and apoptosis. These conditions play essential roles in the pathogenesis and progression of different neuronal conditions in the brain and retina which also includes the premature stages of DR.[61]

At the early onset of the disease, clinical signs such as intraretinal hemorrhages, and microaneurysms are formed (Fig. 16.4). Almost all the patients with type I diabetes, had the disease for 20 years or more[62] and almost 80% of type II diabetes patients[63] have these clinical signs. Pericyte loss from the retinal capillaries also occurs as an earlier sign of the histopathology of DR. This is followed by the loss of endothelial cells of the capillary.[64] Due to the high metabolic requirement of the retinal neurons, a hypoxic condition is created as the capillary cells are lost and this condition induces BRB breakdown and leads to retinal neovascularization.[65,66] With the progress of the disease, the patients with proliferative retinopathy are found to have elevated amounts and sizes of intraretinal hemorrhages along with cotton wool spots which are often seen (Figs. 16.3 and 16.4). Altogether, it results in the local failure of microvascular circulation in the retina, resulting in a condition known as ischemia. In proliferative DR, the formation of new retinal blood vessels occurs that can extend to the vitreous humor and can lead to hemorrhage in the vitreous. This can cause detachment of the retina as well as loss of vision (Fig. 16.3).[67]

Diabetic macular edema (DME) is another important change that occurs in diabetic retinopathy. This condition appears with the blood-retinal barrier breakdown along with the outflow of plasma from the macular small vessels. This causes macular swelling and reabsorption of the plasma fluid elements leading to the formation of hard exudates. DME does not lead to complete visual disability but can cause loss of central vision.[67]

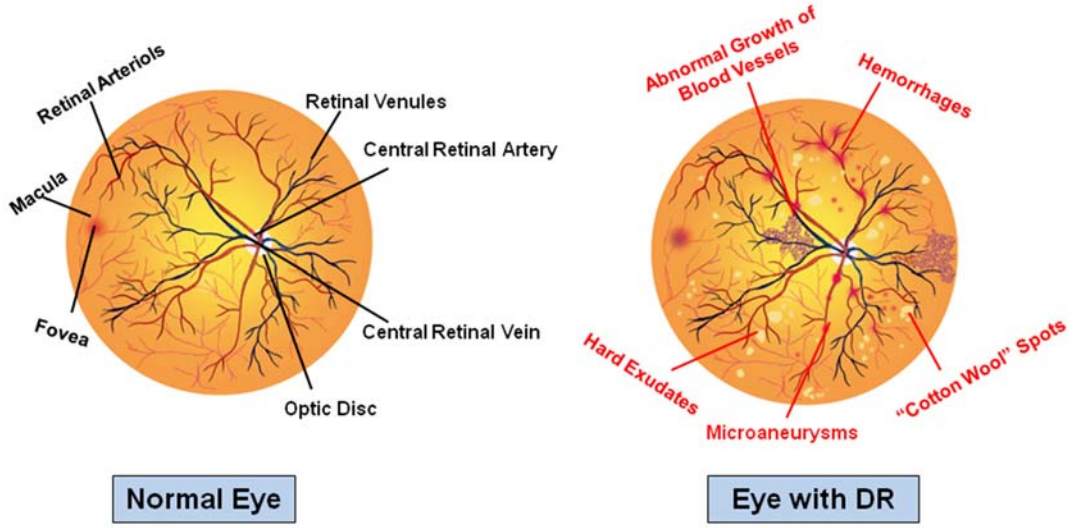

FIGURE 16.4 A comparison between the normal eye and the DR affected eye.

4. Conventional methods of DR treatment

Current treatment strategies of DR involve laser therapy, vitrectomy, and pharmacotherapeutics. However, combinations of two or more strategies are often used to achieve better results.[21] These strategies cannot completely cure DR, but they can slow down the progression of DR by attenuating some of the major symptoms, thereby avoiding early blindness. The conventional treatments of DR involve the following:

4.1 Surgical management

4.1.1 Laser treatment

Laser photocoagulation is a useful treatment of DR that decreases the threat of vision loss.[68] This technique affects the deterioration of unusual blood vessels, reduces oxygen tension, and prevents neovascularization. Laser techniques mainly include (1) Pan-retinal photocoagulation, which applies tiny spots in the retina and slows down the development of new abnormal blood vessels; and (2) Focal laser photocoagulation, which targets each of the leaky blood vessels in the retina.[69]

Although laser treatments are effective in improving visual acuity if done in an appropriate and timely manner, visual complications like loss of central vision, decreased night vision[70] and color vision,[71] reduction in contrast sensitivity,[72] and decreased focus are also reported from various studies. Unusual complications of laser therapy include hemorrhage in the vitreous, retinal detachment, and permanent blindness. These treatment methods may not bring back the lost vision completely as they are destined to prevent further loss of eye sight.[73]

4.1.2 Vitrectomy surgery

Vitrectomy is a surgical method to treat DR by removal of the vitreous gel.[74] It prevents vitreous hemorrhage by removal of the unusually fragile blood capillaries along with the scar tissues. Although vitrectomy is a success, the application of surgical procedures might raise complicated outcomes like eye infection, continuous secretion of tears, cataracts, vitreous hemorrhage, and retinal detachment.[75] Thus it has very limited applications.

4.2 Pharmacotherapy treatments

Pharmacotherapy treatment is used to treat DR. This treatment uses two major types of drugs: (1) VEGF antagonists, (2) corticosteroids. Other compounds can be used alone or in combination.

4.2.1 VEGF inhibitors

VEGF inhibitors act as the antagonists of VEGFs that binds to the receptors and aid abnormal blood vessel formation. Anti-VEGF agents inhibit the proliferation of abnormal blood vessels in the retina and thereby act as a treatment for DR (Fig. 16.5). Currently, four anti-VEGF agents namely Pegaptanib, Ranibizumab, Bevacizumab, and Aflibercept are used for DR management. Pegaptanib is an aptamer that acts as a selective VEGF

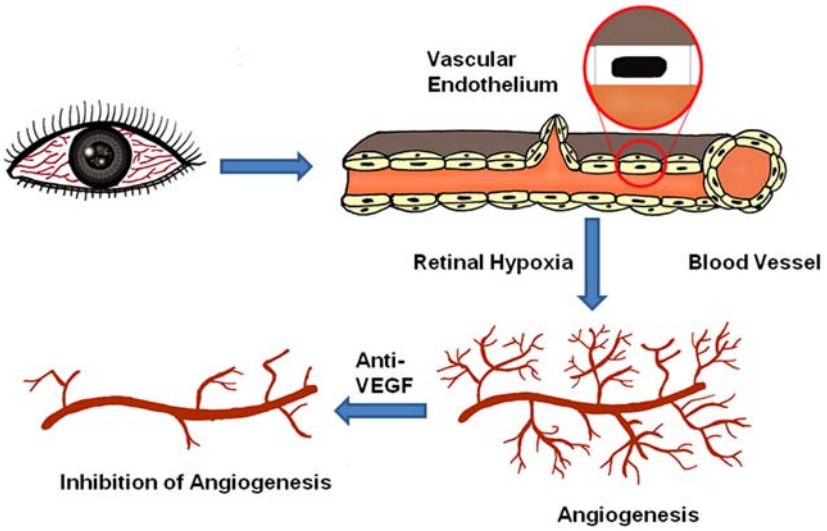

FIGURE 16.5 Treatment strategy using anti-VEGF agents.

inhibitor.[76] Pegaptanib was useful with a few regional and systemic complications; however, the visual outcomes were distressing.[76] This leads to the development of ranibizumab, a humanized monoclonal antibody (Fab) which interacts with the isoforms of VEGF-A and neutralizes them.[77] The use of ranibizumab was soon restricted because of its several ocular problems, like bleeding in the conjunctiva, eye pain, endophthalmitis, and retinal detachment.[78] Ophthalmologists overcome this problem by using another effective therapy like bevacizumab, a full-length humanized monoclonal antibody.[79] Bevacizumab appeared as an "off-label" drug due to its anti-VEGF property for treating DR. Later, another novel anti-VEGF agent, Aflibercept was introduced that binds to the isoforms of VEGF with increased affinity than other agents that act against VEGF.[80] Food and drug administration (FDA) approved this drug to be used for DR patients with diabetic macular edema.

4.2.2 *Corticosteroids*

Corticosteroids possess a potential antiinflammatory effect and are used in treating DR for their ability to decrease the breakdown of the retinal barrier, reduce vascular permeability, downregulate VEGF expression, and show inhibition of matrix metalloproteinases thus preventing the formation of naïve blood vessels.[81,82] Major corticosteroids used to treat DR include dexamethasone, triamcinolone acetonide, and fluocinolone acetonide.[83–85]

4.3 Other treatment strategies

Many treatment strategies can reduce a patient's risk of developing DR. They include (1) Systemic treatment (2) Other medications to treat DR.

4.3.1 *Systemic treatment*

Systemic strategies include methods that are propagated through the circulatory system and may slow down the progress of DR by controlling systemic abnormalities associated

with DR. The strategies may include control of blood sugar, blood pressure, management of hyperlipidemia, and other strategies which are described below. However, the systemic administration of drugs is not that effective as only 1%–2% of the drug can reach the retina.[86]

4.3.1.1 Control of blood sugar

Regulation of glucose within the body is one of the approaches to reducing DR pathogenesis.[87] The intensive control of blood sugar in comparison to the standard glycemic control can decrease the progress of retinopathy by almost one-third.[87,88] These findings suggest the useful effects of intensive glycemic control on the progress of DR.

4.3.1.2 Control of blood pressure

Diabetes is often associated with hypertension. The UK Prospective Diabetes Study (UKPDS) group investigated the effect of intensive blood pressure control and a chance of vascular complexities in type II diabetic patients.[89] Control of blood pressure by captopril, an inhibitor of angiotensin convertase or atenolol, a β-blocker is the important treatment.[90] By reducing blood pressure the retinopathy progression was reduced to 35%. A summary of 9 years study found that the group under intensive blood pressure control had decreased the rate of vision loss by 47% (on The Early Treatment Diabetic Retinopathy Study (ETDRS) chart).[89,91]

4.3.1.3 Managing hyperlipidemia

The Wisconsin Epidemiologic Study of Diabetic Retinopathy (WESDR)[92] along with the ETDRS study[93] investigated the role of serum lipids in chronic type I diabetic patients. It was observed that LDLs and total cholesterol are linked with hard exudate appearance in the retina of DR patients.[94] This suggests that reduction of serum lipids might reduce the development of hard exudates.[93,95] A study showed that treatment of type I diabetes with fenofibrate, a drug that lowers the cholesterol and serum LDL level aids in the reduction of retinopathy progress. However, this investigation also demonstrated that the reduction in DR progression is not dependent on reducing the lipid level. An eye study by the ACCORD suggests lipid-lowering agents such as statins together with fenofibrate decrease retinopathy progression by about one-third.[96,97]

4.3.2 Other treatment strategies

4.3.2.1 PKC inhibitors

Some studies have found ruboxistaurin mesylate act as a potent inhibitor of PKC β2 and oral ruboxistaurin has been found to reduce moderate loss of vision with minimal side effects. However, it is unavailable as a therapeutic agent due to its inefficacy in treatment.[98]

4.3.2.2 Inhibitors of aldose reductase (ARI)

Aldose reductase is a retinal enzyme involved in the polyol pathway that aids in DR progression. ARIs like oral fidarestat and ranirestat was examined in animals that showed a reduction of retinal thickness and thus may play a useful role in managing DR.[99]

4.3.2.3 Antiinflammation agents

Nepafenac, etanercept, meloxicam, and infliximab can reduce inflammatory mediators. In DR, retinal endothelial cells have overexpressed ICAM-1, which result in the attachment of

leukocyte to small vessels of the retina affecting the permeability of BRB. TNF $-\alpha$ inhibitors, like intravitreal infliximab and etanercept, also inhibit leukostasis and breakdown of BRB[100–102].

4.3.2.4 Antioxidants

Diabetes is a metabolic disorder that results in the increased production of superoxide radicals from the mitochondria and activates various pathways for the onset of DR.[103] Several researchers found the use of antioxidants as a strategy to prevent the complications associated with this disease. Clinical investigations found supplementation of vitamin E helps to improve blood flow in the retina.[104] The effect of ubiquinone and other antioxidant therapies was examined in Nonproliferative Diabetic Retinopathy (NPDR). The involvement of oral α-lipoic acid in reducing DR progression was also investigated. These studies found decreased retinal thickness as well as enhanced visual acuity. Calcium dobesilate, a potent antioxidant was reported to slow DR progression with the oral treatment of long duration. Curcumin, quercetin, setarud, luteolin, resveratrol scutellarin, berry anthocyanins, and epigallocatechin gallate are antioxidants that may play a role in slowing down DR progression.[105–110]

4.3.2.5 Carbonic anhydrase inhibitors

Carbonic anhydrase, an important enzyme may also have a role in the progress of DR. Elevated carbonic anhydrase was reported in the vitreous humor of proliferative DR patients.[111] RPE cells as well as Mullar and cone cells contain this enzyme bound to the membrane. The oral administration of an inhibitor of this enzyme such as acetazolamide, dorzolamide, benzolamide causes a reduction in the progression of DR.[112]

4.4 Topical treatment

Topical treatment of ocular diseases has also proven to be advantageous as it minimizes systemic complications and is less invasive. However, the release of the topical agents to the eye posterior segment is quite challenging.[86] In the past few years, several approaches tried designing agents for drug delivery. Efforts were made to increase the contact time of the agents such as the development of gels, ointments, and hydrogels. Topical delivery followed approaches like prodrug formulations, cyclodextrins, permeability enhancers, transscleral or transcorneal penetration, and colloidal drug delivery systems which were found to increase the ocular bioavailability.[113] If ocular bioavailability can be improved, topical treatments can be administered more conveniently and can reduce the treatment cost for eye diseases of the posterior segment.

4.5 Antibody-based therapeutics

Antibody-based therapeutics have always been a useful approach for treating various diseases. Recently retinal treatment strategies have also increased the application of large peptides and protein molecules. However, as these molecules have a large molecular weight, they are unable to reach the inner eye upon topical administration.[114] To avoid this, their administration is performed through highly invasive intravitreal injections leading to patient noncompliance.

4.6 Local treatment for managing diabetic retinopathy

Local treatments such as periocular, intravitreal, peribulbar, subtendon, subconjunctival are used for DR (Fig. 16.6). These involve invasive methods, of which intravitreal drug delivery is currently the most preferred one. However, the side effects of this route are the main disadvantages. The local treatment strategies that are currently used are as follows:

4.6.1 Enzymatic vitreolysis

Enzymatic vitreolysis is the process that uses enzymes to manipulate the vitreous and thus its retinal attachment.[115] Posterior vitreous detachment (PVD) can slow down the progress of DR. Vitreolysis therapy leads to the induction of PVD by vitreolytic agents, thus avoiding surgery. There are mainly two types of vitreolytic agents, which are either liquefactants (cause vitreous liquefaction) or interfactant (cause vitreous separation from the retina). These include tissue plasminogen activator (tPA), microplasmin,[116] plasmin, nattokinase,[117] chondroitinase,[118] hyaluronidase,[119] vitreosolve (nonenzyme), dispase, and RGD-peptide. Intravitreal administration of these agents is important for adjuvant treatment of vitreous surgery.

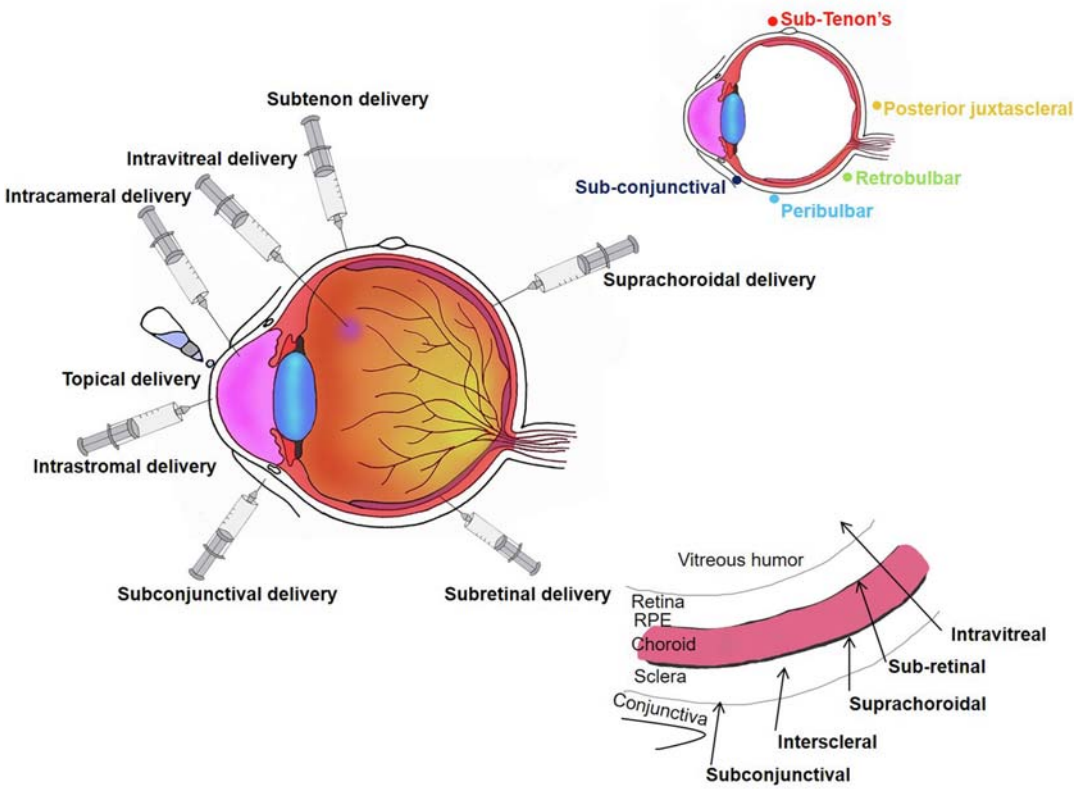

FIGURE 16.6 Various drug delivery routes to different eye regions.

4.6.2 Stem cell therapy

This is a useful strategy to protect the neuronal and vascular network of the diabetic retina.[120] Stem cell belongs to a group of undifferentiated cellular mass that can differentiate into any particular cell type. As the retinal endothelial cells and the pericytes are lost in DR, stem cell therapy can be used in preserving and supporting the abnormal retinal cells and tissues.[121]

4.6.3 Gene therapy

This technique has gained attention due to its ability to control the progress and treatment of retinopathy by investigating the genetic factors affecting retinal oxidative and pathological pathways such as polyol pathway, PKC, hexosamine, and AGEs. They are an effective target for managing DR.[122] Viral or nonviral vectors have been tested for gene transfer into targeted tissues.

5. Limitations of conventional therapy

Well-known strategies to prevent DR involve surgical procedures and pharmacotherapy. Although laser treatment is useful in slowing down DR progress, it has limited specificity and may cause retinal damage leading to blindness.[123] On the other hand, vitrectomy is costly and can only be carried out by specialists. Besides this, the technique has visual distress like detachment of the retina, and vitreous hemorrhage.[124] The limitations lead to the application of new treatment methods using anti-VEGF agents. These agents have large sizes whose entry into the retina is limited.[78] Hence, their administration is done by invasive intravitreal injections, and the treatment required frequent administration for maintaining the efficacy of the drugs. The invasive mode and frequency may lead to ocular complications.[125] When these agents come into the system, they may cause systemic complications such as stroke and myocardial infarction.[126] To overcome these limitations and to avoid the consequences, some implant devices with the properties of sustained-release were developed.[127] But this is another invasive strategy that has its effects like increased intraocular pressure, glaucoma, and cataract.

These limitations of conventional therapy have pushed scientists toward developing different approaches for preventing DR to get advantages such as prolonged contact time, improved penetration, and reduced systemic exposure. This can be achieved by using nanotechnological approaches.

6. Nanoparticles in ocular delivery

The potential application of nanotechnological approaches in optical delivery is a challenge to the corresponding researchers owing to several limitations.[128] The optical barriers are a limitation for penetrating the drugs in the posterior part of the eye. Retinal and corneal epithelium, endothelial cells, and RPE contain tight junctions that limit drug diffusion.[129] Along with this, there are blood-retinal barriers that also limit the delivery of the drug by systemic circulation. Thus, the classical approaches result in very low drug bioavailability. The

bioavailability of some drugs in the eye posterior region can be improved by nanoparticles which also reduce the frequency of invasive strategies and adverse side effects.[130]

In the middle '80s, nanoparticles with polymeric matrices were projected as useful carriers for topical drug administration into the eye.[131] PACA was the first polymeric nanoparticle used in this aspect.[132] From that time onwards several other polymeric compositions have been investigated. Lipid nanoparticles, such as Solid Lipid Nanoparticle (SLN), liposomes, and Nanostructured Lipid Carriers (NLC) are also known for optical drug delivery. They are mainly made up of physiological lipids, which include phospholipids, glycerides, and ceramides, and are biocompatible with or without any toxic effects.[133] To further increase their bioavailability and avoid ocular rejection and mucosal irritation, coating polyethylene glycol on the nanoparticle surface is often done. This strategy is often considered as a preferable substitute for drug delivery to the eye posterior.[134]

Dendrimers are also useful carriers, which entrap the drug molecules in their complex network. Polyamidoamine (PAMAM) is the most frequently used material for producing dendrimers. These systems tend to enhance persistent drug delivery in the eye's posterior part; however, its cytotoxicity is a major disadvantage.[135] Nanoparticles of cationic and bioadhesive materials showed the best retention time at the ocular surface.[136] There are some nanoparticles and nanomaterials used for treating various ocular diseases. They are described in the following section (Fig. 16.7).

7. Nanomaterials for the treatment of DR

7.1 Nanoparticles

7.1.1 Gold NPs

Owing to the specific physicochemical characteristics, gold nanoparticles are widely used in the field of biomedicine, especially for drugs carrier, gene therapy, and photothermal cure of cancer (Fig. 16.8).[137,138] Gold NPs (AuNPs) are synthesized and stabilized by a variety of ligands, which manipulate their characteristics. The ligands for stabilizing gold NPs are specifically selected for the encapsulation of drugs and their release to specific target tissues.[139] Depending on the process of synthesis, AuNPs range from 1 to more than 120 nm.[140] AuNPs bound drugs can be delivered either by covalent bonding, or are encapsulated to the surface by supramolecular interactions. AuNPs are sometimes combined with hydrogels, an approach to couple their characters that lead to a biocompatible drug delivery system.[138]

AuNPs might overcome the limitations of gene delivery associated with viral vectors. It has been seen that the AuNPs are used as transfection agents in the cornea with successful therapeutic doses and did not cause any morphological, toxic, or inflammatory response in vivo.[141] Moreover, the topical administration of AuNPs on the cornea of rabbits did not change their behavior and thus is not detrimental to their visual ability.[141] However, the use of these nanoparticles for a longer time is largely unknown and should undergo clinical trials to understand the pharmacokinetics to make sure that they do not cause toxicity or damage to the eye.

The antiangiogenic properties of gold NPs were first demonstrated by Mukherjee et al. in mouse ears.[142] They showed binding of AuNP to growth factors such as VEGF-165 results in inhibition of their activity and thus the signaling event that follows. Additionally, negatively charged AuNP of 10 nm is found to have the best antiangiogenic characteristics. Kim et al.

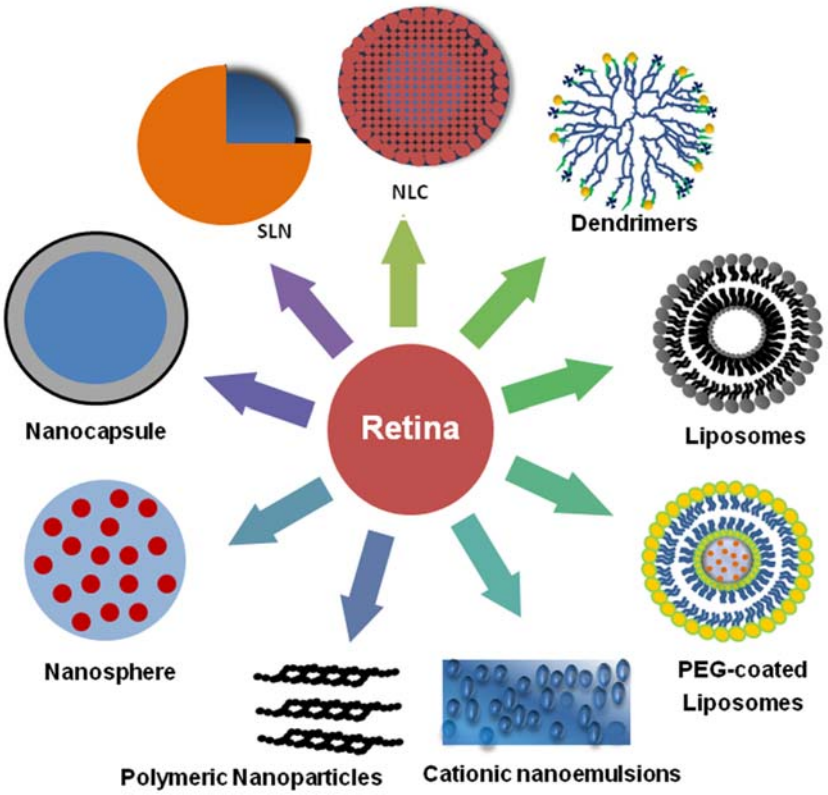

FIGURE 16.7 Different nanomaterials used for targeted drug delivery in the eye posterior.

showed this inhibition in a mouse model of premature retinopathy.[143] Uncontrolled adsorption of protein on nanoparticle surfaces might inhibit their in vivo activity. Synthesis of a bio-inspired protein corona around AuNP by Jo et al. was carried out to mimic the ocular environment.[144] They examined the properties of this complex on HUVEC by doing intravitreal injections in the eyes of mice and beagles. With this corona also, AuNPs were capable of binding with VEGF, and their antiangiogenic properties were also retained, suggesting the interaction of AuNP with tissue-specific protein corona enhances the in vivo properties of the nanoparticles by shielding them from nonspecific adhesion of proteins.

7.1.2 *Silica NPs*

Silicate or silicon dioxide nanoparticles (SiNP) are used to deliver drugs, gene therapy as well as a combined therapy. From the reports of Jo et al., it was found that the SiNPs have antiangiogenic properties which might result from inhibition of VEGF receptor-2 (VEGFR-2) phosphorylation. The study also demonstrated the low cytotoxic effect of SiNPs on neuronal and endothelial cells of the retina.[144] Thus SiNPs can be used to treat retinal neovascularization.

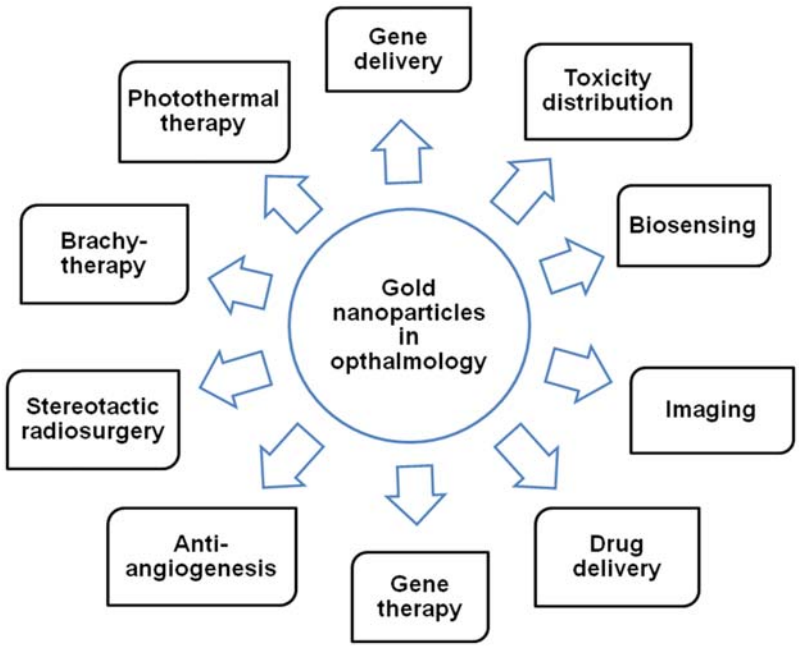

FIGURE 16.8 Application of gold nanoparticles.

7.1.3 *Cerium oxide*

Many of the diseases of the retina such as premature retinopathy, retinitis pigmentosa, diabetic retinopathy, age-induced macular degeneration, and glaucoma are caused by oxidative stress.[145–148] The retina possesses the maximum oxygen metabolism and thus has the risk of generating oxidative damage. Cerium is a rare element and cerium oxide (CeO_2) possesses antioxidant activity. Along with the traditional antioxidant agents, cerium oxide nanoparticles or nanoceria is gaining importance in recent years.[149] CeO_2 nanoparticles have high scavenging activity with very less or no toxicity after drug delivery to the eye.[150] These nanoparticles possess intrinsic antioxidant properties similar to vitamins C and E. In addition, they also have catalytic antioxidant enzymatic potentials of SOD and catalase. The mechanism that underlies its activity is due to the dual oxidation state that depends on reaction conditions.[151] Nanocercia change between Ce^{4+} and Ce^{3+} states, which creates a vacancy for oxygen and thus act as the biological ROS scavenger. Recently it is reported that nanoceria possess anti-inflammatory,[152] neuroprotective,[153] cardioprotective,[154] radioprotective,[155] antiangiogenic,[156] antiinvasive,[157] pro and antioxidative,[158,159] proapoptotic and antiapoptotic properties.[160] In the last few years, researchers have tried to address the potential use of nanoceria as a therapeutic antioxidant for treating diseases caused by oxidative stress.[160] Its small size (of about 5 nm allows it to pass through cell membranes), excellent biocompatibility, and nontoxic nature make it a unique nanoparticle. CeO_2 nanoparticles have the ability to be used as potential carriers of drug delivery agents. Cerium oxide nanoparticles prevent the increased intracellular ROS in the primary culture of rat retinal cells.[161] These nanoparticles

can prevent retinal neovascularization by lowering retinal VEGF levels and thus can be a useful therapeutic approach to treat DR.[162]

7.1.4 Magnetic nanoparticles

The interaction of various drugs with magnetic nanoparticles (MNPs) suggests their use as a promising material for ophthalmic drug delivery.[163] There are different classes of MNPs, which include bimetallic, metallic, and superparamagnetic iron oxide NPs.[164] The reactive surface of MNPs allows modification by bioactive molecules, biocompatible coatings, or targeting moieties thus, increase their target specificity and protect the healthy cells from damage.[165] MNPs are biodegradable, and therefore they are intrinsically safe.

Recently MNPs have been investigated for their ability to function as intraocular nanocarriers for drug delivery.[166] Although, there is no such study reported regarding the effect of MNPs on humans for ocular applications, their usage for ocular treatment has been proposed and evidence from different studies suggests that the iron oxide MNPs are nontoxic to the eye tissues.[167] Studies in Zebrafish and *Xenopus* have shown that MNPs, when injected intraocularly, enter rapidly into the retina and localize persistently within the RPE.[163] When these MNPs are functionalized with recombinant VEGF, they were found to be localized to the choroid.[163] This shows that the binding of MNPs with various bioactive molecules may induce specific targeting in the eye's posterior region.

7.1.5 Polymeric nanoparticles

Polymeric nanoparticles are generated as the synthetic monomers undergo polymerization or by scattering natural macromolecules on synthetic polymeric matrices. Polymeric nanoparticles that are most commonly used include PLA, PLGA, polyvinyl alcohol, chitosan, and PMMA.[168] They are made of solid matrices that either adsorb drugs on their surface or the drugs are loaded in the core. PLGA was popularly used in ophthalmology owing to its biodegradability, nontoxic, nonimmunogenic characteristics.[20] Chitosan is inexpensive, biodegradable, and nontoxic; thus possesses a great interest in polymeric drug delivery systems. Chitosan has strong mucoadhesive properties, thereby showing greater penetrability and sustained release.[169]

Attia Shafie et al. formulated and tested nanoparticles loaded with betamethasone sodium phosphate to treat macular edema.[170] Investigations of these nanoparticles were done to understand their physicochemical characteristics and their in vitro effect demonstrated an initial burst phase which was followed by slow release. Permeability studies were performed in vivo for the optimized formulation of these nanoparticles on the rabbit model, which showed that the nanoparticles are effective in drug delivery to the eye posterior.[21]

7.1.6 Lipid nanoparticles

Nanoparticles based upon lipids are developed to cope up with the limitations of polymeric nanoparticles. Unlike polymeric systems, solid lipid nanoparticles (SLN) contain a solid lipid matrix. The lipid sensitivity of the eye is a major concern, which often restricts the applications of SLN in optical drug delivery. As SLNs are comprised of physiological lipids, they are nontoxic. Another advantage of SLN includes its ability to enhance corneal absorption. These nanoparticles are adhesive which may enhance the retention time and improve ocular bioavailability.[171]

7.1.6.1 Lipid carriers

The second generation of lipid nanoparticles includes nanostructured lipid carriers (NLC), developed to rule out the disadvantages of SLNs.[172] NLCs comprise solids and liquids that are biocompatible along with surfactants and drugs. NLCs are made by incorporating a liquid lipid into a solid lipid matrix which forms a structure having a high amount of crystal imperfections. This ensures enhanced drug accommodation together with the stability of the nanocarrier.[173] Thus NLC has evolved as an efficient ocular delivery system. NLC has several other advantages which include: (1) lipophilic drug encapsulation, to increase their retention time and slow excretion than the conventional formulations, (2) increased ocular adhesion to remove the risk of enzymatic degradation and interaction with epithelial membrane. All these characters depend on the shape, size, surface charge, and lipid components of NLC that interact with the tear film lipid layer, thereby increasing their ocular availability.[174] The affinity of NLC with ocular mucosa may be influenced by its surface properties. Therefore, surface modification can be done to improve the residence time by coating with cationic lipids, cationic polymers, or surfactants to achieve a positively charged system that induces electrostatic interactions with the corneal anionic surface.[175] NLCs are mostly formulated by biological lipids, thereby these nanoparticles show minimal toxicity and excellent tolerance.[176] The ability of mangiferin NLCs to improve ocular bioavailability was studied by Liu et al.[177] Oxidative stress is the major cause of eye diseases like cataracts, DR, and macular degeneration.[178] Mangiferin, a potent antioxidant that also has antiinflammatory and antibacterial activity and is used for the treatment of DR.[179]

7.2 Nanoliposomes

Nanoliposomes are single or multi-layered lipid membranes that surround a hydrophilic core. These are synthetic vesicular systems generated from natural or artificial cholesterol and phospholipids that are nontoxic. Characteristics of a liposome depend on lipid composition, size, the charge on the surface, bilayer fluidity, and the mode of synthesis.[180] Liposomes are preferred for the delivery of therapeutic agents due to their ability to encapsulate hydrophilic molecules inside the core and the hydrophobic drugs remain in bilayers.[181] They have certain advantages as an ocular drug carrier: (1) incorporation of lipophilic and hydrophilic drugs, (2) enhanced permeability of drugs by providing improved retention, (3) increased biocompatibility, (4) controlled drug release, (5) improves bioavailability.[181] Drugs inside the liposomes are protected from enzymatic degradation. Currently, 11 liposomal formulations are available, however, several are under preclinical and clinical trials.[182]

7.3 Niosomes

Similar to liposomes, niosomes are bilayered lamellar structures made of nonionic surfactants that surround a hydrophilic aqueous core.[183] Lamellar structures are favored in ocular targeting because of their stability; cost-effectiveness; easy availability of the raw materials; unlike phospholipids, the surfactants do not require any specific conditions and preventive measures.[184] They provide enhanced durability by preventing the ocular metabolism of drug molecules. Some studies have shown the potential use of niosomes as ophthalmic delivery agents with the advantage of significantly improving the bioavailability and observed no irritation with this formulation.[185] Vyas et al. reported an increased bioavailability of timolol maleate (a

hydrophilic drug) encapsulated in niosomes in comparison to the drug alone.[186] Niosomes were also found to be a potential ophthalmic carrier of gentamicin sulfate. These suggest niosomes be considered as a potential ophthalmic carrier for topical drug administration.[187]

7.4 Nanomicelles

Nanomicelles contain amphiphilic moieties that assemble in an aqueous environment in an ordered structure in which the polar heads are projected outward, and the single-tailed hydrophobic regions are oriented toward the core.[20] Nanomicelles offer unique advantages in ocular drug delivery for their small size and enhanced permeability over ocular epithelia without any irritation.[188] They are either composed of: (1) Anionic (sodium dodecyl sulfate), nonionic (n-dodecyl tetraethylenemonoether), and cationic surfactant (dodecyl trimethylammonium bromide) or (2) polymeric systems.[188]

7.5 Nanoemulsions

Nanoemulsion is an oil-in-water emulsion, in which the droplets are formed from a liquid lipid core surrounded by a lipid monolayer.[189] The use of surfactants stabilizes these structures and results in increased permeability, which facilitates drug uptake in the deeper ocular layers.[190] Thus nanoemulsions provide a faster effect with smaller doses, resulting in minimal ocular side effects, and increasing patient compliance.[191] However, nanoemulsions are not well suited for persistent drug release.[192] Incorporation of nanoemulsions into *in situ*-forming gels, the polymeric substances that form a gel in the eye upon administration due to the phase transition characteristics, an increase in the retention time, and improved therapeutic performance may be achieved.[193]

7.6 Nanogels

Nanogels are nanoscale systems of lipophobic polymers, loaded with both hydrophobic and hydrophilic drugs.[194] The sustained release of the administered drugs can be achieved by controlling the rate of degradation of the cross-links.[20] Nanogels are known to have the potential to bypass the barriers in the eye and thus can be used for retinal drug delivery.[195] Currently, nanogels have promising strategies for the delivery of ocular drugs and thus act as a feasible alternative to the eye drops used conventionally for treating various eye diseases.[196]

7.7 Cyclodextrins (CD)

Cyclodextrin-based nanosystems are capable of delivering drugs from the eye's surface to the posterior region.[113] The molecule is composed of a hydrophilic exterior surrounding a hydrophobic core that captures a variety of molecules, starting from apolar to polar molecules.[197] CD has been proposed as a new attractive biomaterial to obtain hydrogels. This combines the ability of CDs to form inclusion complexes with the swelling property of hydrogels.[198] The use of nanosystems based on CD for increased stability, and enhanced bioavailability of loteprednol etabonate as an effective treatment for ocular allergic conjunctivitis.[199] Therapeutics based on cyclodextrin derivatives are a potential route to target ocular diseases.[200]

7.8 Dendrimer

These are highly branched, synthetic polymeric nanoparticles that range from 2 to 10 nm in diameter.[201] They are soluble in water and chemically modifiable macromolecule systems composed of three components: (1) a core at the center, (2) an external surface containing functional groups, and (3) an interior dendritic structure.[202] They have certain advantages: (1) encapsulates hydrophobic drugs into the core cavities, (2) cannot be easily taken by the RES for their size and low polydispersibility index, (3) improved solubility, permeability, and retention time (4) improved biocompatibility, (5) enhanced targeting.[21] PAMAM is the main component from which dendrimers are prepared. Drugs are captured in polymeric dendrimers through covalent bonds, ionic interactions, hydrogen bonding, or hydrophobic interactions.[20] Dendrimers are capable of delivering a drug to the eye posterior. However, the presence of functional groups may cause cytotoxicity, which is a major limitation of these nanoparticles.

7.9 Quantum dots (QDs)

These nanoparticles have a significant impact on nanotechnological applications due to their wide use in various fields such as physics, chemistry, and biology.[203] They possess a nanocrystalline structure having a size of 2−6 nm and with semiconductor properties. The nanocrystalline structure is formed by heavy metals such as cadmium selenide at the core which is surrounded by an unreactive zinc sulfide shell.[204] Sometimes an outer coating is also present that contains various bioactive molecules with specific functions. QDs possess unique optical and fluorescence properties as a result of their small size and composition which cannot be seen in traditional fluorophores. The unique properties of QDs include (1) a high signal-noise ratio, (2) minimum photobleaching, and (3) wide absorption spectra with narrow emission spectra.[205] Thus, these nanoparticles are often used as imaging agents to label retinal neuronal cells, glial cells, and endothelial cells. Currently, a novel approach using QDs is under development which involves neuronal activation by light-driven stimulation of photoresponsive substances. A recent study suggested that management of retinal degeneration is possible by using a silicon-based QD having the ability to move electrical stimulus to the retinal cells.[206]

8. Nanotechnological approaches to treat DR

8.1 Neuroprotectant-loaded nanoparticles

Endogenous neuroprotectants have an excellent capacity to block some of the important pathological pathways of DR, however, their effects are short-term and thus repeated administration would be necessary.[207] Thus, neuroprotectants loaded on nanoparticles may be a useful strategy to administer them to the retina to improve treatment outcomes.[207] Various studies have addressed to design and characterize NPs for the treatment of DR.[208] The studies have also checked the probability of NPs targeting neuroprotective agents to the diabetic retina. Several reports have suggested that the administration of Octriotide (OCT) functionalized MNPs inhibit cell proliferation, migration, and tube formation induced by VEGF in

different models of DR.[209] Additionally, ex vivo retinal explants have been shown to decrease retinal cell apoptosis by oxidative stress under the treatment of MNPs functionalized with OCT.[210] It was also found that OCT combined MNPs enable sustained release of OCT. All the studies reported that the functionalization does not alter the bioactivity of OCT, as the functionalized OCT also showed the same effects as free OCT. Similar investigations have also been carried out with neurotrophin NGF and a neuropeptide PACAP.[207]

8.2 Subretinal and systemic delivery systems

Subretinal delivery of gene and drug carriers has been developed to overcome the ocular barriers of the vitreous.[211] Ocular gene delivery through subretinal injection was investigated by Naash et al.[212] It was shown that the use of compact DNA nanoparticles can restore the function of cone cells to a normal level along with improved rod cell function as compared to subretinal administration of the DNA alone. The results along with the clinical safety[213] of the nanoparticles after subretinal administration allow their potential use in gene delivery for managing various ocular diseases. For the delivery of different agents to the posterior segment through BRB, the systemic route has also been studied.[214] The inner BRB or iBRB possesses tight junctions, which prevent the entry of systemic drugs into the ocular space. To overcome this limitation a novel approach was developed by Humphries et al. that uses RNAi-mediated suppression for the reversible opening of the tight junctions.[215] This allowed the therapeutics with low molecular weight to be delivered to the retinal outer layer but does not allow molecules above 1 kDa.

Surface-modification of PLGA nanoparticles by transferrin and an RGD peptide (arginine-glycine-aspartic acid) was done for the delivery of an anti-VEGF plasmid.[216] Systemic incorporation of these RGD-functionalized nanoparticles into the CNV rat model was able to affect retinal neovascularization. Thus, surface modification of nanoparticles allowed gene delivery to the outer segments of the photoreceptors, and the RPE and REC cells were better than the nanoparticles that have not undergone functionalization.

8.3 Intravitreal delivery systems

Intravitreal delivery enables the delivery of drugs or particles directly to the vitreous humor allowing them to diffuse or penetrate further to the retina.[217] A report by Behar-Cohen et al. suggested preferential localization of PLA nanoparticles (310 nm) in the RPE of Lewis rats by intravitreal administration even after 4 months from a single injection.[218] Thus, the formulation of nanoparticles is important to prevent the quick clearance of drugs and molecules in the retina and vitreous for prolonged delivery.[219,220] The use of steroid and nonsteroid drugs in several retinal diseases because of antiinflammatory, antiangiogenic, and neuroprotective abilities is often limited to their solubility problems. This limitation causes their early elimination or accumulation in ocular tissues resulting in local toxicity, increased intraocular pressure as well as degeneration of the optic nerve.[221] A strategy was developed by Kannan and Iezzi for retinitis pigmentosa to deliver a steroid known as fluocinolone acetonide (FA) by using PAMAM dendrimers as a targeted carrier for sustained drug delivery. This showed their biodistribution depending on the disease pathology and selected

localization in the retinal microglial cells.[222] Moreover, neuroprotective effects of these dendrimer-FA conjugates were also seen, which were found to be more useful than free drugs at a relatively low concentration (~20-fold lower). Such strategies of treatment with improved drug sustainability may help in reducing the incidence of intravitreal injections and improve drug efficiency by targeted delivery.

8.4 Antiangiogenic nanoparticles

A wide range of retinal disorders are associated with angiogenesis and are termed Angiogenesis-related blindness (ARB). These include diabetic retinopathy, retinopathy of prematuration (ROP), and age-related macular degeneration (AMD).[223] Conventional treatments of ARB involved surgical and focal treatments, like cryotherapy and laser photocoagulation. Recently intravitreal administration of antibodies against VEGF is used to treat pathologic angiogenesis. However, these methods have several limitations as it requires repeated injections due to relatively short duration which may lead to injection-related complications.[224,225]

Nanoparticles are thought to overcome these limitations by improved bioavailability.[224] Several nanoparticles are examined for their antiangiogenic effects.[226] The pioneering work on the gold nanoparticles to evaluate their antiangiogenic properties was done by Bhattacharya et al. From in vitro studies, it is found that the gold nanoparticle's antiangiogenic properties derived from the inhibition of glycoproteins like VEGF165 and bFGF which binds to heparin.[142,227] Various reports also suggest that the gold nanoparticles also can prevent retinal neovascularization by inhibiting the activation of the VEGF-2 receptor.[143] In addition, in vitro studies on bovine RPE cells suggested gold NPs inhibit VEGF-induced angiogenesis by blocking the Src pathway,[228] a kinase involved in the VEGF-induced proliferation in vivo.[229] Silica nanoparticles have antiangiogenic effects on retinal neovascularization which suggest the importance of size, shape, mass, as well as background material of NP, which is an important factor while determining antiangiogenic effects.[230] Furthermore, silver nanoparticles also inhibit proliferation as well as migration of the endothelial cells induced by VEGF and mechanisms thought to induce apoptosis.[231] Antiangiogenic property is also seen in nanoceria. Nanoceria causes reduction of ROS level and regression of neovascular lesions.[162] Recently, the antiangiogenic potential of the titanium oxide nanoparticles was also checked and it was seen that intravitreal administration of TiO_2 nanoparticles at a nontoxic dose may reduce the vascular tufts.[232]

However, the frequent administration of these inorganic nanoparticles may have toxic effects as they are nonbiodegradable and are not eliminated easily from the body. Although, the application of one injection may be tolerable frequent applications may lead to accumulation and decomposition of the nanoparticles with time which may create problems in the sensitive neural retina.[233]

8.5 Retinal degeneration

The degeneration of the retina is also a target of nanoparticle-based therapies in retinopathy. Currently, no definite cure exists for retinal degeneration except for antioxidant

treatment. Nanocercia were shown to prevent photoreceptor cell degeneration induced by light by decreasing the ROS level in the retinal cells.[234] Various studies in this regard suggest that these small nanoparticles mimic antioxidant enzymes to inhibit the production of ROS.[235]

8.6 Nanoparticles for optical gene therapy

Gene therapy targets the cause rather than the symptoms of a disease after the insertion of oligonucleotides to a particular site within the genome.[236] Gene therapy approaches either introduce corrective genes or block the expression of malfunctioned genes. However, gene therapy approaches face substantial problems due to the nonavailability of safe and efficient viral and nonviral vectors. The eye serves as an excellent organ for gene therapy because of its several outstanding features. First, it has a well-compartmentalized structure that allows the delivery of nanoparticles precisely to the specific eye tissues, which minimizes their systemic exposure.[237] Secondly, the ocular tissue contains a stable cell population which may provide adequate longevity with highly efficient transduction.[237] Lastly, due to the immune privilege of the eye, an immunogenic response can be avoided mostly.[238] Various nanoparticle-based model systems of gene therapy, as well as gene delivery, are being examined for treating retinal and choroidal neovascularization.[239] Currently, gene therapy is mainly used to regulate VEGF expression. The two most prominent strategies were used: (1) to increase the expression of VEGF-capturing molecules or (2) to directly decrease VEGF expression or manipulate the signaling pathways associated with VEGF.[240] Marano and his coworkers first described the use of intraocular drug delivery by nanomaterials to decrease the expression of VEGF. With the help of a synthetic lipid-lysine dendrimer, they delivered an anti-VEGF sense oligonucleotide to choroidal lesions. These complex nanomaterials were able to inhibit choroidal neovascularization (CNV) for some months and were also found to be distributed all over the retina up to the RPE without any toxic effects.[241] Similar effects were seen after intravascular administration of a siRNA targeted to VEGFR-1 mRNA, loaded in PEGylated cationic liposomes was able to reduce the CNV area.[242] PLGA nanoparticles have been investigated extensively for delivering plasmids encoding antiangiogenic proteins loaded on biodegradable PLGA nanoparticles. After administration, these nanoparticles are hydrolyzed and their payload is released for a sustained period.[243] Moreover, the PLGA matrix protects the incorporated plasmid from degradation by the nucleases.[244] Intravitreal administration of a plasmid that codes for HIF-1α shRNA, loaded on PLGA nanoparticles causes a significant reduction in leakage from neovascular lesions. HIF-1α controls transcription of VEGF and thus therapeutic interference of HIF leads to downregulation of VEGF expression.[245]

8.7 Nanoparticle-mediated drug delivery

The complex anatomy and physiological barriers present in the eye often limit the delivery of drugs and in a conventional system, it is often affected by poor bioavailability in the eye.[129] Recent advancements in nano-based delivery systems have the potential to overcome these limitations. Nanocarrier-based ocular drug delivery has three major aims that are: (1) to enhance the drug permeability, (2) to control drug release, and (3) to manipulate the

nanocarrier's surface with specific target molecules.[246] Although various types of nanocarriers have been examined for optical drug delivery, the application of polymeric and lipid nanoparticles has the most potential and their use could transform ocular therapy, especially for the disease of the eye posterior segment.[247]

Nanoparticle-based delivery systems allow sustained drug release from nanocarriers (Fig. 16.9), thereby improving their bioavailability. Moreover, after loading the drug on a nano-based system, their aqueous solubility is greatly influenced which prevents degradation.[248] Controlled release of the drugs has the potential to increase the interval between intravitreal injections and thereby have great ocular applications. Intravitreal administration of dexamethasone-loaded PLGA nanoparticles was found to prevent leakage from CNV lesions.[249] Corticosteroids can be used as a therapeutic agent; however, the surface area-volume ratio is quite high for these nanoparticles resulting in rapid release of the high amount of glucocorticoid and thus it was not possible to achieve their sustained release.[250] The same kind of effect was also seen in the subconjunctival application of the budesonide-loaded PLA nanoparticles.[251] A micellar system was synthesized by Oh and his coworkers. This consists of hyaluronate and a water-insoluble antagonist of VEGFR-1, which was able to inhibit choroidal neovascularization (CNV) as compared to the antagonist alone.[252] The vascular leakage could be further reduced by loading genistein, an isoflavonoid interfering with VEGF in the micelles.[253] Controlled drug release from nanoparticles also gives an additional advantage of lowering the toxicity that may arise from high concentrations of the drug. Doxorubicin (DXR) is such an agent that suppresses HIF-1α, having a strong antiangiogenic potential.[254] Although DXR is effective in preventing neovascularization in the eye, it also exerts deleterious effects on the function of the retina.[255] The retinal toxicity was diminished when synthesized in PEG-PSA nanoparticles but retained the antiangiogenic properties.[255] Other investigations used a delivery method to the eye posterior, in which aerosolized nanoparticles were added to the gas during the gas exchange phase of vitrectomy in the porcine eyes. This method has improved the delivery of a variety of pharmacotherapeutic agents for the treatment of various ocular disorders.[21]

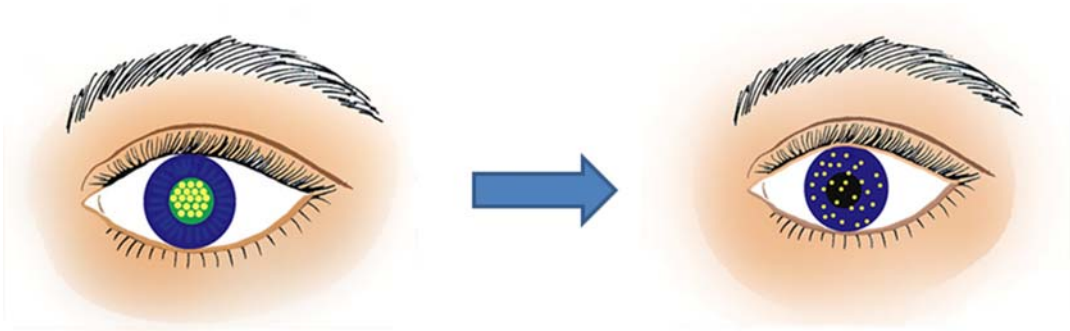

FIGURE 16.9 Application of drug-loaded nanoparticles. After some time the drug molecules are diffused throughout the cornea.

9. Toxicity of nanoparticles in retinopathy

The retina as a multilayered structure consists of three nucleated cell layers and two layers of plexiform.[223] When the light comes to the retina, it is transformed into electrical signals by photoreceptor cells and gets transmitted to the optic nerve.[256] The external factors such as infectious organisms or the therapeutic agents, often damage the cells participating in the phototransduction process and thus deteriorating the visual response. Thus before the clinical applications, each candidate nanoparticle should be evaluated to not have any definite toxicity on the retina.[235] In the case of retinopathy, the toxicological properties are studied in association with the therapeutic effect of the nanoparticles. Thus, there are very few studies on the nanoparticle toxicity aspects. Previous reports on nanoparticle application in retinopathy have shown no definite toxic effect on the retina as confirmed by the histological examinations as well as electroretinography, which is a measurement of the electrical responses in the retina.[235] There are several studies on the toxicity of polymeric nanoparticles based on types, concentrations, and tail length.[257,258] One of the studies showed that the intravitreal administration of gold nanoparticles at minimal concentrations did not induce any toxicity on the retina or optic nerve.[259] In another study, DNA-compacted PEG nanoparticles for treating retinal degeneration, subretinal administration of the nanoparticles at lower concentration induce neither the lymphocyte infiltration nor increase inflammatory cell markers.[213] Hafeli et al. suggested that iron nanoparticles coated with short polyethyleneoxide tails showed more toxicity compared to the nanoparticles with long tails.[257] Alteration of surface characteristics reduces toxic effects on endothelial cells and RPE. Prow et al. showed the usefulness as well as safety of the magnetic nanoparticles along with the chitosan and PCEP nanoparticles[258] by examining the abnormalities of RPE, neuroinflammation, and retinal degeneration. They further proved the intravitreal, as well as subretinal administration of the magnetic nanoparticles, did not show any toxicity in the retina.

9.1 Factors affecting toxicity

Various factors can affect nanoparticle toxicity in the ocular tissues which include size, shape, physicochemical characters, dosage, assessment time, and biodistribution of nanoparticles in the eye.[260,261] Although more studies have emphasized their formulation efficacy, many studies also focus on histology-based toxicity evaluations, along with immunohistochemistry, neuroinflammation, and neuronal toxicity.[235] Besides the factors affecting the nanoparticles' toxicity, magnitude and concentration are two main factors that might have important roles. Administration of the nanoparticles should also be done at a particular concentration to ensure aimed effects with minimal toxicity. Nanoparticle surface charge also affects the toxicity and integrity of the blood–neuronal barrier.[262] The neutral and anionic nanoparticles at low concentrations do not have any toxic effect on the integrity of BBB. However, anionic and cationic nanoparticles at higher concentrations exerted alterations in BBB.[263] In this context, iron and carbon black nanoparticles did not cause intracellular ROS formation even at higher concentration.[264] Zinc oxide nanoparticles cause dose-dependent toxic effects.[265] The safety of the nanoparticles for optical gene delivery was compared by Lutty et al.[258] Intravitreal and subretinal injection of PCEP and magnetic nanoparticles do not cause

any inflammation or pathological effect on the retina. Goldberg et al. demonstrated various sizes of magnetic nanoparticles on ocular toxicity after intravitreal administration of dextran-coated magnetic nanoparticles.[167]

The ocular biodistribution of the nanoparticles along with the disease has a cumulative effect on nanoparticle toxicity. In a rat model, PAMAM dendrimers were readily cleared from the healthy eyes after intravitreal injection. In a diseased retina, the dendrimers were localized in the microglial cells of the retina.[266] Neuroinflammation might be another contributor to dendrimer toxicity. ODN-1, an anti-VEGF oligonucleotide conjugated with a lipophilic dendrimer made of amino acids was injected intravitreally into rat eyes to inhibit laser-induced CVD. Dendrimer-ODN-1 do not show any increase in the inflammation-related antigens and was biocompatible as seen by immunohistochemistry.[241] The intravitreal route requires a much lower dose compared to the systemic route thus helps to reduce nanoparticle toxicity. Henceforth, by synthesizing nanoparticles of various sizes, physicochemical properties and modified surface properties can be done to minimize their toxicity.[235,267]

10. Conclusion

Diabetic retinopathy appears as a consequence of diabetic complications and is a major cause of vision loss throughout the world. The high economic burden of its treatment along with some complications such as cataracts, tear in the eye, glaucoma make the disease difficult to treat. Furthermore, the route of administration, the carrier molecules, are the shortcomings for treatment efficiency. Besides this, the current treatment methods are invasive, painful, and can restore the lost vision only partially. With the development of nanotechnology, many nanomaterials have been created to treat various ocular diseases. Nanomaterials, due to their small size can cross important ocular barriers that often limit ocular delivery. Hence, the ocular drugs can be delivered to the eye's posterior region, the potential site of DR. Furthermore, complex nanoformulations combining the antioxidative and antiangiogenic properties of various nanoparticles with gene therapy can be developed to treat or prevent the onset of DR. Various trials in the nonhuman model followed by a clinical trial in humans will help to treat DR without much side effects.

Acknowledgments

SM is thankful to MHRD for financial support. MM lab is supported by Grant No. BT/PR21857/NNT/28/1238/2017, EMR/2017/003054, Odisha DBT 3325/ST(BIO)-02/2017.

References

1. F. Toyoda, et al., Effect of ranirestat, a new aldose reductase inhibitor, on diabetic retinopathy in SDT rats 2014, J Diabetes Res, 2014, p. 672590.
2. A.D. Association, Diagnosis and classification of diabetes mellitus, Diabetes Care 32 (Suppl. 1) (2009) S62–S67.
3. D.M. Maahs, et al., Epidemiology of type 1 diabetes, Endocrinol Metabol Clin 39 (3) (2010) 481–497.
4. B. Fletcher, M. Gulanick, C. Lamendola, Risk factors for type 2 diabetes mellitus, J Cardiovasc Nurs 16 (2) (2002) 17–23.
5. T.A. Buchanan, A.H. Xiang, Gestational diabetes mellitus, J Clin Invest 115 (3) (2005) 485–491.

6. M.J. Fowler, Microvascular and macrovascular complications of diabetes, Clin Diabetes 26 (2) (2008) 77–82.
7. J.L. Edwards, et al., Diabetic neuropathy: mechanisms to management, Pharmacol Ther 120 (1) (2008) 1–34.
8. M. Porta, F. Bandello, Diabetic retinopathy, Diabetologia 45 (12) (2002) 1617–1634.
9. J.L. Gross, et al., Diabetic nephropathy: diagnosis, prevention, and treatment, Diabetes Care 28 (1) (2005) 164–176.
10. D.S.W. Ting, G.C.M. Cheung, T.Y. Wong, Diabetic retinopathy: global prevalence, major risk factors, screening practices and public health challenges: a review, Clin Exp Ophthalmol 44 (4) (2016) 260–277.
11. S.K. Paikra, J. Bag, M. Mishra, Effect of drugs and nanoformulation on ocular cells in various disease states, in: Nanoformulations in human health, Springer, 2020, pp. 259–283.
12. F. Mulvey, Eye anatomy, eye movements and vision, in: Gaze interaction and applications of eye tracking: advances in assistive technologies, IGI Global, 2012, pp. 10–20.
13. GÜRSU, E. and K. BERBEROĞLU, Mechanisms in the eye.
14. R.L. Gregory, Eye and brain: the psychology of seeing, vol. 80, Princeton university press, 2015.
15. M. Campbell, P. Humphries, The blood-retina barrier, in: Biology and regulation of blood-tissue barriers, Springer, 2013, pp. 70–84.
16. J.I. Alvarez, T. Katayama, A. Prat, Glial influence on the blood brain barrier, Glia 61 (12) (2013) 1939–1958.
17. G. Bergers, S. Song, The role of pericytes in blood-vessel formation and maintenance, Neuro Oncol 7 (4) (2005) 452–464.
18. E. Vecino, et al., Glia–neuron interactions in the mammalian retina, Prog Retin Eye Res 51 (2016) 1–40.
19. R. Simó, et al., The retinal pigment epithelium: something more than a constituent of the blood-retinal barrier—implications for the pathogenesis of diabetic retinopathy, J Biomed Biotechnol 2010 (2010).
20. U.B. Kompella, et al., Nanomedicines for back of the eye drug delivery, gene delivery, and imaging, Prog Retin Eye Res 36 (2013) 172–198.
21. K. Selvaraj, et al., Current treatment strategies and nanocarrier based approaches for the treatment and management of diabetic retinopathy, J Drug Target 25 (5) (2017) 386–405.
22. K.M. Sampat, S.J. Garg, Complications of intravitreal injections, Curr Opin Ophthalmol 21 (3) (2010) 178–183.
23. R.D. Jager, et al., Risks of intravitreous injection: a comprehensive review, Retina 24 (5) (2004) 676–698.
24. P.U. Dugel, F. Bandello, A. Loewenstein, Dexamethasone intravitreal implant in the treatment of diabetic macular edema, Clin Ophthalmol 9 (2015) 1321.
25. A. Grzybowski, et al., 2018 Update on intravitreal injections: euretina expert consensus recommendations, Ophthalmologica 239 (4) (2018) 181–193.
26. R.N. Frank, Potential new medical therapies for diabetic retinopathy: protein kinase C inhibitors, Am J Ophthalmol 133 (5) (2002) 693–698.
27. I. G Obrosova, P. F Kador, Aldose reductase/polyol inhibitors for diabetic retinopathy, Curr Pharmaceut Biotechnol 12 (3) (2011) 373–385.
28. J.L. Wilkinson-Berka, et al., An antisense oligonucleotide targeting the growth hormone receptor inhibits neovascularization in a mouse model of retinopathy, Mol Vis 13 (2007) 1529–1538.
29. S. Rangasamy, P.G. McGuire, A. Das, Diabetic retinopathy and inflammation: novel therapeutic targets, Middle East Afr J Ophthalmol 19 (1) (2012) 52.
30. Z. Weiwei, R. Hu, Targeting carbonic anhydrase to treat diabetic retinopathy: emerging evidences and encouraging results, Biochem Biophys Res Commun 390 (3) (2009) 368–371.
31. B. Wang, et al., Effects of RAS inhibitors on diabetic retinopathy: a systematic review and meta-analysis, Lancet Diabetes Endocrinol 3 (4) (2015) 263–274.
32. J. El Annan, P.E. Carvounis, Current management of vitreous hemorrhage due to proliferative diabetic retinopathy, Int Ophthalmol Clin 54 (2) (2014) 141.
33. S.K. Murthy, Nanoparticles in modern medicine: state of the art and future challenges, Int J Nanomed 2 (2) (2007) 129.
34. D. Chenthamara, et al., Therapeutic efficacy of nanoparticles and routes of administration, Biomater Res 23 (1) (2019) 1–29.
35. M.J. Mitchell, et al., Engineering precision nanoparticles for drug delivery, Nat Rev Drug Discov 20 (2) (2021) 101–124.
36. T.A. Ciulla, A.G. Amador, B. Zinman, Diabetic retinopathy and diabetic macular edema: pathophysiology, screening, and novel therapies, Diabetes Care 26 (9) (2003) 2653–2664.

37. S.L. Jyothi, N. Vishal Gupta, Diabetic retinopathy: an inclusive review on current treatment and management approaches, Asian J Pharmaceut Clin Res 11 (11) (2018).
38. T.W. Gardner, et al., Diabetic retinopathy: more than meets the eye, Surv Ophthalmol 47 (2002) S253–S262.
39. C. Hudson, The clinical features and classification of diabetic retinopathy, Ophthalmic Physiol Opt 16 (1996) S43–S48.
40. M. Brownlee, The pathobiology of diabetic complications: a unifying mechanism, Diabetes 54 (6) (2005) 1615–1625.
41. M. Merlak, et al., Expression of vascular endothelial growth factor in proliferative diabetic retinopathy, Coll Antropol 32 (2) (2008) 39–43.
42. J.L. Wilkinson-Berka, C. Wraight, G. Werther, The role of growth hormone, insulin-like growth factor and somatostatin in diabetic retinopathy, Curr Med Chem 13 (27) (2006) 3307–3317.
43. S. Rangasamy, et al., A potential role for angiopoietin 2 in the regulation of the blood–retinal barrier in diabetic retinopathy, Investig Ophthalmol Vis Sci 52 (6) (2011) 3784–3791.
44. H.L. Brooks, et al., Vitreous levels of vascular endothelial growth factor and stromal-DerivedFactor 1 in patients with diabetic retinopathy and cystoid macular edema beforeand after intraocular injection of triamcinolone, Arch Ophthalmol 122 (12) (2004) 1801–1807.
45. A. Hueber, et al., Basic fibroblast growth factor mRNA, bFGF peptide and FGF receptor in epiretinal membranes of intraocular proliferative disorders (PVR and PDR), Int Ophthalmol 20 (6) (1997) 345–350.
46. Y. Katsura, et al., Hepatocyte growth factor in vitreous fluid of patients with proliferative diabetic retinopathy and other retinal disorders, Diabetes Care 21 (10) (1998) 1759–1763.
47. A.M. Joussen, et al., TNF-α mediated apoptosis plays an important role in the development of early diabetic retinopathy and long-term histopathological alterations, Mol Vis 15 (2009) 1418.
48. M.C. Mocan, S. Kadayifcilar, B. Eldem, Elevated intravitreal interleukin-6 levels in patients with proliferative diabetic retinopathy, Can J Ophthalmol 41 (6) (2006) 747–752.
49. C. Wilkinson, et al., Proposed international clinical diabetic retinopathy and diabetic macular edema disease severity scales, Ophthalmology 110 (9) (2003) 1677–1682.
50. D.S. Fong, et al., Retinopathy in diabetes, Diabetes Care 27 (Suppl. 1) (2004) s84–s87.
51. R.L. Engerman, Pathogenesis of diabetic retinopathy, Diabetes 38 (10) (1989) 1203–1206.
52. G.H. Bresnick, et al., Retinal ischemia in diabetic retinopathy, Arch Ophthalmol 93 (12) (1975) 1300–1310.
53. L. Wu, et al., Classification of diabetic retinopathy and diabetic macular edema, World J Diabetes 4 (6) (2013) 290.
54. D.A. Antonetti, R. Klein, T.W. Gardner, Diabetic retinopathy, N Engl J Med 366 (13) (2012) 1227–1239.
55. R. Frank, Retinopathy D. Diabetic retinopathy, N Engl J Med 350 (2004) 48–58.
56. M. Brownlee, Biochemistry and molecular cell biology of diabetic complications, Nature 414 (6865) (2001) 813.
57. R. Simo, C. Hernandez, Neurodegeneration in the diabetic eye: new insights and therapeutic perspectives, Trends Endocrinol Metabol 25 (1) (2014) 23–33.
58. J. Tang, T.S. Kern, Inflammation in diabetic retinopathy, Prog Retin Eye Res 30 (5) (2011) 343–358.
59. J.L. Wilkinson-Berka, A. Agrotis, D. Deliyanti, The retinal renin–angiotensin system: roles of angiotensin II and aldosterone, Peptides 36 (1) (2012) 142–150.
60. R.A. Kowluru, P.-S. Chan, Oxidative stress and diabetic retinopathy, vol. 2007, Experimental diabetes research, 2007.
61. S.X. Zhang, et al., Endoplasmic reticulum stress and the unfolded protein responses in retinal degeneration, Exp Eye Res 125 (2014) 30–40.
62. R. Klein, et al., The Wisconsin Epidemiologic Study of Diabetic Retinopathy: II. Prevalence and risk of diabetic retinopathy when age at diagnosis is less than 30 years, Arch Ophthalmol 102 (4) (1984) 520–526.
63. R. Klein, et al., The Wisconsin Epidemiologic Study of Diabetic Retinopathy: III. Prevalence and risk of diabetic retinopathy when age at diagnosis is 30 or more years, Arch Ophthalmol 102 (4) (1984) 527–532.
64. T. Kuwabara, D.G. Cogan, Retinal vascular patterns: VI. Mural cells of the retinal capillaries, Arch Ophthalmol 69 (4) (1963) 492–502.
65. P. Henkind, Ocular neovascularization. The Krill memorial lecture, Am J Ophthalmol 85 (3) (1978) 287–301.
66. A. Patz, Clinical and experimental studies on retinal neovascularization: XXXIX Edward Jackson memorial lecture, Am J Ophthalmol 94 (6) (1982) 715–743.
67. R.N. Frank, Diabetic retinopathy, N Engl J Med 350 (1) (2004) 48–58.

68. D.R.S.R. Group, Photocoagulation treatment of proliferative diabetic retinopathy: clinical application of Diabetic Retinopathy Study (DRS) findings, DRS Report Number 8, Ophthalmology 88 (7) (1981) 583–600.
69. A.S. Neubauer, M.W. Ulbig, Laser treatment in diabetic retinopathy, Ophthalmologica 221 (2) (2007) 95–102.
70. P.W. Russell, R. Sekuler, C. Fetkenhour, Visual function after pan-retinal photocoagulation: a survey, Diabetes Care 8 (1) (1985) 57–63.
71. J. Birch, A. Hamilton, Xenon arc and argon laser photocoagulation in the treatment of diabetic disc neovascularization. Part 2. Effect on colour vision, Trans Ophthalmol Soc U K 101 (1) (1981) 93–99.
72. P.K. Khosla, et al., Contrast sensitivity in diabetic retinopathy after panretinal photocoagulation, Ophthalmic Surgery, Lasers and Imaging Retina 25 (8) (1994) 516–520.
73. D.S. Fong, A. Girach, A. Boney, Visual side effects of successful scatter laser photocoagulation surgery for proliferative diabetic retinopathy: a literature review, Retina 27 (7) (2007) 816–824.
74. G.Y. Fujii, et al., A new 25-gauge instrument system for transconjunctival sutureless vitrectomy surgery, Ophthalmology 109 (10) (2002) 1807–1812.
75. D. Newman, Surgical management of the late complications of proliferative diabetic retinopathy, Eye 24 (3) (2010) 441.
76. S.A. Doggrell, Pegaptanib: the first antiangiogenic agent approved for neovascular macular degeneration: GRAGOUNDAS ES, ADAMIS AP, CUNNINGHAM ET et al.: pegaptanib for neovascular age-related macular degeneration, N Engl J Med 351 (2004) 2805–2816. Expert opinion on pharmacotherapy, 2005. 6(8): pp. 1421–1423.
77. P.J. Rosenfeld, et al., Ranibizumab for neovascular age-related macular degeneration, N Engl J Med 355 (14) (2006) 1419–1431.
78. S. Day, et al., Ocular complications after anti–vascular endothelial growth factor therapy in medicare patients with age-related macular degeneration, Am J Ophthalmol 152 (2) (2011) 266–272.
79. N. Ferrara, et al., Discovery and development of bevacizumab, an anti-VEGF antibody for treating cancer, Nat Rev Drug Discov 3 (5) (2004) 391.
80. A.N. Economides, et al., Cytokine traps: multi-component, high-affinity blockers of cytokine action, Nat Med 9 (1) (2003) 47.
81. S. Matsuda, et al., Vascular endothelial growth factor reduced and connective tissue growth factor induced by triamcinolone in ARPE19 cells under oxidative stress, Investig Ophthalmol Vis Sci 46 (3) (2005) 1062–1068.
82. T.A. Ciulla, et al., Corticosteroids in posterior segment disease: an update on new delivery systems and new indications, Curr Opin Ophthalmol 15 (3) (2004) 211–220.
83. A. Martidis, et al., Intravitreal triamcinolone for refractory diabetic macular edema, Ophthalmology 109 (5) (2002) 920–927.
84. B.D. Kuppermann, Sustained-release dexamethasone intravitreal implant for treatment of diabetic macular edema, Expet Rev Ophthalmol 6 (1) (2011) 11–20.
85. P.A. Kurz, et al., Injectable intraocular corticosteroids, in: Surgical management of inflammatory eye disease, Springer, 2008, pp. 5–16.
86. T.R. Thrimawithana, et al., Drug delivery to the posterior segment of the eye, Drug Discov Today 16 (5–6) (2011) 270–277.
87. A.S. Group, A.E.S. Group, Effects of medical therapies on retinopathy progression in type 2 diabetes, N Engl J Med 363 (3) (2010) 233–244.
88. U.P.D.S. Group, Intensive blood-glucose control with sulphonylureas or insulin compared with conventional treatment and risk of complications in patients with type 2 diabetes (UKPDS 33), The lancet 352 (9131) (1998) 837–853.
89. U.P.D.S. Group, Tight blood pressure control and risk of macrovascular and microvascular complications in type 2 diabetes: ukpds 38, BMJ Br Med J (Clin Res Ed) 317 (7160) (1998) 703.
90. L. Elving, et al., Captopril and atenolol are equally effective in retarding progression of diabetic nephropathy, Diabetologia 37 (6) (1994) 604–609.
91. R. Klein, B. Klein, Blood pressure control and diabetic retinopathy, BMJ Publishing Group Ltd, 2002.
92. B.E. Klein, et al., The Wisconsin Epidemiologic Study of Diabetic Retinopathy: XIII. Relationship of serum cholesterol to retinopathy and hard exudate, Ophthalmology 98 (8) (1991) 1261–1265.
93. E.Y. Chew, et al., Association of elevated serum lipid levels with retinal hard exudate in diabetic retinopathy: early Treatment Diabetic Retinopathy Study (ETDRS) Report 22, Arch Ophthalmol 114 (9) (1996) 1079–1084.

94. M. Golubovic-Arsovska, Association of dyslipidaemia with macular oedema and hard exudates in diabetic maculopathy, Prilozi 28 (2) (2007) 149–160.
95. T. Chowdhury, et al., The role of serum lipids in exudative diabetic maculopathy: is there a place for lipid lowering therapy? Eye 16 (6) (2002) 689.
96. A. Keech, et al., Effect of fenofibrate on the need for laser treatment for diabetic retinopathy (FIELD study): a randomised controlled trial, Lancet 370 (9600) (2007) 1687–1697.
97. N. Cheung, T. Wong, Fenofibrate and diabetic retinopathy, Lancet 371 (9614) (2008) 721–722.
98. A.D. Association, The effect of ruboxistaurin on visual loss in patients with moderately severe to very severe nonproliferative diabetic retinopathy: initial results of the protein kinase C β inhibitor diabetic retinopathy study (PKC-DRS) multicenter randomized clinical trial, Diabetes 54 (7) (2005) 2188–2197.
99. F. Toyoda, et al., Effect of ranirestat, a new aldose reductase inhibitor, on diabetic retinopathy in SDT rats, Investig. Ophthalmol. Vis. Sci 55 (13) (2014) 1060.
100. A.M. Joussen, et al., Nonsteroidal anti-inflammatory drugs prevent early diabetic retinopathy via TNF-α suppression, Faseb J 16 (3) (2002) 438–440.
101. M.K. Tsilimbaris, et al., The use of intravitreal etanercept in diabetic macular oedema, in: Seminars in ophthalmology, Taylor & Francis, 2007.
102. P.P. Sfikakis, et al., Infliximab for diabetic macular edema refractory to laser photocoagulation: a randomized, double-blind, placebo-controlled, crossover, 32-week study, Diabetes Care 33 (7) (2010) 1523–1528.
103. F. Giacco, M. Brownlee, Oxidative stress and diabetic complications, Circ Res 107 (9) (2010) 1058–1070.
104. R.J. Nardino, Vitamin E for treatment of diabetic retinopathy, vol. 4, AHC Media, 2001, pp. 100–103.
105. O. Tabatabaei-Malazy, B. Larijani, M. Abdollahi, A novel management of diabetes by means of strong antioxidants' combination, J Med Hypotheses Ideas 7 (1) (2013) 25–30.
106. E. Bagli, et al., Luteolin inhibits vascular endothelial growth factor-induced angiogenesis; inhibition of endothelial cell survival and proliferation by targeting phosphatidylinositol 3′-kinase activity, Cancer Res 64 (21) (2004) 7936–7946.
107. Y.H. Kim, et al., Resveratrol blocks diabetes-induced early vascular lesions and vascular endothelial growth factor induction in mouse retinas, Acta Ophthalmol 90 (1) (2012) e31–e37.
108. D. Wang, et al., Scutellarin inhibits high glucose–induced and hypoxia-mimetic agent–induced angiogenic effects in human retinal endothelial cells through reactive oxygen species/hypoxia-inducible factor-1α/vascular endothelial growth factor pathway, J Cardiovasc Pharmacol 64 (3) (2014) 218–227.
109. M. Perossini, Diabetic and hypertensive retinopathy therapy with Vaccinium myrtillus anthocyanosides (Tegens), Ann Ottalmol Clin. Ocul 113 (1987) 1173.
110. H. Lee, et al., Epigalloccatechin-3-gallate inhibits ocular neovascularization and vascular permeability in human retinal pigment epithelial and human retinal microvascular endothelial cells via suppression of MMP-9 and VEGF activation, Molecules 19 (8) (2014) 12150–12172.
111. B.-B. Gao, et al., Characterization of the vitreous proteome in diabetes without diabetic retinopathy and diabetes with proliferative diabetic retinopathy, J Proteome Res 7 (6) (2008) 2516–2525.
112. M.F. Sugrue, Pharmacological and ocular hypotensive properties of topical carbonic anhydrase inhibitors, Prog Retin Eye Res 19 (1) (2000) 87–112.
113. T. Loftsson, D. Hreinsdóttir, E. Stefansson, Cyclodextrin microparticles for drug delivery to the posterior segment of the eye: aqueous dexamethasone eye drops, J Pharm Pharmacol 59 (5) (2007) 629–635.
114. K. Williams, et al., Topically applied antibody fragments penetrate into the back of the rabbit eye, Eye 19 (8) (2005) 910.
115. M. Diaz-Llopis, et al., Enzymatic vitrectomy for diabetic retinopathy and diabetic macular edema, World J Diabetes 4 (6) (2013) 319.
116. M.D. de Smet, et al., Microplasmin: ex vivo characterization of its activity in porcine vitreous, Investig Ophthalmol Vis Sci 50 (2) (2009) 814–819.
117. A. Takano, et al., Posterior vitreous detachment induced by nattokinase (subtilisin NAT): a novel enzyme for pharmacologic vitreolysis, Investig Ophthalmol Vis Sci 47 (5) (2006) 2075–2079.
118. G. Hageman, S. Russell, Chondroitinase-mediated disinsertion of the primate vitreous body, 1994.
119. P.N. Bishop, D. McLeod, A. Reardon, Effects of hyaluronan lyase, hyaluronidase, and chondroitin ABC lyase on mammalian vitreous gel, Investig Ophthalmol Vis Sci 40 (10) (1999) 2173–2178.

120. Y. Huang, V. Enzmann, S.T. Ildstad, Stem cell-based therapeutic applications in retinal degenerative diseases, Stem Cell Rev Reports 7 (2) (2011) 434–445.
121. G. Rajashekhar, Mesenchymal stem cells: new players in retinopathy therapy, Front Endocrinol 5 (2014) 59.
122. J.H. Ting, D.K. Martin, Basic and clinical aspects of gene therapy for retinopathy induced by diabetes, Curr Gene Ther 6 (2) (2006) 193–214.
123. H.R. McDonald, H. Schatz, Visual loss following panretinal photocoagulation for proliferative diabetic retinopathy, Ophthalmology 92 (3) (1985) 388–393.
124. B.M. Doft, et al., Retinal detachment in the endophthalmitis vitrectomy study, Arch Ophthalmol 118 (12) (2000) 1661–1665.
125. K.G. Falavarjani, Q. Nguyen, Adverse events and complications associated with intravitreal injection of anti-VEGF agents: a review of literature, Eye 27 (7) (2013) 787–794.
126. W.Y. Ng, et al., Incidence of myocardial infarction, stroke, and death in patients with age-related macular degeneration treated with intravitreal anti–vascular endothelial growth factor therapy, Am J Ophthalmol 159 (3) (2015) 557–564. e1.
127. A. Loewenstein, Breaking the Burden: a New Way to Deliver Anti-VEGF: an implantable drug reservoir looks to shake up today's successful but untenable protocols, Rev Optom 155 (2) (2018) 60–64.
128. S. Wadhwa, et al., Nanocarriers in ocular drug delivery: an update review, Curr Pharmaceut Des 15 (23) (2009) 2724–2750.
129. R. Gaudana, et al., Ocular drug delivery, AAPS J 12 (3) (2010) 348–360.
130. Y. Weng, et al., Nanotechnology-based strategies for treatment of ocular disease, Acta Pharm Sin B 7 (3) (2017) 281–291.
131. H.-Y. Zhou, et al., Nanoparticles in the ocular drug delivery, Int J Ophthalmol 6 (3) (2013) 390.
132. R. Pignatello, et al., Flurbiprofen-loaded acrylate polymer nanosuspensions for ophthalmic application, Biomaterials 23 (15) (2002) 3247–3255.
133. E. Sánchez-López, et al., Lipid nanoparticles (SLN, NLC): overcoming the anatomical and physiological barriers of the eye–Part I–Barriers and determining factors in ocular delivery, Eur J Pharm Biopharm 110 (2017) 70–75.
134. Y. Wang, et al., Recent advance of nanoparticle-based topical drug delivery to the posterior segment of the eye, Expet Opin Drug Deliv 15 (7) (2018) 687–701.
135. B. Yavuz, et al., In vitro/in vivo evaluation of dexamethasone—PAMAM dendrimer complexes for retinal drug delivery, J Pharmaceut Sci 104 (11) (2015) 3814–3823.
136. A. Khare, et al., Mucoadhesive polymers for enhancing retention in ocular drug delivery: a critical review, Rev Adhesion Adhesives 2 (4) (2014) 467–502.
137. P. Singh, et al., Gold nanoparticles in diagnostics and therapeutics for human cancer, Int J Mol Sci 19 (7) (2018) 1979.
138. A. Khan, et al., Gold nanoparticles: synthesis and applications in drug delivery, Trop J Pharmaceut Res 13 (7) (2014) 1169–1177.
139. D. Ventura-Espinosa, et al., Ligand effects in the stabilization of gold nanoparticles anchored on the surface of graphene: implications in catalysis, J Catal 394 (2021) 113–120.
140. Y.-C. Yeh, B. Creran, V.M. Rotello, Gold nanoparticles: preparation, properties, and applications in bionanotechnology, Nanoscale 4 (6) (2012) 1871–1880.
141. A. Sharma, et al., Polyethylenimine-conjugated gold nanoparticles: gene transfer potential and low toxicity in the cornea, Nanomed Nanotechnol Biol Med 7 (4) (2011) 505–513.
142. P. Mukherjee, et al., Antiangiogenic properties of gold nanoparticles, Clin Cancer Res 11 (9) (2005) 3530–3534.
143. J.H. Kim, et al., The inhibition of retinal neovascularization by gold nanoparticles via suppression of VEGFR-2 activation, Biomaterials 32 (7) (2011) 1865–1871.
144. D.H. Jo, et al., Nanoparticle-protein complexes mimicking corona formation in ocular environment, Biomaterials 109 (2016) 23–31.
145. D. Athanasiou, et al., The cell stress machinery and retinal degeneration, FEBS Lett 587 (13) (2013) 2008–2017.
146. A.J. Payne, et al., Antioxidant drug therapy approaches for neuroprotection in chronic diseases of the retina, Int J Mol Sci 15 (2) (2014) 1865–1886.
147. J.L. Wilkinson-Berka, et al., Reactive oxygen species, Nox and angiotensin II in angiogenesis: implications for retinopathy, Clin Sci 124 (10) (2013) 597–615.

148. S.G. Jarrett, M.E. Boulton, Consequences of oxidative stress in age-related macular degeneration, Mol Aspect Med 33 (4) (2012) 399–417.
149. C. Xu, X. Qu, Cerium oxide nanoparticle: a remarkably versatile rare earth nanomaterial for biological applications, NPG Asia Mater 6 (3) (2014) e90.
150. R. Maccarone, et al., Ophthalmic applications of cerium oxide nanoparticles, J Ocul Pharmacol Therapeut 36 (6) (2020) 376–383.
151. N. Izu, et al., Development of resistive oxygen sensors based on cerium oxide thick film, J Electroceram 13 (1–3) (2004) 703–706.
152. S.M. Hirst, et al., Anti-inflammatory properties of cerium oxide nanoparticles, Small 5 (24) (2009) 2848–2856.
153. A. Estevez, et al., Neuroprotective mechanisms of cerium oxide nanoparticles in a mouse hippocampal brain slice model of ischemia, Free Radic Biol Med 51 (6) (2011) 1155–1163.
154. J. Niu, et al., Cardioprotective effects of cerium oxide nanoparticles in a transgenic murine model of cardiomyopathy, Cardiovasc Res 73 (3) (2007) 549–559.
155. R.W. Tarnuzzer, et al., Vacancy engineered ceria nanostructures for protection from radiation-induced cellular damage, Nano Lett 5 (12) (2005) 2573–2577.
156. S. Giri, et al., Nanoceria: a rare-earth nanoparticle as a novel anti-angiogenic therapeutic agent in ovarian cancer, PLoS One 8 (1) (2013) e54578.
157. L. Alili, et al., Combined cytotoxic and anti-invasive properties of redox-active nanoparticles in tumor–stroma interactions, Biomaterials 32 (11) (2011) 2918–2929.
158. M. Horie, et al., Cellular responses induced by cerium oxide nanoparticles: induction of intracellular calcium level and oxidative stress on culture cells, J Biochem 150 (4) (2011) 461–471.
159. M. Kumari, et al., Toxicity study of cerium oxide nanoparticles in human neuroblastoma cells, Int J Toxicol 33 (2) (2014) 86–97.
160. A. Karakoti, et al., Nanoceria as antioxidant: synthesis and biomedical applications, JOM (J Occup Med) 60 (3) (2008) 33–37.
161. S.V. Kyosseva, J.F. McGinnis, Cerium oxide nanoparticles as promising ophthalmic therapeutics for the treatment of retinal diseases, World J Ophthalmol 5 (1) (2015) 23–30.
162. X. Zhou, et al., Nanoceria inhibit the development and promote the regression of pathologic retinal neovascularization in the Vldlr knockout mouse, PLoS One 6 (2) (2011) e16733.
163. M. Giannaccini, et al., Magnetic nanoparticles: a strategy to target the choroidal layer in the posterior segment of the eye, Sci Rep 7 (2017) 43092.
164. C. Sun, J.S. Lee, M. Zhang, Magnetic nanoparticles in MR imaging and drug delivery, Adv Drug Deliv Rev 60 (11) (2008) 1252–1265.
165. A.K. Gupta, M. Gupta, Synthesis and surface engineering of iron oxide nanoparticles for biomedical applications, Biomaterials 26 (18) (2005) 3995–4021.
166. S. Bucak, B. Yavuztürk, A.D. Sezer, Magnetic nanoparticles: synthesis, surface modifications and application in drug delivery, Recent Adv Novel Drug Carrier Systems 2 (2012) 165–200.
167. H.B. Raju, et al., Evaluation of magnetic micro-and nanoparticle toxicity to ocular tissues, PLoS One 6 (5) (2011) e17452.
168. A. Gagliardi, et al., Biodegradable polymeric nanoparticles for drug delivery to solid tumors, Front Pharmacol 12 (2021) 17.
169. M.J. Alonso, A. Sánchez, The potential of chitosan in ocular drug delivery, J Pharm Pharmacol 55 (11) (2003) 1451–1463.
170. M.A. Attia Shafie, H. Mohammed Fayek, Formulation and evaluation of betamethasone sodium phosphate loaded nanoparticles for ophthalmic delivery, J Clin Exp Ophthalmol 4 (273) (2013) 2.
171. R. Hirlekar, H. Garse, V. Kadam, Solid lipid nanoparticles and nanostructured lipid carriers: a review, Curr Drug Ther 6 (4) (2011) 240–250.
172. N. Naseri, H. Valizadeh, P. Zakeri-Milani, Solid lipid nanoparticles and nanostructured lipid carriers: structure, preparation and application, Adv Pharmaceut Bull 5 (3) (2015) 305.
173. M. Haider, et al., Nanostructured lipid carriers for delivery of chemotherapeutics: a review, Pharmaceutics 12 (3) (2020) 288.
174. A. Seyfoddin, R. Al-Kassas, Development of solid lipid nanoparticles and nanostructured lipid carriers for improving ocular delivery of acyclovir, Drug Dev Ind Pharm 39 (4) (2013) 508–519.

175. L. Gan, et al., Recent advances in topical ophthalmic drug delivery with lipid-based nanocarriers, Drug Discov Today 18 (5–6) (2013) 290–297.
176. Q. Luo, et al., Nanostructured lipid carrier (NLC) coated with Chitosan Oligosaccharides and its potential use in ocular drug delivery system, Int J Pharm 403 (1–2) (2011) 185–191.
177. R. Liu, et al., Nanostructured lipid carriers as novel ophthalmic delivery system for mangiferin: improving in vivo ocular bioavailability, J Pharmaceut Sci 101 (10) (2012) 3833–3844.
178. D.C. Beebe, N.M. Holekamp, Y.-B. Shui, Oxidative damage and the prevention of age-related cataracts, Ophthalmic Res 44 (3) (2010) 155–165.
179. E. Joubert, et al., Effect of species variation and processing on phenolic composition and in vitro antioxidant activity of aqueous extracts of Cyclopia spp.(honeybush tea), J Agric Food Chem 56 (3) (2008) 954–963.
180. A. Akbarzadeh, et al., Liposome: classification, preparation, and applications, Nanoscale Res Lett 8 (1) (2013) 102.
181. G. Bozzuto, A. Molinari, Liposomes as nanomedical devices, Int J Nanomed 10 (2015) 975.
182. W. Park, K. Na, Advances in the synthesis and application of nanoparticles for drug delivery, Wiley Interdisc Rev: Nanomed Nanobiotechnol 7 (4) (2015) 494–508.
183. S. Moghassemi, A. Hadjizadeh, Nano-niosomes as nanoscale drug delivery systems: an illustrated review, J Contr Release 185 (2014) 22–36.
184. R. Muzzalupo, L. Tavano, Niosomal drug delivery for transdermal targeting: recent advances, Res Rep Transdermal Drug Deliv 4 (2015) 23.
185. M. Saettone, et al., Non-ionic surfactant vesicles as ophthalmic carriers for cyclopentolate. A preliminary evaluation, STP Pharma Sci 6 (1) (1996) 94–98.
186. S. Vyas, et al., Discoidal niosome based controlled ocular delivery of timolol maleate, Pharmazie 53 (7) (1998) 466–469.
187. G. Abdelbary, N. El-gendy, Niosome-encapsulated gentamicin for ophthalmic controlled delivery, AAPS PharmSciTech 9 (3) (2008) 740–747.
188. K. Cholkar, et al., Novel nanomicellar formulation approaches for anterior and posterior segment ocular drug delivery, Recent Pat Nanomed 2 (2) (2012) 82–95.
189. J.B. Aswathanarayan, R.R. Vittal, Nanoemulsions and their potential applications in food industry, Front Sustain Food Syst 3 (2019) 95.
190. H.O. Ammar, et al., Nanoemulsion as a potential ophthalmic delivery system for dorzolamide hydrochloride, AAPS PharmSciTech 10 (3) (2009) 808–819.
191. M. Jaiswal, R. Dudhe, P. Sharma, Nanoemulsion: an advanced mode of drug delivery system, 3 Biotech 5 (2) (2015) 123–127.
192. A.M. Al-Halafi, Nanocarriers of nanotechnology in retinal diseases, Saudi J Ophthalmol 28 (4) (2014) 304–309.
193. S. Makwana, V. Patel, S. Parmar, Development and characterization of in-situ gel for ophthalmic formulation containing ciprofloxacin hydrochloride, Res Pharma Sci 6 (2016) 1–6.
194. M. Suhail, et al., Nanogels as drug-delivery systems: a comprehensive overview, Ther Deliv 10 (11) (2019) 697–717.
195. J. Zhang, et al., Charged nanogels efficiently overcome ocular biological barriers, Investig Ophthalmol Vis Sci 52 (14) (2011), pp. 429–429.
196. M. Jamard, T. Hoare, H. Sheardown, Nanogels of methylcellulose hydrophobized with N-tert-butylacrylamide for ocular drug delivery, Drug Delivery Translat Res 6 (6) (2016) 648–659.
197. F. Hapiot, S. Tilloy, E. Monflier, Cyclodextrins as supramolecular hosts for organometallic complexes, Chem Rev 106 (3) (2006) 767–781.
198. A.M. Ribeiro, A. Figueiras, F. Veiga, Improvements in topical ocular drug delivery systems: hydrogels and contact lenses, J Pharm Pharmaceut Sci 18 (5) (2015) 683–695.
199. O.A.E.-A. Soliman, et al., Potential use of cyclodextrin complexes for enhanced stability, anti-inflammatory efficacy, and ocular bioavailability of loteprednol etabonate, AAPS PharmSciTech 18 (4) (2017) 1228–1241.
200. G. Palladino, et al., Visual evoked potentials of Niemann-Pick type C1 mice reveal an impairment of the visual pathway that is rescued by 2-hydroxypropyl-ß-cyclodextrin, Orphanet J Rare Dis 10 (1) (2015) 133.
201. B.K. Nanjwade, et al., Dendrimers: emerging polymers for drug-delivery systems, Eur J Pharmaceut Sci 38 (3) (2009) 185–196.
202. E. Abbasi, et al., Dendrimers: synthesis, applications, and properties, Nanoscale Res Lett 9 (1) (2014) 1–10.

203. R.S. Pawar, P.G. Upadhaya, V.B. Patravale, Quantum dots: novel realm in biomedical and pharmaceutical industry, in: Handbook of nanomaterials for industrial applications, Elsevier, 2018, pp. 621–637.
204. T.M. Samir, et al., Quantum dots: heralding a brighter future for clinical diagnostics, Nanomedicine 7 (11) (2012) 1755–1769.
205. D. Vasudevan, et al., Core–shell quantum dots: properties and applications, J Alloys Compd 636 (2015) 395–404.
206. J.L. Olson, et al., Intravitreal silicon-based quantum dots as neuroprotective factors in a model of retinal photoreceptor degeneration, Investig Ophthalmol Vis Sci 53 (9) (2012) 5713–5721.
207. R. Amato, et al., Nanoparticle-mediated delivery of neuroprotective substances for the treatment of diabetic retinopathy, Curr Neuropharmacol 16 (7) (2018) 993–1003.
208. J.F. Fangueiro, et al., Current nanotechnology approaches for the treatment and management of diabetic retinopathy, Eur J Pharm Biopharm 95 (2015) 307–322.
209. R. Amato, et al., Association of the somatostatin analog octreotide with magnetic nanoparticles for intraocular delivery: a possible approach for the treatment of diabetic retinopathy, Front Bioeng Biotechnol 8 (2020) 144.
210. R. Amato, et al., VEGF as a survival factor in ex vivo models of early diabetic retinopathy, Investig Ophthalmol Vis Sci 57 (7) (2016) 3066–3076.
211. S.M. Conley, M.I. Naash, Nanoparticles for retinal gene therapy, Prog Retin Eye Res 29 (5) (2010) 376–397.
212. X. Cai, et al., Gene delivery to mitotic and postmitotic photoreceptors via compacted DNA nanoparticles results in improved phenotype in a mouse model of retinitis pigmentosa, Faseb J 24 (4) (2010) 1178–1191.
213. X.-Q. Ding, et al., Ocular delivery of compacted DNA-nanoparticles does not elicit toxicity in the mouse retina, PLoS One 4 (10) (2009) e7410.
214. M. Campbell, P. Humphries, Size-selective and in vitro assessment of inner blood retina barrier permeability, in: Permeability barrier, Springer, 2011, pp. 355–367.
215. M. Campbell, et al., An experimental platform for systemic drug delivery to the retina, Proc Natl Acad Sci USA 106 (42) (2009) 17817–17822.
216. S. Singh, et al., Intravenous transferrin, RGD peptide and dual-targeted nanoparticles enhance anti-VEGF intraceptor gene delivery to laser-induced CNV, Gene Ther 16 (5) (2009) 645.
217. H.F. Edelhauser, et al., Ophthalmic drug delivery systems for the treatment of retinal diseases: basic research to clinical applications, Investig Ophthalmol Vis Sci 51 (11) (2010) 5403–5420.
218. J.-L. Bourges, et al., Ocular drug delivery targeting the retina and retinal pigment epithelium using polylactide nanoparticles, Investig Ophthalmol Vis Sci 44 (8) (2003) 3562–3569.
219. J. Gaudreault, et al., Preclinical pharmacokinetics of Ranibizumab (rhuFabV2) after a single intravitreal administration, Investig Ophthalmol Vis Sci 46 (2) (2005) 726–733.
220. S. Gupta, et al., Intravitreal pharmacokinetics of plain and liposome-entrapped fluconazole in rabbit eyes, J Ocul Pharmacol Therapeut 16 (6) (2000) 511–518.
221. E.M. Del Amo, et al., Pharmacokinetic aspects of retinal drug delivery, Prog Retin Eye Res 57 (2017) 134–185.
222. R. Iezzi, et al., Dendrimer-based targeted intravitreal therapy for sustained attenuation of neuroinflammation in retinal degeneration, Biomaterials 33 (3) (2012) 979–988.
223. D.H. Jo, J.H. Kim, J.H. Kim, How to overcome retinal neuropathy: the fight against angiogenesisrelated blindness, Arch Pharm Res (Seoul) 33 (10) (2010) 1557–1565.
224. K.M. Farjo, J.-x. Ma, The potential of nanomedicine therapies to treat neovascular disease in the retina, J Angiogenesis Res 2 (1) (2010) 21.
225. Y. Diebold, M. Calonge, Applications of nanoparticles in ophthalmology, Prog Retin Eye Res 29 (6) (2010) 596–609.
226. B.A. Saeed, et al., Antiangiogenic properties of nanoparticles: a systematic review, Int J Nanomed 14 (2019) 5135.
227. R. Bhattacharya, et al., Gold nanoparticles inhibit VEGF165-induced proliferation of HUVEC cells, Nano Lett 4 (12) (2004) 2479–2481.
228. B. Karthikeyan, et al., Gold nanoparticles downregulate VEGF-and IL-1β-induced cell proliferation through Src kinase in retinal pigment epithelial cells, Exp Eye Res 91 (5) (2010) 769–778.
229. B.P. Eliceiri, et al., Selective requirement for Src kinases during VEGF-induced angiogenesis and vascular permeability, Mol Cell 4 (6) (1999) 915–924.

230. D.H. Jo, et al., Antiangiogenic effect of silicate nanoparticle on retinal neovascularization induced by vascular endothelial growth factor, Nanomed Nanotechnol Biol Med 8 (5) (2012) 784–791.
231. K. Kalishwaralal, et al., Silver nanoparticles inhibit VEGF induced cell proliferation and migration in bovine retinal endothelial cells, Colloids Surf B Biointerfaces 73 (1) (2009) 51–57.
232. D.H. Jo, et al., Anti-angiogenic effect of bare titanium dioxide nanoparticles on pathologic neovascularization without unbearable toxicity, Nanomed Nanotechnol Biol Med 10 (5) (2014) e1109–e1117.
233. R. Hennig, A. Goepferich, Nanoparticles for the treatment of ocular neovascularizations, Eur J Pharm Biopharm 95 (2015) 294–306.
234. J. Chen, et al., Rare earth nanoparticles prevent retinal degeneration induced by intracellular peroxides, Nat Nanotechnol 1 (2) (2006) 142.
235. D.H. Jo, T.G. Lee, J.H. Kim, Nanotechnology and nanotoxicology in retinopathy, Int J Mol Sci 12 (11) (2011) 8288–8301.
236. I.M. Verma, M.D. Weitzman, Gene therapy: twenty-first century medicine, Annu Rev Biochem 74 (2005) 711–738.
237. J. Bainbridge, M. Tan, R. Ali, Gene therapy progress and prospects: the eye, Gene Ther 13 (16) (2006) 1191.
238. J. Bennett, Immune response following intraocular delivery of recombinant viral vectors, Gene Ther 10 (11) (2003) 977.
239. J. Adijanto, M.I. Naash, Nanoparticle-based technologies for retinal gene therapy, Eur J Pharm Biopharm 95 (2015) 353–367.
240. F.-L. Lin, et al., Gene therapy intervention in neovascular eye disease: a recent update, Molecular Therapy, 2020.
241. R. Marano, et al., Dendrimer delivery of an anti-VEGF oligonucleotide into the eye: a long-term study into inhibition of laser-induced CNV, distribution, uptake and toxicity, Gene Ther 12 (21) (2005) 1544.
242. H.-a. Liu, et al., A lipid nanoparticle system improves siRNA efficacy in RPE cells and a laser-induced murine CNV model, Investig Ophthalmol Vis Sci 52 (7) (2011) 4789–4794.
243. J. Panyam, V. Labhasetwar, Biodegradable nanoparticles for drug and gene delivery to cells and tissue, Adv Drug Deliv Rev 55 (3) (2003) 329–347.
244. M.L. Hedley, J. Curley, R. Urban, Microspheres containing plasmid-encoded antigens elicit cytotoxic T-cell responses, Nat Med 4 (3) (1998) 365–368.
245. C. Zhang, et al., Inhibitory efficacy of hypoxia-inducible factor 1α short hairpin RNA plasmid DNA-loaded poly (D, L-lactide-co-glycolide) nanoparticles on choroidal neovascularization in a laser-induced rat model, Gene Ther 17 (3) (2010) 338.
246. R.D. Bachu, et al., Ocular drug delivery barriers—role of nanocarriers in the treatment of anterior segment ocular diseases, Pharmaceutics 10 (1) (2018) 28.
247. S.K. Sahoo, F. Dilnawaz, S. Krishnakumar, Nanotechnology in ocular drug delivery, Drug Discov Today 13 (3–4) (2008) 144–151.
248. S.K. Sahoo, R. Misra, S. Parveen, Nanoparticles: a boon to drug delivery, therapeutics, diagnostics and imaging, in: Nanomedicine in cancer, Pan Stanford, 2017, pp. 73–124.
249. J. Xu, et al., Inhibitory efficacy of intravitreal dexamethasone acetate-loaded PLGA nanoparticles on choroidal neovascularization in a laser-induced rat model, J Ocul Pharmacol Therapeut 23 (6) (2007) 527–540.
250. R.S. Kadam, et al., RETRACTED: influence of choroidal neovascularization and biodegradable polymeric particle size on transscleral sustained delivery of triamcinolone acetonide, Elsevier, 2012.
251. U.B. Kompella, N. Bandi, S.P. Ayalasomayajula, Subconjunctival nano-and microparticles sustain retinal delivery of budesonide, a corticosteroid capable of inhibiting VEGF expression, Investig Ophthalmol Vis Sci 44 (3) (2003) 1192–1201.
252. E.J. Oh, et al., Anti-Flt1 peptide–hyaluronate conjugate for the treatment of retinal neovascularization and diabetic retinopathy, Biomaterials 32 (11) (2011) 3115–3123.
253. B.B. Aggarwal, S. Shishodia, Molecular targets of dietary agents for prevention and therapy of cancer, Biochem Pharmacol 71 (10) (2006) 1397–1421.
254. K. Lee, et al., Anthracycline chemotherapy inhibits HIF-1 transcriptional activity and tumor-induced mobilization of circulating angiogenic cells, Proc Natl Acad Sci USA 106 (7) (2009) 2353–2358.
255. T. Iwase, et al., Sustained delivery of a HIF-1 antagonist for ocular neovascularization, J Contr Release 172 (3) (2013) 625–633.
256. N. Tian, Visual experience and maturation of retinal synaptic pathways, Vis Res 44 (28) (2004) 3307–3316.

257. U.O. Häfeli, et al., Cell uptake and in vitro toxicity of magnetic nanoparticles suitable for drug delivery, Mol Pharm 6 (5) (2009) 1417–1428.
258. T.W. Prow, et al., Ocular nanoparticle toxicity and transfection of the retina and retinal pigment epithelium, Nanomed Nanotechnol Biol Med 4 (4) (2008) 340.
259. S.J. Bakri, et al., Absence of histologic retinal toxicity of intravitreal nanogold in a rabbit model, Retina 28 (1) (2008) 147–149.
260. S. Zhu, et al., Safety assessment of nanomaterials to eyes: an important but neglected issue, Advanced Science, 2019, p. 1802289.
261. A. Sukhanova, et al., Dependence of nanoparticle toxicity on their physical and chemical properties, Nanoscale Res Lett 13 (1) (2018) 44.
262. C.M. Goodman, et al., Toxicity of gold nanoparticles functionalized with cationic and anionic side chains, Bioconjugate Chem 15 (4) (2004) 897–900.
263. P.R. Lockman, et al., Nanoparticle surface charges alter blood–brain barrier integrity and permeability, J Drug Target 12 (9–10) (2004) 635–641.
264. A. Gramowski, et al., Nanoparticles induce changes of the electrical activity of neuronal networks on microelectrode array neurochips, Environ Health Perspect 118 (10) (2010) 1363–1369.
265. X. Deng, et al., Nanosized zinc oxide particles induce neural stem cell apoptosis, Nanotechnology 20 (11) (2009) 115101.
266. S. Kannan, et al., Dendrimer-based postnatal therapy for neuroinflammation and cerebral palsy in a rabbit model, Sci Transl Med 4 (130) (2012), p. 130ra46–130ra46.
267. Q. Xu, S.P. Kambhampati, R.M. Kannan, Nanotechnology approaches for ocular drug delivery, Middle East Afr J Ophthalmol 20 (1) (2013) 26.

CHAPTER

17

Stimuli-responsive self-assembled nanocarriers based on amphiphilic block copolymers for cancer therapy

Mónica Cristina García[1,2]

[1]Universidad Nacional de Córdoba, Facultad de Ciencias Químicas, Departamento de Ciencias Farmacéuticas, Ciudad Universitaria, Haya de la Torre and Medina Allende, Córdoba, Argentina; [2]Consejo Nacional de Investigaciones Científicas y Técnicas, CONICET, Unidad de Investigación y Desarrollo en Tecnología Farmacéutica, UNITEFA, Córdoba, Argentina

1. Introduction

Cancer is one of the most common life-threatening illnesses and is currently among one of the leading causes of death worldwide. Different treatment protocols have been developed, including surgery, radiotherapy, immunotherapy, and chemotherapy.[1] Conventional chemotherapy is the most commonly used approach in cancer treatment and it mainly relies on small molecule anticancer drugs that interact with DNA molecules, modify them and induce cell death in cancer tissues. However, anticancer drugs used in chemotherapy have many disadvantages, such as low solubility, poor pharmacokinetics, including rapid degradation and undesirable biodistribution, low specificity, inefficient cellular uptake, limited targeting, produce severe side effects, and are toxics.[2,3] These limitations have led to the urgency to develop novel strategies to overcome these shortcomings.

In the last few decades, nanomedicine, emerging technology of the 21st century, has been exploiting nanotechnology for several biomedical purposes, mainly disease treatment, diagnosis, molecular imaging, and theragnosis, as well as regenerative medicine and tissue engineering. From the beginning, nanomedicine has been frequently associated with the use of nanoparticles in oncology and it has assumed an important role in cancer therapy based on diverse tailor-made drug delivery systems.[2,4,5]

Among the different types of nanomaterials that have been developed for cancer treatment and diagnosis, polymer-based nanostructures capable of targeting transport and follow-up

Applications of Multifunctional Nanomaterials
https://doi.org/10.1016/B978-0-12-820557-0.00016-3

site-specific controlled drug release have gained great attention.[3,6–11] Polymeric nanomaterials, especially those based on amphiphilic block copolymers (ABCP) have been widely used in nanomedicine applications as contrast/imaging agent carriers, drug delivery systems, and integrated theragnostic platforms owing to their improved biocompatibility, water dispersibility, tunable compositions, extended bloodstream circulation duration, and facile functionalization.[3,7,10,11] Polymer self-assemblies are formed by the association of ABCP that produces different nanostructural arrangements, including micelles, vesicles (also called polymersomes), liquid crystals, and other complex topological structures (Fig. 17.1).[3,10,11]

Self-assembled nanocarriers have been widely used to encapsulate or entrap therapeutic and/or imaging agents due to the enhanced solubility, increased drug efficacy, and reduced drug toxicity and degradation compared with small molecule drugs alone.[3] In particular, stimuli-responsive nanocarriers that response to the local environment of tumor tissue, on the basis of internal or external stimuli of the tumor, has been developed for cancer targeted drug delivery applications and have gained popularity in recent times (Fig. 17.2).[7,8,12]

ABCP-based self-assemblies can accumulate in the tumor microenvironment for enhanced permeability and retention effect (EPR, passive target) or by the union to any receptor overexpressed in tumor cells (active target) (Fig. 17.3). In comparison to the EPR effect in that takes place in passive targeting, active targeting has offered a new direction of modern nanocarrier design, providing extra advantages for targeted cancer therapy.[3] Nanocarriers for

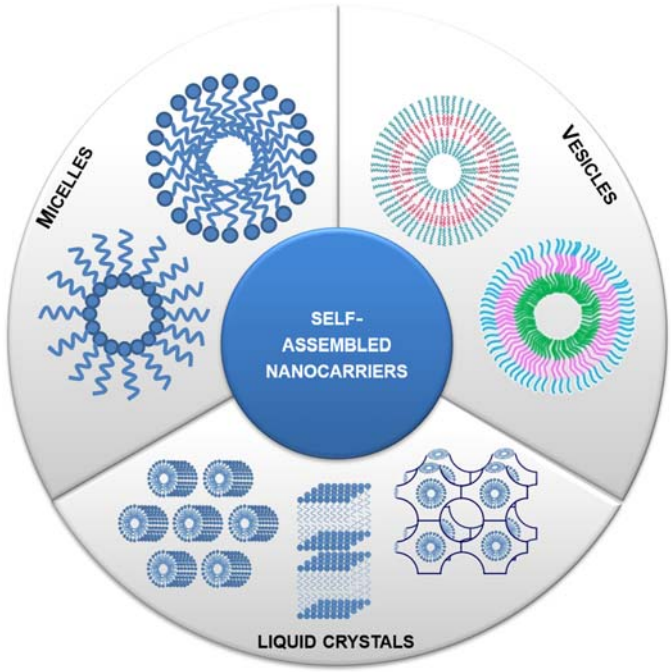

FIGURE 17.1 Schematic structures of some amphiphilic block copolymers-based self-assembled nanocarriers, including typical and reverse polymeric micelles, vesicles, also known as polymersomes based on diblock and triblock copolymers, and hexagonal, lamellar, and cubic liquid crystal mesophases.

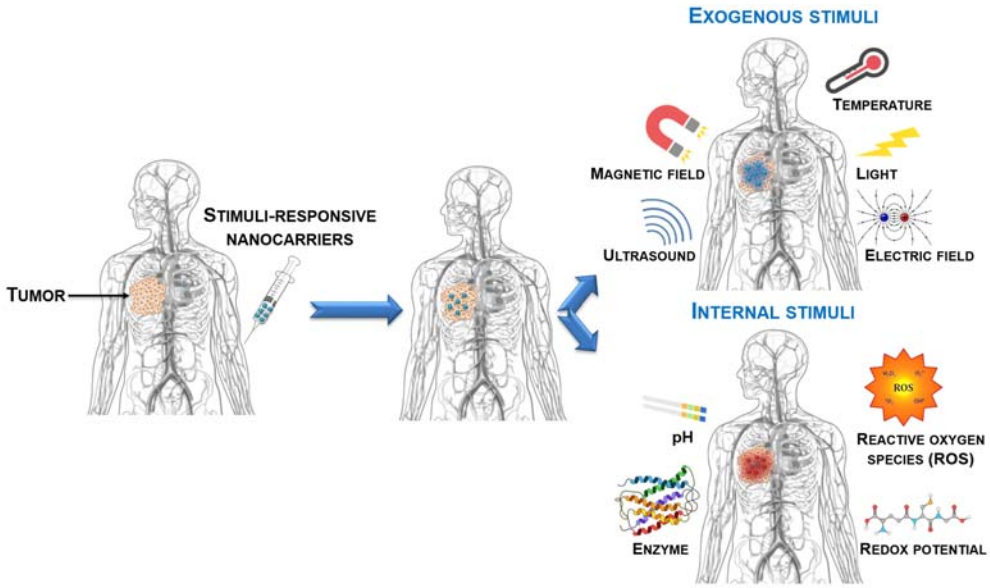

FIGURE 17.2 Schematic representation of stimuli responsiveness utilized in cancer-targeted drug delivery.

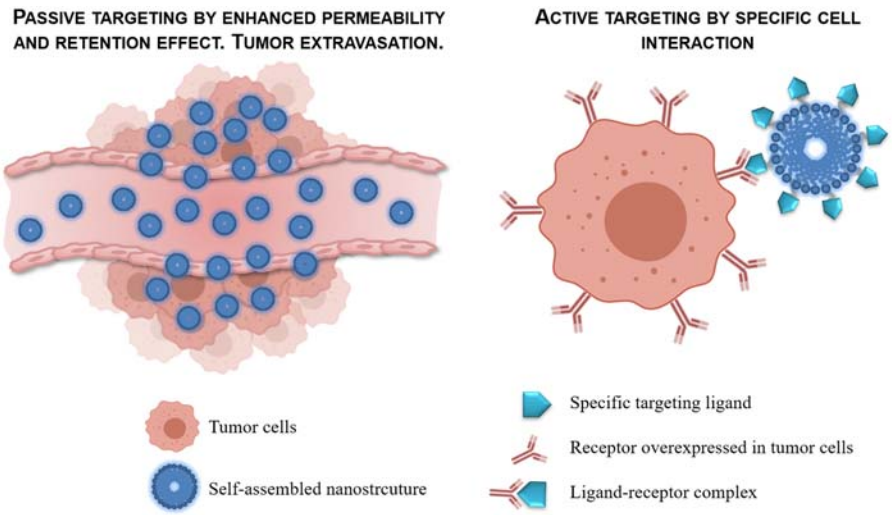

FIGURE 17.3 Schematic representation of passive and active targeting in the tumor microenvironment.

active targeting need to be modified with affinity ligands, namely functional organic molecules, carbohydrates, peptides, antibodies, and aptamers, which can selectively recognize complementary receptors, through specific ligand-receptor interactions, thus promoting intracellular uptake.[13]

In this chapter, the main features regarding the most outstanding contributions in the arena of stimuli-responsive self-assembled nanostructures, mainly focusing on polymersomes, since they have been the subject of several recent researches.[14] The recent advances in their biomedical applications in the treatment of cancer will be highlighted.

2. Amphiphilic block copolymers (ABCP) and self assembled nanocarriers: how and why?

Self-assembly processes are generally low-cost and large-scale techniques, which can be suitable for different purposes, including the development of nanocarriers for biomedical application.[11,15] Simple but effective bottom-up approaches are the base of self-assembly processes. This process starts from the monomers for arriving at the structures nanocarrier, by tailoring experimental parameters that readily and selectively lead to produce different types of nanostructures with novel morphologies and high performance to be applied for therapeutic purposes.[11,16]

Molecular self-assembly raises the spontaneous formation of ordered and well-organized structures. The self-assembly process arises under kinetic and thermodynamic conditions that allow local and specific molecular interactions, including electrostatic or hydrophobic interactions, π-π interactions, hydrogen bonding, and van der Waals forces, which allow keeping the organized molecules at a stable state, thus achieving the minimal energy in the nanostructure.[10,17,18]

As-mentioned, polymer self-assemblies are formed by the association of ABCP. These polymers can be obtained by well-known techniques of copolymerization employing two or three types of comonomers that usually form linear macromolecules in a block distribution of each monomer. The hydrophobic and hydrophilic functional groups present in the comonomer molecules confer the amphiphilic behavior to the obtained ABCP.[11]

Linear di-block (AB), triblock (ABA, BAB, or ABC), multi-block, or star-block copolymers can be prepared,[11,19] where A, B, and C denote distinct blocks.[11,20] Then, ABCP can be considered as a kind of polymer alloy. In general, ABCP is obtained by a combination of hydrophobic biocompatible blocks that usually consist of polyester and poly(amino acids) covalently bonded to a biocompatible hydrophilic block.[21] Poly(ethylene glycol) (PEG) is the most commonly used hydrophilic block because of its adequate properties, which include minimal immunogenicity, high water-solubility, high hydration, and flexibility.[11] ABCP composed by PEG and hydrophobic linear aliphatic polyesters, such as poly(*L*-lactide) (PLA), poly(lactide-*co*-glycolide) (PLGA) and poly(ε-caprolactone) (PCL) has been approved by the Food and Drug Administration (FDA, USA) for therapeutic applications.[22]

As-stated above, ABCP has the ability to assemble into different supramolecular architectures in an aqueous solution aimed at minimizing energetically unfavorable hydrophobe–water interactions. In self-assembly processes novel supramolecular morphologies are obtained, in which molecules assemble themselves without the presence of outside interactions. There are critical geometric and flexibility requirements for the construction of different morphologies, which depend on the inherent molecular curvature and how it influences the packing of the copolymer chains that form the ABCP. Specific self-assembled nanocarriers can be

targeted according to a dimensionless "packing parameter", $p = \frac{v}{a_o \cdot l_c}$, where v is the volume of the hydrophobic chains, a_o is the optimal area of the polar head group, and l_c is the length of the hydrophobic chain(s) of the amphiphilic molecule. Therefore, P value of a given molecule allows the prediction of most likely self-assembled morphology. As a general rule, spherical micelles are most likely when $p \leq \frac{1}{3}$, cylindrical micelles when $\frac{1}{3} \leq p \leq \frac{1}{2}$, and polymersomes $\frac{1}{2} \leq p \leq 1$[11,23] (Fig. 17.4).

Particularly, for self-assembled nanocarriers based on ABCP, not only the p is an important parameter to be considered but also it is convenient to characterize the preferred aggregate morphology by the hydrophilic volume fraction (f), which is defined as the relation between the hydrophilic portion of the polymeric chain and the total molecular mass. In this way, spherical micelles are favored when $f \geq 0.60$, cylindrical micelles when $0.47 \leq f \leq 0.60$, and polymersomes when $0.22 \leq f \leq 0.47$ (Fig. 17.4).[24] Based on experimental evidence, for ABPC containing PEG as a hydrophilic chain, spherical micelles are most likely with a PEG volume fraction $f > 50\%$, cylindrical micelles are favored at $40\% < f < 50\%$, and polymersomes are preferentially formed at $25 < f < 40\%$.[11,25]

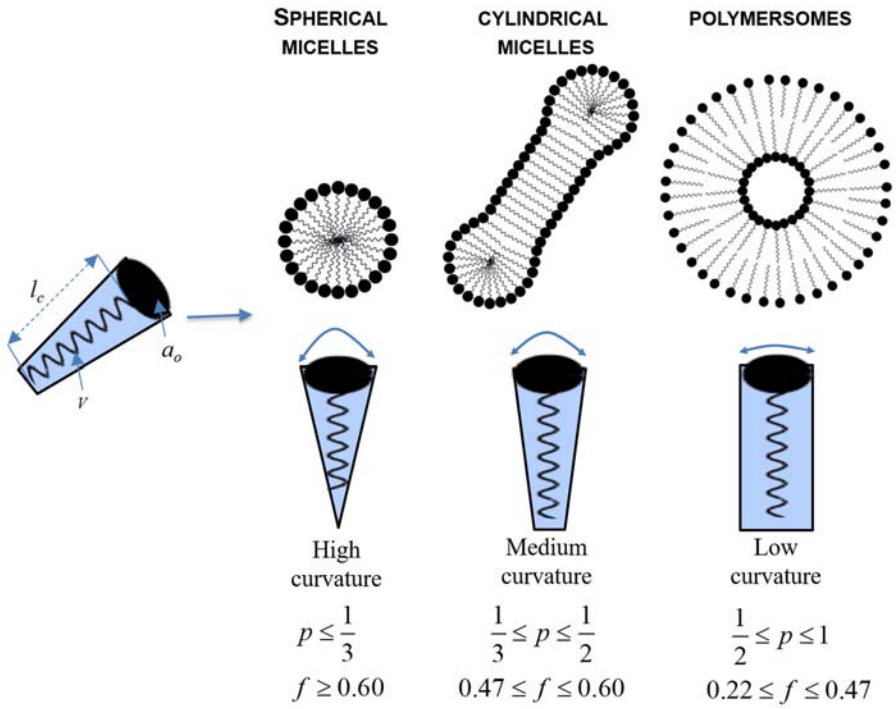

FIGURE 17.4 Interrelations between the self-assembled nanostructures formed by amphiphilic copolymers in aqueous solution and their hydrophilic volume fraction, *f, and* packing parameter, *p*. The type of structure formed is due to the inherent curvature of the molecule, which can be estimated through the calculation of its dimensionless *p*. *Adapted with permission from García MC, Quiroz F. Nanostructured polymers. In Narayan R, editor.* Nanobiomaterials: Nanostructured materials for biomedical applications. *Cambridge, UK: Elsevier: 2018; pp 339–356. Copyright 2018 Elsevier.*

Conventional micelles based on hydrophilic–hydrophobic AB diblock copolymers have been extensively reported. They spontaneously form in aqueous media when the polymer concentration is above the critical micelle concentration.[26] As shown in Figs. 17.1 and 17.4, the structure of a spherical polymeric micelle consists of an external hydrophilic surface and a hydrophobic core. For that reason, these self-assembled nanocarriers can efficiently load hydrophobic drugs and imaging agents in their hydrophobic cores. In addition, they can load hydrophilic drugs coupled or adsorbed to the hydrophilic corona,[9,10,27,28] and, eventually, spherical polymeric micelle can be used as carriers of hydrophobic and hydrophilic payloads. Core-inversible micelles (reverse micelles, Fig. 17.1) have also been reported, which can load hydrophilic drugs in their hydrophilic cores.[10,28] Polymeric micelles present various advantages as nanocarriers, such as high biocompatibility, ease of preparation and load with the drug, and small size (less than 100 nm) that allows deep penetration into tissues, higher stability compared to traditional surfactant-based micelles.[28,29] In cancer therapy, their small size allows them to participate in extravasation through the fenestrations in tumor vessels (**see** Fig. 17.3) and to avoid or limit their uptake by the mononuclear phagocytic system. Hydrophilic surface properties also protect them from immediate recognition and subsequently increase their circulation time in the bloodstream.[30]

Depending on p and f values, spherical micelles pack into cubic liquid crystals, cylindrical micelles form hexagonal liquid crystals, and lamellar aggregates pack as lamellar liquid crystals (Fig. 17.1). Liquid crystals assume a solid crystal character but preserve the mobility of liquids, thus, they are structures in a differential state called mesophase, where the prefix "meso" means "intermediate".[10,31] Moreover, the ordered arrangement of the molecules can increase the viscosity of the system providing an additional advantage for drug delivery systems.[31–33] It has been reported that liquid crystal systems significantly change the release profile of drugs and reduce their toxicity, improving clinical efficiency.[10,31] Another advantage of liquid crystals is that they can be stored for long periods because they are thermodynamically stable.[31]

Under appropriate preparation conditions, ABCP with specific chemical composition will form vesicular assemblies, defined as polymersomes (Figs. 17.1 and 17.4), which have gained great attention in the last 2 decades due to their architecture and advantages compared to their natural lipid counterpart, liposomes.[4,34] Polymersomes exhibit an architecture where the hydrophilic corona of the membrane faces the aqueous core and outer aqueous phase, and the hydrophobic layer of the membrane separates the inner from the outer medium.[4] These self-assembled nanostructures have spherical forms, and in their hydrophilic core can encapsulate water-soluble payloads, while the hydrophobic layer may incorporate lipophilic molecules.[35] Because of their macromolecular nature, the polymeric chains entangle between each other allowing an extra interaction between the copolymers, thus, their higher chemical and physical stability and toughness are superior to liposomes.[10,35,36] Their membrane thickness can be tailored by shifting the hydrophobic ratio of the copolymers. Furthermore, polymersomes are chemically versatile. Their physicochemical properties, including size, polarity, biodegradation, membrane thickness, permeability, stimuli-responsiveness as well as targeting capacity can be modified through the selection of appropriate molecular weight, chemical composition, and proportion between hydrophobic and hydrophilic blocks of the ABCP.[10,25,37] Polymersomes exhibited colloidal stability in aqueous media and tunable and resistant membrane properties, thus they have been explored as nanoplatforms for

therapeutic delivery, due to their ability to encapsulate a wide range of hydrophobic and hydrophilic payloads, such as anticancer drugs, proteins, and genes.[25,36,38] Furthermore, more recent applications include imaging and theragnostic.[39–41] Their use as imaging nanoplatforms has been explored since they provide higher resolution compared to conventional techniques and allow in vivo monitoring of biological pathways and cellular functions, besides being noninvasive.[25,41]

Therefore, the use of ABCP for obtaining self-assembled nanocarriers has been largely explored, since they exhibit the traditional advantages of polymeric materials including flexibility and cost-effectiveness, and extra advantages because of their ability to self-assemble. Moreover, it is possible to obtain control over block functionalities and properties, thus tailoring the nanostructures for required applications.[19] Possible morphologies and functionalities have recently been opened up because of the remarkably diverse and growing range of ABCP architectures that are now available, including those based on stimulus-responsive block copolymers,[23] in which this chapter will focus on.

3. Internal stimuli-responsive self-assembled nanocarriers

Internal stimuli-responsive self-assembled nanocarriers based on ABCP can be prepared to release their payload in a programmed manner to specific intracellular stimuli. These stimuli trigger remarkable changes in the nanocarrier structure, leading to the release of the therapeutic molecules in a particular biological environment. Responsive ABCP-based nanocarriers have been explored for the intracellular delivery of a wide range of anticancer drugs. Even though passive and active targeting strategies (Fig. 17.3) contribute to the accumulation of drug-loaded nanocarriers at an intracellular level, their drug delivery performance can be improved by incorporating appropriate trigger responsiveness in the nanocarrier. In particular, endogenous triggers exploit the characteristics and microenvironment of the tumor, which is completely different from normal tissue physiology. Thus, a range of internal stimuli, including changes in pH, redox state, glucose, and enzyme triggers within tissues and cells, can be utilized.

3.1 pH-responsive self-assembled nanocarriers

pH-responsive nanocarriers have attracted great attention and are one of the most established stimuli-responsive nanocarriers because of the presence of physiological pH gradients within the body. The extracellular pH of a tumor (~6.5–7.2) is slightly lower compared to normal tissues and other biological fluids in physiological conditions (~7.4). pH decreases in intracellular endosomes (pH 5.5–5.0) and lysosomes (pH 4.0–4.5). pH-responsive self-assembled nanocarriers are generally constructed by ABCP with acid-cleavable bonds or ionizable groups designed to carry, deliver, and control the release of payloads to the tumor tissue by exploiting the low pH in the tumor microenvironment.[7,42–46]

As an example, pH-responsive nanocarriers can be formed by ABCP based on hydrolysis-susceptible aliphatic polyesters, such as PLA or PCL, as hydrophobic blocks. For instance, Discher's group reported on biodegradable polymer assemblies prepared with PEG-PCL

and PEG-PLA block copolymers, which were loaded with both paclitaxel and doxorubicin. These pH-responsive nanocarriers exhibited capabilities to permeate and shrink tumors, inducing apoptosis in proportion to the accumulated drug. pH-triggered hydrolytic degradation of the ABCP and polymersomes suffered degradation-induced phase transitions to micelles, which could explain the mechanism for the controlled release of drugs.[38] Later, Deng et al. synthesized a series of novel PEG-b-PCL copolymers methoxy poly(ethylene glycol)-*b*-poly(ε-caprolactone-co-γ-dimethyl maleamidic acid-ε-caprolactone) (mPEG-*b*-P(CL-*co*-DCL)) bearing different amounts of acid-labile β-carboxylic amides on the polyester moiety. These copolymers formed pH-responsive micelles, which were loaded with doxorubicin with a high loading content because of electrostatic interaction. The β-carboxylic amides functionalized micelles showed a negative charge and they were stable in a neutral solution. In acidic conditions (pH 6.0), they quickly changed to positively charged. The pH-triggered negative-to-positive charge reversal, resulting in a very fast drug release in acidic conditions and enhanced cellular uptake by electrostatic absorptive endocytosis as demonstrated in hepatocellular carcinoma cells (HepG2).[47]

Several acid-cleavable linkers, including hydrazone, imine, ortho ester, and acetal have been studied for the preparation of self-assembled nanocarriers based on ABCP. Moreover, nanocarriers with ionizable groups can be also obtained. They usually contain ABCP with weak acidic groups such as carboxylic or sulfonic acids (i.e., poly(acrylic acid), poly(methacrylic acid), among others) and/or weak basic groups such as primary, secondary, or tertiary amine groups (i.e., poly(*β*-amino ester), poly(lysine), poly(histidine), among others), which are sensitive to pH and can suffer changes in conformation or solubility in response to changes in environmental pH *via* ionization (protonation or deprotonation).[7,8,48] These types of linkers can be integrated into the main chain or the pendant chains of the ABCP to prepare self-assembled nanocarriers with tunable degradation kinetics.[42,48–50]

Zhu et al. reported on a coassembly method for the preparation of pH-sensitive nanocarriers, using comb-shaped amphiphilic polymers, i.e., cholate grafted poly(L-lysine) (PLL-CA), with an acid-cleavable amphiphilic PEG−doxorubicin conjugate obtained *via* an acid labile benzoic imine bond. They observed that the permeability of the coassembled polymeric vesicles could be tuned by changing either the PLL-CA/PEG-DOX weight ratio or the environmental pH from 7.4 to 6.5, and destabilization of nanostructures occurred at lower pH values such as 5.0. pH-responsive membrane permeability and triggered dissociation of the nanostructures led to enhance uptake by breast cancer cells (MCF-7) under a condition close to the extracellular environment of solid tumor (pH = 6.5).[49] Wang et al. reported on the preparation of acid-disintegrable nanocarriers based on pH-responsive diblock ABCP for intracellular drug delivery. ABCP were PEG-*b*-poly(2-((((5-methyl-2-(2,4,6-trimethoxyphenyl)-1,3-dioxan-5-yl)methoxy)carbonyl)amino)ethyl methacrylate) (PEG-*b*-PTTAMA). The nanostructures containing cyclic benzylidene acetals in the hydrophobic bilayers were relatively stable under neutral pH, whereas they underwent hydrolysis with the liberation of hydrophobic 2,4,6-trimethoxybenzaldehyde and the simultaneous generation of hydrophilic diol moieties upon exposure to acidic pH milieu. By loading hydrophobic model drug (Nile red) as well as doxorubicin as a hydrophilic drug into the bilayer and aqueous interior of the polymersomes, respectively, the subsequent release of Nile red and doxorubicin was remarkably regulated by the pH of the release media, showing that a lower pH value led to a faster drug release profile. Moreover, these nanostructures were easily taken up by

cervical carcinoma cells (HeLa) and were primarily located in the acidic organelles after internalization, where the pH-responsive cyclic acetal moieties were hydrolyzed and the embedded payloads were therefore released, allowing for the on-demand release of the encapsulants mediated by intracellular pH.[42] Another pH-sensitive PEG-based nanocarrier consist on vesicles based on hydrolytically self-cross-linkable PEG-b- poly(2-diethylamino ethyl methacrylate)-*stat*-3(trimethoxysilyl) propyl methacrylate] (PEG-*b*-P(DEAEMA-*stat*-TMSPMA) copolymer. Polymersomes were formed spontaneously in tetrahydrofuran/water mixtures, with the hydrophilic PEG chains forming the corona and the pH-sensitive P(DEAEMA-*stat*-TMSPMA blocks being located in the membrane walls. The authors demonstrated that nanostructure walls were pH-sensitive. At low pH, protonated P(DEAEMA-*stat*-TMSPMA blocks led the membrane to swell, along with increasing permeability. Also, they found that higher degrees of cross-linking resulted in lower wall permeability.[51]

PEG-based micelles have also been reported. For instance, Huang et al. reported on PEG-poly(acetal urethane) (PAU)-PEG triblock copolymers that readily formed micelles in water (Fig. 17.5). Acetal degradation was accelerated at pH 4.0 and 5.0, indicating their responsiveness to pH changes. Doxorubicin was loaded into the nanostructures and it was released in a controlled and pH-dependent, being faster at lower pH (4.0 > 5.0 > 7.4). Doxorubicin-loaded

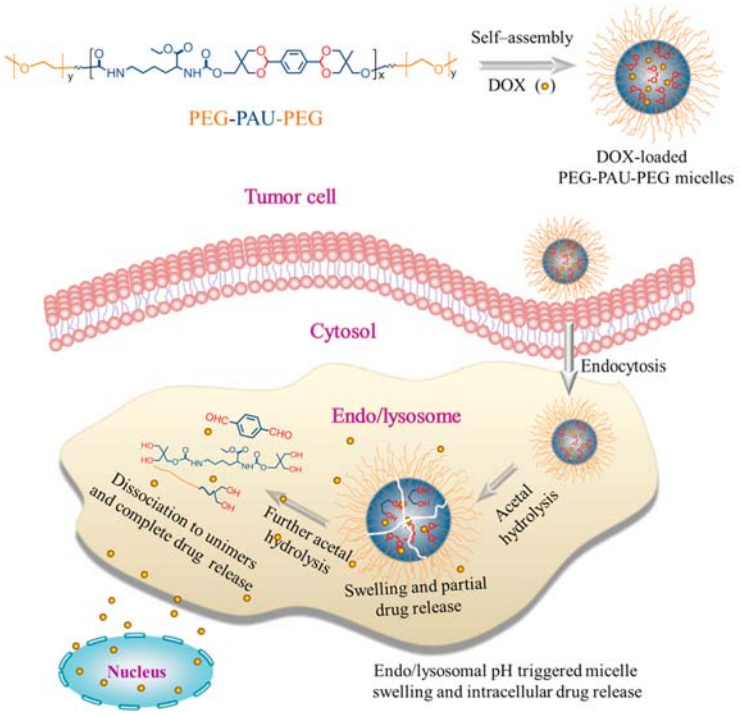

FIGURE 17.5 pH-responsive poly(ethylene glycol)-poly(acetal urethane)-**p**oly(ethylene glycol) (peg-pau-peg) triblock copolymer micelles for intracellular doxorubicin (DOX) delivery. *Reproduced with permission from Huang F, Cheng R, Meng F, Deng C, Zhong Z. Micelles based on acid degradable poly (acetal urethane): preparation, pH-sensitivity, and triggered intracellular drug release. Biomacromolecules 2015;**16**(7):2228–2236. Copyright 2015 American Chemical Society.*

PEG-PAU-PEG micelles showed a high in vitro antitumor activity in both doxorubicin-resistant MCF-7 human breast cancer cells (MCF-7/ADR) and mouse leukemic monocyte macrophage cells (RAW 264.7).[52]

Triblock ABCP has also been widely used to prepare polymersomes. Dan and Ghosh reported on the synthesis of an ABCP by sequential thiol-acrylate Michael addition reaction in one pot. In an aqueous medium, the resulting polymer showed spontaneous vesicular assembly, which disassembled selectively under mild acidic conditions (pH 5.5) resulting in sustained release of encapsulated guest molecules.[53] Zhong's group reported that 2-[3-[5-amino-1-carboxypentyl]-ureido] pentanedioic acid (Acupa)-decorated pH-responsive chimeric polymersomes (Acupa-CPs) efficiently deliver therapeutic proteins into prostate cancer cells. Acupa-CPs were constructed from PEG-*b*-poly(2,4,6-trimethoxybenzylidene-pentaerythritol carbonate)-*b*-poly(succinic acid carbonate) (PEG-PTMBPEC-PSAC) and Acupa-PEG-PTMBPEC-PSAC triblock copolymers. The obtained polymersomes displayed highly efficient loading of both model proteins evaluated (bovine serum albumin and cytochrome C) ant the in vitro release studies showed that protein release was markedly accelerated at mildly acidic pH due to the hydrolysis of acetal bonds in the vesicular membrane. They also studied targeted delivery and anticancer effects of granzyme B (GrB)-loaded Acupa-CPs. These prostate-specific membrane antigen (PSMA)-targeted polymersomes showed a long circulation time in nude mice and showed promising properties as efficient GrB nanocarriers for targeted prostate cancer therapy (Fig. 17.6).[54]

pH-sensitive inversion of polymersomes from poly(acrylic acid)-*b*-polystyrene-*b*-poly(4-vinylpyridine) (PAA-*b*-PS-*b*-P4VP) have also been obtained. pH triggered morphological changes of the triblock copolymer from vesicles to solid spherical aggregates and then back to vesicles. The segregation is based on the difference in repulsive interactions within the PAA or P4VP corona under different pH conditions. At low pH, the P4VP blocks are quaternized, and therefore the repulsive interactions among P4VP chains are increased; the PAA blocks, however, are protonated at low pH and the repulsive interactions among the nonionic PAA blocks are low. Alternately, at high pH, the PAA blocks are neutralized, and the repulsive interactions among PAA coronas are high, whereas the repulsive interactions among the P4VP blocks are low. Asymmetric vesicles with preferentially segregated acidic and basic corona chains could thus be formed by control of the repulsive interaction among corona chains under different pH conditions, i.e., with PAA on the outside at high pH and P4VP outside at low pH. Vesicles with PAA on the outside at high pH can be inverted to P4VP on the outside at low pH, whereas the vesicles are under dynamic conditions.[55]

ABCP constituted by polypeptides are a versatile class of stimuli-responsive building blocks for obtaining self-assembly nanocarriers and they have gained considerable attention for their high biocompatibility, biodegradability, and complex secondary conformations.[48,50] The conformation of the peptide with ionizable side groups can be reversibly manipulated by environmental changes, including pH, ionic strength, temperature, or solvent, which regulate the morphology of peptide-based nanocarriers. Furthermore, ionizable groups can also be used to interact with oppositely charged drugs or bioactive macromolecules *via* electrostatic interactions.[7] Polymersomes fabricated from polypeptide-based ABCP have received a particular name, they are called pepsomes, and have been evaluated for several biomedical applications, including cancer therapy.[48] For instance, poly(glutamic acid) (PGA)- and PLL-based polypeptide block copolymers containing polybutadiene (PBD), polyisoprene (PI), or

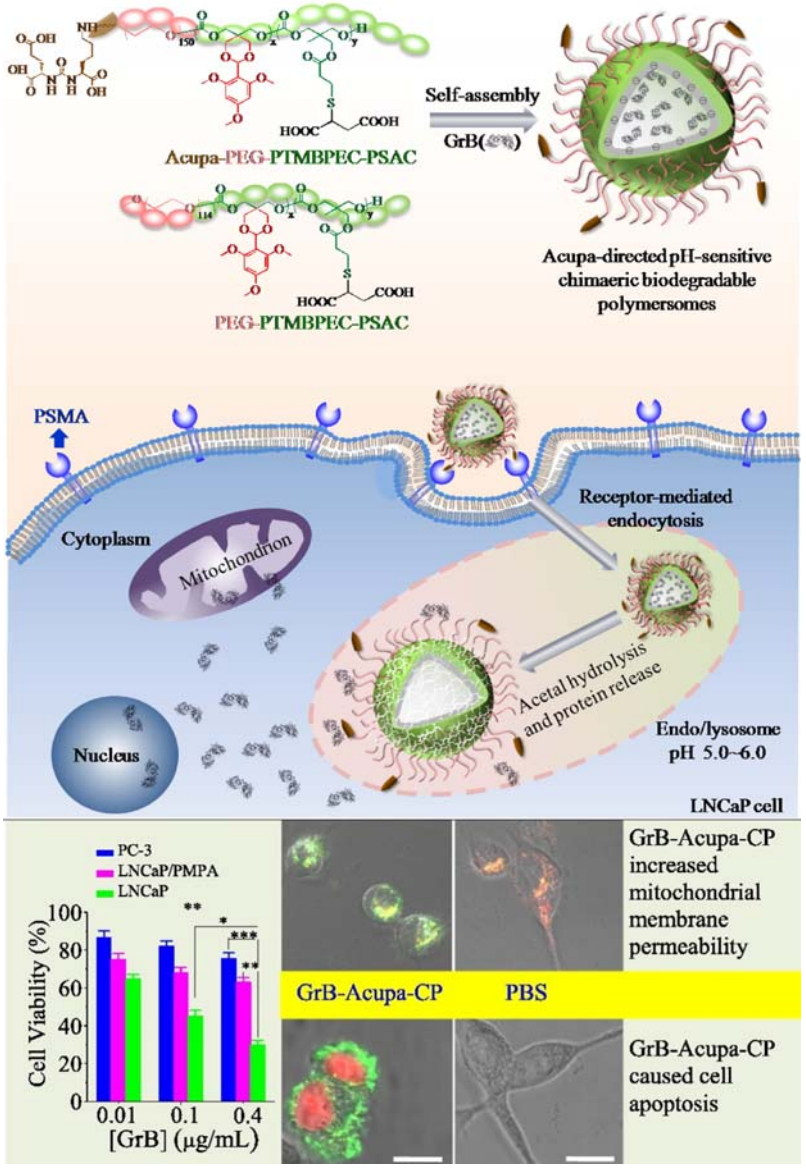

FIGURE 17.6 Schematic illustration on long-circulating prostate-specific membrane antigen (PSMA)-targeting pH-sensitive biodegradable chimeric polymersomes (Acupa-CPs) for active loading and triggered intracellular release of granzyme B (GrB, apoptotic protein) into prostate cancer cells. These nanocarriers efficiently load, deliver and release GrB to PSMA-overexpressing prostate cancer cells, inducing specific and superior anticancer effects. *Reproduced with permission from Li X, Yang W, Zou Y, Meng F, Deng C, Zhong Z. Efficacious delivery of protein drugs to prostate cancer cells by PSMA-targeted pH-responsive chimeric polymersomes. J Control Release 2015;**220**:704–714. Copyright 2015 Elsevier.*

poly(trimethylene carbonate) (PTMC) have been synthetized for preparing pH-responsive polymersomes.[56–58] These nanostructures resulted from a polyelectrolyte corona and a secondary structure of PGA or PLL in the block copolymers. The load of doxorubicin into them was achieved with high loading efficiency and high stability at room temperature, and the drug release rate increased at acidic pH or with increasing temperature.[59] Reversible polymersomes as a function of pH in water have been also produced in moderate acidic or basic aqueous solutions from zwitterionic polypeptide diblock copolymers (PGA-*b*-PLL).[46] Stable pH-sensitive polymersomes have been also obtained by simply mixing a pair of oppositely charged ABCP that contain a PEG block and an ionic block prepared from aniomers and catiomers.[60] This class of polymersomes also received a particular name and they are called polyion complexes or PICsomes, and because of their nature do not require organic solvent for self-assembly into polymersomes and the encapsulation of water-soluble macromolecules is easer compared to conventional polymersomes.[48] Anraku et al. reported on micrometer-sized PICsomes, which were obtained by mixing block aniomer PEG-poly(α,β-aspartic acid) (PEG-P(Asp) and block catiomer PEG-poly([5-aminopentyl]-α,β-aspartamide) (PEG-P(Asp-AP). These PICsomes exhibited tunable membrane permeability by chemical cross-linking of the PIC layer and also showed long circulation in the bloodstream.[60] ABCP based on polypeptides has also been used to prepare pH-responsive micelles. Wang et al. reported on the synthesis of PGA-PLA block copolymers to form doxorubicin-loaded hybrid polymeric micelles to treat melanoma. Drug antitumor activity was regulated by the conformational transition of PGA-*b*-PLA. Under acidic conditions, PGA-*b*-PLA underwent a change in conformation to form channels, which accelerated the doxorubicin release rate. The micelles also showed high targeting and tumor-suppressing ability against melanoma cells (A375) and in vivo studies demonstrated that the micelles with shorter PGA blocks could effectively accumulate in tumor tissues.[61]

The examples above described demonstrating that pH-responsiveness is one of the main stimuli applied in the design of responsive self-assembled nanostructures for cancer therapy.

3.2 Enzyme-responsive self-assembled nanocarriers

Different diseases, including cancer, can cause altered expressions of different enzymes leading to increased concentration of matrix metalloproteinases, hyaluronidase, or cathepsin.[12] Enzyme-responsive nanocarriers exhibited advantageous properties due to the high level of sensitivity, selectivity, and efficiency accompanied by enzymatic conversions for targeted delivery of therapeutic agents at specific sites.[7] Specific enzymatic reactions have been used in the development of stimuli-sensitive nanocarriers that are switched between assembled and disassembled nanostructures.[48,50]

Heise's group synthetized poly(L-glutamic acid-*co*-alanine)-*b*-poly(n-butyl acrylate) (P(GA-co-Ala)-*b*-PBAc) and poly(L-glutamic acid-coalanine)-*b*-polystyrene (P(GA-co-Ala)-*b*-PS) as ABCP with various quantities of L-alanine. Micelles and vesicles were prepared from the deprotected hybrid block copolymers and they studied the effect of peptidases on these nanocarriers. When the self-assembled nanostructures were exposed to elastase and thermolysin enzyme, they suffered degradation depending on the polypeptide composition, exhibiting variable degrees of enzyme-responsiveness. Enzymatic degradation of parts of the

polypeptide block resulted in nanostructure destabilization.[62] Amir's group reported on enzyme-responsive micelles based on ABCP constituted by a linear hydrophilic PEG and a stimulus-responsive dendron with enzyme-cleavable hydrophobic end groups. These amphiphilic PEG-dendron hybrids are self-assembled in water into micelles with a hydrophilic PEG shell and a hydrophobic core. In the presence of the activating enzyme (Penicillin G Amidase from *Escherichia coli*), the hydrophobic end groups cleaved from the dendron, making it more hydrophilic. This change in amphiphilicity resulted in the destabilization of the micellar nanocarriers, leading to their disassembly and release of soluble PEG-dendron hybrids and the encapsulated cargo (Nile Red). The modularity of these PEG-dendron hybrids allowed control over the disassembly rate of the formed micelles by simply tuning the PEG length (Fig. 17.7).[63] Aluri and Jayakannan reported on new classes of enzymatic-biodegradable amphiphilic poly(ester-urethane)s developed from L-tyrosine amino acid resources, which self-assembled into enzyme-responsive nanocarriers. They exhibited excellent encapsulation capabilities for doxorubicin and camptothecin. In vitro drug release studies revealed that the drug-loaded self-assembled nanocarriers were stable under extracellular conditions and they underwent enzymatic-biodegradation exclusively at the intracellular level to release the drugs. Drug-loaded nanocarriers exhibited excellent cell killing in cancer cells as shown in cytotoxicity studies against HeLa cells.[64] Another study performed by Jayakannan's group reported on new classes of biodegradable amphiphilic block and random copolymers based on hydrophilic carboxylic-functionalized PCL (CPCL) and hydrophobic PCL. These polymers were readily dispersible in water, and they were self-assembled into nanocarriers.

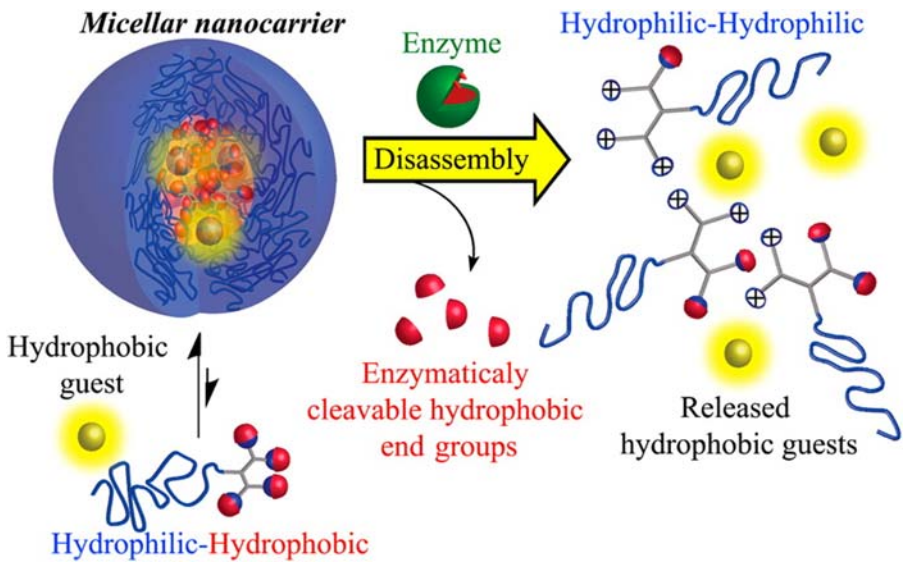

FIGURE 17.7 Schematic representation of the encapsulation of hydrophobic guests in the hydrophobic core of a stimuli-responsive micellar nanocarrier. Upon enzymatic cleavage of the hydrophobic end groups, the nanocarrier disassembles and the guest molecules are released. *Reproduced with permission from Harnoy AJ, Rosenbaum I, Tirosh E, Ebenstein Y, Shaharabani R, Beck R, Amir RJ. Enzyme-responsive amphiphilic PEG-dendron hybrids and their assembly into smart micellar nanocarriers. J Am Chemi Soc 2014;**136**:(21), 7531−7534. Copyright 2014 American Chemical Society.*

They showed excellent capability for loading doxorubicin in the hydrophobic pocket. In vitro drug release kinetics revealed that the self-assembled nanocarriers were stable under physiological conditions, and they exclusively ruptured in the presence of lysosomal esterase enzyme at the intracellular compartments to deliver the drug. The "burst" and "controlled" release of doxorubicin from the nanocarriers was directly controlled by the length and chemical composition of the block and random copolymers. Doxorubicin-loaded nanocarriers killed cancer MCF7 and HeLa cancer cells, demonstrating their usefulness in the treatment of breast and cervical cancers, respectively.[65]

Cathepsin B can be used to cleave certain peptide sequences such as Gly-Phe-Leu-Gly (GFLG). ABCP that contains this peptide sequence can form self-assembled nanostructures with cleavable peptide properties, resulting in the release of the payload. For instance, Feijen's group developed a biodegradable and biocompatible block copolymer of methoxy PEG (mPEG) and poly(D,L-lactide) (PDLLA) in which GFLGF peptide sequence was introduced in between the two blocks(mPEG-pep-PDLLA). The peptide linker was cleavable by the lysosomal enzyme cathepsin B. These ABCP self-assembled into polymersomes in aqueous solutions and disassembled in the presence of the enzyme at pH 5.5, exhibiting rapid release of the model drug acridine orange. Fluorescein isothiocyanate labeled dextran containing polymersomes demonstrated that peptide linkers were cleaved in the lysosomal compartments of the cells, which led to membrane disruption Antiepidermal growth factor receptor-antibody (abEGFR) was immobilized on the surface of polymersomes in order to enhance their cellular uptake by human breast cancer cells ($SKBR_3$). These nanostructures modified with abEGFR demonstrated to be extremely promising as systemic tumor-targeting drug delivery systems since cathepsin B as well as EGF receptors are overexpressed in various tumors (Fig. 17.8).[66] Gu's group reported on an enzyme-responsive PEGylated lysine peptide dendrimer-gemcitabine conjugate based nanocarrier. Owing to the glycyl phenylalanyl leucyl glycine tetra-peptide as an enzyme-cleavable linker to conjugate gemcitabine, the prepared nanostructures were able to release drug significantly faster in the tumor cellular environments, which specifically contain secreted cathepsin B. These self-assembled nanocarriers presented longer intravascular half-life and high accumulation in tumor tissue via the EPR effect, showing excellent antitumor activity on the 4T1 breast tumor model.[67]

The use of GPLGVRGDG peptide sequence was also explored, which cab be cleaved by metalloproteinase enzyme. For instance, Ge's group developed a well-defined enzyme-responsive peptide-linked block copolymer, based on PEG and partially hydrolyzed poly (β-benzyl L-aspartate) (PBLA) linked by the peptide sequence, thus obtaining PEG-GPLGVRGDG-P(BLA-*co*-Asp) ABCP. They self-assembled into micelles and demonstrated to encapsulate doxorubicin efficiently through the synergistic effect of benzyl group-based hydrophobic and carboxyl moiety-based electrostatic interactions. Effective matrix metalloproteinase-2-triggered cleavage of peptide for dePEGylation. Doxorubicin-loaded micelles showed high cellular uptake and cytotoxicity against fibrosarcoma cells that overexpress metalloproteinase-2 (HT1080 cells).[68] Hu's group also reported on metalloproteinase enzymes to cleavage self-assembled nanostructures. They reported on the fabrication of a kind of sandwich-like surface engineered metalloproteinase-responsive nanocarriers, combining the programmable long circulation and targeting properties, which were composed of three layers: detachable PEG out layer, a middle layer of folate ligands, and

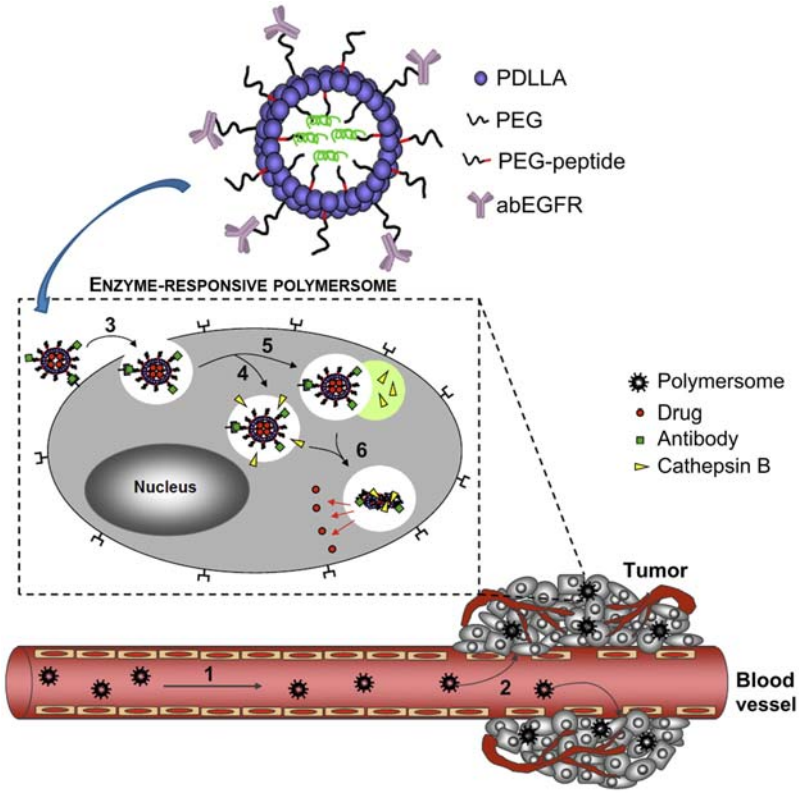

FIGURE 17.8 Schematic illustration of peptide-containing block copolymers for preparing self-assembled nanostructures on anti-epidermal growth factor receptor-antibody (abEGFR) was immobilized to PEG chains. Systemic targeting drug delivery by using abEGFR conjugated and peptide-containing polymersomes in which therapeutic drugs or proteins are present. Long circulating nanostructures can be passively localized in tumor tissue by the enhanced permeation effect (A and B). Antibody-mediated endocytosis (C) followed by enzymatic degradation of polymersomes either in endosomes (D) or in lysosomes (E) may occur especially when lysosomes fuse with endosomes. A rapid release of therapeutic drugs and proteins, which can be triggered by the dissociation of polymersomes as a result of enzymatic degradation (6) will take place. *Reproduced with permission from Lee JS, Groothuis T, Cusan C, Mink D, Feijen J. Lysosomally cleavable peptide-containing polymersomes modified with anti-EGFR antibody for systemic cancer chemotherapy. Biomater 2011;**32**(34):9144–9153. Copyright 2011 Elsevier.*

PCL core. Two kinds of copolymers were synthesized. One of them is composed of longer PEG and PCL with a metalloproteinase-2 and metalloproteinase-9-sensitive linker between PEG and PCL (mPEG-Pep-PCL), and based on PCL-PEG polymer with shorter PEG chain and modified with the tumor cell-specific folate ligand at the end (FA-PEG-PCL). Camptothecin was loaded in the nanocarriers and it was located in the PCL core covered by the folate layer and PEG shell. In vitro studies showed that the inhibition efficiency of tumor cells was dependent on the concentration of the nanocarrier. In the tumor microenvironment, the peptide linker was cleaved by the up-regulated extracellular metalloproteinase 2 and 9, resulting in the detachment of the PEG layer composed of longer PEG chains, consequently allowing

the exposure of the FA layer to enhance the selective binding ability to the melanoma cells (B16) and strengthened the cell internalization, inducing an enhanced antitumor effect. In vivo studies performed in ICR mice demonstrated that upon administration, the nanocarriers are also accumulated in the tumor *via* the EPR effect. Thus, these engineered metalloproteinase-responsive nanocarriers allowed for improving tumor targeting ability, enhanced aggregation of camptothecin in the tumor site, and increase antitumor efficiency.[69]

Pramod et al. prepared polymersomes based on dextran, a polysaccharide, and a renewable-resource alkyl tail. 3-pentadecylphenol and its unsaturated counterpart cardanol, two main components of cashew nut shell liquid were anchored via an aliphatic ester linkage to the dextran backbone through tailor-made synthetic approaches. They self-assembled into polymersomes for dual drug loading and delivering hydrophilic as well as hydrophobic molecules into cells. Rhodamine-B and the polyaromatic anticancer drug camptothecin were selectively loaded in the hydrophilic lumen and hydrophobic membrane, respectively. The aliphatic ester linkage connecting the hydrophobic tail with dextran was demonstrated to be cleaved by esterase under physiological conditions for the fast release of both drugs. The drug-loaded polymersomes demonstrated high cellular uptake as tested on mouse embryonic fibroblast cells.[70] Later, these polymersomes were used to coload doxorubicin and camptothecin. They were capable of preserving the anticancer drugs and release in the presence of the esterase enzyme under physiological conditions. Dual drug-loaded polymersomes demonstrated that both drugs act synergistically to promote the killing of breast cancer (MCF7) and colon cancer (DLD1) cells.[71] Later, Pramod et al. prepared dual stimuli-responsive polymersomes for conjugated and physically loaded doxorubicin delivery in breast cancer cells (MCF7). The pH responsiveness was achieved by the imine chemical linkage and an enzyme cleavable aliphatic ester bond connected the hydrophobic segment at the dextran backbone. The imine chemistry was further exploited to anchor doxorubicin in the dextran backbone, which produced doxorubicin-conjugated dextran polymersomes. The pH and enzyme responsiveness was achieved through acid labile imine linkages and the lysosomal esterase enzyme cleavable aliphatic ester linkage. In vitro studies confirmed the stability of dextran vesicular assemblies under physiological pH conditions and confirmed the cleavage of the acid labile benzylic imine linkage at acidic pH ($\leq$6.0). Also, the esterase enzyme (abundant in lysosomal compartments of cells) assisted the polymersome rupture and the loaded or conjugated drugs were released in intracellular environments. Their results provided new insights into the design of pH- and enzyme-responsive self-assembled nanocarriers for physically loaded and chemically conjugated doxorubicin and its delivery in breast cancer cells.[72]

The ability of enzyme-responsive self-assembled nanocarriers containing chemotherapeutic drugs or proteins to treat tumors is promising and has been explored in the last few years. Even though there are important advances in this arena, the development of enzyme-responsive self-assembled is a relatively new area of research and remains to be tested.[36]

3.3 ROS-responsive self-assembled nanocarriers

The basis of ROS-based stimuli-responsive nanocarriers is the fact that an increase in ROS is associated with abnormal cancer cell growth and reflects a disruption of redox

homeostasis, due either to an elevation of ROS production or to a decline of ROS-scavenging capacity in cancer cells compared to normal cells.[73] Oxidative stress results from the imbalance of ROS generated by aerobic metabolism and antioxidant defenses. Among the theories stating reasons for high ROS in cancer cells, mitochondrial ROS is an important factor, which allows for maintaining growth responses in cancer cells.[74] ROS mostly consists of hydrogen peroxide (H_2O_2), peroxynitrite ($ONOO^-$), hydroxyl radical ($HO\cdot$), superoxide (O_2^-), and singlet oxygen ($^1O_2$), which are produced from various endogenous sources and serve crucial roles in physiological processes, including cellular signaling and proliferation, apoptosis, and immune responses.[3,7] Taking advantage of the abnormal redox states in tumors and considering that pathological sites possess distinctive characteristics from their surroundings, these sites have been considered as targets for site-specific delivery of therapeutic and imaging agents.[7,48] ROS-responsive nanocarriers are an emerging class of nanomaterials in the field of internal biological stimuli.[7]

Napoli et al. reported on the first example of the use of oxidative conversions to destabilize polymersomes. They synthesized triblock copolymer PEG-*b*-poly(propylene sulfide)-*b*-PEG (PEG-*b*-PPS-*b*-PEG). These ABCP self-assembled into unilamellar vesicles in aqueous solutions and could be further oxidatively destabilized. The hydrophobic blocks based on PPS suffered oxidative conversion to a hydrophile block, poly(propylene sulfoxide), and ultimately poly(propylene sulfone). The oxidative process induced morphological changes from stable polymersomes to worm-like micelles to spherical micelles and ultimately to non-associating unimolecular micelles.[75] Later, Hubbell's group prepared ROS-responsive polymersomes based on the block copolymer PEG-*b*-PPS, which were and applied for both antigen (ovalbumin protein) and adjuvant (gardiquimod) delivery to dendritic cell endosomes. Encapsulation of gardiquimod into polymersomes was found to enhance dendritic cell cytokine expression. With the model antigen ovalbumin as a payload, release resulted in a cluster of differentiation 8^+ ($CD8^+$) T cell cross-priming by promoting protein antigen cross-presentation through major histocompatibility complex class I, as indicated by activation of ovalbumin-specific, $CD8^+$ T cells. They observed that polymersomes can function as a vaccine delivery platform for inducing cell-mediated antigen-specific immune responses.[76]

Boronic esters have been widely studied as ROS-sensitive materials for H_2O_2-induced degradation. Liu's group reported on the fabrication of ROS-responsive polymersomes that exhibited intracellular milieu-triggered polymersome bilayer cross-linking, permeability switching, and enhanced imaging/drug release features. During optimization of the chemical design in terms of self-assembling nanostructure morphologies and H_2O_2 response rates, they screened two types of arylboronate derivatives, phenylboronate (PB) and naphthylboronate (NB) esters, and self-immolative linkers of varying spacer lengths. PEG-*b*-PNBMA ABCP was among the four ABCP synthetized the only with self-assembly capabilities. They self-assembled into polymersomes containing aryl boronate ester-capped self-immolative side linkages in the hydrophobic block, followed by surface functionalization with targeting peptides (cell-penetrating peptide CGKRK, Cys-Gly-Lys-Arg-Lys) (Fig. 17.9). Upon cellular uptake, intracellular H_2O_2 triggers the removal of NB capping moieties, followed by self-immolative decaying reactions and generation of primary amine moieties. Extensive amidation reactions then occur due to elevated effective molarity and suppressed amine pKa within hydrophobic bilayer membranes and the equilibrium nature of amine protonation/

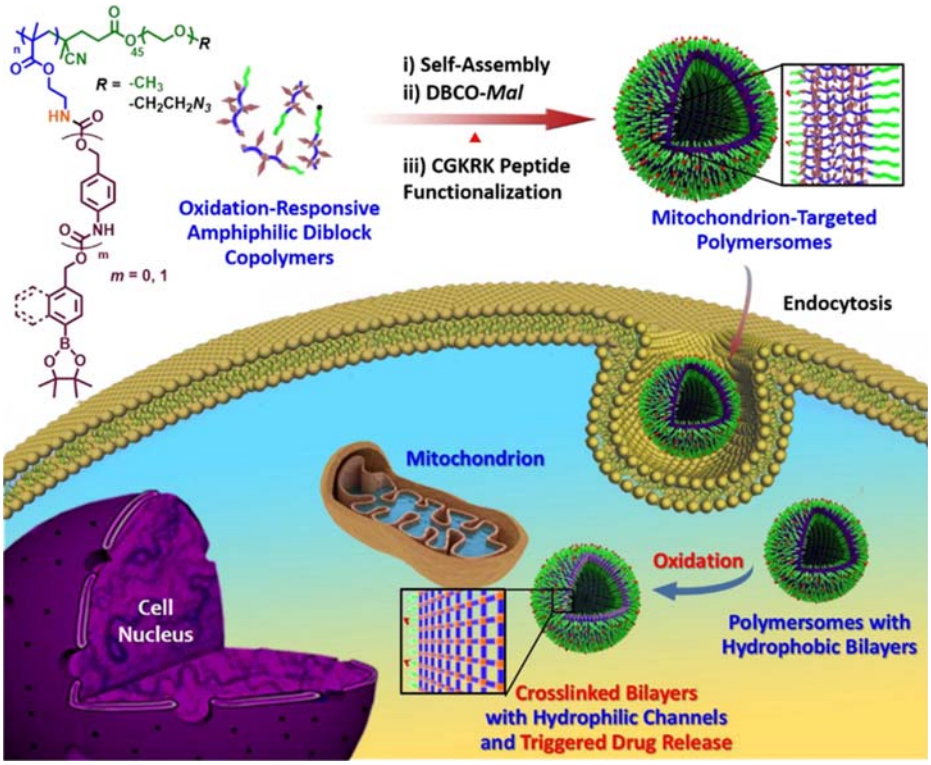

FIGURE 17.9 Schematic representation of the preparation of ROS-responsive polymersomes exhibiting intracellular milieu-triggered vesicle bilayer cross-linking, permeability switching, and enhanced imaging/drug release feature. Mitochondria-targeted reactive polymersomes were obtained through the self-assembly of ABCP containing aryl boronate ester-capped self-immolative side linkages in the hydrophobic block, followed by surface functionalization with targeting peptides. Upon cellular uptake, mitochondrial H_2O_2 triggers cascade decaying reactions and releases primary amine moieties; a prominent amidation reaction then occurs due to suppressed amine pKa within hydrophobic membranes, resulting in concurrent cross-linking and hydrophobic-to-hydrophilic transition of polymersome bilayers inside live cells. *Reproduced with permission from Deng Z, Qian Y, Yu Y, Liu G, Hu J, Zhang G, et al. Engineering intracellular delivery nanocarriers and nanoreactors from oxidation-responsive polymersomes via synchronized bilayer cross-linking and permeabilizing inside live cells. J Am Chem Soc 2016;**138**(33):10452–66. Copyright 2016 American Chemical Society.*

deprotonation, resulting in synchronized bilayer cross-linking and hydrophobic-to-hydrophilic transition of bilayer membranes inside the milieu of live cells. These mitochondria-targeted H_2O_2-reactive polymersomes were also coloaded with doxorubicin and paclitaxel, and sustained drug release was observed as well as cytotoxic activity against HeLa and macrophage-like cells (RAW 264.7).[77]

Li's group reported on the development of a new type of pH/ROS dual-responsive ABCP composed of ortho ester and phenylboronic ester components. This ABCP is self-assembled into micelle-like nanocarriers and their degradation could be modulated by tuning the copolymer composition, the external H_2O_2 concentration, and the pH. Their results indicated that

the phenylboronic ester oxidation rate was faster than the ortho ester hydrolysis rate at neutral pH, and both processes were accelerated with increasing H_2O_2 concentration (Fig. 17.10). These nanocarriers showed promising properties for inflammation-specific drug delivery,[78] thus they may be also promising in the treatment of cancer, since cancer cells, as well as surrounding stromal and inflammatory cells, engage in well-orchestrated reciprocal interactions to form an inflammatory tumor microenvironment.[79]

Recently, Hruby's group synthesized novel, ready-to-use ROS-responsive ABCP with two different spacer chemistry designs to connect a hydrophobic boronic ester-based ROS sensor into the polymer backbone. Polymersomes showed tunable site-specific release of doxorubicin. The reaction with H_2O_2 released an amphiphilic phenol or a hydrophilic carboxylic acid, which impacted polymersome stability and cargo release. They demonstrated that ABCP and polymersomes chemistry influenced the deprotection behavior, showing dependence on ABCP deprotection linkage and H_2O_2 conditions. By spacer chemistry design doxorubicin-loaded ROS-responsive polymersomes could enhance the efficacy of doxorubicin in mice bearing EL4 T cell lymphoma, exhibiting a decrease in tumor growth and prolonged animal survival. Moreover, side effects (weight loss and cardiotoxicity) were also reduced compared to free doxorubicin.[80]

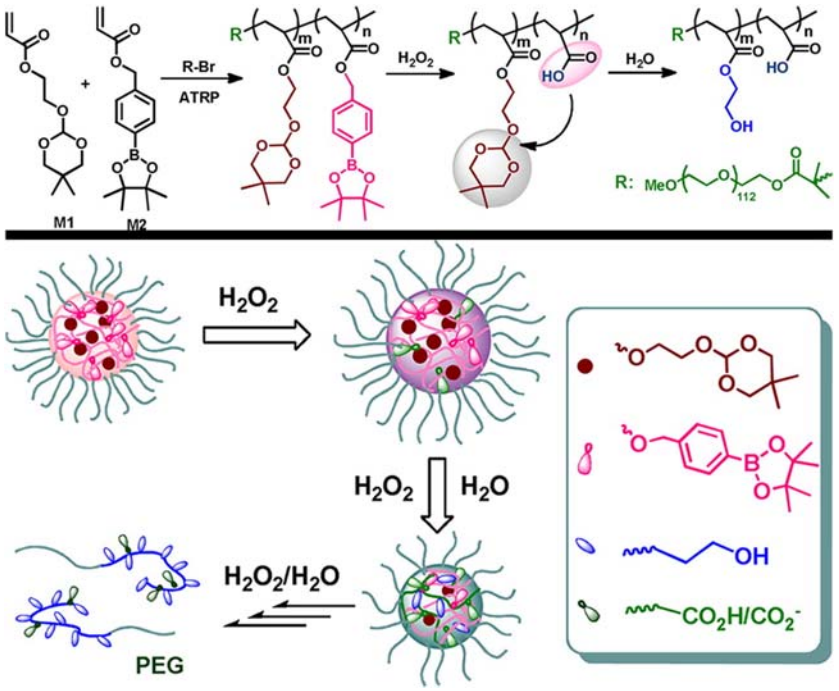

FIGURE 17.10 Schematic representation of the preparation of block copolymers containing a PEG block and a hydrophobic segment composed of different amounts of pendent ortho ester and phenylboronic ester groups, their oxidation and hydrolysis reactions. This ABCP can self-assemble into ROS-responsive micelle-like nanocarriers. *Reproduced with permission Song CC, Ji R, Du F-S, Liang DH, Li ZC. Oxidation-accelerated hydrolysis of the ortho ester-containing acid-labile polymers. ACS Macro Lett 2013;2(3):273−277. Copyright 2013 American Chemical Society.*

Another example of ROS-responsive self-assemblies is the selenium- and tellurium-containing block copolymers. For instance, Zhang's group reported on ABCP diselenide (Se−Se) bonds in the polymer backbone. An ABA-type triblock copolymer was synthetized based on Se−Se-containing polyurethane (PUSeSe) blocks and PEG (PEG-PUSeSe-PEG). This ABCP was capable of self-assembled in water to form ROS-responsive micelles. Se−Se bonds underwent a structural dissociation, inducing the disassembly of the aggregates in the presence of oxidants (i.e., H_2O_2) even in a solution with a very low concentration under mild conditions. These bonds can be oxidized to seleninic acid or reduced to selenol, and in both cases the cleavage of Se−Se bonds induced disassembly of the rhodamine B-loaded micelles. Moreover disassembly of Se−Se bonds was also produced in presence of reductants (i.e., glutathione, GSH).[81] Later, Xu's group focused on another chalcogen element, since tellurium-containing ABCP has become increasingly attractive owing to their unique properties as biomaterials. Tellurium was introduced into ABCP for the fabrication of ultrasensitive ROS-responsive tellurium-containing PEG-PUTe-PEG micelles. In presence of H_2O_2, a fast response of the micelles is produced due to the oxidation of the telluride groups on the backbone into telluroxide groups, which made the micelles more hydrophilic and further leads to swelling of the micelle core.[82] Selenium/tellurium-containing ABCP are emergent materials to develop self-assembled nanocarriers possessing unique stimuli-responsive properties and potential biological functions. For further biomedical applications, their toxicity after degradation needs to be studied more clearly.[83]

ROS-responsive self-assembled nanocarriers have opened up a new direction for the preparation of ABCP capable of backbone cleavage ability and burst release of payload in the tumor microenvironment. However, in vivo studies and clinical trials need to be performed aimed at clearly defining their usefulness for cancer therapy.

3.4 Redox-responsive self-assembled nanocarriers

There is a significant redox potential difference between the intracellular and extracellular microenvironments as well as between tumor and normal tissue. In the extracellular environment, body fluids (e.g., blood), and on the cell surface, the concentration of one of the most prominent reducing agents, GSH is lower (2−20 μM) compared to cytosol and nuclei, where the concentration is higher (10 mM), producing a great reductive microenvironment. The redox potential of cancer cells is 100- to 1000-fold higher than other cells in the human body. Therefore, taking advantage of the local redox state in the tumor microenvironment, and the large difference in redox potential between intracellular and extracellular compartments, redox-responsive self-assembled nanocarriers have been studied for triggered intracellular delivery of a variety of biologically active molecules.[7,50]

Disulfide (SS) bonds can be readily reduced in an intracellular environment due to the thiol-disulfide exchange reaction with GSH, a well-known reducing agent. Disulfide bonds are simply introduced in the middle or side chain of an ABCP or in a cross-linker to provide them redox-responsiveness. The incorporation of disulfide bonds as cross-linkers in the nanostructure allows for improving their stability.[48] Cleavage of these bonds can induce disassembly of the nanocarriers in reductive environments, releasing the payload.[7,36,48,50,84,85]

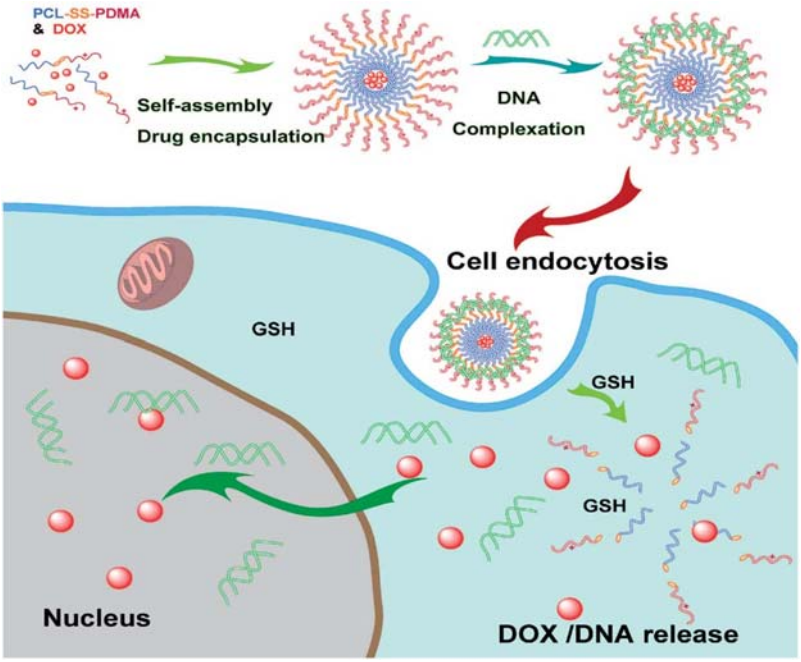

FIGURE 17.11 Schematic illustration of doxorubicin (DOX) encapsulation, DNA condensation, and subsequent intracellular release of the disulfide-linked pcl-*b*-poly(*N*,*N*-dimethylamino-2-ethylmethacrylate) (pcl-SS-pdma) diblock copolymers self-assembled into redox-responsive micelles. *Reproduced with permission from Li Y, Lei X, Dong H, Ren T.Sheddable, degradable, cationic micelles enabling drug and gene delivery. RSC Adv 2014;4(16):8165–8176. Copyright 2014 Royal Society of Chemistry.*

Various redox-responsive self-assembled nanocarriers concerning thiol-triggered intracellular drug release and imaging have already been reported. For instance, Wen et al. reported on doxorubicin-loaded micelles based on PEG-sheddable shell and poly(e-benzyloxycarbonyl-L-lysine) core with a redox-sensitive disulfide linkage (mPEG-SS-PzLL). In the presence of tumor-relevant GSH concentrations, mPEGSS-PzLL micelles underwent shedding of the PEG shell *via* cleavage of disulfide bonds, followed by rapid disassembly of the original micelle structure facilitating efficient release of the encapsulated payload. Doxorubicin-loaded mPEG-SS-PzLL micelles effectively reduced cell viability of human MCF-7 breast cancer cells in a dose-dependent fashion.[84] This shell-detachable strategy was also explored by Ren's group, who developed sheddable, degradable, and cationic micelles based on intermediate disulfide-linked PCL-*b*-poly(*N*,*N*-dimethylamino-2-ethylmethacrylate) (PCL-SS-PDMA) diblock copolymers. These micelles showed GSH-mediated intracellular codelivery of doxorubicin and DNA (Fig. 17.11). The intermediate disulfide linkage was kept intact at the normal condition and showed excellent redox-triggered doxorubicin release and cell uptake eficiency as demonstrated against HeLa cells. Moreover, PCL-SS-PDMA/DNA complexes exhibited 10-fold transfection eficiency in human oral carcinoma cell lines (KB and CAL-27 cells), compared to polyethylenimine (PEI 25K) used as control. Reduction-triggered cleavage by GSH made these sheddable and cationic micelles promising carriers for drug and gene delivery in cancer

therapy.[86] In addition, Wang et al. demonstrated the rapid increase of the free drug concentration in multidrug-resistant cancer cells via the delivery of shell-detachable redox-responsive micelles. These self-assembled nanocarriers were obtained from single disulfide bond-bridged block polymers based on PCL and poly(ethyl ethylene phosphate) (PCL-SS-PEEP). The micelles rapidly released the incorporated doxorubicin in response to the intracellular reductive environment and led to high cellular retention of the doxorubicin in multidrug-resistant MCF-7/ADR breast cancer cells, displaying enhanced cytotoxicity.[87] Luan's group constructed the redox-responsive self-assembled nanocarriers based on the synthesized mPEG-SS-paclitaxel and mPEG-SS-doxorubicin conjugates. The conjugates were amphiphilic and self-assembled into mixed micelles with a precise ratio of the two conjugates in the aqueous solution. In vitro release profile indicated the release of both drugs was synchronized and controlled in the tumor cells, in a reductive environment. Cytotoxicity studies against A549 and B16 cancer cells indicated that mixed micelles exhibited similar anticancer efficacy to combined free drugs. Interestingly, in vivo studies showed the mixed micelle exhibited higher antitumor efficiency in shrinking tumor size compared to free drugs, while reducing systemic toxicity during the treatment.[88] This strategy of preparing conjugates was also explored by Kumar et al., who prepared redox-responsive prodrug nanostructures based on xylan-SS-curcumin conjugate, which could self-assemble in an aqueous medium. They showed excellent redox-responsiveness due to the disulfide linkage and the presence of GSH allowed dual and efficient delivery of 5-fluorouracil and curcumin. cell-viability assays demonstrated that 5-fluorouracil-loaded xylan-SS-curcumin conjugate exhibited enhanced, cell apoptosis induction and inhibition ability in human colorectal cancer (HT-29 and HCT-15) cell lines than the parent drugs.[89] Furthermore, Hu et al. described the synthesis and self-assembly of a particular ABCP based on PEG and a polymerized block of reduction-cleavable camptothecin prodrug monomer (PCPTM) that allowed obtaining PEG-*b*-PCPTM diblock copolymers, termed as polyprodrug amphiphiles. These polymers (>50 wt% camptothecin loading content) can be self-assembled in four different hierarchical organizations (spheres, large compound vesicles, smooth disks, and staggered lamellae with spiked periphery). Among them, the unprecedented staggered lamellae outperformed the other three nanostructure types, exhibiting extended blood circulation duration, the fastest cellular uptake, and unique internalization pathways as evaluated in HepG2 and human lung cancer (A549) cells. The controlled hierarchical organization of polyprodrug amphiphiles and shape-tunable biological performance opened up new horizons for exploring next-generation ABCP-based drug delivery systems with improved efficacy.[90]

Polymersomes sensitive to change in redox potential, often contain disulfide bonds as well. One of the advantages of using redox-responsive polymersomes is that a fine-tuning drug release profile can be provided by changing the number and location of disulfide bonds. Zhong's group developed reversibly stabilized, multifunctional cross-linked dextran nanocarriers based on dextran-lipoic acid derivatives, which self-assembled into polymersomes in water. The addition of a catalytic amount of dithiothreitol yielded stable nanocarriers through a cross-linking of the core. They were loaded with doxorubicin and showed high drug loading efficiency. These redox-responsive polymersomes were stable under extracellular conditions but were rapidly destabilized under reductive environments. A fast de-cross-linking took place as a result of a high concentration of GSH, which produced a reduction-triggered release of doxorubicin in vitro as well as inside tumor cells, demonstrating a rapid and efficient delivery

of doxorubicin into HeLa and RAW 264.7 cell nucleus.[91] Thambi et al. synthesized an ABCP based on three blocks of PEG, PLL and PCL bearing a disulfide bond (PEG-*b*-PLL-SS-PCL), which self-assembled into polymersomes in aqueous media. These nanostructures were coloaded with camptothecin in their membrane and doxorubicin in their aqueous cores. Drugs were released in a sustained manner under physiological conditions, whereas the polymersomes showed triggered release of both drugs in the presence of GSH. These dual drug-loaded self-assembled nanocarriers showed improved cytotoxicity to squamous carcinoma (SCC7) cells.[92] Sun et al. also reported on PEG-containing polymersomes. They developed reduction- and pH-responsive cross-linked polymersomes based on the PEG−PAA−poly(2-(diethyl amino)ethyl methacrylate) (PEG−PAA− PDEA) triblock copolymers, which were further modified with cysteamine to yield the thiol-containing PEG−PAA(SH)−PDEA. These disulfide-crosslinked polymersomes exhibited and were rapidly dissociated in response to GSH at neutral or mildly acidic conditions. These polymersomes were loaded with bovine serum albumin and cytochrome C, and in vitro release studies revealed that protein release was fast under the intracellular-mimicking reducing environment. Cytochrome C-loaded dual-responsive polymersomes induced potent cancer cell apoptosis as observed in MCF-7 and HeLa cells, thus providing an attractive strategy for intracellular protein release.[93] Furthermore, Jia et al. developed reduction-responsive cholesterol-based ABCP. The reduction sensitivity was introduced by the disulfide bridge that linked the hydrophilic PEG block and the hydrophobic PAChol block. PAChol was a smectic liquid crystal polyacrylate-composed of cholesterol monomers. The obtained PEG-SS-PAChol polymersomes showed physical stability because of the presence of cholesterol as cross-linker. Calcein was chosen as a model of hydrophilic molecules to be encapsulated inside PEG-SS-PAChol polymersomes and it was released from them triggered by GSH.[94] Zou et al. reported on tumor-homing, redox-responsive and reversibly crosslinked multifunctional biodegradable polymersomes, which exhibited improved performance that PEGylated liposomal doxorubicin. These self-assembled polymersomes were based on PEG-*b*-poly(trimethylene carbonate-co-dithiolane trimethylene carbonate) (PEG-P(TMC-DTC)) and cyclic peptide cNGQGEQc-functionalized PEG-P(TMC-DTC) (cNGQ-PEG-P(TMC-DTC)). The membrane-forming hydrophobic block consisted of P(TMC) backbone, and a pendant dithiolane ring, which is analogous to lipoic acid. The peptide cNGQ was decorated on the surface. The obtained doxorubicin-loaded redox-responsive polymersomes showed efficient loading and stability with minimal drug leakage under physiological conditions while spontaneous disassembly and quick drug release was produced in response to GSH. They also display efficient receptor-mediated internalization, fast intracellular drug release, and high antitumor activity in $\alpha 3\beta 1$ integrin-overexpressing A549 lung cancer cells. The in vivo pharmacokinetics and biodistribution studies revealed that doxorubicin-loaded cNGQ-decorated polymersomes had a long circulation time and significantly enhanced tumor accumulation compared to PEGylated liposomal doxorubicin and undecorated polymersomes. cNGQ-functionalized polymersomes showed targeted delivery of doxorubicin to subcutaneous as well as orthotopic A549 human lung cancer xenografts in nude mice, resulting in effective tumor suppression, significantly improved survival time, and markedly reduced adverse effects.[95] Folate (FA)-targeted polymersomes have also been reported. For instance, Qin et al. a designed FA-decorated PCL-SS-PEG-SS-PCL based redox-responsive polymersome-based drug nanocarriers for codelivery of doxorubicin and paclitaxel along with P-glycoprotein inhibitor tariquidar. This nanocarrier had a high loading capacity and

enabled simultaneous delivery of three drugs (tariquidar, doxorubicin, and paclitaxel). In vitro cellular uptake, the study demonstrated that tariquidar-containing FA-decorated polymersomes increased drug accumulation into MCF-7/ADR cells via the tariquidar-induced P-glycoprotein efflux inhibition, and further improved targeting to tumor cells due to FA receptor-mediated endocytosis. Doxorubicin and paclitaxel were released into the cytoplasm in responsive to GSH, exerting a synergistic effect and proapoptotic activity against MCF-7/ADR, which was enhanced dramatically along with the administration of tariquidar. This FA-targeted redox-responsive polymersomes loaded with chemotherapeutic drugs and P-glycoprotein inhibitor demonstrated noticeable synergistic effect against human MDR MCF-7 cells and successfully reversed drug resistance, which displayed high potential in overcoming multidrug resistance tumors.[96]

In addition, Bej et al. synthetized two ABA-type ABCP (P1, P2). The hydrophobic B block consisted of a bioreducible segmented poly(disulfide) (PDS), while poly-N-isopropylacrylamide (PNIPAM) or poly(triethylene glycol) methyl ether methacrylate (PTEGMA) served as the hydrophilic A blocks in P1 and P2, respectively (PNIPAM-*b*-PDS-*b*-PNIPAM and PTEGMA-*b*-PDS-*b*-PTEGMA), leading to the formation of polymersomes and micelles, respectively, owing to the difference in the packing parameters. Both self-assembled nanostructures were loaded with doxorubicin and showed comparable encapsulation efficiency. GSH triggered drug release, which was much faster from the polymersomes than micelles owing to the complete degradation of the PDS segment in polymersome morphology unlike in micelle. Doxorubicin-loaded polymersomes showed excellent killing efficiency to the HeLa cells, while doxorubicin-loaded micelles revealed rather poor activity in cancer cells.[97]

Recently, *Wei* et al. reported on redox-responsive doxorubicin-loaded polymersomes based on PEG-P(TMC-DTC) ABCP, which were functionalized with a transferrin-binding peptide CGGGHKYLRW (TBP-polymersomes). These disulfide-crosslinked polymersomes decorated with a transferrin-binding peptide, TBP-polymersomes, could selectively and stably bind transferrin and subsequently mediated targeted doxorubicin delivery to TfR overexpressing HCT-116 colorectal cancer cells in vitro and in vivo, leading to enhanced tumor suppression and reduced off-target side effects (Fig. 17.12).[98] Another recently research on targeted redox-responsive polymersomes was reported by Zhong et al.[99] They designed CD44-targeted chimeric polymersomes encapsulating granzyme B as an artificial killer cell for potent protein therapy of subcutaneous LP1 tumor and bone marrow of orthotopic LP1 multiple myeloma in vivo. Hyaluronic acid-directed reduction-responsive chimeric polymersomes showed high stability, CD44 targetability, and reduction-triggered protein release, thus they emerged as a novel and effective treatment for multiple myeloma.

The described examples of the use of redox-responsive self-assembled nanocarriers demonstrate their great potential in the treatment of cancer. Further in vivo studies are still required since several studies are only limited to evaluating the performance of the nanocarriers in cell lines.

4. Exogenous stimuli-responsive self-assembled nanocarriers

Exogenously triggered nanocarriers can react to external physical stimuli, such as temperature, light, magnetic and electric fields, and ultrasound (Fig. 17.3), thus these stimuli-responsive self-assembled nanocarriers can be remotely controlled for triggering the delivery of the payloads.

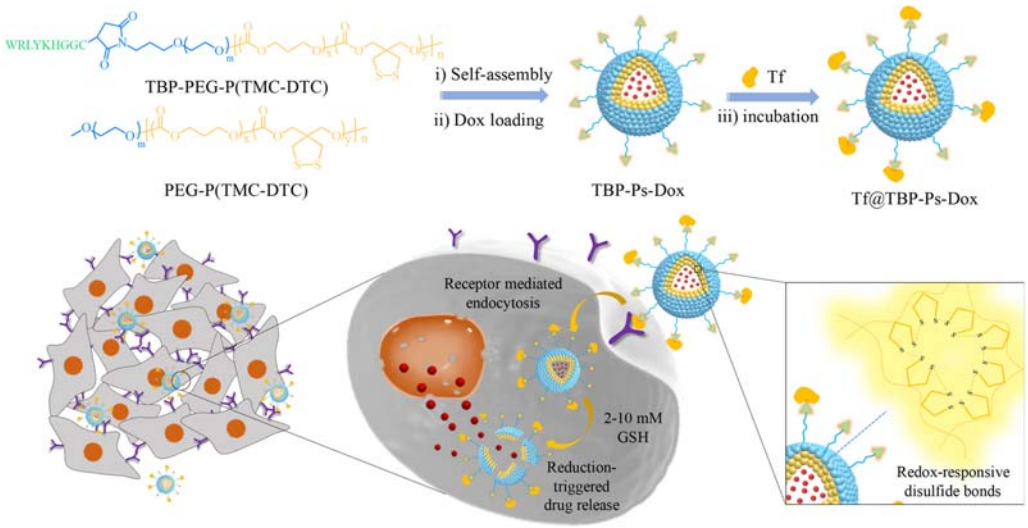

FIGURE 17.12 Schematic illustration of the fabrication of transferrin-bound polymersomal doxorubicin *via* a transferrin-binding peptide (TBP), CGGGHKYLRW. (A) TBP-functionalized polymersomes (TBP-Ps) were self-assembled from peg-*b*-poly(trimethylene carbonate-*co*-dithiolane trimethylene carbonate) (peg-p(tmc-dtc)) and tbp-peg-p(tmc-dtc) ABCP; (B) Doxorubicin (dox) was efficiently loaded into TBP-Ps *via* a pH-gradient method; and (C) incubation with transferrin yielded transferrin-bound polymersomal doxorubicin (tf@tbp-ps-dox). Tf@TBP-ps-dox could not only increase the accumulation and retention in transferrin receptor over-expressing HCT-116 colorectal tumor cells but also enhanced the cellular uptake compared to ps-dox, leading to enhanced efficacy of targeted therapy of colorectal cancer in vivo. *Reproduced with permission from Wei Y, Gu X, Sun Y, Meng F, Storm G, Zhong Z. Transferrin-binding peptide-functionalized polymersomes mediate targeted doxorubicin delivery to colorectal cancer in vivo. J Control Release 2020;**319**:407–415. Copyright 2020 Elsevier.*

4.1 Temperature-responsive self-assembled nanocarriers

Among external stimuli, the temperature is the most widespread and it can be used to trigger the specific responsiveness of self-assembled nanocarriers. Ideally, temperature-responsive nanocarriers should release their cargo between 37 and 42 °C, otherwise undesirable effects may appear above 42 °C.[7] Thermo-sensitive nanocarriers with temperature-response properties have been extensively studied in the 21st century because they are interesting candidates for applications in cancer nanomedicine.[34] Local temperature is slightly higher in solid tumors compared with that of normal tissues; then, drug delivery systems to accumulate into the tumor may be developed by adjusting the thermo-responsiveness of ABPC to be between body temperature and the higher temperature of the tumor.[7,36,100]

Temperature-sensitive polymers display a phase transition at a determined temperature, resulting in changes in their conformation, and solubility as well as in their hydrophilic-hydrophobic balance. Therefore, this type of polymers can change their physical and chemical properties in response to heat.[7] Temperature-responsive polymers can be organized into two main groups. One group is composed of polymers that exhibit an upper critical solution temperature (UCST), and the other group is integrated by polymers that show lower critical solution temperature (LCST), thus they become soluble or insoluble, respectively, upon

heating. Consequently, UCST and LCST are critical temperature points above and below which the polymer and solvent become completely miscible.[101]

Although the most widely studied polymers are relatively temperature insensitive, an extensive range of temperature-responsive ABCP have been obtained by incorporating PNIPAM as block.[7,48,50,100] PNIPAM has a typical LCST of 32 °C; then, this polymer can transit between hydrophilic to hydrophobic when the temperature is switched around this temperature value, which is slightly lower than the physiological temperature. Below LCST, this polymer is soluble and above LCST it is dehydrated and collapsed to an insoluble chain conformation. When PNIPAM is applied as the hydrophobic part of an ABCP, it can self-assemble to form stable nanocarriers at the normal body temperature of 37 °C, while disassembling and rapidly releasing encapsulated payloads at temperatures below 32 °C.[50] For instance, *Li* et al. reported on self-assembled nanocarriers from thermo-sensitive polyion complex (PIC) micelles from diblock copolymer poly(*t*-butyl acrylate-*co*-acrylic acid)-*b*-PNIPAM (P(*t*BA-*co*-AA)-*b*-PNIPAM) and graft copolymer chitosan-*g*-PNIPAM (CS-*g*-PNIPAM). Diblock copolymers self-assembled into micelles in solution. The addition of CS-*g*-PNIPAM induced aggregation of CS onto micelles to form PIC micelles due to the negatively charged and positively charged PAA and CS, respectively. The hydrophobic core encapsulated doxorubicin by hydrophobic interactions and the pH-sensitive PAA-loaded doxorubicin by electrostatic interactions. Reducing pH or increasing ionic strength breaks the interactions between CS/PAA and doxorubicin/PAA triggering drug release. Increasing temperature above LCST, sensitive PNIPAM chains collapsed resulting in the sustained doxorubicin release.[102] Guo's group prepared two types of temperature-responsive biodegradable ABCP, namely poly(N-isopropylacrylamide-*co*-N,N-dimethylacrylamide-*b*-lacitde) and poly(N-isopropylacrylamide-*co*-N,N-dimethylacrylamide-*b*-ε-caprolactone), which showed symmetric hydrophobic blocks. They self-assembled into micelles for further load adriamycin. Drug release and hydrophobic core degradation were enhanced at the simulated tumor tissue condition at pH 5.3 and 40 °C. In accordance, i*n vitro* cytotoxicity assay against stomach cancer (N-87) cells showed enhanced intracellular uptake.[103] Chen et al. reported on P(folate-allylamine-co-NIPA-co-acrylamide-co-octadecyl acrylate) micelles (PFAAM) and P(folate-PEG-acrylic acid-co-NIPA-co-acrylamide-co-octadecyl acrylate) (PFPAM) micelles for active tumor-targeting delivery. Paclitaxel was loaded into the micelles and cytotoxicity assays against A549 and human hepatoma (Bel 7402) cells demonstrated selective tumor targeting efficacy contributed because of the thermal sensitivity and the presence of the folate receptor.[104]

PNIPAM-containing star block copolymers have also been developed to prepare self-assembled nanocarriers. Luo et al. developed a four-arm star multiblock copolymer based on thermosensitive PNIPAM as arms and hydroxyl-terminated polybutadiene (HTPB) as hydrophobic central blocks ($PNIPAM_2$-*b*-HTPB-*b*-$PNIAM_2$). These multiblock copolymers were able readily to form self-assembled micelles for further loading campothecin. Drug release demonstrated thermo-responsiveness, since temperature-induced structural changes were observed in the micelles. Campothecin-loaded micelles showed increased cytotoxic activity against MDA-MB231 human breast cancer cells.[105] Furthermore, Panja et al. reported on temperature-responsive micelles prepared from our-arm star block copolymers, pentaerythritol polycaprolactone-*b*-poly(N-isopropylacrylamide), and pentaerythritol polycaprolactone-*b*-poly(N-vinylcaprolactam), which were tagged with folic acid (PE-PCL-*b*-PNIPAM-FA and

PE-PCL-*b*-PNVCL-FA copolymers) for efficient cancer cell targeting delivery. Doxorubicin was efficiently loaded into the micelles and it was fast released as a response to the change of phase above the LCST, which produced shrinkage of temperature-responsive polymer chains. Doxorubicin-loaded FA-decorated micelles exhibited high cellular uptake and accumulations as demonstrated in FA-overexpressed C6 glioma cells as well as in vivo studies performed in the C6 glioma tumor rat model. Selective tumor accumulation as well as inhibition of tumor growth, without any systemic toxicity, were observed after their intravenous administration (Fig. 17.13).[106]

Regarding temperature-responsive polymersomes, PEG and PNIPAM-based ABCP have been explored. For instance, Yang's group synthesized PEG-*b*-PNIPAM block copolymers that showed temperature-responsive assembly/disassembly of polymersomes. They were stable at body temperature and could load both hydrophilic drugs in the aqueous lumen and hydrophobic molecules in the membrane (e.g., doxorubicin and PKH 26, a red-fluorescent dye, respectively). Fast release of both cargoes occurred at temperatures below 32 °C since the PNIPAM block became hydrophilic. Inducing polymersomes disassemble.[107] Zhong's group prepared water-soluble and temperature-responsive PEG-PAA-PNIPAM triblock copolymers, which quickly self-assembled into polymersomes in an aqueous solution at 37 °C. Formed polymersomes could be readily cross-linked at the interface *via* carbodiimide chemistry, by adding cystamine. Cross-linked polymersomes showed high stability under

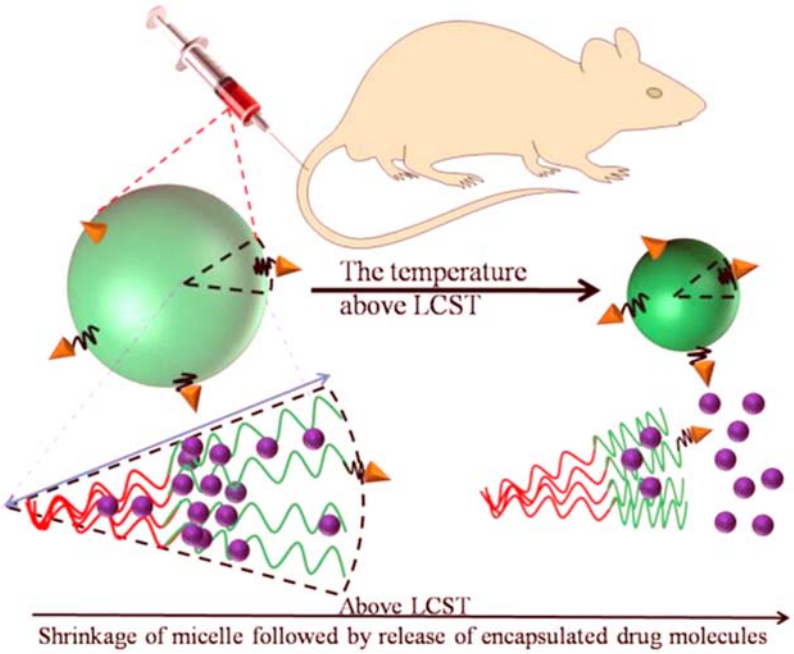

FIGURE 17.13 Schematic representation of temperature-responsive micelles. *Reproduced with permission from Panja S, Dey G, Bharti R, Kumari K, Maiti T, Mandal M, Chattopadhyay S. Tailor-made temperature-sensitive micelle for targeted and on-demand release of anticancer drugs. ACS Appl Mater Interfaces 2016;8(19):12063−12074. Copyright 2016 American Chemical Society.*

different conditions, such as against dilution, organic solvent, high salt conditions, and change of temperature in water. FITC−dextran, selected as a model protein, was loaded into polymersomes and showed high loading efficiency. FITC−dextran was retained within the polymersomes at 25 °C, and dithiothreitol triggered their rapid dissociated because of the reductive environment, mimicking the intracellular environment.[108]

Hydrophobic polymer blocks have also been used to be conjugated with PNIPAM and the obtained copolymers self-assembled into complex morphologies at high temperatures.[48] Moughton and O'Reilly described thermally induced micelles to polymersomes transition for a charged chain end diblock copolymer. They prepared a quaternary amine end-functionalized diblock copolymer based on poly(*tert*-butyl acrylate) and PNIPAM (PtBuA-*b*-PNIPAM). PNIPAM block had this permanently hydrophilic charged quaternary amine as head-group. These block copolymers underwent a temperature-responsive morphology transition from micelles to polymersomes. The authors proposed head-group was a key component to ensure the stability of the diblock copolymer in solution when self-assembled into a nanostructure. They also anticipated that polymersomes may show limited membrane permeability toward positively charged and hydrophilic molecules, which could facilitate their use in temperature-responsive hydrophilic scavenger/encapsulation uses. Moreover, the exterior and interior charged head-group could be explored for binding biologically active molecules, including proteins, DNA, or RNA.[109] In this regard, Mann's group developed protein−polymer conjugates for obtaining temperature-responsive compartments named as proteinosomes. They showed protocellular properties, including selective permeability, membrane-gated internalized enzyme catalysis, guest molecule encapsulation, and protein synthesis *via* gene expression. These nanocarriers could be dispersed in oil or water. Temperature change induced membrane permeability to external substrates, producing an on/off switch for enzymatic reactions inside them.[110]

As described, plenty of PNIPAM-based temperature-responsive nanocarriers have been reported and they have shown promising properties for the treatment of cancer. However, the clinical application of PNIPAM-containing nanocarriers still remains a dilemma, since it has been reported neurotoxicity of acrylamide monomer, as well as lack of complete biocompatibility of PNIPAM, due to i*n vivo* experiments performed in mice have shown systemic toxicity.[111] Over the past decades, numerous efforts have been made for obtaining temperature-responsive nanocarriers other than PNIPAM-based ones. For instance, nanocarriers based on poly(N-vinylcaprolactam) (PVCL),[112,113], poly(trimethylene carbonate)-*b*-PGA,[114] poly(propylene oxide)-*b*-PLL,[115] poly(trans-*N*-(2-ethoxy-1,3dioxan-5-yl)acrylamide),[116] and modified poly(aspartamide)[117,118] have also been reported. To mention some examples, Kharlampieva's group reported on temperature-responsive polymersomes based on PVCL-*b*-polydimethylsiloxane-*b*-PVCL (PVCL-*b*-PDMS-*b*-PVCL) triblock copolymer. The copolymers self-assembled into stable polymersomes at room temperature and were loaded with doxorubicin. Their membrane permeability was controlled by PVCL length, in a temperature range between 37 and 42 °C. Temperatures higher than LCST of PVCL induced gradual polymersome shrinkage or reversible formation of bead-like aggregates that preserved nanocarrier size change. Interestingly, event though temperature triggered morphological changes they were reversible and did not compromise polymersome structural stability. In fact, transient pores were formed in the PVCL-*b*-PDMS-*b*-PVCL polymersome membrane at elevated temperatures, which allowed drug release, which passed

through the hydrophobic PDMS layer, without inducing damage to the polymersome structure (polymersomes remained intact after doxorubicin release). Cytotoxicity studies performed in A549 cells demonstrated that doxorubicin-loaded PVCL-*b*-PDMS-*b*-PVCL polymersomes exhibited a concentration- and time-dependent effect on cell viability.[112] Recently, the same research group synthesized poly (3-methyl-N-vinylcaprolactam)-*b*-poly(N-vinylpyrrolidone) (PMVC-PVPON) diblock copolymers that self-assembled in aqueous media and at room temperature into stable temperature-responsive polymersomes. The decrease in PVPO block length induced variation in LCST of PMVC-PVPON (from 19.2 to 15.2 °C). The polymersomes were loaded with doxorubicin and exhibited high loading capacity and encapsulation efficiency due to hydrophobic interactions between the polymer blocks and doxorubicin. These polymersomes exhibited good structural stability in serum. In vivo studies performed in C57BL/6J mice demonstrated lower cardiotoxicity of doxorubicin from polymersomes compared.[113]

In addition, pH-sensitive tertiary amines-containing ABCP typically have temperature-dependent pK_a. Hence, they have been used to prepare temperature-responsive self-assembled nanostructures.[7] In this way, Agut et al. synthesized a polypeptide-based poly [2-(dimethylamino)ethyl methacrylate]-*b*-PGA (PDMAEMA-*b*-PGA) diblock copolymer, which exhibited responsiveness to pH and temperature changes. They are self-assembled into polymersomes or micelles, depending on the PGA block length. The self-assembly process could be tuned as a function of pH and/or temperature. At pH values near the isoelectric point (IEP), direct or inverse electrostatic polymersomes were generated by electrostatic interactions. At higher pH values, PDMAEMA was uncharged, and the temperature-responsive of the ABCP related to LCST behavior of PDMAEMA (~40 °C). Under basic pH conditions and

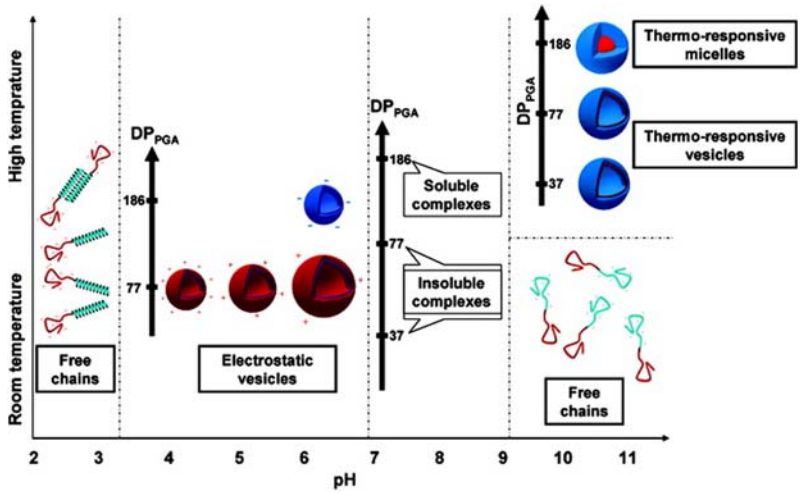

FIGURE 17.14 Schematic representation of the different morphologies obtained from polypeptide-based multi-responsive block copolymers. *Reproduced with permission from Agut W, Brûlet A, Schatz C, Taton D, Lecommandoux S. pH and temperature responsive polymeric micelles and polymersomes by self-assembly of poly [2-(dimethylamino) ethyl methacrylate]-b-poly (glutamic acid) double hydrophilic block copolymers. Langmuir 2010;**26**(13):10546–10554. Copyright 2010 American Chemical Society.*

below its LCST, free chains of ABCP unimers were evidenced, whereas above its LCST the hydrophobicity of PDMAEMA induced self-assembly in a reversible manner (Fig. 17.14).[119] This ABCP are promising to develop anticancer drug-loaded self-assembled nanocarriers for cancer nanomedicine.

Recently, Yang's group developed a novel temperature-polymersome based on nonconjugated and PEGylated poly(amide-imide), which showed unexpected red fluorescence. PEGylation changed from hydrophobic poly(amide-imide) to amphiphilic PEGylated poly(amide-imide). Below LCST, PEG shielded spontaneous self-assembled into polymersomes, whereas above LCST, polymersomes collapsed and phase separation occurred. These polymersomes showed outstanding biostability and photostability as well as prohibited fluorescence quenching, showing promising properties for cell imaging.[120]

As can be observed, different approaches have been studied in the development of temperature-responsive self-assembled nanocarriers. Due to the wide variety of polymers and conjugations that can be explored to prepare new ABCP with thermo-sensitive properties, the horizons in the fabrication of temperature-responsive nanocarriers for cancer therapy are broad.

4.2 Light-responsive self-assembled nanocarriers

Light irradiation, with variable intensity and wavelength, is an easy and cheap exogenous stimulus than has been exploited in the development of photo-responsive self-assembled nanocarriers. Self-assembled can be precisely induced at a specific time and location (spatiotemporal control) upon exposure to certain wavelengths, which can be ultraviolet (UV), near-infrared (NIR), and visible (Vis) light.[7,50,111] Photo-responsive self-assembled nanocarriers are frequently based on ABCP that incorporated photo-sensitive moieties, which behave as light-cleavable linkers or induce light-sensitive degradation or conformational changes.[7]

Release profiles of payloads from these self-assembled nanocarriers can be controlled by adjusting three main parameters, namely intensity light, wavelength, and exposure time. NIR-responsive nanocarriers have been widely studied for biomedical applications since tissue and skin exhibit minimum absorbance in the range of 650−900 nm.[3,7,111] Therefore, photo-responsive nanocarriers show great potential for on-demand drug delivery, accompanied by noninvasive clinical therapy.[7,121]

As mentioned, in the development of light-responsive self-assembled nanocarriers, photosensitive moieties are incorporated into the ABCP, which then self-assembled into nanostructures that exhibit responsiveness to light. After light exposure, these nanocarriers dissemble, dissociate and/or disrupt by photo-induction because of ABCP degradation and/or cleavage of block linkers, or property changes and/or structural modifications are observed because of photo-induction, including changes in hydrophilic-hydrophobic balance and reversible photo-cross-linking.[7,111] Among the different moieties, azobenzene (AZO), 2-diazo-1,2-naphthoquinone (DNQ), spiropyran (SP), *o*-nitrobenzyl (ONB) as well as coumarin derivatives have been the most widely studied in the development of photo-responsive ABCP to make them sensitive to light.[36,48,50,121]

Upon Vis and UV light irradiation, AZO moiety can reversibly change from the *trans* isomer to the *cis* isomer. AZO-containing micelles and polymersomes have been developed for

cancer treatment. For instance, Pearson et al. reported on ABCP containing AZO and β-galactose units, which self-assembled into light-responsive micelles. The use of β-galactose as the hydrophilic shell was intended to target the galectin-3 receptors, which are overexpressed in melanoma cells. Upon UV irradiation, AZO units isomerized quickly to their more polar *cis* isomers, triggering the release of a hydrophobic payload (Nile red). Cytotoxicity studies against human melanoma A375 cells demonstrated that micelles exhibited high cellular uptake, indicating their suitability as nanocarriers for melanoma treatment.[122] Bai et al. synthesized supramolecular prodrug complexes with β-cyclodextrin (β-CD)-acylhydrazone-doxorubicin and studied the targeting of AZO-terminated poly[2-(dimethylamino)ethyl methacrylate] as a building block. They self-assembled into multi-compartment vesicles and complex micelles. Doxorubicin was loaded into them and upon UV-light irradiation exposure, dissociation of β-CD/AZO was induced, leading to a morphology transition, which slightly increased the release rate of doxorubicin. These nanocarriers also exhibited pH-triggered drug release. At pH 5, the release rate increased as a result of the broken acyl hydrazone bond. Cytotoxicity studies performed against MCF-7 cells indicated cellular uptake, suggesting a promising behavior for applications in cancer therapy.[123] AZO-containing polymersomes have also been studied for triggering disruption and disassembly.[124–128] For instance, Blasco et al. developed photo-responsive polymersomes based on AZO-conjugated amphiphilic linear-dendritic block copolymers. They were based on PEG linear segment linked to a fourth generation 2,2-di(hydroxymethyl)propionic acid (bis-MPA) based dendron with 4-isobutyloxyazobenzene units at the periphery, then hydrocarbon chains (C18) were randomly connected to the periphery of the dendron. AZO/C18 ratio influenced the photo-sensitive behavior of the polymersomes as well as the loading of hydrophilic (rhodamine B) and hydrophobic (Nile Red) molecules. UV light was used as an external stimulus to trigger the release of the probes from the nanocarriers, which suffered polymer alterations related to *trans*-to-*cis* isomerization of the AZO moieties.[129–131] Huang's group also reported AZO-containing photo-responsive polymersomes that self-assembled in water. The AZO-based amphiphilic guest itself self-assembled into solid nanoparticles, and upon complexation with water-soluble pillar[6]arene polymersomes were obtained, They exhibited sensitivity to Vis and UV light irradiation, showing reversible transitions between polymersomes and solid nanoparticles with the *trans*-to-*cis* photo-isomerization of the AZO groups after irradiation.[132] Hu et al. reported on giant supramolecular vesicles for photo-responsive and targeted intracellular drug delivery, which were fabricated by hierarchical self-assembly of cucurbit[8]uril used host molecule mixed with maleimide-modified methyl-viologen and hydrophobic 3,4,5-tris(*n*-dodecyloxy) benzoylamide with an AZO moiety. UV light irradiation induced *trans* to *cis* isomerization, photo-triggering reconfiguration of polymersomes to achieve the controlled drug release. The maleimide moiety allowed further functionalization with thiol-containing target molecules, such as RGD peptide or bovine serum albumin. Polymersomes exhibited stability, excellent structural integrity, high drug loading capacity, and photo-switchable drug release in a complex cellular environment. Fast cellular uptake was observed in A549, MDA-MB-231, and prostate cancer cells (PC-3) cancer cells (Fig. 17.15).[133]

SP is a well-known photochromic molecule that has also been evaluated in the development of ABCP. Under Vis or UV light irradiation, SP can suffer reversible isomerization from the hydrophobic ring-closed SP form to the hydrophilic ring-opened merocyanine

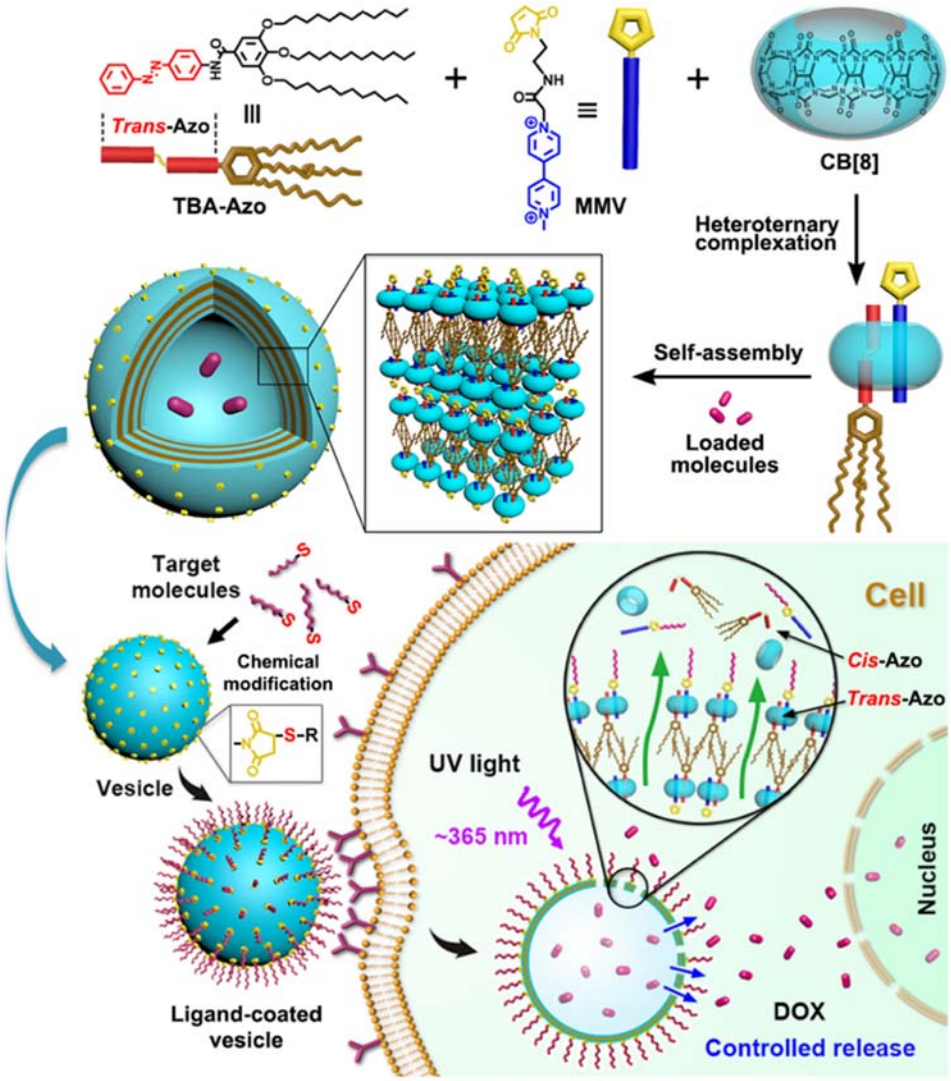

FIGURE 17.15 Schematic representation of the assembly strategy to construct supramolecular vesicles by supra-amphiphiles based on photo-responsive cucurbit[8]uril (CB[8]) heteroternary complexation. They targeted and photo-controlled intracellular drug delivery (UV light irradiation) through surface modification with targeting ligands. *Reproduced with permission from Hu C, Ma N, Li F, Fang Y, Liu Y, Zhao L, Qiao S, Li X, Jiang X, Li T. Cucurbit [8] uril-based giant supramolecular vesicles: highly stable, versatile carriers for photoresponsive and targeted drug delivery. ACS Appl Mater Interfaces 2018;**10**(5):4603–4613. Copyright 2018 American Chemical Society.*

(MC) form, behaving in a wavelength-selective fashion. The photo-tunable isomerization process from SP to MC has been studied to reversibly control the behavior of self-assemblies. For instance, Wang et al. synthesized ethyl cellulose-*g*-poly(2-hydroxyethyl methacrylate)-*g*-poly(spiropyran ether methacrylate) (EC-*g*-PHEMA-*g*-PSPMA) light-sensitive

ABCP, which self-assembled into spherical micelles in aqueous media. Probe pyrene was loaded onto micelles, selected as a poorly water-soluble model drug, and it was observed that its release could be modulated by changing light. Under UV light irradiation, PSPMA became hydrophilic, decreasing the sizes of the micelles, and, after Vis light irradiation, micelles recovered their sizes, depicting reversible behavior.[134] Wang et al. developed photochromic polymersomes that exhibited reversible photo-switchable bilayer permeability. ABCP was based on PEG and PSPA, where SPA is an SP-based monomer containing a unique carbamate linkage. They self-assembled into polymersomes, in which SP moieties underwent reversible photo-triggered isomerization from hydrophobic SP to zwitterionic MC states. This transition was accompanied by changes in membrane polarity and permeability from nonimpermeable to selectively permeable toward noncharged, charged, and zwitterionic small molecule species. Photo-switchable intracellular delivery of hydrophilic small molecules in a spatiotemporal manner was observed in HeLa cells.[135] Recently, Kwangmettatam and Kudernac reported on light-responsive polymersomes based on small amphiphilic molecules bearing two SP moieties and an ethyleneglycol backbone. The self-assembly mechanism involved the self-limiting growth of the MC-containing building blocks. Photo-switching of the protonated MC induced a double diameter of the polymersomes, and this expansion persisted upon irradiation. Once irradiation stopped, the polymersomes shrinked back, following the thermal relaxation to the SP form.[136]

As described, AZO- and SP-containing self-assembled nanocarriers exhibited photoresponsiveness that induce photo-isomerization. On the other hand, ONB-containing ABCP shows a photo-cleavable response upon irradiation. For instance, Jin et al. designed and prepared light-responsive PIC micelles with switchable surface charge. They were based in poly(N,N-dimethyl-N-(2-(methacryloyloxy)ethyl)-N-((2-nitrobenzyl)oxy)-2-oxoethanaminium bromide)-block-poly(carboxybetaine methacrylate) (PDMNBMA-b-PCBMA) block copolymers. These PIC micelles negatively charged FITC-bovine serum albumin and also exhibited pH-responsiveness. Positively charged PDMNBMA blocks transformed to zwitterionic carboxy betaine units upon UV light irradiation, inducing disassembly of the micelles. Furthermore, protein release was fast in the presence of UV irradiation as well as in slightly acid pH (6.5). PIC micelles were efficiently internalized by A549 cells (Fig. 17.16).[137] Liu's group reported on an alternative approach by incorporating light-responsive hydrophobic blocks that activate head-to-tail cascade depolymerization. ABCP was based on degradable poly(-benzyl carbamate) (PBC) block and a hydrophilic PDMA block. They formed self-immolative polymersomes triggered. Different triggers, such as Vis and UV light irradiation, or reductive milieu activated the disintegration of the polymersomes into water-soluble small molecules and hydrophilic blocks.[138] Recently, Yamamoto et al. reported on different photoresponsive polymersomes based on PEG and photocleavable 2-nitrobenzyl compounds bearing alkyne and maleimide functionalities. A fluorophore was loaded into the nanocarriers. near-UV irradiation cleaved at the hydrophobic/hydrophilic interfaces, generating various end groups (succinimide, benzoacetophenone, or carboxylate) at the outer and inner interfaces of the polymersomes, but they preserved their hollow structures even after irradiation. The loaded molecules were released at different rates, depending on the molecular weight as well as the type of hydrophobic polymer; moreover, the presence or absence of the charged end groups also affected the release rate.[139]

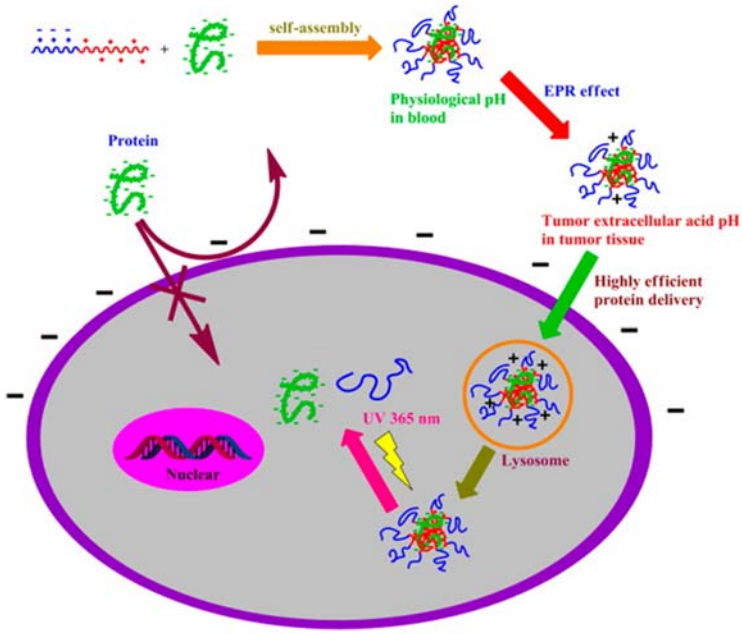

FIGURE 17.16 Schematic representation of light-responsive polyion complex micelles with a switchable surface charge for intracellular delivery of proteins. *Reproduced with permission from Jin Q, Cai T, Wang Y, Wang H, Ji J. Light-responsive polyion complex micelles with a switchable surface charge for efficient protein delivery. ACS Macro Lett 2014;3(7):679−683. Copyright 2014 American Chemical Society.*

The aforementioned examples concerning photo-responsive self-assemblies are based on Vis or UV light irradiation. Although numerous UV light-responsive nanocarriers have exhibited promising properties in vitro, this radiation can only be used for the treatment of illnesses presented in certain regions of the human body, namely eyes or skin, which can be directly irradiated.[7] Moreover, a major drawback of UV irradiation is that the most representative examples used 365 nm wavelength to release the payloads, and this wavelength can damage healthy tissues.[14] For these reasons, several efforts have been made to develop NIR-light-responsive self-assembled nanocarriers. This irradiation exhibits low scattering loss, deep tissue penetration, and minimal harm to healthy tissues.[36,48] Zhang et al. developed doxorubicin-loaded biodegradable micelles prepared by mixing PCL-SS bond-biode gradable photoluminescent polymer (PCL-SS-BPLP) and biotin-PEG-cypate. NIR irradiation induced cypate decomposition, which allowed releasing the drug. Moreover, these micelles also exhibited redox-responsive behavior, and GSH triggered doxorubicin release. Both stimuli synergistically induced HepG2 cell death and apoptosis. In vivo studies performed in C57BL/6 mice with lewis, lung cells demonstrated improved anticancer efficacy of doxorubicin-loaded micelles.[140] NIR-photo-responsive polymersomes have also been developed by including chromophores in the ABCP, which can respond to NIR irradiation.[141−146] Recently, Tang et al. reported NIR light-sensitive polymersomes based on PEG and poly(propylene sulfide) (PSS-PEG). Zinc phthalocyanine (ZnPc), a photosensitizer, was entrapped in

the organic layer while doxorubicin was encapsulated in the aqueous core. Triggered drug release was observed under the NIR irradiation and the polymersomes also exhibited responsiveness to ROS. These nanocarriers exhibit improved efficacy against malignant melanoma (A375) cells and in vivo studies demonstrated excellent antitumor effects by synergistic chemophotodynamic therapy.[147]

Light-responsive self-assembled nanocarriers exhibit great potential for cancer treatment, diagnosis, and theragnosis, and they have also been explored for photothermal and photodynamic therapy, which expand their usefulness for biomedical applications.

4.3 Magnetic-responsive self-assembled nanocarriers

Magnetic-responsive self-assembled nanocarriers have promising properties, including high penetration, noninvasive nature, ease of control, and absence of energy dissipation, which make them useful for biomedical applications, particularly in cancer therapy. For their preparation, commonly ferromagnetic, paramagnetic, or superparamagnetic nanoparticles are incorporated into the self-assemblies. Magnetic-responsive nanocarriers have been explored for magnetically triggered drug delivery and magnetic resonance imaging (MRI). Moreover, the magnetic field can be used for hyperthermia and magnetic guidance, or both combined.[7,36,48,50] Magnetite (Fe_3O_4) and maghemite (γ-Fe_2O_3) are the most commonly used magnetic nanoparticles for preparing self-assembled nanocarriers, since their exhibited high biocompatibility. There are several examples of ABCP-based magnetic-responsive self-assembled since they are based on the combination of magnetic nanoparticles and ABCP capable of self-assembly.[39,148–158] An example that reported on the use of Fe_3O_4 to prepare magnetic-responsive nanocarriers is the work of Pourjavadi et al., who designed magnetic-responsive micelles based on oleic acid-coated Fe_3O_4 nanoparticles and the thermo-responsive PNIPAM-PCL-PNIPAM triblock copolymer. Paclitaxel was loaded and in vitro studies showed controlled drug release at both body and hyperthermia temperature, with increasing release at higher temperatures. Cytotoxicity assays performed in MCF-7 cells showed anticancer activity of paclitaxel-loaded micelles.[159] On the other hand, Oliveira et al. reported on the use of γ-Fe_2O_3, which exhibited superparamagnetic behavior. They synthesized PTMC-*b*-PGA block copolymers that self-assembled into polymersomes. They loaded γ-Fe_2O_3 and doxorubicin for obtaining hybrid magnetic-responsive polymersomes. Upon internalization in HeLa cells, a high-frequency magnetic field was applied (14 mT at 750 kHz), which elicited an increase in cell toxicity due to the higher doxorubicin release (Fig. 17.17).[148]

Magnetic-responsive ABCP-based self-assembled nanocarriers exhibit great potential for magnetic guidance, hyperthermia, triggered drug delivery, and MRI, all biomedical applications with interesting perspectives in cancer therapy and diagnosis.

4.4 Other stimuli-responsive self-assembled nanocarriers

Ultrasound-responsive self-assembled nanocarriers have also been explored in cancer therapy. This is a promising stimulus due to its facile administration, deep tissue penetration (by tuning the frequency, duty cycles, and time of exposure), and low cost. Ultrasound has been

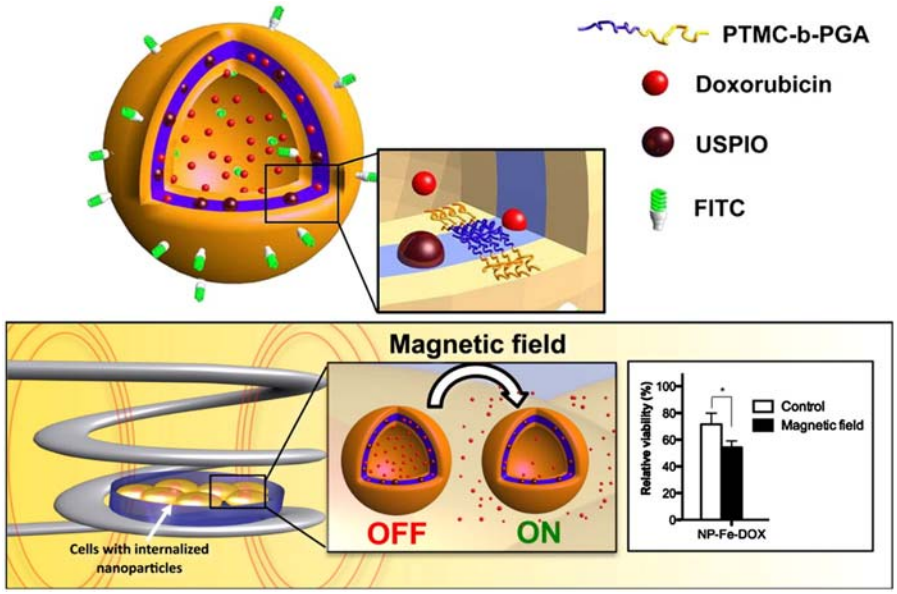

FIGURE 17.17 Schematic representation of doxorubicin (DOX)-loaded magnetic-responsive polymersomes based on poly(trimethylene carbonate)-*b*(L-glutamic acid) (ptmc-*b*-pga) block copolymers and superparamagnetic iron oxide nanoparticles (USPIO; γ-Fe_2O_3). Upon internalization in HeLa cells, polymersomes were exposed to a high-frequency magnetic field that triggered intracellular drug release and increased cytotoxicity. *Reproduced with permission from Oliveira H, Pérez-Andrés E, Thevenot J, Sandre O, Berra E, Lecommandoux S. Magnetic field triggered drug release from polymersomes for cancer therapeutics. J Control Release 2013;**169**(3):165–170. Copyright 2013 Elsevier.*

used as an adjuvant in cancer treatment since it can be a sensitizer to improve chemotherapy and overcome drug resistance.[7,36,48] Some examples include the use of PEG-*b*-PLA block copolymer-based self-assemblies, are under ultrasound-induced bubbles. These air-containing assemblies exhibit potential application for triggered drug release and targeted ultrasound imaging.[160] Moreover, dual stimuli-responsive self-assemblies can be obtained. For instance, Chen and Du synthetized PEG-*b*-poly[2-(diethylamino)ethylmethacrylate-stat-tetrahydrofuranyloxy)ethylmethacrylate] (PEG-*b*-p(DEA-stat-TMA)) triblock copolymers that self-assembled in aqueous medium. The obtained nanocarriers exhibited pH- and ultrasound-responsiveness that induced changes in their size and morphology to trigger drug release.[161]

On the other hand, electric field-responsive self-assembled nanocarriers have shown interesting properties. This stimulus may induce changes in charge or polarity of ABCP, which can alter their chemical composition or structure, thus, disassembly and release of the payload take place.[7,121] Electric field-responsive polymersome based on PEG-ferrocene (PEG-Fc) homopolymers and chain end-decorated PB-ß-cyclodextrins (PS-ß-CD) has been reported. They showed host-guest interaction between Fc and CD and formed reversible diblock copolymers (PS-β-CD/PEG-Fc) that self-assembled into polymersomes. Under +1.5 V electrochemical stimulus, polymersomes suffered disassembly realizing the cargo (rhodamine B).[162] Later, other electric-field-responsive polymersomes were developed

using tetraaniline-PEG, a redox-sensitive amphiphilic rod-coil molecule, which in aqueous media was reduced to leucoemeraldine base able to self-assemble into polymersomes that efficiently load a fluorescein derivative. Upon oxidizing voltage, the polymersome membrane split into smaller micelles, exhibiting a reversible behavior since reassembled to form polymersomes under reducing voltages, behaving as electrically switchable polymersomes.[163]

5. Summary and future challenges

Cancer therapy mainly relies on the use of effective anticancer drugs, but these active small molecules have many disadvantages, which may negatively impact therapeutic success. Some of their undesirable properties can be overcome if they are vesiculated in well-designed nanocarriers. The main goal of research in nanocarriers for therapeutic purposes involves the development of effective and safe treatments for clinic applications. In this sense, several efforts have been made to develop stimuli-responsive ABCP capable of self-assembled into nanocarriers aimed at improving therapies. Taking into account their potentialities, great research focuses has been placed on the comprehensively understanding of their ability to self-assemble into nanostructures as well as the study of their ordered morphologies.

Self-assembled nanostructures have been recognized as one of the key subjects in nanoscience. Self-assembly processes are generally low-cost and large-scale techniques, suitable for different purposes, including biomedical applications in cancer nanomedicine.

In this chapter, various representative examples of stimuli-responsive ABCP-based self-assembled nanocarriers, including internal and external stimuli-driven, and their main applications for cancer therapy were highlighted. The incorporation of stimuli-triggered responsiveness allows self-assembled nanocarriers to recognize changes in the external or internal environment, which trigger the release of the payload, thus, conducting *on-demand* release behavior in spatial-, temporal-, and dose-controlled fashions. Several different stimuli have been studied, such as pH, ROS, enzymes, redox, temperature, light, magnetic and electric fields, and ultrasound, as well as combined stimuli, which may induce modifications in ABCP conformation, their solubility as well as in their hydrophilic-hydrophobic balance, hence inducing destabilization of self-assemblies, leading changes in their structure and immediately releasing the payload.

Even though ABCP-based self-assembled nanocarriers have shown great potential to revolutionize cancer treatment and diagnosis, there are still challenges for their successful translation to clinical applications since limitations continue appearing. More studies regarding biocompatibility, long-term toxicity, and immunogenicity of ABCP and their self-assembled should be performed to define their safety for clinical use. Furthermore, after analyzing the aforementioned examples, it is possible to notice that most stimuli-responsive nanocarriers have been evaluated under relatively static conditions; nevertheless, numerous variables are present in a real situation considering the complexity of the human body. In fact, in the design of targeted nanocarriers that respond to different signals in the tumor microenvironment, a complex scenario must be considered, including long circulation time in the bloodstream, capability to reach the target site, triggered release of the payload,

and, ideally, the biodegradability of the nanocarrier. Therefore, the promising results obtained in vitro or in vivo in small animals even when they are encouraging do not guarantee their further success in vivo in bigger animal models as well as in humans when thinking in clinical use. More advanced in vivo studies are crucial to better understand the interactions between self-assembled nanocarriers and living organisms, and to really define their use and potential clinical translations.

In addition, concerning scalable production as well as the reproducible manufacturing process, significant efforts need to be considered in the design, synthesis, and optimization of ABCP and their subsequent self-assemblies, since a high-performance system that involves simple and reliable manufacturing is always required for translation to clinical use.

References

1. Tran S, DeGiovanni P-J, Piel B, Rai P. Cancer nanomedicine: a review of recent success in drug delivery. *Clin Transl Med* 2017;**6**(1):44.
2. Avramović N, Mandić B, Savić-Radojević A, Simić T. Polymeric nanocarriers of drug delivery systems in cancer therapy. *Pharmaceut* 2020;**12**(4):298.
3. Yin J, Chen Y, Zhang Z-H, Han X. Stimuli-responsive block copolymer-based assemblies for cargo delivery and theranostic applications. *Polym* 2016;**8**(7):268.
4. Salvioni L, Rizzuto MA, Bertolini JA, Pandolfi L, Colombo M, Prosperi D. Thirty years of cancer nanomedicine: success, **f**rustration, and hope. *Cancers* 2019;**11**(12):1855.
5. Pucci C, Martinelli C, Ciofani G. Innovative approaches for cancer treatment: current perspectives and new challenges. *Ecancer Med Sci* 2019;**13**.
6. García MC. Drug delivery systems based on nonimmunogenic biopolymers. In: Parambath A, editor. *Engineering of biomaterials for drug delivery systems. beyond polyethylene glycol*. 1st ed. Cambridge, UK: Woodhead Publishing; 2018.
7. García MC. Stimuli-responsive polymersomes for drug delivery applications. In: Makhlouf ASH, Abu-Thabit NY, editors. *Stimuli responsive polymeric nanocarriers for drug delivery applications*. Cambridge, UK: Elsevier; 2019. p. 345–92.
8. García MC. Ionic-strength-responsive polymers for drug delivery applications. In: Makhlouf ASH, Abu-Thabit NY, editors. *Stimuli responsive polymeric nanocarriers for drug delivery applications*. Cambridge, UK: Elsevier; 2019. p. 393–409.
9. García MC. Nano-and microparticles as drug carriers. In: *Engineering drug delivery Systems*. Cambridge, UK: Elsevier; 2020. p. 71–110.
10. García MC, Aloisio C, Onnainty R, Ullio-Gamboa G. Self assembled nanomaterials. In: Narayan R, editor. *Nanobiomaterials: Nanostructured materials for biomedical applications*. 1st ed. Cambridge, UK: Elsevier; 2018.
11. García MC, Quiroz F. Nanostructured polymers. In: Narayan R, editor. *Nanobiomaterials: Nanostructured materials for biomedical applications*. Cambridge, UK: Elsevier; 2018. p. 339–56.
12. Thomas RG, Jeong YY. Stimuli-responsive nano drug delivery systems for anticancer therapy. In: *Biomimetic nanoengineered materials for advanced drug delivery*. Elsevier; 2019. p. 125–48.
13. Thakkar S, Sharma D, Kalia K, Tekade RK. Tumor microenvironment targeted nanotherapeutics for cancer therapy and diagnosis: a review. *Acta Biomater* 2020;**101**:43–68.
14. Sharma AK, Prasher P, Aljabali AA, Mishra V, Gandhi H, Kumar S, Mutalik S, Chellappan DK, Tambuwala MM, Dua KJDD. *Emerging era of "Somes": Polymersomes as Versatile Drug Delivery Carrier for Cancer Diagnostics and Therapy*. Drug Delivery & Translational Research; 2020.
15. Berbezier I, De Crescenzi M. *Self-Assembly of NanoStructures and NanoMaterials*. Beilstein-Institut; 2015. p. 2190–4286.
16. Fratoddi I, Bearzotti A, Venditti I, Cametti C, Russo M. Role of nanostructured polymers on the improvement of electrical response-based relative humidity sensors. *Sens Actuator B Chem* 2016;**225**:96–108.
17. Habibi N, Kamaly N, Memic A, Shafiee H. Self-assembled peptide-based nanostructures: smart nanomaterials toward targeted drug delivery. *Nano Today* 2016;**11**(1):41–60.

18. Wang F, Akimov YA, Khoo EH, He C. π−π interactions mediated self-assembly of gold nanoparticles into single crystalline superlattices in solution. *RSC Adv* 2015;**5**(110):90766−71.
19. Peponi L, Puglia D, Torre L, Valentini L, Kenny JM. Processing of nanostructured polymers and advanced polymeric based nanocomposites. *Mater Sci Eng R Rep* 2014;**85**:1−46.
20. Davis KA, Matyjaszewski K. ABC triblock copolymers prepared using atom transfer radical polymerization techniques. *Macromol* 2001;**34**(7):2101−7.
21. Letchford K, Burt H. A review of the formation and classification of amphiphilic block copolymer nanoparticulate structures: micelles, nanospheres, nanocapsules and polymersomes. *Eur J Pharm Biopharm* 2007;**65**(3):259−69.
22. Tang Z, He C, Tian H, Ding J, Hsiao BS, Chu B, Chen X. Polymeric nanostructured materials for biomedical applications. *Prog Polym Sci* 2016;**60**:86−128.
23. Blanazs A, Armes SP, Ryan AJ. Self-assembled block copolymer aggregates: from micelles to vesicles and their biological applications. *Macromol Rapid Commun* 2009;**30**(4-5):267−77.
24. Mountrichas G, Petrov P, Pispas S, Rangelov S. Nano-sized polymer structures via self-assembly and co-assembly approaches. In: Fakirov S, editor. *Nano-Size Polymers. Preparation, Properties, Applications*. Switzerland: Springer; 2016. p. 19−48.
25. Guan L, Rizzello L, Battaglia G. Polymersomes and their applications in cancer delivery and therapy. *Nanomed* 2015;**10**(17):2757−80.
26. Zhang Y, Ren T, Gou J, Zhang L, Tao X, Tian B, et al. Strategies for improving the payload of small molecular drugs in polymeric micelles. *J Contr Release* 2017;**261**:352−66.
27. Egusquiaguirre SP, Igartua M, Hernández RM, Pedraz JL. Nanoparticle delivery systems for cancer therapy: advances in clinical and preclinical research. *Clin Transl Oncol* 2012;**14**(2):83−93.
28. Martins AM, Elgaili SA, Vitor RF, Husseini GA. Ultrasonic drug delivery using micelles and liposomes. In: Ashokkumar M, editor. *Handbook of ultrasonics and sonochemistry*. Springer Science+Business Media; 2015.
29. Bobo D, Robinson KJ, Islam J, Thurecht KJ, Corrie SR. Nanoparticle-based medicines: a review of FDA-approved materials and clinical trials to date. *Pharmaceut Res* 2016;**33**(10):2373−87.
30. Steichen SD, Caldorera-Moore M, Peppas NA. A review of current nanoparticle and targeting moieties for the delivery of cancer therapeutics. *Eur J Pharmaceut Sci* 2013;**48**(3):416−27.
31. Calixto G, Bernegossi J, Fonseca-Santos B, Chorilli M. Nanotechnology-based drug delivery systems for treatment of oral cancer: a review. *Int J Nanomed* 2014:3719−35.
32. Malmsten M. *Surfactants and polymers in drug delivery*. CRC Press; 2002.
33. Malmsten M. Phase transformations in self-assembly systems for drug delivery applications. *J Dispersion Sci Technol* 2007;**28**(1):63−72.
34. Mu X, Gan S, Wang Y, Li H, Zhou G. Stimulus-responsive vesicular polymer nano-integrators for drug and gene delivery. *Int J Nanomed* 2019;**14**:5415.
35. Bleul R, Thiermann R, Maskos M. Techniques to control polymersome size. *Macromol* 2015;**48**(20):7396−409.
36. Thambi T, Park JH, Lee DS. Stimuli-responsive polymersomes for cancer therapy. *Biomater Sci* 2016;**4**(1):55−69.
37. Palivan CG, Goers R, Najer A, Zhang X, Car A, Meier W. Bioinspired polymer vesicles and membranes for biological and medical applications. *Chem Soc Rev* 2016;**45**(2):377−411.
38. Ahmed F, Pakunlu RI, Brannan A, Bates F, Minko T, Discher DE. Biodegradable polymersomes loaded with both paclitaxel and doxorubicin permeate and shrink tumors, inducing apoptosis in proportion to accumulated drug. *J Contr Release* 2006;**116**(2):150−8.
39. Sanson C, Diou O, Thevenot J, Ibarboure E, Soum A, Brûlet A, Miraux S, Thiaudière E, Tan S, Brisson A. Doxorubicin loaded magnetic polymersomes: theranostic nanocarriers for MR imaging and magneto-chemotherapy. *ACS Nano* 2011;**5**(2):1122−40.
40. Chiang W-H, Huang W-C, Chang C-W, Shen M-Y, Shih Z-F, Huang Y-F, Lin S-C, Chiu H-C. Functionalized polymersomes with outlayered polyelectrolyte gels for potential tumor-targeted delivery of multimodal therapies and MR imaging. *J Contr Release* 2013;**168**(3):280−8.
41. Pearson R, Avila-Olias M, Joseph A, Nyberg S, Battaglia G. Smart polymersomes: formation, characterisation and. *Smart Mater Drug Deliv* 2013;**1**:179.
42. Wang L, Liu G, Wang X, Hu J, Zhang G, Liu S. Acid-disintegratable polymersomes of pH-responsive amphiphilic diblock copolymers for intracellular drug delivery. *Macromol* 2015;**48**(19):7262−72.

43. Du Y, Chen W, Zheng M, Meng F, Zhong Z. pH-sensitive degradable chimaeric polymersomes for the intracellular release of doxorubicin hydrochloride. *Biomater* 2012;**33**(29):7291–9.
44. Zhan F, Chen W, Wang Z, Lu W, Cheng R, Deng C, Meng F, Liu H, Zhong Z. Acid-activatable prodrug nanogels for efficient intracellular doxorubicin release. *Biomacromol* 2011;**12**(10):3612–20.
45. Li S, Meng F, Wang Z, Zhong Y, Zheng M, Liu H, Zhong Z. Biodegradable polymersomes with an ionizable membrane: facile preparation, superior protein loading, and endosomal pH-responsive protein release. *Eur J Pharm Biopharm* 2012;**82**(1):103–11.
46. Rodríguez-Hernández J, Lecommandoux S. Reversible inside– out micellization of pH-responsive and water-soluble vesicles based on polypeptide diblock copolymers. *J Am Chem Soc* 2005;**127**(7):2026–7.
47. Deng H, Liu J, Zhao X, Zhang Y, Liu J, Xu S, Deng L, Dong A, Zhang J. PEG-b-PCL copolymer micelles with the ability of pH-controlled negative-to-positive charge reversal for intracellular delivery of doxorubicin. *Biomacromol* 2014;**15**(11):4281–92.
48. Hu X, Zhang Y, Xie Z, Jing X, Bellotti A, Gu Z. Stimuli-responsive polymersomes for biomedical applications. *Biomacromol* 2017;**18**(3):649–73.
49. Zhu L, Zhao L, Qu X, Yang Z. PH-sensitive polymeric vesicles from coassembly of amphiphilic cholate grafted poly (l-lysine) and acid-cleavable polymer–drug conjugate. *Langmuir* 2012;**28**(33):11988–96.
50. Che H, van Hest JC. Stimuli-responsive polymersomes and nanoreactors. *J Mater Chem B* 2016;**4**(27):4632–47.
51. Du J, Armes SP. pH-responsive vesicles based on a hydrolytically self-cross-linkable copolymer. *J Am Chem Soc* 2005;**127**(37):12800–1.
52. Huang F, Cheng R, Meng F, Deng C, Zhong Z. Micelles based on acid degradable poly (acetal urethane): preparation, pH-sensitivity, and triggered intracellular drug release. *Biomacromol* 2015;**16**(7):2228–36.
53. Dan K, Ghosh S. One-pot synthesis of an acid-labile amphiphilic triblock copolymer and its pH-responsive vesicular assembly. *Angew Chem Int Ed* 2013;**52**(28):7300–5.
54. Li X, Yang W, Zou Y, Meng F, Deng C, Zhong Z. Efficacious delivery of protein drugs to prostate cancer cells by PSMA-targeted pH-responsive chimaeric polymersomes. *J Contr Release* 2015;**220**:704–14.
55. Liu F, Eisenberg A. Preparation and pH triggered inversion of vesicles from poly (acrylic acid)-b lock-polystyrene-b lock-Poly (4-vinyl pyridine). *J Am Chem Soc* 2003;**125**(49):15059–64.
56. Chécot F, Lecommandoux S, Gnanou Y, Klok HA. Water-soluble stimuli-responsive vesicles from peptide-based diblock copolymers. *Angew Chem* 2002;**114**(8):1395–9.
57. Kukula H, Schlaad H, Antonietti M, Förster S. The formation of polymer vesicles or "Peptosomes" by polybutadiene-b lock-poly (l-glutamate) s in dilute aqueous solution. *J Am Chem Soc* 2002;**124**(8):1658–63.
58. Sanson C, Schatz C, Le Meins J-F o, Brûlet A, Soum A, Lecommandoux Sb. Biocompatible and biodegradable poly (trimethylene carbonate)-b-poly (L-glutamic acid) polymersomes: size control and stability. *Langmuir* 2009;**26**(4):2751–60.
59. Sanson C, Schatz C, Le Meins J-F, Soum A, Thévenot J, Garanger E, Lecommandoux S. A simple method to achieve high doxorubicin loading in biodegradable polymersomes. *J Contr Release* 2010;**147**(3):428–35.
60. Anraku Y, Kishimura A, Oba M, Yamasaki Y, Kataoka K. Spontaneous formation of nanosized unilamellar polyion complex vesicles with tunable size and properties. *J Am Chem Soc* 2010;**132**(5):1631–6.
61. Wang Q-M, Gao Z, Liu S, Fan B, Kang L, Huang W, Jin M. Hybrid polymeric micelles based on bioactive polypeptides as pH-responsive delivery systems against melanoma. *Biomaterials* 2014;**35**(25):7008–21.
62. Habraken GJ, Peeters M, Thornton PD, Koning CE, Heise A. Selective enzymatic degradation of self-assembled particles from amphiphilic block copolymers obtained by the combination of N-carboxyanhydride and nitroxide-mediated polymerization. *Biomacromolecules* 2011;**12**(10):3761–9.
63. Harnoy AJ, Rosenbaum I, Tirosh E, Ebenstein Y, Shaharabani R, Beck R, Amir RJ. Enzyme-responsive amphiphilic PEG-dendron hybrids and their assembly into smart micellar nanocarriers. *J Am Chem Soc* 2014;**136**(21):7531–4.
64. Aluri R, Jayakannan M. Development of l-tyrosine-based enzyme-responsive amphiphilic poly (ester-urethane) nanocarriers for multiple drug delivery to cancer cells. *Biomacromol* 2017;**18**(1):189–200.
65. Malhotra M, Surnar B, Jayakannan M. Polymer topology driven enzymatic biodegradation in polycaprolactone block and random copolymer architectures for drug delivery to cancer cells. *Macromol* 2016;**49**(21):8098–112.
66. Lee JS, Groothuis T, Cusan C, Mink D, Feijen J. Lysosomally cleavable peptide-containing polymersomes modified with anti-EGFR antibody for systemic cancer chemotherapy. *Biomater* 2011;**32**(34):9144–53.

67. Zhang C, Pan D, Li J, Hu J, Bains A, Guys N, Zhu H, Li X, Luo K, Gong Q. Enzyme-responsive peptide dendrimer-gemcitabine conjugate as a controlled-release drug delivery vehicle with enhanced antitumor efficacy. *Acta Biomater* 2017;**55**:153–62.
68. Ke W, Li J, Zhao K, Zha Z, Han Y, Wang Y, Yin W, Zhang P, Ge Z. Modular design and facile synthesis of enzyme-responsive peptide-linked block copolymers for efficient delivery of doxorubicin. *Biomacromol* 2016;**17**(10):3268–76.
69. Yu H, Chen J, Liu S, Lu Q, He J, Zhou Z, Hu Y. Enzyme sensitive, surface engineered nanoparticles for enhanced delivery of camptothecin. *J Contr Release* 2015;**216**:111–20.
70. Pramod P, Takamura K, Chaphekar S, Balasubramanian N, Jayakannan M. Dextran vesicular carriers for dual encapsulation of hydrophilic and hydrophobic molecules and delivery into cells. *Biomacromol* 2012;**13**(11):3627–40.
71. Pramod P, Shah R, Chaphekar S, Balasubramanian N, Jayakannan M. Polysaccharide nano-vesicular multidrug carriers for synergistic killing of cancer cells. *Nanoscale* 2014;**6**(20):11841–55.
72. Pramod P, Shah R, Jayakannan M. Dual stimuli polysaccharide nanovesicles for conjugated and physically loaded doxorubicin delivery in breast cancer cells. *Nanoscale* 2015;**7**(15):6636–52.
73. Trachootham D, Alexandre J, Huang P. Targeting cancer cells by ROS-mediated mechanisms: a radical therapeutic approach? *Nat Rev Drug Discov* 2009;**8**(7):579–91.
74. Sabharwal SS, Schumacker PT. Mitochondrial ROS in cancer: initiators, amplifiers or an Achilles' heel? *Nat Rev Cancer* 2014;**14**(11):709–21.
75. Napoli A, Valentini M, Tirelli N, Müller M, Hubbell JA. Oxidation-responsive polymeric vesicles. *Nat Mater* 2004;**3**(3):183.
76. Scott EA, Stano A, Gillard M, Maio-Liu AC, Swartz MA, Hubbell JA. Dendritic cell activation and T cell priming with adjuvant-and antigen-loaded oxidation-sensitive polymersomes. *Biomater* 2012;**33**(26):6211–9.
77. Deng Z, Qian Y, Yu Y, Liu G, Hu J, Zhang G, Liu S. Engineering intracellular delivery nanocarriers and nanoreactors from oxidation-responsive polymersomes via synchronized bilayer cross-linking and permeabilizing inside live cells. *J Am Chem Soc* 2016;**138**(33):10452–66.
78. Song CC, Ji R, Du F-S, Liang DH, Li ZC. Oxidation-accelerated hydrolysis of the ortho ester-containing acid-labile polymers. *ACS Macro Lett* 2013;**2**(3):273–7.
79. Greten FR, Grivennikov SI. Inflammation and cancer: triggers, mechanisms, and consequences. *Immunity* 2019;**51**(1):27–41.
80. Jäiger Ez, Sincari V, Albuquerque LJ, Jager A, Humajova J, Kucka J, Pankrac J, Paral P, Heizer T, Janouskova O. Reactive oxygen species (ROS)-responsive polymersomes with site-specific chemotherapeutic delivery into tumors via spacer design chemistry. *Biomacromol* 2020;**21**(4):1437–49.
81. Ma N, Li Y, Xu H, Wang Z, Zhang X. Dual redox responsive assemblies formed from diselenide block copolymers. *J Am Chem Soc* 2010;**132**(2):442–3.
82. Wang L, Cao W, Xu H. Tellurium-containing polymers: towards biomaterials and optoelectronic materials. *ChemNanoMat* 2016;**2**(6):479–88.
83. Cao W, Wang L, Xu H. Selenium/tellurium containing polymer materials in nanobiotechnology. *Nano Today* 2015;**10**(6):717–36.
84. Wen HY, Dong HQ, Xie WJ, Li YY, Wang K, Pauletti GM, Shi DL. Rapidly disassembling nanomicelles with disulfide-linked PEG shells for glutathione-mediated intracellular drug delivery. *Chem Commun* 2011;**47**(12):3550–2.
85. Wen H, Li Y. Redox sensitive nanoparticles with disulfide bond linked sheddable shell for intracellular drug delivery. *Med Chem* 2014;**4**:748–55.
86. Li Y, Lei X, Dong H, Ren T. Sheddable, degradable, cationic micelles enabling drug and gene delivery. *RSC Adv* 2014;**4**(16):8165–76.
87. Wang Y-C, Wang F, Sun T-M, Wang J. Redox-responsive nanoparticles from the single disulfide bond-bridged block copolymer as drug carriers for overcoming multidrug resistance in cancer cells. *Bioconj Chem* 2011;**22**(10):1939–45.
88. Zhao D, Wu J, Li C, Zhang H, Li Z, Luan Y. Precise ratiometric loading of PTX and DOX based on redox-sensitive mixed micelles for cancer therapy. *Colloids Surf B Biointerfaces* 2017;**155**:51–60.

89. Kumar B, Priyadarshi R, Deeba F, Kulshreshtha A, Kumar A, Agrawal G, Gopinath P, Negi YS. Redox responsive xylan-SS-curcumin prodrug nanoparticles for dual drug delivery in cancer therapy. *Mater Sci Eng C* 2020;**107**:110356.
90. Hu X, Hu J, Tian J, Ge Z, Zhang G, Luo K, Liu S. Polyprodrug amphiphiles: hierarchical assemblies for shape-regulated cellular internalization, trafficking, and drug delivery. *J Am Chem Soc* 2013;**135**(46):17617−29.
91. Li YL, Zhu L, Liu Z, Cheng R, Meng F, Cui JH, Ji SJ, Zhong Z. Reversibly stabilized multifunctional dextran nanoparticles efficiently deliver doxorubicin into the nuclei of cancer cells. *Angew Chem Int Ed* 2009;**48**(52):9914−8.
92. Thambi T, Deepagan V, Ko H, Lee DS, Park JH. Bioreducible polymersomes for intracellular dual-drug delivery. *J Mater Chem* 2012;**22**(41):22028−36.
93. Sun H, Meng F, Cheng R, Deng C, Zhong Z. Reduction and pH dual-bioresponsive crosslinked polymersomes for efficient intracellular delivery of proteins and potent induction of cancer cell apoptosis. *Acta Biomater* 2014;**10**(5):2159−68.
94. Jia L, Cui D, Bignon J, Di Cicco A, Wdzieczak-Bakala J, Liu J, Li M-H. Reduction-responsive cholesterol-based block copolymer vesicles for drug delivery. *Biomacromol* 2014;**15**(6):2206−17.
95. Zou Y, Meng F, Deng C, Zhong Z. Robust, tumor-homing and redox-sensitive polymersomal doxorubicin: a superior alternative to Doxil and Caelyx? *J Contr Release* 2016;**239**:149−58.
96. Qin Y, Zhang Z, Huang C, Fan F, Liu L, Lu L, Wang H, Liu Z, Yang J, Wang C. Folate-targeted redox-responsive polymersomes loaded with chemotherapeutic drugs and tariquidar to overcome drug resistance. *J Biomed Nanotechnol* 2018;**14**(10):1705−18.
97. Bej R, Sarkar J, Ray D, Aswal VK, Ghosh S. Morphology regulation in redox destructible amphiphilic block copolymers and impact on intracellular drug delivery. *Macromol Biosci* 2018;**18**(7):1800057.
98. Wei Y, Gu X, Sun Y, Meng F, Storm G, Zhong Z. Transferrin-binding peptide functionalized polymersomes mediate targeted doxorubicin delivery to colorectal cancer in vivo. *J Contr Release* 2020;**319**:407−15.
99. Zhong Y, Meng F, Zhang W, Li B, van Hest JC, Zhong Z. CD44-targeted vesicles encapsulating granzyme B as artificial killer cells for potent inhibition of human multiple myeloma in mice. *J Contr Release* 2020;**320**:421−30.
100. Onaca O, Enea R, Hughes DW, Meier W. Stimuli-responsive polymersomes as nanocarriers for drug and gene delivery. *Macromol Biosci* 2009;**9**(2):129−39.
101. Ward MA, Georgiou TK. Thermoresponsive polymers for biomedical applications. *Polym* 2011;**3**(3):1215−42.
102. Li G, Guo L, Meng Y, Zhang T. Self-assembled nanoparticles from thermo-sensitive polyion complex micelles for controlled drug release. *Chem Eng J* 2011;**174**(1):199−205.
103. Li W, Li J, Gao J, Li B, Xia Y, Meng Y, Yu Y, Chen H, Dai J, Wang H. The fine-tuning of thermosensitive and degradable polymer micelles for enhancing intracellular uptake and drug release in tumors. *Biomater* 2011;**32**(15):3832−44.
104. Chen H, Li B, Qiu J, Li J, Jin J, Dai S, Ma Y, Gu Y. Thermal responsive micelles for dual tumor-targeting imaging and therapy. *Nanoscale* 2013;**5**(24):12409−24.
105. Luo Y-L, Yang X-L, Xu F, Chen Y-S, Zhang B. Thermosensitive PNIPAM-b-HTPB block copolymer micelles: molecular architectures and camptothecin drug release. *Colloids Surf B Biointerfaces* 2014;**114**:150−7.
106. Panja S, Dey G, Bharti R, Kumari K, Maiti T, Mandal M, Chattopadhyay S. Tailor-made temperature-sensitive micelle for targeted and on-demand release of anticancer drugs. *ACS Appl Mater Interfaces* 2016;**8**(19):12063−74.
107. Qin S, Geng Y, Discher DE, Yang S. Temperature-controlled assembly and release from polymer vesicles of poly (ethylene oxide)-block-poly (N-isopropylacrylamide). *Adv Mater* 2006;**18**(21):2905−9.
108. Xu H, Meng F, Zhong Z. Reversibly crosslinked temperature-responsive nano-sized polymersomes: synthesis and triggered drug release. *J Mater Chem* 2009;**19**(24):4183−90.
109. Moughton AO, O'Reilly RK. Thermally induced micelle to vesicle morphology transition for a charged chain end diblock copolymer. *Chem Commun* 2010;**46**(7):1091−3.
110. Huang X, Li M, Green DC, Williams DS, Patil AJ, Mann S. Interfacial assembly of protein−polymer nanoconjugates into stimulus-responsive biomimetic protocells. *Nat Commun* 2013;**4**:2239.
111. Johnson RP, Preman NK. Responsive block copolymers for drug delivery applications. Part 1: endogenous stimuli-responsive drug-release systems. In: Makhlouf ASH, Abu-Thabit NY, editors. *Stimuli responsive polymeric nanocarriers for drug delivery applications*, Vol 1. Cambridge, UK: Elsevier; 2018. p. 171−220.
112. Liu F, Kozlovskaya V, Medipelli S, Xue B, Ahmad F, Saeed M, Cropek D, Kharlampieva E. Temperature-sensitive polymersomes for controlled delivery of anticancer drugs. *Chem Mater* 2015;**27**(23):7945−56.

113. Kozlovskaya V, Liu F, Yang Y, Ingle K, Qian S, Halade GV, Urban VS, Kharlampieva E. Temperature-responsive polymersomes of poly (3-methyl-N-vinylcaprolactam)-block-poly (N-vinylpyrrolidone) to decrease doxorubicin-induced cardiotoxicity. *Biomacromol* 2019;**20**(10):3989–4000.
114. Sanson C, Le Meins J-F, Schatz C, Soum A, Lecommandoux S. Temperature responsive poly (trimethylene carbonate)-block-poly (L-glutamic acid) copolymer: polymersomes fusion and fission. *Soft Matter* 2010;**6**(8):1722–30.
115. Naik SS, Ray JG, Savin DA. Temperature-and pH-responsive self-assembly of poly (propylene oxide)-b-poly (lysine) block copolymers in aqueous solution. *Langmuir* 2011;**27**(11):7231–40.
116. Qiao Z-Y, Ji R, Huang X-N, Du F-S, Zhang R, Liang D-H, Li Z-C. Polymersomes from dual responsive block copolymers: drug encapsulation by heating and acid-triggered release. *Biomacromolecules* 2013;**14**(5):1555–63.
117. Hsu SP, Chu IM, Yang JD. Thermo-and pH-Responsive Polymersomes of Poly (α, β-N-substituted-DL-aspartamide) s. *J Appl Polym Sci* 2012;**125**(1):133–44.
118. Lai MH, Jeong JH, DeVolder RJ, Brockman C, Schroeder C, Kong H. Ellipsoidal polyaspartamide polymersomes with enhanced cell-targeting ability. *Adv Funct Mater* 2012;**22**(15):3239–46.
119. Agut W, Brûlet A, Schatz C, Taton D, Lecommandoux S. pH and temperature responsive polymeric micelles and polymersomes by self-assembly of poly [2-(dimethylamino) ethyl methacrylate]-b-poly (glutamic acid) double hydrophilic block copolymers. *Langmuir* 2010;**26**(13):10546–54.
120. Yan J-J, Wang X-Y, Wang M-Z, Pan D-H, Yang R-L, Xu Y-P, Wang L-Z, Yang M. Self-assembling nonconjugated poly (amide-imide) into thermoresponsive nanovesicles with unexpected red fluorescence for bioimaging. *Biomacromol* 2019;**20**(3):1455–63.
121. Li F, Qin Y, Lee J, Liao H, Wang N, Davis TP, et al. Stimuli-responsive nano-assemblies for remotely controlled drug delivery. *J Contr Release* 2020;**322**(14).
122. Pearson S, Vitucci D, Khine YY, Dag A, Lu H, Save M, Billon L, Stenzel MH. Light-responsive azobenzene-based glycopolymer micelles for targeted drug delivery to melanoma cells. *Eur Polym J* 2015;**69**:616–27.
123. Bai Y, Liu CP, Song X, Zhuo L, Bu H, Tian W. Photo-and pH-dual-responsive β-cyclodextrin-based supramolecular prodrug complex self-assemblies for programmed drug delivery. *Chem–Asian J* 2018;**13**(24):3903–11.
124. Lin L, Yan Z, Gu J, Zhang Y, Feng Z, Yu Y. UV-Responsive behavior of azopyridine-containing diblock copolymeric vesicles: photoinduced fusion, disintegration and rearrangement. *Macromol Rapid Commun* 2009;**30**(13):1089–93.
125. Mabrouk E, Cuvelier D, Brochard-Wyart F, Nassoy P, Li M-H. Bursting of sensitive polymersomes induced by curling. *Proc Natl Acad Sci USA* 2009;**106**(18):7294–8.
126. Su W, Han K, Luo Y, Wang Z, Li Y, Zhang Q. Formation and photoresponsive properties of giant microvesicles assembled from azobenzene-containing amphiphilic diblock copolymers. *Macromol Chem Phys* 2007;**208**(9):955–63.
127. Su W, Luo Y, Yan Q, Wu S, Han K, Zhang Q, Gu Y, Li Y. Photoinduced fusion of micro-vesicles self-assembled from azobenzene-containing amphiphilic diblock copolymers. *Macromol Rapid Commun* 2007;**28**(11):1251–6.
128. Jin Q, Liu G, Liu X, Ji J. Photo-responsive supramolecular self-assembly and disassembly of an azobenzene-containing block copolymer. *Soft Matter* 2010;**6**(21):5589–95.
129. Blasco E, Serrano JL, Pinol M, Oriol L. Light responsive vesicles based on linear–dendritic block copolymers using azobenzene–aliphatic codendrons. *Macromol* 2013;**46**(15):5951–60.
130. Blasco E, Piñol M, Oriol L. Responsive linear-dendritic block copolymers. *Macromol Rapid Commun* 2014;**35**(12):1090–115.
131. Blasco E, del Barrio J, Sánchez-Somolinos C, Piñol M, Oriol L. Light induced molecular release from vesicles based on amphiphilic linear-dendritic block copolymers. *Polym Chem* 2013;**4**(7):2246–54.
132. Xia D, Yu G, Li J, Huang F. Photo-responsive self-assembly based on a water-soluble pillar [6] arene and an azobenzene-containing amphiphile in water. *Chem Commun* 2014;**50**(27):3606–8.
133. Hu C, Ma N, Li F, Fang Y, Liu Y, Zhao L, Qiao S, Li X, Jiang X, Li T. Cucurbit [8] uril-based giant supramolecular vesicles: highly stable, versatile carriers for photoresponsive and targeted drug delivery. *ACS Appl Mater Interfaces* 2018;**10**(5):4603–13.
134. Wang B, Chen K, Yang R, Yang F, Liu J. Stimulus-responsive polymeric micelles for the light-triggered release of drugs. *Carbohydr Polym* 2014;**103**:510–9.

135. Wang X, Hu J, Liu G, Tian J, Wang H, Gong M, Liu S. Reversibly switching bilayer permeability and release modules of photochromic polymersomes stabilized by cooperative noncovalent interactions. *J Am Chem Soc* 2015;**137**(48):15262–75.
136. Kwangmettatam S, Kudernac T. Light-fuelled reversible expansion of spiropyran-based vesicles in water. *Chem Commun* 2018;**54**(42):5311–4.
137. Jin Q, Cai T, Wang Y, Wang H, Ji J. Light-responsive polyion complex micelles with switchable surface charge for efficient protein delivery. *ACS Macro Lett* 2014;**3**(7):679–83.
138. Liu G, Wang X, Hu J, Zhang G, Liu S. Self-immolative polymersomes for high-efficiency triggered release and programmed enzymatic reactions. *J Am Chem Soc* 2014;**136**(20):7492–7.
139. Yamamoto S, Yamada T, Kubo G, Sakurai K, Yamaguchi K, Nakanishi J. Preparation of a series of photoresponsive polymersomes bearing photocleavable a 2-nitrobenzyl group at the hydrophobic/hydrophilic interfaces and their payload releasing behaviors. *Polym* 2019;**11**(8):1254.
140. Zhang C, Wang Y, Zhao Y, Liu H, Zhao Y, Li X, Lin Q. Biodegradable micelles for NIR/GSH-Triggered chemophototherapy of cancer. *Nanomater* 2019;**9**(1):91.
141. Yan B, Boyer J-C, Branda NR, Zhao Y. Near-infrared light-triggered dissociation of block copolymer micelles using upconverting nanoparticles. *J Am Chem Soc* 2011;**133**(49):19714–7.
142. Ding H, Lv Y, Ni D, Wang J, Tian Z, Wei W, Ma G. Erythrocyte membrane-coated NIR-triggered biomimetic nanovectors with programmed delivery for photodynamic therapy of cancer. *Nanoscale* 2015;**7**(21):9806–15.
143. Hribar KC, Lee MH, Lee D, Burdick JA. Enhanced release of small molecules from near-infrared light responsive polymer– nanorod composites. *ACS Nano* 2011;**5**(4):2948–56.
144. Lin J, Wang S, Huang P, Wang Z, Chen S, Niu G, Li W, He J, Cui D, Lu G. Photosensitizer-loaded gold vesicles with strong plasmonic coupling effect for imaging-guided photothermal/photodynamic therapy. *ACS Nano* 2013;**7**(6):5320–9.
145. Song J, Cheng L, Liu A, Yin J, Kuang M, Duan H. Plasmonic vesicles of amphiphilic gold nanocrystals: self-assembly and external-stimuli-triggered destruction. *J Am Chem Soc* 2011;**133**(28):10760–3.
146. He J, Zhang P, Babu T, Liu Y, Gong J, Nie Z. Near-infrared light-responsive vesicles of Au nanoflowers. *Chem Commun* 2013;**49**(6):576–8.
147. Tang Q, Hu P, Peng H, Zhang N, Zheng Q, He Y. Near-infrared laser-triggered, self-immolative smart polymersomes for in vivo cancer therapy. *Int J NanoMed* 2020;**15**:137.
148. Oliveira H, Pérez-Andrés E, Thevenot J, Sandre O, Berra E, Lecommandoux S. Magnetic field triggered drug release from polymersomes for cancer therapeutics. *J Contr Release* 2013;**169**(3):165–70.
149. Lecommandoux S, Sandre O, Chécot F, Rodriguez-Hernandez J, Perzynski R. Magnetic nanocomposite micelles and vesicles. *Adv Mater* 2005;**17**(6):712–8.
150. Krack M, Hohenberg H, Kornowski A, Lindner P, Weller H, Förster S. Nanoparticle-loaded magnetophoretic vesicles. *J Am Chem Soc* 2008;**130**(23):7315–20.
151. Yang X, Grailer JJ, Rowland IJ, Javadi A, Hurley SA, Steeber DA, Gong S. Multifunctional SPIO/DOX-loaded wormlike polymer vesicles for cancer therapy and MR imaging. *Biomater* 2010;**31**(34):9065–73.
152. Liu Q, Chen S, Chen J, Du J. An asymmetrical polymer vesicle strategy for significantly improving T 1 MRI sensitivity and cancer-targeted drug delivery. *Macromol* 2015;**48**(3):739–49.
153. Hickey RJ, Haynes AS, Kikkawa JM, Park S-J. Controlling the self-assembly structure of magnetic nanoparticles and amphiphilic block-copolymers: from micelles to vesicles. *J Am Chem Soc* 2011;**133**(5):1517–25.
154. Mart RJ, Liem KP, Webb SJ. Magnetically-controlled release from hydrogel-supported vesicle assemblies. *Chem Commun* 2009;**17**:2287–9.
155. Meeuwissen SA, Kim KT, Chen Y, Pochan DJ, van Hest J. Controlled shape transformation of polymersome stomatocytes. *Angew Chem Int Ed* 2011;**50**(31):7070–3.
156. Van Rhee P, Rikken R, Abdelmohsen L, Maan J, Nolte R, Van Hest J, Christianen P, Wilson D. Polymersome magneto-valves for reversible capture and release of nanoparticles. *Nat Commun* 2014;**5**:5010.
157. Kim KT, Zhu J, Meeuwissen SA, Cornelissen JJ, Pochan DJ, Nolte RJ, van Hest JC. Polymersome stomatocytes: controlled shape transformation in polymer vesicles. *J Am Chem Soc* 2010;**132**(36):12522–4.
158. Roger S, Harmen H, Roeland J, ávan Hest JC, Peter C. Probing morphological changes in polymersomes with magnetic birefringence. *Chem Commun* 2014;**50**(40):5394–6.
159. Pourjavadi A, Mazaheri Tehrani Z, Dastanpour L. Smart magnetic self-assembled micelle: an effective nanocarrier for thermo-triggered paclitaxel delivery. *Int J Polym Mater Polym Biomater* 2019;**68**(12):741–9.

160. Zhou W, Meng F, Engbers G, Feijen J. Biodegradable polymersomes for targeted ultrasound imaging. *J Contr Release* 2006;**116**(2):e62–4.
161. Chen W, Du J. Ultrasound and pH dually responsive polymer vesicles for anticancer drug delivery. *Sci Rep* 2013;**3**:2162.
162. Yan Q, Yuan J, Cai Z, Xin Y, Kang Y, Yin Y. Voltage-responsive vesicles based on orthogonal assembly of two homopolymers. *J Am Chem Soc* 2010;**132**(27):9268–70.
163. Jang HJ, Thambi T, Sivasubramanian M, Byun JH, Ahn JY, Chae SY, Jo D-G, Jeong JH, Lee KC, Park JH. β-cyclodextrin-bearing glycol chitosan for long-acting formulation of an exenatide derivative. *Macromol Res* 2014;**22**(8):816–9.

This page intentionally left blank

CHAPTER

18

Nanoparticles in oral health care: clinical insights and future perspectives

Anurag Satpathy[1,2], *Punyatoya Panda*[2], *Reetuparna Nanda*[2], *Subhashree Priyadarsini*[2] *and Monalisa Mishra*[2]

[1]**Neural Developmental Biology Lab, Department of Life Science, NIT Rourkela, Rourkela, Odisha, India;** [2]**Siksha O Anusandhan University, Bhubaneshwar, Odisha, India**

1. Introduction

Oral health is pivotal to common fitness, wellbeing, and superiority of life. Various oral diseases include dental caries, periodontal diseases, edentulousness, maxillofacial trauma, and oral cancers.[1] These conditions are mostly preventable and can be successfully managed if detected an early stage. In the era of nanoscience, various nano-structured materials are used in diagnosis and treatment purpose.[2] Various innovative products with nanoscale properties are used in oral hygiene products and maxillofacial implants.[3] Thus, nanoscience helps to improve the invasive dentistry.

Nanoparticles (NP) with its variable physicochemical properties offer itself to use it in dental materials.[4–6] Nanoparticles have at least one dimension which is less than 100 nm.[7] Based on the shape, the nanoparticles are classified as 0D, 1D, 2D or 3D.[8] In comparison with the conventional bulk materials, nanoparticles offer improved properties due to their low stability, low coordination and unsatisfied bonds that allow them to interact with other particles effectively and with ease. Additionally, the energy level and the band gap of electrons are altered[9,10] which play a determinant role in particle energy statistics.

Applications of Multifunctional Nanomaterials
https://doi.org/10.1016/B978-0-12-820557-0.00002-3

2. Applications in oral health care: clinical insights

2.1 Oral hygiene

Oral hygiene refers to maintenance of oral cavity, that is, mouth, teeth, and gums clean. Proper oral hygiene helps to maintain a good oral health. To maintain oral hygiene in an infectious mouth, microbial dental plaque and dental calculus needs to be removed.[11] Several studies have reported that poor oral hygiene have an elevated chance of dental caries and periodontal disease. In addition, recent studies have indicated an association between some systemic diseases and poor oral hygiene.

Oral hygiene maintenance is a part of a broader dental discipline which vouches on preventive dentistry. The microbes form biofilm after it get attached to dental pellicle, and consuming proteins, lipids and sugars present within the saliva.[12] Thus, various methods needed to remove bacteria from the teeth. Using nanotechnology, various tools developed which can prevent the biofilm formation within the teeth. Various preventatives include varnishes, mouthwashes and toothpaste which have nanoparticles having antibacterial properties within it. Many nanoparticles prevent bacterial attachment on the tooth surface and thus prevent the formation of biofilm.[13]

2.1.1 Toothbrushes

Toothbrushes are the primary tool with which we mechanically disrupt the dental plaque biofilm.[14] Advances in the tooth brush design have been the subject of research since several decades. That is the reason we keep finding newer types of toothbrushes in the market. Using nanotechnology Kosho Ueshima and Yumeshokunin (a Japanese technology company) have created a toothbrush which does not need any toothpaste. Bristles of the toothbrush are 0.178 mm thick and they are further coated with mineral ions. When the toothbrush is passed over the tooth surface, the ions remove stains and in addition form a protective coating over enamel. The toothbrush can be activated by merely dipping it in water.[15] Raval et al. developed a toothbrush by gold and silver nano-colloidal particles between the bristles which they reported to have improved the mechanical plaque removal. Additionally, it exhibited an antibacterial property leading to significant reduction of periodontal disease.[16]

2.1.2 Dentifrices

More than the types of newer toothbrushes, newer dentifrices are seen occupying the supermarket stores offering a very wide range of active ingredients.[17] Dentifrices contain calcium carbonate as an abrasive agent. Abrasives are the main ingredients of a dentifrice. Thus, alterations in nano-sized calcium carbonate particle will result in differential roughness in toothpastes and their ability to remove stains, added advantage to support tooth remineralization.[18] Dentifrices with calcium carbonate (NPs) and sodium trimetaphosphate (nano-sized) (3%) can promote remineralization of primary carious lesions.[19]

An in vitro experiment showed that the microhardness values of human dental enamel was significantly increased after using dentifrice containing nano-hydroxyapatite (nHA) crystals.[20] For the first time, the toothpaste having nano-hydroxyapatite (nHA) was reported from Japan. The clinical study revealed that the caries reduced to 56% for the school children who brushed with nHA.[21]

Silver containing formulations (Ag) are used to treat variety of infectious diseases since Ag have antimicrobial effects and it is less toxic to humans.[22] Furthermore, the presence of inorganic silver does not disturb the color of the product[23,24] which is a great advantage. Ag can kill various oral bacteria like *Streptococcus mutans*, *Lactobacillus casei*, *Candida albican* and *Staphylococcus aureus*. The antibacterial activity against various mouth bacteria promote silver to be used in various toothpastes.[25–28] The small size of the nanoparticle with extremely large surface area allows it to kill the microorganisms in an efficient way.[28]

Silver ions kill the microorganisms by rupturing the cell wall,[29] cell membrane,[30] and cell envelope.[31,32] The positively charged silver ion further allows the electrostatic attraction between the bacterial cell membrane which is negatively charged. As a result, the bacterial cell membrane ruptured.[33,34] Various silver compounds like AgZ, AgZrPSi, and AgZrP also show effective antimicrobial activity against all oral microorganisms. Thus, these compounds are incorporated in dentifrices of various nano-formulations.[22]

Other than Silver, Zinc Oxide (ZnO), and Titanium Dioxide (TiO_2) NPs also have their potency to kill oral bacteria at certain concentration.[35] Further, Photoactivation of TiO_2 nanoparticles significantly enhances the antimicrobial activity against *Bacteroides fragilis*, *Pseudomonas aeruginosa, Staphylococcus aureus, Salmonella typhimurium*, and *Escherichia coli*.[36] Thus, ZnO and TiO_2 nanoparticles are added in the development of dentifrices, mouthwashes, and other oral hygiene products. These are healthier, innocuous, and effective alternatives to treat bacteria which have antibiotic resistance and can form biofilm.[35]

A dentifrice having nano-silver fluoride (NSF) can prevent *S. mutans* to adhere to the surface. Fluoride ion is known to prevent enamel demineralization by altering the pH for the dissolution of Phosphate as well as Calcium ions in the microbial biofilm and adsorbing on the apatite crystal surfaces. The Fluoride ions replace Calcium ions to form an acid-resistant mineral fluorapatite with low solubility.[37] In addition, fluoride also inhibit the activity of bacteria[38] and acid production by *S. mutans*.[39]

Fluoridated mouth rinses are used in prevention of caries. Fluoride concentration in oral fluids has a profound effect on the progression of dental caries. Sun and Chow et al.[40] in 2008 reported that addition of nano-calcium fluoride having a high reactivity and served as labile Fluoride reservoir helped to reduce caries and decrease dentine permeability.

2.2 Dental caries

Approximately 95% of the people suffer from dental caries irrespective of their age.[41,42] Management of dental caries includes restoration of lost tooth structure and prevention of newly forming carious lesions (Fig. 18.1). Dental caries is a result of loss of organic and inorganic component of tooth due to an acid produced from biofilm of cariogenic bacteria.[43,44] Various bacteria such as *Streptococci mutans* of Lactobacilli species and several actinomyces species have the ability to produce acid. In cariogenic biofilm, the low pH media favors the bacterial growth in that environment.[45]

Nanotechnology is a promising area of technology that is used for the management of dental caries. This is used at restorative level where the lost tooth structure due to cavitation is filled; and popularly it is known as "Dental Fillings." It may also be at the preventive level

FIGURE 18.1 Dental caries affecting the enamel, ddentin, and dental pulp.

to inhibit caries by controlling microbial dental plaque, bacterial acids, and enhance remineralization.

Dental composites form the majority of the dental filling materials since the Dental Amalgam use is decreased due to its toxicity (Figs. 18.2 and 18.3). In a dental composite, three different types of materials are used

1. Organic matrix: It is a polymer formed by polymerization of one or more monomer/oligomers in an organic phase.
2. Inorganic matrix: It is filler of various materials like silica, ceramic, etc. It has various sizes, shapes, and morphologies in its dispersed phase.
3. Organosilane: It is the coupling agent, required for bonding the filler with the organic resin either in interfacial or interphasial phase.

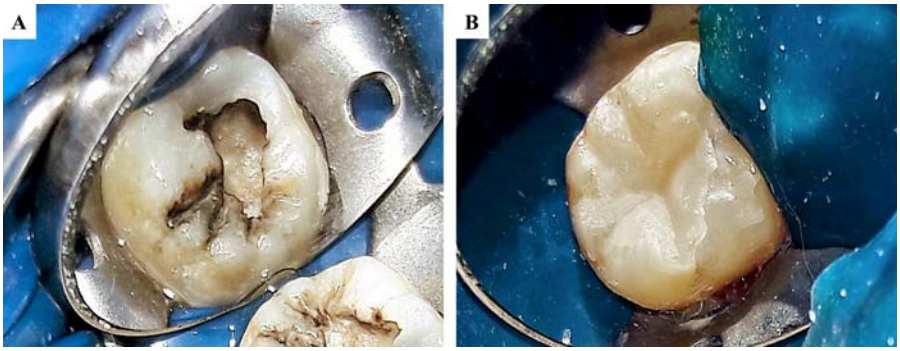

FIGURE 18.2 A: Untreated dental caries of on the occlusal aspect. B: Occlusal dental caries restored with dental composites.

FIGURE 18.3 A: Midline diastema (interdental spacing in the maxillary anterior teeth) B: Midline diastema corrected with dental composites.

Polymerization of the monomers leads to a 3-D P network. Currently used dental composites polymerize to form a hard polymerized composite by exposure of visible light (Wavelength range 400−500 nm). Camphorquinone is a photo initiator (absorption maximum at 468 nm) used by almost all manufacturers.

Acrylic resin monomers allow linear chain polymers to form. To improve the physical property of acrylic resin in 1962 Bis-GMA (bisphenol aglycidyl methacrylate) monomer developed. Early composites were chemically cured with the catalyst, for color stability. Bis-GMA is a composite resin technology. Introduction of light-activated resin material was the major breakthroughs in composite resin technology. Further, reduction in filler particle size and increment of filler load can enhance their applicability. Among the most recent innovations in composites nano-filled materials, in combination with nanometer-sized particles and nano-clusters are used in a conventional resin matrix.

There are several types of nano-fillers which are incorporated either as the sole filler or in combination[46] in dental composites such as silica,[47,48] tantalum ethoxide,[49] zirconia-silica,[50] alumina,[51] nano-fibrillar silicate,[52] titanium oxide,[53] and ordered colloidal particles are also used. In an inorganic phase, the nano-sized organic/inorganic composite are called as nano-composites. The nano-filled composites have excellent resistance, strength, and display superior esthetics with regard to luster and smoothness. Nano-fillers range from 5 to 40 nm. The nano-size allows for the incorporation of larger inorganic phase into the composite. Shapes of the nano-particles such as: nanotubes, nanoclusters, nanofibers, and nanorods plays major role in the mechanical property of the materials. It increases the compressive, microhardness, tensile, and flexural strengths of the material. There is an optical advantage with enhancement of translucency and color mimicking when the particle size is reduced to 20 nm since this size is lesser than the wavelength of visible light spectrum (400−800 nm).

Nano-composites encompass both the nano-hybrid and nano-filled resin-based composites in the context of particle size. The nano-hybrid composite contains pulverized glass fillers and distinct nanoparticles (40−50 nm) while the nano-filled composites have nano-sized filler particle incorporated which are known as “nanomers.” The assemblage of nanomers is termed as “nanoclusters.”

In contrast to the nano-composites, large filler particles 15−20 μm are found in the hybrid composites along with small amount of colloidal silica (0.01−0.05 μm). Anterior restorations demand esthetics; therefore, microfilled composites were developed which have

submicroscopic silicon dioxide particles (approx. 0.04 microns). Although microfilled composite have small-sized fillers that can increase the surface area of the filler particles to several thousand times in comparison with conventional composites. There is a simultaneous increase in the viscosity due to wetting by monomer matrix. This increase in viscosity reduces the percentage filler content to approximately 35 wt%, resulting in reduced strength.[54]

The types of nanoparticles in composite resins have been classified as follows: (1) Type I, (2) Type II.

Type I: It is having two subtypes. Nanometric particles which are dispersed in the resin matrix as single units are designated as subtype 1. Agglomerated nanoparticles clusters are known as the second subtype.

Type II: This type of nanoparticles consists of a cage-like structure which is composed of eight silicon and 12 oxygen atoms. Rather than the agglomerated cluster or being an individual particle, this type of nanoparticle becomes a part of the resin matrix.

Glass-ionomer cement (GIC): GIC containing nanoparticles developed with fluoro aluminum silicate technology (Ketac Nano; 3M ESPE) having size in the range of 1 μm.[55] The inclusion of nano-particles caused superior esthetics and lusture to retain GIC restorations.[56] Among the innovations with involvement of nanotechnology with EQUIA (Easy-Quick-Unique-Intelligent-Aesthetic) system, a nano-filled light-cured varnish (G-Coat Plus, GC Europe, gceurope.com) which is administered on viscous GIC surface (Fuji IX GP Extra, GC Europe). EQUIA system involves inorganic silica nanofillers (having40-nm size and 15 wt.%) propagated in a liquidic condition which results in enhanced wear resistance to avoid water intake and dehydrate and reduced original time of setting. Their superiority to conventional restorations has been validated in a retrospective study.[57]

2.2.1 Dental restorative materials with bioactivity

Composites can be functionalized and made to act more than space-occupying materials. Inorganic fillers in the dental restorative materials can be incorporated with nano-bioactive compounds which will make it clinically viable.

This innovative approach of incorporation of metallic nanoparticles having antimicrobial property and calcium phosphate NPs helps in the mineral balance and management of dental caries and restorative dentistry. The bioactivity, however, depends upon the properties of the nanoparticles.

The bioactivity of the restorative materials in dental caries prevention may be achieved through two pathways:

1. Controlling the mineral loss of tooth.
2. Reduction/modulation of bacterial biofilm production.

2.2.2 Silver nanoparticles

Silver (Ag) has antimicrobial activities[58] and inhibit the respiratory chain of the bacteria and bring alterations in DNA.[59,60] Ag ion interact with sulfhydryl and disulfide groups of bacterial enzyme and alter their metabolism, resulting in cell death. Ag NPs also induce structural abnormalities in microbial cell membrane.[61] The influence of the Ag compounds is dependent on the quantity of silver ions released and their availability for interaction.

Ag decreases the growth of *C. albicans* and *S. mutans*.[62] When silver 2-ethyl hexanoate salt is dissolved in 2-(tert-butylamino) ethyl methacrylate (Ag-TBAEMA), it inhibits the

colony-of *S. mutans* and the mechanical properties also remain unaltered.[63] Incorporation of nano-sized Ag-bromide salt resulted a nanocomposite with a sustained silver ions release and better antibacterial activity against *S. mutans*.[64] Similar antimicrobial activity against *S. mutans* was observed when bioactive glass was incorporated with silver nanoparticles.[65]

Although the combination of fluoride with silver can prevent development of dental caries, it can form tooth discoloration.[66] Another novel silver formulation containing chitosan has inhibitory effects against microorganism *S. mutans*. Apart from inherent antimicrobial property, chitosan has a stabilizing impact on Ag nanoparticles.[67]

2.2.3 Zinc oxide nanoparticles

Zinc oxide (ZnO) was used as a composite resin filler.[68] However, nano-seized ZnO shows toxicity in contrast to both Gram-positive and negative microbes. ZnO can inhibit the growth of bacteria like *S mutans*.[69,70] ZnO when incorporated with resin composite[71] it can significantly reduce the matured microbial biofilm even with addition of 10% ZnO nanoparticles.[72] ZnO nanoparticles were incorporated into flowable composites with an average of 20 nm size. ZnO incorporated composites have more flexural modulus and strength.[73] The antibacterial activity of ZnO incorporated composites against *S. mutans* and *Lactobacillus* was, however lower, in comparison with silver nanoparticles.[64]

2.2.4 Copper oxide (CuO)

There is a gradual demineralization of enamel due to prolonged presence of orthodontic brackets which makes the hypomineralized areas prone to dental caries. Copper Oxide (CuO) can kill various gram-negative and gram-positive species.[74] CuO nanoparticles were incorporated in the orthodontic brackets and dental bonding agents.[75] CuO incorporated orthodontic brackets displayed a significant antimicrobial activity against *S. mutans* biofilm. Incorporation of CuO in the dental bonding agent enhances the bond strength but the tensile strength remains unaltered.[76]

2.2.5 Bioactive glass

Bioactive glass was incorporated in composites with the filler content of about 72%. The bioactive glass composites when exposed to moisture and bacterial challenge displayed higher strength and durability.[77] Bioactive glass in flowable composite significantly decreases the growth of *E. coli* and *S. mutans* and the bond strength also remain unaltered.[78] In presence of bioactive glass composites, bacteria penetration is less in comparison to nonincorporated composites.[79]

2.2.6 Diamond nanoparticles

Incorporation of nano-sized diamond in various materials help to enhances the mechanical as well as antibacterial properties.[80] Silver-loaded functionalized nano-diamonds (Ag/QNDs) was added to a monomer mixture of TEGDMA and Bis-GMA to obtain a dispersion having homogenous property. This dispersion was further observed with an improvement of mechanical properties. Incorporation of 0.3%−1.5% of Ag/QNDs resulted in significant increase in the hardness, strength, and elasticity. Ag/QNDs nanoparticles can prevent the growth and survivability of S. mutans.[81]

2.3 Periodontal disease

Periodontal disease involves a chronic inflammatory tissue change in response to the microbial dental plaque and affects the supporting structures of the tooth (Fig. 18.4). The untreated disease results in progressive destruction and loss of the periodontal complex.[82]

Periodontal disease is conventionally treated by removal of local factors such as microbial plaque and calculus.[83] For conditions with loss of attachment and bone loss, periodontal surgery may be carried out.

Applying nanotechnology-based nano-delivery systems and nano-bio materials, could be a novel approach for treating periodontal diseases which enable drug administration, periodontal pockets retention and proper release of antibacterial agents, which may induce tissue regeneration process.[84]

Two types of inorganic nanoparticles are generally used for periodontal disease treatment:

1. Antimicrobial metallic nanoparticles and numerous nano biomaterials having calcium for bone regeneration.[84]
2. Inorganic nanoparticles are advantageous over the organic antibacterial NPs due to its chemical, long-term stability and thermal resistance.[85]

Inorganic nanoparticles, that is, silver, copper oxide, zinc oxide's activity decreases against oral anaerobic bacteria, namely, *Aggregatibacter actinomycetemcomitans, Prevotella intermedia, Fusobacterium nucleatum, and Porphyromonas gingivalis*.[86]

Inorganic nano-particles kill the bacteria by producing more amount of ROS. Nano-sized heavy metal ions can damage the proteins, DNA and electron transduction of the bacteria.[84] Silver ions are powerful antimicrobial agents since the oxidation of silver nano-particles releases silver ions. Silver ions inhibit the cell growth by binding to the negatively charged bacterial proteins. Antibacterial effect of silver helps to inactivate the enzyme phosphomannose isomerase.[87]

Nonsurgical periodontal therapy includes application of drug at the site of the disease (intrapocket). For this, novel drug delivery systems are constantly developed.[88] The nano-

FIGURE 18.4 Periodontal disease.

tetracycline loaded particles can be uniformly dispersed within a matrix where these particles would gradually biodegraded releasing the drugs for a sustained period of time. Nanocomposite hydrogels based on polyvinyl alcohol, 5% chitosan nano-particles with different proportion of tetracycline prepared by freezing-thawing cycles exhibit inhibition of both gram-negative and gram-positive bacteria.[89] Nanoparticles work when the particulate dispersion size varies from 10 to 1000 nm. Small size facilitate the drug to be entrapped in the nanoparticle matrix.[90] The dispersed particles in the aqueous medium allow it for controlled release with superior steadiness. Furthermore, its small size allows it to reach the unreachable sites in the deep periodontal pocket regions.

Chitosan nanoparticles exhibit differential antimicrobial mechanism of action depending upon their molecular weight.[91] The low molecular weight chitosan nanoparticles can penetrate the bacteria and damage its physiology. High molecular weight chitosan nanoparticles block the nutrient entry into the bacteria by forming a film around it. The chitosan's positive charge allows it to interact with the negative charge of the bacterial cell wall and thus causes damage to the bacteria. The interaction of nanoparticle with the bacterial membrane blocks the nutrition of the bacterial cell with the extracellular matrix. Further, the positive charge contests for the calcium ions at a particular region of the membrane and causes cell death. Chitosan displays antimicrobial property which is effective against periodonto-pathogens like *S. mutans, A. actinomycetemcomitans* and *P. gingivalis*.

Polymersomes have been developed as nano-drug delivery system. Polymersomes were developed to deliver intracellular antimicrobial for *P. gingivalis*.[92] Being amphiphilic block copolymer vesicles Polymersomes have drug encapsulating ability. They have a remarkable ability to enter early cellular endosomes by endocytosis and release the drug by disassembling. Polymersomes proved to be an efficient drug delivery system for antimicrobials that normally find difficulty to enter host cells. Similarly, calcium sulfate beads with tetracycline nanoparticles were incorporated using ionic gelation method for subgingival delivery having bactericidal property for *E.coli* and *S. aureus*.[93]

Nano-fibers of various biodegradable polymers[94] provide huge surface area to volume ratio (up to 103 times), with greater stiffness and tensile strength. Among the various methods to fabricate nano-fibers, electro spinning is the most efficient technique.[95] Drug having both hydrophobic as well as hydrophilic property can be incorporated. An inhibition of growth of *F. nucleatum* and *A. actinomycetemcomitans* was seen with ciprofloxacin containing nanofibers. However, it did not impair the growth of commensals.[96]

Hydroxyapatites nano-crystals are the bone grafting material having more biocompatibility as hydroxyapatites are also found in the natural calcified tissues.[84] They are nontoxic and provide the calcium and phosphate ions for bio mineralization and new bone formation.[97] Nano-hydroxyapatite can also promote the regeneration of periodontal region.[98]

2.4 Malocclusion

Malocclusion in simple terms refers to a misalignment of teeth which is deviation from the normal alignment of teeth in the dental arches. Maligned teeth apart from being visibly unpleasant, often limit the optimum function and can pose a challenge to maintenance of oral health. It is also sometimes referred to crowding, overbite, crossbite, or open bite, etc., depending upon the type of arrangement and relation.

Malocclusion may be limited to dental or maybe skeletal (involving discrepancies of the jaws) is primarily an inherited condition but can be also as a result of oral conditions or trauma. Some oral habits such thumb-sucking, prolonged bottle feeding, mouth-breathing, may also change the shape and structure of the jaws.

Management of malaligned teeth usually involves braces (Fig. 18.5A). Nanotechnology helps to improve the material's property to enhance the orthodontic treatment in terms of the speed and effectiveness of treatment (Fig. 18.5B). For example, by using nanoparticles, better mechanical specifications of the orthodontic archwires and brackets can be achieved.[99–101] Reduction in allergies and corrosion may be achieved by using a nano-coating.[102–104] By using nano-based lubricants, the frictional force between the components can be reduced to facilitate its motion, thus prevent dental affliction.[105] Nanoparticle film composed of nano-ceramics on wires formed of titanium molybdenum alloy, stainless steel and nickel-titanium is also used. Coating enhances the surface topology and decreases the problems associated with friction.[106] Zinc oxide (ZnO) nanoparticles can be used for improvement of the antibacterial and frictional behavior of nickel-titanium alloy.[107] Similarly, ZnO nanoparticles are used as nano-lubricants to coat stainless steel wires. It causes 51% reduction in the frictional energy between the wire and brackets in comparison with the reference wires.[108] Encouraging results were seen by coating of Nickel–Titanium (NiTi)/stainless steel wires by the means of tungsten disulfide (WS2) and Nickel-phosphorous Nanoparticles.

The friction is reduced in a manner which has been proposed by Rapoport et al.[109] and Cizaire et al.[110] Firstly, the nanoparticles act as the spacers between the wire and the slot when there is no angle between them and reduce the coefficient of friction. With an increase in the angle, the friction also increases and the nanoparticles in the coated wires are released due to their exfoliation. The released nano-particles now act as a solid lubricant on the sliding wire. With increase in the load, the rough surfaces come in larger contact. Increased contact squeezes the oral fluids out of the gap between the wire and the slot allowing better functioning of the solid nanoparticle lubricant on the arch wire.

Hollow orthodontic wires with an excellent shape-memory and super elasticity were prepared by ultrasonic spray pyrolysis technique. These wires were first coated via electro spinning with nanoparticles (NiTi/Ni–TiO_2), and then it was followed by removal of wire in order to produce a hollow orthodontic wire. Orthodontic nanorobots interact with cells, which are present in periodontium, cementum region as well as at the site of alveolar

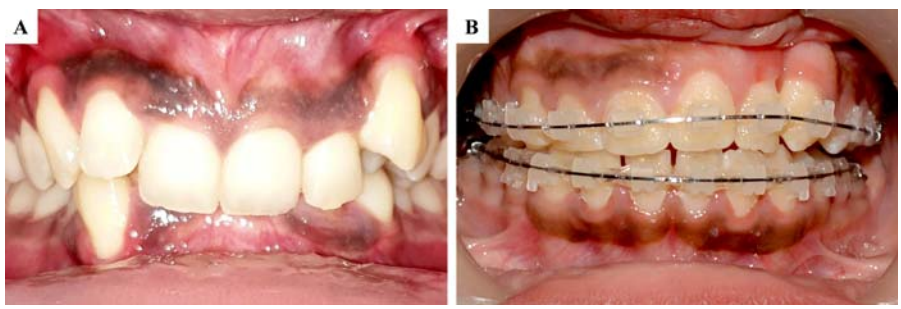

FIGURE 18.5 A: Malalignment of teeth B: Correction of malaligned teeth with ceramic orthodontic braces.

bone, correcting malocclusion by straightening tooth painlessly, correcting vertical reposition and rotations in a single dental office appointment.[2]

Newer development of materials are being focused in order to make them self-disinfecting. Microbial plaque accumulation orthodontic appliances is seen quite commonly. The presence of microbes can lead inflammation of the gingiva, development of white spot lesions, caries, dental infections, and delay in tooth movement.

In order to counter the menace of microbial plaque biofilm, nitrogen-doped titanium dioxide have been utilized. When the nitrogen-doped titanium dioxide is activated, reactive oxygen species (ROS) like OH free radicals, hydrogen peroxide (H_2O_2), superoxide ions (O_2), and peroxyl radicals (HO_2) are formed. ROS can cause damage of nucleic acids, lipids, enzymes and proteins by the means of oxidation reactions. Modifications have also been made with incorporation of Titanium dioxide nanoparticles in the composites used for bonding the orthodontic brackets (Transbond XT).[111] Chitosan nanoparticles with Zinc oxide nanoparticles,[112] Silver with hydroxyapatite nanoparticles[113] and Copper nanoparticles have shown good antibacterial properties.[114]

Silver nanoparticles can be used to coat orthodontic composite resins used to treat malocclusion, for imparting antibacterial properties to it, for avoiding infections and dental caries.[115]

2.5 Missing teeth

Missing teeth is absence of permanent teeth caused mainly by loss of teeth due to tooth decay, tooth injuries, gum diseases. It also includes condition in people born without certain teeth, referred to as congenitally missing teeth, which may be due to certain systemic conditions, like genetic factors, or inherited disorders(Fig. 18.6A).[116] It is otherwise known as hypodontia, which can be defined as the agenesis of one or more teeth, or the congenital absence of teeth. Oligodontia is the absence of six or more congenital permanent teeth.[117] The prevalence of missing teeth also differs with race, age and gender.[118] Wisdom teeth, Upper lateral incisors and secondary premolars, bicuspids are the most common missing teeth.

Management of missing teeth is done by either a removable or a fixed prosthesis to restore form and function such as mastication, speech, and esthetics (Figs. 18.6B and 18.7).[119]

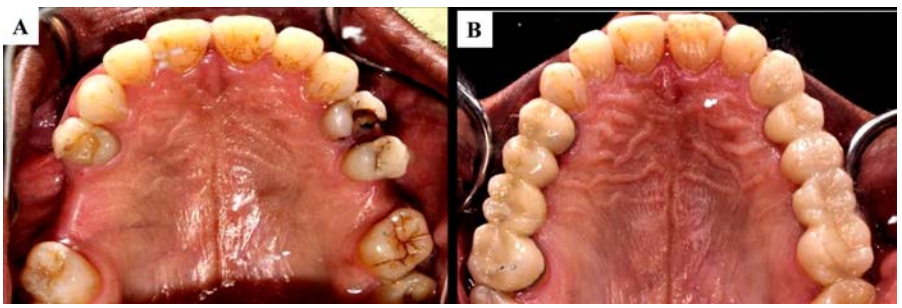

FIGURE 18.6 A: Missing teeth in the maxillary arch B: Replacement of missing teeth with ceramic crowns and bridges.

FIGURE 18.7 Zirconia crowns.

Poly-methylmethacrylate (PMMA) is commonly used for fabrication of denture base. PMMA incorporated into 3D denture base along with Titanium dioxide nanoparticles, shows improved antibacterial characteristics and mechanical properties.[120] Addition of heat-cured PMMA with nano-zirconium oxide, significantly enhances the hardness levels, strength as well as the fracture toughness of the denture base after heat-curing (Fig. 18.8). This was possible because of superior dispersion property of nano-zirconium, its biocompatibility with other organic polymer and because of less aggregation potential.[121,122]

Over the recent years, dental implants have emerged as the preferred and optimum option for rehabilitation of a single or multiple missing teeth in either arches.[123,124] Dental implants

FIGURE 18.8 Treatment partial denture (polymethyl-methacrylate (PMMA)) for replacement of missing teeth.

are titanium (Ti) inserts that have a remarkable ability of osseointegration and have high strength, durability, and biocompatibility.[125] However, sometimes failure occurs due to material, tissue or mechanical factors. Failure to maintain the oral hygiene is a major determinant in the success of dental implant. Conditions such as peri-implantitis, peri-implant mucositis are caused by growth and colonization of gram-negative anaerobes.[126] There is a rise in the implant failures along with rise in the cases of implants. To combat this difficulty, various NPs like Ag,[127–130] copper (Cu),[131] ZnO,[132,133] titanium dioxide (TiO2),[134,135] selenium (Se),[125] and strontium (Sr)[136–138] have been developed which have antibacterial properties(Fig. 18.9A and B).

Ion implantation of silver on Titanium surface demonstrated antimicrobial activity.[139,140] Surface modification of Ti-implants[141,142] exhibited enhanced antibacterial and biocompatibility. Titanium surface modified with coatings has resulted in strong and stable antibacterial activity for a long time.

Dental silicones, the materials which were commonly used for denaturing the soft liners and obturators were coated with various nanoparticles solution, showed better antifungal activity, without altering the denture silicon's hydrophilicity, when immersed in artificial saliva. There was a slow and sustained release soluble chlorhexidine into artificial saliva. These properties can positively influence the longevity and maintenance of the dental prosthesis inside the oral cavity at lower cost.

Luting cements are routinely used for cementation of fixed partial prosthesis. Luting cements impregnated with various nano-particles, can significantly enhances the enamel - dentine bond strength. Because of their small size, those particles can penetrate deeper and bound well to dentinal tubules. Eventually, they reduces the polymerization shrinkage and increases number of elastic modules present in them.[143]

Incorporating ZnO and MgO nanoparticles incorporated luting agents while comparing them to conventional cements of zinc polycarboxylate showed improved compressive and tensile strengths.[143] Also, biaxial flexural, tensile, and compressive strength of glass ionomer cements can be increased significantly by adding fluorapatite/nano-hydroxyapatite particles to them.[144,145]

2.6 Tooth wear

Tooth wear is a result of attrition, erosion, and abrasion, domestication, abfraction of the tooth. Attrition refers to the enamel,/dentin loss.[146] Dental erosion, on the other hand, is the

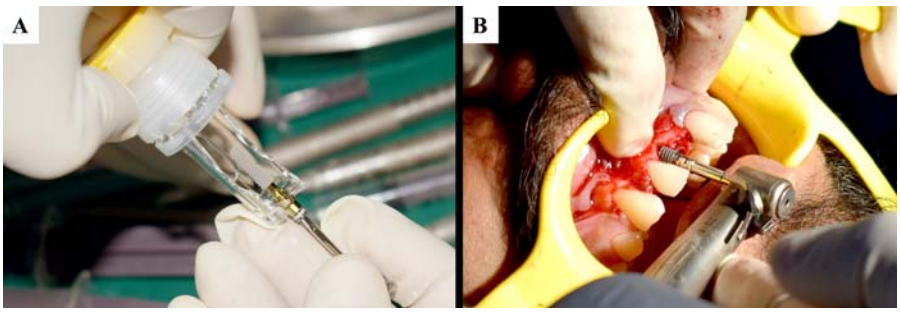

FIGURE 18.9 A: Dental implant (Titanium) B: Dental implant placement.

permanent loss of dental enamel because of the chemical exposure like acidic dissolution beyond the bacterial involvement.[147] Dental erosion and demineralization because of the acids might be intrinsic/extrinsic in their origin.[148,149] Inside the stomach, intrinsic acids are generally originated and those are produced because of the eating disorders, like bulimia nervosa and anorexia[150] or due to improper acidic reflux and regurgitation.[151] Extrinsic sources are the engulfment of acids which are present in dietary components, like fruit juices and carbonated soft drinks.[152] Abrasion is the pathological erosion of dental hard tissue by means of bio-mechanical friction, like brushing of tooth and also because of the aberrant mechanical processes which involve foreign substances, those are repeatedly contact the teeth.[153] Abfraction is also used in relation of tooth wear, causing loss of tooth parts because of the microbial infection due to flexural forces, seen as the wedge-shaped defect occurred at cementoenamel junctional site (CEJ) of a tooth.[154] Attrition is also the most common form of tooth-wear.[155] Erosion is the dental materials loss by means of acidic dissolution having either extrinsic or intrinsic origin, for example, dietary acids/gastric acid.[56]

Nanocomposites are used as fillers to treat tooth wear, which use nano-dimensional filler particles.[156] Those are added to composite resins singly or in a composite form and they can result in indistinctive physical, optical and mechanical properties.[157] Conventional filler are large-sized particles and are made to small size by pinning but this cannot reduce their size to less than 100 nm.[156,158,159] Nanoparticles help to produce the composites with a smoother surface after the polishing there is an increase in the translucency and esthetics.[44] Incorporation of nanoparticles brings good strength, resistance to abrasion along with the retention and improved mechanical properties.[160]

2.7 Dentinal hypersensitivity

Dentinal hypersensitivity, a common problem of the permanent teeth, is mainly caused because of the exposure of dentin to the oral cavity because of the loss of cementrum or enamel. For short duration, it results in acute pain, which is caused because of the presence of exposed dentinal tubules on its surface.[161] The beginning of pain may be triggered by thermal, mechanical or chemical origin, and most commonly by cold stimuli. It may also be caused by acidic foods and fruits, which is the result of a mechanical stimulus.[162] The most common cause for dentinal tubules exposure is the gingival recession, which makes recessed areas more sensible because of the cementum loss, or by exposing dentin. The hypersensitive tooth have eight times more surface density and have twice the diameter of dentinal tubules than that of nonsensitive teeth.[16]

Management of dentinal hypersensitivity involves consistent and reliable treatment need to be developed that can penetrate deep into the dentinal tubules. For this nanoparticles can serve as a solution, unlike conventional sized particles. Nano-sized hydroxyapatite particles are emerged and have enormous applications in dentistry. The nano HAp particles can be used to seal the opening of the dental tubules as they can easily integrate into the tubules. This sealing prevents exposure of the nerves toward external stimuli, thus helping in reduction of hypersensitivity.[163] These HAp NPs have a large surface area, the property that can be exploited to bind them strongly to proteins, and also bacteria and plaque fragments.[164] HAp NPs show high biological activity and can bind effectively to the enamel of the teeth,

preventing exposure of the nerves. They can form an artificial enamel film around the teeth and show bio mimicry.[165] Hence, they are used in different toothpastes and mouth-rinsing solutions for integrating those nanocrystals for the repair of the enamel surfaces. Modified silica NPs are now a days used to treat dentinal hypersensitivity. Having larger pore sizes, higher sorption efficacy of hydrocarbon, higher surface area having well defined structure and hydrothermal/thermal stability, nanoparticles are being researched widely in the recent years.[166,167] Dental nanorobots can offer a quick and permanent treatment to patients.[168]

2.8 Edentulousness

Edentulism is a medical condition of permanent loss of teeth which may be due to several factors (Fig. 18.10A and C). Most of the time, it is accompanied by the scarcity of oral mucosa, salivary glands, and the oral musculature.[169] According to the studies, it is found that edentulism can be a reason for the induction of oral dyskinesia, which can be seen as involuntary, abnormal, patterned orofacial movements.[170,171] It is very common among the older individuals of the population though complete tooth loss has been significantly decreased in the past decade.[172] Polymer poly(methyl methacrylate) (PMMA) is of great rescue to the patients suffering from edentulousness as it is used for manufacturing dentures because of its reliable qualities like ease of processing,[173] repairing,[174] and also its low cost and great acceptability to the patients. PMMA is popular because of its tasteless, odorless properties along with its biocompatibility and esthetic characteristics.[175] Although there are tremendous favorable qualities of PMMA as a denture material it also has a great number of issues like low mechanical resistance,[175] shrinkage of polymer, leaching of monomers which causes allergic reactions.[176] The most important problem with it is the microbial colonization and biofilm formation on the denture surface which can lead to local and systemic infections.[177–179] To control this limitations, nanomaterial is a good option because of its high efficiency as antibacterial agents because of their larger surface area as compared to their size. Thus resulting hyper activity, even in a very small dose.[180] The infection of *Candida albicans* is very common indentures with nanoparticles of silver(Ag)-colloidal[181,182] and nanoparticles solutions of Ag.[183] According to recent studies, the silver nanocomposite with PMMA is beat by the PMMA which are functionalized by TiO_2 nanoparticles, demonstrate better mechanical[184] as well as antibacterial characteristics.[185,186] TiO_2 nanoparticles have antimicrobial activity against both gram-negative and gram-positive bacteria along with fungi. The reason for its wide use is that it is intrinsically environment-friendly and exerts a noncontact biocidal

FIGURE 18.10 A: Edentulous maxillary arch B: Edentulous mandibular arch C: Complete dentures (polymethylmethacrylate (PMMA)).

action.[187] The manufacturing of PMMA/TiO_2 nanocomposites has been achieved by modified sol-gel methods. This ensures a homogenous mixture of TiO_2 nanofillers into PMMA solution. Experiments have shown that addition of TiO_2 nanoparticles modify certain properties of the polymer.[120]

2.9 Discolored teeth

Any dissimilarity from the normal color of the human dentition is known as tooth discolouration. It is frequently complained diseases which differ in terms of severity, appearance, composition. This is a major problem among the people as it disturbs the appearance of the teeth. Tooth color is determined by many intrinsic and extrinsic factors like the light scattering and absorption properties of the enamel and dentine. Sometimes, the color of the denture is affected by the type of food and drinks we take for instance tea is absorbed in the surface of the enamel and gives it an off white appearance. There are two ways of teeth whitening popular, that is, invasive techniques like dental crowns and veneers, and the noninvasive technique like bleaching, etc.

Currently, the most common form of whitening involves the application of a gel containing hydrogen peroxide which bleaches the teeth by removing from the pigment molecules that cause surface discoloration. This is activated by blue light exposure which dramatically speeds the process up. Hydrogen peroxide is cytotoxic and therefore alternatives have been searched for. Titanium dioxide nanoparticles modified with polydopamine however, when applied and exposed to blue light, the nanoparticles produced a whitening effect similar to that of hydrogen peroxide, yet they were much less cytotoxic.[188]

Presently researchers are using Gold nanoparticles (AuNPs) for tooth whitening. According to the researchers, these nanoparticles have potency to be used in this field because of its efficacy in white light irradiation. Researchers have synthesized the nanoparticle using HAuCl4, water and Sodium trihydrate solution. They treated the teeth with black tea for staining and then chose two whitening methods that are H_2O_2 alone and H_2O_2 with AuNPs. When the AuNPs are used as catalyst for H_2O_2 in tooth whitening then they considerably amplified the efficiency of bleaching of H_2O_2.[189] Tooth whitening pastes incorporated with polymeric nanoparticles of carbamide peroxide can enhance the bleaching efficacy and the effectiveness of those whitening pastes.[190]

2.10 Maxillofacial trauma

Maxillofacial trauma involves the injury to the dental and maxillofacial structures (Fig. 18.11). Management is primarily directed toward restoration of form, function, and esthetics.[191] In the treatment of maxillofacial trauma, nanotechnology plays a very crucial role through the help of nanorobotics and nanomaterials.[192]

Administration of profound anesthesia is pivotal to procedures carried out in the management of maxillofacial trauma. An in vivo study explored the application of local anesthetic drug having magnet-directed nanoparticles, such as ropivacaine (MNP/Ropiv) for the production of anesthesia.[193] Researchers engineered about the nanoparticle complexes, which are intravenously injected to ropivacaine which resulted a similar anesthetic effect in

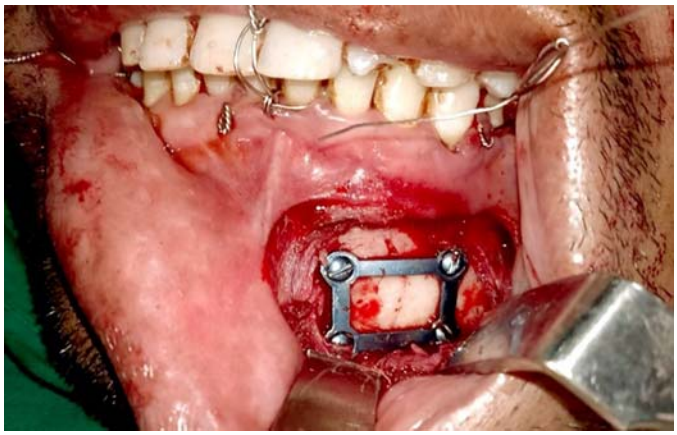

FIGURE 18.11 Open mandibular fracture reduction with mini-plates and mini-screws.

comparison to the conventional. Use of magnets was helpful in accurate anesthesia. Similarly nanocarriers associated with transcriptional transactivator peptide were successfully carried out for ropivacaine skin delivery.[194]

Nanotechnology can be used in the field anesthesia where the patient's gingiva is administered to the colloidal suspension that contains numerous active and dental analgesic nanoparticles. These respond to a stimulus and once they have contact with the tooth of mucosa, the nanoparticles navigate under controlled chemical gradient and temperature differentials to the sensory nerve endings in the gingiva via lamina propria and dental pulp via dentinal tubule. Those nanoparticle-based anesthesia are reversible, fast acting, having no side effects rather than the use of conventional dental anesthetics.[195,196]

In maxillofacial surgery, the implants which are made out of nanoparticles can be applied as dental fillers, as prosthetic implants or as bone replacement materials. These substances exhibit certain advantageous properties like corrosion resistance, surface finish and high deformability. Even the tissues engineered with the natural nanomaterials have the potentiality for absolute reconstruction of patient's craniofacial skeleton and dentition. Nowadays even the nanorobots having diameter of 0.5−3 μm are used at the molecular and cellular level by the clinicians. These robots have several roles for the treatment of diseases, that is, the diagnosis of oral diseases and its application in dental therapeutics, and in dentifrice.[197]

2.11 Maxillofacial cancer

Maxillofacial Cancer is a kind of oral cancer which is now one of the major cancer affecting the human population. There are various cures for the oral and maxillofacial cancers nowadays like radiation therapy, chemotherapy, and reconstructive surgery. Detection of oral cancer has been revolutionized by use of nanotechnology which has enabled detection of even a single cancerous cell in-vivo. Also, it has enabled the delivery of anticancer drugs directly to the cancerous cells. Nanoparticles can enhances and control drugs stability and their delivery, by allowing their constant and uniform release at the place of a dental lesion and eventually

facilitating drug extravasation inside the tumorous system, by shortening its side effects.[198,199] Among the various nanomaterials, which have been used in the management of oral cancers are nano-shells, carbon nanotubes, quantum dots, super magnetic anoparticles, and synthesized nanosponges.[200] Further, antibodies which are specific against cancer cell lines can be isolated. Several kinds of nanoparticles have been found to be suitable for DNA structures probing or for drug/gene delivery, which include liposomes, Polymeric nanoparticles, solid lipid particles, nanocrystals, dendrimers, fullerenes, and other inorganic nanoparticles.[201]

Combinational chemotherapy which is combination of nanomedicine and nanoparticles has expanded the horizon to newer therapeutic approaches that have diminished the tumor cell resistance and reduced unwanted cytotoxicity of normal cells. Doxorubicin encapsulated with a divergent nano-carrier DOX has been used to enhance the targeting of cancerous cells which adheres to epidermal growth factor receptor or folate receptors that are abundantly displayed on the surface of cancerous cells. Both oral and intravenous formulation of Doxorubicin are accessible.[202]

There is also surgical treatment possible which includes routine mandible segmental resection and dissection of radical neck along with sacrifice of the sternocleidomastoid muscle and accessory spinal nerve. With the development in science and technology nanotechnology is another approach for treatment which is now under investigation. In this method of treatment, the monoclonal antibodies are conjugated with nanoparticles, which are reactive toward oral cancer-specific antigens for instance EGFR. In this way, especially nanoparticles will be able to detect and eradicate the oral cancer cells.[203]

3. Conclusions and future perspectives

Clinical applications of nanoparticles in oral healthcare encompass a wide range of areas where continuous research and development is being done globally. Most of the advancements have been seen in the field of treatment of dental caries with dental restorative materials. However, simultaneous advancement is being seen in other areas such as products for maintenance of oral hygiene, drugs and drug delivery systems, dental polymers for dentures, dental implants, materials for dental crowns. Incorporation of nanotechnology into the materials employed in dental regenerative sciences is a promising area for future development of biomaterials for regeneration of lost alveolar bone and enamel.

Acknowledgments

We wish to thank Dr. Smruti Bhusan Nanda, Dr. Sumit Dash, Dr. Harsh Pathak, Dr. Amit Porwal and Dr. Debarchita Sarangi for contributing some of the images used in this chapter.

References

1. Disease GBD, Injury I. Prevalence, Global, regional, and national incidence, prevalence, and years lived with disability for 328 diseases and injuries for 195 countries, 1990-2016: a systematic analysis for the Global Burden of Disease Study 2016. *Lancet* 2017;**390**(10100):1211–59.

2. Aeran H, et al. Nanodentistry: is just a fiction or future. *J Oral Biol Craniofac Res* 2015;**5**(3):207–11.
3. Bhushan J, Maini C. Nanoparticles: a promising novel adjunct for dentistry. *Indian J Dent Sci* 2019;**11**(3):167.
4. Khan I, Saeed K, Khan I. Nanoparticles: properties, applications and toxicities. *Arab J Chem* 2019;**12**(7):908–31.
5. Priyadarsini S, Mukherjee S, Mishra M. Nanoparticles used in dentistry: a review. *J Oral Biol Craniofac res* 2018;**8**(1):58–67.
6. Priyadarsini S, et al. Application of nanoparticles in dentistry: current trends. In: *Nanoparticles in medicine*. Springer; 2020. p. 55–98.
7. Laurent S, et al. Magnetic iron oxide nanoparticles: synthesis, stabilization, vectorization, physicochemical characterizations, and biological applications. *Chem Rev* 2008;**108**(6):2064–110.
8. Tiwari JN, Tiwari RN, Kim KS. Zero-dimensional, one-dimensional, two-dimensional and three-dimensional nanostructured materials for advanced electrochemical energy devices. *Prog Mater Sci* 2012;**57**(4):724–803.
9. Roduner E. Size matters: why nanomaterials are different. *Chem Soc Rev* 2006;**35**(7):583.
10. Buzea C, Pacheco II, Robbie K. Nanomaterials and nanoparticles: sources and toxicity. *Biointerphases* 2007;**2**(4):MR17–71.
11. Hatti S, et al. Biofilm inhibition and antimicrobial activity of a dentifrice containing salivary substitutes. *Int J Dent Hyg* 2007;**5**(4):218–24.
12. Lindh L, et al. Salivary pellicles. In: *Saliva: secretion and functions*. Karger Publishers; 2014. p. 30–9.
13. Allaker R. The use of nanoparticles to control oral biofilm formation. *J Dent Res* 2010;**89**(11):1175–86.
14. Mohanty G, et al. Plaque removal efficacy of toothbrushes with polishing cups—a randomized controlled trial. *Adv Sci Lett* 2016;**22**(2):464–7.
15. Zaccaria JM. *Disposable toothbrush having an edible toothpaste composition*. Google Patents; 1999.
16. AlKahtani RN. The implications and applications of nanotechnology in dentistry: a review. *Saudi Dent J* 2018;**30**(2):107–16.
17. Baishya B, et al. Oral hygiene status, oral hygiene practices and periodontal health of brick kiln workers of Odisha. *J Indian Soc Periodontol* 2019;**23**(2):163–7.
18. Davies R, Scully C, Preston AJ. Dentifrices—an update. *Med Oral Patol Oral Cir Bucal* 2010;**15**(6):e976–82.
19. Danelon M, et al. Effect of toothpaste with nano-sized trimetaphosphate on dental caries: in situ study. *J Dent* 2015;**43**(7):806–13.
20. Ebadifar A, Nomani M, Fatemi SA. Effect of nano-hydroxyapatite toothpaste on microhardness ofartificial carious lesions created on extracted teeth. *J Dent Res Dent Clin Dent Prospects* 2017;**11**(1):14–7.
21. Kani T, et al. Effect to apatite-containing dentifrices on dental caries in school children. *J Dent Health* 1989;**39**(1):104–9.
22. Saengmee-Anupharb S, et al. Antimicrobial effects of silver zeolite, silver zirconium phosphate silicate and silver zirconium phosphate against oral microorganisms. *Asian Pac J Trop Biomed* 2013;**3**(1):47–52.
23. Sekhon BS, Kamboj SR. Inorganic nanomedicine—part 2. *Nanomed Nanotechnol Biol Med* 2010;**6**(5):612–8.
24. Sekhon BS, Kamboj SR. Inorganic nanomedicine—part 1. *Nanomed Nanotechnol Biol Med* 2010;**6**(4):516–22.
25. Percival SL, et al. The antimicrobial efficacy of silver on antibiotic-resistant bacteria isolated from burn wounds. *Int Wound J* 2012;**9**(5):488–93.
26. Song J, et al. Aqueous synthesis of silver nanoparticle embedded cationic polymer nanofibers and their antibacterial activity. *ACS Appl Mater Interfaces* 2011;**4**(1):460–5.
27. Lara HH, et al. Silver nanoparticles are broad-spectrum bactericidal and virucidal compounds. *J Nanobiotechnol* 2011;**9**(1):30.
28. Chaloupka K, Malam Y, Seifalian AM. Nanosilver as a new generation of nanoproduct in biomedical applications. *Trends Biotechnol* 2010;**28**(11):580–8.
29. Lara HH, et al. Bactericidal effect of silver nanoparticles against multidrug-resistant bacteria. *World J Microbiol Biotechnol* 2010;**26**(4):615–21.
30. Li W-R, et al. Antibacterial activity and mechanism of silver nanoparticles on *Escherichia coli*. *Appl Microbiol Biotechnol* 2010;**85**(4):1115–22.
31. Lara HH, et al. Mode of antiviral action of silver nanoparticles against HIV-1. *J Nanobiotechnol* 2010;**8**(1):1.
32. Franci G, et al. Silver nanoparticles as potential antibacterial agents. *Molecules* 2015;**20**(5):8856–74.
33. Sathishkumar M, et al. Cinnamon zeylanicum bark extract and powder mediated green synthesis of nanocrystalline silver particles and its bactericidal activity. *Colloids Surf B Biointerfaces* 2009;**73**(2):332–8.

34. Chen M, et al. Antimicrobial activity and the mechanism of silver nanoparticle thermosensitive gel. *Int J Nanomed* 2011;**6**:2873.
35. Khan ST, Al-Khedhairy AA, Musarrat J. ZnO and TiO 2 nanoparticles as novel antimicrobial agents for oral hygiene: a review. *J Nanoparticle Res* 2015;**17**(6):276.
36. Maness P-C, et al. Bactericidal activity of photocatalytic TiO2 reaction: toward an understanding of its killing mechanism. *Appl Environ Microbiol* 1999;**65**(9):4094–8.
37. ten Cate JM. Contemporary perspective on the use of fluoride products in caries prevention. *Br Dent J* 2013;**214**(4):161–7.
38. Featherstone JD. Prevention and reversal of dental caries: role of low level fluoride. *Community Dent Oral Epidemiol* 1999;**27**(1):31–40.
39. Pandit S, et al. Effect of sodium fluoride on the virulence factors and composition of Streptococcus mutans biofilms. *Arch Oral Biol* 2011;**56**(7):643–9.
40. Sun L, Chow LC. Preparation and properties of nano-sized calcium fluoride for dental applications. *Dent Mater* 2008;**24**(1):111–6.
41. Bowen WH. Do we need to be concerned about dental caries in the coming millennium? *Crit Rev Oral Biol Med* 2002;**13**(2):126–31.
42. Smith D. Dental caries vaccines: prospects and concerns. *Crit Rev Oral Biol Med* 2002;**13**(4):335–49.
43. Marsh PD. Dental plaque as a biofilm and a microbial community–implications for health and disease. *BMC Oral Health* 2006;**6**(Suppl. 1):S14.
44. Acharya S, Satpathy A, Prusty SN. Barriers in the treatment of early childhood caries amongst the general dentists–a cross sectional study in bhubaneswar, odisha, India. *Pesqui Bras em Odontopediatria Clínica Integr* 2018;**18**(1):1–7.
45. Zhan L. Rebalancing the caries microbiome dysbiosis: targeted treatment and sugar alcohols. *Adv Dent Res* 2018;**29**(1):110–6.
46. Garoushi S, et al. Effect of nanofiller fractions and temperature on polymerization shrinkage on glass fiber reinforced filling material. *Dent Mater* 2008;**24**(5):606–10.
47. Wilson KS, Zhang K, Antonucci JM. Systematic variation of interfacial phase reactivity in dental nanocomposites. *Biomaterials* 2005;**26**(25):5095–103.
48. Chen MH, et al. Low shrinkage light curable nanocomposite for dental restorative material. *Dent Mater* 2006;**22**(2):138–45.
49. Furman B, et al. Metal-oxide nanoparticles for the reinforcement of dental restorative resins. *Crit Rev Biomed Eng* 2000;**28**(34):439–43.
50. Mitra SB, Wu D, Holmes BN. An application of nanotechnology in advanced dental materials. *J Am Dent Assoc* 2003;**134**(10):1382–90.
51. Wang Y, et al. High modulus nanopowder reinforced dimethacrylate matrix composites for dental cement applications. *J Biomed Mater Res* 2007;**82**(3):651–7.
52. Tian M, et al. Fabrication and evaluation of Bis-GMA/TEGDMA dental resins/composites containing nano fibrillar silicate. *Dent Mater* 2008;**24**(2):235–43.
53. Wan Q, et al. Light curable dental composites designed with colloidal crystal reinforcement. *Dent Mater* 2008;**24**(12):1694–701.
54. Kramer N, Garcia-Godoy F, Frankenberger R. Evaluation of resin composite materials. Part II: in vivo investigations. *Am J Dent* 2005;**18**(2):75–81.
55. Chandki R, et al. 'Nanodentistry': exploring the beauty of miniature. *J Clin Exp Dent* 2012;**4**(2):e119–24.
56. Moshaverinia A, et al. Effects of incorporation of hydroxyapatite and fluoroapatite nanobioceramics into conventional glass ionomer cements (GIC). *Acta Biomater* 2008;**4**(2):432–40.
57. Friedl K, Hiller KA, Friedl KH. Clinical performance of a new glass ionomer based restoration system: a retrospective cohort study. *Dent Mater* 2011;**27**(10):1031–7.
58. Lansdown ABG. Silver I: its antibacterial properties and mechanism of action. *J Wound Care* 2002;**11**(4):125–30.
59. Brett DW. A discussion of silver as an antimicrobial agent: alleviating the confusion. *Ostomy Wound Manag* 2006;**52**(1):34–41.
60. Ahn S-J, et al. Experimental antimicrobial orthodontic adhesives using nanofillers and silver nanoparticles. *Dent Mater* 2009;**25**(2):206–13.

61. Dickens SH, Flaim GM, Takagi S. Mechanical properties and biochemical activity of remineralizing resin-based Ca−PO4 cements. *Dent Mater* 2003;**19**(6):558−66.
62. Noronha VT, et al. Silver nanoparticles in dentistry. *Dent Mater* 2017;**33**(10):1110−26.
63. Cheng L, et al. Effect of amorphous calcium phosphate and silver nanocomposites on dental plaque microcosm biofilms. *J Biomed Mater Res B Appl Biomater* 2012;**100B**(5):1378−86.
64. Kasraei S, et al. Antibacterial properties of composite resins incorporating silver and zinc oxide nanoparticles onStreptococcus mutansandLactobacillus. *Restor Dent Endod* 2014;**39**(2):109.
65. Chatzistavrou X, et al. Fabrication and characterization of bioactive and antibacterial composites for dental applications. *Acta Biomater* 2014;**10**(8):3723−32.
66. Yee R, et al. Efficacy of silver diamine fluoride for arresting caries treatment. *J Dent Res* 2009;**88**(7):644−7.
67. Arnaud TMS, de Barros Neto B, Diniz FB. Chitosan effect on dental enamel de-remineralization: an in vitro evaluation. *J Dent* 2010;**38**(11):848−52.
68. Bowen RL, Cleek GW. A new series of X-ray-opaque reinforcing fillers for composite materials. *J Dent Res* 2016;**51**(1):177−82.
69. Durner J, et al. Influence of silver nano-particles on monomer elution from light-cured composites. *Dent Mater* 2011;**27**(7):631−6.
70. Fang M, et al. Antibacterial functionalization of an experimental self-etching primer by inorganic agents: microbiological and biocompatibility evaluations. *Biomol Eng* 2007;**24**(5):483−8.
71. Niu LN, et al. Tetrapod-like zinc oxide whisker enhancement of resin composite. *J Dent Res* 2010;**89**(7):746−50.
72. Aydin Sevinç B, Hanley L. Antibacterial activity of dental composites containing zinc oxide nanoparticles. *J Biomed Mater Res B Appl Biomater* 2010;**9999B** [p. NA-NA].
73. Tavassoli Hojati S, et al. Antibacterial, physical and mechanical properties of flowable resin composites containing zinc oxide nanoparticles. *Dent Mater* 2013;**29**(5):495−505.
74. Ren G, et al. Characterisation of copper oxide nanoparticles for antimicrobial applications. *Int J Antimicrob Agents* 2009;**33**(6):587−90.
75. Ramazanzadeh B, et al. Comparison of antibacterial effects of ZnO and CuO nanoparticles coated brackets against Streptococcus mutans. *J Dent* 2015;**16**(3):200−5.
76. Gutierrez MF, et al. Mechanical and microbiological properties and drug release modeling of an etch-and-rinse adhesive containing copper nanoparticles. *Dent Mater* 2017;**33**(3):309−20.
77. Khvostenko D, et al. Mechanical performance of novel bioactive glass containing dental restorative composites. *Dent Mater* 2013;**29**(11):1139−48.
78. Chatzistavrou X, et al. Designing dental composites with bioactive and bactericidal properties. *Mater Sci Eng C Mater Biol Appl* 2015;**52**:267−72.
79. Khvostenko D, et al. Bioactive glass fillers reduce bacterial penetration into marginal gaps for composite restorations. *Dent Mater* 2016;**32**(1):73−81.
80. Mochalin VN, Gogotsi Y. Nanodiamond−polymer composites. *Diam Relat Mater* 2015;**58**:161−71.
81. Cao W, et al. Mechanical property and antibacterial activity of silver-loaded polycation functionalized nanodiamonds for use in resin-based dental material formulations. *Mater Lett* 2018;**220**:104−7.
82. Savage A, et al. A systematic review of definitions of periodontitis and methods that have been used to identify this disease. *J Clin Periodontol* 2009;**36**(6):458−67.
83. Pattnaik S, et al. Clinical and antimicrobial efficacy of a controlled-release device containing chlorhexidine in the treatment of chronic periodontitis. *Eur J Clin Microbiol Infect Dis* 2015;**34**(10):2103−10.
84. Zupancic S, et al. Contribution of nanotechnology to improved treatment of periodontal disease. *Curr Pharmaceut Des* 2015;**21**(22):3257−71.
85. Cevc G, Vierl U. Nanotechnology and the transdermal route: a state of the art review and critical appraisal. *J Contr Release* 2010;**141**(3):277−99.
86. Vargas-Reus MA, et al. Antimicrobial activity of nanoparticulate metal oxides against peri-implantitis pathogens. *Int J Antimicrob Agents* 2012;**40**(2):135−9.
87. Kim T, Hyeon T. Applications of inorganic nanoparticles as therapeutic agents. *Nanotechnology* 2013;**25**(1):012001.
88. Joshi D, et al. Advanced drug delivery approaches against periodontitis. *Drug Deliv* 2014;**23**(2):363−77.

89. Parsa P, Paydayesh A, Davachi SM. Investigating the effect of tetracycline addition on nanocomposite hydrogels based on polyvinyl alcohol and chitosan nanoparticles for specific medical applications. *Int J Biol Macromol* 2019;**121**:1061–9.
90. Garg T, Singh S, Goyal AK. Stimuli-sensitive hydrogels: an excellent carrier for drug and cell delivery. *Crit Rev Ther Drug Carrier Syst* 2013;**30**(5):369–409.
91. Satpathy A, et al. Comparative evaluation of porous chitosan tissue barrier membranes fabricated by two techniques—a stereomicroscopic study. *Adv Sci Lett* 2016;**22**(2):434–6.
92. Wayakanon K, et al. Polymersome-mediated intracellular delivery of antibiotics to treat Porphyromonas gingivalis-infected oral epithelial cells. *Faseb J* 2013;**27**(11):4455–65.
93. Sindhura Reddy N, et al. Tetracycline nanoparticles loaded calcium sulfate composite beads for periodontal management. *Biochim Biophys Acta* 2014;**1840**(6):2080–90.
94. Garg T, et al. Development and characterization of nano-fiber patch for the treatment of glaucoma. *Eur J Pharm Sci* 2014;**53**:10–6.
95. Huang Z-M, et al. A review on polymer nanofibers by electrospinning and their applications in nanocomposites. *Compos Sci Technol* 2003;**63**(15):2223–53.
96. Bottino MC, et al. Biodegradable nanofibrous drug delivery systems: effects of metronidazole and ciprofloxacin on periodontopathogens and commensal oral bacteria. *Clin Oral Invest* 2014;**18**(9):2151–8.
97. Tamai N, et al. Novel hydroxyapatite ceramics with an interconnective porous structure exhibit superior osteoconduction in vivo. *J Biomed Mater Res* 2002;**59**(1):110–7.
98. Horváth A, et al. Histological evaluation of human intrabony periodontal defects treated with an unsintered nanocrystalline hydroxyapatite paste. *Clin Oral Invest* 2013;**17**(2):423–30.
99. Mousavi SM, et al. Effect of esthetic coating on surface roughness of orthodontic archwires. *Int Orthod* 2017;**15**(3):312–21.
100. Tahmasbi S, Ghorbani M, Masudrad M. Galvanic corrosion of and ion release from various orthodontic brackets and wires in a fluoride-containing mouthwash. *J Dent Res Dent Clin Dent Prospects* 2015;**9**(3):159–65.
101. Tahmasbi S, Sheikh T, Hemmati YB. Ion release and galvanic corrosion of different orthodontic brackets and wires in artificial saliva. *J Contemp Dent Pract* 2017;**18**(3):222–7.
102. Mikulewicz M, et al. Transparent orthodontic archwires: a systematic literature review. *Arch Civ Mech Eng* 2017;**17**(3):651–7.
103. Małkiewicz K, et al. Comparative assessment of the corrosion process of orthodontic archwires made of stainless steel, titanium–molybdenum and nickel–titanium alloys. *Arch Civ Mech Eng* 2018;**18**(3):941–7.
104. Arango S, Peláez-Vargas A, García C. Coating and surface treatments on orthodontic metallic materials. *Coatings* 2012;**3**(1):1–15.
105. Katz A, et al. Self-lubricating coatings containing fullerene-like WS2 nanoparticles for orthodontic wires and other possible medical applications. *Tribol Lett* 2006;**21**(2):135–9.
106. Syed SS, et al. A novel method of coating orthodontic archwires with nanoparticles. *J Int Oral Health* 2015;**7**(5):30–3.
107. Kachoei M, et al. Zinc-oxide nanocoating for improvement of the antibacterial and frictional behavior of nickel-titanium alloy. *Nanomedicine (Lond)* 2016;**11**(19):2511–27.
108. Kachoei M, et al. The effect of zinc oxide nanoparticles deposition for friction reduction on orthodontic wires. *Dent Res J* 2013;**10**(4):499–505.
109. Rapoport L, et al. Tribological properties of WS2 nanoparticles under mixed lubrication. *Wear* 2003;**255**(7–12):785–93.
110. Cizaire L, et al. Mechanisms of ultra-low friction by hollow inorganic fullerene-like MoS2 nanoparticles. *Surf Coating Technol* 2002;**160**(2–3):282–7.
111. Lundstrom F, Krasse B. Streptococcus mutans and lactobacilli frequency in orthodontic patients; the effect of chlorhexidine treatments. *Eur J Orthod* 1987;**9**(2):109–16.
112. Banks PA, et al. Fluoride-releasing elastomerics–a prospective controlled clinical trial. *Eur J Orthod* 2000;**22**(4):401–7.
113. Benson PE, Douglas CW, Martin MV. Fluoridated elastomers: effect on the microbiology of plaque. *Am J Orthod Dentofacial Orthop* 2004;**126**(3):325–30.
114. Mattick CR, et al. Fluoride-releasing elastomeric modules reduce decalcification: a randomized controlled trial. *J Orthod* 2001;**28**(3):217–9.

115. Lee SJ, et al. Preparation and characterization of antibacterial orthodontic resin containing silver nanoparticles. *Appl Surf Sci* 2018;**432**:317–23.
116. Nordgarden H, Jensen JL, Storhaug K. Reported prevalence of congenitally missing teeth in two Norwegian counties. *Community Dent Health* 2002;**19**(4):258–61.
117. Jorgenson RJ. Clinician's view of hypodontia. *J Am Dent Assoc* 1980;**101**(2):283–6.
118. Muller TP, et al. A survey of congenitally missing permanent teeth. *J Am Dent Assoc* 1970;**81**(1):101–7.
119. Esposito M, et al. Interventions for replacing missing teeth: different times for loading dental implants. *Cochrane Database Syst Rev* 2013;**21**(3):CD003878.
120. Totu EE, et al. Poly (methyl methacrylate) with TiO2 nanoparticles inclusion for stereolitographic complete denture manufacturing– the fututre in dental care for elderly edentulous patients? *J Dent* 2017;**59**:68–77.
121. Ahmed M, Ebrahim M. Effect of zirconium oxide nano-fillers addition on mechanical properties of heat-polymerized acrylic resin. *Al-Azhar Dent J Girls* 2016;**3**(1):41–8.
122. Gad M, et al. Effect of zirconium oxide nanoparticles addition on the optical and tensile properties of polymethyl methacrylate denture base material. *Int J Nanomed* 2018;**13**:283–92.
123. Satpathy A, et al. Patient awareness, acceptance and perceived cost of dental Implants as a treatment modality for replacement of missing teeth: a survey in Bhubaneswar and Cuttack. *Int J Public Health Dent* 2011;**2**:1–7.
124. Amri R, Saker S. Dental implants therapy: a cross-sectional study of patients' knowledge and awareness. *Br J Med Med Res* 2017;**19**(6):1–9.
125. Liu W, et al. Selenium nanoparticles incorporated into titania nanotubes inhibit bacterial growth and macrophage proliferation. *Nanoscale* 2016;**8**(34):15783–94.
126. Wiedmer D, et al. Antibacterial effect of hydrogen peroxide-titanium dioxide suspensions in the decontamination of rough titanium surfaces. *Biofouling* 2017;**33**(6):451–9.
127. Matsubara VH, et al. Use of silver nanoparticles reduces internal contamination of external hexagon implants by Candida albicans. *Braz Dent J* 2015;**26**(5):458–62.
128. Pokrowiecki R, et al. In vitro studies of nanosilver-doped titanium implants for oral and maxillofacial surgery. *Int J Nanomed* 2017;**12**:4285–97.
129. Liu X, et al. Antibacterial properties of nano-silver coated PEEK prepared through magnetron sputtering. *Dent Mater* 2017;**33**(9):e348–60.
130. Chen P, et al. Fabrication of a silver nanoparticle-coated collagen membrane with anti-bacterial and anti-inflammatory activities for guided bone regeneration. *Biomed Mater* 2018;**13**(6):065014.
131. Vilarrasa J, et al. In vitro evaluation of a multispecies oral biofilm over antibacterial coated titanium surfaces. *J Mater Sci Mater Med* 2018;**29**(11):164.
132. Abdulkareem EH, et al. Anti-biofilm activity of zinc oxide and hydroxyapatite nanoparticles as dental implant coating materials. *J Dent* 2015;**43**(12):1462–9.
133. Memarzadeh K, et al. Nanoparticulate zinc oxide as a coating material for orthopedic and dental implants. *J Biomed Mater Res* 2015;**103**(3):981–9.
134. Westas E, et al. Bactericidal effect of photocatalytically-active nanostructured TiO2 surfaces on biofilms of the early oral colonizer, Streptococcus oralis. *J Biomed Mater Res A* 2017;**105**(8):2321–8.
135. Yang T, et al. Cytocompatibility and antibacterial activity of titania nanotubes incorporated with gold nanoparticles. *Colloids Surf B Biointerfaces* 2016;**145**:597–606.
136. Swain S, Rautray TR, Narayanan R. Sr, Mg, and Co substituted hydroxyapatite coating on TiO_2 nanotubes formed by electrochemical methods. *Adv Sci Lett* 2016;**22**(2):482–7.
137. Chen Y, He F. Fabrication and biological evaluation of the coating co-doped strontium and zinc nanoparticles on porous pure titanium surface by hydrothermal method. *Clin Oral Implants Res* 2019;**30**(S19). pp. 48–48.
138. Lin G, et al. Strontium-incorporated titanium implant surface treated by hydrothermal reactions promotes early bone osseointegration in osteoporotic rabbits. *Clin Oral Implants Res* 2019;**30**(8):777–90.
139. Zhu Y, et al. Hierarchical micro/nanostructured titanium with balanced actions to bacterial and mammalian cells for dental implants. *Int J Nanomed* 2015;**10**:6659.
140. Wang G, et al. Antibacterial effects of titanium embedded with silver nanoparticles based on electron-transfer-induced reactive oxygen species. *Biomaterials* 2017;**124**:25–34.
141. Liu W, et al. Synthesis of TiO2 nanotubes with ZnO nanoparticles to achieve antibacterial properties and stem cell compatibility. *Nanoscale* 2014;**6**(15):9050–62.

142. Li Z, et al. TiO2 nanorod arrays modified Ti substrates promote the adhesion, proliferation and osteogenic differentiation of human periodontal ligament stem cells. *Mater Sci Eng C Mater Biol Appl* 2017;**76**:684–91.
143. Sadat-Shojai M, et al. Hydroxyapatite nanorods as novel fillers for improving the properties of dental adhesives: synthesis and application. *Dent Mater* 2010;**26**(5):471–82.
144. Mohammad Ali K, et al. Synthesis and characterization of nanoparticles and nanocomposite of ZnO and MgO by sonochemical method and their application for zinc polycarboxylate dental cement preparation. *Int Nano Lett* 2011;**1**(1):43–51.
145. Lucas ME, Arita K, Nishino M. Toughness, bonding and fluoride-release properties of hydroxyapatite-added glass ionomer cement. *Biomaterials* 2003;**24**(21):3787–94.
146. Mair LH. Wear in dentistry—current terminology. *J Dent* 1992;**20**(3):140–4.
147. Hemingway CA, et al. Erosion of enamel by non-carbonated soft drinks with and without toothbrushing abrasion. *Br Dent J* 2006;**201**(7):447–50. discussion 439; quiz 466.
148. Milosevic A. Acid erosion: an increasingly relevant dental problem. Risk factors, management and restoration. *Prim Dent J* 2017;**6**(1):37–45.
149. Mahapatra A, et al. Role of salivary pH and flow rate in tooth wear: a clinico-physicochemical study. *Adv Sci Lett* 2016;**22**(2):494–6.
150. Scheutzel P. Etiology of dental erosion—intrinsic factors. *Eur J Oral Sci* 1996;**104**(2 (Pt 2)):178–90.
151. Bartlett DW, et al. A study of the association between gastro-oesophageal reflux and palatal dental erosion. *Br Dent J* 1996;**181**(4):125–31.
152. Lussi A, Jaeggi T, Zero D. The role of diet in the aetiology of dental erosion. *Caries Res* 2004;**38**(Suppl. 1):34–44.
153. Imfeld T. Dental erosion. Definition, classification and links. *Eur J Oral Sci* 1996;**104**(2 (Pt 2)):151–5.
154. Grippo JO. Abfractions: a new classification of hard tissue lesions of teeth. *J Esthetic Dent* 1991;**3**(1):14–9.
155. Rees JS, Somi S. A guide to the clinical management of attrition. *Br Dent J* 2018;**224**(5):319–23.
156. Ghazal M, Hedderich J, Kern M. Wear of feldspathic ceramic, nano-filled composite resin and acrylic resin artificial teeth when opposed to different antagonists. *Eur J Oral Sci* 2008;**116**(6):585–92.
157. Terry DA. Direct applications of a nanocomposite resin system: part 1–The evolution of contemporary composite materials. *Pract Proced Aesthet Dent* 2004;**16**(6):417–22.
158. Ghazal M, Albashaireh ZS, Kern M. Wear resistance of nanofilled composite resin and feldspathic ceramic artificial teeth. *J Prosthet Dent* 2008;**100**(6):441–8.
159. Loyaga-Rendon PG, et al. Compositional characteristics and hardness of acrylic and composite resin artificial teeth. *J Prosthet Dent* 2007;**98**(2):141–9.
160. Nakashima S, et al. Effect of a test dentifrice containing nano-sized calcium carbonate on remineralization of enamel lesions in vitro. *J Oral Sci* 2009;**51**(1):69–77.
161. Rees JS, et al. The prevalence of dentine hypersensitivity in a hospital clinic population in Hong Kong. *J Dent* 2003;**31**(7):453–61.
162. Gillam DG, et al. Comparison of dentine hypersensitivity in selected Occidental and oriental populations. *J Oral Rehabil* 2001;**28**(1):20–5.
163. Khetawat S. Nanotechnology (nanohydroxyapatite crystals): recent advancement in treatment of dentinal hypersensitivity. *JBR J Interdiscip Med Dent Sci* 2015;**3**(3).
164. Vano M, et al. Reducing dentine hypersensitivity with nano-hydroxyapatite toothpaste: a double-blind randomized controlled trial. *Clin Oral Invest* 2018;**22**(1):313–20.
165. Lin K, Wu C, Chang J. Advances in synthesis of calcium phosphate crystals with controlled size and shape. *Acta Biomater* 2014;**10**(10):4071–102.
166. Wu SH, Mou CY, Lin HP. Synthesis of mesoporous silica nanoparticles. *Chem Soc Rev* 2013;**42**(9):3862–75.
167. Chiang YC, et al. A mesoporous silica biomaterial for dental biomimetic crystallization. *ACS Nano* 2014;**8**(12):12502–13.
168. Kumar S, Vijayalakshmi R. Nanotechnology in dentistry. *Indian J Dent Res* 2006;**17**(2):62–5.
169. MacEntee MI, Glick N, Stolar E. Age, gender, dentures and oral mucosal disorders. *Oral Dis* 1998;**4**(1):32–6.
170. Blanchet PJ, et al. Oral dyskinesia: a clinical overview. *Int J Prosthod* 2005;**18**(1).
171. Porwal A, et al. Association of neutral zone position with age, gender, and period of edentulism. *J Prosthodont* 2016;**27**.
172. Douglass CW, Shih A, Ostry L. Will there be a need for complete dentures in the United States in 2020? *J Prosthet Dent* 2002;**87**(1):5–8.

173. El Bahra S, et al. Linear and volumetric dimensional changes of injection-molded PMMA denture base resins. *Dent Mater* 2013;**29**(11):1091–7.
174. Soygun K, Bolayir G, Boztug A. Mechanical and thermal properties of polyamide versus reinforced PMMA denture base materials. *J Adv Prosthodont* 2013;**5**(2):153–60.
175. Vojdani M, Bagheri R, Khaledi AAR. Effects of aluminum oxide addition on the flexural strength, surface hardness, and roughness of heat-polymerized acrylic resin. *J Dent Sci* 2012;**7**(3):238–44.
176. Machado de Andrade I, et al. Effect of chlorhexidine on denture biofilm accumulation. *J Prosthodont* 2012;**21**(1):2–6.
177. Williams DW, et al. Microbial contamination of removable prosthodontic appliances from laboratories and impact of clinical storage. *Br Dent J* 2011;**211**(4):163.
178. Miettinen VM, Vallittu PK. Release of residual methyl methacrylate into water from glass fibre-poly (methyl methacrylate) composite used in dentures. *Biomaterials* 1997;**18**(2):181–5.
179. Akin H, Tugut F, Polat ZA. In vitro comparison of the cytotoxicity and water sorption of two different denture base systems. *J Prosthodont* 2015;**24**(2):152–5.
180. Beyth N, et al. Alternative antimicrobial approach: nano-antimicrobial materials. *Evid Based Complement Alternat Med* 2015;**12**. 2015.
181. Monteiro DR, et al. Silver distribution and release from an antimicrobial denture base resin containing silver colloidal nanoparticles. *J Prosthodont* 2012;**21**(1):7–15.
182. Hamedi-Rad F, et al. Effect of nanosilver on thermal and mechanical properties of acrylic base complete dentures. *J Dent* 2014;**11**(5):495.
183. Wady A, et al. Evaluation of Candida albicans adhesion and biofilm formation on a denture base acrylic resin containing silver nanoparticles. *J Appl Microbiol* 2012;**112**(6):1163–72.
184. Khaled S, et al. Synthesis of TiO2− PMMA nanocomposite: using methacrylic acid as a coupling agent. *Langmuir* 2007;**23**(7):3988–95.
185. Su W, et al. Plasma pre-treatment and TiO2 coating of PMMA for the improvement of antibacterial properties. *Surf Coating Technol* 2010;**205**(2):465–9.
186. Ercan B, et al. Diameter of titanium nanotubes influences anti-bacterial efficacy. *Nanotechnology* 2011;**22**(29):295102.
187. Kummer KM, et al. Effects of different sterilization techniques and varying anodized TiO2 nanotube dimensions on bacteria growth. *J Biomed Mater Res B Appl Biomater* 2013;**101**(5):677–88.
188. Zhang F, et al. Blue-light -activated nano-TiO2@PDA for highly effective and nondestructive tooth whitening. *ACS Biomater Sci Eng* 2018;**4**(8):3072–7.
189. Kakhki NA. Design, synthesis and application of gold nanoparticles in tooth whitening process. *Adv Nanobiotechnol* 2018;**1**(1):4–8.
190. Lima FV, et al. Carbamide peroxide nanoparticles for dental whitening application: characterization, stability and in vivo/in situ evaluation. *Colloids Surf B Biointerfaces* 2019;**179**:326–33.
191. Nahum A. The biomechanics of maxillofacial trauma. *Clin Plast Surg* 1975;**2**(1):59–64.
192. Bhardwaj A, et al. Nanotechnology in dentistry: present and future. *J Int Oral Health* 2014;**6**(1):121.
193. Mantha VRR, et al. Nanoanesthesia. *Anesth Analg* 2014;**118**(6):1355–62.
194. Chen C, You P. A novel local anesthetic system: transcriptional transactivator peptide-decorated nanocarriers for skin delivery of ropivacaine. *Drug Des Devel Ther* 2017;**11**:1941–9.
195. Freitas Jr RA. Nanodentistry. *J Am Dent Assoc* 2000;**131**(11):1559–65.
196. Saravana KR, Vijayalakshmi R. Nanotechnology in dentistry. *Indian J Dent Res* 2006;**17**(2):62–5.
197. Petersen DK, Naylor TM, Ver Halen JP. Current and future applications of nanotechnology in plastic and reconstructive surgery. *Plast Aesthet Res* 2014;**1**:43–50.
198. Mahapatro A, Singh DK. Biodegradable nanoparticles are excellent vehicle for site directed in-vivo delivery of drugs and vaccines. *J Nanobiotechnol* 2011;**9**:55.
199. Brannon-Peppas L, Blanchette JO. Nanoparticle and targeted systems for cancer therapy. *Adv Drug Deliv Rev* 2004;**56**(11):1649–59.
200. Chaturvedi VK, et al. Cancer nanotechnology: a new revolution for cancer diagnosis and therapy. *Curr Drug Metabol* 2019;**20**(6):416–29.
201. Gmeiner WH, Ghosh S. Nanotechnology for cancer treatment. *Nanotechnol Rev* 2015;**3**(2):111–22.

202. Liboiron BD, Mayer LD. Nanoscale particulate systems for multidrug delivery: towards improved combination chemotherapy. *Ther Deliv* 2014;**5**(2):149–71.
203. Wong DT. Salivary diagnostics powered by nanotechnologies, proteomics and genomics. *J Am Dent Assoc* 2006;**137**(3):313–21.This page intentionally left blank

CHAPTER

19

Nebulizer spray delivery of phytopharmaceutical nanosuspension via oral and nasal route: a challenging approach to fight against COVID-19

Abhishek Bhattacharjee[1], *Sabu Thomas*[2] *and Partha Palit*[1]

[1]**Department of Pharmaceutical Sciences, Assam University, Silchar, Assam, India;** [2]**School of Chemical Sciences, Mahatma Gandhi University, Kottayam, Kerala, India**

1. Introduction

The global data on severity and mortality of the coronavirus disease 2019 (COVID-19) pandemic showed that the people of almost all countries and territories have been struggling due to lack of a specific vaccine or effective prophylactic or therapeutic treatment. A commercial vaccine (live attenuated, heat-killed, RNA or subunit) for the community people usually takes time. While, to date, most of the antiviral protease inhibitors and (Ritonavir, Lopinavir, Remdesivir, Hydroxychloroquine, etc.) and specific anti-inflammatory drug used for COVID-19 patients is on trial and error basis. Most cases, patients are unable to recover due to nonspecific drug binding, and adverse drug reaction related to patient's comorbid conditions including organ malfunctioning.[1–5] So, drug target identification, followed by specific drug delivery for rapid healing and protection against devastating severe acute respiratory syndrome coronavirus 2 (SARS-CoV-2), is necessary on an urgent basis.

The SARS-CoV-2, the causative agent of COVID-19, is an enveloped, non-segmented positive-sense single-stranded (ss) RNA virus that contains four structural proteins: Spike (S), Envelope (E), Membrane (M), and Nucleocapsid (N) proteins.[44,6] It is reported that the Spike glycoprotein of this virion harbors a Furin cleavage site, at the boundary between

Applications of Multifunctional Nanomaterials
https://doi.org/10.1016/B978-0-12-820557-0.00017-5

its two subunits, S1/S2, which is activated by the host cell enzyme Furin to make the virus more susceptible to its primary receptor, angiotensin-converting enzyme-2(ACE2).[7] Furin also helps the virion to bind with ACE2 efficiently, via the receptor-binding domain of S-protein, to transmit the virus as stable form and invade the host cell rapidly for further pathogenicity.[8,7] The receptor-binding domain of S-protein after cleavage mediating processing, followed by activation, is responsible for binding with ACE2; In contrast, the interaction of S-protein with host cell ACE2 receptor helps the virus to invade the host cell.[9] The binding affinity of S-protein with ACE-2 is about 10 times higher than other coronaviruses,[10] indicated that CoV-2 infection depends on host cell ACE2 receptor expression. Furthermore, TMPRSS-2 (Transmembrane protease serine 2) fuse and activate the S-protein-ACE2 complex into the host cell endosome, via proteolytic digestion of the S-protein's S2 domain through membrane fusion.[53] This cascade helps to promote the pathogenicity and life-cycle, for which ACE2 and TMPRSS2 can be served as a viable target for nCoV-2 therapy. It has been found that Furin and TMPRSS2 could play a significant role for efficient attachment of cleaved S-protein with host cell ACE2 receptor via activation, priming, and fusion, followed by endosomal internalization to establish pathogenicity through replication, growth, and spread of the infecting virus to another organ. The proteolytic activity of such transmembrane serine protease, before cleavage, activation, and fusion has been exploited by the S-protein of COVID-19 virus toward stronger infection.[11]

In searching for the phyto-compounds, the scientific literature reveals that nature-derived phytopharmaceuticals when active phyto-ingredient is prepared with the suitable and compatible pharmaceutical vehicles and excipients are much more effective and hold promise rather than conventional synthetic or semisynthetic allopathic drug molecule or solo-Phyto molecules to fight against various viral infection (Table 19.1). Some of the phyto-herbal compounds were found to be efficacious against different lethal viral strain such as SARS-COV-1, influenza, MERS coronavirus, Dengue, Japanese encephalitis, Chikungunya, Ebola, human retroviral infection, as suggested by earlier reports. **Curcumin, zingiberene, Ursolic acid, boswellic acid, withanolides, epigallocatechin gallate, glycyrrhizin, piperine, eugenol, and sinigrin** like potential herbal leads had shown profound antimicrobial activity including infection of SARS, influenza, and coronavirus.[13,14]

TABLE 19.1 Detection of microbial strains via biosensor application in various food products.[12]

Target microbes	Transducer signal	Sensor assembly	Bioreceptor	Analytes
Sa. typhimurium; Es coli 0157:H7; *Shi. dysenteriae; Cb. jejuni*	Fluorescence	NRL array sensor (fluorescence- based affinity assay)	Antibody, ganglioside receptors, oligo-saccharide	Food or environmental Samples
Sa. enteric; Li. monocytogens; Es. coli. 0157:H7;	Fluorescence	Antibodies linked viabiotin/ avidinton; optical fibers	Polyclonal antibody for capture antibody; fluorescent monoclonal antibody oraptamera against surface protein Inl	Artificially contaminated meat samples

TABLE 19.1 Detection of microbial strains via biosensor application in various food products.[12]—cont'd

Target microbes	Transducer signal	Sensor assembly	Bioreceptor	Analytes
Es. coli.	Fluorescence	Bioconjugated magnetic beads for capture fluorescent polymeric micelles for reporting	Polyclonal anti-E.coli antibodies	Bacteria in buffer
Es. coli.	Thin-film optical interference Spectroscopy	Antibody- functionalized nanostructure deoxidized porous silicon($PSiO_2$)	Anti-e.coli polyclonal antibody	Bacteria in buffer
Sa. typhimurium	Light scattering	Immunoagglutination assay using anti-Salmonella-conjugated polystyrene microparticles	Anti-salmonella polyclonal antibody	Liquid from processed raw chicken
She. oneidensis	SERS	Silver nanoparticles sandwiched by analyte binding on optical fiber tip	NA	Bacteria in buffer
Es. coli; St. aureus Ba. subtilis	SPR	Long-range SPR antibodieson SAM-gold surface/antibody −functionalized magnetic nanoparticles	potato lectin	Bacteria in serum-spiked buffer

Abbreviations: *Es*: Escherichia; *Ls*: Listeria; *NA*: Not applicable; *Sa*: Salmonella; *SERS*: Surface-enhanced Raman scattering; *She*: Shewanella; *Shi*: Shigella; *SPR*: Surface Plasmon resonance.

However, those phytocompounds have some pharmacokinetic issues related to absorption, bio-availability, first-pass metabolism, for which they not able to hold promise for in vivo potentiality against the infection model, instead of remarkable in vitro results on the viral strain. Therefore, nanotechnology-based anti-COVID drug lead developments are urgently required to keeping up the in vivo stability of the Phyto leads and target-oriented disease management against viral infection and acute inflammation.[15] Nanotechnology oriented drug delivery of the phytopharmaceuticals are needed to be formulated to protect the phytocompounds from in vivo metabolic breakdown into in-active metabolites through oxidation-reduction reaction (Table 19.2).[17]

Secondly, COVID-19 diseases affect the lungs of the patient via ACE2 host cell receptor-mediated pulmonary cellular infection. In this regard, host cell, extracellular **furin proproteinconvertase** and **Transmembrane serine protease (TMPRSS2)** help the virus to get entry inside the cell via membrane fusion, cutting of the spike protein into favourable cleavage side, endocytosis, which further facilitates the viral replication and growth. This phenomenon, in turn, creates pulmonary blood vessels inflammation, vasculitis, lung fibrosis followed by cytokine storm for organ damage in the acute stages.[18] So COVID pandemic demands a safe and effective therapeutic strategy via novel drug delivery system (Fig. 19.1).

As per established scientific knowledge reminds us that nano-suspension-based spray delivery of the lead phytocompounds via intranasal or oral route needs to be highlighted to transport the potential Phyto-drug molecules into the host pulmonary cells of the lungs.[19,20,21,22]

TABLE 19.2 Nanoparticles application in medical sectors.[16]

Nanoparticle	Function	Cell types
Iron oxide nanoparticles	Oxidant by Nox 4 over expression	Myocardium from mice
RNP	Neuroprotective agent (due to its ability to scavenge free radicals	Middle cerebral artery from rats with cerebral ischemia/reperfusion injury
Redox -polymer nano therapeutics	Treatment of the neurodegenerative diseases	Brain from sanescence-accelerated Mouse prone (SAMP8)
WO3 −Pt nanoparticles	Oxidant. Nicotinamide adenine dinucleotide phosphate (NADPH) oxidase biomimetic	Tumor cells
Silver nanoparticles	Oxidant by increasing Nox 4 expression	Human umbilical vein endothelial cells
Silver nanoparticles are used	Increase of hypertension due to a decrease in NO levels	Myocardium from rats
PLGA nanoparticles	Carrier. Treatment for hypertension	Hypertensive rats
Iron oxide, yttrium oxide, cerium oxide, zinc oxide	Proinflammatory	Human vascular endothelial cell line
Nanoparticles based on polyoxalate	Antioxidant and antiinflammatory	Doxorubicin-treated mice heart
Polyketal particles	SOD carrier	Rat myocardium
Nanoceria	Prooxidant. Microvascular dysfunction	Arteriola from rats

PEG, polyethylene glycol; PLGA, copolymerpoly (lactic-co-glycolic acid); RNP, radical-containing nanoparticles; SOD, superoxide dismutase; W03−Pt, platinum tungsten oxide.

Hence, current chapter, our deep insights of nanotechnology-based intranasal or intraoral anti-COVID drug delivery of suitable phytopharmaceuticals as a receptor-ligand on those cellular drug targets will be emphasized to Controlling and eliminating the spread and reoccurrence of this pandemic.

2. The origin of phytocompounds as antiviral agents

To this end, aromatic herbs, herbal teas, culinary spices, and medicinal plants used in the traditional mode of treatments have been regarded as highly promising. As they are safe, effective and nature gifted, easily available as per requirement. Moreover, several bioactive leads like **glycyrrhizin, andrographolide, silymarin, Baicalin, Theaflavin, Azadirachtin, Curcumin, Lycorine, Galantamine, Saikosaponin, Ursolic acid, Rosmarinic acid, and Emodin** have revealed promising effect against different deadly viral infection. During the 2003 SARS outbreak,[23] the efficacy and performance of phyto-therapy and phytomedicine for governing viral infections were exemplified. As such, different countries, including China, Japan, Korea Algeria, are inspiring the use of herbal and medicinal plants in fighting

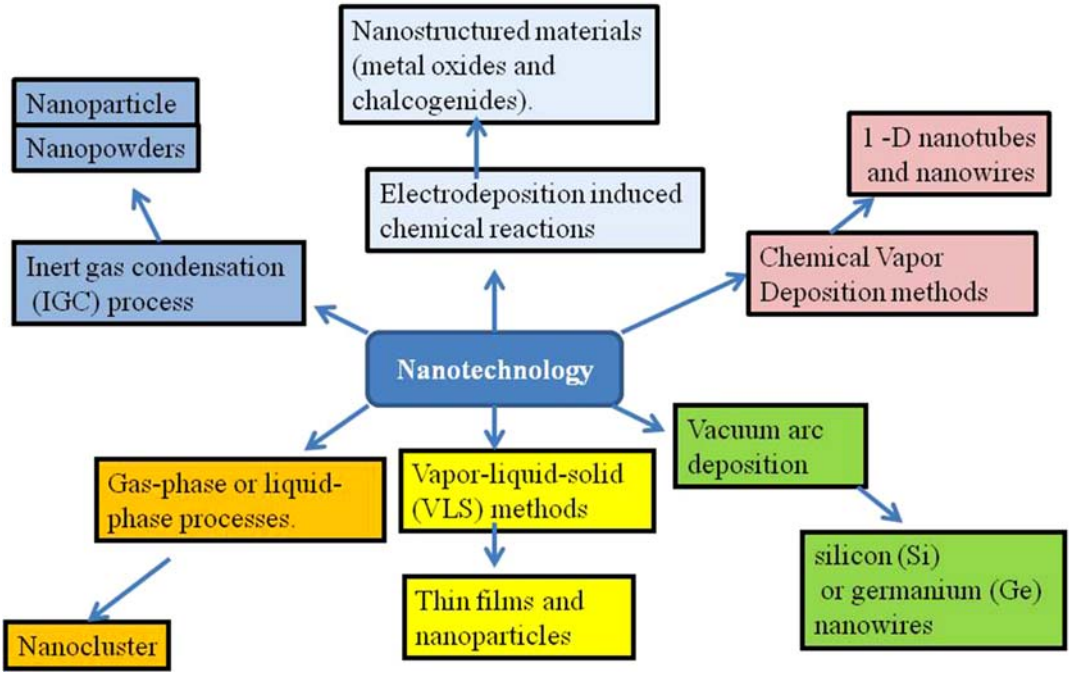

FIGURE 19.1 Nanotechnology approaches for different types of nanoparticles or materials for various sectors.

SARS-CoV-2 infection[23]; Phyto. Res.[24,25,26] After the outbreak of SARS-CoV (2003) and MERS-CoV in 2015, researchers have been energetically trying to discover different antiviral extracts and Phyto-molecules against SARS-CoV. This information had directed a group of experts to screen more than 200 medicinal plants, culinary spices, and aromatic herbs for their antiviral properties against this SARS-CoV strain.[27,28] The antiviral effects of these extracts and lead phyto molecules isolated were dose-dependent. They ranged from low to high concentrations of the extracts, depending on the requirement.[27]

2.1 Background study of phytopharmaceuticals for treatment of respiratory viral infection like influenza, SARS, and MERS coronavirus

An earlier study on traditional and ethnic phyto molecules and their respective extracts, bioactivity guided fraction demonstrated very promising viricidal or host-virus interaction blocking results against the respiratory viral infection particularly in **influenza, SARS, and MERS coronavirus**. Especially, L. radiata exhibited the most potent antiviral activity against the virus strain. These data are in accordance with those of two other research teams, which confirmed that an active compound contained in liquorice roots, i.e., glycyrrhizin, confers an anti-SARS-CoV effect by stopping viral replication.[29] In another study, glycyrrhizin (**Glycyrrhiza glabra, Fabaceae family**) also exhibited antiviral property when tested for its in vitro antiviral activity on 10 different clinical strains of SARS-CoV. **Baicalin**, a constituent of the plant Baikal skullcap (*Scutellariabaicalensis*), has been demonstrated encouraging antiviral

potential against SARS-CoV.[30] So far, in-vitro results of **Baicalin** may not correlate with in-vivo clinical efficacy. Because the oral bio-availability of Baicalin was not satisfactory as per expectation. **Lycorine** is a toxic crystalline alkaloid found in various Amaryllidaceae species and has also confirmed a powerful antiviral effect against SARS-CoV. Several previous investigations suggest that lycorine seems to have broad antiviral properties and has been reported to have an inhibitory action on the Herpes simplex virus (HSV, type I)[31] and Poliomyelitis virus.[32] Other medicinal herbs and plants and culinary spices that have been described to have antiviral properties against SARS-CoV, Influenza, and MERS are Japanese honeysuckle (*Lonicera japonica*), the commonly known Eucalyptus tree, and Korean ginseng (Panax ginseng) the last one through its active secondary metabolite, **ginsenoside-Rb1,**[33] **Sinigrin** and **Hesperidin** have demonstrated impressive antiviral property against SARS-COV-1 and MERS-COV, as well. **Berberine, Quercetin, hypericin, rutin, isoquercetin, Epigallocatechin 3-gallate, Sylimarin, Bromhexine, Coumarins, Gingerols, and Curcumin** are the potential leads derived from various traditional herbs and spices and showed very outstanding antiviral efficacy against respiratory viral infection caused by Influenza virus.[13,34]

2.2 Scope and prospect of phytocompounds for antiviral pharmaceutical dosage form for nano-suspension

Inclusion of microemulsion, emulsion, and liposomes may increase bioavailability. Decrease of size to submicron size, which is recognized as nanosizing, of drugs is also becoming popular nowadays. It could deliver the drug molecules, particularly unstable bioactive phytochemicals, to their locus of action.[35] As an augmentation of solubility of drugs may be an ideal approach for increasing bioavailability via nanosizing drug formulation. This approach may also be quite useful for antiviral drug delivery for treatment, as during viral infection, upper respiratory tract and lungs are being affected by moderate to severe degree. In this context, intranasal or oral nanosuspension based antiviral phytochemicals could confer impressive response for rapid recovery against severe to moderate respiratory syndrome caused by SARS virus. The epithelial surface in the nasal cavity is permeable, and phytochemicals can easily enter. This strategy is appropriate to the drugs which are meant for the nose and lungs. If applied through the nasal cavity, these phyto-leads can circumvent the first-pass metabolism in the liver and plasma enzyme-mediated degradation.

Phyto-chemicals that are not stable in gastric fluid and are harmed during the first-pass metabolism in the liver may be applied by nano-spray based nebulizer dosage form through nasal or oral route. In this way, absorption is slow. This is suitable for drugs given in a low dose for obtaining the desired effect of antiviral response.[36] It is interestingly noted that so many phyto-compounds such as **sinigrin, curcumin, glucoraphanin, allicin, allitridin, and Gingerol** have some limitations at oral-systemic application may due to pharmacokinetic instability.[37] Therefore, nanosuspension coating of potential unstable antiviral phytochemicals can improve the stability, safety, and efficacy for upper respiratory viral infection with high-biological half-life reducing the dose frequency. The report reveals that these novel formulation-based drug deliveries are conveyed to have outstanding advantages over conventional formulations of plant actives and extracts which embrace enhancement of solubility, bioavailability, protection from toxicity, enhancement of pharmacological activity, improved tissue macrophages distribution, sustained delivery, and protection from physical

and chemical degradation.[38] Proposed nano-suspension-based nebulizer drug delivery aims to improve the target specification curb the unwanted side effects of the active phyto-ingredient when used at high levels. Current potent herbs derived phyto molecules such as epigallocatechin gallate, Quercetin, resveratrol and curcumin, silymarin are supposed to be prospecting and productive.[39]

3. The rationality behind choosing nano-suspension based drug delivery for antiviral response in the context of COVID-19

Earlier reports recommend that two potent Phyto molecules curcumin and silymarin had shown fruitful antiviral response against the number of pathogenic deadly viral infection in the in vivo system through nanoparticle-based drug delivery. This nanotechnology-based nano-emulsion or nano-suspension phyto-formulations of the bioactive natural compounds (**curcumin and silymarin)** has remarkably improved the pharmacokinetic parameters to meet significant antiviral response. Because **curcumin** and **silymarin** face lot of issues related to solubility, absorption, cellular drug distribution and first-pass metabolism, for which the bioactivity against the viral infection in the cellular or tissue level have been hindered.[40,41,42] Moreover, viral diseases distress millions of people universally, with a major influence on human health and socioeconomic development. More than 40 million people are exaggerated with human immunodeficiency virus (HIV) alone. SARS, MERS infection caused by influenza, corona, and another deadly virus like Ebola, chikungunya, etc., have taken many lives worldwide in the last 2 years. Hence, present chapter highlights the various nano-carriers (e.g., nano-liposomes, polymeric nanoparticles, solid lipid nanoparticles nano-emulsion, and nano-suspension, etc.) based on tactics that have been discussed in the literature and practically applied in the clinic to combat the different challenges met by the antiviral therapy. The recent developments in smart delivery technologies (e.g., nano-suspension) targeting delivery for site-specific lung mediated delivery of antiviral phytopharmaceuticals at the viral reservoirs are also being discussed in the context of handling of COVID-19 pandemic.[43] Moreover, earlier reports suggested that nano-suspension of lipid nanoparticle carrying suitable active ingredient has been formulated to bypass the lymph node drug insufficiency of the oral combination of the drugs. This nanoparticle formulation demonstrated long-lasting plasma drug profiles and better lymph node drug levels in the macaque in vivo model (Fig. 19.2).

Nanomedicine scientists should take advantage of advanced drug development tools via nano lipid particle-based suspension and followed by animal model's validation to investigate and explore the nanoparticle combination therapeutics of phytopharmaceuticals against COVID-19.[21]

3.1 Expected pharmacological targets for prevention of COVID-19 infection

3.1.1 Host cell surfaced receptor and nano-suspension-based spray drug delivery

The SARS-CoV-2, the causative agent of COVID-19, is an enveloped, nonsegmented positive-sense single-stranded (ss) RNA virus that contains four structural proteins: Spike

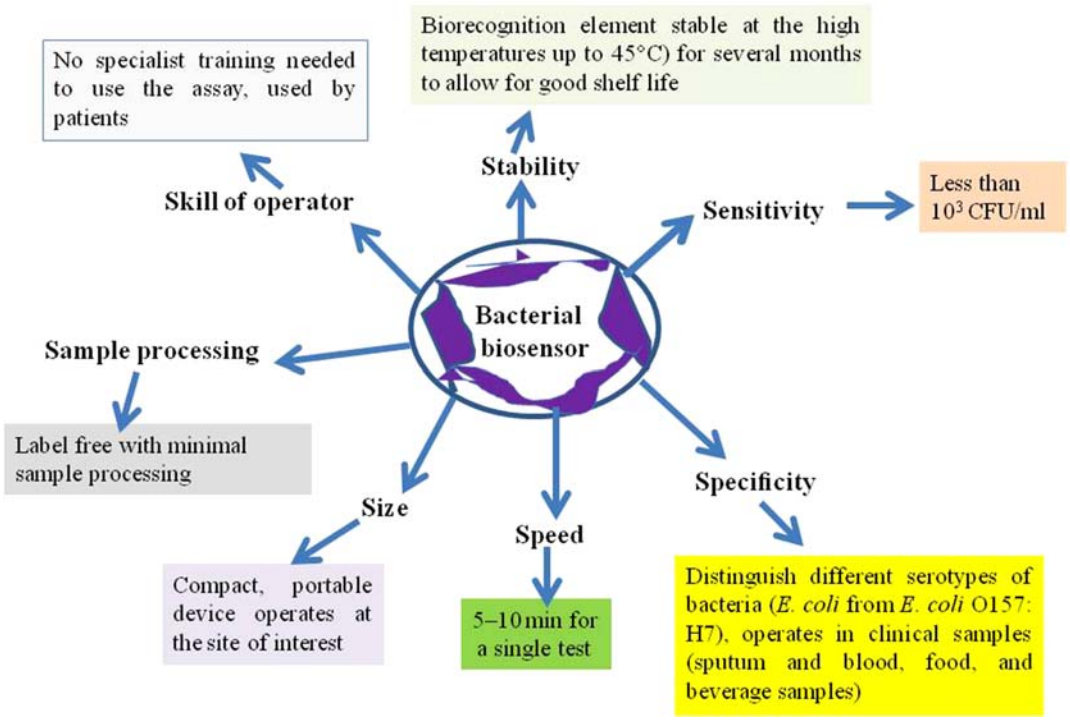

FIGURE 19.2 Bacterial biosensors with their parameters and value or quantity of detection.

(S), Envelope (E), Membrane (M), and Nucleocapsid (N) proteins.[44,6] It has been reported that the Spike glycoprotein of this virion anchorages a Furin cleavage site, at the boundary between its two subunits, S1/S2, which is triggered by the host cell enzyme Furin to make the virus more vulnerable to its primary receptor, angiotensin-converting enzyme-2(ACE2).[7] Furin also aids the virion to bind with ACE2 efficiently, via the receptor-binding domain of S-protein, to transmit the virus as stable form and invade the host cell rapidly for further pathogenicity.[8,7] The receptor-binding domain of S-protein after processing via cleavage, followed by activation, is responsible for binding with ACE2. In contrast, the interaction of S-protein with host cell ACE2 receptor helps the virus to invade the host cell.[9] The binding affinity of S-protein of novel coronavirus with ACE2 is about 10 times higher than other preceding coronaviruses,[10] suggesting that CoV-2 infection depends on host cell ACE2 receptor expression.

Furthermore, TMPRSS2 (Transmembrane protease serine 2) fuse and activate the S-protein-ACE2 complex into the host cell endosome, via proteolytic breakdown of the S-protein's S2 domain through membrane fusion.[11] This phenomenon assists in triggering the pathogenicity and life-cycle, for which ACE2 and TMPRSS2 can be served as a viable target for anti-COVID-19 therapy. It was reported that **Furin** and**TMPRSS2** could play a significant role for efficient attachment of cleaved S-protein with host cell ACE2 receptor via activation, priming, and fusion, subsequently endosomal internalization to establish pathogenicity through replication, growth, exocytosis and spread of the infecting virus to another cellular organ.

The proteolytic activity of such transmembrane serine protease, before cleavage, activation, and fusion has been exploited by the S-protein of COVID-19 virus toward stronger infection.[11] Our current understanding has emphasized on the rational selection of suitable phytopharmaceutical ligand as a potential anti-COVID-19 agent to targeting those host cell receptor proteases to impair the host cell-virus interaction. These could be achieved via nasal or oral nano-suspension spray-based drug delivery of suitable antiviral phytocompounds, to tackle this pandemic panic within a very shortened period.

Moreover, this validated receptor blockers could be delivered specifically via oral or nasal inhaler spray or vapor nano-spray formulation to the corresponding host cell receptor, located at oral mucosa, nasal membrane, and lung cell surface receptor. This tactic could be appropriate; because of the micronized nano-aerosol suspended drug particle would bind to the **Furin** and **TMPRSS2** receptor(s) of the cells in upper respiratory tract very rapidly in a small concentration, via targeted novel drug delivery system. Furthermore, drug formulated in e-cigarette[45] could deliver the active constituent quickly into the lung cell surface receptor for competitive binding to block the virus entry into the host cell. The strategy would provide promising therapeutic intervention toward the emerging insight of prophylactic treatment as supported by the earlier report on the treatment of influenza patient with intranasal or oral delivery of antiviral drug successfully.[46,47] The novel approach of such drug delivery may improve the pharmacokinetic behavior of the antiviral prophylactic or therapeutic agent(s) by enhancing absorption and cell permeability. Drug particle formulated as a harmonious combination of cocktail receptor inhibitors at optimal pharmacologically relevant dose could block the host **Furin**, and **TMPRSS2** receptor located in the target organs esophagus, lungs, as well as in the colon, liver, heart, kidneys, intestine, and pancreas to prevent the entry of the SARS-CoV-2. Additionally, it may diminish the toxicity of the main active ingredient, as well.[48]

Apart from the host cell receptor, several viral targets have been identified so far for therapeutic intervention including mainly **receptor-binding domain (RBD)/Spike protein, N protein, E protein, 3CLpro and RdRp**. The probable inhibitor designing from the Phyto molecules data banks and their subsequent target-oriented nano-drug delivery via nebulizer could be useful for controlling the COVID-19 infection[19,49,50]; The probable phyto molecules as a cocktail combination may be delivered in situ by nano-aerosol suspension inhaler via oral or nasal route rapidly via targeting the above-cited viral protease enzymes for blocking the endosomal viral fusion, replication, growth and infectivity. Hence this plant origin pharmaceutical product for antiviral herbal medicine discovery containing one or more than active ingredients is called as phytopharmaceuticals (Fig. 19.3).

3.1.2 SARS-nCoV-2 drug targets and management via nano colloidal spray suspension

Nano inhalation delivery of the prophylactic or therapeutic phyto molecules coated with copper or silver nanobiomaterials can significantly reduce the outbreak and severity of the infection of COVID-19 in the context of pandemic panic[51] because prevention is better than cure. Moreover, this lethal virus loses its virulence factor and gets deactivated within a short period (1−4 h) upon exposure on copper or silver materials. This strategy of applications aims to control (i) local outbursts of COVID-19 via early-stage home treatment and (ii) lower the risk of ventilator-associated pneumonia (VAP) in hospital ICU. This methodology is to

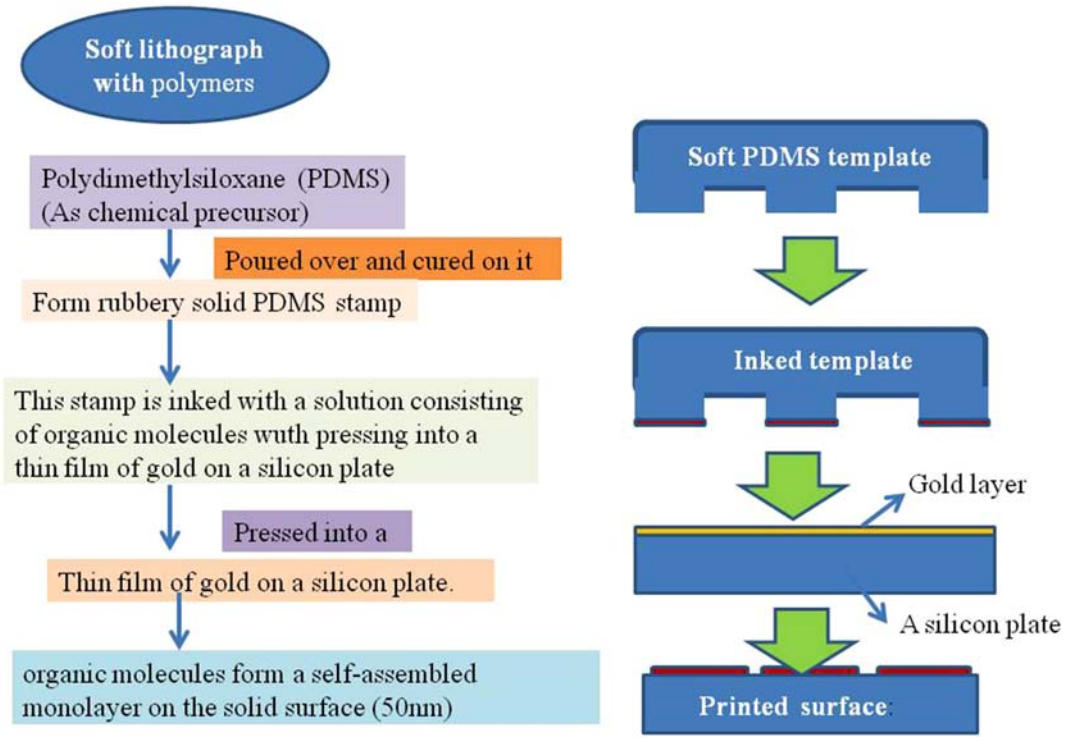

FIGURE 19.3 Schematic diagrams for nanomaterials synthesis.

propose a first-line interference measure with the potential to conquer the proliferation of the viral infection across the respiratory system.

Based on previously published experimental data, on the antiviral effects of a colloidal suspension of silver or copper nanoparticle formulation would be convenient and feasible for achieving antiviral MICof nanomaterial coated phytopharmaceuticals in various respiratory system locations (nasopharyngeal and pulmonary cells). However, efficiency might be depending on (a) the nanoparticle size-dependent required concentration of active phytometabolites (b) the required aerosol delivery characteristics (c) also inhalation time fraction of the normal breathing cycle.

4. Significance of nebulizer-spray for drug delivery against SARS viral infection reference to nCOV-2

Nebulizer based drug delivery is not only effective in mildly symptomatic patients or early prevention of the COVID-19 outbreak, but this aerosolized nano-drug delivery has been found to effective toward the acute and ICU ventilated COVID-19 patients, too.[52,53]

Nebulized nano-drug delivery of active antiviral phyto molecules possesses a robust scientific and biological basis. This strategy recommends urgent investigation of its therapeutic potential, for COVID-19-induced severe acute respiratory syndrome (SARS). COVID-19

SARS creates the typical manifestations of diffuse alveolar injury with extensive pulmonary coagulation activation resulting in fibrin deposition in the microvasculature and formation of hyaline membranes in the air sacs. COVID-19 patients manifest high levels of inflammatory cytokines in plasma and bronchoalveolar lavage fluid and followed by significant coagulopathy. The anticoagulant phytocompounds of nebulized nando-drug delivery may limit fibrin deposition and microvascular thrombosis. Earlier reports suggested that Trials in patients with acute lung injury and related conditions found inhaled anticoagulant or antiinflammatory drug molecules reduced pulmonary dead space, coagulation activation, microvascular thrombosis and clinical deterioration, resulting in increased time free of ventilatory support.

Furthermore, nebulized nano-aerosol suspension holding antiinflammatory, mucolytic, and antiviral Phyto-compounds cocktail, could inactivate the SARS-CoV-2 virus and prevent its entry into mammalian cells, thereby inhibiting pulmonary infection by SARS-CoV-2 as well improve the pharmacokinetic behavior of those plant originated herbal drugs.[54,55,56] Additionally, clinical studies have shown that inhaled nebulizers securely recover outcomes in other inflammatory respiratory diseases and also acts as an effective mucolytic in sputum-producing respiratory patients. It is extensively available and low-cost, which may make this treatment also accessible for low- and middle-income countries. These potentially important therapeutic properties of nebulized nano-inhaler emphasize the necessity for accelerated large-scale clinical trials to examine its potential to diminish mortality in COVID-19 patients.[57–59]

5. Ingredients used in nanosuspensions-based spray nebulizer formulation

5.1 Solubility and stability considerations

If a drug is insoluble or poorly soluble in the common solvents for human consumption, then formulation is usually prepared through nano-suspension. Certain phytochemicals-based drugs get decomposed in the presence of water as an aqueous vehicle and thus cannot be formulated as an aqueous solution. These types of phytopharmaceuticals may be suspended in an alternative nonaqueous vehicle. Prolonged contact between the drug and the dispersion medium might be avoided by formulating a lyophilized suspension which can be freshly prepared with the reconstitution of relevant solvent just before oral administration by the patient. The absorptive properties of fine powders are used in formulating inhalations. Volatile components like menthol or eucalyptus oil if present would be rapidly lost from the solution during use whereas it can be preserved and more prolonged release can be achieved in case of nebulizer-based spray formulation. By using spray nebulizer, the drug can be easily delivered to the target site from the metered device. Vaccines for induction of immunity are often formulated in dispersions of killed microorganisms like in case of cholera, diphtheria, or tetanus vaccine. Thus, the high antigenic stimulus can be provided for a prolonged period which will result in high antibody titer.[60]

5.2 Stabilizers

Stabilizers are the class of excipients that provide stability to the finished dosage form and are broadly classified into antioxidant and antimicrobial preservative. An antioxidant prevents oxidative degradation of the drug present in the formulation. Antioxidant should be compatible with other formulation additives. Before including an antioxidant in a suspension, it is essential to check that its use is not restricted in countries where it desires to sell the formulation. Examples of the effective antioxidant include butylated hydroxy anisole (BHA) and butylated hydroxytoluene (BHT) which are effective at low concentration of 0.02%−0.1% and 0.001% respectively for BHA and BHT. Other examples include tocopherol, EDTA, ascorbic acid, citric acid, etc.

For nanosuspension, a suitable preservative is included in the formulation, particularly if naturally occurring materials are to be used. It will help prevent the growth of microorganisms that may be present in the raw materials or maybe introduced during its use. Preservatives added should be effective against a wide range of bacteria, fungi, yeast, molds, etc., and should be effective at less concentration. Examples of effective preservatives include methylparaben, propylparaben in 10:1 ratio, benzoic acid (0.1%−0.2%), sodium benzoate (0.1%−0.2%), alcohol (15%−20%), glycerine (45%) concentration etc.

5.3 Density modifiers

From the qualitative view of Stoke's law equation, it is seen that lesser is the difference in density between the dispersed nano-sized particles and the dispersion medium lesser will be the tendency to settle down at the bottom. Therefore, similarities in density between these two phases will prevent the sedimentation in nanosuspensions. Thus, the uniform distribution of the drug throughout the dosage form can be achieved. Modification of aqueous phase by addition of a small quantity of glycerol or propylene glycol can be achieved.

5.4 Surfactants and cosurfactants

Surfactants are added in the nanosuspensions to minimize the interfacial tension between the dispersed phase and dispersion medium, which in turn helps to stabilize suspension. Surfactants help to lower the surface free energy of the suspended particles.

5.5 Poloxamers

These are synthetic polymers generally regarded as safe (GRAS) by the Food Drug Administration (FDA) and possess a lot of pharmaceutical applications. Most frequently used poloxamer in pharmaceutical nanosuspensions are poloxamer 188 and poloxamer 407. Hydrophilic-lipophilic ratio, functional group, molecular weight and morphology are the key decisive factors for crystal growth, stability, and their selection as formulation adjuvant in **nanosuspensions.**[61]

5.6 Cellulose derived polymers

Hydroxypropyl methylcellulose (HPMC), hydroxypropyl cellulose (HPC), and hydroxyl ethyl cellulose (HEC) have been widely used as stabilizing agents as well as release modifiers in nanosuspensions. These polymers show steric stabilization of the formulation due to surface adsorbed **hydrophobic groups.**[62]

Organic Solvents-Class three organic solvents such as ethyl alcohol, acetone, butanol, ethyl formate, ethyl ether, ethyl acetate, methyl acetate, methyl ethyl ketone, triacetin which are potentially less toxic to humans are more preferred over conventional hazardous residual solvents.

5.7 Miscellaneous additives

Nanosuspensions like coarse suspensions may contain buffers, osmotic agents, cryoprotective agents, organoleptic agents depending on the type, route of administration and nature of the drug.

6. Preparation methods of nanosuspension

For the preparation of nanosuspensions, two methods are used, namely, the top-down method and the bottom-up method. Under these two basic methods, various methods are utilized for the preparation of nanosuspensions. Wet milling, dry milling, high-pressure homogenization and cogrinding method fall under top-down method, and antisolvent precipitation, liquid emulsion, and sono-precipitation methods fall under bottom-up method.

6.1 Media milling method

Dry milling and wet milling methods fall under the media milling method. In this method, nanosuspensions are prepared by the application of high shearing forces utilizing ball mill or media mill. The size reduction within the milling chamber charged with drug, stabilizer, and vehicle is carried out by application of both impact and attrition forces between the particles and milling chamber. Low energy utilization, ease of scale-up, minimum batch to batch variation and capability to handle large quantities of the material makes this process highly reliable and industry efficient method. This process can be used for both batch and continuous operations. This method is approved by the Food Drug and Administration (FDA). By this method, we can reduce the size of the particles to <200 nm in 30−60 min.[63]

6.2 High-pressure homogenization

In this method, nanosuspensions are prepared by the application of high pressure of 100−1500 bars by passing the materials through a valve that has a small aperture.[64] By this pressure, we can easily convert the micron size ranged particles to nano-ranging particles. For this process, we need the feed materials of micron-size particles to be in the order of preferably <25 μm, and for this, we can use the jet mill for initial size reduction before putting

the feed materials in the homogenizer for further size reduction. In this process, the static pressure reduction due to sudden drop in static velocity of fluids generates cavities, implosion forces and shock waves in the liquid medium breaking down the microparticles to nanoparticles. This process can also be used for batch and continuous operations.

6.3 Precipitation method

In this method, the materials of subcolloidal particle size range are allowed to aggregate into colloidal size range particles by allowing nucleation in a prepared supersaturated solution of drug in a water-miscible organic solvent at optimum temperature and dispersing a small amount of nonsolvent and water under rapid stirring.[12] Rapid nucleation and slow growth rate of crystal size are the decisive factors in the successful production of thermodynamically stable crystal form. Generation of the finely dispersed uniform-sized drug, ease of scale-up and simple and economical process makes the precipitation method industry efficient.

6.4 Emulsion solvent evaporation technique

In this method, initially, the emulsion is formed by first dissolving the drug in an organic solvent and subsequently dispersing it in an aqueous phase containing a surfactant. Further rapid evaporation of the solvent under reduced pressure results in instant production of nanosuspension. Key factors in this method are globule size and concentration of stabilizer.

6.5 Ultrasound-assisted sono-crystallization method

It is a novel method for the preparation of nanosuspensions. In this method, an ultrasound wave is employed in the frequency range of 20−100 Kha, which increases the efficiency of particle size reduction. It is also considered as an effective method for controlling the **nucleation and crystallization process**.[65]

6.6 Cogrinding method

In this method, stable nanosuspensions are prepared by a dry cogrinding technique by using various polymers and copolymers such as Hydroxypropyl methylcellulose (HPMC), polyvinyl pyrrolidone (PVP), polyethene glycol (PEG), **cyclodextrin derivatives, etc.**[66] Controlled stability and enhanced solubility of poorly soluble drugs have been improved by employing this method for preparation **of nanosuspensions**.[60,67]

7. Characterization and evaluation tests

The essential parameters for evaluating nanosuspensions are as follows:

7.1 Mean particle size and particle size distribution

These two parameters are important characterization parameters for nanosuspensions as they govern the physical stability, absorption, dissolution, bioavailability, as well as the

biological performance of the nanosuspensions. The physical stability of nanosuspensions is governed by the polydispersity index (PI). It should be <0.1−0.25, which indicate a impartially narrow particle size distribution, whereas a PI value of >0.5 indicates a broad particle size distribution. Photon correlation spectroscopy (PCS) can be used to determine the mean particle size of nanosuspensions rapidly.[68] Moreover, PCS helps to determine the PI also. <Laser diffractometry (LD) analysis to quantify the nanoparticulate drug particles as well as gives an account of their volume size distribution. LD helps in determining the particles in size range of 0.05−80 μm. The particle size determination by LD analysis is a valuable technique for designing pulmonary as well as parenteral drug delivery systems in case of nanosuspensions. For nanosuspensions, particle size determination can also be undertaken by the Coulter counter method, an essential tool in case of intravenous formulations.[60]

7.2 Crystalline state and particle morphology

A drug might exhibit polymorphism or undergo morphological changes during nanosizing. In order to understand these behavioral changes of a drug substance, it is essential to study their crystalline state and particle morphology. Moreover, when the nanosuspensions are formulated, drug substances undergo size reduction during which amorphous state particles may be generated. Hence, it is essential to study the presence of amorphous drug particles in nanosuspensions. It can be determined by X-ray diffraction (XRD) analysis[69,70] proceedings and also by differential scanning calorimetry (DSC) study. In order to determine the particle morphology, scanning electron microscopy (SEM) is preferred.[70]

7.3 Particle charge (zeta potential)

The physical stability of nanosuspensions is determined by identifying their particle charge or zeta potential, which is governed by the drug itself and stabilizer. Nanosuspensions may be stabilized by stearic and electrostatic stabilization. Zeta potential of 30 mV is desired for good stability in case of electrostatic stabilization whereas a zeta potential of 20 mV is desired for good stability of both steric and electrostatic stabilization.[71]

7.4 Saturation solubility and dissolution

Saturation solubility and dissolution both collectively help to anticipate the in vivo performance of the nanosuspensions. The in vivo performance parameters include the blood profiles, plasma peak and **bioavailability**.[72]

7.5 In vivo biological performance

The investigation of in vivo performance and the formation of the in vitro/in vivo correlation are an integral part of the assessment parameters of any pharmaceutical formulation irrespective of its route of administration and its dosage form. For this, suitable technique has to be employed to determine the surface properties like hydrophilicity or hydrophobicity and protein binding of the formulated nanosuspensions as they decide their in vivo performance in the human body after administration.[72]

8. Component system for intranasal and oral inhaler-based drug delivery systems

In the case of intranasal drug delivery, it is essential to consider the correlation between the formulation, device, and patient. These three factors play an important role in where the drug-loaded droplet deposit in the nasal cavity. The site of deposit of drug particle, either anterior or posterior is considered to be a key parameter for success or failure of nasal drug delivery system.

Nasal spray devices come in a variety of dose and container volumes sizes. They are available in both unit dose as well as multi-dose systems. Actuator plays a crucial role in delivering the desired form of dosage form from the nebulized device. The fill volume is 125 μL for unit dose and 30 mL or more for multidose. Spray volume ranges from 25 to 140 μL. The selection of the spray pump depends on the volume of the formulation. Spray pumps in nebulizers are generally used for the production of both local as well as systemic effect. They are available with a wide range of closures, actuators and other accessories which help them to meet customer requirements. These pumps are used for a wide variety of therapeutic purposes ranging from allergy, pain, intranasal mass vaccination, etc.

The droplet size distribution of the sprayed formulation is important in vitro evaluation test. It can be determined using a laser diffraction pattern study of the sprayed nanodroplets. The droplet size distribution is characterized by the determination of the volume of distribution (Dv_{10}, Dv_{50}, and Dv_{90}), percentage (%) less than 10 μm Dv_{50} stands for volume median diameter. It indicates that 50% of the distribution is contained in droplets that are smaller than this value while the other half is contained in droplets that are larger than this value and so on for Dv_{10} and Dv_{90}.

Spray pattern and plume geometry are important parameters for the performances of pump and nozzle. There are different factors which affect spray pattern and plume geometry, like size and shape of the nozzle, design of the pump, size of metering chamber, and type of formulation.

The spray pattern is tested by noting the distance between the nosepiece and the collection surface for the spray, number of sprays per spray pattern, position of collection surface relative to nosepiece, and visualization procedure.

ViaNase is a liquid dosage form-based drug delivery device which helps in controlled particle dispersion. There are some other interesting devices like OptiMist and DirectHaler, which are devices that are used to target liquid nasal formulations to the nasal cavity as well as the olfactory region. Optimism is a breath-actuated device and has proven to result in more deposition in the nasal cavity than a spray pump.[73,74]

9. Applications of nanosuspension in targeted drug delivery for pulmonary viral infection

Potentially nanosuspensions can overcome various problems associated with conventional dry powder inhalers or suspension type inhalational. Diffusion and dissolution in alveolar fluids, rapid clearance owing to short residence time due to ciliary movement, deposition

in the pharynx, and upper respiratory tract due to aggregation of particles are the common drawbacks of conventional aerosol delivery systems which may be successfully minimized by designing nanosuspension-based nebulizer drug delivery system.

Nanoparticulate nature of the particle can offer quick onset of action due to rapid diffusion and dissolution in the alveolar fluids. Because of their small size, they show a more uniform distribution of the drug in the lungs. At the same time, it will also increase the adhesion of the drug to the mucosal surface will offer prolonged residence time of the drug at the absorption site. Budesonide drug nanoparticles were successfully nebulized using ultrasonic nebulizer technique.[63] Many folds can increase the respirable fraction of drug in case of nebulizer based nanosuspension technology as it is evident from antioxidant coenzyme Q10 nanosuspension stabilized with PEG32 stearate. In vitro cellular cytotoxicity in A549 human lung cells shows no noticeable cytotoxicity for nanosuspensions.[75]

Sometimes it is observed that conversion of nanosuspensions into solid oral and inhalable dosage form may be advantageous to overcome the physical instability associated with their liquid state. For this purpose, spray and freeze-drying techniques are most frequently used. Reconstitution solvents are supplied along with the pack for easy dispersibility of the same just before administration for oral and pulmonary clinical applications.[76]

One study reported that pulmonary aspergillosis could be easily targeted by using nanosuspensions of amphotericin B instead of using its stealth liposomes.[77] Another study at the Freie University of Berlin reported development and characterization of buparvaquone nanosuspensions for pulmonary delivery in the treatment of pneumocystis pneumonia.

Several concepts of nanosuspension formulations have been developed at the Baxter Healthcare Corporation, which can be an excellent choice for treating bioweapon mediated diseases. These concepts suggest that alteration in pharmacokinetic profiles of existing antibiotics can lead to enhanced therapeutic efficacy with reduced side effects. It is evident in the case of nanosuspension formulated with antifungal agent itraconazole. A strategy for dendritic cell vaccine has been developed for use against bio-weapons.[78]

10. Conclusion

Taken together our study, it could be suggested that traditional medicinal herbs and spices derived versatile phytocompounds could be explored to fight against SARS-COV-2 induced lethal pathophysiological immune response and functional disorders. These compounds may confer specific inhibition toward the viral protein-mediated endocytosis, fusion, replication growth due to the presence of secondary metabolic unique pharmacophore scaffolds.

Intranasal or oral inhaler-based nano-suspension of phytometabolites conjugated with targeting ligand, bio-stabilizers must assist the phytopharmaceuticals in reaching and interacting within the locus of pharmacodynamic action into the lungs either viral protease or host cell transmembrane receptor. These nano-phyto formulations of the pharmaceutical product would be very useful and attenuated remarkably the pharmacokinetic unstability related to ADME profile and in vivo compound degradation of phyto molecules after administration.

Our evidenced-based scientific review and the study on therapeutic or prophylactic drug delivery of antiviral phytocompounds suggest that many herbal compounds could successfully reach the targets of SARS-COV-2 life-cycles around the extracellular and intracellular

host cellular receptor sites and airway surfaces via bypassing the untoward effects of active medicament, reducing the recovery time from viral infection and associated pathological disorders. Systemic instability of the active phytomolecules could be avoided through such nano aerosol-based phytopharmaceutical dosage form. These novel strategies of nanopharmaceuticals could improve the antiviral efficacy through the inclusion of **silver or copper nano-powder-based suspended adjuvants**. These technologies also may confer rapid therapeutic action through suitable patient compliance rather than oral tablet, capsule or intravenous injection dosage form for COVID-19 management. It would be noninvasive and painless. These nano-spray inhalers may allow delivery of optimum drug concentrations to the airway surface of the upper respiratory tract for speedy combating of SARS-CoV-2 infection mediated complications. Pressurized metered-dose inhalers could assist in this regard. Jet Nebulizers—Ultrasonic Nebulizers could also successfully deliver the phytocompounds via nano-suspension or emulsion liquid dosage form toward the locus of drug targets. The nebulizer-based nanodrug delivery could easily block the virus-host interaction through the receptor-based attachment for preventing the proliferation of degree of viral infectivity at the cellular level when mild to moderate symptoms of COVID-19 seems to be ascended.

However, the particle size of the nano-suspension and the inhalation techniques adopted by the patient like inspiratory volume, inspiratory flow rate, breath-hold time, breathing rate, and nose versus mouth breathing may trigger or modulate the antiviral response. Moreover, this delivery techniques need to validate in a preclinical or clinical model of COVID-19 with the potential anti-SARS-Cov-2 therapeutic agents(Phyto-molecules) by altering the composition of nano-biomaterial excipients for obtaining better, safe and promising antiviral effect against COVID-19 patient. This respirable nano-carrier is an excellent strategy for antiviral drug delivery of phytopharmaceuticals.

References

1. Lenkens M, de Wit H, Danser AH, Esselink AC, Horikx A, Ten Oever J, van de Veerdonk F, Kramers C. Geneesmiddelen bij COVID-19 [Medication and comedication in COVID-19 patients]. *Ned Tijdschr Geneeskd* 2020;**164**:D4995. Dutch. PMID: 32324352.
2. Zhao H, Wald J, Palmer M, Han Y. Hydroxychloroquine-induced cardiomyopathy and heart failure in twins. *J Thorac Dis* 2018;**10**:E70–3.
3. Zumla A, Chan JF, Azhar EI, Hui DS, Yuen KY. Coronaviruses—drug discovery and therapeutic options. *Nat Rev Drug Discov* 2016;**15**:327–47.
4. Cameron CE, Castro C. The mechanism of action of ribavirin: lethal mutagenesis of RNA virus genomes mediated by the viral RNA-dependent RNA polymerase. *Curr Opin Infect Dis* 2001;**14**:757–64.
5. Carter KL, Do DV. Hydroxychloroquine-induced retinal toxicity. *J Rheumatol* 2020;**47**:632.
6. Drosten C, Preiser W, Günther S, Schmitz H, Doerr HW. Severe acute respiratory syndrome: identification of the etiological agent. *Trends Mol Med* 2003;**9**(8):325–7. https://doi.org/10.1016/s1471-4914(03)00133-3. PMID: 12928032; PMCID: PMC7128529.
7. Walls AC, Park YJ, Tortorici MA, Wall A, McGuire AT, Veesler D. Structure, function, and antigenicity of the SARS-CoV-2 spike glycoprotein. *Cell* 2020;**181**(2):281–92.
8. Coutard B, Valle C, de Lamballerie X, Canard B, Seidah NG, Decroly E. The spike glycoprotein of the new coronavirus 2019-nCoV contains a furin-like cleavage site absent in CoV of the same clade. *Antiviral Res* 2020;**176**:104742. https://doi.org/10.1016/j.antiviral.2020.104742. PMID: 32057769; PMCID: PMC7114094.
9. Li SY, Chen C, Zhang HQ, et al. Identification of natural compounds with antiviral activities against SARS-associated coronavirus. *Antivir Res* 2005;**67**(1):18–23. https://doi.org/10.1016/j.antiviral.2005.02.007.

10. Lau E, Nash CZ, Vogler DR, Cullings KW. Molecular diversity of cyanobacteria inhabiting coniform structures and surrounding mat in a Yellowstone hot spring. *Astrobiology* 2005;**5**(1):83–92.
11. Hoffmann M, Kleine-Weber H, Schroeder S, Krüger N, Herrler T, Erichsen S, et al. Sars-cov-2 cell entry depends on ace2 and tmprss2 and is blocked by a clinically proven protease inhibitor. *Cell* 2020;**181**(2):271–280.e8. https://doi.org/10.1016/j.cell.2020.02.052. PMID: 32142651; PMCID: PMC7102627.
12. Patel VR, Agrawal YK. Nanosuspension: an approach to enhance solubility of drugs. *J Adv Pharm Technol Res* 2011;**2**(2):81.
13. Hensel A, Bauer R, Heinrich M, et al. Challenges at the time of COVID-19: opportunities and innovations in antivirals from nature. *Planta Med* 2020;**86**(10):659–64. https://doi.org/10.1055/a-1177-4396.
14. Langeder J, Grienke U, Chen Y, Kirchmair J, Schmidtke M, Rollinger JM. Natural products against acute respiratory infections: strategies and lessons learned. *J Ethnopharmacol* 2020;**248**:112298. https://doi.org/10.1016/j.jep.2019.1122.
15. Conte R, Marturano V, Peluso G, Calarco A, Cerruti P. Recent advances in nanoparticle-mediated delivery of anti-inflammatory phytocompounds. *Int J Mol Sci* 2017;**18**(4):709. https://doi.org/10.3390/ijms18040709.
16. Puglia C, Lauro MR, Tirendi GG, et al. Modern drug delivery strategies applied to natural active compounds. *Expert Opin Drug Deliv* 2017;**14**(6):755–68. https://doi.org/10.1080/17425247.2017.1234452.
17. Uskoković V. Why have nanotechnologies been underutilized in the global uprising against the coronavirus pandemic? *Nanomedicine* 2020;**15**(17):1719–34. https://doi.org/10.2217/nnm-2020-0163.
18. Shang J, Wan Y, Luo C, et al. Cell entry mechanisms of SARS-CoV-2. *Proc Natl Acad Sci U S A* 2020;**117**(21):11727–34. https://doi.org/10.1073/pnas.2003138117.
19. Basu S, Holbrook LT, Kudlaty K, et al. Numerical evaluation of spray position for improved nasal drug delivery. *Sci Rep* 2020;**10**(1):10568. https://doi.org/10.1038/s41598-020-66716-0. Published 2020 Jun 29.
20. Contini C, EnricaGallenga C, Neri G, Maritati M, Conti P. A new pharmacological approach based on remdesivir aerosolized administration on SARS-CoV-2 pulmonary inflammation: a possible and rational therapeutic application [published online ahead of print, 2020 May 24]. *Med Hypotheses* 2020;**144**:109876. https://doi.org/10.1016/j.mehy.2020.109876.
21. Chauhan G, Madou MJ, Kalra S, Chopra V, Ghosh D, Martinez-Chapa SO. Nanotechnology for COVID-19: therapeutics and vaccine research [published online ahead of print, 2020 Jun 29]. *ACS Nano* 2020. https://doi.org/10.1021/acsnano.0c04006.
22. Weiss C, Carriere M, Fusco L, et al. Toward nanotechnology-enabled approaches against the COVID-19 pandemic. *ACS Nano* 2020;**14**(6):6383–406. https://doi.org/10.1021/acsnano.0c03697.
23. Chen Z, Nakamura T. Statistical evidence for the usefulness of Chinese medicine in the treatment of SARS. *Phytother Res* 2004;**18**(7):592–4. https://doi.org/10.1002/ptr.1485.
24. Cheng PW, Ng LT, Chiang LC, Lin CC. Antiviral effects of saikosaponins on human coronavirus 229E in vitro. *Clin Exp Pharmacol Physiol* 2006;**33**(7):612–6. https://doi.org/10.1111/j.1440-1681.2006.04415.x.
25. Lin LT, Hsu WC, Lin CC. Antiviral natural products and herbal medicines. *J Tradit Complement Med* 2014;**4**(1):24–35. https://doi.org/10.4103/2225-4110.124335.
26. McCutcheon AR, Roberts TE, Gibbons E, et al. Antiviral screening of British Columbian medicinal plants. *J Ethnopharmacol* 1995;**49**(2):101–10. https://doi.org/10.1016/0378-8741(95)90037-3.
27. Boukhatem MN, Setzer WN. Aromatic herbs, medicinal plant-derived essential oils, and phytochemical extracts as potential therapies for coronaviruses: future perspectives. *Plants* 2020;**9**(6):800. https://doi.org/10.3390/plants9060800. Published 2020 Jun 26.
28. CDC SARS response timeline. Available online: http://www.cdc.gov/about/history/sars/timeline.htm. (Accessed 18 March 2020).
29. Cinatl J, Morgenstern B, Bauer G, Chandra P, Rabenau H, Doerr HW. Glycyrrhizin, an active component of liquorice roots, and replication of SARS-associated coronavirus. *Lancet* 2003;**361**(9374):2045–6. https://doi.org/10.1016/s0140-6736(03)13615-x.
30. Chen F, Chan KH, Jiang Y, et al. In vitro susceptibility of 10 clinical isolates of SARS coronavirus to selected antiviral compounds. *J Clin Virol* 2004;**31**(1):69–75. https://doi.org/10.1016/j.jcv.2004.03.003.
31. Renard-Nozaki J, Kim T, Imakura Y, Kihara M, Kobayashi S. Effect of alkaloids isolated from amaryllidaceae on herpes simplex virus. *Res Virol* 1989;**140**(2):115–28. https://doi.org/10.1016/s0923-2516(89)80089-5.
32. Ieven M, Vlietinck AJ, Vanden Berghe DA, et al. Plant antiviral agents. III. Isolation of alkaloids from cliviaminiata regel (Amaryllidaceae). *J Nat Prod* 1982;**45**(5):564–73. https://doi.org/10.1021/np50023a009.

33. Wu CY, Jan JT, Ma SH, et al. Small molecules targeting severe acute respiratory syndrome human coronavirus. *Proc Natl Acad Sci U S A* 2004;**101**(27):10012–7. https://doi.org/10.1073/pnas.0403596101.
34. Yang Y, Islam MS, Wang J, Li Y, Chen X. Traditional Chinese medicine in the treatment of patients infected with 2019-new coronavirus (SARS-CoV-2): a review and perspective. *Int J Biol Sci* 2020;**16**(10):1708–17. https://doi.org/10.7150/ijbs.45538.
35. Roy M, Datta A. Phytochemicals as bioenhancers. In: *Cancer genetics and therapeutics*. Singapore: Springer; 2019.
36. Crowley P, Martini L. Optimising drug delivery: the challenges and opportunities. *On Drug Deliv* 2015:4–11.
37. Shoji Y, Nakashima H. Nutraceutics and delivery systems. *J Drug Target* 2004;**12**(6):385–91. https://doi.org/10.1080/10611860400003817.
38. Ajazuddin SS. Applications of novel drug delivery system for herbal formulations. *Fitoterapia* 2010;**81**(7):680–9. https://doi.org/10.1016/j.fitote.2010.05.001.
39. Wang S, Su R, Nie S, et al. Application of nanotechnology in improving bioavailability and bioactivity of diet-derived phytochemicals. *J Nutr Biochem* 2014;**25**(4):363–76. https://doi.org/10.1016/j.jnutbio.2013.10.002.
40. Ipar VS, Dsouza A, Devarajan PV. Enhancing curcumin oral bioavailability through nanoformulations. *Eur J Drug Metab Pharmacokinet* 2019;**44**(4):459–80. https://doi.org/10.1007/s13318-019-00545-z.
41. Sahibzada MUK, Sadiq A, Khan S, et al. Fabrication, characterization and in vitro evaluation of silibinin nanoparticles: an attempt to enhance its oral bioavailability. *Drug Des Devel Ther* 2017;**11**:1453–64. https://doi.org/10.2147/DDDT.S133806. Published 2017 May 15.
42. Theodosiou E, Purchartová K, Stamatis H, et al. Bioavailability of silymarin flavonolignans: drug formulations and biotransformation. *Phytochemistry Rev* 2014;**13**:1–18. https://doi.org/10.1007/s11101-013-9285-5.
43. Mehendale R, Joshi M, Patravale VB. Nanomedicines for treatment of viral diseases. *Crit Rev Ther Drug Carrier Syst* 2013;**30**(1):1–49. https://doi.org/10.1615/critrevtherdrugcarriersyst.2013005469.
44. de Wit E, van Doremalen N, Falzarano D, Munster VJ. SARS and MERS: recent insights into emerging coronaviruses. *Nat Rev Microbiol* 2016;**14**(8):523–34. https://doi.org/10.1038/nrmicro.2016.81. PMID: 27344959; PMCID: PMC7097822.
45. Breitbarth AK, Morgan J, Jones AL. E-cigarettes-an unintended illicit drug delivery system. *Drug Alcohol Depend* 2018;**192**:98–111. https://doi.org/10.1016/j.drugalcdep.2018.07.031. PMID: 30245461.
46. Peng M, Watanabe S, Chan KWK, He Q, Zhao Y, Zhang Z, et al. Luteolin restricts dengue virus replication through inhibition of the proprotein convertase furin. *Antivir Res* 2017;**143**:176–85.
47. Wong JP, Christopher ME, Viswanathan S, Schnell G, Dai X, Van Loon D, et al. Aerosol and nasal delivery of vaccines and antiviral drugs against seasonal and pandemic influenza. *Expert Rev Respir Med* 2010;**4**(2):171–7. https://doi.org/10.1586/ers.10.15. PMID: 20406083.
48. Remacle AG, Gawlik K, Golubkov VS, Cadwell GW, Liddington RC, Cieplak P, et al. Selective and potent Furin inhibitors protect cells from anthrax without significant toxicity. *Int J Biochem Cell Biol* 2010;**42**:987–95.
49. Khailany RA, Safdar M, Ozaslan M. Genomic characterization of a novel SARS-CoV-2. *Gene Rep* 2020;**19**:100682. https://doi.org/10.1016/j.genrep.2020.100682. PMID: 32300673; PMCID: PMC7161481.
50. Chen H, Lao Z, Xu J, Li Z, Long H, Li D, et al. Antiviral activity of lycorine against Zika virus in vivo and in vitro. *Virol* 2020;**546**:88–97.
51. E.D. Poggio, R.L. McClelland, K.N. Blank, S. Hansen, S. Bansal, A.S. Bomback, et al. Kidney precision medicine project. Systematic review and meta-analysis of native kidney biopsy Complications. Clin J Am Soc Nephrol 2020;15(11):1595–1602. doi:10.2215/CJN.04710420. Erratum in: Clin J Am Soc Nephrol 2021;16(2):293. PMID: 33060160; PMCID: PMC7646247.
52. Eden A, Gashi T, Bergman I, Kompaniets D, Shiran A. COVID-19: how to use a jet nebulizer for drug administration in ventilated patients without putting the Healthcare workers at risk. *Biomed Hub* 2020;**5**(2):1564–7. https://doi.org/10.1159/000508845. Published 2020 Jun 2.
53. Weber AG, Chau AS, Egeblad M, Barnes BJ, Janowitz T. Nebulized in-line endotracheal dornase alfa and albuterol administered to mechanically ventilated COVID-19 patients: a case series. *MedRxiv* 2020. https://doi.org/10.1101/2020.05.13.20087734.
54. Musthaba SM, Ahmad S, Ahuja A, Ali J, Baboota S. Nano approaches to enhance pharmacokinetic and pharmacodynamic activity of plant origin drugs. *Curr Nanosci* 2009;**5**(3):344–52.
55. Usachev EV, Pyankov OV, Usacheva OV, Agranovski IE. Antiviral activity of tea tree and eucalyptus oil aerosol and vapour. *J Aerosol Sci* May 1, 2013;**59**:22–30.

56. Zhou QT, Leung SS, Tang P, Parumasivam T, Loh ZH, Chan HK. Inhaled formulations and pulmonary drug delivery systems for respiratory infections. *Adv Drug Deliv Rev* 2015;**85**:83–99. https://doi.org/10.1016/j.addr.2014.10.022.
57. Chimenti L, Camprubí-Rimblas M, Guillamat-Prats R, et al. Nebulized heparin attenuates pulmonary coagulopathy and inflammation through alveolar macrophages in a rat model of acute lung injury. *Thromb Haemost* 2017;**117**(11):2125–34. https://doi.org/10.1160/TH17-05-0347.
58. Tuinman PR, Dixon B, Levi M, Juffermans NP, Schultz MJ. Nebulized anticoagulants for acute lung injury—a systematic review of preclinical and clinical investigations. *Crit Care* 2012;**16**(2):R70. https://doi.org/10.1186/cc11325. Published 2012 Dec 12.
59. Cornet AD, Hofstra JJ, Vlaar AP, et al. Nebulized anticoagulants limit coagulopathy but not inflammation in *Pseudomonas aeruginosa*-induced pneumonia in rats. *Shock* 2011;**36**(4):417–23. https://doi.org/10.1097/SHK.0b013e31822bcef0.
60. Jacob S, Nair AB, Shah J. Emerging role of nanosuspensions in drug delivery systems. *Biomater Res* 2020;**24**:3. https://doi.org/10.1186/s40824-020-0184-8. Published 2020 Jan 15.
61. Li HY, Seville PC, Williamson IJ, Birchall JC. Dispersibility of spray-dried formulations for pulmonary drug delivery. *J Pharm Pharmacol* 2004;**56**(S1):S10.
62. Mishra B, Sahoo J, Dixit PK. Formulation and process optimization of naproxen nanosuspensions stabilized by hydroxypropyl methylcellulose. *Carbohydr Polym* 2015;**127**:300.
63. Itoh K, Pongpeerapat A, Tozuka Y, Oguchi T, Yamamoto K. Nanoparticle formation of poorly water-soluble drugs from ternary ground mixtures with PVP and SDS. *Chem Pharm Bull (Tokyo)* 2003;**51**(2):171–4. https://doi.org/10.1248/cpb.51.171.
64. Liedtke S, Wissing S, Müller RH, Mäder K. Influence of high-pressure homogenization equipment on nanodispersions characteristics. *Int J Pharm* 2000;**196**(2):183–5.
65. Tran TTD, Tran PHL, Nguyen MNU, Tran KTM, Pham MN, Tran PC, et al. Amorphous isradipine nanosuspension by the sonoprecipitation method. *Int J Pharm* 2014;**474**(1–2):146–50.
66. Wongmekiat A, Tozuka Y, Oguchi T, Yamamoto K. Formation of fine drug particles by cogrinding with cyclodextrins. I the use of β-cyclodextrin anhydrate and hydrate. *Pharm Res (N Y)* 2002;**19**(12):1867–72.
67. Watanabe T, Ohno I, Wakiyama N, Kusai A, Senna M. Stabilization of amorphous indomethacin by co-grinding in a ternary mixture. *Int J Pharm* 2002;**241**(1):103–11.
68. Müller BW, Müller RH. Particle size analysis of latex suspensions and microemulsions by photon correlation spectroscopy. *J Pharmacol Sci* 1984;**73**(7):915–8. https://doi.org/10.1002/jps.2600730713.
69. Müller RH, Benita S, Bohm B, editors. *Emulsions and nanosuspensions for the formulation of poorly soluble drugs*. CRC Press; 1998.
70. Muller RH, Grau MJ. Increase of dissolution rate and solubility of poorly water soluble drugs as nanosuspension. In: *Proc World Meeting APGI/APV, Paris*. **2**; 1998. p. 62–624.
71. Jacobs C, Müller RH. Production and characterization of a budesonide nanosuspension for pulmonary administration. *Pharm Res (N Y)* 2002;**19**(2):189–94. https://doi.org/10.1023/a:1014276917363.
72. Patravale VB, Date AA, Kulkarni RM. Nanosuspensions: a promising drug delivery strategy. *J Pharm Pharmacol* 2004;**56**(7):827–40. https://doi.org/10.1211/0022357023691. PMID: 15233860.
73. Djupesland PG. Nasal drug delivery devices: characteristics and performance in a clinical perspective-a review. *Drug Deliv Transl Res* 2013;**3**(1):42–62. https://doi.org/10.1007/s13346-012-0108-9.
74. Suman JD, Laube BL, Dalby R. Comparison of nasal deposition and clearance of aerosol generated by a nebulizer and an aqueous spray pump. *Pharmaceut Res* October 1, 1999;**16**(10):1648.
75. Rossi I, Sonvico F, McConville JT, Rossi F, Fröhlich E, Zellnitz S, et al. Nebulized coenzyme Q10 nanosuspensions: a versatile approach for pulmonary antioxidant therapy. Eur J Pharmaceut Sci 2018;113:159–170.
76. Malamatari M, Somavarapu S, Taylor KM, Buckton G. Solidification of nanosuspensions for the production of solid oral dosage forms and inhalable dry powders. *Expert Opin Drug Deliv* 2016;**13**(3):435–50.
77. Kohno S, Otsubo T, Tanaka E, Maruyama K, Hara K. Amphotericin B encapsulated in polyethylene glycol-immunoliposomes for infectious diseases. *Adv Drug Deliv Rev* 1997;**24**(2–3):325–9.
78. Jain KK, Jain KK. *The handbook of nanomedicine*. NJ: Humana Press; 2008.

This page intentionally left blank

PART IV

Biomedical applications of nanomaterials

This page intentionally left blank

CHAPTER

20

Bio-nanomaterials and their applications

Mohd Talha[1,2,†], *Nishit Pathak*[3,†], *Sanjib Bhattacharyya*[3] *and Yuanhua Lin*[1,2]

[1]School of New Energy and Materials, Southwest Petroleum University, Chengdu, Sichuan, China; [2]State Key Laboratory of Oil and Gas Reservoir Geology and Exploitation, Southwest Petroleum University, Chengdu, Sichuan, China; [3]Department of Pharmaceutical Science and Chinese Traditional Medicine, Southwest University, Chongqing, China

1. Introduction

Nanomaterials offer ample opportunities to overcome the limitations of conventional bio-materials. The performance of conventionally used biomaterials could significantly enhanced by using of nanoparticles, nanostructured surfaces, and nano-composites.[1,2] Nanomaterials have substantial different physicochemical properties as compare to bulk materials. Several properties of nanomaterials, viz., shape, size, chemical composition, structure of surface and charge, solubility, and aggregation can highly influence their interactions with biological milieu.[3] For instance, single-walled carbon nanotubes (CNTs) having diameters equivalent to the thickness of DNA molecules have established a remarkable potential as high-effciency delivery transporters for biomolecules into cells.[3] The other properties of nanoparticles, such as, high surface to volume ratio, more surface energy, and activity, along with changed wettability could also greatly influence the protein adhesion and the activities of cells.[1,2] Because of nanoscale effects with higher surface area, nanomaterials have been considered as promising tools for the progress of drug delivery, diagnostic biosensors and biomedical imaging.[3] An extensive number of the features of nanoscale materials have offered infinite opportunities for their biomedical applications. Furthermore, nanomaterials can achieve definite therapeutic functions that would be relatively difficult to attain using conventional bio-materials.

[†] M.T. and N. P. contributed equally to this work.

Applications of Multifunctional Nanomaterials
https://doi.org/10.1016/B978-0-12-820557-0.00024-2

The size of nanoparticles (NPs) ranging from the protein level (a few nanometers) to cellular level (submicron size), imitating the extracellular matrix and cell microenvironment and classified tissue structures.[1,2,4] NPs can be employed for personalized cancer care treatment due to use of a size comparable to bio-macromolecules. These can also be employed in cardiovascular treatment, where they established potentials across a number of applications.[5,6] NPs act as drug carrier that can travel via the endothelium of blood vessels for longer circulation. Additionally, certain NPs might be used as contrast agents for magnetic resonance imaging (MRI) and many other bioimaging techniques. None of these tasks could be easily accompanied by using conventional materials. After founding interdisciplinary nanotechnology potentials, it is desired that nanomaterial will syndicate with chemically and clinically applicable fields in the next generation of medical podiums.

This chapter presents some of the recent developments of various nanomaterials in the biomedical field. In particular, we address types of nanomaterials used in medical applications, bioionics as inspired bio-nanomaterials. Finally we focus on applications of nanomaterials in medical arena including nano-coatings, drug releasing ability as well as various therapeutics by magnetic nanoparticles. Due to space constraints, we only cover a limited content; we refer readers to more comprehensive periodicals elsewhere for each topic. The chief emphasis of this chapter is the growth of nanomaterials and their applications in biology and medicine.

2. Types of nanoparticles used in bio-system

Nanoparticles typically form the core of nano-biomaterials. Nano core can be used as a suitable surface for molecular assembly could be composed of either inorganic or polymeric materials. The role of nanomaterials in biology and medicine remains enhanced while the complexities of nanotechnology and human physiology syndicate and fundamental understanding is crucial before thinking about involved applications. In this section, we describe the types of different nanoparticles used in medicine with their specific applications.

2.1 Metallic nanoparticles

Among the various nanomaterials engaged in biomedical research, metallic NPs have been certified to be the most useful and appropriate. Maximum inorganic NPs contain metals, either in the form of elemental metals, viz., Au, Ag, Pt, Co, metal alloys such as FePt, CoPt, etc., metal oxides like Fe_2O_3, TiO_2, etc., or other metal compounds. Such nanoparticles are being revealed for their significant use in biological applications owing to their functional properties, which can be quite different from those of other bulk materials.[7,8] The functional properties of NPs are characterized by the materials along with their size, unique optical signature, and shape. The properties of metallic NPs have been the subject of intense research and grow recently due to the interesting properties of their surface plasmon resonance (SPR). Based on their distinctive physical, optical, and electrical properties, metallic

NPs have established important applications in a wide spectrum of biomedical benefits for example, drug delivery, imaging, sensing and targeting of gene.[9–11] Metallic NPs are applicable as markers for the optical detection of bio-molecules because of their outstanding SPR properties. Some of these NPs also have essential therapeutic potential as antimicrobial and antiplatelet agents.[12]

Gold (Au) NPs have been widely studied for biomedical applications as they display several distinct characteristic features. Au NPs possesses distinctive electronic and optical properties along with chemical inertness and capability to undergo surface functionalization because of the negative charge on their surface.[13] Because of exclusive electronic and optical properties, Au NPs have gained in its use in biosensing, bioimaging and photothermal therapy.[14,15] These properties of Au NPs allow to get easily functionalized with organic molecules thus achieving conjugation with ligands, antibodies or drug molecules for active or passive drug delivery.[16] Au NPs are relatively more bio-orthogonal and less toxic compare to other metal NPs, which makes them comparatively more biocompatible and lucrative option for expanding biological use. The synthesis of Au NPs with diameters ranging from a few to several hundred nanometers is well accepted. Remarkably, it is probable to synthesize not only spherical Au NPs but also other geometries such as rod-shaped particles or hollow shells by using the proper techniques. Like Au, silver (Ag) and its compounds have also been used for medicinal drives since its discovery. Ag NPs have exclusive physicochemical properties like high electrical conductivity, thermal conductivity, optical properties, chemical stability, catalytic activity, and antibacterial properties.[17] These properties have directed the use of Ag NPs in electronic, photonic, antimicrobial, and disinfectant applications.[18] These have extraordinary antimicrobial activity and thus these are chiefly used in the medical industry for textiles, wound dressings and device coatings.

Bimetallic nanoparticles such as iron cobalt (Fe—Co), iron-platinum (Fe—Pt) and iron-nickel (Fe—Ni) possess distinctive chemical and magnetic properties like chemical stability, super paramagnetism, high Curie temperature, and high saturation magnetization along with high X-ray absorption. These characteristics make them significant materials for the use in treatment of hyperthermia, MRI contrast agents, biosensors, and drug delivery.[19,20] Fe—Co oxidize easily and their biocompatibility is debatable, hence generally coated with a biocompatible material to overcome compatibility issue. Metal oxide nanoparticles are also important class of nanoparticles used in biosystem. Titanium dioxide (TiO_2) nanoparticles have exceptional biochemical properties such as biocompatibility, chemical stability, and optical properties which makes it an important material for use in the biomedical applications.[21] It is one of the most broadly employed photo-active nanomaterials worldwide.[22] There are three different forms of TiO_2, viz., anatase, rutile and brookite or combination of the three, each of which can either be exist as crystalline or amorphous. These nanomaterials are a great deal of interest due to their notable properties such as nontoxic behavior and low cost. Silica-based NPs such as SiO_2 have also an essential role in drug delivery and biosensors, due to its size, biocompatibility, surface area, low toxicity, low density, pore volume, and adsorption capacity.[23] These are also used in to diagnose and control diseases as well as correcting genetic disorders.[24] Other metal oxides such as Fe_2O_3, ZnO, zirconia etc. are also used in biomedical application, e.g., ZnO is used for drug delivery and bioimaging, magnetic Fe_2O_3 used in targeted drug delivery and contrast agents in MRI. Their details are beyond the scope of this chapter.

2.2 Carbon-based nanoparticles

One of the most broadly used carbon-based nanomaterials is CNTs because of their significant physical, chemical, and biological properties. CNTs are one-dimensional carbon allotropes that have a large surface area with very good mechanical strength along with ultra-light weight, outstanding chemical and thermal stability, and rich electronic properties. Due to their exceptional physiochemical properties, researchers have explored their potential in biological and biomedical applications.[25,26] CNTs surface could be functionalized simply to bind proteins and nucleic acids, therefore are emerging as advanced constituents in nanoformulations for the delivery of therapeutic molecules.[27]

Graphene is another carbon-based material with many favorable areas of application owing to its large surface area and possibility of easy functionalization, providing prospects for drug delivery. It is a two-dimensional nanoparticle having a single layer of carbon atoms crammed in a honeycomb crystal lattice with sp2 hybridization of carbon. This makes graphene as the thinnest material making a constant crystal lattice without any vacancies or structural dislocations and due to this property graphene has novel physical properties.[28] Certain methods, like chemical exfoliation, yield graphene oxide (GO) rich in hydrophilic oxygen containing functional groups on graphene sheets. GO may be reduced thermally or chemically to formulate reduced graphene oxide (RGO), having fewer oxygen-containing functional groups. In recent years, the mechanical, thermal, electrical, and chemical properties of graphene-based nanoparticles have generated strong attention to scientific community for biomaterials which includes applications in drug and gene delivery, imaging and tissue engineering.[29] However, the use of graphene and its derivatives in the clinic has been restricted because potential of cytotoxicity concern.

Nanodiamond particles (NDs) are a new type of semiconductor quantum dots (QDs) with progressive applications in medicine and biotechnology. NDs have been inspected as single-particle biomarkers for fluorescence imaging.[30] The surface of diamond NDs can also be functionalized to bind proteins and nucleic acids, permitting their use as a carrier for pharmaceutical agents or oligonucleotides.[31] Fullerenes are exclusive carbon allotropes with a polygonal structure made up with 60 carbon atoms exclusively. Nanostructures are described by the occurrence of various points of attachment whose surfaces may be functionalized for tissue binding. Fullerene has good biocompatibility and display low toxicity even at comparatively high dosages. These can be employed as antiviral agents, antibacterial agents and photodynamic agents for anticancer therapy.[32,33]

2.3 Other nanoparticles

Polymeric nanoparticles have colloidal structures composed of synthetic or semisynthetic polymers. Nanoparticles of polymers, viz., polysaccharide chitosan, polylactic acid (PLA), polylactic coglycolic acid (PLGA), and poly-caprolactone have been used as drug carriers.[34,35] The drug is dissolved, attached, entrapped or encapsulated to a polymeric nanoparticle matrix. Hydroxy apatite NPs have been used extensively in medicine and dentistry. It has similar composition with bone and teeth which make it a biocompatible material for the physiological process and present as the chief composition of mineralized tissues of the human body.[36] Liposome is a novel nanostructure for the encapsulation and delivery of

bioactive agents. These are nanoparticles embracing a lipid bilayer membrane surrounding an aqueous interior. Nanoliposome technology deals exciting chances for food technologists in fields including encapsulation and controlled release of food ingredients, also enhanced bioavailability and stability of sensitive materials. The amphiphilic liposome molecules used for the preparation of these molecules have resemblances between the biologic membranes and so have been used for improving the safety and efficacy of new drugs.[37]

3. Bionics as an inspired bio-nanomaterial

Bionics also define by the terms biomimetics, biomimicry, or biogenesis to solve the problem of structure, size, and composition of materials in the scientific field including medicine, electronics, chemistry, and material science, through the mimicking biological processes by the engineering nanostructures. By implementation of bottom-up technique to reboot the concepts and principals to create new material, device and system by enhancing the function and properties of bio-nanomaterials by biomimetic design with potential for an extensive range of applications (sensitive biosensing, detoxification of environmental pollutants, patient tailored therapeutics, etc.).[38] Biogenic material has its origin long time ago, since Leonardo da vinci working on his ships and flying machine, Wright brothers designed plane wing inspired with birds while, Joseph Paxton crystal palace design used the structure of lily pad. But bionics gets officially its name and definition in the 1960 by Jack E. Steele after being formed as a portmanteau from biology and electronics.[39] Biological materials, providing application platforms with complex nano-architectures, are highly functional elements on soft and hard tissues to the macroscale, microscale and nanoscale level with numerous different molecular level of self-assembly, templating, and recognitions motif.[40] Bionics serves as nanoscale biomimics with enhanced properties and functionalities, that is, arranging molecules at the nanoscale via self-assembly. It is possible to combine individual lipids, proteins and DNA units, with their robust synthetic materials known for their sophisticated structure and activity, for example, polymers, porous silica surfaces.[41]

In the various disease inflammations, we can diagnose the disease through inflammation targeting biomimetic nanoparticles.[42,43] Synthetic nanoparticle modified with chorioallantoic membrane, selectins, polymersomes, liposomes, dendrines, hydrogels etc. used as an inflammation targeting biomimetic nanoparticles by targeting cell surface proteins and cell membrane proteins, leukocytes, blood platelets and cancer cells.[44] ZnO and TiO_2 nanoparticles are typically used in cosmetics to white the skin and as sunscreens due to their well dispersed nature and transmit the visible lights.[45] Ref. [46] demonstrate in-vitro the interactions of HIV 1 with Ag NPs. HIV one bind to the sulfur binding residues of glycoprotein knob of host cell. The AgNPs were designed to bind to the same site in the host cell where HIV one compete for tethering and inhibit the binding of HIV one virus. GO/chitosan scaffolds and octacalcium phosphate provide a suitable environment for the enhancement of bone formation due to adorability of bone morphogenetic protein-2 encapsulated with bovine serum albumin NPs and silver NPs and also show the antibacterial properties, cell adhesion and growth.[47] Lanthanide-doped synthetic nanoparticles coated with monolayers of phospholipids with different functional groups are used as a versatile bioprobe in the

various fields.[48] Bio-inspired nanomaterials and techniques is a promising and interdisciplinary approach to the future development of biomimetics, molecular biology, and advanced materials science.

4. Applications of nanomaterials in biology

Nanoparticles have number of applications in the field of medicine. Some applications are shown in Fig. 20.1. Among them some are discussed below:

4.1 Nano-coatings of biomaterials: a smart approach

Currently, nanotechnology is one of the substantial topics in biomaterials research and the generation of a nanostructured surface on biomaterials is a very useful approach to tailor the corrosion resistance, mechanical, and biological properties of the implanted materials. The surface is not only a barrier to resist corrosion and wear, but also serve as a reservoir for loading cargoes carrying drugs, genes, and related nanocarriers. This fascinating strategy establishes a new trend in growth of biomaterials and other medical applications. Several types of bulk materials possess exceptional mechanical properties but may not be compatible with biological tissues and fluids when used in vivo. After surface alteration, properties such as cytocompatibility, osseointegration, and antibacterial traits can be attained selectively and in control manner while the favorable bulk qualities of the materials such as strength, etc., can be unaltered.[49] Modification of surface can improve the stability and at the same time bestow the biomaterials with special functions, including specific cell targeting, in vivo imaging for diagnosis, stimuli-responsive release, drug delivery monitoring, and photo-thermal treatment.[50] When a surface comprises micro and nano-scale topographies in a controlled fashion, the cellular and subcellular functions are modified considerably.[51] In nano-topography, we can experience the interaction between nano surface and cellular factors in the cells at molecular levels. There are lots of cellular function that influence the biological factors like cellular adhesion, kinetic, extracellular matrix-proteins, minerals, migration, deposition, differentiation, proliferation, and changes in gene expression that are easy to measure and experienced

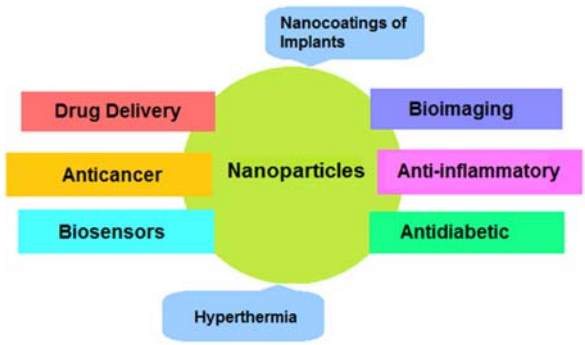

FIGURE 20.1 Applications of nanoparticles in medicine.

at topographical level.[52] Nano-topography changes the morphological responses of cell through nuclear deformation, actin and filament contractility, varying focal adhesion size, composition, and orientation of cells.[53] It is desirable to make drug-eluting implants to deliver drugs locally as a sustained release to improve osseointegration and reduce the healing time after implantation. For instance, nanotubes with a large surface area-to-volume ratio and manageable dimensions are noble candidates for antibacterial agents and carrying and delivering drugs.[54]

Ref. [55] reported that nanosurface roughness have positive influence on activity of cell introduced by acid-etching titanium surface at rat bone-marrow derived osteoblast. Ref. [56] reported micro-nanotopography on the selective melting measure surface, by incorporating the Zn with surface TiO_2 coating by microarc oxidation and subsequent hydrothermal treatment modification of titanium significantly enhance the osteogenesis and antibacterial ability. Ref. [57] demonstrated by in vitro assays and in vivo experiments that the 55 nm nanorod arrays reduced macrophage fusion and formation of Foreign body giant cells (FBGCs) offers a unique means of nanotopography to override biochemical signals and to attenuate fusion by selective mechanosensitivity of biomaterials to limit FBR-associated cell-cell fusion. Graphene-based materials (GBMs), gained substantial interest as nanotopography biomaterials for the coating application and tissue engineering, as discussed above. Due to significant physicochemical properties GBMs, GO and reduced RGO influence cell response, protein, or biomolecular interaction.

4.2 Effective drug release by nanoparticles

Nanotechnology can be utilized to design and develop platform for the drug delivery system to target the particular site. It is also a powerful in vivo technique for the image processing, and controlled release of drug.[58,59] In advance cure of tumors and other biological stimuli biometric nanoparticles play a crucial role.[58] The Food and Drug Administration (FDA) approved some biocompatible nanomaterials such as liposomes, silica NPs, micelles, polymers like polyethylene glycol, PLGA, and redox-sensitive nanocarriers for the drug release after the clinical trial.[60]

In the chemotherapy, stimuli responsive nanocarrier are active participant of drug release specifically respond after external and internal pathological trigger, such as pH value, enzyme, heat, and temperature.[61] The pH sensitive metal ionic nanoparticles and their chemicals groups for the effective drug release maintain the pKa values by pH dependence, accepting and donating protons. A novel pH-sensitive conjugate nanoparticle drug delivery system for doxorubicin (DOX) is made with biocompatible polymer. DOX was released from nanoparticles faster at pH 5.0 than pH 7.4.[62] Hydrogels are one of the controlled drug release polymer that show potential change in their network structure, mechanical strength, swelling behavior, and permeability response to the different tumor stimuli.[63]

ZnO QDs, ZnO CaP, ZnO-folic acid QDs are new kind of multiple functional inorganic nanomaterials for the drug delivery system with controlled drug release having high drug loading capacities, high biocompatibility, and low cytotoxicity.[64,65] The hydrophobic and hydrophilic amino acids are important carrier for design of peptide nanoscaffolds or nanofibers to build robust hydrophobic or hydrophilic drug delivery platform to manage antimicrobial,

antitumor, and antiinflammatory cure.[66] Graphene/GO has been broadly scrutinized as some of the most auspicious biomaterials for biomedicine applications due to their particular properties: chemical and mechanical stability, two-dimensional planar structure, magnificent conductivity, large surface area and superb biocompatibility.[67] Ref. [68] designed nanovesicles, to release the anticancer drug gemcitabine, at the tumor site which overexpress the glutathione and matrix metalloproteinase proteolytic enzyme. Matrix metalloproteinase proteolytic enzyme and glutathione are over expressed in many tumors and metastasis cancer.[69] In drug delivery, nanoparticles offer improved capabilities and performances than conventional therapies, suggesting alternative ways to deliver therapeutics efficiently over various parts of the host body thereby decreasing the side effects related with excessive dosages of highly toxic drugs. Nanoparticles and biomaterials science blend contributing richly in the directions of chemistry and molecular biology to the selective and specific drug delivery or to target cells with a great future applications.

4.3 Magnetic nanoparticles in various disease treatments

Magnetic NPs are widely applied in the field of molecular diagnosis and medicine. Magnetic NPs are easy to prepares and have the unique magnetic properties including nickel, cobalt, iron, silver, gold, and platinum with their metal alloys and metal oxides.[70] Iron oxides and ferrites are commonly used magnetic NPs for diagnose the various disease as demonstrated in Fig. 20.2.[71] The size of 20 nm magnetic NPs shows the surface effects and can carry the high amount of DNA, RNA, proteins, compounds and drugs.[72] Magnetic NPs are nonvirulent, nonimmunogenic, and highly biocompatible. To diagnose all kind of tumors, iron oxides (Fe_2O_3 and Fe_3O_4) and ferrites NPs are widely used because of low cytotoxicity, biodegradability, and the ability to target the multiple receptor site using ligands, and antibodies.[19,71] Ref. [73] reported injecting super magnetic NPs for biomedicine in mouse to see the migration and differentiation of stem cells to understand the mechanism of cancer development.[73] First implied magnetic field for thermotherapy using magnetic NPs against tumor

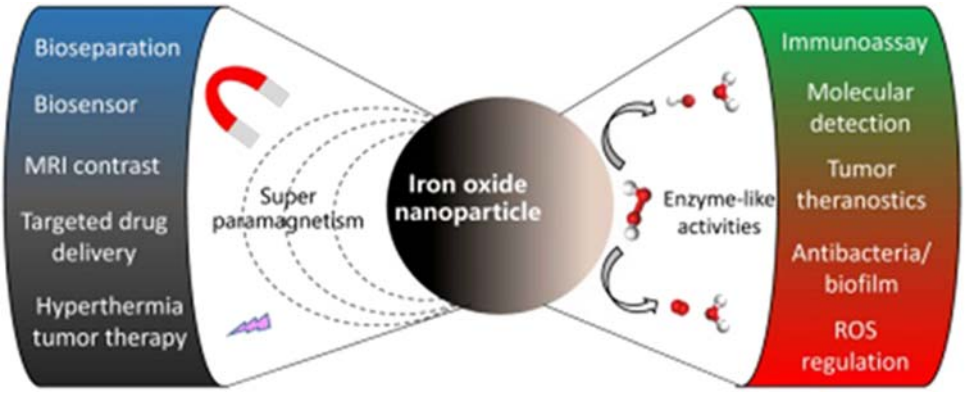

FIGURE 20.2 Typical magnetic properties and novel enzyme-like activity of iron oxide nanoparticles for biomedical applications. *Reproduced with permission from Gao L, Fan K, Yan X. Iron oxide nanozyme: a multifunctional enzyme mimetic for biomedical application. Theranostics. 2017;7:3207–3227.*

thermotherapy was introduced by Ref. [74]. Ref. [75] designed nanoparticles core shell structure based by coating the Mn Zn ferrite NPs with PEG lipid, to diagnose the liver metastasis.

Bifunctional magnetic nanoparticles labeled with antibodies to detect the promising biomarkers β-amyloid-40 and 42 to detect the Alzheimer disease.[76] In the mouse model, the detection of Parkinson's and Huntingdon's disease at the early stage can be diagnosis using MRI by ScFv conjugated supermagnetic iron oxide nanoparticles.[77] In a Nanotheranostic approach the paramagnetic and supermagnetic nanoparticles was used for central nervous system and neurological disorders for targeted delivery to unhealthy regions of brains.[78] In some biomedical applications, we need to use core shell MNPs to assure the biocompatibility and stability of biomolecules.

5. Future of bio-nanomaterials

New generation of bio-nanomaterials science and engineering with many possible applications in medicine has a potential for diagnose and treatments of a variety of life-threatening diseases through specific targeted drug-delivery systems. The benefits of using nano biomaterials are their low toxicity and therefore highly effective. Bio-nanomaterials are playing a crucial role in the field of genetic, molecular biology, cell biology, tissue engineering, and bioimplants, using different kinds of nanoparticles for the development of nanodrugs to target specific site and gene delivery as discussed in this chapter. Many researchers are focused on to developed enhanced and highly durable multifunctional nanoscale-sized platform for the targeted and drug delivery system. Nanoparticle probes include fluorescent biological labels, drug and gene delivery, detection of protein, bio-detection of pathogens, probing of DNA structure, tissue engineering, tumor detection, separation and purification of biological molecules and cells, MRI contrast enhancement and phagokinetic studies.[79,80] The biologically produced nanomaterials are also commercially used for the treatment of neurodegenerations, immunotherapy, cancer detection and diagnose, microbial infections, and many other diseases.[81,82] Nanoimaging techniques have improved signal sensitivity, better spatial resolution, and capable to transmit information on biological systems at molecular and cellular levels.[83] The importance of this research area lies in the progress of an advanced technology that will effect nanoscale approaches designed to probe molecular mechanisms in living cells and molecular imaging.[83] In the field of nano-medicine, the engineered bio-nanomaterials contribute to in vitro and in vivo application for the cellular level to identify the cancer-specific cells and site to deliver the drugs.[84]

Nanoswimmers and nanobots are the future of drug delivery and might be convenient in deliver genes to target tissues at very high adaptability if they carry desired DNA, RNA segments, protein and peptide. These future nanoswimmers and nanobots is perhaps an explanation to some old therapeutic problems in biology and medicine with alluring, less suicidal and more adequate materials. Nanotechnology or its system at the molecular level brings about an all-rounder option, therefore contribute not only for the advancement to current techniques, and rather provide exclusively new appliance and competence. Despite the many aspects regarding the biological potential of nanosystems have been clarified, still there are many concerns prevail regarding the application of metal-based nanoparticles for clinical

purpose. The disadvantage of the nano-systems can be overcome by using more biorthogonal polymers and encapsulating surfactants to cross tissue barrier by improving the biocompatibility of the nanosystems. However, active association among researchers and nanotechnologists can pave the strong development to achieve clinical revolution.

6. Conclusions

The advancements of nanomaterials have been pushed to an exciting research in the field of biomedicine because of their unique properties. The significant basis of using nanomaterials is their large surface area, distinct optical properties, and excellent biocompatibility. In this chapter, we have offered progress in various nanomaterials used in medicine including as well as application of nanomaterials in various disease treatments and effective drug delivery. It can be expected that almost all issues will be resolved with the continuing efforts in regard of treating diseases and improved quality of implanted materials. Nanotechnology is already became an essential part of the medical and clinical applications.

References

1. Liu H, Webster TJ. Nanomedicine for implants: a review of studies and necessary experimental tools. *Biomater* 2007;**28**(2):354–69.
2. Jiang W, Liu H. *Nanocomposites for bone repair and osteointegration with soft tissues*. *Nanocomposites for musculoskeletal tissue regeneration*. 2016. p. 241–57.
3. Dong L, Craig MM, Khang D, Chen C. Applications of nanomaterials in biology and medicine. *J Nanotechnol* 2012;**2012**. https://doi.org/10.1155/2012/816184. Article ID 816184.
4. Rho JY, Kuhn-Spearing L, Zioupos P. Mechanical properties and the hierarchical structure of bone. *Med Eng Phys* 1998;**20**(2):92–102.
5. Falahati M, Attar F, Sharifi M, Saboury AA, Salihi A, Aziz FM, Kostova I, Burda C, Priecel P, Lopez-Sanchez JA, Laurent S, Hooshmand N, El-Sayed MA. Gold nanomaterials as key suppliers in biological and chemical sensing, catalysis, and medicine. *BBA-General Subj* 2020;**1864**:129435.
6. Jiang W, Rutherford D, Vuong T, Liu H. Nanomaterials for treating cardiovascular diseases: a review. *Bioact Mater* 2017;**2**:185–98.
7. Parak WJ, Gerion D, Pellegrino T, Zanchet D, Micheel C, Williams SC, Boudreau R, Le Gros MA, Larabell CA, Alivisatos AP. Biological applications of colloidal nanocrystals. *Nanotechnol* 2003;**14**:R15–27.
8. Carrión CC, Nazarenus M, Paradinas SS, Romero SC, Almendral MJ, Fuentes M, et al. Metal ions in the context of nanoparticles toward biological applications. *Curr Opin Chem Eng.* 2014;**4**:88–96.
9. Murphy CJ, Gole AM, Stone JW, Sisco PN, Alkiany AM, Goldsmith EC, Baxter SC. Gold nanoparticles in biology: beyond toxicity to cellular imaging. *Acc Chem Res* 2008;**41**:1721–30.
10. Daniel MC, Astruc D. Gold nanoparticles: assembly, supramolecular chemistry, quantum - sized - related properties, and applications towards biology, catalysis and nanotechnology. *Chem Rev* 2004;**104**:293–346.
11. Ghosh P, Han G, De M, Kim CK, Rotello VM. Gold nanoparticles in delivery applications. *Adv Drug Deliv Rev* 2008;**60**:1307–15.
12. Shrivastava S, Bera T, Singh SK, Singh G, Ramach-andrarao P, Dash D. Characterization of antiplatelet properties of silver nanoparticles. *ACS Nano* 2009;**3**:1357–64.
13. Patra CR, Bhattacharya R, Mukhopadhyay D, Mukherjee P. Fabrication of gold nanoparticles for targeted therapy in pancreatic cancer. *Adv Drug Deliv Rev* 2010;**62**:346–61.
14. Lepinay S, Staff A, Ianoul A, Albert J. Improved detection limits of protein optical fiber biosensors coated with gold nanoparticles. *Biosens Bioelectron* 2014;**52**:337–44.

15. Meir R, Shamalov K, Betzer O, Motiei M, Horovitz-Fried M, Yehuda R, et al. Nanomedicine for cancer immunotherapy: tracking cancer-specific T-cells in vivo with gold nanoparticles and CT imaging. *ACS Nano* 2015;**9**:6363–72.
16. Khan AK, Rashid R, Murtaza G, Zahra A. Gold nanoparticles: synthesis and applications in drug delivery. *Trop J Pharmaceut Res* 2014;**13**:1169–77.
17. Wei L, Lu J, Xu H, Patel A, Chen ZS, Chen G. Silver nanoparticles: synthesis, properties, and therapeutic applications. *Drug Discov Today* 2015;**20**:595–601.
18. McNamara K, Tofail SAM. Nanoparticles in biomedical applications. *ADV PHY X* 2017;**2**:54–88. https://doi.org/10.1080/23746149.2016.1254570.
19. Seo WS, Lee JH, Sun X, Suzuki Y, Mann D, Liu Z, et al. FeCo/graphitic-shell nanocrystals as advanced magnetic-resonance-imaging and near-infrared agents. *Nat Mater* 2006;**5**:971–6.
20. Lee SJ, Cho JH, Lee C, Cho J, Kim YR, Park JK. Synthesis of highly magnetic graphite-encapsulated FeCo nanoparticles using a hydrothermal process. *Nanotechnology* 2011;**22**:375–603.
21. Yin ZF, Wu L, Yang HG, Su YH. Recent progress in biomedical applications of titanium dioxide. *Phys Chem Chem Phys* 2013;**15**:4844–58.
22. Nguyen PTN, Salim C, Kurniawan W, Hinode H. A non-hydrolytic sol-gel synthesis of reduced graphene oxide/TiO_2 microsphere photocatalysts. *Catal Today* 2014;**230**:166–73.
23. Halas NJ. Nanoscience under glass: the versatile chemistry of silica nanostructures. *ACS Nano* 2008;**2**:179–83.
24. Bitar A, Ahmad NM, Fessi H, Elaissari A. Silica-based nanoparticles for biomedical applications. *Drug Discov Today* 2012;**17**:1147–54.
25. Kam NWS, Liu Z, Dai H. Functionalization of carbon nanotubes via cleavable disulfide bonds for efficient intracellular delivery of siRNA and potent gene silencing. *J Am Chem Soc* 2005;**127**:12492–3.
26. Liu Z, Sun X, Nakayama N, Dai H. Supramolecular chemistry on water - soluble carbon nanotubes for drug loading and delivery. *ACS Nano* 2007;**1**:50–6.
27. Liu Z, Tabakman S, Welsher K, Dai H. Carbon nano-tubes in biology and medicine: in vitro and in vivo detection, imaging and drug delivery. *Nano Res* 2009;**2**:85–120.
28. McIntyre RA. Common nano-materials and their use in real world applications. *Sci Prog* 2012;**95**:1–22.
29. Ahadian S, Ramalingam M, Khademhosseini A. In: Ramalingam M, Wang X, Chen G, Ma P, Cui FZ, editors. *Biomimetics: advancing nanobiomaterials and tissue engineering*. Hoboken, NJ: John Wiely & Sons, Inc.; 2013. p. 279–99 [Chapter 12].
30. Yu SJ, Kang MW, Chang HC, Chen KM, Yu YC. Bright fluorescent nanodiamonds: no photobleaching and low cytotoxicity. *J Am Chem Soc* 2005;**127**:17604–5.
31. Huang H, Pierstorff E, Osawa E, Ho D. Active nano-diamond hydrogels for chemotherapeutic delivery. *Nano Lett* 2007;**7**:3305–14.
32. Schinazi RF, Sijbesma R, Srdanov G, Hill CL, Wudl F. Synthesis and virucidal activity of a water - soluble, configurationally stable, derivatized C60 fullerene. *Antimicrob Agents Chemother* 1993;**37**:1707–10.
33. Tsao N, Kanakamma PP, Luh TY, Chou CK, Lei HY. Inhibition of Escherichia coli - induced meningitis by carboxy fullerene. *Antimicrob Agents Chemother* 1999;**43**:2273–7.
34. Uhrich KE, Cannizzaro SM, Langer RS, Shakesheff KM. Polymeric systems for controlled drug release. *Chem Rev.* 1999;**99**:3181–98.
35. Sailaja AK, Amareshwar P, Chakravarty P. Chitosan nanoparticles as a drug delivery system. *RJPBCS* 2010;**1**:474–84.
36. Priyadarsini S, Mukherjee S, Mishra M. Nanoparticles used in dentistry: a review. *J Oral Biol Craniofac Res* 2018;**8**:58–67.
37. Samad A, Sultana Y, Aqil M. Liposomal drug delivery systems: an update review. *Curr Drug Deliv* 2007;**4**:297–305.
38. Mcalpine MC. *Bionic nanosystems*. Princeton, NJ: Mechanical and Aerospace Engineering Princeton University; 2014.
39. Barthlott W, Rafiqpoor MD, Walter RE. *Bionics and biodiversity—bio-inspired technical innovation for a sustainable future. Biomimetic research for architecture and building construction*. Cham: Springer; 2016. p. 11–55.
40. Tanaka S, Kaneti YV, Septiani NLW, Dou SX, Bando Y, Hossain MSA, et al. A review on iron oxide-based nanoarchitectures for biomedical, energy storage, and environmental applications. *Small Methods* 2019;**3**:1800512.

41. Rasheed T, Nabeel F, Raza A, Bilal M, Iqbal HMN. Biomimetic nanostructures/cues as drug delivery systems: a review. *Mater Today Chem* 2019;**13**:147–57.
42. Park JH, Dehaini D, Zhou J, Holay M, Fang RH, Zhang L. Biomimetic nanoparticle technology for cardiovascular disease detection and treatment. *Nanoscale Horiz* 2020;**5**:25–42.
43. Yang G, Chen S, Zhang J. Bioinspired and biomimetic nanotherapies for the treatment of infectious diseases. *Front Pharmacol* 2019;**10**:751.
44. Kamaly N, Xiao Z, Valencia PM, Radovic-Monero AF, Farokhzad OC. Targeted polymeric therapeutic nanoparticles: design, development and clinical translation. *Chem Soc Rev* 2012;**41**:2971–3010.
45. Lu PJ, Huang SC, Chen YP, Chiueh LC, Shih DYC. Analysis of titanium dioxide and zinc oxide nanoparticles in cosmetics. *J Food Drug Anal* 2015;**23**:587–94.
46. Elechiguerra JL, Burt JL, Morones JR, Bragado AC, Gao X, Lara HH, et al. Interaction of silver nanoparticles with HIV-I. *J Nanobiotechnol* 2005;**3**. https://doi.org/10.1186/1477-3155-3-6.
47. Xie C, Lu X, Han L, Xu J, Wang Z, Jiang L, et al. Biomimetic mineralized hierarchical graphene oxide/chitosan scaffolds with adsorbability for immobilization of nanoparticles for biomedical applications. *ACS Appl Mater Interfaces* 2016;**8**:1707–17.
48. Li LL, Zhang R, Yin L, Zheng K, Qin W, Selvin PR, et al. Biomimetic surface engineering of lanthanide-doped upconversion nanoparticles as versatile bioprobes. *Angew Chem* 2012;**51**:6121–5.
49. Chu PK. Surface engineering and modification of biomaterials. *Thin Solid Films* 2013;**528**:93–105.
50. Zhang L, Li Y, Yu JC. Chemical modification of inorganic nanostructures for targeted and controlled drug delivery in cancer treatment. *J Mater Chem B* 2014;**2**:452–70.
51. Liu X, Chu PK, Ding C. Surface nano-functionalization of biomaterials. *Mater Sci Eng R* 2010;**70**:275–302.
52. Ross AM, Jiang Z, Bastmeyer M, Lahann J. Physical aspects of cell culture substrates: topography, roughness, and elasticity. *Small* 2012;**8**:336–55.
53. Neoh KG, Hu X, Zheng D, Kang ET. Balancing osteoblast functions and bacterial adhesion on functionalized titanium surfaces. *Biomater* 2012;**33**:2813–22.
54. Gao A, Hang R, Huang X, Zhao L, Zhang X, Wang L, et al. The effects of titania nanotubes with embedded silver oxide nanoparticles on bacteria and osteoblasts. *Biomater* 2014;**35**:4223–35.
55. de Oliveira PT, Zalzal SF, Beloti MM, Rosa AL, Nanci A. Enhancement of in vitro osteogenesis on titanium by chemically produced nanotopography. *J Biomed Mater Res A* 2007;**80**:554–64.
56. Xu JY, Chen XS, Zhang CY, Liu Y, Wang J, Deng FL. Improved bioactivity of selective laser melting titanium: surface modification with micro-/nano-textured hierarchical topography and bone regeneration performance evaluation. *Mater Sci Eng C* 2016;**68**:229–40.
57. Kyriakides TR. *Chapter 5 - Molecular events at tissue–biomaterial interface*. *Host response to biomaterials*. Academic Press; 2015. p. 81–116.
58. Liu D, Yang F, Xiong F, Gu N. The smart drug delivery system and its clinical potential. *Theranostics* 2016;**6**:1306–23.
59. Sun C, Jerry SH Lee JSH, Zhang M. Magnetic nanoparticles in MR imaging and drug delivery. *Adv Drug Deliv Rev* 2008;**60**:1252–65.
60. Hassan S, Prakash G, Ozturk AB, Saghazadeh S, Sohail FM, Seo J, et al. Evolution and clinical translation of drug delivery nanomaterials. *Nano Today* 2017;**15**:91–106.
61. Kumar KP, Reddy VC, Kumar SVH, Radhika PR, Sivakumar T. A promising tool for biomolecular nanotechnology–bionanoparticles. *Int J Biomed Nanosci Nanotechnol (IJBNN)* 2012;**2**:207–31.
62. Lu DX, Wen XT, Liang J, Zhang XD, Gu ZW, Fan YJ. Novel pH-sensitive drug delivery system based on natural polysaccharide for doxorubicin release. *Chin J Polym Sci* 2008;**26**:369–74.
63. Gupta P, Vermani K, Garg S. Hydrogels: from controlled release to pH-responsive drug delivery. *Drug Discov Today* 2002;**7**:569–79.
64. Xiang Y, Liu X, Mao C, Liu X, Cui Z, Yang X, et al. Infection-prevention on Ti implants by controlled drug release from folic acid/ZnO quantum dots sealed titania nanotubes. *Mater Sci Eng C* 2018;**85**:214–24.
65. Karimi-Maleh H, Ahanjan K, Taghavi M, Ghaemy M. A novel voltammetric sensor employing zinc oxide nanoparticles and a new ferrocene-derivative modified carbon paste electrode for determination of captopril in drug samples. *Anal Methods* 2016;**8**:1780–8.
66. Habibi N, Kamaly N, Memic A, Shafiee H. Self-assembled peptide-based nanostructures: smart nanomaterials toward targeted drug delivery. *Nano Today* 2016;**11**:41–60.

67. Liu J, Cui L, Losic D. Graphene and graphene oxide as new nanocarriers for drug delivery applications. *Acta Biomater* 2013;**9**:9243–57.
68. Jia L, Zheng JJ, Jiang SM, Huang KH. Preparation, physicochemical characterization and cytotoxicity in vitro of gemcitabine-loaded PEG-PDLLA nanovesicles. *World J Gastroenterol* 2010;**16**:1008.
69. Mondal S, Adhikari N, Banerjee S, Amin SA, Jha T. Matrix metalloproteinase-9 (MMP-9) and its inhibitors in cancer: a Minireview. *Eur J Med Chem* 2020;**194**:112260.
70. Mirza S, Ahmad MS, Shah MIA, Ateeq M. *Chapter 11 - Magnetic nanoparticles: drug delivery and bioimaging applications*. Elsevier; 2020. p. 189–213.
71. Gao L, Fan K, Yan X. Iron oxide nanozyme: a multifunctional enzyme mimetic for biomedical application. *Theranostics* 2017;**7**:3207–27.
72. McBain SC, Yiu HH, Dobson J. Magnetic nanoparticles for gene and drug delivery. *Int J Nanomed* 2008;**3**:169–80.
73. Jin X, Chen K, Huang J, Lee S, Wang J, Gao J, et al. PET/NIRF/MRI triple functional iron oxide nanoparticles. *Biomater* 2010;**31**:3016–22.
74. Jordan A, Wust P, Scholz R, Tesche B, Fahling H, Mitrovics T, et al. Cellular uptake of magnetic fluid particles and their effects on human adenocarcinoma cells exposed to AC magnetic fields in vitro. *Int J Hyperther* 1996;**12**:705–22.
75. Arriortua OK, Garaio E, de la Parte BH, Insausti M, Lezama L, Plazaola F, et al. Antitumor magnetic hyperthermia induced by RGD-functionalized Fe_3O_4 nanoparticles, in an experimental model of colorectal liver metastases. *Beilstein J Nanotechnol* 2016;**7**:1532–42.
76. Yang CC, Yang SY, Chieh JJ, Horng HE, Hong CY, Yang HC, et al. Biofunctionalized magnetic nanoparticles for specifically detecting biomarkers of Alzheimer's disease in vitro. *ACS Chem Neurosci* 2011;**2**:500–5.
77. Liu XG, Lu S, Liu DQ, Zhang L, Zhang LX, Yu XL, et al. ScFv-conjugated superparamagnetic iron oxide nanoparticles for MRI-based diagnosis in transgenic mouse models of Parkinson's and Huntington's diseases. *Brain Res* 2019;**1707**:141–53.
78. Sharma M, Dube T, Chibh S, Kour A, Mishra J, Panda JJ. Nanotheranostics, a future remedy of neurological disorders. *Expet Opin Drug Deliv* 2019;**16**:113–28.
79. LaConte L, Nitin N, Bao G. Magnetic nanoparticle probes. *Mater Today* 2005;**8**:32–8.
80. Wang Z, Ma L. Gold nanoparticle probes. *Coord Chem Rev* 2009;**253**:1607–18.
81. Emerich DF, Christopher GT. Nanotechnology and medicine. *Expet Opin Biol Ther* 2003;**3**:655–63.
82. Boisseau P, Loubaton B. *Nanomedicine, nanotechnology in medicine*. *Comptes Rendus de l'Académie des Sciences*. Elsevier; 2011. p. 620–36.
83. Bennett KM, Jo JI, Cabral H, Bakalova R, Aoki I. MR imaging techniques for nano-pathophysiology and theranostics. *Adv Drug Deliv Rev* 2014;**74**:75–94.
84. Poma A, Giorgio MLD. Toxicogenomics to improve comprehension of the mechanisms underlying responses of in vitro and in vivo systems to nanomaterials: a review. *Curr Genom* 2008;**9**:571–85.

This page intentionally left blank

CHAPTER

21

Can bio-nanotechnology be effective against multi drug resistant (MDR) pathogens?

Divya P. Sukumaran and Mohamed Hatha Abdulla

Department of Marine Biology, Microbiology and Biochemistry, School of Marine Sciences, Cochin University of Science and Technology, Kochi, Kerala, India

1. Introduction

Antibiotic resistance among pathogenic bacteria is one of the serious threats faced by humanity worldwide. The world health organization (WHO) has started several effective actions to contain antibiotic resistance among bacteria such as the Global antimicrobial resistance surveillance system (GLASS), the Global antibiotic research and development partnership (GARDP), and the Interagency coordination group on antimicrobial resistance (IACG).[1] Bacteria are acquiring resistance to most of the currently used antibiotics, including the last resort antibiotics mainly due to overuse or misuse. Many countries have banned the use of antibiotics in various areas to reduce the development of multi drug resistant bacteria. New technologies should be implemented to curb the emergence of life-threatening antibiotic-resistant bacteria. In this context, bio-nanotechnology emerges as a promising one to fight against antibiotic-resistant bacteria.

Nanoparticles (NPs) are reported to posses excellent antibacterial properties, hence considered as a promising alternative to antibiotics and can be used as a drug delivery system, which may reduce the overuse of antibiotics.[2] Nanoparticles coupled with antibiotics act mainly at the site of infection, thus increasing the concentration of antibiotics at the site of bacterium-antibiotic interaction. NP conjugated antibiotics have a lower minimum inhibitory concentration (MIC) compared to the nonconjugated antibiotic against bacteria.[3] Nanoparticles accelerate the effects of commonly used antibiotics by blocking the bacterial efflux pumps.[4] NPs possess a complex antimicrobial mechanism of action and reduce the chance of the development of resistant strains.[5]

Applications of Multifunctional Nanomaterials
https://doi.org/10.1016/B978-0-12-820557-0.00008-4

2. Antibiotic resistance

World Health Organization (WHO) has described antibiotic resistance as one of the greatest threats to human health.[6] Misuse or overuse of antibiotics creates selection pressure leading to the selection and multiplication of drug-resistant mutants. Bacteria are rapidly acquiring antibiotic resistance determinants and disseminated into different environments. The antibiotic-resistant bacteria emerge mainly by three mechanisms (i) horizontal gene transfer events such as conjugation, transduction, and transformation, (ii) genetic mutation, and (iii) recombination.[7] Plasmids, integrons, and transposons are the major mobile genetic elements involved in the dissemination of antibiotic resistance genes. Antibiotics are widely used in clinical medicine, to control diseases in aquaculture and animal production systems as well as growth promoters in animal feeds at subtherapeutic level. Antibiotics released from pharmaceutical manufacturing plants, aquaculture facilities, and animal husbandry facilities may partially degrade and be released into aquatic environments through the release of treated or untreated effluents from waste water treatment plants (WWTP). Clinical settings are considered as the hotspot of antibiotic-resistant bacteria, although various other organically polluted environments could also act as reservoirs of antibiotic-resistant bacteria. These environmental resistant strains can transfer their resistant determinants to human commensal or pathogenic bacteria, leading to more complications in the treatment of infections caused by them.

3. Major classes of antibiotics and their mode of action

World Health Organization has categorized antibiotics into three categories based on their importance to human medicine; (i) Critically important antimicrobials with the highest priority, (ii) Critically important antimicrobials with high priority, (iii) Highly important antimicrobials, (iv) Important antimicrobials.[8] This categorization of antibiotics would lead to better management of antimicrobial resistance by encouraging new research, especially developing new ways to curb antibiotic resistance.

3.1 Cephalosporins

There are five generations of cephalosporins: (i) first generation-cephalexin, cephradine, cefazolin, cephalothin, cephapirin, and cefadroxil; (ii) second generation-cefoxitin, cefuroxime, and cefotetan; (iii) cefotaxime, ceftriaxone, ceftazidime, cefixime, ceftibuten, and cefdinir (iv) fourth generation-cefepime, and cefpirome; (v) fifth generation-ceftobiprole, and ceftaroline. Third, fourth, and fifth generation cephalosporin are considered as critically important antimicrobials with the highest priority. Cephalosporins (first and second generation) and cephamycins are included in the WHO list of highly important antimicrobials.[8]

Inhibition of vital processes such as cell wall synthesis, nucleic acid synthesis, protein synthesis, and impairment of cytoplasmic membrane are the mechanisms of action of beta-lactam antibiotics.[9] Bacteria become resistant by the production of enzymes (extended-spectrum cephalosporinases or Extended spectrum beta-lactamases - ESBLs), which are capable of destroying the four-member beta-lactam ring of the extended-spectrum cephalosporins (third generation). The ESBL enzymes are classified into several types, CTXM,

SHV, and TEM. Bacteria-producing CTX-M enzymes are further divided into five groups based on their amino acid identities: CTX-M1, CTX-M2, CTX-M8, CTX-M9 and CTX-M25. CTX-M-producers are the most prevalent ESBL producers in environmental and clinical settings.[10] There are other ESBLs such as OXA, PER, VEB, BES, GES, SFO, TLA, and IBC, which are minor enzymes.

3.2 Glycopeptides

Vancomycin and teicoplanin are the first-generation glycopeptides antibiotics available for use in humans. Telavancin, dalbavancin, and oritavancin are second-generation glycopeptides, semisynthetic lipoglycopeptide derivatives. Vancomycin and teicoplanin are the glycopeptide antibiotics available for use in humans. The glycopeptide antibiotics are a group of glycosylated cyclic or polycyclic nonribosomal peptides that inhibit Gram-positive bacterial cell wall synthesis by binding to the bacterial D-Ala-D-Ala peptidoglycan binding site.[11] Gram-negative bacilli show an intrinsic mechanism of resistance against glycopeptides, by preventing them from entering the cell and binding to their target sites. Bacteria become resistant to vancomycin by altering the structure of the peptidoglycan precursors. There are six different molecular resistance elements (*VanA*, *VanH*, *VanX*, *VanY*, *VanR*, *VanS*) that confer resistance to vancomycin.[12]

3.3 Macrolides and ketolides

The macrolides and ketolides are broad-spectrum antibiotics. Erythromycin is a first-generation macrolide, while clarithromycin, azalide, and azithromycin are second-generation macrolides. Macrolides are used for the treatment of respiratory infections. Clarithromycin is a commonly prescribed antibiotic that acts by binding to the peptidyltransferase region of the 23S rRNA, inhibiting bacterial protein synthesis.[13] Macrolides are characterized by macrocyclic lactone[14–16] rings with one or more deoxy sugars. Ketolides are semisynthetic derivatives of macrolides, developed to inhibit the macrolide-resistant strains. The mechanism of action of ketolide is similar to that of macrolide, with more affinity for the unmethylated ribosome. Bacteria become resistant to macrolide and ketolide by the mechanisms such as modification of the target site on bacterial ribosomes or efflux via the multidrug efflux pump.

3.4 Polymyxins

Polymyxins are cationic, cyclic-peptide antibiotics. Colistin (polymyxin E) and polymyxin B are commonly used polymyxins. Polymyxins displace Mg^{2+} and Ca^{2+} ions, by the polar and hydrophobic interaction with phosphate groups of the lipopolysaccharides of the bacterial outer membrane. As a result, membrane charge neutralization occurs, leading to disruption of the bacterial outer membranes, resulting in cell death. Polymyxins also have potent antiendotoxin activity and inhibit type II NADH-quinone oxidoreductases in the bacterial cell membrane.[14] Polymyxins are more highly active against many Gram-negative bacteria than Gram-positive bacteria, because of the presence of phospholipids in the membrane of Gram-negative bacteria. Resistance to polymyxin is caused primarily due to alterations of

the negative charge of the outer membrane to prevent the binding of polymyxins. Plasmid-borne *mcr-1* is responsible for a transferable mechanism of polymyxin resistance. There are many variants of *mcr* gene (a gene of the phosphoethanolamine transferase enzyme family).[15] Colistin is considered the "antibiotic of last resort" for treating infections caused by multidrug-resistant Gram-negative bacteria in humans.

3.5 Quinolones

Quinolones and fluoroquinolones are a family of broad-spectrum antibiotics, which are commonly used in the treatment of bacterial infections. The antibiotics include ofloxacin, norfloxacin, ciprofloxacin, moxifloxacin, levofloxacin, nemonoxin, and nalidixic acid. Fluoroquinolone antibiotics are created with the addition of a fluorine group to the quinolone moiety. Quinolone inhibits bacterial DNA gyrase and topoisomerase IV, which is essential for nucleic acid (DNA or RNA) synthesis and intermediary metabolism.

Quinolone resistance is mainly caused by point mutations in the quinolone resistance-determining region (QRDR) of gyrase (*gyrA* and *gyrB*) and topoisomerase (*parC* and *parE*) genes and followed by plasmid-mediated quinolone resistance (PMQR).[15,16] PMQR determinants confer low-level resistance to quinolones. PMQR is mediated by *qnr* genes (encodes pentapeptide repeat protein that protects bacteria), *aac*(6′)-*Ib-cr* (encodes an aminoglycoside acetyltransferase), *oqxAB*, *qepA1,* and *qepA2* genes (encodes efflux pump proteins).

3.6 Aminoglycosides

The antibiotics include streptomycin, gentamicin, kanamycin, netilmycin, tobramicin, and amikacin. Gentamicin is the commonly used aminoglycoside. Aminoglycosides are widely used for the treatment of septicemia, nosocomial respiratory tract infections, complicated urinary tract infections (UTIs), and complicated intraabdominal infections. Gentamicin, tobramycin, and amikacin are frequently prescribed antibiotics in the medical field. Streptomycin is used for treating tuberculosis patients.[17] Aminoglycosides bind irreversibly to the 30S ribosome and inhibit protein synthesis. Aminoglycosides also interference with the cellular electron transport system, inhibition of translation, effects DNA metabolism, and damage cell membranes.

Acquired aminoglycoside resistance can occur through three mechanisms: (i) alterations in membrane permeability, (ii) enzymatic modification, or (iii) alterations in the target site. Enzymatic inactivation plays a major role in aminoglycoside resistance that is either aminoglycoside acetyltransferases (AAC), aminoglycoside adenylyltransferases also named aminoglycoside nucleotidyltransferases (ANT), or aminoglycoside phosphotransferases (APH).[18]

3.7 Ansamycins

Ansamycins are lipophilic macrocyclic antibiotics. Rifampicin, a semisynthetic derivative, is the first line of antibiotics for the treatment of tuberculosis and leprosy. Ansamycins act on bacterial RNA polymerase and inhibits RNA synthesis. Rifapentin, rifamixin, rifalazil, and rifabutin are the other members. Bacteria become resistant to rifamicins by any of the following methods such as (i) duplication of the target, (ii) action of RNA polymerase binding proteins

(RNAP), and (iii) modification of rifampicin binding site by mutation and modification of cell permeability by overexpression of membrane-associated energy-driven efflux pumps.[19,20] WHO has listed ansamycin as a critically important antimicrobial with high priority.[8]

3.8 Carbapenems

Imipenem, imipenem-cilastatin, meropenem, ertapenem, doripenem, panipenem-betamipron, and biapenem are the currently available carbapenems. Carbapenems such as imipenem/cilastatin, meropenem, doripenem, and ertapenem possess a broad spectrum of activity and are commonly used for treating infections caused by multi drug resistant (MDR) bacteria, especially ESBL-resistant pathogens.[21] The properties of carbapenems include small size, ability to form zwitter ion, and high affinity for penicillin-binding proteins. Penicillin-binding proteins (PBPs) also function as transpeptidase enzymes, needed for the synthesis of peptidoglycan. Acylated D-alanyl-D-alanine is the terminal amino acid residue of the peptidoglycan and arbapenems are structurally similar to it. Because of this similarity carbapenem binds to the active site of the PBPs, resulting in the inhibition of transpeptidation of the peptidoglycan layer and disrupting the cell wall synthesis. This leads to autolysis and cell death.[22]

Bacteria become resistant to carbapenems by various mechanisms such as (i) modification of porin expression or alterations in the porin-encoding gene, there bacteria blocking the entry of carbapenems into the cell, (ii) overproduction of efflux pump (overexpression of efflux pumps genes), (iii) production of carbapenemases. There are three classes of carbapenemases namely class A, B, and D. *blaKPC, blaIMI, blaGES, blaNDM,* and *blaOXA-48,* are the genes involved in carbapenem resistance. Carbapenem resistance in Enterobacteriaceae is mainly mediated by NDM-1 and OXA-48.[23]

3.9 Amphenicols

Chloramphenicol, florfenicol, and thiamphenicol are the members of this group. Thiamphenicol and florfenicol are synthetic derivatives of chloramphenicol.[23] Mechanism of action of chloramphenicol is by the inhibition of protein synthesis (binds to the 50S ribosomal subunit and inhibits the peptidyltransferase step). Bacteria acquire resistance against chloramphenicol either by enzymatic inactivation of the drug or nonenzymatically through drug efflux. Chloramphenicol resistance mechanism in Gram-negative bacteria is by plasmid-mediated production of chloramphenicol acetyltransferase.[24]

3.10 Sulfonamides, dihydrofolate reductase inhibitors, and combinations

Sulfonamides are mainly used in human and veterinary medicine. Sulfamethoxazole in combination with trimethoprim (cotrimoxazole) remains an antibiotic alternative in the treatment of several infectious diseases including urinary tract infections.[25] Sulfonamides compete with the structural analog *p*-aminobenzoic acid for binding to dihydropteroate synthase (DHPS), a catalytic enzyme in the folic acid biosynthesis pathway, thus inhibiting the formation of dihydrofolic acid. Sulphonamides inhibit the formation of dihydrofolic acid by competing with the structural analog *p*-aminobenzoic acid for binding to dihydropteroate synthase (DHPS), a catalytic enzyme in the folic acid biosynthesis pathway.[26] Sulfonamide

resistance can result from the acquisition of an alternative DHPS gene (*sul1*, *sul2*, or *sul3* genes), encoding forms of the target dihydropteroate synthase) or mutations in the chromosomal DHPS gene (*folP*).[25,27] The *sul1* gene is a part of the 3′-conserved segment (3′-CS) of class 1 integrons, which are the most frequently detected integrons in gram-negative bacteria.

Trimethoprim inhibits the enzyme dihydrofolate reductase (DHFR) and thereby blocking the synthesis of amino acids and nucleotides.[28] Bacteria acquire resistance by several mechanisms; (i) development of permeability barriers, (ii) efflux pumps, (iii) mutational and regulation changes in target enzymes, and (iv) acquirement of drug-resistant target enzymes.[29]

3.11 Tetracyclines

First-generation tetracyclines include tetracycline, chlortetracycline, and oxytetracycline; and the second-generation ones include minocycline and doxycycline, which are commonly used in the treatment of human and animal infections. Tetracycline inhibits protein synthesis by preventing the binding of aminoacyl-tRNA to the ribosomal acceptor site. Tetracyclines are listed as highly important antimicrobials by WHO, whereas glycylcyclines (third-generation tetracyclines) are listed as critically important antimicrobials with high priority.[8] Glycylcyclines (tigecycline) were developed to overcome problems of resistance to tetracycline.[30] Tetracycline efflux pumps (six groups based on amino acid sequence) are the leading tetracycline resistance mechanism. *tet*(*A*), *tet*(*B*), *tet*(*C*), *tet*(*D*), and *tet*(*E*) are the genes associated with an efflux mechanism.[31]

3.12 Nitrofurantoins

Nitrofurantoins are broad-spectrum antibiotics used for the treatment of urinary tract infections.[32] It belongs to the nitrofuran group, containing one or more nitro groups on a nitroaromatic or nitro heterocyclic background. Nitrofurantoins interfere with enzymes involved in the synthesis of DNA, RNA, and protein, which leads to cell death. Bacteria acquire nitrofurantoin resistance by mutations in *nfsA* or *nfsB*, both of which are encoding oxygen-insensitive nitroreductase.[33]

4. Major antibiotic-resistant bacterial species (WHO priority pathogens list)

World health organization has categorized antibiotic-resistant bacteria into three categories according to the urgency of the need for new research and development: critical, high, and medium priority.[34] The most critical group of multidrug-resistant bacteria that pose a particular threat includes *Acinetobacter*, *Pseudomonas*, and various members of the family Enterobacteriaceae (including *Klebsiella*, *E. coli*, *Enterobacter*, *Serratia*, *Proteus*, *Providencia*, and *Morganella*).[34] These bacteria have acquired resistance to different antibiotics, including last-resort antibiotics such as carbapenems and third-generation cephalosporins. The high-priority categories include *Enterococcus faecium*, *Staphylococcus aureus*, *Helicobacter pylori*, *Campylobacter*, *Salmonellae*, and *Neisseria gonorrhoeae*. *Streptococcus pneumoniae*, *Haemophilus influenzae*, and *Shigella* are included under the medium priority category.[34]

4.1 *Acinetobacter* spp.

Acinetobacter spp. is Gram-negative aerobes. *Acinetobacter baumannii* is the most clinically important pathogen associated with a high level of mortality. *A. baumannii* causes several diseases including blood stream infections, pneumonia, wound infections, urinary tract infections, and skin infections. *A. baumannii* has a longer survival rate in the nosocomial environment such as objects associated with patients and medical staff. The patient-to-patient cross-transmission of *A. baumannii* was also reported.[35] *A baumannii* is intrinsically resistant to many classes of antibiotics, and carbapenem is the drug commonly used to treat infections. At present, carbapenem-resistant *A. baumannii* is the leading cause of concern.[36] Hence carbapenem-resistant *A. baumannii* is included in the WHO priority pathogens list of antibiotic-resistant bacteria as a critical priority for research and development of new and effective antibiotic treatments.[34] Colistin is used for the treatment of carbapenem-resistant bacteria and colistin and carbapenem-resistant *A. baumannii* is a growing problem in clinical settings.[37]

4.2 Pseudomonas aeruginosa

Pseudomonas aeruginosa is Gram-negative aerobic bacilli belonging to the family Pseudomonadaceae. *P aeruginosa* is the leading cause of nosocomial infections, including pneumonia (hospital-acquired pneumonia, ventilator-associated pneumonia), urinary tract infections, wound infections, bacteremia, folliculitis, keratitis, endophthalmitis, otitis, enterocol-itis, and osteomyelitis or meningitis. It is mainly affecting immune-compromised patients, patients undergoing treatment for various diseases, or patients admitted to critical care units.[38]

Type III secretion system is the virulence mechanism effected by *P. aeruginosa*. This secretion system injects potent cytotoxins, including ExoS, ExoT, ExoU, or ExoY into host cells which may result in subsequent cell death and tissue necrosis. ExoU is a major virulence factor of clinical importance. ExoU-producing strains are known as hypervirulent and associated with more severe clinical symptoms.[39] A wide range of antibiotics including aminoglycosides, cephalosporins, fluoroquinolones, monobactams, phosphonic acids, carbapenem, and polymyxins are frequently used to treat *P. aeruginosa* infections. The misuse or overuse of these antibiotics has resulted in the development and dissemination of extremely drug-resistant *P. aeruginosa*. Carbapenem-resistant *P. aeruginosa* is listed in the WHO critical group of multidrug-resistant bacteria.[34]

4.3 Enterobacteriaceae

4.3.1 Escherichia coli

Escherichia coli are usually a commensal, but some strains are emerging as a pathogen. Some strains *Escherichia coli* cause intestinal and extra-intestinal infections in humans and animals. According to Nataro and Kaper, there are six classes of *Escherichia coli* such as enteropathogenic *E. coli* (EPEC), shiga toxin-producing *E. coli* (STEC) or verocytotoxin-producing *E. coli* (VTEC), enterotoxigenic *E. coli* (ETEC), enteroinvasive *E. coli* (EIEC), enteroaggregative *E. coli* (EAEC), and diffusely adhering *E. coli* (DAEC).[40] The extraintestinal pathogenic E. colii (EXPEC) are more prevalent strains associated with urinary tract infections (UPEC), neonatal

meningitis (MAEC), and bacteremia. Enterotoxigenic *E. coli* (ETEC) strains are the leading causes of diarrhea in children living in developing countries and the most common cause of traveler's diarrhea. Shiga toxin-producing *E. coli* (STEC), also called enterohemorrhagic *E. coli* (EHEC), causes hemorrhagic colitis (HC) or hemolytic uremic syndrome (HUS), which is the main cause of acute renal failure in children.[41] Extended-spectrum beta-Lactamase, carbapenem, and clostin-resistant *E. coli* are causing major problems worldwide.

4.3.2 *Klebsiella pneumonia*

Klebsiella pneumonia is a Gram-negative rod, that causes both communities acquired and hospital-acquired infections including pneumonia, urinary tract, intraabdominal infections, liver abscesses, and septicemia. Hospital-acquired pneumonias (HAPs) are more prevalent than community-acquired pneumonias (CAPs). Long-term acute-care hospitals are the breeding ground for hospital-acquired pneumonia.[42] *K. pneumonia* is present in soil and water, also can colonize the human intestinal tract, and then invades into internal organs such as the lungs and liver and causes severe infections. *K. pneumonia* can survive in medical equipment or implants and enters human tissues. *K. pneumonia* gets an entry into lungs and urinary tract through endotracheal intubation and catheter, respectively. The presence of type IV pilus encoded by an integrated conjugative element facilitates the adhering capacity and horizontal gene transfer of these strains. *K. pneumonia* mainly infects immune-compromised groups including the elderly and neonates, but the rapid emergence of hypervirulent and/or multidrug-resistant strains affects healthy individuals.[42] Carbapenem-resistant *Klebsiella pneumonia* (KPC) infections have high mortality rate up to 44%.[43,44]

4.3.3 Enterobacter *spp.*

Bacteria belonging to the Enterobacter genus are gram-negative bacilli. The major species are *Enterobacter cloacae*, *E. aerogenes*, and *E. agglomerans*. *E. cloacae* and *E. aerogenes* are opportunistic pathogens, frequently associated with multidrug-resistance. Infections due to *E. sakazakii* and *E. agglomerans* are much less common than those caused by *E. cloacae* and *E. aerogenes*. *Enterobacter* spp. cause lower respiratory infections (asymptomatic colonization of respiratory secretions, purulent bronchitis, lung abscess, pneumonia, and empyema), skin and soft tissues infections (cellulitis, fasciitis, abscesses, emphysema, myositis, and wound infections), bloodstream and surgical site infections in intensive care facilities, intraabdominal Infections and urinary tract infections.[45] The incubation period varied from 2 h to 20 days. Beta-lactam antibiotics are commonly used for the treatment of *Enterobacter* infections. The prevalence of ESBL and carbapenem-resistant *Enterobacter* in clinical settings would result in the failure of treatment.

4.3.4 Serratia *spp.*

Serratia spp. are Gram-negative bacillus belonging to Enterobacteriaceae family. *Serratia plymuthica*, *Serratia liquefaciens*, *Serratia rubidaea*, *Serratia odorifera*, and *Serratia fonticola* are the members of this genus. *Serescens marcescens* is considered as a major opportunistic bacterial pathogen in this group, which causes nosocomial infections in immunocompromised or critically cared patients, mostly in the neonatal intensive care unit. *Serratia marcescens* rarely causes endophthalmitis. It also causes related to the urinary tract and wound infections. *S. marcescens* also cause infections that occurred in cardiac patients.[46] Third-generation

caphalosoprins and carbapenem resistance is increasing among *Serescens marcescens*. ESBL and carbapenem resistance among these strains cause serious health concerns because *S. marcescens* is intrinsically resistant to colistin, which is the last-resort antibiotics to treat serious infections caused by carbapenem-resistant bacteria.

4.3.5 Proteus, providencia, *and* Morganella *spp.*

The genus *Proteus* contains four species: *P. mirabilis*, *P. vulgaris*, *P. penneri* and *P. myxofaciens. P. mirabilis is* more pathogenic than *P. vulgaris*. These bacteria cause urinary tract infections and chronic renal inflammation. The route of transmission may include nosocomial sources, such as medical devices, surfaces, and intravenous solutions. Third-generation cephalosporins are the most efficient antibiotics against *P. mirabilis*.[47] But due to the over usage of the drug, *P. mirabilis* accounted for 7.4% of the Enterobacteriales with identified ESBL resistance.[48]

Providencia is Gram-negative bacteria that cause nosocomial infections mainly urinary tract infections. There are five species such as *P. rettgeri*, *P. stuartii*, *P. alcalifaciens*, *P. heimbachae.*

P. rettgeri and *P. stuartii* are commonly found in water, soil, and animal reservoirs. *P. rustigianii*, *P. stuartii* and *P. rettgeri* can cause pneumonia, meningitis, endocarditis, wound, and bloodstream infections. Multi drug resistant *Providencia* bacteremia causes high mortality of patients. *Providencia stuartii* and *Proteus mirabilis* coinfection contribute to the increased incidence of urolithiasis and bacteremia.[49] *Proteus*, *providencia,* and *Morganella* spp. colonize in long-term indwelling catheters and cause urinary tract infections. ESBL and carbapenem-resistant *Providencia* species are increasingly reported worldwide.

The genus *Morganella* consists of a single species (*M. morganii*) with two subspecies, namely, *morganii* and *siboni*. *Morganella morganii*, is a commensal found in the intestinal tract of humans and animals associated with diarrheal disease, urinary infections, pyelonephritis, osteomyelitis, peritonitis, abscess, and meningitis. It produces virulence factors, such as urease, hemolysins, and lipopolysaccharide account for infection.[48] ESBL producing *Morganella morganii* is worrisome.

4.3.6 *Enterococcus faecium*

Enterococcus faecium (*E. faecium*) is a gram-positive, facultative anaerobic cocci, member of the gastrointestinal biota of humans and animals. It is considered as an opportunistic pathogen but emerged as an important nosocomial pathogen. *E. faecium* cause hospital-acquired infections, especially endocarditis and bacteremia. The virulence of *E. faecium* is mediated by aggregation substance (*agg* gene), cytolysin (*cyl* gene), collagen binding protein (*acm* gene), enterococcal surface protein (*espfm* gene), gelatinase (*gel* gene), and hyaluronidase (*hyl* gene). *esp* and *hyl* genes play a major role in the colonization (first step of infection) and the progress of nosocomial infections.[50]

Ampicillin, gentamicin, and streptomycin were the drugs of choice for the treatment of *E. faecium* infections. *E. faecium* acquired resistance to many classes of antibiotics and adapted to different hospital environments, leading to the emergence of vancomycin-resistant *E. faecium* (VRE) strains. Prolonged hospitalization and invasive procedures are the risk factors for vancomycin-resistant *E. faecium* (VRE) colonization and implant-related surgical site infections. Patient-to-patient transmission of VRE at healthcare facilities is also a concern. Recently, the prevalence of vancomycin-resistant *E. faecium* has increased worldwide, and WHO has listed vancomycin-resistant *E. faecium* as a serious pathogen.[34]

4.4 Staphylococcus aureus

Staphylococcus aureus is gram-positive cocci, a member of the normal microbiota of anterior nares. These bacteria also colonize in skin, perineum, and pharynx. More than 30% of adult populations are carriers of this bacterium. *S. aureus* can cause community-acquired and hospital-acquired infections including skin infections, pneumonia, surgery wounds, bacteremia, osteomyelitis, impetigo, toxic shock syndrome (TSS), cellulitis, and endocarditis.[51] Nosocomial infection caused by *S. aureus* is a major health challenge. *S. aureus* can survive on medical devices and surfaces. Health workers are the main carriers of this bacterium and antibiotic-resistant *S. aureus* is very common because it cause mainly health-care-associated infection. Penicillin was the initial antibiotic of choice for the treatment. *S. aureus* becomes resistant to penicillin by acquiring *mecA* or *mecC* genes that encodes a novel penicillin-binding protein. These strains are termed meticillin-resistant *S. aureus* (MRSA), the biggest cause of nosocomial infections worldwide. *S. aureus* possesses wide variety of virulence factors such as adhesins and exoproteins. Vancomycin and teicoplanin are last-resort antibiotics for the treatment of MRSA infections. Methicillin-resistant and vancomycin-intermediate or -resistant *Staphylococcus aureus* are included WHO priority pathogen list as a high priority for research.[34]

4.5 Helicobacter pylori

Helicobacter pylori is a Gram-negative bacterium belonging to Helicobacteraceae. *H. pylori* is a gastric pathogen, that causes chronic gastritis, gastric or duodenal ulcers, mucosa-associated lymphoid tissue (MALT) lymphoma, and gastric adenocarcinoma, and iron deficiency anemia. *H. pylori* infections occur as a direct result of human to human, through an oral-oral, gastro-oral, or fecal-oral route. Ninety percent of gastric cancer is due to *H. pylori* infection.[52] Virulence factors involved in pathogenesis are urease C (*ureC*- encodes a phosphoglucosamine mutase that promotes the growth of the bacterial cell wall), cytotoxin-associated A (*cagA*-responsible for inflammation in the gastric mucosa), and vacuolating cytotoxin (*vacA*) gene (damaging the gastric mucosa) and *BabA2* adhesin (membrane protein contributes to the binding activity to the gastric mucosa).

Clarithromycin is the first-line antibiotic used for the treatment of *H. pylori* infection. Clarithromycin is included in the standard triple therapy for 7−10 days for eradication of *H pylori*, which comprises clarithromycin, amoxicillin, and proton pump inhibitor (PPI). The emergence of clarithromycin-resistant strains leads to treatment failure. The prevalence of clarithromycin-resistant strains is increasing worldwide. The triple therapy is not recommended in countries where clarithromycin resistance is more than 15%.[53]

4.6 Campylobacter

Campylobacter spp. are gram negative, rod shaped, and there are 17 species and six subspecies of belonged to the family Campylobacteraceae. *Campylobacter jejuni* and *Campylobacter coli*, are the leading cause of bacterial foodborne gastroenteritis in humans. *C. jejuni* infections also produce bacteremia, septic arthritis, and other extraintestinal symptoms. *Campylobacter* infections are self-limited in humans, characterized as watery or bloody diarrhea, abdominal

cramping, and fever.[54] These species cause more serious symptoms in neonates, elderly and immunosuppressed patients, and need antibiotic treatment. *Campylobacter* infections occur via the consumption of undercooked poultry products, meat, and raw milk. *C. jejuni* is a commensal organism of the intestinal tract of cattle, wild birds, and poultry.

Fluoroquinolone or macrolide is the drug of choice for the treatment of *Campylobacter* gastroenteritis. Emergence of fluoroquinolones −resistant *Campylobacter* spp. is a major concern for public health. Fluoroquinolones are also used in food-producing animals, particularly in poultry, and lead to the development of resistant *Campylobacter* strains. Fluoroquinolone - resistant *Campylobacter* is included in the WHO priority pathogens list of antibiotic-resistant bacteria as a critical priority for research and development.[34]

4.7 *Salmonella* spp.

Salmonella is a Gram-negative, belonging to the family Enterobacteriaceae family, residing in the intestinal tract of various warm- and even cold-blooded animals and humans. *Salmonella* spp. is the major foodborne pathogen. Nontyphoidal *Salmonella* (NTS) strains to cause gastroenteritis. Enteric serotypes Typhi and Paratyphi (Typhoidal *Salmonella*) cause Typhoid (enteric fever) fever.[55] *Salmonella* infection is mainly due to the consumption of contaminated water and food especially seafood and eggs. The incubation period varies from 4 to 72 h after the ingestion of contaminated water or food. Most Nontyphoidal *Salmonella* is self-limiting, but sometimes it becomes life-threatening depending on the serotype and virulence of the strains. These strains cause invasive infections, such as bacteremia, osteomyelitis, and meningitis. Third generations of cephalosporins and fluoroquinolones were used for the treatment of Nontyphoidal *Salmonella* infections. Horizontal gene transfer events lead to genetic changes in *Salmonella*, resulting in the emergence of hypervirulent and antibiotic-resistant strains. More than 2500 *Salmonella* serotypes have been recognized based on a unique combination of somatic O, and flagellar H1 and H2 antigens. *Salmonella* serogroup/serotype B/Typhimurium, and D/Enteritidis cause gastroenteritis and septicemia in humans. Serotype D/Dublin causes gastroenteritis and septicemia in swine, cattle, and sheep. The emergence of ceftriaxone-resistant and fluoroquinolone-resistant Salmonella spp. is a concern. Who has included fluoroquinolone-resistant *Salmonell*a spp in the WHO priority pathogens list.[34]

4.8 Neisseria gonorrhoeae

Neisseria gonorrhoeae a Gram-negative diplococcus (gonococci) causes gonorrhea a sexually transmitted infection, mainly affects the mucosal tissues, including the urethra, cervix, rectum, pharynx, and conjunctiva. *Neisseria gonorrhoeae* invade mucosal surfaces and are able to survive in the presence of human serum. The initial sites for *N. gonorrhoeae* infection are the urethra and the uterine cervix in men and women, respectively. *N. gonorrhoeae* cause symptomatic or asymptomatic infection. This bacterium causes acute urethritis in men. Gonorrhoeae infections in women lead to permanent fallopian tube scarring and blockage resulting in infertility, ectopic pregnancy, and chronic pelvic pain. *N. gonorrhoeae* causes blindness in infants born to mothers who suffered from gonorrhea. *N. gonorrhoeae* cause symptomatic or asymptomatic infection. Sulfonamides and penicillin were the antibiotic agents commonly

used for the treatment of gonorrhea till the emergence of multi drug resistant *N. gonorrhoeae*.[56] At present, ceftriaxone, macrolide, and azithromycin, are commonly recommended in the treatment of gonorrhea, and subsequently, macrolides and cephalosporin-resistant *N. gonorrhoeae* are increasing. *N. gonorrhoeae* acquire resistance by different mechanisms, penicillin resistance is by mutation in genes encoding penicillin-binding protein one and outer membrane protein porin IB, and azithromycin resistance is by overexpression of the efflux pump MtrCDE.[57]

4.9 Streptococcus pneumonia

Streptococcus pneumoniae is the major pathogen that causes community-acquired pneumonia and the leading cause of morbidity and mortality in children younger than 5 years. The mortality rate of *Streptococcal pneumonia* infections ranged from 11% to 20%. *S. pneumonia* also causes bacterial meningitis and otitis media. More than 90 serotypes of *S. pneumoniae* have been recognized based on the chemical composition of the capsular polysaccharide. β-Lactam antibiotics are commonly used treatment for *S. pneumoniae* infections.[58] Emergence of penicillin-nonsusceptible *S. pneumoniae* is by a mutation in the genes coding penicillin-binding protein that catalyze bacterial cell wall production. *S. pneumonia* has increasing resistance to penicillin, macrolides, and fluoroquinolones, which are commonly used for treating community-acquired pneumonia. *S. pneumoniae* carry a variety of virulence factors such as capsular polysaccharide, surface proteins and enzymes, and the toxin pneumolysin. Capsular polysaccharide plays a major role in bacterial virulence including protection from host defense mechanisms, colonization, mucus secretion, restriction of autolysis, and reduced exposure to antibiotics. The emergence of drug-resistant serotypes of *S. pneumonia* creates a significant burden associated with disease management. Penicillin-non susceptible *S. pneumoniae* is included in the WHO priority pathogens list of antibiotic-resistant bacteria.[34]

4.10 Haemophilus influenzae

Haemophilus influenzae is a Gram-negative coccobacillus, facultatively anaerobic belonging to the Family, Pasteurellaceae. *H. influenzae* generally colonize the upper respiratory tract and causes infections such as respiratory infections, bronchitis, epiglottitis, otitis media, sinusitis, and meningitis. *H. influenzae* also cause genitourinary tract infections such as urinary tract infection, pyelonephritis, and prostatitis.[59] *H. influenzae* can be divided into encapsulated groups and nonencapsulated strains are known as nontypeable (NTHie), which cause conjunctivitis-otitis syndrome. There are six serotypes based on the capsule composition (a, b, c, d, e, and f). The capsule polysaccharide is a major virulence factor in pathogenesis and is mainly mediated by the production of capsule polysaccharides. Encapsulated *H. influenzae* serotype b (Hib) is the most virulent serotype causing severe infections including septicemia and meningitis, mainly in children.

Beta-lactams (ampicillin), is the first choice of drug for the treatment of *H. influenzae* infections. *H. influenzae* strains become resistant to ampicillin by two mechanisms (i) Beta-lactamase production (beta-lactamase-positive ampicillin-resistant isolates- BLPAR), (ii) without producing a beta-lactmase by key alterations in penicillin-binding protein 3 (beta-

lactmase-negative ampicillin resistance -BLNAR).[60] Ampicillin-resistant *H. influenzae* is included in the WHO priority pathogens list of antibiotic-resistant bacteria as a critical priority for research and development of new and effective antibiotic treatments.[34]

4.11 *Shigella* spp.

Shigella is Gram-negative bacilli, one of the causative agents of diarrhea. There are four serogroups of *Shigella* spp. on the basis of serological reactions, which are *Shigella dysenteriae* (A), *Shigella flexneri* (B), *Shigella boydii* (C), and *Shigella sonnei* (D). *Shigella* has the ability to invade colonic mucosa and degrade the epithelium. The bacteria enter our bodies through contaminated food or water. The virulence of *Shigella* depends on the plasmid, which is *ipa/mxi-spa* locus. *Shigella* produces *shiga* toxin and enterotoxins. The symptoms include fever, generalized toxicity, anorexia, nausea, crampy abdominal pain, and diarrhea. The incubation period varies from 12 h to 2 days. *Shigella* also causes extra-intestinal infections, including surgical complications, neurologic manifestations, ulvovaginitis, and urinary tract infections.[61] Quinolones and cephalosporins were commonly used to treat shigellosis. Quinolones and cephalosporin-resistant *Shigella* spp. are increasing worldwide. Currently, azithromycin is the choice antibiotic currently used for the treatment. WHO has included fluoroquinolone-resistant *Shigella* spp. in the WHO priority pathogens list. Children under the age of five are more prone to shigellosis.

5. Nano-particles for combating antibiotic resistance

Nanotechnology is a newly emerging field of science providing new insights into different applications in the field of medical science, including antibiotic resistance. Nanoparticles act in different ways against multidrug bacteria, including inhibition of biofilm formation, formation of reactive oxygen species, membrane penetration, inhibition of protein, and nucleic acid synthesis. Nanoparticles can be synthesized by chemical method and green methods. In the chemical method, various chemicals and solvents are used for the synthesis of nanoparticles, which might result in many adverse effects including cytotoxicity. To reduce the adverse effect of the chemical method, scientists have developed the green method, which utilizes different types of plant extracts and microorganisms for the synthesis of nanoparticles. AuNPs, AgNPs, ZnO NPs, CuONPs, Fe_3O_4 NPs, TiO_2 NPs, and MgO NPs can be used as antibacterial agents and as effective drug delivery agents for antibiotic-resistant bacteria.

5.1 Gold (Au) nanoparticles

Gold nanoparticles are widely used in biomedical applications due to their ease of synthesis and properties such as small size, highly stable, biocompatible, noncytotoxic, and interaction with the cell membrane. It can be attached to different antibiotics and used as a drug delivery system. Even though gold nanoparticles (GNPs) are generally regarded as biologically inert, interaction with antibiotics increases their antibacterial properties. The molecular mechanism of action of gold nanoparticles is either by inhibiting the subunit of the ribosome

from binding tRNA or inhibiting ATPase activities to decrease the ATP level, there by collapsing membrane potential, effective against multidrug-resistant Gram-negative bacteria.[62] Gold nanoparticles are effective non-invasive drug carriers for targeting drugs to their site of action. Gold nanoparticles mediated drug delivery increase the concentration of antibiotics at the site of bacterium–antibiotic interaction.

Ref. 63 demonstrated an observable anti-MRSA and VRSA effect of the 30 nm sized AuNPs with the main 100% minimum bactericidal concentration observed at a concentration of 4.5×10^9 (NP/mL). Ref. 64 studied the antimicrobial properties of ultrasmall gold and magnetite-gold nanoparticles (NPs) (stabilized with D, L-methionine, Fe3O4@Au@Met), against multidrug resistant *Acinetobacter baumannii*, *Salmonella enterica* and gram-positive *Staphylococcus aureus* (MSRA), three of 12 the worst bacterial family members included in the World Health Organization (WHO) list.[34] They have determined that the killing efficiency of Au@Met NPs (70 mg/L) probe was 84.4%–58.5% and 89.1%–75.7% against Gram-negative and Gram-positive bacteria, respectively. The presence of single-valent gold (Au^+ ions) on the surface side of gold species (Fe_3O_4@Au@Met NPs, Au@Met nanocrystals) triggers the strong antimicrobial efficiency of Met-capped gold species against drug-resistant bacteria. Gold particles coupled with konjac glucomannan and gelatine can be used for killing superbugs, inhibiting bacterial growth, and promoting wound healing. Gold nanoparticles can amplify the antibacterial activity of gentamicin sulfate.[65] Aminoglycoside antibiotics, ribostamycin, and amikacin forms rod-like self-assembling with negatively charged AuNPs.[66]

Gold nanoparticles (AuNPs) prepared by bacterial exopolysaccharide (EPS) conjugated with a variety of antibiotics exhibited excellent bactericidal activity and reduced MIC and minimum bactericidal concentration (MBC) against MDR Gram-positive and Gram-negative bacteria compared to free drugs.[67] Gold nanoparticles - Amoxicillin conjugates demonstrated enhanced broad-spectrum bactericidal activity against both Gram-positive and Gram-negative bacteria.[68] The antibacterial properties of gold nanoparticles vary depending on their size. Nanocubes-shaped gold particles (AuNCs) are effective bactericidal agents with a 100% inactivation rate. AuNCs were effective against *P. aeruginosa* followed by *E. coli* and *S. Aureus*.[69]

Carbapenems-loaded gold nanoparticles can be used as a delivery system for the therapy of multi-resistant pathogenic infections. Imipenem and meropenem have been conjugated with the surface of citrate-capped gold nanoparticles and the release of imipenem and meropenem from 35 nm gold nanoparticles reached 89% within the first 24 h and reached almost 94% after 72 h.[70] Vanillin-capped gold nanoparticles (VAuNPs) in combination with meropenem or trimethoprim provided 1.5–3-fold better antimicrobial properties against extremely drug-resistant (XDR) *Pseudomonas aeruginosa*.[71] VAuNPs and vanillin can be used as antibiotic adjuvants for inhibiting bacterial efflux pumps to potentiate antibiotics. Ref. 72 found that streptomycin-resistant *Bacillus* becomes highly susceptible to the same antibiotic when combined with gold nanoparticles, opening up windows for the treatment of antibiotic-resistant bacteria with the help of nano particles.

5.2 Silver (Ag) nanoparticles

Silver nanoparticles (Ag NPs) are promising nanoparticles to combat antibiotic-resistant bacteria. The antimicrobial properties of AgNPs can be increased by manipulating the physiochemical properties such as size, shape, surface, concentration, colloidal state, and

oxidation state. Silver nanoparticles having a size in the range of 1−10 nm showed a level of antimicrobial properties against gram-negative and positive bacteria. Silver nanoparticles have different sizes such as nanoplates, nanorods, spherical, and truncated triangular. Nanoplates has the highest antibacterial property than nanorods, and are spherical because surface area holds the largest surface area, which is high in nanoplates makes better interaction with the bacterial cell wall and finally kills the bacteria. The surface coating of AgNPs gives the surface charge, increases the binding tendency toward bacteria, and alters aggregation and dissolution potential. Surface coating plays a major role in designing the antimicrobial AgNPs. The mode of action of silver nanoparticles includes reaction with SH groups of proteins, inhibits respiratory chain enzymes, or interferes with bacterial membrane permeability, causing K^+ loss from the membrane.[73]

An eco-friendly method for synthesizing silver nanoparticles is highly recommended because of noncytotoxic nature of the AgNPS. Ref. 74 synthesized AgNPs from the fungal strain *Phenerochaete chrysosporium*, which was effective against activity against *Pseudomonas aeruginosa*, *Klebsiella pneumoniae*, *Staphylococcus aureus,* and *Staphylococcus epidermidis*. Ref. 75 synthesized silver nanoparticles by filamentous cyanobacteria *Pleclonema* boryanum. AgNps is also synthesized from bacteria such as *Escherichia coli*, *Klebsiella pneumonia*, *Enterobacter cloacae,* etc.[76] Ref. 77 synthesized silver nanoparticles from isolates of *Escherichia hermannii*, *Citrobacter sedlakii,* and *Pseudomonas putida* and it was effective against *K. pneumonia*, *S. epidermidis*, *S. aureus, E. coli,* and *P. aeruginosa*. AgNPs are also synthesized from plant extracts of *Ocimum sanctum*,[78] *Sesuvium portulacastrum*,[79] *Mentha piperita*,[80] etc.

Ref. 81 studied the efficiency of AgNPs in combination with four different antibiotics (amoxycillin, penicillin, gentamicin, and colistin) against several bacteria of veterinary origin. AgNPs are more effective against Gram-negative bacteria than Gram-positive bacteria with the rigid peptidoglycan cell wall. Ref. 82 demonstrated AgNPs in axonnite as a good alternative for other antimicrobials to treat wound infections caused by multidrug-resistant, virulent *Acinetobacter* spp. Silver NPs enhanced the antibacterial activity of cephalosporins (cefotaxime, ceftazidime), a carbapenem (meropenem), quinolones (ciprofloxacin), and aminoglycosides (gentamicin). Conjugated AgNPS and respective antibiotics were highly effective against multi-resistant, beta-lactamase, and carbapenemase-producing *Enterobacteriaceae*.[83] Since AgNPs do not pose a risk of bacterial resistance development, suitable for combinations with antibiotics that are insusceptible to bacterial resistance.

Trimethyl chitosan nitrate-capped silver nanoparticles (TMCN-AgNPs) with positive surface charge were effective against gram-positive, gram-negative, and *A. baumannii* MDR strains at very low concentrations.[84] Ref. 85 found that silver nanoparticles (AgNPs) synthetized on chitosans/montmorillonite nanocomposite films can act by controlling the size/shape of the AgNPs, and inhibited the growth of *Escherichia coli* and *Bacillus subtilis*. AgNPs stabilized by hydrolyzed casein peptides strongly inhibited the biofilm formation of *Escherichia coli*, *Pseudomonas aeruginosa,* and *Serratia proteamaculan*.[86] They also determined the role of porins on the function related to AgNPs and their antibacterial effects. Bacteria deficient in OmpF or OmpC porins (*E. coli* mutant strains) were 4−8 times more resistant to AgNPs as compared to the wild-type strain. Ref. 87 reported that AgNPs and capsaicin could be used for treating ESBL infections caused by *E. coli*. Synthesis of silver nanoparticles using ampicillin (Amp-AgNPs) was found to be effective against sensitive and drug-resistant bacteria.[88] They also checked the biocompatibility of these Amp-AgNPs against cell lines by

using keratinocytes cell lines, which were found to be nontoxic. The use of modified silver nanoparticles with different kinds of antibiotics can be beneficial in combating the emerging threat of antibiotic resistance among bacteria.

5.3 Zinc oxide (ZnO) nanoparticles

Zinc oxide nanoparticles are inexpensive to produce, safe, and can be prepared easily. It has different properties like varied morphology, large surface area to volume ratio, potent antibacterial activity, optic properties, UV filtering properties, antiinflammatory, wound healing, and biocompatibility.[89] ZnO NPs are available in different shapes such as nanoflake, nanoflower, a nanobelt, nanorod, and nanowire. Green synthesis is widely used for the production of ZnO NPs. It is synthesized from bacteria such as *Rhodococcus pyridinivorans*, *B. licheniformis*, *Aeromonas hydrophila*, *Serratia ureilytica* and *Lactobacillus sporogens.* ZnO NPs are also synthesized from different plant species *Azadirachta indica*, *Agathosma betulina*, *Rosa canina*, *E. crassipes*, *Cocus nucifera*, *S. album*, *Nephelium lappaceum* L., *etc*. It can be also synthesized using microalgae and macroalgae.

The antibacterial activity is mainly due to the release of bacteriostatic zinc ions (Zn^{2+}) from the nanoparticle surfaces ZnNPs inhibit glycolysis, transmembrane proton translocation, and acid tolerance in bacteria. The antibacterial activity of ZnO NPs increases with increasing particle concentration, surface area, and decreasing particle size. ZnO nanoparticle can be used for biomaterial applications (endotracheal tube, implanted biomaterials, and catheter applications), which is prone to excessive bacterial growth.[90] Ciprofloxacin-conjugated ZnO nanoparticles (ZN-CIP) exhibited excellent antibacterial activity against clinically isolated multidrug-resistant bacterial strains of *Escherichia coli, Staphylococcus aureus,* and *Klebsiella*.[91] Ref. 92 synthesized ZnO NPs using *C. japonica* plant leaf, which was effective against ESBLs-positive *E. coli* and *P. mirabilis* strains. ZnO NPs have great promise as an antimicrobial agent against ESBLs producing strains. ZnONPs synthesized from fruit extract of *Rosa canina* were effective against bacteria such as *L. monocytogenes*, *E.coli*, and *S.thyphimurium*.[93]

ZnO nanorods encapsulated in chitosan could be synthesized through coprecipitation technique. Ref. 94 studied the attachment of chitosan-capped zinc oxide nanoparticles (ZnO NP) with *Escherichia coli* bacterial outermost cell membrane and their mode of action against these bacteria. Chitosan-capped ZnO nanorods showed higher antibacterial activity compared to that of uncapped ZnO nanomaterial as well as chitosan against *E. coli*. ZnO-NPs potentiate the antimicrobial action of ciprofloxacin and ceftazidime with antibiotics increasing the uptake of these antibiotics.[95] Conjugated ZnO-NPs with ciprofloxacin and ceftazidime were effective against *Acinetobacter baumannii*. Chemically synthesized ZnO-NPs can be developed as an alternative to carbapenem (beta-lactam), which inhibit the growth of carbapenem-resistant *A. baumannii* by producing ROS and causing membrane damage. ZnO-NPs can be used as an alternative drug to carbapenem against this carbapenem-resistant strain of *A. baumannii*.[96] ZnO nanoparticles are also effective against major foodborne pathogens like *Escherichia coli* O157:H7, *Salmonella*, *Listeria monocytogenes*, *Campylobacter jejuni,* and *Staphylococcus aureus*.[97,98] Bacteria-mediated ZnO NPs are proved to be a good novel antimicrobial material.[99] Zinc oxide nanoparticles (ZnO NPs) synthesized from an eco-friendly method using *Aeromonas hydrophila* as a reducing and capping agent was effective against *Pseudomonas aeruginosa* and *Aspergillus flavus*.

5.4 Copper oxide (CuO) nanoparticles

Copper Oxide nanoparticles are robust and have a longer shelf life and show a wide range of physical properties such as high critical temperature, superconductivity, electron correlation effects, and spin dynamics. Cu/Cu_2O NPs can be prepared using physical, biological, and chemical methods. At high concentrations, free Cu^{++} ions exert their antibacterial activity by membrane disruption and reactive oxygen species production, which inhibit both DNA replication and amino acid synthesis in microbes. CuONPs showed excellent antimicrobial activity against *B. subtilis*, *Escherichia coli*, *Pseudomonas aeruginosa*, *Klebsiella pneumonia*, *Enterococcus faecalis*, *Shigella flexneri*, *Salmonella typhimurium*, *Proteus vulgaris*, and *Staphylococcus aureus*.[100–102]

Green synthesis of copper nanoparticles has been carried out using plant extracts such as *Phyllanthus amarus*, *Eucalyptus globules*, *Tecoma castanifolia*, and *Pronus domestic*.[103–106] CuO NPs synthesized from *Phyllanthus amarus* were effective against various multidrug resistance bacteria viz. both Gram-positive (*B. subtilis* and *S. aureus*) and Gram-negative (*E.coli* and *P. aeruginosa*).[103] Terpenoids encapsulated ELE-CuONPs was effective against extended-spectrum beta-lactamases (ESBL) producing *Escherichia coli*, *Pseudomonas aeruginosa*, and methicillin-resistant *Staphylococcus aureus*-1 clinical isolates compared to the bare surface commercial nano-CuO and bulk sized CuO.[104] CuO NPs synthesized from *Tecoma castanifolia* showed significant inhibition on gram-negative bacteria (*E. coli*) and gram-positive bacteria (*S. aureus*).[105] Biosynthetic method of nanoparticles Cu using cyanide- O-3-glucoside as a reducing agent is quick and easy, which had strong antibacterial properties against *Pseudomonas aeruginosa*, *Staphylococcus saprophyticus*, and *Staphylococcus epidermidis*.[106]

High-purity metallic chitosan-copper nanoparticles have been prepared via a chemical method, which was effective against methicillin-resistant *Staphylococcus aureus*, *Bacillus subtilis*, *Pseudomonas aeruginosa*, *Salmonella choleraesuis*, and *Candida albicans*.[107] Ref. 108 synthesized nanoscaled CuO (pure Cu and Cu_2O nanoparticles) by thermal plasma technology, which was effective against meticillin-resistant *Staphylococcus aureus* (MRSA) and *Escherichia coli*. They also compared the efficiency of CuO and nano-Ag against Gram-negative strain and found a greater susceptibility to nano CuO combined with nano-Ag. Ref. 109 synthesized Fe-doped CuO nanoparticles using sol-gel method, which was against pathogenic bacteria *Staphylococcus aureus* and *Staphylococcus epidermidis*. Ref. 110 have developed a simple and low-cost synthesis of CuO and Cu NPs from copper sulfate with chitosan biological macromolecule (CH) as a capped material and corresponding nanocomposite films (CHCuO–CH and CHCu–CH) were developed via the solution casting method. Their study, revealed that the CHCuO NPs and CHCuO–CH film showed a higher inhibition zone against bacteria than the other nanomaterials.

5.5 Iron oxide (Fe_3O_4)

Iron oxide nanoparticles are biocompatible, which makes them an attractive candidate for implementation in biomedicine. Iron oxide nanoparticles have unique properties, such as superparamagnetic behavior, external control, and hypothermal behavior when they are stimulated and under controllable parameters. They can be utilized in the tissue-specific release of therapeutic agents as an effective drug delivery system. The antibacterial activity

of Fe_3O_4 NPs is by the generation of oxygen species (ROS) generation. The free radicals cause depolymerization of polysaccharides, DNA damage, lipid peroxidation, and/or inactivation of enzymes, leading to the inhibition of bacteria.[111]

Ref. 112 synthesized via a novel matrix-mediated method using polyvinylvalcohol (PVA), which showed antibacterial activity against *Staphylococcus aureus*. Ref. 113 synthesized superparamagnetic iron oxide nanoparticles (SPIONs) and used them to kill *Staphylococci* in their biofilm mode of growth. From their study, it is evident that magnetic targeting of SPIONs constitutes a promising alternative for the treatment of costly and recalcitrant biomaterial-associated infections by antibiotic-resistant strains. Ref. 114 synthesized erythromycin-coupled FeNPs and found that the antibacterial effect was improved when the drug was coupled to FeNPs, effective against bacterial cultures of *S. pneumoniae*. Ref. 115 developed doxorubicin (DOX), an anthracycline-loaded iron oxide nanoparticle designed for controlling multidrug-resistant bacteria. DOX-conjugated nanoparticles persisted in drug-resistant cells, indicating that they were not subject to drug efflux. This could provide effective therapy for patients afflicted with deadly drug-resistant cancers. Poly (acrylic acid) (PAA)- coated iron oxide (magnetite) nanoparticles (PAA-MNPs) as efflux inhibitors and used together with rifampicin, found to be effective against *Mycobacterium smegmatis* (close homolog of *M. Tuberculosis*).[116] In presence of PAA-MNP, the efflux inhibition of a rifampicin increases by 3-fold, leading to a similar increase in drug accumulation as compared to that without PAA-MNPs.

5.6 Titanium dioxide (TiO_2)

The antibacterial activity of TiO_2 has been found to be due to a reaction of the TiO_2 surface with water and the formation of ROS on exposure to ultraviolet (UV) irradiation, TiO_2 releases free radicals such as OH, O_{2-}, and HO_{2-}. TiO_2-NPs synthesized through the chemical method have several demerits including toxic chemicals; hence the green method is widely used. Ref. 117 synthesized nano-size titanium dioxide of 20 nm with citric acid and alpha dextrose as double surfactants and the antimicrobial resistance of MRSA against various antibiotics is increased without nano-TiO_2 and decreases with nano-TiO_2. Silver-doped titanium oxide (Ag/TiO_2) spherical nanoparticles showed antibacterial activity against *E. coli*, *C. albicans*, MRSA, and *P. aeruginosa*.[118] Korosi et al.[119] synthesized PF-co-doped anatase TiO_2 nanoparticles(NPs), which showed antibacterial activity against carbapenem-resistant *Klebsiella pneumonia.* The hydrothermal treatment increased the photocatalytic and antibacterial activity of the nanoparticle while PF-co-doping promoted the formation of $OH^{\cdot}$ radicals. Ref. 120 found that PE film incorporated with TiO_2 nanoparticles was more effective in antibacterial activity for *Staphylococcus aureus* and have a good potential to be used as food packaging. Titanium dioxide-polytetrafluorethylene (TiO_2-PTFE) nanocomposite coatings had antibacterial and anticorrosion properties on stainless steel surfaces, which can be used for the development of biomedical metallic implants.[121]

5.7 Magnesium oxide (MgO) nanoparticles

MgO nanoparticles (MgO) can inhibit Gram-positive, Gram-negative bacteria. MgO nanoparticles interact with bacterial cells and cause cell membrane leakage, induce oxidative stress, mainly due to the production of reactive oxygen species (ROS), which leads to cell

death. Biosynthesized MgO NPs at a low concentration are less toxic nanoparticles to human cells. Ref. 122 reported the antimicrobial potency of MgO NPs against a wide spectrum of pathogenic microorganisms such as *Escherichia coli*, *Pseudomonas aeruginos*, *Staphylococcus epidermidis*, *Staphylococcus aureus*, and methicillin-resistant *Staphylococcus aureus* (MRSA). The MgO NPs were more effective against Gram-negative bacteria than Gram-positive bacteria, depending on the cell wall composition. MgO NPs can be used for the production of infection-free medical devices and implants. MgO NPs from endophytic *Streptomyces coelicolor* was found effective against multidrug-resistant pathogens agent including *Shigella flexneri*, *Staphylococcus aureus*, *Streptococcus pneumonia*, and *Klebsiella pneumonia*.[123] MgO NPs are effective and safe antibiofilm agents that inhibit adhesion, biofilm formation, and removal of established biofilms of multidrug-resistant bacteria such as *Escherichia coli*, *Klebsiella pneumonia, and Staphylococcus aureus*.[124] The MgO NPs modified with conventional glass-ionomer cement showed effective antibacterial and antibiofilm activity against *Streptococcus mutans* and *Streptococcus sobrinus*, cariogenic microorganisms, and could be considered for further development as biocompatible antibacterial dental restorative cement.[125]

6. Conclusion

Antibiotic resistance bacteria are a growing threat in the current medical scenario. Whenever a new antibiotic is introduced for the treatment of infections, bacteria acquire resistance by several novel mechanisms, disseminate via horizontal gene transfer into various environments, and create a burden for the control of such bacteria. Nanoparticles are the most promising tools to curb antibiotic-resistant bacteria, which do not allow bacteria to acquire resi stance. AgNPs are considered the most effective nanomaterial against bacteria but other metallic NPs, such as AgNPs, ZnO NPs, CuONPs, Fe_3O_4 NPs, TiO_2 NPs, and MgO NPs, are also effective against multidrug-resistant bacteria. Future studies should be carried out to better understand the mode of action, metabolism, toxic effects, and route of administration of nano particles.

References

1. World Health Organization, Antibiotic Resistance, 2018 [Accessed 01 March 20], https://www.who.int/news-room/fact-sheets/detail/antibiotic-resistance.
2. H.A. Hemeg, Nanomaterials for alternative antibacterial therapy, Int J Nanomed 12 (2017) 8211.
3. A. Gupta, R.F. Landis, V.M. Rotello, Nanoparticle-based antimicrobials: surface functionality is critical, F1000Research 5 (2016).
4. D. Gupta, A. Singh, A.U. Khan, Nanoparticles as efflux pump and biofilm inhibitor to rejuvenate bactericidal effect of conventional antibiotics, Nanoscale Res Lett 12 (1) (2017) 1–6.
5. M.J. Hajipour, K.M. Fromm, A.A. Ashkarran, D.J. de Aberasturi, I.R. de Larramendi, T. Rojo, et al., Antibacterial properties of nanoparticles, Trends Biotechnol 30 (10) (2012) 499–511.
6. World Health Organization, WHO'S first global report on antibiotic resistance reveals serious, worldwide threat to public health, 2014 [Accessed 02 March 20], https://www.who.int/southeastasia/news/detail/30-04-2014-who-s-first-global-report-on-antibiotic-resistance-reveals-serious-worldwide-threat-to-public-health.
7. D.A. Baltrus, Exploring the costs of horizontal gene transfer, Trends Ecol Evol 28 (8) (2013) 489–495.
8. World Health Organization, Critically important antimicrobials for human medicine 5th revision, 2017. Assessed 07:01:20, http://who.int/foodsafety/publications/antimicrobials-fifth/en/.

9. D.J. Tipper, Mode of action of β-lactam antibiotics, Pharmacol therapeut 27 (1) (1985) 1–35.
10. R. Canton, T.M. Coque, The CTX-M β-lactamase pandemic, Curr Opin Microbiol 9 (5) (2006) 466–475.
11. E. Binda, F. Marinelli, G.L. Marcone, Old and new glycopeptide antibiotics: action and resistance, Antibiotics 3 (4) (2014) 572–594.
12. M.S. Butler, K.A. Hansford, M.A. Blaskovich, R. Halai, M.A. Cooper, Glycopeptide antibiotics: back to the future, J Antibiot 67 (9) (2014) 631–644.
13. G.G. Zhanel, M. Dueck, D.J. Hoban, L.M. Vercaigne, J.M. Embil, A.S. Gin, et al., Review of macrolides and ketolides, Drugs 61 (4) (2001) 443–498.
14. Y.D. Bakthavatchalam, A.K. Pragasam, I. Biswas, B. Veeraraghavan, Polymyxin susceptibility testing, interpretative breakpoints and resistance mechanisms: an update, J Glob Antimicrob Resist 12 (2018) 124–136.
15. D.C. Hooper, Mechanisms of action and resistance of older and newer fluoroquinolones, Clin Infect Dis 31 (Supplment_2) (2000) S24–S28.
16. L. Poirel, V. Cattoir, P. Nordmann, Plasmid-mediated quinolone resistance; interactions between human, animal, and environmental ecologies, Front Microbiol 3 (2012) 24.
17. M.L. Avent, B.A. Rogers, A.C. Cheng, D.L. Paterson, Current use of aminoglycosides: indications, pharmacokinetics and monitoring for toxicity, Intern Med J 41 (6) (2011) 441–449.
18. S. Garneau-Tsodikova, K.J. Labby, Mechanisms of resistance to aminoglycoside antibiotics: overview and perspectives, Med Chem Comm 7 (1) (2016) 11–27.
19. A. Tupin, M. Gualtieri, F. Roquet-Baneres, Z. Morichaud, K. Brodolin, J.P. Leonetti, Resistance to rifampicin: at the crossroads between ecological, genomic and medical concerns, Int J Antimicrob Agents 35 (6) (2010) 519–523.
20. P.A. Aristoff, G.A. Garcia, P.D. Kirchhoff, H.H. Showalter, Rifamycins–obstacles and opportunities, Tuberculosis 90 (2) (2010) 94–118.
21. K.M. Papp-Wallace, A. Endimiani, M.A. Taracila, R.A. Bonomo, Carbapenems: past, present, and future, Antimicrob Agents Chemother 55 (11) (2011) 4943–4960.
22. J.N. Kattan, M.V. Villegas, J.P. Quinn, New developments in carbapenems, Clin Microbiol Infect 14 (12) (2008) 1102–1111.
23. a L. Dortet, L. Poirel, F. Al Yaqoubi, P. Nordmann, NDM-1, OXA-48 and OXA-181 carbapenemase-producing *Enterobacteriaceae* in sultanate of Oman, Clin Microbiol Infect 18 (5) (2012) E144–E148;
b T. Nagabhushan, G.H. Miller, K.J. Varma, T. Nagabhushan, G.H. Miller, K.J. Varma, Antibiotics: chloramphenicol and analogues, Van Nostrand's Encyclopedia of Chemistry Hoboken, 2005.
24. S. Schwarz, C. Kehrenberg, B. Doublet, A. Cloeckaert, Molecular basis of bacterial resistance to chloramphenicol and florfenicol, FEMS (Fed Eur Microbiol Soc) Microbiol Rev 28 (2004) 519–542.
25. O. Skold, Sulfonamide resistance: mechanisms and trends, Drug Resist Updates 3 (2000) 155–160.
26. P. Masters, T.A. O'Bryan, J. Zurlo, D.Q. Miller, N.P.G. Joshi, Trimethoprim-sulfamethoxazole revisited, Arch Intern Med 163 (2003) 402.
27. V. Perreten, P.A. Boerlin, New sulfonamide resistance gene (*sul*3) in *Escherichia coli* is widespread in the pig population of Switzerland, Antimicrob Agents Chemother 47 (2003) 1169–1172.
28. P. Huovinen, L. Sundstrom, G. Swedberg, O. Skold, Trimethoprim and sulphonamide resistance, Antimicrob Agents Chemother 39 (1995) 279–289.
29. O. Skold, Resistance to trimethoprim and sulfonamides, Vet Res 32 (3–4) (2001) 261–273.
30. G.G. Zhanel, K. Homenuik, K. Nichol, A. Noreddin, L. Vercaigne, J. Embil, et al., The glycylcyclines, Drugs 64 (1) (2004) 63–88.
31. M.C. Roberts, Tetracycline resistance determinants: mechanisms of action, regulation of expression, genetic mobility, and distribution, FEMS Microbiol Rev 19 (1) (1996) 1–24.
32. C.C. McOsker, P.M. Fitzpatrick, Nitrofurantoin: mechanism of action and implications for resistance development in common uropathogens, J Antimicrob Chemother 33 (Suppl. l_A) (1994) 23–30.
33. C.G. Giske, Contemporary resistance trends and mechanisms for the old antibiotics colistin, temocillin, fosfomycin, mecillinam and nitrofurantoin, Clin Microbiol Infect 21 (10) (2015) 899–905.
34. World Health Organization, WHO publishes list of bacteria for which new antibiotics are urgently needed, 2017 [Accessed 04 March 20], https://www.who.int/news-room/detail/27-02-2017-who-publishes-list-of-bacteria-for-which-new-antibiotics-are-urgently-needed.

35. A.D. Harris, J.K. Johnson, L. Pineles, L.M. O'Hara, R.A. Bonomo, K.A. Thom, Patient-to-patient transmission of *Acinetobacter baumannii* gastrointestinal colonization in the intensive care unit, Antimicrob Agents Chemother 63 (8) (2019) e00392-19.
36. B.A. Evans, A. Hamouda, S.G. Amyes, The rise of carbapenem-resistant *Acinetobacter baumannii*, Curr Pharmaceut Des 19 (2) (2013) 223–238.
37. Y. Snyman, A.C. Whitelaw, S. Reuter, A. Dramowski, M.R.B. Maloba, M. Newton-Foot, Clonal expansion of colistin-resistant *Acinetobacter baumannii* isolates in Cape Town, South Africa, Int J Infect Dis 91 (2020) 94–100.
38. S.L. Gellatly, R.E. Hancock, *Pseudomonas aeruginosa*: new insights into pathogenesis and host defenses, Pathog Dis 67 (2013) 159–173.
39. A.R. Hauser, The type III secretion system of *Pseudomonas aeruginosa*: infection by injection, Nat Rev Microbiol 7 (2009) 654–665.
40. J.P. Nataro, J.B. Kaper, Diarrheagenic *Escherichia coli*, Clin Microbiol Rev 11 (1) (1998) 142–201.
41. L. Beutin, G. Krause, S. Zimmermann, S. Kaulfuss, K. Gleier, Characterization of Shiga toxin-producing *Escherichia coli* strains isolated from human patients in Germany over a 3-year period, J Clin Microbiol 42 (3) (2004) 1099–1108.
42. M.K. Paczosa, J. Mecsas, *Klebsiella pneumoniae*: going on the offense with a strong defense, Microbiol Mol Biol Rev 80 (3) (2016) 629–661.
43. G. Patel, S. Huprikar, S.H. Factor, S.G. Jenkins, D.P. Calfee, Outcomes of carbapenem-resistant *Klebsiella pneumoniae* infection and the impact of antimicrobial and adjunctive therapies, Infect Control Hosp Epidemiol 29 (12) (2008) 1099–1106.
44. M.J. Schwaber, S. Klarfeld-Lidji, S. Navon-Venezia, D. Schwartz, A. Leavitt, Y. Carmeli, Predictors of carbapenem-resistant *Klebsiella pneumoniae* acquisition among hospitalized adults and effect of acquisition on mortality, Antimicrob Agents Chemother 52 (3) (2008) 1028–1033.
45. W.E. Sanders, C.C. Sanders, *Enterobacter* spp.: pathogens poised to flourish at the turn of the century, Clin Microbiol Rev 10 (2) (1997) 220–241.
46. F. Grimont, P.A. Grimont, Serratia. Bergey's Manual of Systematics of Archaea and Bacteria, 2015, pp. 1–22.
47. J. Manos, R. Belas, The genera *Proteus, Providencia*, and *Morganella*, Prokaryotes 6 (2006) 245–269.
48. P.D. Tamma, S.L. Sharara, Z.D. Pana, J. Amoah, S.L. Fisher, T. Tekle, et al., Molecular epidemiology of ceftriaxone-nonsusceptible *Enterobacterales* isolates in an academic medical center in the United States, Open Forum Infect Dis 6 (2019) 353.
49. C.E. Armbruster, S.N. Smith, A. Yep, H.L. Mobley, Increased incidence of urolithiasis and bacteremia during *Proteus mirabilis* and *Providencia stuartii* co-infection due to synergistic induction of urease activity, J Infect Dis 209 (10) (2014) 1524–1532.
50. D. Morrison, N. Woodford, B. Cookson, *Enterococci* as emerging pathogens of humans, J Appl Microbiol 83 (S1) (1997) 89S–99S.
51. S. Krishna, L.S. Miller, Host–pathogen interactions between the skin and Staphylococcus aureus, Curr Opin Microbiol 15 (1) (2012) 28–35.
52. J.C. Atherton, The pathogenesis of *Helicobacter pylori*-induced gastroduodenal diseases, Annu Rev Pathol 1 (2006) 63–96.
53. J. Alarcon-Millan, G. Fernandez-Tilapa, E.M. Cortes-Malagon, C.A. Castanon-Sanchez, J. De Sampedro-Reyes, I. Cruz-del Carmen, et al., Clarithromycin resistance and prevalence of *Helicobacter pylori* virulent genotypes in patients from Southern México with chronic gastritis, Infect Genet Evol 44 (2016) 190–198.
54. N.O. Kaakoush, N. Castano-Rodriguez, H. Mitchell, S.M. Man, Global epidemiology of *Campylobacter* infection, Clin Microbiol Rev 28 (2015) 687–720.
55. J.M. Besser, *Salmonella* epidemiology: a whirlwind of change, Food Microbiol 71 (2018) 55–59.
56. J.W. Tapsall, Antibiotic resistance in *Neisseria gonorrhoeae*, Clin Infect Dis 41 (Suppl. 4) (2005) S263–S268.
57. J.R. Dillon, P. Duck, D.Y. Thomas, Molecular and phenotypic characterization of penicillinase-producing *Neisseria gonorrhoeae* from Canadian sources, Antimicrob Agents Chemother 19 (1981) 952–957.
58. M.R. Jacobs, *Streptococcus pneumoniae*: epidemiology and patterns of resistance, Am J Med 117 (Suppl. 3A) (2004) 3S–15S.
59. B. Stegmayr, A.S. Malmborg, Urinary tract infection caused by *Haemophilus influenzae*. A case report, Scand J Urol Nephrol 22 (1) (1988) 75–77.

60. S. Wen, D. Feng, D. Chen, L. Yang, Z. Xu, Molecular epidemiology and evolution of *Haemophilus influenzae*, Infect Genet Evol (2020) 104205.
61. C. Parsot, P.J. Sansonetti, Invasion and the pathogenesis of *Shigella* infections, in: Bacterial Invasiveness, Springer, Berlin, 1996, pp. 25–42.
62. Y. Cui, Y. Zhao, Y. Tian, W. Zhang, X. Lu, X. Jiang, The molecular mechanism of action of bactericidal gold nanoparticles on *Escherichia coli*, Biomaterials 33 (2012) 2327–2333.
63. S. Omara, MIC and MBC of honey and gold nanoparticles against methicillin-resistant (MRSA) and vancomycin-resistant (VRSA) coagulase-positive *S. aureus* isolated from contagious bovine clinical mastitis, J Genet Eng Biotechnol 15 (1) (2017) 219–230.
64. R. Zalneravicius, A. Mikalauskaite, G. Niaura, A. Paskevicius, A. Jagminas, Ultra-small methionine-capped Au^0/Au^+ nanoparticles as efficient drug against the antibiotic-resistant bacteria, Mater Sci Eng C 102 (2019) 646–652.
65. Y. Zou, R. Xie, E. Hu, P. Qian, B. Lu, G. Lan, et al., Protein-reduced gold nanoparticles mixed with gentamicin sulfate and loaded into konjac/gelatin sponge heal wounds and kill drug-resistant bacteria, Int J Biol Macromol 148 (2020) 921–931.
66. T. Zheng, Y. Li Sip, M. Leong, Q. Huo, Linear self-assembly formation between gold nanoparticles and aminoglycoside antibiotics, Colloids Surf B Biointerfaces 164 (2018) 185–191.
67. Pradeepa, S. Vidya, S. Mutalik, K. Udaya Bhat, P. Huilgol, K. Avadhani, Preparation of gold nanoparticles by novel bacterial exopolysaccharide for antibiotic delivery, Life Sci 153 (2016) 171–179.
68. S. Kalita, R. Kandimalla, K. Sharma, A. Kataki, M. Deka, J. Kotoky, Amoxicillin functionalized gold nanoparticles reverts MRSA resistance, Mater Sci Eng C 61 (2016) 720–727.
69. S. Hameed, Y. Wang, L. Zhao, L. Xie, Y. Ying, Shape-dependent significant physical mutilation and antibacterial mechanisms of gold nanoparticles against foodborne bacterial pathogens (*Escherichia coli, Pseudomonas aeruginosa* and *Staphylococcus aureus*) at lower concentrations, Mater Sci Eng C 108 (2020) 110338.
70. M. Shaker, M. Shaaban, Formulation of carbapenems loaded gold nanoparticles to combat multi-antibiotic bacterial resistance: in vitro antibacterial study, Int J Pharm 525 (1) (2017) 71–84.
71. S. Arya, M. Sharma, R. Das, J. Rookes, D. Cahill, S. Lenka, Vanillin mediated green synthesis and application of gold nanoparticles for reversal of antimicrobial resistance in *Pseudomonas aeruginosa* clinical isolates, Heliyon 5 (7) (2019) e02021.
72. R. Nishanthi, S. Malathi, J.S. Paul, P. Palani, Green synthesis and characterization of bioinspired silver, gold and platinum nanoparticles and evaluation of their synergistic antibacterial activity after combining with different classes of antibiotics, Mater Sci Eng C 96 (2019) 693–707.
73. C.-N. Lok, C.-M. Ho, R. Chen, Q.-Y. He, W.-Y. Yu, H. Sun, et al., Silver nanoparticles: partial oxidation and antibacterial activities, J Biol Inorg Chem 12 (2007) 527–534.
74. M. Saravanan, S. Arokiyaraj, T. Lakshmi, A. Pugazhendhi, Synthesis of silver nanoparticles from *Phenerochaete chrysosporium* (MTCC-787) and their antibacterial activity against human pathogenic bacteria, Microb Pathog 117 (2018) 68–72.
75. M. Lengke, M. Fleet, G. Southam, Biosynthesis of silver nanoparticles by filamentous cyanobacteria from a silver(I) nitrate complex, Langmuir 23 (5) (2007) 2694–2699.
76. A. Shahverdi, S. Minaeian, H. Shahverdi, H. Jamalifar, A. Nohi, Rapid synthesis of silver nanoparticles using culture supernatants of *Enterobacteria*: a novel biological approach, Process Biochem 42 (5) (2007) 919–923.
77. A. Saeb, A. Alshammari, H. Al-Brahim, K. Al-Rubeaan, Production of silver nanoparticles with strong and stable antimicrobial activity against highly pathogenic and multidrug resistant bacteria, Sci World J (2014) 9, 704708.
78. N. Ahmad, S. Sharma, M.K. Alam, V.N. Singh, S.F. Shamsi, B.R. Mehta, et al., Rapid synthesis of silver nanoparticles using dried medicinal plant of basil, Coll Surf B Biointerf 81 (1) (2010) 81–86.
79. A. Nabikhan, K. Kandasamy, A. Raj, N. Alikunhi, Synthesis of antimicrobial silver nanoparticles by callus and leaf extracts from saltmarsh plant, Sesuvium portulacastrum L, Coll Surf B Biointerf 79 (2) (2010) 488–493.
80. D. MubarakAli, N. Thajuddin, K. Jeganathan, M. Gunasekaran, Plant extract mediated synthesis of silver and gold nanoparticles and its antibacterial activity against clinically isolated pathogens, Coll Surf B Biointerf 85 (2) (2011) 360–365.
81. M. Mekalova, V. Aragon, A. Panacek, R. Prucek, R. Zboril, L. Kvitek, Enhanced antibacterial effect of antibiotics in combination with silver nanoparticles against animal pathogens, Vet J 209 (2016) 174–179.

82. M. Lysakowska, A. Ciebiada-Adamiec, L. Klimek, M. Sienkiewicz, The activity of silver nanoparticles (Axonnite) on clinical and environmental strains of *Acinetobacter spp*, Burns 41 (2) (2015) 364–371.
83. A. Panacek, M. Smekalova, R. Vecerova, K. Bogdanova, M. Roderova, M. Kolar, et al., Silver nanoparticles strongly enhance and restore bactericidal activity of inactive antibiotics against multiresistant Enterobacteriaceae, Coll Surf B Biointerf 142 (2016) 392–399.
84. T. Chang, C. Chen, K. Cheng, C. Chin, Y. Chen, X. Chen, et al., Trimethyl chitosan-capped silver nanoparticles with positive surface charge: their catalytic activity and antibacterial spectrum including multidrug-resistant strains of *Acinetobacter baumannii*, Coll Surf B Biointerf 155 (2017) 61–70.
85. J. Gabriel, V. Gonzaga, A. Poli, C. Schmitt, Photochemical synthesis of silver nanoparticles on chitosans/montmorillonite nanocomposite films and antibacterial activity, Carbohydr Polym 171 (2017) 202–210.
86. M. Radzig, V. Nadtochenko, O. Koksharova, J. Kiwi, V. Lipasova, I. Khmel, Antibacterial effects of silver nanoparticles on gram-negative bacteria: influence on the growth and biofilms formation, mechanisms of action, Colloids Surf B Biointerfaces 102 (2013) 300–306.
87. D. Kar, S. Bandyopadhyay, U. Dimri, D. Mondal, P. Nanda, A. Das, et al., Antibacterial effect of silver nanoparticles and capsaicin against MDR-ESBL producing *Escherichia coli*: an in vitro study, Asian Pacific J Trop Dis 6 (10) (2016) 807–810.
88. N. Khatoon, H. Alam, A. Khan, K. Raza, M. Sardar, Ampicillin silver nanoformulations against multidrug resistant bacteria, Sci Rep 9 (1) (2019).
89. L. Zhang, Y. Jiang, Y. Ding, M. Povey, D. York, Investigation into the antibacterial behaviour of suspensions of ZnO nanoparticles (ZnO nanofluids), J Nanoparticle Res 9 (3) (2007) 479–489.
90. J. Seil, T. Webster, Reduced *Staphylococcus aureus* proliferation and biofilm formation on zinc oxide nanoparticle PVC composite surfaces, Acta Biomater 7 (6) (2011) 2579–2584.
91. P. Patra, S. Mitra, N. Debnath, P. Pramanik, A. Goswami, Ciprofloxacin conjugated zinc oxide nanoparticle: a camouflage towards multidrug resistant bacteria, Bull Mater Sci 37 (2) (2014) 199–206.
92. M. Maruthupandy, G. Rajivgandhi, T. Muneeswaran, J. Song, N. Manoharan, Biologically synthesized zinc oxide nanoparticles as nanoantibiotics against ESBLs producing gram negative bacteria, Microb Pathog 121 (2018) 224–231.
93. S. Jafarirad, M. Mehrabi, B. Divband, M. Kosari-Nasab, Biofabrication of zinc oxide nanoparticles using fruit extract of *Rosa canina* and their toxic potential against bacteria: a mechanistic approach, Mater Sci Eng C 59 (2016) 296–302.
94. P. Bhadra, M. Mitra, G. Das, R. Dey, S. Mukherjee, Interaction of chitosan capped ZnO nanorods with *Escherichia coli*, Mater Sci Eng C 31 (5) (2011) 929–937.
95. F. Ghasemi, R. Jalal, Antimicrobial action of zinc oxide nanoparticles in combination with ciprofloxacin and ceftazidime against multidrug-resistant *Acinetobacter baumannii*, J Global Antimicrob Resist 6 (2016) 118–122.
96. V. Tiwari, N. Mishra, K. Gadani, P. Solanki, N. Shah, M. Tiwari, Mechanism of anti-bacterial activity of zinc oxide nanoparticle against carbapenem-resistant *Acinetobacter baumannii*, Front Microbiol 9 (2018) 1218.
97. N. Jones, B. Ray, K. Ranjit, A. Manna, Antibacterial activity of ZnO nanoparticle suspensions on a broad spectrum of microorganisms, FEMS (Fed Eur Microbiol Soc) Microbiol Lett 279 (1) (2008) 71–76.
98. Y. Liu, L. He, A. Mustapha, H. Li, Z. Hu, M. Lin, Antibacterial activities of zinc oxide nanoparticles against *Escherichia coli* O157:H7, J Appl Microbiol 107 (4) (2009) 1193–1201.
99. C. Jayaseelan, A. Rahuman, A. Kirthi, S. Marimuthu, T. Santhoshkumar, A. Bagavan, et al., Novel microbial route to synthesize ZnO nanoparticles using *Aeromonas hydrophila* and their activity against pathogenic bacteria and fungi, Spectrochim Acta Part A Mol & Biomol Spectr 90 (2012) 78–84.
100. M. Ahamed, H. Alhadlaq, M. Khan, P. Karuppiah, N. Al-Dhabi, Synthesis, characterization, and antimicrobial activity of copper oxide nanoparticles, J Nanomater (2014).
101. A. Azam, A. Ahmed, M. Oves, M. Khan, A. Memic, Size-dependent antimicrobial properties of CuO nanoparticles against Gram-positive and -negative bacterial strains, Int J Nanomed 7 (2012) 3527–3535.
102. M. Taran, M. Rad, M. Alavi, Antibacterial activity of copper oxide (CuO) nanoparticles, Pharmaceut Sci 23 (3) (2017) 198–206.
103. N.P.S. Acharyulu, R.S. Dubey, V. Swaminadham, P. Kollu, R.L. Kalyani, S.V.N. Pammi, Green Synthesis of CuO nanoparticles using *Phyllanthus amarus* leaf extract and their antibacterial activity against multidrug resistance bacteria, Int J Eng Res Technol 3 (4) (2014).

104. K. Ali, B. Ahmed, S. Ansari, Q. Saquib, A. Al-Khedhairy, S. Dwivedi, et al., Comparative in situ ROS mediated killing of bacteria with bulk analogue, *Eucalyptus* leaf extract (ELE)-capped and bare surface copper oxide nanoparticles, Mater Sci Eng C 100 (2019) 747–758.
105. G. Sharmila, M. Thirumarimurugan, V. Sivakumar, Optical, catalytic and antibacterial properties of phytofabricated CuO nanoparticles using *Tecoma castanifolia* leaf extract, Optik 127 (19) (2016) 7822–7828.
106. A. Tovar-Corona, M. Lobo-Sanchez, J. Herrera-Perez, R. Zanella, J. Rodriguez-Mora, O. Vazquez-Cuchillo, Green synthesis of copper (0) nanoparticles with cyanidine-O-3-glucoside and its strong antimicrobial activity, Mater Lett 211 (2018) 266–269.
107. M. Usman, M. El Zowalaty, K. Shameli, N. Zainuddin, M. Salama, N. Ibrahim, Synthesis, characterization, and antimicrobial properties of copper nanoparticles, Int J Nanomed 8 (2013) 4467–4479.
108. G. Ren, D. Hu, E. Cheng, M. Vargas-Reus, P. Reip, R. Allaker, Characterisation of copper oxide nanoparticles for antimicrobial applications, Int J Antimicrob Agents 33 (6) (2009) 587–590.
109. A. Pugazhendhi, S.S. Kumar, M. Manikandan, M. Saravanan, Photocatalytic properties and antimicrobial efficacy of Fe doped CuO nanoparticles against the pathogenic bacteria and fungi, Microb Pathog 122 (2018) 84–89.
110. T. Jayaramudu, K. Varaprasad, R. Pyarasani, K. Reddy, K. Kumar, A. Akbari-Fakhrabadi, et al., Chitosan capped copper oxide/copper nanoparticles encapsulated microbial resistant nanocomposite films, Int J Biol Macromol 128 (2019) 499–508.
111. A. Fujishima, T.N. Rao, D.A. Tryk, Titanium dioxide photocatalysis, J Photochem Photobiol C: Photochem Rev 1 (1) (2000) 1–21.
112. N. Tran, A. Mir, D. Mallik, A. Sinha, S. Nayar, T. Webster, Bactericidal effect of iron oxide nanoparticles on *Staphylococcus aureus*, Int J Nanomed 5 (2010) 277.
113. G. Subbiahdoss, S. Sharifi, D. Grijpma, S. Laurent, H. Van Der Mei, M. Mahmoudi, et al., Magnetic targeting of surface-modified superparamagnetic iron oxide nanoparticles yields antibacterial efficacy against biofilms of gentamicin-resistant *staphylococci*, Acta Biomater 8 (6) (2012) 2047–2055.
114. M. Aparicio-Caamano, M. Carrillo-Morales, J.J. Olivares-Trejo, Iron oxide nanoparticle improves the antibacterial activity of erythromycin, J Bacteriol Parasitol 7 (267) (2016) 2.
115. F. Kievit, F. Wang, C. Fang, H. Mok, K. Wang, J. Silber, et al., Doxorubicin loaded iron oxide nanoparticles overcome multidrug resistance in cancer in vitro, J Contr Release 152 (1) (2011) 76–83.
116. P. Padwal, R. Bandyopadhyaya, S. Mehra, Polyacrylic acid-coated iron oxide nanoparticles for targeting drug resistance in mycobacteria, Langmuir 30 (50) (2014) 15266–15276.
117. S.A. Roy, A. Parveen, A.R. Koppalkar, M. Prasad, Effect of nano - titanium dioxide with different antibiotics against methicillin-resistant Staphylococcus aureus, J Biomater Nanobiotechnol 01 (01) (2010) 37–41.
118. T.N. Rao, R.P. Babji, N. Ahmad, R.A. Khan, I. Hassan, et al., Green synthesis and structural classification of *Acacia nilotica* mediated-silver doped titanium oxide (Ag/TiO_2) spherical nanoparticles: assessment of its antimicrobial and anticancer activity, Saudi J Biol Sci 26 (7) (2019) 1385–1391.
119. L. Korosi, B. Bognar, M. Horvath, G. Schneider, J. Kovacs, A. Scarpellini, et al., Hydrothermal evolution of PF-co-doped TiO_2 nanoparticles and their antibacterial activity against carbapenem-resistant *Klebsiella pneumoniae*, Appl Catal B Environ 231 (2018) 115–122.
120. Y. Xing, X. Li, L. Zhang, Q. Xu, Z. Che, W. Li, et al., Effect of TiO_2 nanoparticles on the antibacterial and physical properties of polyethylene-based film, Prog Org Coating 73 (2–3) (2012) 219–224.
121. S. Zhang, X. Liang, G.M. Gadd, Q. Zhao, Advanced titanium dioxide-polytetrafluorethylene (TiO_2-PTFE) nanocomposite coatings on stainless steel surfaces with antibacterial and anti-corrosion properties, Appl Surf Sci 490 (2019) 231–241.
122. N. Nguyen, N. Grelling, C. Wetteland, R. Rosario, H. Liu, Antimicrobial activities and mechanisms of magnesium oxide nanoparticles (nMgO) against Pathogenic bacteria, yeasts, and biofilms, Sci Rep 8 (1) (2018) 16260.
123. S.H. El-Moslamy, Bioprocessing strategies for cost-effective large-scale biogenic synthesis of nano-MgO from endophytic *Streptomyces coelicolor* strain E72 as an anti-multidrug-resistant pathogens agent, Sci Rep 8 (1) (2018) 3820.
124. S. Hayat, S. Muzammil, M. Rasool, Z. Nisar, S. Hussain, A. Sabri, et al., In vitro antibiofilm and anti-adhesion effects of magnesium oxide nanoparticles against antibiotic resistant bacteria, Microbiol Immunol 62 (4) (2018) 211–220.
125. A. Noori, F. Kareem, The effect of magnesium oxide nanoparticles on the antibacterial and antibiofilm properties of glass-ionomer cement, Heliyon 5 (10) (2019) e02568.

CHAPTER

22

Nanomaterials in bioimaging and cell labeling

K. Sapna[1], *P.P. Manzur Ali*[2] *and A.A. Mohamed Hatha*[1]

[1]**Department of Marine Biology, Microbiology and Biochemistry, School of Marine Sciences, Cochin University of Science and Technology, Kochi, Kerala, India;** [2]**MES Mampad College, Malappuram, Kerala, India**

1. Introduction

The word bioimaging or biological imaging is denoted as a noninvasive precision technique for the documentation and recording of information relevant to biological materials using a variety of imaging equipment and processing. Cellular labeling and bioimaging are visualization methods by which recognition and monitoring of information from a biological system is made possible with minimum interference with life processes so that the examined specimen is readily visible from the outside even without physical intervention.[1] Nanomaterials have turned out to be one of the most striking research frontiers in the biomedical grounds with the rapid advancement of combinatorial techniques of bioimaging and nanotechnology.[2,3,4]

2. Challenges of bioimaging and emergence of nanobioimaging

Dramatic improvement of the image processing technology is clearly evident from 1960s to the present. But it was potentially employed for biological applications by researchers in later years of 1980s and in the early 1990s.[5] The advancement of various biological imaging techniques such as X-ray, thermal imaging, X-ray Computed Tomography (CT), hyper spectral imaging, optical, and magnetic resonance imaging (MRI) that are different in principles and equipment, enabled observation of the subcellular structures, cellular process or the ion or metabolite levels as well.[6] Recent advances in bioimaging comprise super-resolution, two-photon Fluorescence Excitation Microscopy (FEM), Fluorescence Resonance Energy Transfer (FRET), and Fluorescence Recovery/Redistribution After Photobleaching

Applications of Multifunctional Nanomaterials
https://doi.org/10.1016/B978-0-12-820557-0.00012-6

(FRAP). However, the limitation in image resolution is a hurdle that is to be evaded for the next generation of bioimaging technology. Emergence of the super-resolution microscopy could achieve betterment of image resolution and resolve the impediments up to a certain extent.[7,8] Nevertheless the complexity of the system and special equipment prerequisite has become barriers for further development in this direction.[9] Despite the great success of Structured Illumination Microscopy (SIM) in resolution enhancement, an expensive hardware and expensive software are essential to surmount the spatial resolution improvement in 2D or 3D.[10] Regardless of many advantages of single bioimaging modality, more basic limitations concerned with the imaging targets, spatial resolution, tissue penetration ability, speed, field of view, biocompatibility, experimental complexity and, imaging sensitivity become vital when reliable and accurate diagnosis are to be achieved. As a result, multimodal imaging technology combining two or more imaging modalities has emerged to provide more reliable and efficient information by combining their potencies.[9,11,12]

It is expected that nanotechnology is able to resolve these problems when combined with various bioimaging techniques, such as MRI, CT, Ultrasound and Optical Imaging (OI). Contrast improvement of image is accomplished by enhancing the specificity of targeted imaging using the unique designed nanoconstructs as contrast agents to improve the imaging effects, thus providing useful information for clinical diagnosis in turn, advance the medical imaging to the next level.[13–16]

3. Scope of nanotechnology in biological imaging

Cell transplantation is an emerging strategy in regenerative medicine in which the self-renewal and differentiation ability of stem cells and progenitor cells are made use of to correct or replace defective cell populations.[17] With proper control, this technology can revolutionize the treatments of myocardial regeneration as well as CNS-related diseases such as spinal cord injury, Parkinson's disease, myelin disorders, and Huntington's disease.[18,19] The immune cell based therapy has promising advancements in the diagnosis, early detection and treatment of cancer malignancy, in which the antitumor power of immune cells, such as T cells, natural killer (NK) cells, B cells, and dendritic cells has been exploited and enhanced in order to ruin the cancerous cells in a highly selective manner.[20]

The main challenge in this highly accepted therapeutic approach was to differentiate between the implanted cells from the host tissue cells and to monitor their survival, migration, differentiation, and regenerative impact in living subjects. Efficient monitoring is crucial for the success of all cell based therapies.[21] Nanoparticles have become the materials of choice in this regard due to their inherent magnetic, optical, or acoustic properties. In addition to this, the prolonged cellular retention time of the nanomaterials offer a large observation casement and therefore makes it possible for longitudinal cell tracking in vivo. Recent progresses in nanotechnology open up an efficient platform for theranostic medicine.[4,22,23,24] Real-time monitoring, minimal or noninvasiveness, and accessibility without tissue destruction are the significant features of nanoparticle (NP)-based theranostics. Moreover, NPs can be effectively used to carry out experiments over an extensive range of time and size scales involved in the imaging procedure.[4,16,23] NPs are categorized as magnetic/metallic NPs [MRI[25,26] in vivo tracking of stem cells,[27]] reporter dyes/fluorophores in the nanoscale

[immunoassays,[28] in vivo fluorescent imaging,[21,29] in vivo stem cell tracking],[27] radiolabeled NPs [Single-Photon Emission Computer Tomography (SPECT), positron emission tomography (PET), Cerenkov luminescence],[30] according to the imaging technique used.

Nanoparticle-based methods are emerging as a powerful technique in cell transplantation therapies for tracking cells in living subjects to monitor the migration and proliferation of implanted cells. This is achieved by loading and then detecting NPs, using corresponding imaging modalities such as MRI, radionuclide imaging [PET and SPECT], and optical imaging at a high spatial and temporal resolution. In this approach, the implanted cells are detached from host cells, which is advantageous over traditional histological methods. Cells loaded with engineered NPs serve as imaging contrast agents, enabling cell tracking. By making use of these attributes, tracking the cell implants in a non-invasive and real-time manner over a long observation period is possible. The NPs can be either directly introduced (non-targeted) or indirectly introduced.[31] This kind of specific targeting using NPs is an effective strategy to lessen the side effects of clinical procedures or drugs.[32] Bioimaging involving Fluorescence, Luminescence, Surface-Enhanced Raman Scattering (SERS), and photoacoustic (PA) signals (Tables 22.1 and 22.2).[4]

TABLE 22.1 Persistent luminescence NPs for bio-imaging and therapy.[4]

Hosts	Dopants	Comments and applications in bio-imaging
Gd_2O_2S	Eu^{3+},Mg^{2+},Ti^{4+}	Fully biocompatible NPs and in vivo imaging
$Ca_3(PO_4)_2$/hydroxyapatite	Mn^{2+},Tb^{3+},Dy^{3+}	Bioimaging applications
$Ca_2Si_5N_8$	Eu^{2+},Tm^{3+}	NPs, functionalization, bioimaging applications, green
$SrAl_2O_4$	Eu^{2+},Dy^{3+}	Emission
$^{Ca}0.2^{Zn}0.9^{Mg}0.9^{Si}2^{O}6$	Mn^{2+},Eu^{2+},Dy^{3+}	NPs, functionalization, pioneer work for bioimaging bioimaging imaging:cancer
		Cancer cells imaging, cell targeting
$^{Ca}1.86^{Mg}0.14^{ZnSi}2^{O}7$	Eu^{2+},Dy^{3+}	FRET and various bio-sensing applications
$CaMgSi_2O_6$	Mn^{2+},Eu^{2+},Pr^{3+}	NPs, functionalization, bio-imaging
$MAlO_3$(M = La,Gd)	Mn^{4+}/Ge^{4+}	Bio-imaging in pork tissue
$GdAlO_3$	Mn^{4+},Ge^{4+}Au Sm^{3+},Cr^{3+}	Trimodality imaging Optical and magnetic dual mode imaging
$ZnGa_2O_4$	Cr^{3+}	NPs, functionalization, bio-imaging(cancer cells imaging),
		Cell targeting, cytotoxicity, visible light NIR
		Photostimulation
		X-rays activation
		Oral administration
		Breast cancer imaging
		Toxicology analysis
		Proto biotic analysis

(*Continued*)

TABLE 22.1 Persistent luminescence NPs for bio-imaging and therapy.[4]—cont'd

Hosts	Dopants	Comments and applications in bio-imaging
$ZnGa_2O_4$ in hollow cavity	Cr^{3+}	Photo dynamic therapies
$ZnGa_2O_4$	Cr^{3+},Gd^{3+}	NPs,functionalization, bimodality optical/ NMRimagingng
$ZnGa_2O_4/SiO_2$	Cr^{3+}	Core-shell structure, drug delivery
$ZnGa_2O_4/Fe_2O_3$	Cr^{3+}	Cell labeling and magnetic vectorization
ZGOCS@m-SiO2@Gd2O3	Cr^{3+}	Multimodal nanoprobes
$Zn_{1.1}Ga_{1.8}Ge_{0.1}O_4/SiO_2$	Cr^{3+},Eu^{3+}	NPs, core-shell structure, drug delivery
$Zn_3Ga_2Ge_2O_{10}$	Cr^{3+}	Imaging of pork tissue, pphotostimulation, cytotoxicity
$Zn_{1.1}Ga_{1.8}$Ge0.1O4@SiO2	Cr^{3+}	Bio-imaging and drug delivery
$^{Zn}1.25^{Ga}1.5^{Ge}$0.25 degrees4	Cr^{3+},Yb^{3+},Er^{3+}	Metastasis tracking, cheo-photodynamic therapy
$^{Zn}1.1^{Ga}1.8^{Ge}$0.1 degree4	Cr^{3+}	Nanothermometry
$Zn_3Ga_2Sn_1O_{10}$	Cr^{3+}	Imaging of goldfish
$^{Zn}2.94^{Ga}1.96^{Ge}2^{O}10$	Cr^{3+},Pr^{3+}	NPs,functionalization
$Zn_3Ga_2Ge_2O_{10}$	Cr^{3+}	Recognition of breast cancer cells
$Zn_3Ga_2GeO_8$	Cr^{3+},Yb^{3+},Er^{3+}	Upconversion
$LiGa_5O_8$	Cr^{3+}/PEG-OCH_3	NPs, functionalization, bio-imaging, visible light stimulation, imaging, Visible light stimulation, Photostimulation
$Ca_3Ga_2Ge_3O_{12}$	Cr^{3+},Yb^{3+},$Tm^{3+}Pr^{3+}$,Yb^{3+}	NIR stimulation, upconversion, in vivo imaging
m-SiO2@Gd3Ga5O12	Cr^{3+},Nd^{3+}	Multimodal imaging and cancer therapy
Sr_2SnO_4	Nd^{3+}	Finger image
$SiO_2/CaMgSi_2O_6$	Eu^{2+},Pr^{3+},Mn^{2+}	Bio-imaging, intraperitoneal injection Photostimulation imaging of pork tissue
$Y_3Al_2Ga_3O_{12}$	Er^{3+},Cr^{3+}	Imaging in the second biological window
$NaYF_4$+$SrAl_2O_4$	Yb^{3+},Tm^{3+}, Eu^{2+},Dy^{3+}	Upconversion and photodynamic therapy
$Sr_2MgSi_2O_7$	Eu^{2+3+},Dy^{3+}	Photodynamic activation Visualization of abdominal inflammation
La3Ga5GeO14@SiO2@Van (Vancomycin)	Cr^{3+},Zn^{2+}	Bio-imaging-guided in vivo and drug delivery
$CaTiO_3$	Pr^{3+},Yb^{3+},Tm^{3+}	Upconverting and guided photo thermal therapy
$ZnSn_2O_4$	Cr^{3+},Eu^{3+}	Cellular and deep tissue imaging
$Sr_3Sn_2O_7$	Nd^{3+}	Second window imaging

TABLE 22.2 Examples of PA contrast agents explored in PA imaging.[4]

Materials		Types of nanoagents	Advantages(+)/Disadvantages (−)
Inorganic	Metallic nanomaterials	Au nanorods; Au nanostars; Au nanocages; Au nanoshell; Au nanovesicles; Au nanoflowers; Ag nanoplates; Palladium nanoplates; Antimony nanoparticles	(+) tunable physiochemical properties; Chemically inert element with reasonable biocompatibility; able to carry cargoes. (−) Non-biodegradability; Suboptimal photothermal stability
	Carbon-based nanomaterials	Carbon nanotubes; Graphenes; Carbon dots	(+) able to carry cargoes; good photothermal stability. (−) nonbiodegradability; heterogeneity
	Transition metal chalcogenides (TMC)-based nanomaterials	CuS; WS_2; MoS_2; FeS; Bi_2S_3; CuSe; Co_9Se_8;Bi_2Se_3	(+)high photothermal conversion efficiency; Good photothermal stability; low cost(−) nonbiodegradability; Contain heavy metal elements
Organic	Dyes	Porphyrin-and Cyanine-based dyes e.g.,Indocyanine green(ICG),IR780, IR825,etc	(+) good biocompatibility/biodegradability (−)poor aqueous solubility Low photothermal stability, Short blood stream circulation half-life
	Polymer-based nanomaterials	Polypyrrole; polyaniline; polydopamine; semiconducting polymers	(+) good biocompatibility and photothermal stability; able to carry cargoes. (−)Their biodegradation behaviors remain unknown

4. Labeling cells with NPs

4.1 Direct labeling

Direct labeling is the approach of loading cells with probes prior to engraftment into the host. This method is comparatively easy and affordable. The NPs can be taken up by cells before implantation which act like dyes to help in monitoring the fate of cells. Detection of probes is possible by relevant imaging modalities. Fluorescent NPs are promising candidates for in vitro and in vivo imaging procedures such as photodynamic therapy and fluorescence resonance energy-based detection.[33] The tracking and monitoring cell-tissue interactions using fluorescent NPs are possible by magnetic resonance technique.

4.2 Indirect labeling

Indirect labeling involves reporter gene (RG)-based cellular tracking and imaging. This is accomplished by either generating traceable activities or producing accumulations of traceable products like fluorescent or bioluminescent proteins or enzymes by means of a transcriptional control component which functions as a biomolecular genetic sensor which can recognize and respond to endogenous transcription factors and transcription regulators

that regulate RG expression. In RG-based cellular labeling and imaging, RG is coupled with a complimentary reporter probe by transfection or transduction which permits for firm, stable and secured tracking of cells.[34] This method allows sustained cellular trafficking but requires sophisticated genetic manipulations.

5. Nanomaterials used for cell labeling/bioimaging applications

When we consider nanomaterials for biological labeling or imaging applications, understanding their electrical, optical, biological, and magnetic properties is essential. Nanoparticles can be broadly categorized in to organic and inorganic. All biopolymers and organic nanomaterials form the nanoplatforms for nanobioimaging and cellular tracking. Nonmetallic NPs are advantageous due to their biocompatibility, functionality at targeted site and ability to bind covalently with the contrasting agents. Superparamagnetic iron oxide nanoparticles (SPIONs) and quantum dots (QDs) are metallic NPs which can be functionalized as imaging materials. Hence, these NPs are effectively altered into nanotheranostics by incorporating therapeutic drugs onto and/or into the nanoplatform. The theranostics applications of nanomaterials were greatly improved by modifying their morphology, surface chemistry and optical properties.[35,36] In view of this, nanomaterials, such as semiconductor nanocrystals,[37] metal complexes,[38–40] surface modified silica,[41,42] and organic dyes[43,44] have been used as probes for diagnosis of cancer. These materials have also been used as imaging probes for visualization of cancer cells, offering an accurate cancer diagnosis via real-time, noninvasive, and high-resolution images, which allows to capture specific information that relates to the tumor metabolism and structure.[45]

This chapter highlights the innovative developments in the field of biological imaging using various nano-based materials such as NPs, quantum dots, nanorods and nanotubes. The primary focus is on the recent contributions of NPs as the carrier for the fabrication of multimodal imaging nanoprobes, as well as corresponding applications in diagnosis and therapy. For easier elucidation, the article is arranged according to the types of the NPs used in bioimaging techniques, performed for various applications.

5.1 Carbon based nanomaterials

Carbon-based nanomaterials (CBN) Consist of carbon dots (CDs), fullerenes, carbon nanotubes (CNTs), graphene (G), graphene oxide (GO) and nanodiamonds (NDDs).[46,47] Surface modification of these different forms of carbon-based NPs provides the opportunity to enhance their properties for employing in various labeling and imaging applications. Their unique optical, electronic, mechanical, and chemical properties increase their potential for imaging and diagnosis of cells or tissues.[48–51]

5.1.1 Carbon nanodots (CNDs)

Carbon dots are clusters of carbon atoms comprising traces of nitrogen and considerable fractions of oxygen and hydrogen with a size of 2–8 nm. Carbon dots were first identified accidently in 2004 from the arc discharge synthesis of carbon nanotubes[52] and shares similar physical and chemical properties with graphene oxide. Hydrophilic CNDs are found to be

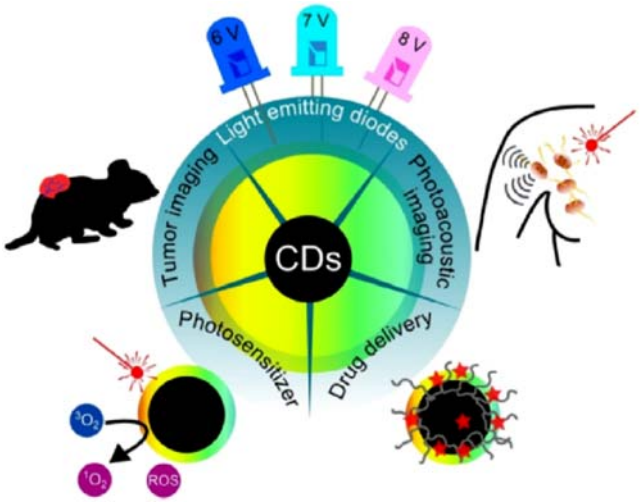

FIGURE 22.1 Application of carbon dots in nanomedicine.[55] *Copyright 2014, Elsevier.*

used extensively in imaging[53] compared to hydrophobic CNDs.[54] Carbon dots exhibits exceptional features for fluorescence labeling and imaging; they are less toxic, easy clearance from the body, low cost, and immune system evasion fairly good biocompatibility and permeability, weak interactions with proteins, resistance to swelling and photobleaching. The unique photoluminiscent and chemical properties among the nanomaterials, CNDs are one of the promising candidate for bioimaging applications (Fig. 22.1).

Molecular signatures of the cells has been exploited for the ell specific imaging using functionalized CNDs. Folate receptor over expression is associated in many caner progression including malignancies of the brain, throat, breast, kidney, lung, ovary, and prostate.[56] Covalently linked folic acid to amine capped carbon dots could differentiate folate receptor over expressing cancer cells from healthy cells. The folic acid composite with CNDs via H bonding quench fluorescence via fast electron transfer and fluorescence recovery is observed upon binding to cervical cancer (HeLa) cells.[57] Similarly, overexpression of transferrin receptor on cancer cell membrane is targeted using Transferrin, an 80-kDa serum glycoprotein. Carbon dots with transferrin is labeled via PEG1500N, 4-arm PEG, and PEIPEG-PEI polymers through R=N=C=NR for tumor cell imaging.[58]

The potential of CNDs for the development noninvasive imaging applications are explored extensively since 2009. Presently, the interest focuses on small animals to study the in vivo limitations of CNDs for fluorescent labeling. The first study to present the feasibility of CNDs were carried out using polyethylene glycol-functionalized CNDs in mice.[59] The fluorescence was observed in the bladder area and ex vivo analysis showed the kidneys were fluorescent whereas the liver not. Similarly, Asp-carbon dots (Asp-CD) used for targeted imaging of glioma cells displayed full-color emission, excellent biocompatibility, and high accumulation in the tumor region. Targeted imaging of glioma is challenging as many contrast agents fail to cross the Blood-Brain Barrier (BBB).[60] Asp-CD injection via the mouse tail vein retained the fluorescence in the glioma 15 min which confirms its capability to cross the BBB. Liposome loaded with CNDs prepared from the hydrothermal treatment of phenyl

propionic acid polymers are another successful method for the MCF-7 tumor imaging in nude mice compared to plain CNDs. Carbon nanodots conjugated with protoporphyrin IX showed that the CNDs are accumulated in the tumor area, 6 h after the injection in a U14 tumor-bearing mice.[61]

5.1.2 Carbon nanotubes (CNTs)

The extraordinary features of Carbon Nanotubes (CNTs) including unique optical, high electrical and thermal conductivity and great tensile strength drowned the attention for many appliations.[62,63] These peculiar characteristics indicate the potential for CNT to use as field emission devices, nanoscale transistors, tips for scanning microscopy, or components for composite materials. Initially CNTs were found not suitable for biomedical applications, because of the insoluble characteristics. Later on it has been established that on surface functionalization, CNTs become highly soluble in water resulting supramolecular complexes with biological macromolecules.[64] A single-walled carbon nanotube (SWNT) is a rolled-up graphene sheet that is composed of benzene-type hexagonal rings of carbon atoms. Single-walled carbon nanotubes emit near-infrared (NIR) fluorescence (700−1300 nm), at which autofluorescence, absorption and scattering by blood and tissue are minimized. This is the most striking property which make SWNTs an excellent candidates for biomedical applications as bioimaging contrast agents[65−67] and biological sensors.[68] The fluorescence detection and imaging of SWNTs offer a powerful tool for tracking the interactions of SWNTs with tissues, cells and organisms. Single-walled carbon nanotubes are capable of covalent linking with visible-wavelength fluorophores that can be readily developed for cancer cell destruction, detection, and dynamic imaging using confocal microscopy. SWNTs and SWNT−streptavidin conjugates could be imaged in human promyelocytic leukemia cells and human T cells by this method.[66] Cell membrane penetration ability of FITC-labeled SWNTs were demonstrated by bioimaging using epifluorescence and confocal microscopy.[67] Cell surface receptors in cancer cell were specifically identified using immunoglobulin G functionalized fluorescently tagged CNTs using confocal microscopy.[69] Presence of multi-walled carbon nanotubes (MWNTs) functionalized with diethylenetriaminepentaacetic dianhydride (DTPA-MWNT) and radiolabeled with indium-111 (111In) in circulation was traced in vivo by dynamic imaging using micro-SPECT scanner.[70]

5.1.3 Fullerenes

Fullerene (C_{60}) is a distinct allotrope of carbon after diamond and graphite discovered in 1985 by Ref. [[71]] Their unique cage like structure, van der Waals diameter of 10.18 Å and electron-deficient nature lead to fascinating properties placed the fullerenes well within the realm of nanotechnology.[72] The carbon−carbon bonds in graphene and carbon nanotubes (CNTs) are sp^2-hybridised whereas sp^3-hybridized in diamond. Fullerenes are made up of a network of both hexagons (1,3,5-cyclohexatriene1) and pentagons ([5]radialene) with a unique hybridization of $sp^{2.278}$ as shown in Fig. 22.2.[73]

Functionalized fullerenes exhibit photothermal and photoacoustic properties. Furthermore, they are biodegradable, water soluble and easily excreted; make them a good choice for imaging and therapy. Water-soluble fullerene derivatives employable in biomedical applications are produced from bioactive compounds that exhibit affinity to certain proteins, nucleic acids or cell receptors such as saccharides or peptides. This is further functionalized

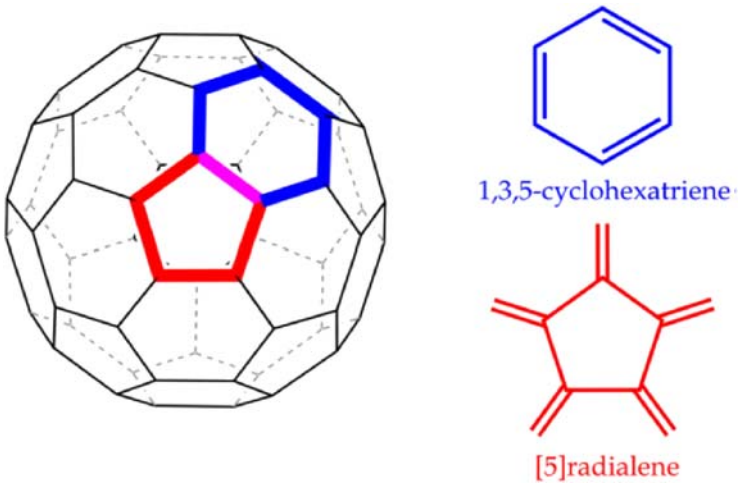

FIGURE 22.2 1,3,5-Cyclohexatriene and [5]radialene sub-units, as found in C60 (double bonds are emitted for clarity). *Reproduced from: Rašović I. Water-soluble fullerenes for medical applications. Mater Sci Technol. 2016;33(7):777–794. https://doi.org/10.1080/02670836.2016.1198114.*

with polar or ionic groups such as hydroxyl, carbonyl or quaternary ammonium salts.[74] Poly hydroxyl fullerenes (PHF) containing chitosan NPs have been studied in the imaging and therapy of cancer. Photoacoustic images of mouse abdominal regions were obtained when the nude mouse subjected to subcutaneous inoculation with BT474 cells (human breast cancer cells). This method showed better contrast with normal cells and no tissue damage caused by LASER irradiation.[75]

MRI is a noninvasive medical imaging technique that can provide visualization of soft tissue with high spatial resolution. High paramagnetic properties and high relaxivity of Gd-based metallofullerenes (Gd-MF) enabled their utilization as MRI contrast agents. In Trimetallic nitride endohedral metallofullerenes (Trimetasphere) is one exceptional class of fullerene molecules used as contrast agent. Here a Gd_3N cluster is encapsulated inside a C_{80} carbon cage referred to as $Gd_3{-}N@C_{80}$ (Fig. 22.3).[76] Gd-containing Trimetasphere contrast agent claimed to have the following properties: the passive uptake of the contrast agent by cells maintaining cell viability and proliferation, and the detection of contrast agent-labeled cells within the lung using non-invasive, high-resolution MRI. Gd-containing Trimetasphere is employed as MRI contrasting agent for in vitro and in vivo imaging and tracking of human amniotic fluid derived stem cells within lung tissue of mice. Gd-containing Trimetasphere specifically binds to damaged lung tissue and perform longitudinal MRI to evaluate the dynamics of cell homing, migration, and clearance.

High-intensity focused ultrasound (HIFU) is a novel noninvasive method used for both local tumor ablation technique and for real-time monitoring of the therapeutic process. Perfluorohexane-encapsulated fullerene nanospheres as dual-mode bioimaging contrast agent has been developed via a vacuum ultrasonic emulsification and centrifugation method. Excellent contrast-enhanced the imaging capabilities of the PFH-C60 nanospheres for ultrasound and CT bimodal bioimaging in dissected bovine livers.[77]

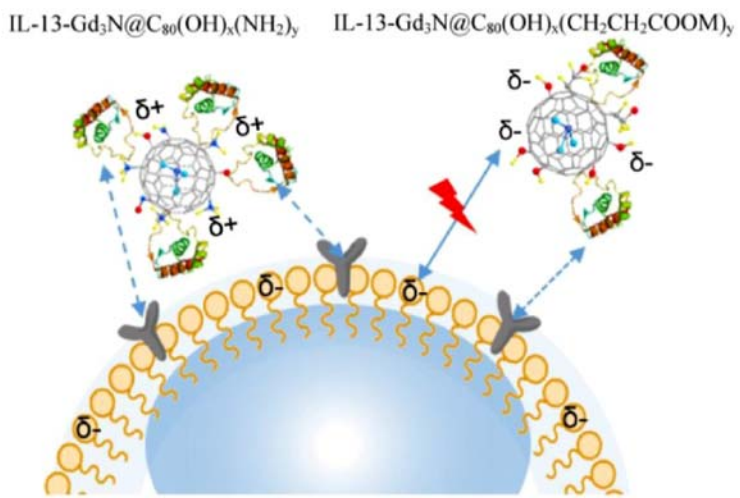

FIGURE 22.3 IL-13-Gd3N@C80(OH)x(NH2)y nanoparticles with positive charges illustrating facile binding to a negatively charged phospholipid bilayer cellular surfaces.[76] *Reprinted (adapted) with permission from reference Li, T, Murphy, S, Kiselev, B, Bakshi, K. S, Zhang, J, Eltahir, et al. A new interleukin-13 amino-coated gadolinium metallofullerene nanoparticle for targeted MRI detection of glioblastoma tumor cells. J Am Chem Soc. 2015;137(24):7881−7888. https://doi.org/10.1021/jacs.5b03991.*

5.2 Iron based nanomaterials

The most extensively used imaging probes are iron oxide NPs (IONPs). They have long been identified as T2 based contrast probes in MRI for cell labeling applications.[78] Iron based NPs of different sizes ranging from 10 to 300 nm with various surface coatings have been identified.[79] Currently available chemical IONPs are Ferumoxide (Endorem_-Europe, Feridex_ in the USA and Japan) and Ferucarbotran (Resovist_-Europe and Japan). Combidex, Ferummoxytol Code 7228 and VSOP−C184 are under clinical trials. In spite of their usefulness in imaging lesions in reticuloendothelial system (RES) organs like liver, spleen, and lymph nodes all these formulas have been used for cell labeling too.[80] These formulas differ in the uptake rate and retention by the cells. Their slight negative charge is the main drawback which is not advantageous for inducing efficient cellular uptake.

Ferritin and MagA are recognized as MRI reporter genes. Their function is to transfer endogenous iron or iron supplements into IONPs.[81] The iron NPs stored in the intracellular protein ferritin causes the relaxation of water molecule which is detected by MRI. Iron NPs are present either in an antiferromagnetic or superparamagnetic form in ferritin cage which will be monitored in MRI. By this way it is possible to recognize any alteration in ferritin content in the heart, liver, spleen, and brain. Deposition of iron in the nerve cell ganglia in the case of neurodegenerative disease like Parkinson's, Alzheimer's and Huntington's diseases is made possible by using MRI. Apart from that the fate of cell grafts in mice cell lines was able to monitor in vivo by MRI using human ferritin heavy chain (hFhc) as an RG, which is proved to be effective as there is no adverse effect on pluripotency of stem cells on expression. Human ferritin heavy chain acts as RG by producing MRI contrast through compensatory upregulation of transferrin receptor and subsequent increase in

cellular iron storage in ferritin bound form. Even after expression the neural differentiation and teratoma formation was effective. To extend the cell trafficking period, ferritin was used in combination with IONPs, which can supply iron atoms to the overexpressed ferritin proteins.[82]

A protein (MagA) found in the magnetotactic bacterium was found to be involved in transferring Fe ions into magnetite (Fe3O4) nanocrystals leading to the formation of NP-containing magnetosomes. In terms of this, MagA protein was identified as a useful agent in reporter gene based imaging because magnetosomes are superior to ferritin in inducing T_2 contrast.[83] The studies on the effect of MagA in mammalian 293FT cells as well as in mouse neuroblastoma N2A cells showed that MagA itself is capable of producing enough NPs to increase the transverse relaxivity or intracellular contrast which can be measured by MRI.[84]

Most well accepted surface coating agent for IONPs is dextran. Chitosan, poly ethylene glycol and polyvinyl alcohol have also been identified as effective coating materials for IONPs.[85,86] Labeling efficiency of SPIONPs on human bone marrow derived mesenchymal stem cells (hBM-MSC) was enhanced by 100% when it was coated with chitosan. The chitosan-SPIONP up to 200 g Fe/mL concentration was proven to be non-toxic. This made in vivo tracking of cells by MRI imaging more easier and efficient.[87] Iron oxide NPs entrapped with chitosan NPs showed an increased uptake under magnetization by Kusa O cell line. The enhanced accumulation in the cells was validated using atomic absorption spectrometry and confocal laser scanning microscopy.[88] Enhancement in the cellular uptake of poly(L-lysine) (PLL) surface-modified IONPs was studied using rat bone marrow stromal cells (rMSCs) and human mesenchymal stem cells (hMSCs). More than 92% cellular uptake was evident with PLL surface modified IONPs, when analyzed by TEM and optical microscopy. The magnetic resonance (MR) images demonstrated the presence of implanted cells in the lesion and at the injection spot.[89] Among the three iron oxide based nanocrystals; Feridex, Resovist, and monocrystalline iron oxide (MION), Feridex and Resovist were found to be more efficient as MRI contrast agents in labeling human mesenchymal stem cells (hMSCs).[90]

In vivo analysis of human hepatic satellite cells to monitor the progress of engraftment process could be effectively carried out using IONPs conjugated with suitable fluorophores.[91] A near-infrared fluorophore (NIRF), IRDye800CW (excitation/emission, 774/789 nm) was found to be promising in tracking of cells by Fe3O4 NPs in mouse macrophage RAW264.7 and later on used to label mammalian cells as its low toxicity was proven. Here the covalent coating of 3-dimercaptosuccinic acid (DMSA) on water-soluble 12 nm IONPs considerably increased the water solubility as well as their NIRF binding.[92,93]

5.3 Gold NPs

Gold NPs are one among the numerous metallic, inorganic NPs that can easily be incorporated and functionalize with biological molecules because of their unique chemical, physical, optical and surface plasmon resonance properties.[94–96] Because of their peculiar surface chemistry, projected biocompatibility, relatively low short-term toxicity and high X-ray absorption coefficient, gold NPs have received significant interest recently for use in multiple imaging technologies.[97] Therefore, gold NPs are well suited as contrast agent for CT and in the development of biosensors.

The two approaches to be employed to functionalize gold NPs are ligand exchange of stabilizers and direct incorporation of a functional stabilizer. In the former, biomolecules containing functional groups such as thiols is substituted by the stabilizer.[98] In the later method, conjugation of biomolecules to the stabilizer molecules, which are already present on gold NPs. The amino acid end groups of the stabilizer are modified by covalent conjugation of ligands.[99,100] The properties of the targeting ligand or stabilizer on the NP has huge influence on the polydispersity, particle size as well as size distribution of metal NPs.[101,102] The development of biocompatible, functionalized gold NPs that specifically target cancer sites has received considerable interest for in vivo imaging applications. Oleyl coated gold nanorods (AuNRs) incorporated with FITC were employed to label COS-7 cells so that the resulting fluorescent cells could be examined using a conventional fluorescence microscope.[103] The positive surface charge and multiple oleyl functionalities facilitate strong interaction of AuNR with cell membrane.

X-ray CT is a commonly used diagnostic imaging tool by which the density differences between the tissues can be visualized. The image contrast of these tissues is provided by X-ray attenuation between soft tissues and electron-dense bone. X-ray contrast agents are used in order to enhance the contrast between different types of tissues, such as normal and cancerous tissue. The commonly used CT contrast enhancers such as highly water-soluble small organic iodinated molecules, have very short imaging time.[104–106] Gold NPs have been identified as valuable X-ray contrast agents showing in vivo stability in blood. PEG-coated gold NPs are capable of imparting antibiofouling properties which in turn extend the systemic circulation.[107] Gum Arabic stabilized gold NPs have been developed by Kattumuri et al. as a potential biocompatible X-ray CT contrast agent.[108] On account of their peculiar features like plasmon-resonant absorption and scattering properties at visible and NIR wavelengths, Gold nanorods are identified as promising candidates in biological imaging. The surface functionalization, optical properties, in vitro and in vivo imaging, and photothermal aspects of gold nanorods make them appropriate to be functionalized with a range of biological molecules such as antibodies, biotin, folic acid, DNA, polyethyleneglycol (PEG), etc.[109] Comparative analysis of CT values demonstrate similarity of AuNPs containing polyethylene glycol-attached dendrimer to a commercial iodine agent, lopamidol, in vitro. Whereas the blood pool imaging of polyethylene glycol-attached dendrimer was observed to be superior to iopamidol. When compared to iopamidol, AuNPs containing polyethylene glycol-attached dendrimer was accumulated more in the liver.[110] Selective targeting of Squamous cell carcinoma (SCC) was achieved with Gold NPs (AuNPs) grown in the PEG-attached dendrimer as potential X-ray CT contrast agent. Popovtzer et al., however, demonstrated the use of gold nanorods as target-specific agents to detect head and neck cancer in vitro with a standard clinical CT.[101] Gold and functional gold NPs are promising candidates for detection of neurological diseases and cancer using CT scanning technology.[111–113] A biocompatible and all-in-one dual-modal nanoprobe developed using Au NPs and NIR emissive semiconducting fluorescence polymers found to be promising as contrast agent for in vivo X-ray CT and fluorescence bioimaging.[113] The CT imaging ability of the BSA-Au cluster was assessed using the commercial iodine-based contrast agent iopromide and compared with BSA-Au clusters (Fig. 22.4).[114] Fig. 22.4A and B depicts Hounsfield Units (HU) values of different concentrations of BSA-Au clusters and iopromide. It is evident that HU values increase with the concentration of the contrast material, with lower concentrations of BSA-Au matching the HU values of much higher concentrations of iopromide (Fig. 22.4A). The slope of HU values versus

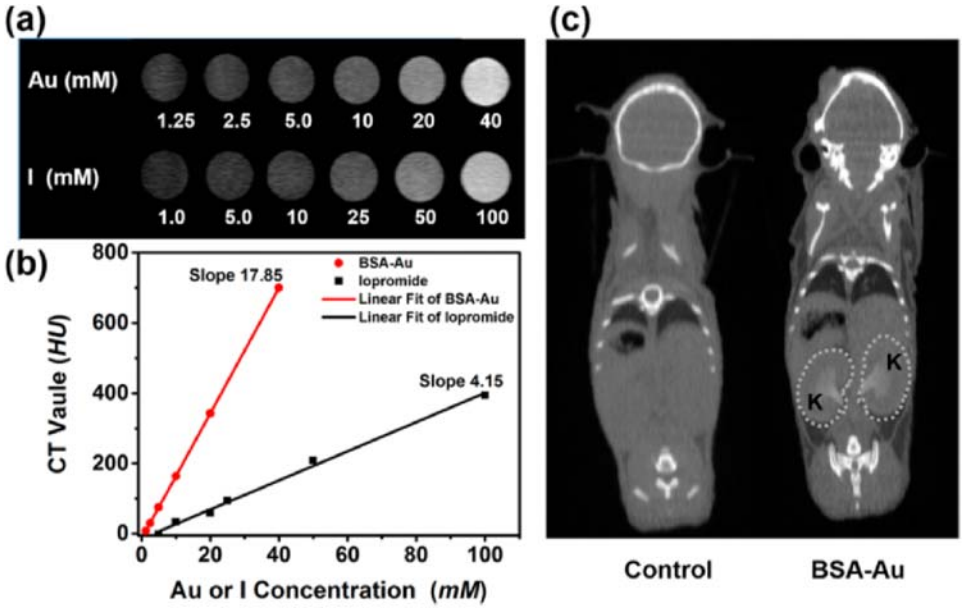

FIGURE 22.4 (A) CT images of BSA-Au clusters (the concentration of au: 1.25, 2.5, 5.0, 10, 20, and 40 mM) with different element concentrations of the iopromide solution (I: 1.0, 5.0, 10, 25, 50, and 100 mM), as contrast agent (B) The graph showing HU values of the BSA-Au cluster and iopromide against Au and I concentrations. (C) Two-dimensional CT images of mice (In vivo) by injecting, saline (left) and BSA-Au cluster (right) 2 h postinjection. The boundaries of the kidneys (D) are indicated with dashed curve.[114] *Reprinted (adapted) with permission from reference Wang, Y, Xu, C, Zhai, J, Gao, F, Liu, R., Gao, L, et.al., Label-free Au cluster used for in vivo 2D and 3D computed tomography of murine kidneys. Anal Chem. 2014;87(1):343−345. https://doi.org/10.1021/ac503887c.*

concentration (Fig. 22.4B) for BSA-Au clusters is 17.85, much steeper than that of iopromide (4.15). These analysis could prove the feasibility of using BSA-Au clusters as a CT contrast agent for in vivo kidney imaging. The BSA-Au clusters-injected mouse can be observed 2 h postinjection compared with the saline-injected control mouse.[114]

5.4 Quantum dots

QDs are fluorescent semiconductor nanocrystals (1−100 nm). The unique physicochemical properties of QDs are increasingly used as fluorophores for in vivo fluorescence imaging applications.[115−118] Quantum dots possess near-unity quantum yields and much greater brightness compared with organic dyes and fluorescent proteins. Broad absorption characteristics, continuous and tunable emission maxima due to quantum size effects, narrow line width in emission spectra, long fluorescence lifetime (5 to >100 ns compared with 1−5 ns in organic dyes) and negligible photobleaching (100−1000 times less than fluorescent dyes) over minutes to hours make QDs a valuable candidate for medical imaging applications.[119] Fluorescence imaging is more advantageous in comparison with other imaging modalities because of its high sensitivity and non-invasive nature. Easy employability with readily available and relatively inexpensive instruments of this method is a significant feature. QDs are potential for in vivo targeting of specific cells (e.g., DNA, labeling neoplastic cells, and cell

membrane receptors) after conjugation with specific bioactive moieties.[120] The size and composition of QDs can be modified synthetically to manage the absorption and emission characteristics. This makes QDs employable for applications in nucleic acid detection, biosensing, and cell labeling. The important barrier for QDs to be used for biological applications is its hydrophobic nature, as many biomolecules have limited solubility and stability in organic solvents.[121–123] However, stability in aqueous conditions and biocompatibility of QDs can be considerably improved with surface modification by ligand exchange or conjugation with surface stabilizers.[98,116] For ligand exchange, heterobifunctional ligands such as mercaptoacetic acid or 3-mercaptopropyl trimethoxy silane containing thiol functionalities are used. Covalent binding of QD with these ligands resulted in improvement of hydrophilicity QD, which is an important aspect for biological applications.[124] The ligand exchange method induce agglomeration which adversely affect the fluorescence efficiency of QDs. Alternate method for surface stabilization include binding with amphiphilic polymers.[125,126] Target specificity of the modified QDs can be established by Conjugating with specific ligands such as peptides, antibodies or small molecules.[127–130] On conjugation with PEG the blood circulation time of QDs is potentially extended which in turn reduced the possibility of nonspecific binding to serum proteins in blood.[131]

Significant accumulation of QD in lungs was noticed when CdSe/Zns QDs coated with PEG and a lung-targeting peptide was investigated in mice.[132] QD based multifunctional NP probe was successfully developed for in vivo imaging of human prostate cancer in mice. In this study the QD based probe was prepared by encapsulating PEGylated QDs using an ABC triblock copolymer as a secondary coating layer, then functionalized by conjugating with a tumor targeting antibody to prostate-specific membrane antigen.[118]

QDs conjugated with arginine-glycine-aspartic acid (RGD) peptide has been used successfully for non-invasive targeted in vivo NIR fluorescence imaging of αvβ3-positive tumor vasculature in a murine xenograft model.[133] Peptide-conjugated QDs are effective as biomarkers for non-invasive targeted in vivo imaging of tumors (Fig. 22.5A).[133] The in vivo fluorescence image of mice with U87MG tumor, treated with QD705-RGD and QD705 is depicted in Fig. 22.5B.[133] Significant accumulation in the liver, bone marrow, and lymph nodes is evident, even 6 h after the injection, where high tumor contrast was also observed.[133]

Quantum dots with different surface coatings retained fluorescence in vivo for at least 4 months where the localization of QDs was supported by the surface coating.[134] QDs coated with monoclonal anti-HER2 antibody in tumors could be efficiently tracked in living mice using a high-speed confocal microscope.[135] Quantum dots modified with PEG-poly(lactic acid) and functionalized with wheat germ agglutinin is a promising candidate as contrast agents for brain imaging.[136] Multiple components such as gadolinium and manganese incorporated to QDs to create multimodal imaging agents to achieve dual mode (fluorescence/magnetic resonance) imaging.[137] The biocompatibility of hydrophobic NIR-QDs (CdSeTe/CdS) can be improved by functionalizing with glutathione and further more with Gd3+-DOTA (DOTA: 1,4,7,10-tetraazacyclododecane-1,4,7,10-tetraacetic acid).[138] Manganese-doped QDs (anti-claudin, anti-mesothelin, or anti-PSCA-coated QDs) have been developed as multimodal targeted probes for confocal spectroscopic imaging to detect pancreatic cancer cells.[137]

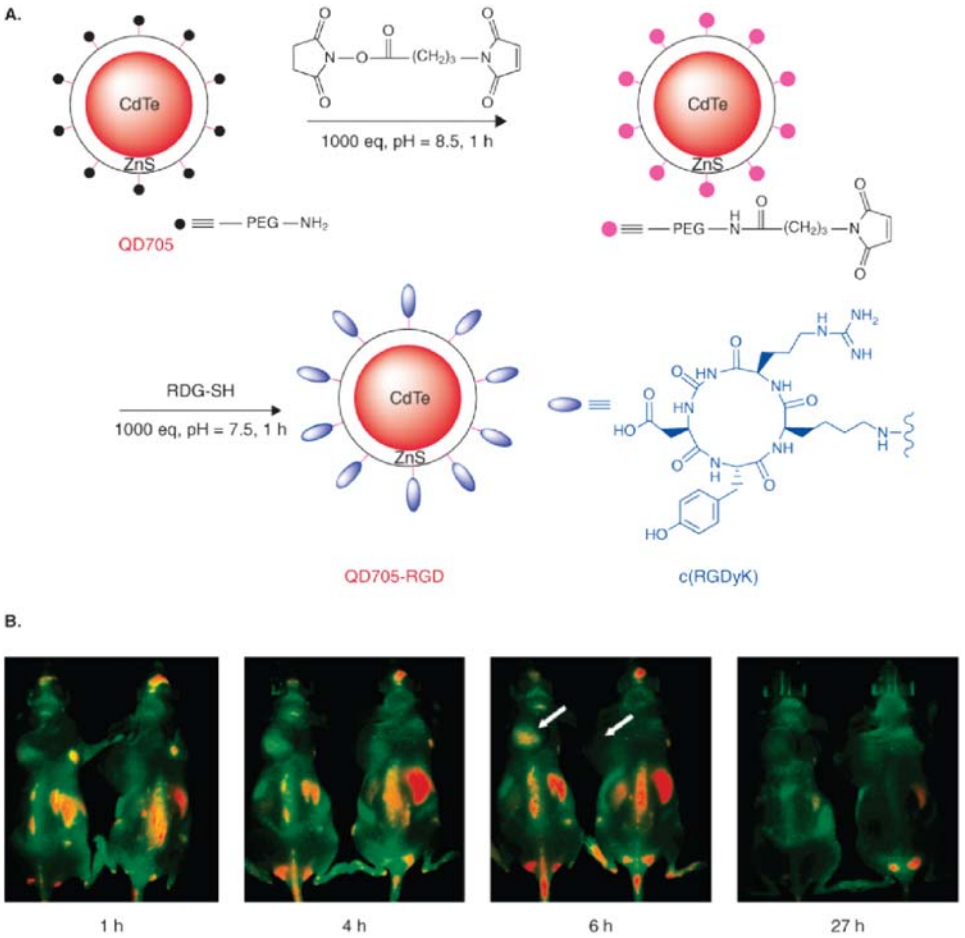

FIGURE 22.5 (A) Synthesis of QD705-RGD by bioconjugation of QD705 and RGD peptide. (B) In vivo NIR fluorescence imaging of U87MG tumor-bearing mice (left shoulder, pointed by white arrows) injected with 200 pmol of QD705-RGD (left) and QD705 (right), respectively. *Reprinted (adapted) with permission from reference Cai W, Shin DW, Chen K, Gheysens O, Cao Q, Wang SX, et al. Peptide-labeled near-infrared quantum dots for imaging tumor vasculature in living subjects. Nano Lett. 2006;6(4):669–676. https://doi.org/10.1021/nl052405t.*

5.5 Semiconductor NPs and Upconversion NPs (UCNPs)

Semiconductor polymer dots (SPDs) are employed in biological imaging in response to their exceptional photophysical characteristics, such as high brightness, good biocompatibility and photostability in comparison with those of organic dyes, QDs and reversibly switchable fluorescent proteins (RSFPs). Semiconductor nanocystals such as CdS, ZnO, TiO2, and CdSe/ZnS core shells, lanthanide-doped upconversion NPs etc. can be employed for MRI, PET/SPECT and CT.[139–141] Lanthanide-doped UCNPs was identified as valuable tools in bioimaging. Their ability to convert low energy near-infrared (NIR) photons into high energy UV or visible emission using multiphoton upconversion processes.[142] Inorganic fluorescent lanthanide ortho

phosphate [EuPO4 ·H2O and TbPO4 · H2O] nanorods can be employed as fluorescent label in cell biology and for cancer detection and diagnosis due to their ability to preserve their fluorescence in human umbilical vein endothelial cells786-O cells and renal carcinoma cells. [143]

Upconversion nanoparticles (UCNPs) are nanoscale particles (diameter 1−100 nm, rare-earth based lanthanide- or actinide-doped transition metals) that are capable of absorbing two or more incident photons of relatively low energy and convert into one emitted photon with higher energy.[144,145] Upconversion NPs have attracted considerable research interest because of their unique optical merits; sharp emissions, large anti-Stokes shifts, long lifetimes, and negligible photobleaching, that make them as ideal candidates for combined applications in biomedical fields including drug delivery, bioimaging, and cancer therapy. Bioimaging with UCNPs involves the excitation of the UCNPs inside a sample and then detecting the frequency-doubled emitted light. In comparison to traditional biolabels, which use Stokes shift processes and require high photon energies,[146] UCNPs utilize an anti-Stokes mechanism that allows for the use of lower energy, less damaging and more deeply penetrating light.[147]

Upconversion NPs are new generation imaging probes[148] that show anti-Stokes emission on exposure of low levels of irradiation in the near-infrared spectral region, where the biological molecules become optically transparent. Sharp emission bandwidth, longer lifetime, tunable emission, high photostability, and low cytotoxicity are the beneficial features of upconversion NPs for cell labeling and imaging applications. Core−shell structured NaYF4 with a uniform silica surface coating and co-doped with lanthanide ions Yb/Er (Silica/NaYF4:Yb,Er) was found to be effective to track transplanted cells in a living mouse model. Tracking was made possible with confocal imaging, spectrophotometry and inductively coupled plasma (ICP) analysis.[149] Using silica/NaYF4:Yb,Er particles, non-invasive imaging of cells became possible within the living subject. Owing to their outstanding optical and physicochemical properties, Lanthanide-doped upconversion NPs have become potential agents for nano-bioimaging applications.[150] Designing of the novel UCNP-based luminescent nanoplatform for whole-body imaging and multimodal cancer imaging in vitro and in vivo is promising applications in this field.[151−153]

5.6 Gadolinium-based NPs

Gadolinium hexanedione NPs (GdH-NPs) was developed as MRI contrast agent to monitor the tissue biodistribution of transplanted stem cells, there by understanding the cellular migration after transplantation. Human mesenchymal stem cells (hMSCs) easily and spontaneously internalized GdH-NPs by endocytotic pathway leading to high accumulation in cells. Then it was easier to track these cells using clinical MR scanners. Gadolinium hexanedione NPs are more advantageous than commercial gadolinium diethylene triamine pentaacetic acid (Gd-DTPA) due to its appropriate size (140 nm), and greater image enhancement ability with low concentration (10 mg/mL). Besides that the GdH-NPs synthesized by microemulsion process were nontoxic and did not affect differentiation potential of hMSCs. TEM results show that GdH-NPs can be used to label hMSCs in vitro without altering cell quality. Data reveals that the new GdH-NPs are promising as stem cell tracking probe which hold better signals in cellular MR image.[154]

Biocompatible nanotemplates (130 nm) on which gadolinium ions (Gd3+) were engineered so as to make a uniform distribution of Gd3+ on the surface. These Gd3+ ions on the surface

make the NPs not only hemocompatible but also increase the accessibility to enzymes thereby inducing relaxivities in the bulk water signal. This feature makes them valuable as next-generation MRI tumor contrast enhancement agents.[155] The water-proton relaxivity properties and intermolecular nanoclustering behavior of gadofullerene derivatives reveals their suitability as MRI contrast-enhancing agents.[156]

When compared to conventionally used contrast agents, the gadofullerenes and gadonanotubes are having high T1 relaxivity and are found to be biologically stable, less toxic and give longer retention time in vivo. Their target specificity can be modified easily as they are more prone to chemical modification with antibodies, peptides, drugs, etc. Possessing many favorable characteristic features such as cellular-translocating abilities,nanosize, superparamagnetism and external derivatization potential, gadofullerins, and gadonanotubes are promising agents to develop as MRI-delivery capsules. Because of their biocompatible nature, long residency time, and less toxicity gadofullerenes and gadonanotubes are potential to be employed in smart MRI, blood-pool, molecular-imaging, and guided-therapy probes to target hypothermia.[157]

Gadolinium (Gd) contrast agent along with nanoconjugates; TiO2 NPs and DNA oligonucleotides were useful as ultrasensitive pH-smart probes for MRI and neutron-capture cancer therapy.[158] A liposomal-based Gd NP called dual- Gd liposomal agent has two candidates, CE-Gd (core-encapsulated Gd liposome) and SC-Gd (surface conjugated Gd liposome). These two together form an entity that is capable of carrying a higher concentration of Gd. Therefore, signal enhancement per particle is greater compared to core-encapsulated and surface-conjugated Gd liposomal agents individually.[159] In vivo studies revealed that dual-Gd liposomal agent has higher T1 relaxivity and higher signal-to-noise and contrast-to-noise ratios for contrast-enhanced magnetic resonance angiography (CE-MRA). Dual-Gd liposomal MRI agent is a promising tool for molecular imaging applications.

5.7 Silica NPs

Two types of silica NPs; solid silica nanoparticles (SiNPs) and mesoporous silica nanoparticles (MSNs) are used for fabricating the multi-modal imaging NPs, according to the merit they have and the objectives to be accomplished. MSNs are found to be good candidate for multimodal bioimaging and theranostics because of their good biocompatibility, long blood circulation time, ease of modification, durability, their chemical inertness, water solubility, optically transparent nature, ease of preparation and free of interference with magnetic radiation, and higher effectiveness in internalization.[160,161] The viability and proliferation of human bone marrow MSCs remained unaltered on internalization of silica NPs conjugated with fluorescein isothiocyanate (FITC). FITC integration into the silica shell facilitated the visualization of multifunctional NP fluorescence. Silica NPs are capable of crossing the endo-lysosomal barrier by retaining their architectonic integrity. SiNPs are promising as novel high-quality fluorescent nanoprobes for biological imaging analysis, particularly for tracking dynamic biological procedures in long-term and realtime fashion. Dynamic monitoring of the cellular behaviors of SiNPs is easier due to its strong and stable fluorescent signals in live cells.[162–165] Silicon nanostructures/nanohybrids with immense potential have been extensively studied and developed for the rational designing of high-quality sensors and probes for bioimaging and biosensing applications.[166–168]

6. Conclusion

The tremendous development and merging of various related disciplines ensured NP based imaging for tracking and monitoring of disease diagnostics and its applications in therapeutics. Many of them are promising agents for fluorescent imaging and some of them have good surface chemistry and absorption capacity to employ in X-ray and CT based imaging. Engineered NPs with precise control over size and composition along with new nanoparticle−conjugates are explored in MRI as contrast agents. Nanotheranostics is an attractive platform where modalities like therapeutics, diagnostics, and stabilizing agents combine to form an all-in-one system with comprehensive features. Hitherto, a multitude of functionalized NPs have been synthesized, further research is required beyond nanoplatform construction such as efficacy, price, clinical safety, and degradation for clinical applications. The major challenges in the usage of NPs for in vivo imaging in humans are efficacy as well as toxicity. For each type of nanomaterial, distribution, accumulation, absorption rate, metabolic clearance, and excretion characteristics are different according to the physicochemical properties and surrounding microenvironment. Surface chemistry, agglomeration, dosage, and way of administration of NPs are other challenges. Reproducibility of these bio-imaging nanoprobes and the binding affinity between different imaging modalities yet to be examined and optimized. Therefore, much more efforts should be paid to address these fundamental challenges to establish nano-based platforms for clinical bioimaging, in turn to develop as theranostic agents.

References

1. Ghamsari MS. Introductory chapter: nano-bioimaging—past, present, and future. In: *State of the art in nano-bioimaging*; 2018. https://doi.org/10.5772/intechopen.74959.
2. Shi J, Votruba AR, Farokhzad OC, Langer R. Nanotechnology in drug delivery and tissue engineering: from discovery to applications. *Nano Lett* 2010;**10**(9):3223−30.
3. Choi HS, Frangioni JV. Nanoparticles for biomedical imaging: fundamentals of clinical translation. *Mol Imaging* 2010;**9**(6):291−310.
4. Yang Y, Wang L, Wan B, Gu Y, Li X. Optically active nanomaterials for bioimaging and targeted therapy. *Front Bioeng Biotechnol* 2019;**7**. https://doi.org/10.3389/fbioe.2019.00320.
5. Vadivambal R, Jayas Digvir S, editors. *Bio-imaging principles, techniques and applications*. Boca Raton: CRC Press; 2016 [Taylor & Francis Group].
6. Bronzino J,D, Peterson D,R, editors. *Biomedical signals, imaging, and informatics*. Boca Raton: CRC Press; 2015 [Taylor & Francis Group].
7. Diaspro A, van Zandvoort MAMJ, editors. *Super-resolution imaging in biomedicine*. Boca Raton: CRC Press, [Taylor & Francis Group]; 2017.
8. Heintzmann R, Huser T. Super-resolution structured illumination microscopy. *Chem Rev* 2017;**117**:13890−908.
9. Peeters Y, Vandenberg W, Duwé S, Bouwens A, Lukeš T, Ruckebusch C, Lasser T, Dedecker P. Correcting for photodestruction in super-resolution optical fluctuation imaging. *Sci Rep* 2017;**7**(1):10470.
10. Demmerle J, Innocent C, North AJ, B all G, Müller M, Miron E, Matsuda A, Dobbie IM, Markaki Y, Schermelleh L. Strategic and practical guidelines for successful structured illumination microscopy. *Nat Protoc* 2017;**12**:988−1010.
11. Lee D-E, Koo H, Sun I-C, Ryu JH, Kim K, Kwon IC. Multifunctional nanoparticles for multimodal imaging and theragnosis. *Chem Soc Rev* 2012;**41**(7):2656−72.
12. Ponsetto JL, Bezryadina A, Wei F, Onishi K, Shen H, Huang E, Ferrari L, Ma Q, Zou Y, Liu Z. Experimental demonstration of localized plasmonic structured illumination microscopy. *ACS Nano* 2017;**11**:5344−50.

13. Cho EC, Glaus C, Chen J, Welch MJ, Xia Y. Inorganic nanoparticle based contrast agents for molecular imaging. *Trends Mol Med* 2010;**16**(12):561–73.
14. Toy R, Bauer L, Hoimes C, Ghaghada KB, Karathanasis E. Targeted nanotechnology for cancer imaging. *Adv Drug Deliv Rev* 2014;**76**:79–97.
15. Arriagada FJ, Osseo-Asare K. Phase and dispersion stability effects in the synthesis of silicananoparticles in a non-ionic reverse microemulsion. *Colloids Surf A* 1992;**69**(2):105–15.
16. Piao Y, Burns A, Kim J, Wiesner U, Hyeon T. Designed fabrication of silica- based nanostructured particle systems for nanomedicine applications. *Adv Funct Mater* 2008;**18**(23):3745–58.
17. Carpenter MK, Frey-Vasconcells J, Rao MS. Developing safe therapies from human pluripotent stem cells. *Nat Biotechnol* 2009;**27**:606–13.
18. Marin-Garcia J, Goldenthal M. Application of stem cells in cardiology: where we are and where we are going. *Curr Stem Cell Res Ther* 2006;**1**(1):1–11. https://doi.org/10.2174/157488806775269052.
19. Bhirde A, Xie J, Swierczewska M, Chen X. Nanoparticles for cell labeling. *Nanoscale* 2011;**3**(1):142–53. https://doi.org/10.1039/C0NR00493F.
20. Ahrens ET, Bulte JWM. Tracking immune cells *in vivo* using magnetic resonance imaging. *Nat Rev* 2013;**13**:755–63.
21. Hart LS, El-Deiry WS. Invincible, but not invisible: imaging approaches toward in vivo detection of cancer stem cells. *J Clin Oncol* 2008;**26**(17):2901–10. https://doi.org/10.1200/jco.2008.16.9573.
22. Wu S, Li Y, Ding W, Xu L, Ma Y, Zhang L. Recent advances of persistent luminescence nanoparticles in bioapplications. *Nanomicro Lett* 2020;**12**(1). https://doi.org/10.1007/s40820-020-0404-8.
23. Fass L. Imaging and cancer: a review. *Mol Oncol* 2008;**2**:115–52.
24. Lim EK, Kim T, Paik S, Haam S, Huh YM, Lee K. Nanomaterials for theranostics: recent advances and future challenges. *Chem Rev* 2015;**115**:327–94. https://doi.org/10.1021/cr300213b.
25. Moonshi SS, Zhang C, Peng H, et al. A unique 19F MRI agent for the tracking of non-phagocytic cells in-vivo. *Nanoscale* 2018;**10**:8226–39.
26. Zhang C, Moonshi SS, Han Y, Puttick S, Peng H, Magoling BJA, et al. PFPE- based polymeric 19F MRI agents: a new class of contrast agents with outstanding sensitivity. *Macromolecules* 2017;**50**(15):5953–63. https://doi.org/10.1021/acs.macromol.7b01285.
27. Rijt Sv, Habibovic P. Enhancing regenerative approaches with nanopaticles. *J R Soc Interface* 2017;**14**(129):20170093. https://doi.org/10.1098/rsif.2017.0093.
28. Runnels JM, Zamiri P, Spencer JA, et al. Imaging molecular expression on vascular endothelial cells by *in vivo* immunofluorescence microscopy. *Mol imaging* 2006;**5**:31–40.
29. Caponetti V, Trzcinski J W, Cantelli A, Tavano R, Papini E, Mancin F, Montalti M. Self-assembled biocompatible fluorescent nanoparticles for bioimaging. *Front Chem* March 28, 2019;**7**:168. https://doi.org/10.3389/fchem.2019.00168.
30. Pratt EC, Shaffer TM, Grimm J. Nanoparticles and radiotracers: advances toward radionanomedicine. *Wiley Interdiscip Rev Nanomed Nanobiotechnol* 2016;**8**(6):872–90. https://doi.org/10.1002/wnan.1402.
31. Ponomarev V. Nuclear imaging of cancer cell therapies. *J Nucl Med* 2009;**50**:1013–6.
32. Scheer A, Kirsch M, Ferenz KB. Perfluorocarbons in photodynamic and photothermal therapy. *J Nanosci nanomed* 2017;**1**:21–7.
33. Chen W. Nanoparticle fluorescence based technology for biological applications. *J Nanosci Nanotechnol* March 2008;**8**(3):1019–51.
34. Gambhir SS, Herschman HR, Cherry SR, Barrio JR, Satyamurthy N, Toyokuni T, et al. Imaging transgene expression with radionuclide imaging technologies. *Neoplasia* 2000;**2**(1–2):118–38. https://doi.org/10.1038/sj.neo.7900083.
35. Xie J, Lee S, Chen X. Nanoparticle-based theranostic agents. *Adv Drug Deliv Rev* 2010;**62**:1064–79.
36. Chen F, Hableel G, Zhao ER, Jokerst JV. Multifunctional nanomedicine with silica: role of silica in nanoparticles for theranostic, imaging, and drug monitoring. *J Colloid Interface Sci* July 1, 2018;**521**:261–79. https://doi.org/10.1016/j.jcis.2018.02.053.
37. Michalet X, Pinaud F, Bentolila L, Tsay J, Doose S, Li J, Sundaresan G, Wu A, Gambhir S, Weiss S. Quantum dots for live cells, in vivo imaging, and diagnostics. *Science* 2005;**307**:538–44.
38. Fernandez-Moreira V, Thorp-Greenwood FL, Coogan MP. Application of d6 transition metal complexes in fluorescence cell imaging. *Chem Commun.* 2010;**46**:186–202.

39. Zhao Q, Li F, Huang C. Phosphorescent chemosensors based on heavy-metal complexes. *Chem Soc Rev* 2010;**39**:3007–30.
40. Zhao Q, Huang C, Li F. Phosphorescent heavy-metal complexes for bioimaging. *Chem Soc Rev* 2011;**40**:2508–24.
41. Yang F, Skripka A, Tabatabaei MS, Hong SH, Ren F, Huang Y, Oh JK, Martel S, Liu X, Vetrone F, Ma D. Magnetic-photoluminescent nanoplatform built from large-pore mesoporous silica. *Chem Mater* 2019;**31**:3201–10.
42. Ding B, Shuai S, Chang Y, Bo T, Meifang W, Ziyong C, et al. Large-pore mesoporous-silica-coated upconversion nanoparticles as multifunctional immunoadjuvants with ultrahigh photosensitizer and antigen loading efficiency for improved cancer photodynamic immunotherapy. *Adv Mater.* 2018;**30**(52):1802479. https://doi.org/10.1002/adma.201802479.
43. Lu X, Zhu W, Xie Y, Li X, Gao Y, Li F, Tian H. Near IR core substituted naphthalenediimide fluorescent chemosensors for zinc ions: ligand effects on PET and ICT channels. *Chem Eur J* 2010;**16**:8355–64.
44. Gu P-Y, Wang Z, Zhang Q. Azaacenes as active elements for sensing and bio applications. *J Mater Chem B* 2016;**44**:7060–74.
45. Zhao H, Liu C, Gu Z, Dong L, Li F, Yao C, Yang D. Persistent luminescent nanoparticles containing hydrogel for targeted, sustained and autofluorescence-free tumor metastasis imaging. *Nano Lett* 2019;**20**(1):252–60. https://doi.org/10.1021/acs.nanolett.9b03755.
46. Bartelmess J, Quinn SJ, Giordani S. Carbon nanomaterials: multifunctional agents for biomedical fluorescence and Raman imaging. *Chem Soc Rev* 2015;**44**:4672–98. https://doi.org/10.1039/C4CS00306C.
47. Patel KD, Singh RK, Kim HW. Carbon-based nanomaterials as an emerging platform for theranostics. *Mater Horiz* 2019;**6**:434–69. https://doi.org/10.1039/C8MH00966J.
48. Goodarzi S, Da Ros T, Conde J, Sefat F, Mozafari M. Fullerene: biomedical engineers get to revisit an old friend. *Mater Today* 2017;**20**:460–80. https://doi.org/10.1016/j.mattod.2017.03.017.
49. Namdari P, Negahdari B, Eatemadi A. Synthesis, properties and biomedical applications of carbon-based quantum dots: an updated review. *Biomed Pharmacother* 2017;**87**:209–22. https://doi.org/10.1016/j.biopha.2016.12.108.
50. Bullock CJ, Bussy C. Biocompatibility considerations in the design of graphene biomedical materials. *Adv Mater Interfac* 2019;**6**:1900229. https://doi.org/10.1002/admi 201900229.
51. Tinwala H, Wairkar S. Production, surface modification and biomedical applications of nanodiamonds: a sparkling tool for theranostics. *Mat Sci Eng C-97* 2019;**97**:913–31. https://doi.org/10.1016/j.msec.2018.12.073.
52. Xu X, Ray R, Gu Y, Ploehn HJ, Gearheart L, Raker K, Scrivens WA. Electrophoretic analysis and purification of fluorescent single-walled carbon nanotube fragments. *J Am Chem Soc* 2004;**126**:12736–7.
53. Esteves da Silva JCG, Gonçalves HMR. Analytical and bioanalytical applicationsof carbon dots. *TrAC Trends Anal Chem* 2011;**30**:1327–36.
54. Mitra S, Chandra S, Kundu T, Banerjee R, Pramanik P, Goswami A. Rapidmicrowave synthesis of fluorescent hydrophobic carbon dots. *RSC Adv* 2012;**2**:12129.
55. Hola K, Zhang Y, Wang Y, Giannelis EP, Zboril R, Rogach AL. Carbon dots emerging light emitters for bioimaging, cancer therapy and optoelectronics. *Nano Today* 2014;**9**(5):590–603.
56. Lu Y, Low PS. Folate-mediated delivery of macromolecular anticancer therapeutic agents. *Adv Drug Deliv Rev* 2002;**54**:675–93.
57. Liu Q, Xu S, Niu C, Li M, He D, Lu Z, Ma L, Na N, Huang F, Jiang H, Ouyang J. Distinguish cancer cells based on targeting turn-on fluorescence imaging byfolate functionalized green emitting carbon dots. *Biosens Bioelectron* 2015;**64**:119–25.
58. Li Q, Ohulchanskyy TY, Liu R, Koynov K, Wu D, Best A, Kumar R, Bonoiu A, Prasad PN. Photoluminescent carbon dots as biocompatible nanoprobes fortargeting cancer cells in vitro. *J Phys Chem C* 2010;**114**:12062–8.
59. Yang ST, Cao L, Luo PG, Lu F, Wang X, Wang H, Meziani MJ, Liu Y, Qi G, Sun YP. Carbon dots for optical imaging in vivo. *J Am Chem Soc* 2009;**131**(32):11308–9. https://doi.org/10.1021/ja904843x.
60. Agarwal S, Sane R, Oberoi R, Ohlfest JR, Elmquist WF. Delivery of molecularly targeted therapy to malignant glioma, a disease of the whole brain. *ExpertRev Mol Med* 2011;**13**:e17.
61. Hua X, Bao Y, Wu F. Fluorescent carbon quantum dots with intrinsic nucleolus targeting capability for nucleolus imaging and enhanced cytosolic and nuclear drug delivery. *ACS Appl Mater Interfaces* 2018;**10**:10664–77.
62. Sadegh H, Shahryari-ghoshekandi R. Functionalization of carbon nanotubes and its application in nanomedicine: a review. *Nanomed J* 2015;**2**:231–48. https://doi.org/10.7508/NMJ.2015.04.001.
63. Iijima S. Helical microtubules of graphitic carbon. *Nat* 1991;**354**(6348):56–8.

64. Al-Jamal WT, Al-Jamal KT, Bomans PH, et al. Functionalized-quantum-dot Liposome hybrids as multimodal nanoparticles for cancer. *Small* 2008;**4**(9):1406–15 [PubMed: 18711753].
65. Bachilo SM, Strano MS, Kittrell C, et al. Structure-assigned optical spectra of single walled carbonnanotubes. *Sci* 2002;**298**(5602):2361–6 [PubMed: 12459549].
66. Kam NWS, Jessop TC, Wender PA, Dai HJ. Nanotube molecular transporters: internalization of carbon nanotube-protein conjugates into mammalian cells. *J Am Chem Soc* 2004;**126**(22):6850–1 [PubMed: 15174838].
67. Pantarotto D, Briand JP, Prato M, Bianco A. Translocation of bioactive peptides across cell membranes by carbon nanotubes. *Chem Commun* 2004;**7**(1):16–7.
68. Dai HJ, Hafner JH, Rinzler AG, Colbert DT, Smalley RE. Nanotubes as nanoprobes in scanning probe microscopy. *Nature* 1996;**384**(6605):147–50. https://doi.org/10.1038/384147a0.
69. Sirdeshmukh R, Teker K, Panchapakesan B. *Functionalization of carbon nanotubes with antibodies for breast cancer detection applications. Proceedings of the International Conference on MEMS, NANO, and Smart Systems*. 2004. p. 48–53.
70. Lacerda L, Soundararajan A, Singh R, et al. Dynamic imaging of functionalized multi- walled carbon nanotube systemic circulation and urinary excretion. *Adv Mater* 2008;**20**(2):225–30.
71. Kroto H, Heath J, O'Brien S, et al. C_{60}: Buckminsterfullerene. *Nature*. 1985;**318**:162–3. https://doi.org/10.1038/318162a0.
72. Taylor R, Walton DRM. The chemistry of fullerenes. *Nature* 1993;**363**(6431):685–93.
73. Rašović I. Water-soluble fullerenes for medical applications. *Mater Sci Technol* 2016;**33**(7):777–94. https://doi.org/10.1080/02670836.2016.1198114.
74. Castro E, Hernandez Garcia A, Zavala G, Echegoyen L. Fullerenes in biology and medicine. *J Mater Chem B* 2017;**5**(32):6523–35. https://doi.org/10.1039/C7TB00855D.
75. Krishna V, Singh A, Sharma P, Iwakuma N, Wang Q, Zhang Q, Knapik J, Jiang H, Grobmyer SR, Koopman B, Moudgil B. Polyhydroxy fullerenes for non-invasive cancer imaging and therapy. *Small* 2010;**6**:2236–41. https://doi.org/10.1002/smll.201000847.
76. Li T, Murphy S, Kiselev B, Bakshi KS, Zhang J, Eltahir, et al. A new interleukin-13 amino-coated gadolinium metallofullerene nanoparticle for targeted MRI detection of glioblastoma tumor cells. *J Am Chem Soc* 2015;**137**(24):7881–8. https://doi.org/10.1021/jacs.5b03991.
77. He K, Ran H, Su Z, Wang Z, Li M, Hao L. Perfluorohexane-encapsulated fullerene nanospheres for dual-modality US/CT imaging and synergistic high- intensity focused ultrasound ablation. *Int J Nanomed* 2019;**14**:519–29. https://doi.org/10.2147/IJN.S184579. Published 2019 Jan 11.
78. Na HB, Song IC, Hyeon T. Inorganic nanoparticles for MRI contrast agents. *Adv Mater* 2009;**21**(21):2133–48. https://doi.org/10.1002/adma.200802366.
79. Zhang C, Liu T, Gao J, Su Y, Shi C. Recent development and application of magnetic nanoparticles for cell labeling and imaging. *Mini Rev Med Chem* 2010;**10**(3):194–203. https://doi.org/10.2174/138955710791185073.
80. Corot C, Robert P, Idee J, Port M. Recent advances in iron oxide nanocrystal technology for medical imaging. *Adv Drug Deliv Rev* 2006;**58**(14):1471–504. https://doi.org/10.1016/j.addr.2006.09.013.
81. Gilad AA, Ziv K, McMahon MT, van Zijl PCM, Neeman M, Bulte JWM. MRI reporter genes. *J Nucl Med* 2008;**49**(12):1905–8. https://doi.org/10.2967/jnumed.108.053520.
82. Pereira SM, Williams SR, Murray P, Taylor A. MS-1 magA. *Mol Imag* 2016;**15**:1–9. https://doi.org/10.1177/1536012116641533.
83. Xie J, Chen K, Chen X. Production, modification and bio-applications of magnetic nanoparticles gestated by magnetotactic bacteria. *Nano Res* 2009;**2**:261–78. https://doi.org/10.1007/s12274-009-9025-8.
84. Zurkiya O, Chan AWS, Hu X. MagA is sufficient for producing magnetic nanoparticles in mammalian cells, making it an MRI reporter. *Magn Reson Med* 2008;**59**(6):1225–31. https://doi.org/10.1002/mrm.21606.
85. Veiseh O, Gunn JW, Zhang M. Design and fabrication of magnetic nanoparticles for targeted drug delivery and imaging. *Adv Drug Deliv Rev* 2010;**62**(3):284–304. https://doi.org/10.1016/j.addr.2009.11.002.
86. Juang J-H, Wang J-J, Shen C-R, Kuo C-H, Chien Y-W, Kuo H-Y, Tsai Z-T, Yen T-C. Magnetic resonance imaging of transplanted mouse islets labeled with chitosan-coated superparamagnetic iron oxide nanoparticles. *Transplant Proc* 2010;**42**(6):2104–8. https://doi.org/10.1016/j.transproceed.2010.05.103.
87. Reddy AM, Kwak BK, Shim HJ, Ahn C, Lee HS, Suh YJ, Park ES. In vivo tracking of mesenchymal stem cells labeled with a novel chitosan-coated superparamagnetic iron oxide nanoparticles using 3.0T MRI. *J Korea Med Sci* 2010;**25**(2):211. https://doi.org/10.3346/jkms.2010.25.2.211.

88. Chaleawlert-umpon S, Mayen V, Manotham K, Pimpha N. Preparation of iron oxide-entrapped chitosan nanoparticles for stem cell labeling. *J Biomater Sci Polym Ed* 2010;**21**(11):1515. https://doi.org/10.1163/092050609x12519805626031.
89. Babic M, Horák D, Trchová M, Jendelová P, Glogarová K, Lesný P, Herynek V, Hájek M, Syková E. Poly(L-lysine)-modified iron oxide nanoparticles for stem cell labeling. *Bioconjug Chem* 2008;**19**:740–50. https://doi.org/10.1021/bc700410z.
90. Kim HS, Oh SY, Joo H,J, Son KR, Song IC, Moon WK. The effects of clinically used MRI contrast agents on the biological properties of human mesenchymal stem cells. *NMR Biomed* 2010;**23**(5):514–22. https://doi.org/10.1002/nbm.1487.
91. Maxwell DJ, Bonde J, Hess DA, Hohm SA, Lahey R, Zhou, Creer MH, Piwnica-Worms D, Nolta JA. Fluorophore-conjugated iron oxide nanoparticle labeling and analysisof engrafting human hematopoietic stem cells. *Stem Cell* 2008;**26**(2):517–24. https://doi.org/10.1634/stemcells.2007-0016.
92. Bertorelle F, Wilhelm C, Roger J, Gazeau F, Ménager C, Cabuil V. Fluorescence-modified superparamagnetic nanoparticles: intracellular uptake and use in cellular imaging. *Langmuir* 2006;**22**(12):5385–91. https://doi.org/10.1021/la052710u.
93. Wilhelm C, Gazeau F. Universal cell labelling with anionic magnetic nanoparticles. *Biomater* 2008;**29**(22):3161–74. https://doi.org/10.1016/j.biomaterials.2008.04.016.
94. Khalil M, Pratama RI, Sujak M, Garry A, Djuhana D, Umar A, Jan BM. Dependence of the photocatalytic reduction of bicarbonate to formic acid by Au–TiO2 on Au morphology and its plasmonic vibrational mode. *Mater Chem Phys* 2020:123018. https://doi.org/10.1016/j.matchemphys.2020.123018.
95. Zhang Y, Zhang C, Xu C, Wang X, Liu C, Waterhouse GIN, et al. Ultra small Au nanoclusters for biomedical and biosensing applications: a mini-review. *Talanta* 2019;**200**:432–42. https://doi.org/10.1016/j.talanta.2019.03.068.
96. Cai WB, Chen XY. Nanoplatforms for targeted molecular imaging in living subjects. *Small* 2007;**3**(11):1840–54 [PubMed: 17943716].
97. Nune SK, Gunda P, Thallapally PK, Lin Y-Y, Laird Forrest M, Berkland CJ. Nanoparticles for biomedical imaging. *Expet Opin Drug Deliv* 2009;**6**(11):1175–94. https://doi.org/10.1517/17425240903229031.
98. Daniel MC, Astruc D. Gold nanoparticles: assembly, supramolecular chemistry, quantum-size related properties, and applications toward biology, catalysis, andnanotechnology. *Chem Rev* 2004;**104**(1):293–346 [PubMed: 14719 978].
99. Pandey P, Singh SP, Arya SK, Gupta V, Datta M, Singh S, Malhotra BD. Application of thiolated gold nanoparticles for the enhancement of glucose oxidase activity. *Langmuir* 2007;**23**(6):3333–7. https://doi.org/10.1021/la062901c.
100. Wangoo N, Bhasin KK, Mehta SK, Suri CR. Synthesis and capping of water- dispersed gold nanoparticles by an amino acid: bioconjugation and binding studies. *J Colloid Interface Sci* 2008;**323**(2):247–54 [PubMed: 18486946].
101. Popovtzer R, Agrawal A, Kotov NA, Popovtzer A, Balter J, Carey TE, Kopelman R. Targeted gold nanoparticles enable molecular CT imaging of cancer. *Nano Lett* 2008;**8**(12):4593–6. https://doi.org/10.1021/nl8029114 [PubMed: 19367807].
102. Wilson R. The use of gold nanoparticles in diagnostics and detection. *Chem Soc Rev* 2008;**37**(9):2028–45 [PubMed: 18762845].
103. Basiruddin S, Saha A, Pradhan N, Jana NR. Functionalized gold nanorod solution via reverse micelle based polyacrylate coating. *Langmuir* 2010;**26**(10):7475–81. https://doi.org/10.1021/la904189a.
104. Yu SB, Watson AD. Metal-based X-ray contrast media. *Chem Rev* 1999;**9**:2353–77 [PubMed: 11749484].
105. Balaszkiewicz P. Synthesis of water-soluble ionic and nonionic iodinated X-ray contrast-media. *Invest Radiol* 1994;**29**:S51–3 [PubMed: 8071045].
106. Galperin A, Margel D, Baniel J, et al. Radiopaque iodinated polymeric nanoparticles for X-ray imaging applications. *Biomater* 2007;**28**(30):4461–8. https://doi.org/10.1016/j.biomaterials.2007.06.032 [PubMed: 17644171].
107. Hainfeld JF, Slatkin DN, Focella TM, Smilowitz HM. Gold nanoparticles: a new X-ray contrast agent. *Br J Radiol* 2006;**79**(939):248–53 [PubMed: 16498039].
108. Kattumuri V, Katti K, Bhaskaran S, et al. Gum Arabic as a phytochemical construct for the stabilization of gold nanoparticles: in vivo pharmacokinetics and X-ray-contrast imaging studies. *Small* 2007;**3**(2):333–41 [PubMed: 17262759].

109. Tong L, Wei Q, Wei A, Cheng J-X. Gold nanorods as contrast agents for biological imaging: surface conjugation, two photon luminescence, and photothermal effects. *Photochem Photobiol* 2009;**85**(1):21–32. https://doi.org/10.1111/j.1751- 1097.2008.00507.x.
110. Kojima C, Umeda Y, Ogawa M, Harada A, Magata Y, Kono K. X-ray computed tomography contrast agents prepared by seeded growth of gold nanoparticle in PEGylated dendrimer. *Nanotechnology* 2010;**21**:245104. https://doi.org/10.1088/0957- 4484/21/24/245104.
111. Shilo M, Reuveni T, Motiei M, Popovtzer R. Nanoparticles as computed tomography contrast agents: current status and future perspectives. *Nanomedicine* 2012;**7**:257–69. https://doi.org/10.2217/nnm.11.190.
112. Reuveni T, Motiei M, Romman Z, Popovtzer A, Popovtzer R. Targeted gold nanoparticles enable molecular CT imaging of cancer: an in vivo study. *Int J Nanomed* 2011;**6**:2859–64. https://doi.org/10.2147/IJN.S25446.
113. Kumar R, Aadil KR, Ranjan S, Kumar VB. Advances of nanotechnology and nanomaterials based strategies for neural tissue engineering. *J Drug Deliv Sci Technol* 2020:101617. https://doi.org/10.1016/j.jddst.2020.101617.
114. Wang Y, Xu C, Zhai J, Gao F, Liu R, Gao L, Zhao Y, Chai Z, Gao X. Label-free Au cluster used for in vivo 2D and 3D computed tomography of murine kidneys. *Anal Chem* 2014;**87**(1):343–5. https://doi.org/10.1021/ac503887c.
115. Xu Y, Wang X, Zhang WL, Lv F, Guo S. Recent progress in two-dimensional inorganic quantum dots. *Chem Soc Rev* 2018;**47**(2):586–625. https://doi.org/10.1039/c7cs00500h.
116. Smith AM, Duan HW, Mohs AM, Nie SM. Bioconjugated quantum dots for in vivo molecular and cellular imaging. *Adv Drug Deliv Rev* 2008;**60**(11):1226–40 [PubMed: 18495291].
117. Choi HS, Liu W, Misra P, Tanaka E, Zimmer JP, Itty Ipe, Bawendi MG, Frangioni JV. Renal clearance of quantum dots. *Nat Biotechnol* 2007;**25**(10):1165–70. https://doi.org/10.1038/nbt1340.
118. Gao X, Cui Y, Levenson RM, Chung LWK, Nie S. In vivo cancer targeting and imaging with semiconductor quantum dots. *Nat Biotechnol* 2004;**22**(8):969–76. https://doi.org/10.1038/nbt994.
119. Resch-Genger U, Grabolle M, Cavaliere-Jaricot S, Nitschke R, Nann T. Quantum dots versus organic dyes as fluorescent labels. *Nat Methods* 2008;**5**(9):763–75. https://doi.org/10.1038/nmeth.1248.
120. Lu ZS, Li CM. Quantum dot-based nanocomposites for biomedical applications. *Curr Med Chem* 2011;**18**:3516–28. https://doi.org/10.2174/092986711796642634.
121. Gerion D, Pinaud F, Williams SC, Parak WJ, Zanchet D, Weiss S, Alivisatos AP. Synthesis and properties of biocompatible water-soluble silica-coated CdSe/ZnS semiconductor quantum dots†. *J Phys Chem B* 2001;**105**(37):8861–71. https://doi.org/10.1021/jp0105488.
122. Roy MD, Herzing AA, Lacerda SHDP, Becker ML. Emission-tunable microwave synthesis of highly luminescent water soluble CdSe/ZnS quantum dots. *Chem Commun* 2008;**14**(18):2106–8.
123. Deng Z, Lie FL, Shen S, Ghosh I, Mansuripur M, Muscat AJ. Water-based route to ligand-selective synthesis of ZnSe and Cd-doped ZnSe quantum dots with tunable ultraviolet A to blue photoluminescence. *Langmuir* 2009;**25**(1):434–42. https://doi.org/10.1021/la802294e.
124. Bruchez Jr M, Moronne M, Gin P, Weiss S, Alivisatos AP. Semiconductor nanocrystals as fluorescent biological labels. *Science* 1998;**281**(5385):2013–6 [PubMed: 9748157].
125. Xu J, Wang J, Mitchell M, Mukherjee P, Jeffries-El M, et al. Organic-inorganic nanocomposites via directly grafting conjugated polymers onto quantum dots. *J Am Chem Soc* 2007;**129**(42):12828–33 [PubMed: 17914821].
126. Anderson RE, Chan WCW. Systematic investigation of preparing biocompatible, single, and small ZnS-capped CdSe quantum dots with amphiphilic polymers. *ACS Nano* 2008;**2**(7):1341–52 [PubMed: 19206301].
127. Bentzen EL, Tomlinson ID, Mason J, Gresch P, Warnement MR, et al. Surface modification to reduce nonspecific binding of quantum dots in live cell assays. *Bioconjugate Chem* 2005;**16**(6):1488–94 [PubMed: 16287246].
128. Xing Y, Chaudry Q, Shen C, et al. Kong KY, Zhau HE, Chung LW, Petros JA, et al. Bioconjugated quantum dots for multiplexed and Quantitative immunohistochemistry. *Nat Protoc* 2007;**2**(5):1152–65 [PubMed: 17546006].
129. Pathak S, Davidson MC, Silva GA. Characterization of the functional binding properties of antibody conjugated quantum dots. *Nano Lett* 2007;**7**(7):1839–45 [PubMed: 17536868].
130. Qian J, Yong KT, Roy I, Ohulchanskyy TY, Bergey EJ, Lee HH, Tramposch KM, He S, Maitra A, Prasad PN. Imaging pancreatic cancer using surface- functionalized quantum dots. *J Phys Chem B* 2007;**111**(25):6969–72 [PubMed: 17552555].
131. Wamement MR, Tomlinson ID, Chang JC, Schreuder MA, Luckabaugh CM, Rosenthal SJ. Controlling the reactivity of ampiphilic quantum dots in biological assays through hydrophobic assembly of custom PEG derivatives. *Bioconjug Chem* 2008;**19**(7):1404–13. https://doi.org/10.1021/bc800104n.
132. Akerman ME, Chan WCW, Laakkonen P, Bhatia SN, Ruoslahti E. Nanocrystal targeting in vivo. *Proc Natl Acad Sci USA* 2002;**99**(20):12617–21 [PubMed: 12235356].

133. Cai W, Shin D-W, Chen K, Gheysens O, Cao Q, Wang SX, Gambhir SS, Chen X. Peptide-labeled near-infrared quantum dots for imagingtumor vasculature in living subjects. *Nano Lett* 2006;**6**(4):669–76. https://doi.org/10.1021/nl052405t.
134. B. Ballou, B.C. Lagerholm, L.A. Ernst, M.P. Bruchez, A.S. Waggoner Noninvasive imaging of quantum dots in mice. *Bioconjug Chem* 2004;**15**(1):79–86. doi:10.1021/bc034153y
135. H. Tada, H. Higuchi, T.M. Wanatabe, N. Ohuchi In vivo real-time tracking of single quantum dots conjugated with monoclonal anti-HER2 antibody in tumors of mice. *Cancer Res* 2007;**67**(3):1138–1144. [PubMed: 17283148]
136. Gao XL, Chen J, Chen J, Wu B, Chen H, Jiang X. Quantum dots bearing lectin-functionalized nanoparticles as a platform for in vivo brain imaging. *Bioconjug Chem* 2008;**19**(11):2189–95. https://doi.org/10.1021/bc8002698.
137. K.T. Yong Mn-doped near-infrared quantum dots as multimodal targeted probes for pancreatic cancer imaging. *Nanotechnol* 2009;**20**(1):015102. [PubMed: 19417242].
138. T. Jin, Y. Yoshioka, F. Fujii, Y. Komai, J. Seki, A. Seiyama Gd3+-functionalized near-infrared quantum dots for in vivo dual modal (fluorescence/magnetic resonance) imaging. *Chem Commun* 2008;**44**:5764–5766. doi:10.1039/b812302k.
139. Duan C, Liang L, Li L, Zhang R, Xu ZP. Recent progress in upconversion luminescence nanomaterials for biomedical applications. *J Mater Chem B* 2018;**6**:192–209.
140. Chandan HR, Schiffman JD, Balakrishna RG. Quantum dots as fluorescent probes: synthesis, surface chemistry, energy transfer mechanisms, and applications. *Sens Actuators B Chem* 2018;**258**:1191–214.
141. I.V. Martynenko, A.P. Litvin, F. Purcell-Milton, A.V. Baranov, A.V. Fedorov, Y.K. Gunko Application of semiconductor quantum dots in bioimaging and biosensing. *J Mater Chem B* 2017;**5**:6701–6727
142. Li Z, Zhang Y, La H, Zhu R, El-Banna G, Wei Y, et al. Upconverting NIR photons for bioimaging. *Nanomaterials* 2015;**5**(4):2148–68.
143. C.R. Patra, R. Bhattacharya, S. Patra, S. Basu, P. Mukherjee, D. Mukhopadhyay Inorganic phosphate nanorods are a novel fluorescent label in cell biology. *J Nanobiotechnol* 2006;**4**(1):11. doi:10.1186/1477-3155-4-11.
144. Reddy KL, Rai M, Prabhakar N, Arppe R, Rai SB, Singh SK, Rosenholm JM, Krishnan V. Controlled synthesis, bioimaging and toxicity assessments in strong red emitting Mn2+ doped NaYF4:Yb3+/Ho3+ nanophosphors. *RSC Adv* 2016;**6**:53698–704. https://doi.org/10.1039/c6ra07106f.
145. Reddy KL, Srinivas V, Shankar KR, Kumar S, Sharma V, Kumar A, Bahuguna A, Bhattacharyya K, Krishnan V. Enhancement of luminescence intensity in red emitting NaYF4:Yb/Ho/Mn upconversion nanophosphors by variation of reaction parameters. *J Phys Chem C* 2017;**121**(21):11783–93. https://doi.org/10.1021/acs.jpcc.7b01334.
146. Chen G, Qiu H, Prasad PN, Chen X. Upconversion nanoparticles: design, nanochemistry, and applications in theranostics. *Chem Rev* 2014;**114**(10):5161–214. https://doi.org/10.1021/cr400425h.
147. Wu X. Upconversion nanoparticles: a versatile solution to multiscale biological imaging. *Bioconjug Chem* 2015;**26**(2):166–75. https://doi.org/10.1021/bc5003967. PMC 4335809. PMID 25254658.
148. Wang F, Banerjee D, Liu Y, Chen X, Liu X. Upconversion nanoparticles in biological labeling, imaging, and therapy. *Analyst* 2010;**135**(8):1839–54. https://doi.org/10.1039/C0AN00144A.
149. Idris NM, Li Z, Ye L, Sim EK, Mahendran R, Ho PC, Zhang Y. Tracking transplanted cells in live animal using upconversion fluorescent nanoparticles. *Biomaterials* 2009;**30**(28):5104–13.
150. Liu C, Ga Z, Zeng J, Hou Y, Fang F, Li Y, Qiao R, Shen L, Lei H, Yang W, Gao M. Magnetic/upconversion fluorescent NaGdF4:Yb,Er nanoparticle-based dual-modal molecular probes for imaging tiny tumors. *In Vivo ACS Nano* 2013;**7**(8):7227–40. https://doi.org/10.1021/nn4030898.
151. Yang D, Li C, Lin J. Multimodal cancer imaging using lanthanide-based upconversion nanoparticles. *Nanomedicine* 2015;**10**(16):2573–91. https://doi.org/10.2217/nnm.15.92.
152. Deng H, Huang S, Xu C. Intensely red-emitting luminescent upconversion nanoparticles for deeptissue multimodal bioimaging. *Talanta* 2018;**184**:461–7.
153. Zhu X, Zhou J, Chen M, Shi M, Feng W, Li F. Core-shell Fe3O4@NaLuF4:Yb,Er/Tm nanostructure for MRI, CT and upconversion luminescence tri-modality imaging. *Biomaterials* 2012;**33**(18):4618–27. https://doi.org/10.1016/j.biomaterials.2012.03.007.
154. Tseng C-L, Shih I-L, Stobinski L, Lin F-H. Gadolinium hexanedione nanoparticles for stem cell labeling and tracking via magnetic resonance imaging. *Biomaterials* 2010;**31**(20):5427–35. https://doi.org/10.1016/j.biomaterials.2010.03.049.
155. Zhu D, White RD, Hardy PA, Weerapreeyakul N, Sutthanut K, Jay M. Biocompatible nanotemplate-engineered nanoparticles containing gadolinium: stability and relaxivity of a potential MRI contrast agent. *J Nanosci Nanotechnol* 2006;**6**:996.

156. Bolskar RD. Gadofullerene MRI contrast agents. *Nanomedicine* 2008;**3**(2):201–13. https://doi.org/10.2217/17435889.3.2.201.
157. Sitharaman B, Wilson LJ. Gadofullerenes and gadonanotubes: a new paradigm for high-performance magnetic resonance imaging contrast agent probes. *J Biomed Nanotechnol* 2007;**3**:342.
158. Paunesku T, Ke T, Dharmakumar R, Mascheri N, Wu A, Lai B, Vogt S, Maser J, Thurn K, Szolc-Kowalska B, Larson A, Bergan RC, Omary R, Li D, Lu Z,R, Woloschak GE. Gadolinium-conjugated TiO_2-DNA oligonucleotide nanoconjugates show prolonged intracellular retention period and T1-weighted contrast enhancement in magnetic resonance images. *Nanomedicine* 2008;**4**(3):201–7.
159. Ghaghada KB, Ravoori M, Sabapathy D, Bankson J, Kundra V, Annapragada A. New dual mode gadolinium nanoparticle contrast agent for magnetic resonance imaging. *PLoS One* 2009;**4**(10):e7628. https://doi.org/10.10371/journal.pone.0007628.
160. Zheng X, Zeng S, Hu J, Wu L, Hou X. Applications of silica-based nanoparticles for multimodal bioimaging. *Appl Spectrosc Rev* 2018;**53**(5):377–94. https://doi.org/10.1080/05704928.2017.1355312.
161. Huang D-M, Hung Y, Ko B-S, Hsu S-C, Chen W-H, Chien, et al. Highly efficient cellular labeling of mesoporous nanoparticles in human mesenchymal stem cells: implication for stem cell tracking. *FASEB J* 2005;**19**(14):2014–6. https://doi.org/10.1096/fj.05-4288fje.
162. Shiohara A, Hanada S, Prabakar S, Fujioka K, Lim TH, Yamamoto K, et al. Chemical reactions on surface molecules attached to silicon quantum dots. *J Am Chem Soc* 2010;**132**:248–53. https://doi.org/10.1021/ja906501v.
163. Shiohara A, Prabakar S, Faramus A, Hsu CY, Lai PS, Northcotea PT, et al. Sized controlled synthesis, purification, and cell studies with siliconquantum dots. *Nanoscale* 2011;**3**:3364–70. https://doi.org/10.1039/c1nr10458f.
164. Cao Z, Peng F, Hu Z, Chu B, Zhong Y, Su Y, et al. In vitro cellular behaviors and toxicity assays of small-sized fluorescent silicon nanoparticles. *Nanoscale* 2017;**9**:7602–11. https://doi.org/10.1039/C7NR0 0530J.
165. Zhou Y, Zhang Y, Zhong Y, Fu R, Wu S, Wang Q, Wang H, Su Y, Zhang H, He Y. The in vivo targeted molecular imaging of fluorescent silicon nanoparticles in *Caenorhabditis elegans*. *Nano Res* 2018;**11**(5):2336–46. https://doi.org/10.1007/s12274- 017-1677-1.
166. Pang JY, Su YY, Zhong YL, Peng F, Song B, He Y. Fluorescent silicon nanoparticle-based gene carriers featuring strong photostability and feeble cytotoxicity. *Nano Res* 2016;**9**:3027–37. https://doi.org/10.1007/s12274-016-1185-8.
167. Nishimura H, Ritchie K, Kasai RS, Goto M, Morone N, Sugimura H, et al. Biocompatible fluorescent silicon nanocrystals for singlemolecule tracking and fluorescence imaging. *J Cell Biol* 2013;**202**:967–83. https://doi.org/10.1083/jcb.201301053.
168. Lai CH, Hütter J, Hsu CW, Tanaka H, Varela-Aramburu S, Cola L, et al. Analysis of carbohydrate-carbohydrate interactions using sugarfunctionalized silicon nanoparticles for cell imaging. *Nano Lett* 2016;**16**:807–11. https://doi.org/10.1021/acs.nanolett.5b04984.

This page intentionally left blank

CHAPTER

23

Biological prospects and potential of nanoparticles in animal nutrition

Vimal Antony Muttathettu[1,2] *and P. Anitha*[1]

[1]College of Veterinary and Animal Sciences, Kerala Veterinary and Animal Sciences University, Mannuthy, Thrissur, Kerala, India; [2]College of Avian Sciences and Management, Kerala Veterinary and Animal Sciences University, Thiruvazhamkunnu, Palakkad, Kerala, India

1. Introduction

Biomedical research has seen several developments in nanoparticles of different materials due to the varied chemical and physical features exhibited.[1] Nanotechnology has very diverse applications in several sectors including agriculture,[2,3] animal production systems,[4] and food systems,[5] with remarkable prospects in animal nutrition.[6] Nanotechnology addresses the reduction in bioavailability,[7] antagonistic reactions,[8] and higher excretion rates[9] effectively as nanoparticles have several unique physical and chemical properties that are different from the normal materials. Nanoparticles possess higher chemical neutrality and physical activity. Bioavailability can also be enhanced by the synthesis of nanoparticles which increases the surface area.[10] There are several natural materials or systems which are in the nanoscale, such as milk with the nanoscale spherical colloid casein micelle,[11] globular proteins in the circulatory fluids,[12] bacteria, viruses, etc. Many materials having a complicated structure in the nanoscale seem to be smooth on gross examination. Nanomaterials existed in the environment, but their presence or beneficial effects were not known earlier which limited their applications. There have been several advances in synthesis and characterization of nanomaterials recently, which have fueled a boom in the study and applications of nanoscale materials.[12]

2. Production of nanoparticles for animal applications

Production of nanoparticles in the laboratory can be achieved through physical, chemical, or biological methods. Each of these methods has their own advantages and disadvantages and is suitable for specific functions.

Applications of Multifunctional Nanomaterials
https://doi.org/10.1016/B978-0-12-820557-0.00011-4

2.1 Physical method

Nanominerals are synthesized by various physical methods which include pulsed laser Ablation, electric arc discharge, gas phase synthesis, physical vapor deposition, chemical vapor deposition, evaporation–condensation, and ball milling-annealing methods. In the physical method pulsed laser ablation, the size of the nanomaterials is controlled using the laser parameters, such as fluence, wavelength, and pulse duration. Vaporization–condensation is a physical method of synthesis which can be done using a tube furnace.[13] Evaporation–condensation can also be done together with laser ablation[14] for physical synthesis.[15] Ball mills are used to grind materials to nanosize for use in livestock nutrition.[16] High-energy ball milling technology exposes a definite quantity of materials to repeated action of hitting balls. This method is used for synthesizing nanominerals, providing higher efficiency than conventionally used mills.[17] Physical methods of synthesis have the advantage of being free from solvent contamination, while there is maximum recovery of nanominerals.[18]

2.2 Chemical method

Chemical methods of synthesis are mostly used to produce nanominerals for animal feed inclusion as it is cheap and less time consuming.[19] Chemical methods have been preferred over physical method because the chemical reduction of mineral salts is more suitable to reduce the particle size. The nanoparticles produced using physical methods have a wider range of particle size, while it is more uniform in chemical methods.[20] Hence, using chemical methods, effective and controlled production of bulk quantity is possible. Reduction of mineral salts by chemical methods is the most convenient way to reduce the size of the particles.[21] However, there is a chance of toxicity caused by the chemicals that are used for synthesis. Hence, eco-friendly chemicals of plant and fungal origin are used as reducing agents to synthesize nanomineral particles and it is called green synthesis.[22] Transition metal colloids can be synthesized by the chemical reduction of transition metal salts, photochemical, sonochemical or thermal decomposition, reduction, displacement of ligands from organometallics, and electrochemical reduction.[20]

The role of zinc oxide (ZnO) in industrial sector has been a topic of research due to its fascinating antibacterial properties. Fabrication of ZnO nanoparticles by sol-gel method has been reported by Husna et al.[23] Mild sol-gel method can be used for the fabrication of ZnO nanoparticles from the precursor of zinc acetate. These ZnO nanoparticles are assessed using Fourier Transform Infrared to find the characteristic peak shown by ZnO. scanning electron microscopy (SEM) is used to study the structure of the nanoparticles and estimate its particle size.

2.3 Biological method

The synthesis of nanoparticles through biological methods can be used for various applications. Nanotechnology critically needs the development of eco-friendly processes which are reliable for the synthesis of nanoparticles of metal oxides.[24] Metal nanoparticles of various shape and size can be synthesized using microorganisms such as bacteria, actinomycetes, fungi, and yeast.[25] Green synthesis of mineral nanoparticles is an efficient, easy, and eco-friendly approach.[19] This process has also been found to reduce the toxicity involved in chemical

synthesis.[26] Methods of biosynthesis of nanoparticles using either plant extracts or microorganisms are now emerging as an effective alternative to the physical and chemical synthetic methods.[27] Several plants, algae, bacteria, fungi, and viruses have been found to be effective for the energy efficient production of mineral nanoparticles that are not toxic and inexpensive.[28]

Synthesizing nanominerals using plant materials is simpler and has an upper hand as there is only a single synthesis procedure, the product recovery is easy from the final solutions, the process is eco-friendly, not toxic, compatible for biomedical applications, and cost effective.[29] Metal nanoparticles have been synthesized successfully from *Carica papaya*,[30] *Aloe vera*,[31] *Avena sativa*,[32] *Sesbania drummondii*,[33] and latex of *Jatropha curcas*.[34] Even though there are several advantages, difficulty in product recovery, maintaining the culture and culture media, and time taken for the formation of nanoparticles are among the main disadvantages of biological method of mineral nanoparticle synthesis.[19]

3. Biomedical applications of nanoparticles

Several promising biomedical applications of nanoparticles that are used extensively are documented here. They have been schematically represented in Fig. 23.1.

3.1 Imaging

There are several research findings showcasing the advantages of nanoparticles in human and animal imaging technologies. The superparamagnetic iron oxide nanoparticles (SPIONs) are increasingly used in magnetic resonance imaging (MRI) of hepatocellular carcinomas. SPIONs are also being applied in magnetic fluid hyperthermia treatment for cancers in addition to their ability for magnetic targeting of drugs.[35] Nanoparticles of iron, gadolinium, and manganese were applied as contrast agents for MRI and positron emission tomography imaging.[36] In a study using a mouse model, biodegradable polybutylene cyanoacrylate–based nanoparticles coated with polysorbate 80 were tried as contrast agent carriers for passing the blood–brain barrier and visualizing amyloid plaques.[37]

3.2 Antimicrobials

The use of nanoparticles in treating bacterial infections is gaining importance. Certain nanopowders have strong antimicrobial properties. They can destroy more than 90% of bacterial species which come in contact. The use of silver and gold nanoparticles for coating surgical implants especially in orthopedic implants has been reported to provide an efficient antimicrobial cover.[38] Moreover, 100 nm nanoparticles of silver and titanium dioxide have been selected as effective coatings for surgical masks due to their antimicrobial effects.[39] Furthermore, the development of effective vaccines against bacteria using antigen-coated nanoparticles is an emerging field in biomedical research.[40]

3.3 Immunology

Calcium phosphate nanoparticles act as adjuvants for viral agents, as a major alternative for aluminum salts.[41] Viral vaccines with calcium phosphate as an adjuvant show a higher immunoglobulin G but a lower immunoglobulin E response when compared with alum-

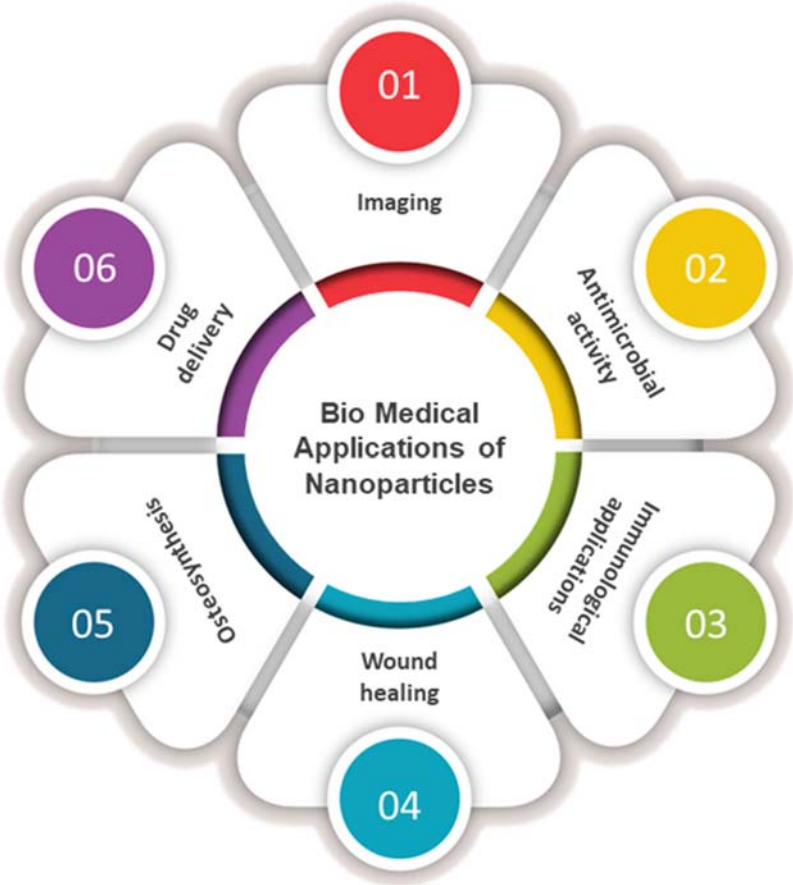

FIGURE 23.1 Biomedical applications of nanoparticles.

based vaccines.[41] Antigen conjugation to the surface of nanoparticles initiated B-cell activation. Nanoparticles coated with cellular membrane have been found to control toxins that damage cell membranes and divert their action far from their targets. This mechanism ensured an effective presentation of the antigen while removing the virulence of the toxin.[40]

3.4 Wound healing

Self-assembling nanofiber scaffolds of peptides enhance the regeneration of axons at the site of an injury. Damaged optic tract was restored in a hamster using peptide nanofiber scaffold presenting a new biomedical technique for repair and restoration of tissues and especially the repair of central nervous system.[42]

3.5 Osteosynthesis

Topographical signals can be transmitted by electrically conductive nanofibers leading to the degradation of the scaffold and simultaneously facilitating the repair of skeletal tissue. These scaffolds can stimulate osteosynthesis while triggering little immune response. There have

been many innovations in the process of manufacturing scaffolds with electrospinning. The hydrophobic characteristics of polymeric nanomaterials have been overcome using surfactants. There have been developments in structure of scaffolds like that of cotton wool. New combinations like chitosan and silk fibroin composites result in the production of proosteogenic proteins like bone morphogenetic protein (BMP-2) which indicates bone stimulating effects.[43]

3.6 Drug delivery

Several nanomedicines have been developed for the treatment and prevention of infectious diseases which affect the nervous system. Antimicrobial drugs which are nano formulated can be used to target the brain endothelial cell receptors promoting its transfer across the blood–brain barrier. The most appropriate ligand is coated on the nano-formulated antimicrobials and it can be administered systemically. It will find and bind to a blood–brain barrier cell or an appropriate carrier cell that would transport it across the barrier. Once it passes the barrier, the drug can be released by the free nanoparticles or macrophages controlling the microbial infection. The infections which affect the central nervous system for which nanomedicines are being developed comprise bacterial meningitis, rabies, malaria, and HIV.[44] Targeted delivery of therapeutic agents to tumors using nanoparticles responsive to magnetic fields improved the drug levels in the tumor compared to drugs with no magnetic property. MRI of viable xenografts and SEM show that silica-coated nanoparticles responsive to magnetic fields can be magnetically guided and their extravasation increased dramatically.[45]

Employment of magnetically responsive nanoparticles (MNPs) for targeting the therapeutics to tumor sites has been reported by Klostergaarda et al.[46] Magnetically responsive nanoparticles, particularly superparamagnetic iron oxides, are reported to enhance the drug levels in the tumor compared to normal drugs in efforts to overcome tumor resistance. Hence, MNPs were injected on mice with orthotopic tumors and tracked by MRI and SEM both indicated successful tumor localization of MNPs. MNPs were also modified with polyethylene glycol (PEG) and the clearance of this compared by estimating signal attenuation in liver due to iron accumulation. The results suggested that PEG substitution could retard the rate of MNP plasma clearance, which may allow greater magnetically enhanced tumor localization.[46]

4. Potential application of nanoparticles in animal production

The use of nanoparticles for applications in animal production has been an emerging field of research. Nanoparticles have several beneficial applications in animal production like molecular biological agents, reproductive aids, diagnostic tools, biocides, drug and nutrient delivery, and nutraceuticals.[47] There are many functionalized nanoparticles which are efficient agents for the cellular transfer of diagnostic and therapeutic compounds.[48] Plasmid encoding, fluorescent reporter nanoproteins can be used for genetic manipulation.[49] Nanoparticle-bound antibodies or lectins recognize damaged spermatozoa via surface markers resulting in their purification.[50] Bacterial cell walls get destabilized by nanopolymers disrupting the homeostasis of the organism making it lethal and resulting in antibacterial action.[51] Antibiotics can be loaded on nanopolymers, which in turn shuttle the antibiotic to the target site or its close proximity.[52] Nanopolymers can be conjugated with metal nanoparticles to obtain a combined nutrient

delivery.[53] Gastric degradation of nutrients can be prevented by nanopolymer encapsulation resulting in increased intestinal absorption.[54] Metal nanoparticles having magnetic properties are used as diagnostic tools for MRI by dispersing them throughout the body.[55] Methotrexate conjugated fluorescent carbon nanoparticles have been successfully used for drug delivery, targeting lung cancer cells for diagnostic imaging.[56] Using surface markers on the spermatozoa that are recognized by nanoparticle-bound antibodies or lectins has shown improvement in the reproductive ability by identifying and removing damaged sperms.[50]

5. Minerals in animal nutrition

Minerals are essential for digestive and biosynthetic processes which lead to the growth of animals. Minerals are classified into two classes based on their dietary requirement. The major or macrominerals are calcium (Ca), phosphorus (P), magnesium (Mg), sodium (Na), potassium (K), sulfur (S), and chloride (Cl) and trace minerals or microminerals, which are iron (Fe), copper (Cu), zinc (Zn), cobalt (Co), selenium (Se), manganese (Mn), and iodine (I).

The macrominerals Ca and P are responsible for improving the texture and tensile strength of the bone in growing animals. Ca plays an important role in making animals metabolically and physiologically active. It is also an integral part of nerve impulses and nerve transmission, blood coagulation, muscle contraction, secretions of the digestive system, and hormonal balance in the body. P is involved in cell wall components and part of cell contents as phospholipids, phospho-proteins, and nucleic acids. Mg is involved in several biochemical processes. The action of this mineral is strongly associated with Ca and P. The Na and K regulate cellular fluid volume, acid base equilibrium, and active transport of nutrients across the cell membrane. Cl is essential for the transport of carbon dioxide and oxygen.

The microminerals Fe, Cu, Zn, Co, Mn, I, and Se are essential for several body functions. The Fe forms an integral part of hemoglobin and is necessary for oxygen transport to the cells. Cu is essential for the synthesis of hemoglobin, heart functions, and bone metabolism. Zinc can reduce the stress in animals and thereby increase milk production. Selenium is added in feed as a potent antioxidant, to enhance the fertility rate and to improve immunity against infectious diseases. Cobalt deficiency has been found to cause rough hair coat, stumbling gait, and reduction in immunity. Manganese deficiency can result in skeletal abnormalities and reproductive inefficiency. Iodine is essential for synthesis of thyroxin, which regulates metabolic rate of body.

Nanominerals used as feed additives in livestock feed yield favorable responses in growth, immunity, and reproduction. It enhances growth, immunity, and improves the feed efficiency of the animals and poultry.

5.1 Nanominerals as feed additives

Mineral intake in adequate levels and its effective absorption is essential for several metabolic functions including immune response to pathogenic challenge, reproduction, and growth. Mineral supplementation is essential in order to achieve optimum production in current animal production systems. The growth and reproduction rate of animals also get reduced due to the deficiency. As the status of trace minerals declines, the immunity and

enzyme functions are also affected. Several experiments on dietary supplementation of nano-minerals and their effects on various metabolic processes are discussed here.

5.1.1 Nano calcium

Ca is a very essential macromineral having vital functions in the body of all animals. It is the most abundant mineral in the body and mostly found in the skeletal system. Dietary intake of calcium carbonate ($CaCO_3$) is very essential for normal bone condition, nerve impulse transmission, muscle contraction, blood clotting, and also maintaining the cell integrity.

Ovariectomized rats, fed with nano Caenriched milk, showed a better total alkaline phosphatase ratio, mineral density in the bones, as well as reduction in bone resorption.[57] Nano $CaCO_3$ supplementation in poultry feed has shown beneficial effects in the growth and production performance with better shell thickness and specific gravity observed in the eggs.[58]

Nano $CaCO_3$, which was studied by inclusion in the purified diet of rat models, was prepared by particle milling for 20 h at 1000 rpm. The particle size obtained was in the range of 2−50 nm. The samples that were examined by X-ray diffraction revealed that the crystalline phase increased with an increase of $CaCO_3$ concentration.[59] Various actions of nano Ca are presented in Table 23.1.

TABLE 23.1 Actions of calcium and copper nanoparticles when used as feed additives in animal feed.

	Mineral	Action	Reference
1	Nano Calcium	1. Ovariectomized rats • better total alkaline phosphatase ratio, mineral density in the bones and reduction in bone resorption 2. Chicken • Better growth, production performance • Better egg shell thickness and egg specific gravity	1. Lei et al (2009) 2. Ganjigohari et al (2017)
2	Nano Copper	1. Turkeys Improved hemoglobin and antioxidant status of fresh breast meat. 2. Chicken (In-ovo injection) • Increase in hematocrit value and improvement in the leukocyte count. • Better body weight gain, feed conversion ratio, carcass content of muscles, and meat characteristics of broiler chicken.	1. Otowski et al (2019) 2. Natalia et al (2015)

5.1.2 Nano copper

Cu is a trace mineral and indispensable in animal nutrition. It has a significant role in synthetic processes like the synthesis of hemoglobin, vasculogenesis, and angiogenesis. It also acts as a catalyst in the metabolic reactions. Cu directly influences the hepatic cholesterol synthesis by reducing hepatic glutathione concentration.[60] Cu is essential for normal functioning of the metabolic reactions in the organism, while its daily requirement is low.

It was found that the digestibility coefficient of Cu, hemoglobin, and the antioxidant status of fresh breast meat increased in turkeys which were fed Cu nanoparticles when compared with those maintained on Cu sulfate supplements.[61]

A comparative study of eggs that are injected in-ovo with 50 ppm colloidal Cu nanoparticles and those injected in-ovo copper sulfate when incubated revealed that the use of colloidal Cu nanoparticles resulted in an increase in hematocrit value, and improvement in the leukocyte count. However, the glucose and cholesterol levels in the serum were reduced. The Cu nanoparticles had a positive effect on body weight gain, feed conversion ratio, carcass content of muscles, and meat characteristics of broiler chicken. Thus, nano Cu may be considered as a potential replacement of Cu salts.[62] The actions of Cu nanoparticles as a feed additive are depicted in Table 23.1.

5.1.3 Nano zinc

Zinc nanoparticles supplemented in feed has been found to enhance growth. It has also improved the feed conversion efficiency in piglets.[63] The growth rate, serum glucose, and alkaline phosphatase in poultry was better on Zn nanoparticle (ZnNP) supplementation.[64] ZnO nanoparticles improve the immunity of the animals, reducing the somatic cell count in subclinical mastitis and increasing the milk production in lactating cows.[65] Broilers orally supplemented with ZnO nanoparticles had a significantly lower serum cholesterol level when compared with the other groups.[66] Incidence of diarrhea is significantly reduced when supplementing ZnO nanoparticles in the diet.[67]

Broiler chicken fed a diet supplemented with nanoparticles of ZnO had high superoxide dismutase and catalase levels but reduced concentration of malondialdehyde (MDA) when compared with the inorganic ZnO fed group. ZnO nanoparticles supplementation in the diet showed a rise in the total lymphocyte count, macrophages, and serum IgY compared to the control, resulting in a better immune status. IgY antibody concentration was observed to be higher in birds supplemented with ZnO nanoparticles. The phagocytic index was also observed to be better in the groups supplemented with ZnO nanoparticles.[68] Broilers supplemented with ZnNPs showed better growth performance, feed conversion ratio, and dressing percentage with a reduction in the cost of production.[69] The functions of Zn nanoparticles have been summarized in Table 23.2.

ZnNPs can change the kinetics of rumen fermentation in ruminants and also alter the percentage of the volatile fatty acids produced.[70] ZnO nanoparticles supplemented in vitro displayed an enhancement in the growth of rumen microbes, microbial protein synthesis in the rumen, and efficiency in energy utilization in the early phase of incubation.[71]

A higher level of Zn concentration in the spermatozoa of buffaloes is essential for their viability and fertility.[72] Zn deficient nutrition can result in reduction in the male fertility due to the poor quality of sperms.[73] Zn-deficient diets were found to cause an increase in

TABLE 23.2 Actions of nano iron and nano selenium when used as additives in animal feed.

3 Nano Zinc	1. Pigs • Improved the feed conversion efficiency in piglets 2. Chicken • Better growth rate, serum glucose and alkaline phosphatase • High superoxide dismutase and catalase levels • Better immune status with increase in the total lymphocyte count, macrophage count and higher serum IgY • Higher phagocytic index 3. Ruminants • Alter the Kinetics of rumen fermentation in ruminants and Percentage of the volatile fatty acids. • Enhancement in the growth of rumen microbes, microbial protein synthesis in the rumen	1. Yang et al (2006) 2. Mishra et al (2014), Hafez et al (2020) 3. Sarker et al (2018), Hackmann et al (2015)

abortions in pregnant sheep.[74] Thus, dietary supplementation of ZnNPs can possibly eliminate these reproductive disturbances and thus improve the economics of farming. A tabular representation of the actions of ZnNPs is given in Table 23.2.

5.1.4 Nano iron

Nano iron (Nano Fe) compounds which were synthesized by scalable flame aerosol technology have better iron bioavailability in vivo in rats when compared to $FeSO_4$. This results in far lesser color change in food matrices than that of conventionally used iron fortifiers. Stainable Fe could not be detected in the gut wall, gut-associated lymphoid tissue, or other tissues of rats which were fed with nano Fe–containing compounds, suggesting no adverse effects. Preparing nanoparticles of Fe compounds having poor water solubility increases their absorption and bioavailability when fed orally, thus improving their nutritional value.[10] Rats fed nano ferric phosphate did not have any adverse histological effects, enabling its use as feed additives.[75]

The better bioavailability of iron nanoparticles added to the feed of poultry is due to the high surface activity and penetration into cells. Various activated processes improve the intracellular metabolism. The broiler chicken feed containing nanoparticles of iron at half the dose of ferric sulfate fulfills the requirement of the birds.[76]

TABLE 23.3 Actions of nano iron and nano selenium when used as additives in animal feed.

4	Nano iron	1. Chicken • Nanoparticles of iron at half the dose of ferric sulfate fulfills the requirement • Increase in the intestinal weight in broilers • Cecum and duodenum length increased • Higher width of the villi in Jejunum	1. Nikonov et al (2011), Laledashti et al (2020)
5	Nano Selenium	1. Better antioxidant properties and lower toxicity 2. Immunostimulating effect 3. Increase in the antifungal activity of bacteria by enrichment 4. Reduce hepatic carcinoma in mice	1. Wang et al (2007) 2. Kojouri et al (2012) 3. Kheradmand et al (2014) 4. Popova (2002)

Feeding of iron nanoparticles in-ovo led to an increase in the intestinal weight in broilers. The caecum and duodenum length increased on in-ovo injection of iron nanoparticles. The width of the villi in jejunum and the surface area were higher in this group of chicken.[77] It has been depicted in Table 23.3.

5.1.5 *Nano selenium*

Selenium is an efficient antioxidant which prevents lipid peroxidation.[78] Hollow spherical selenium nanoparticles (SeNPs) showed antioxidant properties at lower dietary inclusion levels, which reduced the risk of selenium toxicity.[79] SeNPs were shown to have antioxidant properties and lower toxicity than selenomethionine.[80]

SeNPs have shown an immunostimulating potential which is stronger and faster than Na_2SeO_3 when compared with the antioxidant defense system. This is due to an increase in the chemotactic and respiratory burst activities of neutrophils.[81]

The viability of *Candida albicans* in humans has been significantly reduced after exposure to SeNPs-enriched *Lactobacillus* spp. This indicates an increase in the antifungal activity of the bacterial strains by means of enrichment with SeNPs, preventing a pathogenic fungal infection in immunocompromised individuals.[82]

The administration of nanoselenium has been found to reduce hepatic carcinoma in mice.[83] Lung tumor could be prevented by the use of 1,4-phenylenebis (methylene) selenocyanate.[84] Cancer cells sensitized to selenium were found to show better response to conventionally used anticancer drugs. Selenium sensitized prostate cancer cells underwent apoptosis induced by the anticancer drug paclitaxel.[85] Poultry reared on nanoselenium supplemented diets were found to have a higher body weight, better feed consumption, improved immunity status, and good tissue selenium deposition.[84]

Meat type poultry reared on diets supplemented with SeNPs showed an increase in the gutathione peroxidase (GPX), superoxide dismutase (SOD) and catalse, which indicated an improved immune status of the birds.[86] Layer chicken reared with SeNPs supplementation in feed showed also a better cellular and humoral immunity. The inclusion in feed was also found beneficial improving the body weight, feed consumption ratio, antioxidant status, immunity, and tissue Se deposition in grower birds.[87]

The dietary inclusion of SeNPs has a beneficial effect in environmental protection by prevention of pollution caused by the excessive use of inorganic selenium in feed.[88] SeNP supplementation in the diet produced better rumen fermentation and feed utilization in cattle and goat. The rumen microbial activity, activity of digestive microorganisms, and the enzyme activity were found to be improved in the SeNPs.[89] These actions have been summarized in Table 23.3.

5.1.6 Nano silver

Silver nanoparticles (AgNPs) show antibacterial properties against both Gram-positive and Gram-negative bacteria which have encouraged its use as an antibacterial agent in certain coatings.[90] As the size of AgNPs decreases, their efficacy as an antibacterial agent increases caused by an increase in the concentration of Ag + ions produced.[91] AgNPs at a dose of 0.5 mg/kg body weight injected in rabbits resulted in a lower plasma total cholesterol and triglycerides concentration than the values observed in the control rabbits. The treated rabbits had low total antioxidant capacity and high glutathione peroxidase and MDA.[92]

5.1.7 Nano chromium

Chromium (Cr) is an essential trace mineral widely distributed in the body. It acts as a glucose tolerance factor reducing the glucose level in the blood for maintaining normal blood glucose level.[93]

Cr nanocomposites (CrNPs) have high bioavailability due to its high surface area. Pigs supplemented with Cr nanocomposites showed better carcass characteristics, pork quality, and an increase in the Cr deposition in the muscles. The dietary supplementation of CrNPs reduced back fat thickness and carcass fat percentage in pigs. It increased the area of longissimus muscle. The weight of longissimus and semimembranosus muscles significantly increased in the CrNPs fed groups compared to the Cr picolinate. Drip loss in the meat decreased in pigs fed CrNPs.[94]

CrNPs added to feed were found to significantly reduce the serum levels of glucose, urea nitrogen, triglyceride, cholesterol, and non−esterified fatty acid. The total protein, high-density lipoprotein, and lipase activity were significantly higher in pigs offered diets containing CrNPs signifying the favorable health effects. The serum insulin-like growth factor level also increased. The cortisol and insulin levels were significantly reduced. The immunoglobulin M and immunoglobulin G contents in plasma were found higher in the CrNPs supplemented group.[95]

In poultry CrNPs supplementation in diet improved the Cr and Ca accumulation in the liver and egg. It also improved the retention of Zn and Mn in layer chicken.[96] Broilers under heat stress supplemented CrNPs at level of 1000 ppb and Cr picolinate at level of 1500 ppb improved the lymphocyte count and antibody titers against avian influenza and infectious bronchitis[97] (Table 23.4).

TABLE 23.4 Activity of silver and chromium nanoparticles when used as feed additive in animal feed.

6	Nano Silver	1. Antibacterial agent in certain coatings • Antibacterial properties against both Gram-positive and Gram-negative bacteria 2. Rabbit - Oral supplementation • Lower plasma total cholesterol and triglycerides concentration • Low total antioxidant capacity and high glutathione peroxidase and malondialdehyde	1. Strobel and Pratsinis (2007) 2. Abdelsalam et al (2019)
7	Nano Chromium	1. Pigs • Better carcass characteristics, pork quality, and an increase in the chromium deposition in the muscles. • Reduced back fat thickness and carcass fat percentage in pigs. • Decreased drip loss in meat • Higher total protein, high density lipoprotein and lipase activity 2. Chicken • Improved chromium, zinc, magnesium and calcium levels in the liver and egg • Improved the lymphocyte count and antibody titers against Avian Influenza and Infectious Bronchitis in broilers under heat stress • Improved the retention of zinc, iron, and calcium	1. Wang and Xu (2004) 2. Sirirat et al (2013), Farhad and Alireza (2017)

6. Toxicological effects of nanominerals

A critical fact to be considered with engineered nanomaterials is the toxicity. There are many reports where nanomaterials have a negative impact on nontarget organs.[98] Chromic oxide, Cu oxide are some nanomaterials which were reported to cause several adverse effects on nontarget organs leading to critical issues like tissue damage and immune status reduction.[99]

Nanoparticles of graphene oxide and gold were studied for their effects on the kidney in mice after injection for 4 weeks. Serum biochemical examination using the enzymatic method included the kidney function tests, serum creatinine, and urea.[100]

Esraa et al. studied the impact of nanoparticles in animals particularly in weight and kidney condition. Kidney tissues of all groups of mice were subjected to histopathological examination to observe changes in the glomerular and renal tubular epithelial cells. The results of the examination of both the treated and control groups showed no significant changes which suggests that the toxicity, e.g., atrophy of the glomerular and tubular epithelial cells is very low.[100]

Chicken supplemented with nano-ZnO in the feed at the rate of 100 mg/kg produced eggs with very thin shelled eggs. The addition of ZnNPs in feed was found to adversely affect bone mechanical properties like shear force and shear stress force.[101] ZnNPs supplemented lambs showed reversible hepatocyte swelling, while irreversible changes like eosinophilic hepatocyte necrosis and multifocal interstitial nephritis were also observed which are severe toxic changes.[102]

AgNPs were found to be toxic to human lung cells irrespective of the particle coating. Inhalation of AgNPs and the subsequent intracellular release of Ag^+ ions have toxic effects.[103]

7. Conclusion

Nanotechnology has evolved with several developments, with major applications in the livestock industry. The various methods employed for the synthesis of nanoparticles for multiple applications and their environmental effects are discussed in this chapter. Advances in biomedical applications of nanoparticles are elaborated with special reference to the current trends in animal production and the livestock industry. The use of nanoparticles in the tumor therapy, tumor imaging, targeted drug delivery, antimicrobial activity, and surgical implants is dealt with. This chapter also offers an overview of the functions of minerals and applications of nanoparticles in animal nutrition with a detailed insight into nanominerals. There is ample opportunity for further development and research in the field of nutritional supplements. The challenges, safety risks, and limitations associated with the toxicity need to be addressed through further research to enable efficient utilization of nanoparticles in animal nutrition.

References

1. United Nations [August 21, 2014]. *Questions about nanotechnology*. 2012. Available from: https://www.epa.gov/chemical-research/research-nanomaterials.
2. Pramanik P, Krishnan P, Maity A, Mridha N, Mukherjee A, Vikas R. *Application of nanotechnology in agriculture, environmental nanotechnology*vol. 4. Springer; 2020. p. 317–48.
3. Peters RJ, Bouwmeester H, Gottardo S, Amenta V, Arena M, Brandhoff P. Nanomaterials for products and application in agriculture, feed and food. *Trends Food Sci Technol* 2016;**54**:155–64.
4. Pinar TS, Ismail S, Baykalir BG, Mutlu SI, Salem AZM. Nanotechnology and nano-propolis in animal production and health: an overview. *Ital J Anim Sci* 2018;**17**(4):921–30.
5. Dasgupta N, Ranjan S. *Nanotechnology in food sector an Introduction to food grade nanoemulsions*. Springer; 2018. p. 1–18.
6. Gopi M, Pearlin B, Kumar RD, Shanmathy M, Prabakar G. Role of nanoparticles in animal and poultry nutrition: modes of action and applications in formulating feed additives and food processing. *Int J Pharmacol* 2017;**13**:724–31.
7. Gunasekaran T, Haile T, Nigusse T, Dhanaraju MD. Nanotechnology: an effective tool for enhancing bioavailability and bioactivity of phytomedicine. *Asian Pac J Trop Biomed* 2014;**4**(Suppl. 1):S1–7. https://doi.org/10.12980/APJTB.4.2014C980.

8. Liang M, Kohli M, Smith A. *ACS Nano* 2013;**7**(11):9518–25.
9. Longmire M, Choyke PL, Kobayashi H. Clearance properties of nano-sized particles and molecules as imaging agents: considerations and caveats. *Nanomedicine* 2008;**3**(5):703–17. https://doi.org/10.2217/17435889.3.5.703.
10. Hilty FM, Arnold M, Hilbe M. Iron from nanocompounds containing iron and zinc is highly bioavailable in rats without tissue accumulation. *Nat Nanotechnol* 2010;**5**(5):374–80.
11. Fox PF. Milk proteins: general and historical aspects. In: Fox PF, McSweeney PLH, editors. *Advanced dairy chemistry,–volume 1; proteins*. 3rd ed. New York: Kluwer Academic-Plenum Publishers; 2003. p. 1–48.
12. Michael AR. Naturally occurring nanoparticles in food. *Curr Opin Food Sci* 2015;**7**:14–9.
13. Cristina B, Ivan IP. Nanomaterials, and nanoparticles: sources and toxicity. *Biointerphases* 2007;**2**(4):18–71.
14. Ingale AG, Chaudhari AN. Biogenic synthesis of nanoparticles and potential applications:An eco-friendly approach. *J Nanomed Nanotechol* 2013;**4**:165.
15. Iravani S, Korbekandi H, Mirmohammadi SV, Zolfaghari B. Synthesis of silver nanoparticles: chemical, physical, and biological methods. *Res Pharm Sci* 2014;**9**(6):385–406.
16. Cardenas G, Meléndrez M, Cruzat C, Díaz J. Synthesis of tin nanoparticles by physical vapour deposition technique (vd). *Acta Microsci* 2007;**1**:1–2.
17. Koch CC. Synthesis of nanostructured materials by mechanical milling:Problems and opportunities. *Nanostruct Mater* 1997;**9**:13–22.
18. Pentimalli M, Bellusci M, Padella F. High-energy ball milling as a general tool for nanomaterials synthesis and processing. In: Aliofkhazraei M, editor. *Handbook of mechanical nanostructuring*; 2015.
19. Swain PS, Rajendran D, Rao SB, Dominic G. Preparation, and effects of nano mineral particle feeding in livestock: a review. *Vet World* 2015;**8**(7):888–91. https://doi.org/10.14202/vetworld.2015.888-891.
20. Roucoux A, Schulz J, Patin H. Reduced transition metal colloids: a novel family of reusable catalysts. *Chem Rev* 2002;**102**(10):3757–78. 2002.
21. Lane R, Craig B, Babcock W. Materials engineering with nature's building blocks. *AMPTIAC Newslett Spring* 2002;**6**:31–7.
22. Rajendran D, Thulasi A, Jash S, Selvaraju S, Rao SBN. Synthesis, and application of nano minerals in livestock industry. In: Sampath KT, Ghosh J, Bhatta R, editors. *Animal nutrition and reproductive physiology (recent concepts)*. Delhi: Satish Serial Publishing House; 2013. p. 517–30.
23. Husna AM, Krismastuti FSH. Fabrication of zinc oxide nanostructure as antibacterial agent. *AIP Conf Proc* 2019;**2175**:1.
24. Kulkarni N, Muddapur U. Biosynthesis of metal nanoparticles: a review. *J Nanotechnol* 2014;**2014**:8. Article ID 510246.
25. Oremland RS, Herbel MJ, Blum JS, Langley S, Beveridge TJ, Ajayan PM, Sutto T, Ellis AV, Curran S. Structural and spectral features of selenium nanospheres produced by Se-respiring bacteria. *Appl Environ Microbiol* 2004;**70**(1):52–60.
26. Sharma D, Kanchi S, Bisetty K. Biogenic synthesis of nanoparticles: a review. *Arab J Chem* 2019;**12**(8):3576–600.
27. Lee, H-J, Lee G, Jang NR, Yun JH, Song JY, Kim BS, Nano Science and Technology Institute. (2011). Biological synthesis of copper nanoparticles using plant extract. In Nanotechnology conference; Nanotechnology 2011; technical proceedings of the 2011 NSTI Nanotechnology Conference and Expo; NSTI Nanotech 2011 proceedings; Advanced materials, CNTs, particles, films and composites (Vol. 1, pp. 371–374). CRC Press.
28. Shah M, Fawcett D, Sharma S, Tripathy SK, Poinern GEJ. Green synthesis of metallic nanoparticles via biological entities. *Materials* 2015;**8**(11):7278–308.
29. Mittal AK, Uttam YC, Banerjeea C. Synthesis of metallic nanoparticles using plant extracts, Biotech. *Advances* 2013;**31**(2):346–56.
30. Konjari RS, Jacob AA, Jayanthi S, Ramalingam C, Ethiraj AS. Investigation of biogenic silver nanoparticles green synthesized from *Carica papaya*. *Int J Pharm Pharmaceut Sci* 2015;**7**(3):107–10.
31. Sharma S., Kumar K., Aloe-vera leaf extract as a green agent for the synthesis of CuO nanoparticles inactivating bacterial pathogens and dye, J Disp Sci Technol, 42 (13), 1950 1962
32. Amini N, Amin G, Azar ZJ. Green synthesis of silver nanoparticles using Avena sativa L. Extract. *Nano Med Res J* 2017;**2**(1).
33. Sharma NC, Sahi SV, Nath S, Parsons JG, Gardea-Torresde JL, Pal T. Synthesis of plant-mediated gold nanoparticles and catalytic role of biomatrix-embedded nanomaterials. *Environ Sci Technol* 2007;**41**(14):5137–42. https://doi.org/10.1021/es062929a.

34. Bar H, Bhui DK, Sahoo GP, Sarkar P, De SP, Misra A. Green synthesis of silver nanoparticles using latex of Jatropha curcas. *Colloids Surf A Physicochem Eng Asp* 2009;**339**(1–3):134–9.
35. Sharkey J, Starkey Lewis PJ, Barrow M, et al. Functionalized superparamagnetic iron oxide nanoparticles provide highly efficient iron-labeling in macrophages for magnetic resonance-based detection in vivo. *Cytotherapy* 2017;**19**(4):555–69.
36. Shen Z, Wu A, Chen X. Iron oxide nanoparticle based contrast agents for magnetic resonance imaging. *Mol Pharm* 2017;**14**(5):1352–64. https://doi.org/10.1021/acs.molpharmaceut.6b00839.
37. Koffie RM, Farrar CT, Saidi LJ, William CM, Hyman BT, Spires-Jones TL. Nanoparticles enhance brain delivery of blood-brain barrier-impermeable probes for in vivo optical and magnetic resonance imaging. *Proc Natl Acad Sci U S A* 2011;**108**:18837.
38. Bottagisio M, Lovati AB, Galbusera F, Drago L, Banfi G. A precautionary approach to guide the use of transition metal-based nanotechnology to prevent orthopedic infections. *Materials* 2019;**12**:314.
39. Chaitanya B, HiragondaA S, KshirsagaraV V, Dhapteb T, Khannaa P, Joshia PV. Enhanced anti-microbial response of commercial face mask using colloidal silver nanoparticles. *Vacuum* 2018;**156**:475–82.
40. Gao W, Thamphiwatana S, Angsantikul P, Zhang L. Nanoparticle approaches against bacterial infections. *Wiley Interdiscip Rev NanomedNanobiotechnol* 2014;**6**(6):532–47. https://doi.org/10.1002/wnan.1282.
41. He Q, Mitchell AR, Johnson SL, Wagner-Bartak C, Morcol T, Bell SJ. Calcium phosphate nanoparticle adjuvant. *Clin Diagn Lab Immunol* 2000;**7**(6):899–903.
42. Ellis-Behnke R, Liang YX, You SW, Tay DKC, Zhang S, Schneider GE, So KF. Peptide nanofiber scaffold for brain repair and axon regeneration with functional return of vision. Where do we go from? *Nanomed-Nanotechnol Biol Med*. 2006;**2**:317. https://doi.org/10.1016/j.nano.2006.10.151.
43. Kim BR, Nguyen TBL, Min YK, Lee BT. In vitro and in vivo studies of BMP-2-loaded PCL-gelatin-BCP electrospun scaffolds. *Tissue Eng* 2014;**20**:3279.
44. Upadhyay RK. Drug delivery systems, CNS protection, and the blood brain barrier. *BioMed Res Int* 2014:869269.
45. Aihua F, Robert JW, Bryan RS, Joyce M, Chris E, Demir A, Samira G, Shan XW, Sanjiv SG. Fluorescent magnetic nanoparticles for magnetically enhanced cancer imaging and targeting in living subjects. *ACS Nano* 2012;**6**(8):6862–9. https://doi.org/10.1021/nn301670a.
46. Klostergaarda J, Banksonb J, Woodwardc W, Gibsond D, Seeneyd C. Magnetically responsive nanoparticles for vectored delivery of cancer therapeutics. *AIP Conf Proc* 2010;**1311**(1):382–7.
47. Barkalina N, Jones C, Kashir J, Coote S, Huang X, Morrison R, et al. Effects of mesoporous silica nanoparticles upon the function of mammalian sperm in vitro. *Nanomedicine* 2014;**10**(8):59–70.
48. Agarwal S, Zhang Y, Maji S, Greiner A. PDMAEMA based gene delivery materials. *Pharmaceut Res* 2007;**24**:1590–8.
49. Tang JCY, Szikra T, Kozorovitskiy Y, Teixiera M, Sabatini BL, Roska B, Cepko CL. A nanobody-based system using fluorescent proteins as scaffolds for cell-specific gene manipulation. *Cell* 2013;**154**:928–39.
50. Odhiambo JF, DeJarnette JM, Geary TW, Kennedy CE, Suarez SS, Sutovsky M, et al. Increased conception rates in beef cattle inseminated with nanopurified bull semen. *Biol Reprod* 2014;**91**:1–10.
51. Xu LQ, Li NN, Chen JC, Fu GD, Kang E. Quaternized poly(2(dimethylamino)ethyl methacrylate)-grafted agarose copolymers for multipurpose antibacterial applications. *RSC Adv* 2015;**5**:61742–51.
52. Turos E, Reddy GSK, Greenhalgh K, Ramaraju P, Abeylath SC, Jang S, et al. Penicillin-bound polyacrylate nanoparticles: restoring the activity of B-lactam antibiotics against MRSA. *Bioorg Med Chem Lett* 2007;**17**:3468–72.
53. Wang MQ, Wang C, Li H, Du YJ, Tao WJ, Ye SS, et al. Effects of chromium loaded chitosan nanoparticles on growth, blood metabolites, immune traits and tissue chromium in finishing pigs. *Biol Trace Elem Res* 2012;**149**:197–203.
54. Haham M, Ish-Shalom S, Nodelman M, Duek I, Segal E, Kustanovich M, et al. Stability and bioavailability of vitamin D nanoencapsulated in casein micelles. *Food Funct* 2012;**3**:737–44.
55. Soenen SJH, Himmelreich U, Nuytten N, Pisanic TR, Ferrari A, De Cuyper M. Intracellular nanoparticle coating stability determines nanoparticle diagnostics efficacy and cell functionality. *Small* 2010;**6**:2136–45.
56. Ajmal M, Yunus U, Matin A, Haq NU. Synthesis, characterization, and in vitro evaluation of methotrexate conjugated fluorescent carbon nanoparticles as drug delivery system for human lung cancer targeting. *J Photochem Photobiol, A B* 2015;**153**:111–20.
57. Lei Z, Xiaoying Z, Xingguo L. Ovariectomy-associated changes in bone mineral density and bone marrow haematopoiesis in rats. *Int J Exp Pathol* 2009;**90**(5):512–9. https://doi.org/10.1111/j.1365-2613.2009.00661.x.

58. Ganjigohari S, Ziaei N, Ghara A, Tasharrofi S. Nano-calcium carbonate: effect of nano calcium on egg production performance and plasma calcium of laying hens. *J Anim Physiol Anim Nutr* 2017;**102**:225–32.
59. Mulyaningsih N, Tresnasari D, Ramahwati M, Juwono A, Soejoko D, Astuti D. Synthesis and characterization of nano sized CaCO3 in purified diet. *AIP Conf Proc* 2017;**1862**:030066. https://doi.org/10.1063/1.4991170.
60. Kim JW, Chao PY, Allen A. Inhibition of elevated hepatic glutathione abolishes copper deficiency cholesterolemia. *Faseb J* 1992;**6**:2467–71.
61. Otowski K, Ognik K, Kozłowski K. Growth rate, metabolic parameters and carcass quality in turkeys fed diets with different inclusion levels and sources of supplemental copper. *J Anim Feed Sci* 2019;**28**(3):272–81.
62. Natalia MS, Monika Ł, Agnieszka W, Ewa S, Jan N, Abdullah S, Sławomir J, André C. In ovo administration of copper nanoparticles and copper sulfate positively influences chicken performance. *J Sci Food Agric* 2016;**96**(9):3058–62. https://doi.org/10.1002/jsfa.7477. Epub 2015 Oct 29.
63. Yang ZP, Sun LP. Effects of nanometre ZnO on growth performance of early weaned piglets. *J Shanxi Agric Sci* 2006;**3**:024.
64. Mishra A, Swain RK, Mishra SK, Panda N, Sethy K. Growth performance and serum biochemical parameters as affected by nano zinc supplementation in layer chicks. *Indian J Anim Nutr* 2014;**31**(4):384–8.
65. Rajendran D. Application of nano minerals in animal production system. *Res J Biotechnol* 2013;**8**(3):1–3.
66. Sahoo A, Swain RK, Mishra SK, Jena B. Serum biochemical indices of broiler birds fed on inorganic, organic and nano zinc supplemented diets. *Int J Recent Sci Res* 2014a;**5**(11):2078–81.
67. Sahoo A, Swain RK, Mishra SK. Effect of inorganic, organic and nano zinc supplemented diets on bioavailability and immunity status of broilers. *Int J Adv Res* 2014b;**2**(11):828–37.
68. Hafez A, Nassef E, Fahmy M, et al. Impact of dietary nano-zinc oxide on immune response and antioxidant defense of broiler chickens. *Environ Sci Pollut Res* 2020;**27**:19108–14. https://doi.org/10.1007/s11356-019-04344-6.
69. Lina T, Jianyang J, Fenghua Z, Huiying R, Wenli L. Effect of nano-zinc oxide on the production and dressing performance of broiler. *Chin Agric Sci Bull* 2009;**02**.
70. Sarker NC, Keomanivong F, Borhan M, Rahman S, Swanson K. In vitro evaluation of nano zinc oxide (nZnO) on mitigation of gaseous emissions. *J Anim Sci Technol* 2018;**60**:27. https://doi.org/10.1186/s40781-018-0185-5. Published 2018 Nov 9.
71. Hackmann TJ, Firkins JL. Maximizing efficiency of rumen microbial protein production. *Front Microbiol* 2015;**6**:465. https://doi.org/10.3389/fmicb.2015.00465. Published 2015 May 15.
72. Ahmed WM, El-Tohamy MM, Borghese A, Failla S, Barile VL. Zinc profile in blood and semen of breeding buffalo bull with particular emphasis on age variation and semen characteristics. In: *Proceedings of the 5th world buffalo congress, royal palace, Caserta, Italy, 13–16th October. 1997*; 1997. p. 825–8.
73. Colagar AH, Marzony ET, Chaichi MJ. Zinc levels in seminal plasma are associated with sperm quality in fertile and infertile men. *Nutr Res* 2009;**29**(2):82–8.
74. Campbell JK, Mills CF. The toxicity of zinc to pregnant sheep. *Environ Res* 1979;**20**:1–13.
75. Rohner F., Frank O. E., Arnold M, Hilbe M, R. Biebinger, Frank E, Sotiris E. P, Wolfgang L, Richard F. H. and Michael B. Z, Synthesis, characterization, and bioavailability in rats of ferric phosphate nanoparticles, J Nutri 137(3), 614–619
76. Nikonov IN, Folmanis YG, Folmanis GE, et al. Iron nanoparticles as a food additive for poultry. *Dokl Biol Sci* 2011;**440**:328–31.
77. Laledashti MA, Saki AA, Rafati AA, Adolmaleki M. Effect of in-ovo feeding of iron nanoparticles and methionine hydroxy analogue on broilers chickens small intestinal characteristics. *Acta Sci Anim Sci* 2020;**42**.
78. Sadeghian S, Kojouri GA, Mohebbi A. Nanoparticles of selenium as species with stronger physiological effects in sheep in comparison with sodium selenite. *Biol Trace Elem Res* 2012;**146**(3):302–8.
79. Gao X, Zhang J, Zhang L. Hollow sphere selenium nanoparticles: their in vitro anti hydroxyl radical effect. *Adv Mater* 2002;**14**(4):290–3.
80. Wang H, Zhang J, Yu H. Elemental selenium at nano size possesses lower toxicity without compromising the fundamental effect on selenoenzymes: comparison with selenomethionine in mice. *Free Radic Biol Med* 2007;**42**(10):1524–33.
81. Kojouri GA, Sadeghian S, Mohebbi A, MokhberDezfouli MR. The effects of oral consumption of selenium nanoparticles on chemotactic and respiratory burst activities of neutrophils in comparison with sodium selenite in sheep. *Biol Trace Elem Res* 2012;**146**(2):160–6.

82. Kheradmand E, Rafii F, Yazdi MH, Sepahi AA, Shahverdi AR, Oveisi MR. The antimicrobial effects of selenium nanoparticle-enriched probiotics and their fermented broth against Candida albicans. *Daru* 2014;**22**:48.
83. Popova NV. Perinatal selenium exposure decreases spontaneous liver tumorogenesis in CBA mice. *Cancer Lett* 2002;**179**(1):39–42.
84. Sarkar B, Bhattacharjee S, Daware A, Tribedi P, Krishnani K, Minhas P. Selenium nanoparticles for stress-resilient fish and livestock. *Nanoscale Res Lett* 2015;**10**(1):371.
85. Prokopczyk B, Rosa JG, Desai D, et al. Chemoprevention of lung tumorigenesis induced by a mixture of benzo(a)pyrene and 4-(methylnitrosamino)-1-(3-pyridyl)-1-butanone by the organoselenium compound 1,4-phenylenebis (methylene) selenocyanate. *Cancer Lett* 2000;**161**(1):35–46.
86. Prasoon S, Jayanaik V, Malathi CSN, Narayanaswami HD. Effects of dietary supplementation of inorganic, organic and nano selenium on antioxidant status of giriraja chicken. *Int J Curr Microbiol App Sci* 2018;**7**(08):2399–412.
87. Mohapatra P, Swain RK, Mishra SK, Behara T, Swain P, Behura NC, Sahoo G, Sethy K, Bhol BP, Dhama K. Effects of dietary nano—selenium supplementation on the performance of layer-grower birds. *Asian J Anim Vet Adv* 2014;**9**(10).
88. Jia X, Li N, Chen J. A subchronic toxicity study of elemental nano-Se in Sprague Dawley rats. *Life Sci* 2005;**76**:1989–2003.
89. Shi LG, Xun W, Yue W, Zhang C, Ren Y, Liu Q, Wang Q, Shi L. Effect of elemental nano-selenium on feed digestibility, rumen fermentation, and purine derivatives in sheep. *Anim Feed Sci Technol* 2011;**163**:136–42.
90. Strobel R, Pratsinis SE. Flame aerosol synthesis of smart nanostructured materials. *J Mater Chem* 2007;**17**:4743–56.
91. Jackson JB, Halas NJ. Silver nanoshells: variations in morphologies and optical properties. *J Phys Chem B* 2001;**105**:2743–6.
92. Abdelsalam M, Al-Homidan I, Ebeid T, Abou-Emera O, Mostafa M, El-Razik MA, Shehab-El-Deen M, Ghani SA, Fathi M. Effect of silver nanoparticle administration on productive performance, blood parameters, antioxidative status, and silver residues in growing, rabbits under hot climate. *Animals* 2019;**9**(10):845. https://doi.org/10.3390/ani9100845.
93. Schwartz K, Mertz W. Chromium III. Glucose tolerance factor. *Arch Biochem Biophys* 1959;**85**:292–4.
94. Wang MQ, Xu ZR. Effect of chromium nanoparticle on growth performance, carcass characteristics, pork quality and tissue chromium in finishing pigs. *Asian-Australas J Anim Sci* 2004;**17**. https://doi.org/10.5713/ajas.2004.1118.
95. Wang M, Xu Z, Zha L, Lindemann, Merlin. Effects of chromium nanocomposite supplementation on blood metabolites, endocrine parameters, and immune traits in finishing pigs. *Anim Feed Sci Technol* 2007;**139**(1):69–80.
96. Sirirat N, JinJenn L, Tsubg HY, Lien TF. Effect of different levels of nanoparticles chromium picolinate supplementation on performance, egg quality, mineral retention, and tissues minerals accumulation in layer chickens. *J Agric Sci* 2013;**5**(2):150–9. ref.43.
97. Farhad H, Alireza T. Effects of supplemental chromium picolinate and chromium nanoparticles on performance and antibody titers of infectious bronchitis and avian influenza of broiler chickens under heat stress condition. *Vet Res Forum* 2017;**8**(3):259–64.
98. Ivask A, Kurvet I, Kasemets K, Blinova I, Aruoja V, Suppi S. Size-Dependent toxicity of silver nanoparticles to bacteria, yeast, algae, crustaceans and mammalian cells in vitro. *PLoS One* 2014;**9**(7):e102108.
99. Horie M, Keiko N, Endoh N, Kato H, Fujita K, Miyauchi A, Nakamura A, Shinichi K, Yamamoto K, Niki E, Yoshida Y, Iwahashi H. Chromium (III) oxide nanoparticles induced remarkable oxidative stress and apoptosis on culture cells. *Environ Toxicol* 2013;**28**. https://doi.org/10.1002/tox.20695.
100. Esraa HK, Rua K, Majid J. Effect of graphene oxide and gold nanoparticles on kidney parameters of male mice. *AIP Conf Proc* 2020;**2213**:020145. https://doi.org/10.1063/5.0000167.
101. Olgun O, Yildiz AO. Effects of dietary supplementation of inorganic, organic or nano zinc forms on performance, eggshell quality, and bone characteristics in laying hens. *Ann Anim Sci* 2017;**17**(2):463–76.
102. Najafzadeh H, Ghoreishi SM, Mohammadian B, Rahimi E, Afzalzadeh MR, Kazemivarnamkhasti M. Serum biochemical and histopathological changes in liver and kidney in lambs after zinc oxide nanoparticles administration. *Vet World* 2013;**6**:534–7.
103. Gliga A, Skoglund S, OdnevallWallinder I, Fadeel B, et al. Size dependent cytotoxicity of silver nanoparticles in human lung cells: the role of cellular uptake, agglomeration, and Ag release. *Part Fibre Toxicol* 2014;**11**:11.

This page intentionally left blank

CHAPTER

24

Use of lectin-functionalized and lectin-targeted nanoparticles for multiple therapeutic applications

K.R. Rekha Mol and A.A. Mohamed Hatha

Department of Marine Biology, Microbiology and Biochemistry, School of Marine Sciences, Cochin University of Science and Technology, Kochi, Kerala, India

1. Introduction

Carbohydrates are a vital part of fundamental classes of biomolecules present in all cell membranes and walls, their study can help to understand cell biology and to discover new therapeutic and diagnostic approaches. Carbohydrates are involved in many biological processes, such as cell adhesion, cancer metastasis, immune response, and intracellular trafficking, which are guided by carbohydrate-protein interactions.[1] Understanding of the glycosylation pattern variation in intracellular and membrane proteins as well as of proteins in biological fluids have revealed direct links between glycosylation and various pathologies.[2–6] Glycans with huge structural diversity are much less studied compared to proteins and nucleic acids. Therefore, the complicated task of their exploration determines the scope of effective tools for detecting carbohydrate structures and their changes under various physiological and pathological conditions.[7] Because of significant drawbacks in glycan detection and identification methods, the use of carbohydrate-binding proteins becomes a promising tool for their detection and further development of therapeutic agents.

Lectins are a group of nonimmune proteins with at least one catalytic domain that binds either a soluble carbohydrate or the carbohydrate portion of a glycoconjugate noncovalently and reversibly with high specificity.[8] The high affinity and specificity in carbohydrate-lectin interactions are attributed to many factors, such as lectin valence, the structure of binding sites, their spatial arrangement, hydrogen bonding, apolar interactions, extended sites, secondary sites, and the occurrence of residual charged groups in carbohydrates, etc.[9–11] Lectins were first isolated from plants and the advancement of technologies promoted the isolation and purification of numerous lectins from animals, microorganisms, and viruses.[12,13]

Applications of Multifunctional Nanomaterials
https://doi.org/10.1016/B978-0-12-820557-0.00023-0

Furthermore, these proteins are involved in several processes such as cell adhesion, triggering of intracellular signal pathways, protein trafficking, and host-pathogen relation.[14,15]

Nanoparticles (NPs) based therapeutic agents have been widely used to solve various clinical problems after several decades of technological developments.[16] NPs represent a large family of materials and most of the well-studied nanoparticles include Quantum dots, carbon nanotubes, paramagnetic nanoparticles, liposomes, and gold nanoparticles.[17] Several features of these nanomaterials including their diverse size, hydrophilic properties, and charge characteristics allow them to function as carriers for the efficient delivery and absorption of drugs. In favor of their small diameter and sufficient design, nanoparticles can easily be accessed and transported to different body sites such as the blood-brain barrier via the stability in circulation. Moreover, NPs can carry engineered (polymeric NPs) ligand molecules like antibodies or aptamers based on the target, which enables them to recognize specific cells. These features all support the use of NPs for drug delivery.[16,18,19] Various means of therapeutic applications of NPs include drug delivery, gene delivery, vaccine delivery, imaging, and antimicrobial potential.[20–24] Characteristic biocompatibility, nonimmunogenicity, and noncarcinogenicity make NPs harmless warrant tools for gene delivery.[25] Another feature facilitating selective gene targeting is in vivo stability and the lowering of nonspecific uptake. Even though the drugs have good therapeutic potentials, high doses of that may be required due to the availability of low concentrations at the target site resulting in the development of side effects. Thus, the use of a drug delivery system based on NPs enables accelerated transportation to the site of action and prevents rapid clearance of drugs thereby prolonging their existence in the body and reducing side effects.[26]

The focus of research in the designing of functional NPs possesses optical and bio-affinity properties and further efforts for the preparation of functionalized delivery systems, allowing active targeting in the field of diagnosis and therapy.[27] The functionalization of nanomaterials with lectins or carbohydrates results in novel hybrid materials with synergistic properties, which conglomerate the optical, electrical, and/or magnetic properties of the nanoparticle together with the biological activity of the biomolecule.[28] Carbohydrates and lectins linked to several nanostructures, such as dendrimers, fullerenes, carbon nanotubes, metallic nanoparticles, liposomes, polymers, and Quantum dots (QDs), have already been used for protein/glycan detection, cell imaging, cell separation, enzyme immobilization, etc.[28–30] Cellular uptake of ligand-anchored NPs occurs via receptor-mediated endocytosis pathways, where the lectin or carbohydrate ligands linked to the NP is recognized by the specific receptor on the targeted cell surface. Immediately after the ligand-receptor complex formation, it is quickly internalized due to its high binding capacity leading to an efficient cellular uptake of the ligand-conjugated NP by the desired cells. As in the case of functionalization of gold nanoparticles with a Ribosome Inactivating Protein (RIP) such as EHL having high affinity and specificity for Tn antigen on target cells demonstrates an opportunity to standardize Winter Aconite (*Eranthis hyemalis*) plant lectin (EHL)'s biological effects.[31]

Cell surface glycosylation is an inevitable aspect of cell metabolism, as evidenced by the variations in the glycosylation profiles of proteins and lipids on the surface of abnormal cells in comparison to normal cells. Carbohydrate-binding proteins (lectins) specifically binding to those glycoprotein biomarkers can be used for diagnostic purposes. Likewise, carbohydrate-based therapeutic molecules can be developed to specifically target cells via endogenous ligands of the cells. Nanoparticles possess unique physicochemical properties, which are not

intrinsic to the related substances in molecular form, enabling to obtain of engineered structures with multiple desired functions.[32] Hence, lectin or glycan functionalized nanoparticles exploiting the nonimmune, reversible, and specific lectin-carbohydrate interaction can be used for the development of promising agents with strong therapeutic potential.[33–37]

2. Lectins

Lectins are ubiquitous natural proteins specifically and reversibly recognizing and binding carbohydrate complexes being produced by such an ample array of different organisms from viruses to animals.[38–40] The interaction of agglutinins/lectins with biological receptor moieties did not have a catalytic or immune nature. Therefore, carbohydrate-specific antibodies or carbohydrate metabolic enzymes that cause structural changes in carbohydrate molecules when they interaction with them do not belong to the lectin group.[41] These carbohydrate-binding molecules are able to agglutinate various cells (e.g.,.erythrocytes), and the earliest description of the ability to agglutinate erythrocytes was believed to be by Peter Hermann Stillmark in 1888. However, the modern era of lectinomics began almost 100 years later. Structural studies indicated that the carbohydrate-binding activity of lectins was generated by a limited polypeptide segment designated as the carbohydrate recognition domain (CRD) and also, it is not a surprising fact that lectins are widely different in several aspects according to their origin, distinct characteristics such as molecular weight, amino acid sequencing, etc.[8,42,43] Lectins are commonly categorized into two: (1) lectins that are located intracellularly in the luminal compartments (L-type lectins, calnexin, and P-type lectin) and (2) lectins that are secreted or confined to the plasma membrane, function largely outside the cell, e.g., I-type lectins, C-type lectins (e.g., Gal receptors, Man receptors, selectins, or mannan-binding proteins (MBP), or galectins.[44] Even though, all lectins take part in both normal and pathological biological processes and all have varying degrees of interaction with the immune system.[45,46]

The specificity of lectin to recognize carbohydrates through carbohydrate binding sites promotes the identification of cell surfaces attached glycans, glycoconjugates, or free sugars, thereby detecting abnormal cells and biomarkers related to diseased conditions providing interesting results in experimental treatments of immunological diseases, wounds, and cancer. Another type of lectins was reported as modulators and tool markers in vivo and in vitro and also plays a role in the induction of mitosis and immune responses, contributing to resolving infections and inflammations. Other areas where lectins have also been utilized for biomedical applications, including anti-HIV, antitumoral, antimicrobial, antiinflammatory, and antinociceptive activities.[47] Lectins possess a significant role in diagnostics as they serve as powerful tools in immunological studies and can be employed as immunohistochemistry markers in various disease conditions. Lectin-based biosensors are useful for profiling cell types due to the expression of aberrant glycans on diseased and transformed cell surfaces.

Lectin-mediated bioadhesion has been a remarkable characteristic for the development of drug delivery systems and such lectins are frequently used as diagnostic probes and tumor-specific surface markers.[48] Moreover, compared to currently available glycan profile

detection methods, lectin-based assays assure a simple, inexpensive, and rapid alternative for glycosylation screening of protein drugs and for clinical diagnostic purposes.[49–53] The particular strategy of lectin-based Drug Delivery Systems (DDSs) is expected to improve the absorption and bioavailability of poorly absorbable drugs, peptides/proteins along with therapeutic DNA.[54] For lectin-based drug targeting, two strategies are there involving the use of either the oligosaccharide moiety or the lectin as a component of the drug delivery system.[55] Direct lectin targeting or glyco-targeting implicates DDS possessing carbohydrates (oligosaccharides or neoglycoconjugates) directed toward surface endogenous lectins for recognition and internalization by the cell. The reverse lectin targeting approach utilizes exogenous lectins as directing moieties that target whole DDS to glycoproteins or glycolipids expressed on the surface of particular cells.[56,57]

Studies on the purification and characterization of lectins were increased after the development of the affinity chromatography method and the advent of recombinant techniques in the golden era of lectin research including the elucidation of physicochemical properties, amino acid sequences, and 3D structures.[8,13,58–60] The characteristic multivalency of lectin is the main reason behind its strong avidity for glycosylated cell surfaces and also the ability to affect membrane dynamics. Bacterial lectins are able to bind to glycoconjugates on human tissues and are consequently thought to facilitate the first step of infection. The ability of lectins for making membrane invagination indicates that they could also play a vital role in the internalization of intracellular pathogens. In the past decades, there has been an exponential increase in the use of lectins owing to their potential to specifically and selectively target diverse glycosylated biological molecules with good sensitivity and has initiated very promising applications in the field of pharmaceutical sciences.[61–64]

The gastrointestinal route is the most convenient method for the delivery of drugs and vaccines because of its lower costs and patient compliance, and the supply can be made either orally or rectally. Although the formulations such as tablets or capsules are preferred for their relative simplicity, technologically GIT is one of the most challenging routes of administration. It is necessary to overcome diverse physico-chemical barriers that hinder the administration of active molecules orally and may result in poor drug bioavailability. The main obstacles are enzymatic degradation, peristalsis, and stability at acid pH or resistance to penetration on the surface of the mucosa.[65] Variety of approaches are used to deliver drugs locally into the colon via GIT, including time and pH-based systems, enzyme-triggered systems, and pressure-based systems. However, the most effective and specific ones are those methods that rely on biologic principles, such as the methods involving lectins.[66] This technique not only improves drug pharmacokinetics helping to overcome the hurdles toward drug delivery, but also shows several advantages for the patients. The most important ones are the prevention of side effects on healthy tissues and the increase in drug uptake by targeted cells, which permits to reduce the drug dosage.[51] The biorecognitive ligands like lectins possess a high affinity to receptors expressed on targeted biological locations allowing detection of the affected tissue and the release of the drug at its site of action. Because of peculiar features of multivalency and high specificity, the engineering of lectins allows the foundation of novel supramolecular tools, superlectins, neolectins, and Janus lectins with modified architecture, valency, and specificity.

2.1 Lectin-carbohydrate interactions

Structural basics behind the specific lectin-saccharide interactions have been obtained by several studies using X-ray crystallography and other instrumental techniques. Specific biorecognition of lectin-glycoconjugate is similar to that of antibody-antigen or enzyme-substrate interactions, which are mediated by hydrogen bonds, van der Waals interactions, and hydrophobic binding.[8,67–69] For instance, polar and less polar parts of galactose interact with different lectins through hydrogen bonds and hydrophobic interactions respectively.[70–72] Moreover, thermodynamic studies revealed that the dominant forces stabilizing the lectin-sugar complex seem to be hydrogen bonds and van der Waals interactions except for limited electrostatic interactions to specific monosaccharides such as various forms of sialic acid. Many lectins contain two or more carbohydrate-binding sites. The binding of lectins with monosaccharides is stabilized by means of numerous hydrogen bonds, mostly by Asp, Asn, and Gly residues. In general, lectins exhibit low affinity toward carbohydrates ($KD = 10^{-3}$–10^{-4} mol L^{-1}) when compared with antigen-antibody interactions where *KD* is in the subnanomolar range.[72–74] The most high-throughput analytical techniques in glycomics comprising advanced mass spectrometry (MS) combined with liquid chromatography; electrophoresis, and lectin/carbohydrate microarrays have been employed to study binding profiles and distinguished changes in the glycosylation pattern.[75] When compared to techniques such as enzyme-linked lectin assay and lectin microarrays that use labeled systems that generate color or fluorescence, biosensors can operate in a label-free approach reducing consumption of reagents and time (by minimizing steps). Even though the biosensing methods can be electrochemical, optical, mass, and thermal based on the type of signal transduction, electrochemical biosensors are more attractive. Electrochemical biosensors have been constructed using electrodes as sensing surfaces and they are rapid, practical, low-cost, and user-friendly assays and are commonly modified with polymers and nanomaterials (gold, silver, magnetic, etc.) to improve the analytical performance and immobilization of biorecognition elements, such as lectins.[76,77] Techniques such as electrochemical impedance spectroscopy (EIS) and voltammetry are used to measure alterations on the electrode surface and detect ligand-analyte interaction for effective glycoprofiling of a diverse range of samples. EIS measurements occur in accordance with the detection of changes in charge transfer resistance on the sensor surface after the interactions. Instead, voltammetric techniques such as cyclic voltammetry (CV), differential pulse voltammetry (DPV), and square wave voltammetry (SWV) are based on the detection of changes in the current signals generated under the application of potential on the electrode, in presence of a redox probe.[78] Electrochemical lectin-based biosensors are very attractive analytical tools of glycans with innumerous applications, such as cancer diagnostics,[79–81] drug delivery,[82] immunohistological studies,[83] analysis of pathogenic bacteria,[84] anti-HIV research, etc.[85] through detection of biomarkers. Moreover, variation in the spatial distribution of glycans can be analyzed as in the case of *Sambucus nigra* agglutinin (SNA) recognizes sialic acid linked to galactose via an α-2,6 linkage, while *Maackiaa murensis* agglutinin recognizes linkage of sialic acid to galactose via an α-2,3 linkage.

3. Nanoparticles (NPs) as potential therapeutic agents

NPs are made of various materials such as natural or synthetic polymers, lipids latex, ceramic particles, metal particles, and carbon particles. NPs can be used specifically either as carriers of drugs or as therapeutic molecules based on their physical and chemical properties. Nanotechnology is opening new horizons in medical applications as a result of its physicochemical properties, including its chemical composition, size, shape, structure, morphology, and surface properties.[86–88] Various nanoparticles offer considerable promise as quantitation tags for biological assays owing to their significant amplification and unique coding capabilities along with highly sensitive bioaffinity. Reference factors for the selection of nanomaterials in clinical applications are based on their surfaces, which are either hydrophilic or hydrophobic and the exhibition of surface charge and specific ligands.[89] Other than surface characteristics, the size, and shape of a nanoparticle have a key role in its biodistribution in vivo. In most cases, the effects of size have been studied with spherical-shaped particles, and also observed that particles less than 5 nm are rapidly cleared from the circulation through extravasation or renal clearance.[90,91]

The nanoparticle size should be so optimized that it should not escape from the kidney filtration. Drug delivery system-based nanoparticles should be large enough to prevent their speedy discharge into blood capillaries, but they should be small enough to escape from fixed macrophages stuck in the reticuloendothelial system, such as the liver and spleen.[92] Nanoparticles smaller than 10 nm, will be filtered by the kidneys. In addition, they will be captured by the liver if they are larger than 100 nm. Thus, the optimum nanoparticle size for effective in vivo applications is expected to be 10–100 nm. However, in vivo imaging and diagnostic prefers NPs of larger sizes. A larger particle can be selectively delivered to tumor tissues for therapeutic or diagnostic purposes due to enhanced permeability and retention effect.[93–95]

NPs have been studied by scientists to explore their value for clinical applications because of their active role in transporting drugs to the targeted cell as an inevitable part of a drug delivery system. When selecting materials for developing NPs to carry therapeutic agents, several constraints of agents need to be taken into account and overcome including their nonspecific distribution, toxicity, lack of targeting ability, poor solubility in water, and low therapeutic index. Therefore, therapeutic agents must be designed with optimum sizes, shapes, and surface properties to improve biodistribution, solubility, stability, and reduced immunogenicity.[96] For instance, silica-NPs and mesoporous silica NPs (MSNs) are nontoxic, and tasteless, and do not produce pollution levels as that of nonmetallic materials.

Additionally, high absorptivity and good plasticity make them suitable for disease treatment. It is also essential that metabolites or degradation products of NPs do not harm the human body or they must be decomposed and eliminated by the body effectively. For instance, the degradation products of poly (lactic-co-glycolic acid) PLGA-NPs are lactic acid and hydroxy acetic acid, which are also the byproducts of human metabolic pathways, suggesting the advantage of PLGA-NPs can be used in medical applications as biological material with no toxic side effects. It is reported that PLGA-docetaxel-NPs were used to treat breast cancer and their biodegradability and biocompatibility were also observed.[91] The drug concentration at the targeted orthotopic pancreatic ductal adenocarcinoma site increased in mouse models when silica was developed into MSNs further loaded with the antitumor drug oxaliplatin and a specific indoleamine 2,3-dioxygenase inhibitor.[97]

The studies by Refs. 98,99 revealed that gold NPs (Au-NPs) designed to act as a bidentate ligand enhanced the stability of N-heterocyclic carbene (NHC) ligands,[98] and liposomes were utilized for packaging nonwater soluble drugs exploiting their excellent water solubility, are NPs relatively efficient carriers of short genetic sequences that directly insert genes into cells for assembly.[99] Optimized ionizable cationic lipids are a significant factor for the successful phase III clinical trial of lipid NPs (LNPs) siRNA formulation. Furthermore, the Food and Drug Administration (FDA) approved the use of LNPs for the treatment of the hereditary condition transthyretin (TTR) mediated amyloidosis in 2018. At present, numerous ionizable lipids are under clinical research for utilizing in the treatment of various diseases, including cancer and viral infections.[100] Moreover, designing appropriate nano drugs for varied environments is crucial to suit different pathophysiological conditions, such as the spatial variations in the tumor microenvironment (TME) pH. The cationic nature of chitosan molecules containing free amino acids, can easily form salts in acidic solutions making them suitable as drug carriers for antitumor drugs in an acidic TME and for drug release after degradation.[101]

The functionalization of NPs with specific chemical moieties, called as ligands, results in the advent of multifunctional conjugates of immense biomedical applications, especially drug delivery, cancer therapy, tissue engineering, molecular biology, etc.[102] Ligands can be categorized based on their functions, such as stabilization, targeting, imaging, antiimmunogenics, and biocompatibility enhancement. Lectins are proteins found on the surface of certain cell types as receptors for binding specific sugar moieties. For instance, galactose-specific lectins and mannose-6-phosphate-specific lectins are found in the hepatic cells of mammals. Where as, another mannan-binding lectin, is distributed on the surface of immune cells. In addition to their own functions in the liver and immune system, these lectins may be exploited for drug delivery. As a major component of most cell surfaces, carbohydrates such as glycoproteins and glycolipids act as ligands for different receptors such as the lectins and participate in various cell-cell interactions. The ligand-carbohydrate interaction can thus be used in the drug delivery application in two ways.[103] There are two strategies to develop nanoparticle-based therapeutic agents based on lectin-carbohydrate interaction: (i) Direct lectin targeting, where the nanoparticle-bound drug is conjugated to a carbohydrate residue forming a glyconanoparticle drug to target cell surface lectins to achieve better efficacy of the drug. For example, intra-peritoneal administration of a mannan-methotrexate conjugate enhanced antitumor potential in leukemic mice,[104] (ii) In reverse lectin targeting, the nanoparticle is linked to a lectin (i.e., the lectinized nanoparticles), which in turn facilitates targeting of cell surface carbohydrate residues. For example, lectin-attached solid lipid nanoparticles (SLNs) are used in the delivery of insulin.[105]

4. Lectin-linked nanoparticles

Lectins can be used in the biomedical field either as diagnostic agents or as therapeutic agents. Targeted therapy is most probably the most challenging and worthwhile application of lectins in therapy. There are two ways in which lectins are used in targeted therapy, the first method involves the targeting toward cell surface glycans (reverse lectin targeting),

while the second method uses direct lectin targeting (where the targeting agent glycan has an affinity toward endogenous cell lectins).[105] Conventional methods, that have been used for studying carbohydrate-protein interactions were fluorescence spectroscopy-based approaches and enzyme-linked lectinosorbent assays (ELLA).[106,107] An important property of high sensitivity, promotes the most often use of fluorescence labeling in protein-carbohydrate interaction-based assays. However, delay in obtaining results due to the involvement of several time-consuming steps like labeling, incubation, and washing facilitates the rise of NPs as a potential tool with the ease-of-modification and good biocompatibility.[108–110] The functionalization of therapeutic nanoparticle constructs with ligands or biomolecules like lectins or glycans can enable targeted intracellular delivery of drugs, proteins, and genetic materials. Furthermore, NPs protect bioactive molecules from degradation in the physiological environment as well as permit controlled and targeted release of the drug. The emergence of various kinds of uncontrolled/overexpressed glycan moieties like N-acetylglucosamine and sialic acid moieties represent an unusual feature of cancerous cell membranes, and therefore, lectins specifically recognizing glycans (e.g., wheat germ agglutinin (WGA) have been used as drug carriers and potential antineoplastic drugs in biology and medicine.[111–114]

Lack of early diagnosis, drug-resistance, metastasis, and recurrence are major problems that are associated with human malignancies.[39,40] Recently, this has been noticed from cancer statistics data that human cancers are one of the main causes of death as compared to other diseases throughout the globe.[41,115–120] Human malignancies are one of the major concerns for medical health providers. Potential challenging factors related to lectins for successful implementation in therapeutic fields might be their poor stability, unspecific binding, and difficulties in production and purification.[121,122] Moreover, the degree of difference in the expression of glycans or glycan-binding proteins (lectins) could be exploited for the identification of novel biomarkers and might offer novel prospects for therapeutic intervention. In this context, the current study intends to explore the overall relevance and importance of lectin/glycan functionalization of nanoparticles such as AuNps, AgNPs, Magnetic NPs, Quantum dots, liposomes, etc. in the healthcare field for pharmacological delivery of multimeric glycans, lectins or selective inhibitors of lectin-glycan interactions with therapeutic effect.

4.1 Gold nanoparticles (AuNPs)

4.1.1 Lectin linked AuNps

In recent years colloidal gold nanoparticles (AuNPs) have long been exploited in science for their optical properties and are used routinely in both material science and biomedical sciences as bioimaging agents, therapeutic agents, and drug delivery vehicles.[123–126] The possibility to functionalize AuNPs with both therapeutic and imaging agents simultaneously makes them a powerful tool in cellular studies.[31] Gold nanoparticles can be functionalized with the lectin found in the tubers of the Winter Aconite (*Eranthis hyemalis*) plant (EHL) is a Type II Ribosome Inactivating Protein (RIP) with high affinity and specificity for target cells expressed with Tn antigen to fine-tune EHL's biological effects. Results obtained after successful synthesis of bioconjugated citrate gold nanoparticles (AuNPs@Citrate) with EHL indicated that an effective functionalization was attained by the addition of 100 μL of EHL

(1090 ± 40 μg/mL) over 5 mL of AuNPs ([Au^0] = 0.8 mM). The conjugates analyzed by UV-Vis spectroscopy, Dynamic Light Scattering (DLS), Zeta Potential analysis, Transmission Electron Microscopy (TEM), and biological assays on the effect of AuNPs@EHL with *Caenorhabditis elegans*, a free-living nematode commonly used for toxicological studies showed that EHL can be conjugated to gold nanoparticles retaining its elements of biocidal activity.[127]

Another study that has been reported for photodynamic therapy involved a gold nanoparticle functionalized with polyethylene glycol (PEG) conjugated jacalin bearing hydrophobic zinc phthalocyanine photosensitizer (C11Pc) moieties, inferred strong phototoxicity in HT-29 human colorectal adenocarcinoma cells (95%−98%) mainly due to the specific interactions between jacalin and the T-antigen (a Thomsen-Friedenreich antigen) expressed on the cell surface.[128] Cancer cell targeting using the jacalin can selectively deliver C11Pc-PEG gold nanoparticles to HT-29 cells with overexpressed T antigen. MTT viability assay showed that HT-29 colon cancer cell viability was reduced drastically on treatment with the jacalin conjugated nanoparticles compared to the nonconjugated particles. At a nanoparticle concentration of 1.15 μM C11Pc equivalent, jacalin targeted Photodynamic therapy (PDT) led to an exceptional reduction of 10% in HT-29 cell viability while incubation in the dark and nontargeted PDT treatment was noncytotoxic.[129] Similarly, as evidenced by the strong accumulation of *Ricinus communis* agglutinin (RCA) -conjugated gold nanoparticles onto HeLa cells, there is the possibility of the use of such conjugates for developing targeted drug delivery system against cervical cancerous cells.[130]

The ability to synthesize a nanoconjugate with the advantageous ability to bypass the blood-brain barrier (BBB) and selectively target neurons opens the door for numerous applications. It is demonstrated for the first time a three-part AuNP nanoconjugate engineered to deliver drugs, 1,3-dimethylxanthine (THP) and 1,3-dipropyl-8-cyclopentylxanthine (DPCPX), to a specific group of neurons mediated by wheat germ agglutinin (WGA) uptake. The AuNPs acts as a carrier to link the wheat germ agglutinin horse radish peroxidase (WGA-HRP) to the drug via a biodegradable ester bond and after intramuscular injection, the ester bond enables in vivo drug release in the cervical spinal cord and medulla nuclei targeted by WGA-HRP. Several in vivo studies are in progress to fully characterize the dose-response of both THP and DPCPX versions on the nanoconjugate as well as the short and long-term biodistribution and biological effects of the AuNPs. Injection of WGA-nanoconjugates into selected muscles would aid the release of the drug of choice to the associated motoneurons. Hence, there is significant relevance for the application of this potential engineered nanoconjugate across many neuromuscular disease and injury models.[131]

The results obtained by the additional linking of lectins to antibody-functionalized AuNPs for determining the levels of serum glycoprotein biomarkers established a generic platform for rapid, sensitive, and visual detection of glycosylation variations. In this work, an initial dynamic light scattering (DLS) study identified specific glycoprotein-lectin interactions solely present in the serum of hepatocellular carcinoma (HCC) patients compared to healthy controls that showed the altered fucosylation in Serum α-1-Acid glycoprotein. Based on the DLS data, a simple and rapid serological assay was developed by conjugating antibody-coated AuNPs with fucose-binding lectin *Aleuria aurantia* lectin (AAL). As a consequence of the activated aggregation of the AuNP probes in presence of lectin, the plasmon band was shifted from red to blue in response to the enhanced fucosylation of α-1-acid glycoprotein, which colorimetrically reported and made the basis of a rapid visual assay for

hepatocellular carcinoma. This protocol is unique for the detection of glycosylation change in other serum glycoprotein biomarkers in presence of low sample marker concentration (ng/mL), which is having the diagnostic implication in variation analysis of α-1-acid glycoprotein (AGP) -fucosylation in HCC samples.[132,133]

4.1.2 Glycan linked AuNps

The interaction of sugar-chain conjugated nanoparticles with proteins yields aggregates due to multiple sugar-binding sites and can be detected visually and spectroscopically.[134–136] In the past decade, carbohydrates have been increasingly studied due to their ubiquitous nature on the surfaces of proteins and cells, further lectins from various sources are employed for the purpose of glycocode deciphering.[137] Many carbohydrate-functionalized NPs usually immobilized on AuNPs through S–Au binding have been developed as affinity probes to facilitate the detection of carbohydrate-protein interactions like the use of trivalent α-2,6-thio-linked sialic acid ligand-functionalized AuNPs for human influenza virus.[138–140]

For the analysis alone, the use of glycosylated nanomaterials has gained increasing attention in recent years because NPs decorated with glycan structures in a multivalent form similar to the glycocalyx structures on cell surfaces could be used for the detailed study of glycan-lectin interactions.[141,142] In particular studies were done by Jayawardena et al.[116] NPs modified with different saccharide moieties such as lactose, arabinose, cellobiose, sucrose, mannose, glucose, and galactose were able to successfully distinguish four different lectins with different specificities includes Concanavalin A (Con A), soybean agglutinin, *Griffonia simplicifolia* agglutinin, and *Arachis hypogaea* peanut agglutinin by observing a red shift in the λ_{max} of the localized surface plasmon resonance (LSPR) absorption.[116] Such a library-oriented approach of glycan-linked NPs was later used to prepare polymer-stabilized glyco-AuNPs for a rapid, high-throughput, and 96-well microplate-compatible evaluation and identification of pathogenic lectins by taking into account measurements of red-to-blue color shift upon AuNP aggregation, which was monitored by a digital camera.[143] The study involves the functionalization of AuNPs with a mixed monolayer of zinc phthalocyanine and a lactose derivative. For the first time, a carbohydrate was used with a dual purpose, as the stabilizing agent of the AuNPs in aqueous solutions and as the targeting agent for breast cancer cells. The functionalization of the phthalocyanine-AuNPs with lactose led to the production of water-dispersible nanoparticles that are able to generate singlet oxygen and consequent cell death upon irradiation. The targeting ability of lactose toward the galectin-1 receptor on the surface of breast cancer cells was exploited in the in vitro studies with lactose-phthalocyanine functionalized AuNPs. The targeting studies showed the exciting potential of lactose as a specific targeting agent for galactose-binding receptors overexpressed on breast cancer cells.[144]

Worldwide, annual epidemics of seasonal influenza are estimated to be around three to five million cases of severe illness, and annual deaths of up to 650,000 are associated with respiratory diseases.[145] Subtype classification of Influenza A viruses has been done according to the combination of the proteins on their surface; hemagglutinins (HA) and neuraminidases (NA) as an example of H1N1 strain pandemic in 2009.[146] During infection, trimeric hemagglutinins displayed by influenza virus particles bind to sialosides on the surface of their host cells to facilitate internalization and zoonosis (interspecies transmission) can occur due to mutations in the hemagglutinin, enabling avian, porcine and other zoonotic influenza

viruses to infect humans.[147–151] Therefore, the study of hemagglutinin interactions with sialic acids is essential to increase our understanding of this global pathogen and also the discovery of new effective diagnostics and treatments.[152] During infection, the affinity is significantly increased by the cluster glycoside effect due to the multivalent presentation of both the viral hemagglutinin (~200–1000 copies/virus) and sialic acids on the host cell surface.[153,154] Gibson and coworkers have previously reported the development of multivalent gold/polymer hybrids with regard to dissecting glycan binding interactions.[155–158] The aim of this work was to develop a multivalent nanoparticle platform to prevent binding trends of influenza hemagglutinins toward multivalent sialic acid isomers. For that, a library-oriented screening of 27 nanoparticle formulations was done to optimize the size and linker length followed by 2,3- and 2,6-sialyllactosamine attachment to multivalent AuNPs. Colorimetric aggregation assays, DLS, and biolayer interferometry techniques were used to determine the binding affinities. A panel of hemagglutinins comprising human and avian were treated with the particles and results indicated that the multivalent presentation permitted significant cross-binding between human and avian strains, which may aid the discovery of novel tools for infections and zoonosis transmission.[159]

A combined effect of the specific functions of AuNSs, glycopolymer, and Con A facilitated the designing of a successful hybrid nanoplatform (HNP) system, HNP-Con A, for photothermal therapy of liver (HepG2) cancers. The glycopolymer P (DEGMA-*co*-OVNGmix) consists of thermal-responsive monomer, di (ethylene glycol) methyl ether methacrylate (DEGMA), galactose-containing (OVNGal) and glucose-containing (OVNGlu) monomers. Then, the glycopolymer is grafted on the AuNSs surface to form HNP, where OVNGal moiety can specifically recognize the asialoglycoprotein receptor (ACGPR) on hepatocytes, and OVNGlu can specifically recognize Con A. Therefore, the mechanism of action of HNP-Con A system toward liver cancers is in such a way that OVNGal will target the surface of hepatocytes, and then Con A can enter into HepG2 cells to effectively eradicate them. In addition, the heat generated due to the excellent photothermal ability of AuNSs, under near-infrared radiation will kill HepG2 cells as well.[160]

4.2 Silver nanoparticles (AgNPs)

AgNPs are one of the most widely used nanomaterials owing to their exceptional optical, photothermal, electrical, and biological properties. They exhibit profound use in a variety of everyday products, including home appliances, water filters, cosmetics, textiles, and food industry-related items. The most well-known feature of AgNPs is their antimicrobial effect, which favors the use of them also in the medical sector for the production of dressings, catheters, pacemakers, and vascular prostheses. They can also be used as a contrast agent in imaging diagnostics due to their photosensitizing and radiosensitizing properties.[161–164] Related to this, there is a report that revealed the conjugation of AgNPs with antifungal lectins isolated from an edible mushroom, *Agaricus bisporus* (Lange) Pilat. This particular lectin-silver nano conjugates inhibited about 89% of the conidial germination of the fungal pathogen of rice, *Curvularia lunata*. The antifungal activity of the conjugates was far higher other than showed by the individual use of lectins or AgNPs. In another exploration, a noncovalent complex of lectin from the seeds of *Butea monosperma* (BMSL) with AgNP, BMSL-AgNPs (BAgNPs) was prepared to combat uropathogenic *Escherichia coli* biofilms. BMSL is a

tetrameric protein reported to be specific to N-acetyl D-galactosamine, galactose, and lactose.[165,166] Results showed that the glycan recognition potential of lectin BMSL considerably enhanced the antibiofilm and antibacterial activities of AgNps at low concentrations. Moreover, BAgNPs exhibited antibacterial activity by affecting bacterial membrane integrity and imparting oxidative stress to bacteria.[167]

4.3 Magnetic nanoparticles (MNPs)

In recent years, interest in the application of MNPs in various fields like biomedicine and biotechnology has increased due to their effective binding potential of them toward ligands like proteins, peptides, enzymes, antibodies, and drugs. Typically, MNPs are composed of a magnetic core (Fe_2O_3 or Fe_3O_4) and a coating layer, which can be made of biocompatible polymers. In this layer, the functional groups that can easily bind to drug molecules are present, inhibit aggregation, and increase colloidal stability. The most specific property of MNPs, which are made of Fe_2O_3 or Fe_3O_4 core is the response toward an external magnetic field due to superparamagnetism; thereby they could be easily removed or separated from a mixture by the use of a magnetic field. This property is currently most exploited in separation techniques, especially in the separation of cells.[168–171] Validation of specific biological recognition potential of carbohydrates immobilized on MNPs was done using four lectin probes. Different lectins used as probes were Concanavalin A (Con A, a Man selective lectin), Wheat Germ Agglutinin (WGA, a GlcNAc and Sia selective lectin), *Bandeiraea simplicifolia* isolectin (BS-I, a Gal selective lectin and *Tetragonolobus purpureas* Agglutinin (TPA, a Fuc-selective lectin). A normal breast cell line 184B5 and nine types of representative cancer cells were used to study the possibility of using a magnetic glyco-nanoparticle (MGNP)-based system to detect and profile various cell types. Results based on the MR responses suggested active expression of fucose and sialic acid receptors on most of the cell lines under study and the presence of galectins, a family of galactose-specific lectins, GlcNAc receptors, and mannose receptors was also confirmed. The inability of sugar-free nanoprobe NP to bind any cells further established the authenticity of intrinsic carbohydrate-protein interactions as the reason behind the binding.[172]

Lectin-conjugated Fe_2O_3@Au NPs (lectin− Fe_2O_3@Au NPs) were reported to be employed as dual-modality contrast agents for in vivo MR and CT imaging. For that, they produced 22 nm Fe_2O_3@Au NPs, which have a long circulation time, and three lectins (ConA, RCA, and WGA) - Fe_2O_3@ Au NPs have been used to detect colorectal tumors (SW620) in BALB/C nude mice. The experimental results suggested that the lectin− Fe_2O_3@Au NPs had a capacity not only for dual mode MR and CT imaging in vitro but also for MR and CT imaging of colorectal cancer in vivo. Moreover, it was inferred that lectin could also be used as tumor-targeting ligand for synthesizing nanoparticle-based contrast agents.[173]

The latest investigations in this field are now focusing on the theranostic application of lectin-conjugated nanoparticles drug delivery systems with the combined ability to diagnose, deliver a drug and monitor the therapeutic response. In an investigation of using a lectin-conjugated paclitaxel-loaded MNP for leukemia theranostic application, the nanoparticle formulation showed a significantly higher efficacy (~67%) against chronic myelogenous leukemia cells (K562) compared to that of the native paclitaxel. A much longer circulation time

(T1/2 = 15 h) was reported for lectin-coupled paclitaxel nanoparticles related to the native paclitaxel in rats (T1/2 = 5 h).[174]

4.4 Europium doped nanoparticles

Monitoring of epithelial ovarian cancer by using a novel lectin-based approach for the detection of cancer-associated glycosylation of cancer antigen 125 (CA125), well-known mucin - derived cancer marker was reported. For that, highly fluorescent europium (III)-doped nanoparticles (Eu^{+3}-NPs) coated with the macrophage galactose-type lectin (MGL), enabled highly sensitive detection of CA125 marker on ovarian cancer cell line OVCAR-3. The clinical evaluation of the obtained results of the optimized assay based on CA125-MGL interaction exhibited good discrimination between the samples of epithelial ovarian cancer patients and those with endometriosis enabling early detection/screening of ovarian cancer.[175] A lectin-Eu^{+3}-NP dependent approach was utilized for the glycoprofiling of CA15-3 with a panel of 28 lectins in order to identify altered glycosylation of CA15-3 in the blood streams of breast cancer (BC) patients. CA15-3 is a tumor marker commonly used for monitoring patients with advanced BC. Among a panel of 28 lectin- Eu^{+3}-NP preparations tested, only two lectins exhibited satisfactory binding to the BC-associated CA15-3. Those lectins are WGA and recombinant human MGL, which recognize GlcNAc and GalNAc -containing epitopes frequently express on the surface of cancer cells respectively.[176–178] This study suggested that using CA15-3 WGA and CA15-3 MGL Eu^{+3}NPs assays in the plasma of metastatic BC patients were found to be more cancer-specific and more sensitive in distinguishing metastatic BC patients from healthy controls than conventional CA15-3 immunoassay.[179]

Another study demonstrated an effective utilization of spring snowflake *Leucojum vernum* lectin (LVA) - conjugated luminescent GaN: Eu^{+3} nanoparticles and WGA lectin-conjugated fluorescent fluorescein-containing polystyrene nanoparticles for the detection of dying cells (apoptotic and necrotic correspondingly). Because of high specificity, bright fluorescence, and low photobleaching, both types of nanoparticles can be easily applicable in most types of fluorescent microscopy and flow cytometry. Interestingly, an aspect of fluorescence emission in a very narrow red spectral range of GaN: Eu^{+3} nanoparticles, making them a very useful fluorescent nanolabel for multicolor in vivo detection systems.[180]

4.5 Silica NPs

The specific binding property of lectin *Ulex europaeus* Agglutinin-1 (UEA1) toward α-L-fucose has been exploited to distinguish human colorectal adenocarcinomas, adenomas, and polyposis coli from the normal epithelium.[181,182] Fluorescently-labeled mesoporous silica NPs (MSNs) with high surface areas and low systemic toxicities functionalized at its three topologically unique domains developed as targeted endoscopic contrast agents for early detection of polyps and nascent colorectal cancers.[183] For this, fluorescent label fluorescein 5(6)-isothiocyanate (FITC) was first cocondensed into the silica framework of MSNs followed by a coating of the exterior with two different lengths of polyethylene glycol (PEG) to increase their water solubility and diffusion through mucus. Lastly, fluorescent/PEGylated MSNs were coupled with UEA1 targeting premalignant lesions, a very sensitive detection method of early-stage colorectal carcinomas by in vivo imaging techniques.[184] A multifunctional

nanodevice featuring the synergistic properties of selectivity toward human osteosarcoma cells and pH-responsive antitumor drug delivery capability produces an amplification of the antitumor efficacy. This innovative nanodevice is based on doxorubicin (DOX)-loaded MSNs nanoplatforms primarily involve a polyacrylic acid (PAA) polymeric shell, anchored *via* an acid cleavable linker, to avoid early cargo release and provide the characteristic pH-responsive capability. Secondly, a targeting ligand lectin Con A grafted to PAA, to increase the selectivity toward cancer cells while retaining the viability of healthy cells. In vitro assays revealed that the degree of internalization of lectin-conjugated nanosystems into human osteosarcoma cells is two times more than in preosteoblastic cells. Moreover, the antitumor effect is increased up to 8-fold when compared to free drug and 100% antitumor efficacy against osteosarcoma cells compared to healthy bone cells obtained at very small DOX concentrations (2.5 μg mL-1). These outcomes affirm that the synergistic assembly into a unique nanoplatform increases antitumor activity with decreased toxicity toward healthy cells, which founds a new paradigm in targeted bone cancer therapy.[185]

4.6 Poly (lactic-coglycolic acid) PLGA NPs

Natural or synthetic polymers can be used for the synthesis of polymeric nanoparticles; also they can be biodegradable or nonbiodegradable in nature. The type of material used to synthesize nanoparticles determines its performance as a drug delivery agent and its therapeutic potential. The most significant features of these nanoparticles are their size and shape as it has been found that particles with a size of up to 100 nm are most readily absorbed by cells and preferentially their shape should be as spherical as possible. Benefits of the use of such systems include increased bioavailability of drugs, reduced degradation rates, fewer side effects, improved cellular uptake, targeted transport, and efficacy in controlled drug release. Natural polymeric materials include chitosan, collagen, dextran, or alginates and synthetic materials are polylactide (polylactic acid PLL), polycaprolactone (PCL), polyvinyl, polyethylene glycol (PEG), poly (lactic-coglycolic acid) (PLGA) for the production of polymeric nanoparticles.[186,187]

Even though the lectins involved in drug delivery systems possess beneficial anticancer properties, they are typically functionalized with nanoparticles only for the so-called "lectin direct targeting". Development of a nanoparticle formulation of novel WGA-conjugated isopropyl myristate (IPM)-incorporated PLGA nanoparticle for local delivery of paclitaxel to the lung demonstrated a superior in vitro cytotoxicity against A549 and H1299 cells due to an efficient cellular uptake via WGA-receptors.[188] Peanut agglutinin (PNA) and WGA decorated drug-loaded nanoparticles (NPs) were suggested for targeting and selective adhesion to the inflamed tissue in experimental colitis. Lectin-conjugated NPs exhibited a much higher binding and selectivity to inflamed tissue compared to normal NPs. Targeted NPs by using lectins, especially with PNA appear to be a promising tool in future IBD treatment.[189] The intranasal administration of lectin-functionalized PEG-PLGA nanoparticles was reported to be useful for treating schizophrenia. These nanoparticles were loaded with haloperidol and *Solanum tuberosum* lectin (STL). The conjugation of the particles with STL significantly reduced the dose of drug.[190] The WGA-conjugated PLGA nanoparticles with enhanced lectin receptor interaction on the alveolar epithelium can be used for treating tuberculosis.[191]

4.7 Quantum dots

Quantum dots (QDs) represent a class of fluorescent nanomaterials, which has been extensively applied in life science owing to their unique optical properties. These nanocrystals present remarkable beneficial properties such as high resistance to photobleaching and hold active surfaces for conjugations with different molecules, such as antibodies and lectins.[192,193] The abnormal expression of carbohydrates on the cell surface indicates the development of many diseases, pathogenicity, and resistance of microorganisms, making the study of alterations in glycan profile extremely relevant. Therefore, this study reported that green-emitting QDs-Cramoll bioconjugates can be used to evaluate the glucose/mannose content on yeast cell walls of *C. albicans*, *C. glabrata*, and *C. parapsilosis* sensu stricto. To the best of my knowledge, this is the first study that QDs-Cramoll conjugates were applied to analyze the glycocode of *Candida* species since currently available technologies can be considerably laborious. Morphological investigation of yeasts labeled with QDs-Cramoll conjugates indicated that *C. glabrata* (2.7 μm) was smaller when compared to *C. albicans* (4.0 μm) and *C. parapsilosis* sensu stricto (3.8 μm). Also, *C. parapsilosis* population was heterogeneous, presenting rod-shaped blastoconidia. Among all three species, more than 90% of cells were labeled by conjugates and further inhibition and saturation assays indicated that *C. parapsilosis* had a higher level of exposed glucose/mannose than the other two species. Therefore, QDs-Cramoll conjugates can be used as effective fluorescent nanoprobes for the detection of fungal species frequently involved in candidiasis based on glucose/mannose constitution on the cell walls.[194]

In the same way, saccharide-rich structures on the cellular surface of *Candida albicans*, one of the most common opportunistic fungi present in human beings were analyzed by Con A adsorbed on hydrophilic cadmium telluride - mercaptosuccinic acid (CdTe-MSA) QDs (emitting at 600 nm). The specificity of carbohydrate (mannose and glucose) recognition using QDs-ConA aids the dynamic monitoring of the surface expression changes in response to drugs.[195–198] Additionally, fluorescence images and flow cytometry analysis revealed strong labeling of cells due to specific recognition by the bioconjugates, further confirmed when a decrease in the cell labeling was observed after adding methyl-α-D-mannopyranoside. In another study, a similar formulation yielded increased intracellular retention of paclitaxel and an enhanced antiproliferative activity toward colon cancer cells (Caco-2 and HT-29 cells). Further study of the intracellular transport profile using QDs-loaded WGA-PEG nanoparticles in Caco-2 cells demonstrated that the cellular uptake of functionalized nanoparticles begins with the binding of WGA to its cell surface receptor, followed by particle uptake by clathrin and caveolae-mediated endocytosis.[199,200]

4.8 Liposomes

Liposomes are spherical vesicles made of a lipid bilayer with natural or synthetic phospholipids having unique properties as clinically-approved carriers of therapeutic molecules with a range of size between 50 and 300 nm. The nature of phospholipids used for liposome production determines their sensitivities to pH, temperature, or other environmental factors. The main advantages of liposomes are the enrichment of pharmacokinetic properties such as the therapeutic index, reduced side effects, stabilization of encapsulated proteins, and strong in

vitro and in vivo antitumor properties. They show a significant role to improve drug solubility, and can serve as carriers of water-soluble (hydrophilic) molecules inside the liposome body or hydrophobic molecules inside the lipid bilayer.[201–204] In order to increase the effectiveness of liposomes, it is necessary to link amphiphilic molecules such as polyethylene glycol (PEG) to the surface, letting the liposomes reach the site of action.[201] To address some of these features, investigation of a liposomal nanoparticle formulation of *Cratylia mollis* lectin (Cra), a mannose and glucose binding lectin to detect sarcoma 180 in Swiss mice exhibited considerable improvement in the protein stability and delivery. In addition, results showed a significant tumor inhibition percentage (71%) with minimal cytotoxicity compared to free Cra solution (41%).[205]

5. Conclusion

The presented data demonstrate the great significance of lectins with specific glycan recognition potential for the development of both diagnostic and therapeutic agents in the medical field. Different methods of improvement in lectin engineering technologies will reduce certain limitations of lectins due to their proteoinaceous nature or more. Natural or synthetic lectin/glycan technologies including the coupling of nanoparticles will permit the development of novel therapeutic agents with ideal characteristics. Targeted therapy is the most challenging and worthwhile application of lectins/glycan functionalized nanoparticles in therapy. As more studies are conducted, the more unknown specific interactions will be explored and will become available to be utilized for further bioprospecting in the future.

References

1. Reichardt NC, Martín-Lomas M, Penadés S. Glyconanotechnology. *Chem Soc Rev* 2013;**42**:4358–76.
2. Gornik O, Pavić T, Lauc G. Alternative glycosylation modulates function of IgG and other proteins—implications on evolution and disease. *Biochimica et Biophysica Acta (BBA)-General Subjects* 2012;**1820**:1318–26.
3. Lemjabbar-Alaoui H, McKinney A, Yang YW, Tran VM, Phillips JJ. Glycosylation alterations in lung and brain cancer. *Adv Cancer Res* 2015;**126**:305–44.
4. Pu Q, Yu C. Glycosyltransferases, glycosylation and atherosclerosis. *Glycoconj J* 2014;**31**:605–11.
5. Vaidyanathan K, Wells L. Multiple tissue-specific roles for the O-GlcNAc post-translational modification in the induction of and complications arising from type II diabetes. *J Biol Chem* 2014;**289**:34466–71.
6. Zhu Y, Shan X, Yuzwa SA, Vocadlo DJ. The emerging link between O-GlcNAc and Alzheimer disease. *J Biol Chem* 2014;**289**:34472–81.
7. Gabius HJ, André S, Kaltner H, Siebert HC. The sugar code: functional lectinomics. *Biochim Biophys Acta* 2002;**1572**:165–77.
8. Sharon N, Lis H. History of lectins: from hemagglutinins to biological recognition molecules. *Glycobiology* 2004;**14**:53R–62R.
9. Lakhtin VM. Molecular organization of lectins. *Mol Biol* 1994;**28**:245–73.
10. Weis WI, Drickamer K. Structural basis of lectin-carbohydrate recognition. *Annu Rev Biochem* 1996;**65**:441–73.
11. Jesus M, Penadés S. Understanding carbohydrate-carbohydrate interactions by means of glyconanotechnology. *Glycoconj J* 2004;**21**:149–63.
12. Lam SK, Ng TB. Lectins: production and practical applications. *Appl Microbiol Biotechnol* 2011;**89**:45–55.
13. Nascimento KS, Cunha AI, Nascimento KS, Cavada BS, Azevedo AM, Aires-Barros MR. An overview of lectins purification strategies. *J Mol Recogn* 2012;**25**:527–41.

14. Futosi K, Fodor S, Mócsai A. Reprint of Neutrophil cell surface receptors and their intracellular signal transduction pathways. *Int Immunopharm* 2013;**17**:1185–97.
15. Weiss G, Schaible UE. Macrophage defense mechanisms against intracellular bacteria. *Immunol Rev* 2015;**264**:182–203.
16. Ding L, Liu Z, Okweesi Aggrey M, Li C, Chen J, Tong L. Nanotoxicity: the toxicity research progress of metal and metal-containing nanoparticles. *Mini Rev Med Chem* 2015;**15**:529–42.
17. Cai W, Gao T, Hong H, Sun J. Applications of gold nanoparticles in cancer nanotechnology. *Nanotechnol Sci Appl* 2008;**1**:17–32.
18. Danhier F, Ansorena E, Silva J,M, Coco R, Le Breton A, Preat V. PLGA-based nanoparticles: an overview of biomedical applications. *J Contr Release* 2012;**161**:505–22.
19. Pustylnikov S, Sagar D, Jain P, Khan ZK. Targeting the C-type lectins-mediated host-pathogen interactions with dextran. *J Pharm Pharmaceut Sci* 2014;**17**:371.
20. Prabaharan M, Grailer JJ, Pilla S, Steeber DA, Gong S. Amphiphilic multi-arm-block copolymer conjugated with doxorubicin via pH-sensitive hydrazone bond for tumor-targeted drug delivery. *Biomaterials* 2009;**30**:5757–66.
21. Panyam J, Labhasetwar V. Biodegradable nanoparticles for drug and gene delivery to cells and tissue. *Adv Drug Deliv Rev* 2003;**55**:329–47.
22. Bowman K, Sarkar R, Raut S, Leong KW. Gene transfer to hemophilia A mice via oral delivery of FVIII–chitosan nanoparticles. *J Contr Release* 2008;**132**:252–9.
23. Sahoo SK, Misra R, Parveen S. Nanoparticles: a boon to drug delivery, therapeutics, diagnostics and imaging. *Nanomed Cancer* 2017:73–124.
24. Xiao Y, Jaskula-Sztul R, Javadi A, Xu W, Eide J, Dammalapati A, et al. Co-delivery of doxorubicin and siRNA using octreotide-conjugated gold nanorods for targeted neuroendocrine cancer therapy. *Nanoscale* 2012;**4**:7185–93.
25. Saxena A, Mozumdar S, Johri AK. Ultra-low sized cross-linked polyvinylpyrrolidone nanoparticles as non-viral vectors for in vivo gene delivery. *Biomaterials* 2006;**27**:5596–602.
26. Nevozhay D, Kańska U, Budzyńska R, Boratyński J. Current status of research on conjugates and related drug delivery systems in the treatment of cancer and other diseases. *Postepy Higieny Medycyny Doświadczalnej* 2007;**61**:350–60.
27. Basu S, Harfouche R, Soni S, Chimote G, Mashelkar RA, Sengupta S. Nanoparticle-mediated targeting of MAPK signaling predisposes tumor to chemotherapy. *Proc Natl Acad Sci USA* 2009;**106**:7957–61.
28. Seidi F, Jenjob R, Phakkeeree T, Crespy D. Saccharides, oligosaccharides, and polysaccharides nanoparticles for biomedical applications. *J Contr Release* 2018;**284**:188–212.
29. Liu B, Lu X, Ruan H, Cui J, Li H. Synthesis and applications of glyconanoparticles. *Curr Org Chem* 2017;**20**:1502–11.
30. Kottari N, Chabre YM, Sharma R, Roy R. Applications of glyconanoparticles as "sweet" glycobiological therapeutics and diagnostics. In: *Multifaceted development and application of biopolymers for biology, biomedicine and nanotechnology*. Berlin, Heidelberg: Springer; 2013. p. 297–341.
31. Ahmad MZ, Akhter S, Rahman Z, Akhter S, Anwar M, Mallik N, Ahmad FJ. Nanometric gold in cancer nanotechnology: current status and future prospect. *J Pharm Pharmacol* 2013;**65**:634–51.
32. Nikitin MP, Shipunova VO, Deyev SM, Nikitin PI. Biocomputing based on particle disassembly. *Nat Nanotechnol* 2014;**9**:716–22.
33. Shipunova VO, Nikitin MP, Nikitin PI, Deyev SM. *Lectin-based nanoagents for specific cell labelling and optical visualization*. St. Petersburg: International Conference Laser Optics (LO); 2016. pp. S2-37-S2-37.
34. Cunha CRA, Oliveira ADPR, Firmino TVC, Tenório DPLA, Pereira G, Carvalho Jr LB, Fontes A, et al. Biomedical applications of glyconanoparticles based on quantum dots. *Biochimica et Biophysica Acta (BBA)-General Subjects* 2018;**1862**:427–39.
35. Hendrickson OD, Zherdev AV. Analytical application of lectins. *Crit Rev Anal Chem* 2018;**48**:279–92.
36. Pudlarz A, Szemraj J. Nanoparticles as carriers of proteins, peptides and other therapeutic molecules. *Open Life Sci* 2018;**13**:285–98.
37. Jin Y, Hu G, Guo M, Xu J, Wu F, Fan J, Wang X, et al. Nanoparticles targeting macrophages as potential clinical therapeutic agents against cancer and inflammation. *Front Immunol* 2019;**10**:1998. https://doi.org/10.3389/fimmu.2019.01998.

38. Kobayashi Y, Kawagishi H. Fungal lectins: a growing family. In: *Lectins*. New York, NY: Humana Press; 2014. p. 15–38.
39. Vornholt W, Hartmann M, Keusgen M. SPR studies of carbohydrate–lectin interactions as useful tool for screening on lectin sources. *Biosens Bioelectron* 2007;**22**:2983–8.
40. Kilpatrick DC. Animal lectins: a historical introduction and overview. *Biochimica et Biophysica Acta (BBA)-General Subjects* 2002;**1572**:187–97.
41. Rüdiger H, Gabius HJ. Plant lectins: occurrence, biochemistry, functions and applications. *Glycoconj J* 2001;**18**:589–613.
42. Boyd WC. The proteins of immune reactions. In: *The proteins*. Academic Press; 1954. p. 755–844.
43. Ghazarian H, Idoni B, Oppenheimer SB. A glycobiology review: carbohydrates, lectins and implications in cancer therapeutics. *Acta Histochem* 2011;**113**:236–47.
44. Dodd RB, Drickamer K. Lectin-like proteins in model organisms: implications for evolution of carbohydrate-binding activity. *Glycobiology* 2001;**11**:71R–9R.
45. Brewer CF, Miceli MC, Baum LG. Clusters, bundles, arrays and lattices: novel mechanisms for lectin–saccharide-mediated cellular interactions. *Curr Opin Struct Biol* 2002;**12**:616–23.
46. Yau T, Dan X, Ng CCW, Ng TB. Lectins with potential for anti-cancer therapy. *Molecules* 2015;**20**:3791–810.
47. Watanabe Y, Naganuma T, Ogawa T, Muramoto K. Lectins of marine origin and their clinical applications. In: *Antitumor potential and other emerging medicinal properties of natural compounds*. Dordrecht: Springer; 2013. p. 33–54.
48. Majee SB, Biswas GR. Exploring plant lectins in diagnosis, prophylaxis and therapy. *J Med Plants Res* 2013;**7**:3444–51.
49. Blow N. A spoonful of sugar. *Nature* 2009;**457**:618–20.
50. Chen S, Zheng T, Shortreed MR, Alexander C, Smith LM. Analysis of cell surface carbohydrate expression patterns in normal and tumorigenic human breast cell lines using lectin arrays. *Anal Chem* 2007;**79**:5698–702.
51. Hirabayashi J. Concept, strategy and realization of lectin-based glycan profiling. *J Biochem* 2008;**144**:139–47.
52. Hwang GM, Pang L, Mullen EH, Fainman Y. Plasmonic sensing of biological analytes through nanoholes. *IEEE Sensor J* 2008;**8**:2074–9.
53. Kuno A, Uchiyama N, Koseki-Kuno S, Ebe Y, Takashima S, Yamada M, Hirabayashi J, et al. Evanescent-field fluorescence-assisted lectin microarray: a new strategy for glycan profiling. *Nat Methods* 2005;**2**:851–6.
54. Bawa R, Audette GF, Rubinstein I. *Handbook of clinical nanomedicine: nanoparticles, imaging, therapy, and clinical applications*. Pan Stanford; 2016.
55. Gabor F, Bogner E, Weissenboeck A, Wirth M. The lectin–cell interaction and its implications to intestinal lectin-mediated drug delivery. *Adv Drug Deliv Rev* 2004;**56**:459–80.
56. Ensign LM, Cone R, Hanes J. Oral drug delivery with polymeric nanoparticles: the gastrointestinal mucus barriers. *Adv Drug Deliv Rev* 2012;**64**:557–70.
57. Li H, Dong WF, Zhou JY, Xu XM, Li FQ. Triggering effect of N-acetylglucosamine on retarded drug release from a lectin-anchored chitosan nanoparticles-in-microparticles system. *Int J Pharm* 2013;**449**:37–43.
58. Wright CS. The crystal structure of wheat germ agglutinin at 2· 2 Å resolution. *J Mol Biol* 1977;**111**:439–57.
59. Foriers A, Lebrun E, Van Rapenbusch R, de Neve R, Strosberg AD. The structure of the lentil (Lens culinaris) lectin. Amino acid sequence determination and prediction of the secondary structure. *J Biol Chem* 1981;**256**:5550–60.
60. Giga Y, Ikai A, Takahashi K. The complete amino acid sequence of echinoidin, a lectin from the coelomic fluid of the sea urchin *Anthocidaris crassispina*. Homologies with mammalian and insect lectins. *J Biol Chem* 1987;**262**:6197–203.
61. De Mejía EG, Prisecaru VI. Lectins as bioactive plant proteins: a potential in cancer treatment. *Crit Rev Food Sci Nutr* 2005;**45**:425–45.
62. Abdullaev FI, Gonzalez de Mejia E. Antitumor effect of plant lectins. *Nat Toxins* 1997;**5**:157–63.
63. Vojdani A. Lectins, agglutinins, and their roles in autoimmune reactivities. *Altern Ther* 2015;**21**:42–7.
64. van Buul VJ, Brouns FJ. Health effects of wheat lectins: a review. *J Cereal Sci* 2014;**59**:112–7.
65. Agrawal U, Sharma R, Mody N, Dubey S, Vyas SP. Improved oral bioavailability of bioactives through lipid-based nanoarchitectures. In: *Surface Chemistry of Nanobiomaterials*. William Andrew Publishing; 2016. p. 433–62.
66. Minko T. Drug targeting to the colon with lectins and neoglycoconjugates. *Adv Drug Deliv Rev* 2004;**56**:491–509.
67. Lis H, Sharon N. Lectin-carbohydrate interactions. *Curr Opin Struct Biol* 1991;**1**:741–9.

68. Gemeiner P, Mislovičová D, Tkáč J, Švitel J, Pätoprstý V, Hrabárová E, Kožár T, et al. Lectinomics: II. A highway to biomedical/clinical diagnostics. *Biotechnol Adv* 2009;**27**:1–15.
69. Arnaud J, Audfray A, Imberty A. Binding sugars: from natural lectins to synthetic receptors and engineered neolectins. *Chem Soc Rev* 2013;**42**:4798–813.
70. Nelson DL, Cox MM, Lehninger AL. *Principles of biochemistry*. New York: Freeman; 2008.
71. Poget SF, Legge GB, Proctor MR, Butler PJG, Bycroft M, Williams RL. The structure of a tunicate C-type lectin from Polyandrocarpa misakiensis complexed with D-galactose. *J Mol Biol* 1999;**290**:867–79.
72. Wang B, Boons GJ, editors. *Carbohydrate recognition: biological problems, methods, and applications*, vol 13. John Wiley & Sons; 2011.
73. Goldstein II, Poretz RD. Isolation, physicochemical characterization, and carbohydrate—binding specificity of lectins. *The lectins. Properties Functions Appl Biol Med* 2012:233–47.
74. Von der Lieth CW, Lütteke T, Frank M, editors. *Bioinformatics for glycobiology and glycomics: an introduction*. John Wiley & Sons; 2009.
75. Alley Jr WR, Mann BF, Novotny MV. High-sensitivity analytical approaches for the structural characterization of glycoproteins. *Chem Rev* 2013;**113**:2668–732.
76. Santos Silva, dos PM, Barroso Coel LCB, Santos Correia M T dos. Electrochemical biosensing strategies to detect serum glycobiomarkers. *Adv Res* 2016;**6**:1–17.
77. Bahadır EB, Sezgintürk MK. Applications of commercial biosensors in clinical, food, environmental, and biothreat/biowarfare analyses. *Anal Biochem* 2015;**478**:107–20.
78. Liu X, Duckworth PA, Wong DK. Square wave voltammetry versus electrochemical impedance spectroscopy as a rapid detection technique at electrochemical immunosensors. *Biosens Bioelectron* 2010;**25**:1467–73.
79. Quiroga AV, Barrio DA, Añón MC. Amaranth lectin presents potential antitumor properties. *LWT–Food Sci Technol* 2015;**60**:478–85.
80. Panda PK, Mukhopadhyay S, Behera B, Bhol CS, Dey S, Das DN, Bhutia SK, et al. Antitumor effect of soybean lectin mediated through reactive oxygen species-dependent pathway. *Life Sci* 2014;**111**:27–35.
81. Singh RS, Tiwary AK, Kennedy JF. Lectins: sources, activities, and applications. *Crit Rev Biotechnol* 1999;**19**:145–78.
82. Sharon N. Bacterial lectins, cell-cell recognition and infectious disease. *FEBS Lett* 1987;**217**:145–57.
83. Kabir SR, Nabi MM, Nurujjaman M, Reza MA, Alam AK, Zaman R, Uddin MS, et al. *Momordica charantia* seed lectin: toxicity, bacterial agglutination and antitumor properties. *Appl Biochem Biotechnol* 2015;**175**:2616–28.
84. Lindhorst TK. Small molecule ligands for bacterial lectins: letters of an antiadhesive glycopolymer code. In: *Glycopolymer code: synthesis of glycopolymers and their applications*; 2015. p. 1–16. https://doi.org/10.1039/9781782622666-00001.
85. Sato T, Hori K. Cloning, expression, and characterization of a novel anti-HIV lectin from the cultured cyanobacterium, Oscillatoria agardhii. *Fish Sci* 2009;**75**:743–53.
86. Rosi NL, Mirkin CA. Nanostructures in biodiagnostics. *Chem Rev* 2005;**105**:1547–62.
87. Wang J. Nanomaterial-based amplified transduction of biomolecular interactions. *Small* 2005;**1**:1036–43.
88. Penn SG, He L, Natan MJ. Nanoparticles for bioanalysis. *Curr Opin Chem Biol* 2003;**7**:609–15.
89. Sun T, Zhang YS, Pang B, Hyun DC, Yang M, Xia Y. Tailor-made nanoparticles for drug delivery in cancer therapy. *Angew Chem* 2014;**126**:12520–68.
90. Pang L, Qin J, Han L, Zhao W, Liang J, Xie Z, Wang J, et al. Exploiting macrophages as targeted carrier to guide nanoparticles into glioma. *Oncotarget* 2016;**7**:37081.
91. Bowerman CJ, Byrne JD, Chu KS, Schorzman AN, Keeler AW, Sherwood CA, Napier ME. Docetaxel-loaded PLGA nanoparticles improve efficacy in taxane-resistant triple-negative breast cancer. *Nano Lett* 2017;**17**:242–8.
92. Kumar Khanna V. Targeted delivery of nanomedicines. *ISRN Pharmacol* 2012. https://doi.org/10.5402/2012/571394.
93. Alexis F, Pridgen E, Molnar LK, Farokhzad OC. Factors affecting the clearance and biodistribution of polymeric nanoparticles. *Mol Pharm* 2008;**5**:505–15.
94. Caliceti P, Veronese FM. Pharmacokinetic and biodistribution properties of poly (ethylene glycol)–protein conjugates. *Adv Drug Deliv Rev* 2003;**55**:1261–77.
95. Gullotti E, Yeo Y. Extracellularly activated nanocarriers: a new paradigm of tumor targeted drug delivery. *Mol Pharm* 2009;**6**:1041–51.

96. Kim C, Cho EC, Chen J, Song KH, Au L, Favazza C, Wang LV. In vivo molecular photoacoustic tomography of melanomas targeted by bioconjugated gold nanocages. *ACS Nano* 2010;**4**:4559–64.
97. Lu J, Liu X, Liao YP, Salazar F, Sun B, Jiang W, Meng H, et al. Nano-enabled pancreas cancer immunotherapy using immunogenic cell death and reversing immunosuppression. *Nat Commun* 2017;**8**:1–14.
98. Man RW, Li CH, MacLean MW, Zenkina OV, Zamora MT, Saunders LN, Crudden CM, et al. Ultrastable gold nanoparticles modified by bidentate N-heterocyclic carbene ligands. *J Am Chem Soc* 2018;**140**:1576–9.
99. Patel S, Ashwanikumar N, Robinson E, DuRoss A, Sun C, Murphy-Benenato KE, Sahay G, et al. Boosting intracellular delivery of lipid nanoparticle-encapsulated mRNA. *Nano Lett* 2017;**17**:5711–8.
100. Kulkarni JA, Cullis PR, van der Meel R. Lipid nanoparticles enabling gene therapies: from concepts to clinical utility. *Nucleic Acid Therapeut* 2018;**28**:146–57.
101. Rao W, Wang H, Han J, Zhao S, Dumbleton J, Agarwal P, Lu X. Chitosan-decorated doxorubicin-encapsulated nanoparticle targets and eliminates tumor reinitiating cancer stem-like cells. *ACS Nano* 2015;**9**:5725–40.
102. Prud'homme RK, Svenson S. Introduction: benefits and challenges for multifunctional nanoparticles in medicine. In: *Multifunctional nanoparticles for drug delivery applications*. Boston, MA: Springer; 2012. p. 1–5.
103. Kaszuba M, Jones MN. The use of lectins for liposome targeting in drug delivery. In: Rhodes JM, Milton JD, editors. *Lectin methods and protocols. methods in molecular medicine™*. Humana Press; 1998. p. 9. https://doi.org/10.1385/0-89603-396-1:583.
104. Budzynska R, Nevozhay D, Kanska U, Jagiello M, Opolski A, Wietrzyk J, Boratynski J. Antitumor activity of mannan–methotrexate conjugate in vitro and in vivo. *Oncol Res* 2007;**16**:415–21.
105. Gupta A, Gupta RK, Gupta GS. Targeting cells for drug and gene delivery: emerging applicationsof mannans and mannan binding lectins. *J Sci Ind Res (India)* 2009;**68**:465–83.
106. Lee YC. Fluorescence spectrometry in studies of carbohydrate-protein interactions. *J Biochem* 1997;**121**:818–25.
107. McCoy Jr JP, Varani J, Goldstein IJ. Enzyme-linked lectin assay (ELLA): II. Detection of carbohydrate groups on the surface of unfixed cells. *Exp Cell Res* 1984;**151**:96–103.
108. Zeng X, Andrade CA, Oliveira MD, Sun XL. Carbohydrate–protein interactions and their biosensing applications. *Anal Bioanal Chem* 2012;**402**:3161–76.
109. Chen H, Kou X, Yang Z, Ni W, Wang J. Shape- and size- dependent refractive index sensitivity of gold nanoparticles. *Langmuir* 2008;**24**:5233–7.
110. Sperling RA, Gil PR, Zhang F, Zanella M, Parak WJ. Biological applications of gold nanoparticles. *Chem Soc Rev* 2008;**37**:1896–908.
111. Tuccillo FM, De Laurentiis A, Palmieri C, Fiume G, Bonelli P, Borrelli A, Scala G, et al. Aberrant glycosylation as biomarker for cancer: focus on CD43. *BioMed Res Int* 2014. https://doi.org/10.1155/2014/742831.
112. Li M, Song L, Qin X. Glycan changes: cancer metastasis and anti-cancer vaccines. *J Biosci* 2010;**35**:665–73.
113. Kumamoto K, Goto Y, Sekikawa K, Takenoshita S, Ishida N, Kawakita M, Kannagi R. Increased expression of UDP-galactose transporter messenger RNA in human colon cancer tissues and its implication in synthesis of Thomsen-Friedenreich antigen and sialyl Lewis A/X determinants. *Cancer Res* 2001;**61**:4620–7.
114. Pinho SS, Reis CA. Glycosylation in cancer: mechanisms and clinical implications. *Nat Rev Cancer* 2015;**15**:540–55.
115. Boyd WC, Shapleigh E. Specific precipitating activity of plant agglutinins (lectins). *Science* 1954;**119**:419.
116. Varrot A, Basheer SM, Imberty A. Fungal lectins: structure, function and potential applications. *Curr Opin Struct Biol* 2013;**23**:678–85.
117. Taylor ME, Drickamer K, Schnaar RL, Etzler ME, Varki A. *Discovery and classification of glycan-binding proteins. Essentials of glycobiology*. 3rd ed. Cold Spring Harbor (NY): Cold Spring Harbor Laboratory Press; 2015.
118. Peumans WJ, Van Damme JM, Barre A, Rougé P. *Classification of plant lectins in families of structurally and evolutionary related proteins. The molecular immunology of complex carbohydrates—2*. Boston, MA: Springer; 2001. p. 27–54.
119. Fujimoto Z, Tateno H, Hirabayashi J. *Lectin structures: classification based on the 3-d structures. Lectins*. New York: Humana Press; 2014. p. 579–606.
120. Jayawardena HSN, Wang X, Yan M. Classification of lectins by pattern recognition using glyconanoparticles. *Anal Chem* 2013;**85**:10277–81.
121. Li D, Chiu H, Zhang H, Chan DW. Analysis of serum protein glycosylation by a differential lectin immunosorbant assay (dLISA). *Clin Proteonomics* 2013;**10**:12.
122. Gray MP. U.S. Patent No. 3,053,739. Washington, DC: U.S. Patent and Trademark Office, 1962.

123. Dreaden EC, Alkilany AM, Huang X, Murphy CJ, El-Sayed MA. The golden age: gold nanoparticles for biomedicine. *Chem Soc Rev* 2012;**41**:2740–79.
124. Hutter E, Maysinger D. Gold nanoparticles and quantum dots for bioimaging. *Microsc Res Tech* 2011;**74**:592–604.
125. Dykman L, Khlebtsov N. Gold nanoparticles in biomedical applications: recent advances and perspectives. *Chem Soc Rev* 2012;**41**:2256–82.
126. Libralato G, Galdiero E, Falanga A, Carotenuto R, De Alteriis E, Guida M. Toxicity effects of functionalized quantum dots, gold and polystyrene nanoparticles on target aquatic biological models: a review. *Molecules* 2017;**22**:1439.
127. Djafari J, McConnell MT, Santos HM, Capelo JL, Bertolo E, Harvey SC, Fernández-Lodeiro J, et al. Synthesis of gold functionalised nanoparticles with the Eranthis hyemalis lectin and preliminary toxicological studies on *Caenorhabditis elegans*. *Materials* 2018;**11**:1363.
128. Obaid G, Chambrier I, Cook MJ, Russell DA. Targeting the oncofetal Thomsen–Friedenreich disaccharide using Jacalin-PEG phthalocyanine gold nanoparticles for photodynamic cancer therapy. *Angew Chem Int Ed* 2012;**51**:6158–62.
129. Obaid G, Chambrier I, Cook MJ, Russell DA. Cancer targeting with biomolecules: a comparative study of photodynamic therapy efficacy using antibody or lectin conjugated phthalocyanine-PEG gold nanoparticles. *Photochem Photobiol Sci* 2015;**14**:737–47.
130. Wang J, Duan T, Sun L, Liu D, Wang Z. Functional gold nanoparticles for studying the interaction of lectin with glycosyl complex on living cellular surfaces. *Anal Biochem* 2009;**392**:77–82.
131. Zhang Y, Walker JB, Minic Z, Liu F, Goshgarian H, Mao G. Transporter protein and drug-conjugated gold nanoparticles capable of bypassing the blood-brain barrier. *Sci Rep* 2016;**6**:25794. https://doi.org/10.1038/srep25794.
132. Bose PP, Mandal G, Kumar D, Duseja A, Chatterjee BP. Visual detection of serum asialohaptoglobin by plasmonic sandwich ELLSA–a new platform for cirrhosis diagnosis. *Analyst* 2016;**141**:76–84.
133. Bose PP, Chatterjee U, Chatterjee BP. Assessment of altered fucosylation of serum A-1-acid glycoprotein in hepatocellular carcinoma patients by gold-nanoparticle aggregation immunoassay. *Mater Sci Res India* 2018;**15**:263–71.
134. Babu P, Sinha S, Surolia A. Sugar– quantum dot conjugates for a selective and sensitive detection of lectins. *Bioconjugate Chem* 2007;**18**:146–51.
135. Shinchi H, Wakao M, Nakagawa S, Mochizuki E, Kuwabata S, Suda Y. Stable sugar-chain-immobilized fluorescent nanoparticles for probing lectin and cells. *Chem Asian J* 2012;**7**:2678–82.
136. Nakamura-Tsuruta S, Kishimoto Y, Nishimura T, Suda Y. One-step purification of lectins from banana pulp using sugar-immobilized gold nano-particles. *J Biochem* 2008;**143**:833–9.
137. Tkac J, Bertok T, Nahalka J, Gemeiner P. *Perspectives in glycomics and lectin engineering*. *Lectins*. New York, NY: Humana Press; 2014. p. 421–45.
138. Compostella F, Pitirollo O, Silvestri A, Polito L. Glucose-gold nanoparticles: synthesis and applications. *Beilstein J Org Chem* 2017;**13**:1008–21.
139. de la Fuente JM, Barrientos AG, Rojas TC, Rojo J, Cañada J, Fernández A, Penadés S, et al. Gold glyconanoparticles as water-soluble polyvalent models to study carbohydrate interactions. *Angew Chem Int Ed* 2001;**40**:2257–61.
140. Marín MJ, Rashid A, Rejzek M, Fairhurst SA, Wharton SA, Martin SR, Russell DA, et al. Glyconanoparticles for the plasmonic detection and discrimination between human and avian influenza virus. *Org Biomol Chem* 2013;**11**:7101–7.
141. Adak AK, Li BY, Lin CC. Advances in multifunctional glycosylated nanomaterials: preparation and applications in glycoscience. *Carbohydr Res* 2015;**405**:2–12.
142. Yilmaz G, Becer CR. Glyconanoparticles and their interactions with lectins. *Polym Chem* 2015;**6**:5503–14.
143. Richards SJ, Otten L, Gibson MI. Glycosylated gold nanoparticle libraries for label-free multiplexed lectin biosensing. *J Mater Chem B* 2016;**4**:3046–53.
144. Calavia PG, Chambrier I, Cook MJ, Haines AH, Field RA, Russell DA. Targeted photodynamic therapy of breast cancer cells using lactose-phthalocyanine functionalized gold nanoparticles. *J Colloid Interface Sci* 2018;**512**:249–59.

145. Iuliano AD, Roguski KM, Chang HH, Muscatello DJ, Palekar R, Tempia S, Wu P, et al. Estimates of global seasonal influenza-associated respiratory mortality: a modelling study. *Lancet* 2018;**391**:1285–300.
146. World Heath Organisation - Fact Sheet - Influenza (Seasonal). https://www.who.int/news-room/fact-sheets/detail/influenza-(seasonal). Accessed March 10, 2020.
147. Rogers GN, D'Souza BL. Receptor binding properties of human and animal H1 influenza virus isolates. *Virology* 1989;**173**:317–22.
148. Connor RJ, Kawaoka Y, Webster RG, Paulson JC. Receptor specificity in human, avian, and equine H2 and H3 influenza virus isolates. *Virology* 1994;**205**:17–23.
149. Webster RG, Laver WG, Air GM, Schild GC. Molecular mechanisms of variation in influenza viruses. *Nature* 1982;**296**:115–21.
150. Gamblin SJ, Haire LF, Russell RJ, Stevens DJ, Xiao B, Ha Y, Wiley DC, et al. The structure and receptor binding properties of the 1918 influenza hemagglutinin. *Science* 2004;**303**:1838–42.
151. Rogers GN, Paulson JC, Daniels RS, Skehel JJ, Wilson IA, Wiley DC. Single amino acid substitutions in influenza haemagglutinin change receptor binding specificity. *Nature* 1983;**304**:76–8.
152. Gulati S, Lasanajak Y, Smith DF, Cummings RD, Air GM. Glycan array analysis of influenza H1N1 binding and release. *Cancer Biomark* 2014;**14**:43–53.
153. Weis W, Brown JH, Cusack S, Paulson JC, Skehel JJ, Wiley D. C Structure of the influenza virus haemagglutinin complexed with its receptor, sialic acid. *Nature* 1998;**333**:426–31.
154. Lundquist JJ, Toone EJ. The cluster glycoside effect. *Chem Rev* 2002;**102**:555–78.
155. Richards SJ, Gibson MI. Optimization of the polymer coating for glycosylated gold nanoparticle biosensors to ensure stability and rapid optical readouts. *ACS Macro Lett* 2014;**3**:1004–8.
156. Belický Š, Katrlík J, Tkáč J. Glycan and lectin biosensors. *Essays Biochem* 2016;**60**:37–47.
157. Richards SJ, Biggs CI, Gibson MI. *Multivalent glycopolymer-coated gold nanoparticles*. *Macro-Glycoligands*. New York, NY: Humana Press; 2016. p. 169–79.
158. Otten L, Vlachou D, Richards SJ, Gibson MI. Glycan heterogeneity on gold nanoparticles increases lectin discrimination capacity in label-free multiplexed bioassays. *Analyst* 2016;**141**:4305–12.
159. Richards SJ, Baker AN, Walker M, Gibson MI. Polymer-stabilized sialylated nanoparticles: synthesis, optimization and differential binding to influenza hemagglutinins. *Biomacromolecules* 2020;**21**:1604–12.
160. Zheng Y, Zhang Y, Zhang T, Cai H, Xie X, Yang Y, Wu H. AuNSs@ Glycopolymer-ConA hybrid nanoplatform for photothermal therapy of hepatoma cells. *Chem Eng J* 2020;**389**:124460. https://doi.org/10.1016/j.cej.2020.124460.
161. Austin LA, Mackey MA, Dreaden EC, El-Sayed MA. The optical, photothermal, and facile surface chemical properties of gold and silver nanoparticles in biodiagnostics, therapy, and drug delivery. *Arch Toxicol* 2014;**88**:1391–417.
162. Ahmed KBR, Nagy AM, Brown RP, Zhang Q, Malghan SG, Goering PL. Silver nanoparticles: significance of physicochemical properties and assay interference on the interpretation of in vitro cytotoxicity studies. *Toxicol Vitro* 2017;**38**:179–92.
163. Zhang XF, Liu ZG, Shen W, Gurunathan S. Silver nanoparticles: synthesis, characterization, properties, applications, and therapeutic approaches. *Int J Mol Sci* 2016;**17**:1534.
164. Wei L, Lu J, Xu H, Patel A, Chen ZS, Chen G. Silver nanoparticles: synthesis, properties, and therapeutic applications. *Drug Discov Today* 2015;**20**:595–601.
165. Abhilash J, Geethanandan K, Bharath SR, Sadasivan C, Haridas M. Crystallization and preliminary X-ray diffraction analysis of a galactose-specific lectin from the seeds of Butea monosperma. *Acta Crystallogr Sect F Struct Biol Cryst Commun* 2011;**67**:524–6.
166. Abhilash J, Geethanandan K, Bharath SR, Sabu A, Sadasivan C, Haridas M. The crystal structure of a lectin from Butea monosperma: insight into its glycosylation and binding of ligands. *Int J Biol Macromol* 2015;**72**:1376–83.
167. Senthilnathan R, Arunachalam J, Anbazhagan V. Revealing the significance of the glycan binding property of butea monosperma seed lectin for enhancing the antibiofilm activity of silver nanoparticles against uropathogenic *Escherichia coli*. *Bioconjugate Chem* 2020;**31**:139–48.
168. Vaghari H, Jafarizadeh-Malmiri H, Mohammadlou M, Berenjian A, Anarjan N, Jafari N, Nasiri S, et al. Application of magnetic nanoparticles in smart enzyme immobilization. *Biotechnol Lett* 2016;**38**:223–33.
169. Wahajuddin SA. Superparamagnetic iron oxide nanoparticles: magnetic nanoplatforms as drug carriers. *Int J Nanomed* 2012;**7**:3445–71.

170. Chen JP, Yang PC, Ma YH, Tu SJ, Lu YJ. Targeted delivery of tissue plasminogen activator by binding to silica-coated magnetic nanoparticle. *Int J Nanomed* 2012;**7**:5137–49.
171. Li X, Wei J, Aifantis KE, Fan Y, Feng Q, Cui FZ, Watari F. Current investigations into magnetic nanoparticles for biomedical applications. *J Biomed Mater Res* 2016;**104**:1285–96.
172. El-Boubbou K, Zhu DC, Vasileiou C, Borhan B, Prosperi D, Li W, Huang X, et al. Magnetic glyco-nanoparticles: a tool to detect, differentiate, and unlock the glyco-codes of cancer via magnetic resonance imaging. *J Am Chem Soc* 2010;**132**:4490–9.
173. He X, Liu F, Liu L, Duan T, Zhang H, Wang Z, et al. Lectin-conjugated Fe2O3@ Au core@ shell nanoparticles as dual mode contrast agents for in vivo detection of tumor. *Mol Pharm* 2014;**11**:738–45.
174. Singh A, Dilnawaz F, Sahoo SK. Long circulating lectin conjugated paclitaxel loaded magnetic nanoparticles: a new theranostic avenue for leukemia therapy. *PLoS One* 2011;**6**:e26803. https://doi.org/10.1371/journal.pone.0026803.
175. Gidwani K, Huhtinen K, Kekki H, van Vliet S, Hynninen J, Koivuviita N, Lamminmäki U, et al. A nanoparticle-lectin immunoassay improves discrimination of serum CA125 from malignant and benign sources. *Clin Chem* 2016;**62**:1390–400.
176. Hadjialirezaei S, Picco G, Beatson R, Burchell J, Stokke BT, Sletmoen M. Interactions between the breast cancer-associated MUC1 mucins and C-type lectin characterized by optical tweezers. *PLoS One* 2017;**12**:e0175323. https://doi.org/10.1371/journal.pone.0175323.
177. Nollau P, Wolters-Eisfeld G, Mortezai N, Kurze AK, Klampe B, Debus A, Wagener C. Protein domain histochemistry (PDH) binding of the carbohydrate recognition domain (CRD) of recombinant human glycoreceptor CLEC10A (CD301) to formalin-fixed, paraffin-embedded breast cancer tissues. *J Histochem Cytochem* 2013;**61**:199–205.
178. Kubota Y, Fujioka K, Takekawa M. WGA-based lectin affinity gel electrophoresis: a novel method for the detection of O-GlcNAc-modified proteins. *PLoS One* 2017;**12**:e0180714. https://doi.org/10.1371/journal.pone.0180714.
179. Terävä J, Tiainen L, Lamminmäki U, Kellokumpu-Lehtinen PL, Pettersson K, Gidwani K, et al. Lectin nanoparticle assays for detecting breast cancer-associated glycovariants of cancer antigen 15-3 (CA15-3) in human plasma. *PLoS One* 2019;**14**:e0219480. https://doi.org/10.1371/journal.pone.0219480.
180. Bilyy R, Tomyn A, Kit Y, Podhorodecki A, Misiewicz J, Nyk M, Stoika R, et al. Detection of dying cells using lectin-conjugated fluorescent and luminescent nanoparticles. *Mater Werkst: Entwicklung, Fertigung, Prüfung, Eigenschaften und Anwendungen technischer Werkstoffe* 2009;**40**:234–7.
181. Rhodes JM, Black RR, Savage A. Glycoprotein abnormalities in colonic carcinomata, adenomata, and hyperplastic polyps shown by lectin peroxidase histochemistry. *J Clin Pathol* 1986;**39**:1331–4.
182. Yonezawa S, Nakamura T, Tanaka S, Maruta K, Nishi M, Sato E, et al. Binding of Ulex europaeus agglutinin-I in polyposis coli: comparative study with solitary adenoma in the sigmoid colon and rectum. *J Natl Cancer Inst* 1983;**71**:19–24.
183. Cheng SH, Hsieh CC, Chen NT, Chu CH, Huang CM, Chou PT, Lo LW, et al. Well-defined mesoporous nanostructure modulates three-dimensional interface energy transfer for two-photon activated photodynamic therapy. *Nano Today* 2011;**6**:552–63.
184. Chen NT, Souris JS, Cheng SH, Chu CH, Wang YC, Konda V, Lo LW, et al. Lectin-functionalized mesoporous silica nanoparticles for endoscopic detection of premalignant colonic lesions. *Nanomed Nanotechnol Biol Med* 2017;**13**:1941–52.
185. Martínez-Carmona M, Lozano D, Colilla M, Vallet-Regí M. Lectin-conjugated pH-responsive mesoporous silica nanoparticles for targeted bone cancer treatment. *Acta Biomater* 2018;**65**:393–404.
186. Tang M, Lei L, Guo S, Huang W. Recent progress in nanotechnology for cancer therapy. *Chin J Cancer* 2010;**29**:775–80.
187. Mottaghitalab F, Farokhi M, Shokrgozar MA, Atyabi F, Hosseinkhani H. Silk fibroin nanoparticle as a novel drug delivery system. *J Contr Release* 2015;**206**:161–76.
188. Mo Y, Lim LY. Preparation and in vitro anticancer activity of wheat germ agglutinin (WGA)-conjugated PLGA nanoparticles loaded with paclitaxel and isopropyl myristate. *J Contr Release* 2005;**107**:30–42.
189. Diesner SC, Wang XY, Jensen-Jarolim E, Untersmayr E, Gabor F. Use of lectin-functionalized particles for oral immunotherapy. *Ther Deliv* 2012;**3**:277–90.

190. Piazza J, Hoare T, Molinaro L, Terpstra K, Bhandari J, Selvaganapathy PR, Mishra RK. Haloperidol-loaded intranasally administered lectin functionalized poly (ethylene glycol)—block-poly (D, L)-lactic-co-glycolic acid (PEG—PLGA) nanoparticles for the treatment of schizophrenia. *Eur J Pharm Biopharm* 2014;**87**:30—9.
191. Sung JC, Pulliam BL, Edwards DA. Nanoparticles for drug delivery to the lungs. *Trends Biotechnol* 2007;**25**:563—70.
192. Rizvi SB, Ghaderi S, Keshtgar M, Seifalian AM. Semiconductor quantum dots as fluorescent probes for in vitro and in vivo bio-molecular and cellular imaging. *Nano Rev* 2010;**1**:5161. https://doi.org/10.3402/nano.v1i0.5161.
193. Reshma VG, Mohanan PV. Quantum dots: applications and safety consequences. *J Lumin* 2019;**205**:287—98.
194. Oliveira WF, Cabrera MP, Santos NR, Napoleão TH, Paiva PM, Neves RP, Fontes A, et al. Evaluating glucose and mannose profiles in Candida species using quantum dots conjugated with Cramoll lectin as fluorescent nanoprobes. *Microbiol Res* 2020;**230**:126330. https://doi.org/10.1016/j.micres.2019.126330.
195. Tenório DP, Andrade CG, Cabral Filho PE, Sabino CP, Kato IT, Carvalho Jr LB, Santos BS. CdTe quantum dots conjugated to concanavalin A as potential fluorescent molecular probes for saccharides detection in Candida albicans. *J Photochem Photobiol B Biol* 2015;**142**:237—43.
196. Xu X, Ding L, Xue Y, Ju H. A simple fluorescent strategy for in situ evaluation of cell surface carbohydrate with a quantum dot—lectin nanoprobe. *Analyst* 2010;**135**:1906—8.
197. Desai JV, Mitchell AP. *Candida albicans* biofilm development and its genetic control. *Microbial Biofilms* 2015:99—114.
198. Gow NA, Hube B. Importance of the *Candida albicans* cell wall during commensalism and infection. *Curr Opin Microbiol* 2012;**15**:406—12.
199. Wang C, Ho PC, Lim LY. Wheat germ agglutinin-conjugated PLGA nanoparticles for enhanced intracellular delivery of paclitaxel to colon cancer cells. *Int J Pharm* 2010;**400**:201—10.
200. Gao X, Wang T, Wu B, Chen J, Chen J, Yue Y, Jiang X, et al. Quantum dots for tracking cellular transport of lectin-functionalized nanoparticles. *Biochem Biophys Res Commun* 2008;**377**:35—40.
201. Barry JN, Vertegel A. ANanomaterials for protein-mediated therapy and delivery. *Nano Life* 2013;**3**:1343001. https://doi.org/10.1142/S1793984413430010.
202. Wilczewska AZ, Tenerowicz K, Markiewicz KH, Car H. Nanoparticles as drug delivery systems. *Pharmacol Rep* 2012;**64**:1020—37.
203. Kraft JC, Freeling JP, Wang Z, Ho RJ. Emerging research and clinical development trends of liposome and lipid nanoparticle drug delivery systems. *J Pharmaceut Sci* 2014;**103**:29—52.
204. Suntres ZE. Liposomal antioxidants for protection against oxidant-induced damage. *J Toxicol* 2011. https://doi.org/10.1155/2011/152474.
205. Andrade CA, Correia MT, Coelho LC, Nascimento SC, Santos-Magalhães NS. Antitumor activity of Cratylia mollis lectin encapsulated into liposomes. *Int J Pharm* 2004;**278**:435—45.

CHAPTER

25

Construction and application of bionanomaterials

Sonali Naik[1,2], *Arun Torris*[1] *and S. Kiran*[1,2]

[1]Polymer Science and Engineering Division, CSIR-National Chemical Laboratory, Pune, Maharashtra, India; [2]Academy of Scientific and Innovative Research (AcSIR), Ghaziabad, India

1. Bionanomaterials

The science and innovation of biotechnology and nanotechnology have made awesome outcomes in the most recent couple of years which enabled clinicians to better detect, prevent, manage, and treat human disease. Nanotechnology deals with the construction of materials/devices with components at the nanometer (10^{-9} m) scale, whereas biotechnology deals with the use of biological systems/agents/organisms for beneficial use.[1] Bionanomaterials are one of those outcomes from the convergence of biotechnology and nanotechnology. Bionanomaterials are nanoscale molecular materials that are composed partially or fully of biological molecules such as proteins, peptides, enzymes, antibodies, DNA, RNA, lipids, oligosaccharides, viruses, and cells. The interface between biomolecule and nanomaterials can be manipulated by the bio-inspired process to obtain atomic-specific complex bionanomaterials/devices under mild experimental conditions. Furthermore, these materials can perform many explicit tasks that strongly recommend their introduction in the field of drug delivery, diagnostics, biosensing, and bioengineering.

2. History of nanotechnology and nanomaterials

Even though the management of materials at atomic and molecular scales seems to be a profoundly modern concept, the history of nanotechnology dates back to the ancient era, particularly in the development of nanocomposite[2] (Fig. 25.1). The artisans at these periods were unaware of nanoparticles, still, the presence of Au Cu and Ag nanoparticles were detected in the potteries which dated back to the fourth century. Lycurgus cup a decorative roman treasure has been detected with the presence of gold-silver alloyed nanoparticles in

Applications of Multifunctional Nanomaterials
https://doi.org/10.1016/B978-0-12-820557-0.00009-6

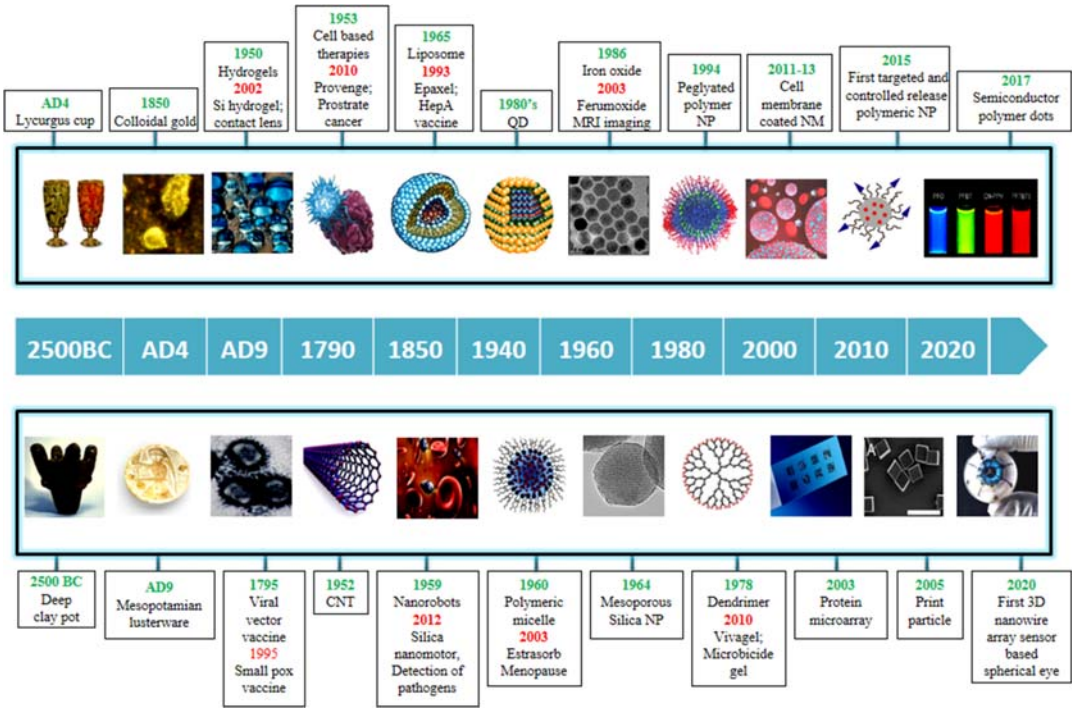

FIGURE 25.1 Schematic representation on the evolution of nanomaterials, green font represents the discovery period and the red font indicates the FDA approval period.

glass due to which it exhibited different colors in presence of light. Some other relevant citing dates back to the 9th century which involves the usage of nanoparticles for generating a glittering effect on the surface of pots. Most of these ancient marvels contained homogeneously dispersed Au, Ag, and Cu nanoparticles in the glassy matrix. Even these days, pottery from the middle ages and renaissance often retains a distinct gold- or copper-colored metallic glitter. The scientific understanding of nanomaterial came much later in the 18th century. One of the first scientific reports was authored by Micheal Faraday in 1857 on the synthesis of the colloidal solution of Au nanoparticles. This is considered one of the first scientific researchers into nanoscience and nanotechnology because of his remarkable discovery of the Faraday–Tyndall effect due to the scattering of light by colloidal particles. Over the years, the application of nanomaterials in biomedicine has vastly increased and the introduction of organic, inorganic, and carbon-based materials further enhanced their role for medical applications (Fig. 25.2).

3. Design of bionanomaterials

Bionaonomaterial fabrication involves the usage of biological resources and mechanisms for constructing nanodevices suitable for biomedical applications. So techniques having a

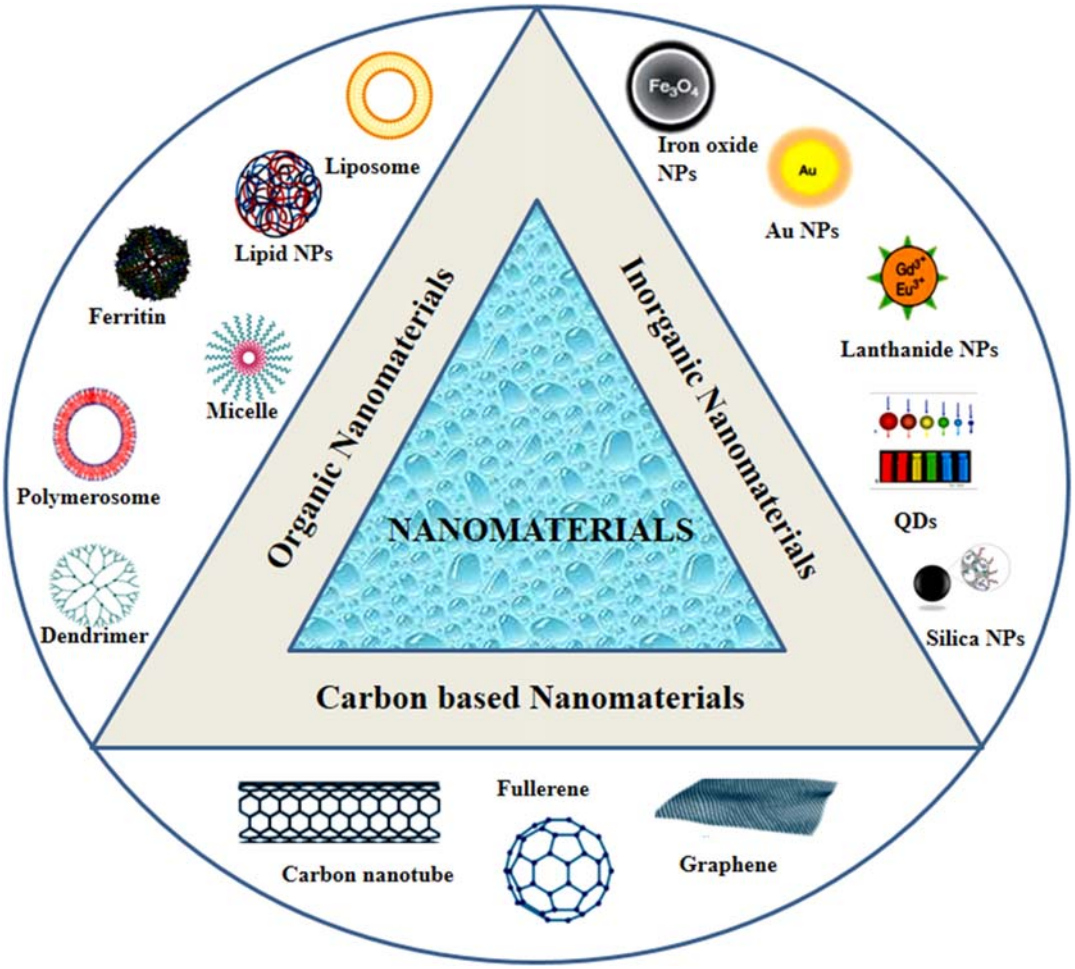

FIGURE 25.2 Schematic representation of the classification of nanomaterials.

great degree of control on the overall structure and chemistry which is deprived of any undesired side reaction usually preferred. Bottom-up self-assembly is one such promising technique that utilizes weak and specific interaction to achieve the required functionality and structure for nanofabrication is widely followed. Self-assembly plays a major role in bionanofabrication where noncovalent interactions such as hydrogen bonding, pi-pi interaction, electrostatic interaction, and van der Waals interactions are intricate in the formation of well-defined and stable hierarchical arrangements. Even though the individual interaction is weak, mutual interaction between the molecules leads to a very stable structure. DNA, protein, peptide, virus, enzymes are the key players for the design of bioinspired nanomaterials which can be self-assembled to create zero-dimensional (0D), one-dimensional (1D), and two-dimensional (2D) to three-dimensional (3D) architectures (Fig. 25.3).[3–6] Furthermore, these

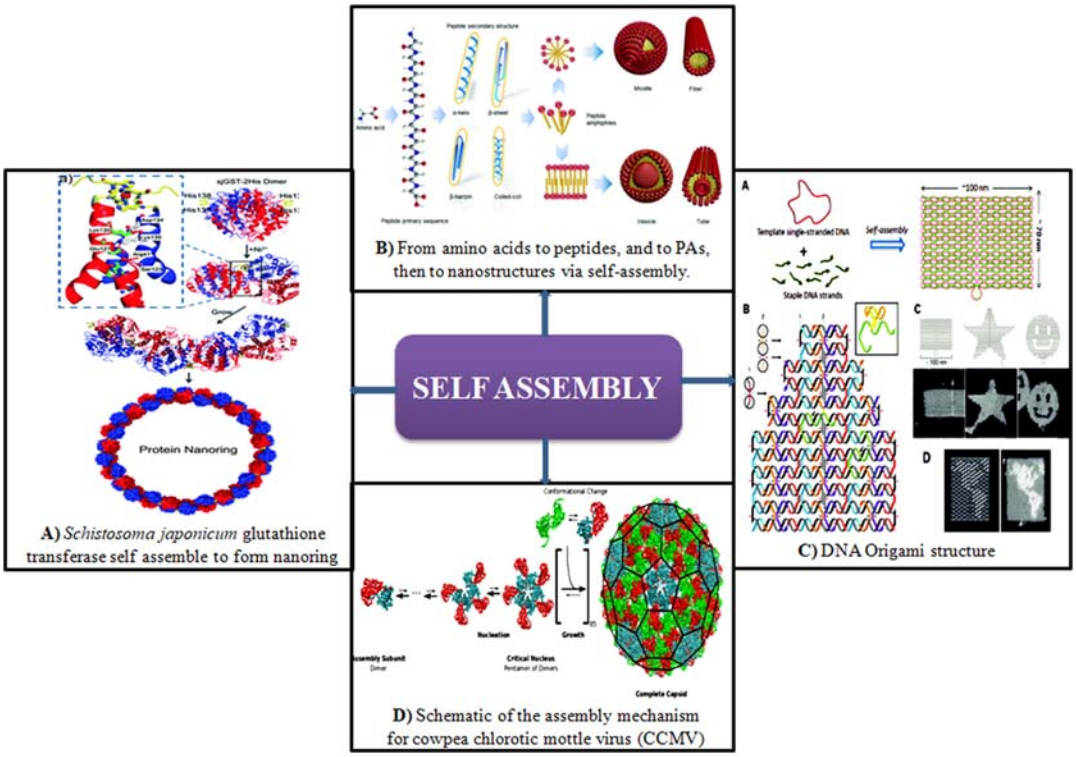

FIGURE 25.3 Self-assembled bionanomaterials (A) proteins (B) peptides (C) DNA (D) virus.

biomolecules can self-assemble by molecule-molecule interactions, molecule-material recognition, molecule-mediated, nucleation and growth, and molecule-mediated reduction/oxidization to create hybrid nanomaterials.[7]

Engineered protein assemblies were found attractive for future applications due to their large scale biosynthesis ability and their biofunctionality and biocompatibility. Proteins, as the elemental base of living organisms, play major roles in the process of functions and activities in living organisms. Proteins are composed of 20 basic building blocks of amino acids which aid in performing complex folds with other proteins to form supramolecular self-assemblies having delicate architectures and versatile functionalities. Furthermore, feature such as inherent biocompatibility, biofunctionality, and bioavailability makes protein assemblies attractive for future biomedical applications. Several strategies such as symmetry strategies, template strategies, crosslinking strategies, and supramolecular strategies have been commonly employed to develop different dimensionality protein self-assembly.[8] From zero-dimensional nanoparticles (nanospheres, and rings), 1D materials (nanowires), 2D materials (nanostructured protein films, metal coordinated proteins), to 3D materials (protein crystal and hydrogels) were created by the self-assembly of proteins.[8–10] Some of the recent work involves the construction of protein-based nanoparticles for anticancer applications. Nanoparticles sizes ranged from 60 to 500 nm and showed a distinct killing effect on the

cancer cells, such as MCF-7 and H460 cells, and exhibited IC_{50} of 260 ng/mL when applied to H460 cells.[11] Another recent example involves the development of protein nanocages that penetrate airway mucus and tumor tissue. Ferritin heavy-chain nanocages functionalized with polyethylene glycol was synthesized and on administration rapidly penetrated both mucus barriers and tumor tissues in vitro and in vivo and selectively entered cancer cells.[12]

Peptide-based self-assembly was extensively studied for the past few decades in the field of bioscience due to good biocompatibility and functionalities. Intermolecular forces and environmental factors such as temperature, solvent polarity, solution pH, ionic strength, photo irradiation, metal ion complexation, and enzymatic reactions[13] influence the nature of nanostructures generated by peptide self-assembly.[14,15] These factors lead peptide to self-assemble to nanostructures such as nanofibers, nanobelts, nanoribbons, nanotubes, hydrogels, and vesicles,[12] cyclic peptides normally stack into nanotubes,[12] and branched peptides often form micelles or vesicles.[12] These self-assembled nanostructures were exploited as cargo for transporting drugs, DNA, and proteins. In a recent example, Subramaniyam S et al. reported the effect of concentration in developing different nanostructures from short peptide having the sequence of BOC-Phe-Phe-Glu-$(OH)_2$ through the self-assembly. Spherical assemblies, nanotubes, and necklace-like supramolecular architectures were fabricated by controlling the concentration and incubation time. Furthermore, the spherical units were able to encapsulate small molecules and deliver them into cells, thus representing their potential for drug delivery applications.[16] Ziqi Wang et al.[17] reported recognition–reaction–aggregation cascade procedure for the construct of the peptide-based superstructure which could specifically promote the penetrability of renal cancer cell membranes and promote the delivery of the drug, ultimately achieving chemosensitization in vitro and in vivo.

DNA molecule is considered one of the most promising platforms for constructing new generation nanoscale architectures especially because of its programmability and structural stability.[18–25] In particular, many studies reported the design of DNA-based bionanomaterials such as DNA tiles,[26–28] DNA origami,[18,29] DNA bricks,[30] wireframe structures,[31,32] and crystals.[33] DNA origami is one of the most promising methods which involved the folding of DNA to create arbitrary shapes of DNA nanostructures, owing to its high biocompatibility and biosecurity.[34,35] Origami methods have found specific applicability in constructing a wide variety of 2D and 3D nano-objects. Furthermore, studies involved the construction of DNA based hydrogels. When compared to most synthetic or natural polymer hydrogels thus developed showed unique properties such as minimal toxicity, designability, precise recognition, and structural rigidity. Increasing development in the field of DNA nanotechnology has escalated the possible applications of developing, nanomechanical devices, computing systems, and programmable/autonomous molecular machines from DNA nanostructures.[36] However, scaling up the dimension of DNA nanostructures is often challenging. Strategies such as the solution and environment-dependent assembly of preassembled origami building blocks and DNA tiles,[37–41] and seed-mediated algorithmic assembly are currently employed to generate scalable nanopatterns. With ever-growing improvements using structural DNA nanotechnology, we can easily forecast a rewarding future in the generation of DNA templates with arbitrarily prescribed morphologies. Furthermore other than examples mentioned here viruses, enzymes, and phospholipid[39,40] also showed promising results in creating flexible and distinct architecture bionanomaterials through self-assembly. Utilization of biomolecules and bioinspired process such as self-assembly can offer potential strategies to build highly complex bionanomaterials which can meet the ever-growing needs in future bionanotechnology applications.

IV. Biomedical applications of nanomaterials

4. Nanorobots

Nanorobots (NR) are engineered controllable nanomachines/devices fabricated from nanoscale components having a size range from 0.1 to 10 μm. NR is a promising area developed by the fusion of nanotechnology and engineering and is expected to deliver great improvements in the field of medicine.[42] The advantages of NR include miniature dimension, lesser mass, higher thrust-to-weight ratio, high flexibility, and high sensitivity. Further because of the miniaturized version it can be easily introduced into the circulatory system utilizing catheters or other openings in the human body. Furthermore, NR can be easily programmed for specific biological tasks which can lead to better diagnosis procedures with minimum invasive procedures.

4.1 Classification of the nanorobotic systems

Based on the origin nanorobots can be categorized into natural/biological, artificial, and biohybrid types. The natural/biological NR, are fabricated using proteins, viruses, bacteria, DNA, and cells where synthetic polymers and noble metals and nonmetals are used to fabricate artificial NR. Both natural and artificial NR entities offer many functional advantages. The practical applicability of artificial NR is still limiting due to low energy efficiency, flexibility, and major concern over the lack of degradation, and biocompatibility with living cells. Even though natural/biological-based NR exhibited outstanding biocompatibility, biodegradability, along with accuracy, and controllability, the stability of these materials in the biological medium is a concern. Overall artificial based NR was lacking adequate compatibility with living cells while natural NR suffers from limited stability, this led to the development of biohybrid NR by merging the adequate properties both artificial and biological materials.

Based on the energy source used for propulsion artificial NR can be classified in two, one in which energy for propulsion is generated by a chemical process and other by physical process. The propulsion system of NR has a strong impact on their performances such as functioning environment, transport velocity, motion control, and biocompatibility,etc., which in turn can affect their overall performance in biological systems. Mechanical energy required for the propulsion of NR is generated by the consumption of fuel in the case of chemically propelled NR. Up to this period, a large number of chemically/biochemically propelled NR were reported which includes bimetallic nanorods, multiple-layer tubes, and Janus particles.[43] While physical stimuli such as magnetic, optical, electrical, and acoustic fields are used for propulsion in physically powered NR. So the necessity of high concentration chemical fuel and toxicity problems arising from the utilization of chemical fuel in the case of chemically propelled NR, and the requirement of high physical energy in the form of UV light, ultrasound, or magnetism for physically propelled NR are some of the negative side effects related to the usage of NR for clinical application. Despite the significant advance in the field, there is a rising demand for developing NR with precise geometries, fabrication methods, motion control, and biologically compatible fuel.[44,45]

4.2 Applications of nanorobots

Nanorobots have been utilized for numerous applications such as diagnosis, minimally invasive surgery, and especially in the field of targeted drug delivery, among many. Precise navigation, constant monitoring, and maneuverability to complex regions of a biological system by minimally invasive techniques make nanorobots as a key contender for the intended application.

4.2.1 Drug delivery

Nanorobots of natural/biological, artificial, and hybrid origin with cargo towing abilities have been extensively utilized for active drug delivery in the cellular level, and a tremendous sign of progress has been made in the previous few years. Passive drug delivery utilizes the flow of systemic circulation to carry drugs to the targeted area and ultimately they lack navigation ability for precisely targeted delivery. Since NR has the potential to promptly transport and deliver therapeutic agents directly to the site of application, thereby it will lead to improved therapeutic efficacy and aid in reducing systemic side effects due to toxicity induced by drugs. Recently, numerous studies have proven the cargo-carrying ability and therapeutical functions of NR, some of which involve the guided transport of drug-loaded liposomes,[46] pancreatic cancer cells,[47] and nucleic acids[48] among many. Drugs were mainly loaded into the NR by layer-by-layer, encapsulation, physical adsorption, electrostatic interaction, and so on.[48] Chemical or physical propulsion techniques were normally exploited to steer the drug-loaded NR to a programmed destination. On reaching the intended destination, physiological environments (e.g., pH) or external fields (e.g., NIR light, ultrasound, and magnetic fields) will trigger and aid in the release of encapsulated drugs.[43]

4.2.2 Delivery of therapeutics for cancer treatment

Cancer has been a major health problem worldwide and is the second leading cause of death. Targeting and delivery of drugs to the tumor site with reduced side effects is still a concern. Because of the miniature size and ease of transportability in the vascular system, many multifunctional nanoparticles were utilized to improve the tumor-targeting efficiency. Even though a wide variety of nanoparticles were developed many are in the early stages and the success of these nanoparticles in clinical practice remains questionable. So studies were conducted for the development of precise and active materials that can be self-propelled, actively targeted, and can penetrate the bio-barrier at the clinical level. Miniature size, precise payload-carrying facility, and ease of transportability in the vascular system paved the way to the introduction of NR for biomedical applications.[49–52]

Chemically propelled NR has been widely utilized for active drug delivery, and fantastic development has been made in the past few years. H_2O_2 is commonly used as the propulsion fuel and mechanisms such as bubble propulsion, self-electrophoresis, and self-diffusiophoresis were involved in the propulsion of these chemically powered nanomachines.[53,54] Numerous studies were reported on the development of chemically powered NR, especially for cancer therapy. One such study involves the practice of template-assisted layer-by-layer (LBL) assembly for the development of chemically propelled nanoporous polymer multilayer tubular nanomotor. This chemically propelled NR utilizes H_2O_2 as fuel for its navigation. Furthermore, this study highlights these bubble-propelled nanomotors are capable enough

to deliver the loaded drugs such as doxorubicin hydrochloride to cancer cells with the aid of chemical fuel and external magnetic field. Saloni et al.[55] reported the construction of Fe_3O_4 nanoparticles conjugated self-propelling NR loaded with an anticancer drug, doxorubicin hydrochloride. NR exhibited better tissue penetration, control, and improved pharmacokinetics makes it a superior approach in targeted cancer therapy. The above-developed nanobots demonstrated better self-propulsion not only in high ionic media but also in other biological media. Nanomotors with chemotactic behavior were developed for anticancer drug delivery. The nanomotor is based on a polymer somestomatocyte functionalized with platinum nanoparticles which are capable of acting as cargo for anticancer drugs such as doxorubicin. Further, this study demonstrates that platinum loaded nanosized polymer stomatocytes showed effective drug loading capability and also display chemotactic behavior in the presence of hydrogen peroxide gradients.[52]

Most of the earlier reported NR are made up of synthetic polymers and noble metals limiting them meeting the needs of biomedical applications due to its poor biodegradability and biocompatibility. So more efforts were set to construct NR with improved biocompatibility.[56–58] One such study involves the development of chemically propelled, biodegradable, and functionalized NR by template-assisted layer-by-layer assembly. The NR assembly is made of bovine serum albumin/poly-L-lysine incorporated with gold particles embedded in gelatin hydrogel.NR showed promising results in effective anticancer drug encapsulation and controlled delivery to cancer cells with the aid of near-infrared light.[59] Thus developed protein-based nano-rockets are biodegradable and can be effectively maneuvered to the targeted site making it a reliable platform for the next generation of NR in the biomedical field. Further studies involved the utilization of plant products to develop biodegradable plant-based swimmers have been reported, but its ability for drug delivery applications has yet to be demonstrated.[60] These examples successfully demonstrate the in-vitro drug delivery of chemically propelled NR. Other than drugs these chemically propelled NR are exploited for the pick-up, transport, and release of various cargoes such as cancer cells,[47] nucleic acids,[48] polymer particles,[61] and bacteria.[62] However, the fundamental problem concerning the applicability of NR toward clinical application lies in the toxicity on using H_2O_2 as the main fuel, complex preparation technique, and poor biocompatibility.[63]

Physical propelled NR are promising alternatives in this aspect, as they rely on chemical free propulsion forces, which will be safer for biomedical applications as no toxic chemicals utilized for propulsion. Ultrasound energy with little harm to the human body is widely used for biomedical applications.[64] Ultrasonic energy is derived from a high-frequency sound wave can trigger and regulate the speed of NR. Acoustic NR can autonomously convert local ultrasound energy into mechanical motion, which helps to control direction and speed independently. Furthermore different modes of movements such as axial propulsion and spinning about their axis can be achieved by applying different ultrasonic frequencies making it an interesting technique to control the movement of NR.[65] Taking advantage of the influence of ultrasound studies was conducted to regulate and modulate the speed of NR by physical propulsion. Various studies involved in the development of ultrasound-driven NR for imaging and drug delivery applications. Garcia-Gradilla et al.[65] demonstrated the construction and transportation of ultrasound powered nanowire motors to cancer cells and the rapid release of drug by NIR-light exposure. Wei Wang et al.[56] demonstrated the construction of that nanoporous gold NR about 300 nm and the ultrasonic propulsion of rod-shaped

nanomotors inside living HeLa cells. The nanoporous gold structure enabled the near-infrared light controlled release of the drug by photothermal effects. Furthermore, these studies highlight that the propulsion does not require chemical fuels or high-power ultrasound thus provide a new insight for propelling the NR without affecting the viability of fuels. But the applicability of ultrasound propulsion in vivo environment has to be still addressed as its propulsion capability will be hindered due to the influence of reflection, refraction, and attenuation of ultrasound.

Magnetic nanomaterials are of increasing interest in biomedical applications such as cancer treatment, magnetic resonance imaging contrast, cell tracking, and others. This extreme interest arises because of their biocompatibility, ease of maneuverability, and its applicability in various therapeutic applications.[56,66] Compared with other external field-driven motors, magnetically powered NR are particularly promising as miniaturized engines for biomedical applications as they can perform complex therapeutic maneuvers while obviating fuel requirements under magnetic actuation and without adversely affecting the tissues.[67–69] So efforts were carried out to understand cargo-towing capability magnetic nanomotors by fuel-free technique. For example, magnetically guided NR was used toward the delivery of fluorouracil medication for reducing tumor growth in a mice model. Fe and Pd entities were used to construct NR by template-assisted electrodeposition and external magnetic fields were used to draw FePd nanowires to the site of application. The drug release was externally triggered, allowing the nanorobotic platform to distribute a high amount of the therapeutic agent in a localized area of the tumor triggering cell death exclusively in this region.[70,71]

Fuel-free flexible magnetic nickel–silver nano-swimmers for targeted drug delivery was introduced by Gao et al.[56] Applicability of nano-swimmers is demonstrated by directing the delivery of drug-loaded particles to HeLa cancer cells in biological media. These fuel-free nanomotors have been shown the capability in pick-up and transport of various drug carriers to the predetermined destination through a planned route, which represents a novel approach toward transporting cargos in a target-specific manner. These recent results highlight the importance involved in using low toxic functional magnetic NR which can be triggered magnetically for both targeting and inducing cancer cell apoptosis. Despite the significant advancements and understanding in the design of both physically and chemically propelled NRas advanced cargo transport systems, several challenges still exist for their practical in-vivo use.[72] So various biohybrid-based NR has been designed and studied for targeted delivery of payloads. In one such study, magnetotactic bacterias, which have the capability to produce magnetic iron oxide nanoparticles naturally, were utilized as a potential career (Fig. 25.4). Further, a carbodimide-based bioconjugation method was utilized to covalently bind amine containing molecules of bacteria to carboxylated liposomes loaded with therapeutic payloads. In vitro studies reviewed that these biohybrid systems were effective in delivering an active substance to the solid tumor without altering intrinsic bacterial motility and their behavior under a controlled magnetic field.[73]

Felfoul et al.[74] demonstrated magneto-aerotactic bacteria can effectively be used to develop NR which can be actively used to improve drug delivery in tumor hypoxic regions. The study indicated that magneto-aerotactic containing a chain of magnetic iron-oxide nanocrystals tend to swim along local magnetic field lines and toward low oxygen concentrations to transport drug-loaded nanoliposomes into hypoxic regions of the tumor. However, the potential

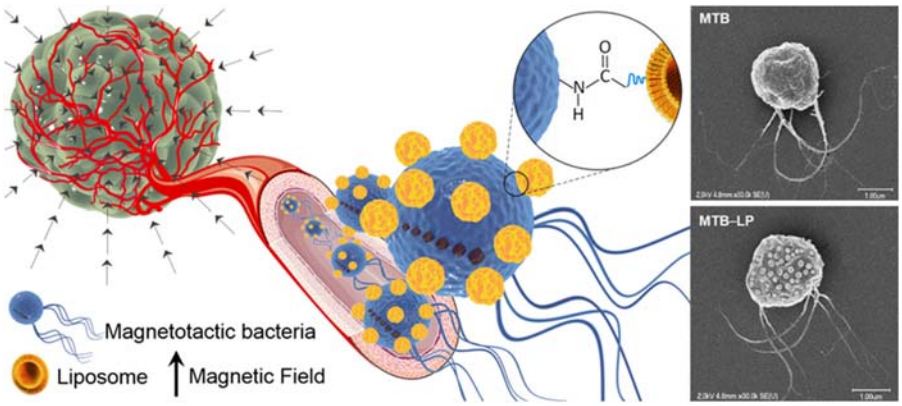

FIGURE 25.4 Schematic representation of self-propelled magnetotactic bacteria and its microscopic images.[73]

toxicity of bacteria to the human body and the controlled drug release from the bacteria-based robot has yet to analyze.

DNA molecule is considered one of the most promising platforms for constructing new generation mechanical molecular devices that can precisely sense and respond to molecular triggers.[75] Many reports indicate that a tetrahedral framework of nucleic acid could aid as a favorable nanocarrier for many antitumor drugs, especially due to its high biocompatibility and biosecurity.[76–78] These advances have triggered the biological application of DNA nanostructures, most notable advancement involves the construction of DNA NR and employing them as drug-delivery nano-vehicles for cancer treatment. DNA origami method which involved the folding of DNA to create arbitrary shapes was commonly employed to design and produce DNA nanostructures platforms with controlled size, shape, and spatial addressability[79–82] for biological applications.[83–91]

Origami technique along with self-assembly was utilized for developing tube-shaped DNA NR programmed to transport and deliver payloads such as thrombin solely to tumor sites in a controlled fashion into tumor vessels to induce thrombosis for tumor therapy (Fig. 25.5). Hollow tubular DNA nanorobot (19×90 nm) was constructed by binding thrombin in the cavity of tubular, which protected the thrombin molecule from being interfered with the external environment. Only at the site of application, the nanobot gets opened exposing the contained thrombin molecules and activating localized coagulation. Invivo experiments on mouse model revealed that thrombin incorporated nanorobot was effective in generating confined coagulation to selectively block tumor blood vessels, thus inhibiting tumor growth. This developed NR proves to be safe and inert material for the precise transfer of thrombin and other drugs in cancer therapy.[92]

WenjuanWaet. al. report the construction of DNA framework-based intelligent nanorobot for selective lysosomal degradation of tumor-specific proteins on cancer cells. These DNA

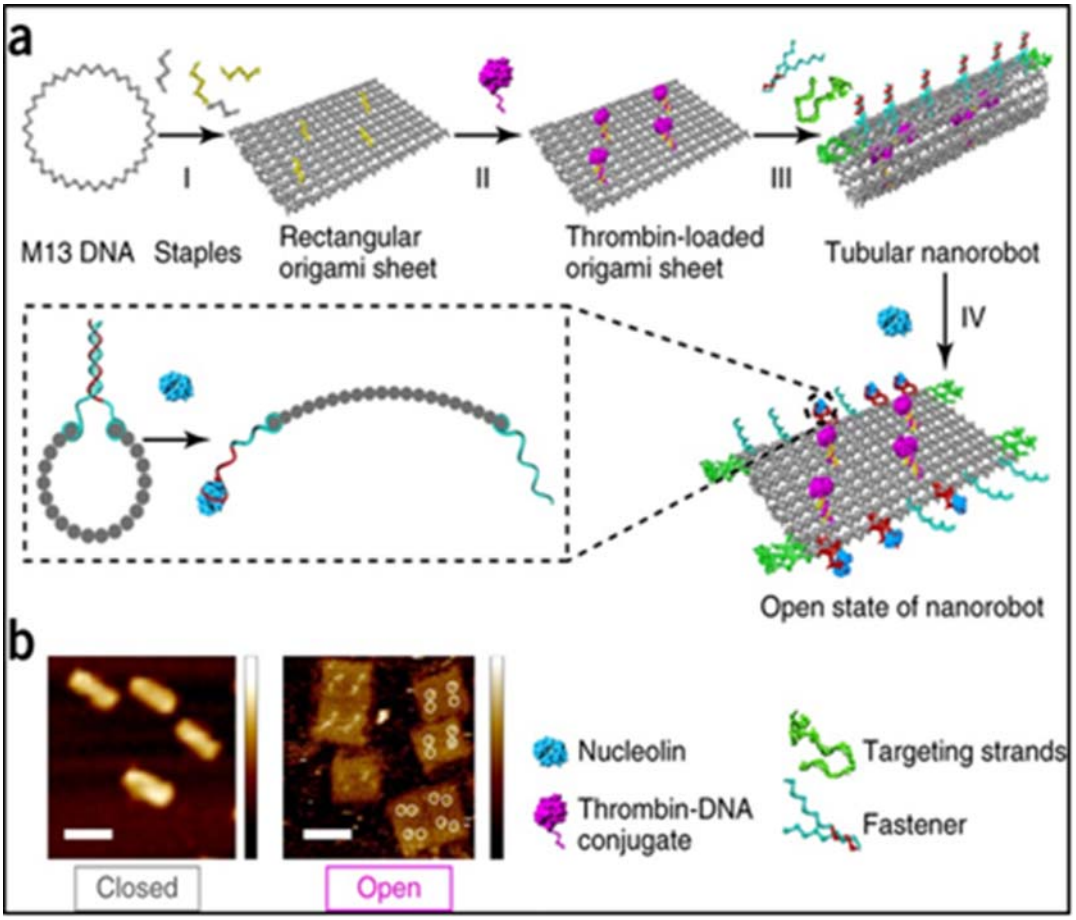

FIGURE 25.5 (A) Schematic illustration on the construction and mechanism of action of the thrombin-loaded DNA nanorobot (B) atomic force microscopy of closed (left) and opened states (right) of DNA nanorobot.[92]

nanorobots were capable of targeting breast cancer cells and inducing the lysosomal degradation of the membrane protein. Further studies of these DNA nanorobots in a mouse model revealed that these NR structures can enhance stability and prolonged blood circulation time of anchored aptamers thereby inducing lysosomal degradation with higher efficiency. Hence DNA based NR sheds new light on targeted drug delivery/protein degradation for precision cancer therapy.[92]

With intensive research efforts, significant progress has been achieved in developing NR in the last 2 decades. The outcome of these studies indicates the potential of NR in improving

medical treatment producers. Despite the remarkable progress in the field, many hurdles have to be overcome to be practically applied for clinical application. Speed, efficiency, nature of fuel for propulsion, cargo towing property, maneuverability in viscous media such as blood and biocompatibility have to further improve before moving to clinical translation of NR.

5. Biochip technology

Concerning implantable bioelectronics, miniaturization is considered the state of the art in electrochemical biodevices. The encouraging progress in the field of nanotechnology which is once used for the construction of computer chips for extended time has led to envisage the development of so-called biochips. Biochips are a kind of miniaturized laboratory that is composed of a set of diminished microarrays that are used to analysis or detection of biological species and molecule.[93] Millions of sensors present in the chip enable it to perform multiple experiments to be executed at the same time to obtain high throughput in less time making them preferably suited to encounter the demands of biological molecules. Furthermore, the introduction of microfluidic assay simplified and automated of tedious laboratory task without compensating the sensitivity of biochip. Moreover, the advantage of these miniaturized devices is the ease of integration of common techniques such as electrophoresis, mass spectrometry, luminescence, electrical signal, and magnetism with a biochip.

Initially, biochip technology was utilized for monitoring fisheries; currently, it covers almost all the areas related to healthcare applications. The overall market size of biochips is estimated to grow at a CAGR of 18.4% from 2015 to 2020 to reach $17.75 billion by 2020.[94] In 1993, the Food and Drug Administration passed the Safe Medical Devices Registration Act of 1993, requiring all artificial body implants to have "implanted" identification—the biochip. Currently, most medical devices and implants are loaded with a biochip. In the late 1980s, the first DNA microarray was commercialized by Affymetrix. Agilent Technologies, Inc., CombiMatrix Corporation, Affymetrix, SynVivo, Euroimmun, Bio-Rad Laboratories, Inc., Cepheid Inc., Fluidigm Corporation, GE Healthcare, Hoffman-La-Roche Ltd. are some of the many key and niche players in the field of biochips. Currently, diverse types of biochips are available which are suitable for diagnosis, drug development, gene detection, chromosomal location analysis, DNA methylation, miRNA, and alternative splicing arrays, pharmaceutical, biotech, and agrochemical industries.[95]

Microarray and transducer are the two important components of any biochip. Microarray's major role is to detect various biomolecules. Microarrays are a network of sensors modified with sensing molecules either physically or chemically. The transducer converts the molecular sensing mechanism into an understandable output that could be understood by the operator. The rapid improvement in the field of nanotechnology provides a promising platform for incorporating enzymes into nanosystems to improve the overall selectivity and sensitivity. Various efforts were put forward to develop low-cost miniaturized biochip by the incorporation of nanomaterial along with microfluidic technique. A key advantage to the use of nanoparticles for fabricating biochip is their large surface area to volume ratio compared to that of bulk materials. The results of these studies indicated the incorporation of functional nanomaterial will aid in the development of biochip with low expenditure and high sensitivity.[96]

Many metals and nonmetals nanoparticles were utilized for the development of biosensors. Some of the studies involve the usage of metals like gold, silver, palladium, rhodium, platinum titanium, zinc, and various forms of carbon such as CNT and graphene for the fabrication of biochip. Some studies involve the utilization of various carbon forms such as the detection of dopamine, glucose,[97] and even for the detection of nutrition in the soil. Nanowires of zinc oxide and titanium were used to detect pH conditions in the environment, whereas nanotubes of nickel oxide nanorods[98] were utilized for detecting total cholesterol in human blood. Nanoparticles that exhibited biocompatibility such as gold, silver, iron, palladium, rhodium, platinum, etc., were utilized for functionalizing groups like proteins, peptides, ligands, DNA, fatty acids, and plasmids for aiding the sensing of biomolecules.[99–101] Even though many noble metals can be utilized for developing biosensors, gold nanoparticles stand out due to their unique surface chemistry, high electron densities, chemical inertness, and their possession of good electrical and optical properties.[102,103] Incorporation of gold nanoparticles aided in improving the overall sensitivity and biomarker targetability due to its high surface to volume ratio. So gold nanoparticles embedded biochips were commonly fabricated which aided as a sensing platform for a vast number of analytes such as detection of glucose level,[104,105] cardiovascular diseases, and detection of antigen responsible for cancer[106–110] Fig. 25.6.

One of the most promising applications of the biochip is the early-stage detection and identification of cancer-associated biomarkers.[111] Rosetta, Febit, and Protagen some of the leading companies to explore biochip utilization for cancer diagnosis. Nanoparticles along with microfluidic platforms led to multiplex assay aiding in the detection of a panel of protein biomarkers thus improving the overall reliability in cancer diagnosis.[112–115] Nanoparticles of metals such as gold, silver, nanoparticles of different dimensions of a magnetic material like iron, various form of carbon nanomaterial, quantum dots coated with antibodies or oligonucleotides have been investigated for cancer biomarker detection,[116–118] toxicity level in water,[101] detection of hydrogen peroxide released from living cells.[119,120]

Biochip technology was utilized for the detection and diagnosis of severe physiological diseases. During the few last decades, dramatic progress was made in the field of fabricating biochip which is capable of investigating the molecular mechanisms of human emotion in real time using body fluids such as blood, saliva, urine, or sweat (Fig. 25.7).[121]

Studies were even carried out for the development of simplified and cost-effective biochips which led to the progress in creating cantilever biochip and paper-based biochip. Many advantages could be pointed out for these modified biochips. Cantilevers-based biochip does not require external electronics or power labeling or any signal transducer for fluorescent molecule for operation. Furthermore, microfabrication of cantilever systems exhibited superior property over earlier microcantilevers.[122,123]

The deflection of microcantilever was analyzed to detect the concentration of the analyte and it is commonly used for the detection of DNA sequences or antibody-antigen bindings. There were certain reports regarding the developments of low-cost paper-based biochips were cellulose micro-/nanofiber matrices of paper substrate provide huge advantages in both microfluidic platform and 3D hierarchical backbone for incorporating metal nanomaterials. Various fabricating method for paper-based biochips involves direct printing, photolithography, and 3D printing. In which direct printing technique can produce submillimeter resolution thus developed biochips were utilized for the detection of glucose, iron, and

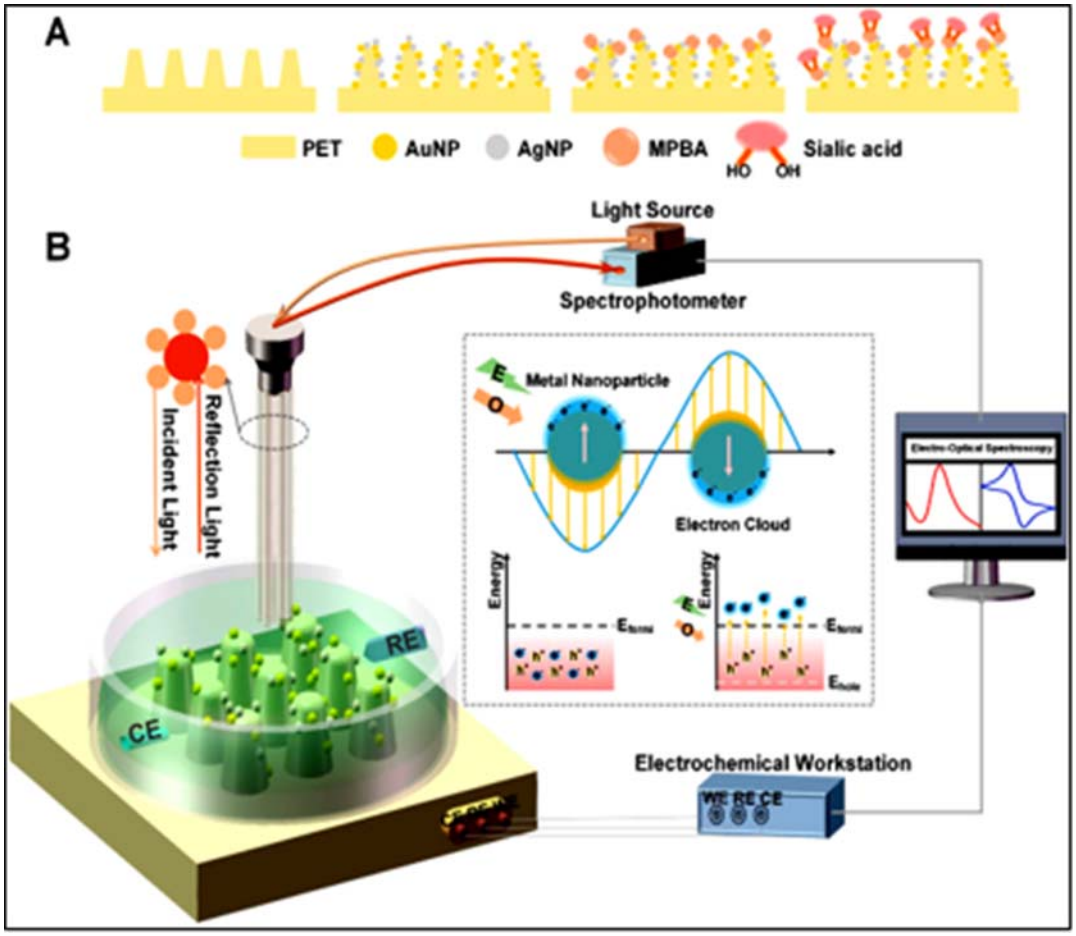

FIGURE 25.6 The nanochip-based dynamic electro-optical spectroscopy system. (A) Fabrication and functionalization of the nanochip. (B) The apparatus of the system and the schematic representation.

various biomolecule. When compared to direct printing, photolithography enabled high-resolution and photo-resistant patterning.[124]

However, 2D microfluidic devices still have limitations in their capabilities. 3D configuration of paper-based biochips microfluidic devices has successfully demonstrated densely packed microfluidic channels as well as multiple detections of biomolecules.[125] A study has indicated that paper-based 3D microfluidic devices enable the detection of multiple reagents such as glucose and bovine specific albumin in artificial urine solution.[126] The furthermore unique configuration of metal nanostructures can be deployed by simple methods such as drop and drying, immersing, thermal evaporation, and inkjet-printing on cellulose micro-/

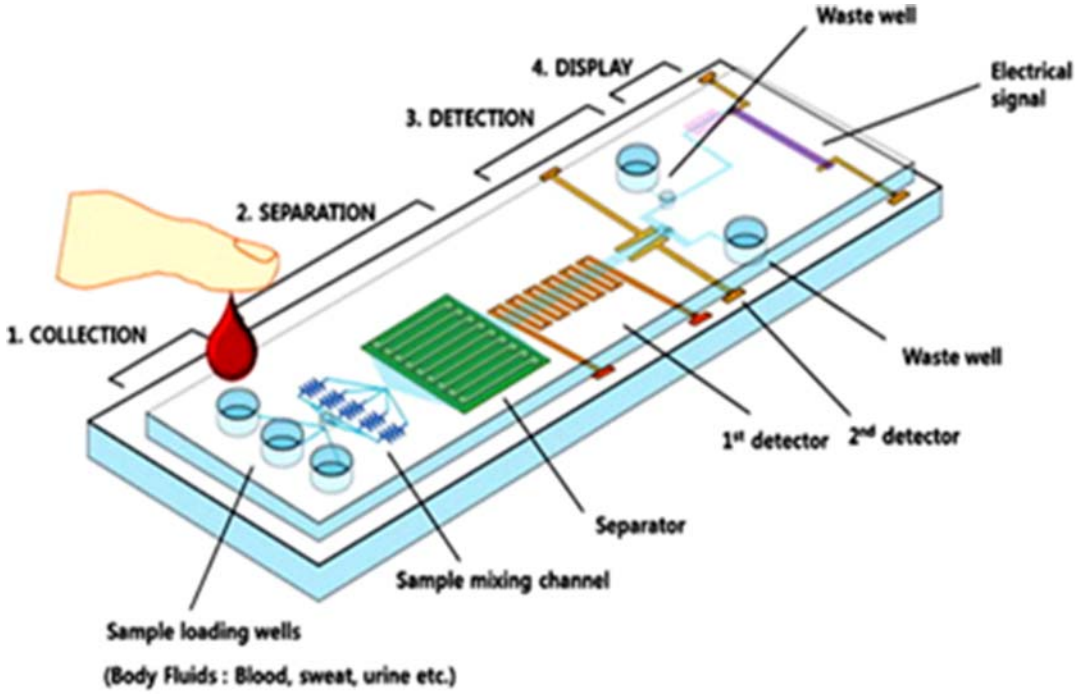

FIGURE 25.7 Schematic drawing of emotion-on-a-chip.[121]

nanofiber matrices which secures generation of multiple plasmonic hotspots for highly sensitive detection of biomolecules.[127]

For the early detection of disease, especially at the point-of-care, there is an ever-increasing need and demand for a novel and more efficient diagnostic tools.[128] The phenomenal capability of nano-sized materials to exhibit unique physiochemical characteristics in contrast to bulk material has opened new gateways to downstream the development and fabrication of novel materials suitable for detection and diagnosis that were not possibly evident in the past. Biochips are one of the outputs of the ever-blooming area of nanotechnology. Biochips offer many attractive analytical features and represent promising candidates for future clinical diagnostics. This fully integrated total analysis system leverages microelectronic components, microfabrication techniques, and nanotechnology that offers diagnostic accuracy equal to laboratory-confined reference methods. Incorporation of microfluidics with biochips has added the following advantages such as multiplex assay and simultaneous separation of the targeted biomolecules for detection. Despite good progress in multiplexed sensing, further advances are still needed to handle hundreds of biomarkers in short turnaround times with minimum or no cross-reaction between the affinity ligands and target biomolecules. This biochip research undoubtedly represents progress for advanced disease detection.

6. Bionanomaterials for diagnostics

The diagnostics in the biomedical scenario involves the study of procedures that provides information for screening, diagnosis, and detection of diseases. Nanomaterial based disease diagnostics have become an increasingly relevant alternative to traditional techniques. Bionanomaterials designed for diagnostics involves nanomaterials, partially or fully derived from biological resources, intended for the screening, diagnosis as well as detection of diseases.[129] Classifications of bionanomaterials for diagnostics are given in Fig. 25.8.

6.1 Proteins and peptides

6.1.1 Albumin nanoparticles

Jeong et al. reported the preparation of human serum albumin (HSA) nanoparticles, conjugated with photo-sensitizer, as an efficient targeting agent for photodynamic therapy.[130] EDC coupling method was employed for the conjugation of photo-sensitizer onto HSA, resulting in the formation of HSA-photosensitizer nanoparticles. These albumin nanoparticles form self-assembled structures in aqueous media and were nontoxic in their native state. They exhibited enhance tumor-specific bio-distribution, which aids them to adversely affect the tumor site with singlet oxygen, generated by the photo-sensitizer upon laser irradiation.[131]

6.1.2 Layer-by-layer protein architectures

Takahashi et al. reviewed the layer-by-layer (LBL) approach for the construction of protein architectures, such as avidin and biotin.[132] The binding between avidin and biotin is high and resembles covalent bonds. LBL deposition of avidin and biotin on the surfaces of optical

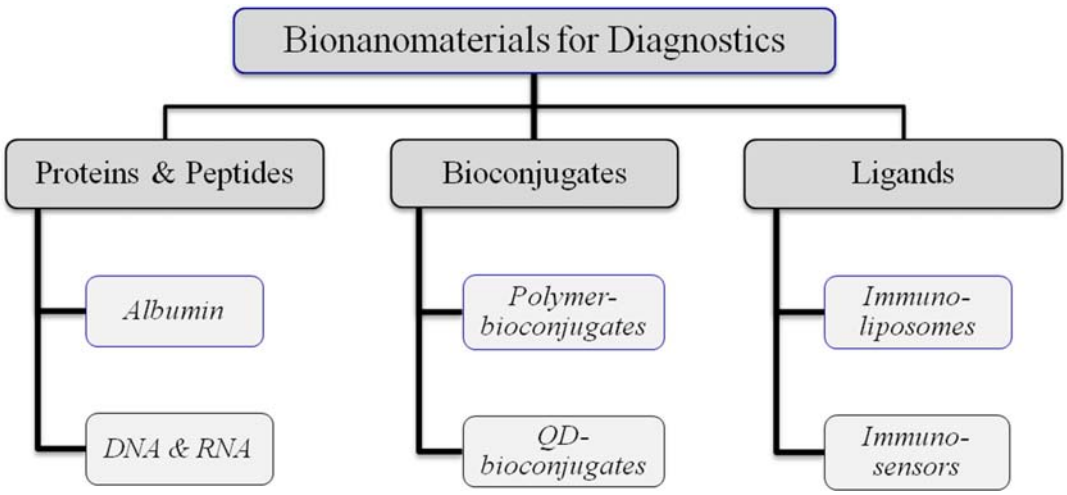

FIGURE 25.8 Classification of bionanomaterials for diagnostic applications.

probes and electrodes results in the formation of optical and electrochemical biosensors. They help to tag DNA and proteins with activated biotin derivatives.

6.2 Bioconjugates

6.2.1 Polymer bioconjugates

Mansur et al. have devised a polymer bioconjugate-based core-shell system to target and image αvβ3 integrin receptors of cancer cells.[133] Chitosan was covalently bound onto RGD peptide using a cross-linker and was later used to cap CdS quantum dots (QDs). Chitosan layer enhances the solubility of QDs, thereby forming a shell on its surface in aqueous media at ambient temperature. These core-shell structures were effective at specific targeting integrin, when assayed in vitro, using noncancerous human embryonic kidney cell lines and cancerous sarcoma osteogenic-derived cell lines.[134]

6.2.2 Quantum dot bioconjugates

Quantum dot (QD) bioconjugates represents one of the major interfaces of biotechnology and nanotechnology, where the unique optical property of QDs in combination with various biomolecules adds more promising applications in cellular imaging and labeling.[135] Such inorganic—biological hybrids can enhance the bioavailability and long-term stability of QDs.

QD bioconjugates were prepared by the conjugation of inorganic nanostructures with biomolecules such as proteins, peptides, DNA, etc. Generally, three conjugation schemes are following for attaching proteins on to the surface of QDs. First one is EDC (1-ethyl-3-(3-dimethylaminopropyl) carbodiimide) condensation, where amine functional groups on proteins reacts with carboxy groups on the surfaces of QDs. Second approach is the direct binding of proteins on to the surface of QDs using thiolated peptides or polyhistidine (HIS) residues. Third approach is the noncovalent self-assembly, where proteins were chemically modified to induce physical attraction with the functional moieties on the surface of QDs. Resulting conjugates reflects the combined attributes of both inorganic nanomaterials and biomolecules.

Medintz et al. reported the combination of ~20 Maltose binding proteins (44 kDa) to each QDs possessing 6-nm diameter.[137] Such multifunctional inorganic—biological hybrids can act as nanoscaffold, housing several biomolecules and functions as a chemical sensor. Chan et al. labeled ZnS-capped CdSe QDs with the protein transferrin by the reaction between carboxyl groups on the surface of QDs with that of amine in protein[136] (Fig. 25.9). These hybrid bioconjugates were easily transported into HeLa cells by receptor-mediated endocytosis and showed ultrasensitive detection at single-dot level, which helps to image molecular trafficking in living cells. Similarly, self-assembly of CdSe−ZnS QD bioconjugates was studied by Mattoussi et al.[138] In this study, chimeric fusion proteins were electrostatically conjugated to the oppositely charged QDs with high quantum yield and retention of biological activity. However, in this approach, the presence of charged species or interaction domain might impart challenges in the functions of QD bioconjugates, by disturbing the electrostatic balance between QD and protein.

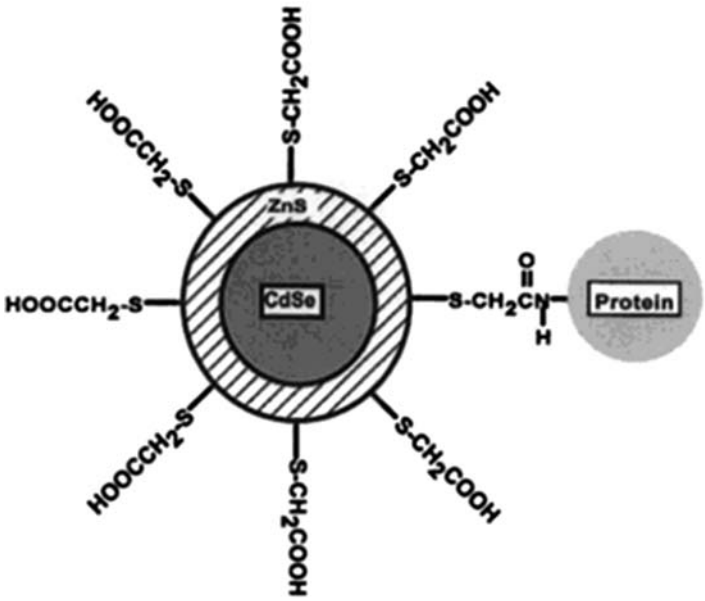

FIGURE 25.9 Schematic of a ZnS-capped CdSe QD covalently coupled to a protein by mercaptoacetic acid.[136]

6.3 Ligands

6.3.1 Immuno-liposomes

Liposomes are well-known pharmaceutical carriers, with phosphor-lipid based bi-layered structures and are one of the widely used agents for the delivery of therapeutic agents with solubility issues. However, one of the major drawbacks of liposomes is fast elimination from systemic circulation and their deposition in the liver.[139]

One of the solutions for faster systemic elimination of liposomes is designing targeted-liposomes, with specific ligands, attached to their surface, which can discriminate and bind onto cells of interest. Torchilin has reported the modification of liposomes with immuno-globulins (Ig), which are attached onto the surface of liposomes or inserted into the liposomal membrane, without affecting the integrity of liposomes or activity of the antibody.[140] Modified liposomes were able to accumulate in the area within the body where an attached antibody recognizes and binds its antigen.

6.3.2 Immuno-sensors

Immuno-assay is the quantification of antibody or antigen concentrations, derived from specific recognition interactions. It is considered as one of the major analytical technique adopted widely in clinical diagnostics and bio-sensing. New generation of bionanomaterials, which possess the ability to identify or "sense" the presence of specific biomolecules, has paved the way for the development of immuno-sensors. These advanced sensors could provide very vital information about early disease diagnosis, by utilizing immune reagent recognition elements.[141]

A silicon nanowire array-based immuno-sensor was developed by Zhang et al., to address cardiovascular diseases. This silicon nanowire array detects the cardiac biomarkers such as human cardiac troponin-T, creatine kinase-MM and creatine kinase-MB in serum, in a label-free approach, with femtomolar sensitivity.[142]

7. Bionanomaterials for regenerative medicine

Nanotechnology has been looked upon as a solution to many key questions evolving around the biological systems to be revealed and with higher expectations toward the future.[143] Regenerative medicine (RM) focuses on replacing or regenerating cells, tissues or organs in human body, mainly to restore their normal function. This objective may be achieved either by stimulating bodies own inherent repair mechanisms or by implanting tissues or organs, grown outside the body when body loses its own ability to repair. RM involves various approaches and tools, depending upon the problem to the addressed. This branch of medicine has been projected as a potential solution to alleviate shortage of organs for donation.[144]

Three major pillars of RM are cell therapy, biological agents, and biomaterials, applied independently or in combination (Fig. 25.10).[145] Recently research advances in stem cells and their therapies have gained attention and momentum in various RM approaches and constitute a major domain of cell-based therapies adopted so far. They showed higher potential in addressing injuries and damages caused by various degenerative diseases, chronic diabetes, as well as aging.[146] Driven by multiple microenvironmental cues and their stimulation, stem cells renew by themselves, within a definite time period and differentiate further onto specialized cells and tissue. Thus, they demonstrated their potential in addressing the replacement or regeneration of damaged cells and tissues in an organ.[147] Various regulating

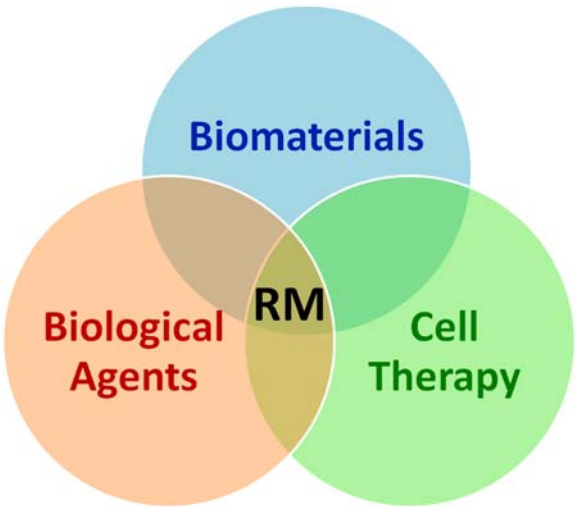

FIGURE 25.10 Three major pillars constituting regenerative medicine (RM).

biological agents such as growth factors, signaling molecules, extracellular matrices (ECMs), etc., aids stem cells and play a critical role in modulating the behavior of stem cells, during the regeneration process.[148]

Nanostructures and bionanomaterials play a major role in intrinsic interaction with higher specificity toward various biological systems involved in RM. One of their unique properties lies in controlling stem cell signals and to analyze them further to study the mechanisms involved in adult stem cell behavior.[149] In this section, we have summarized bionanomaterials employed for RM, addressing their important roles in tracking, imaging, vascularization, and repair of degenerated tissues (Fig. 25.11).

7.1 Tracking and imaging cellular events

Nanomaterials are coupled with biomolecules in controlled conditions by employing interdisciplinary approaches to monitor and support the regeneration process. For example, iron nanoparticles coated with dextran are used for tracking and studying stem cells with MRI tools.[150] Bio-mimetic coating helps the nanomaterials to enhance their solubility and attain long-term stability. Further, they are easily internalized onto the cytoplasm, with higher labeling efficiency and provide real-time signals to the diagnostic tools. They possess higher sensitivity than conventional gadolinium-based contrast agents and monitor the migration of stem cells at their site of implantation. Magnetic-sorting techniques help to retrieve stem cells from the excised tissues, such as spleen and bone marrow.[151] Analysis of these excised tissues provide valuable information about the distribution and differentiation of stem cells and contributes toward significant clinical and research implications.

Conjugation of iron oxide nanoparticles with antitrasnferin receptor monoclonal antibody helps to design new generation of antibody-functionalized bionanomaterials. These nanomaterials were used to target transferring receptors on the surface of progenitor cells, thereby labeling them for monitoring the progress of regeneration in the central nervous system.[152]

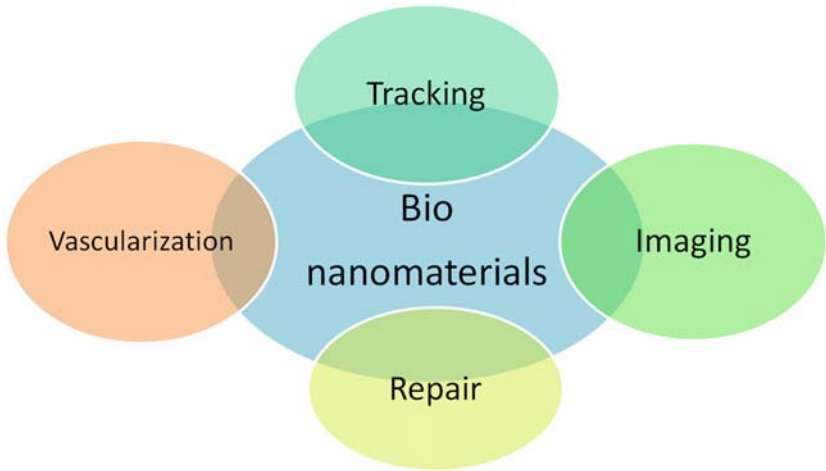

FIGURE 25.11 Overall functionality of bionanomaterials in RM.

Neurotransplantation of these nano-systems helped to track the extent of myelination in nerve tissues. QDs or semiconductor nanocrystals integrated with biomolecules has opened an array of opportunities to track and image the progress of tissue regeneration. Molecular dynamics of integrin molecules responsible for the osteogenic differentiation of stem cells were studied by QDs conjugated with integrin antibodies. These bionanomaterials also provided accurate optical identification of these critical integrin molecules involved in the bone regeneration process. Similarly QDs conjugated with arginine-glycine-aspartic acid peptide were used to label human mesenchymal stem cells (hMSCs) which provided their long-term labeling as well as monitoring their differentiation onto various substages to form adipogenic cells.[153]

7.2 Vascularization and repair of tissues

Self-assembled peptide nanofibers were designed to integrate revascularization process in dental pulp tissue.[154] Synthetic scaffold containing the peptide nanofibers mimics the natural ECM thereby enhancing the cell−cell and cell−matrix interactions. Simultaneously, the delivery of growth factors such as vascular endothelial growth factor and encapsulation of dental pulp stem cells in these peptide scaffold induced in vivo angiogenesis in the artificial teeth implanted in a mice.

7.3 Translation of bionanomaterials

Even though fundamental science has been enriched with wide number of innovations in the past, as evidenced by tremendous progress in the development of various nanomaterials for RM, the number of marketed products is still a major concern, as compared to that of traditional medicine. Rational design as well as strict evaluation of bionanomaterials could improve their efficacy and minimize potential concerns. Safety concerns are one of the major bottle-necks involved in the translation of bionanomaterials for various biomedical applications.[155] Systematic comparison of nanomaterials during the clinical trials are hard tasks due to the variation in the particle size, surface properties and stability, tumor properties, pharmaco-kinetics analysis, etc. Significant and seamless collaborative efforts among various research groups, investors, and regulatory authorities are essential for the commercialization of clinically used bionanomaterials.

We summarized the role of bionanomaterials in various tissue regeneration processes such as imaging, tracking, repair, and regeneration. New imaging techniques and modalities are also reported in line with the evolving process of bionanomaterials. Synthesis techniques of these nano-systems need to be evolved to enhance their sensitivity and reproducibility, which helps them further in their translation from lab to the bed side. With the increasing number of new bionanomaterials developed in this domain of medicine, they could have a major impact on the translation of these novel techniques for better healthcare management of the human race.

8. Conclusion

Advances in nano-biotechnology allow the utilization of both biotechnology and nanotechnology to fabricate novel, complex nano-sized materials for the well-being of humankind. Smart, functional nanomaterials provide an adaptable platform in exploring several chronic illnesses and management in a more noninvasive route. Bionanomaterials of complex architecture, functionality, dimensions along with improved selectivity, sensitivity, and cargo targeting capability are suitable for therapeutic use. However, the drawbacks on scale-up and concerns regarding side effects associated with the in vivo applicability of these newly developed bionanomaterials remain questionable. According to the current scenario, the enhancement of surface properties is a key step in developing smart materials for medical use. The benefits and drawbacks associated with the relevancy of bionanomaterials for therapeutic application should be investigated intensely during future investigations.

References

1. Y.-C. Lee, J.-Y. Moon, Introduction to bionanotechnology, 2020.
2. S. Hassan, G. Prakash, A. Bal Ozturk, S. Saghazadeh, M.F. Sohail, J. Seo, R.D. Mehmet, Y.S. Zhang, K. Ali, Evolution and clinical translation of drug delivery nanomaterials, Nano Today 15 (2017) 91−106.
3. M. Endo, Y. Yangyang, H. Sugiyama, DNA origami technology for biomaterials applications, Biomater Sci 1 (2013) 347−360.
4. Z. Song, X. Chen, X. You, K. Huang, A. Dhinakar, Z. Gu, J. Wu, Self-assembly of peptide amphiphiles for drug delivery: the role of peptide primary and secondary structures, Biomater Sci 5 (2017) 2369−2380.
5. J.D. Perlmutter, M.F. Hagan, Mechanisms of virus assembly, Annu Rev Phys Chem 66 (2015) 217−239.
6. Y. Bai, Q. Luo, W. Zhang, M. Lu, J. Xu, H. Li, J. Liu, Highly ordered protein nanorings designed by accurate control of glutathione S-transferase self-assembly, J Am Chem Soc 135 (2013) 10966−10969.
7. C. Gong, S. Sun, Y. Zhang, L. Sun, Z. Su, A. Wu, G. Wei, Hierarchical nanomaterials via biomolecular self-assembly and bioinspiration for energy and environmental applications, Nanoscale 11 (10) (2019) 4147−4182.
8. Y. Bai, Q. Luo, J. Liu, Protein self-assembly via supramolecular strategies, Chem Soc Rev 45 (10) (2016) 2756−2767.
9. I.W. Hamley, Protein assemblies: nature-inspired and designed nanostructures, Biomacromolecules 20 (2019) 1829−1848.
10. Y. Wang, P. Katyal, J.K. Montclare, Protein-engineered functional materials, Adv Healthcare Mater 8 (2019) 1801374.
11. L. Hong, J. Zhao, A. Wang, L. Qi, W. Cui, Supramolecular assembly of protein-based nanoparticles based on tumor necrosis factor-related apoptosis-inducing ligand (TRAIL) for cancer therapy, Colloids Surf A Physicochem Eng Asp 590 (2020) 124486.
12. X. Huang, J. Chisholm, J. Zhuang, Y. Xiao, G. Duncan, X. Chen, S. Jung, J. Hanes, Protein nanocages that penetrate airway mucus and tumor tissue, Proc Nat Acad Sci 114 (2017) E6595−E6602.
13. X. Hu, M. Liao, H. Gong, L. Zhang, H. Cox, T.A. Waigh, J.R. Lu, Recent advances in short peptide self-assembly: from rational design to novel applications, Curr Opin Colloid Interface Sci 45 (2020) 1−13.
14. K. Sato, M.P. Hendricks, L.C. Palmer, S.I. Stupp, Peptide supramolecular materials for therapeutics, Chem Soc Rev 47 (2018) 7539−7551.
15. A. Dasgupta, D. Das, Designer peptide amphiphiles: self-assembly to applications, Langmuir 35 (2019) 10704−10724.
16. S. Sivagnanam, A. Arul, S. Ghosh, A. Dey, S. Ghorai, P. Das, Concentration-dependent fabrication of short-peptide-based different self-assembled nanostructures with various morphologies and intracellular delivery property, Mater Chem Front 3 (2019) 2110−2119.
17. Z. Wang, H.-W. An, D. Hou, M. Wang, X. Zeng, R. Zheng, L. Wang, K. Wang, H. Wang, W. Xu, Adv Mater 31 (2019) 1807175.
18. P.W. Rothemund, Folding DNA to create nanoscale shapes and patterns, Nature 440 (2006) 297−302.
19. L. Liang, J.-W. Shen, Q. Wang, Molecular dynamics study on DNA nanotubes as drug delivery vehicle for anticancer drugs, Colloids Surf B Biointerfaces 153 (2017) 168−173.

20. H. He, J. Dai, Y. Meng, et al., Self-assembly of DNA nanoparticles through multiple catalyzed hairpin assembly for enzyme-free nucleic acid amplified detection, Talanta 179 (2018) 641–645.
21. S. Bi, Y. Dong, X. Jia, M. Chen, H. Zhong, B. Ji, Self-assembled multifunctional DNA nanospheres for biosensing and drug delivery into specific target cells, Nanoscale 7 (16) (2015) 7361–7367.
22. Mohammed AM, Velazquez L, Chisenhall A, Schiffels D, Fygenson DK, Schulman R. Self-assembly of precisely defined DNA nanotube superstructures using DNA origami seeds. Nanoscale 2017;9:522–526.
23. A.M. Maier, W. Bae, D. Schiffels, J.F. Emmerig, M. Schiff, T. Liedl, Self-assembled DNA tubes forming helices of controlled diameter and chirality, ACS Nano 11 (2017) 1301–1306.
24. H.H. Zhang, W.J. Wang, N. Hagen, I. Kuzmenko, M. Akinc, A. Travesset, S. Mallapragada, D. Vaknin, Self-assembly of DNA functionalized gold nanoparticles at the liquid-vapor interface, Adv Mater Interfaces 3 (2016) 1600180.
25. M.M. Bhanjadeo, A.K. Nayak, U. Subudhi, Surface-assisted DNA self-assembly: an enzyme-free strategy towards formation of branched DNA lattice, Biochem Biophys Res Commun 485 (2) (2017) 492–498.
26. T. Fu, N. Seeman, DNA double-crossover molecules, Biochemistry 32 (1993) 3211–3220.
27. E. Winfree, F. Liu, L.A. Wenzler, N.C. Seeman, Design and self-assembly of two-dimensional DNA crystals, Nature 394 (1998) 539–544.
28. P.W.K. Rothemund, et al., Design and characterization of programmable DNA nanotubes, J Am Chem Soc 126 (2004) 16344–16352.
29. S.M. Douglas, et al., Self-assembly of DNA into nanoscale three-dimensional shapes, Nature 459 (2009) 414–418.
30. Y. Ke, L.L. Ong, W.M. Shih, P. Yin, Three-dimensional structures self-assembled from DNA bricks, Science 338 (2012) 1177–1183.
31. F. Zhang, et al., Complex wireframe DNA origami nanostructures with multi-arm junction vertices, Nat Nanotechnol 10 (2015) 779–784.
32. E. Benson, et al., DNA rendering of polyhedral meshes at the nanoscale, Nature 523 (2015) 441–444.
33. J. Zheng, et al., From molecular to macroscopic via the rational design of a self-assembled 3D DNA crystal, Nature 461 (2009) 74–77.
34. M.R. Jones, N.C. Seeman, C.A. Mirkin, Programmable materials and the nature of the DNA bond, Science 347 (2015) 1260901.
35. M.R. Jones, N.C. Seeman, C.A. Mirkin, Programmable materials and the nature of the DNA bond, Spherical Nucleic Acids (2020) 167–197.
36. H. Li, J.D. Carter, T.H. LaBean, Nanofabrication by DNA self-assembly, Mater Today 12 (2009) 24–32.
37. A. Aghebat Rafat, T. Pirzer, M.B. Scheible, A. Kostina, F.C. Simmel, Surface-assisted large-scale ordering of DNA origami tiles, Angew Chem Int Ed 53 (2014) 7665–7668.
38. S. Woo, P.W.K. Rothemund, Self-assembly of two-dimensional DNA origami lattices using cation-controlled surface diffusion, Nat Commun 5 (2014) 4889.
39. Y. Suzuki, M. Endo, H. Sugiyama, Lipid-bilayer-assisted two-dimensional self-assembly of DNA origami nanostructures, Nat Commun 6 (2015) 8052.
40. Y. Sato, M. Endo, M. Morita, M. Takinoue, H. Sugiyama, S. Murata, S.-I.M. Nomura, Y. Suzuki, Environment-dependent self-assembly of DNA origami lattices on phase-separated lipid membranes, Adv Mater Interfaces 5 (2018) 1800437.
41. Y. Chen, W. Sun, C. Yang, Z. Zhu, Scaling up DNA self-Assembly, ACS Appl Bio Mater 3 (2020) 2805–2815.
42. M.T. Nistor, A.G. Rusu, Chapter 3—nanorobots with applications in medicine, in: Micro and nanotechnologies, polymeric nanomaterials in nanotherapeutics, Elsevier, 2019, pp. 123–149.
43. M. Luo, Y. Feng, T. Wang, Micro-/nanorobots at work in active drug delivery, Adv Funct Mater 28 (2018) 1706100.
44. H. Wang, P. Martin, Fabrication of micro/nanoscalemotors, Chem Rev 115 (2015) 8704–8735.
45. R. Dong, Y. Cai, Y. Yang, W. Gao, B. Ren, Photocatalytic micro/nanomotors: from construction to applications, Acc Chem Res 51 (2018) 1940–1947.
46. D. Kagan, R. Laocharoensuk, M. Zimmerman, C. Clawson, S. Balasubramanian, D. Kang, D. Bishop, S. Sattayasamitsathit, L. Zhang, J. Wang, Rapid delivery of drug carriers propelled and navigated by catalytic nanoshuttles, Small 6 (2010) 2741–2747.

47. S. Balasubramanian, D. Kagan, C.-M. Jack Hu, S. Campuzano, M.J. Lobo-Castañon, N. Lim, D.Y. Kang, M. Zimmerman, L. Zhang, J. Wang, Micromachine-enabled capture and isolation of cancer cells in complex media, Angew Chem Int Ed 50 (2011) 4161–4164.
48. D. Kagan, S. Campuzano, S. Balasubramanian, G.-U.F. FilizKuralay, J. Wang, Functionalized micromachines for selective and rapid isolation of nucleic acid targets from complex samples, Nano Lett 11 (2011) 2083–2087.
49. Z. Jin, K.T. Nguyen, G. Go, B. Kang, H.-K. Min, S.-J. Kim, Y. Kim, H. Li, C.-S. Kim, S. Lee, S. Park, K.-P. Kim, M.H. Kang, J. Song, P. Jong-Oh, E. Choi, Multifunctional nanorobot system for active therapeutic delivery and synergistic chemo-photothermal therapy, Nano Lett 19 (2019) 8550–8564.
50. Z. Wu, X. Lin, X. Zou, J. Sun, Q. He, Biodegradable protein-based rockets for drug transportation and light-triggered release, ACS Appl Mater Interfaces 7 (2014) 250–255.
51. C. Peters, M. Hoop, S. Pané, B.J. Nelson, C. Hierold, Degradable magnetic composites for minimally invasive interventions: device fabrication, targeted drug delivery, and cytotoxicity tests, Adv Mater 28 (2016) 533–538.
52. F. Peng, Y. Tu, J.C.M. van Hest, D.A. Wilson, Self-guided supramolecular cargo-loaded nanomotors with chemotactic behavior towards cells, Angew Chem Int Ed 54 (2015) 11662–11665.
53. D. Kagan, M.J. Benchimol, J.C. Claussen, E. Chuluun-Erdene, S. Esener, J. Wang, Acoustic droplet vaporization and propulsion of perfluorocarbon-loaded microbullets for targeted tissue penetration and deformation, Angew Chem Int Ed 51 (2012) 7519–7522.
54. S. Sengupta, M.E. Ibele, A. Sen, Fantastic voyage: designing self-powered nanorobots, Angew Chem Int Ed 51 (2012) 8434–8445.
55. S.S. Andhari, R.D. Wavhale, K.D. Dhobale, et al., Self-propelling targeted magneto-nanobots for deep tumor penetration and pH-responsive intracellular drug delivery, Sci Rep 10 (2020) 4703.
56. W. Gao, D. Kagan, O.S. Pak, C. Clawson, S. Campuzano, E. Chuluun-Erdene, E. Shipton, E.E. Fullerton, L. Zhang, E. Lauga, J. Wang, Cargo towing fuel-free magnetic nanoswimmers for targeted drug delivery, Small 8 (2012) 460–467.
57. F. Mou, C. Chen, Q. Zhong, Y. Yin, H. Ma, J. Guan, Autonomous motion and temperature-controlled drug delivery of Mg/Pt-poly(N-isopropylacrylamide) Janus micromotors driven by simulated body fluid and blood plasma, ACS Appl Mater Interfaces 6 (2014) 9897–9903.
58. L. Soler, S. Sanchez, Catalytic nanomotors for environmental monitoring and water remediation, Nanoscale 6 (2014) 7175–7182.
59. Z. Wu, X. Lin, X. Zou, J. Sun, Q. He, Biodegradable protein-based rockets for drug transportation and light-triggered release, ACS Appl Mater Interfaces 7 (2015) 250–255.
60. L. Sonntag, J. Simmchen, V. Magdanz, Nano-and micromotors designed for cancer therapy, Molecules 24 (2019) 3410.
61. K.M. Manesh, M. Cardona, R. Yuan, M. Clark, D. Kagan, S. Balasubramanian, J. Wang, Template-assisted fabrication of salt-independent catalytic tubular microengines, ACS Nano 4 (2010) 1799–1804.
62. S. Campuzano, J. Orozco, D. Kagan, M. Guix, W. Gao, S. Sattayasamitsathit, J.C. Claussen, A. Merkoçi, J. Wang, Bacterial isolation by lectin-modified microengines, Nano Lett 12 (2012) 396–401.
63. Z. Wu, Y. Wu, W. He, X. Lin, J. Sun, Q. He, Self-propelled polymer-based multilayer nanorockets for transportation and drug release, Angew Chem Int Ed 52 (2013) 7000–7003.
64. W. Wang, S. Li, L. Mair, S. Ahmed, T.J. Huang, T.E. Mallouk, Acoustic propulsion of nanorod motors inside living cells, Angew Chem Int Ed 53 (2014) 3201–3204.
65. V. Garcia-Gradilla, S. Sattayasamitsathit, F. Soto, F. Kuralay, C. Yardımcı, D. Wiitala, M. Galarnyk, J. Wang, Ultrasound-propelled nanoporous gold wire for efficient drug loading and release, Small 10 (2014) 4154–4159.
66. X.-Z. Chen, M. Hoop, E.S. FajerMushtaq, C. Hu, B.J. Nelson, P. Salvador, Recent developments in magnetically driven micro- and nanorobots, Appl Mater Today 9 (2017) 37–48.
67. L. Zhang, K.E. Peyer, B.J. Nelson, Artificial bacterial flagella for micromanipulation, Lab Chip 10 (2010) 2203–2215.
68. L. Zhang, J.J. Abbott, D. Lixin, B.E. Kratochvil, D. Bell, B.J. Nelson, Artificial bacterial flagella: fabrication and magnetic control, Appl Phys Lett 94 (2009) 064107.
69. A. Ghosh, P. Fischer, Controlled propulsion of artificial magnetic nanostructured propellers, Nano Lett 9 (2009) 2243–2245.

70. M. Hoop, A.S. Ribeiro, D. Rösch, P. Weinand, N. Mendes, F. Mushtaq, X.-Z. Chen, Y. Shen, C.F. Pujante, J. Puigmartí-Luis, J. Paredes, B.J. Nelson, A.P. Pêgo, S. Pané, Mobile magnetic nanocatalysts for bioorthogonal targeted cancer therapy, Adv Funct Mater 28 (2018) 1705920.
71. S. Sánchez, L. Soler, J. Katuri, Chemically powered micro- and nanomotors, Angew Chem Int Ed 54 (2015) 1414–1444.
72. A. Serrà, G. Vázquez-Mariño, J. García-Torres, M. Bosch, E. Vallés, Magnetic actuation of multifunctional nanorobotic platforms to induce cancer cell death, Adv Biosys 2 (2018) 1700220.
73. S. Taherkhani, M. Mohammadi, S. Martel, M. Tabrizian, Covalent binding of nanoliposomes to the surface of magnetotactic bacteria for the synthesis of self-propelled therapeutic agents, ACS Nano 8 (2014) 5049–5060.
74. O. Felfoul, M. Mohammadi, S. Taherkhani, et al., Magneto-aerotactic bacteria deliver drug-containing nanoliposomes to tumour hypoxic regions, Nat Nanotechnol 11 (2016) 941–947.
75. J. Li, C.H. Fan, H. Pei, J.Y. Shi, Q. Huang, Smart drug delivery nanocarriers with self-assembled DNA nanostructures, Adv Mater 25 (2013) 4386–4396.
76. M. Liu, W. Ma, Q. Li, D. Zhao, X. Shao, Q. Huang, L. Hao, Y. Lin, Aptamer-targeted DNA nanostructures with doxorubicin to treat protein tyrosine kinase 7-positive tumours, Cell Prolif 52 (2019) e12511.
77. K.R. Kim, D.R. Kim, T. Lee, J.Y. Yhee, B.S. Kim, I.C. Kwon, D.R. Ahn, Drug delivery by a self-assembled DNA tetrahedron for overcoming drug resistance in breast cancer cells, Chem Commun (Cambridge, UK) 49 (2013) 2010–2012.
78. X. Xie, X. Shao, W. Ma, D. Zhao, S. Shi, Q. Li, Y. Lin, Overcoming drug-resistant lung cancer by paclitaxel loaded tetrahedral DNA nanostructures, Nanoscale 10 (2018) 5457–5465.
79. C.G. Park, M.A. Kwon, J.K. Song, D.M. Kim, Cell-free synthesis and multifold screening of Candida Antarctica lipase B (CalB) variants after combinatorial mutagenesis of hot spots, Biotechnol Prog 27 (2011) 47–53.
80. A.P. Alimov, A. Khmelnitsky, P.N. Simonenko, A.S. Spirin, A.B. Chetverin, Cell-free synthesis and affinity isolation of proteins on a nanomole scale, Biotechniques 28 (2000) 338–344.
81. J.-H. Ahn, J.-W. Keum, D.-M. Kim, High-throughput, combinatorial engineering of initial codons for tunable expression of recombinant proteins, J Proteome Res 7 (2008) 2107–2113.
82. M.C. Jewett, J.R. Swartz, Rapid expression and purification of 100 nmol quantities of active protein using cell-free protein synthesis, Biotechnol Prog 20 (2004) 102–109.
83. J.C.W. ArnazRanji, B. Bradley C., M.C. Jewett, Chapter 15 - transforming synthetic biology with cell-free systems, in: Huimin Zhao (Ed.), Synthetic Biology, Academic Press, 2013, pp. 277–301.
84. W. Ma, Y. Zhan, Y. Zhang, X. Shao, C.M. XuepingXie, W. Cui, L. Qian, J. Shi, L. Jiang, C. Fan, Y. Lin, An intelligent DNA nanorobot with in vitro enhanced protein lysosomal degradation of HER2, Nano Lett 19 (2019) 4505–4517.
85. Y. Shimizu, A. Inoue, Y. Tomari, T. Suzuki, T. Yokogawa, K. Nishikawa, et al., Cell-free translation reconstituted with purified components, Nat Biotechnol 19 (2001) 751–755.
86. E.D. Carlson, R. Gan, C.E. Hodgman, M.C. Jewett, Cell-free protein synthesis: applications come of age, Biotechnol Adv 30 (2012) 1185–1194.
87. R.K. Saiki, D.H. Gelfand, S. Stoffel, S.J. Scharf, R. Higuchi, G.T. Horn, et al., Primer-directed enzymatic amplification of DNA with a thermostable DNA polymerase, Science 239 (1988) 487–491.
88. T.-W. Kim, I.-S. Oh, J.-H. Ahn, C.-Y. Choi, D.-M. Kim, Cell-free synthesis and in situ isolation of recombinant proteins, Protein Expr Purif 45 (2006) 249–254.
89. M. Bujara, M. Schumperli, R. Pellaux, M. Heinemann, S. Panke, Optimization of a blueprint for in vitro glycolysis by metabolic real-time analysis, Nat Chem Biol 7 (2011) 271–277.
90. F. Katzen, G. Chang, W. Kudlicki, The past, present and future of cell-free protein synthesis, Trends Biotechnol 23 (2005) 150–156.
91. I. Usón, G.M. Sheldrick, Advances in direct methods for protein crystallography, Curr Opin Struct Biol 9 (1999) 643–648.
92. S. Li, Q. Jiang, S. Liu, et al., A DNA nanorobot functions as a cancer therapeutic in response to a molecular trigger in vivo, Nat Biotechnol 36 (2018) 258–264.
93. P. Cui, S. Wang, Application of microfluidic chip technology in pharmaceutical analysis: a review, J Pharm Anal 9 (2019) 238–247.
94. Report by markets and markets research private Ltd as on June 2020.

95. R. Bumgarner, Overview of DNA microarrays: types, applications, and their future, Curr Protoc Mol Biol 101 (2013) [Chapter 22]:Unit-22.1.
96. E. Sackmann, A. Fulton, D. Beebe, The present and future role of microfluidics in biomedical research, Nature 507 (2014) 181–189.
97. R.M. Iost, F.C.P.F. Sales, M.V.A. Martins, M.C. Almeida, F.N. Crespilho, Glucose biochip based on flexible carbon fiber electrodes: in vivo diabetes evaluation in rats, Chemelectrochem 2 (2015) 518–521.
98. M.A. Ali, P.R. Solanki, M.K. Patel, H. Dhayani, V.V. Agrawal, R. John, B.D. Malhotra, A highly efficient microfluidic nano biochip based on nanostructured nickel oxide, Nanoscale 5 (2013) 2883–2891.
99. L. Xu, H. Yu, S. Michael, S.-J.H. Akhras, S. Osterfeld, R.L. White, Giant magnetoresistive biochip for DNA detection and HPV genotyping, Biosens Bioelectron 24 (2008) 99–103.
100. X. Ma, Y. Wu, S. Jin, Y. Tian, X. Zhang, Y. Zhao, L. Yu, X.J. Liang, Gold nanoparticles induce autophagosome accumulation through size-dependent nanoparticle uptake and lysosome impairment, ACS Nano 5 (2011) 8629–8639.
101. S. Loyprasert, P. Thavarungkul, P. Asawatreratanakul, B. Wongkittisuksa, C. Limsakul, P. Kanatharana, Label-free capacitive immunosensor for microcystin-LR using self-assembled thioureamonolayer incorporated with Ag nanoparticles on gold electrode, Biosens Bioelectron 24 (2008) 78–86.
102. M. José, Paloma yáñez-sedeño, araceli González-Cortés, Gold nanoparticle-based electrochemical biosensors, Electrochim Acta 53 (2008) 5848–5866.
103. J. Zhang, L. Mou, X. Jiang, Surface chemistry of gold nanoparticles for health-related applications, Chem Sci 11 (2020) 923–936.
104. G.R. Koirala, E.-S. Kim, R. Dhakal, Z. Chuluunbaatar, Y.H. Jo, S.-S. Kim, N.-Y. Kim, Microfabricated passive resonator biochip for sensitive radiofrequency detection and characterization of glucose, RSC Adv 8 (2018) 33072–33079.
105. S.H. Baek, C.Y. Park, M.W. Kim, R. Shi, S. Kumar Kailasa, T.J. Park, Cu-nanoflower decorated gold nanoparticles-graphene oxide nanofiber as electrochemical biosensor for glucose detection, Mater Sci Eng C 107 (2020) 107.
106. S. Li, J. Liu, Y. Lu, L. Zhu, C. Li, L. Hu, J. Li, J. Jiang, S. Low, Mutual promotion of electrochemical-localized surface plasmon resonance on nanochip for sensitive sialic acid detection, Biosens Bioelectron 117 (2018) 32–39.
107. X. Li, M. Yu, Z. Chen, X. Lin, Q. Wu, A sensor for detection of carcinoembryonic antigen based on the polyaniline-Au nanoparticles and gap-based interdigitated electrode, Sensor Actuator B Chem 239 (2017) 874–882.
108. B.B. Nunna, D. Mandal, J.U. Lee, et al., Detection of cancer antigens (CA-125) using gold nano particles on interdigitated electrode-based microfluidic biosensor, Nano Converg 6 (3) (2019).
109. S.S. RaginiRaghav, Core–shell gold–silver nanoparticles based impedimetricimmunosensor for cancer antigen CA125, Sensor Actuator B Chem 220 (2015) 557–564.
110. K.K. Adhikari, E.S. Kim, N.Y. Kim, Multiparameter microwave characterization and probing of ultralow glucose concentration using a microfabricated biochip, Micromachines 7 (93) (2016).
111. J. Matsuzaki, T. Ochiya, Circulating microRNAs and extracellular vesicles as potential cancer biomarkers: a systematic review, Int J Clin Oncol 22 (2017) 413–420.
112. C. Yu, J. Irudayaraj, Multiplex biosensor using gold nanorods, Anal Chem 79 (2007) 572–579.
113. E. Zeidan, S. Li, Z. Zhou, et al., Single-multiplex detection of organ injury biomarkers using SPRi based nano-immunosensor, Sci Rep 6 (2016) 36348.
114. Z. Cheng, N. Choi, R. Wang, et al., Simultaneous detection of dual prostate specific antigens using surface-enhanced Raman scattering-based immunoassay for accurate diagnosis of prostate cancer, ACS Nano 11 (2017) 4926–4933.
115. D.U. Yu-Lin, M.O. Liu-Ting, Y.I. Ya-Sha, Q.I.U. Li-Ping, W.-H. TAN, Aptamers from cell-based selection for bioanalysis and bioimaging, Chin J Anal Chem 45 (2017) 1757–1765.
116. B. Adam, H. Brian Halsall, W.R. Heineman, Microfluidic immunosensor systems, Biosens Bioelectron 20 (2005) 2488–2503.
117. S. Hanash, S. Pitteri, V. Faca, Mining the plasma proteome for cancer biomarkers, Nature 452 (2008) 571–579.
118. P. Juzenas, W. Chen, Y.-P. Sun, M. Alvaro Neto Coelho, R. Generalov, N. Generalova, I.L. Christensen, Quantum dots and nanoparticles for photodynamic and radiation therapies of cancer, Adv Drug Deliv Rev 60 (2008) 1600–1614.

119. H. Jans, Q. Huo, Gold nanoparticle-enabled biological and chemical detection and analysis, Chem Soc Rev 41 (2012) 2849–2866.
120. Z.-M. Lyu, X.-L. Zhou, X.-N. Wang, P. Li, L. Xu, E.-H. Liu, Miniaturized electrochemiluminescent biochip prepared on gold nanoparticles-loaded mesoporous silica film for visual detection of hydrogen peroxide released from living cells, Sensor Actuator B Chem 284 (2019) 437–443.
121. J.-H. Lee, Y. Hwang, K.-A. Cheon, Emotion-on-a-chip (EOC): evolution of biochip technology to measure human emotion using body fluids, Med Hypotheses 79 (2012) 827–832.
122. S.P. Fodor, R.P. Rava, X.C. Huang, A.C. Pease, C.P. Holmes, C.L. Adams, Multiplexed biochemical assays with biological chips, Nature 364 (1993) 555–556.
123. C.A. Rowe, L.M. Tender, M.J. Feldstein, J.P. Golden, S.B. Scruggs, B.D. MacCraith, J.J. Cras, F.S. Ligler, Array biosensor for simultaneous identification of bacterial, viral, and protein analytes, Anal Chem 71 (1999) 3846–3852.
124. M. Sher, R. Zhuang, U. Demirci, W. Asghar, Paper-based analytical devices for clinical diagnosis: recent advances in the fabrication techniques and sensing mechanisms, Expert Rev Mol Diagn 17 (2017) 351–366.
125. J. Ma, S. Yan, C. Miao, L. Li, W. Shi, X. Liu, Y. Luo, T. Liu, B. Lin, W. Wu, Y. Lu, Paper microfluidics for cell analysis, Adv Healthcare Mater 8 (2019) 1801084.
126. A.K. Yetisen, M. Safwan, C.R. Lowe, Paper-based microfluidic point-of-care diagnostic devices, Lab Chip 13 (2013) 2210–2251.
127. M.S. KatarzynaRatajczak, High-performance modified cellulose paper-based biosensors for medical diagnostics and early cancer screening: a concise review, Carbohydr Polym 229 (2020) 115463.
128. H. Inan, M. Poyraz, F. Inci, M.A. Lifson, M. Baday, B.T. Cunningham, U. Demirci, Photonic crystals: emerging biosensors and their promise for point-of-care applications, Chem Soc Rev 46 (2017) 366–388.
129. D. Quesada-González, A. Merkoçi, Nanomaterial-based devices for point-of-care diagnostic applications, Chem Soc Rev 47 (13) (2018) 4697–4709.
130. (a) H. Jeong, M. Huh, S.J. Lee, H. Koo, I.C. Kwon, S.Y. Jeong, K. Kim, Photosensitizer-conjugated human serum albumin nanoparticles for effective photodynamic therapy, Theranostics 1 (2011) 230–239;
(b) Q. Chen, C. Wang, Z. Zhan, W. He, Z. Cheng, Y. Li, Z. Liu, Near-infrared dye bound albumin with separated imaging and therapy wavelength channels for imaging-guided photothermal therapy, Biomaterials 35 (28) (2014) 8206–8214;
(c) Q. Chen, C. Liang, X. Wang, J. He, Y. Li, Z. Liu, An albumin-based theranostic nano-agent for dual-modal imaging guided photothermal therapy to inhibit lymphatic metastasis of cancer post surgery, Biomaterials 35 (34) (2014) 9355–9362.
131. (a) G. Gao, Y.-W. Jiang, W. Sun, Y. Guo, H.-R. Jia, X.-W. Yu, G.-Y. Pan, F.-G. Wu, Molecular targeting-mediated mild-temperature photothermal therapy with a smart albumin-based nanodrug, Small 15 (33) (2019) 1900501;
(b) W.Z. Xinzhe Yu, D. Yang, J. Gu, Z. Guo, H. Li, D. Fu, C. Jin, Triple-functional albumin-based nanoparticles for combined chemotherapy and photodynamic therapy of pancreatic cancer with lymphatic metastases, Int J Nanomed 12 (2017) 6771–6785.
132. S. Takahashi, K. Sato, J.-I. Anzai, Layer-by-layer construction of protein architectures through avidin–biotin and lectin–sugar interactions for biosensor applications, Anal Bioanal Chem 402 (5) (2012) 1749–1758.
133. A.A.P. Mansur, S.M. de Carvalho, H.S. Mansur, Bioengineered quantum dot/chitosan-tripeptide nanoconjugates for targeting the receptors of cancer cells, Int J Biol Macromol 82 (2016) 780–789.
134. V.S. Madamsetty, A. Mukherjee, S. Mukherjee, Recent trends of the bio-inspired nanoparticles in cancer theranostics, Front Pharmacol 10 (1264) (2019).
135. I.L. Medintz, H.T. Uyeda, E.R. Goldman, H. Mattoussi, Quantum dot bioconjugates for imaging, labelling and sensing, Nat Mater 4 (6) (2005) 435–446.
136. W.C.W. Chan, S. Nie, Quantum dot bioconjugates for ultrasensitive nonisotopic detection, Science 281 (5385) (1998) 2016–2018.
137. I.L. Medintz, A.R. Clapp, H. Mattoussi, E.R. Goldman, B. Fisher, J.M. Mauro, Self-assembled nanoscale biosensors based on quantum dot FRET donors, Nat Mater 2 (9) (2003) 630–638.
138. H. Mattoussi, J.M. Mauro, E.R. Goldman, G.P. Anderson, V.C. Sundar, F.V. Mikulec, M.G. Bawendi, Self-assembly of CdSe–ZnS quantum dot bioconjugates using an engineered recombinant protein, J Am Chem Soc 122 (49) (2000) 12142–12150.
139. (a) V.P. Torchilin, Recent advances with liposomes as pharmaceutical carriers, Nat Rev Drug Discov 4 (2) (2005) 145–160;
(b) Q. Chen, H. Ke, Z. Dai, Z. Liu, Nanoscale theranostics for physical stimulus-responsive cancer therapies, Biomaterials 73 (2015) 214–230.

140. (a) V.P. Torchilin, Liposomes as targetable drug carriers, Crit Rev Ther Drug Carrier Syst 2 (1) (1985) 65–115;
(b) O.N. Oliveira, R.M. Iost, J.R. Siqueira, F.N. Crespilho, L. Caseli, Nanomaterials for diagnosis: challenges and applications in smart devices based on molecular recognition, ACS Appl Mater Inter 6 (17) (2014) 14745–14766.
141. (a) J. Ezzati Nazhad Dolatabadi, M. de la Guardia, Nanomaterial-based electrochemical immunosensors as advanced diagnostic tools, Anal Methods 6 (12) (2014) 3891–3900;
(b) J. Wang, G. Chen, H. Jiang, Z. Li, X. Wang, Advances in nano-scaled biosensors for biomedical applications, Analyst 138 (16) (2013) 4427–4435.
142. G.-J. Zhang, K.T.C. Chai, H.Z.H. Luo, J.M. Huang, I.G.K. Tay, A.E.-J. Lim, M. Je, Multiplexed detection of cardiac biomarkers in serum with nanowire arrays using readout ASIC, Biosens Bioelectron 35 (1) (2012) 218–223.
143. T.A. Taton, Nanotechnology: boning up on biology, Nature 412 (6846) (2001) 491–492.
144. (a) S. Verma, A.J. Domb, N. Kumar, Nanomaterials for regenerative medicine, Nanomedicine 6 (1) (2011) 157–181;
(b) Š. Kubinová, E. Syková, Nanotechnologies in regenerative medicine, Minim Invasive Ther Allied Technol 19 (3) (2010) 144–156;
(c) R. Langer, Perspectives and challenges in tissue engineering and regenerative medicine, Adv Mater 21 (32–33) (2009) 3235–3236.
145. (a) C.V. Rahman, A. Saeed, L.J. White, T.W.A. Gould, G.T.S. Kirby, M.J. Sawkins, C. Alexander, F.R.A.J. Rose, K.M. Shakesheff, Chemistry of polymer and ceramic-based injectable scaffolds and their applications in regenerative medicine, Chem Mater 24 (5) (2012) 781–795;
(b) S. Martino, F. D'Angelo, I. Armentano, J.M. Kenny, A. Orlacchio, Stem cell-biomaterial interactions for regenerative medicine, Biotechnol Adv 30 (1) (2012) 338–351;
(c) I.O. Smith, X.H. Liu, L.A. Smith, P.X. Ma, Nanostructured polymer scaffolds for tissue engineering and regenerative medicine, Wirley Interdiscip Rev Nanomed Nanobiotechnol 1 (2) (2009) 226–236;
(d) M.E. Furth, A. Atala, M.E. Van Dyke, Smart biomaterials design for tissue engineering and regenerative medicine, Biomaterials 28 (34) (2007) 5068–5073.
146. J.M.W. Slack, Stem cells in epithelial tissues, Science 287 (5457) (2000) 1431–1433.
147. (a) Y. Liang, P. Walczak, J.W.M. Bulte, The survival of engrafted neural stem cells within hyaluronic acid hydrogels, Biomaterials 34 (22) (2013) 5521–5529;
(b) D. Logeart-Avramoglou, K. Oudina, M. Bourguignon, L. Delpierre, M.-A. Nicola, M. Bensidhoum, E. Arnaud, H. Petite, In vitro and in vivo bioluminescent quantification of viable stem cells in engineered constructs, Tissue Eng C Methods 16 (3) (2010) 447–458.
148. J.S. Odorico, D.S. Kaufman, J.A. Thomson, Multilineage differentiation from human embryonic stem cell lines, Stem Cell 19 (3) (2001) 193–204.
149. A.S. Mao, D.J. Mooney, Regenerative medicine: current therapies and future directions, Proc Natl Acad Sci USA 112 (47) (2015) 14452–14459.
150. R. Lawaczeck, M. Menzel, H. Pietsch, Superparamagnetic iron oxide particles: contrast media for magnetic resonance imaging, Appl Organomet Chem 18 (10) (2004) 506–513.
151. M. Lewin, N. Carlesso, C.-H. Tung, X.-W. Tang, D. Cory, D.T. Scadden, R. Weissleder, Tat peptide-derivatized magnetic nanoparticles allow in vivo tracking and recovery of progenitor cells, Nat Biotechnol 18 (4) (2000) 410–414.
152. I.D. Duncan, E.A. Milward, Glial cell transplants: experimental therapies of myelin diseases, Brain Pathol 5 (3) (1995) 301–310.
153. (a) J. Zhu, L. Zhou, F. XingWu, Tracking neural stem cells in patients with brain trauma, N Engl J Med 355 (22) (2006) 2376–2378;
(b) H. Chen, I. Titushkin, M. Stroscio, M. Cho, Altered membrane dynamics of quantum dot-conjugated integrins during osteogenic differentiation of human bone marrow derived progenitor cells, Biophys J 92 (4) (2007) 1399–1408;
(c) B.J. Muller-Borer, M.C. Collins, P.R. Gunst, W.E. Cascio, A.P. Kypson, Quantum dot labeling of mesenchymal stem cells, J Nanobiotechnol 5 (1) (2007) 9;
(d) B.S. Shah, P.A. Clark, E.K. Moioli, M.A. Stroscio, J.J. Mao, Labeling of mesenchymal stem cells by bioconjugated quantum dots, Nano Lett 7 (10) (2007) 3071–3079.
154. K.M. Galler, J.D. Hartgerink, A.C. Cavender, G. Schmalz, R.N. D'Souza, A customized self-assembling peptide hydrogel for dental pulp tissue engineering, Tissue Eng 18 (1–2) (2011) 176–184.
155. S. Mitragotri, D.G. Anderson, X. Chen, E.K. Chow, D. Ho, A.V. Kabanov, J.M. Karp, K. Kataoka, C.A. Mirkin, S.H. Petrosko, J. Shi, M.M. Stevens, S. Sun, S. Teoh, S.S. Venkatraman, Y. Xia, S. Wang, Z. Gu, C. Xu, Accelerating the translation of nanomaterials in biomedicine, ACS Nano 9 (7) (2015) 6644–6654.

CHAPTER

26

Medical device associated-biofilm eradication strategies: use of multi-functional nanomaterials

Akshit Malhotra[1,3], *Giuvanni Mutton*[2], *Suchitra Rajput Chauhan*[4], *Vincent Semetey*[2] *and Ashwini Chauhan*[1,3]

[1]**Department of Microbiology, Tripura University (A Central University), Tripura, India;** [2]**Chimie ParisTech, PSL University, CNRS, Institut de Recherche de Chimie Paris, Paris, France;** [3]**Invisiobiome, New Delhi, Delhi, India;** [4]**Centre for Advanced Materials and Devices (CAMD), School of Engineering and Technology, BML Munjal University, Kapriwas, Haryana, India**

1. Introduction

Biofilms are complex communities of microbes found on biotic or abiotic surfaces embedded in genetically and physiologically diverse extracellular polymeric substances (EPS). Prokaryotes were studied as free-flowing single colony entities for a great range of understanding of microbial life before we began to study the biofilm mode of microbial development. The understanding of the biofilm lifestyle of bacteria is recent though observations of this cooperative model have been quite early. As early as 1650, Antonie van Leeuwenhoek described the ability of prokaryotes to form adherent colonies before the term "biofilm" was coined by William Costerton in 1977 when he observed bacteria to have more adhered to the bottom rocks than to exist as freely flowing in an Alpine Lake.

As bacteria switch to a biofilm mode of living as part of it's adaptive response to survive in different contrasts of environments, various distinct characteristics are expressed. These properties include protection for bacterial cells from antibacterial agents, nutrient limitations, host immunologic defense systems, and other hostile factors. Several phenotypic and genotypic characteristics of bacterial cells in biofilms are distinct from their planktonic counterparts

Applications of Multifunctional Nanomaterials
https://doi.org/10.1016/B978-0-12-820557-0.00019-9

and are responsible for the recalcitrance of antibiotics. The multi-factorial resistance is due to the presence of biofilm-specific multi-drug resistance efflux pumps and the formation of persister cells inside the biofilm matrix.[1]

Biofilms have significantly influenced the medical field and have several implications in healthcare settings. As we understand the role of commensal bacterial biofilms as a pathological barrier in our gastrointestinal tract and on our skin, the relevance of studying the biofilm mode of bacterial development in clinical settings has grown tremendously. It has been found that alterations in the protective barriers can enhance the susceptibility to pathogenic bacteria. Microbial biofilms infect wounds resulting in delayed healing and form scars. In stomach infections caused due to gastric ulcers, *Helicobacter pylori* biofilms have been known to erode the stomach lining. In cystic fibrosis non-removal mucus in the lungs leads to biofilm infection with additional morbidity and patient death. More importantly, nosocomial pathogens i.e., harmful microbes present in hospital settings, have shown biofilm-forming abilities and multi-drug resistance. In clinical settings, microbial contamination on a wide variety of surfaces, mainly medical devices and implants results in over-usage of resources while the associated infections are linked to complications, disease burden, morbidities, and mortality.[2]

Bacteria and other microbes have the tendency to adhere to surfaces such as indwelling medical devices and synthetic polymers, and eventually form bacterial colonies and mature biofilms acting as a reservoir of pathogens. The eventual dispersal of bacterial cells from mature biofilm leads to the dissemination of pathogens, systematic infection, and transmission. It is extremely difficult to eradicate the biofilm communities due to their multifactorial recalcitrance toward therapeutic interventions. Therefore, it is indeed essential to develop long-lasting preventive solutions to avoid the development of nosocomial infections on surfaces of medical importance, primarily, medical devices and implants.

Biofilms have been found to contaminate endotracheal tubes, vascular access catheters, and urinary catheters. Also, ventricular assist devices, prosthetic valves, and pacemakers have been shown to develop biofilm-associated complications over the period of their use. Dental caries and orthodontal infections in dental care are certain implications of biofilms, which were identified much early while the understanding of biofilm infections in other clinical settings is recent Fig. 26.1.

The contemporary rise in antimicrobial resistance of nosocomial pathogens along with their biofilm-forming ability has rendered device-associated infections to be "Achilles Heel" of healthcare. Present-day antibiotics are no longer effective in eradicating biofilms and, thus, the development of new antibiotics offers more gloom than the lure. Advancements in Nanotechnology and its applications to develop nano-patterned and nano-textured surfaces have emerged to be an interesting alternative to explore to enable enhanced prevention of bacterial attachment. Surface-modified implants not only improve tissue integration and healing but also keep microbial species at bay.

As this volume of the series, gives a fascinating glimpse of cutting-edge multi-disciplinary applications of multi-functional nanomaterials in diverse fields such as military applications, energy generation and storage, animal nutrition, membrane distillation, biorefinery and more, this chapter attempts to highlight key progress that nanomaterials have made in eradicating microbial infections in hospital settings primarily in events of medical device implantation.

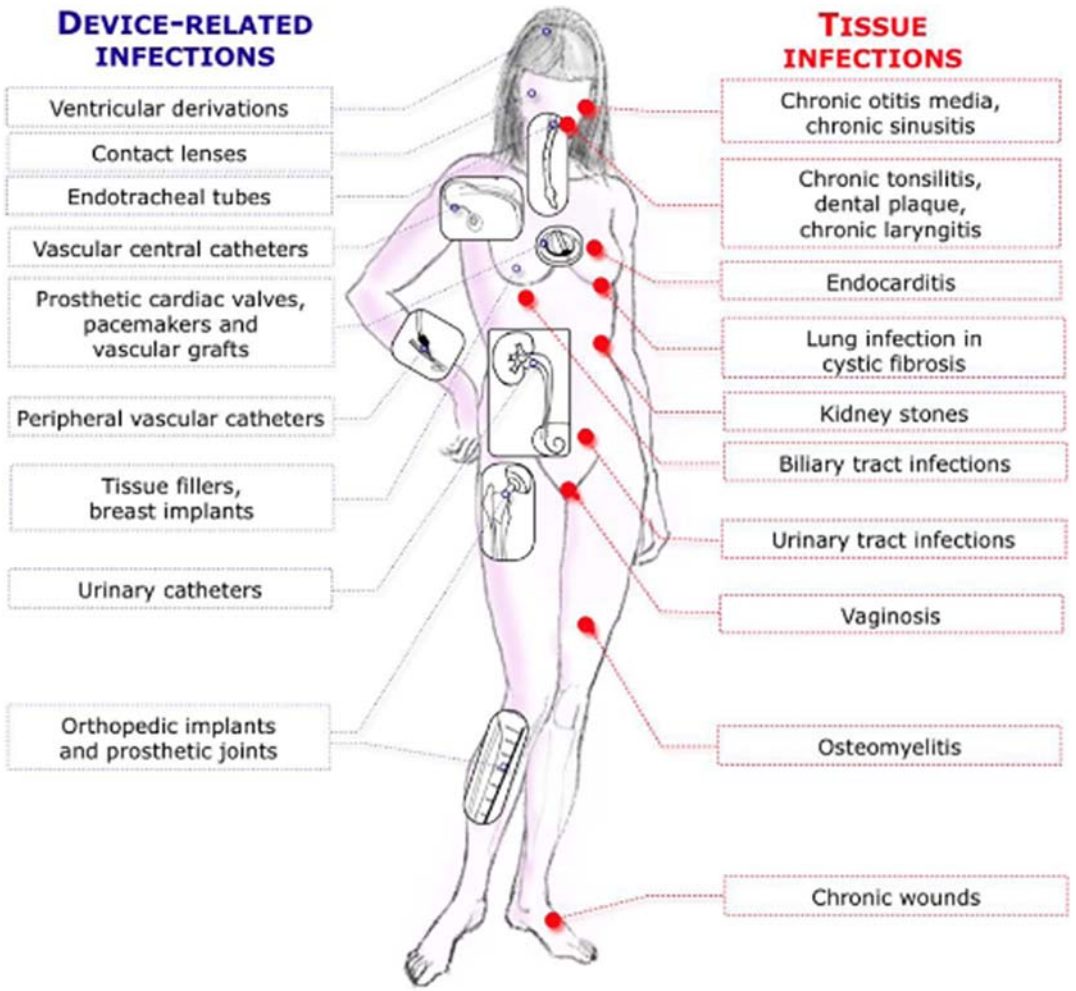

FIGURE 26.1 Biofilm infections occur in diverse medical devices and tissues in the human body. *This figure is taken from Lebeaux, D, Chauhan, A, Rendueles, O, Beloin, C. From in vitro to in vivo models of bacterial biofilm-related infections.* Pathogens *2013;2:288–356.*

This chapter exclusively brings an in-depth understanding of biofilms: origin and prevalence, their architecture: how they form and what they do, an overview of biomedical complications, the current advances in applications of nanomaterials to develop antifouling surfaces of medical devices and implants, and at the end, key future perspectives to guide our move forward in the realm of applications of nanomaterials in developing surfaces preventing device-associated infections. It is our hope that this chapter in the volume "Applications of Multi-functional Nanomaterials" will attract attention from interdisciplinary researchers as well as clinicians actively engaged in the field of nosocomial infections, surface science, microbiology, biomedical engineering, polymer science, and nanotechnology.

2. Biofilms: origin and prevalence

We have understood bacteria as a unicellular life form. The lifestyle of bacteria in synthetic media and laboratory conditions has shaped our understanding of it as a single colony structure. Also, we have studied bacteria in a traditional system where bacterial cells are freely swimming around in a liquid medium composed of tailored nutrients. Such studies have indeed benefitted us by expanding our awareness of bacterial morphology, physiology, genetics, metabolic activities, disease pathogenesis, and many other aspects.

Interestingly, bacteria rarely exist in nature as simple creatures. They tend to exist in nature as complex communities and behave much differently than free-flowing bacteria. While existing in communities, bacteria display properties different than those studied when they are in planktonic form.

In nature, for example, bacteria exist in aggregates and granular forms on substrates in the aquatic environment[3] and waste-water treatment digesters.[4] The lifestyle of bacteria when it exists in communities is believed to play an important role in various biogeochemical cycles of the biosphere.[5] Biofilms are also found in harsh-unusual environments such as acid mine drainage where due to acidic conditions pH is very low and bacterial biofilms help in regulating the sulfur cycle.[6] In our daily lives, we come across dental caries due to plaque formation over our teeth and fouling in kitchen sinks, all due to the formation of microbial assemblages over numerous surfaces.

Biofilms are communities of microorganisms attached to a surface or adhered to cells or both, encapsulated and surrounded by the matrix composed of self-synthesized extracellular polymeric substances (EPS). This mode of microbial lifestyle is an eventual development of the "microbial get-together", which could consist of single or multiple species.

Almost a 100 years back, people observed biofilm spoil the substrates such as those of marine ships.[5] Today, due to advancements in microscopy and imaging techniques, the advent of microelectrodes and modeling, we have been able to profoundly understand biofilms at molecular levels. All such efforts have helped us to understand that biofilms are just not only slime encapsulations of microbes but rather well coordinated, cooperative, and communicating structures adapting to varied physiological conditions of environments.

Biofilms on a micro-scale are cities comprising bacteria dwelling in huge structures. These cities are also powered by communication and interactions just like people around us interact with each other for basic necessities inhabiting physical spaces such as tall buildings. The matrix of the biofilm offers a different physio-chemical environment inside it where cells communicate and interact with each other distinctly. This communication is influenced by conditions in the biofilm matrix and external environmental cues. The understanding of the matrix properties, the role of intercellular interactions inside the matrix, and the sustenance of biofilm lifestyle with continuous adaptation to the external environment enable us to elucidate mechanisms that make biofilms recalcitrant and difficult to eradicate.[7–9]

3. Architecture of biofilms

3.1 How do biofilms form and disassociate: friend-ing and unfriend-ing the surface?

In the presence of environmental cues (stimuli), microbes begin to interact with surfaces that are available around them. The attachment of microbes to a substrate is a concerted

phenomenon determined by microbial cell surface characteristics, substratum's properties, and surrounding liquid conditions. The attachment process consists of reversible and irreversible steps.

To understand the ecological, health, and economic impact and relevance of surface-associated communities, we must understand how bacteria adhere to the substrates such as skin, medical devices, marine ships, kitchen sinks, human teeth, tissues, etc. Bacterial adherence has been widely studied in the context of liquid-solid interfaces.

Surface-associated bacterial life commences when bacteria sense environmental stimuli or factors. These environmental signals differ from one bacteria to another. Some bacteria will form surface-associated communities under any circumstances like *P. aeruginosa* whereas *Vibrio cholerae* grows only when additional nutritional components are present. Other than the growth factors (nutritional cues) acting as environmental stimuli, there are other factors in whose response bacteria start to find a surface for adhesion such as a change in pH, osmolarity, temperature, and oxygen.[10] Adhesion onto a surface leads them to develop biofilm mode of lifestyle resulting in their better survival and sustenance.

When the bacteria sense any kind of environmental stimuli, they attempt to attach to the surface around them in a reversible and irreversible form. Bacteria along with other blood cells (in the case of medical devices) are in Brownian motion and under the influence of gravitational and surrounding hydrodynamic forces. This keeps them in contact with surfaces where they interact for adhesion and colonization. Depending on the change in numerous gradients such as pH, temperature, nutrition, oxygen, ions, etc., they respond to attractive and repelling forces that they experience with the substratum. The properties of the substrate such as surface wettability, mechanical properties (elastic modulus and tensile strength), and surface chemistry along with the characteristics of the surrounding media determine bacterial adhesion. In this process, motile bacteria may exploit their flagellar movement to overcome forces that take them away from surfaces such as hydrodynamic forces of liquid or repulsive forces of the substrate where it tries to adhere.[11] In response to the nutrient gradient, chemotaxis also promotes bacterial adhesion onto a surface.[12]

The initial attachment being reversible is an interplay of the properties of the substrate and liquid media, and the environmental cues that bacteria experience when it is freely-flowing around. Bacteria do not commit themselves to the surface while all such initial movements and surface interactions are reversible if they find better nutrient availability elsewhere or get removed off the surface by hydrodynamic forces.

The irreversible and strong attachment to the surface takes place using additional adhesins and adhesive organelles. *P. aeruginosa* uses type IV pili (i.e., multi-subunit adhesive organelles) to mediate its motility through liquid media[13] while *E. coli* uses type 1 fimbriae to mediate adhesion on the surface.[14,15] They help bacteria to firmly hold onto the surface after, which the bacteria self synthesizes and organizes large EPS-encapsulated structures. The multi-layered growth of thick biofilms occurs due to a large amount of EPS accumulation, which could result in a film with a smooth surface[16] or a complex and a typical one i.e., bacterial aggregates with water channels.[17]

We must understand that while bacteria are responding to the environment and surfaces around them as part of their adaptation and survival mechanisms, it also undergoes a lot of genetic changes evident from the genes transcribed specifically and differently during biofilm formation.[13,18] These different gene expressions are driven by transcription factors that promote events of surface association and secretion of extracellular polymer substances like carbohydrates, amino acids, extracellular DNA, and lipids. As EPS molecules are synthesized,

bacteria irreversibly adhere onto the surface. Once the initial layer of biofilm is formed comprising EPS matrix entrapping bacterial microcolonies, more bacterial cells (same or different species) from the liquid media around it come over to join the "microbial get-together" and form "mushroom"-like structures or even, flat monolayers. Depending on the metabolism and aero-tolerance, bacteria are arranged in different layers of biofilm, such as anaerobic bacteria settle in lower layers to avoid exposure to oxygen. In order to perform specialized functions, bacteria communicate using quorum sensing systems among the same or different species, also referred to ascross-talk" to perform specialized functions. We have discussed this in detail in the next section. As the production of more layered structures takes place with more EPS secreted, biofilm becomes mature and gradually disperses entrapped bacteria.

Dispersal in biofilms is vital for bacteria to survive, expand and reproduce. Biofilm deattachment (dispersal) may occur by a physical process, environmental stress cues, or gene expressions favoring dispersal. Biofilms are continuously exposed to varied shear stress, hydrodynamic forces and flow velocity of liquid fluids around and bacteria continue to passively disperse. The detachment by physical forces is mainly by shearing, sloughing, and abrasion. These physical processes are discussed in detail by Brading and coworkers.[19] More than the physical processes, which cause the passive dispersal of bacteria from biofilm to planktonic lifestyle, it is the environmental changes that cause bacteria to shift to planktonic mode. Inside the mature biofilm structure, there are several events, which trigger bacteria inside the assemblage to disperse due to the increase in toxic by-products, change in nutrient composition, fluctuations in gradients of pH and oxygen, and various other stress conditions.[20] Due to nutritional depletion, in P. fluorescens, the production of EPS lyase increases to mediate biofilm dispersal[21] and due to oxygen-limitation, dispersal occurs in *P. putida* biofilms.[22] At the same time, it is not possible to generalize nutrient depletion to cause biofilm dispersal as nutrient abundance can assist dispersal such as in environmental *Acinetobacter* sp. biofilms.[23]

The process of detachment enables bacteria to either move out of nutrient-deficit environment or take advantage of available nutrients to enhance metabolism, reproduce and disperse for expansion.[24] It is possible for the process of biofilm dispersal to be genetically orchestrated other than the process being environmentally induced. Biofilm dispersal is based on periodic disassociation of the biomass from the substrate where nutrient depletion doesn't trigger dispersal and thus, is a genetically orchestrated event such as in *P. putida*.[25]

3.2 What do bacterial biofilms do?

3.2.1 Cross talk: quorum sensing

Bacteria respond to the change in the density of certain chemical compounds by activating a particular gene cascade. Also, bacteria secrete chemical compounds, which as chemical signals cause other bacteria to respond. This ability to respond to chemical signals and as well generate chemical signals establishes communication across the membranes with even different microbial species. This communication occurs inside the bacterial biofilm and across it as well even with mixed bacterial species. Besides, making the biofilm architecture robust, the EPS polymeric network also facilitates better communication due to the close proximity of bacteria and, thus, diverse cellular changes over a period of time.

There are mainly three types of quorum sensing systems that are well-studied. The first one is found in gram-negative bacteria consists of LuxI/LuxR-based quorum sensing system. Acyl-homoserine lactone is signaling molecule, capable of diffusing across the cell membrane, which is synthesized using LuxI protein. As more bacterial cells synthesize AHL, indicating an increase in cell density, it binds with LuxR protein. This complex formation of AHL-LuxR initiates the transcription of certain genes, which creates biofilm mature. Here, LuxR acts as a transcriptional regulator. Genes responsible for biofilm formation are upregulated with help of LuxR-AHL complex where AHL production plays a key role in the transcriptional regulation of LuxR. And, the AHL production is driven by LuxI, therefore the process is called LuxI/LuxR quorum sensing system.

The second QS system involves peptides of varying lengths that act as QS signaling molecules and this system of communication is shown to exist in Gram-positive bacterial species. Such as in *S. pneumoniae* a 17-residue peptide is responsible for quorum sensing.[26] Third group of signaling molecules consists of autoinducer-2, boron-furan-derived signal molecules, which are found in Gram-positive and Gram-negative bacteria.

Not only do bacteria communicate using quorum sensing with the same species cells, but they also communicate with the cells of other species and as well kingdoms. We can get a deep understanding through dedicated reviews discussing them in detail.[27,28]

QS systems have been known to regulate various physiological processes such as secretion of virulence factors, antibiotic resistance, biofilm formation, and more.[29] Many studies demonstrate that in absence of quorum sensing systems, the grown biofilms are susceptible to antibiotics such as tobramycin and kanamycin treatment, H_2O_2 treatment, SDS, immune cells phagocytosis.[30,31] This is well explained by an example: in one of the strains of *P. aeruginosa* PAO1, LuxI/LuxR quorum sensing system is found to be responsible for eDNA formation, and in absence of eDNA, biofilms show susceptibility to detergents such as SDS.[32]

3.2.2 *Recalcitrance: a powerplay of characteristics in biofilms*

Bacteria display prolonged survival against antibiotics in a biofilm lifestyle unlike being susceptible in planktonic mode. It has been shown that disinfectants such as sodium hypochlorite needs to be 600 times more concentrated to be effective to inhibit *S. aureus* biofilms than to inhibit *S. aureus* planktonic cells.[33] Biofilm mode of bacterial development in medical settings is difficult to treat and causes recurrent infections and morbidities. The ability of bacteria in biofilms to tolerate, resist and persist in presence of a wide range of antibiotics is due to multiple factors and characteristics specific to the biofilm lifestyle of bacteria.

a. Slowed Growth Rate and Persister Cells: Bacterial cells in biofilms are metabolically inactive owing to scarce oxygen and nutrient content. Antibiotics that target metabolic events and processes like cell growth, and cell division to disrupt bacterial growth are ineffective due to the presence of dormant cells. β-lactams are used to target dividing cells but they don't work when treated to *E. coli* biofilms due to metabolically dormant cells.[34] The subpopulation of cells in biofilm matrix, whose growth rate is extremely slow and develop phenotypic variations, known as persisters are neither dead nor metabolically active and are a reservoir of infectious pathogens as they get activated when they disperse from biofilm matrix.[35]

b. EPS Matrix Protection: Suci and colleagues reported that the penetration ability of ciprofloxacin was dramatically reduced in *P. aeruginosa* biofilm.[36] In *K. pneumoniae* biofilm, ampicillin's tolerance is shown by Anderl and colleagues due to reduced penetration capability of ampicillin.[37] This is because EPS matrix, consisting of charged polysaccharides and eDNA, plays a significant role in entrapping the antibiotic and limiting it's reach to the bacterial life inside biofilms. Besides conferring antibiotic resistance to the biofilm, the EPS matrix also gives overall physical protection to the sessile communities. Lied et al. concluded that biofilms escaped human leukocyte killing due to the presence of alginate exopolysaccharide in the EPS matrix while it's absence resulted in killing biofilm bacteria.[38]

c. Efflux Pumps: Efflux Pumps enable bacteria to flush out intracellular toxins including antibiotic drugs. These pumps are protein complexes that are expressed in planktonic cells while the genes encoding the efflux pumps are found to be upregulated in biofilm lifestyle. Zhang et al. have shown that a specific gene i.e., PA 1874–77 in *P. aeruginosa* was responsible for efflux pump formation and found to be upregulated in the biofilm of *P. aeruginosa* leading to enhanced resistance toward antibiotics.[39]

d. Horizontal Gene Transfer: High frequency of horizontal gene transfer occurs in biofilm bacteria. We have seen in the case of *S. aureus* that the biofilm lifestyle promotes plasmid transfer and results in antimicrobial resistance owing to plasmid-mediated conjugation process of gene transfer.[40]

4. Medical biofilms: complications in medical devices

The usage of medical devices, such as voice prostheses, artificial organs, contact lenses, catheters, and hip and knee implants, has become an integral component of modern medicine to restore and enhance the biological function of any component of the body, assist in therapeutic interventions to treat diseases in the body and monitor various body functions. The global market of biomaterials that are implanted is expected to touch $133 billion by 2022.[41]

The surface of medical devices, which indwell or are implanted in patients are known to be associated with bacterial attachment, formation of complex communities, and the subsequent persistent infections.[42] Biofilm-forming abilities of bacteria present in critical care settings present a significant challenge besides the risk of contagious spread in patients to cause systemic infections.[43] The EPS matrix of biofilm shows high resistance to antibiotics, environmental stresses, and clearance by the host-immune system, causing chronic infections.[44]

The formation of conditioning films on indwelling medical device surfaces as a function of physical and chemical properties of the surface and surrounding liquid facilitates bacterial adhesion on medical device surfaces.[45] The surface characteristics such as roughness at the microscale level and environmental conditions such as the gradients of nutrients pH, temperature and osmolarity also determine the species-specific formation of surface-associated communities on medical devices. For instance, *Enterococcus* spp. and *E. coli* are dominant species found in CAUTI infections while *S. aureus* is widely reported to be present in central venous catheter-associated infections. As medical devices are exposed to blood circulation, the formation of a layer of albumin, glycoproteins, immunoglobulins, fibronectin, and host proteins

takes place attracting nonspecific (such as van der waals, coulomb, and strong hydrophobic interactions) and specific receptor-ligand interactions. In medical devices, within a few days depending on species, biofilms reach maturation.[46]

Microbes in planktonic lifestyle swim in random Brownian motion and hydrodynamic forces in local physiological and interstitial fluids before meeting the biomaterial surface. We can call the process of initial adhesion an "interplay" or "tri-lateral" (host-device-microbe) interaction of host factors including immune response, microbial properties as a result of activities such as gene expressions of motility encoding genes, adhesins/autolysins expression and quorum sensing, and device material properties. Biofilm lifestyle commences when microbes encounter and respond to the challenges for survival and adaptation. When free-flowing bacteria come across the surface of medical devices, they explore it with help of flagella, cilia, or fimbria. Bacteria may find the surface to be either deposited with plasma proteins as part of the conditioning process or immunocytes as part of the immune response to the biomaterial depending on the delay of contamination after implantation. Bacteria form specific and irreversible contact with the surface to mark the onset of biofilm aggregation and disease pathogenesis (Fig. 26.2)

Infections resulting from microbes present in hospital settings are termed nosocomial infections, while infections in medical devices constitute 50% of such nosocomial infections.[47] Biofilm infections in medical devices can arise from the skin of the patient, the skin of the critical care worker or from the surrounding clinical settings. The most common pathogens to cause infections in medical devices are Gram-positive bacteria with *S. epidermidis* involved in every 8 of 10 reported cases.[48] The other Gram-positive bacteria associated with biofilm infections in medical devices include *Enterococcus faecalis* and *Staphylococcus aureus* while Gram-negative bacteria include *Klebsiella pneumoniae*, *Escherichia coli*, *Proteus mirabilis* and *Pseudomonas aeruginosa*.[47]

Device-associated infections are excruciatingly notorious in patients with compromised immune systems and who are already receiving critical care.[49] Biofilms reduce device's

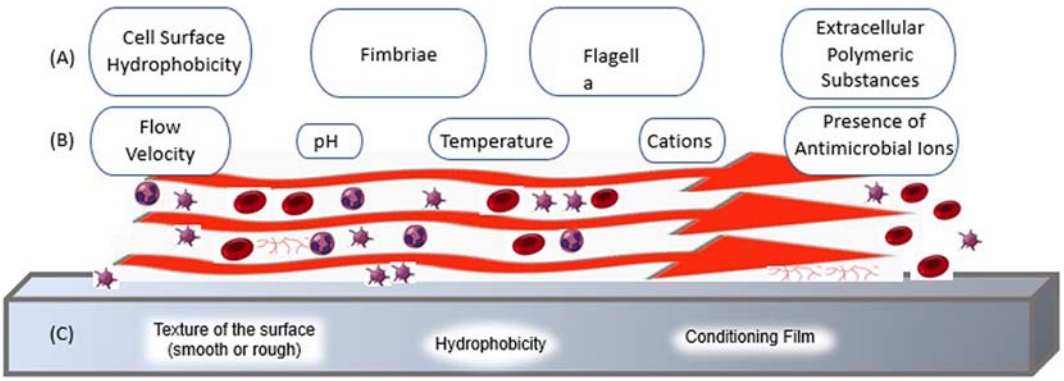

FIGURE 26.2 Schematic to show different parameters affecting the biofilm formation and eventually the anti-biofilm strategies. (A) Different bacterial components playing role in surface contact; (B) Blood factors affecting bacterial adhesion leading to biofilm formation; (C) Surface properties of medical device.

functionality or mechanical failure leading to device's painful removal and replacement.[50] Such complications in medical devices cause extended patient stays, increased cost-burden due to overuse of resources and morbidities resulting in mortality.[51]

Biofilm infections due to their multi-factorial recalcitrance (as discussed above) are difficult to eradicate and treat. Several research efforts are done to develop preventive strategies to avert the formation of surface-associated communities on surfaces of medical devices.

5. Application of nanomaterials to reduce the risk of device-associated infections

At the nanoscale, materials display several unique characteristics, which we don't find when they are in the bulk state. Compared to both micro and bulk, nanosized materials show quantum confinement effect.[52] The effect is observed if the size of the particle is small in comparison to the wavelength of the electron. Quantum Dots (QDs) due to their small size (~10 nm or less) exhibit difference in optical and electronic properties compared to bulk, like quantum size-dependent luminescence and nonlinear optical properties of silicon quantum dots/SiO_2 multilayer.[53] It is known that the bandgap of group II–VI semiconductors becomes narrower as the constituting atoms become heavier. In the case of nanoparticles with diameters of 2–10 nm, the bandgap is increased due to the quantum size effect compared with the bulk semiconductor.[54] The tuneable optical properties of QDs based on their size are leading to a variety of applications including bioimaging, solar cells, LEDs, diode lasers, and transistors. In biological context, the small size (less than 100 nm) of nanomaterials enables them to interact with the cell wall of bacteria. Apart from small sizes, diverse shapes, and morphologies (wires, rods, sheets, etc.), nanomaterials possess unique bioactive features also due to high surface-to-volume ratios resulting in prolonged surface contact and better chemical reactivities. This also makes them be appropriately used as drug-loading carriers and targeting entities along with their permeating nature.

Antibacterial nanomaterials i.e., materials having intrinsic bactericidal properties, ranging from metal and metallic oxide nanoparticles, carbon nanotubes and fullerenes, and a monolayer of antifouling polymers or such materials may act as a carrier (or releaser) of antibacterial agents such as nitric oxide (NO) and antibiotics. Also, their shape and surface charge effectively cause cell death due to disruption of the cell membrane. Metal and metallic oxide nanoparticles (NPs) are among the most commonly studied and applied for antiinfection applications. Numerous metal and metal oxide NPs, such as silver NPs, gold NPs, selenium NPs, titanium dioxides (TiO_2) NPs, zinc oxide (ZnO) NPs, and magnesium oxide (MgO) NPs, have shown a broad-spectrum of antimicrobial properties against both Gram-positive and Gram-negative bacteria.[55] Several nanocarriers such as mesoporous silica, liposome, polymeric NPs, etc. have been also developed as well to better deliver and control the release of classical antimicrobial drug improving their action.[56]

There are several mechanisms shown by nanomaterials that exhibit their biocidal character. The surface charge of nanomaterials,[57] their particle size,[58] cell membrane alterations[59] caused by them, their ability to interfere in the metabolic pathway,[60] disrupting the cell's respiratory chain,[61] causing peroxidation of lipids,[62] different morphologies,[63] uncoiling of DNA,[64] ROS production,[65] nitrosation of thiols of proteins.[66] The biocidal nature of

nanomaterials is mostly due to utilization of multiple mechanisms. The exact mechanism by which nanoparticles exert their antimicrobial activity is not well-understood due to complications involved while studying planktonic bacteria and nanomaterial each separately from physicochemical standpoint as both systems individually (bacterial cell and nanomaterial) are sophisticated and complex. The biofilm lifestyle of bacteria is a further complex microenvironment to study the interaction of nanoparticles. There are several approaches using different organic and inorganic nanoparticles, nanotextured surfaces, and nanocomposites.

5.1 Polymeric nanoparticles

Polymeric Nanoparticles are increasingly gaining interest among researchers to use it as drug delivery vehicles due to its several characteristics such as ease of preparation, simple to functionalize, stabile during periods of storage, and controlled release behavior.[67] Polylactic-co-glycolic acid (PLGA) nanoparticles were used to load antibiofilm hydrogel xylitol to improve it's penetration in the biofilm matrix of bacterial wound infection.[68]

Interestingly, polymeric NPs are also applied as coatings on the surface of medical devices, which are susceptible to device-associated infections. The sustained and controlled release of nitric oxide (NO) is achieved using hydrogel/trehalose composite nanoparticles (10 nm)[66] to prevent *S. aureus* biofilm formation on glass surfaces (30% reduction in adhesion). Further, the ability of NO-np to eradicate biofilms on the surfaces of the medical device i.e., CVC is investigated both in vitro and in vivo resulting in a significant reduction of biofilm cell viability.[69] This study presents both prophylactic and therapeutic application of NO-releasing hydrogel/trehalose composite NPs. Several derivatives of quaternary ammonium polyethyleneimine (QA-PEI) nanoparticles have been evaluated as biocidal additives in dental implant materials due to their antibacterial and biocompatible properties.[70] When incorporated in dental implant base material, QA-PEI NPs have shown significant antibiofilm activity in vivo along with biocidal activity toward broad spectrum salivary bacteria. This is achieved by incorporating very low concentration of QPEI NPs (1% w/w) in dental resin composite potentially triggering stress on the biofilms that later form on dental implants.[71] In another study, researchers used biocompatible NPs to coat the polyethylene (PE) surfaces relevant to minimal-invasive medical instruments that can be removed for cleaning the device for effective sterilization and stop any circulation of infectious pathogens in future use. This is achieved by depositing cetyl palmitate and silicium (Sicarstar) nanoparticles using anisothermal physical plasma (in low-pressure discharge regime) on the PE surface. The developed nano layers show no cytotoxicity to the keratinocyte cell line and exhibit 2–3 log reduction of *S. aureus* and *P. aeruginosa* bacterial colonization.[72]

Polymer NPs provide a low cytotoxic, therefore, more biocompatible platform along with long-lasting nature and antibacterial properties. However, studies are missing to evaluate the interactions of these polymers with host factors and resultant surface properties.

5.2 Silver nanomaterials

The capabilities of silver compounds to be used as a disinfectant has been identified long back. Recently, antibiotic resistance has been found to be associated with chronic bacterial

infections, particularly biofilms. Silver's intriguing antimicrobial character across a wide range of Gram-negative and Gram-positive bacteria have resulted in tremendous research on silver nanomaterials. Also, silver nanomaterials have been extensively explored to develop coatings on the substrates and surface modifications in the base materials that are used to manufacture medical implants, devices, instruments, and surfaces relevant in hospital settings.

Glass surfaces were immobilized with self-assembled monolayers of AgNPs to prevent biofilm formation. This method of modifying the surface consisted of presilanization of the glass surface with (3-aminopropyl) triethoxysilane and the subsequent AgNPs (9 nm) monolayer formation with help of noncovalent interactions between $-NH_2$ groups and silver atoms. AgNPs exhibited significant antibiofilm activity against strong adherent, methicillin-resistant, and biofilm-forming pathogenic bacterial strain, which was isolated from a patient with sepsis due to intravascular catheter-associated infection. Also, in the same study, AgNP-monolayers showed stability in an aqueous medium, prolonged release, and minimal detachment of AgNPs from the surface.[73] In another approach, uniform distribution of silver nanoparticles over the silicon polymer surface along with the effective release of silver ions is achieved. Organic complexes of silver are dissolved in supercritical carbon dioxide and later exposed to hydrogen gas, which further results in the decomposition of organometallic precursors of silver and ultimately, resulting in the homogenous distribution of silver nanoparticles. It was found that after surface modification and formation of conditioning film over it, the silver ions were still able to release and show antimicrobial property.[74] Further improvement for controlled and long-lasting release of silver is established while composing antimicrobial denture materials by adding AgNPs (60 nm) to polymethyl-methacrylate (PMMA) resin, which is used to develop dentures. An antimicrobial denture base polymer with long-lasting silver release with greater diffusion into the PMMA denture resin was developed, which can prevent denture stomatitis and several disease complications related to oral mucosal tissues in people who wear complete denture[75] Moreover, several strategies have employed silver nanoparticles and incorporated them directly upon the surface of medical devices such as to study the translation of antimicrobial and antifouling nature of AgNPs in the application.

Plastic catheters (PE-BAX polyamide 20 gauge catheters) are coated with a thin layer of AgNPs with sustained release of Ag^+ ions eluting even after 10 days in vivo implantation. The coating exhibited significant antimicrobial activity and prevented biofilm-forming ability over a broad range of microbes including *S.* aureus, coagulase-negative staphylococci, *E. coli*, *Enterococcus* spp. and *Candida albicans*.[76] In another study, urinary catheters are coated using Ag-PTFE (silver-polytetrafluoroethylene) nanocomposite. AgNPs with size 50−200 nm is incorporated into the PTFE matrix. The combined improved effect of the Ag-PTFE nanocomposite displays both antiadhesive and antibacterial activity against both Gram-negative *E. coli* and Gram-positive *S. aureus*. The antiinfection capability of Ag-PTFE coated urinary catheter assessed in in vitro bladder model was promising while improving the working life of silicone urinary catheter from 6 to 40 days. Moreover, good biocompatibility was associated with the use of Ag-PTFE coating with fibroblast cell lines.[77] Further, the antiencrustation ability of Ag-PTFE nanocomposite coatings results in lesser resistance and blockages inside urinary catheter.[78] Surgical sutures dip coated by AgNPs (2−5 nm in size) displayed antiadhesive activity resulting in reduced adhesion of *S. aureus* cells. Moreover, the silver ions continue to release >30 days

indicating long-term release ability and noncytotoxicity to eukaryotic cell lines.[79] AgNPs synthesized by Mussel-inspired green synthesis have been used to apply on commercial Central Venous Catheters. Besides, dopamine after getting auto-oxidized forms adhesive polydopamine films on inorganic and organic materials. Catechol groups in polydopamine films act as reducing agents to generate AgNPs. CVCs treated with dopamine solution followed by treatment with silver nitrate solution leads to AgNPs production. The coating of the medical device i.e., CVC with 30−50 nm spherical size AgNPs display concentration-dependent antibacterial activity. The eukaryotic cell's (host cells) cytocompatibility is poor at higher doses and good at lower doses, which can be further investigated in vivo studies.[80]

Silver has been used as an effective antibacterial agent over the past several decades in various forms such as metallic silver, silver salts, and colloidal silver. Silver Nanoparticles are extensively applied in cosmetics, textiles, wound dressings, food packaging films, water remediation, and electronic devices that significantly contribute to human and environmental exposure.

In the application of silver as an alternative to antibiotics, bacterial resistance against ionic silver is well established. Silver ionic resistance has been shown to comprise of $Ag+$ reduction to a neutral oxidation state where silver is no longer toxic to bacteria and, another mechanism where Ag^{+}/H^{+} chemiosmotic antiporters or P-type adenosine triphosphatases cause efflux of Ag^{+} inside the bacterial cells.[81] As well, silver nanoparticles result in bacterial resistance i.e., mediated by elimination of silver ions.[82] There are few recent studies, which explore bacterial resistance due to AgNPs. In one study Panáček and colleagues[83] elucidated the mechanism of silver nanoparticles due to the production of flagellin (bacterial flagellum protein) causing aggregation of silver NPs while another study attributes the resistance due to flagellum-based motility instead of aggregation of nanoparticles.[84]

Interestingly, gram-positive bacteria have not shown so far any resistance to AgNPs, which covers a broad range of clinically relevant and drug-resistant bacterial strains. This includes a wide range of nonmotile bacteria *S. aureus*, several types of *Streptococci* and *Acinetobacter*, and even *P. aeruginosa*, which switches to a nonmotile phenotype in late and chronic infections.[85] Though bacterial resistance mechanisms are currently investigated and surrounded by debate, it is somehow clear that their widespread application can contribute toward global antimicrobial resistance.

5.3 Titanium oxide nanomaterials

Titanium offers several properties, which makes it favourable material to design medical implants from showing more resistance to bacterial colonization than steel to display, in its oxide form, strong mechanical strength, biocompatibility, and chemical stability.[86]

TiO_2 nanotubes were fabricated using electrochemical anodization and further loaded with bone morphogenetic proteins (BMP2), which help in osteoblast differentiation and bone healing. Chitosan's layer and Alginate dialdehyde conjugated with gentamicin's layer was alternatively coated on BMP2-loaded Titanium nanotubes with help of spin coating layer-by-layer. This layer-by-layer assembly showed the antibacterial property and good biocompatibility with osteoblast cells. The antibacterial activity shows a modest two-log reduction. This coating demonstrated in vitro differentiation of osteoblasts, improved

alkaline phosphatase activity, enhanced mineralization capability, and promoted osteogenic-relative gene expression and all these events are associated with the bone healing process.[87]

In another report, Titanium oxide nanotube arrays (30 or 80 nm) also synthesized using anodization on titanium substrates significantly reduced colonization of *S. epidermidis*. Also, the adhesion of C3H10T1/2 cells with osteogenic potential, which morphologically similar to fibroblasts and functionally similar to mesenchymal stem cells (help in repairing bone/cartilage tissues).[88]

5.4 Zinc oxide nanomaterials

Zinc Nanomaterials are the second most exploited metal nanoscale materials after silver in the context of their antibacterial and antibiofilm activity. A unique advantage of the use of zinc nanomaterials is their cytocompatibility with eukaryotic cells while exhibiting antimicrobial activity comparable to AgNPs.[89]

The development of ZnO Nanoparticles coatings on glass surfaces deposited by sonochemistry was explored to prevent bacterial colonization. The coated surface produced hydroxyl radicals, which limited bacterial activity and showed no biofilm growth for 10 days.[90] ZnO NPs (5 nm) were deposited on titanium plates exhibiting nanoscale topography using sonochemistry. The impact of different Ti nanoscale topography (a periodic structure like Titania nanotube vs. a non-periodic structure like Titania Nanoleaf), as well as ZnONPs incorporated with these nanostructures in reducing bacterial adhesion and promoting cellular viability, was studied. The antibacterial activity of ZnO NPs was concentration-dependent. The antimicrobial mechanism of ZnO NPs was through membrane damage as well as through the release of Zn^{2+} ions.[91] In another strategy to modify the base material of orthopedic implant, ZnO nanomaterials are combined with nanohydroxyapatite and later, deposited on titanium discs (dental implant substrate) using an electrohydrodynamic deposition. A homogenous and uniformly coated surface of ZnO and HA NPs (20−100 nm) along with their composite mixtures could be coated onto the surface of titanium discs. The growth of biofilm was monitored over 4 days on the surfaces coated with antimicrobial nanoparticles. Besides, the composite (nZnO + nHA) displayed negligible antimicrobial activity while leading to significant biofilm growth reduction. The composite coating reduced the overall number of bacteria and possibly inhibited microbial growth and thus, preventing the biofilm growth to reach a steady state. There are multiple modes of actions of the composite coatings, which altogether result in distinct growth events of bacterial biofilm, which were not explored in this application of ZnO nanomaterials.[92] In another strategy, ZnO Nanoparticles along with gallic acid and chitosan have been used to develop coating formulation for contact lenses. Silicon hydrogel contact lenses can be coated in a one-step high-intensity ultrasound coating process with chitosan, gallic acid, and ZnO Nanoparticles simultaneously to result in an antibacterial surface. The nanocomposite coating on a contact lens is multi-functional with properties like antioxidant and antibacterial to pathogenic *S. aureus* and biocompatible as it doesn't induce damage to human cells.[93]

Interestingly, the doping of Zn has been done in CuO to result in Zn:CuO nanoparticles for applying coatings over the surfaces of artificial teeth, contact lenses, and pediatric catheters. Zn:CuO nanoparticles (30 nm) were also used to create a coating via a sonochemical

deposition process during which the artificial tooth. Zn:CuO NPs displayed antibacterial efficacy in presence of *S. mutans* by disrupting the cell membrane integrity causing intracellular ROS generation. Moreover, 88% reduction in biofilm formation was observed with Zn:CuO coating.[94] $Zn_{0.11}Cu_{0.89}O$ (Zn−CuO) nanoparticles (30−65 nm) were also used to confer antibacterial activity to contact lenses. Zn-doped CuO composite was formed and coated in contact lenses using sonochemistry. The significant reduction of adhesion of *S. epidermidis* and *P. aeruginosa* was observed while the leaching profile of ions from nanoparticles was low. Several physical properties such as refractive index, oxygen permeability, softness, and biocompatibility have to be explored to establish well-characterized contact-less coating with potential activity to reduce contact-less associated microbial keratitis.[95] Zn-doped CuO nanoparticles were coated on silicone pediatric catheters using ultrasound nanofabrication. Along with stability and low leaching levels, the coating significantly inhibited biofilm activity with a maximum inhibition of 99.5% for *P. mirabilis*. Biocompatibility, in terms of eukaryotic cell cytotoxicity, irritation potential, and cytokine secretion levels, was evaluated for the coated catheters in vitro and various histopathological and biochemical parameters were assessed in vivo, revealing no toxicity and abnormalities. The coating upon assessments in in vitro experiments shows a 99.5% reduction in viable bacterial cells, implying that there are still more than 10^5 bacterial cells after the killing of the rest of the cells. In order to evaluate the robustness of coatings to be able to kill bacteria effectively, a high dose inoculum in vivo over a long duration of catheterization is important to validate the promise of coatings to prevent CAUTI in rabbits.[96] The period of catheterization in the study is 7 days during which the coated catheters didn't show any incidence of bacteria, unlike the uncoated catheters where more than 10^5 bacteria were found to be present.

5.5 Nanotextured surfaces

It is possible to develop nanostructured surfaces, which prevent bacterial adhesion and do not release biocides or inhibiting agents for killing microbes, thus, employing a passive approach to reduce the risk of infectious microbial fouling. There are several limitations associated with surface coatings and modifications such as bacterial resistance against antimicrobial coating agents, available for release over a limited period of time, and the durability of the modified surface is short term. Nanotextured surfaces involve the creation of specific patterned surfaces at the nanoscale either due to introducing nanopatterns or nano-size objects (such as particles, micelles, vesicles, and tubes) over micropatterned surfaces. Several research studies have been pursued in this direction, which can be broadly categorized as surfaces inspired by nature such as antifouling diamond nanocones mimicking cicada fly wings[97] or synthetic micro- and nanostructured surfaces having roughness that mimics natural patterns.

Shark's skin like micropattern is done to design antibiofouling surface and developed upon endotracheal tubes to result in 99% prevention in bacterial adhesion and reduced biofilm formation of *S. aureus* and *P. aeruginosa*.[98] In another strategy, cicada fly wings were mimicked on titanium surfaces and mechanically kill *P. aeruginosa* bacteria by causing stretch in cell walls by nanospikes to result into cell puncturing. Cicada wing-inspired nanowires are designed on clinically relevant titanium surfaces with the help of an alkaline hydrothermal process to eradicate gram-negative motile cells.[99]

Silicon nanopillars have been patterned to develop a high aspect ratio surface using a deep reactive ion etching technique involving C_4F_6 gas in the deposition cycle and O_2 and SF_6 gases in the etch cycle. The random interspacing of silicon nanopillars enhanced surface hydrophobicity and resulted in 86% killing of bacteria.[100] Further, in order to improve the biocidal activity of the nanotextured surface, additional deposition of quaternary polymer brushes,[101] copper and silver nanoparticles[102] were used to deposit upon silicon nanopillars. The silicon nanopillars are functionalized with lysozyme entrapping polymer brushes to develop a contact-killing surface for bacteria adhering to the surface.[103] Nanotextured-based antifouling surfaces may involve: (1) functionalization of nanopatterned architecture with antimicrobial agents, (2) preventing adhesion with surface roughness (hydrophobic surfaces), (3) biocidal surface by formation of nanopillars (or patterned deposition of nanoobjects). Though these strategies present minimal risk of causing resistance or decline in long-term biocidal behavior, unfortunately, these processes are not scaled for medical devices so far and limited investigation of bactericidal nature is done in presence of host factors and in vivo models.

5.6 On-demand release based coatings

Traditional biocidal coatings face certain limitations. First, long-term exposure to biocides leads to a decrease in killing efficiency due to the lesser release of biocides than their minimum inhibitory concentrations and the emergence of antibiotic resistance. Second, the longer release of biocides results in toxicity to local mammalian cells and tissues. Antifouling coatings with the bacteria-responsive release, which only releases the biocidal agent in response to bacteria and remains inert in it's absence, can overcome the limitations of traditional coatings. Self-defensive coatings triggered by bacterial microenvironment responses are recently gaining attention among researchers to explore their potential to be used as coatings for preventing device-associated infections. During biofilm formation, there is a change in the microenvironment of bacterial cells such as concentration of enzymes, pH, and virulence factors.[104] These factors that influence biofilm formation can be used as "triggers" or stimuli agents to switch on the antibacterial nature of bacteria by either releasing loaded antibiotics or exposure to immobilized biocidal groups.

Metal ion coordination polymer is used to develop release systems and responsive drug loading coatings, which can potentially be used for bone implants. Titania nanotubes (TNTs) are loaded with AgNPs and antibacterial agents (ibuprofen or vancomycin) and further sealed with 1, 4-bis(imidazole-1-ylmethyl)benzene i.e., metal coordination polymer. The formation of intermediate coordination bonds with metal ions in this system is sensitive to changes in pH. Upon bacteria-induced acidification, the cleavage of the coordination bond leads to the release of encapsulated antimicrobial agents. In addition to this, the release of metal ions from the synthesized responsive system resulted in enhanced antimicrobial and osteoblast proliferation activities.[105] In another strategy, a multi-functional coating was developed to reduce the risk of biofilm colonization (by local release of Tannic acid, oxidant, and gentamicin sulfate, antibiotic) and improve bone healing despite oxidative stress on Ti-based

surfaces. The approach involved the combination of chitosan-polycaprolactone nanofibers along with polyelectrolyte multilayers of tannic acid and gentamicin sulfate.[106] Toxin-triggered release nanostructures are developed in response to specific secreted virulence factors by pathogenic bacteria. Aminocellulose nanospheres are synthesized sonochemically and incorporated on silicon surfaces using layer-by-layer (LbL) assembly with help of hyaluronic acid. The study compares LbL constructs that are made using nanospheres of amino cellulose and their bulk forms and observe the same antibiofilm effect with fewer multilayers of amino cellulose nanospheres. The hyaluronic acid gets degraded by pyocyanin secreted by *P. aeruginosa* causing the release of amino cellulose nanospheres. The polycationic amino cellulose nanospheres, act upon degradation caused by *P. aeruginosa* to prevent biofilm formation on the commercially available Foley Catheter.[107]

It should be noted that these emerging coatings need more understanding of the synergistic mechanism that they promise, which should be validated in long-term in vivo biofilm models. It is important that these coatings besides being durable and robust should also promote antithrombotic and osteogenic properties.

6. Future perspectives: nano-micro-macro: a complex interplay

The application of nanomaterials struggles with associated toxicities in the host system and the environment. Long-term robustness needs to be validated to understand the impact of the host-response on the mode of action of nanomaterials. The application of nanomaterials upon the medical device and it's characterization in preclinical settings is not well explored in proportion to the studies, which show promise at preliminary and limited-controlled experimental setups.

Nanomaterials have been widely used to assess, improve and engineer their antibacterial and antibiofilm abilities. Many interesting findings encourage their exploration as potential antimicrobial agents to treat and prevent chronic biofilm infections over routine antibiotics. Researchers from multi-disciplines are widely exploring a solution to the clinical challenge posed by the biofilm lifestyle of microbes. Nanomaterials-mediated strategies driven by mechanistic actions happening at "nanoscale" face a considerable challenge for application in "multicellular" host species to combat notorious biofilm lifestyle of "micro"-bes for achieving a "macro"-level impact, which is to improve patient outcomes. It is extremely important to involve multi-disciplinary perspectives of clinicians, microbiologists, chemists, nanotechnologists, etc. with relevant in vitro and in vivo models taking into close consideration of various host-factors, medical device characteristics, and features of microbial lifestyle,[108] unlike the contemporary studies, which overlook some critical perspectives and relevant study designs.

Acknowledgments

AC would like to thank UGC-BSR (F.30-487/2019(BSR)), DST-Nanomission (DST/NM/NB/2018/203), ICMR (OMI/20/2020-ECD-1) and SERB-CRG (CRG/2021/001974) for the funding support. AM would like to acknowledge the fellowship support from DST-Nanomission Project (DST/NM/NB/2018/203).

References

[1] Bhowmik A, Malhotra A, Jana S, Chauhan A. Biofilm formation and pathogenesis. In: Nag M, Lahiri D, editors. *Analytical methodologies for biofilm research*. US: Springer; 2021. p. 3–37. https://doi.org/10.1007/978-1-0716-1378-8_1.

[2] Chauhan A, et al. Preventing biofilm formation and associated occlusion by biomimetic glycocalyxlike polymer in central venous catheters. *J Infect Dis* 2014;**210**:1347–56.

[3] Geesey GG, Richardson WT, Yeomans HG, Irvin RT, Costerton JW. Microscopic examination of natural sessile bacterial populations from an alpine stream. *Can J Microbiol* 1977;**23**:1733–6.

[4] MacLeod FA, Guiot SR, Costerton JW. Layered structure of bacterial aggregates produced in an upflow anaerobic sludge bed and filter reactor. *Appl Environ Microbiol* 1990;**56**:1598–607.

[5] Hall-Stoodley L, Costerton JW, Stoodley P. Bacterial biofilms: from the natural environment to infectious diseases. *Nat Rev Microbiol* 2004;**2**:95–108.

[6] Edwards KJ, Bond PL, Gihring TM, Banfield JF. An archaeal iron-oxidizing extreme acidophile important in acid mine drainage. *Science* 2000;**287**:1796–9.

[7] Lebeaux D, et al. pH-mediated potentiation of aminoglycosides kills bacterial persisters and eradicates in vivo biofilms. *J Infect Dis* 2014;**210**:1357–66.

[8] Singh BP, Ghosh S, Chauhan A. Control of bacterial biofilms for mitigating antimicrobial resistance. In: Panwar H, Sharma C, Lichtfouse E, editors. *Sustainable agriculture reviews 46: mitigation of antimicrobial resistance vol 1 tools and targets*. Springer International Publishing; 2020. p. 147–76. https://doi.org/10.1007/978-3-030-53024-2_7.

[9] Singh BP, Ghosh S, Chauhan A. Development, dynamics and control of antimicrobial-resistant bacterial biofilms: a review. *Environ Chem Lett* 2021;**19**:1983–93.

[10] Toole GO, Kaplan HB, Kolter R. Biofilm formation as microbial development. *Annu Rev Microbiol* 2000;**54**:49–79.

[11] Toutain CM, Caizza NC, Zegans ME, O'Toole GA. Roles for flagellar stators in biofilm formation by *Pseudomonas aeruginosa*. *Res Microbiol* 2007;**158**:471–7.

[12] Schmidt J, et al. The *Pseudomonas aeruginosa* chemotaxis methyltransferase CheR1 impacts on bacterial surface sampling. *PLoS One* 2011;**6**:1–11.

[13] Klausen M, Aaes-Jørgensen A, Molin S, Tolker-Nielsen T. Involvement of bacterial migration in the development of complex multicellular structures in *Pseudomonas aeruginosa* biofilms. *Mol Microbiol* 2003;**50**:61–8.

[14] Chauhan A, Sakamoto C, Ghigo J-M, Beloin C. Did I pick the right colony? Pitfalls in the study of regulation of the phase variable antigen 43 adhesin. *PLoS One* 2013;**8**:e73568.

[15] Martinez JJ, Mulvey MA, Schilling JD, Pinkner JS, Hultgren SJ. Type 1 pilus-mediated bacterial invasion of bladder epithelial cells. *EMBO J* 2000;**19**:2803–12.

[16] Wimpenny JWT, Colasanti R. A unifying hypothesis for the structure of microbial biofilms based on cellular automaton models. *FEMS (Fed Eur Microbiol Soc) Microbiol Ecol* 1997;**22 1–2216**.

[17] Costerton JW, Lewandowski Z. Microbial biofilms. *Annu Rev Microbiol* 1995;**49**:711–45.

[18] Morici LA, Carterson AJ, Wagner VE, Frisk A. *Pseudomonas aeruginosa AlgR represses the rhl quorum-sensing system in a biofilm-specific manner*. 2007. p. 7752–64.

[19] Brading MG, Jass J, Lappin-Scott HM. Dynamics of bacterial biofilm formation. In: Lappin-Scott H, Costerton J, editors. *Microbial biofilms*. vols 46–63. Cambridge: Cambridge University Press; 1995. https://doi.org/10.1017/cbo9780511525353.004.

[20] Karatan E, Watnick P. Signals, regulatory networks, and materials that build and break bacterial Biofilms.pdf. *Microbiol Mol Biol Rev* 2009;**73**:310–47.

[21] Allison DG, Ruiz B, Sanjose C, Jaspe A, Gilbert P. Extracellular products as mediators of the formation and detachment of Pseudomonas fluorescens biofilms. *FEMS Microbiol Lett* 1998;**167**:179–84.

[22] Applegate DH, Bryers JD. Effects of carbon and oxygen limitations and calcium concentrations on biofilm removal processes. *Biotechnol Bioeng* 1991;**37**:17–25.

[23] James GA, Korber DR, Caldwell DE, Costerton JW. Digital image analysis of growth and starvation responses of a surface- colonizing Acinetobacter sp. *J Bacteriol* 1995;**177**:907–15.

[24] Kaplan JB. Biofilm dispersal: mechanisms, clinical implications, and potential therapeutic uses. *J Dent Res* 2010;**89**:205–18.

[25] Gjermansen M, Nilsson M, Yang L, Tolker-Nielsen T. Characterization of starvation-induced dispersion in Pseudomonas putida biofilms: genetic elements and molecular mechanisms. *Mol Microbiol* 2010;**75**:815–26.
[26] Cvitkovitch DG, Li Y-H, Ellen RP. Quorum sensing and biofilm formation in Streptococcal infections. *J Clin Invest* 2003;**112**:1626–32.
[27] McNab R, Lamont RJ. Microbial dinner-party conversations: the role of LuxS in interspecies communication. *J Med Microbiol* 2003;**52**:541–5.
[28] Moos WH, et al. Microbiota and neurological disorders: a gut feeling. *Biores Open Access* 2016;**5**:137–45.
[29] Irie Y, Parsek MR. Quorum sensing and microbial biofilms. *Curr Top Microbiol Immunol* 2008;**322**:67–84.
[30] Hentzer M, et al. Inhibition of quorum sensing in *Pseudomonas aeruginosa* biofilm bacteria by a halogenated furanone compound. *Microbiology* 2002;**148**:87–102.
[31] Bjarnsholt T, et al. *Pseudomonas aeruginosa* tolerance to tobramycin, hydrogen peroxide and polymorphonuclear leukocytes is quorum-sensing dependent. *Microbiology* 2005;**151**:373–83.
[32] Allesen-Holm M, et al. A characterization of DNA release in *Pseudomonas aeruginosa* cultures and biofilms. *Mol Microbiol* 2006;**59**:1114–28.
[33] Luppens SBI, Reij MW, Van der Heijden RWL, Rombouts FM, Abee T. Development of a standard test to assess the resistance of *Staphylococcus aureus* biofilm cells to disinfectants. *Appl Environ Microbiol* 2002;**68**:4194–200.
[34] Ashby MJ, Neale JE, Knott SJ, Critchley IA. Effect of antibiotics on non-growing planktonic cells and biofilms of *Escherichia coli*. *J Antimicrob Chemother* 1994;**33**:443–52.
[35] Lewis K. Persister cells, dormancy and infectious disease. *Nat Rev Microbiol* 2007;**5**:48–56.
[36] Suci PA, Mittelman MW, Yu FP, Geesey GG. Investigation of ciprofloxacin penetration into *Pseudomonas aeruginosa* biofilms. *Antimicrob Agents Chemother* 1994;**38**:2125–33.
[37] Anderl JN, Franklin MJ, Stewart PS. Role of antibiotic penetration limitation in *Klebsiella pneumoniae* biofilm resistance to ampicillin and ciprofloxacin. *Antimicrob Agents Chemother* 2000;**44**:1818–24.
[38] Leid JG, et al. The exopolysaccharide alginate protects *Pseudomonas aeruginosa* biofilm bacteria from IFN-γ-Mediated macrophage killing. *J Immunol* 2005;**175**:7512–8.
[39] Zhang L, Mah TF. Involvement of a novel efflux system in biofilm-specific resistance to antibiotics. *J Bacteriol* 2008;**190**:4447–52.
[40] Savage VJ, Chopra I, O'Neill AJ. *Staphylococcus aureus* biofilms promote horizontal transfer of antibiotic resistance. *Antimicrob Agents Chemother* 2013;**57**:1968–70.
[41] *Global implantable biomaterials market outlook (2014–2022)*. New york: Reportlinker. PR Newswire; 2015.
[42] Sabina C, et al. Biofilms formed by gram-negative bacteria undergo increased lipid A palmitoylation, enhancing in vivo survival. *mBio* 2014;**5**. e01116-14.
[43] Chauhan A, et al. A rat model of central venous catheter to study establishment of long-term bacterial biofilm and related acute and chronic infections. *PLoS One* 2012;**7**:e37281.
[44] Høiby N, Bjarnsholt T, Givskov M, Molin S, Ciofu O. Antibiotic resistance of bacterial biofilms. *Int J Antimicrob Agents* 2010;**35**:322–32.
[45] Chauhan A, Lebeaux D, Ghigo J-M, Beloin C. Full and broad-spectrum in vivo eradication of catheter-associated biofilms using gentamicin-EDTA antibiotic lock therapy. *Antimicrob Agents Chemother* 2012;**56**:6310–8.
[46] Donlan RM. Biofilms and device-associated infections. *Emerg Infect Dis* 2001;**7**:277–81.
[47] Harris LG, Richards RG. Staphylococci and implant surfaces: a review. *Inj* 2006;**37**.
[48] Von Eiff C, Heilmann C, Peters G. New aspects in the molecular basis of polymer-associated infections due to staphylococci. *Eur J Clin Microbiol Infect Dis* 1999;**18**:843–6.
[49] Stressmann Franziska A, et al. Comparative analysis of bacterial community composition and structure in clinically symptomatic and asymptomatic central venous catheters. *mSphere* 2017;**2**. e00146-17.
[50] Lebeaux D, et al. Management of infections related to totally implantable venous-access ports: challenges and perspectives. *Lancet Infect Dis* 2014;**14**:146–59.
[51] Guggenbichler JP, Assadian O, Boeswald M, Kramer A. Incidence and clinical implication of nosocomial infections associated with implantable biomaterials—catheters, ventilator-associated pneumonia, urinary tract infections. *GMS Krankenhaushygiene Interdiszip* 2011;**6**. Doc18.
[52] Zhirnov Vv, Cavin RK. Chapter 2 - Basic physics of ICT. In: Zhirnov Vv, Cavin RK, editors. *Microsystems for bioelectronics (Second Edition)*. William Andrew Publishing; 2015. pp. 19–49.

[53] Zhang P, et al. Quantum size-dependent luminescence and nonlinear optical properties of silicon quantum dots/SiO_2 multilayer. *Opt Laser Technol* 2023;**157**:108706.
[54] Neikov OD, Yefimov NA. Chapter 9 - Nanopowders. In: Neikov OD, Naboychenko SS, Yefimov NA, editors. *Handbook of non-ferrous metal powders (Second Edition)*. Elsevier; 2019. p. 271e311.
[55] Vallet-Regí M, González B, Izquierdo-Barba I. Nanomaterials as promising alternative in the infection treatment. *Int J Mol Sci* 2019;**20**.
[56] Edson JA, Kwon YJ. Design, challenge, and promise of stimuli-responsive nanoantibiotics. *Nano Converg* 2016;**3**.
[57] El Badawy AM, et al. Surface charge-dependent toxicity of silver nanoparticles. *Environ Sci Technol* 2011;**45**:283–7.
[58] Morones JR, et al. The bactericidal effect of silver nanoparticles. *Nanotechnology* 2005;**16**:2346–53.
[59] Warnes SL, Caves V, Keevil CW. Mechanism of copper surface toxicity in *Escherichia coli* O157:H7 and Salmonella involves immediate membrane depolarization followed by slower rate of DNA destruction which differs from that observed for Gram-positive bacteria. *Environ Microbiol* 2012;**14**:1730–43.
[60] Iavicoli I, Fontana L, Leso V, Bergamaschi A. The effects of nanomaterials as endocrine disruptors. *Int J Mol Sci* 2013;**14**:16732–801.
[61] Sotiriou GA, Pratsinis SE. Antibacterial activity by nanosilver particles. *Mater Res Soc Symp Proc* 2011;**1413**:1–6.
[62] Hong R, Kang TY, Michels CA, Gadura N. Membrane lipid peroxidation in copper alloy-mediated contact killing of *Escherichia coli*. *Appl Environ Microbiol* 2012;**78**:1776–84.
[63] Pal S, Tak YK, Song JM. Does the antibacterial activity of silver nanoparticles depend on the shape of the nanoparticle? A study of the gram-negative bacterium *Escherichia coli*. *Appl Environ Microbiol* 2007;**73**:1712–20.
[64] Sondi I, Salopek-Sondi B. Silver nanoparticles as antimicrobial agent: a case study on *E. coli* as a model for Gram-negative bacteria. *J Colloid Interface Sci* 2004;**275**:177–82.
[65] Santo CE, et al. Bacterial killing by dry metallic copper surfaces. *Appl Environ Microbiol* 2011;**77**:794–802.
[66] Friedman A, et al. Susceptibility of gram-positive and -negative bacteria to novel nitric oxide-releasing nanoparticle technology. *Virulence* 2011;**2**:37–41.
[67] Cheow WS, Hadinoto K. Antibiotic polymeric nanoparticles for biofilm-associated infection therapy. *Methods Mol Biol* 2014;**1147**:227–38.
[68] Anjum A, Chung P-Y, Ng S-F. PLGA/xylitol nanoparticles enhance antibiofilm activity via penetration into biofilm extracellular polymeric substances. *RSC Adv* 2019;**9**:14198–208.
[69] Radu MM, et al. Sustained nitric oxide-releasing nanoparticles interfere with methicillin-resistant *Staphylococcus aureus* adhesion and biofilm formation in a rat central venous catheter model. *Antimicrob Agents Chemother* 2016;**61**. e02020-16.
[70] Chrószcz M, Barszczewska-Rybarek I. Nanoparticles of quaternary ammonium polyethylenimine derivatives for application in dental materials. *Polym* 2020;**12**.
[71] Beyth N, Yudovin-Farber I, Perez-Davidi M, Domb AJ, Weiss EI. Polyethyleneimine nanoparticles incorporated into resin composite cause cell death and trigger biofilm stress in vivo. *Proc. Natl. Acad. Sci. U. S. A.* 2010;**107**:22038–43.
[72] Lukowski G, et al. Renewable nano-structured coatings on medical devices prevent the transmission of clinically relevant pathogens. *Surf Coating Technol* 2019;**366**:227–37.
[73] Taglietti A, et al. Antibiofilm activity of a monolayer of silver nanoparticles anchored to an amino-silanized glass surface. *Biomater* 2014;**35**:1779–88.
[74] Furno F, et al. Silver nanoparticles and polymeric medical devices: a new approach to prevention of infection? *J Antimicrob Chemother* 2004;**54**:1019–24.
[75] Monteiro DR, et al. Silver distribution and release from an antimicrobial denture base resin containing silver colloidal nanoparticles. *J Prosthodont* 2012;**21**:7–15.
[76] Roe D, Karandikar B, Bonn-Savage N, Gibbins B, Roullet J, baptiste. Antimicrobial surface functionalization of plastic catheters by silver nanoparticles. *J Antimicrob Chemother* 2008;**61**:869–76.
[77] Zhang S, et al. Enhanced antibacterial and antiadhesive activities of silver-PTFE nanocomposite coating for urinary catheters. *ACS Biomater Sci Eng* 2019. https://doi.org/10.1021/acsbiomaterials.9b00071.
[78] Wang L, et al. In-vitro antibacterial and anti-encrustation performance of silver-polytetrafluoroethylene nanocomposite coated urinary catheters. *J Hosp Infect* 2019;**103**:55–63.
[79] Ho CH, Odermatt EK, Berndt I, Tiller JC. Long-term active antimicrobial coatings for surgical sutures based on silver nanoparticles and hyperbranched polylysine. *J Biomater Sci Polym Ed* 2013;**24**:1589–600.

[80] Wu K, Yang Y, Zhang Y, Deng J, Lin C. A ntimicrobial activity and cytocompatibility of silver nanoparticles coated catheters via a biomimetic surface functionalization strategy. *Int J Nanomed* 2015;**10**:7241–52.
[81] Li XZ, Nikaido H, Williams KE. Silver-resistant mutants of *Escherichia coli* display active efflux of Ag+ and are deficient in porins. *J Bacteriol* 1997;**179**:6127–32.
[82] Graves JLJ, et al. evolution of silver nanoparticle resistance in *Escherichia coli*. *Front Genet* 2015;**6**:42.
[83] Panáček A, et al. Bacterial resistance to silver nanoparticles and how to overcome it. *Nat Nanotechnol* 2018;**13**:65–71.
[84] Stabryla LM, et al. Role of bacterial motility in differential resistance mechanisms of silver nanoparticles and silver ions. *Nat Nanotechnol* 2021;**16**:996–1003.
[85] Sally D, et al. Phosphatidylinositol-(3,4,5)-Trisphosphate induces phagocytosis of nonmotile *Pseudomonas aeruginosa*. *Infect Immun* 2018;**86**:e00215–8.
[86] Geetha M, Singh AK, Asokamani R, Gogia AK. Ti based biomaterials, the ultimate choice for orthopaedic implants—a review. *Prog Mater Sci* 2009;**54**:397–425.
[87] Tao B, et al. BMP2-loaded titania nanotubes coating with pH-responsive multilayers for bacterial infections inhibition and osteogenic activity improvement. *Colloids Surf B Biointerfaces* 2019;**177**:242–52.
[88] Peng Z, et al. Dual effects and mechanism of TiO2 nanotube arrays in reducing bacterial colonization and enhancing C3H10T1/2 cell adhesion. *Int J Nanomed* 2013;**8**:3093–105.
[89] Punjabi K, et al. Efficiency of biosynthesized silver and zinc nanoparticles against multi-drug resistant pathogens. *Front Microbiol* 2018;**9**:2207.
[90] Applerot G, et al. ZnO nanoparticle-coated surfaces inhibit bacterial biofilm formation and increase antibiotic susceptibility. *RSC Adv* 2012;**2**:2314–21.
[91] Elizabeth E, Baranwal G, Krishnan AG, Menon D, Nair M. ZnO nanoparticle incorporated nanostructured metallic titanium for increased mesenchymal stem cell response and antibacterial activity. *Nanotechnol* 2014;**25**.
[92] Abdulkareem EH, et al. Anti-biofilm activity of zinc oxide and hydroxyapatite nanoparticles as dental implant coating materials. *J Dent* 2015;**43**:1462–9.
[93] Hoyo J, Ivanova K, Guaus E, Tzanov T. Multifunctional ZnO NPs-chitosan-gallic acid hybrid nanocoating to overcome contact lenses associated conditions and discomfort. *J Colloid Interface Sci* 2019;**543**:114–21.
[94] Eshed M, Lellouche J, Gedanken A, Banin E. A Zn-doped CuO nanocomposite shows enhanced antibiofilm and antibacterial activities against Streptococcus mutans compared to nanosized CuO. *Adv Funct Mater* 2014;**24**:1382–90.
[95] Tuby R, et al. Fabrication of a stable and efficient antibacterial nanocoating of Zn-CuO on contact lenses. *ChemNanoMat* 2016;**2**:547–51.
[96] Shalom Y, Perelshtein I, Perkas N, Gedanken A, Banin E. Catheters coated with Zn-doped CuO nanoparticles delay the onset of catheter-associated urinary tract infections. *Nano Res* 2017;**10**:520–33.
[97] Fisher LE, et al. Bactericidal activity of biomimetic diamond nanocone surfaces. *Biointerphases* 2016;**11**:11014.
[98] May RM, et al. Micro-patterned surfaces reduce bacterial colonization and biofilm formation in vitro: potential for enhancing endotracheal tube designs. *Clin Transl Med* 2014;**3**:e8.
[99] Diu T, et al. Cicada-inspired cell-instructive nanopatterned arrays. *Sci Rep* 2014;**4**:7122.
[100] Hasan J, Raj S, Yadav L, Chatterjee K. Engineering a nanostructured "super surface" with superhydrophobic and superkilling properties. *RSC Adv* 2015;**5**:44953–9.
[101] Wang H, et al. High antibacterial efficiency of pDMAEMA modified silicon nanowire arrays. *Colloids Surf B Biointerfaces* 2011;**83**:355–9.
[102] Fellahi O, et al. The antimicrobial effect of silicon nanowires decorated with silver and copper nanoparticles. *Nanotechnology* 2013;**24**:495101.
[103] Wei T, Yu Q, Zhan W, Chen H. A smart antibacterial surface for the on-demand killing and releasing of bacteria. *Adv. Healthc. Mater.* 2016;**5**:449–56.
[104] Wei T, Yu Q, Chen H. Responsive and synergistic antibacterial coatings: fighting against bacteria in a smart and effective way. *Adv. Healthc. Mater.* 2019;**8**:1801381.
[105] Wang T, et al. Metal ion coordination polymer-capped pH-triggered drug release system on titania nanotubes for enhancing self-antibacterial capability of Ti implants. *ACS Biomater Sci Eng* 2017;**3**:816–25.
[106] Sutrisno L, et al. Construction of three-dimensional net-like polyelectrolyte multilayered nanostructures onto titanium substrates for combined antibacterial and antioxidant applications. *J Mater Chem B* 2018;**6**:5290–302.

[107] Francesko A, et al. Bacteria-responsive multilayer coatings comprising polycationic nanospheres for bacteria biofilm prevention on urinary catheters. *Acta Biomater* 2016;**33**:203–12.
[108] Chauhan A, Ghigo J-M, Beloin C. Study of in vivo catheter biofilm infections using pediatric central venous catheter implanted in rat. *Nat Protoc* 2016;**11**:525–41.
[109] Lebeaux D, Chauhan A, Rendueles O, Beloin C. From in vitro to in vivo models of bacterial biofilm-related infections. *Pathog* 2013;**2**:288–356.

CHAPTER

27

Nano-biomaterials for therapeutic and diagnostic applications

Thillaichidambaram Muneeswaran[1], *Muthuchamy Maruthupandy*[1], *Thirumalaisamy Vennila*[2], *Sathyavathi Sundararaju*[3] and *Franck Quero*[1,4]

[1]Laboratorio de Nanocelulosa y Biomateriales, Departamento de Ingeniería Química, Biotecnología y Materiales, Facultad de Ciencias Físicas y Matemáticas, Universidad de Chile, Santiago, Chile; [2]Department of Chemistry, Sri Sairam Engineering College, Chennai, Tamil Nadu, India; [3]Department of Pathology, Division of Pathology Sciences, Sidra Medicine, Doha, Qatar; [4]Millennium Nucleus on Smart Soft Mechanical Metamaterials, Santiago, Chile

1. Introduction

Nanotechnology is an extensively developing field of interdisciplinary science that deals with materials in the size range of 1−100 nm[1] called nanomaterials (NMs). It includes nanoparticles (NP), quantum dots (QDs), carbon nanotubes (CNTs), graphene, and their composites. [2−4] Synthesis of NMs with different morphology, structure, size, and their application for the welfare of humanity as a whole is the prime objective of the nanoscience and technology. In the past decade, researchers have paid more attention to nanoparticles owing to their unique attributes such as size, shape, and large surface to volume ratio among others.[5,6] With these unique features, nanomaterials have shown better properties including chemical stability, thermal conductivity, catalytic reactivity, nonlinear optical performance compared to their bulk materials.[7,8]

Besides, NMs could be synthesized with adjustable characteristic properties according to applications and needs.[9] NMs were found to be relevant for a variety of applications in various fields of science and technology but not limited to optical, biomedical, chemical, and energy sciences.[3,6,10−14] Among the various applications of NMs, their utilization in the biomedical field is well established and much attention has been paid in all aspects of their biological applications.[15] NMs can be classified as carbon-based, metallic, metal oxides,

Applications of Multifunctional Nanomaterials
https://doi.org/10.1016/B978-0-12-820557-0.00029-1

ceramics, semiconductors, polymeric, and lipid-based NMs.[16,17]Among this classification, metal and metal oxide nanoparticles (MO NPs) have been shown to have potential applications in engineering, agriculture, sensors, and medicine.[18,19]

In particular, metal and metal oxide NPs play a vital role in biomedical applications including antimicrobial therapy, cancer therapy, and diagnostics of several diseases, as well as biochemical sensors, bio-assay, tumor-imaging, drug delivery, and pharmaceutical treatment procedures.[20,21] Hence, various novel metal NMs such as gold, silver, zinc, copper, iron, and their oxide NPs with different shapes and sizes have been synthesized for potential application in therapeutic and diagnosis.[2,6,20,22] Here, we discuss the biological syntheses of some metal and metal oxide nanoparticles as well as polymeric and liposomal NMs and their essential insights and limitations in diagnostic and therapeutic potential for antimicrobial, targeted drug delivery, and immune therapy.

2. Biologically synthesized metal and metal oxide nanoparticles

MO NPs are synthesized by combining oxides of metals from groups 3−12 of the periodic table.[23,24] Generally, MO NPsare prepared via physical methods such as spray pyrolysis,[25,26] ultra-sonication[27] or chemical vaporization.[28,29] Similarly, chemical methods such as sol-gel,[30] hydrothermal,[31] microwave assisted,[32] solvothermal,[33] oxidation-reduction, and chemical precipitation[17,34,35] can also be used to synthesis MO NPs.[36] NPs synthesized via chemical methods are relatively toxic and were found to have, consequently, limited biomedical applications.[19,37] Besides, the solvents and other chemicals used for synthesis are hazardous to the environment that profoundly affects the ecosystem.[19,38] In addition, the yield of chemical and physical methods is low, inhibits particle growth at some point, and generates unstable NPs.[39,40] Interestingly, green syntheses of metal and MO NPs has been recommended as alternative routes to chemical syntheses and put into practice.[39]

Green synthesis refers to the eco-friendly synthesis of MO NPs using plants, microorganisms, and or by their constituents such as lipids, enzymes, carbohydrates, and proteins.[39,41] In some cases, nontoxic, renewable materials, and biodegradable waste products have also been used to synthesis MO NPs.[42] The selection of the primary materials for green synthesis is crucial for adequate stabilization, where natural compounds are desired to act as capping agents to passivate the surface of MO NPs.[6,37,41] Biologically assisted synthesis routes were found to improve the biocompatibility of the synthesized MO NPs.[3,43] Moreover, natural compounds including proteins can serve as reducing, stabilizing, and capping agents thus enhancing the physical and chemical properties and biocompatibility of MO NPs enables for biomedical applications.[44,45] MO NPs are synthesized in two steps referred to as nucleation and growth. For the synthesis of NPs, their respective salts (e.g., Ag NPs—$AgNO_3$, Au NPs—$HAuCl_4$) are added individually to the plant extract or biomass of microbes such as bacteria, fungi, algae, plants (Fig. 27.1).[37,41,46–48]

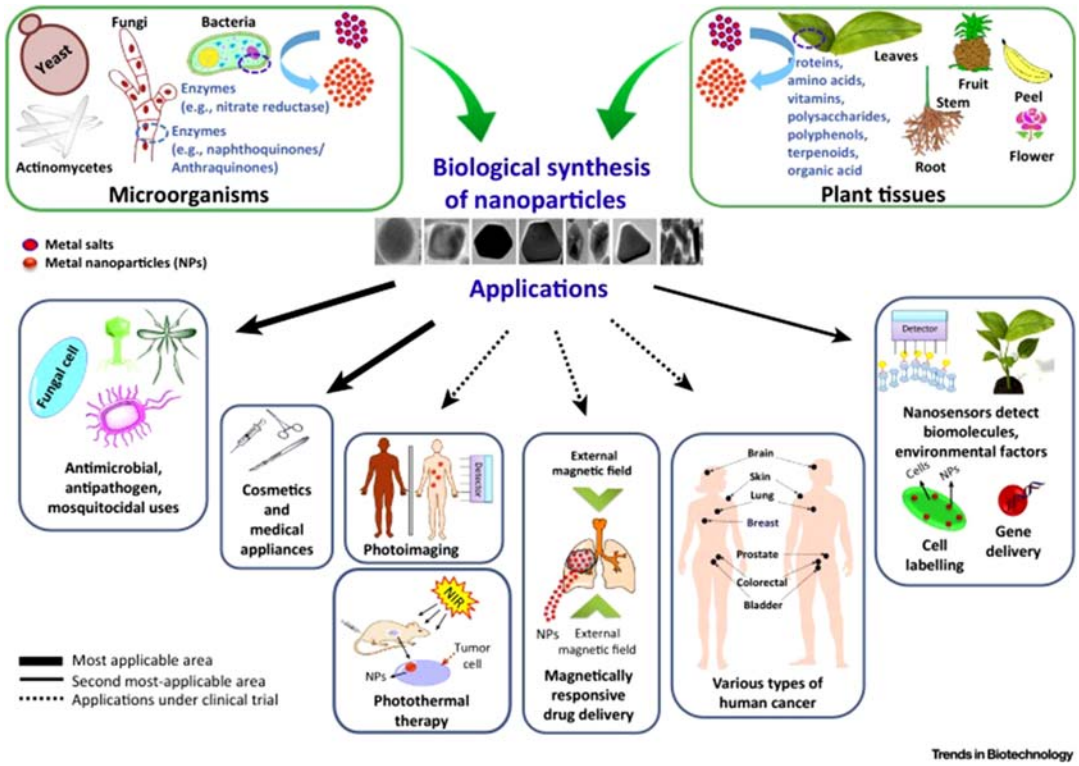

FIGURE 27.1 Metal nanoparticle (NP) biological syntheses and their applications in biomedical and environmental fields. Ag NPs have a wide spectrum of antimicrobial activities and are mostly used as biomedicine, whereas Zn and Ti NPs as cosmetics. Similarly, Ag, Zn, and other metal NPs possess antimicrobial property and are utilized in food packaging, wound dressings, catheters for drug delivery, and other products. In parallel, biological NPs are used as biosensors to detect various biomolecules in environment and agriculture fields. NPs are also used in targeted drug delivery, gene transport, and labelling plant and animals cells for diagnosis. Studies on the development of various NPs for photothermal therapy, magnetically active drug delivery, and photoimaging are ongoing.

2.1 Microbial biosynthesis

Microbial synthesis of metal NPs may be intracellular or extracellular. In the case of extracellular synthesis, the selected metal salts are reduced under the enzymatic action of extracellular enzymes produced by the microbes. In the case of intracellular synthesis, the metallic ions are transported inside the cell, engulfed and reduced to NP and finally excreted out or stored inside the cells.[20,48,49] The properties of the resulting NPs depend highly on the microbial species used during their synthesis.

2.1.1 Bacteria and actinomycetes

Due to their fast growth rate, simple handling and genetically modifiable feature for the bio-mineralization of metals through genetic engineering, bacteria are highly preferable over other methods for the synthesis of metal NPs.[49,50] Bacteria can cope with stress conditions by developing intracellular sequestration of metals, efflux pumps, change in metal ion concentration, and extracellular precipitation.[51] In 1980, Beveridge and Murray reported

the first extracellular bacterial synthesis of NPs by *Bacillus subtilis* that deposited gold NPs on their cell wall. Since then, several studies have reported the ability of bacteria to synthesize NPs as briefly discussed by.[49] Srivastava and Constanti[52] showed intracellular synthesis of Pd, Ag, Rh, Ni, Fe, Co, Pt, and Li NPs by *Pseudomonas aeruginosa*, without addition of any external substance for the formation of NPs.Bacterial strains including *Escherichia coli, B. subtilis, Bacillus megaterium, P. aeruginosa, Klebsiella pneumoniae, Bacillus cereus, Alteromonas, and Ochrobactrum* have been widely used and reported for the synthesis of NPs.[49,51,53] Active biofilms of *Shewanella loihica* PV-4 were found to be able to synthesize ultrasmall (from two up to7 nm) palladium and platinum NPs.[54] *Bacillus brevis* was found to synthesis spherical silver NPs within the diameter size range of 41−62 nm.[55] Recently, marine bacteria were also reported for the synthesis of metal NPs such as silver and gold using *Stenotrophomonas*[56] and copper NPs using *Kocuriaflava*.[57]

Actinomycetes are the repository of novel secondary metabolites and extracellular enzymes.[58] Actinomycetes were also evaluated to obtain NPs by extracellular or intracellular synthesis. Successful synthesis of AgNPs was reported by Otari et al.[59] using *Rhodococcus NCIM*, which paved the way for the synthesis of NPs using actinomycetes. Since then, several groups of researchers have been focusing on the use of acinomycetes for NPs synthesis. AgNPs were synthesized by *Streptomyces* sp. LK-3,[60] *Streptacidiphilus durhamensis*,[61] whereas *Streptomyces griseoruber* and *Streptomyces capillispiralis* Ca-1 were used, respectively, for the synthesis of copper and gold NPs.[62,63] Rajivgandhi et al.[64] reported the synthesis of zinc oxide nanosheets using *Nocardiopsis* sp. GRG1.

2.1.2 Fungi and yeast

Recently, fungal- and yeast-mediated synthesis of metal NPs have been reported as promising approaches for synthesizing NPs since they tolerate, accumulate metals, and their mass cultivation is possible at low cost. Similar to bacterial biosynthesis of metal NPs, fungal mediated synthesis can be either intracellular or extracellular.[65] In addition, size and shape of NPs depend on whether biomass or cell free extract is used for the synthesis.[66] Several reports are available for the synthesis of AgNPs using fungal strains such as *Fusarium oxysporum, Schizophyllum radiatum, Penicillium diversum,* and *Trichoderma harzianum*.[67−70] Similarly, yeast strains such as *Yarrowia lipolytica* NCYC789, *Candida utilis* NCIM 3469, *Saccharomyces cerevisiae*, were also used for AgNPs synthesis.[71−73] Next to AgNPs, AuNPs were prominently synthesized using fungal (e.g., *Rhizopusoryzae, Aspergillus niger, Fusarium oxysporum*)[74−76] and yeast strains (*Candida utilis, Yarrowia lipolytica* NCIM3589)[77−79,80] used *Aspergillus flavus* to synthesis TiO_2 NPs. *Aspergillus fumigatus* were used for the extracellular synthesis of ZnO NPs.[81] Detailed information on the synthesis of metal and MONPs and the factors affecting the synthesis using fungal and yeast strains and their applications were described by Boroumand Moghaddam et al.[65,82] Gajendran et al.[83], Chhipa, H.[84] and Parkash et al.[85]

2.2 Protein or enzyme-based biosynthesis

Microbial enzyme-based NPs synthesis has also been investigated. This method delivers NPs with various size and shape, and usage of different enzyme resulted in different NPs and reaction rate. Besides, during microbial-based synthesis, NPs are bound with the microbial biomass, which requires laborious separation and high cost purification steps.[86,87] The positively charged metal ions (e.g., Ag^+) are able to adsorb onto the negatively charged

surface of the protein through electrostatic interaction. Electron transfer between the metal ion and the protein proceeds and induces the formation of metal NPs.[87,88] In the same way, peptides were also used as reducing and capping agent for the synthesis of metal NPs[87,89,90] and in some cases peptides served as template for the crystal growth of metal NPs.[91]

2.3 Algal-based biosynthesis

According to Fawcett et al.,[92] algae could hyperaccumulate heavy metals and modify them into simple forms and represent a potential source of bioactive compounds such as antioxidants and pigments including carotenoids, chlorophylls, and phycobilins. The presence of carbohydrates, proteins, minerals, oil, fats, and polyunsaturated fatty acids[93] makes them a vital source for the synthesis of NPs. These active compounds both act as reducing and stabilizing agents. The synthesis of NPs may be done by using actively growing cells or dead cells as well as residual biomass or cell free extracts.[94,95] *Chlorella vulgaris* has shown good ability to synthesis Ag and AuNPs using growing and dead cells, respectively.[96,97] Several mechanisms of synthesis have been proposed but the exact mechanism is still elusive. Dahoumane et al.[80] proposed NADH-mediated synthesis of NPs, where electrons from NADH can reduce metal ions. The presence of monosaccharides and polysaccharides, that are present in algae, possess functional groups such as aldehyde, ketone, and hydroxyl groups that act as reducing agents.[98,99] Pigments, such as chlorophyll, fucoxanthin, and riboflavin, act as reactive molecules and trap light; electrons from H_2O that are produced during photosynthesis act as electron donor that can reduce metals.[100,101]

Polysaccharides were extracted from the marine algal biomass and used for the synthesis of metal NPs. Several marine algae including *Pterocladia capillacea*, *Jania rubens*, *Ulva faciata*, and *Colpomenia sinuosa* were used for the synthesis of NPs.[102] Extracts of *Sargassum ilicifolium* were used for the synthesis of AgNPs.[103] The synthesis of NPs based on algae was reviewed briefly by Khanna et al.[102] and Bao and Lan.[94] Arsiya et al.,[104] used crude extract of *Chlorella vulgaris* and Sayadi et al.[105] used *Spirulina platensis* to synthesis Pd NPs. MO NPs such as iron oxide, copper oxide and zinc oxide have been extensively synthesized by using macroalgae. Zinc oxide (ZnO) nanoflowers and cadmium sulfide NPs were prepared from cell free extracts of *Chlamydomonas reinhardtii* by Rao and Gautam[106] and Rao, and Pennathur[107] ZnO NPs were synthesized using *S. muticum*.[30,108] Momeni and Nabipour[109] used *S. bovinum* for the synthesis of octahedral palladium NPs having diameter size between 5 and 10 nm.

2.4 Plant-based biosynthesis

As reported by Mittal et al.,[110] plant-based syntheses of NPs are typically carried out at room temperature and can be accomplished within minutes or can last for a few hours. The compounds present in the extract first reduce the metal salt, which leads to the synthesis of NPs. In addition, these compounds adsorbed onto the surface of the NPs and ensured their stability.[111–114] By following color changes of the reaction media, the successful formation of the respective NPs could be confirmed. Theoretical simulations (e.g., density functional theory (DFT) and molecular dynamics (MD) simulations) have predicted the special binding of a particular phytochemical on metal oxide facets and as a result, the morphology of MONPs

was predicted.[4] Due to the numerous phytochemicals present in plant-extracts, it is difficult to find the exact mechanism of formation using phytochemicals.[115,116]

Several preparation methods can be adopted for the synthesis of single, multimetal NPs and MONPs. Leaf extracts of *Polyalthia longifolia, Catharanthus roseus, Azadirachta indica, Aloe vera,* and *Nerium oleander* were used for the synthesis of AgNPs.[112,117–120] Huang et al.[121] reported the synthesis of Ag and AuNPs using leaf extracts of *Cinnamomum camphora*. Elia et al.[122] used extracts of *Salvia officinalis, Lippia citriodora, Pelargonium graveolens,* and *Punica granatum* for the synthesis of AuNPs. Similarly, leaf extracts of *Evolvulus alsinoides*, bark extracts of *Eucommia ulmoides* and root extracts of *Salvadora persica* were used for synthesizing PdNPs as reported by Gurunathan et al.[77], Duan et al.[123] and Khan et al.[124], respectively. Recently, detailed plant mediated synthesis of nanomaterials was published elsewhere.[115,125,126] CuO NPs were synthesized by using gum obtained from *Sterculia* tree.[127] Ellagic acid extracted from Korean rambutan peel was used for the synthesis of chain-like ZnO.[14] Flower extracts of *Cassia auriculate*[128] and *Vitex negundo*[129] were used for the synthesis of ZnO NPs. Several NMs such as iron, iron oxide, copper, copper oxide, gold, silver, zinc, and zinc oxide were synthesized widely for numerous applications discussed briefly elsewhere.[12,16,130–135] Sometimes, the synthesized NPs are impure, and purification is necessary by either filtration or dialysis. In a study, metal NPs were converted to MONPs after purification by decomposing the NPs (prepared from the sources as described in Sections 2.1–2.4) at relatively high temperature.[136]

Biosynthesis of NPs depends on the solvent used for extraction, reaction temperature, pressure, mixing ratio of the reactants, and pH of the reaction medium. The presence of several chemical moieties in the molecular structure of phytochemicals such as ketones, aldehydes, flavones, amides, terpenoids, carboxylic acids, phenols, and ascorbic acids makes plants excellent choices to synthesis NPs.[137] With respect to microbial synthesis, the selected microbes have to be maintained in the culture media, which is costly and more laborious compared to plant-based synthesis. Also, it is possible to synthesis NPs of small sizes (between 1 and 100 nm)[138] by using plants and sometimes NPs having larger sizes (100–500 nm) were also obtained.[120,139,140] In addition, chemical substances derived from plants are easily available, which promotes rapid synthesis. Finally, the use of plant extracts results in more stable NPs and is suitable for environmentally friendly large-scale synthesis.[141]

3. Polymeric and liposomal nanocarriers

Most of the drugs showing in vitro potency are poorly soluble or insoluble in water, which restricts their usage in clinical applications.[142] These drugs can be conjugated onto surfaces or encapsulated inside the carrier's system to improve their solubility, bioavailability, and biodistribution.[143] The development of nanotechnology offers a wide range of applications in medicine not limited to several diseases including cancer. In this context, NPs have been used as carriers for therapeutic substances such as small drugs, genes, protein-peptides, and imaging contrast agent in diagnosis.[144] Controlled release of these substances is achieved by adequate formulation of the matrix or external stimuli such as pH and/or temperature.[145]

Nano-carriers ensure high bioavailability of the drug by evading reticulo endothelial system. Their small size guarantees high therapeutic efficacy by means of site targeted

delivery.[124,146,147] Properties including circulating durability and stability, targeting capacity, response to stimuli, and diagnostic ability can be improved by surface modification or conjugation with antibodies.[148] For instance, the bioavailability and site specificity of NPs improved while NPs maintained their ability to deliver specific antibody aptamer with improved cancer activity.[147] Nanocarriers are broadly classified as polymer-based or lipid-based systems according to the material used for their preparation. Generally, polymeric nanoparticles, polymeric micelles, dendrimers (polymers), liposomes, solid lipid nanoparticles (lipids), and metal (gold, silver) NPs have shown ability for use as nanocarriers.[147]

3.1 Polymeric nanocarriers

Polymer-based NPs can be made of biodegradable polymers and have been widely evaluated as carriers of drugs, proteins, and DNA to target cells and tissues. These are highly preferable owing to their structural and long-term storage stability, long half-life in blood stream, and high controllable release capability.[149] The use of polymeric nanoparticles (PNPs) as drug carriers has been studied since 1980s. Since then, several PNPs have been developed and mostly used for delivering low molecular weight drugs, proteins, plasmid, and antisense DNA as well as short interfering RNA.[150,151] The preparation of PNPs and their application has been reviewed in detail by Sawdon et al.[152], Kreuter[153] and Amoabediny et al.[154]

PNPs can be prepared using biodegradable, amphiphilic, biocompatible copolymers approved by the Food and Drug Administration. The polymers may be natural (e.g., chitosan, gelatin, sodium alginate and albumin[155] or synthetic (e.g., polylactides (PLA), polyglycolides poly(vinyl alcohol), poly(acrylic acid), polyacrylamide, and polyethylene glycol (PEG)).[155–157] For improving their stability and ability to control the release of drugs, PNPs can be mixed with ligands and antigens.[157] For instance, PEG can be conjugated with polymers for enhancing its immune-compatibility, bioavailability.[158] PNPs can be synthesized using the preformed polymer or synthesized directly during the process of polymerization. Direct polymerization is achieved by microemulsion, mini-emulsion, surfactant free emulsion, and interfacial polymerization. PNPs can be prepared with preformed polymer and dispersed with drugs to avoid toxic, unreactive residues, and unreacted monomers during the polymerization.[159] Solvent evaporation, nanoprecipitation, emulsification/solvent diffusion (ESD), high-pressure homogenization, salting out, dialysis, and spray drying are some of the methods used for the synthesis of PNPs from preformed polymers. Detailed preparation of PNPs and their functionalities can be found elsewhere.[147,156,160,161]

3.2 Liposomal nanocarriers

Liposomes are biocompatible vesicles, hydrophobic and hydrophilic in nature, usually spherical ($\geq$30 nm to micrometers) in shape and typically prepared from cholesterol and natural phospholipids used carriers of drugs.[162] Lipid-based colloidal carriers are nontoxic and used as an alternative to toxic polymeric systems. They are made of one or more lipid bilayers, in which the polar groups are arranged inside or outside of the adjacent aqueous phase. They can be used to encapsulate both hydrophilic and hydrophobic drugs.[163] Lipid composition, surface charge size, and the method of preparation determine the characteristic

features of liposomes. Moreover, the rigidity and charge of the bilayer depends on the components forming the bilayer. For example, unsaturated phosphatidylcholine from egg or soybean phosphatidylcholine (natural origin) is highly permeable and less stable compared with saturated phospholipids with long acyl chains that are rigid and impermeable in nature.[162,164]

Liposomes are smaller (0.025 μm) to larger (2.5 μm) with one or more bilayers. The size affects the circulation half-life of liposome and the amount of drugs encapsulated inside the liposome affected by the size and number of layers. Liposomes are categorized based on their size and number of bilayers as unilamellar (one bilayer) and multilamellar vesicles (more than one bilayer).[165,166] The preparation of liposomes is typically done in following stages: (1) drying down lipids from organic solvent, (2) dispersing the lipid in aqueous media, (3) purifying the resultant liposome, and (4) analyzing the final product.[165,167] Recently,[165] have extensively reviewed the preparation methods of liposomes. Composite liposomes and their drug delivery were published elsewhere[168] for more detailed information about liposomes and their types. Drugs can be loaded into liposomes either passively or actively. In passive loading, the drug is encapsulated along with liposome formation, whereas in active loading, drugs are loaded after liposome formation. The loading efficiency of hydrophobic drugs depends on the solubility of the drug in the liposome membrane. Water-soluble drugs can be effectively loaded by changing pH.[168,169]

More recently, niosomes made of nonionic or amphiphilic surfactants were developed. These are more stable than liposomes and have shown to possess increased transdermal drug delivery ability and were successful used as targeted drug delivery system. Niosomes can be made with or without cholesterol or other lipids.[170] Both liposomes and niosomes provide similar benefits. Niosomes, however, are cheaper and highly stable compared to liposomes.[170] By combining niosome and liposome, biocompatible liponiosome (<150 nm) was developed having the advantages of both carriers. These were found to possess the ability to deliver high amount of both hydrophilic and/or hydrophobic drugs.[171]

4. Metal and metal oxide nanoparticles for antimicrobial therapy

Antibiotics are widely used to combat microbial infections and are considered as one of the major inventions in pharmaceuticals. Recently, however, multidrug resistance (MDR) among the pathogens is considered as common phenomenon and most pathogens have been developing resistance against almost all the available antibiotics. The prevalence of drug resistance threatens the life of humans and become one of the major health or economic issues of the globe in the 21st century.[172] The unique nature of nanomaterials could be potentially utilized to limit and manage the global crisis of emerging microbial pathogens and could contribute to the development of efficient therapeutic solutions. Hence, researches have been focusing on nanomaterials to treat these MDR pathogens and more particularly metal or MO NPs. Researchers involved in the evaluation of nanoparticle as antibiotic have reported that the engineered NPs could efficiently combat MDR strains.[173,174] These NPs are highly stable, durable, and some of them possess low toxicity to mammalian cell lines.[175] By targeting multiple biological molecules including protein and DNA, metal, and MO NPs can act as antimicrobial

agent against MDR pathogens. According to Baptista et al.,[176] and Naveed et al.,[177] MDR pathogens inactivate antibiotics by enzyme, decrease cell permeability, modify target sites/enzymes, and increase efflux via overexpression of efflux pumps for the development of resistance. NPs have the ability to overcome these mechanisms and eliminate the bacterial infections and also inhibit the evolution of resistance.[178] Furthermore, they can improve the activity of several antibiotics by having synergism. For instance, the functionalization of fluoroquinolone with Au NPs was found to improve their efficiency against MDR *Escherichia coli* infections.[174]

Several mechanisms of action have been proposed including biofilm inhibition, activation of host immune system, ROS generation, lipid peroxidation, cell wall/cell membrane damage, inhibition of enzymes, RNA, protein synthesis and proteolysis.[179–181] Also, antitubercular drugs encapsulated by PLG NPs have completely cleared infectious bacteria from the organs of mice. Moreover, the expressions of spaP, gbpB, gtfB, gtfC, ldh, comD, comE, and luxS of *S. mutans* were remarkably downregulated when treated with Ag/ZnO.[182] Similarly, chitosan and chitosan/ZnO nanocomposites have altered the gene expression of quorum-sensing-dependent-virulence factors by repressing LasI and RhlI gene of multidrug resistant *P. aeruginosa*.[183] The chemical moieties present onto bacterial cell wall such as carboxyl, amide, phosphate, and hydroxyl groups act as anchoring sites where the oxide NPs interact, generating ROS and, as a result, induce bacterial death.[180,184] The antibacterial activity is highly depending on the size of the NPs where the activity increases upon decreasing NPs size due to the increasing specific surface area. The importance of shape in the antimicrobial activity, however, cannot be predicted, although limited reports are available. In addition, the mechanism of action is dependent of surface chemistry of NPs.[185] The combined effect of size, shape, ζ-potential, ligands, and material on the mechanism of action of NPs against bacteria is still elusive.[180,186] Singh et al.[37] have reviewed in detail the antimicrobial activity of biologically synthesized metal NPs (Fig. 27.2).

The biological synthesis of these important NPs derived from different natural and renewable resources is discussed in the previous Sections 2.1–2.4. Silver, gold, zinc, copper, silver oxide (Ag_2O), copper oxide (CuO), iron oxide (Fe_2O_3), magnesium oxide (MgO), titanium oxide (Ti_2O), and ZnO are some of the extensively studied metal and MO NPs for their antimicrobial activity.[37,185] Among these metals and MO NPs, silver or its ionic forms have shown the greatest effect on bacteria killing[187] with multiple modes of actions; hence, it was extensively studied and used to treat MDR pathogens.[188] Silver NPs have been used as nanocarriers as well as for the administration of drugs and antibiotics along with silver, showing enhanced effect against MDR pathogens.[189,190] AgNPs possess antibacterial activity against pathogens such as Methicillin resistant *Staphylococcus aureus (MRSA),* Erythromycin resistant *Streptococcus pyogens,* Ampicillin resistant *Escherichia coli,* Vancomycin resistant *Staphylococcus aureus*.[191]

Ag NPs are highly reactive and show high affinity with sulfur group of proteins, enzymes that collapse bacterial cell structure, increase cell permeability and inactivate enzymes. It also binds with DNA and denatures DNA, thereby interrupting replication that leads to cell death.[192–194] Ag NPs have been used as antibacterial, antiviral, and antimycotic agents[195] and coated onto the blades, needles and also on venal, urinary, and drainage catheters.[54]Ag NPs synthesized using fungal strains such as *Fusarium oxysporum, Macrophomina phaseolina* and bacterial strains such as *Xanthomonas* spp, *Sinomonas mesophila* MPKL 26 showed activity

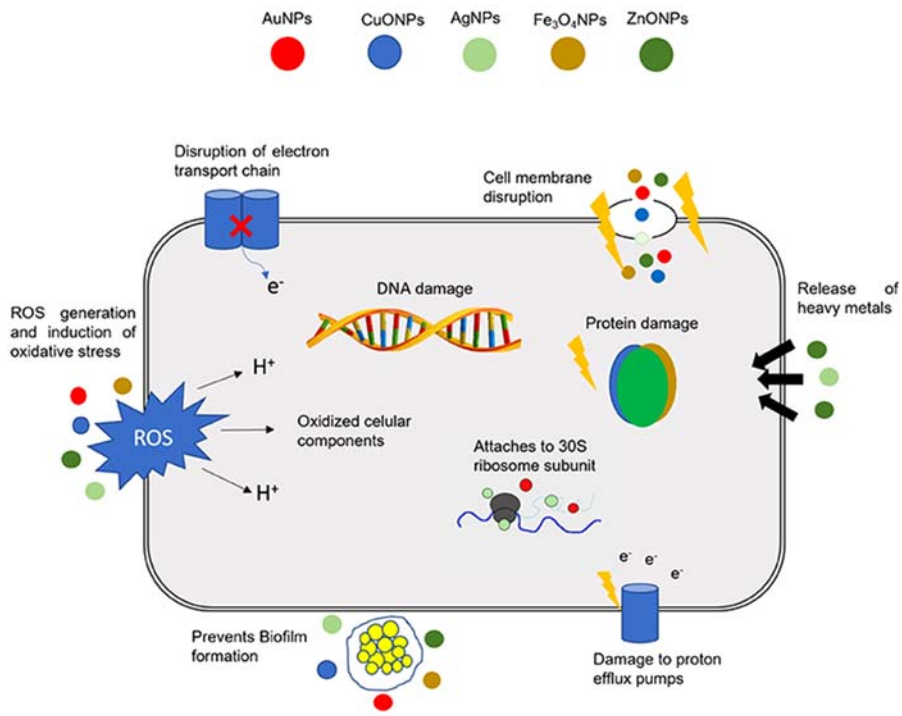

FIGURE 27.2 Plausible mechanism of actions of nanoparticles (NPs) in bacterial cells. The synchronized action of various mechanisms of nanoparticles that exert antibacterial activity may have a significant influence in combatting MDR bacteria.

against MRSA and beta-lactamase producing strains, ampicillin, and chloramphenicol resistant *E. coli, P. aeruginosa,* and *S. aureus*, respectively.[196–199] Cubic, triangular, spherical, and fiber-like shaped AgNPs synthesized by using leaf extract of *Solanum nigrum* and other plant species showed antibacterial activity against six MDR bacterial strains and antibiofilm activity against *P. aeruginosa* and *S. epidermidis*.[200–202] According to Das et al.[39] and Dash et al.[200]; AgNPs synthesized using leaf extract of *Ocimum gratissimum, Cinnamomum tamala* generated intercellular ROS that effectively kills MDR *E. coli* and *S. aureus* cells. Alavi et al.[203] showed that Ag NPs synthesized using *Protoparmeliopsis muralis* was highly effective against planktonic and biofilms of *S. aureus* ATCC 43,300 (MDR), *E. coli* ATCC 25,922 and *P. aeruginosa* ATCC 27,853 than Cu, TiO_2, ZnO, and Fe_3O_4 MO NPs.

Similar to Ag NPs, Au NPs have also been widely used as antibacterial agent against clinical pathogens due to their high biocompatibility. Au NPs can be used alone or incorporated with biomolecules such as collagen, chitosan, or with antibiotics or antibodies.[37,204] For instance, the incorporation of ampicillin was found to increase the antibacterial effect of AuNPs against ampicillin bacteria.[205] Au NPs enters the cell, destabilize ATP synthase as well as cell membrane potential that results in cell death. Furthermore, the multivalence of ligand functionality of AuNPs efficiently makes them interact with cell surface of the bacteria.[206] AuNPs synthesized using the methanolic leaf extract of *Clitoria ternatea* showed strong activity against MDR gram-positive (*S. aureus, S. epidermidis*) and gram-negative bacteria

(*E. coli*, *P. aeruginosa*) and showed QS-based antibiofilm activity.[207] Nontoxic and biocompatible AuNPs prepared from aqueous peel extract of *Musa paradisiaca* showed antibiofilm activity against antibiotic resistant (MARS) gram-positive *Enterococcus faecalis*.[208] Boda et al.[209] utilized Au nanoclusters against planktonic and biofilm forming MDR pathogenic *Staphylococci*. Au NPs possess synergism when loaded along with antibiotics. For instance, lysozyme-capped Au NCs (Lys-Au NCs) with β-lactam antibiotic ampicillin (Lys-Au NCs-Amp) revert the MRSA resistance and also kills the nonresistant bacterial strains.[210] Gandhi and Khan[211] developed bacitracin-templated Au nanoclusters to combat MDR pathogens. Mohamed[212] synthesized ampicillin-loaded AuNPs that showed potential activity against ampicillin-resistant bacterial strains including *MRSA, P. aeruginosa, Enterobacter aerogenes* by reducing the level of beta-lactamase and inhibiting transmembrane pump that catalyzes drug efflux.

Zinc and zinc oxide NPs (ZnO NPs) have been used as antibacterial and antifungal agents. Several studies demonstrated their good biocompatibility and low toxicity.[37,213] The bacterial surface possesses proteins, and the cell walls are composed of polysaccharides and tiechoic acid, which helps bacteria to thrive in host defense and harsh environmental conditions. These are charged molecules and surface modified ZnO NPs specifically elicit damage on the cell wall of the bacteria.[214] ZnONPs showed antibacterial activity against *E. coli, Listeria monocytogenes, Salmonella,* and *S. aureus*.[213,215] ZnO NPs are highly conductive and hence absorbs more UV light, which causes desorption of oxygen from its surfaces that enhances the interaction of ZnO with bacteria. The level of ROS was found to be higher when ZnO NPs were illuminated with UV light and showed efficient antibacterial activity.[216,217] UV light illuminated ZnO NPs were found to show increased oxidative stress against cells by producing superoxide, hydroxyl, and singlet oxygen radicals. Extracellularly synthesized ZnONPs by using the supernatant of *Escherichia hermannii* showed antibacterial activity against urinary tract infective MDR pathogenic strains of *E. coli* and *K. pneumoniae*. The authors showed that the ZnONPs interacted with the cell wall of the bacteria and destabilized it by ROS production, leading to cell death.[218] Similarly, Maruthupandy et al.[203] synthesized ZnO NPs using *Camellia japonica* leaf extract, which showed inhibitory effect against extended spectrum β lactamases (ESBLs) producing clinical strains of *E. coli* and *P. mirabilis* with minimal inhibitory concentration (MIC) percentages of 83% and 81% at 100 μg/mL, respectively. Likewise, ZnO NPs synthesized using root extract of *Raphanussativus* showed higher antimicrobial activity against *Escherichia fergusonii* (MDR) and *Escherichia coli* strains than chemically synthesized ZnO NPs.[154] Most of the virulence genes are down regulated in the presence of ZnO NPs, which confirms the effective treatment of ZnO NPs.[118]

Likewise, iron oxide (FeO) NPs showed activity against human pathogens such as *S. aureus, S. enterica*, *P. mirabilis, E. coli, P. aeruginosa, Pasteurella multocida, P. aeruginosa* and *S. typhi* and plant pathogen *Ralstoniasolanacearum* synthesized using plants *G. jasminoides, L. inermis, Skimmia laureola,* and *M. oleifera*.[219–221] Fe-based NPs were also used as coating materials for medical devices and textiles against bacterial and fungal infections. Furthermore, they possess similar advantages compared to other metal NPs and in addition they can be recovered from the environment using magnets owing to their magnetic properties.[222,223] In the same way, Muthukumar et al.[224] synthesized FeO NPs using *Azadirachta indica* leaf extract and tested their antibacterial and antibiofilm activity against *P. aeruginosa, S. aureus, K. pneumoniae* L. *sphaericus, and B. safensis*. The study showed that these FeO NPs were

more active against gram-positive than gram-negative bacteria due to the presence of thick peptidoglycan layer onto the surface of gram-positive bacteria. FeO NPs were also found to inhibit more efficiently the biofilm formation of gram-negative bacteria than gram-positive bacteria since the NPs could efficiently diffuse when the hydrophilic bacterial surface turned into hydrophobic surface that attracts the NPs.[225] Very recently, FeONPs synthesized using *R. tuberosa* leaf extract were coated onto cotton fabric and were found to be active against *K. pneumoniae*, *E. coli* and *S. aureus* bacterial strains. They suggested that the synthesized FeO NPs could be used as coating materials onto the readymade fabrics, uniforms, and laboratory coats used in hospitals.[226] The positively charged FeO NPs tend to attach onto the surface of the negatively charged cell wall of the bacteria, resulting in increased attachment of NPs and destabilization of cell wall inducing bacterial death.[227]

Copper-based NPs are semiconductors that have a narrow band gap; Cu and copper oxide (CuO) NPs have been shown to have antimicrobial activity toward wide ranges of bacterial and fungal pathogens via ROS mediated mechanism.[228] Rajivgandhi et al.[229] successfully used CuO NPs synthesized using leaf extract of *Camilla japonica* against ESBL producing urinary tract infecting pathogens such as *P. aeruginosa* and *K. pneumoniae*. CuO NPs act on the bacterial cells and alters the intracellular signaling pathways that controls the oxidative stress, leading to cell lysis.[230] Ashajyothi et al.[231] synthesized Cu and ZnONPs extracellularly using *Enterococcus faecalis* and tested antibiotic activity against clinical pathogens *E. coli, K. Pneumonia, methicillin-resistant S. aureus (MRSA)*and non-clinical strains*P. aeruginosa MTCC 741, S. flexneri MTCC 1457,* and *E. faecalis NCIM 5025*. They found that both NPs were active against both gram-positive and gram-negative pathogens and also inhibited the biofilm formation of all pathogens except *P. aeruginosa.* They concluded that Cu NPs are more effective than ZnO NPs. Studies from several researchers suggested that Cu NPs were highly active against MDR*P. aeruginosa* and *MRSA* pathogenic strains, similarly to the activity of AgNPs.[232,233] According to Meghana et al.[234]; CuO NPs always generate ROS that specifically affects the chromosomal DNA rather than other molecules that highlighted the particle specific activity of CuO.

Titanium dioxide (TiO_2) NPs are chemically stable, nontoxic, and possess wide applications. They are more particularly used in the formulation of cosmetics owing to their UV radiation absorption ability.[235] TiO_2 NPshave shown to have antibacterial activity against most bacteria.[63] Similar to previously discussed metals and MO NPs,TiO_2NPs also generate ROS and kill bacteria by adhering onto the surface of the bacterial cell wall and produce ROS that act on phospholipids present on the cell wall of the bacteria by lipid peroxidation.[236] This destabilizes cell membrane and causes damage to the cellular components, particularly on DNA and is followed by cell death.[237–239] Very few reports are available on the preparation of TiO_2 NPs using biological materials for antimicrobial applications. TiO_2 NPs prepared from *Psidium guajava, Prunus yedoensis* showed bactericidal property against *E. coli and S. aureus*.[240,241] TiO_2 NPs synthesized using *Aloe barbadensis mill* were active against *P. aeruginosa* PAO1.[242] Likewise, Subhapriya et al.[243] synthesized TiO_2 NPs using *T. foenum-graecum* leaf and showed effective activity against *Y. enterocolitica, P. vulgaris, E. faecalis, P. aeruginosa, S. faecalis, S. aureus, B. subtilis, E. coli and fungus C. albicans*. TiO_2 NPs also synthesized using *Streptomyces* sp. HC1 showed antimicrobial activity toward several pathogens such as *E. coli, S. aureus, C. albicans, and A. niger* and antibiofilm activity against *P. aeruginosa*.[244]

Other than these metals, several metals NPs such as aluminum, palladium (Pd), selenium (Se), and cerium were also evaluated as antimicrobial agents. PdNPs[245] and cerium NPs[246] synthesized using peel extract of *M. oleifera* showed antibacterial activity against *E. coli* and *S. aureus*. Pd NPs synthesized using *F. decipiens* leaf extract and *C. guianensis* fruit extract were effective against several human pathogens and the effect was found to be oxidative stress mediated.[247,248] Se NPs synthesized using bacterial sources such as *B. licheniformis* JS2,[249] *S. maltophilia, B. mycoide*,[250] *S. aureus, P. aeruginosa*, and *E. coli*[251] showed potential activity against bacteria and fungus, and on their biofilm formation. Even if antibacterial effects have been proven in preclinical studies, evaluation of therapeutic efficacy in clinical trials and the safety of NP systems is essential.[186] The economic impact of clinical translation of NPs must be addressed with regard to their therapeutic efficacy.[186,252]

5. Targeted drug delivery and disease diagnosis

Recent researchers have been mainly focusing on developing compounds from natural resources to find novel drugs for treating major diseases such as cancer, diabetes, heart diseases, inflammatory, and microbial diseases due to their least toxicity, side effects, cost, and higher efficiency.[253] These active materials often delivered with larger delivery systems, which have several limitations such as low biocompatible, toxic, poorly soluble, unstable, poor bioavailable, targeted delivery issue, and tone effect, and side effects of medicines. To overcome these pitfalls, NPs have been developed as delivery systems and offer time-controlled or targeted-delivery of drugs.[137] NPs increase the bioavailability and stability of the drug as well as the delivery drugs at specific sites and consequently increases the efficiency of delivery systems.[129] Furthermore, NPs are smaller in size and it could deliver various genes, vaccines, proteins, hydrophobic and hydrophilic drugs to the different part of the body including brain, arterial walls, lymphatic system, liver, spleen, lungs.[254,255] The rate of degradation and drug release could be easily adjusted by using polymers.[256] Polymeric and liposomal NPs-based delivery systems are briefly discussed in Section 3.

Liposomes were the first developed and approved nano-carrier based on lipids that can deliver inorganic NPs such as gold and iron NPs, which increases their used for drug delivery, imaging and other treatments.[129,205,257] Also, the addition of NPs could increase the bioavailability and control the release of drugs. For site specific drug delivery applications, metal as well as organic, inorganic, and polymeric nanomaterials were used particularly for delivering poorly soluble and least absorption drugs.[258,259] These systems were designed to deliver the drugs at specific place or for controlled release of the drug at specific sites and to overcome the opsonization/sequestration of phagocytosis.[260] Nanostructures convey drugs either by self-delivery or passive delivery. In self-delivery, the drugs are directly linked with the carrier to facilitate the delivery whereas in passive delivery the drugs are loaded hydrophobically in the inner cavity of the nanostructure. These were found to encounter the specific site and release the planned amount of drug since lower amount of drug was encapsulated in hydrophobic environment.[162] It is possible to deliver drugs using NPs and the loading of drugs into the NPs are classified as active or passive targeting. In active targeting, the drugs are loaded with the delivery system that carry site-specific antibodies or

peptides, which could bind onto the receptors of the particular site. The drugs delivery system circulates in the blood stream and delivers the drug in a particular site due to changes in pH, temperature, molecular site or/and shape.[41,261] Mostly, these drug delivery systems are used for treating cancer.

Drug, gene and protein delivery of Au NPs have been reviewed by researchers.[41,262,263] Similar to liposomes, Au NPs can deliver several recombinant proteins, DNA, vaccines, and antibiotics. AuNPs have been used for treatment of cancer therapy and successfully crossed the blood brain barrier when loaded with human serum albumin. In addition, this was achieved due to the lower surface charge, albumin layer, and the capacity to absorb huge amount of creatine.[264] Antibiotics are typically loaded onto AuNPs via ionic or covalent bond, and the ampicillin functionalized AuNPs were found to be able to revert the drug resistance of the MDR pathogens.[265] Also, functionalization of Au NPs with ampicillin, streptomycin, and kanamycin demonstrated efficient antibacterial activity.[244,266] AuNPs provide uniform size, similar surface properties, and increased biocompatibility when encapsulated in alginic acid-poly[2-(diethylamino)ethyl methacrylate] monodisperse hybrid nanospheres. Human colorectal LoVo cancer cells uptake more these negatively charged nanospheres and hence were used as optical sensor for tumor imaging along with inhibition.[267]

Conjugating AuNPs with 2,5-diphenyltetrazole and methacrylic acid, shifted AuNPs plasmon resonance to near infrared (NIR), which increases the photothermal efficiency of breast cancer treatment.[268] Recently, [58] showed the delivery of small molecules for targeting lymphocytes and Dhanya et al.[269] observed better transfection efficiency when arginine conjugated AuNPs were caped with starch and polyethyleneimine. Munsell et al.[270] developed efficient histone-inspired scaffolds using AuNPs adorned with histone motifs for delivering genes and chromatin analysis. In another study, noncovalently conjugated AuNPs-siRNA covered with a lipid layer efficiently delivered siRNA into cell, followed by specific gene silencing.[271] In MCF-7 cells, lipid-coated AuNPs showed nearly 85% of gene transfection efficiency facilitated by folic acid (FA) based ligands.[272] Iron oxide NPs have been extensively used as cancer therapeutic agent with high degree of specificity. It is possible to control the particle through external magnetic field that improves the release of dexamethasone acetate in vivo.[43] A study by Jain et al.[273] clearly demonstrated the biosafety of these magnetic NPs while testing them intravenously. These were found mostly in the liver and spleen rather than in other organs. Similarly, long-term exposure of magnetic NPs did not exert oxidative stress in the cell or change liver enzyme levels suggesting good biocompatibility. Paclitaxel-loaded chitosan oligosaccharide (PTX-COS) stabilized AuNPs could deliver and release drug by pH dependent manner. The synthesized PTX-COS AuNPs showed strong cytotoxicity against MDA-MB-231 cells by means apoptosis. The increased ROS generation and altered mitochondrial membrane potential (MMP) level caused cell death (Fig. 27.3).[274]

Nanoscaled diagnostics offer new alternatives for portable and sensitive health monitoring that can guide the use of nanoscale immunotherapies. As metal-based nanoparticles (gold, silver and silica) and polymer-based nanoparticles (chitosan, dextran, polyethylene glycol (PEG) and polylactic-co-glycolic acid (PLGA)) possess photo-based imaging ability. These can act as nanocarriers to deliver various fluorescent dyes or photosensitizers for photoimaging and therapeutic applications including magnetic resonance imaging (MRI) and optical imaging to photothermal therapy (PTT) and chemotherapy.[2] In early 90s′, iron oxide

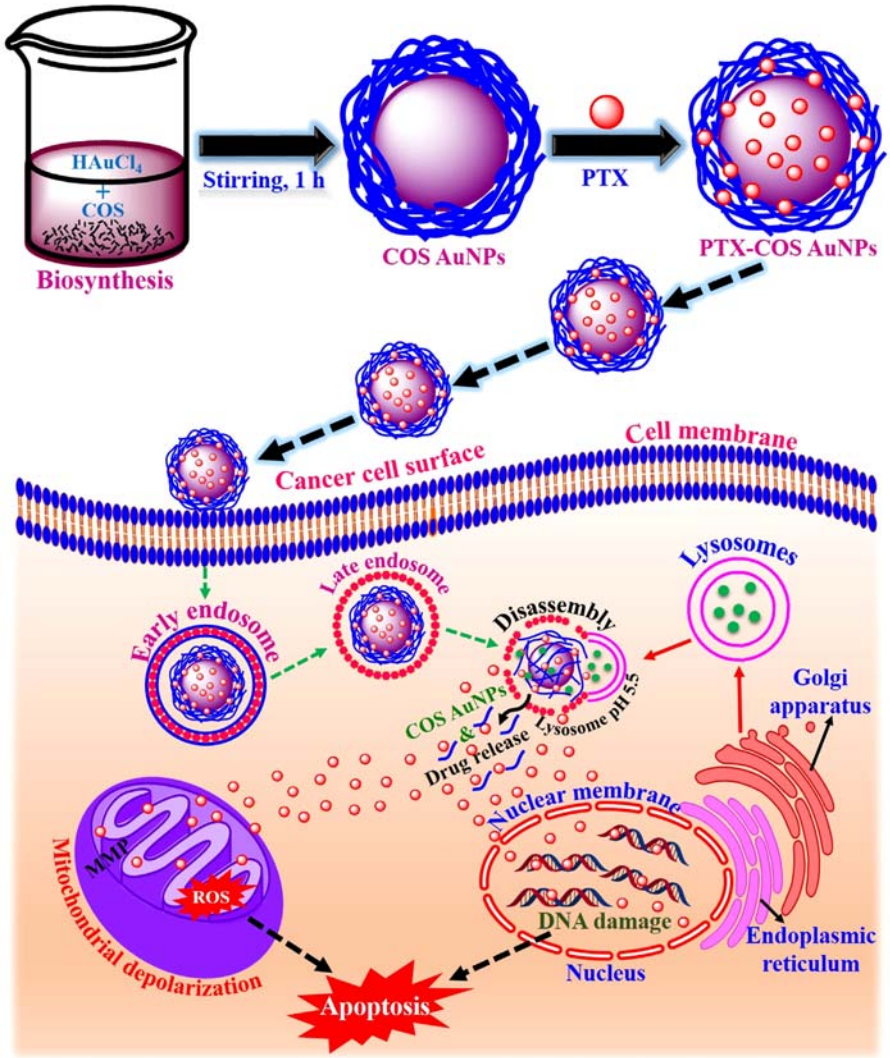

FIGURE 27.3 A general strategy for the biosynthesis of gold nanoparticles (Au NPs) using chitosan oligosaccharide, followed by loading of paclitaxel (PTX) on stabilized Au NPs made of chitosan oligosaccharide (COS Au NPs), and a potential mechanism for cellular uptake and mode of action of paclitaxel-loaded COS Au NPs in MDA-MB-231 cancer cells.

nanoparticles with magnetic properties have been used as vascular contrast agent for MRI.[275] AuNPs have been functionalized for the detection of biological molecules (DNA and proteins), heavy metals, and glucose as well as microbes.[276–278] In 2008, Huang et al. developed optically responsive gold nanorod (GNR)-elastin-like polypeptide (ELP) nanoassemblies that showed phase transition and aggregation of NPs upon NIR irradiation, which could be used for drug sensor and drug delivery.

PEGylated AuNPs showed Raman scattering efficiency increased by 14−15 orders of magnitude, which could be applied for detecting cancer cells in animals.[279] Similarly, PEGylated AuNPs demonstrated ability for imaging tumor and blood cells since they can be easily distributed and stabilized in aqueous solutions.[280] It was shown that size, shape, and structure of Au NPs affect their scattering property. Very recently, biocompatible deferrioxamine conjugated to PEGylated Mn(II) complex gold nanoparticles could be used as dual imaging system in MRI and CT scan and also effective against 4T1 breast tumor-bearing BALB/c mice.[281] Similarly, AuNPs in the size range of 30−100 nm were found to scatter light strongly, which can be detected using dark-field microscopy imaging.[282] Huang and El-Sayed[282] prepared spherical AuNPs (40 nm) conjugated with epidemic growth factor (EFGR). After 4 min of exposure to laser light, head and neck cancers could be detected. Tabrizi et al.[283,284] developed inexpensive and highly selective electrochemical aptasensors based on MWCNTS-PdNano/Ptca and Au@AgNPs for counting leukemic lymphoblast and adenocarcinoma gastric cancer cells. AuNPs modified with PEG and polyethylmethacrylate (PEMA) showed efficient tumor detection when used along with antitumor drug daunorubicin.[285] Recently, a brief review on application of gold NPs in cancer therapy and diagnosis is published elsewhere.[286]

6. Nano-vaccination and immunotherapy

Vaccination is an important achievement of medical science that helps human beings to survive against several epidemics and pandemics. Vaccines induce immune response and provide lifelong protection and it may contain inactivated, killed, or attenuated microbes. The main objectives of effective vaccines design are successful presentation of antigens to antigen presenting cells (APC), the ability of APCs to process antigens[287,288] and present them to T-cells along with MHC and other costimulatory cells.[289] APC internalize and process antigens and hence matures and migrates to lymph nodes and present the antigen to T-Cells. Development of new vaccines for emerging infectious diseases and improvement of existing vaccines against specific diseases is the major concern of pharmaceutical industries.[290] Vaccines failed, however, to protect some patients and also pose health risk due to reversal of virulence.[291] In addition, vaccines should also induce immune response to cancer, HIV, malaria, and tuberculosis. Nanotechnology has been recently involved into vaccine development to overcome the drawbacks of conventional vaccination progress by developing nanocarrier-based delivery systems to increase cellular and humoral immune responses and slow release of targeted delivery. Scientists believed that nanovaccines could overcome pathogen-mediated evasion of the immune response and induce specific cytotoxic T-lymphocyte (CTL; activated CD^{8+} T cell).[292,293] Nanoparticles used as adjuvants can facilitate the uptake of vaccine antigen by APCs and achieve efficient antigen recognition and presentation to target specific receptors onto the cell surface to stimulate selective and specific immune responses.[294]

In the last 2 decades, several particles with different physicochemical characteristics have been evaluated for delivering antigens, such as (co)polymers, liposomes, mesoporous silica, chitosan, and particle size and found to control the immunological fate of their biodistribution, pharmacokinetics, efficacy, and cellular internalization.[295−299] Usually, NP based vaccines target Dendritic Cells (DC) and sometimes targets lymph nodes with APCs

that eliminates premature antigen presentation.[300] Nanovaccines itself elicit themselves immune response however the immune response is not enough to maintain its activity and also tumor- or tissue-infiltrating ability of T cells. Hence, combination of nanovaccines and immune modulators could be used as a therapeutic agent. For example, combination of nano disc vaccine and anti-PD-1, anti-CTLA-4 can destroy cancer cells.[301] Similarly, antigens were combined with several Inorganic NMs such as gold NPs, quantum dots, silica NPs, carbon nanotubes, and iron oxide NPs and subsequently used as vaccines to stimulate immune response against infectious disease.[302–307]

Use of Poly (lactic-co-glycolic acid) (PLGA) as a nanocarrier for imaging, drug targeting and therapy have gained more attention due to their biocompatibility and degradation potential. Cisplatin-loaded poly(L-glutamic acid)-g-methoxy poly(lactic-co-glycolic acid) nanoparticles were developed for treating lung cancer[308] and their recent advancement has been reviewed by Farooq et al.[309] Similarly, spherical PLGA-NPs were used to encapsulate an inactivated Swine influenza virus (SwIV) H1N2 antigens and tested for treating swine flu.[310] Several types of formulations have been recently developed for various diseases, suitable vaccine formulations, toxicity assessment, drug solubility rate, and saturation but storage seems to be a challenge.[164,311] Chitosan and pullulan (natural biopolymer-based nanodelivery systems) have been tested on animals as vaccine and adjuvant delivery systems and the results revealed that vaccination doses of the antigen entrapped in nanoparticles via intranasal induced higher systemic and mucosal antibody responses. Likewise, chitosan NPs loading plasmid DNA encoding nucleocapsid protein of Severe Acute Respiratory Syndrome Coronavirus (SARS-CoV) for nasal immunization in mice has been studied.[312] Therefore, nanocarrier-based delivery systems could provide a suitable route of administration of vaccine molecules and enhance cellular uptake thereby resulting in the induction of innate and adaptive immune responses against infectious diseases.[313] Development of multifunctional nanovaccines significantly increased stability, sustained release of antigens, lowered immunotoxicity, increased target-specificity, facilitated modification of nanoparticle surfaces and ability to codeliver antigens along with adjuvants that may potentially be used more broadly for the prevention and treatment of infectious disease and cancer.[314] For instance, GNPs contains high-mannoside-type oligosaccharides (P1@HM) and HLA-A*0201-restricted HIV-peptides showed increased DC activity that resulted in high level of HIV-specific CD^{4+} and CD^{8+} T-cell proliferation and cytokine secretion. The results of the study would be promising approach for improving HIV vaccines (Fig. 27.4).[315]

In animal models, gold NPs are effective immunotherapeutic against several contagious diseases including HIV, malaria, listeria, and parasitic diseases.[302,316–319] Additionally, the size-dependent effect of AuNP has been tested against its response on viral proteins (NP-displayed foot-and-mouth disease related peptide).[320] In a study, codelivery of AuNPs with ovalbumin (OVA) was found to stimulate Toll-like receptor 9 (TLR9), in which the immunization with AuNps along with treated DCs showed reduced viral removal than mice immunized with DC and control.[307] AuNPs are considered as Class B Select Agent and were found to protect the immunized animals against Burkholderia mallei when conjugated with LPS and protein carrier.[321]

Cancer cells are surrounded by immunosuppressive microenvironment that restricts the immune system to recognize and kill cancer cells. Hence, treating cancer even in the era of

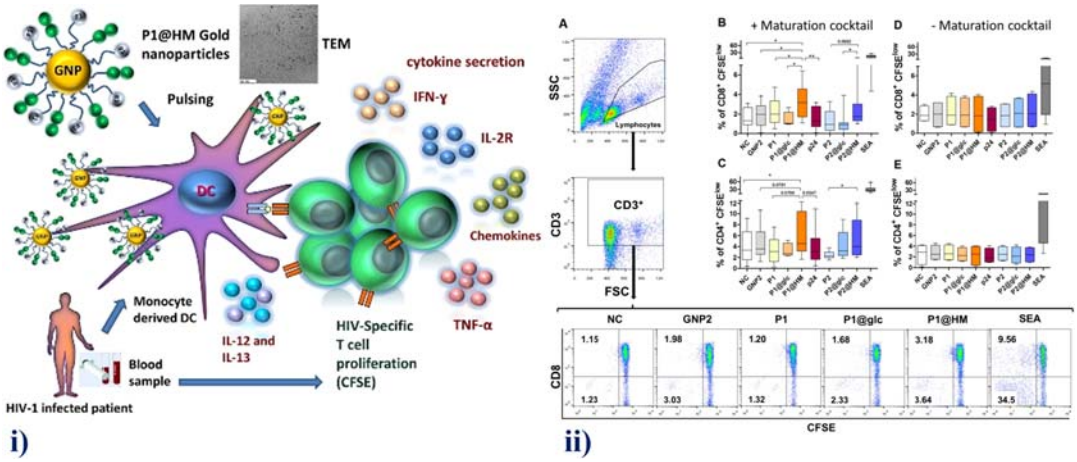

FIGURE 27.4 (i) Representation of the development of GNP formulation conjugated with HLA-restricted HIV peptides and mannosides, and loaded with dendritic cells for the enhancement of HIV-specific T-cell responses. (ii). Response of cell in terms of T-cell proliferation in response to autologous MDDC pulsed with peptide@manno GNPs.

the advanced science is still a challenge. Further, the available methods including chemotherapy radiation have several side effects.[302] Recently, researchers found that the delivery of OVA and cytosine-phosphate-guanine (CpG) motif on polypropylene sulfide NPs delayed tumor growth of thymoma cell line.[322] Iron oxide NPs are superparamagnetic particles, which could be used to target immune signals because it can evade biological barriers and visualized using high-contrast MRI at cellular level.[323,324] Being magnetic and owing to their ability to imaging eliciting immune signal, iron oxide NPs can be used as immunotherapeutic agents against several diseases particularly to cancer. For instance, dimercaptosuccinic acid (DMSA)-coated magnetic NPs were found to possess ability for adsorbing the antitumorigenic cytokine IFN.[323] Similarly, iron oxide–zinc oxide core–shell NPs were used to target DCs for cancer therapy and imaging applications (Fig. 27.5).[325]

7. Conclusions and future perspectives

The biologically synthesized metal and metal oxide NPs possess interesting advantages compared to the chemically synthesized NPs, which include biocompatibility, low cost, and environmental friendliness. As discussed above, metal and metal oxide NPs have potential biomedical applications in treating infections and targeted drug delivery systems. Also, functionalization of these NPs could be used as nanovaccine and improved immunotherapy cancers and diseases. However, knowledge on the bioactive material responsible for the formation of NPs during biosynthesis is still limited since the biological molecules are responsible for both biocompatibility and stability, and more information on this is needed for the biofabrication of desired NPs. Several groups of researchers have been focusing on the largescale production of biosynthesis of smaller sizes with reproducibility and commercialization. Large-scale production biosynthesized NPs are still at its infancy and still need improvement and optimization. Though metal and MO NPs are effective against drug

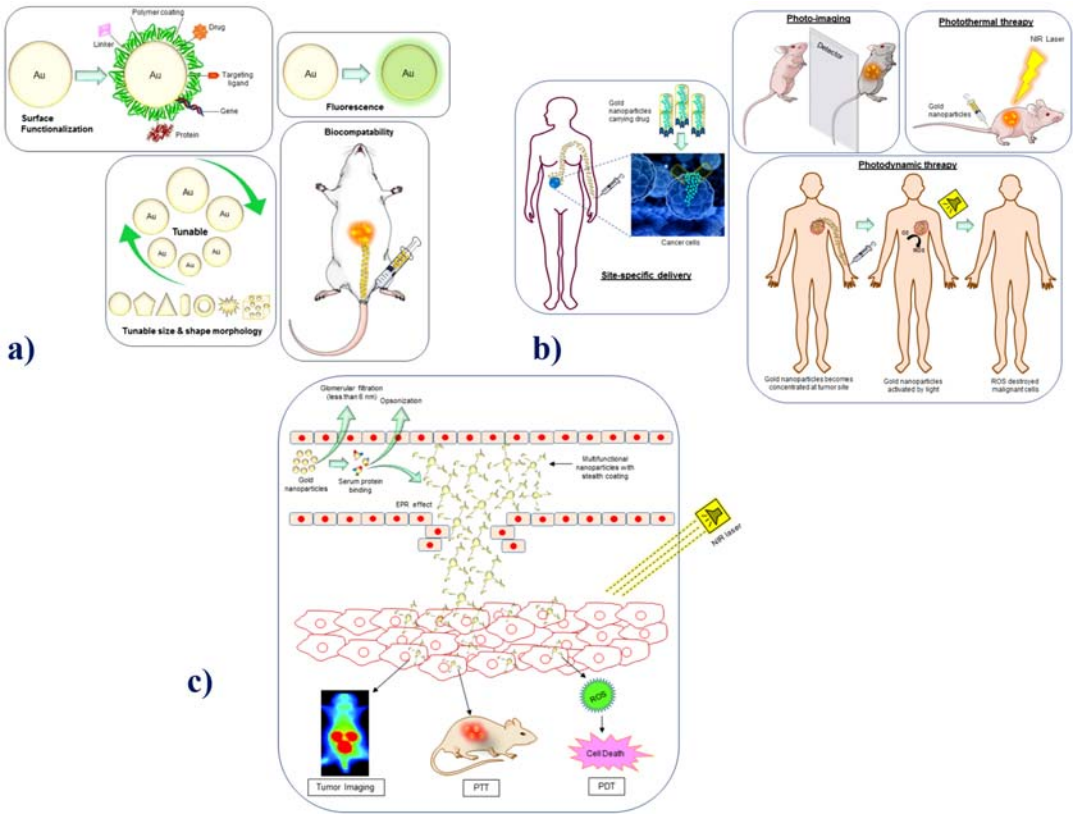

FIGURE 27.5 a) Key features of gold nanoparticles (Au NPs). B) Various methods of detection and treatment of cancer using Au NPs. C) Systemic administration of multifunctional Au NPs for photothermal therapy (PTT), photodynamic therapy (PDT), and cancer bioimaging. NIR = near infra-red, ROS= reactive oxygen species.

resistant pathogens, information on their metabolism, clearance, toxicity, and in-depth knowledge on the pharmacokinetics/pharmacodynamics is very limited. Further, the environmental fate and behavior of the NPs is not yet fully understood.

Functionalization of NPs with ligands can be accomplished by means of surface modifications that enable them to interact with biological molecules and make them as important tool in nanomedicine. These nanomedicines have several advantages not limited to site targeted drug delivery, controlled drug release, stability, improved bioavailability, and biocompatibility compared to conventional medicines. They could be potentially used as vaccines immunotherapeutics and early diagnosis of diseases. Some are already available in the market and in some in clinical trials. However, these are only efficient at preclinical stages. Only very few of them successfully translated to clinics. Other ones are already available in the market, but their clinical translation is a major hurdle. The clinical trial framework for the nanomedicine must be improved to ensure quality and safety of nanomedicine. The encapsulated drugs have higher half lives in the body, but their long-term side effect of the nanomedicine needs

to be deeply studied. Further, detailed toxicological profile of these nanomedicines is essential, and more research should focus on these aspects before clinical trials. Development of nanocarriers is also an important factor for the translation of these medicines to clinics. Collaborative interdisciplinary research all over the world is necessary for clinical use of these NPs as therapeutics and diagnosis.

Acknowledgments

The authors gratefully acknowledge financial support from CONICYT/FONDECYT (Nos. 3190072, 3180128 and 1200675). Acknowledgments are also extended to the "Nuclei for Smart Soft Mechanical Metamaterials" grant funded by the Millennium Science Initiative of the Ministry of Economy, Development, and Tourism.

References

1. ISO C. TS 27687:. *2008—Nanotechnologies—Terminology and definitions for nano-objects—Nanoparticle, nanofibre and nanoplate* 2008.
2. Elkodous MA, El Sayyad GS, Abdelrahman IY, El Bastawisy HS, Mohamed AE, Mosallam FM, Nasser HA, Gobara M, Baraka A, Elsayed MA, et al. Therapeutic and diagnostic potential of nanomaterials for enhanced biomedical applications. *Colloids Surf B: Biointerf* 2019.
3. Singh J, Dutta T, Kim K-H, Rawat M, Samddar P, Kumar P. 'Green'synthesis of metals and their oxide nanoparticles: applications for environmental remediation. *J Nanobiotechnol* 2018;**16**(1):84.
4. Yuliarto B, Septiani NLW, Kaneti YV, Iqbal M, Gumilar G, Kim M, Na J, Wu KC-W, Yamauchi Y. Green synthesis of metal oxide nanostructures using naturally occurring compounds for energy, environmental, and biorelated applications. *New J Chem* 2019;**43**(40):15846.
5. Iravani S. Green synthesis of metal nanoparticles using plants. *Green Chem* 2011;**13**(10):2638.
6. Annu, A. A.; Ahmed, S. J. H. o. E. Green synthesis of metal, metal oxide nanoparticles, and their various applications. 2018, 1.
7. Agarwal H, Kumar SV, Rajeshkumar S. A review on green synthesis of zinc oxide nanoparticles—An ecofriendly approach. *Res Effi Tech* 2017;**3**(4):406.
8. Kalpana V, Devi Rajeswari V. A review on green synthesis, biomedical applications, and toxicity studies of ZnO NPs. *Bioinorganic Chem Appl* 2018;**2018**.
9. Shanker U, Jassal V, Rani M, Kaith BS. *Towards green synthesis of nanoparticles: from bio-assisted sources to benign solvents. A review* 2016;**96**(9):801—35.
10. Luo X, Morrin A, Killard AJ, Smyth MR. Application of nanoparticles in electrochemical sensors and biosensors. *Electroanal: Int J Devoted Funda Prac Aspects Electroanalysis* 2006;**18**(4):319.
11. Sharma D, Kanchi S, Bisetty K. Biogenic synthesis of nanoparticles: a review. *Arabian J Chem* 2019;**12**(8):3576.
12. Wen Z-Q, Li G, Ren D. Detection of trace melamine in raw materials used for protein pharmaceutical manufacturing using surface-enhanced Raman spectroscopy (SERS) with gold nanoparticles. *Appl Spectros* 2011;**65**(5):514.
13. Xia Y, Yang H, Campbell CT. Nanoparticles for Catalysis. *Acc Chem Res* 2013;**46**(8).
14. Yuvakkumar R, Suresh J, Saravanakumar B, Nathanael AJ, Hong SI, Rajendran V. Rambutan peels promoted biomimetic synthesis of bioinspired zinc oxide nanochains for biomedical applications. *Spectrochimica Acta Part A: Mole Biomole Spectros* 2015;**137**:250.
15. Kumar VV, Anthony SP. *Surface chemistry of nanobiomaterials*. Elsevier; 2016.
16. Khan I, Saeed K, Khan I. Nanoparticles: properties, applications and toxicities. *Arabian J Chem* 2019;**12**(7):908.
17. Zikalala N, Matshetshe K, Parani S, Oluwafemi OS. Biosynthesis protocols for colloidal metal oxide nanoparticles. *Nano-Struct Nano Obj* 2018;**16**:288.
18. Chavali MS, Nikolova MP. Metal oxide nanoparticles and their applications in nanotechnology. *SN Appl Sci* 2019;**1**(6):607.
19. Jeevanandam J, Chan YS, Danquah MK. Biosynthesis of metal and metal oxide nanoparticles. *ChemBioEng Rev* 2016;**3**(2):55.
20. Das M, Chatterjee S. *Green synthesis, characterization and applications of nanoparticles*. Elsevier; 2019.

21. McNamara K, Tofail SA. Nanoparticles in biomedical applications. *Adv Phys: X* 2017;**2**(1):54.
22. Sadowski Z, Pawlowska A. *Nanotechnology applied to pharmaceutical technology*. Springer; 2017.
23. Gangwar J, Gupta BK, Srivastava AK. Prospects of emerging engineered oxide nanomaterials and their applications. *Defence Sci J* 2016;**66**(4).
24. Raghunath A, Perumal E. Metal oxide nanoparticles as antimicrobial agents: a promise for the future. *Int J Antimicrob Agents* 2017;**49**(2):137.
25. Nazari P, Gharibzadeh S, Ansari F, Nejand BA, Eskandari M, Kohnehpoushi S, Ahmadi V, Salavati-Niasari M. Facile green deposition of nanostructured porous NiO thin film by spray coating. *Mat Lett* 2017;**190**:40.
26. Nazari RR, Taloobaghi HE, Eshghi H. Crystalline phase evolution in nanostructured copper sulfide thin films prepared by spray pyrolysis method: the effect of annealing. *Mat Sci-Poland* 2017;**35**(3):673.
27. Saikia JP, Paul S, Konwar BK, Samdarshi SK. Ultrasonication: enhances the antioxidant activity of metal oxide nanoparticles. *Colloids Surf B: Biointerf* 2010;**79**(2):521.
28. An W-J, Thimsen E, Biswas P. Aerosol-chemical vapor deposition method for synthesis of nanostructured metal oxide thin films with controlled morphology. *J Phy Chem Lett* 2010;**1**(1):249.
29. Golmohammadi M, Ahmadi SJ, Towfighi J. Catalytic cracking of heavy petroleum residue in supercritical water: study on the effect of different metal oxide nanoparticles. *J Supercritical Fluids* 2016;**113**:136.
30. Azizi S, Ahmad MB, Namvar F, Mohamad R. Green biosynthesis and characterization of zinc oxide nanoparticles using brown marine macroalga Sargassum muticum aqueous extract. *Mat Lett* 2014;**116**:275.
31. Hayashi H, Hakuta Y. Hydrothermal synthesis of metal oxide nanoparticles in supercritical water. *Materials* 2010;**3**(7):3794.
32. Herring NP, Panda AB, Abou Zeid K, Almahoudi SH, Olson CR, Patel A, El-Shall M. *Metal oxide nanomaterials for chemical sensors*. Springer; 2013.
33. Chen Y, Zhang J, Wang Z, Zhou Z. Solvothermal synthesis of size-controlled monodispersed superparamagnetic iron oxide nanoparticles. *Appl Sci* 2019;**9**(23):5157.
34. Arabi M, Ghaedi M, Ostovan A. Engineering. Development of a lower toxic approach based on green synthesis of water-compatible molecularly imprinted nanoparticles for the extraction of hydrochlorothiazide from human urine. *ACS Sustain Chem Eng* 2017;**5**(5):3775.
35. Duan H, Wang D, Li Y. Green chemistry for nanoparticle synthesis. *J Coll Stud Retent* 2015;**44**(16):5778.
36. Nikam A, Prasad B, Kulkarni A. Wet chemical synthesis of metal oxide nanoparticles: a review. *CrystEngComm* 2018;**20**(35):5091.
37. Singh A, Gautam PK, Verma A, Singh V, Shivapriya PM, Shivalkar S, Sahoo AK, Samanta SK. Green synthesis of metallic nanoparticles as effective alternatives to treat antibiotics resistant bacterial infections: a review. *Biotechnol Rep (Amst)* 2020;**25**:e00427.
38. Molnár Z, Bódai V, Szakacs G, Erdélyi B, Fogarassy Z, Sáfrán G, Varga T, Kónya Z, Tóth-Szeles E, Szűcs R. Green synthesis of gold nanoparticles by thermophilic filamentous fungi. *Scient Reports* 2018;**8**(1):1.
39. Das B, Dash SK, Mandal D, Ghosh T, Chattopadhyay S, Tripathy S, Das S, Dey SK, Das D, Roy S. Green synthesized silver nanoparticles destroy multidrug resistant bacteria via reactive oxygen species mediated membrane damage. *Arabian J Chem* 2017;**10**(6):862.
40. Rajput N. Methods of preparation of nanoparticles-a review. *Int J Adv Eng Technol* 2015;**7**(6):1806.
41. Paul P, Pattnaik Y, Panda PK, Jha E, Verma SK, Suar M. *Green methods for wastewater treatment*. Springer; 2020.
42. Virkutyte J, Varma RS. Green synthesis of metal nanoparticles: biodegradable polymers and enzymes in stabilization and surface functionalization. *Chem Sci* 2011;**2**(5):837.
43. Augustine R, Hasan A. Technology. Emerging applications of biocompatible phytosynthesized metal/metal oxide nanoparticles in healthcare. *J Drug Delivery Sci Tech* 2020:101516.
44. Mukherjee P, Roy M, Mandal B, Dey G, Mukherjee P, Ghatak J, Tyagi A, Kale S. Green synthesis of highly stabilized nanocrystalline silver particles by a non-pathogenic and agriculturally important fungus T. asperellum. *Nanotechnology* 2008;**19**(7):075103.
45. Wypij M, Golinska P. *Bioinspired Metal Nanoparticles with Special Reference to Mechanism. In Nanotechnology Applied To Pharmaceutical Technology*. Cham: Springer; 2017. pp. 3–29.
46. Katas H, Moden NZ, Lim CS, Celesistinus T, Chan JY, Ganasan P, Suleman Ismail Abdalla S. Biosynthesis and potential applications of silver and gold nanoparticles and their chitosan-based nanocomposites in nanomedicine. *J Nanotechnol* 2018;**2018**.
47. Renuka R, Devi KR, Sivakami M, Thilagavathi T, Uthrakumar R, Kaviyarasu K. Biosynthesis of silver nanoparticles using phyllanthus emblica fruit extract for antimicrobial application. *Biocat Agri Biotechnol* 2020:101567.

48. Sathyavathi S, Manjula A, Rajendhran J, Gunasekaran P. *Biosynthesis and characterization of mercury sulphide nanoparticles produced by Bacillus cereus MRS-1*. 2013.
49. Gahlawat G, Choudhury AR. A review on the biosynthesis of metal and metal salt nanoparticles by microbes. *RSC Adv* 2019;**9**(23):12944.
50. Faramarzi MA, Sadighi A. Insights into biogenic and chemical production of inorganic nanomaterials and nanostructures. *Adv Colloid Interface Sci* 2013;**189**:1.
51. Iravani S. Bacteria in nanoparticle synthesis: current status and future prospects. *Int Sch Res Notices* 2014. https://doi.org/10.1155/2014/359316.
52. Srivastava SK, Constanti M. Room temperature biogenic synthesis of multiple nanoparticles (Ag, Pd, Fe, Rh, Ni, Ru, Pt, Co, and Li) by *Pseudomonas aeruginosa* SM1. *J Nanoparticle Res* 2012;**14**(4):831.
53. Sathyavathi S, Manjula A, Rajendhran J, Gunasekaran P. Extracellular synthesis and characterization of nickel oxide nanoparticles from Microbacterium sp. MRS-1 towards bioremediation of nickel electroplating industrial effluent. *Bioresour Technol* 2014;**165**:270.
54. Chernousova S, Epple M. Silver as antibacterial agent: ion, nanoparticle, and metal. *Angewandte Chemie Int Ed* 2013;**52**(6):1636.
55. Saravanan M, Barik SK, MubarakAli D, Prakash P, Pugazhendhi A. Synthesis of silver nanoparticles from Bacillus brevis (NCIM 2533) and their antibacterial activity against pathogenic bacteria. *Microb Pathogene* 2018;**116**:221.
56. Malhotra A, Dolma K, Kaur N, Rathore YS, Mayilraj S, Choudhury AR. Biosynthesis of gold and silver nanoparticles using a novel marine strain of Stenotrophomonas. *Biosource Technol* 2013;**142**:727.
57. Kaur H, Dolma K, Kaur N, Malhotra A, Kumar N, Dixit P, Sharma D, Mayilraj S, Choudhury AR. Marine microbe as nano-factories for copper biomineralization. *Biotechnol Bioprocess Eng* 2015;**20**(1):51.
58. Yang C, Qian R, Xu Y, Yi J, Gu Y, Liu X, Yu H, Jiao B, Lu X, Zhang W. Marine actinomycetes-derived natural products. *Curr Topics Med Chem* 2019.
59. Otari S, Patil R, Nadaf N, Ghosh S, Pawar S. Green biosynthesis of silver nanoparticles from an actinobacteria Rhodococcus sp. *Mat Lett* 2012;**72**:92.
60. Karthik L, Kumar G, Kirthi AV, Rahuman A, Rao KB. LK3 mediated synthesis of silver nanoparticles and its biomedical application. *Bioprocess Biosys Eng* 2014;**37**(2):261.
61. Buszewski B, Railean-Plugaru V, Pomastowski P, Rafińska K, Szultka-Mlynska M, Golinska P, et al. *o. m., immunology; infection. Antimicrobial activity of biosilver nanoparticles produced by a novel Streptacidiphilus durhamensis strain* 2018;**51**(1):45.
62. Hassan SE-D, Fouda A, Radwan AA, Salem SS, Barghoth MG, Awad MA, Abdo AM, El-Gamal MS. Endophytic actinomycetes Streptomyces spp mediated biosynthesis of copper oxide nanoparticles as a promising tool for biotechnological applications. *JBIC J Biol Inorganic Chem* 2019;**24**(3):377.
63. Ranjitha V, Rai VR. Actinomycetes mediated synthesis of gold nanoparticles from the culture supernatant of Streptomyces griseoruber with special reference to catalytic activity. *3 Biotech* 2017;**7**(5):299.
64. Rajivgandhi G, Maruthupandy M, Muneeswaran T, Anand M, Manoharan N. Antibiofilm activity of zinc oxide nanosheets (ZnO NSs) using Nocardiopsis sp. GRG1 (KT235640) against MDR strains of gram negative *Proteus mirabilis* and *Escherichia coli*. *Process Biochem* 2018;**67**:8.
65. Boroumand Moghaddam A, Namvar F, Moniri M, Azizi S, Mohamad R. Nanoparticles biosynthesized by fungi and yeast: a review of their preparation, properties, and medical applications. *Molecules* 2015;**20**(9):16540.
66. Shankar SS, Ahmad A, Pasricha R, Sastry MJ. Bioreduction of chloroaurate ions by geranium leaves and its endophytic fungus yields gold nanoparticles of different shapes. *J Mat Chem* 2003;**13**(7):1822.
67. Ganachari SV, Bhat R, Deshpande R, Venkataraman A. Extracellular biosynthesis of silver nanoparticles using fungi Penicillium diversum and their antimicrobial activity studies. *BioNanoSci* 2012;**2**(4):316.
68. Hamedi S, Ghaseminezhad M, Shokrollahzadeh S, Shojaosadati SA. Controlled biosynthesis of silver nanoparticles using nitrate reductase enzyme induction of filamentous fungus and their antibacterial evaluation. *Artif Cells Nanomed Biotechnol* 2017;**45**(8):1588.
69. Metuku RP, Pabba S, Burra S, Gudikandula K, Charya MS. Biosynthesis of silver nanoparticles from Schizophyllum radiatum HE 863742.1: their characterization and antimicrobial activity. *3 Biotech* 2014;**4**(3):227.
70. Rajput S, Werezuk R, Lange RM, McDermott MT. Fungal isolate optimized for biogenesis of silver nanoparticles with enhanced colloidal stability. *Langmuir* 2016;**32**(34):8688–97.
71. Apte M, Sambre D, Gaikawad S, Joshi S, Bankar A, Kumar AR, Zinjarde S. Psychrotrophic yeast Yarrowia lipolytica NCYC 789 mediates the synthesis of antimicrobial silver nanoparticles via cell-associated melanin. *Amb Express* 2013;**3**(1):32.

72. Korbekandi H, Mohseni S, Mardani Jouneghani R, Pourhossein M, Iravani S. Biosynthesis of silver nanoparticles using *Saccharomyces cerevisiae*. *Artif Cells Nanomed Biotechnol* 2016;**44**(1):235.
73. Waghmare SR, Mulla MN, Marathe SR, Sonawane KD. Ecofriendly production of silver nanoparticles using Candida utilis and its mechanistic action against pathogenic microorganisms. *3 Biotech* 2015;**5**(1):33−8.
74. Das SK, Das AR, Guha AK. Gold nanoparticles: microbial synthesis and application in water hygiene management. *Langmuir* 2009;**25**(14):8192.
75. Xie J, Lee JY, Wang DI, Ting YP. High-yield synthesis of complex gold nanostructures in a fungal system. *J Phys Chem C* 2007;**111**(45):16858.
76. Zhang X, He X, Wang K, Yang X. Different active biomolecules involved in biosynthesis of gold nanoparticles by three fungus species. *J Biomed Nanotechnol* 2011;**7**(2):245.
77. Pimprikar P, Joshi S, Kumar A, Zinjarde S, Kulkarni S. Influence of biomass and gold salt concentration on nanoparticle synthesis by the tropical marine yeast Yarrowia lipolytica NCIM 3589. *Colloids Surf B: Biointerf* 2009;**74**(1):309.
78. Rajakumar G, Rahuman AA, Roopan SM, Khanna VG, Elango G, Kamaraj C, Zahir AA, Velayutham K. Fungus-mediated biosynthesis and characterization of TiO2 nanoparticles and their activity against pathogenic bacteria. *Spectrochimica Acta Part A: Mole Biomole Spectros* 2012;**91**:23.
79. Raliya R, Biswas P, Tarafdar J. TiO2 nanoparticle biosynthesis and its physiological effect on mung bean (Vigna radiata L.). *Biotechnol Reports* 2015;**5**:22.
80. Dahoumane SA, Yéprémian C, Djédiat C, Couté A, Fiévet F, Coradin T, Brayner R. A global approach of the mechanism involved in the biosynthesis of gold colloids using micro-algae. *J Nanoparticle Res* 2014;**16**(10):2607.
81. Raliya R, Tarafdar JC. ZnO nanoparticle biosynthesis and its effect on phosphorous-mobilizing enzyme secretion and gum contents in Clusterbean (Cyamopsis tetragonoloba L.). *Agri Res* 2013;**2**(1):48.
82. Siddiqi KS, Husen A. *Fabrication of metal nanoparticles from fungi and metal salts: scope and application* 2016;**11**(1):1−15.
83. Gajendran B, Varier KM, Liu W, Yao Y, Raman J, Ben-David Y, Li Y, Chinnasamy A. *Biological synthesis of nanoparticles and their applications*. CRC Press; 2019.
84. Chhipa H. *Mycosynthesis of nanoparticles for smart agricultural practice: a green and eco-friendly approach*. *Green synthesis, characterization and applications of nanoparticles.* Elsevier; 2019. pp. 87−109.
85. Parkash V, Gaur A, Agnihotri R. *Nanotechnology for food, agriculture, and environment*. Springer; 2020.
86. Gholami-Shabani M, Shams-Ghahfarokhi M, Gholami-Shabani Z, Akbarzadeh A, Riazi G, Ajdari S, Amani A, Razzaghi-Abyaneh M. Enzymatic synthesis of gold nanoparticles using sulfite reductase purified from *Escherichia coli*: a green eco-friendly approach. *Process Biochem* 2015;**50**(7):1076.
87. Palomo JM, Filice M. Biosynthesis of metal nanoparticles: novel efficient heterogeneous nanocatalysts. *Nanomaterials* 2016;**6**(5):84.
88. Das SK, Khan MMR, Guha AK, Naskar N. Bio-inspired fabrication of silver nanoparticles on nanostructured silica: characterization and application as a highly efficient hydrogenation catalyst. *Green Chem* 2013;**15**(9):2548.
89. Kracht S, Messerer M, Lang M, Eckhardt S, Lauz M, Grobéty B, Fromm KM, Giese B. Electron transfer in peptides: on the formation of silver nanoparticles. *Angewandte Chemie Int Ed* 2015;**54**(10):2912.
90. Unal Gulsuner H, Ceylan H, Guler MO, Tekinay AB. Multi-domain short peptide molecules for in situ synthesis and biofunctionalization of gold nanoparticles for integrin-targeted cell uptake. *ACS Appl Mat Interf* 2015;**7**(20):10677.
91. Naik RR, Stringer SJ, Agarwal G, Jones SE, Stone MO. Biomimetic synthesis and patterning of silver nanoparticles. *Nat Mater* 2002;**1**(3):169.
92. Fawcett D, Verduin JJ, Shah M, Sharma SB, Poinern GE. A review of current research into the biogenic synthesis of metal and metal oxide nanoparticles via marine algae and seagrasses. *J Nanosci* 2017;**2017**.
93. Michalak I, Chojnacka K. Algae as production systems of bioactive compounds. *Eng Life Sci* 2015;**15**(2):160.
94. Bao Z, Lan CQ. Advances in biosynthesis of noble metal nanoparticles mediated by photosynthetic organisms−A review. *Colloids Surf B: Biointer* 2019:110519.
95. Bhuyar P, Rahim MHA, Sundararaju S, Ramaraj R, Maniam GP, Govindan N. Synthesis of silver nanoparticles using marine macroalgae Padina sp. and its antibacterial activity towards pathogenic bacteria. *Beni-Suef U J Basic Appl Sci* 2020;**9**(1):1.
96. Luangpipat T, Beattie IR, Chisti Y, Haverkamp RG. Gold nanoparticles produced in a microalga. *J Nanoparticle Res* 2011;**13**(12):6439.
97. Satapathy S, Shukla SP, Sandeep K, Singh AR, Sharma NJJ. *o. a. p. Evaluation of the performance of an algal bioreactor for silver nanoparticle production* 2015;**27**(1):285.

98. Castro L, Blázquez ML, Muñoz JA, González F, Ballester A. Biological synthesis of metallic nanoparticles using algae. *IET Nanotechl* 2013;**7**(3):109.
99. Pettegrew C, Dong Z, Muhi MZ, Pease S, Mottaleb MA, Islam MR. Silver nanoparticle synthesis using monosaccharides and their growth inhibitory activity against gram-negative and positive bacteria. *Int Sch Res Notices* 2014.
100. Bao Z, Lan CQ. Mechanism of light-dependent biosynthesis of silver nanoparticles mediated by cell extract of Neochloris oleoabundans. *Colloids Surf B: Biointer* 2018;**170**:251.
101. Jena J, Pradhan N, Dash BP, Panda PK, Mishra BKJJoSCS. Pigment mediated biogenic synthesis of silver nanoparticles using diatom Amphora sp. and its antimicrobial activity 2015;**19**(6):661.
102. Khanna P, Kaur A, Goyal D. Algae-based metallic nanoparticles: synthesis, characterization and applications. *J Microbiol Methods* 2019;**163**:105656.
103. Roy S, Anantharaman P. Biosynthesis of Silver Nanoparticles by Sargassum Ilicifolium (Turner) C. Agardh with their antimicrobial activity and potential for seed germination. *J Appl Phys Nanotechnol* 2018;**1**(1):2.
104. Arsiya F, Sayadi MH, Sobhani SJML. *Green synthesis of palladium nanoparticles using Chlorella vulgaris* 2017;**186**:113.
105. Sayadi MH, Salmani N, Heidari A, Rezaei MR. Interfaces. Bio-synthesis of palladium nanoparticle using Spirulina platensis alga extract and its application as adsorbent. *Surf Interf* 2018;**10**:136.
106. Rao MD, Gautam P. Synthesis and characterization of ZnO nanoflowers using C hlamydomonas reinhardtii: a green approach. *Environ Prog Sustain Ener* 2016;**35**(4):1020.
107. Rao MD, Pennathur G. Green synthesis and characterization of cadmium sulphide nanoparticles from Chlamydomonas reinhardtii and their application as photocatalysts. *Mat Res Bull* 2017;**85**:64.
108. Sanaeimehr Z, Javadi I, Namvar F. Antiangiogenic and antiapoptotic effects of green-synthesized zinc oxide nanoparticles using Sargassum muticum algae extraction. *Cancer Nanotechnol* 2018;**9**(1):3.
109. Momeni S, Nabipour I. A simple green synthesis of palladium nanoparticles with Sargassum alga and their electrocatalytic activities towards hydrogen peroxide. *Appl Biochem Biotechnol* 2015;**176**(7):1937.
110. Mittal AK, Chisti Y, Banerjee UC. Synthesis of metallic nanoparticles using plant extracts. *Biotechnol Adv* 2013;**31**(2):346.
111. Ahmad F, Ashraf N, Ashraf T, Zhou R-B, Yin D-C. Biological synthesis of metallic nanoparticles (MNPs) by plants and microbes: their cellular uptake, biocompatibility, and biomedical applications. *App Microbiol Biotechnol* 2019;**103**(7):2913.
112. Ahmed S, Saifullah, Ahmad M, Swami BL, Ikram S. Green synthesis of silver nanoparticles using Azadirachta indica aqueous leaf extract. *J Rad Res Appl Sci* 2016;**9**(1):1.
113. Jassal V, Shanker U, Gahlot S, Kaith B, Iqubal MA, Samuel P. Sapindus mukorossi mediated green synthesis of some manganese oxide nanoparticles interaction with aromatic amines. *Appl Phys* 2016;**122**(4):271.
114. Roy P, Das B, Mohanty A, Mohapatra S. Green synthesis of silver nanoparticles using Azadirachta indica leaf extract and its antimicrobial study. *Appl Nanosci* 2017;**7**(8):43.
115. Ankamwar B, Kirtiwar S, Shukla AC. *Advances in pharmaceutical biotechnology*. Springer; 2020.
116. Ishak NM, Kamarudin S, Timmiati S. Green synthesis of metal and metal oxide nanoparticles via plant extracts: an overview. *Mat Exp Res* 2019;**6**(11):112004.
117. Ponarulselvam S, Panneerselvam C, Murugan K, Aarthi N, Kalimuthu K, hangamani S. Synthesis of silver nanoparticles using leaves of Catharanthus roseus Linn. G. Don and their antiplasmodial activities. *Asian Pacific J Trop Biomed* 2012;**2**(7):574.
118. Prasad T, Elumalai E. Biofabrication of Ag nanoparticles using Moringa oleifera leaf extract and their antimicrobial activity. *Asian Pacific J Trop Biomed* 2011;**1**(6):439.
119. Roni M, Murugan K, Panneerselvam C, Subramaniam J, Hwang J-S. Evaluation of leaf aqueous extract and synthesized silver nanoparticles using Nerium oleander against *Anopheles stephensi* (Diptera: culicidae). *Parasitol Res* 2013;**112**(3):981.
120. Tippayawat P, Phromviyo N, Boueroy P, Chompoosor A. Green synthesis of silver nanoparticles in aloe vera plant extract prepared by a hydrothermal method and their synergistic antibacterial activity. *PeerJ* 2016;**4**:e2589.
121. Huang J, Li Q, Sun D, Lu Y, Su Y, Yang X, et al. Biosynthesis of silver and gold nanoparticles by novel sundried Cinnamomum camphora leaf. *Nanotechnology* 2007;**18**(10):105104.
122. Elia P, Zach R, Hazan S, Kolusheva S, Porat Ze, Zeiri Y. Green synthesis of gold nanoparticles using plant extracts as reducing agents. *Int J Nanomed* 2014;**9**:4007.
123. Gurunathan S, Kim E, Han JW, Park JH, Kim J-H. Green chemistry approach for synthesis of effective anticancer palladium nanoparticles. *Molecules* 2015;**20**(12):22476.

124. Albanese A, Tang PS, Chan WC. The effect of nanoparticle size, shape, and surface chemistry on biological systems. *Annual Rev Biomed Eng* 2012;**14**:1.
125. Benelli G. Plant-mediated biosynthesis of nanoparticles as an emerging tool against mosquitoes of medical and veterinary importance: a review. *Parasitol Res* 2016;**115**(1):23.
126. Dauthal P, Mukhopadhyay M. Noble metal nanoparticles: plant-mediated synthesis, mechanistic aspects of synthesis, and applications. *Indus Eng Chem Res* 2016;**55**(36):9557.
127. Nguyen NH, Padil VVT, Slaveykova VI, Černík M, Ševců A. Green synthesis of metal and metal oxide nanoparticles and their effect on the unicellular alga Chlamydomonas reinhardtii. *Nanoscale Res Lett* 2018;**13**(1):1.
128. Ramesh P, Rajendran A, Meenakshisundaram M. Green syntheis of zinc oxide nanoparticles using flower extract cassia auriculata. *J Nanosci Nanotechnol* 2014;**2**(1):41–5.
129. Jahangirian H, Lemraski EG, Webster TJ, Rafiee-Moghaddam R, Abdollahi Y. A review of drug delivery systems based on nanotechnology and green chemistry: green nanomedicine. *Int J Nanomed* 2017;**12**:2957.
130. Chung I-M, Park I, Seung-Hyun K, Thiruvengadam M, Rajakumar G. Plant-mediated synthesis of silver nanoparticles: their characteristic properties and therapeutic applications. *Nanoscale Res Lett* 2016;**11**(1):40.
131. Ebrahiminezhad A, Zare-Hoseinabadi A, Sarmah AK, Taghizadeh S, Ghasemi Y, Berenjian A. Plant-mediated synthesis and applications of iron nanoparticles. *Mol Biotechnol* 2018;**60**(2):154.
132. Hameed S, Iqbal J, Ali M, Khalil AT, Abbasi BA, Numan M, Shinwari ZK. Green synthesis of zinc nanoparticles through plant extracts: establishing a novel era in cancer theranostics. *Mat Res Exp* 2019;**6**(10):102005.
133. Joshi A, Sharma A, Bachheti RK, Husen A, Mishra VK. *Nanomaterials and plant potential*. Springer; 2019.
134. Rajeshkumar S, Menon S, Kumar SV, Tambuwala MM, Bakshi HA, Mehta M, Satija S, Gupta G, Chellappan DK, Thangavelu L, et al. Antibacterial and antioxidant potential of biosynthesized copper nanoparticles mediated through Cissus arnotiana plant extract. *J Drug Delivery Sci Technol* 2019;**197**:111531.
135. El Shafey AM. Green synthesis of metal and metal oxide nanoparticles from plant leaf extracts and their applications: *a review* 2020;**9**(1):304–39.
136. Sundrarajan M, Ambika S, Bharathi K. Plant-extract mediated synthesis of ZnO nanoparticles using Pongamia pinnata and their activity against pathogenic bacteria. *Adv Power Technol* 2015;**26**(5):1294.
137. Hamidi M, Azadi A, Rafiei P. Hydrogel nanoparticles in drug delivery. *Adv Drug Deliv Res* 2008;**60**(15):1638.
138. Parveen K, Banse V, Ledwani L. *AIP conference proceedings*. 2016. pp. 020048.
139. Teow S-Y, Wong MM-T, Yap H-Y, Peh S-C, Shameli K. Bactericidal properties of plants-derived metal and metal oxide nanoparticles (NPs). *Molecules* 2018;**23**(6):1366.
140. Thatoi P, Kerry RG, Gouda S, Das G, Pramanik K, Thatoi H, Patra JK. Photo-mediated green synthesis of silver and zinc oxide nanoparticles using aqueous extracts of two mangrove plant species, Heritiera fomes and Sonneratia apetala and investigation of their biomedical applications. *J Photochem Photobiol B: Biol* 2016;**163**:311.
141. Vijayaraghavan K, Ashokkumar T. Plant-mediated biosynthesis of metallic nanoparticles: a review of literature, factors affecting synthesis, characterization techniques and applications. *J Environ Chem Eng* 2017;**5**(5):4866.
142. Merisko-Liversidge EM, Liversidge GG. Drug nanoparticles: formulating poorly water-soluble compounds. *Taxicol Pathol* 2008;**36**(1):43.
143. Sawant RR, Torchilin VP. Multifunctional nanocarriers and intracellular drug delivery. *Curr Opinion Solid State Mat Sci* 2012;**16**(6):269.
144. Kim BY, Rutka JT, Chan WC. Nanomedicine. *N Engl J Med* 2010;**363**(25):2434.
145. Soppimath KS, Tan DW, Yang YY. pH-triggered thermally responsive polymer core–shell nanoparticles for drug delivery. *Adv Mat* 2005;**17**(3):318.
146. Dave V, Tak K, Sohgaura A, Gupta A, Sadhu V, Reddy KR. Lipid-polymer hybrid nanoparticles: synthesis strategies and biomedical applications. *J Microbiol Methods* 2019.
147. Hadinoto K, Sundaresan A, Cheow WS. Lipid–polymer hybrid nanoparticles as a new generation therapeutic delivery platform: a review. *European J Pharmaceut Biopharmaceut* 2013;**85**(3):427.
148. Torchilin V. Multifunctional and stimuli-sensitive pharmaceutical nanocarriers. *European J Pharmaceut Biopharmaceut* 2009;**71**(3):431.
149. Shah R, Eldridge D, Palombo E, Harding I. *Lipid nanoparticles: production, characterization and stability*. Springer; 2015.
150. Miyata K, Christie RJ, Kataoka K. Polymeric micelles for nano-scale drug delivery. *React Func Poly* 2011;**71**(3):227.
151. Nasir A, Kausar A, Younus A. Engineering. A review on preparation, properties and applications of polymeric nanoparticle-based materials. *Poly-Plastics Technol Eng* 2015;**54**(4):325.
152. Sawdon AJ, Peng C-A. Polymeric micelles for acyclovir drug delivery. *Colloids Surf B: Biointerf* 2014;**122**:738.

153. Kreuter J. Drug delivery to the central nervous system by polymeric nanoparticles: what do we know? *Adv Drug Delivery Rev* 2014;**71**:2.
154. Kumar AK, Saila ES, Narang P, Aishwarya M, Raina R, Gautam M, Shankar EG. Biofunctionalization and biological synthesis of the ZnO nanoparticles: the effect of Raphanus sativus (white radish) root extract on antimicrobial activity against MDR strain for wound healing applications. *Inorganic Chem Comm* 2019;**100**:101.
155. Nagavarma B, Yadav HK, Ayaz A, Vasudha L, Shivakumar H. Different techniques for preparation of polymeric nanoparticles-a review. *Asian J Pharm Clin Res* 2012;**5**(3):16.
156. Amoabediny G, Haghiralsadat F, Naderinezhad S, Helder MN, Akhoundi Kharanaghi E, Mohammadnejad Arough J, Zandieh-Doulabi B. Overview of preparation methods of polymeric and lipid-based (niosome, solid lipid, liposome) nanoparticles: a comprehensive review. *I J Polym Mat Polym Biomat* 2018;**67**(6):383.
157. Pallerla S, Prabhakar B. Review on polymers in drug delivery. *American J Pharmtech Res* 2013;**3**:900.
158. Owens III DE, Peppas NA. Opsonization, biodistribution, and pharmacokinetics of polymeric nanoparticles. *Int J Pharmaceut* 2006;**307**(1):93.
159. Delplace V, Couvreur P, Nicolas J. Recent trends in the design of anticancer polymer prodrug nanocarriers. *Poly Chem* 2014;**5**(5):1529.
160. Nelemans LC, Gurevich L. Drug delivery with polymeric nanocarriers—cellular uptake mechanisms. *Materials* 2020;**13**(2):366.
161. Venditti I. Morphologies and functionalities of polymeric nanocarriers as chemical tools for drug delivery: a review. *J King Saud Univ-Sci* 2019;**31**(3):398.
162. Lu H, Wang J, Wang T, Zhong J, Bao Y, Hao H. Recent progress on nanostructures for drug delivery applications. *J Nanomat* 2016;**2016**.
163. Shehata T, Ogawara K-i, Higaki K, Kimura T. Prolongation of residence time of liposome by surface-modification with mixture of hydrophilic polymers. *Int J Pharm* 2008;**359**(1−2):272.
164. Lung P, Yang J, Li Q. Nanoparticle formulated vaccines: opportunities and challenges. *Nanoscale* 2020;**12**(10):5746.
165. Has C, Sunthar P. A comprehensive review on recent preparation techniques of liposomes. *J Liposome Res* 2019;vol. 1.
166. Sharma A, Sharma US. Liposomes in drug delivery: progress and limitations. *Int J Pharmaceut* 1997;**154**(2):123.
167. Akbarzadeh A, Rezaei-Sadabady R, Davaran S, Joo SW, Zarghami N, Hanifehpour Y, Samiei M, Kouhi M, Nejati-Koshki K. Liposome: classification, preparation, and applications. *Nanoscale Res Lett* 2013;**8**(1):102.
168. Mufamadi MS, Pillay V, Choonara YE, Du Toit LC, Modi G, Naidoo D, Ndesendo VM. A review on composite liposomal technologies for specialized drug delivery. *J Drug Delivery* 2011:2011.
169. Allen C, Dos Santos N, Gallagher R, Chiu G, Shu Y, Li W, Johnstone S, Janoff A, Mayer L, Webb M. Controlling the physical behavior and biological performance of liposome formulations through use of surface grafted poly (ethylene glycol). *Biosci Reports* 2002;**22**(2):225.
170. Weber S, Zimmer A, Pardeike J. Solid lipid nanoparticles (SLN) and nanostructured lipid carriers (NLC) for pulmonary application: a review of the state of the art. *European J Pharmaceut Biopharmaceut* 2014;**86**(1):7.
171. Naderinezhad S, Amoabediny G, Haghiralsadat F. Co-delivery of hydrophilic and hydrophobic anticancer drugs using biocompatible pH-sensitive lipid-based nano-carriers for multidrug-resistant cancers. *RSC Adv* 2017;**7**(48):30008.
172. World Health Organization (W.H.O). *Antimicrobial resistance: global report on surveillance*. World Health Organization; 2014.
173. Alavi M, Rai M. Recent advances in antibacterial applications of metal nanoparticles (MNPs) and metal nanocomposites (MNCs) against multidrug-resistant (MDR) bacteria. *Expert Rev Anti-Infec Therapy* 2019;**17**(6):419.
174. Gupta A, Saleh NM, Das R, Landis RF, Bigdeli A, Motamedchaboki K, Campos AR, Pomeroy K, Mahmoudi M, Rotello VM. Synergistic antimicrobial therapy using nanoparticles and antibiotics for the treatment of multidrug-resistant bacterial infection. *Nano Futures* 2017;**1**(1):015004.
175. Deravi LF, Swartz JD, Wright DW. The biomimetic synthesis of metal oxide nanomaterials. In: Kumar CSSR, editor. *Nanotechnologies for the Life Sciences*; 2010. https://doi.org/10.1002/9783527610419.ntls0137.
176. Baptista PV, McCusker MP, Carvalho A, Ferreira DA, Mohan NM, Martins M, et al. *Nano-strategies to fight multidrug resistant bacteria—A Battle of the Titans* 2018;**9**:1441.
177. Naveed M, Chaudhry Z, Bukhari SA, Meer B, Ashraf H. *Antibiotics and antimicrobial resistance genes in the environment*. Elsevier; 2020.
178. Slavin YN, Asnis J, Häfeli UO, Bach H. Metal nanoparticles: understanding the mechanisms behind antibacterial activity. *J Nanobiotechnol* 2017;**15**(1):65.

179. Gupta A, Mumtaz S, Li C-H, Hussain I, Rotello VM. Combatting antibiotic-resistant bacteria using nanomaterials. *J Coll Stud Retent* 2019;**48**(2):415.
180. Lee N-Y, Hsueh P-R, Ko W-C. Nanoparticles in the treatment of infections caused by multidrug-resistant organisms. *Front Pharmacol* 2019;**10**:1153.
181. Sangave PC, Matkar NM, Suvarna V. *Model organisms to study biological activities and toxicity of nanoparticles*. Springer; 2020.
182. Huang Q, Wang S, Sun Y, Shi C, Yang H, Lu Z. Effects of Ag/ZnO nanocomposite at sub-minimum inhibitory concentrations on virulence factors of Streptococcus mutans. *Archives Oral Biol* 2020;**111**:104640.
183. Badawy MSE, Riad OKM, Taher F, Zaki SA. Chitosan and chitosan-zinc oxide nanocomposite inhibit expression of LasI and RhlI genes and quorum sensing dependent virulence factors of *Pseudomonas aeruginosa*. *Int J Biolog Macromol* 2020;**149**:1109.
184. Omoike A, Chorover J, Kwon KD, Kubicki JD. Adhesion of bacterial exopolymers to α-FeOOH: inner-sphere complexation of phosphodiester groups. *Langmuir* 2004;**20**(25):11108.
185. Kadiyala U, Kotov NA, Van Epps JS. Antibacterial metal oxide nanoparticles: challenges in interpreting the literature. *Curr Pharmaceuti Des* 2018;**24**(8):896.
186. Zazo H, Colino CI, Lanao JM. Current applications of nanoparticles in infectious diseases. *J Cont Release* 2016;**224**:86.
187. Seil JT, Webster TJ. Antimicrobial applications of nanotechnology: methods and literature. *Int J Nanomed* 2012;**7**:2767.
188. Cheng G, Dai M, Ahmed S, Hao H, Wang X, Yuan Z. Antimicrobial drugs in fighting against antimicrobial resistance. *Front Microbiol* 2016;**7**:470.
189. Singh R, Smitha M, Singh SP. The role of nanotechnology in combating multi-drug resistant bacteria. *J Nanosci Nanotechnol* 2014;**14**(7):4745.
190. Yount NY, Yeaman MR. Emerging themes and therapeutic prospects for anti-infective peptides. *Ann Rev Pharmacol Toxicol* 2012;**52**:337.
191. Das CA, Kumar VG, Dhas TS, Karthick V, Govindaraju K, Joselin JM, Baalamurugan J. Antibacterial activity of silver nanoparticles (biosynthesis): a short review on recent advances. *Biocat Agricult Biotechnol* 2020:101593.
192. Rai M, Deshmukh S, Ingle A, Gade A. Silver nanoparticles: the powerful nanoweapon against multidrug-resistant bacteria. *J Appl Microbiol* 2012;**112**(5):841.
193. Jazmine Silvero C M, Rocca DM, de la Villarmois EA, Fournier K, Lanterna AE, Perez MF, Becerra MC, Scaiano JC. Selective photoinduced antibacterial activity of amoxicillin-coated gold nanoparticles: from one-step synthesis to in vivo cytocompatibility. *ACS Omega* 2018;**3**(1):1220.
194. Theophel K, Schacht VJ, Schlüter M, Schnell S, Stingu C-S, Schaumann R, Bunge M. The importance of growth kinetic analysis in determining bacterial susceptibility against antibiotics and silver nanoparticles. *Front Microbiol* 2014;**5**:544.
195. Vadlapudi V, Amanchy R. Phytofabrication of silver nanoparticles using Myriostachya wightiana as a novel bioresource, and evaluation of their biological activities. *Brazilian Arch Biol Technol* 2017;**60**.
196. Chowdhury S, Basu A, Kundu S. Green synthesis of protein capped silver nanoparticles from phytopathogenic fungus Macrophomina phaseolina (Tassi) Goid with antimicrobial properties against multidrug-resistant bacteria. *Nanoscale Res Lett* 2014;**9**(1):1.
197. Manikprabhu D, Cheng J, Chen W, Sunkara AK, Mane SB, Kumar R, Hozzein WN, Duan Y-Q, Li W-J. Sunlight mediated synthesis of silver nanoparticles by a novel actinobacterium (Sinomonas mesophila MPKL 26) and its antimicrobial activity against multi drug resistant *Staphylococcus aureus*. *J Photochem Photobiol B: Biol* 2016;**158**:202.
198. Scandorieiro S, de Camargo LC, Lancheros CA, Yamada-Ogatta SF, Nakamura CV, de Oliveira AG, Andrade CG, Duran N, Nakazato G, Kobayashi RK. Synergistic and additive effect of oregano essential oil and biological silver nanoparticles against multidrug-resistant bacterial strains. *Front Microbiol* 2016;**7**:760.
199. Silva Santos K, Barbosa AM, Pereira da Costa L, Pinheiro MS, Oliveira MBPP, Ferreira Padilha F. Silver nanocomposite biosynthesis: antibacterial activity against multidrug-resistant strains of *Pseudomonas aeruginosa* and Acinetobacter baumannii. *Molecules* 2016;**21**(9):1255.
200. Dash SS, Samanta S, Dey S, Giri B, Dash SK. Rapid green synthesis of biogenic silver nanoparticles using cinnamomum tamala leaf extract and its potential antimicrobial application against clinically isolated multidrug-resistant bacterial strains. *Biolog Trade Element Res* 2020;**1**.

201. Jinu U, Jayalakshmi N, Anbu AS, Mahendran D, Sahi S, Venkatachalam P. Biofabrication of cubic phase silver nanoparticles loaded with phytochemicals from Solanum nigrum leaf extracts for potential antibacterial, anti-biofilm and antioxidant activities against MDR human pathogens. *J Cluster Sci* 2017;**28**(1):489.
202. Prasannaraj G, Venkatachalam P. Enhanced antibacterial, anti-biofilm and antioxidant (ROS) activities of biomolecules engineered silver nanoparticles against clinically isolated gram positive and gram negative microbial pathogens. *J Cluster Sci* 2017;**28**(1):645.
203. Maruthupandy M, Rajivgandhi G, Muneeswaran T, Song J-M, Manoharan N. Biologically synthesized zinc oxide nanoparticles as nanoantibiotics against ESBLs producing gram negative bacteria. *Microb Pathogene* 2018;**121**:224.
204. Rajendran NK, Kumar SSD, Houreld NN, Abrahamse H. A review on nanoparticle based treatment for wound healing. *J Drug Delivery Sci Technol* 2018;**44**:421.
205. Chavan C, Kamble S, Murthy A, Kale S. Ampicillin-mediated functionalized gold nanoparticles against ampicillin-resistant bacteria: strategy, preparation and interaction studies. *Nanotechnology* 2020;**31**(21):215604.
206. Guerrini L, Alvarez-Puebla RA, Pazos-Perez N. Surface modifications of nanoparticles for stability in biological fluids. *Materials* 2018;**11**(7):1154.
207. Vanaraj S, Jabastin J, Sathiskumar S, Preethi K. Production and characterization of bio-AuNPs to induce synergistic effect against multidrug resistant bacterial biofilm. *J Cluster Sci* 2017;**28**(1):227.
208. Vijayakumar S, Vaseeharan B, Malaikozhundan B, Gopi N, Ekambaram P, Pachaiappan R, Velusamy P, Murugan K, Benelli G, Kumar RS. Therapeutic effects of gold nanoparticles synthesized using Musa paradisiaca peel extract against multiple antibiotic resistant *Enterococcus faecalis* biofilms and human lung cancer cells (A549). *Microb Pathogene* 2017;**102**:173.
209. Boda SK, Broda J, Schiefer F, Weber-Heynemann J, Hoss M, Simon U, Basu B, Jahnen-Dechent W. Cytotoxicity of ultrasmall gold nanoparticles on planktonic and biofilm encapsulated gram-positive staphylococci. *Small* 2015;**11**(26):3183.
210. Kalita S, Kandimalla R, Bhowal AC, Kotoky J, Kundu S. Functionalization of β-lactam antibiotic on lysozyme capped gold nanoclusters retrogress MRSA and its persisters following awakening. *Scient Reports* 2018;**8**(1):1.
211. Gandhi H, Khan S. Biological synthesis of silver nanoparticles and its antibacterial activity. *J Nanomed Nanotechnol* 2016;**7**(2):1000366.
212. Mohamed MA. Myco-engineered gold nanoparticles from Jahnula aquatica coated with ampicillin/amoxicillin and their antibacterial and anticancer activity against cancer cells. *Biotechnol Lett* 2020;**42**(1):151.
213. Jones N, Ray B, Ranjit KT, Manna AC. Antibacterial activity of ZnO nanoparticle suspensions on a broad spectrum of microorganisms. *FEMS Microbiol Lett* 2008;**279**(1):71.
214. Sirelkhatim A, Mahmud S, Seeni A, Kaus NHM, Ann LC, Bakhori SKM, Hasan H, Mohamad D. Review on zinc oxide nanoparticles: antibacterial activity and toxicity mechanism. *Nano Micro Lett* 2015;**7**(3):219.
215. Liu Y, He L, Mustapha A, Li H, Hu Z, Lin M. Antibacterial activities of zinc oxide nanoparticles against *Escherichia coli* O157: h7. *J Appl Microbiol* 2009;**107**(4):1193.
216. Wang ZL. Zinc oxide nanostructures: growth, properties and applications. *J Phys: Conden Matt* 2004;**16**(25):R829.
217. Zhang L, Ding Y, Povey M, York D. ZnO nanofluids—A potential antibacterial agent. *Prog Natural Sci: Mat Int* 2008;**18**(8):939.
218. El-Rab SMG, Abo-Amer AE, Asiri AM. *Biogenic synthesis of ZnO nanoparticles and its potential use as antimicrobial agent against multidrug-resistant pathogens*. 2020.
219. Aisida SO, Madubuonu N, Alnasir MH, Ahmad I, Botha S, Maaza M, Ezema FI. Biogenic synthesis of iron oxide nanorods using Moringa oleifera leaf extract for antibacterial applications. *Appl Nanosci* 2020;**10**(1):305.
220. Alam T, Khan RAA, Ali A, Sher H, Ullah Z, Ali M. Biogenic synthesis of iron oxide nanoparticles via Skimmia laureola and their antibacterial efficacy against bacterial wilt pathogen Ralstonia solanacearum. *Mat Sci Eng: C* 2019;**98**:101.
221. Naseem T, Farrukh MA. Antibacterial activity of green synthesis of iron nanoparticles using Lawsonia inermis and Gardenia jasminoides leaves extract. *J Chem* 2015;**2015**.
222. Gupta AK, Gupta M. Synthesis and surface engineering of iron oxide nanoparticles for biomedical applications. *Biomaterials* 2005;**26**(18):3995.
223. Makarov VV, Makarova SS, Love AJ, Sinitsyna OV, Dudnik AO, Yaminsky IV, Taliansky ME, Kalinina N. Biosynthesis of stable iron oxide nanoparticles in aqueous extracts of Hordeum vulgare and Rumex acetosa plants. *Langmuir* 2014;**30**(20):5982.

224. Muthukumar H, Chandrasekaran NI, Mohammed SN, Pichiah S, Manickam MJ. Iron oxide nano-material: physicochemical traits and in vitro antibacterial propensity against multidrug resistant bacteria. *J Indus Eng Chem* 2017;**45**:121.
225. Hajipour MJ, Fromm KM, Ashkarran AA, de Aberasturi DJ, de Larramendi IR, Rojo T, Serpooshan V, Parak WJ, Mahmoudi M. Antibacterial properties of nanoparticles. *Trends Biotechnol* 2012;**30**(10):499.
226. Vasantharaj S, Sathiyavimal S, Senthilkumar P, LewisOscar F, Pugazhendhi A. Biosynthesis of iron oxide nanoparticles using leaf extract of Ruellia tuberosa: antimicrobial properties and their applications in photocatalytic degradation. *J Photochem Photobiol B: Biol* 2019;**192**:74.
227. Madivoli ES, Kareru PG, Maina EG, Nyabola AO, Wanakai SI, Nyang'au J. Biosynthesis of iron nanoparticles using Ageratum conyzoides extracts, their antimicrobial and photocatalytic activity. *Appl Sci* 2019;**1**(5):500.
228. Ekthammathat N, Thongtem T, Thongtem S. Antimicrobial activities of CuO films deposited on Cu foils by solution chemistry. *Appl Surf Sci* 2013;**277**:211.
229. Rajivgandhi G, Maruthupandy M, Muneeswaran T, Ramachandran G, Manoharan N, Quero F, Anand M, Song J-M. Biologically synthesized copper oxide nanoparticles enhanced intracellular damage in ciprofloxacin resistant ESBL producing bacteria. *J Anim Morphol Physiol* 2019;**127**:267.
230. Ulloa-Ogaz AL, Piñón-Castillo HA, Muñoz-Castellanos LN, Athie-García MS, Ballinas-Casarrubias MDL, Murillo-Ramirez JG, Flores-Ongay LÁ, Duran R, Orrantia-Borunda E. Oxidative damage to *Pseudomonas aeruginosa* ATCC 27833 and *Staphylococcus aureus* ATCC 24213 induced by CuO-NPs. *Environ Sci Poll Res* 2017;**24**(27):22048.
231. Ashajyothi C, Harish KH, Dubey N, Chandrakanth R. Antibiofilm activity of biogenic copper and zinc oxide nanoparticles-antimicrobials collegiate against multiple drug resistant bacteria: a nanoscale approach. *J Nanostr Chem* 2016;**6**(4):329.
232. Cherian T, Ali K, Saquib Q, Faisal M, Wahab R, Musarrat J. Cymbopogon citratus functionalized green synthesis of CuO-nanoparticles: novel prospects as antibacterial and antibiofilm agents. *Biomolecules* 2020;**10**(2):169.
233. Kruk T, Szczepanowicz K, Stefańska J, Socha RP, Warszyński P. Synthesis and antimicrobial activity of monodisperse copper nanoparticles. *Colloids Surf B: Biointerf* 2015;**128**:17.
234. Meghana S, Kabra P, Chakraborty S, Padmavathy N. Understanding the pathway of antibacterial activity of copper oxide nanoparticles. *RSC Adv* 2015;**5**(16):12293.
235. Trouiller B, Reliene R, Westbrook A, Solaimani P, Schiestl RH. Titanium dioxide nanoparticles induce DNA damage and genetic instability in vivo in mice. *Cancer Res* 2009;**69**(22):8784.
236. Wong M-S, Chu W-C, Sun D-S, Huang H-S, Chen J-H, Tsai P-J, Lin N-T, Yu M-S, Hsu S-F, Wang S-L. Visible-light-induced bactericidal activity of a nitrogen-doped titanium photocatalyst against human pathogens. *Appl Environ Microbiol* 2006;**72**(9):6111.
237. Besinis A, De Peralta T, Handy RD. The antibacterial effects of silver, titanium dioxide and silica dioxide nanoparticles compared to the dental disinfectant chlorhexidine on Streptococcus mutans using a suite of bioassays. *Nanotoxicol* 2014;**8**(1):1.
238. Foster HA, Ditta IB, Varghese S, Steele A. Photocatalytic disinfection using titanium dioxide: spectrum and mechanism of antimicrobial activity. *Appl Microbiol Biotechnol* 2011;**90**(6):1847.
239. Hirakawa K, Mori M, Yoshida M, Oikawa S, Kawanishi S. Photo-irradiated titanium dioxide catalyzes site specific DNA damage via generation of hydrogen peroxide. *Free Radical Res* 2004;**38**(5):439.
240. Manikandan V, Velmurugan P, Jayanthi P, Park J-H, Chang W-S, Park Y-J, Cho M, Oh B-T. Biogenic synthesis from Prunus× yedoensis leaf extract, characterization, and photocatalytic and antibacterial activity of TiO 2 nanoparticles. *Res Chem Intermed* 2018;**44**(4):2489.
241. Santhoshkumar T, Rahuman AA, Jayaseelan C, Rajakumar G, Marimuthu S, Kirthi AV, Velayutham K, Thomas J, Venkatesan J, Kim S-K. Green synthesis of titanium dioxide nanoparticles using Psidium guajava extract and its antibacterial and antioxidant properties. *Asian Pacific J Trop Med* 2014;**7**(12):968.
242. Rajkumari J, Magdalane CM, Siddhardha B, Madhavan J, Ramalingam G, Al-Dhabi NA, Arasu MV, Ghilan A, Duraipandiayan V, Kaviyarasu KJ, et al. Synthesis of titanium oxide nanoparticles using Aloe barbadensis mill and evaluation of its antibiofilm potential against *Pseudomonas aeruginosa* PAO1. *J Photochem Photobiol* 2019;**201**:111667.
243. Subhapriya S, Gomathipriya P. Green synthesis of titanium dioxide (TiO2) nanoparticles by Trigonella foenum-graecum extract and its antimicrobial properties. *Microb Pathegene* 2018;**116**:215.
244. Saha B, Bhattacharya J, Mukherjee A, Ghosh A, Santra C, Dasgupta AK, Karmakar P. In vitro structural and functional evaluation of gold nanoparticles conjugated antibiotics. *Nanoscale Res Lett* 2007;**2**(12):614.

245. Surendra T, Roopan SM, Arasu MV, Al-Dhabi NA, Rayalu GM. RSM optimized Moringa oleifera peel extract for green synthesis of M. oleifera capped palladium nanoparticles with antibacterial and hemolytic property. *J Photochem Photobiol B: Biol* 2016;**162**:550.
246. Surendra T, Roopan SM. Photocatalytic and antibacterial properties of phytosynthesized CeO2 NPs using Moringa oleifera peel extract. *J Photochem Photobiol B: Biol* 2016;**161**:122.
247. Gnanasekar S, Murugaraj J, Dhivyabharathi B, Krishnamoorthy V, Jha PK, Seetharaman P, Vilwanathan R, Sivaperumal S. Antibacterial and cytotoxicity effects of biogenic palladium nanoparticles synthesized using fruit extract of Couroupita guianensis Aubl. *J Appl Biomed* 2018;**16**(1):59.
248. Sharmila G, Fathima MF, Haries S, Geetha S, Kumar NM, Muthukumaran CJ. Green synthesis, characterization and antibacterial efficacy of palladium nanoparticles synthesized using Filicium decipiens leaf extract. *J Mole Struc* 2017;**1138**:35.
249. Sonkusre P, Cameotra SS. Biogenic selenium nanoparticles inhibit *Staphylococcus aureus* adherence on different surfaces. *Colloids Surf B Biointerf* 2015;**136**:1051.
250. Cremonini E, Zonaro E, Donini M, Lampis S, Boaretti M, Dusi S, Melotti P, Lleo MM, Vallini G. Biogenic selenium nanoparticles: characterization, antimicrobial activity and effects on human dendritic cells and fibroblasts. *Microb Biotechnol* 2016;**9**(6):758.
251. Medina Cruz D, Mi G, Webster T. Synthesis and characterization of biogenic selenium nanoparticles with antimicrobial properties made by *Staphylococcus aureus*, methicillin-resistant *Staphylococcus aureus* (MRSA), *Escherichia coli*, and *Pseudomonas aeruginosa*. *J Biomed Mat Res Part A* 2018;**106**(5):1400.
252. Duncan R, Gaspar R. Nanomedicine (s) under the microscope. *Mole Pharmaceut* 2011;**8**(6):2101.
253. Patra JK, Das G, Fraceto LF, Campos EVR, del Pilar Rodriguez-Torres M, Acosta-Torres LS, Diaz-Torres LA, Grillo R, Swamy MK, Sharma S. Nano based drug delivery systems: recent developments and future prospects. *J Nanobiotechnol* 2018;**16**(1):71.
254. Costa JP, Carvalho S, Jesus S, Soares E, Marques AP, Borges O. Optimization of chitosan-α-casein nanoparticles for improved gene delivery: characterization, stability, and transfection efficiency. *AAPS PharmSciTech* 2019;**20**(3):132.
255. Zepeda-Cervantes J, Cruz-Reséndiz A, Sampieri A, Carreón-Nápoles R, Sánchez-Betancourt JI, Vaca L. Incorporation of ORF2 from Porcine Circovirus Type 2 (PCV2) into genetically encoded nanoparticles as a novel vaccine using a self-aggregating peptide. *Vaccine* 2019;**37**(14):1928.
256. Gao J, Xu Y, Zheng Y, Wang X, Li S, Yan G, Wang J, Tang R. pH-sensitive carboxymethyl chitosan hydrogels via acid-labile ortho ester linkage as an implantable drug delivery system. *Carbohydrate Poly* 2019;**225**:115237.
257. Huang C-L, Hsieh W-J, Lin C-W, Yang H-W, Wang C-K. Multifunctional liposomal drug delivery with dual probes of magnetic resonance and fluorescence imaging. *Ceramics Int* 2018;**44**(11):12442.
258. Krauel K, Pitaksuteepong T, Davies NM, Rades T. Entrapment of bioactive molecules in poly (alkylcyanoacrylate) nanoparticles. *American J Drug Delivery* 2004;**2**(4):251.
259. Mirza AZ, Siddiqui FA. Nanomedicine and drug delivery: a mini review. *Int Nano Lett* 2014;**4**(1):94.
260. Blanco E, Shen H, Ferrari M. Principles of nanoparticle design for overcoming biological barriers to drug delivery. *Nature Biotechnol* 2015;**33**(9):941.
261. Kumari A, Kumar V, Yadav S. Nanotechnology: a tool to enhance therapeutic values of natural plant products. *Trends Med Res* 2012;**7**(2):34.
262. Khan A, Rashid R, Murtaza G, Zahra A. Gold nanoparticles: synthesis and applications in drug delivery. *Trop J Pharmaceut Res* 2014;**13**(7):1169.
263. Sengani M, Grumezescu AM, Rajeswari VD. Recent trends and methodologies in gold nanoparticle synthesis—A prospective review on drug delivery aspect. *OpenNano* 2017;**2**:37.
264. López-Viota J, Mandal S, Delgado AV, Toca-Herrera JL, Möller M, Zanuttin F, Balestrino M, Krol S. Electrophoretic characterization of gold nanoparticles functionalized with human serum albumin (HSA) and creatine. *J Colloid Interf Sci* 2009;**332**(1):215.
265. Brown AN, Smith K, Samuels TA, Lu J, Obare SO, Scott ME. Nanoparticles functionalized with ampicillin destroy multiple-antibiotic-resistant isolates of *Pseudomonas aeruginosa* and Enterobacter aerogenes and methicillin-resistant *Staphylococcus aureus*. *Appl Environ Microbiol* 2012;**78**(8):2768.
266. Bhattacharya D, Saha B, Mukherjee A, Santra CR, Karmakar P. Gold nanoparticles conjugated antibiotics: stability and functional evaluation. *Nanosci Nanotechnol* 2012;**2**(2):14.
267. Guo R, Li R, Li X, Zhang L, Jiang X, Liu B. Dual-functional alginic acid hybrid nanospheres for cell imaging and drug delivery. *Small* 2009;**5**(6):709.

268. Xia H, Gao Y, Yin L, Cheng X, Wang A, Zhao M, Ding J, Shi H. Light-Triggered covalent coupling of gold nanoparticles for photothermal cancer therapy. *ChemBioChem* 2019;**20**(5):667.
269. Dhanya G, Caroline D, Rekha M, Sreenivasan K. Histidine and arginine conjugated starch-PEI and its corresponding gold nanoparticles for gene delivery. *Int J Biolog Macromole* 2018;**120**:999.
270. Munsell EV, Fang B, Sullivan MO. Histone-mimetic gold nanoparticles as versatile scaffolds for gene transfer and chromatin analysis. *Bioconjugate Chem* 2018;**29**(11):3691.
271. Poletaeva J, Dovydenko I, Epanchintseva A, Korchagina K, Pyshnyi D, Apartsin E, Ryabchikova E, Pyshnaya I. Non-covalent associates of siRNAs and AuNPs enveloped with lipid layer and doped with amphiphilic peptide for efficient siRNA delivery. *Int J Mole Sci* 2018;**19**(7):2096.
272. Du B, Gu X, Han X, Ding G, Wang Y, Li D, Wang E, Wang J. Lipid-coated gold nanoparticles functionalized by folic acid as gene vectors for targeted gene delivery in vitro and in vivo. *ChemMedChem* 2017;**12**(21):1768.
273. Jain TK, Reddy MK, Morales MA, Leslie-Pelecky DL, Labhasetwar V. Biodistribution, clearance, and biocompatibility of iron oxide magnetic nanoparticles in rats. *Mole Pharmaceut* 2008;**5**(2):316.
274. Manivasagan P, Bharathiraja S, Bui NQ, Lim IG, Oh J. *Paclitaxel-loaded chitosan oligosaccharide-stabilized gold nanoparticles as novel agents for drug delivery and photoacoustic imaging of cancer cells* 2016;**511**(1):367−79.
275. Weissleder R, Elizondo G, Wittenberg J, Rabito C, Bengele H, Josephson L. Ultrasmall superparamagnetic iron oxide: characterization of a new class of contrast agents for MR imaging. *Radiology* 1990;**175**(2):489.
276. Chang C-C, Chen C-P, Wu T-H, Yang C-H, Lin C-W, Chen C-Y. Gold nanoparticle-based colorimetric strategies for chemical and biological sensing applications. *Nanomaterials* 2019;**9**(6):861.
277. Sun J, Lu Y, He L, Pang J, Yang F, Liu Y. Colorimetric sensor array based on gold nanoparticles: design principles and recent advances. *TrAc Trends Analy Chem* 2019:115754.
278. Zhang G. Functional gold nanoparticles for sensing applications. *Nanotechnol Rev* 2013;**2**(3):269.
279. Qian X-M, Nie SM. Single-molecule and single-nanoparticle SERS: from fundamental mechanisms to biomedical applications. *J Coll Stud Retent* 2008;**37**(5):912.
280. Zhou B, Zheng L, Peng C, Li D, Li J, Wen S, Shen M, Zhang G, Shi X. Synthesis and characterization of PEGylated polyethylenimine-entrapped gold nanoparticles for blood pool and tumor CT imaging. *ACS Appl Mat Interf* 2014;**6**(19):17190.
281. Yaghoobi F, Torabi M, Kefayat A, Ghahremani F, Farzadniya A. Therapeutic effect of deferrioxamine conjugated to PEGylated gold nanoparticles and complexed with Mn (II) beside the CT scan and MRI diagnostic studies. *Colloids Surf A: Physicochem Eng Aspects* 2019;**583**:123917.
282. Huang X, El-Sayed MA. Gold nanoparticles: optical properties and implementations in cancer diagnosis and photothermal therapy. *J Adv Res* 2010;**1**(1):13.
283. Tabrizi MA, Shamsipur M, Saber R, Sarkar S, Sherkatkhameneh N. Flow injection amperometric sandwich-type electrochemical aptasensor for the determination of adenocarcinoma gastric cancer cell using aptamer-Au@ Ag nanoparticles as labeled aptamer. *Electrochimca Acta* 2017;**246**:1147.
284. Tabrizi MA, Shamsipur M, Saber R, Sarkar S. Flow injection amperometric sandwich-type aptasensor for the determination of human leukemic lymphoblast cancer cells using mwcnts-pdnano/ptca/aptamer as labeled aptamer for the signal amplification. *Analy Chimica Acta* 2017;**985**:61.
285. Song M, Wang X, Li J, Zhang R, Chen B, Fu D. Effect of surface chemistry modification of functional gold nanoparticles on the drug accumulation of cancer cells. *J Biomed Mat Res* 2008;**86**(4):942.
286. Sayyadi K, Rahdar A, Esmaili N, Sayyadi J. Application of gold nanoparticles in cancer diagnosis and therapy: a mini-review. *Adv Nanochem* 2019;**1**(2):47.
287. Strassburg MA. The global eradication of smallpox. *American J Infect Control* 1982;**10**(2):53.
288. World Health Organization (WHO). 2018 assessment report of the Global Vaccine Action Plan: strategic advisory group of experts on immunization. *World Health Organization* 2018.
289. Serda RE. Particle platforms for cancer immunotherapy. *Int J Nanomed* 2013;**8**:1683.
290. Look M, Bandyopadhyay A, Blum JS, Fahmy T. Application of nanotechnologies for improved immune response against infectious diseases in the developing world. *Adv Drug Delivery Rev* 2010;**62**(4−5):378.
291. Germain RN. Vaccines and the future of human immunology. *Immunity* 2010;**33**(4):441.
292. Rappuoli R, Aderem A. A 2020 vision for vaccines against HIV, tuberculosis and malaria. *Nature* 2011;**473**(7348):463.
293. van der Burg SH, Arens R, Ossendorp F, van Hall T, Melief C. Vaccines for established cancer: overcoming the challenges posed by immune evasion. *Nat Rev Cancer* 2016;**16**(4):219.
294. Mehrabi M, Dounighi NM, Mohammadi M, Masoudi A. Nanoparticles and vaccine development. *Pharmaceut Nanotechnol* 2020;**8**(1):6.

295. Borges O, Cordeiro-da-Silva A, Romeijn SG, Amidi M, de Sousa A, Borchard G, Junginger HE. Uptake studies in rat Peyer's patches, cytotoxicity and release studies of alginate coated chitosan nanoparticles for mucosal vaccination. *J Controlled Rel* 2006;**114**(3):348.
296. Horisawa E, Kubota K, Tuboi I, Sato K, Yamamoto H, Takeuchi H, Kawashima Y. Size-dependency of DL-lactide/glycolide copolymer particulates for intra-articular delivery system on phagocytosis in rat synovium. *Pharmaceut Res* 2002;**19**(2):132.
297. Mahony D, Cavallaro AS, Stahr F, Mahony TJ, Qiao SZ, Mitter N. Mesoporous silica nanoparticles act as a self-adjuvant for ovalbumin model antigen in mice. *Small* 2013;**9**(18):3138.
298. Oussoren C, Storm G. Liposomes to target the lymphatics by subcutaneous administration. *Adv Drug Delivery Rev* 2001;**50**(1−2):143.
299. Wang J, Byrne JD, Napier ME, DeSimone J. More effective nanomedicines through particle design. *Small* 2011;**7**(14):1919.
300. Wang C, Ge Q, Ting D, Nguyen D, Shen H-R, Chen J, Eisen HN, Heller J, Langer R, Putnam D. Molecularly engineered poly (ortho ester) microspheres for enhanced delivery of DNA vaccines. *Nat Mat* 2004;**3**(3):190.
301. Kuai R, Sun X, Yuan W, Xu Y, Schwendeman A, Moon J. Subcutaneous nanodisc vaccination with neoantigens for combination cancer immunotherapy. *Bioconjugate Chem* 2018;**29**(3):771.
302. Hess KL, Medintz IL, Jewell CM. Designing inorganic nanomaterials for vaccines and immunotherapies. *Nano Today* 2019;**27**:73−98.
303. Hu Z, Song B, Xu L, Zhong Y, Peng F, Ji X, Zhu F, Yang C, Zhou J, Su Y. Aqueous synthesized quantum dots interfere with the NF-κB pathway and confer anti-tumor, anti-viral and anti-inflammatory effects. *Biomaterials* 2016;**108**:187.
304. Pusic K, Aguilar Z, McLoughlin J, Kobuch S, Xu H, Tsang M, Wang A, Hui G. Iron oxide nanoparticles as a clinically acceptable delivery platform for a recombinant blood-stage human malaria vaccine. *FASEB J* 2013;**27**(3):1153.
305. Versiani AF, Astigarraga RG, Rocha ES, Barboza APM, Kroon EG, Rachid MA, Souza DG, Ladeira LO, Barbosa-Stancioli EF, Jorio A. Multi-walled carbon nanotubes functionalized with recombinant Dengue virus 3 envelope proteins induce significant and specific immune responses in mice. *J Nanobiotechnol* 2017;**15**(1):26.
306. Zhao K, Rong G, Guo C, Luo X, Kang H, Sun Y, Dai C, Wang X, Wang X, Jin Z. Synthesis, characterization, and immune efficacy of layered double hydroxide@ SiO2 nanoparticles with shell-core structure as a delivery carrier for Newcastle disease virus DNA vaccine. *Int J Nanomed* 2015;**10**:2895.
307. Zhou Q, Zhang Y, Du J, Li Y, Zhou Y, Fu Q, Zhang J, Wang X, Zhan L. Different-sized gold nanoparticle activator/antigen increases dendritic cells accumulation in liver-draining lymph nodes and CD8+ T cell responses. *ACS Nano* 2016;**10**(2):2678.
308. Shi C, Yu H, Sun D, Ma L, Tang Z, Xiao Q, Chen X. Cisplatin-loaded polymeric nanoparticles: characterization and potential exploitation for the treatment of non-small cell lung carcinoma. *Acta Biomater* 2015;**18**:68.
309. Farooq MA, Aquib M, Farooq A, Haleem Khan D, Joelle Maviah MB, Sied Filli M, Kesse S, Boakye-Yiadom KO, Mavlyanova R, Parveen A, et al. Recent progress in nanotechnology-based novel drug delivery systems in designing of cisplatin for cancer therapy: an overview. *Arti Cells Nanomed Biotechnol* 2019;**47**(1):1674.
310. Dhakal S, Hiremath J, Bondra K, Lakshmanappa YS, Shyu D-L, Ouyang K, Kang K-i, Binjawadagi B, Goodman J, Tabynov K. Biodegradable nanoparticle delivery of inactivated swine influenza virus vaccine provides heterologous cell-mediated immune response in pigs. *J Controlled Res* 2017;**247**:194.
311. Jaafar-Maalej C, Elaissari A, Fessi H. Lipid-based carriers: manufacturing and applications for pulmonary route 2012;**9**(9):1111−27.
312. Raghuwanshi D, Mishra V, Das D, Kaur K, Suresh MR. Dendritic cell targeted chitosan nanoparticles for nasal DNA immunization against SARS CoV nucleocapsid protein. *Mole Pharmaceut* 2012;**9**(4):946.
313. Pati R, Shevtsov M, Sonawane A. Nanoparticle vaccines against infectious diseases. *Front Immunol* 2018;**9**:2224.
314. Fu B, Huang X, Deng J, Gu D, Mei Q, Deng M, Tang S, Lü M. Application of multifunctional nanomaterials in cancer vaccines. *Oncol Reports* 2018;**39**(3):893.
315. Climent N, García I, Marradi M, Chiodo F, Miralles L, Maleno MJ, et al. Loading dendritic cells with gold nanoparticles (GNPs) bearing HIV-peptides and mannosides enhance HIV-specific T cell responses. *Nanomedicine: Nanotechnology, Biology and Medicine* 2018;**14**(2):339−51.
316. Assis NR, Caires AJ, Figueiredo BC, Morais SB, Mambelli FS, Marinho FV, Ladeira LO, Oliveira SC. The use of gold nanorods as a new vaccine platform against schistosomiasis. *J Control Res* 2018;**275**:40.

317. Calderon-Gonzalez R, Frande-Cabanes E, Teran-Navarro H, Marimon JM, Freire J, Salcines-Cuevas D, Fariñas MC. Gnp-gapdh1-22 nanovaccines prevent neonatal listeriosis by blocking microglial apoptosis and bacterial dissemination. *Oncotarget* 2017;**8**(33):53916.
318. Gianvincenzo PD, Calvo J, Perez S, Álvarez A, Bedoya LM, Alcamí J, Penadés S. Negatively charged glyconanoparticles modulate and stabilize the secondary structures of a gp120 V3 loop peptide: toward fully synthetic HIV vaccine candidates. *Bioconjugate Chem* 2015;**26**(4):755.
319. Kaba SA, Brando C, Guo Q, Mittelholzer C, Raman S, Tropel D, Aebi U, Burkhard P, Lanar DE. A nonadjuvanted polypeptide nanoparticle vaccine confers long-lasting protection against rodent malaria. *J Immunol* 2009;**183**(11):7268.
320. Chen Y-S, Hung Y-C, Lin W-H, Huang GS. Assessment of gold nanoparticles as a size-dependent vaccine carrier for enhancing the antibody response against synthetic foot-and-mouth disease virus peptide. *Nanotechnology* 2010;**21**(19):195101.
321. Gregory AE, Judy BM, Qazi O, Blumentritt CA, Brown KA, Shaw AM, Torres AG, Titball RW. A gold nanoparticle-linked glycoconjugate vaccine against Burkholderia mallei. *Nanomed Nanotechnol Biol Med* 2015;**11**(2):447.
322. De Titta A, Ballester M, Julier Z, Nembrini C, Jeanbart L, Van Der Vlies AJ, Swartz MA, Hubbell JA. Nanoparticle conjugation of CpG enhances adjuvancy for cellular immunity and memory recall at low dose. *Proceed Nat Acad Sci* 2013;**110**(49):19902.
323. Mejías R, Pérez-Yagüe S, Gutiérrez L, Cabrera LI, Spada R, Acedo P, Serna CJ, Lázaro FJ, Villanueva Á, del Puerto Morales M. Dimercaptosuccinic acid-coated magnetite nanoparticles for magnetically guided in vivo delivery of interferon gamma for cancer immunotherapy. *Biomaterials* 2011;**32**(11):2938.
324. Moore A, Grimm J, Han B, Santamaria P. Tracking the recruitment of diabetogenic CD8+ T-cells to the pancreas in real time. *Diabetes* 2004;**53**(6):1459.
325. Cho N-H, Cheong T-C, Min JH, Wu JH, Lee SJ, Kim D, Yang J-S, Kim S, Kim YK, Seong S-Y. A multifunctional core−shell nanoparticle for dendritic cell-based cancer immunotherapy. *Nat Nanotechnol* 2011;**6**(10):675.
326. Gericke M, Pinches A. Biological synthesis of metal nanoparticles. *Hydrometallurgy* 2006;**83**(1−4):132.
327. Duan L, Li M, Liu H. Biosynthesised palladium nanoparticles using Eucommia ulmoides bark aqueous extract and their catalytic activity. *IET Nanotechnol* 2015;**9**(6):349.
328. Khan M, Albalawi GH, Shaik MR, Khan M, Adil SF, Kuniyil M, Alkhathlan HZ, Al-Warthan A, Siddiqui MRH. Miswak mediated green synthesized palladium nanoparticles as effective catalysts for the Suzuki coupling reactions in aqueous media. *J Saudi Chem Soc* 2017;**21**(4):450.
329. Akbar S, Tauseef I, Subhan F, Sultana N, Khan I, Ahmed U, Haleem KS. An overview of the plant-mediated synthesis of zinc oxide nanoparticles and their antimicrobial potential. *Inorg Nano-Metal Chem* 2020;**1**.
330. Butoescu N, Jordan O, Burdet P, Stadelmann P, Petri-Fink A, Hofmann H, Doelker E. Dexamethasone-containing biodegradable superparamagnetic microparticles for intra-articular administration: physicochemical and magnetic properties, in vitro and in vivo drug release. *European J Pharmac Biopharmac* 2009;**72**(3):529.

This page intentionally left blank

CHAPTER

28

Polymeric nanoparticles for biomedical applications

S. Malathi[1,2], *S. Narayana Kalkura*[2] *and S. Balasubramanian*[1]

[1]Department of Inorganic Chemistry, University of Madras, Chennai, Tamil Nadu, India; [2]Crystal Growth Centre, Anna University, Chennai, Tamil Nadu, India

1. Introduction

Cancer includes a range of diseases that arise as a result of the unregulated growth of malignant cells, which have the potential to invade or spread to other body parts. According to American Cancer Society statistics, 1.8 million new cancer cases have been diagnosed, and 606,520 cancer deaths are estimated for 2020 in the United States.[1] The term "cancer" refers to uncontrolled cellular growth and multiplication resulting from a cell phenotype that produces growth signals and is insensitive to antigrowth signals. Such cells have unlimited replicative potential, evade apoptosis, induce angiogenesis, and stimulate invasion and metastasis.[2] There are many types of cancer with few typical or common characteristics, so its treatment is incredibly challenging. Most chemotherapy drugs in the market are difficult to administer directly, and many are toxic to healthy tissues and produce undesirable side effects. To overcome these limitations, recent advances in nanoparticle-based cancer drug delivery present a promising strategy to achieve high therapeutic efficiency of anticancer agents by providing protection during circulation and enhancing their bioavailability.[3] Nanotechnology is the science that usually deals with the size range from a few manometers (nm) to several hundred nm, depending on their intended use.[4] It has been the area of interest over the last decade for developing precise drug delivery systems as it offers numerous benefits to overcome the limitations of conventional formulations.[5,6] It is very promising both in cancer diagnosis and treatment since it can enter the tissues at molecular level. Nanoparticles are attractive vehicles for anticancer agents, because of their controlled drug release and tumor selective properties.

Applications of Multifunctional Nanomaterials
https://doi.org/10.1016/B978-0-12-820557-0.00028-X

Although a variety of nanoplatforms is currently available, nanoparticle fabrication using natural or synthetic biodegradable polymeric nanomaterials has attracted much attention in drug delivery research because of their ability to precisely control and allow sustained release of encapsulated drugs. The most employed polymers are PLGA, PLA, PGA, PCL, poly (D, L-lactide), chitosan, and PLGA-PEG.[7–11] PLGA has been in safe clinical use since its approval by the FDA in 1969. PLGA particles for drug release were approved in 1989 (Lupron Depot) and since then have been commonly used due to their controlled release properties for eliciting a persistent therapeutic effect.[12] PLGA nanoparticles can be prepared using an emulsion solvent diffusion method, where during the particle preparation process, target drugs can be effectively entrapped in the precipitated rigid core of nanoparticles. PLGA nanoparticles are attractive candidates for tumor targeted therapy and imaging. Incorporating and encapsulating drugs in PLGA matrices enables their slow release over a prolonged period of time, which leads to a reduced frequency of dose administration, reduced discomfort, and peak associated adverse effects. This results in protection of the drug or bioactive principle within the body, and maintenance of its more constant blood levels. These benefits eventually increase overall patient compliance. Among different polymers, poly (lactic-co-glycolic) acid [PLGA] has been extensively used in biomedical applications. Another important benefit of using polymers and nanoparticles as drug carriers derives from their ability to increase the water solubility of hydrophobic drugs, extend the circulation of drugs in the blood, and suppress or eliminate fast renal excretion. Together, the use of drug carriers dramatically increases organ or cell-specific drug accumulation[13,14] and opens up the possibility of controlled activation (i.e., release) of the delivered drug where the therapeutic effect is required, for example, in tumor cells. Selective activation in this way could prevent the drug's toxicity from affecting normal tissues and cells, mitigating or eliminating any harmful side effects it might otherwise have.

Curcuma longa is a medicinal plant that has been used in traditional Chinese and Indian Ayurvedic medicines for thousands of years.[15] The potential anticancer properties of curcumin were first reported in 1985, where investigators found both turmeric extract and pure curcumin were cytotoxic to human lymphocytes, leukemic cells, and Dalton's lymphoma cells. In this report, the authors concluded that the cytotoxic component found in the turmeric extract was curcumin.[16] Curcumin has been studied as a therapeutic agent for a multitude of disorders including inflammatory and autoimmune conditions, diabetes, skin conditions, neurological and psychiatric disorders, and cancer.[17] Several in vitro investigations demonstrate that curcumin inhibits cancer cells growth (IC50; 50% cell growth inhibition) at concentration of 5–30 μM,[18–21] resembling cisplatin and gem-citabine (chemotherapeutic drug) concentrations. Because of its exceptional medicinal value, a total of 68 clinical trials have been registered with clinicaltrials.gov (as of April 16, 2020) in which most of them are targeting cancer. Curcumin has an extremely safe profile in both animals and humans.[22,23] So far, all the preclinical and clinical results from oral administration of curcumin have revealed extremely poor bioavailability, typically in nanomolar concentrations.[24–26] A classic example is a pharmacokinetic study involving healthy humans which found that only 1.73 ± 0.19 and 2.30 ± 0.26 μg mL^{-1} of curcumin (Cmax) was present in serum levels even after a high oral dose of 10 and 20 g curcumin, respectively.[27] This suggests curcumin undergoes extensive

metabolic changes in the intestine and liver. Polymeric nanoparticles were used to overcome these issues.[28–31]

This chapter summarizes the recent development and application of PLGA/curcumin nanoformulations in anticancer therapy. We first discuss about PLGA synthesis and their physicochemical properties and fabrication of PLGA nanoparticles and curcumin-loaded PLGA nanoparticles and highlighting their functional properties toward different cancer types. In this chapter, we have given an overview of research in the field of anticancer drug delivery using PLGA nanocarriers and hurdles that need to be overcome.

2. Synthesis of PLGA copolymer

The poly (lactic-co-glycolic) acid (PLGA) was prepared by modifying the procedure reported by Wang et al.[32] PLGA can be synthesized by melt-polycondensation and ring-opening polymerization. The process for the preparation of PLGA has a strong influence on the physicochemical properties of the resultant product. A general schematic representation of various steps of the experimental protocol to the synthesis of PLGA copolymer is indicated in Fig. 28.1. In the present investigation three different catalysts, viz., tin powder, stannous chloride, and stannous octoate were used for PLGA copolymer synthesis.

The low molecular weight PLGA copolymers synthesized by simple modification by melt poly condensation have been reported by Ajioka et al.[33] The synthesis of copolymers of DL-lactic acid and glycolic acid is illustrated in Fig. 28.2. In this method, PLGA with high molecular weight can be prepared after a relatively long reaction period at 130°C under high vacuum in diphenyl ether medium. However, removal of the solvent from the final product is difficult, and hence the product is likely to be contaminated with the solvent. Thus, it was thought that polycondensation should preferably be carried out in the limitations arising from the use of azeotropic solvents[34–36].

The alternate protocol (Fig. 28.3) in which stannous chloride was employed as a catalyst without azeotropic distillation was adopted. The yield of PLGA is comparatively low in this method when compared to that of stannous octoate as a catalyst (Fig. 28.4). Stannous octoate is preferred for biomedical applications because of the high reaction rate of the polymerization, the low degree of racemization even at high temperatures and its low toxicity.[37,38] $Sn(oct)_2$ is a highly efficient commercial catalyst and a food additive permitted in numerous countries.[39] Although there are a variety of catalysts available such as antimony compounds, zinc compounds, and alkoxides, stannous octoate is preferred because it is approved by the FDA as a food stabilizer.[40] In addition, stannous octoate is commercially available, easy to handle and soluble in common organic solvents and cyclic monomers. The PLGA was obtained by direct melt polycondensation of DL-lactic acid and glycolic acid through esterification mechanism initiated by $Sn(oct)_2$ under high vacuum (Fig. 28.4). The PLGA copolymers are freely soluble in chloroform, tetrahydrofuran, dichloromethane, toluene, and dimethyl sulfoxide.

However, these copolymers are partially soluble in solvents such as dimethyl formamide, ethanol, methanol, and acetone and are completely insoluble in diethyl ether and water. Drug delivery using di-block PLGA copolymers invariably makes use of medium and high

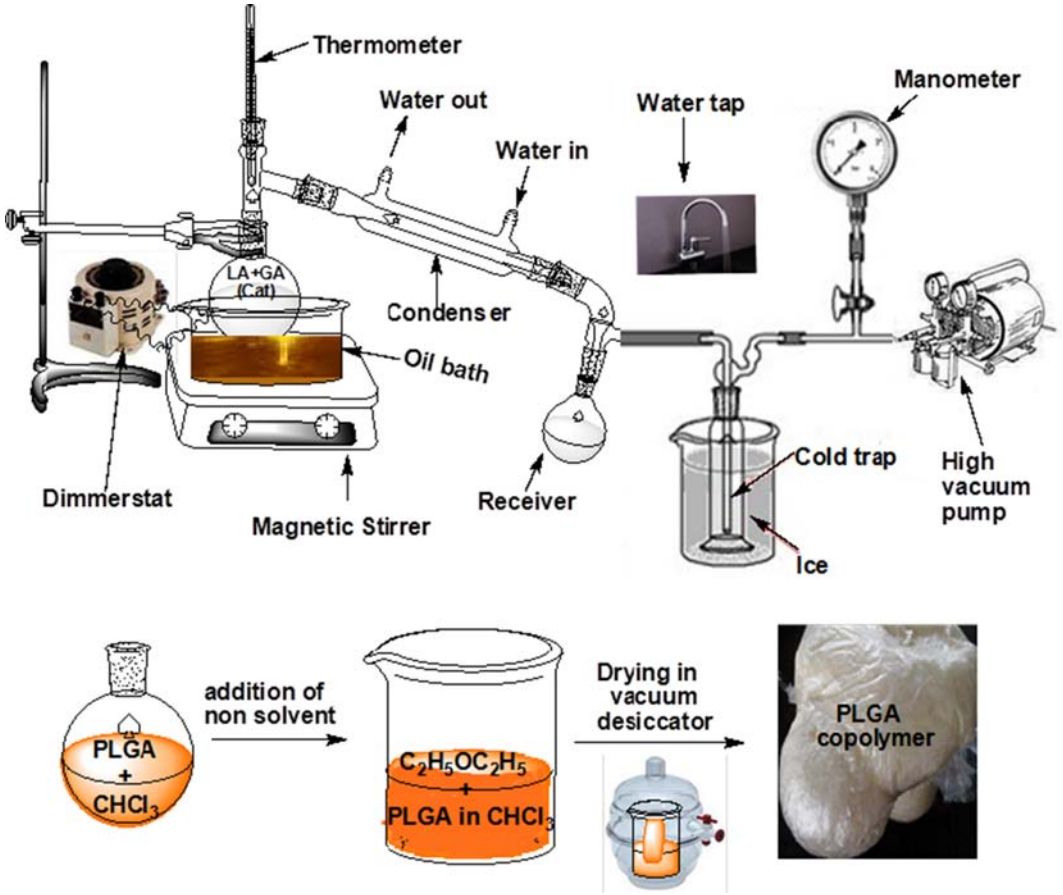

FIGURE 28.1 Schematic representation of synthesis of PLGA copolymer.

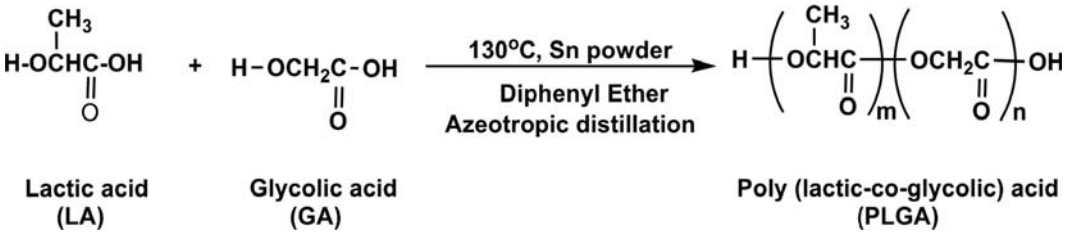

FIGURE 28.2 Schematic representation of synthesis of PLGA copolymer using Sn powder catalyst.

molecular weight (20–70 KDa) systems. However, the drug loading and release behavior profile of both hydrophilic and hydrophobic drugs with low molecular weight polymeric systems have not been explored yet. Besides, in most of the studies the PLGA copolymer with only 50/50 ratio has been employed and the efficacy of these systems with other LA, GA ratios has not been completely understood.

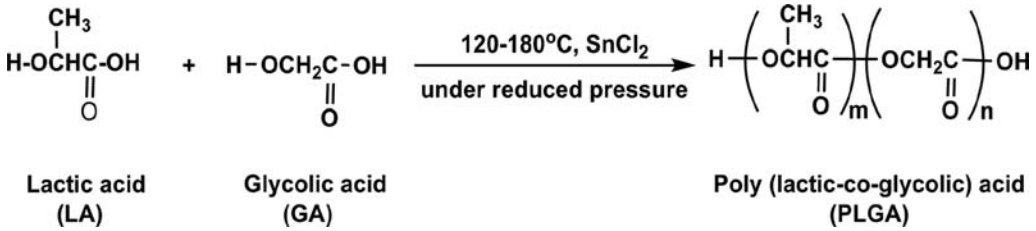

FIGURE 28.3 Schematic representation of synthesis of PLGA copolymer using SnCl2 catalyst.

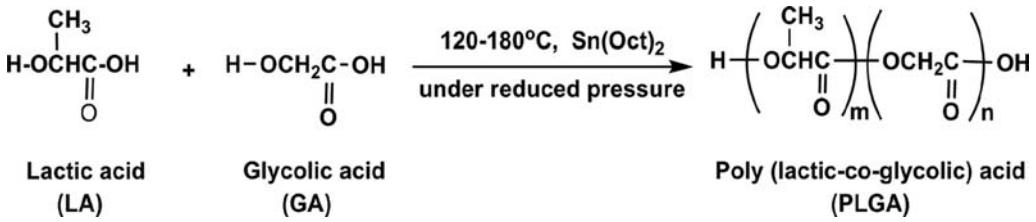

FIGURE 28.4 Schematic representation of synthesis of PLGA copolymer using $Sn(oct)_2$ catalyst.

The optimized method to prepare 10 different ratios of PLGA, viz., PLG1:95/05, PLG2:90/10, PLG3:85/15, PLG4:80/20, PLG5:75/25, PLG6:70/30, PLG7:65/35, PLG8:60/40, PLG9:55/45, and PLG10:50/50 is provided in Fig. 28.4. Wu et al. have reported a series of PLGA copolymers with various molar ratios of lactic to glycolic acid (85/15, 75/25 and 65/35) with different molecular weights (13,000−14,000).[41]

3. Characteristics of PLGA

PLGA is a copolymer of lactic acid and glycolic acid, and it is accepted by the food and drug administration (FDA) of the United States, owing to its biodegradability and biocompatibility. Poly (lactic-co-glycolic acid) (PLGA) PLGA copolymers are aliphatic polyesters composed of varying proportions of lactic and glycolic acids. Different PLGA products are available in the market. PLGA is the most frequently used biodegradable polymer in the controlled (Drug Delivery Systems) DDSs. PLGA with less than 70% lactic acid will be amorphous in nature, which is preferable for controlled drug release applications because of its low mechanical strength and high biodegradability where increased lactic acid percentage (>70%) often results in crystalline PLGA with high mechanical strength for use in other biomedical and tissue engineering applications.[42]

Molecular weight and polydispersity index are the key factors which influence the mechanical strength of PLGA as well as its ability to be formulated as a drug delivery carrier and controlling its degradation rate and hydrolysis. However, the type of drug being used also affects the release rate. Crystallinity also affects swelling behavior, mechanical strength, and capacity to undergo hydrolysis, as well as biodegradation rate. PLGA has an inherent viscosity of 0.5−0.8 mPa. PLGA copolymers are largely amorphous and exhibit a glass

transition temperature (Tg) in the range of 40−60°C. It shows glassy behavior and possesses a rigid chain structure. PLGA can be processed into any shape and size and is capable of encapsulating molecules of varied sizes[43−45]. PLGA is readily soluble in most of the organic solvents. When the more crystalline PGA is copolymerized with PLA, the resultant PLGA has a lower degree of crystallinity and a higher hydration rate and hydrolysis. Assuming generalization, the higher the PGA content, the faster is the degradation. However, PLGA (50:50) does not comply with this rule and exhibits faster degradation. Boury et al. have investigated bovine serum albumin (BSA) release from 10 μm microspheres prepared with 50:50 PLGA of two different molecular weights (15 and 87 kDa). A quasi-absence of burst effect was observed with the lowest molecular weight polymer, but it was followed by an incomplete release after 1 month. With the higher molecular weight PLGA, a high initial release of BSA was recorded in the first hours and thereafter, the remainder of the encapsulated BSA was completely released over the following 15 days.[46] Makino et al. showed pulsatile drug release in high molecular weight PLGAs. At lower molecular weight (19,000), a relatively constant release profile was obtained; increasing molecular weight to 23,000−44,000 and 74,000 decreased the linearity of release.[47]

The degree of crystallinity and melting point is related to molecular weight. Commercially available PLGA polymers are usually characterized in terms of intrinsic viscosity, which is directly related to their molecular weight.[43,45,48] PLGA is known to be a biocompatible and nontoxic polymer. These properties were first established by the production of biodegradable sutures. Dexon (PGA) and Vicryl L-PLGA (8:92) are biodegradable sutures that have a history of clinical use older than 30 years. The physicochemical properties of a polymer affect the host response to a polymeric implant. PLGA implantation studies in the bone or soft tissues of animals have shown either nil or very mild inflammatory responses that ease out with time. Thus, no toxicity or allergic responses were reported with PLGA.[45,49−51] The following are lead suppliers of Good Manufacturing Practice (GMP) grade PLA, PGA, and PLGA: Purac, Birmingham Polymers, Boehringer Ingelheim, Alkermes, Sigma Aldrich Chemical Company and Polyscience. Other suppliers include Mitsui Chemicals, cater to local niche markets. Birmingham polymers have a range of PLGA copolymers priced at approximately $38−47 per gram. PLA and PLGA represent nontraditional excipients in the pharmaceutical industry. While the present demand for these polymers is limited, a significant growth potential exists, primarily driven by the development and advances in PLGA drug delivery systems. The first FDA-cleared PLGA product was the Lupron Depot drug-delivery system (TAP Pharmaceutical Products, Lake Forest, Illinois) a controlled release device for the treatment of advanced prostate cancer that used biodegradable microspheres of 75:25 lactide/glycolide to administer leuprolide acetate over a period of 4 months (replacing daily injections).

4. Method of preparation of PLGA nanoparticles

Several methods for polymeric nanoparticle production have been developed, which generally include two main steps. The first step is to prepare an emulsified system, and this is common to all the methods used. The nanoparticles are formed during the second step, which varies according to the method used. In general, the principle of the second

step gives its name to the method. Some methods do not require the preparation of an emulsion prior to obtaining the nanoparticles and are based on spontaneous precipitation of a polymer or through self-assembly of macromolecules.[52] The commonly used methods for preparation of PLGA nanoparticles are:

1. Emulsification solvent evaporation[53]
2. Emulsification solvent diffusion[54]
3. Emulsification reverse salting-out[54]
4. Nanoprecipitation[55]

The emulsification solvent evaporation is one of the most frequently used methods among the above methods.

4.1 Emulsion solvent evaporation

4.1.1 Single (oil/water) evaporation method

In the single emulsion method (oil-in water), PLGA is gradually first dissolved in dichloromethane, which constitutes the organic phase.[56–63] Hydrophobic drug is added to this organic phase in a glass tube. The tube is vortexed until the drug is homogenously dispersed. Then this solution is added to a large volume of water in the presence an emulsifier or capping agent (e.g., polyvinyl alcohol [PVA], Tocopherol polyethylene glycol 1000 succinate [TPGS], Polyethylene glycol [PEG]) and homogenized using an Ultra-Turrax homogenizer or by using an ultrasonicator at 0°C. After this step, the emulsion is poured into a beaker and stirred uncovered with a magnetic stirrer until the organic solvent is completely evaporated at room temperature. This process allows the nanoparticles to harden. Once the organic solvents are removed, the nanoparticles are collected by repeated centrifugation and/or dialysis.

4.1.2 Double emulsion (water/oil/water) evaporation method

In the double emulsion method,[64–74] aqueous phase is prepared by dissolving an appropriate amount of the hydrophilic drug in deionized water. Then this solution is added dropwise into the organic phase containing PLGA polymer dissolved in organic solvent under high-speed vortexing/stirring to obtain a water-in-oil primary emulsion. This primary emulsion is then added to an aqueous solution containing emulsifier (e.g., PVA, PEG, TPGS), and ultrasonicated in an ice bath or homogenized at high-speed using Ultra Turrax for the appropriate time. The organic solvent is then allowed to evaporate, as described in the single emulsion procedure. The nanoparticles are then washed, centrifuged, lyophilized, and collected. It is important to note that the choice of organic solvents, emulsifier concentration, and stirring speed will impact the final nanoparticle size and drug loading. Fig. 28.5 shows the schematic illustration of hydrophilic drug-encapsulated PLGA nanoparticles synthesis using water-oil-water emulsion method.

4.2 Properties of PLGA nanoparticles

Characterization becomes a prerequisite for understanding the properties of the nanoparticles. Several parameters can provide insight into the properties of the nanoparticles. First

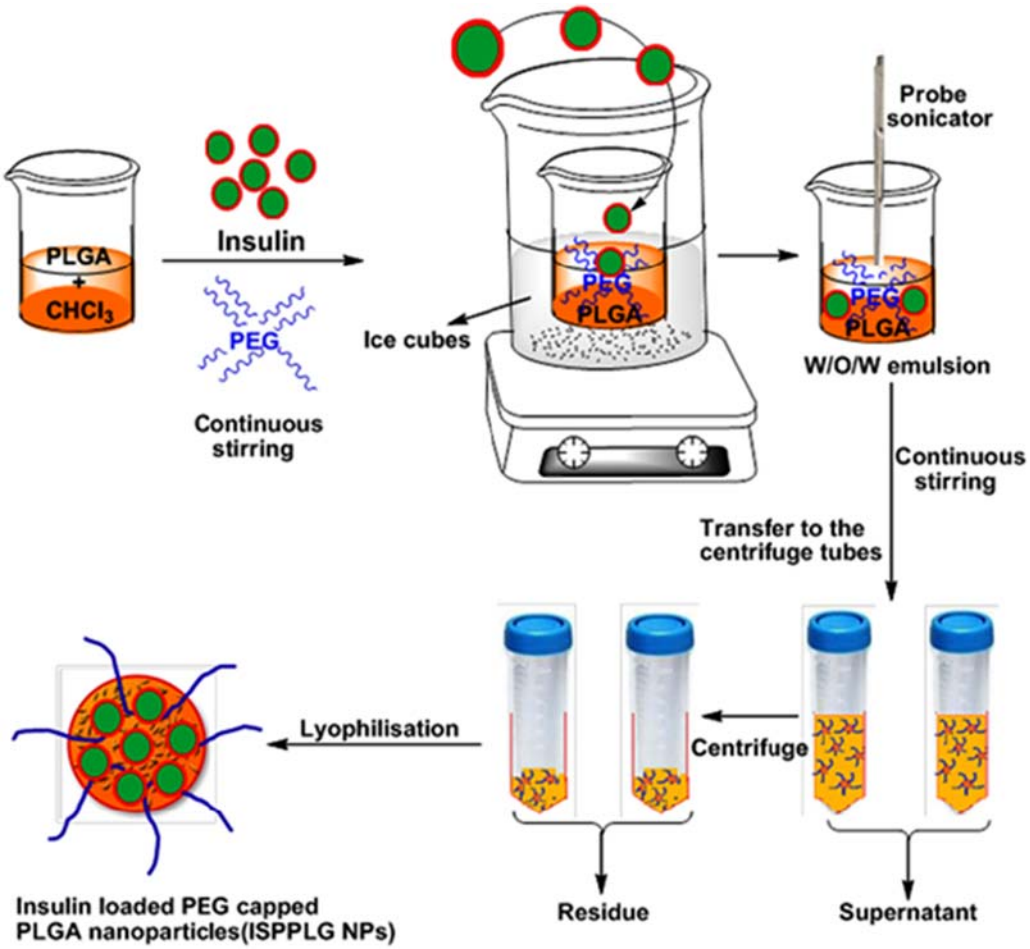

FIGURE 28.5 Schematic illustration of hydrophilic drug encapsulated PLGA nanoparticles.

and foremost, size helps determine the efficacy of the nanoparticles, release profile, and degradation pattern. Dynamic light scattering, scanning electron microscopy, transmission electron microscopy, and atomic force microscopy can be used to determine parameters such as size, shape. Distribution, and morphology of the nanoparticle. It has also been reported that the higher molecular weight of the polymer has an adverse effect on the particle size, encapsulation efficiency, and degradation rate.[75] The chain length of the polymer represents the molecular weight of the polymer, thus reflecting the chemical nature of the polymer, that is, its hydrophobic or hydrophilic nature. It is well known that polymers with shorter chain length are hydrophobic and have a faster degradation rate. However, polymers with a longer chain length are generally hydrophilic in nature and have a shorter degradation rate. Thus, the molecular weight of the polymer plays a crucial role in deciding the release kinetics of the drug.[76] Size exclusion chromatography is useful in determining the molecular

weight of the polymer.[77] It has also been observed that the in vitro and in vivo release characteristics of the drug are affected by the physical state of both the drug and polymer. The muco-adhesion, nanoparticle constancy and intracellular trafficking are greatly dependent on the zeta potential.[78] The biodistribution of the nanoparticles is greatly dependent upon their hydrophobic nature. Various studies have corroborated that the retention time of hydrophilic particles is more than that of hydrophobic particles.[79] Techniques such as water contact angle measurement and hydrophobic interaction chromatography may be used to determine the hydrophobicity and hydrophilicity of the nanoparticles, respectively.[80] The surface chemistry can be analyzed with a variety of techniques such as X-ray photoelectron spectroscopy, Fourier transform infrared spectroscopy, and nuclear magnetic resonance spectroscopy.[81]

5. Cancer

Cancer is the leading cause of death worldwide, and its treatment has been a major concern for researchers and doctors. Severe side effects of prominent anticancer drugs have forced the research community to explore delivery vehicles to achieve drug delivery specifically to the cancer site. Among these, nanoparticles emerged as the most potential candidates. But of various metallic and inorganic nanocarriers explored for the purpose of drug delivery, none are without any toxic effect to normal cells. Such a scenario shifted focus of delivery vehicle research to biocompatible and nontoxic carriers leading to polymeric nanocarriers.

There are several common strategies for targeting specific cancer cells to inhibit tumor development, progression, and metastasis without causing severe side effects.[82] In addition to the chemically synthesized anticancer agents, several anticancer compounds with different modes of action have been extracted from plant sources, such as Taxus brevifolia, Catharanthus roseus, Betula alba, Cephalotaxus species, Erythroxylum previllei, Vincarosia, Curcuma longa, and many others.[83] Among them, curcumin is the most important component of the rhizomes of Curcuma longa L. (turmeric)[84] and was extracted from turmeric in pure crystalline form for the first time[85] in 1870.

5.1 Curcumin: from ancient medicine (Indian solid gold)

The polyphenol curcumin (Fig. 28.6) is the active ingredient in the herbal remedy and dietary spice turmeric (Curcuma longa Linn). This vibrant yellow spice, derived from the rhizome of the plant,[86] has a long history of use in traditional medicines of China and India.[87]

Curcumin has a surprisingly wide range of beneficial properties, including antiinflammatory, antioxidant, chemopreventive. and chemotherapeutic activity (Fig. 28.7). The pleiotropic activities of curcumin derive from its complex chemistry as well as its ability to influence multiple signaling pathways, including survival pathways such as those regulated by NF-kB, Akt, and growth factors as well as cytoprotective pathways dependent on Nrf2. Curcumin is a free radical scavenger and hydrogen donor and exhibits both pro- and antioxidant activity. It also binds metals, particularly iron and copper, and can function as an iron chelator. Curcumin is remarkably nontoxic and exhibits limited bioavailability. Curcumin

FIGURE 28.6 Different sources of curcumin and its structure.

FIGURE 28.7 Pictorial representation of therapeutic potential of curcumin.

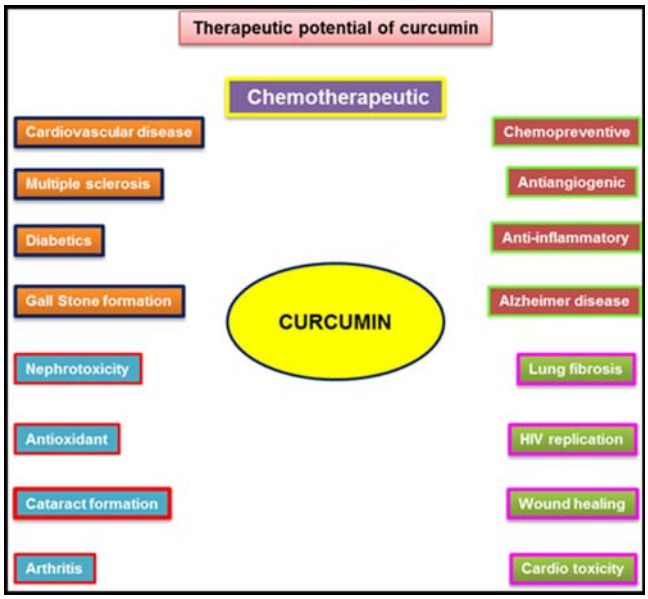

exhibits great promise as a therapeutic agent and is currently in human clinical trials for a variety of conditions including multiple myeloma, pancreatic cancer, myelodysplastic syndromes, colon cancer, psoriasis. and Alzheimer's disease.

Curcumin and its derivatives have received immense attention in the past 2 decades due to their biofunctional properties such as antitumor, antioxidant, and antiinflammatory activities.[88] These properties are attributed to the key elements in the curcumin structure.[89] Therefore, a great deal of scientific work has shed light on the structure activity relationship (SAR) of curcumin to improve its physiochemical and biological properties. Due to the importance of cancer as a leading cause of death and the ongoing quest for more efficient and less toxic anticancer agents, the focus is on the anticancer activity of curcumin.

5.2 PLGA/curcumin nanoformulation in anticancer therapy

Curcumin, the active ingredient of turmeric, has remarkable antitumor activity against various cancers. However, it has poor absorption and low bioavailability; thus, to cross the blood–brain barrier and reach tumor tissue, it needs to be transferred to tumor site by special drug delivery systems, such as nanoparticles. PLGA is a biocompatible member of the aliphatic polyester family of biodegradable polymers. For this reason, it has long been a fashionable choice for drug delivery applications, particularly since it has been FDA-approved for administration in humans under different pharmaceutical formulations. In this context, PLGA-based nanovectors present well-documented advantages for drug delivery purposes, as their self-assembled matrix enhance drug stability and protection from degradation induced by the external environment. Moreover, at the nanoscale size, nanoparticles can easily penetrate cancer tissues through the "enhanced permeation and retention" (EPR) effect; in this way, the sustained release of the cargo from the polymer matrix could enhance therapies improving the drug pharmacodynamic profiles (Table 28.1).

TABLE 28.1 PLGA/curcumin nanoformulations for the treatment of different cancers and their outcome.

PLGA/curcumin nanoformulations for the treatment of different cancers (publication titles)	Outcome	References
Breast cancer		
Intracellular drug release from curcumin-loaded PLGA nanoparticles induces G2/M block in breast cancer cells	PLGA nanoparticles (NPs) release curcumin intracellularly inducing time- and dose-dependent inhibition of proliferation via a G2/M block even at low concentrations of drug. The study of intracellular degradation of NPs associated with a specific G2/M blocking effect on MCF7 breast cancer cells caused by curcumin release in the cytoplasm provided direct evidence on the mechanism of action. PLGA NPs proved to be completely safe, suggesting a potential utilization of this nanocomplex to improve the intrinsically poor bioavailability of curcumin for the treatment of severe malignant breast cancer.	[93]
EGFR-targeting PLGA-PEG nanoparticles as a curcumin delivery system for breast cancer therapy	Effective delivery of an anticancer agent, curcumin, into EGFR-expressing MCF-7 cells in vitro and in vivo. Curcumin-loaded NPs gave rise to reduced phosphoinositide 3-kinase signaling, decreased cancer cell viability, attenuated drug clearance from the circulation, and suppressed tumor burden.	[94]
Hybrid nanoparticles coated with hyaluronic acid lipoid for targeted co-delivery of paclitaxel and curcumin to synergistically eliminate breast cancer stem cells	Fabrication of bCSC (breast cancer stem cell)-targeting codelivery system (HA-Hybrid NPs) by attaching a lipoid (HA-HDA) to the surface of hydrophobic PLGA NPs to codeliver the widely used chemotherapy agent PTX and the selective inhibitor of cancer stem cells (CSCs) curcumin (CUR). bCSC-targeted HA-Hybrid NP provides a potential strategy for enhancing breast cancer therapeutic efficiency.	[95]
Gemcitabine co-encapsulated with curcumin in folate decorated PLGA	Nanosuspension to enhance its anticancer potentiality synergistically.	[96]

(*Continued*)

TABLE 28.1 PLGA/curcumin nanoformulations for the treatment of different cancers and their outcome.—cont'd

PLGA/curcumin nanoformulations for the treatment of different cancers (publication titles)	Outcome	References
nanoparticles; a novel approach to treat breast adenocarcinoma	The folate conjugated dual drug formulations. Folate conjugated curcumin and gemcitabine loaded nanoparticles (FCGNPs) gave better results in suppressing the pgy-1 gene and also showed higher cellular uptake, cytotoxicity, apoptosis, and cell cycle arrest. The in vivo therapeutic efficacy of FCGNPs was higher compared to unconjugated and respective single-drug formulations.	
GANT61 and curcumin loaded PLGA nanoparticles for GLI-1 and PI3K/Akt mediated inhibition in breast adenocarcinoma	The NPs induced cytotoxic effects to breast cancer cells followed by cell death via autophagy and apoptosis, reduction in their target protein expression along with compromising the self-renewal property of CSCs. The dual-drug NPs provide a novel perspective on the aid of existing anticancer nanomedicine therapies to target a heterogeneous tumor mass effectively.	[97]
Methotrexate and curcumin co-encapsulated PLGA nanoparticles as a potential breast cancer therapeutic system: in vitro and in vivo evaluation	Methotrexate and curcumin could be efficiently encapsulated in PLGA. Codelivery of methotrexate and curcumin inhibits progression of breast cancer. Curcumin enhances the loading efficacy of methotrexate in PLGA NPs.	[98]
An in vivo study for targeted delivery of curcumin in human triple negative breast carcinoma cells using biocompatible PLGA microspheres conjugated with folic acid	Curcumin-loaded PLGA microspheres induce apoptosis in human triple-negative breast cancer cells by upregulating cleaved caspase-3 and downregulating p-AKT. Effective vehicle for delivery of hydrophobic drugs to the folate overexpressed cancer cells.	[99]
pH-sensitive polymeric nanoparticles of mPEGPLGA-PGlu with hybrid core for simultaneous encapsulation of curcumin and doxorubicin to kill the heterogeneous tumor cells in breast cancer	Use of CURDOX-NPs is a potentially useful therapeutic strategy for refractory breast cancer. The percentage of CSCs in tumor significantly decreased in control group.	[100]
PLGA-CTAB curcumin nanoparticles: Fabrication, characterization, and molecular basis of anticancer activity in triple negative breast cancer cell lines (MDA-MB-231 cells)	Effective delivery of curcumin in TNBC cancer cells and opens new frontiers in clinical cancer chemotherapy. Evaluation of PLGA-CTAB curcumin NP anticancer efficacy and the underlying mechanism in triple-negative breast cancer cell lines (MDA-MB-231 cells).	[101]
Nano-encapsulated metformin-curcumin in PLGA/PEG inhibits synergistically growth and hTERT gene expression in human breast cancer cells	Coencapsulation of metformin (Met) and curcumin (Cur) in PEGylated PLGA NPs and evaluation of their therapeutic efficacy on T47D breast cancer cells. Met−Cur−PLGA/PEG NPs exhibit synergistic antiproliferative effect and significantly arrest the growth of cancer cells ($P < .05$). Met−Cur−PLGA/PEG NPs based combinational therapy holds promising potential toward the treatment of breast cancer.	[102]

TABLE 28.1 PLGA/curcumin nanoformulations for the treatment of different cancers and their outcome.—cont'd

PLGA/curcumin nanoformulations for the treatment of different cancers (publication titles)	Outcome	References
Chemopreventive efficacy of curcumin loaded PLGA microparticles in a transgenic mouse model of HER-2 positive breast cancer	Curcumin treatment decreases mammary VEGF levels significantly. PLGA microparticles enhance tumorigenesis. This method can decrease the overall dose of curcumin and allow the development of sustained release curcumin dosage forms as a practical approach to cancer chemoprevention. PLGA microparticle administration was shown to be associated with higher plasma lactic acid levels and increased activation of NF-κB.	[103]
Fabrication of curcumin encapsulated PLGA nanoparticles for improved therapeutic effects in metastatic cancer cells	Encapsulation of curcumin in poly(lactic-co-glycolide) (PLGA) NPs, in the presence of poly(vinyl alcohol) and poly(L-lysine) stabilizers using nanoprecipitation method. Nano-CUR6 (optimized curcumin nanoformulations) shows improved anticancer potential in cell proliferation and clonogenic assays compared to free curcumin. Therapeutic efficacy of curcumin may be enhanced by PLGA NP formulations, and tumor-specific targeted delivery of curcumin is made feasible by coupling of anticancer antibody to the NPs.	[104]
Anticancer efficiency of curcumin-loaded mesoporous silica nanoparticles/nanofiber composites for potential postsurgical breast cancer	Curcumin incorporated into the mesoporous silica NPs (CUR@MSNs) were embedded into the randomly oriented bead-free electrospun poly(lactic-co-glycolic acid) nanofibers (PLGA NFs) and exhibited a sustained and prolonged drug release profile. Higher cytotoxicity and lower migration with increased apoptosis induction were detected in the cells treated with CUR@MSNs/PLGA NFs.	[105]
The remarkable role of emulsifier and chitosan, dextran, and PEG as capping agents in the enhanced delivery of curcumin by nanoparticles in breast cancer cells	The encapsulation efficiency of curcumin by PLGA NPs with different capping agents such as chitosan, PEG, and dextran and emulsifier lies in the range of 82%–89% and the antioxidant activity is 80%. The in vitro anticancer activity of PLGA NPs embedded with curcumin and different capping agents on MCF-7 indicates that they are more effective in arresting cell growth. The cellular uptake of TPGS emulsified dextran capped curcumin encapsulated PLGA NPs is much higher when compared to that of PLGA NPs with other capping agents, emulsifier, and free curcumin.	[106]
Targeted nanocurcumin therapy using Annexin A2 antibody improves tumor accumulation and therapeutic efficacy against highly metastatic breast cancer	The in vivo targeting potential as well as combinatorial therapeutic potential of Annexin A2 (AnxA2) antibody-conjugated curcumin loaded poly(lactic-co-glycolic acid) (PLGA) NPs (AnxA2-CPNP) against metastatic breast cancer cells are enhanced.	[107]

(*Continued*)

TABLE 28.1 PLGA/curcumin nanoformulations for the treatment of different cancers and their outcome.—cont'd

PLGA/curcumin nanoformulations for the treatment of different cancers (publication titles)	Outcome	References
Blood cancer		
Coformulation of doxorubicin and curcumin in poly-(D, L-lactide-co-glycolide) nanoparticles suppresses the development of multidrug resistance in K562 cells	CUR helps in the inhibition of expression of the hybrid gene bcr/abl leading to increasing efficacy of formulation in K562 cells. Effective delivery of the payload to the cells by NPs, and combination therapy with doxorubicin (DOX) and curcumin (CUR) produced more potential therapeutic effects. The combination of DOX and CUR in NP formulation can be utilized as a novel treatment regimen for chronic myeloid leukemia.	[113]
Microfluidic assisted nanoprecipitation of PLGA nanoparticles for curcumin delivery to leukemia Jurkat cells	Size tuneable synthesis of Cur-PLGA NP is less than 100 nm in diameter with a narrow size distribution and excellent colloidal stability. Cur-PLGA NP is a nontoxic and effective delivery system for curcumin, which enhances anticancer activity of curcumin against leukemia Jurkat cells compared to native curcumin.	[114]
Colon cancer		
Real-time label-free targeting assessment and in vitro characterization of curcumin-loaded poly-lactic-co-glycolic acid nanoparticles for oral colon targeting	CPLGA NPs (200 nm) (curcumin-loaded poly-lactic-co-glycolic acid) surface-coated with chitosan (CS) for gastrointestinal mucosa adhesion, wheat germ agglutinin (WGA) for colon targeting, or GE11 peptide for tumor colon targeting. C-PLGA NP formulations exhibit good colloidal stability in synthetic gastrointestinal fluids.	[117]
Co-delivery of camptothecin and curcumin by cationic polymeric nanoparticles for synergistic colon cancer combination chemotherapy	Combined delivery of camptothecin (CPT) and CUR in a single NP enhances synergistic effects of the two drugs. Combinational application of CPT and CUR with a one-step-fabricated codelivery system for effective colon cancer combination chemotherapy.	[118]
The kinetics and release behavior of curcumin loaded pH-responsive PLGA/chitosan fibers with antitumor activity against HT-29 cells	Poly(lactide-glycolide)/chitosan loaded with curcumin nanofiber (PLGA/CS/Cur) was developed by electrospinning technique. The incorporated curcumin was well-dispersed and maintained crystalline form in PLGA/CS fiber matrix by hydrogen bonding. At pH 7.4, the release followed Fickian diffusion mechanism; while at pH 2.0, the release followed the coexistence of diffusion and erosion mechanisms. The amount of Cur released at pH 2.0 was much higher than that at pH 7.4. As a result, the nanofibers demonstrated higher anticancer activity at acidic environment.	[119]

TABLE 28.1 PLGA/curcumin nanoformulations for the treatment of different cancers and their outcome.—cont'd

PLGA/curcumin nanoformulations for the treatment of different cancers (publication titles)	Outcome	References
Enhanced drug retention, sustained release, and anti-cancer potential of curcumin and indole-curcumin analog-loaded polysorbate 80-stabilized PLGA nanoparticles in colon cancer cell line SW480	Indole-incorporated curcumin analog and curcumin loaded PLGA NPs had a size range of 50–150 nm diameter. Nanoformulation preserved the drug from degradation in wide ranges of pH environments. NPs treatment against SW480 cancer cell line triggered nuclear fragmentation, cell cycle blockade, inhibition of apoptosis, and metastatic biomarkers.	[120]
Chitosan/carboxymethylcellulose-stabilized poly(lactide-co-glycolide) particles as bio-based drug delivery carriers	CS/NaCMC-covered-PLGA particles showed colloidal stability, over a wider pH range when compared to CS-covered-PLGA particles. Curcumin, a model hydrophobic drug, was encapsulated into the particles up to 10 wt% of PLGA. The CS/NaCMC-covered-PLGA particles loaded with curcumin showed delayed release in mildly acidic conditions and faster release in neutral and basic conditions. Cytotoxicity experiments carried out with human colorectal carcinoma cells yielded good results.	[121]
Factorial design formulation optimization and in vitro characterization of curcumin loaded PLGA nanoparticles for colon delivery	In vitro cellular uptake studies with HT-29 cells showed that the optimized curcumin-loaded PLGA NP exhibited a much higher cellular uptake of curcumin (i.e., 7.01 ± 0.33 μg/106 cells) than a native curcumin solution (3.74 ± 0.56 μg/106 cells).	[122]
Passively targeted curcumin-loaded PEGylated PLGA nanocapsules for colon cancer therapy in vivo	Use of PLGA-based polymeric oil-core nanocapsules (NCs) for curcumin loading and delivery to colon cancer in mice after systemic injection. Castor oil-core PLGA-based NC achieves high drug loading efficiency (≈18% w(drug)/w (polymer)%) compared to previously reported NCs. Curcumin-loaded NCs internalize more efficiently in CT26 cells than the free drug and exert therapeutic activity in vitro, leading to apoptosis and blocking the cell cycle.	[123]
Lung cancer		
Dual release of angiostatin and curcumin from biodegradable PLGA microspheres inhibit Lewis lung cancer in a mice model	Codelivery of angiostatin and curcumin by PLGA microspheres for the synergistic treatment of lung cancer. Dual-drug loaded microspheres exhibit a higher antiproliferative activity in endothelial cells but not in HepG2 cell. Dual-drug loaded Ms (As–Cur–PLGA-Ms) exhibit higher antitumor activity when compared to single-drug loaded Ms (AS–PLGA-Ms and Cur–PLGA-Ms).	[127]

(*Continued*)

TABLE 28.1 PLGA/curcumin nanoformulations for the treatment of different cancers and their outcome.—cont'd

PLGA/curcumin nanoformulations for the treatment of different cancers (publication titles)	Outcome	References
A comparison between PLGA-PEG and NIPAAm-MAA nanocarriers in curcumin delivery for hTERT silencing in lung cancer cell line	Comparison between PLGA-PEG and NIPAAm-MAA nanocarriers in delivery of curcumin and also in levels of hTERT (Telomerase reverse transcriptase) silencing in lung cancer cell line (calu-6). Curcumin loaded PLGA-PEG decreases hTERT expression levels more than that of curcumin loaded NIPAAm-MAA and free curcumin. Curcumin loaded PLGA-PEG can be a useful nano-based carrier for delivery of curcumin to fight lung cancer.	[128]
The effects of nanoencapsulated curcumin-Fe_3O_4 on proliferation and hTERT gene expression in lung cancer cells	By encapsulation of curcumin-Fe3O4, cytotoxicity of the drug substantially increased for all concentrations. Expression level of the hTERT in A549 lung cancer cell lines was reduced with increasing concentrations in both pure and nanoencapsulated curcumin. Compared to pure form, nanoencapsulated curcumin caused further decline in the expression levels of the gene.	[129]
Ovarian cancer		
Photodynamic therapy of ovarian carcinoma cells with curcumin-loaded biodegradable polymeric nanoparticles	Curcumin-loaded biodegradable PLGA NPs (CUR-NPs) exhibit better physicochemical properties such as stability in the presence of light and improved serum stability compared to free curcumin. Nanoformulation facilitates the use of higher amounts of curcumin and shows strong apoptotic effects on tumor cells. Formulation of CUR-NPs for photodynamic therapy.	[132]
Core–shell microencapsulation of curcumin in PLGA microparticles: programmed for application in ovarian cancer therapy	Liquid-driven coflow focusing (LDCF)-CUR-loaded PLGA microparticles (CPMs) exhibit high therapeutic potential in the treatment of peritoneal cancers, such as ovarian, that reside in the peritoneal cavity. Pharmacokinetics of LDCF-CPMs shows slow systemic absorption with longer mean residence time (MRT). IP delivery of CUR can expose the ovarian tumor to higher concentration for a longer duration by programming the thickness of the shell.	[133]
Evaluation of the efficacy of paclitaxel with curcumin combination in ovarian cancer cells	PLGA-phospholipid-PEG NPs containing Taxol and CUR have improved solubility and stability together with a slow-release effect. CUR is found to overcome the MDR of tumor cells by elevating the paclitaxel concentration in the tumor cells to improve the antitumor activity of this combination.	[134]

TABLE 28.1 PLGA/curcumin nanoformulations for the treatment of different cancers and their outcome.—cont'd

PLGA/curcumin nanoformulations for the treatment of different cancers (publication titles)	Outcome	References
Cervical cancer		
Curcumin entrapped folic acid conjugated PLGA–PEG nanoparticles exhibit enhanced anticancer activity by site specific delivery	Curcumin entrapped NPs of PLGA–PEG copolymer which were conjugated with folic acid (PPF copolymer) are useful for site-specific targeting since many cancer cells exhibit external folic acid binding receptors.	[135]
Curcumin nanoformulation for cervical cancer treatment	Poly(lactic-co-glycolic acid) based curcumin NP formulation (nano-CUR) is compared with free CUR. Nano-CUR effectively inhibits cell growth, induces apoptosis, and arrests the cell cycle in cervical cancer cell lines.	[136]
A novel curcumin-loaded PLGA micromagnetic composite system for controlled and pH-responsive drug delivery	Magnetic microspheres (MMS) exhibit excellent superparamagnetism displaying a saturated magnetism (24.4 emu/g). Microspheres (MS) and MMS were spherical in shape along with a smooth surface of mean diameter of 0.5 and 1 μm, respectively. MIONP content in MMS was 23.74 wt%. MMS have a pH-induced drug-releasing asset with a cumulative CUR releasing efficiency of 73.25%, and they have cytotoxicity against HeLa cell lines with a significant potency.	[137]
Brain tumor		
Effects of curcumin loaded PLGA nanoparticles on the RG2 rat glioma model	Evaluation of the antitumor activity of curcumin on glioblastoma tissue in the rat glioma-2 (RG2) tumor model. Intratumoral administration of curcumin-loaded poly((lactic-co-glycolic acid)-1,2-distearoyl-glycerol-3-phospho-ethanolamine-N-[methoxy (polyethylene glycol)-2000]) ammonium salt PLGA-DSPE-PEG hybrid NPs is effective against glioblastoma.	[138]
Evaluation of targeted curcumin (CUR) loaded PLGA nanoparticles for in vitro photodynamic therapy on human glioblastoma cell line	Enhancement of the photodynamic efficiency of curcumin (CUR) on glioblastoma tumor cells. MAb-CUR-PLGA NPs exhibit more effective photodynamic toxicity (56% vs. 24%) on the DKMG/EGFRvIII cells. Anti-EGFRvIII MAb-CUR-PLGA NPs have the potential as targeted drug delivery system for PDT in the overexpressed EGFRvIII tumor cells.	[139]
Preparation of curcumin-loaded PLGA nanoparticles and investigation of its cytotoxicity effects on human glioblastoma U87MG cells	CUR-PLGA-NPs have high cytotoxicity effects compared to free CUR in U87MG cell line. Half maximal inhibitory concentration (IC50) after cell incubation for 72 h was 57.99 and 32.90 μg/mL for free CUR and CUR-PLGA-NPs, respectively.	[140]

(*Continued*)

TABLE 28.1 PLGA/curcumin nanoformulations for the treatment of different cancers and their outcome.—cont'd

PLGA/curcumin nanoformulations for the treatment of different cancers (publication titles)	Outcome	References
Skin cancer		
Fabrication of nanopatterned PLGA films of curcumin and TPGS for skin cancer	Curcumin-loaded tocopherol polyethylene glycol 1000 succinate stabilized poly(lactic-co-glycolic acid) nanopatterned films (CTP-NPFs) show good in vitro cytotoxicity toward human skin cancer cell line (A431) when compared to that of unpatterned films. CTP-NPFs effectively reduce the progression of cancer cells in vivo, in the skin carcinogenesis. Nanopatterned films can be used as an alternate treatment for skin cancer.	[146]
Effects of nano-encapsulated curcumin-chrysin on telomerase, MMPs and TIMPs gene expression in mouse B16F10 melanoma tumor model	Nano-combination of curcumin and chrysin into PLGA NPs with a one-step fabricated codelivery system may be a promising and convenient approach to improve their efficiency in melanoma cancer therapy.	[147]
Liver cancer		
Formulation, characterization and evaluation of curcumin-loaded PLGA-TPGS nanoparticles for liver cancer treatment	Curcumin-loaded (PLGA/TPGS) NPs successfully internalized by HepG2 cells play a synergistic role in inhibiting the growth of hepatocellular carcinoma cells. Curcumin-loaded (PLGA/TPGS) NPs provide a promising platform for the treatment of liver cancer.	[151]
Studying the effect of physically adsorbed coating polymers on the cytotoxic activity of optimized bisdemethoxycurcumin loaded-PLGA nanoparticles	Study on the effect of different physically adsorbed coating, using PEG 4000, Tween 80, and Pluronic F68 to impart a hydrophilic stealth character to the surface. Physically adsorbed coating polymers on the cytotoxic activity of optimized bisdemethoxycurcumin (BDMC)-loaded PLGA NPs were investigated. Coated NPs show the highest inhibition of malignant cells viability.	[152]
Curcumin-loaded poly(L-lactide-co-glycolide) microbubble-mediated sono-photodynamic therapy in liver cancer cells	CUR-PLGA MBs are spheres with smooth surface and an average size of 3.7 μm. Drug entrapment efficiency and drug-loading capacity were 74.29 ± 2.60% and 17.14 ± 0.60%, respectively. CUR-PLGA MBs have good biocompatibility with normal L02 cells and were almost noncytotoxic to HepG2 cells. Potential mechanism was related to the mitochondrial membrane potential loss and increased production of intracellular reactive oxygen species.	[153]
Erythrocyte membrane cloaked curcumin-loaded nanoparticles for enhanced chemotherapy	RBCM-p-PLGA@Cur NPs possess potent antitumor activity in a murine H22 xenograft cancer model in terms of reduced tumor volume and mass, as well as inducing apoptosis of tumor cells, and have no observable systemic toxicity.	[154]

TABLE 28.1 PLGA/curcumin nanoformulations for the treatment of different cancers and their outcome.—cont'd

PLGA/curcumin nanoformulations for the treatment of different cancers (publication titles)	Outcome	References
Prostate cancer		
Impregnation of curcumin into a biodegradable (poly-lactic-co-glycolic acid, PLGA) support, to transfer its well-known in vitro effect to an in vivo prostate cancer model	Curcumin-impregnated PLGA is significantly more active (approximately twofold increase) with respect to oral curcumin, which supports its use for subcutaneous administration for prostate cancer (PCa) therapy. A suitable approach for solid pancreatic tumors due to well tolerated in loco-regional application.	[159]
Anticancer activity of curcumin loaded PLGA nanoparticles on PC3 prostate cancer cells	Investigation of the toxic effect of encapsulation of Cur in PLGA (poly lactic-co-glycolic acid) nanospheres (NCur) on PC3 human cancer prostate cell. NCur has considerable cytotoxic activity more than that of Cur on PC3 cell lines, which is mediated by induction of both apoptotic and autophagic processes. High potential as an adjuvant therapy for clinical application in prostate cancer.	[160]
Optimization and scale up of microfluidic nanolipomer production method for preclinical and potential clinical trials	PLGA polymer concentration of 10 mg/mL and a DSPE-PEG lipid concentration of 10% w/v provided optimal size, PDI, and stability. High encapsulation efficiency of 58.8% and drug loading of 4.4% were achieved at 7.5% w/w initial concentration of curcumin/PLGA polymer. The process of developing nanolipomers using high-flow microfluidic system with optimal characteristics is significant as the same optimized parameters used for small batches could be translated into manufacturing large-scale batches for clinical trials through parallel flow systems.	[161]
Pancreatic cancer		
Evaluation of curcumin loaded chitosan/PEG blended PLGA nanoparticles for effective treatment of pancreatic cancer	Curcumin-loaded poly(D,L-lactide-co-glycolide) (PLGA) NPs and surface coated with chitosan and PEG (CNPs) to achieve optimum therapeutic effect. Superior cytotoxicity, enhanced antimigratory, anti-invasive, and apoptosis-inducing ability of CNPs in metastatic pancreatic cancers.	[166]
Formulation, characterization and evaluation of curcumin loaded PLGA nanospheres for cancer therapy	Curcumin loaded PLGA nanospheres exert more pronounced effect on the cancer cells as compared to free curcumin.	[28]
Colorectal cancer		
Co-delivery of curcumin and chrysin by polymeric nanoparticles inhibit synergistically growth and hTERT gene expression in human colorectal cancer cells	Curcumin (Cur) and Chrysin (Chr) co-encapsulated in PEGylated PLGA NPs (Cur–Chr–PLGA/PEG NPs) exhibit synergistic antiproliferative effect and arrest the growth of cancer cells significantly.	[169]

(*Continued*)

TABLE 28.1 PLGA/curcumin nanoformulations for the treatment of different cancers and their outcome.—cont'd

PLGA/curcumin nanoformulations for the treatment of different cancers (publication titles)	Outcome	References
	Nanocombinational application of the natural herbal substances with a one-step fabricated codelivery system for effective colorectal cancer combinational chemotherapy. Cur−Chr−PLGA/PEG NPs decline hTERT expression in all concentration ($P < .05$).	
Epithelial cell adhesion molecule aptamer functionalized PLGA-lecithin-curcumin-PEG nanoparticles for targeted drug delivery to human colorectal adenocarcinoma cells	Apt-CUR NPs demonstrate superior antiproliferation activity in HT29 colon cells than that of free CUR at the same concentration. They exhibit a stronger cytotoxic effect in EpCAM + HT29 cells when compared to that of EpCAM-HEK293T cells.	[170]

5.2.1 *Breast cancer*

Breast cancer is the most threatening and commonly diagnosed cancer, and it is responsible for 25% of all cancer cases and 15% of all cancer deaths among females across the globe.[90] The existing chemotherapies or radiotherapy has shown limited to moderate success in breast cancer.[91] However, among all breast cancers, triple-negative breast cancer (TNBC) is the most aggressive, metastatic, and hardest to treat due to nonresponsiveness to hormone-dependent therapies or therapies which target (human epidermal growth factor) HER-2 receptors.[92] Receptors overexpressed in breast tumor cells, such as human epidermal growth factor receptor-2 (HER2), EGFR, vascular endothelial growth factor receptor (VEGFR), and insulin −like growth factor I receptor, are being targeted using specific ligands/drugs. This approach is being utilized in formulating targeted nanoparticles systems for drug delivery.

Paolo Verderio et al. have developed curcumin-loaded PLGA nanovectors which result in the PLGA nanoformulation and curcumin drug release inside the cytoplasm of MCF7 breast cancer cells leading to a controlled inhibition of cell proliferation induced by curcumin-triggered cycle arrest.[93] Jin et al. have demonstrated[94] that the anticancer effect of free Cur on primary tumor burden can be enhanced through its delivery bound to target PLGA-PEG NPs. In vitro data suggest that the addition of EGFR-targeting GE11 peptides to Cur-NPs can substantially enhance the delivery of Cur to EGFR-expressing tumor cells and subsequently improve both the inhibition of PI3K signaling and the level of apoptotic tumor cell death. The rapid accumulation of Cur in MCF-7 cells following its delivery in the form GE11-Cur-NPs suggests that Cur uptake occurs via active receptor-mediated endocytosis as well as passive uptake through the cell membrane in vitro. It follows that such drug delivery strategies could therefore be used to enhance the impact of clinically approved breast cancer therapies (e.g., cyclophosphamine). Their findings support the development of novel drug delivery strategies that enhance the delivery of anticancer agents to tumor tissue; this

could be achieved by targeting specific tumor cell receptors (in breast cancer and other cancer types) and by using cell-specific peptides or membranes possibly following tumor sensitization. Although the Cur-loaded NPs seem nontoxic in tumor-bearing mice (as evidenced by the absence of visible side-effects, animal lethality, and change in circulating inflammatory cytokines vs. healthy mice), full dose-dependent toxicology studies in humans are lacking. It is encouraging, however, that free Cur as well as these types of NPs are well-tolerated in cancer patients.[94] Zhe Yanga et al., have synthesized a hyaluronic acid lipoid by conjugating n-hexadecylamine (HDA) to the carboxyl group of hyaluronic acid (HA), which can be attached to the surface of hydrophobic PLGA nanoparticle cores via the hexadecyl anchors to construct a bCSC (breast cancer stem cell)-targeting vehicle with core-shell structure for codelivering PTX(Paclitaxel) and CUR(curcumin) (Fig. 28.8A). Through the targeting capacity of HA layer, the formed HA-Hybrid NPs could effectively accumulate in tumors and associate with bCSCs. Additionally, the PTX- and CUR-loaded HA-Hybrid NPs not only inhibited the proliferation and migration of breast cancer cells in vitro but also effectively enhanced the efficacy of breast tumor growth suppression by simultaneously eliminating the non-bCSCs and bCSCs.[95]

Curcumin (CUR) and Gemcitabine (GEM) coencapsulated PLGA nanoparticles (CGNPs) were fabricated and evaluated in terms of particle size, zeta potential, drug encapsulation, and release. CGNPs were fabricated with folic acid (FCGNPs) to actively target tumors overexpressing folate receptors. The cellular uptake and cytotoxicity were evaluated on both folate positive MDA-MB-231 and MCF-7 cell lines, out of which MDA-MB-231 gave a better response. Apoptosis assay and cell cycle damage also increased in MDA-MB-231 cell lines

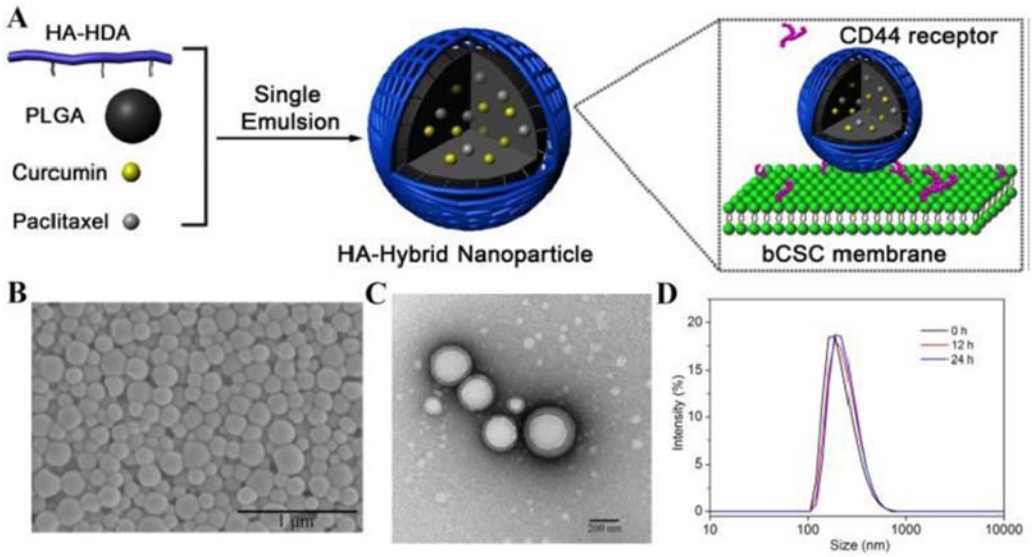

FIGURE 28.8 (A) Schematic illustration of composition/structure of the HA-Hybrid NPs, and their binding to CD44 on breast cancer stem cells (bCSCs). (B) The SEM image and (C) TEM image of the HA-Hybrid NPs. (D) the particle size distribution of the HA-Hybrid NPs incubated in PBS (pH = 7.4, 0.01M) containing 10% FBS at different time intervals.

after treatment with FCGNPs. In vivo tumor accumulation and antitumor effect were observed on the MDA-MB-231 xenografts in nude mice. It is expected that CGNPs decorated with folic acid, that is, FCGNPs will be a novel codelivery system to overcome drug resistance and toxicity and to enhance the therapeutic efficacy of GEM in folate positive tumors. Folate conjugated single (CUR/GEM) and dual (CUR + GEM) drug-loaded nanoformulations were prepared and evaluated for P-glycoprotein-1 (pgy-1) gene resistance, followed by in vitro cellular uptake and cytotoxicity assay in cells.[96] Ankita et al. have developed a combination strategy for inhibiting the Hh/Gli-EGFR signaling pathway in heterogeneous breast cancer cells by encapsulating a Hh/Gli small molecule antagonist GANT61 and an EGFR inhibitor curcumin inside PLGA nanoparticles (NPs) as shown in Scheme 28.1. This dual drug combination of GANT61 and curcumin PLGA NPs could be an exciting approach in the arsenal of existing anticancer nanomedicine therapies for the treatment and management of breast cancer that will kill all the bulk tumor cells and CSCs together by targeting EGFR and Hh pathway thus minimizing the recurrence of the deadly disease.

The PLGA nanoparticles were prepared for codelivery of methotrexate (MTX) and CUR and characterized by their particles size, morphology, drug encapsulation efficiencies, release patterns, cell cytotoxicity, and in vivo efficacy. Altering MTX and CUR quantity leads to particle size of 142.3 ± 4.07 nm with MTX encapsulation efficiency of $71.32 \pm 7.8\%$ and CUR encapsulation efficiency of $85.64 \pm 6.3\%$. These particles showed significantly higher cytotoxicity in comparison with free MTX or CUR or even their solo-loaded formulations. The in vivo results showed the synergic effect of MTX and CUR codelivery on inhibiting the progression of breast cancer.[98] Curcumin encapsulated PLGA microsphere has been designed by

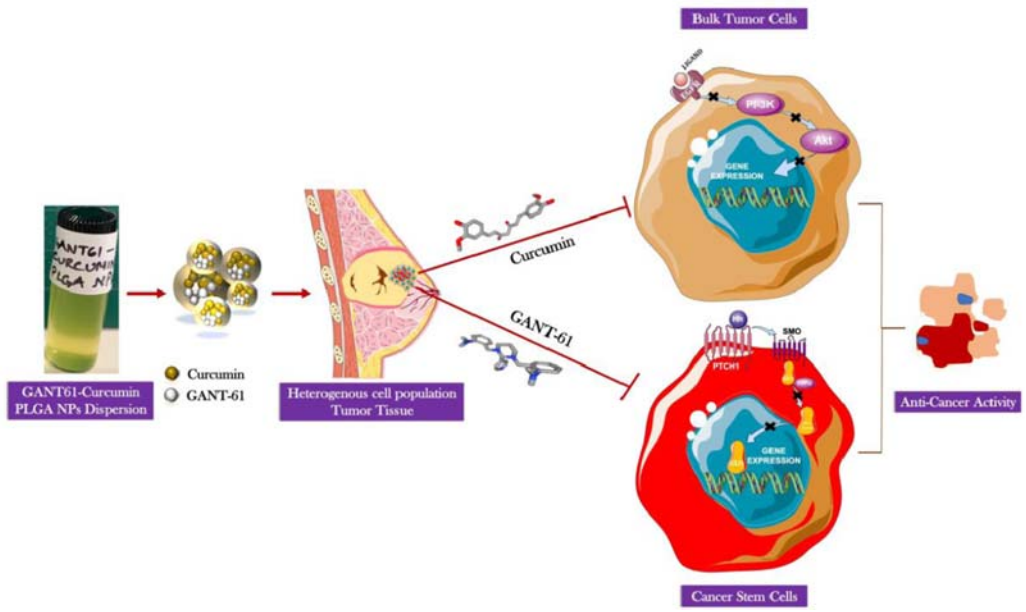

SCHEME 28.1 Therapeutic targeting of heterogeneous breast tumor mass which has an aberrant activation of the Hedgehog and EGFR signaling pathways by GANT61-curcumin PLGA NPs.[97]

simple single emulsion method for mediating the delivery of hydrophobic curcumin to the triple negative breast cancer cells (TNBC). These microspheres induce DNA damage and perturb mitochondria membrane, causing apoptosis mediated cell death. The Western blot studies reveal upregulation of p27, the negative regulator of cyclin-dependent kinase, and p-AKT is down regulated which leads to the cellular arrest. For curtailing the cytotoxicity toward normal cells, these microspheres are targeted to cancer cells by conjugating them with folic acid (PLGA@CCM@FA). The folic acid conjugated PLGA microsphere shows more cytotoxic effects toward the TNBCs than the nonconjugated ones. The in vitro results are also replicated in the in vivo BALB/C mice models. In triple negative breast cancer cell bearing BALB/C models, the group of mice treated with PLGA@CCM@FA showed more tumor regression patterns than the other groups.[99]

A pH-sensitive dual drug-loaded nanoparticle curcumin (CUR) and doxorubicin (DOX) (CURDOX-NPs) was prepared by using monomethoxy (polyethylene glycol)-b-P (D, L-lactic-co-glycolic acid)-b-P (L-glutamic acid) (mPEG-PLGA-PGlu) polymer to simultaneously target the breast cancer stem cells and the differentiated tumor cells. The particle size, surface potential, morphology and drug-loading capability of CURDOX-NPs were carefully characterized in vitro. The effective antitumor effect of CURDOX-NPs was also confirmed by in vitro and in vivo. The ability of CURDOX-NPs to kill the heterogeneous tumor cells in tumor tissues was also evaluated in vitro tumor spheroid and in vivo xenograft mice model.[100] Fabrication of small positively charged Cur NPs by nanoprecipitation method by using PLGA as a carrier and hexadecyltrimethylammonium bromide (CTAB) as a surfactant/surface charge modifier, and subsequent characterization of the physicochemical properties, drug-controlled release, and cellular incorporation of Cur nanoparticles (CN) have been reported and their anticancer potential and underlying mechanism in human TNBC MDA-MB-23 have been investigated.[101] The coencapsulation of Cur and Met in PEGylated PLGA nanoparticles (NPs) and evaluation of their anticancer effect against human breast cancer cell line T47D have been reported.[102] The efficacy of curcumin-loaded PLGA microparticles in a transgenic mouse model of HER-2+ breast cancer, Balb-neuT has been examined. The effect of curcumin treatment on tumor multiplicity, growth and angiogenesis was determined.[103] To develop a uniform curcumin encapsulated PLGA nano-formulation, different amounts of poly (vinyl alcohol) (PVA)/poly(L-lysine) (PLL) were screened. An optimized nanoparticle formulation of curcumin (nano-CUR6) exhibited superior cellular uptake, retention, and release in cancer cells. The anticancer potential of this curcumin nanoparticle formulation was examined in highly metastatic ovarian and breast cancer cells. In addition, effects of this formulation on molecular pathways associated with apoptosis were investigated. The antibody conjugation abilities of this nano-formulation for antibody guided delivery of drugs to cancer cells have also been generated[104].

Curcumin-loaded mesoporous silica nanoparticles (CUR@MSNs) were incorporated in bead-free electrospun PLGA nanofibers with a sustained and extended curcumin release profile. In addition, MCF-7 cells treated with CUR@MSNs/PLGA NFs showed enhanced cytotoxicity and decreased migration as well as increased apoptotic induction.[105] The investigations carried out by the author's research group at the University of Madras demonstrated that the bioavailability of curcumin was considerably increased by poly (lactic-co-glycolic) acid [PLGA (60/40)] nanoparticles with different capping agents such as Chitosan, Dextran and PEG and emulsifier (Tocopherol Poly (Ethylene Glycol) 1000 Succinate: TPGS) with good drug loading

and delivery performance. The encapsulation efficiency of curcumin by PLGA NPs with different capping agents such as Chitosan, PEG, and Dextran and emulsifier lies in the range of 82%–89%, and the antioxidant activity is 80%.[106] Annexin A2 (AnxA2) antibody-conjugated curcumin loaded poly(lactic-co-glycolic acid) (PLGA) nanoparticles (AnxA2-CPNP) clearly indicated that the cell-surface expression of AnxA2 increases during breast cancer progression with very high expression in highly malignant cancer cells and basal expression in nonmalignant cells. Cell viability, plasmin generation, and wound healing assays reveal that AnxA2-CPNPs effectively inhibited cell proliferation, invasion, and migration, key elements for cancer growth and metastasis.[107]

5.2.2 Blood cancer

Leukemia is a clonal disorder originated in the bone marrow during hematopoiesis and is characterized by the unregulated proliferation of poorly differentiated white blood cells. Classification of the disease is based on the type of cell affected (myeloid or lymphoid) and the degree of cell proliferation (acute or chronic) (epigenetics of hematopoiesis and hematological malignancies).[108] In 2020, approximately 60,530 estimated new cases of leukemia and 23,100 estimated deaths will occur in the United States.[109] Chronic myeloid leukemia (CML) is a good example of how hematological diseases have greatly benefited from the advance of cytogenetic and molecular methodologies. It was the first cancer in which a unique causative chromosomal abnormality was identified, t(9; 22) (q34; q11)—Philadelphia chromosome (Ph)—and the associated BCR-ABL1 gene, providing a specific target for disease treatment[110–112]. Tyrosine kinase inhibitors (TKIs) target the dysregulated kinase activity of the fusion protein encoded by BCR-ABL1 (Imatinib discontinuation in chronic myeloid leukemia patients with undetectable BCR-ABL transcript level).

The coadministration of DOX and CUR in PLGA NPs can promote the cytotoxicity by both the drugs in vitro in leukemic cells. It increased the therapeutic concentration of DOX inside the nucleus, by inhibition of nuclear efflux of DOX by CUR in K562 cells. Moreover, CUR helps in downregulation of both MDR1 and BCL-2 expression helping in stimulation of further cell death induced by DOX in K562 cells. Both the drugs combined induced a number of apoptotic pathways, leading to higher expression of a number of apoptotic proteins. RT-PCR results illustrate that the synergistic effect of both the drugs on apoptosis induction may help in downregulation of bcr/abl gene in K562 cells. Thus, DOX and CUR exhibited a synergistic inhibitory effect on the cell growth of K562, which may provide combinatorial strategies in cancer therapy.[113] Mandy et al. have demonstrated size tuneable synthesis of Cur-PLGA NP by microfluidic hydrodynamic flow method. The resulting Cur-PLGA NPs are less than 100 nm in diameter with a narrow size distribution and excellent colloidal stability. Cur- PLGA NPs significantly inhibit the degradation of curcumin with the rate of degradation of $1.1 \pm 0{:}4\%$ h-1. Microfluidic synthesized Cur-PLGA NP is a nontoxic and effective delivery system for curcumin, in particular, it enhances anticancer activity of curcumin against leukemia Jurkat cells compared to native curcumin.[114]

5.2.3 Colon cancer

Colon cancer, the third-most common malignant tumor, is associated with high mortality, accounting for more than 1.4 million new cases and over half a million deaths worldwide annually.[115] Current therapeutic approaches for colon cancer treatment include surgery,

chemotherapy, and radiotherapy. Of these modalities, chemotherapy is the most effective method.[116] Curcumin-loaded PLGA NPs were successfully prepared and coated with chitosan, WGA (wheat germ agglutinin) and GE11(a dodeca peptide) to yield drug carriers for ameliorating curcumin delivery to HT-29 colon cancer cells.[117] Stability studies revealed a good colloidal stability of the coated curcumin-loaded PLGA NPs (C-PLGA NPs) formulations in synthetic gastrointestinal fluids. The NP interactions and cell uptake were studied by means of QCM combined with SLBs and SPR combined with living cells. The QCM and SPR techniques in combination with biomimetic sensing layers were found to be successful tools to investigate the targeting properties of NPs. These innovative techniques allowed in fact for elucidating a few aspects of NP/cell interactions and uptake providing for the correlation between the nature of the coating and the cell selectivity. The results showed that CS-coated CPLGA NPs can interact with the cells by nonspecific electrostatic mechanisms, while WGA- and GE11-coated CPLGA NPs mediate active recognition of specific cell targets.

Cationic PLGA NPs were employed as carriers to codeliver CPT (camptothecin) and CUR for colon cancer combination chemotherapy.[118] The resultant NPs had desirable diameters and size distribution, and a slightly positive zeta-potential. Studies on drug release and cellular uptake of this codelivery system showed that both drugs were effectively taken up by cells and released simultaneously. Cationic CPT/CUR-NPs exhibited clear synergistic effects against Colon-26 cells. Furthermore, these synergistic effects depended on drug ratios, with NPs with a CPT/CUR ratio of 4: 1 showing the highest anticancer activity toward Colon-26 cells. These studies unambiguously demonstrate that dual-drug-loaded NPs act in a synergistic manner to effectively reduce the dose of drug required.

The nanofibers of poly(lactide-glycolide)/chitosan loaded with curcumin (PLGA/CS/Cur) was developed by electrospinning technique for controlled cur delivery. At pH 7.4, the release followed Fickian diffusion mechanism; while at pH 2.0, the release followed the coexistence of diffusion and erosion mechanisms. The amount of Cur released at pH 2.0 was much higher than that at pH 7.4. Hence, the nanofibers exhibited higher anticancer activity at acidic environment and have the potential as a pH responsive vehicle for the controlled drug delivery.[119] Indole-incorporated curcumin analogue and curcumin loaded PLGA nanoparticles were synthesized by solvent evaporation. technique.

The nanoparticle treatment against human colon cancer cell line SW480 triggered nuclear fragmentation, cell cycle blockade, inhibition of apoptosis and metastatic biomarkers. These drug-loaded nanoparticles may be potent nano-formulations against colon cancer because of its ability to tolerate extreme pH environments, thus having potential of oral drug-delivery.[120] PLGA colloidal particles stabilized by complexes of two oppositely charged polysaccharides, chitosan (cationic, CS) and sodium CM-cellulose (anionic, NaCMC), displayed pH-dependent characteristic. The CS/NaCMC-covered-PLGA particles loaded with curcumin showed delayed release in mildly acidic conditions and faster release in neutral and basic conditions. Cytotoxicity experiments were carried out with human colorectal carcinoma cells.[121] The properties of the optimized curcumin loaded PLGA nanoparticles predicted by the 23 factorial design approach correlated very well with the experimental determinations. In vitro cellular uptake studies with HT-29 cells showed that the optimized curcumin-loaded PLGA nanoparticle exhibited a much higher cellular uptake of curcumin (i.e., 7.01 ± 0.33 μg/106 cells) than a native curcumin soln. (3.74 ± 0.56 μg/106 cells).[122] Poly (lactic-co-glycolic acid) (PLGA)—based polymeric oil-cored nanocapsules (NCs) for

curcumin loading and delivery to colon cancer in mice after systemic injection. Formulations of different oil compositions are prepared and characterized for their curcumin loading, physico-chemical properties, and shelf-life stability. The results indicate that castor oil-cored PLGA-based NC achieves high drug loading efficiency (≈18% w(drug)/w(polymer)%) compared to previously reported NCs. Curcumin-loaded NCs internalize more efficiently in CT26 cells than the free drug, and exert therapeutic activity in vitro, leading to apoptosis and blocking the cell cycle.[123]

5.2.4 *Lung cancer*

Lung cancer is an aggressive deadly disease worldwide. As a leading cancer type, the global incidence of lung cancer is rising by 0.5% per year, and the mortality from lung cancer is expected[124] to be over 50% by 2020. Thus, there are urgent needs to exploit new specific drugs or novel therapeutic methods for lung cancer treatment. It has been well established that tumor growth, including lung cancer, is critically dependent on angiogenesis for nutrients and oxygen supply. Therefore, antiangiogenesis has been regarded as a promising therapeutic strategy for clinical therapy of cancer.[125,126] PLGA microspheres (MS) showed an optimizing potential as a long-term delivery system. The cytotoxicity of the human dermal microvascular endothelial cells (HMEC-1) was significantly increased by AS−Cur−PLGA-Ms. Furthermore, codelivery of angiostatin (As) and curcumin (Cur) by PLGA Ms significantly inhibited the tumor growth in vivo.[127] Poly (N-isopropylacrylamide-co-methacrylic acid) (PNIPAAm-MAA) is one of the hydrogel copolymers utilized in the drug delivery system for cancer therapy. Roointan et al. have reported two nanocarriers Poly (lactic-co-glycolic acid)-Polyethylene glycol (PLGA-PEG) and N-Isopropylacrylamide-methacrylic acid (NIPAAm-MAA) in delivery of curcumin and also in levels of human telomerase reverse transcriptase (hTERT) silencing in lung cancer cell line (calu-6). Telomerase reverse transcriptase (abbreviated to TERT, or hTERT in humans) is a catalytic subunit of the enzyme telomerase. The MTT results demonstrated that the IC50 values of curcumin loaded nanocarriers were in lower concentrations than free curcumin. The hTERT expression levels were decreased by curcumin loaded PLGA-PEG more than curcumin loaded NIPAAm-MAA and free curcumin. The curcumin loaded PLGA-PEG can be a useful nano-based carrier for delivery of anticancer agents such as curcumin to fight lung cancer.[128]

Curcumin-loaded PLGA-PEG-Fe3O4 nanoparticles and comprise the effects of pure curcumin and curcumin-nanomagnetic encapsulated in PLGA-PEG on cell cytotoxicity and hTERT gene expression in A549 lung cancer cell line. IC50 of pure curcumin and nano-encapsulated curcumin during 24, 48, and 72 h was obtained as 50.5, 49.1, and 48.3 μM and 23.7, 13.6, and 7.3 μM, resp. Moreover, nano-encapsulated curcumin showed time-dependent cytotoxic effect on A549 cell line during 24, 48, 72 h in comparison with pure curcumin.[129]

5.2.5 *Ovarian cancer*

Ovarian cancer is one of the most dismal malignancies in women.[130] The principal site of which remains the peritoneal cavity. An effective approach of therapeutic strategies includes cytoreductive surgery followed by chemotherapies.[131] IP (intraperitoneal) delivery of these chemotherapeutics might provide the possibility to accumulate high concentration at the tumor site within the peritoneum for prolonged time. Dual et al. exploited curcumin-loaded biodegradable PLGA nanoparticles (CUR-NP) for photodynamic therapy using a custom

manufactured prototype low power LED device. CUR-NPs exhibit better physicochemical properties compared to free curcumin, such as improved serum stability. Furthermore, hemocompatibility of curcumin was improved through polymeric encapsulation, minimizing the risk of hemorrhages in patients. Curcumin, which elsewise is safe for normal cells, showed cytotoxic effects on tumor cells upon irradiation at a low intensity therefore selectively inhibiting tumor growth. Since production of ROS (Reactive oxygen species) occurs only upon irradiation of the intracellular photosensitizer, tumor tissues can be targeted with precision. Using LED as an irradiation source offers several advantages such as portability, durability, and economical compared to lasers. Moreover, LED's can irradiate a relatively larger area, which could be beneficial for the treatment of large tumors or even skin cancer.[132]

Dwivedi et al. have established a novel liquid-driven coflow focusing (LDCF) process to fabricate curcumin (CUR)-loaded poly (lactic-co-glycolic acid) (PLGA) microparticles (CPMs). The LDCF-CPMs reveal the physiochemical stability with sustained release profile corresponding to 95% CUR release over a period of 14 days in an in vitro release medium. Moreover, LDCF-CPMs were testified for cytotoxicity against SKOV-3 ovarian cancer cell lines and peritoneal delivery advantages by animal experiments. The pharmacokinetics of LDCF-CPMs in rats following IP injection shows slow systemic absorption with mean residence time (MRT) of 13.54 h in comparison with 9.82 and 6.74 h for single emulsion SE-CPMs and free CUR, respectively. In addition, IP delivery of CUR can expose the ovarian tumor to higher concentration for a longer duration by programming the thickness of the shell. The study provides compelling evidence for LDCF-CPMs having high therapeutic opportunity in the treatment of peritoneal cancers, such as ovarian, that reside in the peritoneal cavity.[133] Zeng et al. have evaluated the efficacy of paclitaxel combined with curcumin (CUR) against drug resistance in ovarian cancer cells. PLGA-phospholipid-PEG nanoparticles were prepared using the nano precipitation method. Adrenomedullin (ADM), an autocrine/paracrine factor produced by both stromal cells and cancer cells, was used to induce the A2780 cell line (human ovarian cancer cell line) to establish the model of the multidrug resistance (MDR) cell line, and the protein activity of P-glycoprotein (P-gp) in the A2780 cell line and A2780/ADM resistant cell line was determined using Western blot analysis. The prepared nanoparticles were uniform in size (100 nm), and round in shape. The results of the protein trace printing experiment showed that the P-gp content of the drug-resistant cell line was significantly reduced by the CUR nanoparticles. PLGA-phospholipid nanoparticles containing Taxol and CUR have improved solubility and stability together with a slow-release effect. In addition, CUR was able to overcome the MDR of tumor cells by elevating the paclitaxel concentration in the tumor cells to improve the antitumor activity of this combination.[134]

5.2.6 Cervical cancer

Cervical cancer is the second most common cancer and the largest cancer killer among women in most developing countries including India. Although various drugs have been developed for cervical cancer, treatment with these drugs often results in a number of undesirable side effects, toxicity, and multidrug resistance (MDR). Also, the outcomes for cervical cancer patients remain poor after surgery and chemo radiation. Jisha et al. have reported that curcumin entrapped nanoparticles of PLGA−PEG copolymer which were conjugated with folic acid (PPF copolymer) for site specific targeting exhibit enhanced anticancer activity,

since many cancer cells exhibit external folic acid binding receptors. In vitro release kinetics measurements of the drug from the nanoparticles showed a controlled release pattern up to 5 days. The MTT assay depicted a high amount of cytotoxicity of PPF nanocurcumin in HeLa cells. Cellular uptake studies demonstrated the efficacy of surface engineering with folate over free nanoparticles. The AO/EB staining, DAPI staining, and clonogenic assay (in vitro cell survival assay based on the ability of a single cell to grow into a colony) of the nanoparticles confirm the efficacy and mechanism by which the cytotoxicity was induced.[135] Mohd et al. have reported poly(lactic-co-glycolic acid)-based curcumin nanoparticle formulation (Nano-CUR) is compared to free CUR. Nano-CUR effectively inhibits cell growth, induces apoptosis, and arrests the cell cycle in cervical cancer cell lines. Nano-CUR treatment modulated the entities such as miRNAs, transcription factors and proteins associated with carcinogenesis. Moreover, Nano-CUR effectively reduced the tumor burden in a preclinical orthotopic mouse model of cervical cancer by decreasing oncogenic miRNA-21, suppressing nuclear β-catenin and abrogating expression of E6/E7 HPV oncoproteins including smoking compound benzo[a]pyrene (BaP) induced E6/E7 and IL-6 expression. These superior preclinical data suggest that nano-CUR may be an effective therapeutic modality for cervical cancer[136](Fig. 28.9).

Ayyanar et al. have synthesized the biodegradable PLGA microspheres (MS) containing magnetic iron oxide nanoparticles (MIONPs) with curcumin by the emulsion solvent evaporation method. The curcumin drug release profiles resulted that the MMS have a pH-induced drug-releasing asset with a cumulative drug releasing efficiency of 73.25%. The microspheres have cytotoxicity against HeLa cell lines with a significant potency that is promising for targeted chemotherapeutic applications.[137]

5.2.7 *Brain cancer*

Malignant brain cancer treatment is limited by a number of constraints, including the blood−brain barrier, transport within the brain interstitium, difficulties in delivering therapeutics specifically to tumor cells, the highly invasive quality of gliomas, and drug resistance. As a result, the prognosis for patients with high-grade gliomas is poor and has improved little in recent years. Nanomedicine approaches have been developed in the laboratory, with some technologies being translated to the clinic, in order to address these issues.

Significant cytotoxicity on RG2(rat glioma-2 tumor model) cells by curcumin-loaded PLGA-DSPE-PEG [poly(lactic-co-glycolic acid)-1,2-distearoyl-glycerol-3-phospho-ethanolamine-N-[methoxy (polyethylene glycol)-2000] ammonium salt] nanoparticles have been reported. Intratumoral applications of curcumin alone and curcumin-loaded nanoparticles both decrease tumor size (from66.6 ± 44.6 to 34.9 ± 21.7mm3, $P = .028$), but curcumin-loaded nanoparticles were more effective in reduction of tumor size than intratumoral curcumin injection alone Clinical studies should also be implemented for common use of curcumin-loaded PLGADSPE-PEG nanoparticles in the treatment of glioblastoma patients in clinical practice.[138]

Jamali et al. have reported that antibody conjugated biodegradable PLGA nanoparticles were developed to enhance the photodynamic efficiency of curcumin (CUR) on glioblastoma tumor cells. The effect of monoclonal antibody (MAb) on the tyrosine phosphorylation of EGFRvIII after photodynamic therapy (PDT) was assessed. The immunoreactivity of the antibody in MAb-PLGA NPs was preserved during the process of conjugation. The selective

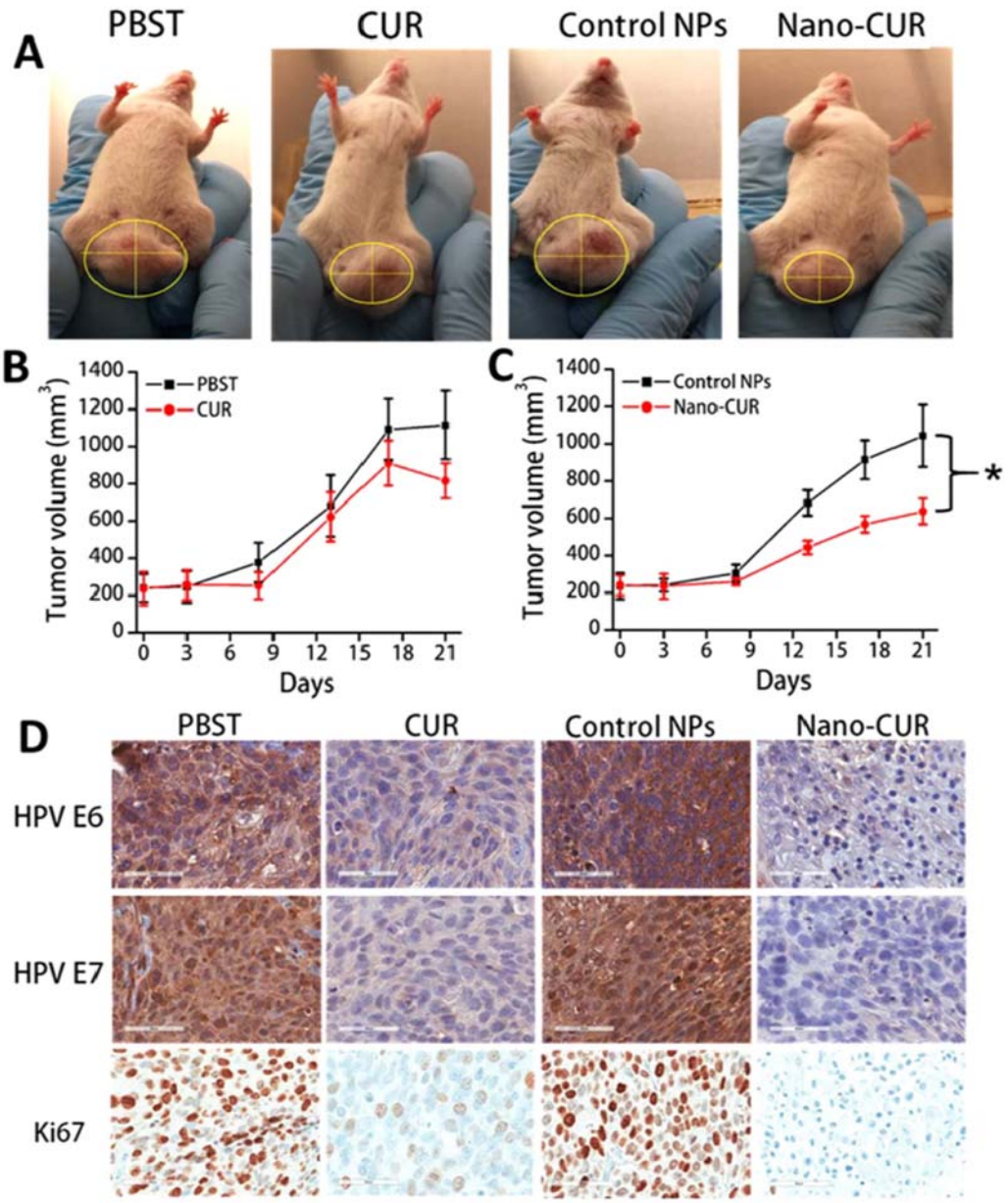

FIGURE 28.9 Tumor formation in female nude mice by injecting four million CaSki cells. (A–C) Nano-CUR was able to reduce the tumor burden by a considerable amount as compared to free CUR. Error bars show SEM; N = 6; *$P < .05$. (D) Immunohistochemical (IHC) analysis showed that CUR and Nano-CUR were effective in suppressing the expression of HPV oncogenic proteins E6 and E7 and cell proliferation marker Ki67 in mice. Original magnification 400X.

cellular internalization of MAb-PLGA NPs (FITC or CUR loaded) into the DKMG/EGFRvIII cells (EGFRvIII overexpressed human glioblastoma cell line) in comparison with DK-MG^{low} (human glioblastoma cell line with low level of EGFRvIII) was also confirmed. MAb-CUR-PLGA NPs were able to show more effective photodynamic toxicity (56% vs. 24%) on the DKMG/EGFRvIII cells compared to CUR-PLGA NPs. These results suggest that the anti-EGFRvIII MAb-CUR-PLGA NPs have potential of targeted drug delivery system for PDT in the overexpressed EGFRvIII tumor cells.[139]

Curcumin loaded PLGA nanoparticles (CUR-PLGA-NPs) as a drug delivery system to overcome the limitation of hydrophobicity of CUR as well as to investigate its toxicity effect on human glioblastoma U87MG cells compared to free CUR has been reported. The cytotoxicity studies on U87MG cell line indicated that CUR-PLGA-NPs had high cytotoxicity effects compared to free CUR. The half maximal inhibitory concentration (IC50) after cell incubation for 72 h was 57.99 μg/mL and 32.90 μg/mL for free CUR and CUR-PLGA-NPs, respectively.[140]

5.2.8 Skin cancer

Cutaneous malignancy is one of the major types of skin cancers that is lethal.[141] According to the World Cancer report, around 30% of cancers diagnosed in the recent past are skin cancer.[142] Like many other cancers, there are no specific preventive measures for skin cancer.[143] There are few drugs available for the treatment of skin cancer, but their toxic side effects on the vital organs limits their use.[144,145] Malathi et al. have developed poly (lactic-co-glycolic acid) (PLGA) nanopatterned films (NPFs) through poly dimethyl siloxane (PDMS) cast molding technique and explored its therapeutic efficacy in combination with curcumin and tocopherol poly (ethylene glycol) 1000 succinate (TPGS). Poly (lactic-co-glycolic) acid nanopatterned films (CTP-NPFs) showed good in vitro cytotoxicity toward human skin cancer cell line (A431) when compared to that of unpatterned films. CTP-NPFs effectively reduced the progression of cancer cells in vivo, in the skin carcinogenesis model in Swiss albino mice induced by 7, 12-Dimethylbenz[a]anthracene (DMBA)/croton oil.[146] Curcumin (Cur) and Chrysin (Chr), two natural anticancer drugs, coencapsulated in PLGA-PEG nanoparticles (NPs) showed the highest melanoma tumor growth inhibition was detected for CurChr NPs, followed by CurChr = Cur NPs > Cur > Chr NP > Chr.[147]

5.2.9 Liver cancer

Liver is the largest solid organ of the human body and bears some important functions. The occurrence of malignant liver tumors will lead to life-threatening consequences. Liver cancer is the sixth most fatal cancer in the world, which is usually treated by surgery.[148] Since most patients are diagnosed at advanced stages, effective nonsurgical treatment, such as systemic chemotherapy, is urgently needed.[149] At present, the most active single drugs for liver cancer include adriamycin, sorafenib, 5-fluorouracil, and cisplatin. However, with a response rate of only 10%, they have no significant effect on the overall survival rate. This may be due to the toxicity and poor response resulted from chemoresistance.[150] Chen et al. have reported the preparation of curcumin-loaded (PLGA/TPGS) NPs by emulsification and solvent evaporation method. Curcumin-loaded (PLGA/TPGS) NPs could be successfully internalized by HepG2 cells and play a synergistic role in inhibiting the growth of hepatocellular carcinoma

cells. They exhibit high target organ accumulation, superior antitumor efficiency, and lower toxicity in vivo.[151]

The effect of different physically adsorbed polymer coating (Tween 80, PEG 4000 and Pluronic F68) on the cytotoxic activity of optimized bis(dimethoxy)curcumin (BDMC) loaded-PLGA nanoparticles has been investigated. BDMC-loaded PLGA nanoparticles depend on the polymer type, polymer concentration and PVA concentration. Coated NPs showed the highest inhibition of malignant cells viability compared to the uncoated NPs and free BDMC where the IC50 of Pluronic-F68 coated NPs was 0.54 ± 0.01 μg/mL. The augmented effect against malignant cells poses these particles as a successful cancer remedy.[152]

Curcumin (CUR) loaded PLGA microbubble(MB) mediated sono-photodynamic therapy (SPDT) (CUR-PLGA-MB-SPDT) in HepG2 liver cancer cells was reported. Transmission electron microscopy revealed pyroptosis and apoptosis in the CUR-PLGA-MB-SPDT group; the potential mechanism was related to the mitochondrial membrane potential loss and increased production of intracellular reactive oxygen species.[153] Curcumin-loaded porous PLGA nanoparticles (NPs) were prepared, and surface modified with red blood cell membranes (RBCM) to yield biomimetic RBCM-p-PLGA@Cur NPs. In vitro studies showed that drug release from nonporous PLGA NPs was slow and that much of the drug remained trapped in the NPs. RBCM-p-PLGA@Cur NPs possess potent antitumor activity in a murine H22 xenograft cancer model (in terms of reduced tumor volume and mass, as well as inducing apoptosis of tumor cells) and have no observable systemic toxicity.[154]

5.2.10 *Prostate cancer*

Prostate cancer is the most frequently diagnosed cancer and the leading cause of cancer deaths among males worldwide. The best lines of defense, viz., radiation therapy and chemotherapy are unsatisfactory due to the untoward side effects on healthy cell and the problem of drug resistance[155–158]. Gracia et al. have reported that curcumin impregnated PLGA administered subcutaneously to PCa xenografts shows a clear and robust antitumor effect, with the bioavailability and controlled release of the curcumin are likely to be responsible for an increase in antitumor responses compared with oral administration.[159] The toxic effect of encapsulation of Cur in PLGA nanospheres (NCur) on PC3 human cancer prostate cell has been reported. The effects of MTT assays revealed that the NCur at the concentration of 25 μg/mL for 48 h were able to exert a more pronounced effect on the PC3 cells as compared to free Cur. Apoptotic index was significantly increased in NCur-treated cells compared to free Cur. The percentage of autophagic cells (LC3- II positive cells) was also significantly increased in NCur treatment in comparison to free Cur. These data indicate that the NCur has considerable cytotoxic activity more than Cur on PC3 cell lines, which is mediated by induction of both apoptotic and autophagic processes. Thus, NCur has high potential as an adjuvant therapy for clinical application in prostate cancer.[160]

The curcumin loaded nanolipomers (PLGA-DSPE-PEG) were fabricated using a microfluidic synthesis method under high flow parameters. Functional assessment of uptake of the nanolipomers in C4–2B prostate cancer cells showed increased uptake at 24 h. The nanolipomer was more effective in the cell viability assay compared to free drug. In vivo retention in mice of these nanolipomers revealed retention for up to 2 h and were completely cleared at 24 h.[161]

5.2.11 Pancreatic cancer

Pancreatic cancer is the fourth most predominant cancer with high patient mortality rate and the incidence of the disease is approximately equal to the annual deaths.[162,163] More than 85% of patients diagnosed are at an advanced tumor stage (either locally spread or metastasized to distant organs) with a median survival of 8−12 months in locally advanced stage and 3−6 months in metastatic stage.[164] Thus, metastasis of cancer cells to distant organs is considered as one of the major causes of therapeutic failure and high incidence of death in pancreatic cancer.[165] Arya et al. have explored the above approach to formulate curcumin-loaded Poly D, L-lactide-co-glycolide (PLGA) NPs and further surface coated it with chitosan and PEG (CNPs) with the anticipation to reduce the limitations associated with native curcumin delivery for achieving an optimum therapeutic effect. The NPs are of nanometer range having smooth and spherical surface morphology and with an efficient loading of curcumin. In vitro, cellular studies revealed superior cytotoxicity, enhanced antimigratory, antiinvasive, and apoptosis-inducing ability of CNPs in metastatic pancreatic cancer in comparison to a native counterpart.[166] Mukerjee et al. have demonstrated robust intracellular uptake of the curcumin loaded PLGA nanospheres in the cells. Cell viability studies revealed that the curcumin-loaded nanospheres were able to exert a more pronounced effect on the cancer cells as compared to free curcumin.[28]

5.2.12 Colorectal cancer

Current therapeutic attitudes for colorectal cancer therapy include surgery, chemotherapy, and radiotherapy. Of these modalities, chemotherapy is the most efficient approach. However, application of a single chemotherapeutic agent usually fails to attain appropriate cancer remission due to the development of drug resistance, heterogeneity of cancer cells, and adverse effects as a result of high and/or repeated administration.[167,168] To overcome these issues and for better therapeutic effectiveness, combinational chemotherapy has been approved in clinics as an initial cancer therapy regimen. Copolymers of PLGA/PEG were employed as carriers to codelivery of Cur and Chr(chrysin) into Caco-2 cells for colorectal cancer combination chemotherapy. Combinational nanoformulation of Cur−Chr was capable of killing Caco-2 cancer cells (human epithelial colorectal adenocarcinoma cancer cells.) more quickly than either treatment alone, thereby potentially this strategy can reduce cytotoxicity and patient side effects. Moreover, the codelivery of Cur and Chr by PLGA/PEG nanocarrier suppresses hTERT expression more efficiently relative to the delivery of either Cur or Chr at the same concentrations, indicating synergism.[169] Li et al. have synthesized CUR-NPs (curcumin-loaded lipid-polymer-lecithin hybrid nanoparticles) and functionalized with ribonucleic acid (RNA) aptamers (Apts) against epithelial cell adhesion molecule (EpCAM) for targeted delivery to colorectal adenocarcinoma cells. The encapsulation of CUR in Apt-CUR-NPs resulted in the increased bioavailability of delivered CUR over a period of 24 h compared to that of free CUR in vivo. These results show that the EpCAM Apt-functionalized CUR-NPs enhance the targeting and drug delivery of CUR to colorectal cancer cells.[170]

6. Conclusions

We have summarized the recent development and application of PLGA/curcumin nanoformulations in anticancer therapy. PLGA synthesis, their physicochemical properties, fabrication of PLGA nanoparticles, and curcumin-loaded PLGA nanoparticles are discussed. Their functional properties toward different cancer types such as breast cancer, blood cancer, colon cancer, lung cancer, ovarian cancer, cervical cancer, brain tumor, skin cancer, liver cancer prostate cancer, pancreatic cancer, and colorectal cancer are highlighted.

The drug delivery and therapeutics is one which is complex and continually evolving. Numerous challenges associated with biomedical applications, whether through drug delivery or engineering, include but are not limited to an understanding of the cellular environment, safety, and toxicity issues, scale up for large-scale manufacturing, and cost burdens. A strategy that addresses most of these concerns would be a boon to drug delivery and biomedical engineering.

PLGA has been one of the most popular polymers since its approval by the USFDA and EMA. It represents a unique class of polymers useful in medicine and holds great promise for future biomedical applications and provides the benefits of a minimally invasive strategic regenerative medication. It can be invariably tailored to meet the demands of specific therapies and controlled drug deliveries by modifying its lactide/glycolide ratio. Its biodegradability, biocompatibility, and minimal toxicity make it a safe choice for applications in bone tissue engineering, cancer therapeutics, vaccine and gene delivery, brain-related disorders, and several other biomedical uses. More detailed studies on the mechanism of action of the PLGA-based strategies, their functionalities, in vivo evaluation, pharmacokinetic modeling, biodistribution, and toxicity assessment are required. These findings should be validated and reproducible in clinical trials. More laboratory leads should find their way to successful clinical trials and demonstrate therapeutic benefit and proof of efficacy in these trials.

Acknowledgment

One of the authors (SM) thanks the University Grants Commission, India for the award of Dr. D. S. Kothari Post-Doctoral Fellowship [No.F.4-2/2006 (BSR)/CH/18−19/0122]. One of the authors (SNK) thanks the University Grants Commission, India for the award of the UGC-BSR Faculty Fellowship [No.F.4-5(11)2019 (BSR)].

References

1. Siegel RL, Miller KD, Jemal A. Cancer statistics, 2020. *CA A Cancer J Clin* 2020;**70**(1):7−30.
2. Lammers T, Kiessling F, Hennink WE, Storm G. Drug targeting to tumors: principles, pitfalls and (pre-) clinical progress. *J Contr Release* 2012;**161**(2):175−87.
3. Amreddy N, Babu A, Muralidharan R, Panneerselvam J, Srivastava A, Ahmed R, Mehta M, Munshi A, Ramesh R. Recent advances in nanoparticle-based cancer drug and gene delivery. *Adv Cancer Res* 2018;**137**:115−70.
4. Peer D, Karp JM, Hong S, Farokhzad OC, Margalit R, Langer R. Nanocarriers as an emerging platform for cancer therapy. *Nat Nanotechnol* 2007;**2**(12):751−60.
5. Malam Y, Loizidou M, Seifalian AM. Liposomes and nanoparticles: nanosized vehicles for drug delivery in cancer. *Trends Pharmacol Sci* 2009;**30**(11):592−9.

6. Kumar BS, Lutful M, Nanoemulsions A. Increasing possibilities in drug delivery. *Eur J Nanomed* 2013;**5**(2):97–110.
7. Alexis F, Pridgen E, Molnar LK, Farokhzad OC. Factors affecting the clearance and biodistribution of polymeric nanoparticles. *Mol Pharmacol* 2008;**5**(4):505–15.
8. Chan JM, Valencia PM, Zhang L, Langer, Farokhzad OC. Polymeric nano particles for drug delivery. *Methods Mol Biol* 2010;**624**:163–75.
9. Gupta M, Agrawal GP, Vyas SP. Polymeric nanomedicines as a promising vehicle for solid tumor therapy and targeting. *Curr Mol Med* 2013;**13**(1):179–204.
10. Parveen S, Sahoo SK. Polymeric nanoparticles for cancer therapy. *J Drug Target* 2008;**16**(2):108–23.
11. Sinha R, Kim GJ, Nie S, Shin DM. Nanotechnology in cancer therapeutics: bioconjugated nanoparticles for drug delivery. *Mol Cancer Therapeut* 2006;**5**(8):1909–17.
12. Swain S, Sahu PK, Beg S, Babu SM. Nanoparticles for cancer targeting current and future directions. *Curr Drug Deliv* 2016;**13**(8):1290–302.
13. Zhu X, Zeng X, Zhang X, Cao W, Wang Y, Chen H, Wang T, Hsiang-I T, Zhang R, Chang D, He S, Mei L, Shi X. The effects of quercetin-loaded PLGA-TPGS nanoparticles on ultraviolet B-induced skin damages in vivo. *Nanomedicine* 2016;**12**(3):623–32.
14. Hillery AM, Lloyd AW, Swarbrick J. In: *Drug delivery and targeting for pharmacists and pharmaceutical scientists*. London: Taylor & Francis Inc; 2001.
15. Gupta SC, Patchva S, Koh W, Aggarwal BB. Discovery of curcumin, a component of golden spice, and its miraculous biological activities. *Clin Exp Pharmacol Physiol* 2012;**39**(3):283–99.
16. Kuttan R, Bhanumathy P, Nirmala K, George MC. Potential anticancer activity of turmeric (Curcuma longa). *Cancer Lett* 1985;**29**(2):197–202.
17. Kocaadam B, Sanlier N. Curcumin, an active component of turmeric (Curcuma longa), and its effects on health. *Crit Rev Food Sci Nutr* 2017;**57**(13):2889–95.
18. Bar-Sela G, Epelbaum R, Schaffer M. Curcumin as an anti-cancer agent: review of the gap between basic and clinical applications. *Curr Med Chem* 2010;**17**(3):190–7.
19. Basnet P, Skalko-Basnet N. Curcumin: an anti-inflammatory molecule from a curry spice on the path to cancer treatment. *Molecules* 2011;**16**(6):4567–98.
20. Wilken R, Veena MS, Wang MB, Srivatsan ES. Curcumin: a review of anti-cancer properties and therapeutic activity in head and neck squamous cell carcinoma. *Mol Cancer* 2011;**10**:12.
21. Yallapu MM, Jaggi M, Chauhan SC. Curcumin nanoformulations: a future nanomedicine for cancer. *Drug Discov Today* 2012;**17**(1–2):71–80.
22. Shankar TN, Shantha NV, Ramesh HP, Murthy IA, Murthy VS. Toxicity studies on turmeric (Curcuma longa): acute toxicity studies in rats, guineapigs & monkeys. *Indian J Exp Biol* 1980;**18**(1):73–5.
23. Lao CD, Ruffin IV MT, Normolle D, Heath DD, Murray SI, Bailey JM, Boggs ME, Crowell J, Rock CL, Brenner DE. Dose escalation of a curcuminoid formulation. *BMC Compl Alternative Med* 2006;**6**:10.
24. Bansal SS, Goel M, Aqil F, Vadhanam MV, Gupta RC. Advanced drug delivery systems of curcumin for cancer chemoprevention. *Cancer Prev Res* 2011;**4**(8):1158–71.
25. Huang Q, Yu H, Ru Q. Bioavailability and delivery of nutraceuticals using nanotechnology. *J Food Sci* 2010;**75**(1):R50–7.
26. Anand P, Kunnumakkara AB, Newman RA, Aggarwal BB. Bioavailability of curcumin: problems and promises. *Mol Pharm* 2007;**4**(6):807–18.
27. Vareed SK, Kakarala M, Ruffin MT, Crowell JA, Normolle DP, Djuric Z, Brenner DE. Pharmacokinetics of curcumin conjugate metabolites in healthy human subjects. *Cancer Epidemiol Biomarkers Prev* 2008;**17**(6):1411–7.
28. Mukerjee A, Vishwanatha JK. Formulation, characterization and evaluation of curcumin loaded PLGA nanospheres for cancer therapy. *Anticancer Res* 2009;**29**(10):3867–75.
29. Braden ARC, Vishwanatha JK, Kafka E. *Formulation of active agent loaded activated PLGA nanoparticles for targeted cancer nano-therapeutics*. United States patent, US: University of North Texas Health Science Center at Fort Worth; 2008. 20080253961.
30. Anand P, Nair HB, Sung B, Kunnumakkara AB, Yadav VR, Tekmal RR, Aggarwal BB. Design of curcumin loaded PLGA nanoparticles formulation with enhanced cellular uptake, and increased bioactivity in vitro and superior bioavailability in vivo. *Biochem Pharmacol* 2010;**79**(3):330–8.

31. Cartiera MS, Ferreira EC, Caputo C, Egan ME, Caplan MJ, Saltzman WM. Partial correction of cystic fibrosis defects with PLGA nanoparticles encapsulating curcumin. *Mol Pharm* 2010;**7**(1):86–93.
32. Wang ZY, Zhao YM, Wang F, Wang JJ. Syntheses of poly (lactic acid-co-glycolic acid) serial biodegradable polymer materials via direct melt polycondensation and their characterization. *Applied Polymer Science* 2006;**99**(1):244–52.
33. Ajioka M, Enomoto K, Suzuki K, Yamaguchi A. The basic properties of poly (lactic acid) produced by the direct condensation polymerization of lactic acid. *J Environ Polym Degrad* 1995;**3**:225–34.
34. Ajioka M, Suizu H, Higuchi C, Kashima T. Aliphatic polyesters and their copolymers synthesized through direct condensation polymerization. *Polym Degrad Stabil* 1998;**59**(1–3):137–43.
35. Moon SI, Lee CW, Taniguchi I, Miyamoto M, Kimura Y. Melt solid polycondensation of L-lactic acid: an alternative route to poly (L-lactic acid) with high molecular weight. *Polymer* 2001;**42**(11):5059–62.
36. Takahashi K, Taniguchi I, Miyamoto M, Kimura Y. Melt solid polycondensation of glycolic acid to obtain high-molecular-weight poly (glycolic acid). *Polymer* 2000;**41**(24):8725–8.
37. Deasy PB, Finan MP, Meegan MJ. Preparation and characterization of lactic/glycolic acid polymers and copolymers. *J Microencapsul* 1989;**6**(3):369–78.
38. David RW, Ramani N, Jeffrey JK. Reversible kinetics and thermodynamics of the homopolymerization of l-lactide with 2-ethylhexanoic acid tin (II) salt. *Macromolecules* 1997;**30**(23):7075–85.
39. Dong CM, Qiu KY, Gu ZW, Feng XF. Synthesis of poly (D ,L -lactic acid-*alt* -glycolic acid) from D ,L -3-methylglycolide. *J Polym Sci Polym Chem Ed* 2000;**38**(23):4179–84.
40. Kowalski A, Duda A, Penczek S. Mechanism of cyclic ester polymerization initiated with tin (II) octoate. Macromolecules fitted with tin (II) alkoxide species observed directly in MALDI–TOF spectra. *Macromolecules* 2000;**33**(3):689–95.
41. Wu XS, Wang NJ. Synthesis, characterization, biodegradation, and drug delivery application of biodegradable lactic/glycolic acid polymers. Part II: biodegradation. *J Biomater Sci Polym Ed* 2001;**12**(1):21–34.
42. Habraken W, Wolke J, Mikos A, Jansen J. Injectable PLGA microsphere/calcium/phosphate cements: physical properties and degradation characteristics. *J Biomater Sci Polym Ed* 2006;**17**(9):1057–74.
43. Houchin ML, Topp EM. Physical properties of PLGA films during polymer degradation. *J Appl Polym Sci* 2009;**114**(5):2848–54.
44. Park PIP, Jonnalagadda S. Predictors of glass transition in the biodegradable poly lactide and poly-lactide-co-glycolide polymers. *J Appl Polym Sci* 2006;**100**(3):1983–7.
45. Avgoustakis K. *Poly lactic-co-glycolic acid (PLGA). Encyclopedia of biomaterials and biomedical engineering*. Taylor & Francis; 2005. Available from: https://doi.org/10.1081/E-EBBE-120013950.
46. Boury F, Marchais H, Proust JE, Benoit JP. Bovine serum albumin release from poly (α-hydroxy acid) microspheres: effects of polymer molecular weight and surface properties. *J Contr Release* 1997;**45**(1):75–86.
47. Makino G, Mogi T, Ohtake N, Yoshida M, Ando S, Nakajima T. Pulsatile drug release from poly (lactide-co-glycolide) microspheres: how does the composition of the polymer matrices affect the time interval between the initial burst and the pulsatile release of drugs? *Colloids and Surfaces B: Biointerfaces* 2000;**19**(2):173–217.
48. Danhier F, Ansorena E, Silva JM, Coco R, Le Breton A, Préat V. PLGA based nanoparticles: an overview of biomedical applications. *J Contr Release* 2012;**161**(2):505–22.
49. Anderson JM, Shive SM. Biodegradation and biocompatibility of PLA and PLGA microspheres. *Adv Drug Deliv Rev* 1997;**28**(1):5–24.
50. Tiainen J, Soini Y, Tormala. lactide/polyglycolide 80/20 screws take more than 11/2 years to resorb in rabbit cranial bone. *J Biomed Mater Res B Appl Biomater* 2004;**70**(1):49–55.
51. Vert M, Christel P, Chabot F, Leray J. Bioresorbable plastic materials for bone surgery. In: Hastings GW, Ducheyne P, editors. *Macromolecular biomaterials*. Boca Raton, FL: CRC Press; 1984. p. 119–42.
52. Vauthier C, Bouchemal K. Methods for the preparation and manufacture of polymeric nanoparticles. *Pharmaceut Res* 2009;**26**(5):1025–58.
53. Anton N, Benoit JP, Saulnier P. Design and production of nanoparticles formulated from nano-emulsion templates-A Review. *J Contr Release* 2008;**128**(3):185–99.
54. Moinard-Chécot D, Chevalier Y, Briançon S, Fessi H, Guinebretière S. Nanoparticles for drug delivery: review of the formulation and process difficulties illustrated by the emulsion-diffusion process. *J Nanosci Nanotechnol* 2006;**6**(9–10):2664–81.

55. Ibrahim H, Bindschaedler C, Doelker E, Buri P, Gurny R. Aqueous nanodispersions prepared by a salting-out process. *Int J Pharm* 1992;**87**(1−3):239−46.
56. Nahar M, Jain NK. Preparation, characterization and evaluation of targeting potential of amphotericin B-loaded engineered PLGA nanoparticles. *Pharmaceut Res* 2009;**26**(12):2588−98.
57. Özcan I, Azizoğlu E, Senyiğit T, Özyazici M, Özer Ö. Comparison of PLGA and lecithin/chitosan nanoparticles for dermal targeting of betamethasone valerate. *J Drug Target* 2013;**21**(6):542−50.
58. Yin P, Wang Y, Qiu YY, Hou LL, Liu X, Qin J, Duan Y, Liu P, Qiu P, Li1 Q. Bufalin-loaded mPEG-PLGAPLL-cRGD nanoparticles: preparation, cellular uptake, tissue distribution, and anticancer activity. *Int J Nanomed* 2012;**7**:3961−9.
59. Matthaus C, Schubert S, Schmitt M, Krafft C, Dietzek B, Schubert US, Popp J. Resonance Raman spectral imaging of intracellular uptake of β- carotene loaded poly(D, L-lactide-co-glycolide) nanoparticles. *ChemPhysChem* 2013;**14**(1):155−61.
60. Ibrahim MM, Abd-Elgawad AE, Soliman OA, Jablonski MM. Nanoparticle-based topical ophthalmic formulations for sustained celecoxib release. *J Pharmaceut Sci* 2013;**102**(3):1036−53.
61. Xu A, Yao M, Xu G, Ying J, Ma W, Li B, Jin Y. A physical model for the size-dependent cellular uptake of nanoparticles modified with cationic surfactants. *Int J Nanomed* 2012;**7**:3547−54.
62. Khalil NM, do Nascimento TCF, Casa DM, Dalmolin LF, Cristina de Mattos A, Hoss I, Romano MA, Mainardes RA. Pharmacokinetics of curcumin-loaded PLGA and PLGA-PEG blend nanoparticles after oral administration in rats. *Colloids Surf, B* 2013;**101**:353−60.
63. Aksungur P, Demirbilek M, Denkbas EB, Unlu N. Comparative evaluation of cyclosporine A/HPBCD incorporated PLGA nanoparticles for development of effective ocular preparations. *J Microencapsul* 2012;**29**(6):605−13.
64. Liu P, Yu H, Sun Y, Zhu M, Duan Y. A mPEG-PLGAb-PLL copolymer carrier for adriamycin and siRNA delivery. *Biomaterials* 2012;**33**(17):4403−12.
65. Varshochian R, Jeddi-Tehrani M, Mahmoudi AR, Khoshayand MR, Atyabi F, Sabzevari A, Esfahani MR, Dinarvand R. The protective effect of albumin on bevacizumab activity and stability in PLGA nanoparticles intended for retinal and choroidal neovascularization treatments. *Eur J Pharmaceut Sci* 2013;**50**(3−4):341−52.
66. Wang Y, Li P, Kong L. Chitosan-modified PLGA nanoparticles with versatile surface for improved drug delivery. *AAPS PharmSciTech* 2013;**14**(2):585−92.
67. Abdelghany SM, Quinn DJ, Ingram RJ, J. R, Gilmore BF, Donnelly RF, Taggart CC, Scott CJ. Gentamicin loaded nanoparticles show improved antimicrobial effects towards *Pseudomonas aeruginosa* infection. *Int J Nanomed* 2012;**7**:4053−63.
68. Lecaroz C, Gamazo C, Renedo MJ, Blanco-Prieto MJ. Biodegradable micro- and nanoparticles as long-term delivery vehicles for gentamicin. *J Microencapsul* 2006;**23**(7):782−92.
69. Alonso-Sande M, des Rieux A, Fievez V, Sarmento B, Delgado A, Evora C, Remuñán-López C, Préat V, Alonso MJ. Development of PLGA-mannosamine nanoparticles as oral protein carriers. *Biomacromolecules* 2013;**14**(11):4046−52.
70. Malathi S, Balasubramanian S. Synthesis of biodegradable polymeric nanoparticles and their controlled drug delivery for tuberculosis. *J Biomed Nanotechnol* 2011;**7**(1):150−1.
71. Malathi S, Balasubramanian S. Rifampicin-Loaded Poly(lactic-co-glycolic) acid microspheres: synthesis, characterization, delivery and their antimicrobial studies. *J Bionanoscience* 2011;**5**(1):47−52.
72. Malathi S, Rachita L, Purna Sai K, Balasubramanian S. Synthesis and characterization of biodegradable Poly (lactic-co-glycolic) acid polymer for treatment of melanoma. *Colloids Surf, B* 2014;**117**:128−34.
73. Malathi S, Nanthakumar P, Pandiyan V, Balasubramanian S. Novel PLGA based nanoparticles for the oral delivery of insulin. *Int J Nanomed* 2015;**10**:2207−18.
74. Saravanan S, Malathi S, Sesh PSL, Selvasubramanian S, Balasubramanian S, Pandiyan V. Hydrophilic poly (ethylene glycol) capped poly (lactic-co-glycolic) acid nanoparticles for subcutaneous delivery of insulin in diabetic rats. *Int J Biol Macromol* 2017;**95**:1190−8.
75. Young J, Chong SC, Sung HK, Kyung SK, Sun K, Yong HS, Jae WN. Preparation of poly(dl-lactide-co-glycolide) nanoparticles without surfactant. *J Appl Polym Sci* 2001;**80**(12):2228−36.
76. Mittal G, Sahana DK, Bhardwaj V, Ravi Kumar MN. Estradiol loaded PLGA nanoparticles for oral administration: effect of polymer molecular weight and copolymer composition on release behavior in vitro and in vivo. *J Contr Release* 2007;**119**(1):77−85.

77. Garinot M, Fievez V, Pourcelle V, Stoffelbach F, des Rieux A, Plapied L, Theatee I, Freichels H, Jérôme C, Marchand-Brynaert J, Schneider Y-J, Préat V. PEGylated PLGA-based nanoparticles targeting M cells for oral vaccination. *J Contr Release* 2007;**120**(3):195–204.
78. Esmaeili F, Ghahremani MH, Esmaeili B, Khoshayand MR, Atyabi F, Dinarvand R. PLGA nanoparticles of different surface properties: preparation and evaluation of their body distribution. *Int J Pharm* 2008;**349**(1–2):249–55.
79. Bala I, Hariharan S, Kumar MN. PLGA nanoparticles in drug delivery: the state of the art. *Crit Rev Ther Drug Carrier Syst* 2004;**21**(5):387–422.
80. Zhang Z, Feng SS. The drug encapsulation efficiency, in vitro drug release, cellular uptake and cytotoxicity of paclitaxel-loaded poly(lactide)-tocopheryl polyethylene glycol succinate nanoparticles. *Biomaterials* 2006;**27**(21):4025–33.
81. Yang A, Yang L, Liu W, Li Z, Xu H, Yang X. Tumor necrosis factor alpha blocking peptide loaded PEG-PLGA nanoparticles: preparation and in vitro evaluation. *Int J Pharm* 2007;**331**(1):123–32.
82. Umar A, Dunn BK, Greenwald P. Future directions in cancer prevention. *Nat Rev Cancer* 2012;**12**(12):835–48.
83. Gupta AP, Khan S, Manzoor MM, Yadav AK, Sharma G, Anand R, Gupta S. Chapter 10-Anticancer curcumin: natural analogues and structure-activity relationship. *Stud Nat Prod Chem* 2017;**54**:355–401.
84. Alibeiki F, Jafari N, Karimi M, Peeri Dogaheh H. Potent anti-cancer effects of less polar Curcumin analogues on gastric adenocarcinoma and esophageal squamous cell carcinoma cells. *Sci Rep* 2017;**7**(1):2559.
85. Goel A, Kunnumakkara AB, Aggarwal BB. Curcumin as "Curecumin": from kitchen to clinic. *Biochem Pharmacol* 2008;**75**:787–809.
86. Kçhler FE. *Kçhler's Medizinal-Pflanzen in naturgetreuen Abbildungen mit kurz erl uterndem Texte:* Atlas zur Pharmacopoea germanica. *Germany*. 1883.
87. Untermhaus G, Ammon H, Wahl MA. Pharmacology of Curcuma longa. *Planta Med* 1991;**57**(1):1–7.
88. Nagahama K, Utsumi T, Kumano T, Maekawa S, Oyama N, Kawakami J. Discovery of a new function of curcumin which enhances its anticancer therapeutic potency. *Sci Rep* 2016;**6**:30962.
89. Aggarwal BB, Deb L, Prasad S. Curcumin differs from tetrahydrocurcumin for molecular targets, signaling pathways and cellular responses. *Molecules* 2014;**20**(1):185–205.
90. Torre LA, Bray F, Siegel RL, Ferlay J, Lortet JT, Jemal A. Global cancer statistics, 2012. *CA A Cancer J Clin* 2012;**65**(2):87–108.
91. Vijayalakshmi A, Kumar PR, Priyadarsini SS, Meenaxshi C. In vitro antioxidant and anticancer activity of flavonoid fraction from the aerial parts of Cissus quadrangularis Linn. against human Breast carcinoma cell lines. *J Chem* 2013;**9**:1–9.
92. War SA, Kim B, Kumar U. Human somatostatin receptor-3 distinctively induces apoptosis in MCF-7 and cell cycle arrest in MDA-MB-231 breast cancer cells. *Mol Cell Endocrinol* 2015;**413**:129–44.
93. Paolo V, Paolo B, Miriam C, Laura P, Davide P. Intracellular drug release from curcumin-loaded PLGA nanoparticles induces G2/M block in breast cancer cells. *Biomacromolecules* 2013;**14**(3):672–82.
94. Jin H, Pi J, Zhao Y, Jiang J, Li T, Zeng X, Yang P, Evans C, Cai J. EGFR-targeting PLGA-PEG nanoparticles as a curcumin delivery system for breast cancer therapy. *Nanoscale* 2017;**9**(42):16365–74.
95. Zhe Y, Na S, Rui C, Chenyang Z, Jie L, Zhongmin T. Hybrid nanoparticles coated with hyaluronic acid lipoid for targeted co-delivery of paclitaxel and curcumin to synergistically eliminate breast cancer stem cells. *J Mater Chem B* 2017;**5**(33):6762–75.
96. Ria M, Ramkrishna S, Brahamacharry P, Julekha K, Shantanu G, Mita CD. Gemcitabine co-encapsulated with curcumin in folate decorated PLGA nanoparticles; a novel approach to treat breast adenocarcinoma. *Pharmaceut Res* 2020;**37**(3):56.
97. Ankita B, Sindhu CP, Ankit KR, Vivekanandan P, Yoshikata N, Toru M, Sakthi Kumar D. GANT61 and curcumin loaded PLGA nanoparticles for GLI-1 and PI3K/Akt mediated inhibition in breast adenocarcinoma. *Nanotechnology* 2020;**31**(18):185102.
98. Vakilinezhad MA, Amini A, Dara T, Alipour S. Methotrexate and Curcumin co-encapsulated PLGA nanoparticles as a potential breast cancer therapeutic system: in vitro and in vivo evaluation. *Colloids Surf, B* 2019;**184**:110515.
99. Kunal P, Dipranjan L, Pravat Kumar P, Shubham R, Souravi B, Ananya D, Kuladip J, Parimal K. An in vivo study for targeted delivery of curcumin in human triple negative breast carcinoma cells using biocompatible PLGA microspheres conjugated with folic acid. *J Nanosci Nanotechnol* 2019;**19**(7):3720–33.

100. Jian-Dong Y, De-Li ZG, Meng-Qi T, Meng-Ting L, Xia-Fang X, Xing T, Ying-Zheng Z, He-Lin X. pH-sensitive polymeric nanoparticles of mPEG PLGA-PGlu with hybrid core for simultaneous encapsulation of curcumin and doxorubicin to kill the heterogeneous tumor cells in breast cancer. *Artif Cell Nanomed Biotechnol* 2018;**46**(1):302–13.
101. Meena R, Kumar S, Raj kumar, Gaharwar US, Rajamani P. PLGA-CTAB curcumin nanoparticles: fabrication, characterization and molecular basis of anticancer activity in triple negative breast cancer cell lines (MDA-MB-231 cells). *Biomed Pharmacother* 2017;**94**:944–54.
102. Raana F, Younes P-S, Mehdi D, Shahrzad J, Javid L-A, Hadi S, Vahid S-I, Nosratollah Z. Nano-encapsulated metformin-curcumin in PLGA/PEG inhibits synergistically growth and hTERT gene expression in human breast cancer cells. *Artif Cell Nanomed Biotechnol* 2018;**46**(5):917–25.
103. Alex EG, Komal S, Brenda K, Jayanth P. Chemopreventive efficacy of curcumin-loaded PLGA microparticles in a transgenic mouse model of HER-2-positive breast cancer. *Drug Delivery and Translational Research* 2018;**8**(2):329–41.
104. Murali MY, Brij KG, Meena J, Subhash CC. Fabrication of curcumin encapsulated PLGA nanoparticles for improved therapeutic effects in metastatic cancer cells. *J Colloid Interface Sci* 2010;**351**(1):19–29.
105. Mohebian Z, Babazadeh M, Zarghami N, Mousazadeh H. Anticancer efficiency of curcumin-loaded mesoporous silica nanoparticles/nanofiber composites for potential postsurgical breast cancer. *J Drug Deliv Sci Technol* 2021;**61**:102170.
106. Malathi S, Arunkumar P, Premkumar K, Balasubramanian S. The remarkable role of emulsifier and chitosan, dextran and PEG as capping agents in the enhanced delivery of curcumin by nanoparticles in breast cancer cells. *Int J Biol Macromol* 2020;**162**:748–61.
107. Mukerjee A, Ranjan AP, Vishwanatha JK. Targeted nanocurcumin therapy using Annexin A2 antibody improves tumor accumulation and therapeutic efficacy against highly metastatic breast cancer. *J Biomed Nanotechnol* 2016;**12**(7):1374–92.
108. Hu D, Shilatifard A. Epigenetics of hematopoiesis and hematological malignancies. *Gene Dev* 2016;**30**(18):2021–41.
109. https://cancerstatisticscenter.cancer.org/#!/cancer-site/Leukemia.
110. Vinhas R, Cordeiro M, Pedrosa P, Fernandes AR, Baptista PV. Current trends in molecular diagnostics of chronic myeloid leukemia. *Leuk Lymphoma* 2017;**58**(8):1791–804.
111. Campiotti L, Suter MB, Guasti L, Piazza R, Gambacorti-Passerini C, Grandi AM, Squizzato A. Imatinib discontinuation in chronic myeloid leukaemia patients with undetectable BCR-ABL transcript level: a systematic review and a meta-analysis. *Eur J Cancer* 2017;**77**:48–56.
112. Patel AB, Wilds BW, Deininger MW. Treating the chronic-phase chronic myeloid leukemia patient: which TKI, when to switch and when to stop? *Expet Rev Hematol* 2017;**10**(7):659–74.
113. Ranjita M, Sanjeeb KS. Coformulation of doxorubicin and curcumin in Poly-(D, L-lactide-co-glycolide) nanoparticles suppresses the development of multidrug resistance in K562 cells. *Mol Pharm* 2011;**8**(3):852–66.
114. Mandy H, Leung M, Amy QS. Microfluidic assisted nanoprecipitation of PLGA nanoparticles for curcumin delivery to leukemia Jurkat cells. *Langmuir* 2018;**34**(13):3961–70.
115. Twelves C, Wong A, Nowacki MP, Abt M, Burris H, Carrato A, Cassidy J, Cervantes A, Fagerberg J, Georgoulias V, Husseini F, Jodrell D, Koralewski P, Kröning H, Maroun J, Marschner N, McKendrick J, Pawlicki M, Rosso R, Schüller J, Seitz J, Stabuc B, Tujakowski J, Hazel GV, Zaluski J, Scheithauer W. Capecitabine as adjuvant treatment for stage III colon cancer. *N Engl J Med* 2005;**352**(26):2696–704.
116. Liu C, Zhao G, Liu J, Ma N, Chivukula P, Perelman L, Okada K, Chen Z, Gough D, Yu L. Novel biodegradable lipid nano complex for siRNA delivery significantly improving the chemosensitivity of human colon cancer stem cells to paclitaxel. *J Contr Release* 2009;**140**(3):277–83.
117. Mohamed AA, Alma K-H, Teemu S, Timo O, Isabella MM, Antonio R, Hatem RI, Mohsen IA, Paolo C, Marjo Y, Ahmed MS, Francesca M, Stefano S, Tapani V. Real-Time label-free targeting assessment and in vitro characterization of curcumin loaded Poly-lactic-co-glycolic acid nanoparticles for oral colon targeting. *ACS Omega* 2019;**4**(16):16878–90.
118. Bo X, Xiaoying S, Moon KH, Emilie V, Mingzhen Z, Didier M. Co-delivery of camptothecin and curcumin by cationic polymeric nanoparticles for synergistic colon cancer combination chemotherapy. *J Mater Chem B* 2015;**3**(39):7724–33.

119. Chen M, Li L, Xia L, Jiang S, Kong Y, Chen X, Wang H. The kinetics and release behaviour of curcumin loaded pH-responsive PLGA/chitosan fibers with antitumor activity against HT-29 cells. *Carbohydr Polym* 2021;**265**:118077.
120. Sufi SA, Hoda M, Pajaniradje S, Mukherjee V, Coumar SM, Rajagopalan R. Enhanced drug retention, sustained release, and anti-cancer potential of curcumin and indole-curcumin analog-loaded polysorbate80-stabilized PLGA nanoparticles in colon cancer cell line SW480. *Int J Pharm* 2020;**588**:119738.
121. Inphonlek S, Sunintaboon P, Leonard M, Durand A. Chitosan/carboxymethylcellulose stabilized poly(lactide-co-glycolide) particles as bio-based drug delivery carriers. *Carbohydr Polym* 2020;**242**:116417.
122. Akl MA, Kartal-Hodzic A, Oksanen T, Ismael HR, Afouna MM, Yliperttula M, Samy AM, Viitala T. Factorial design formulation optimization and in vitro characterization of curcumin-loaded PLGA nanoparticles for colon delivery. *J Drug Deliv Sci Technol* 2016;**32**(Part-A):10−20.
123. Klippstein R, Wang JT-W, El-Gogary RI, Bai J, Mustafa F, Rubio N, Bansal S, Al-Jamal WT, Al-Jamal K. Passively targeted curcumin- loaded PEGylated PLGA nanocapsules for colon cancer therapy in vivo. *Small* 2015;**11**(36):4704−22.
124. Gibelin C, Couraud S. Somatic alterations in lung cancer: do environmental factors matter? *Lung Cancer* 2016;**100**:45−52.
125. Folkman J. Is angiogenesis an organizing principle in biology and medicine? *J Pediatr Surg* 2007;**42**(1):1−11.
126. Folkman J. Antiangiogenesis in cancer therapy-endostatin and its mechanisms of action. *Exp Cell Res* 2006;**312**(5):594−607.
127. Yue C, Xiaoguang Y, Yannan W, Jingwen Y, Yin W, Chunlei Y, Yanxin H, Yongli B, Luguo S, Yuxin L. Dual release of angiostatin and curcumin from biodegradable PLGA microspheres inhibit Lewis lung cancer in a mice model. *RSC Adv* 2016;**6**(112):111440−6.
128. Roointan A, Sharifi-Rad M, Badrzadeh F, Sharifi-Rad J. A comparison between PLGA-PEG and NIPAAm-MAA nanocarriers in curcumin delivery for hTERT silencing in lung cancer cell line. *Cell Mol Biol* 2016;**62**(9):51−6.
129. Sadeghzadeh H, Pilehvar-Soltanahmadi Y, Akbarzadeh A, Dariushnejad H, Sanjarian F, Zarghami N. The effects of nanoencapsulated curcumin-Fe3O4 on proliferation and hTERT gene expression in lung cancer cells. *Anti Cancer Agents Med Chem* 2017;**17**(10):1363−73.
130. Siegel R, Ma J, Zou Z, Jemal A. Cancer statistics. 2014. *CA A Cancer J Clin* 2014;**64**(1):9−29.
131. Marchini S, Fruscio R, Clivio L, Beltrame L, Porcu L, Fuso Nerini I, Cavalieri D, Chiorino G, Cattoretti G, Mangioni C, Milani R, Torri V, Romualdi C, Zambelli A, Romano M, Signorelli M, di Giandomenico S, D'Incalci M. Resistance to platinum-based chemotherapy is associated with epithelial to mesenchymal transition in epithelial ovarian cancer. *Eur J Cancer* 2013;**49**(2):520−30.
132. Lili D, Michael RA, Shashank RP, Jens S, Mohammed AS, Carsten E, Udo B. Photodynamic therapy of ovarian carcinoma cells with curcumin-loaded biodegradable polymeric nanoparticles. *Pharmaceutics* 2019;**11**(6):282.
133. Dwivedi P, Yuan S, Han S, Mangrio FA, Zhu Z, Lei F, Ming Z, Cheng L, Liu S, Si T, Xu RX. Core-shell microencapsulation of curcumin in PLGA microparticles: programmed for application in ovarian cancer therapy. *Artif Cell Nanomed Biotechnol* 2018;**46**(3):481−91.
134. Zeng L, Yuan-Yuan Z, Zhao-Yuan L, Si-Qing N. Evaluation of the efficacy of paclitaxel with curcumin combination in ovarian cancer cells. *Oncol Lett* 2016;**12**(5):3944−8.
135. Jisha JP, Arun K, Thulasidasan T, Ruby John A, Nandan CD, Ashwanikumara N, Vinod Kumar GS. Curcumin entrapped folic acid conjugated PLGA−PEG nanoparticles exhibit enhanced anticancer activity by site specific delivery. *RSC Adv* 2015;**5**(32):25518−24.
136. Mohd SZ, Neeraj C, Murali MY, Rishi KG, Diane MM, Sonam K, Mohammed S, Sheema K, Nadeem Z, Meena J, Subhash CC. Curcumin nanoformulation for cervical cancer treatment. *Sci Rep* 2016;**6**:20051.
137. Ayyanaar S, Kesavan MP, Sivaraman G, Maddiboyina B, Annaraj J, Rajesh J, Rajagopal G. *A novel curcumin-loaded PLGA micromagnetic composite system for controlled and pH-responsive drug delivery, Colloids and Surfaces, A: physicochemical and Engineering Aspects*, vol. 573; 2019. p. 188−95.
138. Orunoğlu M, Kaffashi A, Pehlivan SB, Sahin S, Söylemezoğlu F, Oğuz K,K, Mut M. Effects of curcumin-loaded PLGA nanoparticles on the RG2 rat glioma model. *Mater Sci Eng C* 2017;**78**:32−8.
139. Zahra J, Mehdi K, Sedigheh MH, Neda E, Saeideh A, Fatemeh I, Hemen M-S, Maliheh P. Evaluation of targeted curcumin (CUR) loaded PLGA nanoparticles for in vitro photodynamic therapy on human glioblastoma cell line. *Photodiagnosis Photodyn Ther* 2018;**23**:190−201.

140. Arzani H, Adabi M, Mosafer J, Dorkoosh F, Khosravani M, Maleki H, Nekounam H, Kamali M. Preparation of curcumin-loaded PLGA nanoparticles and investigation of its cytotoxicity effects on human glioblastoma U87MG cells. *Biointerface Res App Chem* 2019;**9**(5):4225–31.
141. Jung HS, Kong WH, Sung DK, Lee MY, Beack SE, Keum DH, Kim KS, Yun SH, Hahn SK. Nanographene oxide-hyaluronic acid conjugate for photothermal ablation therapy of skin cancer. *ACS Nano* 2014;**8**(1):260–8.
142. WHO website (www.who.int) assessed on 1 September 2015.
143. ASCO's patient information website-Cancer.Net (www.cancer.net).
144. Sporn MB, Suh N. Chemoprevention of cancer. *Carcinogenesis* 2000;**21**(3):525–30.
145. Wilson MA, Schuchter LM. Chemotherapy for melanoma. *Cancer Treat Res* 2016;**167**:209–29.
146. Malathi S, Pavithra PS, Sridevi S, Verma RS. Fabrication of nanopatterned PLGA films of curcumin and TPGS for skin cancer. *Int J Pharm* 2020;**578**:119100.
147. Tavakoli F, Jahanban-Esfahlan R, Seidi K, Jabbari M, Behzadi R, Pilehvar-Soltanahmadi Y, Zarghami N. Effects of nano-encapsulated curcumin-chrysin on telomerase, MMPs and TIMPs gene expression in mouse B16F10 melanoma tumour model. *Artif Cell Nanomed Biotechnol* 2018;**46**(2):75–86.
148. Altekruse SF, McGlynn KA, Reichman ME. Hepatocellular carcinoma incidence, mortality, and survival trends in the United States from 1975 to 2005. *J Clin Oncol* 2009;**27**(9):1485–91.
149. Villanueva A, Llovet JM. Targeted therapies for hepatocellular carcinoma. *Gastroenterology* 2011;**140**(5):1410–26.
150. Asghar U, Meyer T. Are there opportunities for chemotherapy in the treatment of hepatocellular cancer? *J Hepatol* 2012;**56**(3):686–95.
151. Chen XP, Li Y, Zhang Y, Li GW. Formulation, characterization and evaluation of curcumin- loaded PLGA-TPGS nanoparticles for liver cancer treatment. *Drug Des Dev Ther* 2019;**13**:3569–78.
152. Mina M, Rania MH, Ahmed SG, Samar M. Studying the effect of physically adsorbed coating polymers on the cytotoxic activity of optimized bisdemethoxycurcumin- loaded PLGA nanoparticles. *J Biomed Mater Res* 2017;**105**(5):1433–45.
153. Zhu J-X, Zhu W-T, Hu J-H, Yang W, Liu P, Liu Q-H, Bai Y-X, Xie R. Curcumin-loaded Poly(L-lactide-co-glycolide) microbubble-mediated sono-photodynamic therapy in liver cancer cells. *Ultrasound Med Biol* 2020;**46**(8):2030–43.
154. Xie X, Wang H, Williams GR, Yang Y, Zheng Y, Wu J, Zhu L-M. Erythrocyte membrane cloaked curcumin-loaded nanoparticles for enhanced chemotherapy. *Pharmaceutics* 2019;**11**(9):429.
155. Shi M, Cai Q, Yao L, Mao Y, Ming Y, Ouyang G. Antiproliferation and apoptosis induced by curcumin in human ovarian cancer cells. *Cell Biol Int* 2006;**30**(3):221–6.
156. Gonzalo ML, Isaacs WB. Molecular pathways to prostate cancer. *J Urol* 2003;**170**(6):2444–52.
157. Hayat MJ, Howlader N, Reichman ME, Edwards BK. Cancer statistics, trends, and multiple primary cancer analyses from the Surveillance, Epidemiology and End Results (SEER) program. *Oncol* 2007;**12**(1):20–37.
158. Richie JP. Anti-androgens and other hormonal therapies for prostate cancer. *Urology* 1999;**54**(6A):15–8.
159. Gracia E, Mancini A, Colapietro A, Mateo C, Gracia I, Festuccia C, Carmona M. Impregnation of curcumin into a biodegradable (Poly-lactic-co-glycolic acid, PLGA) support, to transfer its well known in vitro effect to an in vivo prostate cancer model. *Nutrients* 2019;**11**(10):2312.
160. Seyed S, Mohammadreza A, Ali K, Layasadat K, Mahmoud O, Abbas H-M. Anticancer activity of curcumin-loaded PLGA nanoparticles on PC3 prostate cancer cells. *Iran J Pharm Res (IJPR)* 2017;**16**(3):868–79.
161. Gdowski A, Johnson K, Shah S, Gryczynski I, Vishwanatha J, Ranjan A. Optimization and scale up of microfluidic nanolipomer production method for preclinical and potential clinical trials. *J Nanobiotechnol* 2018;**16**(1):12.
162. Nieto J, Grossbard ML, Kozuch P. Metastatic pancreatic cancer 2008: is the glass less empty? *Oncol* 2008;**13**(5):562–76.
163. Sun C, Ansari D, Andersson R, Wu DQ. Does gemcitabine-based combination therapy improve the prognosis of unresectable pancreatic cancer? *World J Gastroenterol* 2012;**18**(35):4944–58.
164. Long J, Luo G, Liu C, Cui X, Satoh K, Xiao Z, Zhang B, Xu J, Ni Q, Li M, Yu X. Development of a unique mouse model for pancreatic cancer lymphatic metastasis. *Int J Oncol* 2012;**41**(5):1662–8.
165. Fujii T. Extended lymphadenectomy in pancreatic cancer is crucial. *World J Surg* 2013;**37**(8):1778–81.
166. Geetanjali A, Manasi D, Sanjeeb Kumar S. Evaluation of curcumin loaded chitosan/PEG blended PLGA nanoparticles for effective treatment of pancreatic cancer. *Biomed Pharmacother* 2018;**102**:555–66.

167. Ciombor K, Wu C, Goldberg R. Recent therapeutic advances in the treatment of colorectal cancer. *Annu Rev Med* 2015;**66**:83–95.
168. Ricciardiello L, Bazzoli F, Fogliano V. Phytochemicals and colorectal cancer prevention—myth or reality? *Nat Rev Gastroenterol Hepatol* 2011;**8**(10):592–6.
169. Javid L-A, Younes P-S, Mehdi D, Shahriar A, Raana F, Shahrzad J, Nosratollah Z. Co-delivery of curcumin and chrysin by polymeric nanoparticles inhibit synergistically growth and hTERT gene expression in human colorectal cancer cells. *Nutr Cancer* 2017;**69**(8):1290–9.
170. Li L, Xiang D, Shigdar S, Yang W, Li Q, Lin J, Liu K, Duan W. Epithelial cell adhesion molecule aptamer functionalized PLGA-lecithin-curcumin-PEG nanoparticles for targeted drug delivery to human colorectal adenocarcinoma cells. *Int J Nanomed* 2014;**9**:1083–96.

Further reading

1. Harivardhan RL, Patrick C, editors. *Macromolecular anticancer therapeutics*. New York: Springer; 2010.

This page intentionally left blank

CHAPTER

29

Bio-nanomaterials: applications and utility in agricultural and medical field

Rajesh Srivastava[1], *Ruby Varghese*[2] *and Ann Rose Abraham*[3]

[1]Department of Biotechnology, GIT, Gitam Institute of Technology and Management (GITAM), Visakhapatnam, Andhra Pradesh, India; [2]Department of Chemistry, School of Sciences, Jain Deemed to be University, Bangalore, Karnataka, India; [3]Department of Physics, Sacred Heart College (Autonomous), Thevara, Kochi, Kerala, India

Abbreviations

Ar Argon
ATR-ATIR Attenuated Total Reflection Fourier Transform Infrared Spectroscopy
C3N4 Graphitic
CBNs Carbon Based Nanomaterials
CLP Classification, labeling, and packaging
CNMs Carbon Nanomaterials
CNTs Carbon Nanotubes
$Co_2(CO)_7$ Cobalt Carbonyls or **W $(CO)_6$:** Tungsten Carbonyls
EC European Commission
ELASA Enzyme Linked Immune Sorbent Assay
Es *Escherichia*
Fe $(CO)_5$ Iron Carbonyls
Fe/C Iron/Carbon
Fe/Co Iron/Cobalt
HA Hyaluronic Acid
He Helium
kHz Kilohertz
Ls *Listeria*
MBNs Metals-Based Nanomaterials
MBs/MNPs Microbubbles/metal Nanoparticles
MGOTNs Magnetic Graphene Oxide Titanate Nanomaterial
MOFs Metal–Organic Framework
MWCNTs MultiWalled CNTs

Applications of Multifunctional Nanomaterials
https://doi.org/10.1016/B978-0-12-820557-0.00021-7

NA Not Applicable
NDs Nanodiamonds
NIC Normalized Impedance Change
NPs Nanoparticles
NT Nanotechnology
OTA Ochratoxin A
PDMS Polydimethylsiloxane
PEG Polyethylene Glycol
PLGA Copolymer Poly (Lactic-co-Glycolic Acid)
PN Photocatalytic Nanomaterials
QDs Quantum Dots
R&D Research and Development
REACH Restriction of Chemicals
RNP Radical-Containing-Nanoparticles
Sa *Salmonella*
SERS Silver-coated Microstructured Substrates
SERS Surface-enhanced Raman Scattering
She *Shewanella*
Shi *Shigella*
SOD Superoxide Dismutase
SPR Surface Plasmon Resonance
SWCNTs Single-walled CNTs
TiO_2 Titanium dioxide
UCNPs Upconverting Nanoparticles
WO3−Pt Platinum Tungsten Oxide

1. Introduction

In modern and competitive markets, advanced technologies have influenced food products and food processing industries. Consumers demand fresh, authentic, convenient, and flavored rich food products. Enhanced shelf life, maintenance of freshness of food, and safety are important factors that determine competitiveness in this era. Nanotechnology involves the creation and manipulation of molecules at the nanoscale (1−100 nm).[1]

Environmental pollutants from the oil industry have been raising great concern over the years. In this regard, nanoparticles (NPs) have been a crucial and emerging tool for the detection of pollutants (such as aromatic carbon, polyphenols, or toxic gases) from oil refineries. Ochratoxin A detection using enzyme-linked immunosorbent assay (ELISA) or chromatic assay technique consumed more time and money. NPs-based sensors have helped in the determination of polyphenol, aromatics compounds, or toxic gas concentration at optimal conditions. In this sensor development, quantum dots and NPs have shown potential for new generation detection devices with the introduction of innovative sensors used at low-level contaminant detection based on electrochemical properties.[2]

Mycotoxin (ochratoxin A ~ OTA) produced by *Aspergillus* or *Penicillium* species is reported to affect the kidney, liver, and brain of both humans and animals. With advanced technology, even a trace amount of mycotoxin can be detected using nanoparticles with biosensing functions. A biosensor constitutes a bioreceptor, transducer, signal processor, and digital display. The bio-receptors in biosensors can be antibodies/nanobodies, peptides, aptamers/GNases, or MTP. Several nanomaterials with multifaceted properties are reported to act as receptors such as CNMs, MBs/MNPs, QDs, UCNPs, or MOFs.[3]

Similar to mycotoxins, pathogenic bacteria cause great losses in agriculture. Virulence is the ability of any microorganism to contaminate the host and cause disease. Bacterial flagella contribute to the virulence of pathogenic nature which causes bacterial infection and transmission. Many nanomaterial-based biosensors are developed to detect bacterial infection. One such example is nanopores with ionic impendence of electrolyte, which are used for the detection of antibody-pathogen interaction that is monitored by impedance spectra with analysis of normalized impedance change (NIC at 1 kHz).[3,4] This detection method has estimated the number of E. *coli* O157: H7 in $10-10^5$ CFU per ml at the detection limit (10 cfu/ml). While determining the milk quality, this nanopore with hyaluronic acid (HA) is reported to successfully detect *E. coli* O157: H7. It is also helpful in detecting nontargeted bacterial species such as *Staphylococcus aureus*, *Bacillus cereus,* or nonpathogenic *E. coli* DHα strain.[4]

Agriculture and food go hand in hand, hence infection in poultry farm animals not only inflate the mortality rate but also deflate the economy. A portable stand-alone biosensor can be used as a diagnostic tool in detecting meningitis or in determining/preventing contagious diseases caused by bacteria.[5]

Technology is a double-edged sword, if not used cautiously can result in a great disaster. Deliberately or unintentionally, exposure to the toxic affluents may cause an adverse effect on abiotic and biotic factors which makes up our ecosystem, such as lead depositions in wastewater and radioactive effluents from the nuclear industry to the water body or the land can lead to inevitable situations[6–8]. Nanomaterials can be the answer to be dealt with such chaotic situations. Magnetic graphene oxide titanate composite nanomaterial (MGOTNs) are suitable for rapid or effective absorption of Pb^{2+} ions from wastewater due to their efficient absorption, recyclability, or easy magnetic separation stability for purification of toxic lead elements from contaminated wastewater.[9] Likewise, semiconductor nanosensors with radioactive like Boron can be used in environmental monitoring by removing uranium from radioactive wastewater with graphene oxide.[10]

With the development of nanotechnology, there is a revolution in the field of food, agriculture, and the environment due to the introduction of smart and active packaging, nanosensors, nanopesticides or nanofertilizers, which helped in improving food quality, providing quality control, facilitates crop growth, and monitoring the environmental condition. Further high performance and low toxic nature of nanomaterials can also address the active fuel development via the application of nanotechnology.[7,8] Paramount of regulation and legislation has regulated the manufacturing, processing, application, or disposal of nanomaterial, and it needs to put effort into strengthening the public awareness and acceptance of novel nanoenabled foods or agriculture products.[8] In this chapter, the authors will discuss recent development in nanomaterials and their synthesis with their application in different sectors.

2. Nanomaterials

Multiple sensitive, reliable, and efficient techniques/assays such as enzyme-linked immunosorbent assay (ELISA) and chromatographic analysis are explored meticulously to detect the target molecules/contaminants/adulterants, but these detection techniques are time-consuming, require expensive equipment, highly skillful operator or elaborated preparative steps.[5,6]

Year-long experimentation and validation have made the scientific community converge the traditional fields of chemistry, biology, and physics to form a new field known as nanotechnology. Nanotechnology is defined as the systematic study of small sizes of materials with natural or synthetic origins having properties dependent on the length scale in nanometers (dimensions of 1−100 nm).[1,2] Nanotechnology has played a significant role in food, agriculture, and the environment. This technology has developed nanoscale materials with a controlled delivery system, improved food quality, and safety, facilitated the detection of environmental contaminants, and provides crop safety with the assurance of betterment of human life and development of the economy by holding on to the value of sustainable development.[11]

With the advent of recombinant DNA technology which relies on molecular biology techniques, the problem of world hunger to an extent can be solved by genetic modification in crops. While nanotechnology has helped in providing future development of more precise and effective methods which created manipulated food polymers or polymeric assemblies for improved quality and food safety.[11−13] It has helped the creation of novel and précised defined materials that have promised properties of self-assembly, self-healing, or maintaining capabilities.[1] NPs have exhibited increased sensitivity or selectivity that can be used as sensor devices for their detection.[14−16] Biosensors have shown great potential for accurate, sensitive, portable, and fast detection in the food industry, textile industry, biomedical industry, and environmental treatment technologies.[3] The addition of nanomaterials to the high-performance electrochemical sensing platforms can not only be used for the detection of target molecules but also provides catalytic effect, conductivity, and cytocompatibility.[1,2] Owing to their high surface-to-volume ratio, pollutants can easily adsorb to the electrode surface by completing the redox reaction processes.[17−19]

Globally, Food contamination resulting from a pathogenic microorganism is a severe public health issue that results in food-borne diseases which affect human beings every year. One such causative agent is *Escherichia coli*. Conventionally, atomic force microscopy is used to analyze the morphology of flagella of *Escherichia coli*, or the swarming plate method was applied for pH-dependent changes in bacterial motility,[6,7] as the virulence is caused by bacterial flagella. Both of which are costly and laborious techniques. Recently, a simple and rapid method was developed with commercially available alumina nanoporous membrane containing hyaluronic acid (HA). This membrane has permitted the successful immobilization of antibodies and thus helps in the detection of harmful *E. coli* O157: H7.[3,4]

Nanomaterials can be used extensively in the agriculture sector.[19] The potential or capabilities of nanomaterials are involved with the improvement of seed germination and protection from pathogens or in detecting pesticide residue.[18] Nanomaterials with photocatalytic properties have been reported to attract the attention of emerging resources, utilized in agriculture

applications. Certain nanomaterials such as biocompatible titanium dioxide (TiO_2) with photocatalytic activity (TiO_2-PN) are a model benefit that can address the global environmental challenges or issues faced by farmers. Under high salinity levels, the incorporation of TiO_2 mitigated the deteriorating agronomical trait and elevated antioxidant levels in *Dracocephalum moldavica*. Application of lower concentrations of TiO_2 via roots or leaves of the crops has been known to positively impact crop performance through stimulating the activity of various enzymes, elevating chlorophyll content and enhancing photosynthesis, facilitating increased nutrient uptake, strengthening stress tolerance, and increasing crop yield and quality.[8,9,20,21] Still, many scientific reports have stated the nanotoxicology associated with the usage of TiO_2, hence farmers should be well educated by promoting risk assessment and innocuous practices of TiO_2 nanomaterials.[22]

The implementation of Nanotechnology in bioremediation has been vastly studied. Loaded magnetite nanoparticles, such as Magnetic graphene oxide-titanate composites (MGO-TNs) can reduce secondary pollution via adsorbing pollutants.[21,22] Adsorption mechanisms of composite nanomaterials are exhibited with ion exchange and surface complexation processes. And batch adsorption equipment had shown the maximum adsorption capacity (3.23×10^2 mg/g for Pb^{+2}) by use of MGO-TNs composite. Further, removal efficiency has retained at 90% after completing six cycles of the adsorption-desorption process.[6,9]

Radioactive pollutants can be found in wastewater, freshwater, soil, or any ecosystem as they may cause health issues or irreparable damage to the living system. A highly selective and sensitive Nano-based sensor such as Gold nanoparticles (e.g., DNAzyme-Gold Nanoparticle), and Silver nanoparticles (citrate-stabilized silver nanoparticles)[23] are used to detect uranyl ions. Detection of uranyl ions by different sensors has been discussed intuitively via understanding the different capabilities of methods of uranyl ion detection.[11,20]

The release of nanoparticles into the environment should be diligently handled. European Commission (EC) has provided specific recommendations for nanomaterials, and everything is precisely mentioned in the EC regulation—REACH (Registration, Evaluation, Authorization, and Restriction of Chemicals) and CLP (Classification, Labeling, and Packaging). Based on regulations, nanomaterials can be natural, manufactured materials containing particles in unbound or aggregates or agglomerate states with 50% or more particle size distribution in the 1-100 nm range. In specific cases for the environment, health, or competitiveness state, the size distribution threshold (50% or more value) can be replaced between the 1%–50% range.[13,14]

Nanomaterials have been vastly studied in the biomedical field such as fluorescent biological labels, drug delivery, antigen-antibody detection, forensic cases, regenerative study, tumor biology, separation, and analytical techniques.[24] Engineering approaches modified, and designed nanomaterials, with specific functions, targeted to the medical field. There is a report available on fullerenes, graphene flakes, and single-wall carbon nanotubes (CNTs) with an external dimension of 1 nm or below. These nanomaterials can be generated in a natural state from volcanic, ash, soot from a forest fire, or unintentional byproducts of combustion processes (during welding, diesel engine).[16,17] Similarly, Hybrid nanomaterials such as organic–organic or organic–inorganic which include lipid polymer, clay-carbon, and metal-oxide-based nanohybrids are applied for a promised platform for therapeutic due to their tuning ability through a combination of functional components.[17,18] The following sections will discuss the type of nanomaterials as shown in Fig. 29.1.

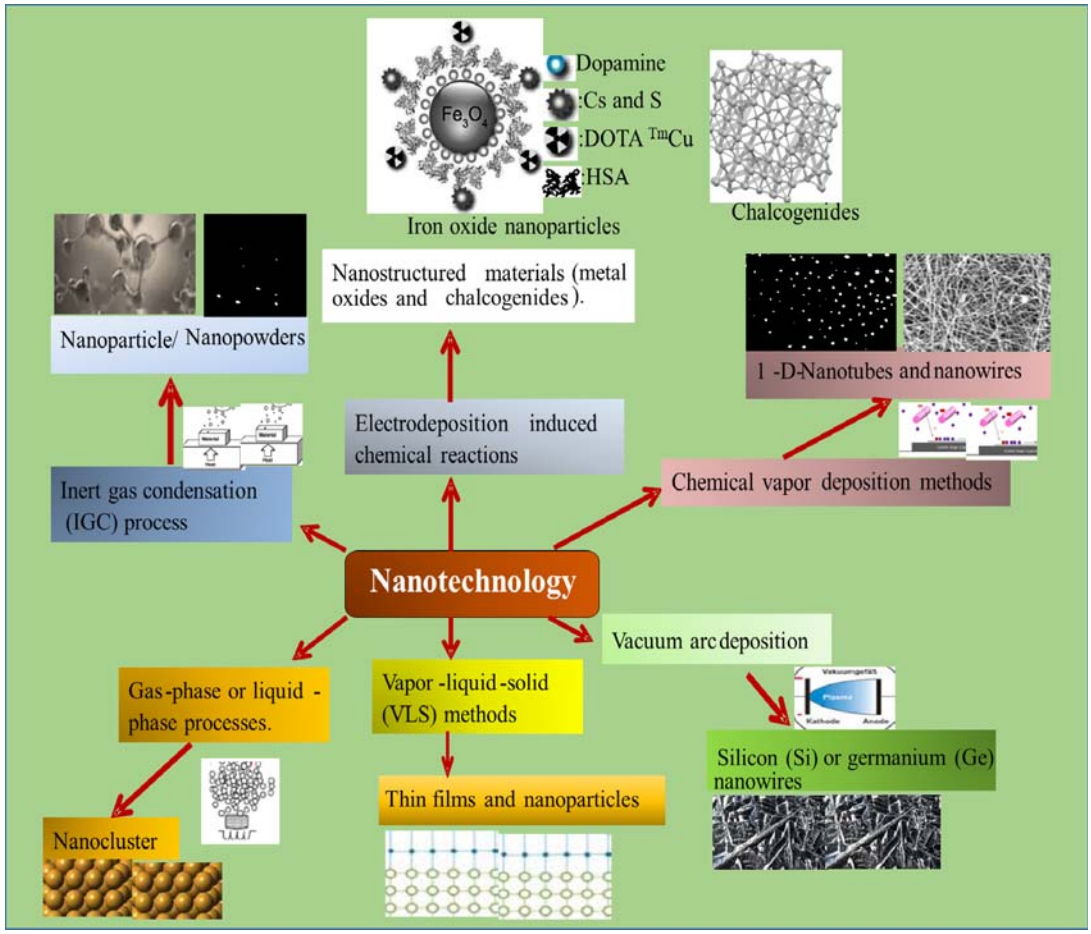

FIGURE 29.1 Nanotechnology approaches for different types of nanoparticles or materials for various sectors.

3. Nanomaterials types or categories

3.1 Carbon-based nanomaterial (CBNs)

This nanomaterial is made up of carbon in form of a hollow sphere, ellipsoids, or tubes. Spherical or ellipsoidal forms of this carbon nonmaterial are known as fullerenes whereas cylindrical form is referred to as nanotubes and all these forms of carbon-based nanomaterials are shown many potential applications such as improved films or coating, stronger or lighter materials construction with application in electronics. These materials have exhibited great versatility due to being chemically combined with other forms of carbon-based

nanomaterials. It has shown different ranges of elements for the formation of covalent bonds. It can exhibit excellent characteristics like high density or high hardness.[24]

Innumerous studies are carried out by employing carbon-based nanomaterial with a wide variety of structures for multiple applications. Nanomaterials based on graphene and CNTs have imparted positive influences on mitigating environmental issues. In this regard, hydrogen photoelectrogenesis processes devices, batteries, clean energy generation from the oxygen reduction reaction, degradation of organic pollutants, or sensor development can be achieved from various applications of carbon-based nanomaterials (CBNs).[15–19,21–25]

Magnetic carbon nanocages are created from cheap carbon sources like lignin at low temperatures by carbonization processes. This developed hybrid carbon-based nanomaterial (CBNs) which is stabilized by covalent bond (van Der Waals force) interactions is used as efficient and recycled absorbent materials for the removal of dye wastes from textile wastewater.[23] Detailed study needed to be carried out to evaluate the application of CBN such as their synthesis or characterization to be implemented in the vast horizon of technological development with no adverse effects on the ecosystem.[25,26]

The carbon shell is reported to protect the iron cores against oxidation responsible for the high degree of crystallinity. Spherical-shaped Carbon shell encapsulating iron nanoparticles has superparamagnetic properties which have been applied potentially in drug delivery systems.[26,27] The exhibition of the band gap of carbon and boron nitride double-wall heteronanotubes (C-BN-DWHNTs) with different chirality and sizes and tuning by intertube distances is reported to have wide medical applications. This material has imposed an electric field of zig-zag nature with the further possibility of future electronic and electrooptic nanodevice applications.[27,28] Advanced CBN as biomimetic materials is utilized as scaffolds for tissue regeneration.[29]

Apart from drug delivery, CBN can act as substrates for nerve cell regeneration or active cell guidance, or as supramolecular architecture for mimicking the extracellular environment which reduces the inflammatory response in brain implants. CNTs graphene or nanodiamonds (NDs) are found as highly promising nanomaterials.[30]

3.1.1 *Carbon nanotubes (CNTs)*

CNTs are a group of promising nanomaterials with multifaceted properties, because they are biologically active, spatially designed, and biomimetic.[31,32] In 1991, the first CNTs were developed and reported, these hollow cylinders made of graphene are classified into single-walled (SWCNTs), double-walled (DWCNTs) or multi-walled (MWCNTs) layers of graphene. SWCNTs exhibit metallic or semiconductive properties, which can be altered or modified by external electric fields,[33] while MWCNTs exhibit metallic behavior.

CNTs can be synthesized by three methods: chemical vapor depositions, arc-discharge, and Laser-ablation method.[32] Their electronic properties are dependent mainly on geometric

parameters (diameters or chiral angles). Diameters of chiral angles are also determined by the magnitude or direction of the chiral vectors.[32,33]

3.1.2 Nanodiamonds (NDs)

These are sp3-hybridized carbon nanoparticles (diameter <20 nm) with crystal domains and diamondoid-like topology, and tetrahedral configuration. Nanodiamonds (NDs) are versatile nanomaterials due to their physio-chemical and mechanical properties such as extreme hardness, low friction coefficient, high mobility, and thermal conductivity. NDs are chiefly synthesized from an oxygen-deficient complex mixture of trinitrotoluene and hexogen-like explosives when detonated in a close chamber process.[34,35] NDs are extensively explored in the biomedical field due to their low cytotoxicity, stable fluorescence, facile functionalization, biocompatibility, and other basic properties. It has been widely studied in drug delivery, bioimaging, and regenerative biology such as biomimetic scaffolds, and as fillers in tissue engineering.[34]

3.1.3 Graphene

It is a mono-atomic, two-dimensional, sheet of sp2 hybridized carbon atoms arranged as a honeycomb lattice. It has been isolated from graphite in 2004.[36] Graphene has attained a lot of attention from the scientific community due to its unique chemical, physical, optical, magnetic, thermal, and mechanical properties such as high electron mobility, ambipolar electric field effect, and ballistic condition of electronic charge carrier.[37] Hence, it has been widely studied in various fields including electronics, energy, catalysis, sensing, and biomedical fields.[38]

Graphene is a good example of allotrope carbon and contains a single atomic graphite layer, which exists in two-dimensional planner sheets. It is mainly made up of nonmetal but as its properties are similar to semi-conducting metal, it is usually known as quasi-metal. In graphene nanomaterials, each carbon is covalently bonded (in sp2 hybridized mode) to form hexagons.[39] Each hexagon in the graphene sheet is exhibited to have two pi electrons in a delocalized form which allows for efficient electricity conduction. The holes in the structure are reported to transfer photons in an unimpeded form which provides high thermal conductivity. Graphene in nanoelectronic forms is reported for the fabrication of high-quality graphene in large volume production.[39,40] Different methods are employed for generating graphene with exfoliation of it by mechanical, chemical, or thermal reduction with chemical vapor deposition.[40,41]

3.2 Metals-based nanomaterials (MBNs)

These types of nanomaterials include quantum dots, nanogold, nanosilver, or metal oxides (titanium dioxide). A quantum dot is a closely packed semiconductor crystal, with a size ranging from a few nanometers to 100 nanometers. Size changes in quantum dots are reported to modify their optical properties.[42] Metal-based nanoparticles (MBPs) are reported to synthesize from organometallic precursors by using gas phase synthesis via pyrolysis processes. MBPs can be incorporated in Biosensor (Fig. 29.2), and can also be used to commercially prepare nanopowder (powder mean size$\sim$ 6−100 nm) which has multiple activities.[43]

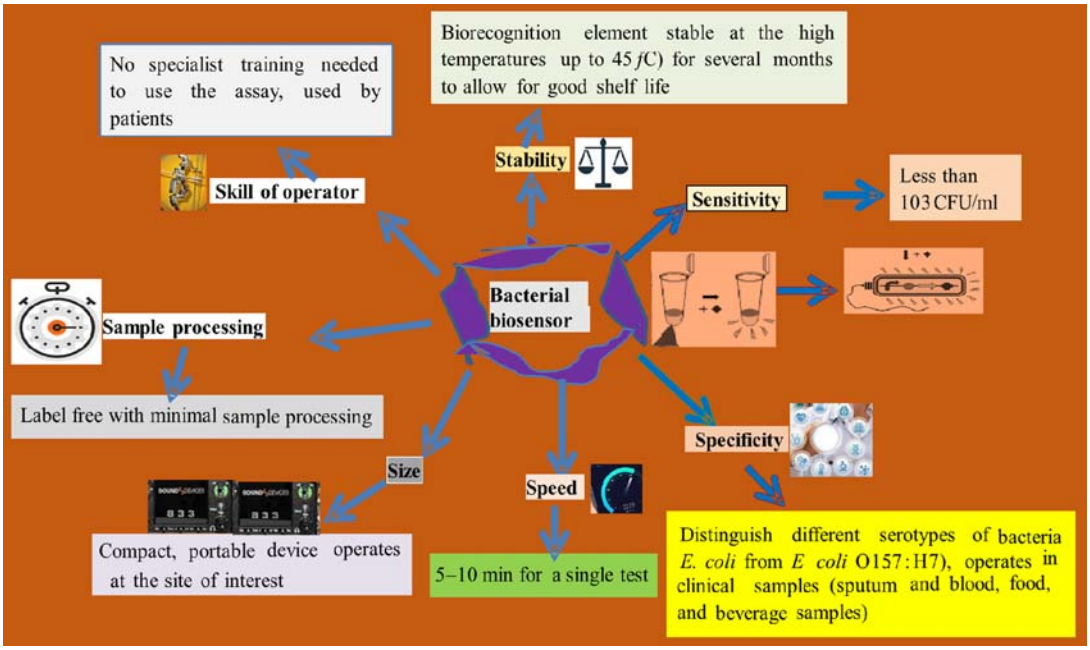

FIGURE 29.2 Bacterial biosensors with their parameters and value or quantity of detection.

Many numbers of metal-based nanopowders are reported by incorporating metals such as Fe, Co, Fe/Co alloy, or Fe/C. Mechanism of nanoparticles (NPs) formation to synthesize nanopowders will influence the experimental parameters that affect the shape, size, distribution, structures, and chemical or phase composition of oxide carbon or organic coated nanoparticles.[44] Metal nanopowder can be used to improve the performance of solid rocket propellants, as sensors, cosmetic applications, and so on.[45,46]

3.3 Dendrimers nanomaterial

Generally, dendrimers are synthesized using either a divergent or a convergent method. By the implementation of either of the method, the resultant will be an outward grown dendrimer from a multifunctional core molecule. This core molecule reacts with any monomer molecules containing one reactive and two dormant groups, producing a first-generation dendrimer.[47] Their surface has numerous chain ends that can be tailored to perform specific chemical functions such as catalysis while its core can be used for drug delivery applications.[5,47,48]

As mentioned earlier dendrimers can be synthesized by either convergent or divergent methods. The divergent approach is a kind of primitive method where gradually building blocks are added to the arms. It is a time-consuming and exhaustive method. In the convergent method, the synthesis of each branch with requisite sizes is predetermined; hence, it begins with the molecular structure and ultimately ends up with the outermost arm of the final

dendrimer.[49,50] Among both the approaches, the convergent approach is preferable due to its precision with minimal defects and ease in purifying desired product.[51] Due to prominent properties such as multisurface functional groups, polyvalency, self-assembly, and electrostatic interaction with the desired compound, dendrimers can be used for targeted drug delivery, as sensors in diagnostic tools, in mitigating environmental pollutants such as polyamidoamine (PAMAM)-based dendrimer can be used to treat wastewater, removal of inorganic and organic pollutant, sensing, and capturing CO_2 and its conversion.[52]

3.4 Composites nanomaterials

Fabrication of two nano-sized materials through weak interactions such as van der Waals, hydrogen bonding, or weak electrostatic interactions, produces composite material.[53,54] Some of the discrete inorganic units of nanocomposite materials are polymer matrix—discontinuous reinforcement (nonlayered) nanocomposites, metal matrix nanocomposites (MMNC), and ceramic matrix nanocomposites.[54,55] Nanocomposites exhibit a synergistic effect due to the addition of multiple components of the nanomaterials.[55] Hence, these nanomaterials exhibit versatile properties such as a high surface-to-volume ratio for embedding biomolecules such as biocatalysts, high mechanical strength with prominent electrical conductivity, redox reactivity, and catalytic activity. Nanocomposite materials are investigated as transducer materials for enzymes-based nanoelectronic devices.[56–59] It has been extensively studied in the biomedical field such as imaging, targeted drug delivery, batteries, gas sensing, and artificial implants.[6–9,59] Because they acquiesce to biological functionalization, these nanomaterials are also utilized in the detection of cancerous cells[10] and host-pathogen interaction in plants[11,58]

4. Application of nanoparticles

Versatile nanomaterials are reported to be used as food packaging materials by providing quality assurance and safety to the food. Nanomaterial used in the development of food-grade polymers has shown the enhanced or extend shelf life of carbonated beverages as alternative glass bottles or expensive cans usages.[19] Silver nanoparticles are known for their antibacterial property, hence can be used in food-grade polymers developed to construct food cans to prevent bacterial contamination.[24] Sensors made of nanoparticles are developed for direct detection of bacteria in canned food or other contaminants that can report from the surface of food at the packaging plant.[25]

Nanosensors can help in the point of packaging testing with the reduction of contamination from grocery store shelves. Nanoparticles can be used in delivering vitamins or other nutrients through food or beverages without any loss in taste or appearance which can be achieved by encapsulating nutrients that can be easily circulated in blood streams with the promised rate of elevated nutrient bioabsorption[34,38] and Tables 29.1 and 29.2 showed the application of nanoparticles in biosensors. Nanosensors can also be used to sense analytes of the ultra-low range such as pesticides, metal ions, and toxic effluents released in water, soil, and air, and Fig. 29.3 shows the application of bionanoparticles in multiple sectors.

TABLE 29.1 Detection of microbial strains via biosensor application in various food products.[60]

Target microbes	Transducer signal	Sensor assembly	Bioreceptor	Analytes
Sa. typhimurium; Es coli 0157:H7; *Shi. dysenteriae; Cb. jejuni*	Fluorescence	NRL array sensor (fluorescence-based affinity assay)	Antibody, ganglioside receptors, oligo-saccharide	Food or environmental samples
Sa. enteric; Li. monocytogens; Es. coli. O157:H7;	Fluorescence	Antibodies linked viabiotin/ avidinton; optical fibers	Polyclonal antibody for capture antibody; fluorescent monoclonal antibody oraptamera gainst surface protein inl	Artificially contaminated meat samples
Es. coli.	Fluorescence	Bioconjugated magnetic beads for capture fluorescent polymeric micelles for reporting	Polyclonal anti-E.coli antibodies	Bacteria in buffer
Es. coli.	Thin-film optical interference spectroscopy	Antibody- functionalized nanostructure doxidized porous silicon(PSiO2)	Anti-e.coli polyclonal antibody	Bacteria in buffer
Sa. Typhimurium	Light scattering	Immunoagglutination assay using anti-Salmonella-conjugated polystyrene microparticles	Anti-salmonella polyclonal antibody	Liquid from processed raw chicken
She. Oneidensis	SERS	Silver nanoparticles sandwiched by analyte binding on optical fiber tip	NA	Bacteria in buffer
Es. coli; St. aureus Ba. subtilis	SPR	Long-range SPR aantibodies on SAM-gold surface/antibody-functionalized magnetic nanoparticles	, potato lectin	Bacteria in serum-spiked buffer

Es, Escherichia; *Ls*, Listeria; *NA*, Not applicable; *Sa*, Salmonella; *SERS*, *Shi*, Shigella; Surface-enhanced Raman scattering; *She*, Shewanella; *SPR*, Surface Plasmon resonance.

TABLE 29.2 Nanoparticles application in medical sectors.[48]

Nanoparticle	Function	Cell types
Iron oxide nanoparticles	Oxidant by nox 4 overexpression	Myocardium from mice
RNP	Neuroprotective agent due to its ability to scavenge free radicals	Middle cerebral artery from rats with cerebral ischemia/reperfusion injury
Redox-polymer nanotherapeutics	Treatment of the neurodegenerative diseases	Brain from senescence-accelerated mouse prone (SAMP8)
WO3−Pt nanoparticles	Oxidant. Nicotinamide adenine dinucleotide phosphate (NADPH) oxidase biomimetic	Tumor cells
Silver nanoparticles	Oxidant by increasing nox 4 expression	Human umbilical vein endothelial cells

(*Continued*)

TABLE 29.2 Nanoparticles application in medical sectors.[48]—cont'd

Nanoparticle	Function	Cell types
Silver nanoparticles are used	Increase of hypertension due to a decrease in NO levels	Myocardium from rats
PLGA nanoparticles	Carrier. Treatment for hypertension	Hypertensive rats
Iron oxide, yttrium oxide, cerium oxide, zinc oxide	Proinflammatory	Human vascular endothelial cell line
Nanoparticles based on polyoxalate	Antioxidant and antiinflammatory	Doxorubicin-treated mice heart
Polyketal particles	SOD carrier	Rat myocardium
Nanoceria	Prooxidant. Microvascular dysfunction	Arteriola from rats

PEG, polyethylene glycol; *PLGA*, copolymer poly (lactic-co-glycolic acid); *RNP*, radical-containing-nanoparticles; *SOD*, superoxide dismutase; *WO3−Pt*, platinum tungsten oxide.

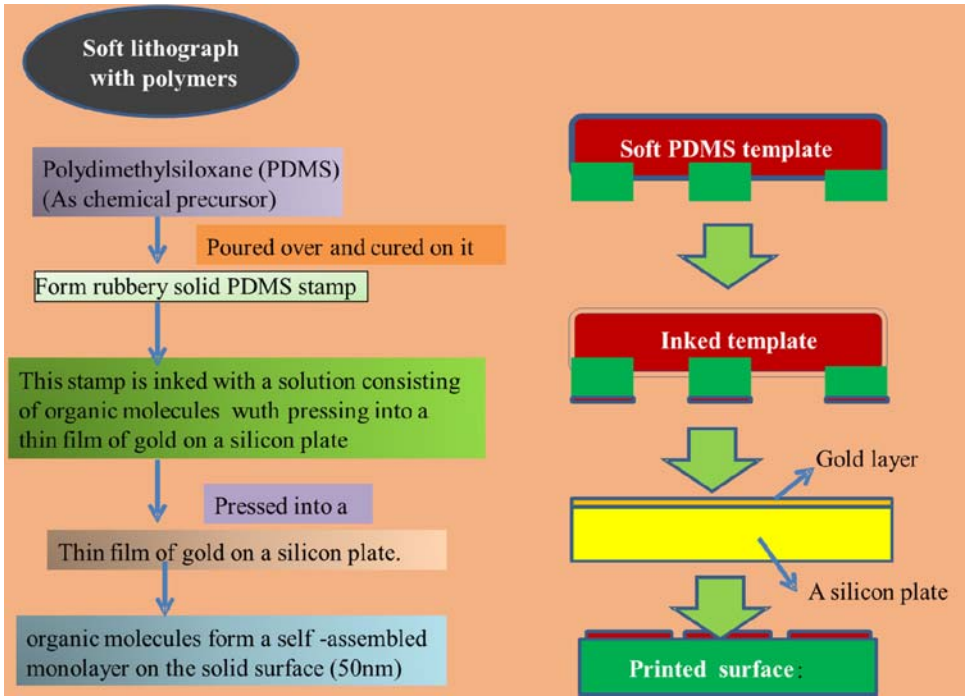

FIGURE 29.3 Schematic diagrams for nanomaterials synthesis.

5. Conclusions

Nanotechnology is opening vast avenues for future development with its precise and effective methods that can be used in technological advancement by pertaining to sustainability. Nanomaterials have been created by the exploitation of various natural or synthetic materials with the dimension of 1−100 nm size. Nanomaterials synthesis is reported by applying top-down and bottom-up approaches, and it is found in the form of fibers, tubes, and other specific forms that are used in food processing, medical or pharmaceutical, agricultural sector, etc. The best yield or productivity of crops can enhance by nanotechnology approaches. Developed MGO-TNs material has shown hierarchical structure and large surface area with good adsorption performance, recyclability, or easy magnetic separation stability for purification of toxic lead elements from contaminated wastewater. Nanomaterials with photocatalytic properties have been reported to attract the attention of emerging resources, utilized in agriculture applications, and currently developed biocompatible titanium dioxide (TiO_2) contained photocatalytic posses nanomaterials (TiO_2-PN). Uranium sensors in different modes have been reported with the rapid development of the nuclear industry and this sensor has helped in the detection of a series of radioactive pollutants. Detailed research should be carried out as the full potential in the field of agriculture, food, medicine, and environmental protection is yet to be comprehended, and hopefully, there will be a gradual movement from theoretical knowledge toward the application regime by pertaining to sustainability for the betterment of our planet.

References

1. Chhabra H, Kumar M. Size and shape dependent equation of state for nanomaterials with application to bulk materials. *J Phys Chem Solid* 2020;**139**:109308.
2. Saleh TA, Fadillah G, Saputra OA. Nanoparticles as components of electrochemical sensing platforms for the detection of petroleum pollutants: a review. *Trend Anal Chem* 2019;**118**:194−206.
3. Alhamoud Y, Yang D, Selorm S, Kenston F, Liu G, Liu L, Zhou H, Ahmed F, Zhao J. Advances in biosensors for the detection of ochratoxin A: Bioreceptors, nanomaterials, and their applications. *Biosens Bioelectron* 2019;**141**:111418.
4. Joung CK, Kim HN, Lim MC, Jeon TJ, Kim HY, Kim YR. A nanoporous membrane-based impedimetric immunosensor for label-free detection of pathogenic bacteria in whole milk. *Biosens Bioelectron* 2013;**44**:210−5.
5. Ahmed A, Rushworth JV, Hirst NA, Millner PA. Biosensors for whole-cell bacterial detection. *Clin Microbiol Rev* 2014;**27**(3):631−46.
6. Sharma H, Mutharasan R. Review of biosensors for foodborne pathogens and toxins. *Sensor Actuator B Chem* 2013;**183**:535−49.
7. Chang KC, Cheng SJ, Chen YC, Huang HR, Liou JW. Nanoscopic analysis on pH induced morphological changes of flagella in *Escherichia coli*. *J Microbiol Immunol Infect* 2013;**46**(6):405−41.
8. He X, Deng H, Hwang HM. The current application of nanotechnology in food and agriculture. *J Food Drug Anal* 2019;**27**(1):1−2.
9. Yang X, Guo N, Yu Y, Li H, Xia H, Yu H. Synthesis of magnetic graphene oxide-titanate composites for eficient removal of Pb(II) from wastewater: performance and mechanism. *J Environ Manag* 2020;**256**:109943.
10. Hassan T. Development of nanosensors in nuclear technology. *AIP Conf Proc* 2017;**1799**:040001.
11. Biju V. Chemical modifcations and bioconjugate reactions of nanomaterials for sensing, imaging, drug delivery and therapy. *Chem Soc Rev* 2014;**43**(3):744−64.
12. Seabra AB, Paula AJ, De Lima R, Alves OL, Durán N. Nanotoxicity of graphene and graphene oxide. *Chem Res Toxicol* 2014;**27**(2):159−68.

13. Werengowska-Ciećwierz K, Wiśniewski M, Terzyk AP, Furmaniak S. The chemistry of Bioconjugation in nanoparticles-based drug delivery system. *Adv Condens Matter Phys* 2015;**2015**(198175):27.
14. Nel A, Xia T, Mädler L, Li N. Toxic potential of materials, at the nanolevel. *Science* 2006;**311**(5761):622–7.
15. Salata OV. Applications of nanoparticles in biology and medicine. *J Nanobiotechnol* 2004;**2**(1):1–6.
16. Ma J, Zhang J, Xiong Z, Yong Y, Zhao XS. Preparation, characterization and antibacterial properties of silver-modifed graphene oxide. *J Mater Chem* 2011;**21**(10):3350–2.
17. García MC, Uberman PM. Nanohybrid filler-based drug-delivery system. In: Mohapatra SS, Ranjan S, Dasgupta N, Mishra RK, Thomas S, editors. *Nanocarriers for Drug Delivery,Nanoscience and Nanotechnology in Drug Delivery. Micro and Nano Technologies*. Elsevier Inc.; 2019. p. 43–79 [Chapter 2].
18. Varghese RJ, Sakho EM, Parani S, Thomas S, Oluwafemi OS, Wu J. Introduction to nanomaterials: synthesis and applications. In: Thomas S, Sakho EHM, Kalarikkal N, Oluwafemi SO, Wu J, editors. *Nanomaterials for Solar Cell Applications*. Elsevier Inc.; 2019. p. 75–95 [Chapter 3].
19. Khot LR, Sankaran S, Maja JM, Ehsani R, Schuster EW. Applications of nanomaterials in agricultural production and crop protection: a review. *Crop Protect* 2012;**35**:64–70.
20. Wu X, Huang Q, Mao Y, Wang X, Wang Y, Hu Q, Wang H, Wang X. Sensors for determination of uranium: a review. *Trends Anal Chem* 2019;**89**–**11**:118.
21. Rodríguez-González V, Terashima C, Fujishima A. Applications of photocatalytic titanium dioxide-based nanomaterials in sustainable agriculture. *J Photochem Photobiol C Photochem Rev* 2019;**49**–**6**:40.
22. Chaudhary IJ, Singh V. Titanium dioxide nanoparticles and its impact on growth, biomass and yield of agricultural crops under environmental stress: a review. Research. *J Nanosci Nanotechnol* 2020;**10**(1):1–8.
23. Wu P, Hwang K, Lan T, Lu Y. A DNAzyme-gold nanoparticle probe for uranyl ion in living cells. *J Am Chem Soc* 2013;**135**(14):5254–7.
24. Liu Y, Dong X, Chen P. Biological and chemical sensors based on graphene materials. *Chem Soc Rev* 2012;**41**(6):2283–307.
25. dos Santos MC, Maynart MC, Aveiro LR, da Paz EC, Pinheiro VS. Carbon-based materials: recent advances, challenges, and perspectives reference module in materials. *Sci Mater Eng* 2017.
26. Siqueira JR, Oliveira ON. Carbon-based nanomaterials. *Nanostructures* 2017:233–49.
27. Xia D, Otyepka M, Li X, Liu W, Zheng Q. Carbon-based materials at nanoscale. Hindawi publishing. *Corp J Nanomater* 2015;**750242**:2.
28. Sun H, You X, Denge J, Chen X, Yang Z, Ren J, Peng H. Novel graphene/carbonnanotube composite fibers for efficient wire-shaped miniature energy device. *Adv Mater* 2014;**26**(18):2868–73.
29. Ge C, Du J, Zhao L, Wang L, Liu Y, Li D, Yang Y, Zhou R, Zhao Y, Chai Z, Chen C. Binding of blood proteins to carbon nanotubes reduces cytotoxicity. *Proc Natl Acad Sci U S A* 2011;**108**(41):16968–73.
30. Monaco AM, Giugliano M. Carbon-based smart nanomaterials in biomedicine and neuroengineering. *Beilstein J Nanotechnol* 2014;**5**:1849–63.
31. Krüger A, Kataoka F, Ozawa M, Fujino T, Suzuki Y, Aleksenskii AE, Vul AY, Ōsawa E. Unusually tight aggregation in detonation nanodiamond: identification and disintegration. *Carbon* 2005;**43**:1722–30.
32. Bottino MC, Thomas V, Schmidt G, Vohra YK, Chu TMG, Kowolik MJ, Janowski GM. Recent advances in the development of GTR/GBR membranes for periodontal regeneration—a materials perspective. *Dent Mater* 2012;**28**(7):703–21.
33. Novoselov KS, Geim AK, Morozov SV, Jiang D, Zhang Y, Dubonos SV, Grigorieva IV, Firsov AA. Electric field effect in atomically thin carbon films. *Science* 2004;**306**:666–9.
34. Qin JX, Yang XG, Lv CF, Li YZ, Liu KK, Zang JH, et al. Nanodiamonds: synthesis, properties, and applications in nanomedicine. *Mater Des* 2021;**210**:110091.
35. Fang L, Ohfuji H, Irifune T. A novel technique for the synthesis of nanodiamond powder. *J Nanomater* 2013;**201845**:4.
36. Guillou CL, Brunet F, Irifune T, Ohfuji H, Rouzaud JN. Nanodiamond nucleation below 2273 K at 15 GPa from carbons with different structural organizations. *Carbon* 2007;**45**(3):636–48.
37. Bhuyan MSA, Uddin MN, Islam MM, Bipasha FA, Hossain SS. Synthesis of graphene. *Int Nano Lett* 2016;**6**(2):65–83.
38. Ghosal K, Sarkar K. Biomedical applications of graphene nanomaterials and beyond. *ACS Biomater Sci Eng* 2018;**4**(8):2653–703.

39. Wu ZS, Ren W, Gao L, Zhao J, Chen Z, Liu B, Tang D, Yu B, Jiang C, Cheng HM. Synthesis of graphene sheets with high electrical conductivity and good thermal stability by hydrogen arc discharge exfoliation. *ACS Nano* 2009;**3**:411–7.
40. Subrahmanyam KS, Panchakarla LS, Govindaraj A, Rao CNR. Simple method of preparing graphene flakes by an arc-discharge method. *J Phys Chem C* 2009;**113**:4257–9.
41. Bolotin KI, Sikes KJ, Jiang Z, Klima M, Fudenberg G, Hone J, Kim P, Stormer HL. Ultrahigh electron mobility in suspended graphene. *Solid State Commun* 2008;**146**:351–5.
42. Chandran SP, Chaudhary M, Pasricha R, Ahmad A, Sastry M. Synthesis of gold nanotriangles and silver nanoparticles using Aloe vera plant extract. *Biotechnol Prog* 2006;**22**:577–83.
43. Vasilieva ES, Tolochko OV, Yudin VE, Kim D, Lee DW. *Production and application of metal-based nanoparticles*. Paris: France. ENS; 2006. p. 73–8. ffhal-00166768f, https://hal.archives-ouvertes.fr/hal-00166768/document.
44. Du L, Jiang H, Liu X, Wang E. Biosynthesis of gold nanoparticles assisted by *Escherichia coli* DH5a and its application on direct electrochemistry of hemoglobin. *Electrochem Commun* 2007;**9**:1165–70.
45. Gardea-Torresdey JL, Gomez E, Peralta-Videa JR, Parsons JG, Troiani H, Jose-Yacaman M. Alfalfa sprouts: a natural source for the synthesis of silver nanoparticles. *Langmuir* 2003;**19**:1357–61.
46. He S, Guo Z, Zhang Y, Zhang S, Wang J, Gu N. Biosynthesis of gold nanoparticles using the bacteria *Rhodopseudomonas capsulata*. *Mater Lett* 2007;**61**:3984–7.
47. Mauricio MD, Guerra-Ojeda S, Marchio P, Valles SL, Aldasoro M, Escribano-Lopez I, Herance JR, Rocha M, Vila JM, Victor VM. Nanoparticles in medicine: a focus on vascular oxidative stress. *Oxid Med Cell Longev* 2018;**6231482**:20.
48. Novoselov KS, Jiang D, Schedin F, Booth TJ, Khotkevich VV, Morozov SV, Geim AK. Two-dimensional atomic crystals. *Proc Natl Acad Sci U S A* 2005;**102**:10451–3.
49. Gilles ER, Frechet JMJ. Dendrimers and dendritic polymers in drug delivery. *Drug Discov Today* 2005;**10**:35–43.
50. Cacialli F, Samorì P, Silvac C. Supramolecular architectures. *Mater Today* 2004;**7**(4):24–32.
51. Stiriba S-E, Frey H, Haag R. Dendritic polymers in biomedical applications: from potential to clinical use in diagnostics and therapy. *Angew Chem Int Ed* 2002;**41**:1329–34.
52. Viltres H, López YC, Leyva C, Gupta NK, Naranjo AG, Acevedo–Peña P, Kim KS. Polyamidoamine dendrimer-based materials for environmental applications: a review. *J Mol Liq* 2021;**334**:116017.
53. Ramesan MT, Suhailath K. *Role of Nanoparticles on Polymer Composites. Micro and Nano Fibrillar Composites (MFCs and NFCs) from Polymer Blends*. Woodhead Publishing Series in Composites Science and Engineering Elsevier B.V.; 2017. p. 301–32.
54. Camargo PHC, Satyanarayana KG, Wypych F. Nanocomposites: synthesis, structure, properties and new application opportunities. *Mater Res* 2009;**12**:1–39.
55. Sajad D, Shah MA, Sheikh NA, Butt MM. *Applications of Nanocomposites, a Review*. United States: EnPress Publisher, LLC; 2018. p. 1–21. 10.24294/can.v0i0.875. t: https://www.researchgate.net/publication/325114474.
56. Benzait Z, Yuca N. Synergistic effect of carbon nanomaterials on a cost-effective coral-like Si/rGO composite for lithium ion battery application. *Electrochim Acta* 2020;**339**:135917.
57. Hassan T, Salam A, Khan A, Khan SU, Khanzada H, Wasim M, Kim IS. Functional nanocomposites and their potential applications: a review. *J Polym Res* 2021;**28**(2):1–22.
58. Pan L, Liu J, Shi J. Cancer cell nucleus-targeting nanocomposites for advanced tumor therapeutics. *Chem Soc Rev* 2018;**47**(18):6930–46.
59. Facure MH, Schneider R, Mercante LA, Correa DS. A review on graphene quantum dots and their nanocomposites: from laboratory synthesis towards agricultural and environmental applications. *Environ Sci J Integr Environ Res: Nano* 2020;**7**(12):3710–34.
60. Hodge P. Polymer science branches out. *Nature* 1993;**362**(6415):18–9.

This page intentionally left blank

PART V

Environmental applications

This page intentionally left blank

CHAPTER

30

Enhanced cocatalysis of bimetallic nanostructures for catalytic and photocatalytic applications

Aadil Bathla and Bonamali Pal

School of Chemistry and Biochemistry, Thapar Institute of Engineering & Technology, Patiala, Punjab, India

1. Introduction

Catalysis is an important factor in developing a sustainable world and found a wide range of applications in different sectors, products, and processes. Catalysis term arises from the Greek words kata, which means down and lyein means release. During the 16th-17th centuries, different catalytic reactions were carried out, for example, synthesis of vinegar using ethanol oxidation, formation of soap with fat hydrolysis, dehydration of ethanol to form diethyl ether, and many other reactions. Haber successfully synthesized ammonia using iron as a catalyst and received a Nobel Prize in 1919. Paul Sabatier used nickel (Ni) as a catalyst for the hydrogenation of different unsaturated organic compounds and received a Nobel Prize in 1919.[1–3] Catalyst is considered as the backbone of various scientific and industrial applications, as it is being responsible for the conversion, yield, and selectivity of chemical transformation and also effectively used in the area of pharmaceuticals, environmental remediation, petro-chemistry, etc. Once the concept of catalysis had been established, the next question was how the catalyst works.

A catalyst in a chemical reaction increases the rate of the reaction by forming the bond with reactant molecules and allowing them to react in order to form the desired final product. After the product formation, it is detached from the catalyst surface and leaves the catalyst unaffected and available for the next catalytic process (Fig. 30.1). In other words, the catalyst process can be described as a cyclic process, initially, it participates in the reaction and is recovered back in its original form at the end of the cycle.[4,5]

In a chemical reaction, reactants' molecules required some activation energy to form products. This activation energy is considered as barrier height for a chemical reaction. The

Applications of Multifunctional Nanomaterials
https://doi.org/10.1016/B978-0-12-820557-0.00013-8

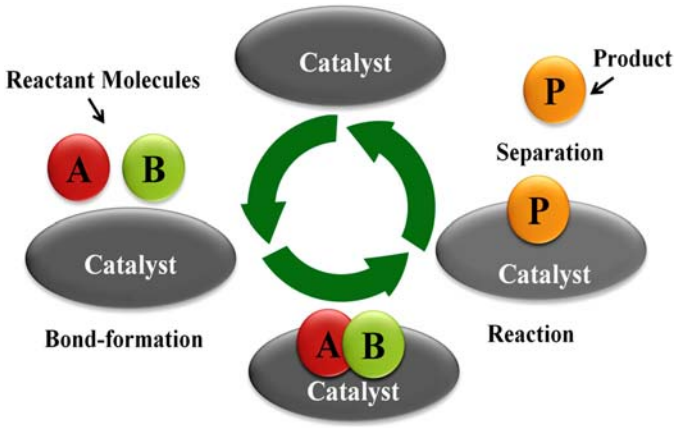

FIGURE 30.1 The schematic diagram showing how a catalyst works in a chemical reaction.

reactant molecules have to cross this barrier height in order to form the product molecules. If the barrier height is large only a few reactant molecules collide with each other and cross the barrier to form a transition state. Reactant molecules having lower activation energy (E_a) cannot pass through the transition state and are unable to form the desired product. In the presence of a catalyst, more reactant molecules are converted into products because the catalyst provides an alternate route for the reaction that requires lower activation energy. The new route results in bond rearrangements and allows large fractions of reactant molecules with sufficient energy to pass through the transition state to form product molecules.[5,6] Hence catalyst helps to cross the barrier in two or more steps and increases the rate of a reaction without changing the overall standard Gibbs free energy required for the reaction (Fig. 30.2).

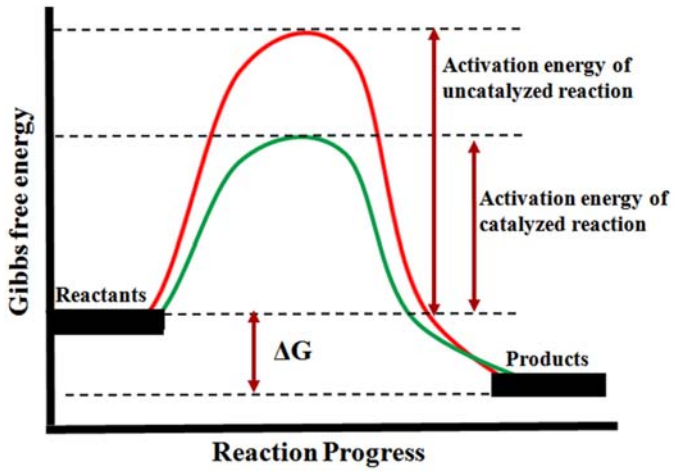

FIGURE 30.2 Effect of catalyst on the activation energy of the reaction.

2. Types of catalysts

2.1 Positive and negative catalysts

The chemical spices, which accelerate or speed up the rate of a chemical reaction are known as positive catalysts. For example, in the decomposition of $KClO_3$ (potassium trioxochlorate), MnO_2 (manganese dioxide) acts as a positive catalyst. The positive catalysts found various applications in chemical industries.

$$2KClO_3(s) \xrightarrow{MnO_2} 2KCl(s) + 3O_2(g)$$

There are many different substances that slow down the chemical process. When these substances are added to the reaction mixture instead of increasing, they retard or inhibit the reaction rate. These are known as negative catalysts or inhibitors and the process is known as negative catalysis. For example, the decomposition rate of H_2O_2 (hydrogen peroxide) can be retarded by H_3PO_4 (tetraoxophosphate(V) acid). Also, ethanol solution (2%) inhibits the oxidation of $CHCl_3$ (trichloromethane) by air.

2.2 Catalytic promoters and inhibitors

There are certain substances that do not act as a catalyst but affect the rate of a chemical reaction by disturbing the catalytic efficiency of the catalyst. For example, Fe is used as a catalyst for ammonia synthesis in the Haber process. The catalytic efficiency of Fe can be enhanced by adding a certain amount of Al_2O_3 and Mo. The substances, which accelerate or increase the efficiency of the catalyst are termed as promoters. However, there are various substances that retarded the efficiency of the catalysts and are known as inhibitors or catalytic poisons. H_2S (Hydrogen sulfide), As_2O_3 (arsenic oxide), HCN (hydrogen cyanide) and Hg (mercury) salts work as inhibitors.

2.3 Homogenous and heterogeneous

In the catalysis process, it is a very important as well as challenging task to identify the active metal species, which is responsible for the catalytic reaction. Based on the solubility parameters and critical phase of catalyst and reactant, catalysis is conventionally classified into two categories: Homogeneous and Heterogeneous catalysis.

In Homogeneous catalysis, the catalyst operates or accelerates the reaction process in a similar phase as that of the reactant molecules. Most of the homogenous catalytic reactions are carried out in the liquid phase.[7–9] There are many catalytic and industrial important reactions that involve the use of homogenous catalyst.

(1) Acid catalysis, (2) Esterification, (3) Liquid phase hydrogenation of C═C, (4) Reduction of NO_2 to NH_2 group, (5) Carbonylations, (6) Polymerization and Metathesis (7) Oxidation and many more.

2.3.1 Advantages

- XHomogeneous catalysts are highly active as well as selective toward the formation of the desired product.
- Reactants and catalysts are in the same phase (liquid) as a result they promote the reaction rate with higher efficiency.

- Homogeneous catalysts in the liquid phase are easily characterized by different spectroscopy techniques.
- Homogeneous catalysts are more preferable for exothermic reactions.

2.3.2 *Disadvantages*

In spite of a large number of catalytic applications, there are also some limitations associated with homogeneous catalysis.

- Catalytic activity is governed by its reusability. Homogenous catalysts are difficult to separate from the reaction mixture and recycled for other reactions.
- Homogenous catalysis is highly temperature dependent and exhibited poor activity and selectivity at a higher temperature.

Heterogeneous catalysis is widely employed for various industrial applications specifically in petrochemicals, pharmaceuticals, and agrochemical industries. In heterogeneous catalysis, the catalyst operates the reaction in different phases as that of the reactant molecules, and adsorption of reactant molecules takes place on the surface of the catalyst. In the adsorption process, the gas or liquid phase reactant molecules are stuck to the surface active sites of the catalyst. Thus, a chemical reaction occurs at the catalyst surface and after completion of the reaction, the product molecules are desorbed from the catalyst surface.[10–12] Hydrogenation of C=C, C=O, degradation of toxic organic pollutants, and many other industrially important chemical reactions are carried out using heterogeneous catalysis.

3. Cocatalysis

The activity of the catalyst can be increased by the addition of a small quantity of second chemical material called cocatalyst or promoter in cooperative catalysis. Cocatalysts provide different active sites and reaction paths for surface catalytic reactions. The physicochemical properties of cocatalyst like structure, and surface area affect the rate and nature of surface reactions.[13,14] Fig. 30.3 shows the effect of cocatalyst in the ammonia synthesis using Haber's process. A small amount of Al_2O_3 on the Fe surface provides a new reaction pathway that requires the smallest activation energy for N_2 dissociation and results in a higher amount of ammonia formation.

In photochemical reactions, loading metal cocatalysts is the most popular way to increase the activity of the semiconductor photocatalyst. The cocatalyst deposited on the surface of the semiconductor effectively binds the reactant molecules and promotes the adsorption of these molecules on the surface. Cocatalyst act as a sink for photogenerated electron and hole pairs and improve the photocatalytic efficiency of the semiconductor.[15,16] Coinage metals (Ag, Au, Cu, Pt) are widely used as cocatalysts.[17–19] Because of localized surface plasmon resonance (LSPR), impregnation of these coinage metals on the surface of the semiconductors shifts the spectral response of photocatalysts in the visible region. Also, depositions of these metals result in the formation Schottky barrier and retard the recombination rate of photogenerated electrons and holes, and enhance the charge separation. When a photocatalyst or semiconductor is illuminated with a light source the electrons are excited from the valence band

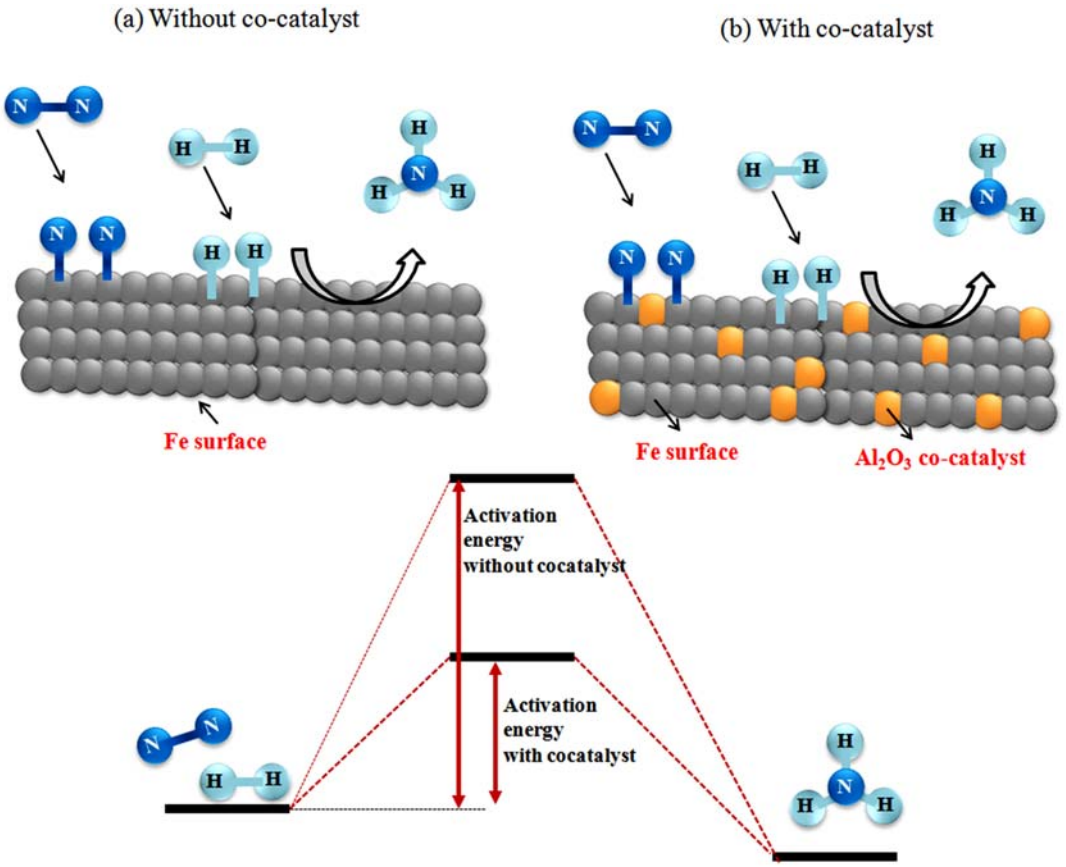

FIGURE 30.3 Effect of cocatalyst on ammonia synthesis reaction.

(VB) to the corresponding conduction band (CB) of the semiconductor. This results in the formation of photogenerated electrons in the conduction band and holes are generated in the valence band. The deposited noble metal cocatalyst, entrap the photo-excited electrons because the Fermi energy level of coinage metal is always lower than the semiconductor. Thus, the cocatalyst improves the charge separation by hindering the recombination of photogenerated charge carriers and improves the photocatalytic efficiency of the semiconductor.[20–22] Fig. 30.4 shows the schematic diagram of how a cocatalyst works after being deposited on the surface of the semiconductor.

3.1 Silica (SBA-15) supported transition metal nanoparticles as a cocatalyst

Mesoporous materials because of their specific morphology and high porosity have received remarkable attention for biosensor, adsorption, drug delivery, catalytic and photocatalytic applications. Among various mesoporous materials, SBA-15 is considered to be a promising material as it shows a higher specific area, uniform pore size distributions, and

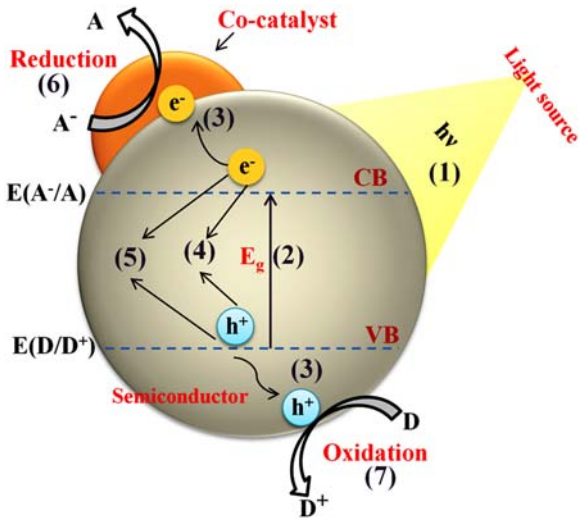

FIGURE 30.4 Role of cocatalyst in different stages: (1) light capturing (2) photo-excitation (3) charge separation and transfer (4) recombination of charge carriers (5) recombination surface charge carriers (6) photocatalytic reduction (7) photocatalytic oxidation.

high thermal stability. It has been observed that due to lower acidic strength, the pure or bare SBA-15 shows poor catalytic activity. Different strategies like deposition of metal/metal oxides, and doping of $-NH_2$, $-SH$ functional groups have been employed in order to enhance the catalytic activity of SBA-15. The deposition of different metals like Au, Ag, Pd, and Pt by physical adsorption or chemical adsorption on the surface of SBA-15 is a promising and widely used approach to increase the catalytic efficiency of SBA-15. However, for many years, Au was considered to be inert till the exciting discovery made by Haruta et al.[23] and Hutching et al.[24] that revolutionized the field of catalysis on Au-based catalysts. Shu et al.[25] prepared a heterogeneous Au catalyst by stirring SBA-15 in a CH_2Cl_2 solution of PH_3PAuBF_4 to form a homogeneous Au complex followed by its reduction with ascorbic acid to form Au nanoparticles. Ma et al.[26] synthesized Ag/SBA-15 nanocomposites by varying the Ag loading (4%−16%) using the impregnation method for oxidation of benzyl alcohol to benzaldehyde. Szegedi et al.[27] reported the formation of Ag nanoparticle-loaded mesoporous silica nanostructures using the pulsed laser ablation (PLA) method for the oxidation of toluene. Fuku et al.[28] employed microwave-assisted alcohol reduction method for the formation of highly dispersed Ag nanospheres (∼4 nm) and nanorods (∼9 nm in diameter) within the channels of SBA-15. Strzalka et al.[29] proposed an efficient, fast, and interesting approach for the synthesis of Ag nanostructures (nanospheres ∼4 nm and nanowires ∼50 nm depending on Ag loading) supported on mesoporous silica with controlled morphology and composition using tollen's reagent as Ag source. Similarly, Compared with Au and Ag metals, Cu/CuO have also demonstrated great capacity as redox catalysts due to being cheaper, easily accessible, and exhibiting exceptional electrochemical and catalytic properties.[30–32]

3.2 Zeloite-supported metal nanoparticles as a cocatalyst

It has been observed that the smallest size particles show higher catalytic activity than the large size particles. Metal nanoparticles show higher activity because of their small size and higher surface-to-volume ratio but have lower thermal stability, which hinders their catalytic efficiency under harsh reaction conditions. Zeolites are promising candidates for the encapsulation of metal nanoparticles. Generally, postsynthesis method is used to introduce metal nanoparticles in zeolite cavities. Various metals like Re (rhenium), Mo (molybdenum), and W (tungsten), which are unable to form a cationic complex in the solution, can be encapsulated in the zeolites in an acidic medium. The Au nanoparticles encapsulated silicalite-1 showed higher activity for ethanol oxidation in the gas phase and displayed superior selectivity (98%) for benzaldehyde. Pt-supported beta zeolite exhibited longer stability and activity toward the toluene combustion (check). The mesoporous zeolite exhibited higher stability, activity, and 100% selectivity than the commercially used microporous zeolite (Pt-R/beta), which becomes inactive after 6 h of the reaction. Direct decomposition of nitric oxide (NO) to nitrogen (N_2) and oxygen (O_2) has been achieved by Cu encapsulated ZSM-5. It is observed that the rate of selective reduction of NO to N_2 is inhibited by SO_2, H_2O, and O_2. However, it is observed that the addition of hydrocarbons, which act as reducing agents significantly increases the decomposition of NO. In comparison to amorphous oxides, mesoporous zeolites provide different surface active sites for metal nanoparticle encapsulation. Thus, the heterojunction of metal nanoparticles with hierarchical zeolites is considered as a promising approach for a large number of industrial applications.[33,34]

4. Photocatalysis

Catalysis is a phenomenon in which a certain chemical substance accelerates the rate of transformation of reactant molecules into products without being consumed in the chemical reaction. That chemical substance is recognized as a catalyst that speeds up the rate of a reaction by providing an alternate path of lower activation energy. Photocatalysis is a reaction in which light is used to activate a substance in order to increase the rate of a chemical reaction. Thus, photocatalysis is defined as the acceleration of a chemical reaction by direct light irradiation or by the irradiation of a catalyst.

4.1 Principle of photocatalysis

Generally, semiconductor materials are used as photocatalysts for various photocatalytic applications. When a semiconductor is illuminated with light radiations, adsorption of photons takes place. If the band gap energy of the semiconductor is equal to or smaller than the photon's energy then electrons are excited from the valence band of the semiconductor to the corresponding conduction band. The excitation of electrons simultaneously results in the generation of the positive hole (h^+) in valence band (schematically shown in Fig. 30.5).

$$h\nu + \text{Semiconductor} \rightarrow h^+ + e^-$$

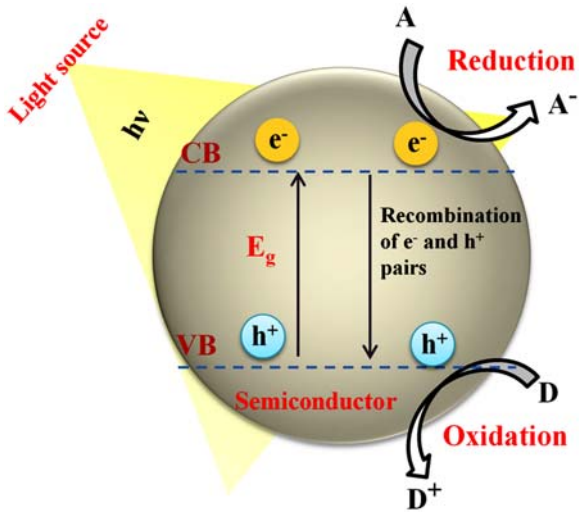

FIGURE 30.5 Photochemical process of semiconductor.

Two possibilities are there after the formation of photogenerated electrons and hole pairs in the conduction band and valence band respectively. (1) In absence of an appropriate scavenger, recombination of photogenerated charge carriers (e^{-}-h^{+}) takes place. Because scavenger entrapped the photogenerated holes and enhances the charge separation. (2) Prevention of charge carriers takes place if the photogenerated electrons and hole pairs undergo a redox reaction with the substance that is adsorbed on the surface of the semiconductor. The life span of photogenerated electron and hole pairs is very small (a few nanoseconds) but this time is long enough to promote the photo-redox reaction. The necessary condition for a semiconductor to be photo-active is the redox-potential of the photogenerated electrons in the conduction band should be sufficiently negative. In a similar way, the redox-potential of photogenerated holes in the valence should sufficiently be positive. Based on this the adsorbed oxygen can be reduced to superoxide radicals by photogenerated electrons and photogenerated holes result in the formation of hydroxyl radicals, which can further oxidize different organic pollutants.

4.2 Metal oxide photocatalyst

Metal oxides such as TiO_2, ZnO, MgO, Fe_2O_3, etc. are widely used as effective photocatalysts for a large number of applications. Out of various metal oxides, TiO_2 is a viable, nonpoisonous, exceptionally steady, encouraging semiconductor material and finds various catalytic applications in different research areas.[35–38] The significant disadvantage in regards to titanium dioxide is a wide band gap energy (3.2 eV), which restrains its photocatalytic performance under the visible region. Different strategies have been made by the researchers to manufacture effective M-TiO_2 heterocomposite containing diverse plasmonic metals (Cu, Au, and so on.) that viably actuate and improve the photocatalytic action of TiO_2 under visible region.[39] Monga et al.[40] demonstrated the synthesis, characterization and photocatalytic activity of bimetallic Cu@Au

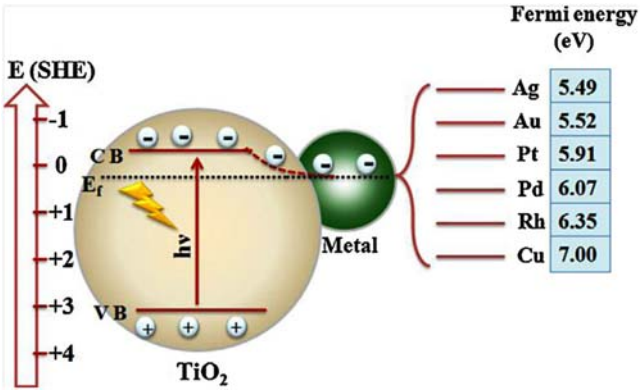

FIGURE 30.6 Charge transfer process and Fermi level equilibration at metal-$Ti0_2$ heterojunction. *Reprinted with permission from Kaur et al.* [43] *Copyright @2015 Elsevier.*

and inverse Au@Cu core-shell nanostructure imparted to TiO_2 for effective nitro-aromatic reduction under visible light. Crake et al.[41] revealed that TiO_2/C_3N_4 nanocomposite exhibited remarkable photo-reduction efficiency toward gaseous CO_2 under UV-Visible light illumination. Likewise, Au−Pt stacked TiO_2 nanosheets were employed for photocatalytic hydrogen production via water splitting under solar radiations.[42]

In photocatalytic reaction, the deposited metal act as a sink for the photogenerated electrons present in the CB (conduction band) of titanium oxide, and the photogenerated holes initiate the oxidation of molecules adsorbed on the surface of the TiO_2. Therefore, metal-TiO_2 heterojunction is a promising material for enhanced photooxidation processes. The rate of charge transfer process generally depends upon the relative placement of conduction and valence bands and also upon the work function of deposited metal species. The metal deposited on the surface of titanium dioxide forms a Schottky barrier, which traps the photogenerated electrons, hinders the recombination of electron and hole pairs, and improves the charge separation and thereby improving the charge separation efficiency for enhanced oxidation−reduction rate of the surface adsorbed organic substrates. The size of deposited metal, nature, composition, and reduction potential (E^o) influence the charge separation and Fermi level equilibration in M-TiO_2 composites[43–45] (Fig. 30.6).

5. Transition metal nanocatalysis

Nowadays, nanocatalysis involving the use of metal nanoparticles as a catalyst has gained significant attention for various industrial applications. The nanoparticles of transition metals (Ni, Pd, Au, Ag, Cu, and Zn) are effectively used as a catalyst for various organic transformation reactions i.e., hydrogenation of nitro-aromatics, C−C bond formation, C−H functionalization, oxidation-reduction reactions. The small size, large surface area, and high surface-to-volume ratio of the metal nanoparticles result in the effective interaction of nanoparticles with reactant molecules even under mild reaction conditions and improve the yield and selectivity of the reaction. The optical and electronic properties of metal

nanoparticles are highly dependent on different physical and chemical parameters. Thus, the catalytic performance of metal nanoparticles can be controlled or improved by varying the size, shape, composition, and surface morphology of the nanoparticles. The Au nanoparticles having different morphological appearances i.e., nanospheres, nanorods, triangular, hexagonal, etc. are found to have different yield and selectivity for the same catalytic/photocatalytic reaction. Monga et al.[46] reported the synthesis of Au nanoparticles having different morphology nanospheres and nanorods. It is found that both nanoparticles exhibited different optical and electronic properties. The Au nanospheres show a surface plasmon band at 536 nm, conversely, Au nanorods showed a surface plasmon band at 679 nm. It is observed that Au nanorods exhibited a higher percentage yield for the reduction of p-nitrophenol and p-nitrobenzoic acid relative to Au nanospheres credited to the higher exposed catalytic surface area of Au nanorods. The size and morphological appearance of metal nanoparticles can be altered by changing the experimental conditions, for example by varying the composition, surfactant ratio, reducing/capping agents, temperature, and time interval for their synthesis. It is observed that by varying the weight ratio of PVP (polyvinylpyrrolidone) with respect to Ni, the size of Ni nanoparticles is varied from 10−12 to 3−5 nm. The Ni nanoparticles having an average size between 3 and 5 nm were found to have higher activity for Suzuki Miyaura cross-coupling reaction and also have higher yield and selectivity for the catalytic hydrogenation of cinnamaldehyde and croton aldehyde compared to large size Ni nanoparticles.[47]

In spite of the large number of catalytic applications, a single monometallic nanocatalyst is not able to accomplish the desired activity and selectivity for the reactions. The monometallic Ag nanoparticles are found to have limited practical applications because of their higher affinity toward the oxidation and agglomeration process, which affects the optical and catalytic properties of Ag nanoparticles. A large number of surfactants, capping agents like ligands, and polymers have been used in order to improve the stability and aggregation of these metal nanoparticles. Presently, the coating of one metal nanoparticle with a layer of another metal resulting in the formation of bimetallic nanostructure has gained tremendous attention among researchers. The coating of Ag nanoparticles with the layer of Au nanoparticles prevents the oxidation of Ag nanoparticles and improves the chemical stability as an electronic transition between the two metallic elements arises due to the difference in electron affinity and electro-negativity values of two different metal atoms.

6. Importance of bimetallic over monometallic nanoparticles

Bimetallic core-shell nanocomposites consisting of two different metals (Au@Ag, Ag@Au, Pd@Ni, Au@Cu, Pd@Cu, Au@Pd) have attained particular interest in the area of catalysis/photocatalysis. These bimetallic nanocatalysts exhibited superior optical, structural, and physiochemical properties relative to their respective parent metals. The improvement in their catalytic performance arises due to

1. the electronic or ligand effect in which charge transfer occurs between two different metals resulting in the modification of electronic properties of the first metal (Fig. 30.7)

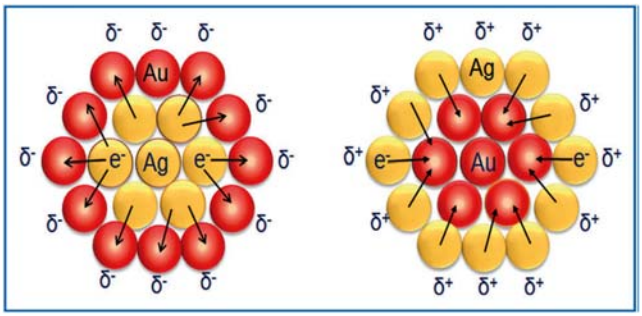

FIGURE 30.7 Interfacial charge transfer process between two different metals. *Reprinted with permission from Monga et al. [55]. Copyright @2015 Royal Society of Chemistry.*

2. An ensemble or geometric effect in which the addition of second metal on the surface of the first metal provides new surface active sites. Fig. 30.8 shows the color transformation and change observed in optical properties of core@shell nanostructure as the concentration of shell precursors increases.[48]
3. Each metal element promotes different elementary reaction steps resulting in a bifunctional mechanism. Monga et al.[46] explored the effect of shapes of bimetallic Au@Ag nanostructures resulting in superior photo-activity for the nitro aromatic reduction than the monometallic counterparts.

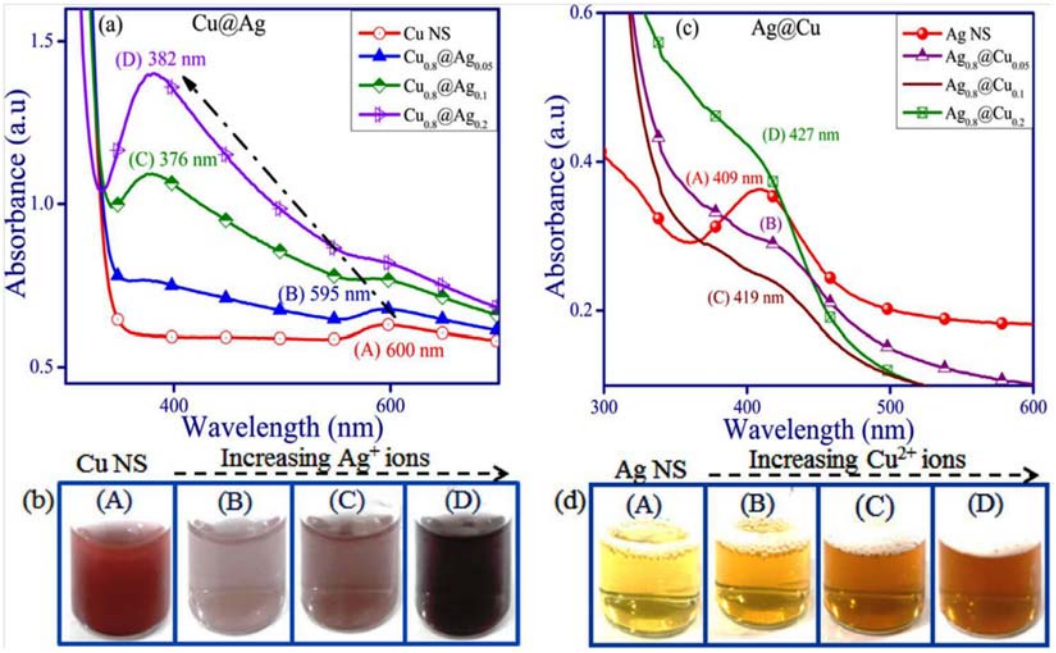

FIGURE 30.8 Effect of increasing (A–B) Ag deposition onto Cu nanospheres and (C–D) Cu deposition onto Ag nanospheres with corresponding change in color intensity. *Reprinted with permission from Monga et al. [48]. Copyright @2017 Elsevier.*

Different strategies have been employed like photochemical, successive reduction, microwave-polyol, template, potentiostatic, electrochemical deposition, and two-step reduction in order to form bimetallic nanostructure. Depending upon the synthetic approach two metals can adopt either core@shell or alloy nanostructure. Among various heterostructures like alloy, dumbbell, and hollow core-shell nanostructure, bimetallic core-shell nanostructures are promising nanocatalysts for a large number of catalytic reactions. However, one pot coreduction method based on galvanic displacement reaction is widely employed for the synthesis of core-shell nanostructures. In this case, two metallic precursors are added simultaneously and the reduction potentials of metals play a significant role in determining the final structural design. Metals having dissimilar reduction potentials are reduced in a consecutive manner in the presence of suitable reducing agents (Ascorbic acid, Hydrazine, $NaBH_4$, etc.). Metal ions with more positive reduction potential tend to be reduced at a faster rate and serve as a core whereas metals with lower potential are reduced later and make a shell over the core metal nanoparticles leading to the formation of the core-shell nanostructure. Jiang et al.[49] reported the formation of Au@Ag core-shell nanostructure by galvanic interaction caused by the difference in reduction potentials of the two soluble metal salts (E^0 $Ag^+/Ag = +0.80$ eV vs. SHE; E^0 $Au^{3+}/Au = +0.93$ eV vs. SHE). Similarly, Tang et al.[50] studied the galvanic interaction between Au and Pd metal ions leading to the formation of Au@Pd core-shell nanostructure based on their reduction potential (E^0 $Au^{2+}/Au = +1.42$ eV vs. SHE; E^0 $Pd^{2+}/Pd = +0.91$ eV vs. SHE). The bimetallic nanostructures of noble metals (Au, Ag, Cu, etc.) are broadly investigated because of their enhanced surface plasmon resonance in the visible region, identical crystal structure (FCC), and simplistic synthesis technique. The bimetallic core-shell nanostructure of Au@Ag and reverse core-shell Ag@Au with a different morphological appearance like spheres, rods, cubic, wires, octahedrons and many more have been synthesized by different researchers. It was observed that the chemical and different electronic properties of bimetallic core-shell nanostructure can be modified by changing the nature of core/shell atoms, by varying the core/shell thickness. Monga et al.[40] reported the difference in catalytic behavior observed by altering the core and shell thickness in Au@Ag and reverse Ag@Au core-shell nanostructure. The difference in chemical properties arises due to the fact that both metal atoms (Au, Ag) have different work functions, and also by covering the core region of Au atoms by Ag shell affected the physical properties of nanostructure like dispersion in various liquids, alteration in zeta potential values, which govern overall electro-kinetic properties of the bimetallic nanostructure.

7. Metal-semiconductor (TiO_2) photocatalysis

The photocatalytic hydrogenation of organic compounds using semiconductor photocatalysis attracted a lot of interest. The selective hydrogenation of C═O (carbonyl group) is an essential step for various applications and is widely used in the synthesis of different drugs, chemicals pesticides, and polymers. Both mono/bimetallic nanocatalysts have been used for this purpose, but bimetallic nanoparticles achieve significant interest among researchers because of their advanced physicochemical properties. The deposition of these monometallic/bimetallic nanoparticles (NPs) on the surface of the semiconductor (TiO_2) improves the photocatalytic efficiency of the semiconductor. The impregnated monometallic/bimetallic

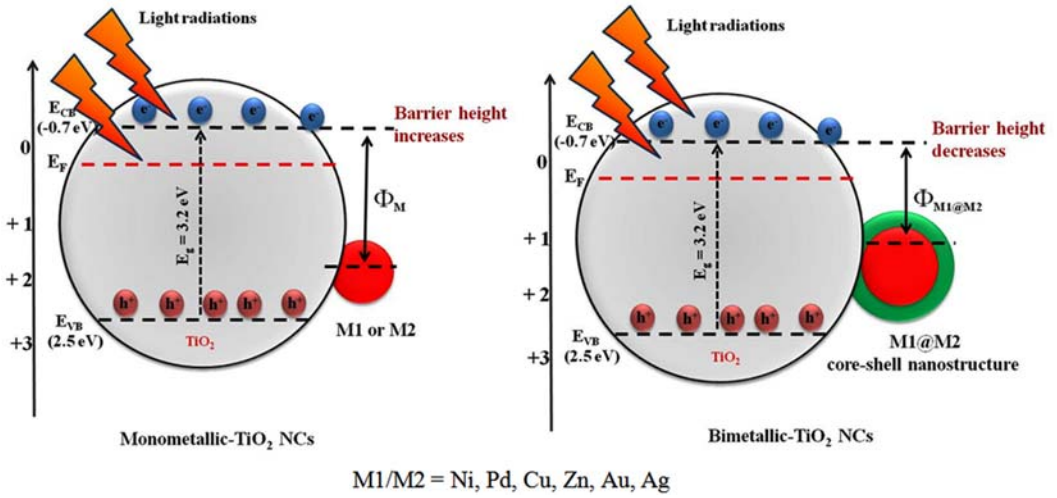

FIGURE 30.9 Charge transfer process in case of mono/bimettalic-TiO_2 nanocomposites.

nanoparticles act as a photo-sensitizer and enhance the charge transfer process from the conduction band of the semiconductor to the surface of the metal nanoparticle (NP). Therefore, metal/semiconductor hetero-junction becomes a key factor for making a highly active photocatalyst. Shiraishi et al.[51] reported the photocatalytic production of hydrogen peroxide from ethanol using Au−Ag bimetallic loaded TiO_2 photocatalyst. Monga et al.[40] reported the cocatalytic effect of bimetallic Cu−Au core-shell nanostructure impregnated on TiO_2 for the photo-reduction of nitro aromatic compounds and photo-oxidation of salicylic acid. Similarly, Ge et al.[52] studied visible light-driven photocatalytic reduction of water using Au−Pd bimetallic nanoparticles deposited on graphitic carbon nitride. The enhancement in the catalytic performance of bimetallic nanocomposites occurred due to a shift in their work function relative to monometallic ones. This led to an increase in the life span of charge carriers and facilitate the charge transfer process from the CB of TiO_2 and enriches the electron density over the M1@M2 reaction active center. The charge transfer process occurred in the case of bimetallic core-shell nanostructure and a TiO_2 nanocomposite as shown in Fig. 30.9.

7.1 Enhanced photocatalytic activity of bimetallic deposited TiO_2 photocatalyst

The deposition of bimetallic nanostructure on the surface of titanium oxide improves the photocatalytic performance of TiO_2 in several ways: (1) when a photocatalyst is illuminated with light radiations, it captures the photoexcited conduction electrons (CB) of TiO_2 and retard electron-hole recombination. (2) It promotes the formation of superoxide radicals by transferring photoexcited electrons to the adsorbed oxygen molecules. (3) It prevents the aggregation of titanium dioxide nanoparticles. (4) The synergistic interaction between two different metals and bimetallic-TiO_2 heterojunction increases the stability of the material and improves the interfacial charge transfer process for various catalytic reactions.

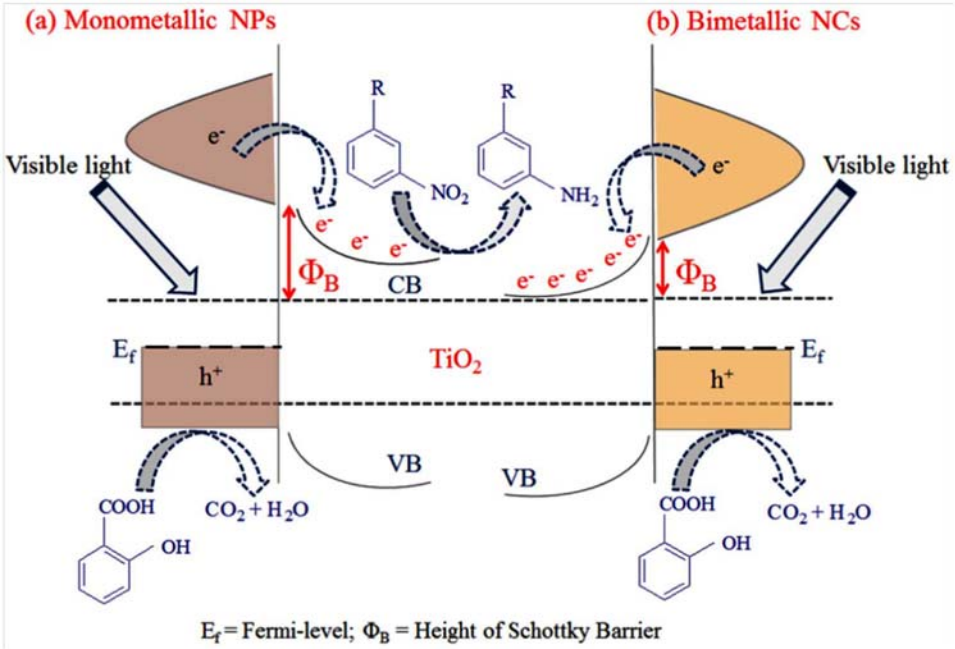

FIGURE 30.10 Possible mechanism for the reduction of nitro compounds using (A) monometallic (B) bimetallic TiO_2 nanocomposites under visible light. *Reprinted with permission from Monga et al. [48]. Copyright @2017 Elsevier.*

Fig. 30.10 represents the mechanism for the photooxidation of salicylic acid and photoreduction of the nitro compound using mono/bimetallic-TiO_2 nanocomposites. The photoexcited electrons in the conduction band (CB) of TiO_2 are used for the reduction of adsorbed oxygen molecules to superoxide radicals. The holes generated in the valence band of TiO_2 promote the photodegradation of salicylic acid. From the above mechanism, the rate-determining step for the photocatalytic reaction is the transfer of electrons from metal nanoparticles to TiO_2. In a photocatalytic process, the photoexcited electrons have to overcome the Schottky barrier (ΦB) formed at the metal-TiO_2 heterojunction. It was observed that depositing the metal on the surface of another metal resulted in the lowering of work function and Schottky barrier height compared to monometallic ones. As a result, bimetallic-TiO_2 nanocomposites promote the efficient charge transfer for various organic transformation reactions as compared to monometallic counterparts and displayed higher activity and selectivity for the reaction.[48]

8. Preparation and characterization techniques

8.1 Galvanic replacement method

Various methods like photochemical, successive reduction, template synthesis, potentiostatic, electrochemical deposition, and two-step reduction have been employed to

synthesize core-shell nanostructures. These methods resulted in the formation of alloy and other hetero-nanostructures. However, one pot coreduction method based on galvanic displacement reaction is widely employed for the synthesis of core-shell nanostructures. In this case, two metallic precursors are added simultaneously and the reduction potentials of metals played a significant role in determining the final structural design. Metals having dissimilar reduction potentials are reduced in a consecutive manner in the presence of suitable reducing agents (ascorbic acid, hydrazine, sodium borohydride, etc.). Metal ions with more positive reduction potential tend to be reduced at a faster rate and serve as a core whereas metals with lower potential are reduced later and make a shell over the core metal nanoparticles leading to the formation of core-shell nanostructure.[53,54] The formation of Pd@Au core-shell nanostructures was carried out by using coreduction method (based on galvanic interaction between Pd and Au metal atoms). In a standard process, an aqueous mixture of $PdCl_2$ (2 mM, 8.5 mL), 100 mg of ascorbic acid, PVP (66.6 mg), and KBr (60 mg) is added into a round bottom flask (50 mL). The subsequent blend was preheated at 110°C for 1 hour followed by the addition of $HAuCl_4$ solution (3 mL, 3 mM). After the addition of HAuCl4 in the response blend, the response temperature was sloped to 200°C and maintained for another 1h utilizing refluxing. The galvanic interaction between Pd and Au metal atoms led to the construction of a core-shell nanostructure composed of Pd core and Au shell.[39]

8.2 Seed mediated growth method

The catalytic activity of metal nanoparticles is highly surface-dependent and can be tuned by modifying the size, shape, and composition of the material. The seed-mediated growth method is a promising and widely used method to synthesize different shape metal nanoparticles. Monga et al.[40] reported the synthesis of core@shell and inverse core@shell of Ag, Au, and Cu using the seed growth method.

8.2.1 Formation of Cu@Au core-shell nanostructure

The as-prepared Cu nanospheres were used as a seed for the deposition of Au in order to form a bimetallic core-shell nanostructure. In a standard procedure, 426 μL of Cu nanospheres were diluted with an aqueous solution containing 1 wt% of polyvinylpyrrolidone (PVP) followed by the addition of different amounts of Au aqueous solution ($HAuCl_4.3H_2O$, 0.01 M). To initiate the reduction of Au over Cu core, 0.1 mL of ascorbic acid (0.1 M) was added to the mixture. The pH of the reaction mixture was maintained at $\sim$8–9 pH by adding 0.2 mL of an aqueous solution of NaOH (0.1 M). The synthesized Cu@Au nanostructure was washed several times with water and ethanol and redispersed in a known amount of distilled water.[40]

8.2.2 Fabrication of inverse Au@Cu core-shell nanostructure

A similar procedure (as reported above) was used to synthesize the inverse Au@Cu core-shell nanostructure. 610 μL aqueous solution of Au nanosphere was added to an aqueous solution containing 1 wt% of polyvinylpyrrolidone (PVP) followed by the addition of different amounts of Cu aqueous solution ($CuSO_4.5H_2O$, 0.01 M). 5 mL of hydrazine

monohydrate was added to initiate reduction of Cu over Au core followed by the addition of 11 mL of NaOH solution (1M). The synthesized Cu@Au nanostructure was washed several times with water and ethanol and redispersed in a known amount of distilled water.[40]

8.3 Wet impregnation method

8.3.1 Synthesis of mono/bimetallic-TiO_2 nanocomposites

The Pd@Au−TiO_2 nanocomposites were synthesized via the wet impregnation method. 200 mg of presynthesized titanium dioxide nanospheres were dispersed in 30 mL of distilled water. Add 1wt% of mono/bimetallic nanoparticles and the resulting suspension was kept under continuous magnetic stirring for 24h to get Pd/Au−TiO_2 nanocomposite.[39]

9. Characterizations

9.1 UV-visible spectroscopy

The optical absorption properties of metal nanoparticles were determined by UV-Vis absorption spectroscopy. The principle of this instrument is that when the sample is exposed to light (having suitable energy for electronic transition within the molecule), the required energy is absorbed and the transition of electrons takes place from the lower to the higher energy level. In Fig. 30.11A Ag nanospheres show a significant surface plasmon band at 414 nm. It was observed that on increasing the composition of Au shell thickness from 10, 20−30 μL, the intensity of absorption band red-shifted to 490, 508, and 550 nm respectively. It was

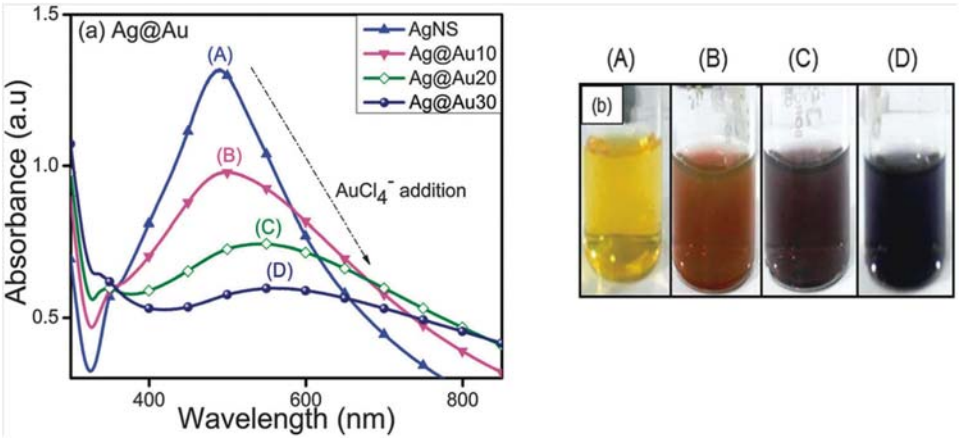

FIGURE 30.11 (A) Effect of increasing Au-shell thickness over Ag nanospheres (NS) (B) corresponding changes observed in the color intensity. *Reprinted with permission from Monga et al. [55]. Copyright @2015 Royal Society of Chemistry.*

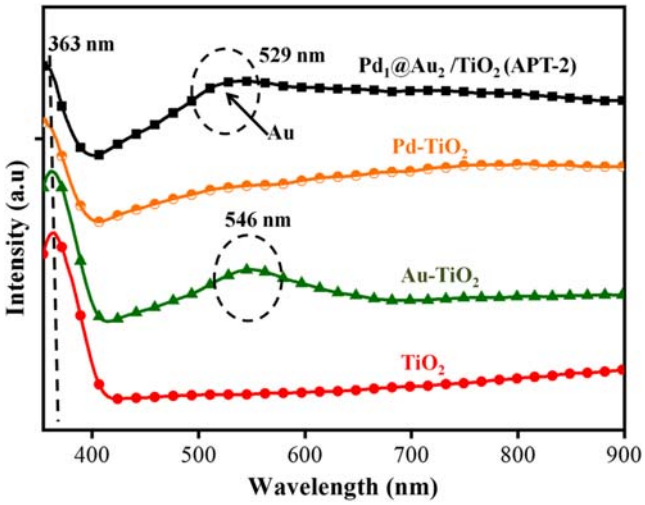

FIGURE 30.12 DRS (diffused reflectance spectroscopy) analysis of mono (Pd, Au) and bimetallic ($Pd_1@Au_2$) $-TiO_2$ (APT-2) nanocomposites. *Reprinted with permission from Bathla et al. [39]. Copyright @2020 Elsevier.*

predicted that morphological changes observed in Ag nanospheres arise due to the deposition of Au (as a shell) over the Ag nanospheres (as a core). This evidence is further supported by a corresponding change in color intensity from yellow to light orange to purple and blue as represented in Fig. 30.11B.[55]

9.2 Diffused reflectance spectroscopy (DRS)

The optical absorption characteristics of bare and Pd/Au$-TiO_2$ nanocomposites can be analyzed using DRS (diffused reflectance spectroscopy). A sharp intensive peak was observed at 363 nm, which corresponds to the bare TiO_2 nanosphere (NS) (Fig. 30.12). Relative to pristine titanium dioxide nanospheres, gold nanoparticles exhibited an absorption edge at 546 nm. However, in bimetallic-TiO_2 nanocomposite ($Pd_1@Au_2/TiO_2$, APT-2) the absorption edge is blue-shifted to 529 nm as shown in Fig. 30.12.[39]

9.3 Electron microscopy

Electron microscopy techniques like transmission electron microscopy (TEM), high resolution-TEM (HRTEM), and scanning electron microscopy (SEM) are used to examine the morphological characters like the shape and statistical distribution of particle size. From the TEM images, the size of bare Au nanospheres was found to be lies in the range of 10−16 nm (Fig. 30.13A). When Ag ions are deposited on the surface of as-prepared Au nanospheres, a layer of thickness ~3−4 nm (Fig. 30.13B−C) was observed suggestion the formation of core-shell nanostructure where Au acts as a core and Ag as shell.[55] On further addition of Ag nanoparticles thickness of shell increased to ~8−10 nm Fig. 30.13D.

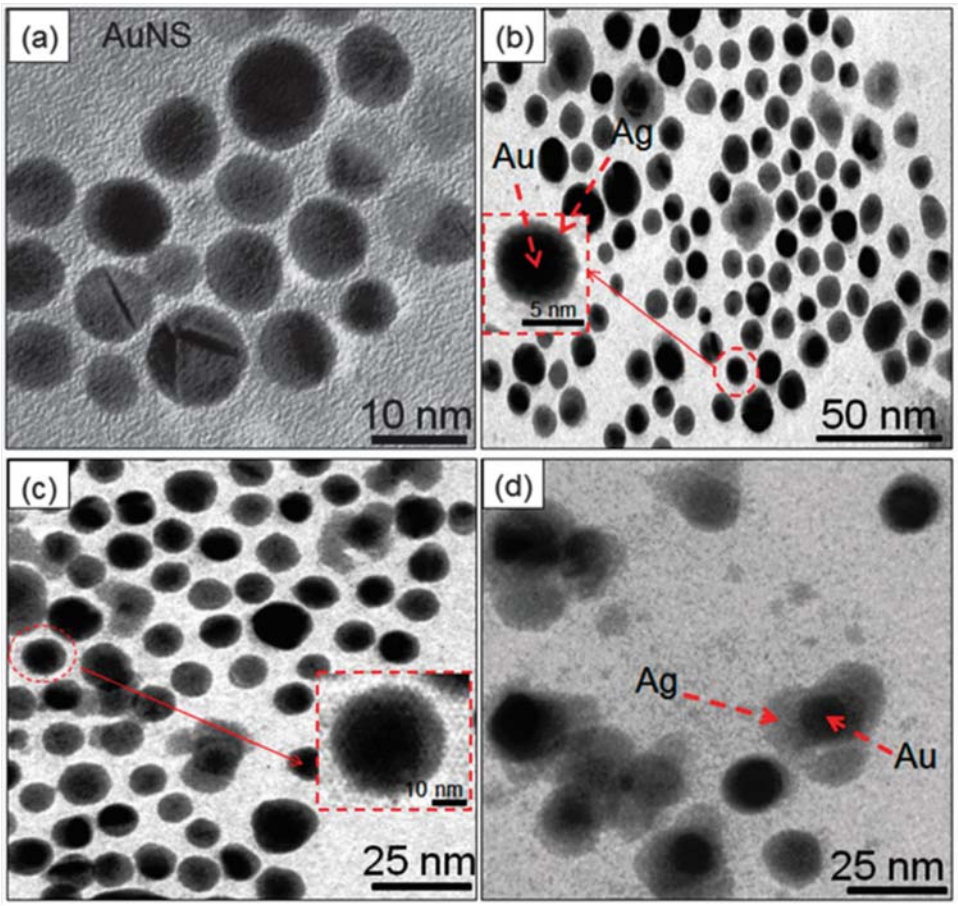

FIGURE 30.13 TEM images of (A) Au nanospheres and (B–D) Au@Ag core-shell nanocomposites of varying Ag-shell thicknesses. *Reprinted with permission from Monga et al. [55]. Copyright @2015 Royal Society of Chemistry.*

The morphological appearance of Pd@Au core-shell nanostructures was further evaluated by STEM through EDS elemental mapping (Fig. 30.14). The STEM images (Fig. 30.14A and B) displayed a significant luminance contrast indicating a distinctive boundary between the Pd core and Au shell. Since the atomic density of Au is much higher than Pd; Fig. 30.14C shows the high intensity of Au over the shell region (shown in red color) and Pd showed a higher intensity in the core region (shown in green color, Fig. 30.14D) indicating the formation of Pd@Au nanostructure.[39]

9.4 X-ray powder diffraction (XRD)

The phase structural, facet design, polymorphism, and unit cell properties were studied by X-ray diffraction with Cu Kα at 1.54 A^{o} operating at 13–45 kV and the diffraction angle was set between 10°–80° with 5°/min rise. The samples for the XRD were finely ground in a mortar pestle

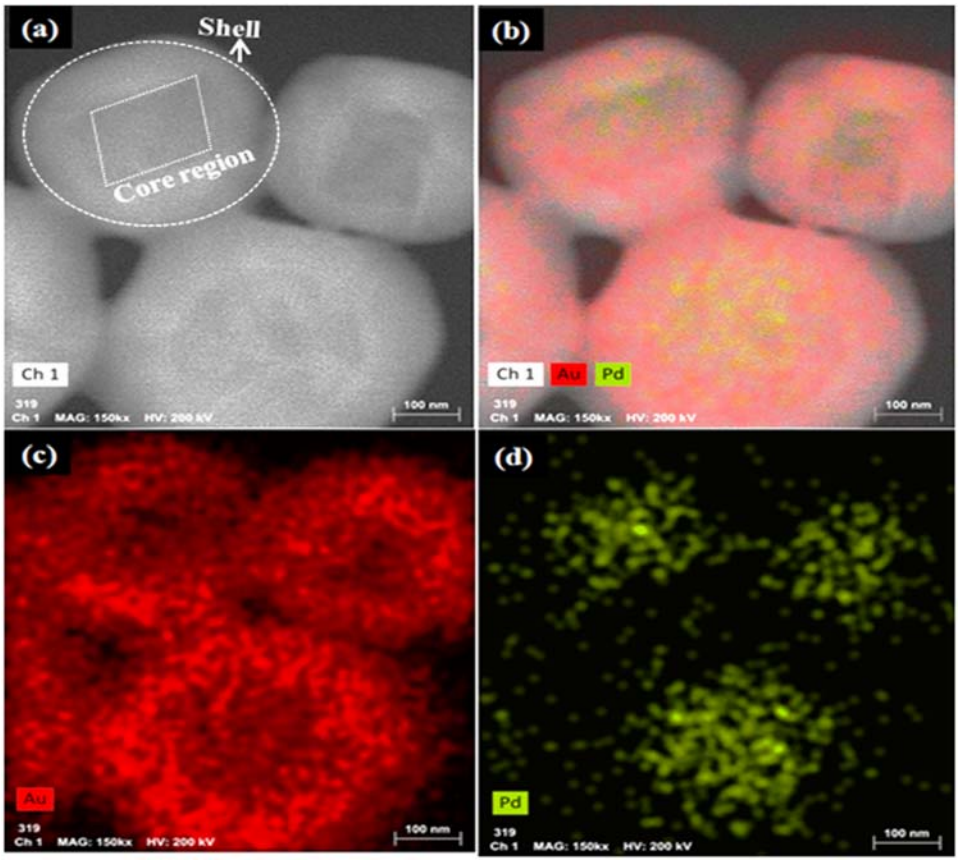

FIGURE 30.14 Scanning transmission electron microscopy (STEM) and energy-dispersive X-ray spectroscopy (EDS) mapping of Pd@Au core-shell nanostructure. *Reprinted with permission from Bathla et al. [39]. Copyright @2020 Elsevier.*

before analysis. Fig. 30.15 shows the XRD analysis of standard titanium dioxide (P25) and as-prepared titanium dioxide nanosheets. The diffraction peaks of titanium dioxide (P25) were found to be identical to the anatase phase (JCPDS 01-089-4921). The high-intensity XRD peaks occur at 25.41° (101), 38.07° (004), 48.19° (200), 55.15° (105), and 60.27° (204) correspond to different lattice planes. The presence of (004) lattice plane at 38.07° clearly suggests the development of (001) faceted titanium dioxide nanosheets. The nonexistence of (001) diffraction peak in standard titanium dioxide (P25) is due to a number of structural factors of TiO_2.[54]

9.5 X-ray photoelectron spectroscopy (XPS)

The surface chemistry, quantitative elemental composition, and oxidation state were studied by XPS technique. The titanium (2p) spectrum (Fig. 30.16A) is consist of two different deconvoluted peaks whose center lie at 458.2 and 464.1 eV respectively.[39,56] The difference between Ti $2p_{3/2}$ and $2p_{1/2}$ signals was found to be 5.9 eV suggesting the existence of a +4 oxidation state of

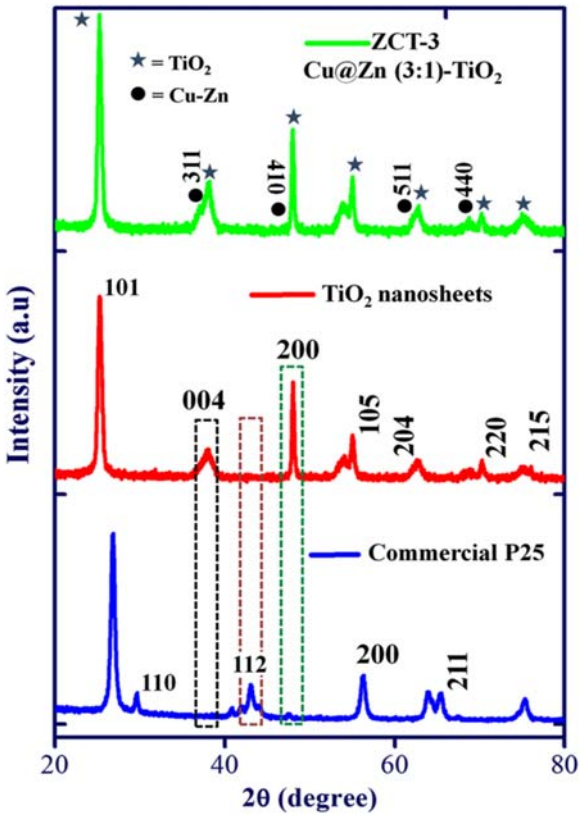

FIGURE 30.15 X-ray diffraction pattern of P25, TiO_2 nanosheets, and Cu@Zn−TiO_2 nanocomposite. *Reprinted with permission from Bathla et al. [54]. Copyright @2019 Elsevier.*

Ti. The O1s spectra deconvoluted into three different peaks corresponding to O^{2-} (529.6 eV), O−H binding (531.5 eV), and O_2 (free oxygen, 533.5eV) respectively (Fig. 30.16B).[39,57] The high-resolution XPS spectrum of palladium 3d (Fig. 30.16C) consists of two different deconvoluted peaks, which were assigned to Pd $3d_{5/2}$ (335.3 eV) and $3d_{3/2}$ (341.9 eV) respectively suggesting the occurrence of Pd $^{(0)}$. A noticeable shoulder peak at 336.6 eV was also observed indicating that Pd nanoparticles also exist in the Pd^{2+} chemical state.[39,58] Similarly, the core level gold 4f spectrum (Fig. 30.16D) consists of two deconvoluted peaks centered at 82.9 eV ($4f_{5/2}$) and 86.8 eV ($4f_{7/2}$), which were assigned to the metallic state of gold ($Au^{(0)}$).[39,59]

10. Applications

10.1 Photocatalytic activity of Pd@Au-TiO_2

The combination of Pd and Au as a core-shell nanostructure exhibited brilliant optical, catalytic, and photocatalytic properties. These Pd@Au−TiO_2 nanocomposites were studied for the selective hydrogenation of unsaturated aldehydes under catalytic/photocatalytic reaction

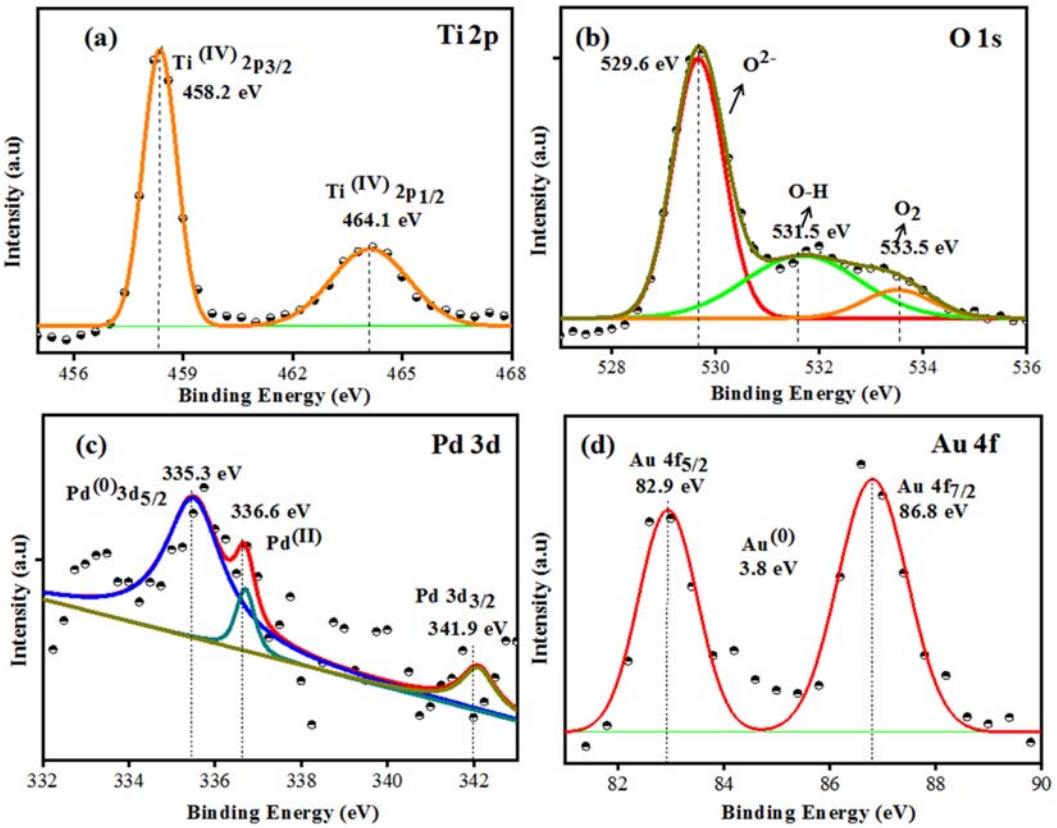

FIGURE 30.16 XPS (X-ray photoelectron spectroscopy) analysis of (A) Ti, (B) O, (C) Pd, (D) Au. *Reprinted with permission from Bathla et al. [39]. Copyright @2020 Elsevier.*

conditions. Fig. 30.17 shows a histogram indicating the comparative % yield obtained for the cinnamaldehyde (CAL) hydrogenation carried out under catalytic/photocatalytic experimental conditions. The APT-2 ($Pd_1@Au_2/TiO_2$) photocatalyst displayed a superior percentage yield (98%) toward the selective hydrogenation of cinnamaldehyde to cinnamyl alcohol than APT-1 ($Pd_1@Au_1/TiO_2$) (67%) and APT-3 ($Pd_1@Au_3/TiO_2$) (83%) under solar radiations. The synergy between Pd@Au and TiO_2 enhanced the charge separation process and facilitate the effective charge transfer at the bimetallic-TiO_2 hetero-junction. As a result, higher selectivity and yield for cinnamaldehyde hydrogenation were observed for bimetallic Pd−Au/TiO_2 than monometallic ones. Moreover, under catalytic conditions, the superior catalytic performance of bimetallic $Pd_1@Au_2/TiO_2$ (APT-2) nanostructure occurred because TiO_2 support provides a higher surface area for adsorption of reactant molecules.[39]

10.2 Photocatalytic activity of Cu@Zn-TiO_2

The selective hydrogenation of quinoline was carried out by using bimetallic Cu@Zn core-shell nanostructure. It was found that nanostructure showed higher activity and selectivity relative to monometallic Cu/Zn nanoparticles. Moreover, when Cu@Zn acted as a cocatalyst

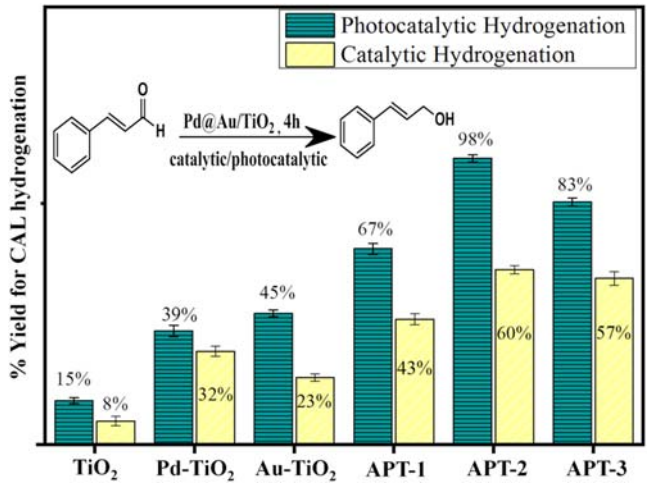

FIGURE 30.17 The % yield obtained for cinnamaldehyde hydrogenation (catalytic/photocatalytic) using different catalyst. *Reprinted with permission from Bathla et al. [39]. Copyright @2020 Elsevier.*

after deposition on the surface of TiO_2, it showed a higher percentage yield for quinoline hydrogenation under visible light. The quinoline hydrogenation reaction was carried out using different controlled reaction conditions. It was found that Cu@Zn/TiO_2 having a higher Cu weight ratio with respect to Zn (Cu:Zn, 3:1) exhibited a higher rate constant of $k = 2.1 \times 10^{-1}$ h^{-1} for quinoline hydrogenation. In the standard procedure, the hydrogenation of quinoline was performed under rough reaction conditions and involved the usage in very harsh conditions (high temperature, solvents, and bases). Therefore, Cu@Zn/TiO_2 nanocomposites could be an effective photocatalyst for selective quinoline hydrogenation.[54]

10.2.1 Possible mechanism for the selective hydrogenation of quinoline

When Cu@Zn/TiO_2 was exposed to visible radiations, the electrons from the valence band (VB) were migrated to the corresponding conduction band (CB) of titanium dioxide. The deposited Cu@Zn nanostructure act as cocatalyst and initiates the charge transfer process and enhances electrons flow to the catalytic active sites of Cu@Zn. The expected mechanism for the selective hydrogenation of quinoline is represented in Fig. 30.18. First, there is a 1,4 hydride addition, which leads to the formation of quinolin-1-ium cation followed by 1,2 hydride addition resulting in the formation of 3,4-dihydroquinolin-1-ium cation or 1,4-dihydroquinoline (Fig. 30.18) and then lastly transformed into 1,2,3,4-tetrahydroquinoline. Synergistic interaction among Cu and Zn at Cu@Zn−TiO_2 interface leads to the barrier height reduction, which efficiently enhances the charge transfer process for the selective hydrogenation of quinoline relative to the monometallic counterparts.[54]

10.3 Catalytic activity of Au@Ag and Ag@Au core-shell nanostructure

Fig. 30.19A shows the amount of NA (3-nitroaniline) and PDA (1,3-phenylenediamine) produced from DNB (1,3-dinitrobenzene) using different mono/bimetallic Au@Ag and Ag@Au core-shell nanostructure. It was observed that with the addition of an aqueous

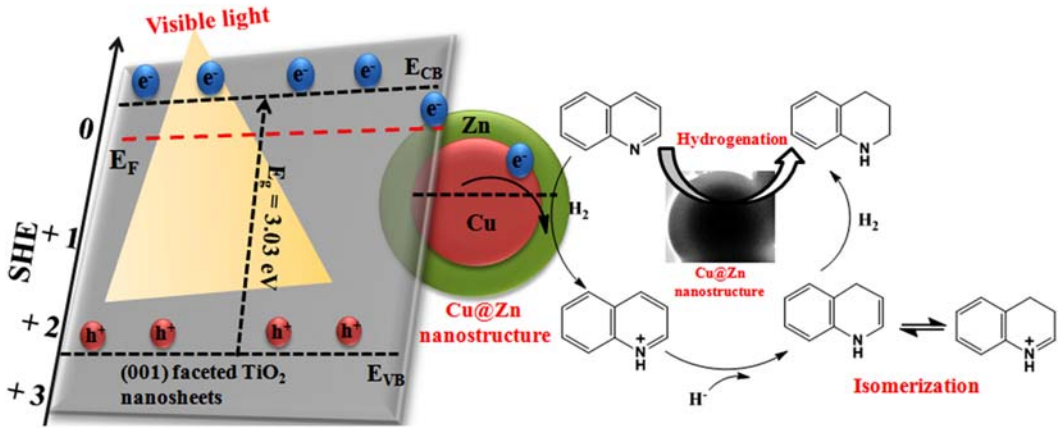

FIGURE 30.18 The possible reaction mechanism for the quinoline hydrogenation under visible light. *Reprinted with permission from Bathla et al. [54]. Copyright @2019 Elsevier.*

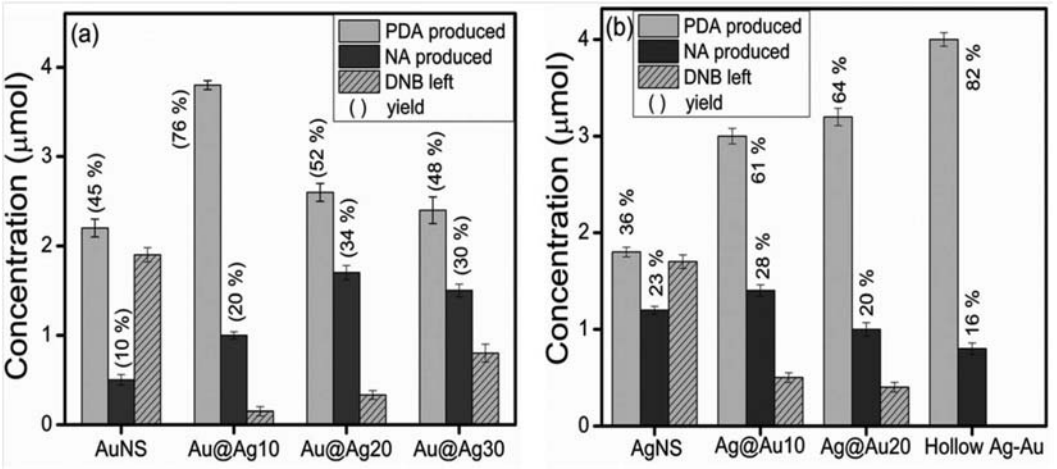

FIGURE 30.19 Amount of 3-nitroaniline (NA) and 1,3-phenylenediamine (PDA) produced from 1,3-dinitrobenzene (DNB) reduction by different mono/bimetallic (A) Au@Ag and (B) Ag@Au core-shell nanocomposites. *Reprinted with permission from Monga et al. [55]. Copyright @2015 Royal Society of Chemistry.*

solution of Ag (10 mL) over Au nanospheres the percentage yield of PDA was increased (70%) relative to bare monometallic Au nanospheres (45%). On further increase in Ag weight ratio, the percentage yield increased to 52% in the case of Au@Ag20 but reduced to 48% in the case of Au@Ag30 nanostructure. This might arise due to the fact that with an increase in Ag weight ratio, the separation between Ag-shell and Au-core increases results in weaker electronic interaction between Au@Ag30 nanostructure. Similarly, Fig. 30.19B shows the percentage yield of PDA obtained after catalytic reduction using Ag@Au core-shell nanostructure. It was found that hollow bimetallic Ag@Au showed higher catalytic activity and percentage yield (82%) as compared to mono and bimetallic

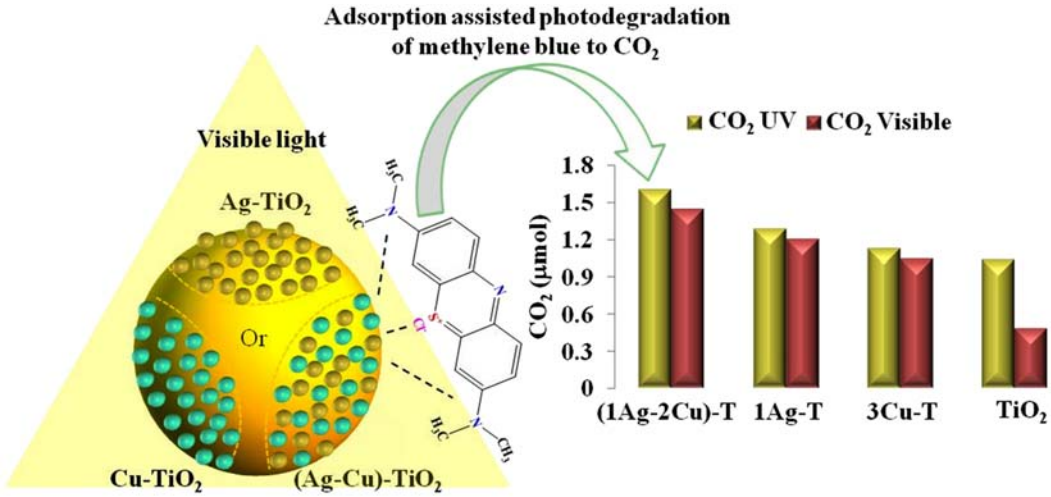

FIGURE 30.20 Comparative CO_2 evolution using mono/binary Ag−Cu−TiO_2 nanocomposite under UV/Visible light. *Reprinted with permission from Bhardwaj et al. [60]. Copyright @2018 Elsevier.*

Au@Ag core-shell nanostructure. The hollow core-shell provides a higher surface area and more catalytic active sites than other mono/bimetallic nanostructures and showed higher activity in PDA formation.[55]

10.4 Photoactivity of binary Ag−Cu/TiO_2 nanocomposites

In this study, codeposited binary Ag−Cu/TiO_2 nanocomposites were examined for adsorption and photocatalytic activities in comparison to Ag/Cu−TiO_2 monometallic nanocomposites. Under UV light illumination, the different weight percentages of Ag and Cu were photo deposited on the surface of titanium oxide in an inert atmosphere. The characteristics SPR band observed at 480 nm and at 640 nm for Ag and Cu respectively. From the TEM analysis, the particle size was found be lie in the 10−20 nm range. It was observed that binary Ag−Cu/TiO_2 nanocomposite displayed higher quenching of photoluminescence intensity relative to mono metallic Ag/Cu−TiO_2 nanocomposite. Moreover, binary Ag−Cu/TiO_2 showed higher activity for the photocatalytic degradation of methylene blue and salicylic acid under different light sources (UV and Visible light (Fig. 30.20)).[60]

11. Conclusion

In concluding remark, bimetallic nanostructures are successfully used as catalysts/cocatalyst for different applications. Pd@Au, Cu@Zn core-shell nanostructures are systematically examined for the selective hydrogenation of cinnamaldehyde and quinoline under light radiation respectively and displayed higher activity and selectivity than corresponding monometallic ones. Similarly, Ag@Au core-shell, Au@Ag inverse core-shell, and binary Ag−Cu/TiO_2

nanocomposites are effectively used as photocatalysts for degradation, photo-oxidation, and reduction of different organic pollutants. Thus, the bimetallic-TiO_2 nanocomposite is an effective and a potential candidate for the selective hydrogenation of unsaturated aldehydes and other industry-relevant compounds that works in a viable, simple, and greener way.

References

1. Lindström B, Pettersson LJ. *Cattech* 2003;**7**:130–8.
2. Wisniak J. *Educación Química* 2010;**21**:60–9.
3. Robertson A. *Platinum Metals Rev* 1975;**19**:64–9.
4. Kakaei K, Esrafili MD, Ehsani A. *In introduction to catalysis*. Elsevier; 2019. p. 1–21.
5. Chorkendorff I, Niemantsverdriet JW. *Concepts of modern catalysis and kinetics*. John Wiley & Sons; 2017.
6. Hagen J. *Industrial catalysis: a practical approach*. John Wiley & Sons; 2015.
7. Van Leeuwen PW. *Homogeneous catalysis: understanding the art*. Springer Science & Business Media; 2006.
8. Misono M, Nojiri N. *Appl Catal* 1990;**64**:1–30.
9. Chauvel A, Delmon B, Hölderich WF. *Appl Catal, A* 1994;**115**:173–217.
10. Deutschmann O, Knözinger H, Kochloefl K, Turek T. *Ullmann's encyclopedia of industrial chemistry*. 2000.
11. Boudart M. *J Mol Catal* 1985;**30**:27–38.
12. Cook E. *In Peregrine Phillips, the inventor of the contact process for sulphuric acid*. Nature Publishing Group; 1926.
13. Chou H, Hwang B, Sun C. *New and future developments in catalysis*. 2013. p. 217–70.
14. Khan M, Al-Oufi M, Toseef A, Nadeem M, Idriss H. *Catal Lett* 2018;**148**:1–10.
15. Yeh T-F, Cihlář J, Chang C-Y, Cheng C, Teng H. *Mater Today* 2013;**16**:78–84.
16. Jang JS, Ham DJ, Lakshminarasimhan N, yong Choi W, Lee JS. Appl Catal. *A* 2008;**346**:149–54.
17. Tanaka A, Sakaguchi S, Hashimoto K, Kominami H. *ACS Catal* 2013;**3**:79–85.
18. Lin H-Y, Yang H-C, Wang W-L. *Catal Today* 2011;**174**:106–13.
19. Reichert R, Jusys Z, Behm RJr. *J Phy Chem,C* 2015;**119**:24750–9.
20. Wen J, Xie J, Chen X, Li X. *Appl Surf Sci* 2017;**391**:72–123.
21. Ni M, Leung MK, Leung DY, Sumathy K. *Renew Sustain Energy Rev* 2007;**11**:401–25.
22. Nozik AJ. *Appl Phy Lett* 1977;**30**:567–9.
23. Haruta M, Kobayashi T, Sano H, Yamada N. *Chem Lett* 1987;**16**:405–8.
24. Hutchings GJ. *J Catalysis* 1985;**96**:292–5.
25. Shu X-Z, Nguyen SC, He Y, Oba F, Zhang Q, Canlas C, Somorjai GA, Alivisatos AP, Toste FD. *J Am Chem Soc* 2015;**137**:7083–6.
26. Ma L. *Chin J Catal* 2014;**35**:108–19.
27. Szegedi Á, Popova M, Valyon J, Guarnaccio A, De Stefanis A, De Bonis A, Orlando S, Sansone M, Teghil R, Santagata A. *Appl Phy, A* 2014;**117**:55–62.
28. Fuku K, Hayashi R, Takakura S, Kamegawa T, Mori K, Yamashita H. *Angew Chem Int Ed* 2013;**52**:7446–50.
29. Zienkiewicz-Strzałka M, Deryło-Marczewska A, Skorik YA, Petrova VA, Choma A, Komaniecka I. *Int JF Mol Sci* 2020;**21**:166.
30. Sareen S, Mutreja V, Singh S, Pal B. *RSC Advan* 2015;**5**:184–90.
31. Sareen S, Mutreja V, Pal B, Singh S. *Micropor Mesopor Mater* 2015;**202**:219–25.
32. Sareen S, Mutreja V, Singh S, Pal B. *J Colloid Interface Sci* 2016;**461**:203–10.
33. Farrusseng D, Tuel A. *New J Chem* 2016;**40**:3933–49.
34. Komvokis VG, Iliopoulou EF, Vasalos IA, Triantafyllidis KS, Marshall CL. *Appl Catal, A* 2007;**325**:345–52.
35. Rohani S, Ziarati A, Ziarani GM, Badiei A, Bürgi T. *Catal Sci Technol* 2019;**9**:3820–7.
36. Pradenas M, Yáñez J, Ranganathan S, Contreras D, Santander P, Mansilla HD. *Water Environ Res* 2019;**91**:157–64.
37. Edelmannová M, Lin K-Y, Wu JC, Troppová I, Čapek L, Kočí K. *Appl Surf Sci* 2018;**454**:313–8.
38. Boro B, Gogoi B, Rajbongshi B, Ramchiary A. *Renew Sustain Energy Rev* 2018;**81**:2264–70.
39. Bathla A, Pal B. *Sol Energy* 2020;**205**:292–301.
40. Monga A, Bathla A, Pal B. *Sol Energy* 2017;**155**:1403–10.

41. Crake A, Christoforidis KC, Godin R, Moss B, Kafizas A, Zafeiratos S, Durrant JR, Petit C. *Appl Catal, B* 2019;**242**:369–78.
42. Rather RA, Pooja D, Kumar P, Singh S, Pal B. *J CleanProd* 2018;**175**:394–401.
43. Kaur J, Singh R, Pal B. *J Mol Catal, A* 2015;**397**:99–105.
44. Kaur R, Pal B. *Appl Catal, A* 2015;**491**:28–36.
45. Kaur R, Pal B. *New J Chem* 2015;**39**:5966–76.
46. Monga A, Pal B. *Colloid Surface A* 2015;**481**:158–66.
47. Bathla A, Pal B. *ChemistrySelect* 2018;**3**:4738–44.
48. Monga A, Rather RA, Pal B, Sol. *Energy Mater Sol Cells* 2017;**172**:285–92.
49. Jiang H-L, Akita T, Ishida T, Haruta M, Xu Q. *J Am Chem Soc* 2011;**133**:1304–6.
50. Fu G, Liu Z, Chen Y, Lin J, Tang Y, Lu T. *Nano Res* 2014;**7**:1205–14.
51. Tsukamoto D, Shiro A, Shiraishi Y, Sugano Y, Ichikawa S, Tanaka S, Hirai T. *ACS Catal* 2012;**2**:599–603.
52. Han C, Gao Y, Liu S, Ge L, Xiao N, Dai D, Xu B, Chen C. *Int J Hydro Energy* 2017;**42**:22765–75.
53. Bathla A, Pal B. *J Ind Eng Chem* 2018;**67**:486–96.
54. Bathla A, Pal B. *J Ind Eng Chem* 2019;**79**:314–25.
55. Monga A, Pal B. *New J Chem* 2015;**39**:304–13.
56. Chen N, Deng D, Li Y, Liu X, Xing X, Xiao X, Wang Y. *Sci Rep* 2017;**7**:7692.
57. Su C, Liu L, Zhang M, Zhang Y, Shao C. *CrystEngComm* 2012;**14**:3989–99.
58. Kibis L, Titkov A, Stadnichenko A, Koscheev S, Boronin A. *Appl Surf Sci* 2009;**255**:9248–54.
59. Jiang Z, Zhang W, Jin L, Yang X, Xu F, Zhu J, Huang W. *J Phy Chem, C* 2007;**111**:12434–9.
60. Bhardwaj S, Pal B. *Advan Powder Technol* 2018;**29**:2119–28.

CHAPTER

31

Nanomaterials incorporated electrospun membranes for membrane distillation

Noel Jacob Kaleekkal and Sruthi Gopal

Membrane Separation Group, Department of Chemical Engineering, National Institute of Technology Calicut, Kozhikode, Kerala, India

1. Introduction

Membranes have attracted significant attention as a potential technology for desalination of brine/seawater, wastewater treatment, gas purification, recovery of valuable material, separation processes in the food processing and pharmaceutical industry.[1,2] The demand for high-quality water has spurred advancements in membrane technology, which has proven vital for sustainable water recovery among various competing options.[3] The IUPAC defines a membrane as a "Structure, having lateral dimensions much greater than its thickness, through which transfer may occur under various driving forces." The membrane processes classified according to the driving-force of transport is as follows: (1) pressure gradient-ultrafiltration,[4] nanofiltration,[5] reverse osmosis (RO),[6] etc., (2) concentration gradient dialysis,[7] membrane extraction, supported/emulsion liquid membranes,[8] etc., (3) electrical gradient-electrodialysis,[9] electrofiltration,[10] electrochemical ion-exchange,[11] etc., (4) thermal gradient-membrane distillation (MD),[12] etc., (5) osmotic pressure gradient-forward osmosis,[13] pressure retarded osmosis,[14] etc., and (6) a combination of 1–5.[15,16]

2. Membrane distillation

The term "MD" was coined more than 55 years ago; however, this technology is still in its early stages. It is interesting to note that while most membrane separation processes are isothermal, MD is an exception to this as the driving force is the thermal gradient across

Applications of Multifunctional Nanomaterials
https://doi.org/10.1016/B978-0-12-820557-0.00025-4

the membrane.[17] MD is a unique separation process in which heat and mass transport occur simultaneously, and a vapor-liquid equilibrium exists across a microporous hydrophobic membrane. This process involves a hot saline solution in the feed side of the membrane and a cold pure distillate (water) in the permeate side with the vapor permeating through the membrane. The distinctive hydrophobic nature of the membrane prevents liquid entry and permits only the volatile component (vapor) to diffuse across the dry membrane pore.[18] The water vapor flux is proportional to the vapor pressure difference existing on both sides, and this driving force is produced by maintaining a transmembrane temperature difference or by lowering the pressure in the permeate side using vacuum/sweep gas.[19] The surface energy of the membrane plays a vital role in achieving separation as the pores should not be wetted operation. Hence, to remove solutes from aqueous streams, the polymeric membranes used are inherently hydrophobic or modified suitably to improve the surface hydrophobicity.[20]

MD is far superior as opposed to competing technologies due to the following reasons: (1) MD can achieve theoretically 100% rejection of all nonvolatile components including inorganic ions, macromolecules, etc., (2) can handle feeds at higher temperatures (while operates at lower temperatures as compared to thermal desalination processes like evaporation) (3) lower operating pressures as compared to RO (Where applied pressure must be several times greater than osmotic pressure) (4) can handle high salinity feeds, (5) mechanical stability requirement is lower as compared to RO/NF membranes and (6) able to utilize waste-heat and low-grade energy sources.[21] As a result, there are a large number of researchers focusing on all aspects of the MD technology, including membrane materials and configurations,[22] heat and mass transfer modeling,[23] fouling and its mitigation,[24] heat recovery and utilization of low energy sources,[25] integrated MD systems,[26] process applications[27] etc. Apart from original research, there are critical reviews on general MD and[28] and specific facets[29] available in the literature. The number of publications related to MD is given in Fig. 31.1 (Source: Scopus search).

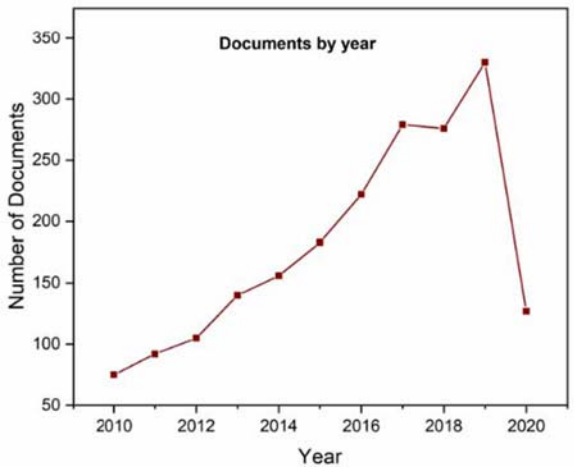

FIGURE 31.1 No of documents published related to MD during the last 10 years.

Over the last 30 years, desalination has proven to be a viable alternative water supply, and the majority (87% global) of the desalination plants use multistage flash (MSF) distillation or RO. The energy requirement for employing MD for desalination of highly salty feeds with a latent heat recovery system lies somewhere in between RO and MSF.

Theoretically, to produce a quantity of 1 m^3 of deionized water, the RO process requires 2−3 times of the ΔG_{sep} for sea-water desalination, and a thermal process would utilize 600 times ΔG_{sep} assuming no latent heat is recovered. For high salinity feeds, the energy consumption (ΔG_{sep}) by MD is more significant than that required to desalinate seawater; however, this is only a small fraction of the latent heat.[30] Further, MD requires minimum/no pretreatment even for produced water,[31] can utilize low-grade energy, is independent of feed concentrations and operates at lower temperature/pressure.[32] Low-grade energy requirement allows it to utilize renewable energy sources - solar, geothermal, tidal, wind etc., or even colocating the MD units in close proximity to industrial facilities and power generation systems to take advantage of the waste heat. Hybrid systems integrating MD with other separation methods are also being explored to improve water recovery.[33]

Due to these factors, MD can be employed for wastewater treatment in textile industries, breweries, tanneries, etc., as it can remove organic matter, heavy metals, and other contaminants from wastewater. Application of MD in treating nuclear waste, concentrating fruit juices and recovery of commercially valuable products like enzymes and proteins have also been reported.[34] The unavailability of a suitable membrane and its high energy consumption are the two major factors causing hindrance in the commercialization of the MD process.[18] For the membrane, the constraints include wetting of the membrane pores over long periods of operation, reduced permeability, complications in fabricating a stable and efficient membrane with adequate mechanical strength and antifouling ability.[19] The deposition of organic, inorganic, and colloidal substances and accumulation of biofilm in the pores results in fouling which further reduces the permeate quality.

The full potential of the MD process can be realized if high-flux sustainable membranes are synthesized, novel applications and process integration are explored.

2.1 MD configurations

There are mainly four different types of configurations generally used. The schematic representations are given in Fig. 31.2.

3. State-of-the-art research in membrane distillation

The entire process of MD is subject to continuous improvement progressively, aiming to eliminate the drawbacks discussed earlier. The studies for MD have been primarily based on (i) improving the membrane configurations, (ii) coupling of MD with other processes, (iii) augmenting the energy consumption by waste heat utilization or by using renewable energy sources, and (iv) membrane modifications. This chapter focuses on membrane modifications using nanomaterials.

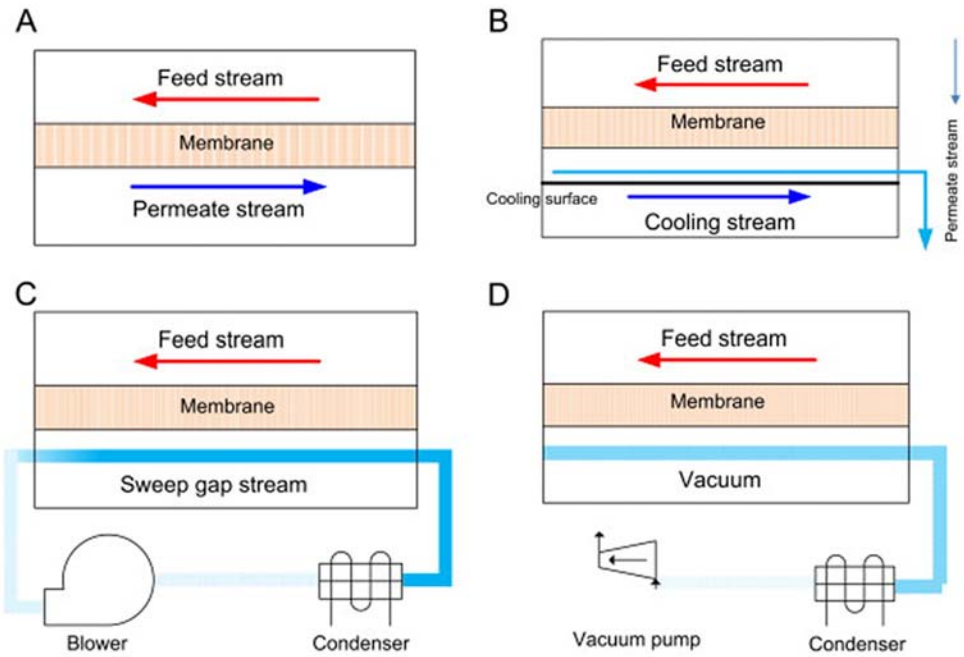

FIGURE 31.2 Illustration of a basic MD configurations: (A), DCMD, (B) AGMD, (C) SGMD, and (D) VMD from.[18]

4. Electrospinning as a method for fabrication of membranes

The principle underlying the electrospinning process is the uniaxial elongation of a viscoelastic polymer solution under an applied electric field caused by repulsive electrostatic forces. This technology gained popularity as it can produce electrospun mats with a tunable fiber diameter ranging from few microns to nanometre scale. The controllable pore size, high surface to volume ratio, and large porosity of the nanofibrous membranes make it attractive in various applications, including MD.[35] Fig. 31.3 shows a schematic representation of the electrospinning setup. Electrospinning consists of three main components: (i) a high voltage DC power source, (ii) a syringe needle containing the polymer solution with a needle; mounted on a syringe pump, and (iii) grounded metallic flat plate or rotating drum as a collector.

Initially, the polymer solution bought to the tip of the needle (using the pump) forms a drop at the tip due to the viscosity and surface tension of the solution. On applying an electric field, the hemispherical droplet-shaped polymer solution at the tip elongates to form a cone termed as Taylor cone. Further increase in this voltage (greater than critical voltage, generally around 5–40 kV) overcomes the surface tension forces causing the solution to eject out from the tip, and the fluid gets transformed into a jet undergoing stretching and thinning traveling toward the grounded collector.

The solvent evaporates as the jet travels in the air, leaving behind a charged polymer fiber that aligns randomly on the collector, forming an electrospun mat (membrane). The mat is then further dried at a specified temperature before being used for any application.[37]

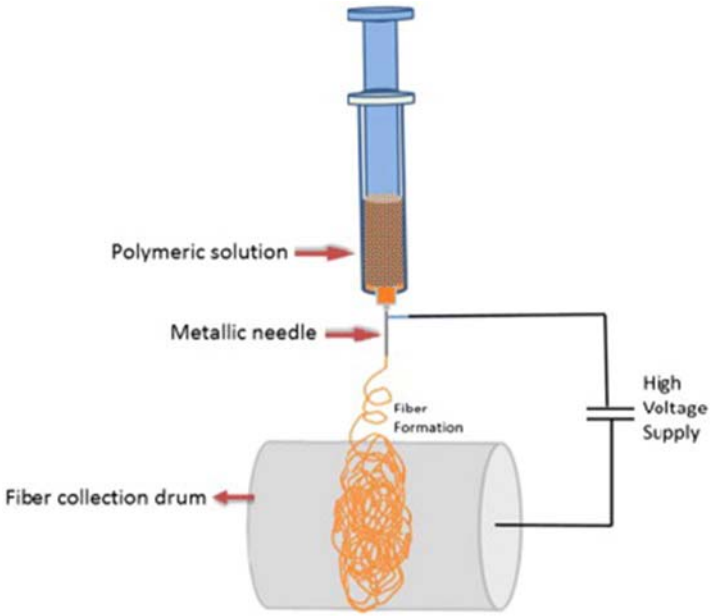

FIGURE 31.3 Schematic of electrospinning setup.[36]

Electrospinning emerged as a suitable fabrication technique that can produce membranes having greater hydrophobicity with excellent porosity.[38] The electrospun membranes offer a precision control in pore size, morphology, fiber diameter/thickness[39] with a three-dimensional interconnected porous structure.[35] Electrospinning is a cost-efficient method to produce highly porous membranes from a wide variety of polymers. Electrospun membranes can be successfully functionalized with other organic/inorganic materials and quickly deposited over surfaces like metal, glass, microfibrous mats etc. Hydrophobic polymers such as polypropylene (PP), polytetraflouroethylene (PTFE), polyethylene (PE), polyvinylidiene fluoride (PVDF) are some of the most widely explored in MD. Electrospun membranes using styrene butadiene styrene (SBS) was reported to be a cost-effective alternative compared to PTFE membranes. The electrospun membranes exhibited larger pore sizes, stable flux for longer runs (120 h), and salt rejection of 99.8% (from seawater).[40] Electrospun polystyrene nanofibrous membranes were also explored in the DCMD process, and the membranes displayed an excellent porosity of 86% and a modest flux of 31.17 kg/m^2 hr.[41] Ref. 12 synthesized a triple-layered membrane prepared by electrospinning PVDF on either side of a commercial (DuPont) nanofibrous PES support tested in the DCMD set-up.

Electrospun membranes, however, face significant challenges—membrane wetting and fouling. Incorporating nanomaterials is an excellent method to achieve membrane characteristics such as antiwetting, antimicrobial, selfcleaning, superhydrophobicity, etc.[42]

With the advent of nanotechnology, electrospinning has become an up-and-coming and versatile technology for membrane fabrication.[43]

4.1 Electrospinning parameters

Several reports give an idea about the influence of electrospinning parameters on nanofiber properties and are given in Table 31.1.[37] Figs. 31.4 and 31.5 illustrate the SEM images of various electrospun membranes.

TABLE 31.1 Factors affecting the morphology and structure of electrospun nanofibers.

Electrospinning parameter	Effect on morphology and structure of the membranes/fibers
Solution parameters	
Viscosity (polymer concentration)	Optimal range. Low viscosity leads to electrospraying and too high viscosity leads to drying of solution at the tip (nonuniform fibers with beads). Within optimal range, increase in viscosity/concentration increases the fiber diameter.
Molecular weight	Increasing molecular weight decreases formation of beads and droplets as it aids in better stretching and entanglement.
Solution conductivity	Increasing conductivity aids in reducing fiber diameter and may produce broader distribution of fibers. Ionic salts are added to improve solution conductivity.
Surface tension	No relationship can be predicted. Generally, lower surface tension is preferred as it decreases the resistance of the solution. Surfactants are employed to increase surface tension.
Solvent volatility	Higher solvent volatility produces pores and microvoids on the fibers, further increasing its surface area.
Process parameters	
Voltage differential	The effect of voltage difference is ambiguous. Greater applied voltage is shown to yield thinner fibers. The range of operation has been reported between 10 and 35 kV in most cases. Higher ΔV can lead to bead formation.
Flow rate	Lower flow rate yields narrower fibers and the increase in flow rate is observed to increase fiber diameter, with beads being formed and/or the fibers are not completely dry. 0.5 mL/h to 3 mL/h.
Distance between needle tip and collector	Reported distance is between 13 and 30 cm. At optimum distance the collected fiber is completely dried. At distances too short or too far the formation of beads becomes prominent.
Collector	Metal flat-plate or rotating drums are widely used. Rotating drums can help to produced aligned fibers.
Environmental parameters	
Temperature	A high temperature favors the formation of thin fibers due to the reduction in viscosity. 23–32°C.
Humidity	High relative humidity is seen to produce pores on fibers due to the microphase separation. Low humidity produces smooth fibers and the relative humidity is maintained between 25% and 50%.

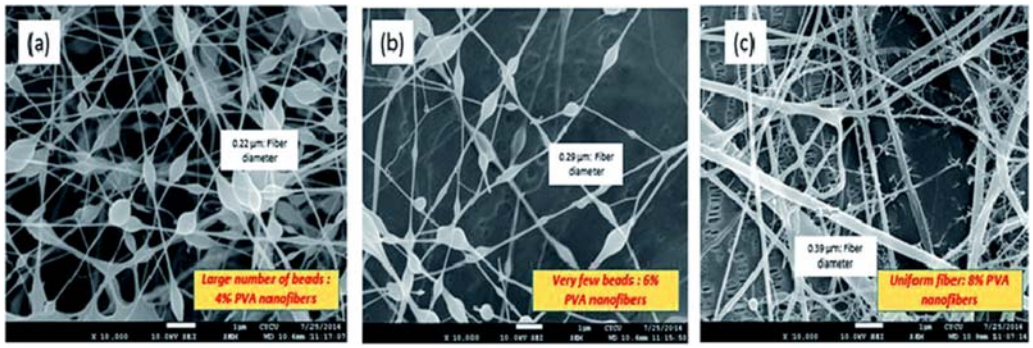

FIGURE 31.4 SEM micrographs of PVA nanofibers indicating the effect of polymer concentration on fiber quality and fiber diameter (A) 4% PVA (B) 6% PVA (C) 8% PVA [M_w: 146,000−186 000, 99+% hydrolyzed, solvent used: deionized water. *Republished with permission of RSC Adv., 2016, from Ray SS, Chen SS, Li CW, Nguyen NC, Nguyen HT. A comprehensive review: electrospinning technique for fabrication and surface modification of membranes for water treatment application.* RSC Adv *2016;**6**, (88):85495−85514. http://10.1039/c6ra14952a, permission conveyed through Copyright Clearance Center, Inc.*

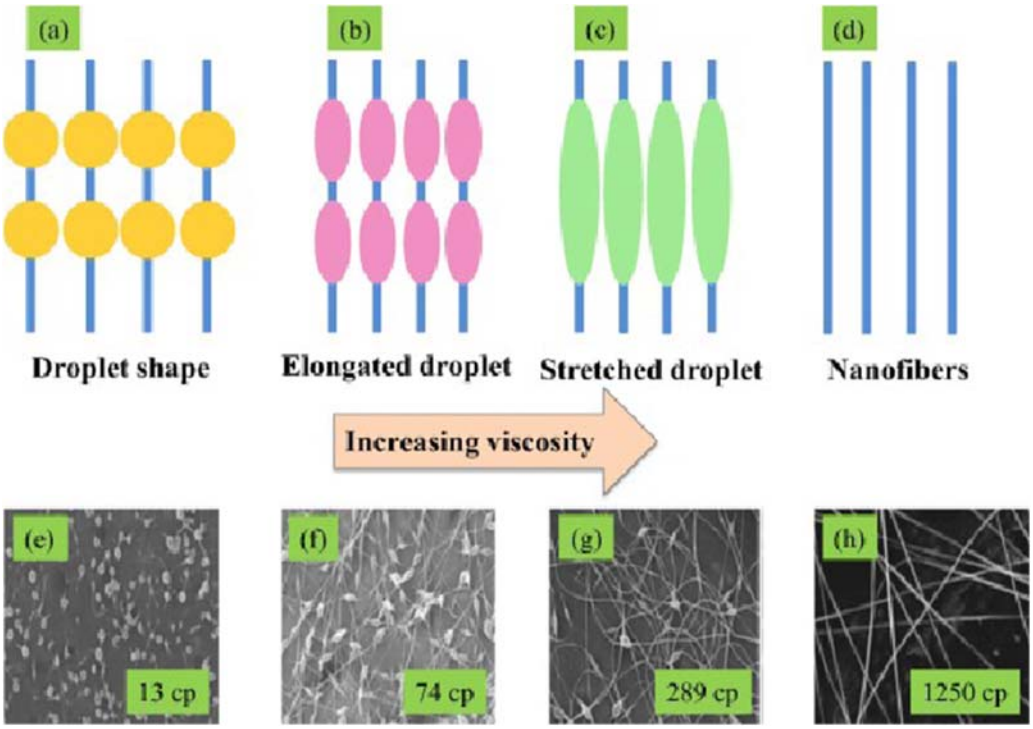

FIGURE 31.5 Variation in morphology of electrospun nanofibers of PEO with viscosity: (A−D) schematic and (E−H) SEM micrographs. *From Haider A, Haider S, and Kang IK, A comprehensive review summarizing the effect of electrospinning parameters and potential applications of nanofibers in biomedical and biotechnology,* Arab J Chem, *2018;**11**(8):1165−1188, http://10.1016/j.arabjc.2015.11.015.*

5. Nanoparticles incorporated electrospun membranes for MD

Electrospinning has been employed for MD due to the current trend of employing nanofibrous membranes in desalination and water treatment. Nanoparticles are being incorporated into these membranes in order to overcome some of the inherent limitations of pristine polymer membranes. These membranes are reported to have higher efficiency, reduced pore wetting, and are less prone to fouling.

Nanoparticles can increase the tensile strength or prevent heat conduction in the membrane, leading to improved mechanical and thermal stability. Roughness is an important factor that determines the antiwetting capability of the membranes. It promotes hydrophobicity. Nanomaterials increase the surface roughness of membranes due to the presence of numerous air pockets. Self-cleaning methods inspired by nature can be conferred to membranes via functionalizing with nanomaterials.[45] Generally, a particle with external dimensions or internal pore structures in the range of 1−100 nm are classified as nanoparticles and possess distinct physical/chemical properties. A nanomaterial can be classified as zero-dimensional/one dimensional/two-dimensional if all/two/one of the dimensions satisfy the above criterion.[46] Wetting and fouling are the significant factors that cause hindrance in the long-term stability of membranes. The antimicrobial property of nanoparticles is responsible for preventing biofouling. The improvement in membrane properties leads to an increase in flux as well as rejection rate. Functional nanomaterial inclusion into membranes improves membrane permeability, fouling resistance, mechanical, and thermal stability.

Even though there is an increased interest in using nanomaterials in electrospun membranes for MD is still under reshaping for extensive studies. Superhydrophobic electrospun membranes were formed with the incorporation of nanoparticles in the polymeric membrane. Nanoparticles exhibit a high surface area and increased physical and chemical activity (reactivity and absorptivity), making them desirable for membrane processes. These nanofillers used are primarily inorganic. They are mixed with the polymer and have substantial surface area. Nanoparticle doses required for the water treatment are low, making their application relatively economical.[47]

6. Role of nanoparticles to enhance the performance of electrospun membranes

6.1 Silica nanoparticles (SiNPs)

Silica nanoparticles are widely employed due to their availability, ease of synthesis, thermal stability, high surface area with a broad particle size distribution. The SiO_2 nanoparticles are inherently hydrophilic due to hydrogen bonds between the hydroxyl group of water and SiO_2. The particles have to be made hydrophobic to enhance the membrane hydrophobicity and improve its dispersion in nonpolar solvent (as in colloidal electrospinning).[48] Fig. 31.6 shows the superhydrophobicity of functionalized silica. The high density of −OH groups facilitates the functionalization of the SiO_2 using the silane/fluoro silane coupling agents. These coupling agents are characterized by long-chain bulky alkyl groups (may contain F), which

FIGURE 31.6 Image showing the comparison of surface wettability between silica (B & D) and OTS modified silica (C & E). *Reprinted from Li X, Yu X, Cheng C, Deng L, Wang M, Wang X. Electrospun superhydrophobic organic/inorganic composite nano fi brous membranes for membrane distillation. 2015 http://10.1021/acsami.5b06509 copyright (2015) American Chemical Society.*

form self-assembled layers on SiO_2, thereby conferring water repellent properties and rendering them hydrophobic for use in membrane preparation.[49] Alternatively, postfabrication, fluoropolymers are anchored onto the electrospun membranes (containing SiO_2 nanoparticles) via dip-coating rendering the membranes superhydrophobic. These fluoropolymer modifications are popular due to their superior hydrophobic characteristics, low surface energy, chemical resistance, mechanical stability, and thermal stability.[50]

Superhydrophobic membranes suppress mineral scaling due to a surface-bound air layer, which decreases the contact area between the feed solution and the membrane. The reduced contact diminishes the sites required for interfacial crystallization at the liquid−solid interface.[51] SiO_2 incorporated electrospun membranes were investigated for seawater desalination, brackish water treatment, and recovery of water from oil-containing wastewater in either DCMD or VMD modes. PVDF or its copolymer PVDF-HFP wase used to prepare electrospun membranes (incorporated with SiO_2) for desalination in DCMD. The SiO_2 NPs were modified using silane modifiers- OTMS[49,52,53], ODTS, CI-DMOS,[52] 17-FAS,[51] PDMS.[54] All the membranes displayed excellent rejection (>99.9%), exhibited high water contact angle values (>150−170), and permeate fluxes (ranging from 28 to 46 LMH) much greater than the pristine membranes. Ref. 55 developed a lotus-like roughness on polyimide nanofibrous membrane using a mussel inspired strategy (polydopamine). The SiO_2 nanoparticles were electrostatically anchored on the membrane surface, which was then made hydrophobic by the immersion in FAS.

The prepared membranes were superhydrophobic with a water contact angle of 152°, a modest high-water flux of 31 $Lm^{-2}h^{-1}$ and a 100% salts rejection. In addition, the membranes could withstand hot water feed and displayed a high LEP. The hydrophilic cellulose acetate polymer was investigated in DCMD for seawater desalination. In order to render the

membrane hydrophobic, the incorporation of TEOS functionalized SiO_2[56] and dip coating the Si/CA membrane using PDTS[50] was some of the techniques employed.

Aerogels are highly porous ultralight materials that have low thermal conductivity. The addition of silica aerogel (SiAG) into the PVDF matrix improved the thermal efficiency of the electrospun membranes in DCMD. The SiAG lowered the thermal conductivity of the membranes from 0.111 to 0.083 W/mK, which accounted for a 150% increase in thermal efficiency.[57] OTMS-SiNPs included PVDF electrospun membrane investigated for brackish water desalination in a DCMD configuration was superhydrophobic confirmed by a water contact angle of 156°, and a permeate flux of 37 LMH was reported.[49] The vacuum membrane distillation (VMD) mode has also been explored for desalination. The mechanism of surface functionalization of the PVDF−SiO_2 nanofiber membrane introduced into the FAS solution is due to the successive condensation reactions between the OH groups found in the SiO_2 nanoparticles and the Si−O−alkyl groups of the silane.[58] The surface modification can be seen from the AFM image (Fig. 31.7). The surface wettability of the modified membrane was altered due to the increased surface roughness and lower surface free energy.

Another application of the MD process is water recovery from wastewater containing oil/water emulsions. One of the approaches was to prepare a multiscale textured surface consisting of a hydrophobic PTFE base and hydrophilic nanocomposite fibrous networks comprising of cellulose acetate (CA) and SiNPs. While treating oil-containing feed composite membranes with a multiscale textured surface consisting of the hydrophobic substrate and a hydrophilic top layer are found to mitigate oil fouling in MD. Owing to its inherent hydrophilicity, silica serves as an excellent additive while fabricating the hydrophilic fibrous networks required for the top surface. The attachment of oil and the spreading of an oil droplets on a hydrated surface were significantly diminished by the presence of the hydration layer. The foulant,

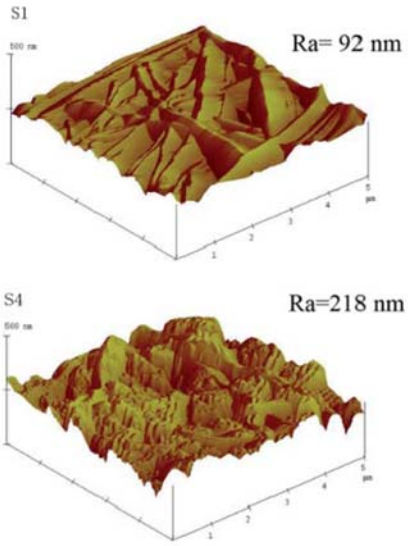

FIGURE 31.7 AFM image of FAS surface-functionalized SiO_2-PVDF membrane with 0wt% & 8 wt.% SiO_2. *Adapted from Dong Z, Ma X, Xu Z, Gu Z. RSC Advances, 2015:67962−67970. http://10.1039/c5ra10575g.*

"oil" could be removed by washing with DI water. The membranes operated in a DCMD mode exhibited a water flux of around 20 LMH using a synthetic saline crude oil as feed.[59]

The formation of a reentrant structure at the surface was seen to impart superhydrophobicity (1760), thereby minimizing the effect of foulants on the PVDF membrane surface. These omniphobic PVDF membranes were prepared by electrostatic interaction between the hydrophilic silica nanoparticles (SiNPs) and polystyrene (PS) microsphere, followed by fluorination using FAS was used to treat saline oily wastewater in a DCMD mode.[60] Yuan Liao and his coworkers studied the effect of small and large modified silica nanoparticles incorporated into PVDF nanofibrous membranes. These membranes were superior in terms of flux (~18.1 LMH), porosity, and water contact angle.[61]

A single-scale reentrant structure was formed by mono-axial electrospinning, and one with a multiscale reentrant structure was created by coaxial electrospinning. Silica nanoparticles were used as the sheath solution to create electrospun fibers with nanoscale roughness on individual fibers. A super amphiphilic membrane electrospun silica-based membrane was modified with fluoroalkyl silane to acquire low surface energy. The membranes with SiNPs showed better antiwetting properties.[62] The details of works using silica NPs are given in Table 31.2.

6.2 Carbon nanomaterials

Carbon nanotubes are one of the most versatile types of carbon nanomaterial being explored as a material of interest in many diverse applications. Theoretically, it is a rolled-up layer of graphene sheet containing sp^2 hybridized carbon forming a cylinder. It can arrange to form concentric cylinders (1−10 nos) with an interlayer spacing ranging from 0.34 to 0.39 nm.[63] When a CNT consists of a single graphene sheet, it is referred to as a single-wall CNT (SWCNT), and when it comprises more than one layer of concentric cylinders held together by van der Waals attractions, it is known as a multiwall CNT (MWCNT). Its hydrophobic nature, tensile strength, and elasticity are some of the reasons they are employed as fillers in preparing polymeric membranes.

Mitra's group (Fig. 31.8) explored MD and put forth several transport mechanisms across a porous membrane containing CNTs. Incorporating CNTs increases the membrane hydrophobicity, decreasing the pore wetting, thus enhancing water vapor transport across the membrane. The hydrophobic nanotubes can allow the diffusion of vapor by Fickian, Knudsen or molecular diffusion. Moreover, their smooth surface also enhances mass transport via diffusion or adsorption-desorption. The nanotubes' high thermal conductivity helps limit the concentration polarization within the membrane pores, thus ensuring constant high flux.[64]

The addition of CNTs leads to a bead formation on the membrane surface, which further increases the surface roughness. The increased surface roughness results in a higher water contact angle.[65] The antifouling studies (organic, inorganic, and bio-foulants) of a dual-layer membrane consisting of (i) a hydrophobic base layer prepared by electrospinning using PVDF polymer with organically modified (silane) SiO_2 and (ii) a hydrophilic top layer prepared by electrospinning carboxylated multiwalled carbon nanotubes (f-MWCNTs) with silver nanoparticles (AgNPs) were carried out. It was revealed that the f-MWCNTs/AgNPs coating significantly reduced the deposition and cake formation on the surface of the membrane (Fig. 31.9). Ag NP's and MWCNT's combined imparted biocidal properties to the

TABLE 31.2 List of works using silica NP's incorporated electrospun membranes for MD.

Nanoparticle: Silica										
Polymer used	**Functionalization of NP**	**MD mode**	**Membrane configuration**	**Application**	**LEP**	**WCA**	**Fiber dia and membrane thickness**	**Pore size and porosity**	**Flux**	**Rejection %/solute rejected**	**Refs**
CA	Fluorination by immersing in PDTS solution	DCMD	Flat sheet	Desalination	–	155.6 ± 3.9°	330.5 ± 83.2 nm & 243.6 ± 2.5 μm	0.35 ± 0.07 μm & 78.4 ± 3.1%	13.6 kg/m^2hr	99.99%	[50]
PVDF	Silanization using OTMS	DCMD	Flat sheet	Desalination	–	156 ± 6°	–	–	37.1 LMH	99.9%	[49]
CA	Functionalized using TEOS	DCMD	Flat sheet	Desalination	58 kPa	150.6 ± 4.0°	- & 52 μm	1 μm & 89.8%	46.3 LMH	99.99%	[56]
PVDF	Modified through silanization using OTMS, ODTS, CI-DMOS	DCMD	Flat sheet	Desalination,	80.1 ± 3.9 kPa	162.6± 1.8°	986 ± 344 nm & 132 μm	1.41 μm& 78.5 ± 2.9%	34.2 LMH	>99.9%	[52]
PVDF	Silanization using OTMS	DCMD	Flat sheet	Desalination organic/protein recovery/bacterial effluent	-	151 ± 7°	- & 116 μm	1.26 ± 0.03 μm &80%	42 LMH	97.2%	[53]
PVDF-HFP	Flouroalkysilanization using 17-FAS	DCMD	Flat sheet	Desalination	-	157.19°	420 ± 180 nm &174 ± 2 μm	- & 80.7 ± 1.2%	45.6 LMH	>99%	[51]
PVDF	Silica fumes dispersed on PVDF/PDMS mixture	DCMD	Flat sheet	Desalination	0.72 ± 0.04 bar	170°± 1°	- & 55±2 μm	1.5 ± 0.01 μm& (88 ± 2) %	28 kg/m^2 hr	99.99%	[54]
PVDF	Silica aerogel	DCMD	Flat sheet	Desalination	1.57 ± 0.05 bar	78.62 ± 0.9°	- &325 ± 3 μm	0.485 μm&60.19 ± 1.47%	12.5 LMH	99.99%	[57]
PI	Flourination	DCMD	Flat sheet	Desalination	42 kPa	152°	375 ± 25 nm& 105±4 μm	2.23 μm& -	31 LMH	99.99%	[55]

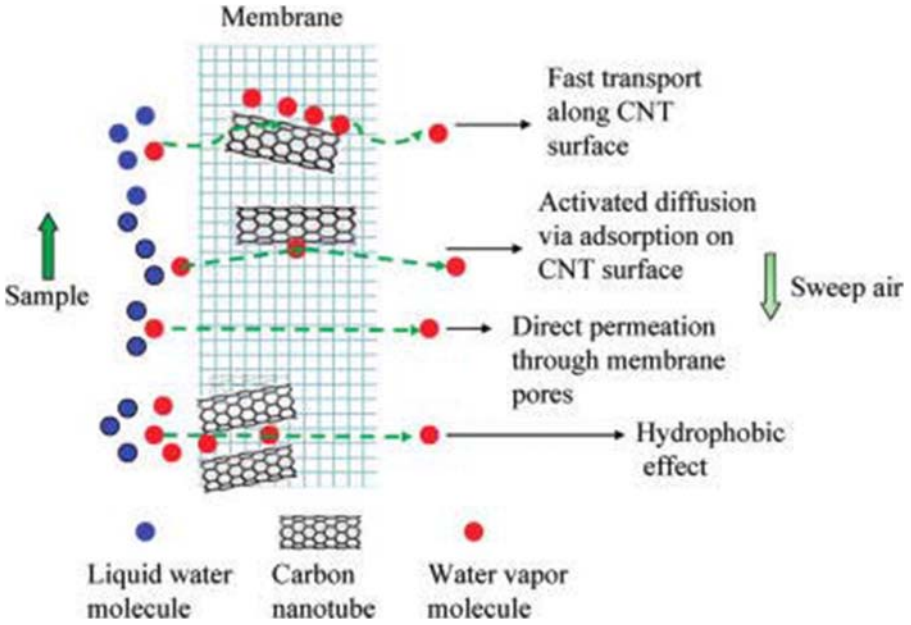

FIGURE 31.8 Schematic diagram showing the mechanism of transport through CNT in MD. *Reprinted from Gethard K, Sae-Khow O, Mitra S. Water desalination using carbon-nanotube-enhanced membrane distillation.* ACS Appl Mater Interfaces *2011;3(2):110–114, http://10.1021/am100981s copyright (2010) American Chemical Society.*

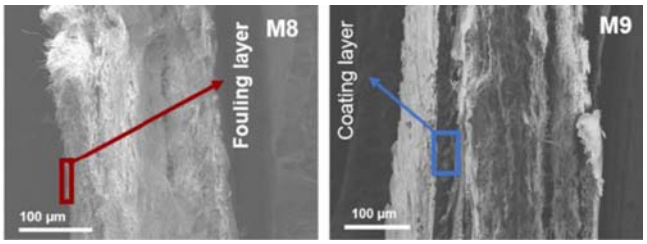

FIGURE 31.9 Crossectional view of alginate fouled uncoated (M8) and CNT/Ag nanoparticle coated (M9) modified SiO_2 PVDF membrane. *From Nthunya LN, Gutierrez L, Nxumalo EN, Verliefde AR, Mhlanga SD, and Onyango MS, f-MWCNTs/AgNPs-coated superhydrophobic PVDF nanofibre membrane for organic, colloidal , and biofouling mitigation in direct contact membrane distillation,* J Environ Chem Eng *2020;8(2):103654, http://10.1016/j.jece.2020.103654.*

membranes against thermophilic bacteria in the feed. However, this hydrophilic coating led to a decline in the permeate flux (16–17 LMH) when compared to the pristine membrane (36–42 LMH).[66]

In a similar study, the f-MWCNTs/AgNPs hydrophilic active layer enhanced resistance to bovine serum albumin (BSA) adhesion, and the protein rejection was> 99.98%. A decline in flux (by 27%) was observed in this case as well.[53]

Many reports indicate that coating the superhydrophobic membrane using a hydrophilic layer is a viable and promising one-step solution to address membrane fouling. The presence

of a hydrophilic layer on the membrane surface helps form hydrogen bonds with water molecules, creating a thin layer of water molecules between the membrane and the bulk solutions. This layer will reduce the undesirable adhesion or adsorption of foulants on the membrane surface.[67]

The incorporation of TiO_2-CNTs into the electrospun PVDF-HFP membrane increased productivity by 13.7%−46% when the feed concentrations were 36,000−9000 ppm.[68]

Recovery of valuable compounds from wastewater and utilizing them in suitable industries make the process profitable and sustainable. Using the MD process, J. Guo et al. [78] recovered ammonia, a major pollutant in industrial, agricultural and municipal wastewater streams. The recovered ammonia is available for use in fertilizer industries. A mixture of Nafion ionomer and fluorinated MWCNTs was incorporated into a PVDF-HFP nanofibrous membrane used in this process exhibited a permeate flux (ammonia) of 46.5 LMH using the DCMD. Superhydrophobic electrospun polyvinylidene fluoride-co-hexafluoropropylene (PcH) incorporated with 1-5 wt.% CNTs[69] and a triple-layer nanocomposite PcH-PES-PcH/CNTs membranes[70] were also evaluated for seawater desalination using DCMD. The highest VMD flux of 20 g/m^2 CNTs coated membrane was 28.4 kg/m^2 h for a 3.5 wt.% NaCl feed.[71]

Graphene, graphene oxide (GO), and partially reduced graphene oxide (r-GO) form a 2-D class of carbon materials that are of great interest. Graphene is particularly suitable for MD application due to its hydrophobic nature and antifouling nature.[72] However, GO is inherently hydrophilic and has many functional groups that serve as excellent reactive sites for covalent functionalization. The chemical functionalization of GO is carried out to overcome the Van-der-Waals forces and to promote better dispersion in organic solvents rendering them hydrophobic. Fluoropolymers like perfluorooctyltriethoxysilane (FTES) can also modify the GO promoting enhanced interfacial affinity with the polymer matrix through entanglement.[73] r-GO is hydrophobic due to the high density of carbon atoms arranged in a hexagonal honeycomb lattice-type structure, and this formation enables the sorption of water vapor alone.[74]

Graphene materials impart antibacterial/microbial properties, which could be explained by the stress on the cell wall induced by the sharp edges of graphene nanosheets, causing the intercellular material to leak out. Another explanation could be that the GO acts as a terminal electron acceptor drawing electrons from the microorganisms leading to ROS-independent oxidative stress.[67]

The incorporation of hydrophobic graphene materials into PES/PVDF[75] Polyvinylidene fluoride-co-hexafluoropropylene[72,74] and PVDF[73] electrospun nanofibrous membranes were investigated in three modes: DCMD, AGMD, and VMD. It can be confirmed that incorporating these nanomaterials improved membrane porosity enhanced the water contact angle and showed excellent (>99.9%) NaCl rejection.

A zero-dimensional carbon material, graphene quantum dots (GQDs) are nano-scaled pieces of graphene itself having relatively lesser size than GO, and they have also been investigated in membranes employed for MD.

A. Jafari et al.[76] reported an improved permeate flux and outstanding salt rejection (99.7%) using GQDs/PVDF nanofibrous membrane in AGMD mode. The incorporation of activated carbon nanoparticles provided additional functionalities for PVDF -HFP membrane and delivered better DCMD performance with an ultrahigh flux of 45.6 LMH.[77] The details of works, including carbon-based nanomaterials incorporated electrospun membranes, are given in Table 31.3.

TABLE 31.3 List of works using carbon-based nanomaterials incorporated electrospun membranes for MD.

Nanoparticle: Carbon										
Polymer used	**Functionalization of NP**	**MD mode**	**Membrane configuration**	**Application**	**LEP**	**WCA**	**Fiber dia and membrane thickness**	**Pore size and porosity**	**Flux**	**Rejection %/solute rejected**	**Refs**
PVDF (with silane modified SiO_2)	Ag + carboxylated MWCNT'S	DCMD	Flat sheet	Industrial effluent treatment	-	164°	-	2.5 μm & -	17 LMH	99%	[66]
PES/PcH	MWCNT's	DCMD	Flat sheet	Desalination	1.8 bar	144±2°	347 nm&107 ± 2.8 μm	0.55 ± 0.03 μm & 91 ± 1.8%	22.2 kg/m^2hr	100%	[70]
PVDF	FTES functionalized GO	VMD	Flat sheet	Desalination	233.9 ± 7.3 kPa	140.5°	51.1 ± 11.0 nm &26 ± 2 μm	171.2 ± 16.8 nm &96.8 ± 1.2%	36.4 kg/m^2hr	99.9%	[73]
PES/PVDF	Graphene nanoplates	DCMD	Flat sheet	Desalination	85 kPa	132.3 ± 0.8°	0.356 ± 0.05 μm &142 ± 1.8 μm	0.379 ± 0.09 μm& 88 ± 1.5%	16.6kg/m^2hr	99%	[75]
PVDF	Carboxylated MWCNT'S	DCMD	Flat sheet	Desalination, protein separation	-	57±4°	- &135 μm	0.65 ± 0.02 μm& 80%	13.1 LMH	99.8%	[53]
PVDF	Carboxylated MWCNT'S	DCMD	Flat sheet	Desalination	-	63 ± 4°	-	-	14.7 LMH	99.63%	[49]
Nafion ionomer incorporated PVDF-HFP	Flourinated MWCNT'S	DCMD	Flat sheet	Ammonia recovery	1.39 ± 0.06 bar	138.7°	0.3 μm & 104 ± 0.19 μm	0.42 ± 0.01 μm & 89.7 ± 1.02%	46.5 LMH	66.2%	[78]
PVDF-HFP	TiO_2 + CNT's	DCMD	Flat sheet	Desalination	0.81 bar	139 ± 2.0°	0.43 ± 0.05 μm & 73 μm	0.46 ± 0.05 μm & 86 ± 1.2%	17.3 kg/m^2hr	99%	[68]
PVDF	Graphene quantum dots	AGMD	Flat sheet	Desalination	135.6 ± 3.2 kPa	121 ± 0.95°	289.79 ± 62.3 nm & 193.7 ± 2.5 μm	4.9 nm & 92 ± 1.2%	17.6 kg/m^2 h	99.7%	[76]

(*Continued*)

TABLE 31.3 List of works using carbon-based nanomaterials incorporated electrospun membranes for MD.—cont'd

Nanoparticle: Carbon											
Polymer used	**Functionalization of NP**	**MD mode**	**Membrane configuration**	**Application**	**LEP**	**WCA**	**Fiber dia and membrane thickness**	**Pore size and porosity**	**Flux**	**Rejection %/solute rejected**	**Refs**
PVDF	CNT's	VMD	Flat sheet	Desalination	186 kPa	156°	294 nm & 101 ± 3.0 μm	0.19 μm& 70.2%	28.4 kg/ m^2 h	>99.9%	[71]
PVDF-HFP	Activated carbon NP'S	DCMD	Flat sheet	Desalination	1.36 ± 0.04 bar	142.7 ± 0.6°	- & 200 ± 2.2 μm	0.787 ± 0.036 μm & 90.5 ± 1.7%	45.6 LMH	99.95%	[77]
PVDF-HFP	Reduced graphene oxide (GO)	DCMD	Flat sheet	Desalination	103.42 kPa	139°	166 ± 145 nm & -	0.47 μm & 76.45%	20.37 kg/ m^2h	99.97%	[74]

6.3 Metal- metal oxides

TiO_2 nanoparticles are the most widely employed as they can aid in the removal/photocatalytic degradation of dyes, detergents, surfactants, cyanides, organic chlorinated compounds, phenols, aromatics, pesticides and heavy metals (arsenic, cadmium, lead, etc.). TiO_2 NPs in polymeric membranes have also been associated with improved thermal and mechanical strength up to specific blend proportions.[47] The hydrophobicity of the membrane is one of the most important factors which determine the efficiency of MD performance. Therefore, it is important to modify the nanoparticles' surface and diminish their hydrophilic character.[79] Low surface energy fluorosilanes such as Perfluoro dodecyl trichlorosilane (FTCS),[80] perfluoro octyl triethoxysilane (FTES/PFTS)[81,82] etc. are commonly reported for the modification of TiO_2 nanoparticles. Electrospraying hydrophobic TiO_2 over PVDF-HFP electrospun membranes was reported to provide 99.99% rejection of NaCl when tested in DCMD mode. The water-repelling nature and self-cleaning tendency of the modified membranes were commendable.[81] The use of coaxial spinneret and multi-spinneret to include FTES-TiO_2 is another technique explored to prepare membranes with antiwetting properties with stable permeate flux.[83] The AFM image (Fig. 31.10) of the surface clearly shows the surface modification of the PVDF membrane on incorporating TiO_2.

ZnO is another photocatalyst that has been employed to prepare nanocomposite PTFE electrospun membranes for VMD application.[84]

The Ag NPs has a unique ability to resist the growth of bacteria and biofilms on membrane surfaces and make them suitable for long-term stable operations.[85] The generation of reactive oxygen species (ROS) and oxidative stress were the two primary mechanisms responsible for Ag nanoparticle's toxicity or antibacterial activity. In MD applications Ag NPs are mainly used along with f-MWCNT's, forming a hydrophilic layer that helps mitigate oil fouling.[66]

Silver nanoparticle (noble metal) showcases a unique phenomenon where it can convert light directly to heat due to an effect termed plasmon-induced hot-electron transfer (PHET). Xiong Li et al.[86] demonstrated a unique ultraviolet light-driven MD using a PVDF/Ag photothermal nanofibrous composite membrane (Fig. 31.11).

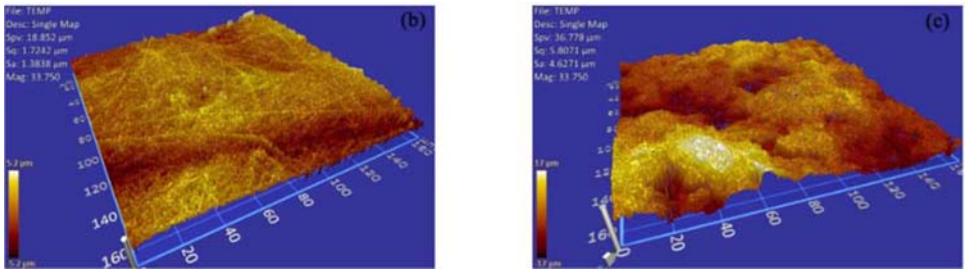

FIGURE 31.10 AFM image of unmodified and TiO_2-FTCS surface modified PVDF ENM. *From Ren LF, Xia F, Chen V, Shao J, Chen R, and He Y, TiO2-FTCS modified superhydrophobic PVDF electrospun nanofibrous membrane for desalination by direct contact membrane distillation,* Desalination *2017;**423** (September):1–11, http://10.1016/j.desal.2017.09.004.*

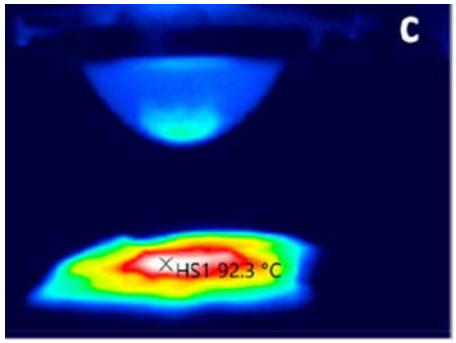

FIGURE 31.11 IR thermal images upon irradiation of UV light for 60 s on Ag incorporated PVDF membrane. *Reprinted from Ye H et al., Silver nanoparticle-enabled photothermal nanofibrous membrane for light-driven membrane distillation.* Ind Eng Chem Res *2019;**58**(8):3269−3281, http://10.1021/acs.iecr.8b04708. copyright (2019) American Chemical Society.*

At 20% Ag loading, the membrane could provide a high-efficiency heat source (∼60%) for heating the feed solution, and this configuration could be operated without any auxiliary heating.

The drawback of incorporation of silver nanoparticles in MD membranes is that they may leach out of the matrix over time, or during synthesis, the NPs may get deposited on the membrane surface, blocking the pores, which eventually could lead to a decline in the permeate flux.[87]

The infrared induced photothermal effect was pronounced in the PVDF/Antimony doped Tin oxide hybrid nanofibrous membranes used in VMD. The modified membranes exhibited low-temperature polarization, and permeate flux of 27 LMH was reported.[88]

Alumina NPs are widely reported to enhance permeability, provide superior antifouling ability and augment the mechanical strength of the membrane.[46] Alumina is inherently hydrophilic, and the presence of a large number of −OH groups provide sites for functionalization with highly branched hydrocarbons to render it hydrophobic. Hydrophilic alumina nanoparticle incorporated membranes are generally employed in an AGMD configuration as opposed to the DCMD configuration. This could be to avoid the heat loss by conduction due to the high thermal conductivity of alumina (∼28 W/mK).[89]

Heavy metals, even in low concentrations, pose a severe threat to the environment and human health. The eventual build-up of heavy metals in human tissues occurs over time and leads to damage that eventually causes harmful physiological effects. The Al_2O_3 NPs embedded PVDF membrane in the AGMD mode could remove 99% of heavy metals -Pb, Cd, Cr, Cu, Ni.[90] A 100% lead rejection was reported in a similar study using a PVDF electrospun membrane incorporated with isostearyl acid-modified Al_2O_3 NPs.[91] More details about metal and metal oxide incorporated electrospun membranes for MD are given in Table 31.4.

TABLE 31.4 List of works using metal oxide nanoparticles incorporated electrospun membranes for MD.

Nanoparticle: Metal oxide											
Polymer used	**NP/functionalization**	**MD mode**	**Membrane configuration**	**Application**	**LEP**	**WCA**	**Fiber dia and membrane thickness**	**Pore size and porosity**	**Flux**	**Rejection %/solute rejected**	**Refs**
PVDF	Al_2O_3 functionalized with isostearyl acids	AGMD	Flat sheet	Heavy metal rejection	21 Psi	150°	172 nm & 130 μm	0.55 μm & 88.1%	23 LMH	>99%	[90]
PVDF	Al_2O_3	AGMD	Flat sheet	Heavy metal rejection	25 Psi	154°	236 nm & 115 ± 0.82 μm	0.39 μm & 87.5%	18.67 LMH	99.99%	[89]
PVDF	$AgNO_3$ (Ag NP's)	DCMD	Flat sheet	Desalination	1.55 ± 0.04 bar	148 ± 2.1°	0.34 μm & -	0.31 μm & 67.5 ± 1.8%	2.5 kg/ m^2hr	>99%	[86]
PVDF-HFP	FTES functionalized TiO_2	DCMD	Flat sheet	Desalination	96.37 ± 1.7 kPa	149± 2.8°	296 ± 74 nm & 100±8 μm	0.7567 μm & 91.6%	37.8 kg/ m^2hr	99.99%	[82]
PVDF-HFP	FTES functionalized TiO_2	DCMD	Flat sheet	Desalination	90.5 ± 3.6 kPa	153.4°	231 ± 139 nm& 231 ± 139 μm	0.76 ± 0.05 μm & 89.8 ± 1.9%	40 LMH	99.99%	[83]
PVDF-HFP	PFTS functionalized TiO_2	DCMD	Flat sheet	Desalination	1.10 bar	155°	398 nm&125 μm	0.75 μm& 85%	38.7 ± 1.105 LMH	>99%	[81]

TABLE 31.5 List of works using other some important nanoparticles incorporated electrospun membranes for MD.

Nanoparticle: Others										
Polymer used	**NP/ functionalization**	**MD mode**	**Membrane configuration**	**Application**	**LEP**	**WCA**	**Fiber dia and membrane thickness**	**Pore size and porosity**	**Flux**	**Rejection %/solute rejected**	**Refs**
PVDF	MOF Iron-BTC	DCMD	Flat sheet	Desalination	82.73 kPa	138.06 ± 2.18°	445.58 ± 166.92 nm &79.99 ± 13.59 μm	0.63 ± 0.18 μm & 66.24%	2.87 kg/ m^2 h	99.99%	[92]
Psf	PTFE NP's	DCMD	Flat sheet	Desalination	100.3 kPa	155°	491 nm & 551.6 ± 3.6 μm	- & 84.1 ± 0.9%	44.8kg/ m^2hr	99.99%	[95]

6.4 Metal-organic framework (MOF)

These are coordination complexes with metal cations surrounded by organic ligands with high specific surface area and porous structure. The organic-inorganic coordination is responsible for the unique properties of MOF. MOFs are generally used in gas separation and are not suitable for water treatment because of their instability, with certain exceptions-zirconium and iron complexes.

Superhydrophobic PVDF membrane fabricated with MOF (iron 1,3,5-benzenetricarboxylate) displayed a high water contact angle (~140 degrees), a moderately high LEP (82.73 kPa) with a 99.99% NaCl rejection in a DCMD mode.[92]

6.5 Other nanoparticles

Suitable nanoparticles such as aerogels,[93] nanoclay,[94] PTFE nanoparticle[95] etc. have also been employed as additives in various electrospun membranes to be employed for MD. Nanoclay improves the mechanical properties and thermal stability of polymer membranes as well as imparts a hydrophobic nature.

Details of some other commonly used nanoparticles incorporated electrospun membranes are given in Table 31.5.

7. Conclusion

This chapter focuses on the state-of-the-art development of electrospun nanofibrous membranes modified with nanoparticles for MD applications. MD is a promising alternative for water recovery and seawater desalination. The MD process is robust and can remove 100% of the total dissolved solids, withstand high salinity feed streams, and operates at a lower temperature (compared to thermal processes) and pressure (compared to RO). The standard MD configurations and the modifications of the process configurations have been discussed in detail. Electrospinning is a novel technology to produce nanofibrous membranes and has been proven successful in developing highly porous membranes with excellent hydrophobicity. Though significant variations of electrospinning techniques are being investigated, upgrading this technique to an industrial scale remains a challenge. The advent of nanotechnology in developing novel membranes is a significant achievement, fueling the chances of the commercialization of MD. It offers novel opportunities to revolutionize approaches toward drinking water treatment by enhancing the multi-functionalities like antiwetting and antifouling. Surface modifications via functionalization of nanoparticles render superhydrophobicity. The primary concern is the release of nanomaterials from water treatment systems into drinking water and soil during the end disposal and the hazards it may cause. The number of researchers investigating MD is rising. With this current trend, the possibility of addressing some of these issues raised will no longer be a pipe dream, making MD a competing technology for water recovery and seawater desalination.

References

1. Saleem H, Trabzon L, Kilic A, Zaidi SJ. Recent advances in nanofibrous membranes: production and applications in water treatment and desalination. *Desalination* 2020;**478**(August 2019):114178. https://doi.org/10.1016/j.desal.2019.114178.
2. Pendergast MM, Hoek EMV. A review of water treatment membrane nanotechnologies. *Energy Environ Sci* 2011;**4**(6):1946–71. https://doi.org/10.1039/c0ee00541j.
3. Ali A, Drioli E, Macedonio F. Membrane engineering for sustainable development: a perspective. *Appl Sci* 2017;**7**(10). https://doi.org/10.3390/app7101026.
4. Arumugham T, Amimodu RG, Kaleekkal NJ, Rana D. Nano CuO/g-C 3 N 4 sheets-based ultrafiltration membrane with enhanced interfacial affinity, antifouling and protein separation performances for water treatment application. *J Environ Sci (China)* 2019;**82**:57–69. https://doi.org/10.1016/j.jes.2019.03.001.
5. Liu TY, Liu ZH, Zhang RX, Wang Y, Van der Bruggen B, Wang XL. Fabrication of a thin film nanocomposite hollow fiber nanofiltration membrane for wastewater treatment. *J Membr Sci* 2015;**488**:92–102. https://doi.org/10.1016/j.memsci.2015.04.020.
6. Raza MA, et al. PVA/TEOS crosslinked membranes incorporating zinc oxide nanoparticles and sodium alginate to improve reverse osmosis performance for desalination. *J Appl Polym Sci* 2019;**136**(22):1–10. https://doi.org/10.1002/app.47559.
7. Chérif M, et al. Reconstituted and brackish waters desalination by neutralization dialysis process with ion-exchange membranes. *Desalin Water Treat.* 2017;**65**:52–9. https://doi.org/10.5004/dwt.2017.20286.
8. Henmi M, et al. Self-organized liquid-crystalline nanostructured membranes for water treatment: selective permeation of ions. *Adv Mater* 2012;**24**(17):2238–41. https://doi.org/10.1002/adma.201200108.
9. Gahlot S, Sharma PP, Jha PK, Kulshrestha V. Effective desalination of brackish water by electrodialysis using SPANI composite cation exchange membranes. *ChemistrySelect* 2017;**2**(28):8886–92. https://doi.org/10.1002/slct.201701200.
10. Yang GCC, Tang PL, Yen CH. Removal of micropollutants from municipal wastewater by graphene adsorption and simultaneous electrocoagulation/electrofiltration process. *Water Sci Technol* 2017;**75**(8):1882–8. https://doi.org/10.2166/wst.2017.074.
11. Wang Z, et al. An electrochemically switched ion exchange process with self-electrical-energy recuperation for desalination. *Separ Purif Technol* 2020;**239**:116521. https://doi.org/10.1016/j.seppur.2020.116521.
12. M. Al-furaiji, J. T. Arena, J. Ren, N. Benes, and A. Nijmeijer, "Triple-layer nanofiber membranes for treating high salinity brines using direct contact membrane distillation."
13. Azadi F, Karimi-Jashni A, Zerafat MM. Desalination of brackish water by gelatin-coated magnetite nanoparticles as a novel draw solute in forward osmosis process. *Environ Technol (United Kingdom)* 2020;**3330**. https://doi.org/10.1080/09593330.2020.1717642.
14. Wan CF, Jin S, Chung TS. Mitigation of inorganic fouling on pressure retarded osmosis (PRO) membranes by coagulation pretreatment of the wastewater concentrate feed. *J Membr Sci* 2019;**572**(August 2018):658–67. https://doi.org/10.1016/j.memsci.2018.11.051.
15. Emadzadeh D, Matsuura T, Ghanbari M, Ismail AF. Hybrid forward osmosis/ultrafiltration membrane bag for water purification. *Desalination* 2019;**468**(June). https://doi.org/10.1016/j.desal.2019.114071.
16. Li M, Li K, Wang L, Zhang X. Feasibility of concentrating textile wastewater using a hybrid forward osmosis-membrane distillation (FO-MD) process: performance and economic evaluation. *Water Res* 2020;**172**:115488. https://doi.org/10.1016/j.watres.2020.115488.
17. Nagy E. "*Membrane distillation*," basic equations mass transp. *through a membr. Layer, no. MD*. 2019. p. 483–96. https://doi.org/10.1016/B978-0-12-813722-2.00019-4.
18. Wang P, Chung T. Recent advances in membrane distillation processes : membrane development , con fi guration design and application exploring. *J Membr Sci* 2015;**474**(January):39–56. https://doi.org/10.1016/j.memsci.2014.09.016.
19. Rezaei M, Warsinger DM, H. L. V J, Duke MC, Matsuura T, Samhaber WM. Wetting phenomena in membrane distillation : mechanisms , reversal , and prevention. *Water Res* 2018;**139**:329–52. https://doi.org/10.1016/j.watres.2018.03.058.
20. El-Bourawi MS, Ding Z, Ma R, Khayet M. A framework for better understanding membrane distillation separation process. *J Membr Sci* 2006. https://doi.org/10.1016/j.memsci.2006.08.002.

21. Khayet M. Membranes and theoretical modeling of membrane distillation: a review. *Adv Colloid Interface Sci* 2011;**164**(1–2):56–88. https://doi.org/10.1016/j.cis.2010.09.005.
22. Camacho LM, et al. *Advances in membrane distillation for water desalination and purification applications*. Switzerland: Water; 2013. https://doi.org/10.3390/w5010094.
23. Qtaishat M, Matsuura T, Kruczek B, Khayet M. *Heat and mass transfer analysis in direct contact membrane distillation* 2008;**219**:272–92. https://doi.org/10.1016/j.desal.2007.05.019.
24. Zhong W, Ji C, Li H, Hou J, Chen V. Fouling mitigation in submerged VMD for the treatment of brackish groundwater concentrates with transverse vibration and crystallizer. *Desalination* 2018;**426**(July 2017):32–41. https://doi.org/10.1016/j.desal.2017.10.024.
25. González D, Amigo J, Suárez F. Membrane distillation : perspectives for sustainable and improved desalination. *Renew Sustain Energy Rev* 2017;**80**(April 2016):238–59. https://doi.org/10.1016/j.rser.2017.05.078.
26. Wang KY, Teoh MM, Nugroho A, Chung TS. Integrated forward osmosis-membrane distillation (FO-MD) hybrid system for the concentration of protein solutions. *Chem Eng Sci* 2011;**66**(11):2421–30. https://doi.org/10.1016/j.ces.2011.03.001.
27. Adham S, Hussain A, Matar JM, Dores R, Janson A. Application of Membrane Distillation for desalting brines from thermal desalination plants. *Desalination* 2013;**314**:101–8. https://doi.org/10.1016/j.desal.2013.01.003.
28. Alkhudhiri A, Darwish N, Hilal N. Membrane distillation: a comprehensive review. *Desalination* 2012. https://doi.org/10.1016/j.desal.2011.08.027.
29. Zhang Y, Peng Y, Ji S, Li Z, Chen P. Review of thermal ef fi ciency and heat recycling in membrane distillation processes. *DES* 2015;**367**:223–39. https://doi.org/10.1016/j.desal.2015.04.013.
30. Deshmukh A, et al. Membrane distillation at the water-energy nexus: limits, opportunities, and challenges. *Energy Environ Sci* 2018;**11**(5):1177–96. https://doi.org/10.1039/c8ee00291f.
31. Ghaffour N, Soukane S, Lee JG, Kim Y, Alpatova A. Membrane distillation hybrids for water production and energy efficiency enhancement: a critical review. *Appl Energy* 2019;**254**(August):113698. https://doi.org/10.1016/j.apenergy.2019.113698.
32. Ali A, Tsai JH, Tung KL, Drioli E, Macedonio F. Designing and optimization of continuous direct contact membrane distillation process. *Desalination* 2018;**426**(October 2017):97–107. https://doi.org/10.1016/j.desal.2017.10.041.
33. Ullah R, et al. Energy e ffi ciency of direct contact membrane distillation. *Desalination* 2018;**433**(January):56–67. https://doi.org/10.1016/j.desal.2018.01.025.
34. Tijing LD, Woo YC, Choi JS, Lee S, Kim SH, Shon HK. Fouling and its control in membrane distillation-A review. *J Membr Sci* 2015. https://doi.org/10.1016/j.memsci.2014.09.042.
35. Dong ZQ, hua Ma X, Xu ZL, You WT, bing Li F. Superhydrophobic PVDF-PTFE electrospun nanofibrous membranes for desalination by vacuum membrane distillation. *Desalination* 2014;**347**:175–83. https://doi.org/10.1016/j.desal.2014.05.015.
36. Ahmed FE, Lalia BS, Hashaikeh R. A review on electrospinning for membrane fabrication: challenges and applications. *Desalination* 2015;**356**:15–30. https://doi.org/10.1016/j.desal.2014.09.033.
37. Ray SS, Chen S, Nguyen NC, Nguyen HT. *1 introduction*. 2019. p. 247–73.
38. Dehghan SF, et al. Optimization of electrospinning parameters for polyacrylonitrile-MgO nanofibers applied in air filtration. *J Air Waste Manag Assoc* 2016;**66**(9):912–21. https://doi.org/10.1080/10962247.2016.1162228.
39. Ray SS, et al. Casting of a superhydrophobic membrane composed of polysulfone/Cera flava for improved desalination using a membrane distillation process. *RSC Adv* 2018;**8**(4):1808–19. https://doi.org/10.1039/c7ra12474k.
40. Duong HC, Chuai D, Woo YC, Shon HK, Nghiem LD, Sencadas V. A novel electrospun, hydrophobic, and elastomeric styrene-butadiene-styrene membrane for membrane distillation applications. *J Membr Sci* 2018;**549**(November 2017):420–7. https://doi.org/10.1016/j.memsci.2017.12.024.
41. Ke H, et al. Electrospun polystyrene nanofibrous membranes for direct contact membrane distillation. *J Membr Sci* 2016;**515**:86–97. https://doi.org/10.1016/j.memsci.2016.05.052.
42. Ray SS, Chen SS, Li CW, Nguyen NC, Nguyen HT. A comprehensive review: electrospinning technique for fabrication and surface modification of membranes for water treatment application. *RSC Adv* 2016;**6**(88):85495–514. https://doi.org/10.1039/c6ra14952a.
43. Selatile MK, Ray SS, Ojijo V, Sadiku R. Recent developments in polymeric electrospun nanofibrous membranes for seawater desalination. *RSC Adv* 2018;**8**(66):37915–38. https://doi.org/10.1039/C8RA07489E.

44. Haider A, Haider S, Kang IK. A comprehensive review summarizing the effect of electrospinning parameters and potential applications of nanofibers in biomedical and biotechnology. *Arab J Chem* 2018;**11**(8):1165–88. https://doi.org/10.1016/j.arabjc.2015.11.015.
45. Pan CY, et al. Electrospun nanofibrous membranes in membrane distillation: recent developments and future perspectives. *Separ Purif Technol* 2019;**221**(September 2018):44–63. https://doi.org/10.1016/j.seppur.2019.03.080.
46. Ike IA, Orbell JD, Duke M. *Nanoparticle incorporation into desalination and water treatment membranes-potential advantages and challenges*. Elsevier Inc.; 2017.
47. Lu H, Wang J, Stoller M, Wang T, Bao Y, Hao H. *An overview of nanomaterials for water and wastewater treatment*. 2016. vol. 2016.
48. Li X, Yu X, Cheng C, Deng L, Wang M, Wang X. *Electrospun superhydrophobic organic/inorganic composite nano fi brous membranes for membrane distillation*. 2015. https://doi.org/10.1021/acsami.5b06509.
49. Nthunya LN, et al. Fouling-resistant PVDF nanofibre membranes for the desalination of brackish water in membrane distillation. *Separ Purif Technol* 2019;**228**(March):115793. https://doi.org/10.1016/j.seppur.2019.115793.
50. Hou D, Ding C, Fu C, Wang D, Zhao C, Wang J. Electrospun nanofibrous omniphobic membrane for anti-surfactant-wetting membrane distillation desalination. *Desalination* 2019;**468**(August 2018):114068. https://doi.org/10.1016/j.desal.2019.07.008.
51. Su C, Horseman T, Cao H, Li Y, Lin S. *Robust superhydrophobic membrane for membrane distillation with excellent scaling resistance*. 2019. https://doi.org/10.1021/acs.est.9b04362.
52. Nthunya LN, Gutierrez L, Verliefde R, Mhlanga SD. *Enhanced flux in direct contact membrane distillation using superhydrophobic PVDF nanofibre membranes embedded with organically modified SiO 2 nanoparticles*. 2019. https://doi.org/10.1002/jctb.6104. no. June.
53. Nthunya LN, et al. Superhydrophobic PVDF nanofibre membranes coated with an organic fouling resistant hydrophilic active layer for direct-contact membrane distillation. *Colloids Surfaces A Physicochem. Eng. Asp.* 2019;**575**(December 2018):363–72. https://doi.org/10.1016/j.colsurfa.2019.05.031.
54. Liao Y, Zheng G, Jeanne J, Tian M, Wang R. Development of robust and superhydrophobic membranes to mitigate membrane scaling and fouling in membrane distillation. *J Membr Sci* 2020;**601**(December 2019):117962. https://doi.org/10.1016/j.memsci.2020.117962.
55. Zhu Z, et al. *Dual-bioinspired design for constructing membranes with superhydrophobicity for direct contact membrane distillation*. 2018. https://doi.org/10.1021/acs.est.7b06227.
56. Dizge N, Shaulsky E, Karanikola V. Electrospun cellulose nanofibers for superhydrophobic and oleophobic membranes. *J Membr Sci* 2019;**590**(June):117271. https://doi.org/10.1016/j.memsci.2019.117271.
57. Li K, Wang K, Zhang Y, Liu H, Wang J. A polyvinylidene fluoride (PVDF)–silica aerogel (SiAG) insulating membrane for improvement of thermal efficiency during membrane distillation. *J Membr Sci* 2020;**597**(September):117632. https://doi.org/10.1016/j.memsci.2019.117632.
58. Dong Z, Ma X, Xu Z, Gu Z. *RSC advances*. 2015. p. 67962–70. https://doi.org/10.1039/c5ra10575g.
59. Hou D, Wang Z, Wang K, Wang J, Lin S. Composite membrane with electrospun multiscale-textured surface for robust oil-fouling resistance in membrane distillation. *J Membr Sci* 2018;**546**(September 2017):179–87. https://doi.org/10.1016/j.memsci.2017.10.017.
60. Zheng R, Chen Y, Wang J, Song J, Li X, He T. Preparation of omniphobic PVDF membrane with hierarchical structure for treating saline oily wastewater using direct contact membrane distillation. *J Membr Sci* 2018;**555**(December 2017):197–205. https://doi.org/10.1016/j.memsci.2018.03.041.
61. Liao Y, Wang R, Fane AG. *Fabrication of Bioinspired Composite Nano fi ber Membranes with Robust Superhydrophobicity for Direct Contact Membrane Distillation*. 2014.
62. Silica- CES, Huang Y, Wang Z, Hou D, Lin S. Author's accepted manuscript coaxially electrospun superamphiphobic silica-based membrane for anti-surfactant-wetting membrane distillation. *J Membr Sci* 2017. https://doi.org/10.1016/j.memsci.2017.02.044.
63. Eatemadi A, et al. Carbon nanotubes: properties, synthesis, purification, and medical applications. *Nanoscale Res Lett* 2014;**9**(1):1–13. https://doi.org/10.1186/1556-276X-9-393.
64. Gethard K, Sae-Khow O, Mitra S. Water desalination using carbon-nanotube-enhanced membrane distillation. *ACS Appl Mater Interfaces* 2011;**3**(2):110–4. https://doi.org/10.1021/am100981s.
65. Atif R, Inam F. Reasons and remedies for the agglomeration of multilayered graphene and carbon nanotubes in polymers. *Beilstein J Nanotechnol* 2016;**7**(1):1174–96. https://doi.org/10.3762/bjnano.7.109.

66. Nthunya LN, Gutierrez L, Nxumalo EN, Verliefde AR, Mhlanga SD, Onyango MS. f-MWCNTs/AgNPs-coated superhydrophobic PVDF nanofibre membrane for organic , colloidal , and biofouling mitigation in direct contact membrane distillation. *J Environ Chem Eng* 2020;**8**(2):103654. https://doi.org/10.1016/j.jece.2020.103654.
67. Mahmoud KA, Mansoor B, Mansour A, Khraisheh M. Functional graphene nanosheets: the next generation membranes for water desalination. *Desalination* 2015;**356**:208–25. https://doi.org/10.1016/j.desal.2014.10.022.
68. Elmarghany MR, El-Shazly AH, Salem MS, Sabry MN, Nady N. Novel membrane suitable for membrane distillation: effect of mixed nanofillers on the membrane performance. *Key Eng Mater* 2019;**801**:325–30. KEM doi: 10.4028/www.scientific.net/KEM.801.325.
69. Tijing LD, et al. Superhydrophobic nanofiber membrane containing carbon nanotubes for high-performance direct contact membrane distillation. *J Membr Sci* 2016;**502**:158–70. https://doi.org/10.1016/j.memsci.2015.12.014.
70. Elmarghany MR, et al. Triple-layer nanocomposite membrane prepared by electrospinning based on modified PES with carbon nanotubes for membrane distillation applications. *Membranes* 2020;**10**(1):1–19. https://doi.org/10.3390/membranes10010015.
71. Yan KK, Jiao L, Lin S, Ji X, Lu Y, Zhang L. Superhydrophobic electrospun nanofiber membrane coated by carbon nanotubes network for membrane distillation. *Desalination* 2018;**437**(February):26–33. https://doi.org/10.1016/j.desal.2018.02.020.
72. Woo YC, et al. W5ater desalination using graphene-enhanced electrospun nanofiber membrane via air gap membrane distillation. *J Membr Sci* 2016;**520**:99–110. https://doi.org/10.1016/j.memsci.2016.07.049.
73. Li H, Shi W, Zeng X, Huang S, Zhang H, Qin X. Improved desalination properties of hydrophobic GO-incorporated PVDF electrospun nanofibrous composites for vacuum membrane distillation. *Separ Purif Technol* 2020;**230**(February 2019):115889. https://doi.org/10.1016/j.seppur.2019.115889.
74. Chen T, Soroush A, Rahaman MS. Highly hydrophobic electrospun reduced graphene oxide/poly(vinylidene fluoride-co-hexafluoropropylene) membranes for use in membrane distillation. *Ind Eng Chem Res* 2018;**57**(43):14535–43. https://doi.org/10.1021/acs.iecr.8b03584.
75. Salem MS, El-Shazly AH, Nady N, Elmarghany MR, Sabry MN. PES/PVDF blend membrane and its composite with graphene nanoplates: preparation, characterization, and water desalination via membrane distillation. *Desalin. Water Treat.* 2019;**166**:9–23. https://doi.org/10.5004/dwt.2019.24611.
76. Jafari A, Kebria MRS, Rahimpour A, Bakeri G. Graphene quantum dots modified polyvinylidenefluride (PVDF) nanofibrous membranes with enhanced performance for air Gap membrane distillation. *Chem. Eng. Process. - Process Intensif.* 2018;**126**(2010):222–31. https://doi.org/10.1016/j.cep.2018.03.010.
77. Zhao L, Wu C, Lu X, Ng D, Truong YB, Xie Z. Activated carbon enhanced hydrophobic/hydrophilic dual-layer nanofiber composite membranes for high-performance direct contact membrane distillation. *Desalination* 2018;**446**(August):59–69. https://doi.org/10.1016/j.desal.2018.09.002.
78. Guo J, et al. Enhanced ammonia recovery from wastewater by Nafion membrane with highly porous honeycomb nanostructure and its mechanism in membrane distillation. *J Membr Sci* 2019;**590**(July). https://doi.org/10.1016/j.memsci.2019.117265.
79. Theron J, Walker JA, Cloete TE. Nanotechnology and water treatment: applications and emerging opportunities. *Crit Rev Microbiol* 2008;**34**(1):43–69. https://doi.org/10.1080/10408410701710442.
80. Ren LF, Xia F, Chen V, Shao J, Chen R, He Y. TiO2-FTCS modified superhydrophobic PVDF electrospun nanofibrous membrane for desalination by direct contact membrane distillation. *Desalination* 2017;**423**(September):1–11. https://doi.org/10.1016/j.desal.2017.09.004.
81. Seyed Shahabadi SM, Rabiee H, Seyedi SM, Mokhtare A, Brant JA. Superhydrophobic dual layer functionalized titanium dioxide/polyvinylidene fluoride-co-hexafluoropropylene (TiO2/PH) nanofibrous membrane for high flux membrane distillation. *J Membr Sci* 2017;**537**(April):140–50. https://doi.org/10.1016/j.memsci.2017.05.039.
82. Lee EJ, An AK, He T, Woo YC, Shon HK. Electrospun nanofiber membranes incorporating fluorosilane-coated TiO2 nanocomposite for direct contact membrane distillation. *J Membr Sci* 2016;**520**:145–54. https://doi.org/10.1016/j.memsci.2016.07.019.
83. Lee EJ, An AK, Hadi P, Lee S, Woo YC, Shon HK. Advanced multi-nozzle electrospun functionalized titanium dioxide/polyvinylidene fluoride-co-hexafluoropropylene (TiO2/PVDF-HFP) composite membranes for direct contact membrane distillation. *J Membr Sci* 2017;**524**(August 2016):712–20. https://doi.org/10.1016/j.memsci.2016.11.069.

84. Huang QL, Huang Y, Xiao CF, You YW, Zhang CX. Electrospun ultrafine fibrous PTFE-supported ZnO porous membrane with self-cleaning function for vacuum membrane distillation. *J Membr Sci* 2017;**534**(399):73–82. https://doi.org/10.1016/j.memsci.2017.04.015.
85. Kunduru KR, Nazarkovsky M, Farah S, Pawar RP, Basu A, Domb AJ. *Nanotechnology for water purification: applications of nanotechnology methods in wastewater treatment*. 2017. no. January.
86. Ye H, et al. Silver nanoparticle-enabled photothermal nanofibrous membrane for light-driven membrane distillation. *Ind Eng Chem Res* 2019;**58**(8):3269–81. https://doi.org/10.1021/acs.iecr.8b04708.
87. Nthunya LN, et al. A review of nanoparticle-enhanced membrane distillation membranes : membrane synthesis and applications in water treatment. *J Chem Technol Biotechnol* 2019;**94**(9):2757–71. https://doi.org/10.1002/jctb.5977.
88. Huang Q, Gao S, Huang Y, Zhang M, Xiao C. Study on photothermal PVDF/ATO nanofiber membrane and its membrane distillation performance. *J Membr Sci* 2019;**582**(April):203–10. https://doi.org/10.1016/j.memsci.2019.04.019.
89. Attia H, Johnson DJ, Wright CJ, Hilal N. Robust superhydrophobic electrospun membrane fabricated by combination of electrospinning and electrospraying techniques for air gap membrane distillation. *Desalination* 2018;**446**(August):70–82. https://doi.org/10.1016/j.desal.2018.09.001.
90. Attia H, Johnson DJ, Wright CJ, Hilal N. Comparison between dual-layer (superhydrophobic–hydrophobic) and single superhydrophobic layer electrospun membranes for heavy metal recovery by air-gap membrane distillation. *Desalination* 2018;**439**(January):31–45. https://doi.org/10.1016/j.desal.2018.04.003.
91. Attia H, Alexander S, Wright CJ, Hilal N. Superhydrophobic electrospun membrane for heavy metals removal by air gap membrane distillation (AGMD). *Desalination* 2017;**420**(July):318–29. https://doi.org/10.1016/j.desal.2017.07.022.
92. Yang F, Efome JE, Rana D, Matsuura T, Lan C. Metal-organic frameworks supported on nanofiber for desalination by direct contact membrane distillation. *ACS Appl Mater Interfaces* 2018;**10**(13):11251–60. https://doi.org/10.1021/acsami.8b01371.
93. Lee EJ, Deka BJ, An AK. Reinforced superhydrophobic membrane coated with aerogel-assisted polymeric microspheres for membrane distillation. *J Membr Sci* 2019;**573**(May 2019):570–8. https://doi.org/10.1016/j.memsci.2018.12.019.
94. Prince JA, Singh G, Rana D, Matsuura T, Anbharasi V, Shanmugasundaram TS. Preparation and characterization of highly hydrophobic poly(vinylidene fluoride) - clay nanocomposite nanofiber membranes (PVDF-clay NNMs) for desalination using direct contact membrane distillation. *J Membr Sci* 2012;**397–398**:80–6. https://doi.org/10.1016/j.memsci.2012.01.012.
95. Khayet M, Wang R. Mixed matrix polytetrafluoroethylene/polysulfone electrospun nanofibrous membranes for water desalination by membrane distillation. *ACS Appl Mater Interfaces* 2018;**10**(28):24275–87. https://doi.org/10.1021/acsami.8b06792.

CHAPTER

32

Application of multifunctional carbon-based silver nanocomposites for environmental remediation

Laxmi Gayatri Sorokhaibam, Mary R. Louis and Sandeep Chaudhary

Department of Chemistry, Visvesvaraya National Institute of Technology Nagpur, Nagpur, Maharashtra, India

Abbreviations

AC activated carbon
Ag@AC silver-loaded activated carbon
AgNPs silver nanoparticles
AOPs advanced oxidation processes
B Temkin constant
BET Brunner-Emmet and Teller
bT constant associated with the heat of adsorption in J mol^{-1}
C_0 concentration of dye in mg L^{-1} before adsorption
C_e concentration of dye in mg L^{-1} after adsorption
FEG-SEM field emission gun scanning electron microscopy
FT-IR Fourier transform infrared
HR-TEM high-resolution transmission electron microscopy
Ibu ibuprofen
K_F Freundlich constant in $(mg.g^{-1}\ (L.mg^{-1})^{\ 1/n})$
K_L Langmuir constant in L mg^{-1}
K_T Temkin isotherm constant in L g^{-1}
MFM/C multifunctional materials or composites
n adsorption intensity
NSAID nonsteroidal antiinflammatory drugs
PCPPs pharmaceutical and personal care products
ppt parts per trillion
q_e adsorption capacity in mg g^{-1} at equilibrium
q_{max} maximum monolayer capacity

Applications of Multifunctional Nanomaterials
https://doi.org/10.1016/B978-0-12-820557-0.00022-9

R gas constant
R^2 coefficient of determination
RB-4 reactive blue 04
RhB rhodamine B
R_L the separation factor
Rpm revolutions per minute
RR-120 reactive Red 120
SAED selected area diffraction
SEM-EDAX scanning electron microscopy (SEM) with Energy dispersive x-ray analysis
T temperature in Kelvin
TEM transmission electron microscopy
TG-DTA thermogravimetric and differential thermal analysis
XRD X-ray diffraction
λ_{max} wavelength of maximum absorbance

1. Introduction

Wastewater treatment forms an important part of environmental remediation, and reuse of recycled water can solve the scarcity of fresh water to a certain extent. A very limited portion (~0.03%) of the total Earth's water content is available for human consumption.[1] Agricultural, industrial, and domestic human activities have adversely affected the availability and quality of the present water resources. Thus, the huge utilization of freshwater for industrialization and domestic activities in addition to the ever-increasing pollution of freshwater bodies may lead to the inevitable scarcity of this resource.

Industries such as textile industries consume a substantially huge quantity of fresh water in their production and processing activities and generate a huge volume of highly contaminated wastewaters.[2,3] Dyes are a notorious class of molecules present in such wastewater systems constituting 10%–15% of the total quantity of dyes used. The spike in demand for attractively colored products has led to increased application of these dyes in several sectors like textiles, leather, dyestuff, plastic, paper, printing, food, pharmaceuticals, research laboratories, cosmetics, etc.[4,5] These colorant molecules tend to impart color to water even in their minute concentrations[6] and are known to have a highly stable and complex structure. These dyes are known to interfere with the ecosystem in several ways by decreasing the intensity of sunlight that penetrates the colored water, affecting the life cycle of aquatic flora and fauna,[7] which deteriorate the environment and affect human and aquatic life when released into the natural water systems.[1,3] Many of them are associated to carcinogenic, and mutagenic potential in addition to their ability to cause other medical complications.[8,9] Hence, removal of these toxic dyes from wastewater before their discharge is highly essential.[10]

The other class of common organic pollutants is pharmaceutical and personal care products (PCPPs)[11] which belong to a new group of emerging contaminants. These compounds seek their path into the wastewater streams through human and veterinary consumption or application as medicines, fungicides, and disinfectants used for industrial, agricultural, and household purposes and through excreta.[12] Ibuprofen (Ibu) is an important and widely prescribed drug for conditions such as rheumatoid arthritis as

nonsteroidal antiinflammatory drugs (NSAID) and for relief from pain and fever as antipyretic and analgesic drugs.[12,13] The complete removal of PCPPs faces several challenges, of which lack of awareness of the effect and intensity of toxicity that arise from long-lasting exposure to very low concentration (parts per trillion) and high-transformation rates of such molecules are known. The diverse class of molecules in terms of their physical and chemical properties increases the difficulties in preparing an effective treatment strategy.[14] Also, the recognition of new molecules as PCPPs are increasing on a regular basis with an enhanced detection technology (detection range of sub-ppt, i.e., $ng.dm^{-3}$).[12] The NSAID in wastewater systems has known to cause several conditions such as degenerative, renal, and necrotic changes on the vertebrates. There is also evidence of the effect of NSAID in the water on both vertebrate and invertebrate form of life causing defects in the reproductive functions, affecting the growth of the fungal and bacterial species, damaging the genetic and systemic properties of some mussels and fish species, and disrupting the cytogenetic properties in freshwater bivalves.[13] Ibu has been detected in water streams in high concentrations in the $\mu g\ L^{-1}$, hence, necessitating its removal from the aqueous streams.

Therefore, to tackle the problem of freshwater scarcity and to prevent contamination of the available freshwater bodies, wastewater treatment using an effective method that may require the development of advanced materials is highly desirable. There are various biological and chemical processes available for wastewater treatment and dye removal strategies. Some of these technologies are adsorption, membrane filtration, ion exchange, catalytic degradation, flocculation, and advanced oxidation processes, etc.[15,16] Most of these processes are either cost-intensive or require higher energy inputs, huge capital investments, or sophisticated setups that hinder the acceptance of wastewater treatment strategies, especially in developing nations. Among the several techniques, the adsorption process appears to be a promising technique with the capability of rendering higher efficiency, economic feasibility, and simplicity in operation.[17] In this technique, the most versatile adsorbent in water and wastewater treatment is activated carbon (AC).[18] AC has a relatively stable chemical structure and a high surface area with well-developed porosity, which may provide binding sites for various organic contaminants.[19] Also, the lack of hydrophilic functional groups is one of the limitations of activated carbon. There is scope to enhance the efficiency of these carbon materials through surface modification of the activated carbons, imparting various functionalities either through impregnation/doping/loading or by using biomass material that has inherent properties for wastewater treatment.

A variety of surface properties and surface chemistry may be achieved by suitable surface modification strategies. Suitably designed nanocomposites may act as multifunctional adsorbent materials in wastewater treatment strategies.[20] The suitable and well-planned fabrication and modeling of the surface of the AC may provide us with multifunctional properties that can target multiple pollutants for effective remediation of the wastewater. The modification methods may yield several routes to enhance and impart several properties in one composite material, which may prove superior in wastewater treatment strategies. The chemical/physical modification methods are known to alter the surface properties and textures of the activated carbon. The preparation of nanocomposite by tailoring the surface of the AC with nanoparticles (NPs)

may prove beneficial in providing the combined effect of the efficient conventional adsorbent (AC) and the promising future generation adsorbent (NPs). The ultimate purpose is to utilize multifunctional materials for eliminating several diversified pollutants from the wastewaters.

Hence, in this chapter, the role of multifunctional silver-loaded activated carbon (Ag@AC) in wastewater treatment strategies is presented through the preparation and application in removalof Rhodamine B (RhB), Reactive blue-04 (RB-4), Reactive red-120 (RR-120), and Ibuprofen (Ibu). The details and rate of the removal of the pollutants through the adsorption isotherms and kinetics studies were also deduced.

1.1 Multifunctional adsorbents

Multifunctional adsorbents are formed by combining two or more different materials (or phases) to produce a single material that behaves as a homogenous entity and has predictable and reproducible properties.[21] The composite material/multifunctional adsorbent often has properties that are different from the individual components. With appropriate design, a composite combines the best qualities of each component, producing a material with properties that are superior to its pristine form. They also find applications in catalytic, electric, batteries, capacitors,[22] etc.

Multifunctional materials or composites (MFM/C) in wastewater treatment technology and strategies have gained benevolent recognition in the current time.[23] The conventional techniques and materials usually are designed to tackle one particular target pollutant, which limits their application. Hence, with the introduction of MFM/C, benefits such as new technology with huge flexibility and surplus surface engineering alternative methods can be achieved.[23] Through proper modification of high surface area substrates like activated carbon, a newer and wide variety of properties of MFM/C may be achieved. Some multifunctional materials were prepared as composites of reduced graphene oxide, titanium oxide and silver nanoparticles (AgNPs) were used to fabricate the silicon nitride and polyethersulfone ceramic matrix to achieve desalination, dye removal and antibacterial properties in a thin film structure .[24] The high surface area and antimicrobial graphene oxide were loaded with photocatalytic TiO_2 and antimicrobial silver. The strategic loading of the cationic quaternary ammonium salts— 3-(trimethoxysilyl)-propyldimethyloctadecyl ammonium chloride and poly(vinyl-N-hexylpyridinium bromide)— were used to fabricate the AC surface for the removal of microbial contaminants: *Escherichia coli (E. coli)*, *Staphylococcus aureus (S. aureus)*, and organic pollutant phenol.[25] The biological AC was loaded with magnetic cobalt ferrites to target the removal of methylene blue dye, and the magnetic properties ensured efficient removal of the spent adsorbent after application.[26] Thus, for the removal of various pollutants of different kinds, suitably engineered materials prove to be potentially useful. A graphical representation of the preparation and application of multifunctional adsorbent is represented below:

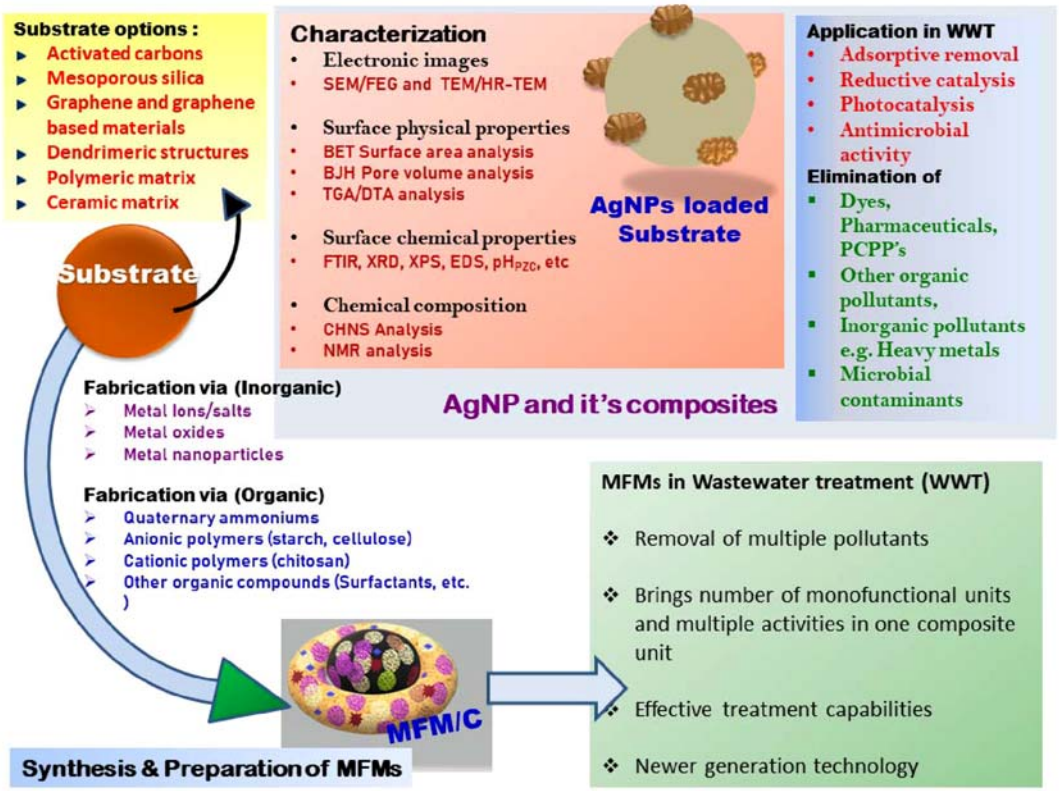

1.1.1 *Role of AgNPs in multifunctional adsorbents*

NPs have displayed a good potential to be promising adsorbents in wastewater treatment strategies and techniques and may be used to modify the surface of the AC, yielding a superior-quality nanocomposite. They may act as super-adsorbent materials because of their increased surface-to-volume ratio with a reduction in their size from bulk to nano dimensions.[27] They are known to display several attractive properties such as an ordered structure with a high aspect ratio, ultralightweight, high mechanical strength, electrical and thermal conductivity, and high specific surface area.[28] Similarly, AgNPs are also known to have distinctive physicochemical properties and broad bactericidal and fungicidal activities.[29] These NPs may be loaded on the surface of the AC to form nanocomposites.[30] The controlled release of AgNPs has particularly been advantageous in preserving the antimicrobial property for a longer duration.[31]

Thus, multifunctional materials may suitably be prepared by loading AgNPs on a suitable substrate. As discussed earlier, AgNPs are themselves known to exhibit multifunctional nature owing to their several unique and inherent properties like photosensitivity, photocatalytic, optical, catalysis, and electrical properties than the metallic silver.[32] The smaller size of AgNPs causes hindrance in their easy application, recycle and reuse, and hence the preparation of silver nanocomposites is a useful alternative. Due to these reasons, silver nanocomposites have high environmental implications. AgNPs and their composites also have the added advantage of their biocompatibility with the eukaryotic cells and high antibacterial, antiviral, and antifungal activity in comparison to other metal NPs.[33] So, these AgNPs may serve in providing a safe strategy to decorate and fabricate a suitable substrate that may participate in environmental remediation through the potential for removal of a wide range of pollutants. The antimicrobial activity of the silver nanocomposites further contributes towards the disinfection of water systems. Several methods for effective AgNPs preparation for effective wastewater treatment have been reported. The AgNPs reduced and stabilized by the rhizome of taro were utilized in the catalytic degradation of the organic pollutants like nitroarenes: picric acid, 4-nitroaniline, 4-nitrophenol, 2-nitrophenol,; and azo dyes: methyl orange, congo red, methyl red and RhB.[34] Silver-loaded graphene oxide composite was prepared to obtain multifunctional properties to achieve adsorptive removal of malachite green and ethyl violet dyes, catalytic degradation for 2-nitroaniline elimination along with antimicrobial activity against both gram-negative and gram-positive bacteria *E. coli* and *S. aureus*, respectively.[35] Similarly, our recent work on AgNPs stabilized by aqueous leave extract of *Tabernaemontana divaricata,* were decorated on the surface of AC prepared from the pods of *Delonix regia* to obtain antibacterial activity against *Bacillus subtilis* and *E. coli*, antifungal activity against *Candida albicans,* and organic dye removal like RhB dye[36] is also one approach toward utilizing nanocomposites for targeting multiple pollutants.

1.1.2 Silver nanocomposites for environmental application

Nanocomposite as an adsorbent will prove as an efficient adsorbent because of the increase in their surface-to-volume ratio with the reduction of the size of the adsorbent particle from bulk to nano dimensions,[37] and it also has many attractive properties such as an ordered structure with a high aspect ratio, ultralightweight, high mechanical strength, electrical and thermal conductivity, and high specific surface area, etc. Among the nanoparticles, AgNPs are gaining more importance because of their antimicrobial and antiviral properties[49] as discussed earlier. The application of Ag nanocomposites for different pollutant systems and its efficiency is given in Table 32.1.

1.2 Target pollutants

There are different types of pollutants present in industrial wastewater like synthetic dyes (cationic and anionic), organic pollutants (pesticides, pharmaceuticals, and phenols, etc.), and biological pollutants (e.g., bacteria— *E. coli* and *B. subtilis*, fungus— *C. albicans* and other pathogenic microbial populations). The textile industry consumes a substantial amount of water in its manufacturing processes, particularly in the dyeing and finishing operations of the

TABLE 32.1 Efficiency of Ag nanoparticle composites in dye removal.

Adsorbent	System	Maximum adsorption capacity	References
AC-AgNPLs	Crystal violet	87.2	38
AgNP-CMSs	Methylene blue	250	39
Ag-NP-AC	Sunset yellow	37.03	40
Ag-NPs-AC	Methylene blue	71.4	40
SNP-AC	Direct yellow 12	454.54	41
Ag-NPs-AC	Congo red	66.7	42
GO-Ag	Malachite green Ethyl violet	143 72	35
Ag-NPs-AC	Methylene blue	172.22	43
Silver nanoparticles loaded corncob adsorbent	Tannery effluent Dairy canteen	238 251 210	44
Ag-NPs-coated AC beads	Congo red	64.80	45
Ag-Np-AC	Eosin yellow	285.7	46
AgCl-NRs-AC	Methylene blue	227.27	47
Ag-NP-AC	Methylene blue	75.2	48
Ag-NP-AC	Bromophenol	200	49

plants. The wastewater from textile plants is classified as the most polluting of all the industrial sectors, considering the volume generated as well as the effluent composition.[50] RR-120 and RhB are important dyes which are widely used in the textile industries.[51] They are also used in cosmetics, such as lipsticks and soap, as a coloring agent. The toxicity of these dyes has been evaluated in several biological systems.[52] The dye was reported to induce growth retardation and liver damage, erythrocyte hemolysis, and suppression of the immune response in isolated spleen cells. Pharmaceutical products like Ibu belong to the class of emerging contaminants[53] which are widely used for their medicinal applications leading to their occurrence in the natural environment through medicinal effluents or pharmaceutical industry wastes. Ibuprofen, 2-[4-(2-methylpropyl)phenyl] propanoic acid is used as an anti-inflammatory drug/analgesic[53,54] and often reported in dilute concentrations of less than 1 ppb. Though they have not been regulated by environmental pollution control agencies, yet their potential effect on living organisms is nonetheless. Hence, the development of multifunctional adsorbents to target the removal of different contaminants simultaneously is growing attention in recent years.

As for the experimental methodology, the initial and residual concentrations of the chemical pollutants may be measured using a UV-visible spectrophotometer at their absorbance

TABLE 32.2 Chemical specification of pollutants under study.

Properties	Rhodamine B (RhB)	Reactive red 120 (RR-120)	Reactive blue 04 (RB-4)	Ibuprofen sodium salt (Ibu)
Other names	Brilliant pink B	Triazine dye red	Procion blue	Advil
Type	Cationic dye	Anionic dye	Anthraquinone	PCPPs
Molecular formula	C28H31ClN2O3	C44H24Cl2N14O20S6Na6	C23H14Cl2N6O8S2	C13H17NaO2
Molecular weight ($gmol^{-1}$)	479.02	1470	637.43	228.26
Solubility (gL^{-1})	15	70	45	20
χ_{max} (nm)	554	535	591	222
Procured from	Sigma-Aldrich	Sigma-Aldrich	Alfa Aesar	Sigma-Aldrich

maximum as provided in Table 32.2. The working standard solutions of the target pollutants were prepared from the stock solutions of 500 mg L^{-1} by subsequent dilution method to the required concentration. All experiments were repeated in triplicates to ensure the reproducibility and accuracy of the data generated.

1.3 Preparation of Ag@AC

The AC procured from Merck; India was utilized as the base support. For the fabrication on the surface of AC with silver, 10 mL of $AgNO_3$ (0.03M) was mixed with 10 mL of Na_2CO_3 (2.5 mM), and the mixture was constantly stirred for 1 h to yield white precipitates of Ag_2CO_3. The reducing agent, $NaBH_4$ (1 mM, 2 mL), and stabilizing agent, starch solution (2%, 20 mL) were added with constant stirring and heating at 60°C for ~1.5 h. The details of chemicals used for the preparation of the composite were silver nitrate ($AgNO_3$, purity = 99.9%; Alfa Aesar), sodium borohydride ($NaBH_4$, purity = 97.10%), sodium carbonate (Na_2CO_3, purity = 99.55%; Merck), and starch $\{(C_6H_{10}O_5)_n\}$. All chemicals were used without further purification and solutions were prepared in ultrapure water from the Milli-Q Elga system (Millipore) for all experiments. A color change from white to brown was observed, indicating the formation of reduced silver.[11] To this brown-colored solution (Fig. 32.1), 7 g of AC was added, and the mixture was heated at 60°C for ~1.5 h with intermittent mixing yielding Ag@AC. Later, the Ag@AC was placed in a furnace for 1.5 h at 300°C. The resultant carbon was further characterized and its potential application in dye removal was investigated. The resultant material is referred to hereafter as Ag@AC.

The efficiency of various silver nanoparticle-loaded nanocomposites toward different dye removal is summarized in Table 32.2.

FIGURE 32.1 Brown coloration indicating the formation of AgNPs.

2. Adsorbent characterization

AC and Ag@AC were characterized to understand the surface composition, morphology, and thermal stability using Fourier transform infrared (FT-IR), X-ray diffraction (XRD), Thermogravimetric and differential thermal analysis (TG-DTA), HITACHI TG/DTA 7200), Scanning electron microscopy (SEM) with Energy dispersive x-ray analysis (SEM-EDAX), TEM and Brunner-Emmet and Teller (BET) surface analysis. FTIR spectra of AC and Ag@AC were examined to determine the functional groups present on their surface to understand their possible role in the interaction and removal of the dye contaminants. The spectra were recorded in transmittance mode using Shimadzu Spectrophotometer with 40 scans and a resolution rate of 4 cm^{-1} in the range of 400−4000 cm^{-1}. The samples were prepared using dry FTIR grade KBr powder in a ratio of 1:100. The XRD patterns for both the samples were obtained using an X-ray diffractometer (Panalytical's X'Pert Pro) with a wavelength of 1.54Å (Cμ K-α1), equipped with nickel beta filter and an X'Celerator solid-state detector and 2θ range of 5−100 degrees. The SEM images were recorded with a 10,000 times magnification by the scanning electron microscope (FEI, QUANTA 200-3D). The TEM micrograph was obtained by dripping the Ag@AC dispersed in isopropanol, followed by ultrasonication for 30 min, and dried on the copper grid which was then characterized on TEM-EDX (Tecnai T-20) at 200 eV. The surface area of the prepared adsorbent was characterized by Quantachrome Sorptometer using the nitrogen adsorption-desorption method where the prior degassed finely powdered sample was analyzed at −196°C. The specific surface area was calculated by the BET isotherm model, while the total pore volume and the average size were determined by the Barrett-Joyner-Halenda (BJH) method. To determine the thermal stability of the AC and Ag@AC, TG analysis was performed in the temperature range of 40°C−800°C under a nitrogen flow of 200 mL per min at the heating rate of 10°C per minute.

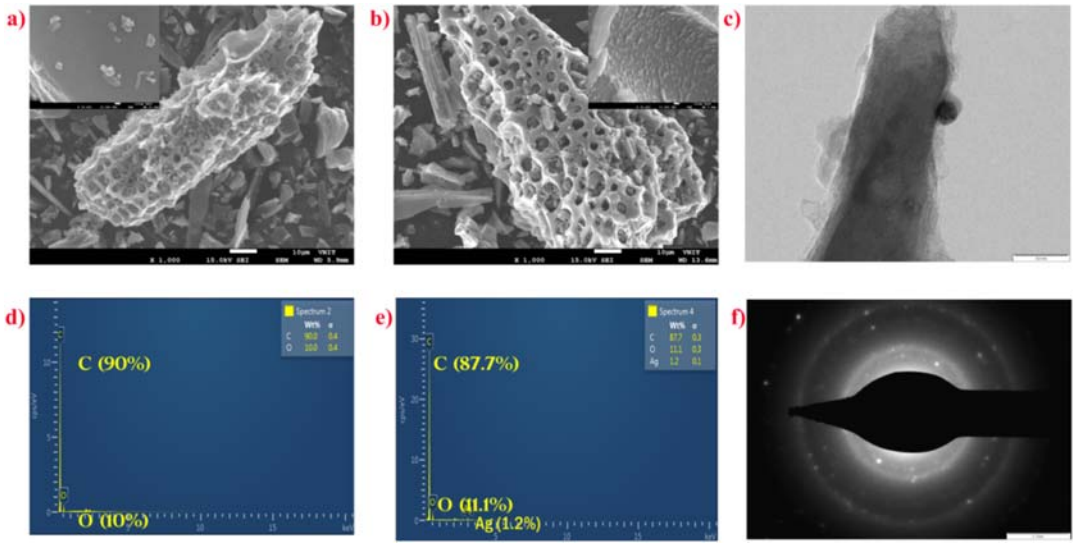

FIGURE 32.2 The electron microscopic studies: (A) FE-SEM images of AC, (B) FE-SEM images of Ag@AC, (C) HR-TEM images of Ag@AC, (D) EDAX spectra of AC (E) EDAX spectra of Ag@AC (F) SAED pattern of Ag@AC.

2.1 FE-SEM and EDX analysis results

Fig. 32.2A and B illustrate the electron microscopic images of AC and Ag@AC. The dark spots on the HR-TEM image of Ag@AC in Fig. 32.2C prove the successful loading of AgNPs on the carbon surface. The Field emission gun scanning electron microscopy images and EDAX data of AC and Ag@AC are given in Fig. 32.2D and E. As seen from Fig. 32.2, both AC and Ag@AC have a rough and porous surface. The image further illustrates that the silver modification of AC has resulted in a more heterogeneous nature and well-developed pores at the Ag@AC surface. This silver is expected to further aid in the removal of pollutants with synergistic action with that of the AC's carbon base.

The confirmation of the presence of silver at the Ag@AC surface may be obtained from its EDAX spectra which show successful Ag loading (1.20%). Other elements carbon (87.70%) and oxygen (11.10%) were also present. It is also observed that the AC surface lacked trace metals but was rich in carbon (90.00%) along with oxygen (10.00%) (Fig. 32.2D). Thus, the EDAX data presented in (Fig. 32.1E) also supports the successful fabrication of AC surface to develop Ag@AC.

2.2 HR-TEM analysis

The Transmission electron microscopy (TEM) image of Ag@AC (Fig. 32.2C) shows that the prepared composite had both lighter and darker regions. The darker regions indicate the presence of denser moieties like metallic structures. In this case, it may represent the denser silver-loaded at the carbon surface while the porous carbon structure is represented by the lighter region seen in the HR-TEM (High-resolution TEM) images. The successful modification of the AC carbon surface with silver may hence be understood.

TABLE 32.3 Surface area and pore characteristics of AC and Ag@AC.

Property	AC	Ag@AC
Surface area	523.45 $m^2 g^{-1}$	855.40 $m^2 g^{-1}$
Pore volume	0.3318 $cm^3 g^{-1}$	0.4773 $cm^3 g^{-1}$
Pore size	35.294 Å	34.174 Å

The selected area electron diffraction, i.e., Selected area diffraction (SAED) data (Fig. 32.2F) suggests the presence of both amorphous and crystalline structures in the Ag@AC. The diffused rings and the bright spots observed in the SAED data represent the amorphous carbon surface and the crystalline loaded silver, respectively. The data suggests that the amorphous carbon embeds silver in its polycrystalline form.

2.3 Surface and surface area analysis

The surface area of the AC greatly influences its adsorption capacity and efficiency. It is generally seen that the AC with the high surface area may have high adsorption capacity for a particular adsorbate. Thus, the surface pore structure and pore distribution analysis of the AC is highly essential. The surface area of the AC and the silver-loaded carbon material were 523.45 $m^2 g^{-1}$ and 855.40 $m^2 g^{-1}$ respectively as observed from Table 32.3. The fabrications of the surface of the AC lead to the increase in surface area which may be attributed to the increased porosity. It is also seen that the pore volume of the Ag@AC had a higher value compared to that of AC with values of 0.3318 $cm^3 g^{-1}$ and 0.4773 $cm^3 g^{-1}$,respectively. The hysteresis loop in the nitrogen adsorption curve indicates that the pores present on both the carbon material have a mesoporous structure (Fig. 32.3A and B). The pore diameter as obtained from the BJH model indicated a decrease in the pore diameter upon modification of AC which may be well understood from the fact that the AgNPs occupied the surface of the AC to form Ag@AC (Fig. 32.3C and D). Hence, it is expected that the carbon composite (Ag@AC) had superior surface properties than the AC. Ag@AC is mesoporous and crystalline, having a very high surface area (855.40 $m^2 g^{-1}$), high thermal stability, and greater porosity, which are very useful in the removal of organic and microbial pollutants in real water.

2.4 XRD analysis results

The XRD data were collected for AC and Ag@AC is presented in Fig. 32.4. The XRD pattern of AC shows two prominent and broader peaks around 24.03° and 44.00° which indicate the amorphous carbon structure of the AC in addition to some sharper peaks. The sharper peaks may be due to the presence of some crystalline structures at the carbon surface. The XRD pattern of Ag@AC (Fig. 32.4A) in comparison to AC showed some new peaks which may indicate the successful fabrication of the AC surface to form Ag@AC. A strong peak at 32.27° may be due to the presence of silver oxide moieties.[55] Also, the weaker and

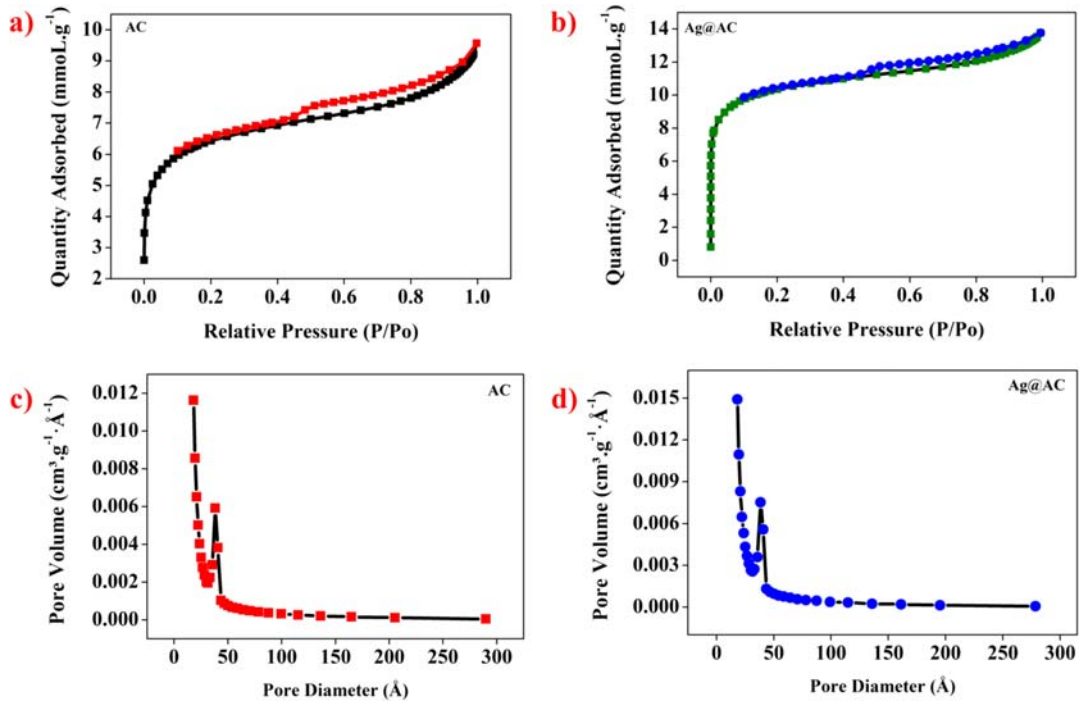

FIGURE 32.3 Surface characteristic analysis: (1) nitrogen adsorption-desorption isotherms (A) AC and (B) Ag@AC; (2) BJH method for the pore size distribution (C) AC (D) AG@AC.

short peaks at 54.85 and 67.65 degrees indicate the presence of Ag_2O at the surface of Ag@AC as indicated by the previously reported work.[55,56] The peaks at 32.27 degrees, 54.85 degrees, and 67.65 degrees represent (111), (220), and (222) planes of cubic Ag_2O. The changes in the two XRD patterns highlight the successful incorporation interaction of silver at the AC surface to form the Ag@AC surface. These changes in the XRD pattern offer qualitative evidence of the deposition of silver over the surface of the AC.

2.5 FT-IR spectra

The FT-IR spectra of AC and Ag@AC (Fig. 32.4B) give information about the chemical composition and its surface functional group characteristics. On loading with silver at the AC surface, some slight changes in the FT-IR spectra were observed as seen in Fig. 32.4B. This may be due to the interaction of silver at the AC surface. Several peaks were observed in the IR spectrum of both AC and Ag@AC. The peaks at 3727.08 cm^{-1} and 3430.17 cm^{-1} represent the free and hydrogen-bonded hydroxyl groups denoting the alcoholic, and phenolic and/or carboxyl functional groups.[57] The peaks around 2882.68 cm^{-1}, 1433 cm^{-1}, and 1345.34 cm^{-1} may be assigned to the absorption by the $-CH_3$ and $-CH_2$ group stretching and bending absorption. The peaks around 1617 cm^{-1} represent the presence of $-C{=}C$ or $-COO$ stretching. The presence of the aromatic group skeletal stretching may be observed at

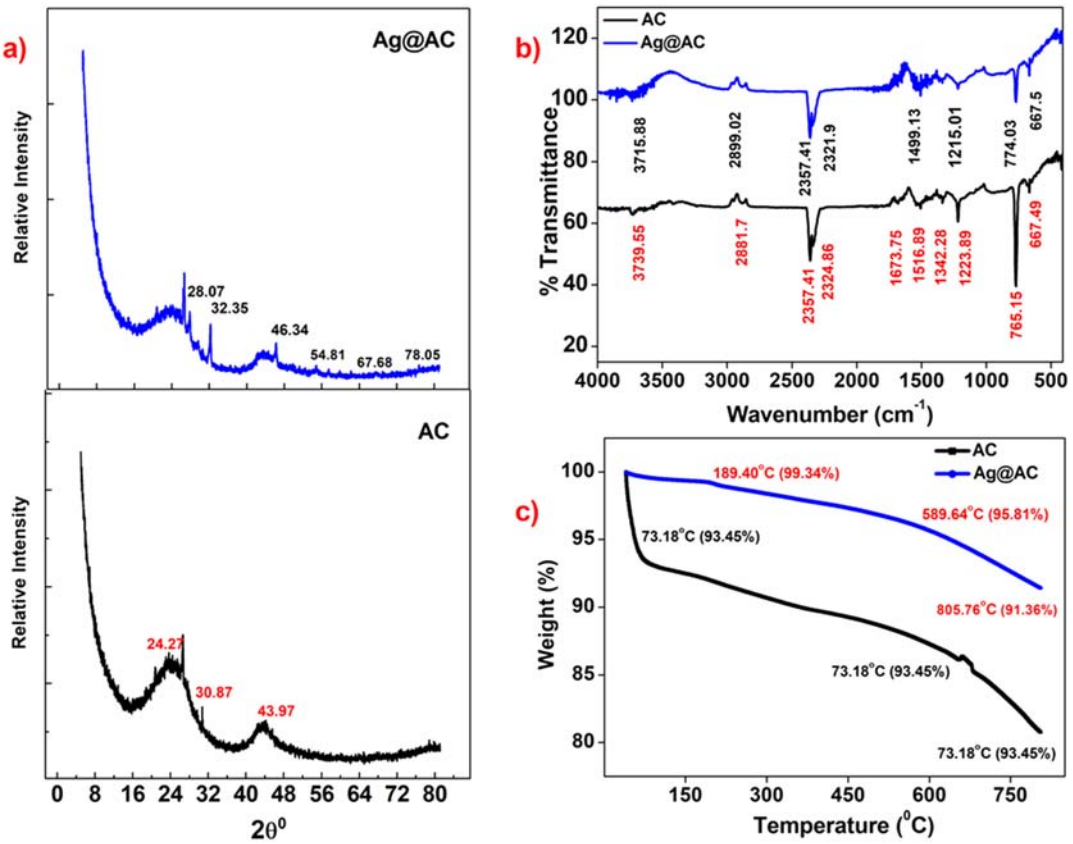

FIGURE 32.4 Characterization results of AC and Ag@AC (A) XRD pattern (B) FTIR spectra, and (C) TG curve of AC and Ag@AC.

around 1514.77 cm^{-1}.[58] Long-chain CH_2 may be inferred from the peaks present around 772.09 cm^{-1} while C—O stretching may be seen at around 1217.8 cm^{-1}. The FT-IR spectra of both the carbons i.e., AC and Ag@AC show the presence of functional groups containing C, H, and O. The minor shifts in the peak position between the two FT-IR spectra were observed, which indicated successful fabrication of the AC surface to form Ag@AC.

2.6 TG-DTA results

The thermal stability of AC and Ag@AC was investigated using TG-DTA. The thermogram is represented in Fig. 32.4C. The TG-DTA analysis demonstrates that the prepared silver-loaded carbon had higher thermal stability than AC, as shown in Fig. 32.4c. From the TG-DTA curve, it was observed that the composite carbon remained stable even at higher temperatures with a comparatively lower loss of the carbon content. The AC thermogram reveals that about 7.8% weight loss at around 115.9°C while 20% of the weight loss at around 800°C was observed. In the case of Ag@AC, at 225.5°C only 1.1% loss was recorded while

8.5% was lost at around 800°C. This reveals the higher thermal stability of Ag@AC than the pristine carbon AC. Thus, it may be observed that the thermal stability of the prepared material was enhanced to some extent in the case of Ag@AC compared to AC itself.

3. Adsorption studies

The batch study comprised of investigating the role of Ag@AC in the removal of several cationic and anionic dyes and one particular and common pharmaceutical compound from their aqueous solution. The experiment involved contacting 20 mL of 50 mg L^{-1} initial concentration solutions with varying predetermined dosage (1 g L^{-1}–15 g L^{-1}) of AC as well as Ag@AC. The adsorption was carried out in 150 mL screw-capped conical flasks placed on a rotating surface shaker incubator at 37.4°C at 100 rpm for a total contact time of 5h. Kinetics of removal for target the pollutants were also investigated by contacting an optimized dose of 300 mg of Ag@AC for the varying periods (0–300 min) at 37.4°C under continuous agitation at 100 rpm.

After completion of the experiment, the carbon-free supernatant was collected by filtering out the carbon through the Whatman filter paper. The residual dye concentration in the filtrate was determined by a UV-visible spectrophotometer at their respective wavelengths of maximum absorbance (λ_{max}) values. Later, the efficiency of Ag@AC was recorded in the form of the percentage removal and the adsorption capacity of the adsorbents. The calculations were done using Eqs. (32.1) and (32.2), respectively.

$$\%\ \text{Removal} = (C_0 - C_e) \times 100/C_0 \tag{32.1}$$

$$q_e = (C_0 - C_e) \times V/w \tag{32.2}$$

Where, C_0 and C_e are the concentration of dye in mg L^{-1} before and after adsorption, V is the volume of dye solution in L and w is the weight of the adsorbent in g, respectively.

4. Adsorption isotherm studies

The adsorption isotherm plot explains the distribution of concentration of adsorbate molecules between both the phases (bulk and the adsorbent surface) at a constant temperature. They may yield several parameters that inform about the pollutant-carbon surface interactions. Langmuir, Freundlich, and Temkin adsorption isotherms were applied to understand the surface-pollutants interactions involved in the adsorptive removal of the pollutants at the Ag@AC surface, and the data is represented in Table 32.4.

4.1 Langmuir adsorption isotherm

Langmuir adsorption isotherm usually explains the monolayer adsorption of adsorbate molecules at the surface of the adsorbent, which is assumed to be a homogenous surface

in nature with a finite number of equivalent energy sites. The isotherm fails to recognize the importance of other interactions, e.g., those established between the adsorbed neighboring molecules and diffusion of the molecules at the adsorbent surface. It is well known that the Langmuir model generally explains the chemisorption interactions and is beneficial to express the maximum monolayer capacity (q_{max}) of an adsorbent for a particular adsorbate. The two Langmuir isotherm constants K_L (Langmuir constant in L mg^{-1}) and q_{max} (maximum monolayer adsorption capacity per unit mass of adsorbent) may be derived from the values of slope and intercept obtained from plotting the linear equation given in Eq. (32.3). The value of K_L yields information about the favorability of the adsorption process through the value of the separation factor (R_L), which is calculated using Eq. (32.4)

$$\frac{C_e}{q_e} = \frac{1}{K.q_{max}} + \frac{C_e}{q_{max}} \tag{32.3}$$

$$R_L = \frac{1}{1 + K_L C_0} \tag{32.4}$$

where q_e is the adsorption capacity in mg g^{-1} at equilibrium, and C_0 and C_e are the concentrations of adsorbates in mg L^{-1} initially and at equilibrium. R_L is the separation factor and its values ranging between 0 and 1 indicate a favorable adsorption process. In the present study, R_L values were found to be within this range indicating a favorable adsorption process. The R_L value is an important factor that yields information about the feasibility of the adsorption process. The adsorption process may be favorable ($0 < R_L <$), unfavorable ($R_L > 1$), linear ($R_L = 1$), or irreversible ($R_L = 0$). The regression coefficient values show that the Langmuir adsorption isotherm shows the best fit to explain the adsorption of RR dyes at the AC and Ag@AC carbon surface. The calculated q_{max} values for RR at the Ag@AC surface are given in Table 32.4 and are found to be close to the experimental value of 24 mg g^{-1}. This indicates a monolayer formation of RR at the adsorbent surface, which may be understood from the high molecular weight and huge molecular structure. The adsorption of other molecules on the Ag@AC surface had a poor value of the regression coefficient.

4.2 Freundlich adsorption isotherm

Freundlich adsorption isotherm assumes the heterogeneous surface of the adsorbent resulting from the difference in the energies of the active sites available for the adsorbate interaction. This results in the different affinities of the sites toward the adsorbate molecules. The model also considers the weak physical interactions between the neighboring adsorbate molecules, which may lead to multilayer formation. The linearized Freundlich adsorption isotherm is indicated in Eq. (32.5)

$$\ln q_e = \ln K_F + \frac{1}{n} \ln C_e \tag{32.5}$$

where, K_F (mg g^{-1} (L $mg^{-1})^{1/n}$) is the Freundlich constant and n is a dimensionless quantity known as the adsorption intensity. The value of 'n' indicates the feasibility of the process of

adsorption in the specified adsorption system, where $0 < 1/n < 1$ shows feasible adsorption. The $n > 1$ value refers to the unfeasible process of adsorption. The values of $1/n$ in the cases of RR-120, RB-04, and Rh-B indicates a favorable interaction at the Ag@AC surface, while the mechanism behind the Ibu surface interaction remains unclear, which is also clear from their R^2 (coefficient of determination) values. the Freundlich adsorption isotherm holds good in the case of RB-4 and Rh-B removal by the Ag@AC (Table 32.4).

4.3 Temkin adsorption isotherm

Temkin adsorption isotherm holds well when solutes from solutions have an intermediate concentration (i.e., excluding solutions with low and high concentrations) adhere to a heterogeneous surface. The model takes into consideration the participation of the adsorbate and adsorbent interactions in the adsorption process. The model assumes a linear decrease in the heat of adsorption (rather than the exponential decrease) of all molecules present in the layer, with increasing coverage. The model also represents a uniform distribution of binding energies up to a certain maximum binding energy.[59] The linear equation of the Temkin adsorption isotherm is given in Eq. (32.6)

$$q_e = B \ln K_T + B \ln C_e \tag{32.6}$$

where K_T in L g^{-1} is the Temkin isotherm constant and B is constant and is indicated in Eq. (32.7).

$$B = \frac{RT}{b_T} \tag{32.7}$$

where R is the gas constant (8.314 J mol^{-1} K^{-1}) and T is the temperature in Kelvin, and b_T in J mol^{-1} is a constant associated with the heat of adsorption. The positive values of b represent the endothermic adsorption process, while negative values indicate exothermic interactions. The values of b_T also indicate the types of interactions (physisorption, ion-exchange, and chemisorption) governing the adsorption process.

From Table 32.4, the positive values of b_T indicate endothermic reactions involved in the removal of all the pollutants at the Ag@AC surfaces. From the R^2-values, it may be seen that the Temkin adsorption isotherm holds good in explaining the Ibu removal at the Ag@AC surface.

5. Removal of cationic dye

The adsorbent dosage affects the adsorption process by increasing the adsorption sites. Hence, it is essential to study the effect of the increasing adsorbent dosage on the adsorption behavior of the material. The removal of Rh-B with the increasing dosage of Ag@AC was evaluated and results are given in Fig. 32.6. It was observed that ~99% removal was achieved even in cases of low dosage (~2 g L^{-1}). The adsorption isotherm revealed the type II nature of the adsorption where the adsorbate occupies the mesoporous sites.

TABLE 32.4 Parameters of the adsorption isotherm for the different targets at the surface of Ag@AC.

		Adsorption isotherm constants			
		RR-120	**RB-4**	**Rh-B**	**Ibu**
Experimental outcomes	%Removal				
	Dosage				
	q_e				
Langmuir	R^2	0.996	0.797	0.713	0.03
	q_{max} (mg g^{-1})	28.52	32.87	29.26	−35.04
	K_L (g L^{-1})	0.734	0.26	13.15	−0.12
	R_L	0.027	0.072	0.002	−0.20
Freundlich	R^2	0.807	0.965	0.951	0.746
	K_F ((mg g^{-1}) (L $mg^{-1})^{1/n}$)	10.19	7.14	48.83	4.28
	$1/n$	0.422	0.55	0.51	1.50
Temkin	R^2	0.862	0.850	0.749	0.910
	K_T (L g^{-1})	5.66	2.68	51.03	0.002
	B	5.05	5.93	4.74	0.91
	b_T (J. mol^{-1})	509.94	434.52	543.82	2832.77

The increase in contact time allows more interaction between the adsorbate and the adsorbent surface, thus affecting the adsorption performance of an adsorbent. The carbon-free filtrate collected after filtration on completion of the specified time interval of shaking was analyzed spectrophotometrically to calculate the residual dye concentration. A kinetic study on the removal of Rh-B dye was found to be instantaneous and fast, where maximum adsorption was obtained in the initial 5 min exposure. Hence, the rate of removal was found to be constant at the Ag@AC surface at different periods of contact between the adsorbate and the adsorbent.

6. Removal of anionic dyes

Ag@AC also demonstrated a good decolorizing property against the group of dyes belonging to the anionic and refractory reactive group of dyes. The effect of increasing adsorbent dosage in the removal of two reactive dyes, i.e., RR-120 and RB-4 showed that with

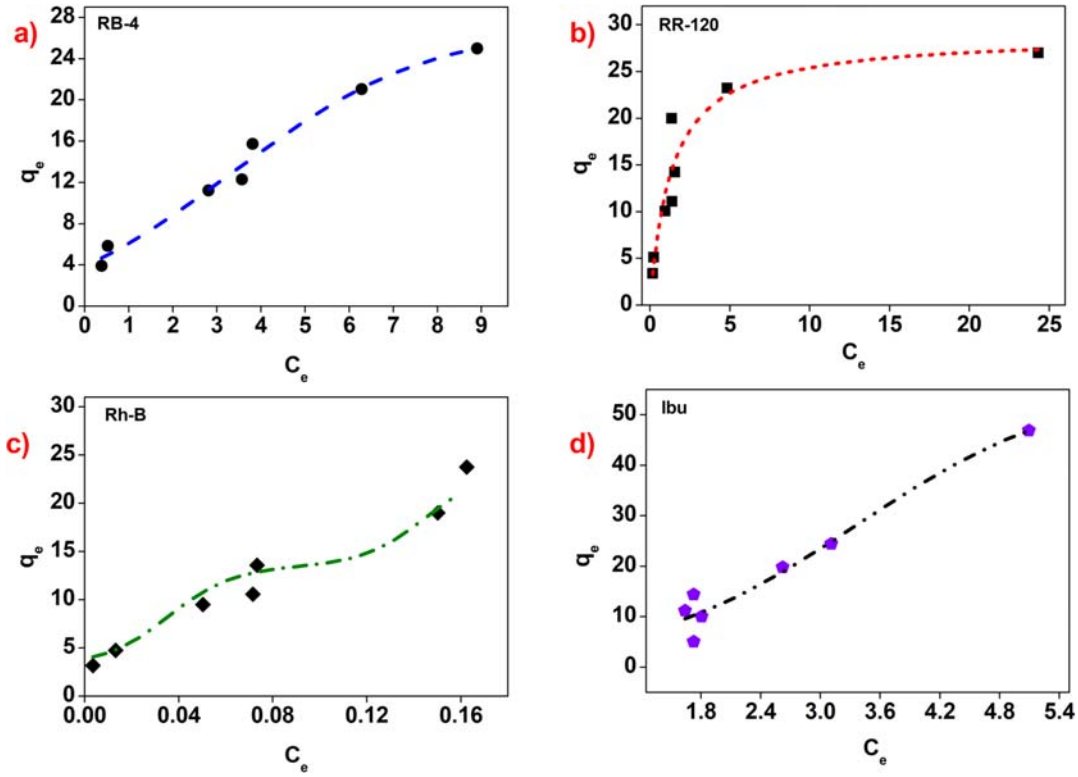

FIGURE 32.5 Adsorption isotherm plots for the adsorptive removal of pollutants at the Ag@AC surface.

increased dosage, there was an increase in the percentage removal of both the pollutants by Ag@AC. At lower adsorbent dosage (2–3.5 g L^{-1}) Ag@AC could remove about 93%–98% and 83%–93% of the RR-120 and RB-4 dyes, respectively. While at higher dosage the performance of both dyes was more or less constant. This may be due to the surplus availability of adsorption sites at a higher dosage for the incoming adsorbates. The maximum removal of ~99%–100% of RR-120 and RB-4 dye was achieved at a 15 g L^{-1} dosage of Ag@AC. The maximum adsorption capacity (q_e) was found to be 23.24 mg g^{-1} and 25 mg g^{-1}, respectively for RR-120 and RB-4 dye (Table 32.5).

7. Removal of ibuprofen

The adsorption study on the surface interaction of Ag@AC on the removal of Ibu showed that Ag@AC could effectively remove the Ibu molecules from the solution. About 96% removal of Ibu was achieved at a dosage of 3.5 g L^{-1}. It was observed that with increasing dosage the percentage removal of Ibu was slightly decreased, which may be due to the weaker interactions prevailing between the adsorbate molecules and the adsorbent. The adsorption isotherm pattern (Fig. 32.5) also supports this speculation by indicating multilayer

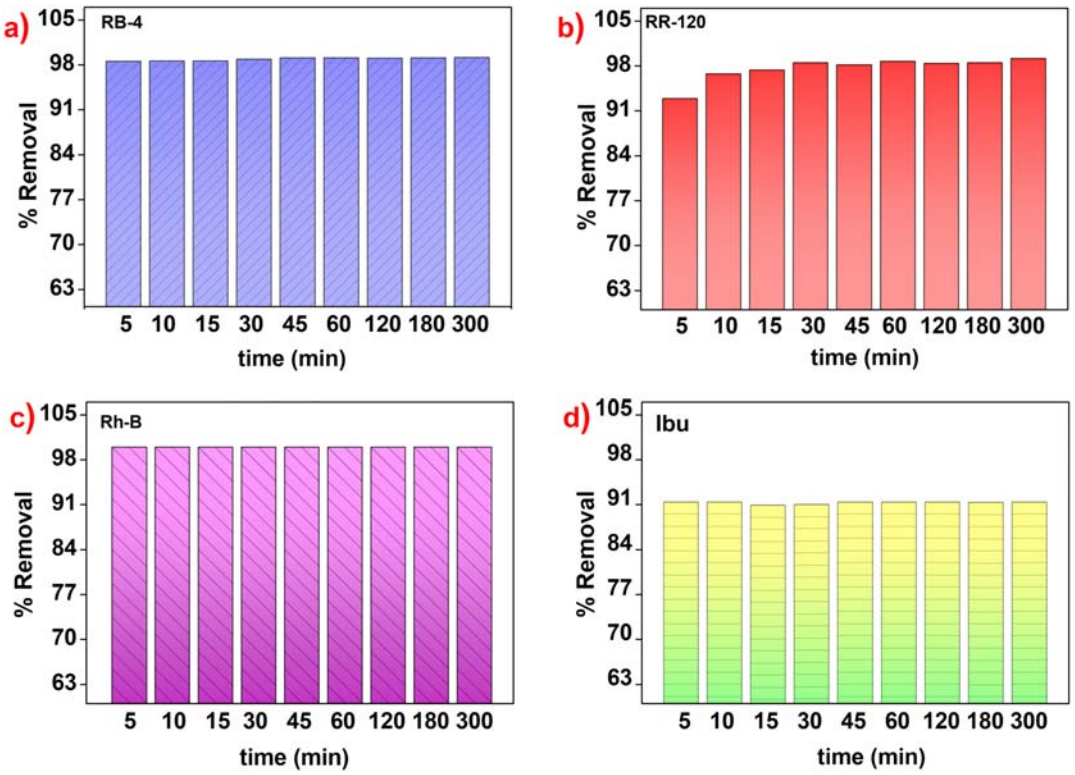

FIGURE 32.6 Application of Ag@AC in removal dyes and PCPPs from aqueous solutions.

TABLE 32.5 Comparative adsorption capacities of commercial adsorbent and Ag@AC.

	Adsorption capacity (mg g^{-1})	
Target pollutants	**AC**	**Ag@AC**
RR	19	25.5
RB	22	24.6
Rh-B	47	47
Ibu	–	47

formation at the Ag@AC surface. The adherence of the layer of Ibu formed at a distance from the surface may be due to weak physical interactions guided by the concentration gradient of Ibu from bulk to the surface. Hence, at a higher dosage, some reverse processes might be prevailing.

8. Summary

This chapter reports the development of a multifunctional (Ag@AC), which was prepared by fabrication of the surface of the commercially available AC with starch-stabilized AgNPs. The successful loading along with the physical and chemical properties of Ag@AC were determined from various sophisticated characterization techniques as discussed in the chapter. Ag@AC exhibited improved physical properties such as an increased surface area with well-developed pores and better temperature stability than the nascent carbon. The HR-TEM images reveal the successful deposition of the dense, metallic AgNPs on the amorphous and porous carbon substrate. About a 63.4% increase in the surface area (m^2g^{-1}) was observed on the fabrication of the nascent AC to form Ag@AC. The enhanced surface properties of Ag@AC provided more efficient binding sites for the incoming pollutants, as exhibited from the increased pollutant removal performance. The multifunctional nature of Ag@AC can be successfully proposed by the experimental evidence of the removal of organic pollutants like dyes and pharmaceuticals (in batch mode) and literature that proposes the antimicrobial and other unique properties of AgNPs and nanocomposites. The future work may be directed toward probing this developed material toward the disinfection of water, adding further to its multifunctional properties. The cationic dye RhB, anionic dyes RR-120, and RB-4 and a pharmaceutical Ibu were selected for the present work. The adsorptive removal studies were undertaken and a good removal efficiency with a fast rate of adsorption of all the three dyes and Ibu was observed. Around 2 g L^{-1}, 3.5 g $L^{-1,}$ and 15 g L^{-1} of Ag@AC were required to achieve maximum removal of cationic dyes, anionic dyes, and pharmaceutical target compounds. The adsorption was instantaneous for the Rh-B and Ibu removal requiring nearly 5 min exposure to remove 99% and 91.1% of the respective initial concentration. The bulky reactive dyes required 30 min exposure time to achieve maximum removal of both RR-120 and RB-4 dyes. Thus, Ag@AC could effectively remove organic pollutants like dyes and pharmaceuticals through a simple process of adsorption. The probable mechanism, rate, and effect of experimental conditions like dosage and contact time on the efficiency of Ag@AC surface were studied. The discussion satisfactorily indicates the multifunctional nature of the adsorbent prepared by loading silver on the activated carbon, Ag@AC. Hence, silver loading on AC provides a suitable route to prepare multifunctional adsorbent materials for effective water purification. The need for the development of multifunctional adsorbents with the potential for targeting multiple pollutants is highly demanding in view of environmental remediation.

Acknowledgments

The authors would like to acknowledge Sophisticated Analytical Instrumentation Facility (SAIF) center, Panjab University, SAIF IIT Madras, SAIF STIC, Cochin, for various material characterization support and Zakiullah Zaidi for his technical guidance. We would also like to thank the 'Characterization facility', Department of Chemistry, VNIT, Nagpur, under DST-FIST (Sanction No. SR/FST/CSI-279/2016(C)). Lastly, the work was partly funded by the Department of Science & Technology—Science & Engineering Research Board (DST-SERB) (Grant no. ECR/2017/000221) Government of India.

References

1. Deniz F. Adsorption properties of low-cost biomaterial derived from Prunus amygdalus L. for dye removal from water. *Sci World J* 2013;**2013**. https://doi.org/10.1155/2013/961671.
2. Ebrahimian Pirbazari A, Saberikhah E, Badrouh M, Emami MS. Alkali treated foumanat tea waste as an efficient adsorbent for methylene blue adsorption from aqueous solution. *Water Resour Ind* 2014;**6**:64–80. https://doi.org/10.1016/j.wri.2014.07.003.
3. Wang J, Zhu H, Hurren C, Zhao J, Pakdel E, Li Z, Wang X. Degradation of organic dyes by P25-reduced graphene oxide: influence of inorganic salts and surfactants. *J Environ Chem Eng* 2015;**3**(3):1437–43. https://doi.org/10.1016/j.jece.2015.05.008.
4. Zhao YG, Li XP, Yao SS, Zhan PP, Liu JC, Xu CP, Lu YY, Chen XH, Jin MC. Fast throughput determination of 21 allergenic disperse dyes from river water using reusable three-dimensional interconnected magnetic chemically modified graphene oxide followed by liquid chromatography-tandem quadrupole mass spectrometry. *J Chromatogr A* 2016;**1431**:36–46. https://doi.org/10.1016/j.chroma.2015.12.089.
5. Constantin M, Asmarandei I, Harabagiu V, Ghimici L, Ascenzi P, Fundueanu G. Removal of anionic dyes from aqueous solutions by an ion-exchanger based on pullulan microspheres. *Carbohydr Polym* 2013;**91**(1):74–84. https://doi.org/10.1016/j.carbpol.2012.08.005.
6. Amin MT, Alazba AA, Shafiq M. Adsorptive removal of reactive black 5 from wastewater using bentonite clay: isotherms, kinetics and thermodynamics. *Sustain Times* 2015;**7**(11):15302–18. https://doi.org/10.3390/su71115302.
7. González JA, Villanueva ME, Piehl LL, Copello GJ. Development of a chitin/graphene oxide hybrid composite for the removal of pollutant dyes: adsorption and desorption study. *Chem Eng J* 2015;**280**:41–8. https://doi.org/10.1016/j.cej.2015.05.112.
8. Mahida VP, Patel MP. Removal of some most hazardous cationic dyes using novel poly (NIPAAm/AA/N-allylisatin) nanohydrogel. *Arab J Chem* 2016;**9**(3):430–42. https://doi.org/10.1016/j.arabjc.2014.05.016.
9. Debnath S, Kitinya J, Onyango MS. Removal of Congo red from aqueous solution by two variants of calcium and iron based mixed oxide nano-particle agglomerates. *J Ind Eng Chem* 2014;**20**(4):2119–29. https://doi.org/10.1016/j.jiec.2013.09.041.
10. Han Y, Li H, Liu M, Sang Y, Liang C, Chen J. Purification treatment of dyes wastewater with a novel microelectrolysis reactor. *Separ Purif Technol* 2016;**170**:241–7. https://doi.org/10.1016/j.seppur.2016.06.058.
11. Devi TB, Mohanta D, Ahmaruzzaman M. Biomass derived activated carbon loaded silver nanoparticles: an effective nanocomposites for enhanced solar photocatalysis and antimicrobial activities. *J Ind Eng Chem* 2019;**76**:160–72. https://doi.org/10.1016/j.jiec.2019.03.032.
12. Mestre AS, Pires J, Nogueira JMF, Carvalho AP. Activated carbons for the adsorption of ibuprofen. *Carbon N Y* 2007;**45**(10):1979–88. https://doi.org/10.1016/j.carbon.2007.06.005.
13. Salem NA, Yakoot SM. Non-steroidal anti-inflammatory drug, ibuprofen adsorption using rice straw based biochar. *Int J Pharmacol* 2016;**12**(7):729–36. https://doi.org/10.3923/ijp.2016.729.736.
14. Delgado LF, Charles P, Glucina K, Morlay C. Adsorption of ibuprofen and atenolol at trace concentration on activated carbon. *Separ Sci Technol* 2015;**50**(10):1487–96. https://doi.org/10.1080/01496395.2014.975360.
15. Rajabi HR, Arjmand H, Kazemdehdashti H, Farsi M. A comparison investigation on photocatalytic activity performance and adsorption efficiency for the removal of cationic dye: quantum dots vs. Magnetic nanoparticles. *J Environ Chem Eng* 2016;**4**(3):2830–40. https://doi.org/10.1016/j.jece.2016.05.029.
16. Mittal A, Mittal J, Malviya A, Kaur D, Gupta VK. Adsorption of hazardous dye crystal violet from wastewater by waste materials. *J Colloid Interface Sci* 2010;**343**(2):463–73. https://doi.org/10.1016/j.jcis.2009.11.060.
17. Jauris IM, Fagan SB, Adebayo MA, Machado FM. Adsorption of acridine orange and methylene blue synthetic dyes and anthracene on single wall carbon nanotubes: a first principle approach. *Comput Theor Chem* 2016;**1076**:42–50. https://doi.org/10.1016/j.comptc.2015.11.021.
18. Demarchi CA, Chahm T, Martins BA, Debrassi A, Nedelko N, Ślawska-Waniewska A, Dłuzewski P, Dynowska E, Greneche JM, Rodrigues CA. Adsorption of reactive red dye (RR-120) on nanoadsorbent O-Carboxymethylchitosan/γ-Fe2O3: kinetic, equilibrium and factorial design studies. *RSC Adv* 2016;**6**(41):35058–70. https://doi.org/10.1039/c6ra04249j.
19. Tzvetkov G, Mihaylova S, Stoitchkova K, Tzvetkov P, Spassov T. Mechanochemical and chemical activation of lignocellulosic material to prepare powdered activated carbons for adsorption applications. *Powder Technol* 2016;**299**:41–50. https://doi.org/10.1016/j.powtec.2016.05.033.

20. Tan KB, Vakili M, Horri BA, Poh PE, Abdullah AZ, Salamatinia B. Adsorption of dyes by nanomaterials: recent developments and adsorption mechanisms. *Separ Purif Technol* 2015:229–42. https://doi.org/10.1016/j.seppur.2015.07.009.
21. Saharan VK, Badve MP, Pandit AB. Degradation of reactive red 120 dye using hydrodynamic cavitation. *Chem Eng J* 2011;**178**:100–7. https://doi.org/10.1016/j.cej.2011.10.018.
22. Badve MP, Bhagat MN, Pandit AB. Microbial disinfection of seawater using hydrodynamic cavitation. *Separ Purif Technol* 2015;**151**:31–8. https://doi.org/10.1016/j.seppur.2015.07.020.
23. Song Y, Jiang H, Bi H, Zhong G, Chen J, Wu Y, Wei W. Multifunctional bismuth oxychloride/mesoporous silica composites for photocatalysis, antibacterial test, and simultaneous stripping analysis of heavy metals. *ACS Omega* 2018;**3**(1):973–81. https://doi.org/10.1021/acsomega.7b01590.
24. Abadikhah H, Naderi Kalali E, Khodi S, Xu X, Agathopoulos S. Multifunctional thin-film nanofiltration membrane incorporated with reduced graphene oxide@TiO2@Ag nanocomposites for high desalination performance, dye retention, and antibacterial properties. *ACS Appl Mater Interfaces* 2019;**11**(26):23535–45. https://doi.org/10.1021/acsami.9b03557.
25. Shi Z, Neoh KG, Kang ET. Antibacterial and adsorption characteristics of activated carbon functionalized with quaternary ammonium moieties. *Ind Eng Chem Res* 2007;**46**(2):439–45. https://doi.org/10.1021/ie0608096.
26. Chen H, Yang Y, Wei J, Xu J, Li J, Wang P, Xu J, Han Y, Jin H, Jin D, Peng X, Hong B, Ge H, Wang X. Cobalt ferrites/activated carbon: synthesis, magnetic separation and catalysis for potassium hydrogen persulfate. *Mater Sci Eng B Solid-State Mater Adv Technol* 2019;**249**(September):114420. https://doi.org/10.1016/j.mseb.2019.114420.
27. Geethapriya D, Barathan S. Optimisation of the conditions involved in the preparation of activated carbon from mosambi peel and the evaluation of antibacterial activity of nano-sized activated carbon, silver nano-particles, and silver impregnated activated carbon. *Int J ChemTech Res* 2017;**10**(1):540–9.
28. Karthik C, Radha KV. Silver nanoparticle loaded activated carbon: an escalated nanocomposite with antimicrobial property. *Orient J Chem* 2016;**32**(1):735–41. https://doi.org/10.13005/ojc/320182.
29. Ki YY, Jeong HB, Chul WP, Hwang J. Antimicrobial effect of silver particles on bacterial contamination of activated carbon fibers. *Environ Sci Technol* 2008;**42**(4):1251–5. https://doi.org/10.1021/es0720199.
30. Louis MR, Sorokhaibam LG, Chaudhary SK, Bundale S. Silver-loaded biomass (Delonix regia) with anti-bacterial properties as porous carbon composite towards comprehensive water purification. *Int J Environ Sci Technol* 2020;**17**(4):2415–32. https://doi.org/10.1007/s13762-019-02528-8.
31. Ficai A, Grumezescu AM. In: Ficai A, Grumezescu AM, editors. *Nanostructures for antimicrobial therapy: nanostructures in therapeutic medicine series*. Elsevier; 2017.
32. Khan ZUH, Khan A, Shah A, Wan P, Chen Y, Khan GM, Khan AU, Tahir K, Muhammad N, Khan HU. Enhanced photocatalytic and electrocatalytic applications of green synthesized silver nanoparticles. *J Mol Liq* 2016;**220**:248–57. https://doi.org/10.1016/j.molliq.2016.04.082.
33. Keshari AK, Srivastava R, Singh P, Yadav VB, Nath G. Antioxidant and antibacterial activity of silver nanoparticles synthesized by cestrum nocturnum. *J Ayurveda Integr Med* 2018;**1–8**. https://doi.org/10.1016/j.jaim.2017.11.003.
34. Ismail M, Khan MI, Khan SB, Akhtar K, Khan MA, Asiri AM. Catalytic reduction of picric acid, nitrophenols and organic azo dyes via green synthesized plant supported Ag nanoparticles. *J Mol Liq* 2018;**268**:87–101. https://doi.org/10.1016/j.molliq.2018.07.030.
35. Naeem H, Ajmal M, Beenish R, Tul S, Farooq M, Siddiq M. Facile synthesis of graphene oxide – silver nanocomposite for decontamination of water from multiple pollutants by adsorption , catalysis and antibacterial activity. *J Environ Manag* 2019;**230**:199–211. https://doi.org/10.1016/j.jenvman.2018.09.061.
36. Louis MR, Sorokhaibama LG, Bhandari VM, Bundale S. Multifunctional activated carbon with antimicrobial property derived from delonix regia biomaterial for treatment of wastewater. *J Environ Chem Eng* 2018;**6**(1):169–81. https://doi.org/10.1016/j.jece.2017.11.056.
37. AbdEl-Salam AH, Ewais HA, Basaleh AS. Silver nanoparticles immobilised on the activated carbon as efficient adsorbent for removal of crystal violet dye from aqueous solutions. A kinetic study. *J Mol Liq* 2017;**248**:833–41. https://doi.org/10.1016/j.molliq.2017.10.109.
38. Chen Q, Wu Q. Preparation of carbon microspheres decorated with silver nanoparticles and their ability to remove dyes from aqueous solution. *J Hazard Mater* 2015;**283**:193–201. https://doi.org/10.1016/j.jhazmat.2014.09.024.

39. Ghaedi M, Heidarpour S, Nasiri Kokhdan S, Sahraie R, Daneshfar A, Brazesh B. Comparison of silver and palladium nanoparticles loaded on activated carbon for efficient removal of methylene blue: kinetic and isotherm study of removal process. *Powder Technol* 2012;**228**:18–25. https://doi.org/10.1016/j.powtec.2012.04.030.
40. Ghaedi M, Sadeghian B, Pebdani AA, Sahraei R, Daneshfar A, Duran C. Kinetics, thermodynamics and equilibrium evaluation of direct yellow 12 removal by adsorption onto silver nanoparticles loaded activated carbon. *Chem Eng J* 2012;**187**:133–41. https://doi.org/10.1016/j.cej.2012.01.111.
41. Ghaedi M, Biyareh MN, Kokhdan SN, Shamsaldini S, Sahraei R, Daneshfar A, Shahriyar S. Comparison of the efficiency of palladium and silver nanoparticles loaded on activated carbon and zinc oxide nanorods loaded on activated carbon as new adsorbents for removal of Congo red from aqueous solution: kinetic and isotherm study. *Mater Sci Eng C* 2012;**32**(4):725–34. https://doi.org/10.1016/j.msec.2012.01.015.
42. Van HT, Nguyen TMP, Thao VT, Vu XH, Nguyen TV, Nguyen LH. Applying activated carbon derived from coconut shell loaded by silver nanoparticles to remove methylene blue in aqueous solution. *Water Air Soil Pollut* 2018;**229**(12). https://doi.org/10.1007/s11270-018-4043-3.
43. Thamilselvi V, Radha KV. Silver nanoparticle loaded corncob adsorbent for effluent treatment. *J Environ Chem Eng* 2017;**5**(2):1843–54. https://doi.org/10.1016/j.jece.2017.03.020.
44. Pal J, Deb MK. Efficient adsorption of Congo red dye from aqueous solution using green synthesized coinage nanoparticles coated activated carbon beads. *Appl Nanosci* 2014;**4**(8):967–78. https://doi.org/10.1007/s13204-013-0277-y.
45. Ravanan M, Ghaedi M, Ansari A, Taghizadeh F, Elhamifar D. Comparison of the efficiency of Cu and silver nanoparticle loaded on supports for the removal of eosin y from aqueous solution: kinetic and isotherm study. *Spectrochim Acta Part A Mol Biomol Spectrosc* 2014;**123**:467–72. https://doi.org/10.1016/j.saa.2013.12.049.
46. Nekouei F, Kargarzadeh H, Nekouei S, Keshtpour F, Makhlouf ASH. Novel, facile, and fast technique for synthesis of AgCl nanorods loaded on activated carbon for removal of methylene blue dye. *Process Saf Environ Protect* 2016;**103**:212–26. https://doi.org/10.1016/j.psep.2016.07.010.
47. Ghaedi M, Roosta M, Ghaedi AM, Ostovan A, Tyagi I, Agarwal S, Gupta VK. Removal of methylene blue by silver nanoparticles loaded on activated carbon by an ultrasound-assisted device: optimization by experimental design methodology. *Res Chem Intermed* 2018;**44**(5):2929–50. https://doi.org/10.1007/s11164-015-2285-x.
48. Ghaedi M, Ghayedi M, Kokhdan SN, Sahraei R, Daneshfar A. Palladium, silver, and zinc oxide nanoparticles loaded on activated carbon as adsorbent for removal of bromophenol red from aqueous solution. *J Ind Eng Chem* 2013;**19**(4):1209–17. https://doi.org/10.1016/j.jiec.2012.12.020.
49. Yao L, Zhang L, Wang R, Chou S, Dong ZL. A new integrated approach for dye removal from wastewater by polyoxometalates functionalized membranes. *J Hazard Mater* 2016;**301**:462–70. https://doi.org/10.1016/j.jhazmat.2015.09.027.
50. Huang Z, Wu P, Gong B, Yang S, Li H, Zhu Z, Cui L. Preservation of glutamic acid-iron chelate into montmorillonite to efficiently degrade reactive blue 19 in a fenton system under sunlight irradiation at neutral PH. *Appl Surf Sci* 2016;**370**:209–17. https://doi.org/10.1016/j.apsusc.2016.02.126.
51. Gogate PR, Pandit AB. A review of imperative technologies for wastewater treatment I: oxidation technologies at ambient conditions. *Adv Environ Res* 2004;**8**(3–4):501–51. https://doi.org/10.1016/S1093-0191(03)00032-7.
52. Ranc B, Faure P, Croze V, Simonnot MO. Selection of oxidant doses for in situ chemical oxidation of soils contaminated by polycyclic aromatic hydrocarbons (PAHs): a review. *J Hazard Mater* 2016:280–97. https://doi.org/10.1016/j.jhazmat.2016.03.068.
53. Michael I, Achilleos A, Lambropoulou D, Torrens VO, Pérez S, Petrović M, Barceló D, Fatta-Kassinos D. Proposed transformation pathway and evolution profile of diclofenac and ibuprofen transformation products during (sono)photocatalysis. *Appl Catal B Environ* 2014;**147**:1015–27. https://doi.org/10.1016/j.apcatb.2013.10.035.
54. Madhavan J, Grieser F, Ashokkumar M. Combined advanced oxidation processes for the synergistic degradation of ibuprofen in aqueous environments. *J Hazard Mater* 2010;**178**(1–3):202–8. https://doi.org/10.1016/j.jhazmat.2010.01.064.
55. Reddy PN, Reddy MHP, Pierson JF, Uthanna S. Characterization of silver oxide films formed by reactive RF sputtering at different substrate temperatures. *ISRN Opt* 2014:1–7. https://doi.org/10.1155/2014/684317.
56. Kim MJ, Kim S, Park H, Huh YD. Morphological evolution of Ag2O microstructures from cubes to octapods and their antibacterial activities. *Bull Kor Chem Soc* 2011;**32**(10):3793–5. https://doi.org/10.5012/bkcs.2011.32.10.3793.

57. Puchana-Rosero MJ, Adebayo MA, Lima EC, Machado FM, Thue PS, Vaghetti JCP, Umpierres CS, Gutterres M. Microwave-assisted activated carbon obtained from the sludge of tannery-treatment effluent plant for removal of leather dyes. *Coll Surfaces A Physicochem Eng Asp* 2016;**504**:105–15. https://doi.org/10.1016/j.colsurfa.2016.05.059.
58. Sepúlveda LA, Cuevas FA, Contreras EG. Valorization of agricultural wastes as dye adsorbents: characterization and adsorption isotherms. *Environ Technol (United Kingdom)* 2015;**36**(15):1913–23. https://doi.org/10.1080/09593330.2015.1016119.
59. Moradi O, Maleki MS. Removal of COD from dairy wastewater by MWCNTs: adsorption isotherm modeling. *Fullerenes Nanotub Carbon Nanostruct* 2013;**21**(10):836–48. https://doi.org/10.1080/1536383X.2011.613547.

Further reading

1. Ficai A, Grumezescu AM. In: Ficai A, Grumezescu AM, editors. *Nanostructures for antimicrobial therapy: nanostructures in therapeutic medicine series*. Elsevier; 2017.

Index

Note: Page numbers followed by "*f*" indicate figures and "*t*" indicate tables.

B

C

D

E

F

G

H

N

O

T

APPLICATIONS OF MULTIFUNCTIONAL NANOMATERIALS

Edited by Sabu Thomas, Nandakumar Kalarikkal, and Ann Rose Abraham

Applications of Multifunctional Nanomaterials showcases the major applications of highly promising nanosystems that are currently evolving as next-generation nanobots, memory or energy devices, or even nanocarriers for drug delivery. This includes energy harvesting applications using nanomaterials, nanosuspensions in fight against COVID-19, nanofilms for photodetection, electromagnetic interference (EMI) shielding applications, and even role of nanomaterials in biofilm eradication and also environmental protection. The vast energy applications of nanomaterials including energy generation, storage, energy saving, and EMI shielding will be an innovative and ground-breaking theme of the book. Functionalized magnetic nanoparticles for drug delivery, magnetic hyperthermia, sutures, cancer therapy, dentistry, animal nutrition, and other biomedical and bioengineering applications are discussed in detail.

Key Features

- Illustrates in brief the major scientific impacts offered by nanomaterials, one-dimensional (1D) nanofibers, and 2D nanomaterials.
- Highlights the energy applications, electromagnetic interference shielding, industrial applications, environmental applications, and biomedical and healthcare applications of nanomaterials.
- Exemplifies applications of ferromagnetic and multiferroic nanomaterials, inorganic nanomaterials, carbon nanomaterials, 1D fibers and 2D layered materials, and nanofluids.

About the Editors

Prof. Sabu Thomas, an outstanding Alumnus of IIT, Kharagpur, is one of India's most renowned scientists in the area of Polymers. After completing his PhD from IIT Kharagpur (1984–1987), he joined Mahatma Gandhi University as a Lecturer in 1997 and later became the Vice Chancellor of the University. He has taken up a large number of visiting assignments abroad. Under his leadership, the University has been ranked 713th by TIME, 30th in NIRF, and the best university in Kerala.

Dr. Nandakumar Kalarikkal is a Senior Professor (Former Director and Chair) at the School of Pure and Applied Physics and Former Director and Joint Director of the International and Inter University Centre for Nanoscience and Nanotechnology of Mahatma Gandhi University, Kottayam, Kerala, India. His research activities involve applications of nanostructured materials, laser plasma, computational nanoscience, and phase transitions. He is a Fulbright Fellow and the recipient of research fellowships and associateships from prestigious government organizations such as the Department of Science and Technology and Council of Scientific and Industrial Research of the Government of India.

Ann Rose Abraham, PhD, is currently an Assistant Professor at the Department of Physics, Sacred Heart College (Autonomous), Thevara, Kochi, Kerala, India. Dr. Abraham received MSc, MPhil, and PhD degrees in Physics from the School of Pure and Applied Physics, Mahatma Gandhi University, Kerala, India. Her PhD thesis was on the "Development of Hybrid Multiferroic Materials for Tailored Applications." She is an expert in the fields of condensed matter physics, nanomagnetism, multiferroics, and polymeric nanocomposites. She has a good number of publications to her credit in many peer-reviewed, high-impact journals of international repute and is the editor of numerous books.

ELSEVIER elsevier.com/books-and-journals

Material Science

ISBN 978-0-12-820557-0

9 780128 205570